

Vol. 21, No. 4, December, 2022

ISSN (Print): 0972-6268; ISSN (Online) : 2395-3454

# NATURE ENVIRONMENT & POLLUTION TECHNOLOGY

*A Multidisciplinary, International Journal  
on Diverse Aspects of Environment*



**Technoscience Publications**

website: [www.neptjournal.com](http://www.neptjournal.com)



# Technoscience Publications

A-504, Bliss Avenue, Balewadi,  
Opp. SKP Campus, Pune-411 045  
Maharashtra, India

[www.neptjournal.com](http://www.neptjournal.com)

## Nature Environment and Pollution Technology

(An International Quarterly Scientific Research Journal)

### EDITORS

**Dr. P. K. Goel (Chief Editor)**

Former Head, Deptt. of Pollution Studies  
Y. C. College of Science, Vidyanagar  
Karad-415 124, Maharashtra, India

**Dr. K. P. Sharma**

Former Professor, Deptt. of Botany  
University of Rajasthan  
Jaipur-302 004, India

**Managing Editor :** Mrs. Apurva Goel Garg, C-102, Building No. 12, Swarna CGHS, Beverly Park, Kanakia, Mira Road (E) (Thane) Mumbai-401107, Maharashtra, India

**Published by :** Mrs. T. P. Goel, Technoscience Publications, A-504, Bliss Avenue, Balewadi, Pune-411 045, Maharashtra, India

**E-mail :** [contact@neptjournal.com](mailto:contact@neptjournal.com); [operations@neptjournal.com](mailto:operations@neptjournal.com)

### INSTRUCTIONS TO AUTHORS

#### Scope of the Journal

The Journal publishes original research/review papers covering almost all aspects of environment like monitoring, control and management of air, water, soil and noise pollution; solid waste management; industrial hygiene and occupational health hazards; biomedical aspects of pollution; conservation and management of resources; environmental laws and legal aspects of pollution; toxicology; radiation and recycling etc. Reports of important events, environmental news, environmental highlights and book reviews are also published in the journal.

#### Format of Manuscript

- The manuscript (*mss*) should be typed in double space leaving wide margins on both the sides.
- First page of *mss* should contain only the title of the paper, name(s) of author(s) and name and address of Organization(s) where the work has been carried out along with the affiliation of the authors.

*Continued on back inner cover...*

# Nature Environment and Pollution Technology

Vol. 21, No. (4), December 2022

## CONTENTS

1. **Xinjie Yu, Xiongfei Cai, Ji Wang, Shuai Zhang, Shuai Zhao and Die Xu**, Bioaccessibility and Health Risk Assessment of Heavy Metals in Dust of the Urban Areas of Guiyang, Guizhou, China 1471-1480
2. **Jing Zhang, Haihua Jing, Kebao Dong, Jiaqi Ma and Zexu Jin**, Effect of Drip Irrigation Under Mulch on Nitrogen Transport in Deep Soil Layers in an Agricultural Region of the Xiliao River Plain, China 1481-1490
3. **Manish Kumar Mandal and Bala Ramudu Paramkusam**, Analysis of Alkali-Induced Soil Heaving in Non Expansive Soil Using Electrokinetic Model 1491-1505
4. **M. Arthy and B. R. Phanikumar**, Statistical Analysis and Modeling of Trivalent Chromium Ion Adsorption by Green-Mediated Iron Nanoparticles 1507-1517
5. **R. Ramanathan, L. Abdullah, M. S. Syed Mohamed and M.H.F.M Fauadi**, A Review of User-Centred Design Methods for Designing a Portable Oil Spill Skimmer 1519-1529
6. **S. R. Hariprakash and T. Prakash**, A Review on Microalgae Biofuel Production and use in CI Engine Applications 1531-1541
7. **L. S. Cao, H. Xu and H. Li**, Effect of Greening Trees on Thermal Comfort of the Pedestrian Streets in Hot Summer and Cold Winter Regions in China 1543-1552
8. **Namrata and N. D. Wagh**, A Review on Atmospheric Dispersion System for Air Pollutants Integrated with GIS in Urban Environment 1553-1563
9. **W. M. W. Rozita, S. Zamtira, FI. Mohd, T. L. Mohd, I. A. Nurul, I. A. W. Muhammad and S. Mazrura**, Air Pollution, Cardiovascular and Respiratory Admissions in Klang Valley, Malaysia - Finding the Effects 1565-1573
10. **B. S. Rajyaguru, A. Varma, A. C. Kharkwal and J. Singh**, Enhancement of Xanthan Biosynthesis Using Medicinal Herbs - A Novel Approach 1575-1585
11. **Safaa K. Hashim Al-Khalaf, Ahmed Samir Naje, Zaid Abed Al-Ridah and Haider M. Zwain**, Environmental Modelling of Ionic Mass Transfer Coefficient in a Unique Electrocoagulation Reactor 1587-1597
12. **Chitrakara Hegde and Rahul Ribeiro**, Preparation and Characterization of Hydrophobic Membranes and Their Seawater Desalination Performance Study by Direct Contact Membrane Distillation 1599-1608
13. **Dashuang Liang, Wenping Liu and Yugang Zhao**, Optimal Models for Plant Disease and Pest Detection Using UAV Image 1609-1617
14. **Shefali Arora**, The Inherent Grave Consequences of Glacial Retreat 1619-1627
15. **Ramzi H. Amran, Mamdoh T. Jamal, Arulazhagan Pugazhendi, Mamdouh Al-Harbi and Saba Bowrji**, Petroleum Hydrocarbon Degradation and Treatment of Automobile Service Station Wastewater by Halophilic Consortia Under Saline Conditions 1629-1637
16. **Dharmendra Kumar Singh and Nawal Kishore**, Geoelectrical Sounding to Identify Sub-surface and Groundwater State at Village Banauli, Singrauli District, Madhya Pradesh, India 1639-1647
17. **C. K. Fu, Y. Fang, C. Y. Yang, C. G. Chen and L. X. Wang**, Investigation of Adsorption of Heavy Metal Ions on C<sub>3</sub>N<sub>4</sub> Nanosheets by Batch and Microscopic Methods 1649-1656
18. **N. Siddiqui, T. Faiyaz and V. S. Tari**, Ganga and Yamuna Rivers: Through the Lens of the National Green Tribunal 1657-1664
19. **I.W. Supartha, A. Roifiq, I.W. Susila, I.M. Damriyasa, M. Tulung, I.K.W. Yudha, I.W.E.K. Utama and P. A. Wiradana**, Population Structure of Thrips parvispinus Karny (Thysanoptera: Thripidae) and Population Abundance of Predatory Insect on Red Chili (*Capsicum annum* L.) Treated with Imidacloprid Insecticide 1665-1671
20. **N. Vasudha and P. Venkateswara Rao**, Identification of Dominant Air Pollutants Over Hyderabad Using Principal Component Analysis (PCA) 1673-1680
21. **K. A. Viraj Miyuranga, U. S. P. R. Arachchige, D. Thilakarathne, R. A. Jayasinghe and N. A. Weerasekara**, Impact of the Chemical Composition of Oil for Biodiesel Production to Reduce Environmental Pollution 1681-1687
22. **Yogyata Srivastava, Abhishek Chauhan, S. B. Singh and Tanu Jindal**, Impact of Environmental Pollutants on Alzheimer's Disease: A Review 1689-1695
23. **L. Quiñones-Huatangari, F. H. Fernandez-Zarate and A. E. Huaccha-Castillo**, Nitrous Oxide Emissions Generated in Coffee Cultivation: A Systematic Review 1697-1703
24. **Jonmenjoy Barman, Subhom Narjinary, Sankar Biswas, Brototi Biswas and Ratnaprabha Jadhav**, Elephant Habitat Suitability Analysis of Alipurduar District, West Bengal Using Geospatial Technology 1705-1712
25. **Nella Yulia Sari and Fida Rachmadiarti**, Potency of *Jatropha integerrima* Jacq., *Hibiscus rosa-sinensis* L. and *Ruellia tweediana* as Absorbants of Lead (Pb) in Air 1713-1720
26. **R. R. Lohar and C. P. Hase**, Sustainable Production of Soybean (*Glycine max* L.) Crop Through Chemical Fertilizers and Organic Manures Along with the Improvement in Soil Health 1721-1728
27. **Fauzan Ali Ikhsan, Bambang Setioko and Atiek Suprapti**, Water Sustainability Concept of Hindu Javanese Community Settlements Toward Global Climate Change Resilience in the Indonesia Mountainous Area 1729-1737
28. **P. Negi, R. Thakur, K. Manral, K. Tomar, B. S. Rawat, B. Ramola and Waseem Ahmad**, Coated Controlled-Release Fertilizers: Potential Solution for Sustainable Agriculture 1739-1745

29. **A. A. Elewee and M. Sh. Aswood**, Estimation of Indoor Radon Concentration in Some Houses in Al-Shatra District, Dhi-Qar Governorate, Iraq 1747-1752
30. **M. K. Yadav and A. K. Srivastava**, Effective Mixer Design an Important Factor In SSCR Systems for Reduction of NO<sub>x</sub> from Exhaust of Diesel Engines 1753-1760
31. **A. Ma'ruf and S. Hartati**, Production and Characterization of Nano-Chitosan from Blood Clamshell (*Anadara granosa*) by Ionic Gelation 1761-1766
32. **Sudhir Kumar Chaturvedi**, Health Impact Assessment of Air Pollution in India During COVID-19 Lockdown by Using Satellite Remote Sensing and Deep Learning 1767-1774
33. **Shikha Arya, Prabhawati Tiwari, Alok Sagar Gautam and Manish Sharma**, Aeropalynology of *Parthenium hysterophorus* L. in Relation to Meteorological Parameters from Srinagar Valley of Garhwal Himalaya, Uttarakhand 1775-1781
34. **N. N. Abdulqader, B. S. Isgör, A. N. Genç, Enver Güler and Vahide Cansu Seymenoglu**, Modeling Surface Water Quality and Nutrient Correlation with Sediment Oxygen Demand at Dam Water Reservoirs 1783-1806
35. **M. Kaur, A. Bhatnagar, O. Dhillon and A. S. Yadav**, Genotoxic Effects of Rice-Agrochemicals on *Channa punctatus* (Bloch) and *Cyprinus carpio* (Linnaeus) Using Micronucleus Assay and Alkaline Single Cell Gel Electrophoresis 1807-1815
36. **Irrinki Hemalatha, Dakamari Harika and Manoj Kumar Karnena**, Sustainable Nano-Bioremediation Approaches for the Treatment of Polluted Soils 1817-1826
37. **J. Zhang, L. Xia, R. Han and W. Wei**, Comparison of As(III) Adsorption by Nanomagnetic Fe<sub>3</sub>O<sub>4</sub>, Activated Carbon and Modified Activated Carbon 1827-1835
38. **Shilpa A. Veerabhadranavar and B. Venkatesh**, An Assessment of Future Predictions of Rainfall Using GCM Projections in the Western Ghats Region of India 1837-1845
39. **Feifei Wang, Jinlu Guo, Yufei Quan, Sumin Wang and Qiguan Wang**, Recent Advances in Electrocatalytic Nitrogen Reduction to Produce Ammonia Under Ambient Conditions 1847-1855
40. **Yanwei Yang, Weiguo Sun and Chi Li**, Research on the Governance of Rural Environmental Pollution in Heilongjiang Province Based on the Environmental Kuznets Curve 1857-1864
41. **R. Kanimozhi, D. Arvind Prasath, R. Dhandapani and Santhosh Sigamani**, Response Surface Optimization of Culture Conditions of *Microcystis* sp. to Enhance its Biomass Production and Explore its Potential as Antimicrobials 1865-1873
42. **O.H. Aremu, C.O. Akintayo, S.M. Nelana, M.J. Klink and O.S. Ayanda**, Optimization of Influential Parameters for the Degradation of Metronidazole Contained in Aquaculture Effluent via Sonocatalytic Process: Kinetics and Mechanism 1875-1885
43. **S. Talwar, K. Bamel, Prabhavathi and A. Mal**, Effect of High Temperature on Reproductive Phase of Plants: A Review 1887-1892
44. **N.D. Permatasari, J.E. Witoyo, M. Masruri, S.S. Yuwono and S.B. Widjanarko**, Application of a Two-Level Full Factorial Design for the Synthesis of Composite Bioplastics from Durian Seed Flour and Yellow Konjac Flour Incorporating Ethanolic Extract of *Syzygium myrtifolium* Leaves and its Characterization 1893-1901
45. **P. Agrawal, A. Agrawal and A. K. Patel**, Community Level Physiological Profiling of Microbial Communities Influencing Mine Spoil Genesis in Chronosequence Coal Mine Overburden Spoil 1903-1912
46. **M.A.H. Bhuiyan and M.A. Darda**, The COVID-19 Pandemic and Sustainable Tourism Development 1913-1919
47. **S. Rajalakshmi, B. Mythili Gnanamangai, D. Vinoth Kumar, V. Sri Santhya, M. Priya, R. Mary Josephine, Ashutosh Kumar Srivastava, R. Sudhakaran and M. A. Deepa**, Green Campus Audit Procedures and Implementation to Educational Institutions and Industries 1921-1932
48. **O. J. Oyebode and J. A. Otoko**, Medical Waste Management and Design of a Low-Cost Incinerator for Reduction of Environmental Pollution in a Multi-System Hospital 1933-1942
49. **P. Chaitanya, Era Upadhyay, Desh Deepak Singh and Virendra Singh**, Effective Contribution of Air Pollutants to Physiological and Psychological Human Diseases: A Systematic Review 1943-1954
50. **J.A. Vásquez-Contreras, M.R. Castañeda-Chávez, O.P. Castellanos-Onorio, V. Alcántara-Méndez, P. Zuñiga-Ruíz, A. García-Saldaña and M. Díaz-González**, Radiological Study of Water for Human Use and Consumption in Rural Areas of the Central Zone of the State of Veracruz, Mexico 1955-1962
51. **S. K. Verma, A. D. Prasad and M. K. Verma**, An Assessment of Ongoing Developments in Water Resources Management Incorporating SWAT Model: Overview and Perspectives 1963-1070
52. **Ibrahim Abdelfattah, Wael Abdelwahab and Ashraf M. El-Shamy**, Environmental Remediation of Contaminated Wastewater with Ammonium Using Clay-Based Adsorbents 1971-1982
53. **Reema Mandal, Anirban Das, A. K. Sudheer, Rajnee Ranjan and Mahesh Gaddam**, Fluorid Contamination of Groundwater from Semi-Arid Regions of Western India 1983-1994
54. **N. Sunaedi, S. P. Hadi and A. N. Bambang**, Payment for Environmental Services in Indonesia: Mutually Beneficial Watershed Environmental Management Model 1995-2004
55. **A.M.A. Bahar, M. Muhammad, M. T. Anees and M. M. A. Khan**, Development of Flood Vulnerability and Risk Indices for Kelantan District, Peninsular Malaysia 2005-2014

The Journal  
is  
Currently  
Abstracted  
and  
Indexed  
in:

CAB Abstracts, U.K.

Ulrich's (Refereed) database

Zetoc

J-Gate

Centre for Research Libraries

Connect Journals (India)

Research Bible (Japan)

Elektronische  
Zeitschriftenbibliothek (EZB)

CNKI Scholar (China National  
Knowledge Infrastructure)

AGRIS (UN-FAO)

CNKI Scholar (China National Knowledge Infrastructure)

Scopus CiteScore (2021) 0.70

Scopus®, SJR (0.169) 2021

Index Copernicus (2021) = 111.68

Chemical Abstracts, U.S.A.

Indian Science Abstracts,  
New Delhi, India

Pollution Abstracts, U.S.A.

Elsevier Bibliographic  
Databases

Paryavaran Abstract,  
New Delhi, India

Zoological Records

Electronic Social and Science  
Citation Index (ESSCI)

Indian Citation Index (ICI)

CrossRef (DOI)

EBSCO: Environment Index™

Google Scholar

DOAJ

Environment Abstract, U.S.A.

ProQuest, U.K.

WorldCat (OCLC)

British Library

Indian Science

JournalSeek

SHERPA/RoMEO

Directory of Science

CSA: Environmental Sciences and Pollution Management

Access to Global Online Research in Agriculture (AGORA)

Present in UGC-CARE List (Group II)

UDL-EDGE (Malaysia) Products like *i*-Journals, *i*-Focus and *i*-Future

[www.neptjournal.com](http://www.neptjournal.com)

# Nature Environment and Pollution Technology

## EDITORS

### Dr. P. K. Goel (Chief Editor)

Former Head, Deptt. of Pollution Studies  
Yashwantrao Chavan College of Science  
Vidyanagar, Karad-415 124  
Maharashtra, India

### Dr. K. P. Sharma

Former Professor, Ecology Lab, Deptt. of Botany  
University of Rajasthan  
Jaipur-302 004, India  
Rajasthan, India

**Managing Editor:** Mrs. Apurva Goel Garg, C-102, Building No. 12, Swarna CGHS, Beverly Park, Kanakia, Mira Road (E) (Thane) Mumbai-401107, Maharashtra, India (**E-mail: [operations@neptjournal.com](mailto:operations@neptjournal.com)**)

**Business Manager:** Mrs. Tara P. Goel, Technoscience Publications, A-504, Bliss Avenue, Balewadi, Pune-411 045, Maharashtra, India (**E-mail: [contact@neptjournal.com](mailto:contact@neptjournal.com)**)

## EDITORIAL ADVISORY BOARD

1. **Dr. Prof. Malay Chaudhury**, Department of Civil Engineering, Universiti Teknologi PETRONAS, Malaysia
2. **Dr. Saikat Kumar Basu**, University of Lethbridge, Lethbridge AB, Canada
3. **Dr. Sudip Datta Banik**, Department of Human Ecology Cinvestav-IPN Merida, Yucatan, Mexico
4. **Dr. Elsayed Elsayed Hafez**, Deptt. of of Molecular Plant Pathology, Arid Land Institute, Egypt
5. **Dr. Dilip Nandwani**, College of Agriculture, Human & Natural Sciences, Tennessee State Univ., Nashville, TN, USA
6. **Dr. Ibrahim Umaru**, Department of Economics, Nasarawa State University, Keffi, Nigeria
7. **Dr. Tri Nguyen-Quang**, Department of Engineering Agricultural Campus, Dalhousie University, Canada
8. **Dr. Hoang Anh Tuan**, Deptt. of Science and Technology Ho Chi Minh City University of Transport, Vietnam
9. **Mr. Shun-Chung Lee**, Deptt. of Resources Engineering, National Cheng Kung University, Tainan City, Taiwan
10. **Samir Kumar Khanal**, Deptt. of Molecular Biosciences & Bioengineering, University of Hawaii, Honolulu, Hawaii
11. **Dr. Sang-Bing Tsai**, Zhongshan Institute, University of Electronic Science and Technology, China
12. **Dr. Zawawi Bin Daud**, Faculty of Civil and Environmental Engg., Universiti Tun Hussein Onn Malaysia, Johor, Malaysia
13. **Dr. Srijan Aggarwal**, Civil and Environmental Engg. University of Alaska, Fairbanks, USA
14. **Dr. M. I. Zuberi**, Department of Environmental Science, Ambo University, Ambo, Ethiopia
15. **Dr. Prof. A.B. Gupta**, Dept. of Civil Engineering, MREC, Jaipur, India
16. **Dr. B. Akbar John**, Kulliyah of Science, International Islamic University, Kuantan, Pahang, Malaysia
17. **Dr. Bing Jie Ni**, Advanced Water Management Centre, The University of Queensland, Australia
18. **Dr. Prof. S. Krishnamoorthy**, National Institute of Technology, Tiruchirapally, India
19. **Dr. Prof. (Mrs.) Madhoolika Agarwal**, Dept. of Botany, B.H.U., Varanasi, India
20. **Dr. Anthony Horton**, Envirocarb Pty Ltd., Australia
21. **Dr. C. Stella**, School of Marine Sciences, Alagappa University, Thondi -623409, Tamil Nadu, India
22. **Dr. Ahmed Jalal Khan Chowdhury**, International Islamic University, Kuantan, Pahang Darul Makmur, Malaysia
23. **Dr. Prof. M.P. Sinha**, Dumka University, Dumka, India
24. **Dr. G.R. Pathade**, H.V. Desai College, Pune, India
25. **Dr. Hossam Adel Zaqoot**, Ministry of Environmental Affairs, Ramallah, Palestine
26. **Prof. Riccardo Buccolieri**, Deptt. of Atmospheric Physics, University of Salento-Dipartimento di Scienze e Tecnologie Biologiche ed Ambientali Complesso Ecotekne-Palazzina M S.P. 6 Lecce-Monteroni, Lecce, Italy
27. **Dr. James J. Newton**, Environmental Program Manager 701 S. Walnut St. Milford, DE 19963, USA
28. **Prof. Subhashini Sharma**, Dept. of Zoology, University of Rajasthan, Jaipur, India
29. **Dr. Murat Eyvaz**, Department of Environmental Engg. Gebze Inst. of Technology, Gebze-Kocaeli, Turkey
30. **Dr. Zhihui Liu**, School of Resources and Environment Science, Xinjiang University, Urumqi, China
31. **Claudio M. Amescua García**, Department of Publications Centro de Ciencias de la Atmósfera, Universidad Nacional Autónoma de México
32. **Dr. D. R. Khanna**, Gurukul Kangri Vishwavidyalaya, Haridwar, India
33. **Dr. S. Dawood Sharief**, Dept. of Zoology, The New College, Chennai, T. N., India
34. **Dr. Amit Arora**, Department of Chemical Engineering Shaheed Bhagat Singh State Technical Campus Ferozepur -152004, Punjab, India
35. **Dr. Xianyong Meng**, Xinjiang Inst. of Ecology and Geography, Chinese Academy of Sciences, Urumqi, China
36. **Dr. Sandra Gómez-Arroyo**, Centre of Atmospheric Sciences National Autonomous University, Mexico
37. **Dr. Manish Sharma**, Research and Development Cell, Bahra University, Shimla Hills, Shimla, India
38. **Dr. Wen Zhang**, Deptt. of Civil and Environmental Engineering, New Jersey Institute of Technology, USA



# Bioaccessibility and Health Risk Assessment of Heavy Metals in Dust of the Urban Areas of Guiyang, Guizhou, China

Xinjie Yu, Xiongfei Cai, Ji Wang<sup>†</sup>, Shuai Zhang, Shuai Zhao and Die Xu

School of Geographic and Environmental Sciences, Guizhou Normal University, Guiyang, 550025, China

<sup>†</sup>Corresponding author: Ji Wang; chuliu0610@163.com (Xinjie Yu)

Nat. Env. & Poll. Tech.  
Website: [www.neptjournal.com](http://www.neptjournal.com)

Received: 27-10-2021

Revised: 07-01-2022

Accepted: 24-01-2022

## Key Words:

Urban Dust  
Heavy metals  
Bioaccessibility  
Health risk

## ABSTRACT

To investigate what health risks the heavy metals in dust will bring to the human body after they enter humans through different exposure pathways- breathing inhalation and hand-to-mouth ingestion, this study took the old urban area of Guiyang as the study area to grasp the heavy metal concentrations of surface dust, in recreative squares main streets, hospitals, residential areas, and schools in the urban area, and the bioaccessibility in the simulated lung and simulated gastrointestinal. The results showed that the concentrations of Cu, Pb, Zn, Cd, Ni, and Cr in the dust were higher than the background values. Particularly, the Zn concentration exceeded the background value by 9.71 times. The bioaccessibility results indicated that the most soluble heavy metals in the simulated lung, simulated stomach, and simulated intestine were Zn, Ni, and Cu, respectively, and the bioaccessibility of most heavy metals was significantly higher in the gastric phase than that in the intestinal phase, and only the bioaccessibility of Cu was higher in the intestinal phase than that in the gastric phase. The linear results fit showed that the total amount of heavy metals alone could not be used for predicting the human intake of heavy metals in the dust. Human health risk assessment based on bioaccessibility showed that children had higher non-carcinogenic and carcinogenic risks than adults in terms of both hand-to-mouth ingestion and respiratory inhalation exposure pathways, but none of these figures exceeded the limit values.

## INTRODUCTION

Cities are now where people spend the majority of their time, and their rapid development has led to numerous environmental health problems (Li et al. 2019a). As an inorganic pollutant, heavy metals are featured by bioconcentration and difficult degradation and can cause a variety of hazards after entering the human body through different exposure pathways (Tang et al. 2017). Dust is an important carrier for the attachment of heavy metals and various pollutants. Since dust is at a different environmental interface and can bring important source-sink effects (Renata et al. 2021). Therefore, many scholars have studied the sources and spatial distribution of heavy metals in dust, and most of the findings show that the sources of heavy metals in dust are mainly related to vehicle exhaust emissions, wear and tear of the vehicles, and aging of pavement materials, while the spatial distribution is related to the source of pollution (Han et al. 2020, Yu et al. 2021, Jose et al. 2021).

Bioaccessibility refers to the ratio of the amount of contaminants released in the gastrointestinal fluid to the total amount after the contaminants in the soil and food enter the human digestive system. Compared with the traditional

assessment methods, bioaccessibility can more accurately reflect the heavy metals in the human body scientifically and reasonably. There has been a lot of research on bioaccessibility at home and abroad, but the researches mainly focus on soil heavy metals and metal mining areas, etc. (Du et al. 2020, Sultana et al. 2020). Although the bioaccessibility of heavy metals in dust has been reported, the simulated digestion phase is only limited to the gastrointestinal phase, and there are few studies on the bioaccessibility of the simulated respiratory system in vitro. Therefore, this study used in vitro simulated human digestive system and respiratory system to conduct the bioaccessibility study, and it is significant to carry out a health risk assessment on the urban populations based on bioaccessible concentration.

With the rapid development of the economy and the continuous expansion of urban transportation, Guiyang's ecological and environmental problems have become increasingly prominent. The main objective of this study was to evaluate the total heavy metal concentrations in Guiyang city. In vitro simulation method was used to simulate the leaching of heavy metals from dust in human lungs and gastrointestinal tract respectively, to explore the bioaccessibility of heavy metals. Finally, according to the bioaccessibility of heavy

metals in different stages, these data could be used to conduct non-carcinogenic and carcinogenic health risk assessment studies for adults and children in the city.

## MATERIALS AND METHODS

### Study Area

Guiyang city (106°07'-107°17'N, 26°11'-27°22'E), as it is known in Fig. 1, is located in the central part of the Guizhou province. The old urban areas of Guiyang City were selected for this research: Yunyan District and Nanming District. These old urban areas have been developed for a long period, and there have been historical residues of heavy metals in the dust on the surface of old urban areas due to the expansion of traffic and the construction of a large number of high-rise buildings in its long history course. Therefore, urban residents living in the old city are facing potential health risks from dust and heavy metal exposure.

### Sampling and Sample Preparation

A total of 71 dust sampling points were shown in Fig. 1. The sampling sites covered recreative squares, main streets, hospitals, residential areas, schools, and other areas where most people locate. The dust samples are collected from April to May 2021, and it was ensured that the humidity in the city was not high and the weather was clear during the sampling period. All dust samples were packed in individually labeled polyethylene sealed plastic bags and were transported back to the laboratory for processing afterward. Before the experiment, extra materials, such as hairs, sand, grit, and plant residues, were removed from samples through a 1mm nylon

screen. Finally, samples were sieved through a 200  $\mu\text{m}$  mesh nylon screen, labeled, and prepared to be tested.

### Gamble Analysis

In vitro simulated respiratory system mainly uses the Gamble analysis method (Zoitos et al. 1997). The simulated lung fluid was added to each reactor with a solid-liquid ratio of 1:1000, and the temperature was kept at 37°C, the normal temperature of the human body. The solution oscillated at 100  $\text{r}\cdot\text{min}^{-1}$  for 24 h in a constant-temperature oscillator, centrifuged at 5,000  $\text{r}\cdot\text{min}^{-1}$  for 10min, and filtered through a 0.45  $\mu\text{m}$  filter membrane. Finally, the contents of Cu, Pb, Zn, Cd, Ni, and Cr in the filtrate were measured by inductively coupled plasma mass spectrometry (ICP-MS, PerkinElmer NexION 2000).

### Physiologically-Based Extraction Test (PBET) Analysis

The PBET method has become the most typical in vitro method for simulating the digestive system (Ruby et al. 1993). The method was based on the physiological characteristics of the human body to simulate the digestion stage of the stomach and the absorption stage of the small intestine. The simulated gastric liquid was added to each reactor at a 1:100 solid-to-liquid ratio and was oscillated in a constant-temperature oscillator at 100  $\text{r}\cdot\text{min}^{-1}$  for 1 h. In the intestinal phase, saturated  $\text{NaHCO}_3$  solution was added until the pH of the solution reached 8.0, and then 0.14 g of bile salt and 0.04 g trypsin were added into the constant, and the mixture oscillated under the same conditions as the simulated stomach for 4 h. Then the supernatant was collected, centrifuged, and filtered.

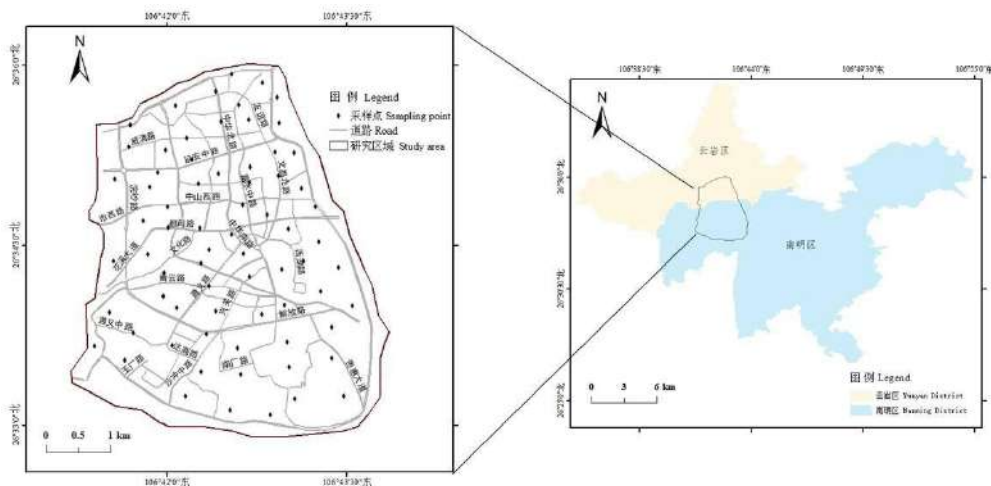


Fig. 1: Sampling points and map of the study area.



Bioaccessibility in the gastric or intestinal stages could be calculated based on the following equation:

$$BAC(\%) = \frac{C_{IV} \times V_{IV}}{T_S \times M_S} \times 100\% \quad \dots(1)$$

Where *BAC* is the bioaccessibility for heavy metals; *C<sub>IV</sub>* means the concentration of heavy metals in the soluble state in the lung dissolution, gastric digestion, and intestinal absorption phases for the simulated experiment (mg.L<sup>-1</sup>); *V<sub>IV</sub>* refers to the volume for the reaction solution in each reactor (L); *T<sub>S</sub>* is the total amount for heavy metals in the sample (mg.kg<sup>-1</sup>); *M<sub>S</sub>* is the mass for the sample in the reactor (kg).

### Human Health Risk Assessment

Considering that human exposure to heavy metals in the dust is mainly through two exposure routes respiratory inhalation and hand-to-mouth ingestion, this study was mainly based on the bioaccessibility of simulated lungs and simulated gastrointestinal tracts to calculate the average daily exposure and the corresponding non-carcinogenic and carcinogenic risks for adults and children under these two routes. the average daily exposure (ADD) and risk values were mainly calculated in the following form:

$$ADD_{inh} = \frac{C_{dust} \times InhR \times EF \times ED}{PEF \times BW \times AT} \quad \dots (2)$$

$$ADD_{ing} = \frac{C_{dust} \times IngR \times EF \times ED \times CF}{BW \times AT} \quad \dots (3)$$

The physical meaning and values of the specific formula parameters are listed in Table 1.

Heavy metals accumulate in the human body under different exposure pathways and cause chronic non-carcinogenic risks. Cd, Ni, and Cr mainly cause cancer in people. The human health risks caused by respiratory inhalation, hand-oral ingestion, and dermal exposure in this study are expressed as HI and CR, respectively (USEPA 2007).

$$HQ = \frac{ADD}{RfD} \quad \dots (4)$$

$$HI = \sum HQ_i \quad \dots (5)$$

$$CR = \sum ADD_i \times SF_i \quad \dots (6)$$

where HQ (Hazard Quotient) is the single non-carcinogenic risk; *RfD* means the reference dose at different pathways (mg.kg<sup>-1</sup>.d<sup>-1</sup>). HI represents the total non-carcinogenic risk due to all heavy metals; CR (Cancer Risk) represents the total carcinogenic risk due to all heavy metals; SF refers to the slope for carcinogenicity (mg.kg<sup>-1</sup>.d<sup>-1</sup>).

The Environmental Protection Agency (EPA) believes the risk is low when HQ or HI < 1 and some non-carcinogenic risk is produced when HQ or HI > 1; the carcinogenic risk is negligible when CR is below 10<sup>-6</sup>, within the acceptable range, that is, between 10<sup>-6</sup> and 10<sup>-4</sup>, and above 10<sup>-4</sup>, the carcinogenic risk can be regarded as a serious one. The physical meaning and values of the specific formula parameters are listed in Table 2.

### Data Analysis

The data were compiled by Excel 2016, and the spatial

Table 1: Parameter values in average daily intake calculation models of heavy metals.

Parameter	Physical meaning	Unit	Child	Adult
<i>C<sub>dust</sub></i>	The concentration of heavy metals in dust	mg.kg <sup>-1</sup>	—	—
<i>IngR</i>	Daily intake rate	mg.kg <sup>-1</sup>	100	200
<i>InhR</i>	Inhalation rate	m <sup>3</sup> .d <sup>-1</sup>	5.6	16.5
<i>EF</i>	Exposure frequency	day.year	180	180
<i>ED</i>	Exposure time	year	6	24
<i>PEF</i>	Dust emission factor	m <sup>3</sup> .kg <sup>-1</sup>	1.36×10 <sup>9</sup>	m <sup>3</sup> .kg <sup>-1</sup>
<i>CF</i>	Conversion factor	/	1×10 <sup>-6</sup>	
<i>BW</i>	Average weight	kg	14.9	58.6
<i>ABS</i>	Skin absorption factor	/	0.001	
<i>SA</i>	Exposed skin surface area	cm <sup>2</sup>	4350	1600
<i>AF</i>	Average exposure time	/	0.2	0.2
<i>AT</i> (non-carcinogens)	Average exposure time	day	365×6	365×24
<i>AT</i> (carcinogens)	Average exposure time	day	365×70	365×70

Table 2: Reference doses for non-cancer metals and slope factors for carcinogenic metals.

Elements	<i>RfD<sub>ing</sub></i>	<i>RfD<sub>inh</sub></i>	<i>SF<sub>ing</sub></i>	<i>SF<sub>inh</sub></i>
Cu	4.00E-02	4.00E-02	-	-
Pb	3.50E-03	3.50E-03	-	-
Zn	0.3	0.3	-	-
Cd	1.00E-03	1.00E-03	6.1	6.30
Ni	2.00E-02	2.06E-02	-	0.84
Cr	3.00E-03	2.86E-05	-	42.0

distribution for sampling points was performed by ArcGIS 10.2. The visualization of the data was plotted by OriginPro 8.0. The fitting relationship between the total amount of heavy metals in dust and the bioaccessibility in different simulation stages was performed by SPSS 16.0. The degree of fit could reflect the correlation between the total amount and the bioaccessible amount.

## RESULTS AND DISCUSSION

### Total Metal Concentration

The concentrations of Cu, Pb, Zn, Cd, Ni, and Cr in 71 dust samples in this study were shown in Fig. 2 and Table 3. From Table 3, all heavy metal concentrations of dust were significantly above the background values, which were 5.16, 1.82, 9.71, 2.92, 3.41, 4.99, and 1.72 times the background values, respectively. The concentrations were ranked as follows: Zn > Cu > Cr > Ni > Pb > Cd. Although the concentration of Pb in this study exceeded the background value, it was significantly reduced compared with previous studies on heavy metals in urban road dust. It could be speculated that the Pb concentration in this study was less than limited levels probably because of the widespread use of unleaded gasoline. However, the reason why it was higher than the background value might be due to the relatively long development his-

tory of the old city, some of the Pb was deposited in the dust or might be related to the wear of automobile materials (Zheng et al. 2020). Among the investigated heavy metals, Zn content significantly exceeded the standard of other heavy metals. According to our analysis, the main sampling sites in this study were located near the main roads and parking lots of residential areas. Some studies suggested that the high concentration of Zn was related to the wear and tear of car parts and tires (Goix et al. 2016). According to the statistical principle, the larger the coefficient of variation (C.V), the greater the degree of dispersion of the pollutant, and the greater the influence of external factors. From Table 3, it could be seen that the coefficient of variation was ranked from high to low as Pb > Cd > Zn > Cr > Cu > Ni so it could be seen that Pb, Cd, and Zn showed a higher level of variation, indicating that these three heavy metals were uniformly distributed spatially compared with each other and were more influenced by external factors. At the same time, the conclusion in this study is consistent with the conclusion drawn by Fan et al. (2020).

### In Vitro Stimulation of the Respiratory System

The bioaccessibility of Cu, Pb, Zn, Cd, Ni, and Cr in the simulated lung was shown in Fig. 3 and Table 4. Among the six elements involved in this study, Cr had the lowest

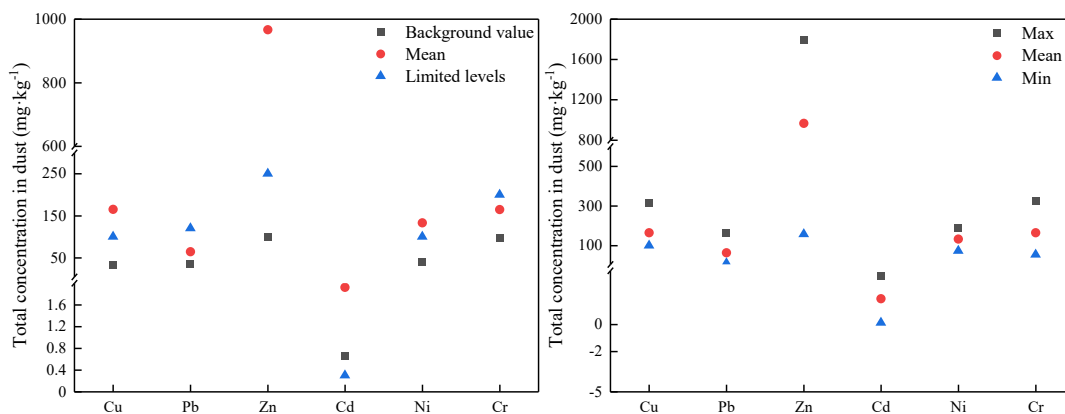


Fig. 2: Total heavy metals in dust in this study.

Table 3: Concentrations of heavy metals ( $\text{mg.kg}^{-1}$ ) in surface dust.

Element	Minimum	Maximum	Median	Mean $\pm$ SD	C.V. [%]	Background value
Cu	100.67	315.72	156.98	$165.41 \pm 47.37$	28.64	32.0
Pb	11.24	163.34	45.82	$64.41 \pm 44.28$	68.76	35.2
Zn	157.44	1793.91	996.21	$966.61 \pm 373.19$	38.61	99.5
Cd	0.13	3.62	1.99	$1.924 \pm 0.89$	46.41	0.659
Ni	73.72	187.52	127.82	$133.26 \pm 26.39$	19.81	39.1
Cr	54.91	325.86	162.64	$164.86 \pm 53.69$	32.57	95.9

bioaccessibility (3.81%) and Zn had the highest bioaccessibility (38.97%). The high dissolution of Zn in simulated lungs might be related to the special characteristic of Zn. Studies had shown that car tire wear is an important source of ZnO in dust, and the low bioaccessibility of Cr might also be related to the occurrence of ZnO (Adachi & Tainoshu 2004). Some researchers extracted different forms of Cr using Tessier sequential extraction method and found that Cr was mainly in the insoluble residual fraction and the soluble fraction was relatively low. Therefore, the bioaccessibility of Cr in simulated lung fluid was the smallest. In this study, the bioaccessibility of Cd in simulated lung fluid was similar to that of Cr and was at a lower level (Li et al. 2019b). However, some studies had shown that the bioaccessibility of Cd in simulated lungs was at a higher level. The reason for the difference may be related to the components in the simulated lung fluid, pH, extraction time, and the source of Cd (Zhang et al. 2019). The bioaccessibility percentages of

the other three heavy metals Cu, Pb, and Ni in the simulated lung were 12.99%, 15.51%, and 10.54%, respectively.

### In Vitro Stimulation of the Digestive System

In this study, the bioaccessibility of heavy metals in dust in the simulated stomach and intestine stage was shown in Fig. 3 and Table 4. It could be seen that the bioaccessibility of Cu, Pb, Zn, Cd, Ni, and Cr in the stomach and intestine of 71 samples. Table 4 summarized the range, average concentration, and median of the bioaccessibility of heavy metals in dust samples. The heavy metals with high bioaccessibility in the gastric phase were Cu, Zn, Cd, and Ni, which all were more than 40%. Cr had the lowest dissolution rate of 4.19%. In the intestinal phase, the average of heavy metals bioaccessibilities was as follows: Cu>Zn>Ni>Cd>Pb>Cr. Compared with the bioaccessibility of the gastric phase, the bioaccessibility in the intestinal phase was significantly reduced, Pb bioaccessibility decreased from 23.89% to 13.26%, Zn

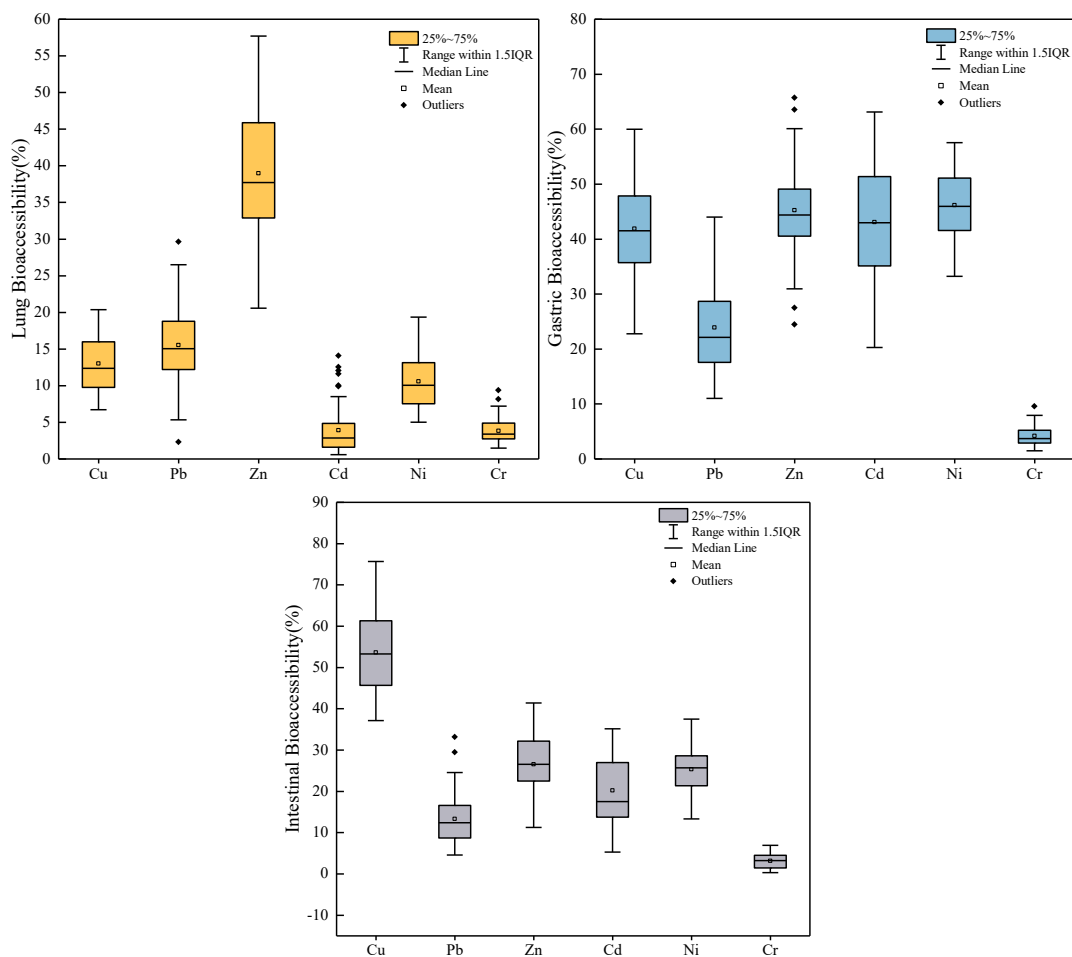


Fig. 3: The percentage for bioaccessibility of each heavy metal at different simulation stages.

Table 4: Bioaccessibility of heavy metals in the lung phase, gastric phase, and intestinal phase of dust.

Heavy metals	Lung [%]			Gastric [%]			Intestinal [%]		
	Range	Median	Mean	Range	Median	Mean	Range	Median	Mean
Cu	6.68-20.36	12.36	12.99	22.77-59.98	41.46	41.85	37.13-75.66	53.26	53.62
Pb	2.26-29.61	15.01	15.51	10.98-43.96	22.11	23.89	4.57-33.14	12.37	13.26
Zn	20.54-57.69	37.67	38.97	24.43-65.69	44.35	45.22	11.25-41.36	26.51	26.49
Cd	0.57-14.03	2.82	3.88	20.26-63.10	42.96	43.07	5.29-35.14	17.46	20.17
Ni	4.99-19.34	10.04	10.54	33.22-57.51	45.91	46.16	13.27-37.46	25.64	25.32
Cr	1.47-9.33	3.39	3.81	1.47-9.51	3.68	4.19	0.27-6.87	3.21	3.09

bioaccessibility from 45.22% to 26.49%, Cd bioaccessibility from 43.07% to 20.17%, and Ni from 46.16% to 25.32%. The bioaccessibility of Cr from the stomach stage to the intestine stage changed little, while Cu increased from 41.85% in the stomach stage to 53.62% in the intestine stage. In general, the bioaccessibility of most heavy metals was significantly higher in the gastric stage than in the intestinal stage. Some research showed that heavy metals, such as Pb, Zn, Cd, and Ni, were more active and easily soluble and digested under acidic conditions in the stomach (Soltani et al. 2021, Zhao et al. 2020). After the heavy metals dissolved in the gastric stage (acidic) enter the intestinal stage (alkaline), the adsorption and precipitation reaction occurred and the solubility of heavy metals decreased. The small degree of

change in Cr might be mainly because Cr was mainly in the form of residues and the dissolution rate was not high in simulated human gastrointestinal fluid (Li et al. 2019b). The reason for the increased Cu bioaccessibility was that Cu could be complex with trypsin and bile salts, thus showing a higher solubility effect in the intestinal absorption phase (Xu et al. 2018).

### Relationships Between the Bioaccessibility and the Total Concentrations

The linear relationships between the total amount of Cu, Pb, Zn, Cd, Ni, and Cr in dust and bioaccessibility in the simulated lung phase, gastric phase, intestinal phase were presented in Fig. 3, Fig. 4, Fig. 5. Linear coefficients ( $R^2$ ) of the total

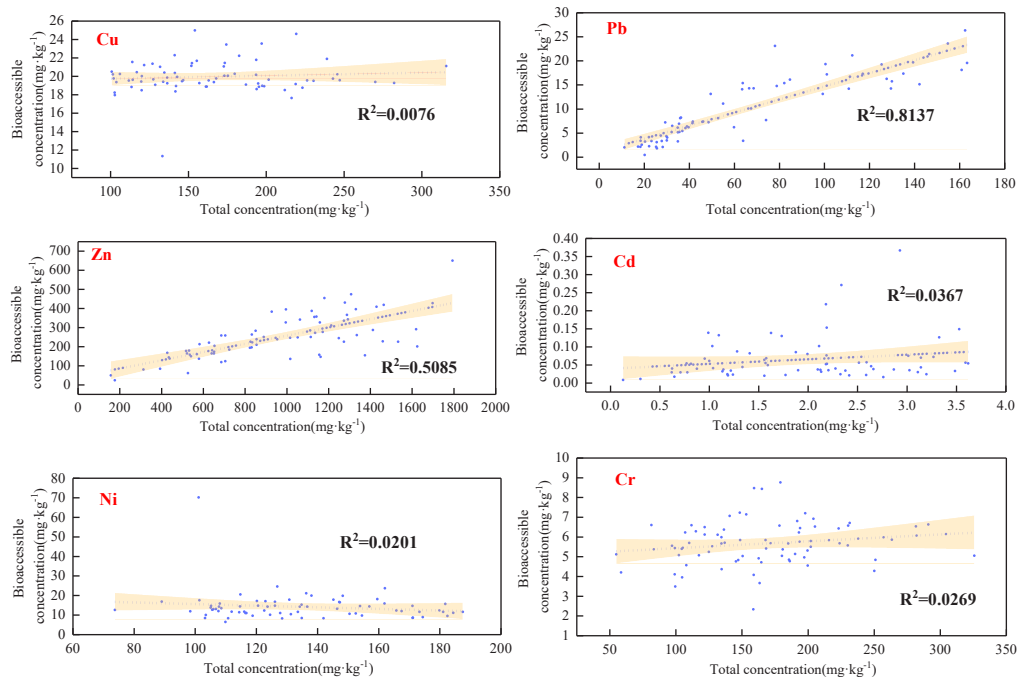


Fig. 4: Linear fit of the lung phase.

amount of each heavy metal in the dust and bioaccessibility in the simulated lung phase were 0.0076, 0.8137, 0.8044, 0.0367, 0.0201, and 0.0269, respectively. Only the total amount of Pb ( $R^2=0.8137$ ) and Zn ( $R^2=0.8044$ ) showed a significant correlation with the concentration of the lung fluid extract, while other heavy metals had no significant linear relationship with the total concentration. The linear coefficients ( $R^2$ ) of each heavy metal in the gastric phase were 0.6057, 0.8003, 0.8074, 0.6868, 0.7151, and 0.1168, respectively. The concentration of Pb, Zn, and Ni in the gastric fluid extract stage showed good correlations with the total amount in dust, Cu and Cd showed moderately positive correlation, and there was no significant correlation for Cr. The linear coefficients ( $R^2$ ) of each heavy metal in the simulated intestinal phase were 0.6279, 0.6276, 0.5085, 0.4501, 0.4135, and 0.1244, respectively, and the total amount of heavy metals showed a moderately positive correlation with the concentration of the intestinal extract stage except for Cr. It could be seen from the linear fit relationships in different phases that the total amount of Pb and Zn could only be used to simply estimate the digestive dissolution in the human lung and stomach, but most of the total heavy metals could not greatly affect the bioaccessibility. Since human mainly intakes heavy metals through the intestine, therefore, the previous health risk using the total amount of heavy metals had some errors and could not accurately reflect the absorption of heavy metals in the human body or carcinogenic and non-carcinogenic risk values (Sun et al. 2018).

### Health Risk Assessment of Heavy Metals Based on Bioaccessibility

According to Table 5, the average daily non-carcinogenic exposure for children was higher than that for adults in both pathways, and the daily average non-carcinogenic was also higher than that for adults. The daily average exposure of non-carcinogenic heavy metals for hand-to-mouth intake was shown as follows: Zn>Cu>Ni>Pb>Cr>Cd. Zn could reach 8.29E-04, and Cd was the smallest among all these heavy metals, reaching 1.21E-06. Thus, in comparison, the number of heavy metals absorbed in the intestine was higher, and the non-carcinogenic risk by hand-oral intake was also much higher than that through respiratory inhalation (Shahab et al. 2018). However, the non-carcinogenic risks for Cu, Pb, Zn, Cd, Ni, and Cr in both exposure pathways did not exceed 1, which was below the standard values, indicating that no non-carcinogenic risks were caused. Although both children and adults had the highest daily average exposure to Zn by these two pathways among all these metals, Pb was the non-carcinogenic element with the greatest risky value in the non-carcinogenic risk assessment results. According to Table 3, children had the highest average daily exposure of Ni for children reached 4.99E-10 under the respiratory inhalation pathway, the total carcinogenic risk for children was 6.38E-07 under the two pathways, and the total carcinogenic risk value for adults was 8.71E-10. Furthermore, the carcinogenic risk values of Cd, Ni, and Cr for children were

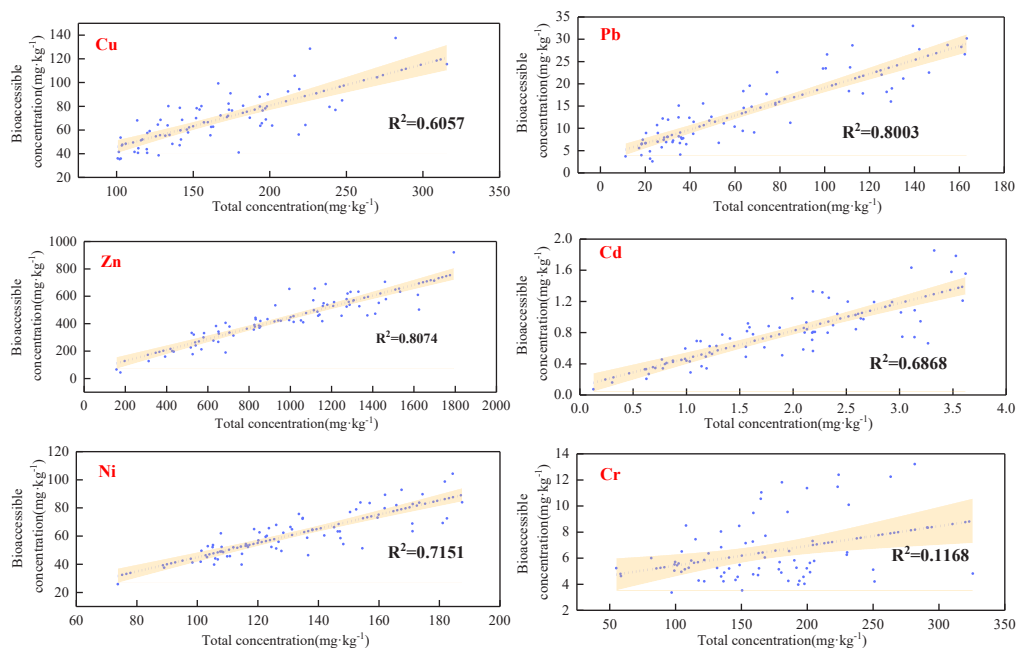


Fig. 5: Linear fit of the gastric phase.

Table 5: Health risk assessment on heavy metals based on bioaccessibility in dust for adults and children.

Heavy metals	Children					Adults				
	ADD <sub>ing</sub>	HQ <sub>ing</sub>	ADD <sub>inh</sub>	HQ <sub>inh</sub>	HI	ADD <sub>ing</sub>	HQ <sub>ing</sub>	ADD <sub>inh</sub>	HQ <sub>inh</sub>	HI
Hazard quotient(HQ) /mg·kg <sup>-1</sup> ·d <sup>-1</sup>										
Cu	1.48E-04	3.69E-03	2.72E-09	6.80E-08	3.69E-03	7.51E-05	1.88E-03	2.04E-09	5.09E-08	1.88E-03
Pb	2.51E-05	7.15E-03	1.34E-09	3.84E-07	7.15E-03	1.27E-05	3.64E-03	1.01E-09	2.88E-07	3.64E-03
Zn	8.29E-04	2.76E-03	5.29E-08	1.76E-07	2.76E-03	4.22E-04	1.41E-03	3.96E-08	1.32E-07	1.41E-03
Cd	1.21E-06	1.22E-03	8.77E-12	8.77E-09	1.22E-03	6.17E-07	6.18E-04	6.57E-12	6.57E-09	6.18E-04
Ni	1.12E-04	5.58E-03	1.94E-09	9.43E-08	5.58E-03	5.67E-05	2.84E-03	1.46E-09	7.07E-08	2.84E-03
Cr	1.62E-05	5.41E-03	7.68E-10	2.68E-05	5.44E-03	8.25E-06	2.75E-03	5.75E-10	2.01E-05	2.77E-03
Total	1.13E-03	2.58E-02	5.97E-08	2.75E-05	2.58E-02	5.75E-04	1.31E-02	4.47E-08	2.06E-05	1.32E-02
Cancer risk(CR)/ mg·kg <sup>-1</sup> ·d <sup>-1</sup>										
Cd	1.04E-07	6.35E-07	7.52E-13	4.74E-12	6.35E-07	6.01E-14	3.67E-13	2.25E-12	1.42E-11	1.46E-11
Ni	—	—	1.67E-10	1.40E-10	1.40E-10	—	—	4.99E-10	4.19E-10	4.19E-10
Cr	—	—	6.58E-11	2.76E-09	2.76E-09	—	—	1.97E-10	8.28E-09	8.28E-09
Total	1.04E-07	6.35E-07	2.34E-10	2.90E-09	6.38E-07	6.01E-14	3.67E-13	6.98E-10	8.71E-09	8.71E-09

6.35E-07, 1.40E-10, and 2.76E-09, respectively. According to the calculation results, the carcinogenic risk of children could also be ignored. The carcinogenic risk values of Cd, Ni, and Cr in adults reached 1.46E-11, 4.19E-10, and 8.28E-09 respectively, which the risk of cancer in adults was negligible based on the calculation results. Based on the evaluation results, although the non-carcinogenic and carcinogenic risks did not reach the risk values, the exposure to heavy metals

was highest under the hand-to-mouth pathway of ingestion, so people who need to travel should take protective measures, such as wearing a mask and washing hands regularly.

## CONCLUSIONS

In this study, the total amount of Cu, Pb, Zn, Cd, Ni, and Cr in surface dust in the old urban area of Guiyang city was

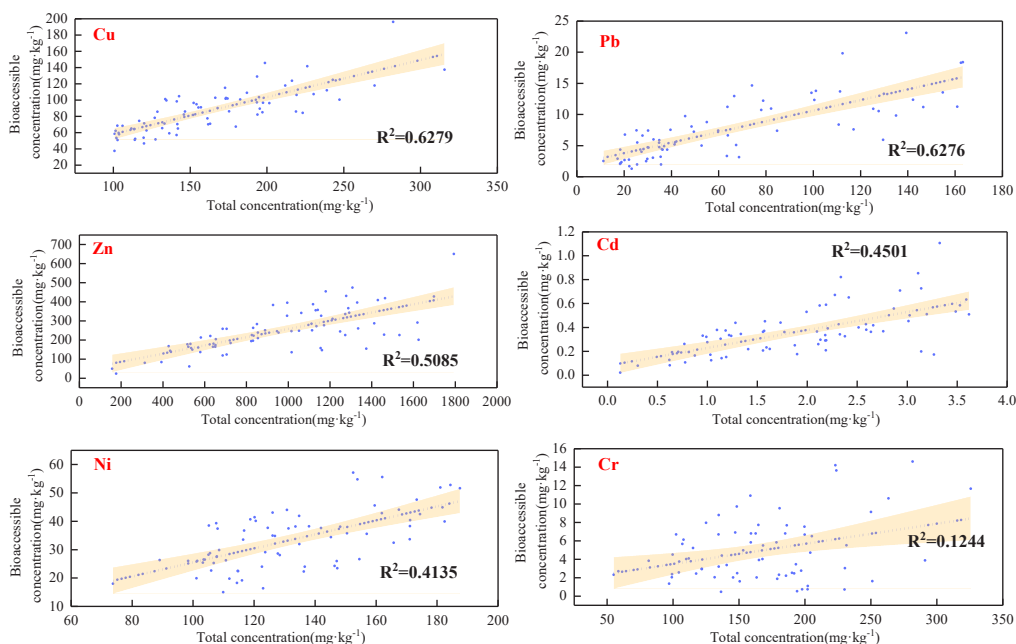


Fig. 6: Linear fit of the intestinal phase.

investigated. The study aimed to study the bioaccessibility and health risk assessment of the two exposure routes of inhalation and hand-to-mouth ingestion were studied. The results indicated that (1) The total amounts of Cu, Pb, Zn, Cd, Ni, and Cr in surface dust in the old urban area of Guiyang exceeded the background values of Guizhou Province, showing different degrees of pollution. Especially, the extent of Zn exceeded the standard greatly, 9.71 times the background value. The coefficient of variation indicated that Pb, Zn, and Cd were mainly disturbed by human activities and external factors. (2) Subsequently, bioaccessibility experiments on heavy metals in dust were conducted in the simulated lung, stomach, and intestine. According to the results, among the heavy metals with the highest dissolution in the simulated lung stage, Zn (38.97%) had the highest bioaccessibility and Cr (3.81%) had the lowest dissolution. In the gastric phase, the highest bioaccessibility was Ni (46.16%) and the lowest dissolution was Cr (4.19%). In the intestinal phase, Cu (53.62%) had the highest bioaccessibility while Cr (3.09%) had the lowest dissolution. (3) Thirdly, a linear fit was shown between the total amount of heavy metals in dust and the bioaccessible amount of Pb and Zn in different simulation stages, which proved that only the bioaccessibility of Pb and Zn had a better correlation with the total amount in the simulated lung and gastric phases. In the simulated intestine stage, the heavy metals had no significant correlation with the total amount in this study, showing that the total amount of heavy metals alone could not help predict the human intake of heavy metals in the dust. (4) The results of health risk assessment based on bioaccessibility showed that the non-carcinogenic and carcinogenic risks for children were higher than those of adults under both hand-to-mouth intake and respiratory inhalation exposure pathways, and the non-carcinogenic and carcinogenic risk values for Cu, Pb, Zn, Cd, Ni, and Cr did not exceed the limits, indicating that the health risks of children and adults in this region were within acceptable limits. However, the non-carcinogenic and carcinogenic risks did not reach risk values, the risk under the hand-to-mouth pathway was higher than those under the respiratory inhalation pathway so people living in this urban area need to take certain protective measures.

## ACKNOWLEDGEMENT

This research was supported by the National Natural Science Foundation of China (grant no. 41807336) and the Science and Technology Plan Project of Guizhou (grant no. [2019]1231).

## REFERENCES

Li, Y.B., Fang, F.M., Lin, Y.S., Wang, Y., Kuang, Y. and Wu, M. H. 2019a.

- Heavy metal contamination and health risks of indoor dust around Xinqiao Mining Area, Tongling, China. *J. Hum. Ecol. Risk Assess.*, 26: 46-56.
- Tang, Z., Miao, C., Cheng, J., Jing, J. and Li, Y. 2017. Contamination and health risks of heavy metals in street dust from a coal mining city in Eastern China. *J. Ecotox. Environ. Safe.*, 138: 83-91.
- Renata, M.N., Figueiredo, A.M.G., Oliveira, C.E.S. and Babinski, M. 2021. Urban contamination sources in tunnel dust from So Paulo city: Elemental and isotopic characterization. *J. Atmos. Environ.*, 254: 118188.
- Han, Q., Wang, M., Cao, J., Gui, C. and Liu, Y. 2020. Health risk assessment and bioaccessibilities of heavy metals for children in soil and dust from urban parks and schools of Jiaozuo, China. *J. Ecotox. Environ. Safe.*, 191: 110157.
- Yu, B., Lu, X.W., Fan, X.Y., Fan, P., Zuo, L., Yang, Y.F. and Wang, L.Q. 2021. Analyzing environmental risk, source, and spatial distribution of potentially toxic elements in the dust of residential area in Xi'an urban area, China. *J. Ecotox. Environ. Safe.*, 208: 111679.
- Jose, J., Srimuruganandam, B. 2021. Application of micro-morphology in the physical characterization of urban road dust. *J. Particology*, 54: 146-155.
- Du, H.L., Yin, N.Y., Cai, X.L., Wang, P.F., Li, Y. and Fu, Y.Q. 2020. Lead bioaccessibility in farming and mining soils: The influence of soil properties, types and human gut microbiota. *J. Sci. Total Environ.*, 708: 135227.
- Sultana, M.S., Wang, P.F., Yin, N.Y., Rahman, M.H., Du, H.L., Cai, X.L., Fu, Y.Q. and Cui, Y.S. 2020. Assessment of nutrients' effect on the bioaccessibility of Cd and Cu in contaminated soil. *J. Ecotox. Environ. Safe.*, 202: 110913.
- Zoitos, B.K., Meringo, A. and Rouyer, E. 1997. In vitro measurement of fiber dissolution rate relevant to persistence at neutral pH: An interlaboratory round robin. *J. Inhal. Toxicol.*, 9(6): 525-540.
- Ruby, M.V., Davis, A. Link, T.E., Schoof, R., Chaney, R.L., Freeman, G.B. and Bergstrom, P. 1993. Development of an in vitro screening test to evaluate the in vivo bioaccessibility of ingested mine-waste lead. *J. Environ. Sci. Technol.*, 27: 2870-2877.
- USEPA. 2007. Guidance for Evaluating the Oral Bioaccessibility of Metals in Soils for Use in Human Health Risk Assessment. OSWER 9285-7-80. Office of Solid Waste and Emergency Response, Washington, DC.
- Zheng, N., Hou, S., Wang, S., Sun, S. and Li, X. 2020. Health risk assessment of heavy metals in street dust around a zinc smelting plant in China based on bioaccessibility and bioaccessibility. *J. Ecotox. Environ. Safe.*, 197: 110617.
- Goix, S., Uzu, G., Oliva, P., Barraza, F., Calas, A., Castet, S., Point, D., Masbou, J., Duprey, J.L. and Huayta, C. 2016. Metal concentration and bioaccessibility in different particle sizes of dust and aerosols to refine metal exposure assessment. *J. J. Hazard. Mater.*, 317: 552-562.
- Fan, X.Y., Lu, X.W. and Liu, H.M. 2020. Pollution and source analysis of heavy metals in surface dust from Xian university campuses. *J. Environ. Sci.*, 41(08): 3556-3562.
- Adachi, K. and Tainoshu, Y. 2004. Characterization of heavy metal particles embedded in tire dust. *J. Environ. Int.*, 30(8): 1009-1017.
- Li, L., Xing, W., Zhao, Q., Scheckel, K.G. and Zheng, L. 2019b. Inhalation bioaccessibility of Cd, Cu, Pb, and Zn and speciation of Pb in particulate matter fractions from areas with different pollution characteristics in Henan province, China. *J. Ecotox. Environ. Safe.*, 175: 192-200.
- Zhang, M., Li, X., Yang, R., Wang, J., Ai, Y., Gao, Y., Zhang, Y., Zhang, X., Yan, X. and Liu, B. 2019. Multipotential toxic metals accumulated in urban soil and street dust from Xining city, NW China: Spatial occurrences, sources, and health risks. *J. Arch. Environ. Contam. Toxicol.*, 76(2): 308-330.
- Soltani, N., Keshavarzi, B., Moore, F., Cave, M. and Golshani, R. 2021. In vitro bioaccessibility, phase partitioning, and health risk of potentially toxic elements in the dust of an iron mining and industrial complex. *J. Ecotox. Environ. Safe.*, 212: 111972.

- Zhao, L.S., Yu, R.L., Yan, Y., Cheng, Y. and Huang, H. 2020. Bioaccessibility and provenance of heavy metals in the park dust in a coastal city of southeast China. *J. Appl. Geochem.*, 123: 104798.
- Xu, L.L., Jiao, L., Hong, Z.Y., Zhang, Y.R., Du, W.J., Wu, X., Chen, Y.T., Deng, J.J., Hong, Y.W. and Chen, J.S. 2018. Source identification of PM<sub>2.5</sub> at a port and an adjacent urban site in a coastal city of China: Impact of ship emissions and port activities. *J. Sci. Total Environ.*, 634: 1205-1213.
- Sun, L.Q., Sun, C.Y., Liu, F. and Bao, X.M. 2018. Health risk assessment of oral bioaccessibility of heavy metal in soil from coalfield in Huaibei City, China. *J. Hum. Ecol. Risk Assess.*, 25: 2045-2055.
- Shahab, A.D., Mahin, K., Majid, A. and Mojgan, Y. 2018. Pollution and health risk assessment of heavy metals in agricultural soil, atmospheric dust, and major food crops in Kermanshah province, Iran. *J. Ecotox. Environ. Safe.*, 163: 153-164.





# Effect of Drip Irrigation Under Mulch on Nitrogen Transport in Deep Soil Layers in an Agricultural Region of the Xiliao River Plain, China

Jing Zhang, Haihua Jing, Kebao Dong<sup>†</sup>, Jiaqi Ma and Zexu Jin

College of Water Conservancy, Shenyang Agricultural University, Shenyang, Liaoning, 110866, China

<sup>†</sup>Corresponding author: Kebao Dong; dongkebao@126.com

Nat. Env. & Poll. Tech.  
Website: [www.neptjournal.com](http://www.neptjournal.com)

Received: 22-08-2021

Revised: 24-11-2021

Accepted: 24-12-2021

## Key Words:

Transport of water and nitrogen

Drip irrigation

Mulch

NO<sub>3</sub>-N

NH<sub>4</sub>-N

Groundwater pollution

Xiliao river plain

## ABSTRACT

In the agricultural region of the Xiliao River Plain, drip irrigation under mulch has been widely implemented. It not only saves irrigation water, but also changes the structure of the underlying surface of agricultural land, which affects the local hydrological cycle to a certain extent, and makes the process of nitrogen transportation in soil with new characteristics. This study analyzed the distribution of NH<sub>4</sub>-N, NO<sub>3</sub>-N, and NO<sub>2</sub>-N in different soil depths during the whole growth period under three underlying surface conditions, including drip irrigation under mulch, border irrigation, and bare area through field in-situ observation experiment, and analyzed the influence of drip irrigation under mulch on nitrogen transport in deep soil layers. The results showed that under the soil properties of the experimental area, drip irrigation under mulch creates more water to enter the deep soil layers, which was beneficial to alleviate the downward trend of local groundwater level to a certain extent. The average content of NH<sub>4</sub>-N and NO<sub>3</sub>-N under drip irrigation under mulch was higher than that under border irrigation. The average content of NH<sub>4</sub>-N under drip irrigation under mulch was 1.24 mg.kg<sup>-1</sup> in soil depths of 80-300 cm, and 0.97 mg.kg<sup>-1</sup> under border irrigation. The average content of NO<sub>3</sub>-N under drip irrigation under mulch was 2.73 mg.kg<sup>-1</sup> in soil depths of 80-300 cm, and 1.99 mg.kg<sup>-1</sup> under border irrigation. The increment of NH<sub>4</sub>-N and NO<sub>3</sub>-N distribution in deep soil layers under drip irrigation under mulch was greater than that under border irrigation, and the increment of NO<sub>3</sub>-N content is significantly greater than that under border irrigation. Soil water content has a significant impact on the contents of NH<sub>4</sub>-N and NO<sub>3</sub>-N. It indicated that compared with traditional border irrigation, drip irrigation under mulch was beneficial to alleviate the downward trend of local groundwater, but it would increase the risk of nitrogen pollution in local groundwater.

## INTRODUCTION

The Xiliao River Plain is located in the western part of north-east China, most of which is in the semi-arid area, with low annual rainfall and high evaporation, relatively poor surface water, and abundant groundwater which is easy to exploit and utilize. With the development of agriculture, industry, and economy in the region, the lack of surface water can hardly meet the needs of normal production and life, and the rich local groundwater resources become the main source of water supply in the region (Zhong et al. 2018). Long-term sustainable utilization of groundwater is the basis of economic development and agricultural production in this region. Therefore, ascertaining the characteristics of groundwater recharge and the safety of groundwater quality is critical to the effective management of local water resources and the ecosystem that depends on groundwater. (Macdonald & Edmunds 2014, Zhang & Wang 2021)

Research shows that groundwater nitrogen pollution is a common environmental problem in China, and the concentration of NO<sub>3</sub>-N in shallow groundwater is close to 10 mg.L<sup>-1</sup> (the maximum pollution scale of EPA in the United States). Excessive use of nitrogen and phosphorus in agricultural production in an irrigated farming area will cause groundwater pollution through eluviating. (Hansen et al. 2017, Soldatova et al. 2021) Compared with non-point source pollution of surface water, the pollution of groundwater by nitrogen and phosphorus is more serious to human health in the Xiliao River Plain, where groundwater is the main source of water supply. At present, the Xiliao River Plain is faced with many water resources problems, such as river drying up, surface water pollution, groundwater overexploitation, etc. (Zhong et al. 2018). Groundwater quality in some areas of the basin has been polluted to different degrees, especially nitrogen pollution, the detection rate, and the variation trend both show an upward trend, and three kinds of nitrogen (NH<sub>4</sub>-N, NO<sub>3</sub>-N,

NO<sub>2</sub>-N) are often detected at the same time. The potential threat of nitrogen pollution to groundwater security is more serious in an irrigated farming area of the Xiliao River Plain where groundwater is the main source of water.

Eluviation is considered to be one of the main ways of nitrogen loss in agricultural production, especially in irrigation systems of farmland. The results showed that precipitation and irrigation amount influenced the eluviation process of nitrogen and phosphorus (Williams et al. 2021, Hao et al. 2015), nitrogen eluviation is easy to occur in places with high nitrogen application rate and shallow rooting depth (Halvorson et al. 2008, Fan et al. 2010). The transport process of NO<sub>3</sub>-N is related to soil properties (Liu et al. 2021, Iqbal et al. 2019). The clay layer in the soil profile tends to form saturated soil, which is conducive to delaying and attenuating the process of water infiltration, to reduce the amount of NO<sub>3</sub>-N leaching into groundwater (Li et al. 2018). In addition, the time point of fertilization and type of fertilizer, the type of land use, and the thickness of the percolation zone also significantly affected the storage of soil nitrogen salts and the concentration of groundwater nitrogen salts (Robertson et al. 2017, Suchy et al. 2018). With the increasing demands for water in irrigation areas and the development of irrigation technology, under the background of “Water-saving and grain-increasing”, drip irrigation under mulch has been widely promoted in the Xiliao River Plain (Wang et al. 2014). Drip irrigation under mulch is a technology combining film mulching and drip irrigation, which makes the limited water cycle between soil and mulching, and changes the original hydrological cycle (Wang et al. 2014, Jia et al. 2021). The large-scale promotion of drip irrigation under mulch has also changed the underlying surface conditions in an irrigated farming area of Xiliao River to a certain extent, and new characteristics of water transport and solute transport have emerged. Therefore, the study on the characteristics of solute transport under drip irrigation under mulch is helpful to more comprehensively evaluate the comprehensive effect of drip irrigation under mulch as a water-saving measure.

At present, the research on drip irrigation under mulch mainly focuses on crop yield, effective water utilization coefficient, and salt and water utilization above the root length of crops, while less attention is paid to the storage, movement, and attenuation process of inorganic nitrogen in deep soil layers (Mil et al. 2018, Chen et al. 2015). Because of the difficulty of sampling, the potential reserves and retention time of inorganic nitrogen in deep soil layers have not been determined, posing a potential threat to the quality of future groundwater in some areas (Ascott et al. 2017). At present, numerous methods have been applied to monitor the characteristics of water and solutes, such as field in-situ

experiments, monitoring equipment (time domain reflectometry, etc.) (Aharoni et al. 2017), and tracer experiments and stable isotopes (Xiang et al. 2019). Field in-situ experiment is widely used because of their authenticity and accuracy.

The experimental area of this study is located in the Jianping Irrigation Experimental Station, Chaoyang City, Liaoning Province, China. Through field, in-situ observation experiments, the soil water content, and nitrogen content in different soil depths under three kinds of soil surface conditions, including drip irrigation under mulch, border irrigation, and bare area were observed during the whole crop growth period. The main objectives of this study were to (1) describe, analyze the effects of drip irrigation under mulch on different distribution characteristics of soil water and nitrogen content, and (2) analyze the effect of drip irrigation under mulch on nitrogen migration. From the perspective of hydrology and water resources, this paper reflects a more comprehensive evaluation of the performance of drip irrigation under mulch in the hydrologic cycle and provides more references for making water resource development strategies in similar areas.

## MATERIALS AND METHODS

### Site Description

The experimental area is located in the Jianping Irrigation Experimental Station, Chaoyang City, Liaoning Province, China (E119°18', N 41°47'), on the east bank of the Lao-Ha River and has an elevation of 461m. It is located in the transitional zone of oceanographic monsoon climate to a continental climate, which belongs to the semi-arid monsoon continental climate. This area is a typical semi-arid area with the characteristics of a vertical hydrological cycle. Rainfall rarely forms surface runoff, and the infiltration is intense. Rainfall is the main source of groundwater recharge. The average annual rainfall is 440mm, 80% of the rainfall is concentrated from June to August. The average annual evapotranspiration is 1800-2100mm, and the evaporation is the largest in April-June, accounting for 45%-50% of the total annual evaporation. The sunshine duration is long, and the annual average sunshine duration is 2868-3111h. The average temperature for many years is 5-6°C. The hydrologic cycle and climate-related characteristics of the experimental area are representatives, which can represent the Xiliao River basin.

Field irrigation methods in the experimental area are mainly border irrigation and drip irrigation under mulch. The soil is dominated by loamy sandy soil and sandy with some sandy loam interbedded between layers. The concentrations of inorganic nitrogen (NH<sub>4</sub>-N, NO<sub>3</sub>-N, NO<sub>2</sub>-N) in ground-

water were  $0.590 \text{ mg}\cdot\text{L}^{-1}$ ,  $12.889 \text{ mg}\cdot\text{L}^{-1}$ , and  $0.004 \text{ mg}\cdot\text{L}^{-1}$ , respectively. Among them, the  $\text{NO}_3\text{-N}$  concentration exceeds the maximum pollution scale of THE US EPA. According to the actual local planting situation, maize (Liaodan 1211) was selected as the research object in this experiment.

### Design of Experiments

In the planting area of the experimental area, two irrigation methods were set, one was drip irrigation under mulch and the other was border irrigation. At the same time, the bare area (non-planted crops) was set as blank control, and there were three kinds of underlying surface forms. To exclude the error caused by soil spatial variability and experimental contingency, the experiment was repeated several times. Due to the impermeability of drip irrigation and mulching under the plastic film and the rain-catching effect of furrows, water will move sideways (Zhang & Wang 202). In the drip irrigation area under mulch, two monitoring sections were set up, namely, the middle position of plastic film (MPF) and the middle position of furrow (MF). Water infiltration under drip irrigation was changed from one-dimensional infiltration to two-dimensional infiltration. To eliminate errors, the moisture and solute contents were calculated using MBF and MF. A separate monitoring section, called MBI, MBA, is set up in border irrigation and flat bare areas, respectively, as shown in Fig. 1.

The experiment began on April 29, 2019, and ended on October 22, 2019. Border irrigation was carried out irrigation before sowing on May 9, with the irrigation amount of  $600 \text{ m}^3\cdot\text{hm}^{-2}$ , sowing on May 15, and seedling on May 25. Drip irrigation under mulch was carried out irrigation before sowing on May 9, with the irrigation amount of  $300 \text{ m}^3\cdot\text{hm}^{-2}$ , sowing on May 9, and seedling on May 21. Border irrigation was applied with DAP (diammonium phosphate) (N 18%)  $187.5 \text{ kg}\cdot\text{hm}^{-2}$  on May 15 and urea (N 46%)  $375.0 \text{ kg}\cdot\text{hm}^{-2}$  on June 28. Drip irrigation under mulch was applied with DAP (N 18%)  $187.5 \text{ kg}\cdot\text{hm}^{-2}$  and slow-release fertilizer (N

20%)  $450.0 \text{ kg}\cdot\text{hm}^{-2}$  on May 9. To explore the characteristics of soil water and inorganic nitrogen migration in different growth periods of crops, typical time points of crop growth were selected for measurement, namely, April 29 (Initial state), June 5 (Early stage of crop growth), July 9 (Rapid growth stage of crop growth), August 23 (Middle stage of crop growth) and October 10 (Late stage of crop growth). The rainfall, irrigation, and sampling time points during the test are shown in Fig. 2.

### Design and Measurement

During the experiment, the groundwater level in the experimental area was maintained at about 320 cm. To better explore the characteristics of water and solute transport between crop roots and groundwater levels in deep soil layers, the research depth was set at 300 cm. Soil samples at different depths were sampled with a soil sampler, and soil samples were taken every 20 cm To eliminate the errors caused by soil spatial variability and experiment contingency, repeated tests and multiple selection sites were carried out.

The soil mass moisture content was measured by oven drying method and converted to soil volume water content, the formula is shown below.

$$\theta_m = \frac{M_w}{M_s} \quad \dots(1)$$

$$\theta_v = \theta_m \cdot \frac{\rho_b}{\rho_w} \quad \dots(2)$$

Where  $\theta_m$  is the soil mass moisture content ( $\text{g}\cdot\text{g}^{-1}$ ),  $\theta_v$  is the soil volume water content ( $\text{cm}^3\cdot\text{cm}^{-3}$ ),  $M_w$  is the mass of water in the sample (g),  $M_s$  is the mass of soil in the sample (g).  $\rho_b$  is soil bulk density ( $\text{g}\cdot\text{cm}^{-3}$ ),  $\rho_w$  is the bulk density of water,  $\rho_w = 1.0 \text{ g}\cdot\text{cm}^{-3}$ .

The soil samples were extracted with KCL solution and analyzed with Auto Discrete Analyzers (CleverChem380) for  $\text{NH}_4\text{-N}$  (lower detection limit  $0.005 \text{ mg}\cdot\text{L}^{-1}$ ),  $\text{NO}_3\text{-N}$  (lower

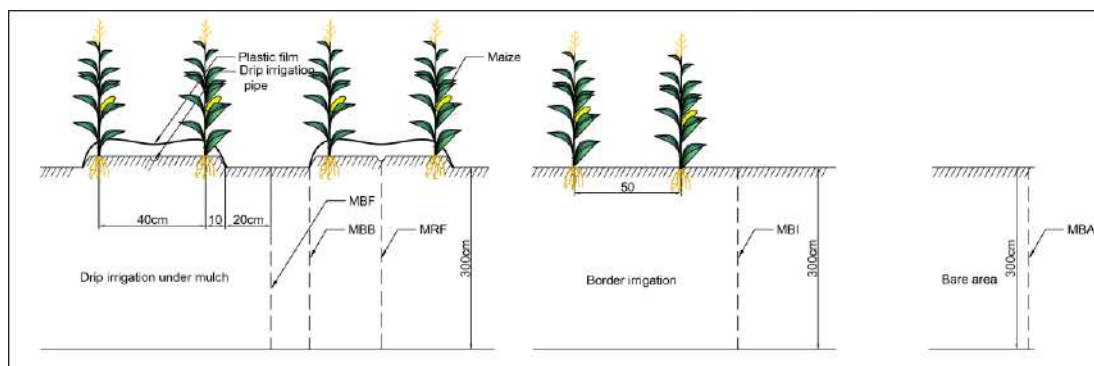


Fig. 1: Soil water content and solute observation profile.

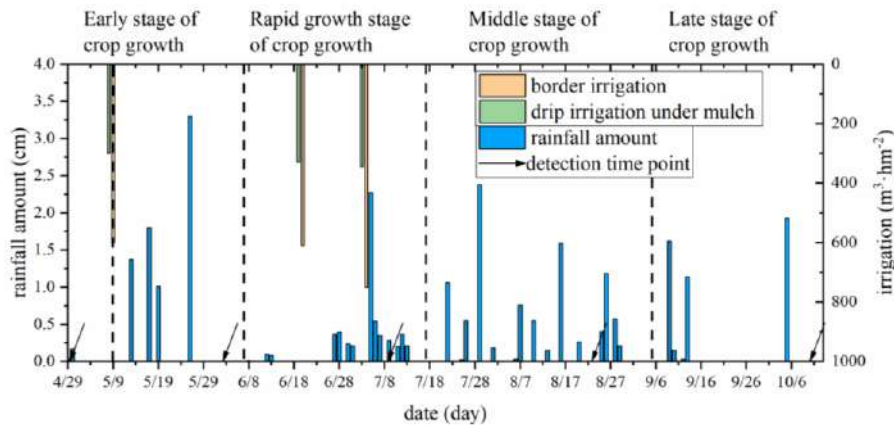


Fig. 2 Rainfall and irrigation records in 2019.

detection limit  $0.003 \text{ mg}\cdot\text{L}^{-1}$ ), and  $\text{NO}_2\text{-N}$  (lower detection limit  $0.002 \text{ mg}\cdot\text{L}^{-1}$ ). Use the following formula to make the conversion.

$$\theta_m = \frac{M_w}{M_s} \quad \dots(3)$$

Where  $C$  is soil solute concentration ( $\text{mg}\cdot\text{kg}^{-1}$ ),  $C_T$  is the concentration of sample solution ( $\text{mg}\cdot\text{L}^{-1}$ ),  $v$  is the volume of KCL solution (mL),  $M_s$  is the mass of soil in the sample (g).

## RESULTS

### Soil Property

Undisturbed soil was taken from 0-40cm, 40-70 cm, 70-110 cm, 110-250 cm, and 250-300 cm in the test area, and the basic physical properties of soil (bulk density, field capacity, and saturated soil water content) were obtained through experiments. Soil particle analysis was carried out to determine the soil type according to the American soil classification standard. The test results are shown in Table 1. The soil texture in the test region is mainly loamy sandy soil and sandy, with some sandy loam interbedded between layers. From the results of soil particle analysis, it can be seen that the sand content in the experimental area is large and the infiltration capacity is strong. Previous studies have also proved that the soil in the experimental area has a strong infiltration capacity.

Table 1: Physical properties of soil in the test area.

Soil depth (cm)	Volume weight [ $\text{g}\cdot\text{cm}^{-3}$ ]	Field capacity [ $\text{cm}^3\cdot\text{cm}^{-3}$ ]	Saturated soil water content [ $\text{cm}^3\cdot\text{cm}^{-3}$ ]	Soil type
0-40	1.54	0.21	0.44	Loamy sand
40-70	1.65	0.35	0.44	<u>Sandy loam</u>
70-110	1.59	0.24	0.43	Sand
110-250	1.62	0.14	0.41	Sand
250-300	1.51	0.10	0.36	Sand

### Soil Water Content

The distribution of soil water content with soil depth in border irrigation, drip irrigation under mulch, and the bare area are shown in Fig. 3.

Since the roots of maize are mainly distributed in 0-80cm soil, the ability of root water uptake in the region below 80 cm was relatively weak, the soil was divided into two parts with a limit of 80 cm. Above 0-80 cm, the water content of drip irrigation under film was high. At 40 cm, the maximum water content of drip irrigation under mulch was 24.54%, which was greater than that of bare area (22.39%) and far greater than that of border irrigation (17.91%). At 80cm-300 cm, the average water content of drip irrigation under mulch was 7.94%, which was close to that of bare area (7.68%) and greater than that of border irrigation (6.35%). Soil water content firstly increases and then decreases. The reason for this phenomenon is related to soil properties at different depths. The soil at the depth of 40 cm had better water preservation, while the soil below 80 cm had better infiltration capacity.

The results showed that the water content of drip irrigation under mulch was higher than border irrigation in the soil about 40 cm and below 80 cm. The reason for this phenomenon was that under the influence of the local hydrological cycle, the film mulching did not reduce the infiltration amount

of rainfall and made the water vapor circulation under the film, which reduced the evaporation of soil water to a certain extent. Due to the rain-catching effect of ridging, more water is absorbed into the deep soil under the comprehensive influence of the strong infiltration capacity of the local soil. Compared with border irrigation, drip irrigation under mulch could save about 50% of irrigation water and get more water into deep soil, which was beneficial to the process of groundwater infiltration and recharge, and alleviated the downward trend of local groundwater level to a certain extent.

### The Content of $\text{NH}_4\text{-N}$

The distribution of  $\text{NH}_4\text{-N}$  content with soil depth in border irrigation, drip irrigation under mulch, and bare area during the whole growth period is shown in Fig. 4.

As can be seen from Fig. 4, the contents of  $\text{NH}_4\text{-N}$  in the soil under the three underlying surface conditions all decreased gradually with the increase of soil depth. Under drip irrigation under mulch, the average content of  $\text{NH}_4\text{-N}$  was  $2.85 \text{ mg.kg}^{-1}$  at 0-80 cm depth and  $1.24 \text{ mg.kg}^{-1}$  at 80 cm-300 cm depth during the crop growth period. Under border irrigation, the average content of  $\text{NH}_4\text{-N}$  was  $1.90 \text{ mg.kg}^{-1}$  at 0-80 cm and  $0.97 \text{ mg.kg}^{-1}$  at 80 cm -300 cm. Under bare area the average content of  $\text{NH}_4\text{-N}$  was  $1.44 \text{ mg.kg}^{-1}$  at 0-80cm and  $0.55 \text{ mg.kg}^{-1}$  at 80-300 cm. This was because the solute transport was easily affected by soil properties, the shallow soil layers in the experimental area contained much more clay and silt than the deep soil layers. The negatively charged colloids in the shallow soil layers tended to adsorb the positively charged  $\text{NH}_4\text{-N}$  ions, thus hindering the further downward movement of  $\text{NH}_4\text{-N}$ , resulting in a higher content of  $\text{NH}_4\text{-N}$  in the shal-

low soil layers. Only when the soil water content was close to the saturated water content or reached the upper limit of the adsorption capacity of colloidal particles,  $\text{NH}_4\text{-N}$  would be driven by infiltration to the deep soil layers.

During the whole growth period, the average content of  $\text{NH}_4\text{-N}$  in 0-300cm under drip irrigation under mulch was  $1.63 \text{ mg.kg}^{-1}$ , which was higher than that under border irrigation ( $1.20 \text{ mg.kg}^{-1}$ ). However, due to the lack of nitrogen fertilizer supplement, the content of  $\text{NH}_4\text{-N}$  in flat bare land was low and hardly changed over time, with the average content maintained at about  $0.77 \text{ mg.kg}^{-1}$ . The reason for this phenomenon was that the film mulching reduced the ammonia volatilization from the surface soil, and at the same time, drip irrigation under mulch got more water into the soil due to the rain-catching effect and impermeability of plastic film. The leaching effect was increased. This caused more  $\text{NH}_4\text{-N}$  to migrate from the surface to the deep soil layers.

### The Content of $\text{NO}_3\text{-N}$

The distribution of  $\text{NO}_3\text{-N}$  content with soil depth in border irrigation, drip irrigation under mulch, and bare area during the whole growth period are shown in Fig. 5.

As can be seen from Fig. 5, the contents of  $\text{NO}_3\text{-N}$  in the soil under the three underlying surface conditions all increased with the increase of soil depth, and there was an obvious increase process at 60cm-120cm. Under drip irrigation under mulch, the average content of  $\text{NO}_3\text{-N}$  was  $0.37 \text{ mg.kg}^{-1}$  in 0-80 cm and  $2.73 \text{ mg.kg}^{-1}$  in 80 cm – 300 cm during the crop growth period. Under border irrigation, the average content of  $\text{NO}_3\text{-N}$  was  $0.16 \text{ mg.kg}^{-1}$  in 0-80 cm and

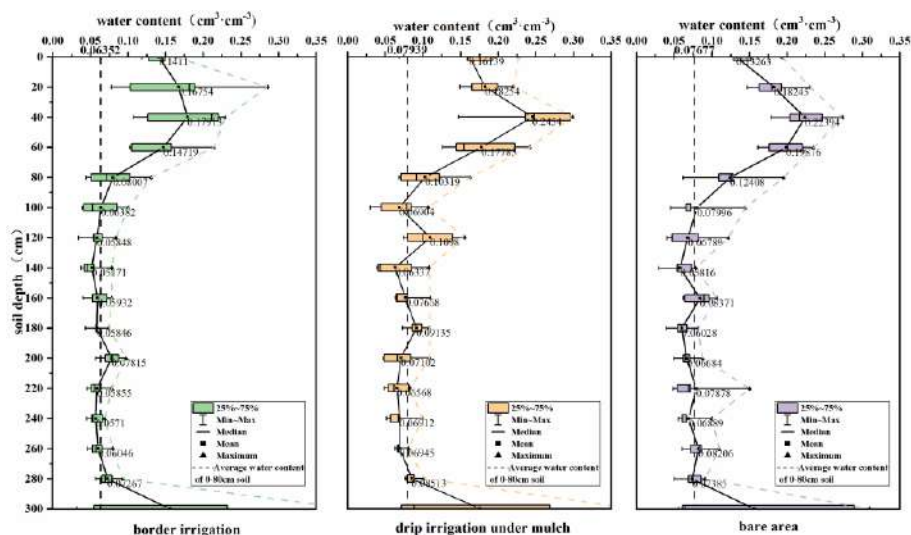


Fig. 3: Distribution of water content.

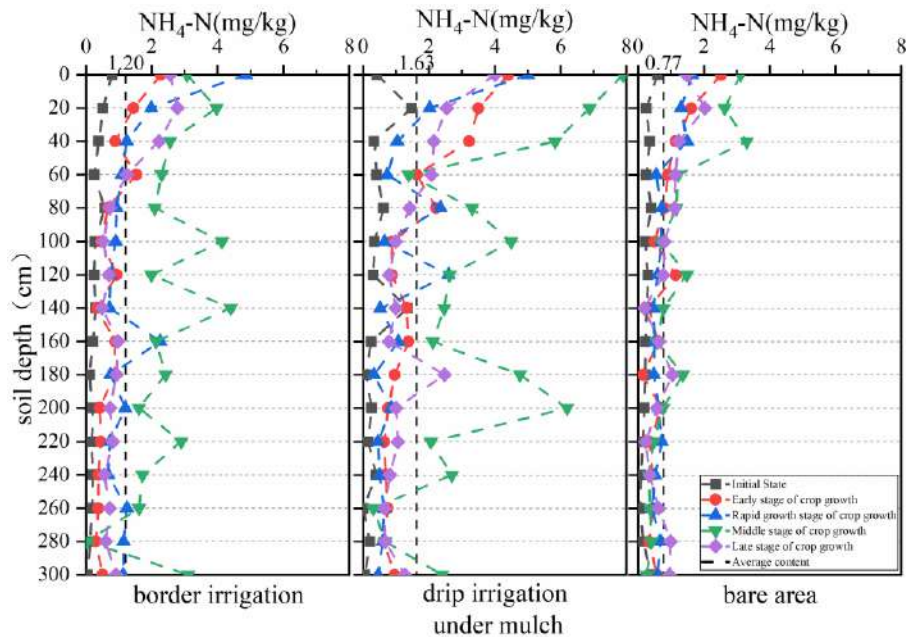


Fig. 4: Distribution of  $\text{NH}_4\text{-N}$  content.

1.99  $\text{mg}\cdot\text{kg}^{-1}$  in 80 cm-300 cm. Under border irrigation, the average content of  $\text{NO}_3\text{-N}$  was 0.08  $\text{mg}\cdot\text{kg}^{-1}$  at 0-80cm and 0.86  $\text{mg}\cdot\text{kg}^{-1}$  at 80-300cm. This was because the soil property in the experimental area was relatively sandy, with a strong ability for infiltration. The leaching effect of rainfall and

irrigation was strong, which made a large amount of  $\text{NO}_3\text{-N}$  in the shallow soil layers migrate to the deep soil layers. At the same time, considering the absorption and utilization of crops, the  $\text{NO}_3\text{-N}$  content in shallow soil layers was less, while the  $\text{NO}_3\text{-N}$  content in deep soil layers was more.

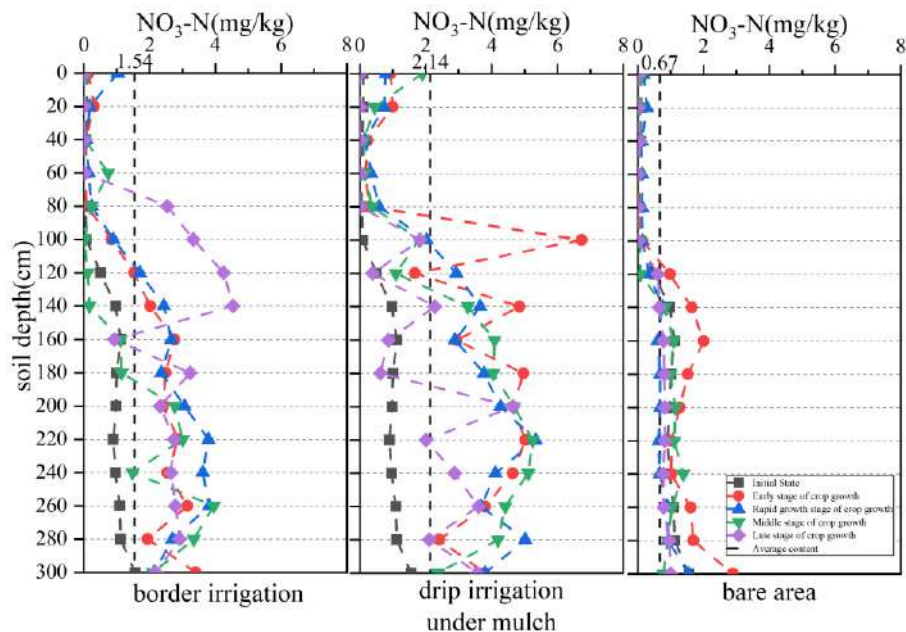


Fig. 5: Distribution of  $\text{NO}_3\text{-N}$  content.

During the whole growth period, the average content of  $\text{NO}_3\text{-N}$  in 0-300cm under drip irrigation under mulch was  $2.14 \text{ mg.kg}^{-1}$ , which was higher than that under border irrigation ( $1.54 \text{ mg.kg}^{-1}$ ). However, due to the lack of nitrogen fertilizer supplement, the content of  $\text{NO}_3\text{-N}$  in flat bare land was low, and changed little over time, with the average content maintained at about  $0.67 \text{ mg.kg}^{-1}$ . This was because drip irrigation under mulch made more water enter the soil, enhanced the leaching effect, and made more  $\text{NO}_3\text{-N}$  migrate to the deep soil layers.

### The Content of $\text{NO}_2\text{-N}$

The distribution of  $\text{NO}_2\text{-N}$  content with soil depth in border irrigation, drip irrigation under mulch, and bare area during the whole growth period are shown in Fig. 6.

As can be seen from Fig. 6, the contents of  $\text{NO}_2\text{-N}$  under the three underlying surface conditions hardly changed with the increase of soil depth, and the contents of  $\text{NO}_2\text{-N}$  fluctuated only in the surface soil above 40cm at different growth stages. The content of  $\text{NO}_2\text{-N}$  in the soil below 40cm was unchanged and low.

In drip irrigation under mulch, border irrigation, and bare land, the  $\text{NO}_2\text{-N}$  content was  $0.040 \text{ mg.kg}^{-1}$ ,  $0.035 \text{ mg.kg}^{-1}$  and  $0.031 \text{ mg.kg}^{-1}$ , respectively. As the content of  $\text{NO}_2\text{-N}$  in soil was low, and as an intermediate product of nitrification and denitrification, it was unstable in soil, so no further discussion would be made.

## DISCUSSION

### Relationship Between Inorganic Nitrogen Content and Water Content

"Salt with water" is the basic law of solute transport. Drip irrigation under mulch changed the underlying surface of farmland. Under the comprehensive effects of local soil properties and the characteristics of the hydrological cycle in a semi-arid area, new characteristics appeared in the process of water infiltration, that was, more water entered deep soil under drip irrigation under mulch. Therefore, exploring the relationship between inorganic nitrogen and water content is crucial to understand the process of nitrogen transport in the experimental area.

The relationship between the average content of  $\text{NH}_4\text{-N}$  and  $\text{NO}_3\text{-N}$  and the average water content was obtained by weighting the content of  $\text{NH}_4\text{-N}$  and  $\text{NO}_3\text{-N}$  and water content. The results are shown in Fig. 7 and Fig. 8.

As can be seen from Fig. 7, there was no clear correlation between  $\text{NH}_4\text{-N}$  content and water content in the soil above 60cm. In the soil below 60cm, the content of  $\text{NH}_4\text{-N}$  and water fluctuated in some areas, but the overall change trend with soil depth was the same. This was because there were many factors affecting the content of  $\text{NH}_4\text{-N}$  in shallow soil layers, including the application of nitrogen fertilizer and ineffective volatilization, the effects of root absorption and utilization, rainfall, irrigation, and the negatively charged

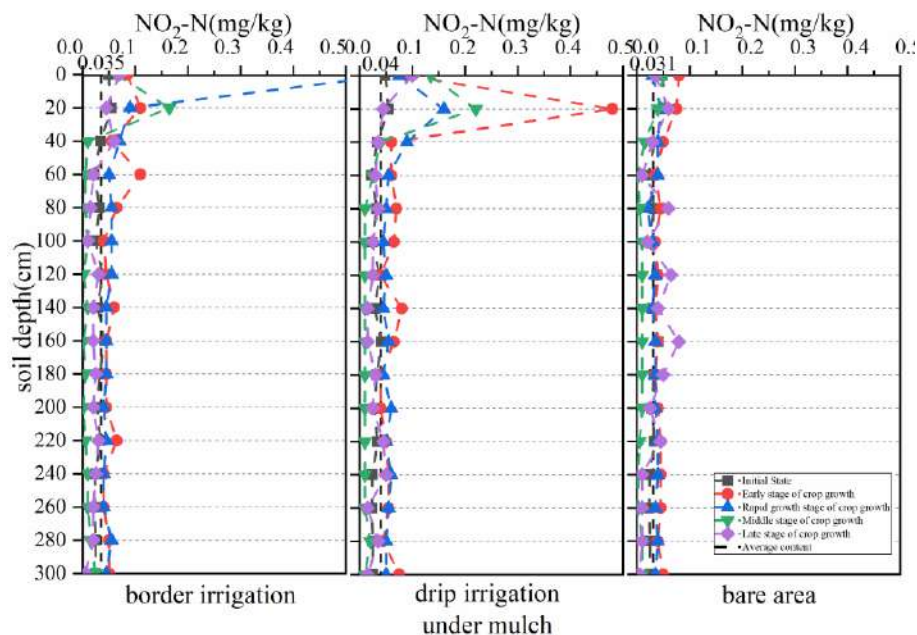


Fig. 6: Distribution of  $\text{NO}_2\text{-N}$  content.

colloidal adsorption in shallow soils, which all affected the migration of  $\text{NH}_4\text{-N}$ . Therefore, there was no clear correlation between the content of  $\text{NH}_4\text{-N}$  in the shallow soil layers and water content. However, for the deep soil layers, the soil properties of each layer were the same, which were mainly sand particles, and the colloidal adsorption is weak. The infiltration of soil water becomes the main factor affecting the migration of  $\text{NH}_4\text{-N}$ . Therefore, the variation trend of  $\text{NH}_4\text{-N}$  content with soil depth was consistent with the variation trend of water content with soil depth.

As can be seen from Fig. 8, there was no clear correlation between  $\text{NO}_3\text{-N}$  content and water content in the soil above 80 cm. The variation trend of  $\text{NO}_3\text{-N}$  content and water content in the soil below 80cm was the same as the soil depth. The reason for this result was the same as that for  $\text{NH}_4\text{-N}$ , except that the soil in the experimental area was sandy and there was no clay layer with a certain thickness in the shallow soil layers. During irrigation or rainfall, saturated soil could not be formed in the shallow layer to delay and attenuate water infiltration, so  $\text{NO}_3\text{-N}$  in the shallow layer

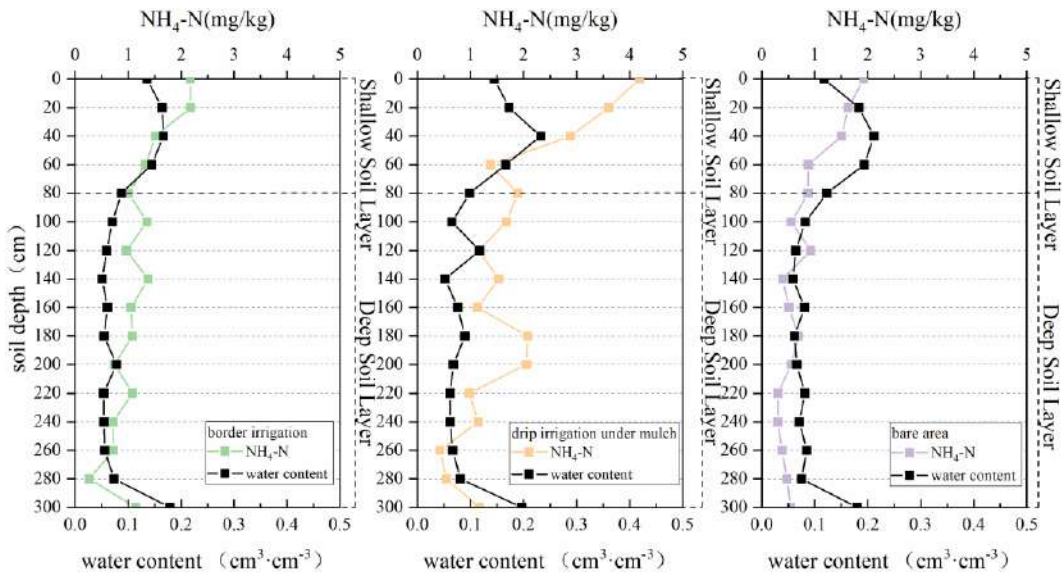


Fig. 7: Distribution of  $\text{NH}_4\text{-N}$  content and water content.

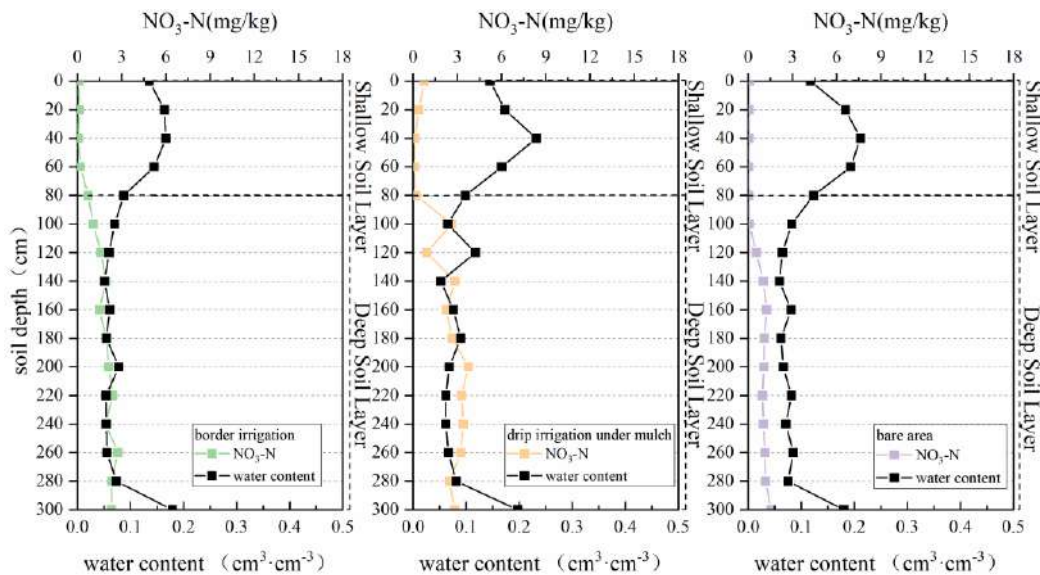


Fig. 8: Distribution of  $\text{NO}_3\text{-N}$  content and water content.



rapidly migrated to the deep layer, and the content of  $\text{NO}_3\text{-N}$  increased with the increase of soil depth.

### The Change of $\text{NH}_4\text{-N}$ and $\text{NO}_3\text{-N}$ Content at Different Depths

The content of  $\text{NH}_4\text{-N}$  and  $\text{NO}_3\text{-N}$  in each growth period was weighted, and the initial state content value was subtracted to obtain the change of  $\text{NH}_4\text{-N}$  and  $\text{NO}_3\text{-N}$  content in each growth period. The vertical migration of soil inorganic nitrogen could be reflected by the changes of  $\text{NH}_4\text{-N}$  and  $\text{NO}_3\text{-N}$  contents at different depths. The content changes of  $\text{NH}_4\text{-N}$  and  $\text{NO}_3\text{-N}$  at different depths under drip irrigation under mulch and border irrigation are shown in Fig. 9. Due to the lack of nitrogen fertilizer application, the change value of soil  $\text{NH}_4\text{-N}$  and  $\text{NO}_3\text{-N}$  content was small, so it was not further discussed.

As can be seen from Fig. 9, in the soil above 80cm, the change of  $\text{NO}_3\text{-N}$  content under drip irrigation under mulch and border irrigation was small, but the increased value of  $\text{NH}_4\text{-N}$  content under drip irrigation under mulch was significantly greater than that under border irrigation.

In the soil below 80cm, the change value of  $\text{NH}_4\text{-N}$  content under drip irrigation under mulch and border irrigation decreased with the increase of soil depth. Although the increase of  $\text{NH}_4\text{-N}$  content under drip irrigation under mulch was slightly greater than that under border irrigation, the increase of  $\text{NH}_4\text{-N}$  content under two conditions below 220 cm was almost the same. It can be seen that with the increase of groundwater depth, the amount of  $\text{NH}_4\text{-N}$  entered into groundwater will gradually decrease. When the depth of groundwater is more than 220cm, the amount of  $\text{NH}_4\text{-N}$

entered into groundwater under the two conditions is almost the same.

In the soil depth range of 80cm-220 cm, the change value of  $\text{NO}_3\text{-N}$  content under drip irrigation under mulch and border irrigation increased with the increase of soil depth and decreased with the increase of depth below 220 cm. However, in the whole interval below 80cm, the increment of  $\text{NO}_3\text{-N}$  content under drip irrigation under mulch was significantly greater than that under border irrigation. It can be seen that when the local groundwater depth is less than 220 cm, the amount of  $\text{NO}_3\text{-N}$  entered into the groundwater will gradually decrease. When the depth of groundwater is more than 220cm, the amount of  $\text{NO}_3\text{-N}$  entered into groundwater decreases with the increase of groundwater depth. The amount of  $\text{NO}_3\text{-N}$  entered into groundwater under drip irrigation under mulch was significantly greater than that under border irrigation.

It is worth noting that the  $\text{NO}_3\text{-N}$  and  $\text{NH}_4\text{-N}$  distributed in the area between the soil level below 80cm and the groundwater level above cannot be effectively utilized by crops, and will move further to the groundwater under the leaching effect of rainfall and irrigation. In this area, the contents of  $\text{NH}_4\text{-N}$  and  $\text{NO}_3\text{-N}$  in drip irrigation under mulch were higher than those in border irrigation. The promotion of drip irrigation under the mulch will increase the risk of nitrogen pollution in local groundwater.

### CONCLUSION

Compared with traditional border irrigation, drip irrigation under mulch not only saved irrigation water but also made more water infiltrate into deep soil layers, which increased

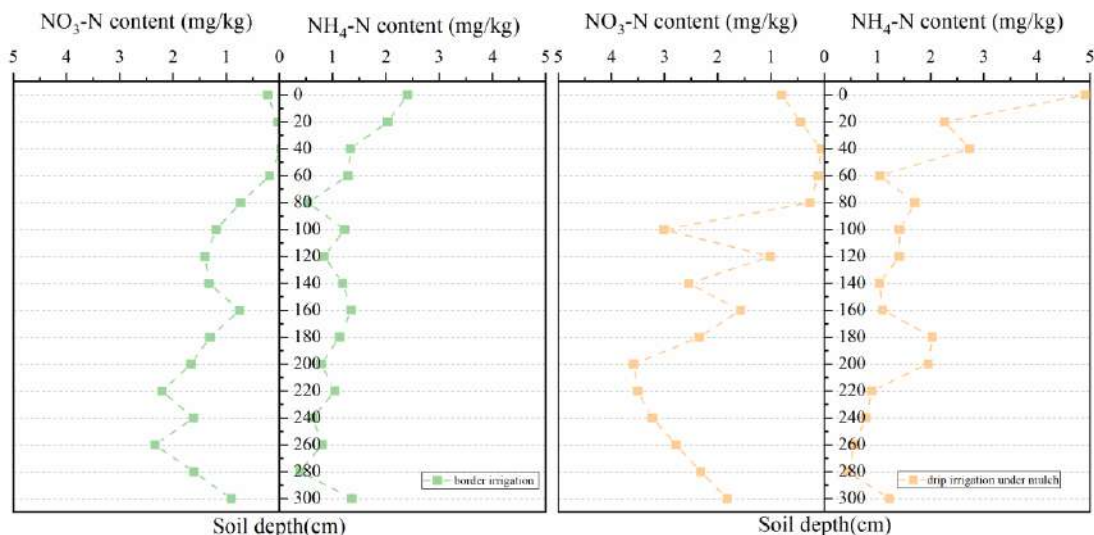


Fig. 9: Distribution of changes in  $\text{NH}_4\text{-N}$  and  $\text{NO}_3\text{-N}$  contents.

the infiltration recharge of groundwater and had a positive effect on alleviating the decrease of local groundwater level.

The average content of  $\text{NH}_4\text{-N}$  and  $\text{NO}_3\text{-N}$  under drip irrigation under mulch was higher than that under border irrigation because drip irrigation under mulch increased the infiltration of water into the deep soil, it intensified the leaching effect of irrigation and rainfall on inorganic nitrogen. This phenomenon was especially obvious in deep soil layers. The average content of  $\text{NH}_4\text{-N}$  was  $1.24 \text{ mg}\cdot\text{kg}^{-1}$  at 80 cm–300 cm under drip irrigation under mulch and  $0.97 \text{ mg}\cdot\text{kg}^{-1}$  under border irrigation. The average content of  $\text{NO}_3\text{-N}$  was  $2.73 \text{ mg}\cdot\text{kg}^{-1}$  at 80 cm–300 cm under drip irrigation under mulch and  $1.99 \text{ mg}\cdot\text{kg}^{-1}$  under border irrigation.

According to the analysis of the relationship between soil  $\text{NH}_4\text{-N}$ ,  $\text{NO}_3\text{-N}$  contents, and water content, the deep soil layers' water content has been significantly impacted by the contents of  $\text{NH}_4\text{-N}$  and  $\text{NO}_3\text{-N}$ . The change value of  $\text{NH}_4\text{-N}$  content in deep soil layers decreased with the increase of soil depth. The change value of  $\text{NO}_3\text{-N}$  content increased with the increase of soil depth above 220cm and decreases with the increase of soil depth below 220 cm. The increment of  $\text{NH}_4\text{-N}$  and  $\text{NO}_3\text{-N}$  contents in deep soil layers under drip irrigation under mulch was greater than that under border irrigation, and the increment of  $\text{NO}_3\text{-N}$  content was significantly greater than that under border irrigation.

This study analyzed the distribution of  $\text{NH}_4\text{-N}$ ,  $\text{NO}_3\text{-N}$ , and  $\text{NO}_2\text{-N}$  in different soil depths during the whole growth period under three underlying surface conditions, including drip irrigation under mulch, border irrigation, and bare area through field in-situ observation experiment, and analyzed the influence of drip irrigation under mulch on inorganic nitrogen transport in deep soil layers. The results showed that drip irrigation under mulch saved the amount of irrigation water and increased the amount of groundwater recharge, but increased the risk of nitrogen pollution in local groundwater. From the perspective of hydrology and water resources, this paper provides a more comprehensive evaluation of the performance of drip irrigation under mulch in the hydrological cycle and also provides more basis for similar areas to formulate water resources development strategies.

## ACKNOWLEDGEMENTS

The authors acknowledge the public science and technology research funds project of the National Ministry of Water Resources. The granted research is titled “Study of key technology of hydrologic cycle and aquatic safety in the semi-arid region (201501031)”. The authors would like to thank the anonymous reviewer for the helpful comments, which improved the quality of the manuscript.

## REFERENCES

- Aharoni, I., Siebner, H. and Dahan, O. 2017. Application of vadose-zone monitoring system for real-time characterization of leachate percolation in and under a municipal landfill. *Waste Manag.*, 67: 203–213.
- Ascott, M.J., Gooddy, D. C., Wang, L., Stuart, M.E., Lewis, M.A., Ward, R.S. and Binley, A.M. 2017. Global patterns of nitrate storage in the vadose zone. *Nature Commun.*, 8(1): 1–7.
- Chen, C.R., Xu, Z.H., Zhang, S.L. and Keay, P. 2005. Soluble organic nitrogen pools in forest soils of subtropical Australia. *Plant Soil*, 277(1): 285–297.
- Fan, J., Hao, M. and Malhi, S.S. 2010. Accumulation of nitrate N in the soil profile and its implications for the environment under dryland agriculture in northern China: A review. *Canad. J. Soil Sci.*, 90(3): 429–440.
- Halvorson, A.D., Bartolo, M.E., Reule, C.A. and Berrada, A. 2008. Nitrogen effects on onion yield under drip and furrow irrigation. *Agro. J.*, 100(4): 1062–1069.
- Hansen, B., Thorling, L., Schullehner, J., Termansen, M. and Dalgaard, T. 2017. Groundwater nitrate response to sustainable nitrogen management. *Sci. Rep.*, 7(1): 1–12.
- Hao, C., Yan, D., Xiao, W., Shi, M., He, D. and Sun, Z. 2015. Impacts of typical rainfall processes on nitrogen in typical rain field of black soil region in Northeast China. *Arab. J. Geosci.*, 8(9): 6745–6757.
- Iqbal, A., He, L., Khan, A., Wei, S., Akhtar, K., Ali, I. and Jiang, L. 2019. Organic manure coupled with inorganic fertilizer: An approach for the sustainable production of rice by improving soil properties and nitrogen use efficiency. *Agronomy*, 9(10): 651.
- Jia, Q., Shi, H., Li, R., Miao, Q., Feng, Y., Wang, N. and Li, J. 2021. Evaporation of maize crop under mulch film and soil covered drip irrigation: field assessment and modeling on West Liaohe Plain, China. *Agric. Water Manag.*, 253: 106894.
- Li, S., Zhang, Y., Yan, W. and Shangguan, Z. 2018. Effect of biochar application method on nitrogen leaching and hydraulic conductivity in silty clay soil. *Soil Till. Res.*, 183: 100–108.
- Liu, S., Qin, T., Dong, B., Shi, X., Lv, Z. and Zhang, G. 2021. The influence of climate, soil properties and vegetation on soil nitrogen in sloping farmland. *Sustainability*, 13(3): 1480.
- Macdonald, D.M. and Edmunds, W.M. 2014. Estimation of groundwater recharge in weathered basement aquifers, southern Zimbabwe: A geochemical approach. *Appl. Geochem.*, 42: 86–100.
- Robertson, W.M., Böhlke, J.K. and Sharp, J.M. 2017. Response of deep groundwater to land use change in desert basins of the Trans Pecos region, Texas, USA: Effects on infiltration, recharge, and nitrogen fluxes. *Hydrol. Process.*, 31(13): 2349–2364.
- Soldatova, E., Dong, Y., Li, J., Liu, Y., Zan, J., Boeckx, P. and Sun, Z. 2021. Nitrogen transformation and pathways in the shallow groundwater–soil system within agricultural landscapes. *Environ. Geochem. Health*, 43(1): 441–459.
- Suchy, M., Wassenaar, L.I., Graham, G. and Zebarth, B. 2018. High-frequency  $\text{NO}_3\text{-}$  isotope ( $\delta^{15}\text{N}$ ,  $\delta^{18}\text{O}$ ) patterns in groundwater recharge reveal that short-term changes in land use and precipitation influence nitrate contamination trends. *Hydrol. Earth Syst. Sci.*, 22(8): 4267–4279.
- Wang, Z., Jin, M., Šimůnek, J. and van Genuchten, M.T. 2014. Evaluation of mulched drip irrigation for cotton in arid Northwest China. *Irrigation Science*, 32(1): 15–27.
- Williams, G.T., Jenkins, S.F., Lee, D.W. and Wee, S.J. 2021. How rainfall influences tephra fall loading—an experimental approach. *Bull. Volcanol.*, 83(6): 1–13.
- Xiang, W., Si, B.C., Biswas, A. and Li, Z. 2019. Quantifying dual recharge mechanisms in the deep unsaturated zone of Chinese Loess Plateau using stable isotopes. *Geoderma*, 337: 773–781.
- Zhang, Z. and Wang, W. 2021. Managing aquifer recharge with multi-source water to realize sustainable management of groundwater resources in Jinan, China. *Environmental Science and Pollution Research*, 28(9): 10872–10888.
- Zhong, Y., Zhong, M., Feng, W., Zhang, Z., Shen, Y. and Wu, D. 2018. Groundwater depletion in the West Liaohe River Basin, China and its implications revealed by GRACE and in situ measurements. *Rem. Sens.*, 10(4): 493.



# Analysis of Alkali-Induced Soil Heaving in Non-Expansive Soil Using Electrokinetic Model

Manish Kumar Mandal\* and Bala Ramudu Paramkusam\*†

\*Department of Civil Engineering, Indian Institute of Technology (Banaras Hindu University), Varanasi, India

†Corresponding author: Bala Ramudu Paramkusam; pbramudu.civ@itbhu.ac.in

Nat. Env. & Poll. Tech.  
Website: [www.neptjournal.com](http://www.neptjournal.com)

Received: 30-12-2021

Revised: 20-02-2022

Accepted: 24-02-2022

## Key Words:

Alkali-induced heaving  
Electrokinetic  
Heaving pressure  
Geotechnical properties

## ABSTRACT

An attempt has been made in this paper to conduct an Electrokinetic (EK) enhanced large-scale model study to analyze the heaving phenomena observed in fields. The application of the EK technique on fields to study alkali-induced heaving has been simulated in the laboratory using a rectangular and circular model. The EK technique was mainly employed to facilitate alkali soil interaction. Analysis of the geometry of the model boundary on the various physiochemical as well as geotechnical properties of the soil was conducted. Before that, a simple heaving analysis was also performed in an oedometer without the EK technique. Compare to the maximum heaving of 5.55% observed in the oedometer the soil in EK-equipped circular and rectangular models showed the heaving of 5.42% and 4.21% respectively. The heaving pressure recorded for the oedometer was  $67.5 \text{ t.m}^{-2}$  while for the circular and rectangular models these values were  $37.7 \text{ t.m}^{-2}$  and  $18.8 \text{ t.m}^{-2}$  respectively. Further, the value of unconfined compressive strength of soil decreases from 141 kPa to 80 kPa after interaction with alkali and the decrease was more prominent in the circular EK model. However, there was an increase in the friction angle and a decrease in cohesion value after alkali interaction. The structural alteration due to alkali solution was examined by SEM and XRD analysis.

## INTRODUCTION

Electrokinetic (EK) is a newly developed technique for soil stabilization. Casagrande first introduced this method in 1940 to stabilize railway embankments (Casagrande 1949). This technique is based on three basic principles, electromigration, i.e., transport of material due to movement of charged ions, electrophoresis i.e., movement of dispersed particles, and electroosmosis i.e., movement of pore fluid across a porous material. Since the movement of fluid is a big challenge in the case of heterogeneous or low permeable soil, all these phenomena involve the application of voltage gradient across the material. The electrokinetic technique is the best suitable method for injecting pore fluids in such soils under a potential gradient (Alshawabkeh & Bricka 2000).

For in-situ stabilization of soil/sites, the EK technique can be a great option for civil engineers. It may involve minimal disturbance to the existing structures, unlike conventional methods, which are expensive, time-consuming, and maybe challenging to implement at developed sites. The potential of the EK technique is being investigated by several researchers in context to their vital role in various geotechnical solutions such as rapid dewatering of clayey soil which have very high

moisture retention capacity (Dizon & Orazem 2020, Jian et al. 2019, Liu et al. 2018, Martin et al. 2019, Shang 1997, Shen et al. 2020) chemical stabilization of low shear strength soil (Estabragh et al. 2019, 2020, Moayedi et al. 2014, Nordin et al. 2013, Lakshmi & Sivaranjani 2014), bio-grouting of soft soil to improve its geotechnical properties (Keykha & Asadi 2017, Keykha et al. 2014, 2015) and removal of heavy metals from the soils (Cameselle et al. 2021, Kim et al. 2001, Ma et al. 2018, Sivapullaiah et al. 2015, Yi et al. 2017). The efficiency of the EK technique is a function of several parameters such as the electrode materials (Méndez et al. 2012, Xiao & Zhou 2019), spacing between the electrode (Rittirong et al. 2008, Turer & Genc 2005, Wan et al. 2021), voltage gradient (Fu et al. 2019, Mu'azu et al. 2016) and rate of chemical addition. It has been reported that out of metals and non-metals which are generally used as electrodes, metal electrodes are more efficient. However, it also has several drawbacks, such as its proneness to corrosion on exposure to an acidic environment which may also lead to soil pollution. To overcome such problems, several experimental investigations were carried out by wrapping the electrodes with polymeric materials. Among various materials, geotextiles were proved to be satisfactorily efficient in reducing the

corrosion of the electrodes (Azhar et al. 2018, Glendinning et al. 2005).

Furthermore, alkali contamination in soils is also a problem that has been receiving great concern owing to its detrimental effects on the existing structures. Alkali contamination causes heaving of the soils and may also impact their engineering properties (Ashfaq et al. 2019, Irfan et al. 2018; Reddy et al. 2017, Vindula & Chavali 2018, Vindula et al. 2019). It has also been reported that alkali contamination causes mineralogical and morphological changes in the soil matrix (Chavali et al. 2017, Sivapullaiah & Manju 2005, Sivapullaiah et al. 2010). A number of works have been reported to study alkali-induced heaving (Chavali et al. 2017, Reddy et al. 2017). All the studies reported till now were conducted at small scale set up in oedometer apparatus. But in practical scenarios, there can be significant variations in the implementation of the process and the results too. For instance, inundation of alkali solution through the soil specimen is possible on a small scale. However, in large-scale models, fluid transport through the sample can be difficult because of the low permeability of the soil. To the author's knowledge, no work has been conducted till now to study the alkali-induced heaving of soil using the EK technique in a large-scale model.

In this paper, an attempt has been made to conduct EK equipped large-scale model study to analyze the heaving

phenomena observed in fields. The effect of the model geometry has also been taken into account by using a rectangular and circular-shaped model. The results were compared in terms of percentage heaving and heaving pressure. Further, the effect of boundary geometry in EK-equipped models was analyzed in terms of variations in voltage. The effect of alkali interaction using the EK technique on the engineering properties of the soil was also compared for both models.

## MATERIALS AND METHODS

### Soil

In the present study, the soil samples were collected by open excavation upto a depth of 3 m from the natural ground level at the Banaras Hindu University Campus. Wet sieving was performed in which the soil sample was first washed through a 75 $\mu$ m sieve and the fraction coarser and finer than 75 $\mu$ m were collected and oven dried separately. Following it, mechanical sieving and hydrometer methods were used as per (Astm D6913-04R2009 2004) to analyze coarser fractions and finer fractions respectively. A semi-log curve was plotted between the percentage finer and diameter of a particle in mm as shown in Fig. 1. Based on the Unified Soil Classification System (USCS), the soil was classified as CL (Clay with low plasticity). Before the experiment, the collected soil samples were oven-dried and sieved. The physical properties

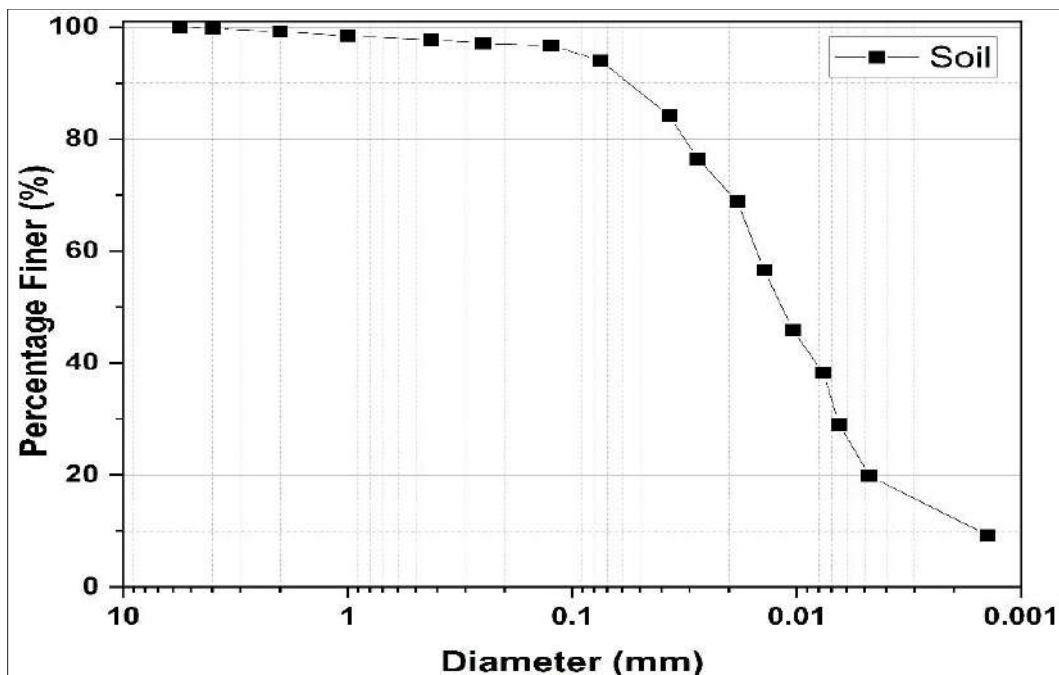


Fig. 1: Particle size distribution curve of soil.

Table 1: Geotechnical properties of test soil.

Property	Soil	Standards
Specific Gravity	2.5	ASTM D854 - 14
Liquid limit (%)	35	
Plastic limit (%)	22.23	ASTM D4318 - 17
Plasticity index (%)	12.77	
Clay	12	
Silt	80	ASTM D6913 / D6913M - 17
Sand	8	
Maximum dry density ( $\text{g.cc}^{-1}$ )	1.66	
Optimum moisture content (%)	16.4	ASTM D698-12
Unconfined compressive strength (kPa)	141.25	ASTM D2166 / D2166M - 16
Cohesion (kPa)	55	
The angle of friction ( $^{\circ}$ )	13	ASTM D2850 - 15

Table 2: Chemical composition of test soil (XRF analysis).

Mineral	SiO <sub>2</sub>	Al <sub>2</sub> O <sub>3</sub>	TiO <sub>2</sub>	Fe <sub>2</sub> O <sub>3</sub>	MnO	MgO	CaO	Na <sub>2</sub> O	K <sub>2</sub> O	P <sub>2</sub> O <sub>5</sub>
Percentage Composition	62.6	15.89	0.81	7.55	0.06	7.36	0.65	0.36	3.53	0.07

and chemical composition of soil are listed in Table 1 and Table 2 respectively.

### Experimental Set-up and Test Procedure

The whole experimental analysis was conducted in three different sets up the details of each type of experimental setup are explained in detail in the subsequent sections.

### Oedometer Test

One dimensional free swell test was performed in Oedometer in accordance with ASTM D2166 (2020) to study the heaving behavior of soil inundated with 16 M NaOH solution. The virgin soil was compacted in the consolidation ring of 6 cm diameter and 2 cm height at the density corresponding to the optimum moisture content. Porous stones with filter papers were placed on both sides of the soil specimen extruded in the ring after compaction, which is then placed into the oedometer assembly. The soil sample is inundated with 16

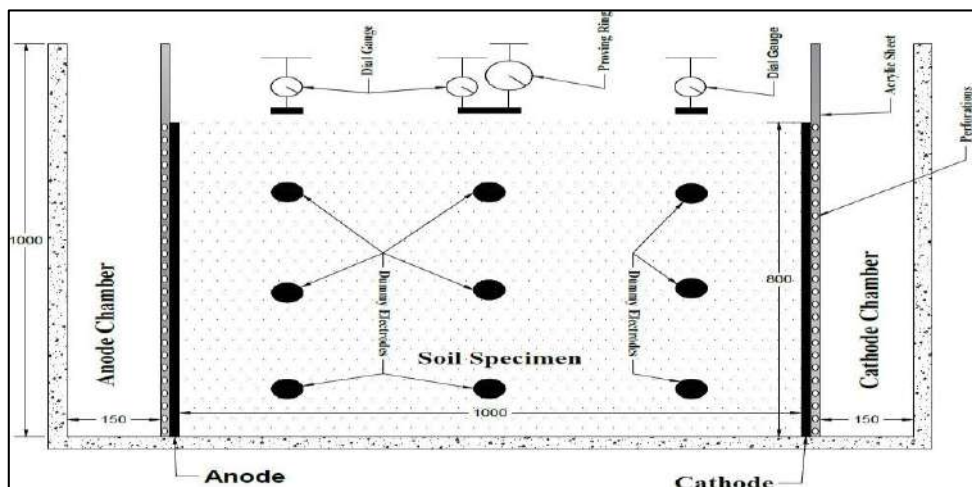


Fig. 2: Elevation view of the rectangular electrokinetic model.

M NaOH solution and is kept free from any type of load application. Here, in this case, the flow of NaOH as the pore fluid takes place without the effect of any potential gradient. Soon after the interaction with NaOH, the soil starts heaving. The amount of heaving in the vertical direction with the time was recorded using a dial gauge. The test was continued till the time no significant change in dial gauge reading was observed with time. The percentage heaving in the vertical direction was then calculated as the ratio of the actual heaving to the initial height of the specimen.

The principle mechanism behind heaving due to alkali interaction is the increase in the pH of the soil which leads to an increase in negative charge on the surface of the soil. These charges create greater repulsion between the soil particles and thus cause heaving (Paulose et al. 2017).

### Rectangular Electrokinetic Model

The second phase of the experiment involved a large-scale model testing in studying the heaving behavior of alkali-interacted soil. The movement of the NaOH as the pore fluid takes place under the influence of an electric potential gradient. The schematic of the elevation and plan of the model testing tank has been shown in Fig. 2 and Fig. 3. Fig. 4 shows the image of a rectangular EK model showing the position of the dummy electrode, dial gauge, and proving ring. The testing tank was rectangular with dimensions of 1300 mm × 750 mm × 1000 mm fabricated brick masonry. The tank was divided transversally into three parts comprising three chambers, namely, the anode chamber, the cathode chamber, and the soil chamber. The length of the soil chamber was 1000 mm,

while that of both the electrolyte chambers was 150 mm. A 20 mm thick perforated acrylic sheet was placed between the electrolyte chamber and soil chamber to ensure a uniform flow of the electrolyte. The top surface was kept open where the soil heaving was measured. The electrodes were made up of a brass net sandwiched between two geotextile sheets which were then fixed against the acrylic sheets. This brass net was used to apply a voltage gradient between the anode and cathode. A potential difference of 100 V across the two ends of the soil chamber was maintained throughout the experiment. The effect of NaOH on the percentage heaving, heaving pressure, voltage, unconfined compressive strength, and shear behavior of the soil was evaluated across the soil specimen.

Dial gauges were placed at nine different locations at the top soil surface as shown in Fig. 4(b), to measure the surface heaving. The nine-dial gauge was placed in sets of three at a distance of 250 mm, 500 mm, and 750 mm from the anode. Three proving rings were placed at the central line to measure the heaving pressure exerted by the soil. The voltage sensors 9 in number, were placed inside the soil sample to measure voltage and temperature change throughout the experiment as shown in Fig 4(a). The voltage sensors can be regarded as dummy electrodes.

### Circular Electrokinetic Model

The third phase of the experiment was conducted in a large-scale circular model made of RCC, the elevation and plan of which are shown in Fig. 5 and Fig. 6, respectively.

The anode, cathode, and soil chambers were in the form of three concentric compartments. The outermost chamber

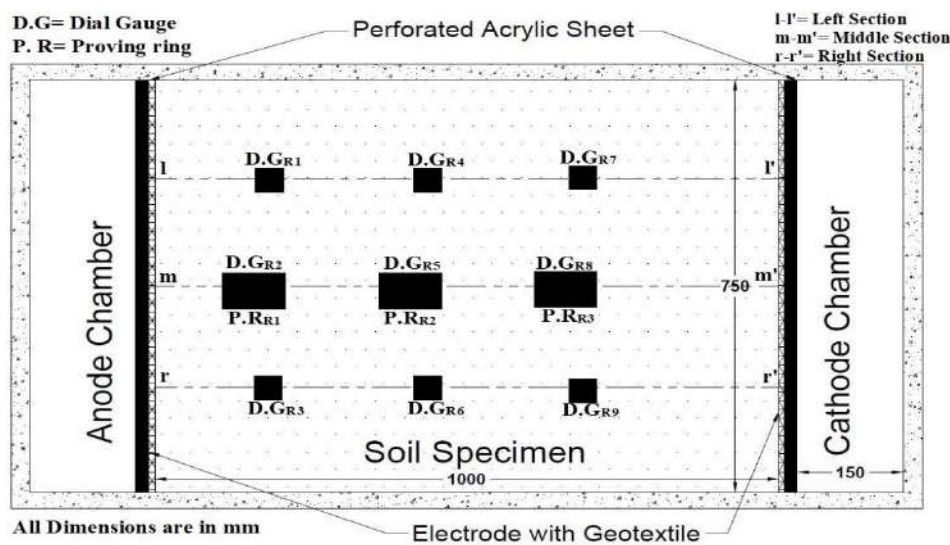


Fig. 3: Plan view of the rectangular electrokinetic model.



Fig. 4: Rectangular EK model image (a) Soil chamber installed with dummy electrode (b) Soil chamber with D.G. and P.R.

was the anode chamber. The middle compartment was for soil specimens, while the inner compartment was the cathode chamber. The diameter of the soil compartment and anode chamber was 600 mm and 150 mm, respectively, as shown in Fig. 6, while the height of the tank was 750 mm. The flow of the fluid was radially inwards from the anode chamber to the cathode chamber. Perforations were made on the walls of the anode chamber for the uniform flow of solution. Like

in the case of a rectangular setup, the electrodes were made by sandwiching a brass net between two Geosynthetic sheets and were placed on the inner wall surface of the soil chamber.

Fig. 7 shows the image of a circular EK model with a dummy electrode, dial gauge, and proving ring. Dial gauge and proving rings were placed at the top surface of the soil for measuring the heaving and heaving pressure, respectively. As

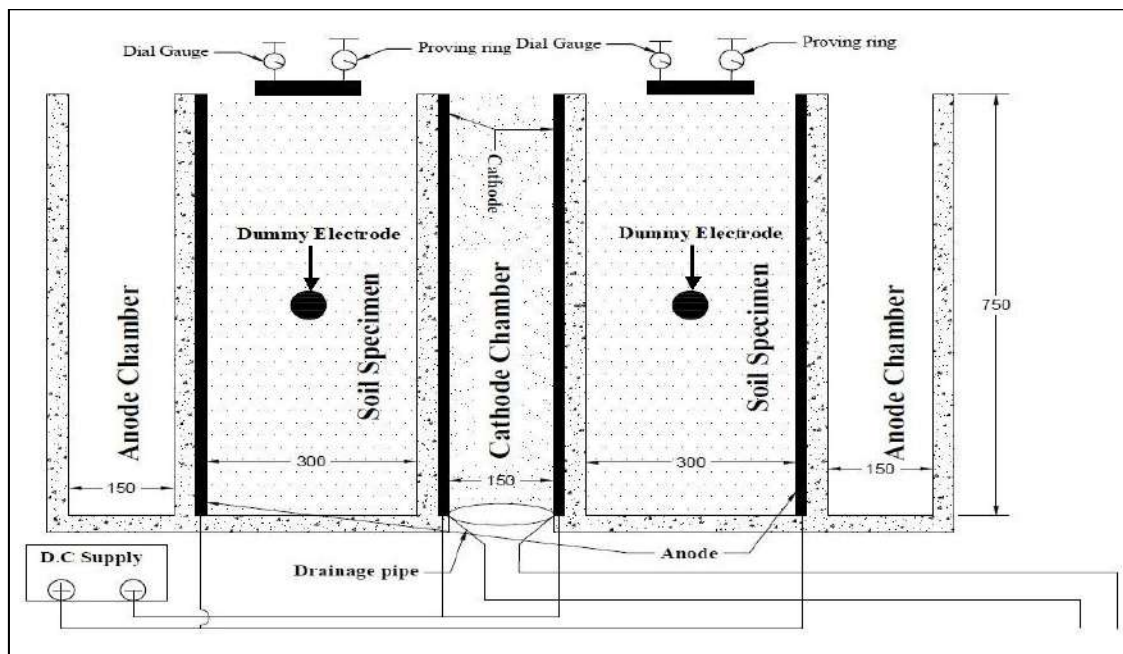


Fig. 5: Elevation view of a circular electrokinetic model.

can be seen from Fig. 7(c), the four dial gauges were placed at the mid-point of the anode and cathode. Furthermore, four voltage sensors were placed at the mid-depth just below the four dial gauges to monitor the change in the voltage and temperature sensors as shown in Fig 7(b). The cathode chamber was connected to a drain pipe at the bottom from where the electrolyte was drained out at regular intervals, while the anode chamber was refilled at regular intervals.

### Sample Preparation

Preparation of the soil bed in the testing tank was a challenging task as any sort of non-homogeneity was not desirable. The soil bed was prepared at the bulk density corresponding

to the optimum moisture content. A pre-calculated amount of soil was mixed with the water corresponding to the OMC, and this soil was compacted in the tank in 5 layers. The bottom two layers were given a little less compactive effort as compared to the upper one to incorporate the settlement due to overburden stresses. Once the soil bed was prepared, Cone Penetration Test (CPT) was conducted at different locations to check for uniformity in the prepared soil bed. The results were plotted in terms of penetration of the cone in mm per blow which is termed as Dynamic Penetration Index (DPI). In the case of the rectangular tank, CPT tests were conducted at the four corners, while in the case of the circular tank, it was conducted at two diametrically opposite

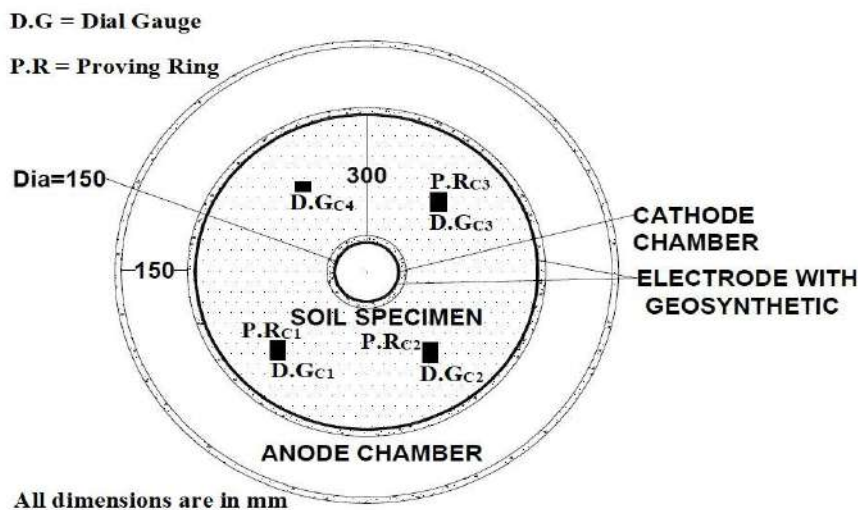


Fig. 6: Plan view of circular EK model.

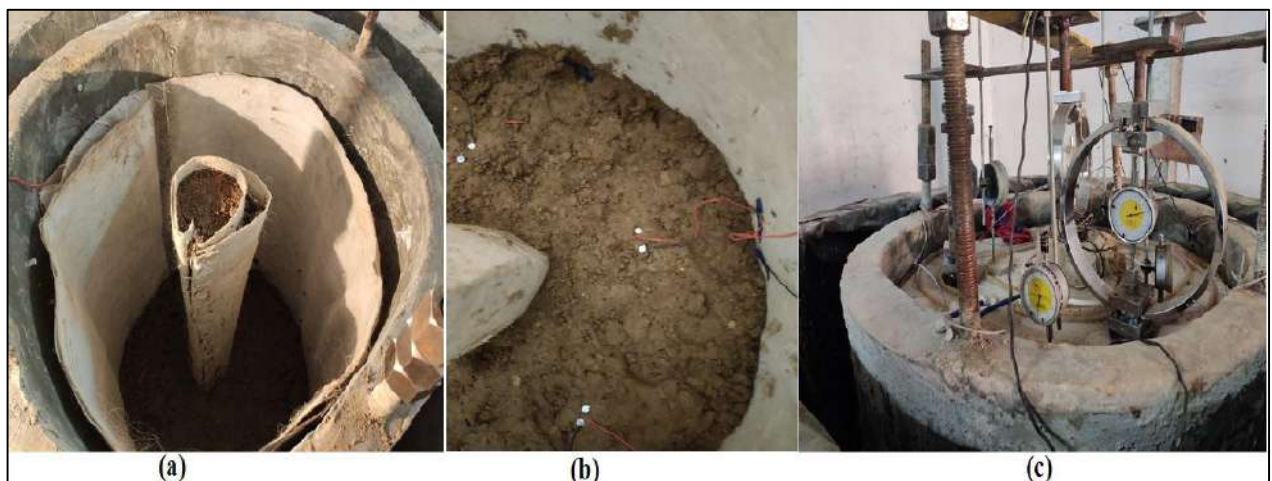


Fig. 7: Circular EK model (a) soil chamber (b) soil with dummy electrode (c) soil with D.G and P.R.



points. The results of the tests are shown in Fig. 8. Fig. 8(a) shows the CPT results for the rectangular model, while Fig. 8(b) shows the CPT results for the circular model. The CPT profiles for both types of the model were almost uniform for all locations except a slight decrease was observed at the bottom owing to the densification due to overburden stresses.

**RESULTS AND DISCUSSION**

**Surface Heaving**

The time vs heaving profiles for all the three test setups are shown in Fig. 9, Fig. 10, and Fig. 11. The soil sample was mixed thoroughly with distilled water at optimum moisture content and compacted statically to the desired depth to achieve density nearest to maximum dry density. Fig. 9 shows the percentage heaving with time recorded in the oedometer tests. The heaving showed a continuous increase with time.

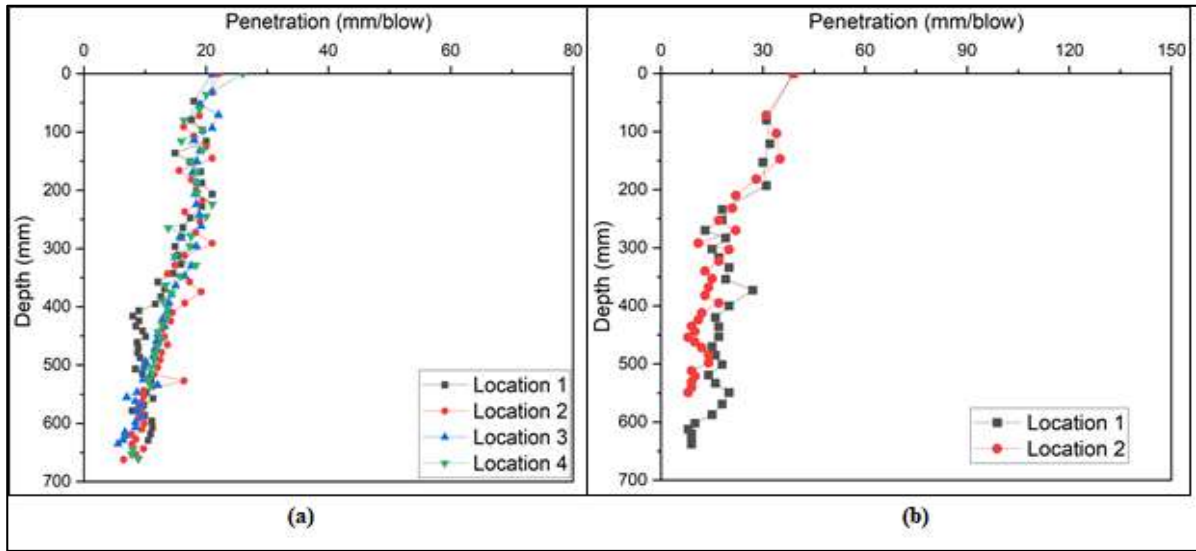


Fig. 8: CPT Test results for (a) Rectangular model and (b) Circular model.

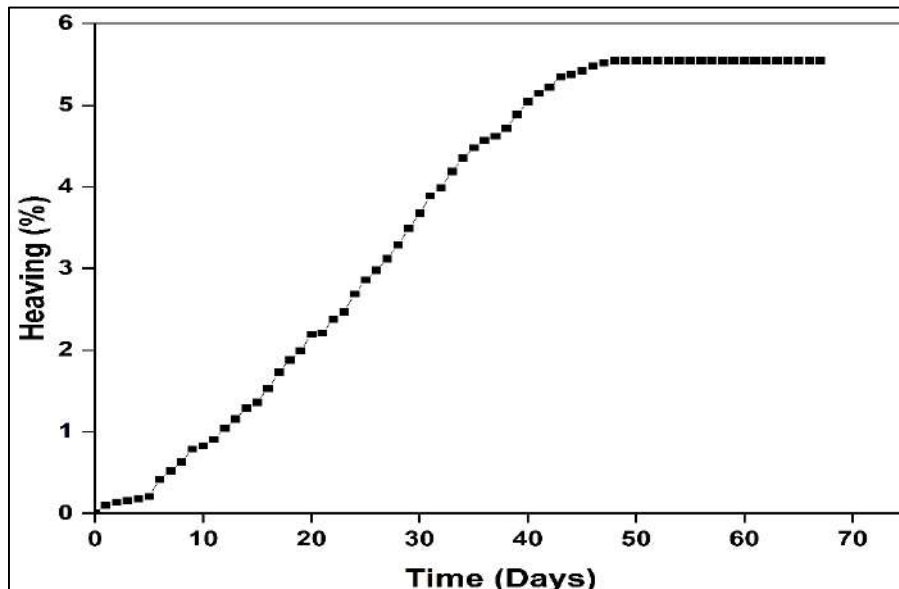


Fig. 9: Heave in soil inundated with 16 M NaOH solution in Oedometer test.

The maximum percentage of heaving was 5.55% which was achieved in approximately 40 days after which no significant heaving was observed. Similarly, Fig. 10 shows the heaving recorded in the nine-dial gauges in the rectangular electro-kinetic test setup. The graph is evidence of an obvious increase in the heaving with time for all the dial gauges. However, when the distance from the anode was increased, the percentage of heaving decreased. The maximum value of heaving in the case of rectangular test setup was 4.39% which was observed in the dial gauges nearest to the anode. The reason could be attributed to the fact that the soil nearer to the anode gets rapidly interacted with NaOH as the flow of the electrolyte is from anode to cathode. Further, it was

also observed that the heaving shown by the dial gauges at the edges was slightly higher than those at the middle for a fixed distance from the anode. The possible reason behind this particular observation could be that the flow of electrolytes along the model boundaries would be faster due to less resistance offered at the soil-boundary interface. The time-heaving profile obtained from the four dial gauges in the circular test setup is shown in Fig. 11. It was seen that the heaving in the case of the circular electro-kinetic model was increasing sharply with increasing interaction time. The maximum heaving observed, in this case, was 5.42%. The heaving in the four dial gauges did not show much deviation since the radial inward flow of electrolyte causes uniform

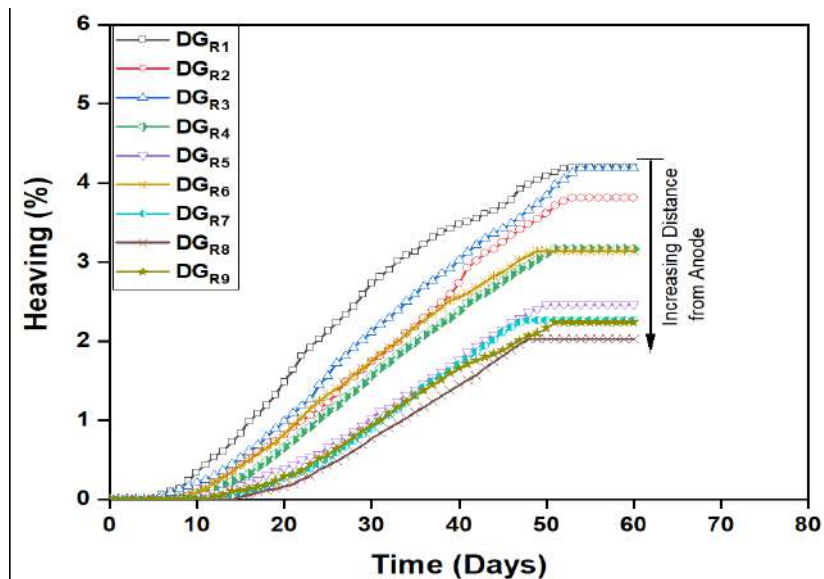


Fig. 10: Heave in soil inundated with 16 M NaOH solution in rectangular EK model.

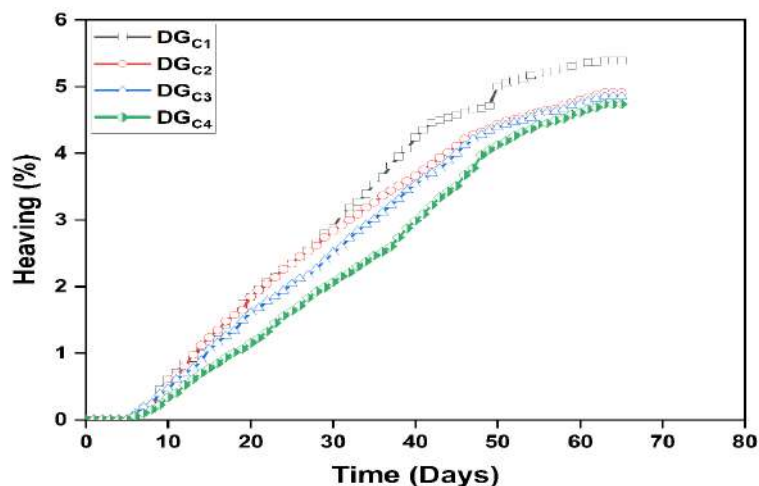


Fig. 11: Heave in soil inundated with 16 M NaOH solution in circular EK model.

soil-alkali interaction at a particular radial distance from the anode.

It is also worth noticing that the rate of heaving, represented by the slope of the time-heaving curves, is maximum in the case of the circular model where the electrolyte flow was radial. Moreover, the rate of heaving in the case of an oedometer increases initially and becomes constant after 25-30 days. In the case of the rectangular model, the rate of heaving increases initially up to 30-35 days, reduces thereafter, and becomes constant after 50-55 days. Unlike in the above two experiments, the rate of heaving in the case of the circular model shows a sharp increase with time and did not show any reduction up to 60 days.

A comparison of the percentage heaving in the case of all the three setups is shown in Fig. 12. From the fig. it can be observed that the percentage heaving was maximum in the case of the oedometer test followed by the circular EK model and then the rectangular EK model. When heave is considered, the soil weight contributes an additional component of vertical load (Merifield et al. 2009). It could be possible that in the case of the large-scale EK models, a portion of the heaving at the bottom layers is suppressed by the overburden pressure of the overlying soil. This effect would not be prominent in the case of an oedometer as a relatively very less amount of soil is used in the specimen.

### Heaving Pressure

The heaving pressure in EK models was measured through a proving ring which is placed on the surface at three different

locations which are already shown in their respective plans. On the other hand, the heaving pressure in the oedometer is the total amount of load required to bring back the deflection in the dial gauge to its original position. A comparative bar chart depicting the heaving pressure obtained for all both EK tests is shown in Fig.13. Again, the maximum heaving pressure was observed in the oedometer test which is  $67.5 \text{ t.m}^{-2}$  while the heaving pressure in the circular EK model and rectangular EK model is about  $37.8 \text{ t.m}^{-2}$  and  $18.8 \text{ t.m}^{-2}$  respectively. The heaving pressure in all three proving rings in the circular model is approximately the same while in the case of the rectangular model, the heaving pressure reduces as the distance from the anode increases.

### Comparison of Rectangular and Circular EK Model

The sections that follow give a comparison of the variation of the various factors in the rectangular EK model and the circular EK model.

### Variation of Electric Potential

The plot of the electric potential versus time as measured during the EK tests in rectangular and circular EK models are shown in Fig. 14 and Fig. 15 respectively. The electric potential was measured using voltage sensors at the mid-depth just below the dial gauges. Fig.14 shows the variation of electrical potential in the rectangular EK model. The recorded electric potential showed a decrease in moving from anode to cathode. The electric potential increases as the flow start from the anode to the cathode and then decreases with the precipitation of sodium ions across the soil specimen.

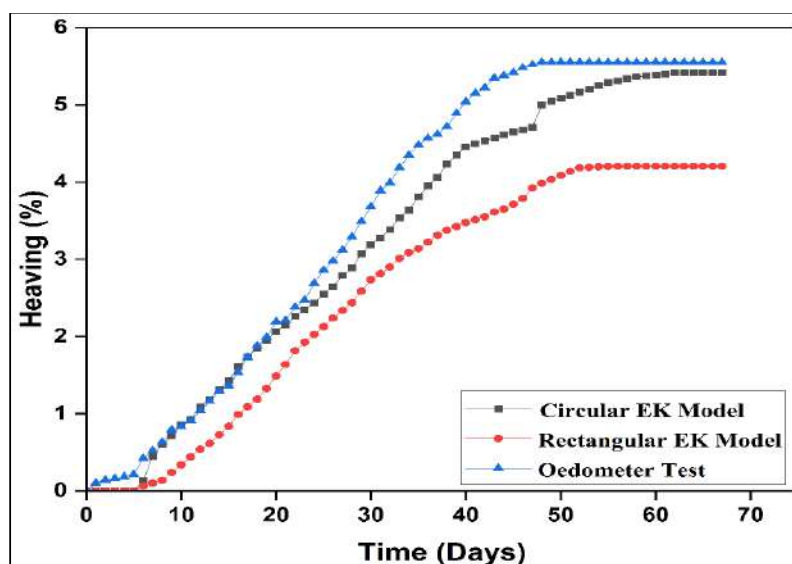


Fig. 12: Effect of model boundaries on percentage heaving.

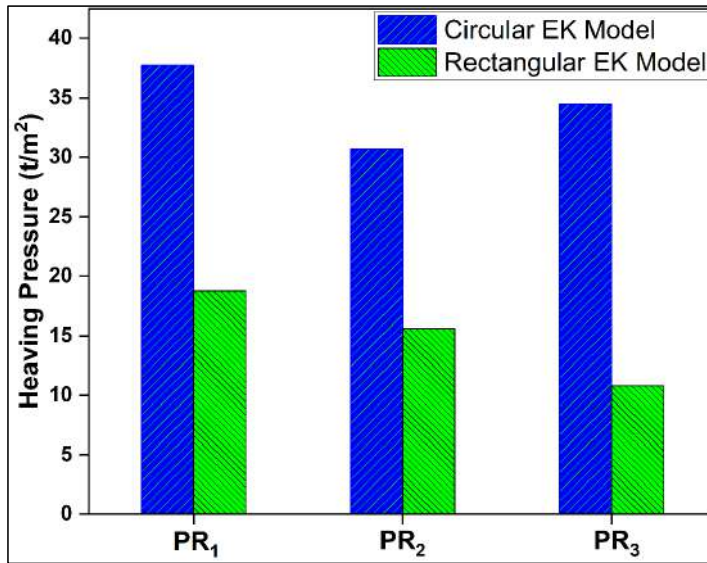


Fig. 13: Heaving pressure in soil due to alkali interaction in EK tests.

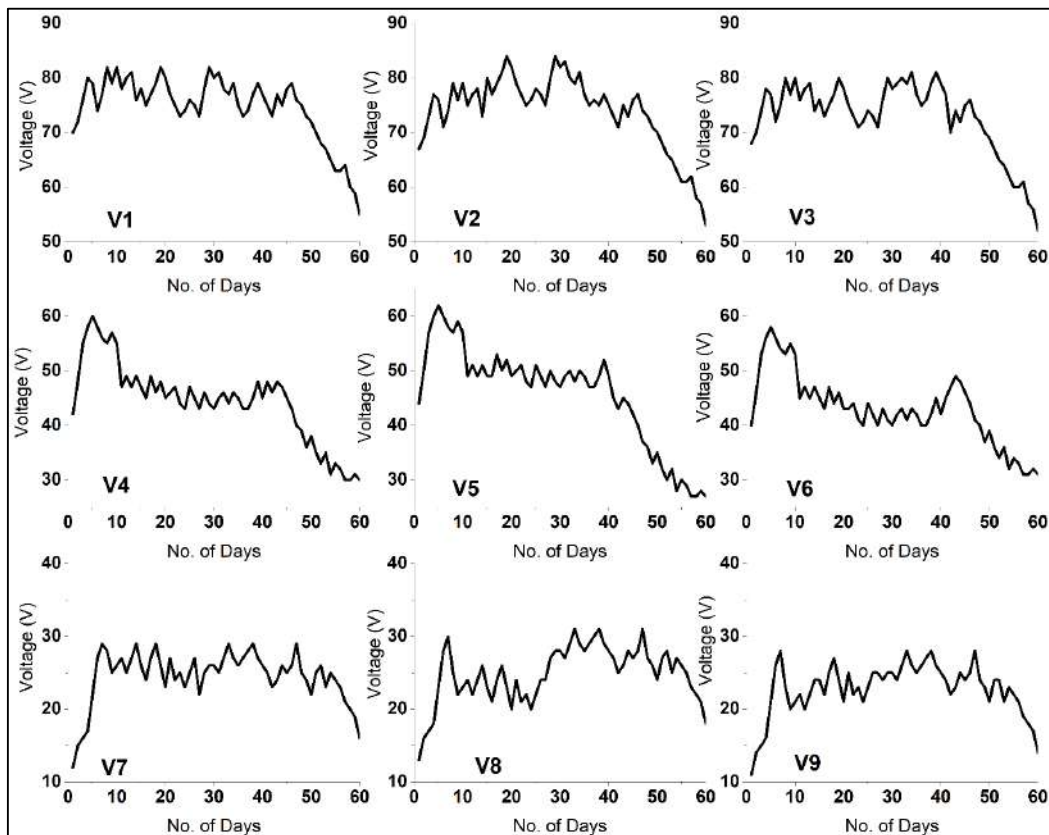


Fig. 14: Variation of Electrical potential in rectangular EK model.

However, a non-uniformity in electric potential variation was observed due to the non-uniform flow of electrolytic solution in the soil sample. This non-uniformity in flow may occur due to the large volume of soil and non-uniform precipitation of sodium ions in the soil sample.

Likewise, Fig. 15 depicts that in the circular EK model, a similar electric potential profile was observed with time for all four locations which indicates the uniformity in flow at every location. As the experiment continues, the electrical potential increases due to the movement of ions from the anode to the cathode. After 15 days, a linear decrement in electrical potential was observed with time which occurs due to the precipitation of sodium hydroxide into the soil. After the precipitation of sodium hydroxide, the electric potential becomes constant across the soil sample. Therefore, it is apparent that the change in electrical potential of the circular EK model was approximately the same, however in the rectangular EK model the electrical potential varies as we move from anode to cathode.

**Unconfined Compressive Strength**

The unconfined compressive strength (UCS) test was

conducted in accordance with ASTM D2166 (2016) to analyze the change in the strength of soil specimens after alkali interaction. The UCS value of the virgin soil conducted before its interaction with NaOH was found to be 141 kPa. Fig. 16(a) shows the UCS values of alkali interacted soil in a circular EK model collected from the mid-depth below the location of dial gauges. The UCS value was in the range of 84-93 kPa for all four specimens after an interaction period of 60 days. Similarly, Fig. 16(b) shows the UCS value of alkali interacted soil in a rectangular EK model collected from the mid-depth below the location of dial gauges. The UCS values were in the range of 90 to 124 kPa after an interaction period of 60 days. The samples collected from the mid-section showed the highest UCS value as compared to the left and right sections. This particular observation can be related to the percentage of heaving where the lowest heaving was observed at the midsection.

The reduction in UCS value with respect to virgin soil after alkali interaction can be attributed to the dissolution of clay minerals in an alkaline environment and the formation of new compounds (Sivapullaiah & Manju 2005). From the UCS graph of circular and rectangular EK models, it was

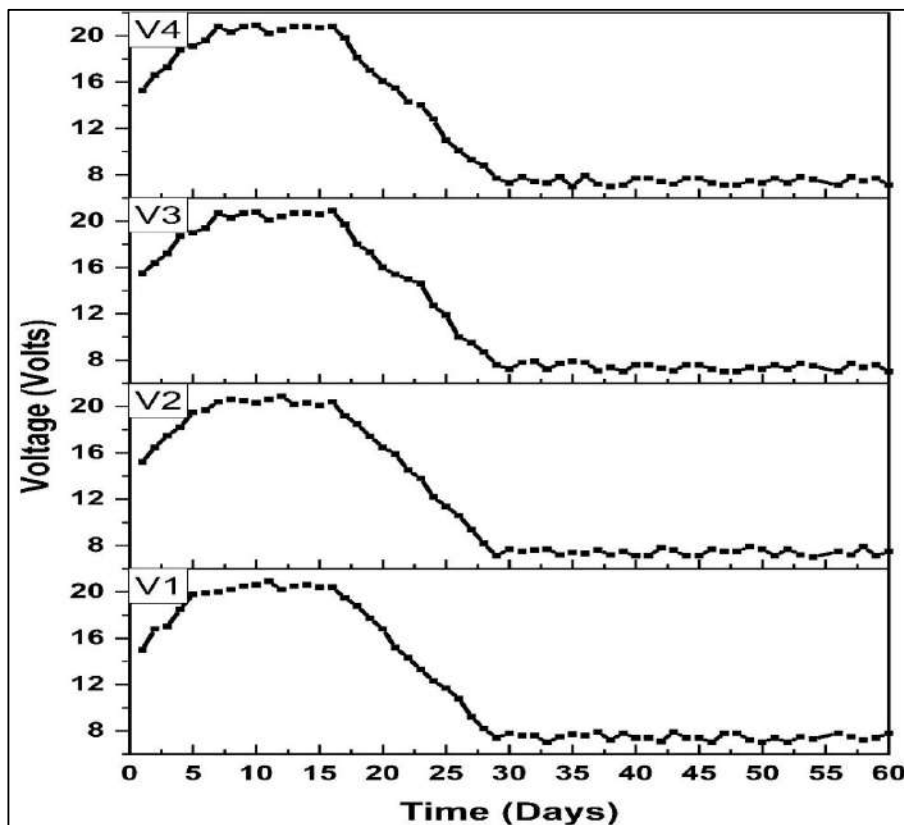


Fig. 15: Variation of Electrical potential in circular EK model.

also observed that the UCS value in the circular model at all four sampling points was similar whereas, in a rectangular model, the reduction in the UCS values was less pronounced on moving from anode to cathode. This was because the intensity of the alkali interaction was not the same at all the points at a given time as the flow of electrolyte from anode to cathode causes the electrolyte to reach different sampling points at different times.

**Shear Strength Parameters**

Unconsolidated Undrained triaxial tests were also conducted in accordance with ASTM D2850 (2015) at the collected

specimens at three confining stresses of 50 kPa, 100 kPa, and 150 kPa. The shear strength parameters calculated from the obtained results for the rectangular EK model are shown in Fig. 17. Fig. 17 (a) shows the variation of friction angle with the distance from the anode along all three sections. The cohesion and internal friction angle of an un-interacted soil sample is obtained at 55 kPa and 13°. The interaction of NaOH causes an increase in the friction angle. The friction angle is reduced as the distance from the anode increases. Furthermore, the cohesion decreased as the interaction of the NaOH increased as can be seen from Fig. 17(b). Higher decrement in cohesion values was found for the samples nearer to the anode. These

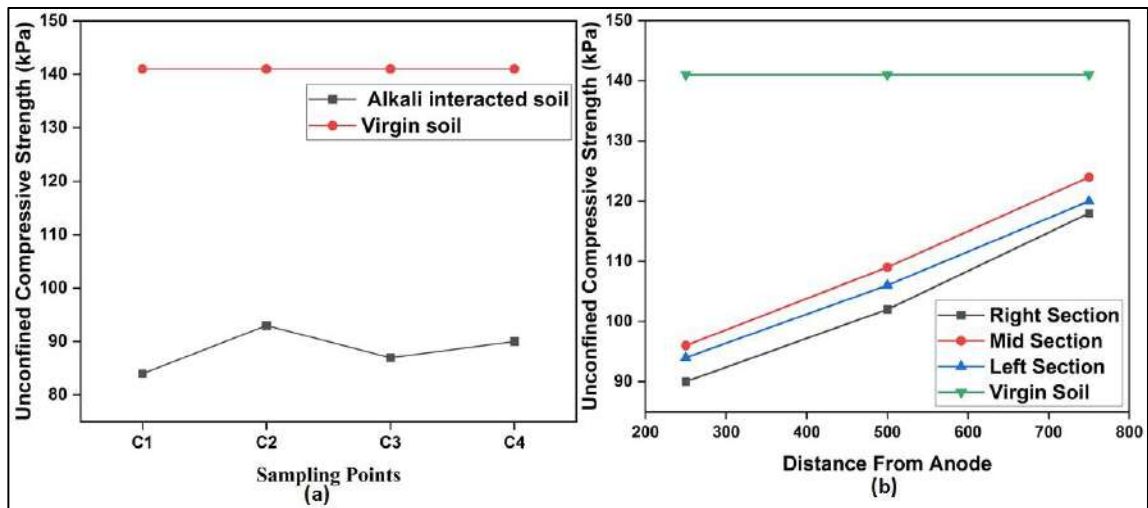


Fig. 16: Variation of UCS in (a) circular EK model and (b) rectangular EK model.

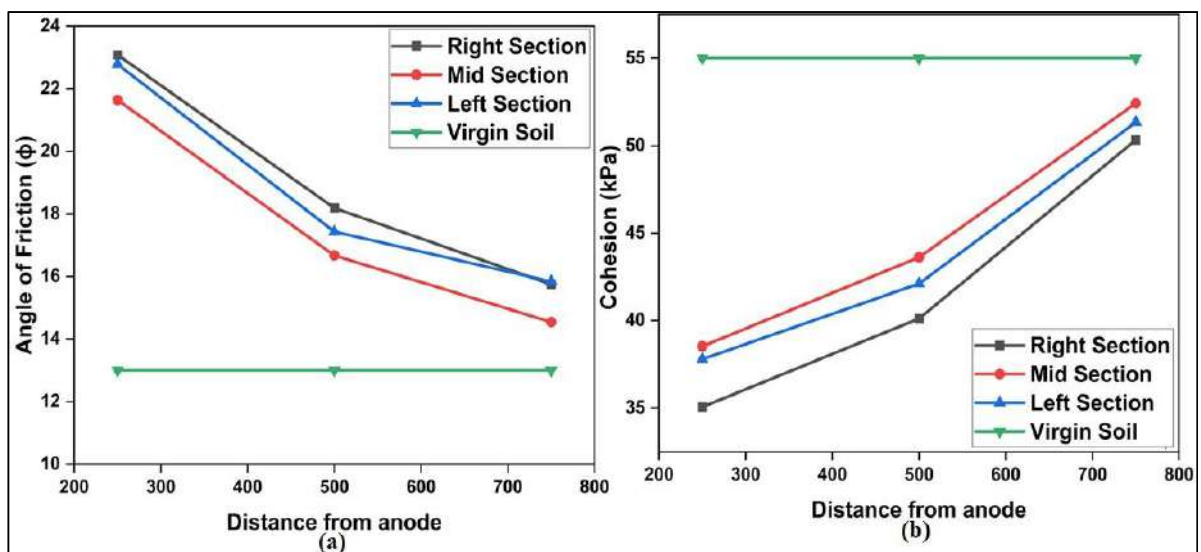


Fig. 17: Variation of (a) Angle of Friction (b) Cohesion in rectangular EK model.

changes in cohesion values decrease as the distance from the anode increases. Similarly, Fig. 18(a) and Fig. 18(b) show the variation of friction angle and cohesion respectively for the circular EK model. The values of friction angle and cohesion were almost similar for all the soil samples. However, there was a definite change in the cohesion as well as in the friction angle of the soil after its interaction with NaOH.

In an attempt to find the possible reason behind such a change in the friction angle and cohesion, it was realized that the pH value is a vital parameter that may potentially influence the mechanical response of the clayey soils. As reported by (Gratchev & Sassa 2009), the edge surface of the clay particle is highly dependent on pH. In a highly alkaline

medium when pH is very high, these edges become more negative due to the adsorption of OH<sup>-</sup> ions. This induces the face-to-face association of the particles which is responsible for the change in the shear strength parameters.

**Scanning Electron Microscopy**

The morphological changes in the soil matrix under alkali interaction were studied by scanning electron microscopy. After the interaction period of 60 days, samples were collected for SEM analysis. The SEM images of the virgin soil and the soil interacting with 16M NaOH solution are shown in Fig. 19. Distinct flaky particle structure of the virgin soil can be observed in Fig 19 (a). The SEM image of soil interacting

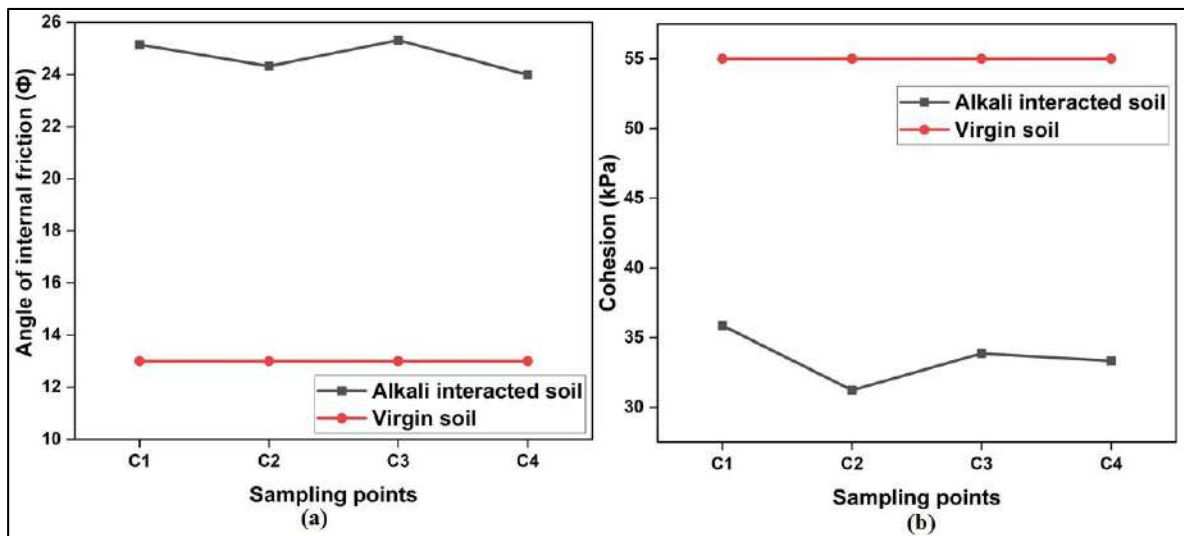


Fig. 18: Variation of (a) Angle of Friction (b) Cohesion in circular EK model.

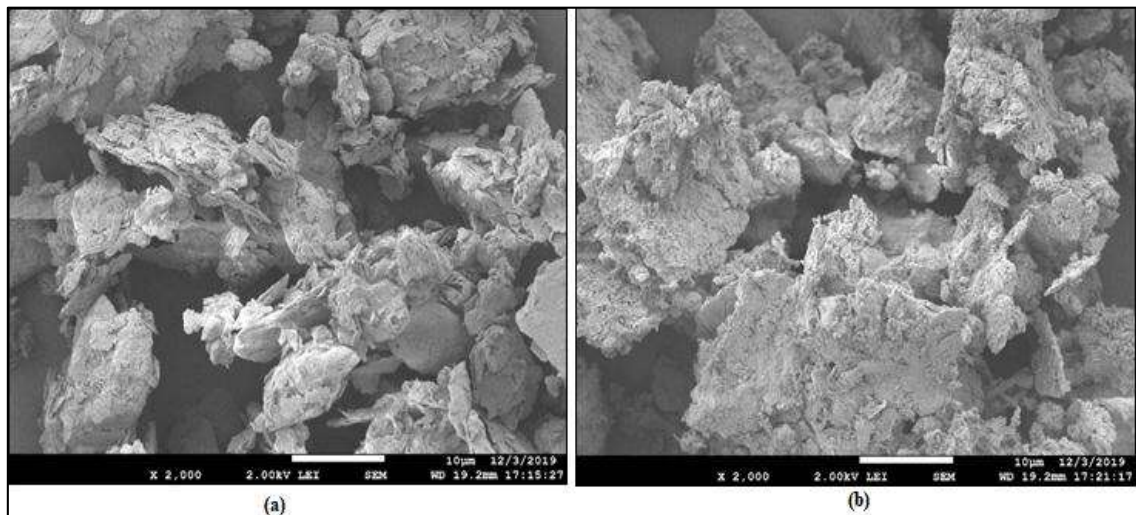


Fig. 19: SEM images of virgin soil (a) Virgin soil (b) Alkali interacted soil.

with alkali shown in Fig. 19(b) shows some disintegration or weathering. This morphological change in the soil supports the formation of a new compound due to alkali interaction which causes heaving.

### X-ray Diffraction Analysis

XRD analysis was performed to check for the formation of any new products in the soil after its interaction with the 16M NaOH solution. The soil specimens were collected soon after the completion of the 60 days interaction period. These specimens were dried and ground to a fine powder with a mortar and pestle. X-ray diffractometer was used to scan the sample and identify the mineral composition of the soil specimen corresponding to XRD peak position and intensities using JCPDS software. The X-Ray diffraction patterns for virgin and alkali interacted soil are shown in Fig 20. New peaks corresponding to NASH have been observed by the XRD analysis which is a mineral of zeolite group (Sodium aluminum silicate hydrate) which is responsible for the heaving of soil.

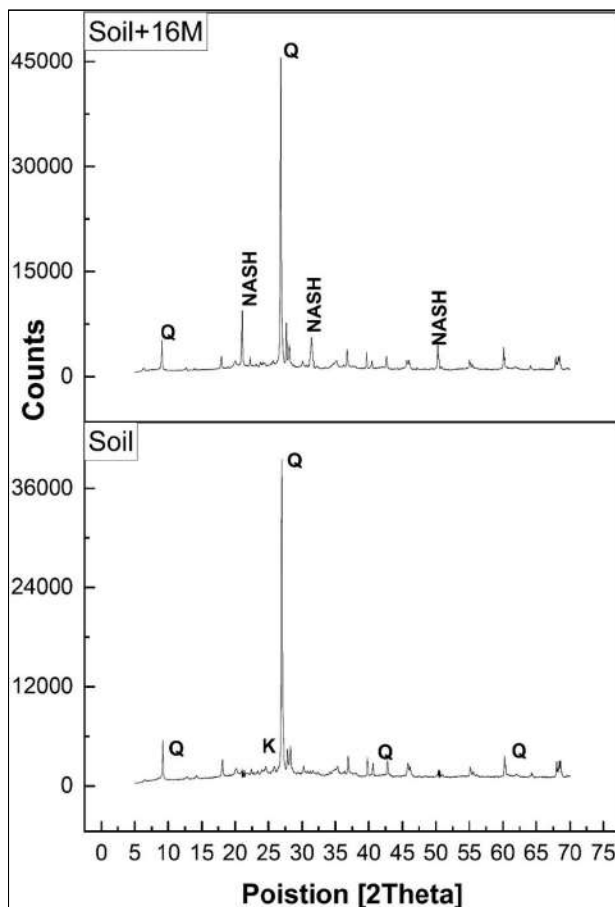


Fig. 20: X-ray diffraction analysis of soil and soil inundated with 16 M NaOH solution.

### CONCLUSIONS

The following conclusions can be drawn from the experimental analysis conducted in the present study:

- Interaction of soil with an alkali causes an unexpected heaving in the soil. The maximum percentage of heaving due to alkali interaction was observed in the oedometer test followed by the circular EK model and rectangular EK model. More uniform alkali interaction was achieved in the case of the circular EK model when compared to the rectangular EK model in low permeable soil.
- A considerable decrease in the unconfined compressive strength of the virgin soil was observed after its interaction with the alkali solution. In the case of the rectangular EK model, the effect of alkali on the UCS value was reduced as the distance from the anode was increased.
- Variation of electrical potential with time in the soil shows the flow of alkali solution into the soil is uniform in the case of the circular EK model.
- Alkali interaction causes an increase in the friction angle and a decrease in cohesion value. The respective change was directly proportional to the intensity of the alkali interaction which is a function of the time of interaction and flow of the electrolyte.

### REFERENCES

- Alshawabkeh, A.N. and Bricka, R.M. 2000. Basics and applications of electrokinetic remediation. *Environ. Sci. Pollut. Control Ser.*, 61: 95-112.
- Ashfaq, M., Heeralal, M. and Reddy, P.H.P. 2019. A Study on Strength Behavior of Alkali-Contaminated Soils Treated with Fly Ash: Recycled Waste Materials. Springer, Singapore., pp. 137-143.
- ASTM D2166/D2166M. 2016. Standard Test Method for Unconfined Compressive Strength of Cohesive Soil. The Annual Book of ASTM Standards, PA., 1-6.
- ASTM D2166/D2166M. 2020. Standard Test Methods for One-Dimensional Consolidation Properties of Soils. The Annual Book of ASTM Standards, PA., 1-10.
- ASTM D2850. 2015. Standard test method for unconsolidated-undrained triaxial compression test on cohesive soils. ASTM International, West Conshohocken, PA, USA.
- ASTM D4318. 2010. Standard Test Methods for Liquid Limit, Plastic Limit, and Plasticity Index of Soils. ASTM International, West Conshohocken, PA. 1-14.
- ASTM D6913-04R. 2009. Standard Test Methods for Particle-Size Distribution (Gradation) of Soils Using Sieve Analysis. ASTM International, West Conshohocken, PA., 61-35.
- ASTM D698. 2003. Standard Test Methods for Laboratory Compaction Characteristics of Soil Using Standard Effort. The Annual Book of ASTM Standards, PA., 1-11.
- ASTM D854. 2000. Standard Test Methods for Specific Gravity of Soil Solids by Water Pycnometer. ASTM International, West Conshohocken, PA. 1-7.
- Azhar, A.T.S., Jefferson, I., Madan, A., Abidin, M.H.Z. and Rogers, C.D.F.



2018. Electrokinetic stabilization method of soft clay in the pure system using the electrokinetic geosynthetic electrode. *J. Phys. Conf. Ser.*, 995(1): 012109.
- Cameselle, C., Gouveia, S. and Cabo, A. 2021. Enhanced electrokinetic remediation for the removal of heavy metals from contaminated soils. *Appl. Sci.*, 11(4): 1799.
- Casagrande, I.L. 1949. Electro-osmosis in soils. *Geotechnique*, 1(3): 159-177.
- Chavali, R.V.P., Vindula, S.K., Babu, A. and Pillai, R.J. 2017. Swelling behavior of kaolinitic clays contaminated with alkali solutions: a micro-level study. *Appl. Clay Sci.*, 135: 575-582.
- Dizon, A. and Orazem, M.E. 2020. Advances and challenges of electrokinetic dewatering of clays and soils. *Curr. Opin. Electrochem.*, 22: 17-24.
- Estabragh, A.R., Moghadas, M., Javadi, A.A. and Abdollahi, J. 2019. Stabilization of clay soil with polymers through electrokinetic technique. *Euro. J. Environ. Civil Eng.*, 12: 1-19.
- Estabragh, A.R., Moghadas, M., Javadi, A.A. and Abdollahi, J. 2020. Stabilization of clay soil by ion injection using an electrical field. *Proceed. Instit. Civil Eng. Ground Improve.*, 15: 1-13.
- Fu, H., Yuan, L., Wang, J., Cai, Y., Hu, X. and Geng, X. 2019. Influence of high voltage gradients on electrokinetic dewatering for Wenzhou clay slurry improvement. *Soil Mech. Found. Eng.*, 55(6): 400-407.
- Glendinning, S., Jones, C.J. and Pugh, R.C. 2005. Reinforced soil using cohesive fill and electrokinetic geosynthetics. *Int. J. Geomech.*, 5(2): 138-146.
- Gratchev, I.B. and Sassa, K. 2009. Cyclic behavior of fine-grained soils at different pH values. *J. Geotech. Geoenviron. Eng.*, 135(2): 271-279.
- Irfan, M., Chen, Y., Ali, M., Abrar, M., Qadri, A. and Bhutta, O. 2018. Geotechnical properties of effluent-contaminated cohesive soils and their stabilization using industrial by-products. *Processes*, 6(10): 203.
- Jian, Z., Yanli, T., Cunyi, L. and Xiaonan, G. 2019. Experimental study of electro-kinetic dewatering of silt based on the electro-osmotic coefficient. *Environ. Eng. Science.*, 36(6): 739-748.
- Keykha, H.A. and Asadi, A. 2017. Solar-powered electro-bio-stabilization of soil with ammonium pollution prevention system. *Adv. Civil Eng. Mater.*, 6(1): 360-371.
- Keykha, H.A., Huat, B.B. and Asadi, A. 2014. Electrokinetic stabilization of soft soil using carbonate-producing bacteria. *Geotech. Geol. Eng.*, 32(4): 739-747.
- Keykha, H.A., Huat, B.B. and Asadi, A. 2015. Electro-bio grouting stabilization of soft soil. *Environ. Geotech.*, 2(5): 292-300.
- Kim, S. O., Moon, S. H. and Kim, K. W. 2001. Removal of heavy metals from soils using enhanced electrokinetic soil processing. *Water Air Soil Pollut.*, 125(1): 259-272.
- Lakshmi, P.R. and Sivaranjani, N. 2014. Chemical stabilization of soft clay soil using the electrokinetic method. *IOSR J. Mech. Civil Eng.*, 11(2): 34-37.
- Liu, Y., Xie, X., Zheng, L. and Li, J. 2018. Electroosmotic Stabilization on Soft Soil: Experimental Studies and Analytical Models (A historical review). *Int. J. Electrochem. Sci.*, 13: 9051-9068.
- Ma, Y., Li, X., Mao, H., Wang, B. and Wang, P. 2018. Remediation of hydrocarbon-heavy metal co-contaminated soil by electrokinetics combined with biostimulation. *Chem. Eng. J.*, 353: 410-418.
- Martin, L., Alizadeh, V. and Meegoda, J. 2019. Electro-osmosis treatment techniques and their effect on dewatering of soils, sediments, and sludge: A review. *Soils Found.*, 59(2): 407-418.
- Méndez, E., Pérez, M., Romero, O., Beltrán, E.D., Castro, S., Corona, J.L. and Bustos, E. 2012. Effects of electrode material on the efficiency of hydrocarbon removal by an electrokinetic remediation process. *Electrochim. Acta*, 86: 148-156.
- Merifield, R.S., White, D.J. and Randolph, M.F. 2009. Effect of surface heave on the response of partially embedded pipelines on clay. *J. Geotech. Geoenviron. Eng.*, 135(6): 819-829.
- Moayedi, H., Kassim, K.A., Kazemian, S., Raftari, M. and Mokhberi, M. 2014. Improvement of peat using Portland cement and electrokinetic injection technique. *Arab. J. Sci. Eng.*, 39(10): 6851-6862.
- Moayedi, H., Kassim, K.A., Kazemian, S., Raftari, M. and Mokhberi, M. 2014. Improvement of peat using Portland cement and electrokinetic injection technique. *Arab. J. Sci. Eng.*, 39(10): 6851-6862.
- Nordin, N.S., Tajudin, S.A. and Kadir, A.A. 2013. Stabilization of soft soil using electrokinetic stabilization method. *Int. J. Zero Waste Gen.*, 1(1): 5-12.
- Ou, C.Y., Chien, S.C. and Chang, H.H. 2009. Soil improvement using electro-osmosis with the injection of chemical solutions: field tests. *Canad. Geotech. J.* 46(6): 727-733.
- Paulose, S., Reddy, P.H.P. and Jayakumar, K.V. 2014. Swell potential studies on soils contaminated with NaOH solutions. *Proceed. Indian Geotech. Conf.*, 18-20.
- Reddy, H.P., Prasad, C.R.V. and Pillai, R.J. 2017. Swelling of natural soil subjected to acidic and alkaline contamination. *Period. Polytech. Civil Eng.*, 61(3): 611-620.
- Rittirong, A., Shang, J.Q., Mohamedelhassan, E., Ismail, M.A. and Randolph, M.F. 2008. Effects of electrode configuration on electrokinetic stabilization for caisson anchors in calcareous sand. *J. Geotech. Geoenviron. Eng.*, 134(3): 352-365.
- Shang, J.Q. 1997. Electrokinetic dewatering of clay slurries as engineered soil covers. *Canad. Geotech. J.*, 34(1): 78-86.
- Shen, Y., Shi, W., Li, S., Yang, L., Feng, J. and Gao, M. 2020. Study on the Electro-Osmosis Characteristics of Soft Clay from Taizhou with Various Saline Solutions. *Advances in Civil Engineering*.
- Sivapullaiah, P.V. and Manju, K. 2005. Kaolinite-alkali interaction and effects on basic properties. *Geotech. Geol. Eng.*, 23(5): 601-614.
- Sivapullaiah, P.V., Prakash, B.S.N. and Suma, B. N. 2015. Electrokinetic removal of heavy metals from soil. *J. Electrochem. Sci. Eng.*, 5(1): 47-65.
- Sivapullaiah, P.V., Sankara, G. and Allam, M.M. 2010. Mineralogical changes and geotechnical properties of an expansive soil interacted with a caustic solution. *Environ. Earth Sci.*, 60(6): 1189-1199.
- Turer, D. and Genç, A. 2005. Assessing the effect of electrode configuration on the efficiency of electrokinetic remediation by sequential extraction analysis. *J. Hazard. Mater.*, 119(1-3): 167-174.
- Vindula, S.K. and Chavali, R.V.P. 2018. Role of fly ash in control of alkali induced swelling in kaolinitic soils: a micro-level investigation. *Int. J. Geotech. Eng.*, 12(1): 46-52.
- Vindula, S.K., Chavali, R.V.P., Reddy, P.H.P. and Srinivas, T. 2019. Ground granulated blast furnace slag to control alkali-induced swell in kaolinitic soils. *Int. J. Geotech. Eng.*, 13(4): 377-384.
- Wan, Y., Zhai, J. and Wang, A. 2021. Comparative study on electrode arrangement in electrokinetic remediation of contaminated soil. *Nature Environ. Pollut. Technol.*, 20(1): 221-227.
- Xiao, J. and Zhou, S. 2019. Effect of electrode materials on electrokinetic remediation of uranium-contaminated soil. *IOP Conf. Ser. Earth Environ. Sci.*, 300(3): 032074.
- Yi, X.U., Liang, X., Yingming, X.U., Xu, Q.I.N., Huang, Q., Lin, W.A.N.G. and Yuebing, S.U.N. 2017. Remediation of heavy metal-polluted agricultural soils using clay minerals: A review. *Pedosphere*, 27(2): 193-204.





# Statistical Analysis and Modeling of Trivalent Chromium Ion Adsorption by Green-Mediated Iron Nanoparticles

M. Arthy\*† and B. R. Phanikumar\*\*

†Department of Energy and Environmental Engineering, Saveetha School of Engineering, Saveetha Institute of Medical and Technical Sciences, Chennai, India

\*\*Department of Civil Engineering, SRKR Engineering College, Bhimavaram, Andhra Pradesh, India

†Corresponding author: M. Arthy; ramamaruthi1288@gmail.com

Nat. Env. & Poll. Tech.  
Website: [www.neptjournal.com](http://www.neptjournal.com)

Received: 10-08-2021

Revised: 10-11-2021

Accepted: 16-11-2021

## Key Words:

Trivalent chromium  
Zero-valent iron nanoparticles  
Magnetic iron nanoparticles  
Principal component analysis  
Partial least squares  
Agglomerative hierarchical clustering

## ABSTRACT

In this study, the adsorption of trivalent chromium ions by green-mediated iron nanoparticles was studied statistically. The effect of independent variables such as pH, temperature, time, adsorbent dosage, and initial metal ion concentration on uptake capacity and removal efficiency were examined. Multiple linear regression (MLR), principal component analysis (PCA), partial least squares (PLS), and principal component regression (PCR) are effectively applied for the analysis and modeling of adsorption data. The value of  $p$  in Bartlett's sphericity test was proved to be less than 0.05 which indicates that the principal component analysis could be useful for adsorption data. The AHC analysis showed that among all variables, the contribution of pH was high in the adsorption of trivalent chromium ions by ZVIN and MIN nanoparticles. The value of  $R^2$  in statistical modeling of adsorption of trivalent chromium ions by ZVIN particles was high in PCR (0.981) than in MLR (0.945) and PLS (0.752) models. Similarly, for MIN particles, the  $R^2$  value of PCR (0.982) was higher than the MLR (0.943) and PLS (0.742) models. The analysis of goodness of fit statistics showed that the PCR model effectively predicted the uptake capacity and removal efficiency more than MLR and PLS models.

## INTRODUCTION

Heavy metals are defined as metals with high atomic weight or high density (Briffa et al. 2020). Heavy metal discharge from various industrial activities is of global environmental challenge. The heavy metal ions such as Cr(VI), As(III) and Pb (II) that are present in wastewater have dangerous impacts on life. Especially, pollution by chromium ions is more common in developing countries. The chromium ions are widely used in many industrial processes such as leather tanning, electroplating, metal coating, etc. (Sun et al. 2016). Currently, a lot of tons of Cr-bearing solid or liquid wastes are getting discharged from anthropogenic sources (Bedemo et al. 2016). The methods such as chemical precipitation, coagulation, flocculation, Electrochemical treatment (ECT), Electrocoagulation, Electro-flotation, Electro-oxidation, Ion-exchange, Membrane filtration, Electrodialysis, Bioremediation, and Phytoremediation have been widely used for the removal of chromium ions from aqueous solutions. However, these methods have some major drawbacks such as low efficiency, high-energy requirements, production of toxic sludges, and sensitive operating conditions. Compared to other techniques, the adsorption process has revealed

a higher percentage of metal ion removal from water and wastewater hence it is widely used for the treatment of industrial effluents and solid or liquid waste containing complex metal ions (Abdolali et al. 2014). The commercially available adsorbents have been widely used for the removal of chromium ions from the aqueous solution (Renu et al. 2017). In recent times, nanoparticles are receiving more attention than conventional materials in the adsorption process due to their high surface area and faster adsorption rates. Carbon-based nanomaterials, carbon nanotubes, graphene, and metal oxide-based nanomaterials have been widely used as adsorbents for the removal of heavy metals from water and wastewater (Sadegh et al. 2017).

The nanoparticles can be synthesized using various physical and chemical processes however the green synthesis of nanoparticles is getting wider attention among researchers and scientists. The green synthesis of nanoparticles does not require any toxic substances. It consumes less energy and produces safer products and by-products (Usman et al. 2019). Generally, plant extract, enzymes, microorganisms, and organic wastes are used as reducing agents for the production of nanoparticles. However, the prediction of the

adsorption data with statistical tools is very limited. Few studies such as the adsorption of boron on calcium alginate gel beads (Ruiz et al. 2013), Zinc ion adsorption on mango leaf powder (Kaushal & Singh 2017), ascorbic acid removal by activated carbon (Ozdemir & Onal 2013) were reported. In this study, the tea waste extract was used as a reducing agent for the synthesis of ZVIN and MIN nanoparticles. The ZVIN and MIN particles were then tested for their efficacy in the adsorption of trivalent chromium ions. The main aim of this research is to statistically analyze the adsorption data of chromium ions by ZVIN and MIN nanoparticles.

## MATERIALS AND METHODS

### Materials

The chemicals such as chromium (III) nitrate nonahydrate [ $\text{Cr}(\text{NO}_3)_3 \cdot 9\text{H}_2\text{O}$ ], ferric chloride ( $\text{FeCl}_3$ ), ammonia ( $\text{NH}_4\text{OH}$ ), and sodium dodecyl sulfate ( $\text{NaC}_{12}\text{H}_{25}\text{SO}_4$ ) were used in the experimental program. They were obtained from SDFCL (Sdfine-Chem Limited) and all were analytical reagent grade. The tea waste, sugarcane bagasse, and neem leaves were collected from Vellore, Tamil Nadu, India. The statistical analysis was performed using XLSTAT and SPSS software.

### Preparation of Nanoparticles

The Zerovalent Iron Nanoparticles (ZVIN) and Magnetic Iron oxide Nanoparticles (MIN) were green synthesized using effective and novel methods. The detailed preparation of nanoparticles was explained in our previous study (Arthy & Phanikumar 2016). Fig. 1 shows the schematic representation of the synthesis of nanoparticles. Briefly, the ZVIN nanoparticles were prepared by mixing 17 mL of 0.1% SDS with 100 mL of tea waste extract (2.6 g of tea waste was boiled in 100 mL of DIW), and the solution was continuously stirred at a temp of 60°C. To the above mix, 0.1 N  $\text{FeCl}_3$  was added till the color of the solution changed from orange to black. After color changes, the solution was stirred for 15 min and was oven-dried at 80°C for 24 h. The dried particles were washed several times with ethanol and water and again it was oven-dried at 80°C. The MIN nanoparticles were prepared by adding 15 mL of 0.1% sodium dodecyl sulfate solution to 5mL of Iron/tea solution (2g of tea waste was boiled in 100mL of 0.2M  $\text{FeCl}_3$  solution). To the above solution, 50 mL of 16.5% of ammonia was added dropwise by continuously stirring it at 60°C. The solution turned black immediately. The particles were separated using the magnet and coated with neem leaf extract (6.7 g of fresh neem leaves were boiled in 100 mL of DIW). The particles were then washed several times with water and ethanol and were oven-dried at 80°C for 15 h.

## Characterization of Nanoparticles

The nanoparticles were characterized using UV-Visible spectroscopy, BET surface area analysis, XRD, FTIR, SEM, EDX, AFM, VSM, and  $\text{pH}_{\text{pzc}}$ . The size of the nanoparticles was found to be 53.7 nm and 16.3 nm respectively for ZVIN and MIN. The instrumentation analysis of ZVIN and MIN was reported in our previous work (Arthy & Phanikumar 2016, Arthy & Phanikumar 2015).

### Batch Adsorption Tests

The effect of independent variables such as adsorbent dosage, pH, time, initial metal ion concentration, and temperature was studied on the adsorption response of uptake capacity (mg/g) and removal efficiency (%). The batch adsorption process was carried out by varying the independent variables such as adsorbent dosage (0.05 to 0.125 g), pH (2-7), time (5-120 min), initial metal ion concentration (50-300 ppm), and temperature (30, 45 and 60°C). The metal ion concentration after the adsorption process was measured using Varian AA240 atomic adsorption spectrometer (Arthy & Phanikumar 2015). The metal ion uptake capacity and removal efficiency of ZVIN and MIN was calculated using the following equations:

$$\text{Uptake Capacity } (q_e, q_t) = [C_i - C_e] / M_i \times V \quad \dots(1)$$

$$\text{Removal Efficiency } Y (\%) = ([C_i - C_e] / C_i) \times 100 \quad \dots(2)$$

Where V is the volume of solution (mL), M is the mass of the dry adsorbent (g), and  $C_i$  and  $C_e$  are the initial and equilibrium concentrations of  $\text{Cr}^{3+}$  in the aqueous solution (mg/L). All the experiments were performed in duplicate and the mean values were considered for analysis.

### Principal component analysis (PCA) and Agglomerative Hierarchical Clustering (AHC)

PCA is a dimensionality reduction method that is used to reduce the dimensions of a large data set. Reducing the number of variables will reduce the accuracy of the data set whereas reducing the dimensionality will still contain most of the information in the data set.

Before performing PCA and HCA, the data must be standardized using the following equation:

$$Z = (X - \mu) / \sigma \quad \dots(3)$$

Where X is the score of original variables,  $\mu$  is the arithmetic mean of the variable and  $\sigma$  is the standard deviation of the variable (Frescura et al. 2020). In this study, the Z score was calculated using SPSS software. To access the differences and similarities between the factors, HCA was used. PCA performs the principle component analysis on the adsorption data set which converts the original data into new variables called principal components.

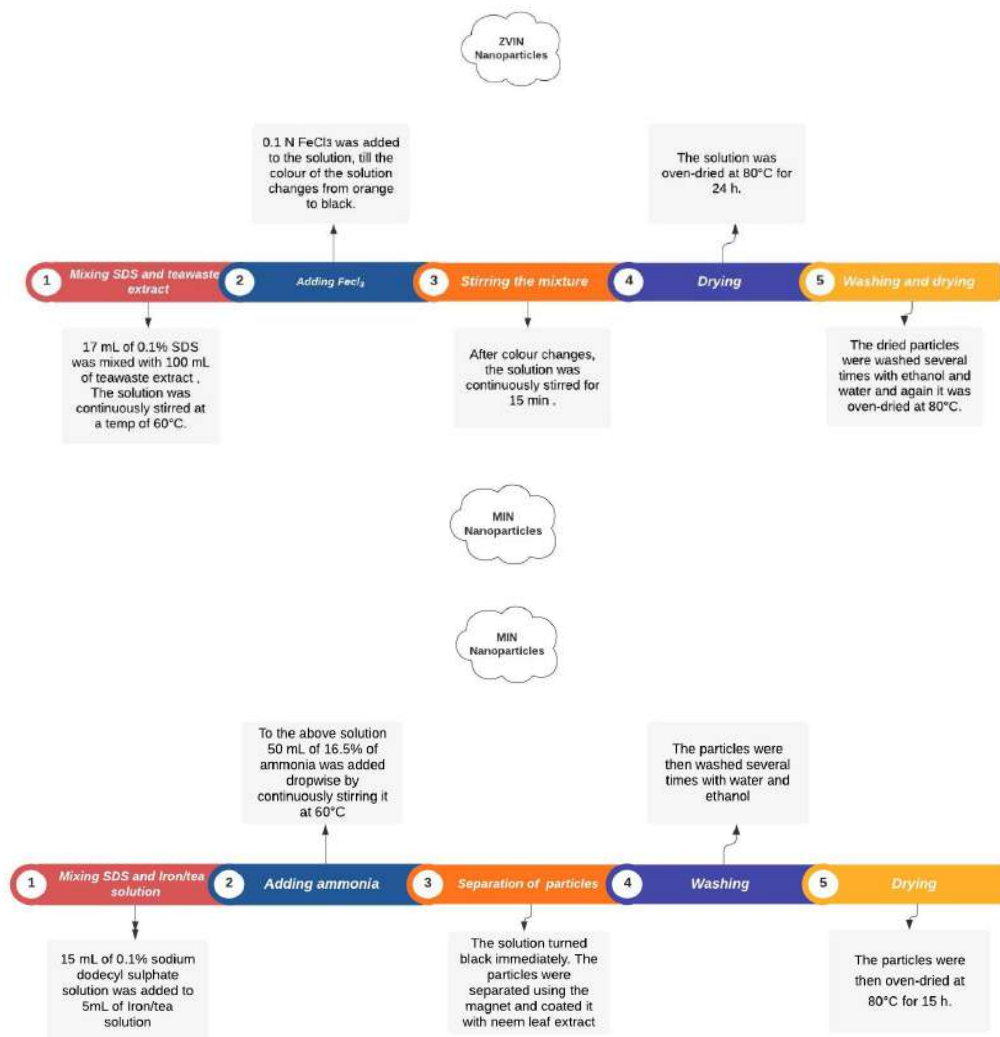


Fig. 1: Synthesis of ZVIN (a) and MIN (b) Nanoparticles.

### Statistical Prediction of Adsorption Data

The prediction of uptake capacity and removal efficiency was done by different models MLR, PLS, and PCR. Multivariate analysis is an efficient tool for developing a quantitative relationship, between the predictor variables X (pH, initial metal ion concentration, temperature, time, and adsorbent dosage) and a dependent variable Y (uptake capacity, removal efficiency). In this study, the generalized equation of MLR and PLS model was given by equation 4 whereas the generalized equation for PCR is given by equation 5.

$$\text{Uptake capacity/Removal Efficiency} = \beta_0 + \beta_1 \times \text{pH} + \beta_2 \times \text{Time} + \beta_3 \times \text{Initial metal ion conc} + \beta_4 \times \text{temperature} + \beta_5 \times \text{adsorbent dosage} \quad \dots(4)$$

$$\text{Uptake capacity/Removal Efficiency} = \beta_0 + \beta_1 \times F_1 + \beta_2 \times F_2 + \beta_3 \times F_3 + \beta_4 \times F_4 + \beta_5 \times F_5 \quad \dots(5)$$

where,

$\beta_0 - \beta_5$  represents the coefficients estimated by MLR, PLS, and PCR models

### RESULTS AND DISCUSSION

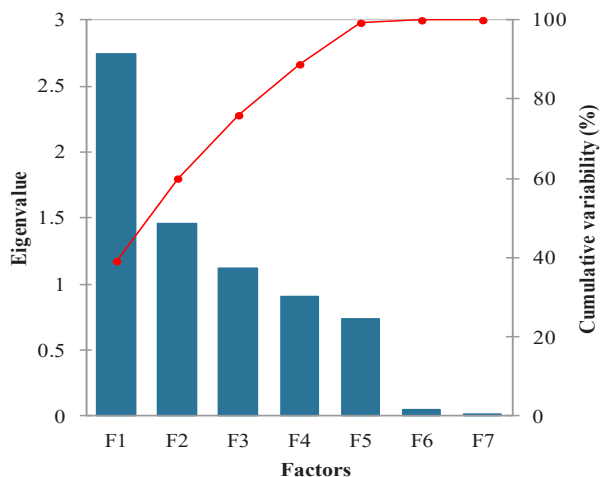
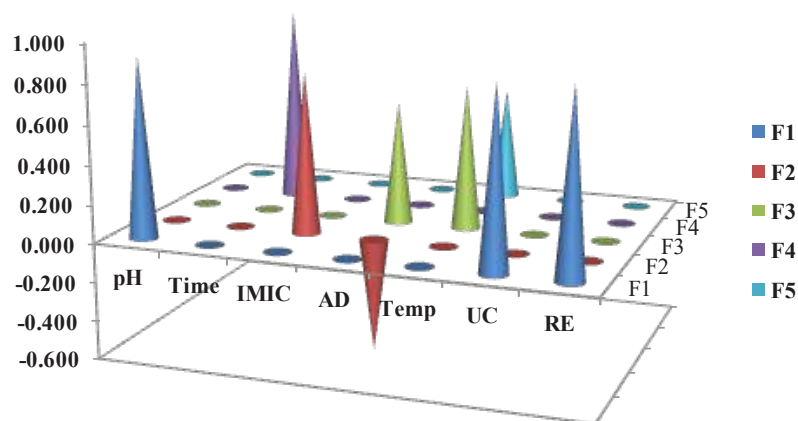
The maximum experimental uptake capacity of ZVIN and MIN were found to be 231.19 and 232.59 mg/g respectively. The removal efficiency of ZVIN and MIN were found to be 92.6% and 93% respectively (Arthy & Phanikumar 2016).

### Analysis of Data

### Principal Component Analysis (PCA)

A principal component consists of a score vector and a loading vector. The score vector contains information on how the adsorbents are related to each PC. Loading vectors define the reduced dimension space and contain information on how the variables relate to each PC (Alvarez-Uriarte et al. 2011). The influence of variables such as pH, initial metal ion concentration, temperature, time, adsorbent dosage, uptake capacity, and removal efficiency on factors is given by factor loadings. It helps in the identification of the most important variables which has a significant influence (positive or negative) on the factors. The factor loading higher than 0.5 was assumed to be significant (Alvarez-Uriarte et al. 2011). Hence, the factor loading of less than 0.5 was not reported in this study. Fig. 2(a) illustrates the factor loading of ZVIN particles on the adsorption of trivalent chromium ions. Factor 1 has high positive loading for pH (0.921), uptake capacity (0.911) and removal efficiency (0.929). Factor 2 has high

positive loading for initial metal ion concentration (0.826) and high negative loading for adsorbent dosage (-0.578). Factor 3 has high positive loading for adsorbent dosage (0.624) and temperature (0.735). Factors 4 and 5 have high positive loading for time (0.998) and temperature (0.577) respectively. Fig. 2(b) shows the scree plot of ZVIN particles, totally of seven factors were extracted for the adsorption of trivalent chromium ions using ZVIN particles. The Eigenvalue of the factors were found to be 2.743, 1.380, 1.098, 1.001, 0.733, 0.042 and 0.004 respectively for factor 1, factor 2, factor 3, factor 4, factor 5, factor 6 and factor 7. The percentage of variability was found to be 39.188%, 19.717%, 15.682%, 14.293%, 10.47%, 0.593% and 0.057% respectively for factor 1, factor 2, factor 3, factor 4, factor 5, factor 6 and factor 7. Fig. 2(c) illustrates the factor loading of MIN-particles on the adsorption of trivalent chromium ions. Factor 1 has high positive loading for pH (0.934), uptake capacity (0.907), and removal Efficiency (0.934). Factor 2 has high positive loading



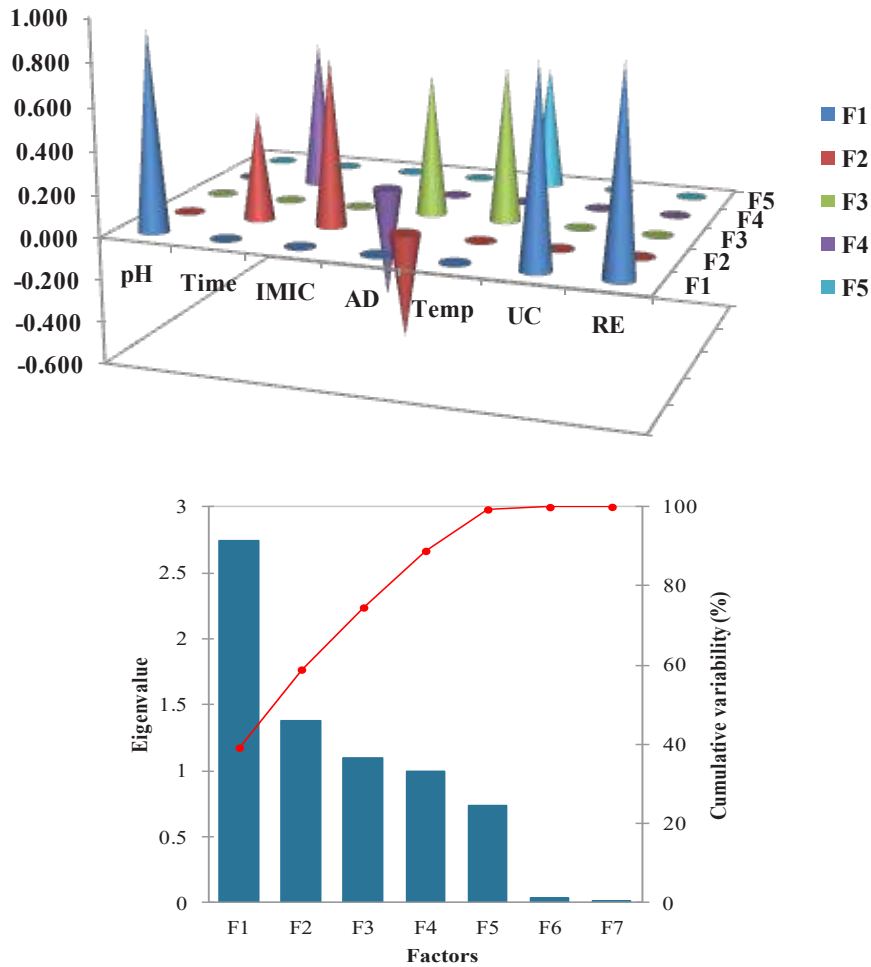


Fig. 2: Loading plot of ZVIN (a) and MIN (c) and Scree plot of ZVIN (b) and MIN (d).

for time (0.508) Initial metal ion concentration (0.785) and negative loading for adsorbent dosage (-0.5). Factor 3 has high positive loading for adsorbent dosage (0.661) and temperature (0.724). Factor 4 has high positive loading on time (0.701) and negative loading on initial metal ion concentration (-0.552). Factor 5 has high factor loading on temperature (0.584). Fig. 2(d) shows the scree plot of MIN- particles which resulted in seven factors, the Eigenvalues of the factors were found to be 2.738, 1.460, 1.120, 0.899, 0.734, 0.045, and 0.004 respectively for factor 1, factor 2, factor 3, factor 4, factor 5, factor 6 and factor 7. The percentage of variability was found to be 39.117%, 20.859%, 15.999%, 12.847%, 10.481%, 0.647% and 0.050% respectively for factor 1, factor 2, factor 3, factor 4, factor 5, factor 6 and factor 7.

Eigenvalues indicate the importance of the factors. Thus, the factors with an Eigen value greater than one were

assumed to be significant. Similarly, the percentage of variability should also be greater than 10 (Alvarez-Urriarte et al. 2011). Hence, the number of factors retained for ZVIN and MIN was found to be 4 and 3 respectively. For ZVIN and MIN particles, Factor 3 showed high positive loading for temperature when compared with Factor 5 hence it is not considered. The cumulative variance of ZVIN and MIN were found to be 88.88% (four factors) and 75.97% (three factors), while the minimum decisive factor of the satisfactory analysis is 70% (Cvejanov & Skrbic 2017, Scitutto et al. 2017).

**Agglomerative Hierarchical Clustering (AHC)**

Agglomerative hierarchical clustering is an iterative classification method, which clusters the dissimilarities between objects together. The type of dissimilarity depends on the nature of the data and the subject studied. The result of AHC is shown in the dendrogram which shows the progressive

Table 1: AHC Result analysis by class of ZVIN.

Class	1	2
Objects	14	4
Sum of weights	14	4
Within-class variance	6.074	1.466
Minimum distance to the centroid	0.698	0.319
Average distance to the centroid	2.141	0.918
Maximum distance to the centroid	3.695	1.518

grouping of data. From the dendrogram, the appropriate number of classes into which the data can be grouped can be identified. In this study, the ward's agglomeration method and Euclidean distance of dissimilarity were chosen.

Fig. 3(a) and 3(b) show the dendrogram of ZVIN and MIN particles respectively. The dendrogram has been majorly classified into two clusters C1 and C2 for both ZVIN and MIN particles. The AHC was used to examine the different operating conditions of adsorbents in the removal of trivalent chromium ions. The elements belonging to the same group are similar to each other and the elements in different groups are heterogeneous in relation to the same variables (Vandeginste 1998). In this study, cluster C2 belongs to the observations on pH for both ZVIN and MIN particles. The cluster C1 belongs to the observations of other input variables like time, temperature, initial metal ion concentration, and adsorbent dosage. The result indicates that, when compared with other independent variables, the pH influences more the removal of trivalent chromium ions by ZVIN and MIN nanoparticles. Table 1 and Table 2 show the AHC result by class respectively for ZVIN and MIN particles. The C2 is more homogeneous than the C1. This is validated by the result of the Within-class variance shown in Table 1 and Table 2 of ZVIN and MIN. The within-class variance of C1 is found to be 6.074 and 3.646 respectively for ZVIN and MIN which is higher than C2.

## Modeling of Adsorption Data

### Multiple Linear Regression Analysis

The purpose of multiple linear regression is used to learn the relationship between the predictor variable and the dependent variable. In linear regression, models of the unknown parameters are estimated from the data using linear models. Linear regression has many practical applications such as prediction, forecasting...etc. It can be used to fit a predictive model to an observed set of input  $x$  and output  $y$  values. The generalized equation of MLR is given by equation 6.

$$Y_i = \beta_0 + \beta_1 X_1 + \dots + \beta_n X_n \quad \dots(6)$$

Where,  $\beta_i$  ( $i = 0, \dots, n$ ) are the parameters generally esti-

Table 2: AHC Result analysis by class of MIN.

Class	1	2
Objects	16	4
Sum of weights	16	4
Within-class variance	3.646	1.436
Minimum distance to centroid	0.176	0.308
Average distance to centroid	1.480	0.914
Maximum distance to centroid	3.636	1.520

mated by least squares and  $X_i$  ( $i = 1, \dots, n$ ) are the explanatory variables (predictors) (Sousa et al. 2007). Multiple linear regression analysis (MLR) is one of the most widely used methodologies for expressing the dependence of a response variable on several independent variables. Despite its success in many applications, the regression approach can face serious difficulties when the independent variables are correlated with each other (McAdams et al. 2000). Multicollinearity, or high correlation among the independent variables in a regression equation, can make it difficult to correctly identify the most important contributors to a physical process. In this study, the linear regression was calculated using the 'Forward' model. Eq. 7 and 9 show the MLR model for uptake capacity of ZVIN and MIN respectively whereas Eq. 8 and 10 show the MLR model for removal efficiency of ZVIN and MIN respectively.

$$\text{Uptake capacity of ZVIN} - 0.789 \text{ pH} + 0.525 \text{ IMIC} - 0.351 \text{ Adsorbent dosage} \quad \dots(7)$$

$$\text{Removal Efficiency of ZVIN} - 0.949 \text{ pH} \quad \dots(8)$$

$$\text{Uptake capacity of MIN} - 0.792 \text{ pH} + 0.510 \text{ IMIC} - 0.346 \text{ Adsorbent dosage} \quad \dots(9)$$

$$\text{Removal Efficiency of MIN} - 0.95 \text{ pH} \quad \dots(10)$$

### Principal Component Regression

Principal component regression (PCR) combines principal component analysis (PCA) and multiple linear regression (MLR). In PCR, instead of directly using dependent variables on the explanatory variables, the principal components of explanatory variables are used as regressors. The principal components with higher variances are selected as regressors. The PCR is used to overcome the multicollinearity problem. Eq. 11 shows the generalized equation of PCR.

$$Y_i = \beta_0 + \beta_1 F_1 + \dots + \beta_n F_n \quad \dots(11)$$

Where,  $\beta_i$  ( $i = 0, \dots, n$ ) are the parameters generally estimated by least squares and  $F_i$  ( $i = 1, \dots, n$ ) are the factors calculated by principal component analysis. Eq. 12 and 14 show the PCR model for uptake capacity of ZVIN and MIN respectively whereas Eq. 13 and 15 show the PCR model for removal efficiency of ZVIN and MIN respectively. In



Table 3: Statistical analysis of uptake capacity by ZVIN and MIN nanoparticles.

Uptake Capacity	ZVIN			MIN		
	MLR	PCR	PLS	MLR	PCR	PLS
Observations	18	18	18	20	20	20
Sum of weights	18	18	18	20	20	20
DF	14	15	16	16	16	18
R <sup>2</sup>	0.945	0.981	0.752	0.943	0.982	0.742
Adjusted R <sup>2</sup>	0.934	0.978	0.513	0.932	0.978	0.521
MSE	0.066	0.022	0.234	0.068	0.022	0.245
RMSE	0.257	0.148	0.484	0.261	0.148	0.495
MAPE	29.328	27.011		41.409	39.142	
DW	0.985	0.631		1.015	0.649	
Cp	3.482	4.737		3.265	4.000	
AIC	-45.398	-66.078		-50.183	-72.865	
SBC	-41.836	-63.407		-46.200	-68.882	
PC	0.086	0.027		0.086	0.028	

this study, the linear regression of principal components was calculated using the ‘Forward’ model.

Uptake capacity of ZVIN -  $0.534 \times F1 + 0.321 \times F2 \dots(12)$

Removal Efficiency of ZIVN -  $0.545 \times F1 - 0.270 \times F2 \dots(13)$

Uptake capacity of MIN -  $0.534 \times F1 + 0.303 \times F2 - 0.124 \times F3 \dots(14)$

Removal Efficiency of MIN -  $0.549 \times F1 - 0.224 \times F2 + 0.117 \times F3 \dots(15)$

**Partial Least Square**

Partial least square is a rapid, well-organized, and best regression method based on covariance. It is a technique that decreases the predictors to a lesser set of uncorrelated components and achieves least square regression on these components, instead of on the original data. PLS is used to find a relationship between explanatory variables (X) and independent variables (y). The generalized equation for PLS is given by the following equation

$Y=Xb \dots(16)$

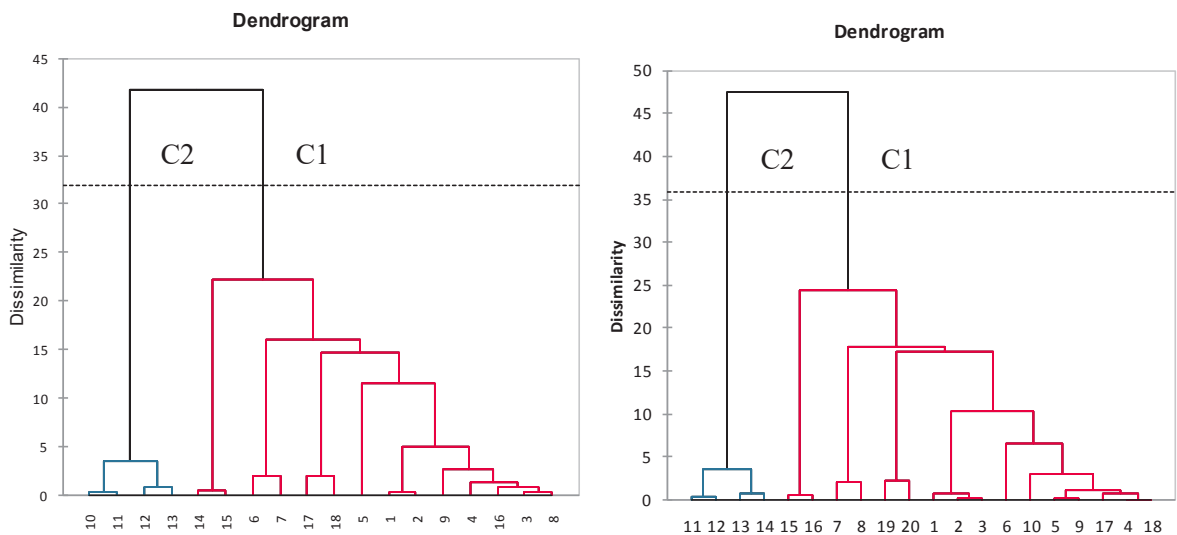


Fig. 3: Dendrogram obtained from AHC of ZVIN (a) and MIN (b) particles.

Table 4: Statistical analysis of Cr<sup>3+</sup> ion removal by ZVIN and MIN nanoparticles.

Removal Efficiency	ZVIN			MIN		
	MLR	PCR	PLS	MLR	PCR	PLS
Observations	18	18	18	20	20	20
Sum of weights	18	18	18	20	20	20
DF	16	15	16	18	16	18
R <sup>2</sup>	0.901	0.970	0.790	0.902	0.965	0.794
Adjusted R <sup>2</sup>	0.895	0.966	0.473	0.897	0.958	0.466
MSE	0.105	0.034	0.199	0.103	0.042	0.195
RMSE	0.325	0.184	0.446	0.321	0.204	0.442
MAPE	148.729	110.638		53.343	33.135	
DW	0.990	1.069		1.152	1.245	
Cp	3.070	2.403		2.195	4.000	
AIC	-38.635	-58.233		-43.553	-60.098	
SBC	-36.854	-55.562		-41.562	-56.115	
PC	0.124	0.042		0.119	0.052	

Where  $b$  is the calibration vector. Eq. 17 and 19 show the PLS model for uptake capacity of ZVIN and MIN respectively whereas Eq. 18 and 20 illustrate the PLS model for removal efficiency of ZVIN and MIN respectively.

Uptake capacity of ZVIN -  $0.766 \times \text{pH} + 0.038 \times \text{Time} + 0.121 \times \text{IMIC} - 0.199 \times \text{Adsorbent dosage} + 0.232 \times \text{Temperature}$  ... (17)

Removal Efficiency of ZVIN -  $0.785 \times \text{pH} + 0.039 \times \text{Time} + 0.124 \times \text{IMIC} - 0.204 \times \text{Adsorbent dosage} + 0.238 \times \text{Temperature}$  ... (18)

Uptake capacity of MIN -  $0.773 \times \text{pH} - 0.058 \times \text{Time} + 0.116 \times \text{IMIC} - 0.186 \times \text{Adsorbent dosage} + 0.206 \times \text{Temperature}$  ... (19)

Removal Efficiency of MIN -  $0.8 \times \text{pH} - 0.06 \times \text{Time} + 0.120 \times \text{IMIC} - 0.192 \times \text{Adsorbent dosage} + 0.213 \times \text{Temperature}$  ... (20)

### Comparison of MLR, PCR and PLS Models

#### Goodness of Fit

Tables 3 and 4 show the statistical analysis of the adsorption data by ZVIN and MIN respectively. The DF represents the number of degrees of freedom, which indicate that the number of independent values, can vary in a study without breaking any constraint. The DF of MLR, PCR, and PLS was given in Tables 3 and 4. The values indicated that the PCR and PLS model has high degrees of freedom when compared with MLR for both uptake capacity and removal efficiency of ZVIN and MIN nanoparticles. The R<sup>2</sup> is interpreted as the

amount of the variability of the dependent variable explained by the model. The better fit of the model should have the value of R<sup>2</sup> close to 1. In this study, the R<sup>2</sup> value of PCR was found to be greater than in other models. Similarly, the adjusted R<sup>2</sup> value is also greater for the PCR model (Tables 3 and 4). The mean of the squares of the error (MSE) is the average squared difference between the predicted values and the actual values. The Root Mean Square Error (RMSE) is the standard deviation of the residuals. The values closer to zero are better hence, the MSE and RMSE values of the PCR model were found to be less when compared with MLR and PLS models. The mean absolute percentage error (MAPE) is a measure of the prediction accuracy of forecasting methods. The result shows that the PCR model has less MAPE value than MLR (Tables 3 and 4).

Durbin-Watson (DW) is a test for autocorrelation in the residuals from a statistical regression analysis. DW statistic value always lies between 0 and 4. If the result lies between 0 and <2 there is a positive autocorrelation. If the value is 2 there is no autocorrelation detected in the sample. If the value lies between >2 and 4 it is negative autocorrelation. In this study, the value suggests a positive correlation for both ZVIN and MIN nanoparticles (Tables 3 and 4). Mallows Cp coefficient evaluates the accuracy and bias of the full model to the models with a subset of the predictors. The Mallows Cp value should be close to the number of predictors plus the constant. The nearer the Cp coefficient to the predictor variable, the less the model is biased. The value of Cp of ZVIN and MIN on uptake capacity and removal efficiency

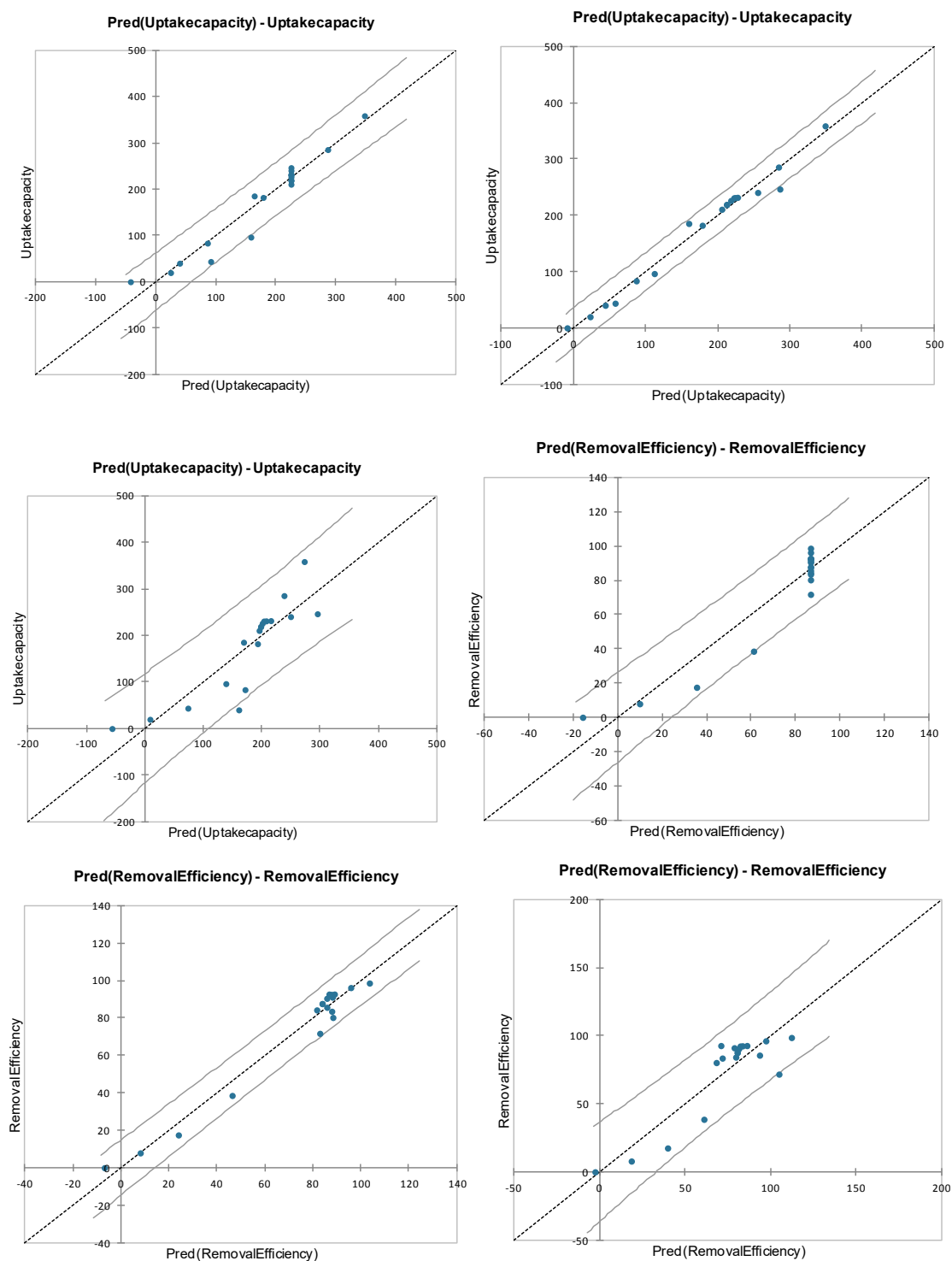


Fig. 4: Variation of predicted values on uptake capacity (a, b, c) and removal efficiency (d, e, f) of ZVIN nanoparticles by MLR (a, d), PCR (b, e) and PLS(c, f) models.

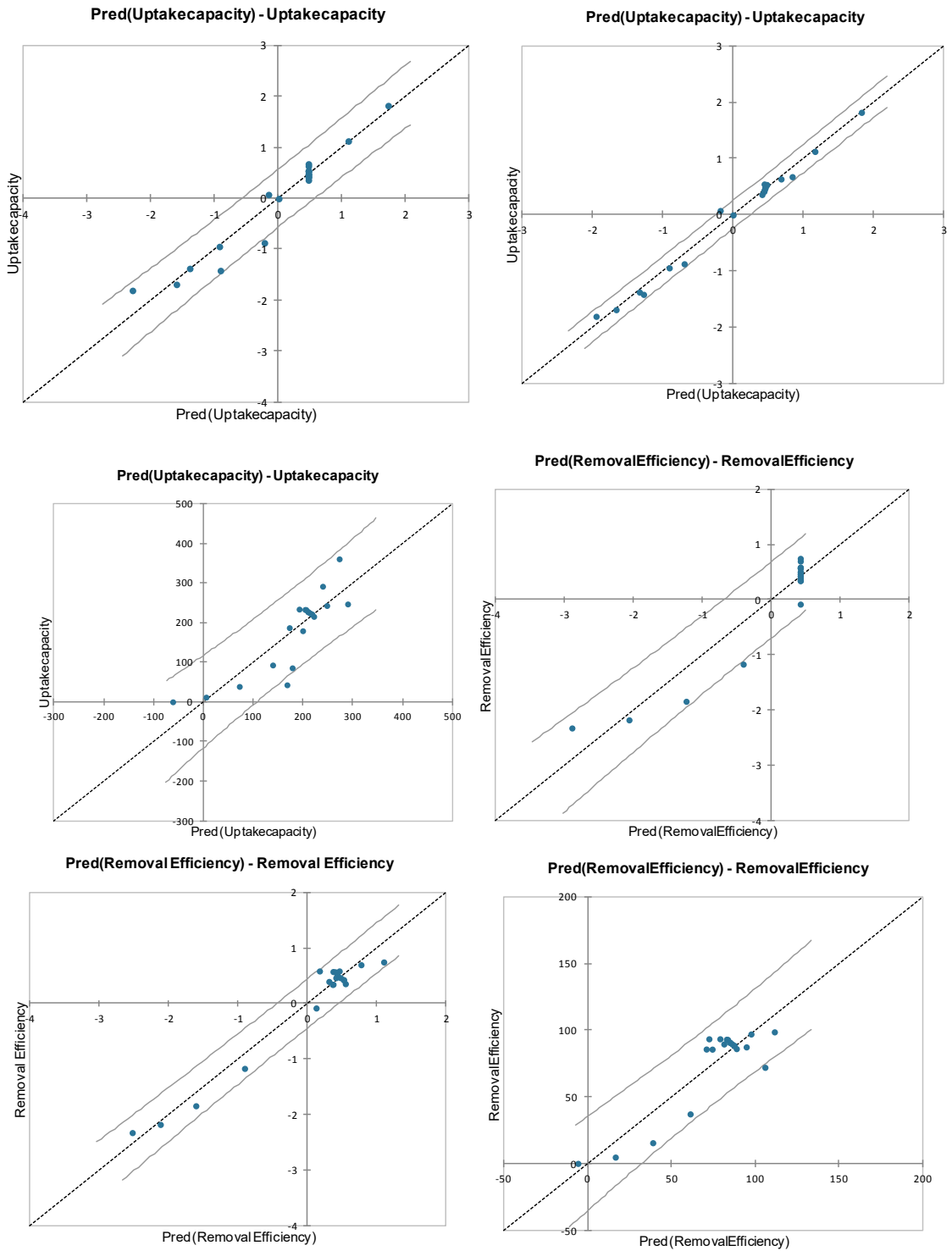


Fig. 5: Variation of predicted values on uptake capacity (a, b, c) and removal efficiency (d, e, f) of MIN nanoparticles by MLR (a, d), PCR (b, e) and PLS(c, f) models.

indicated that both MLR and PCR models are less biased. Akaike's information criterion (AIC) is an estimator of prediction error. AIC estimates the amount of information lost by the model. It is used to compare the quality of the model. Schwarz's Bayesian Criterion (SBC) is a decisive factor for model selection, the model with the lowest BIC is chosen. Table 3 and 4 shows the PCR model has fewer AIC and SBC values than the MLR model for both uptake capacity and removal efficiency of ZVIN and MIN nanoparticles. Amemiya's prediction criterion (PC) is similar to adjusted  $R^2$ , where, it penalizes more heavily than adjusted R-square. The value of PC is less for the PCR model when compared to the MLR model for both ZVIN and MIN nanoparticles on the removal of  $Cr^{3+}$  ions.

Thus the analysis of goodness of fit indicates that the PCR model is best suited for the prediction of uptake capacity and removal efficiency for MLR, PCR, and PLS models.

### Prediction of Uptake Capacity and Removal Efficiency

Fig. 4 and 5 show the variation of predicted values on uptake capacity and removal efficiency of ZVIN and MIN nanoparticles by MLR, PCR, and PLS models. The figures show that the PCR model has effectively predicted the uptake capacity and removal efficiency of ZVIN and MIN nanoparticles.

### CONCLUSION

In this paper, two statistical analysis techniques (PCA and HCA) and three statistical modeling techniques (PCR, MCR, and PLS) were applied to the adsorption data. These data analysis tools enhance the understanding of the adsorption process. PCA and HCA were applied to identify the chief contribution of independent variables in the removal of  $Cr^{3+}$  ions from an aqueous solution. The results indicated that among all variables, the contribution of pH in the removal of  $Cr^{3+}$  ions from an aqueous solution was found to be high. PCR, MLR, and PLS were used for the prediction of adsorption data. The analysis of goodness of fit for MLR, PCR, and PLS models indicates that the PCR model is best suited for the prediction of uptake capacity and removal efficiency.

### ACKNOWLEDGEMENT

The authors are thankful to the VIT University, Vellore for providing sufficient facilities to carry out this research work.

### REFERENCES

Abdolali, A., Guo, W.S., Ngo, H.H., Chen, S.S., Nguyen, N.C. and Tung, K.L. 2014. Typical lignocellulosic wastes and by-products for bio-sorption process in water and wastewater treatment: A critical review. *Bioresour. Technol.*, 160: 57-66.

Agarwal, R.M. and Singh, K. 2017. Heavy metal removal from wastewater using various adsorbents: A review. *J. Water Reuse Desal.*, 7(4): 384-419.

Alvarez-Uriarte, J.I., Iriarte-Velasco, U., Chimen-Alanis, N. and Gonzalez-Velasco, J.R. 2011. Application of principal component analysis to the adsorption of natural organic matter by modified activated carbons. *Sep. Sci. Technol.*, 46(14): 2239-2249.

Arthy, M. and Phanikumar, B.R. 2016. Efficacy of iron-based nanoparticles and nano-biocomposites in the removal of  $Cr^{3+}$ . *J. Hazard. Toxic. Radioact. Waste*, 20(3): 1-28.

Arthy, M. and Phanikumar, B.R. 2015. Immobilization of chromium in tannery sludge using iron-based nanoparticles and nanobiocomposites. *Water Air Soil Pollut.*, 226: 204.

Bedemo, A., Chandravanshi, B.S. and Zewge, F. 2016. Removal of trivalent chromium from aqueous solution using aluminum oxide hydroxide. *Springer Plus*, 5(1): 1288.

Briffa, J., Sinagra, E. and Blundell, R. 2020. Heavy metal pollution in the environment and their toxicological effects on humans. *Heliyon.*, 6: e04691.

Chatfield, C. and Collin, A.J. 1980. Introduction to multivariate analysis. Chapman and Hall/ Methuen, New York.

Cvejanov, J.D and Skrbic, B.D. 2017. Application of principal component and hierarchical cluster analyses in the classification of Serbian bottled waters and comparison with waters from some other European countries. *J. Serb. Chem. Soc.*, 82(6): 711-721.

Frescura, L.M., de Menezes, B.B., Duarte, R. and da Rosa M.B. 2020. Application of multivariate analysis on naphthalene adsorption in aqueous solutions. *Environ. Sci. Pollut. Res. Int.*, 27(3): 3329-3337.

Karpuzcu, M. and Senes, S. 1987. Design of Monitoring Systems for Water Quality by Principal Component Analysis: A Case Study. Proceedings of the International Symposium on Environmental Management. Environment, 1987, Istanbul, pp. 673-690.

Kaushal, A. and Singh, S.K. 2017. Critical analysis of adsorption data statistically. *Appl. Water Sci.*, 7: 3191-3196.

McAdams, H.T., Crawford, R. and Hadder, G.R. 2000. A Vector Approach to Regression Analysis and its Application to Heavy-Duty Diesel Emissions. Society of Automotive Engineers, Inc., Warrendale, Pennsylvania, United States, pp. 1-18.

Ozdemir, C.S. and Onal, Y. 2013. Statistical analysis of equilibrium and kinetic data for ascorbic acid removal from aqueous solution by activated carbon. *Desalin. Water Treat.*, 51(22-24): 4658-4665.

Ruiz, M., Roset, L., Demey, H., Castro, S., Sastre, A.M. and Perez, J.J. 2013. Equilibrium and dynamic studies for adsorption of boron on calcium alginate gel beads using principal component analysis (PCA) and partial least squares (PLS). *Mater. Sci. Technol.*, 44(5): 349-514.

Sadegh, H., Ali, G.A.M., Gupta, V.K., Makhlof, A.S.H., Shahryari-Ghoshehendi, R., Nadagouda, M.N., Sillanpaa, M. and Megiel, E. 2017. The role of nanomaterials as effective adsorbents and their applications in wastewater treatment. *J. Nanostruct. Chem.*, 7 (1): 1-14.

Sciutto, G., Oliveri, P., Prati, S., Catelli, E Bonacini, I and Mazzeo, R. 2017. A multivariate methodological workflow for the analysis of FTIR chemical mapping applied to historic paint stratigraphies. *Int. J. Anal. Chem.*, 2017: 1-12.

Sousa, S.I.V., Martins, F.G., Alvim-Ferraz, M.C.M. and Pereira, M.C. 2007. Multiple linear regression and artificial neural networks based on principal components to predict ozone concentrations. *Environ. Model Softw.*, 22(1): 97-103.

Sun, S., Ma, J., Liu, W. and Chen, K. 2016. Gram-grade Cr(vi) adsorption on magnetite/carbon hybrid architectures. *RSC Adv.*, 6 (34): 28435-28441.

Usman, A.I., Aziz, A.A. and Noqta, O.A. 2019. Green sonochemical synthesis of gold nanoparticles using palm oil leaves extracts. *Mater. Today Proc.*, 7: 803-807.

Vandeginste, B. G. M., Massart, D. L., Buydens, L. M. C., De Jong, S., Lewi, P. J. and Smeyers-Verbeke, J. 1998. Handbook of Chemometrics and Qualimetrics Cluster Analysis. Elsevier, Amsterdam, p. 57.





# A Review of User-Centred Design Methods for Designing a Portable Oil Spill Skimmer

R. Ramanathan\*, L. Abdullah\*†, M. S. Syed Mohamed\* and M.H.F.M Fauadi\*

\*Faculty of Manufacturing Engineering, Universiti Teknikal, Malaysia Melaka, 76100 Durian Tunggal, Melaka, Malaysia

†Corresponding author: lokman@utem.edu.my

Nat. Env. & Poll. Tech.  
Website: [www.neptjournal.com](http://www.neptjournal.com)

Received: 20-10-2021

Revised: 07-02-2022

Accepted: 10-02-2022

### Key Words:

Analytical hierarchy process  
Conceptual design selection  
Product development process  
Pairwise comparison  
Oil spill skimmer

## ABSTRACT

Boom and skimmer are mechanical techniques in Oil Spill Response and Recovery (OSRR) that collect oil from the water surface. However, there are several drawbacks of using boom and skimmer, such as the oil could pass over the boom during strong wind and high tides. Moreover, the currently available oil skimmer designed by the engineers is heavy-duty; in consequence, it is ineffective in shallow water. Thus, there is a need to develop a portable oil spill skimmer to complement the current drawbacks. Several journals on the fabrication of the oil spill skimmer were reviewed. Findings from literature shows that the development of oil spill skimmer lacks user requirements when designing a portable oil spill skimmer. This article provides a systematic review of Kansei Engineering and the Analytical Hierarchy Process in the product development process. Therefore, Kansei Engineering and Analytical Hierarchy Process (AHP) can be incorporated in the early stage of designing a portable oil spill skimmer. This paper also includes the application of Kansei Engineering and AHP in design research articles. Findings from observed articles indicate a lack of design and development technologies relating to products for environmental protection; the AHP and Kansei Engineering application is somewhat lacking. Moreover, the fabrication of an oil spill skimmer focuses more on technical specifications and includes fewer user requirements. As a result, the characteristics such as ease of use, robustness, and safety cannot be evaluated. The AHP and Kansei Engineering methodology can be extended to the design and manufacture of products for environmental protection.

## INTRODUCTION

A mechanism for removing oil that floats on a liquid surface is known as an oil skimmer. Depending on the technical configuration, it is used for a variety of purposes, including the remediation of oil spills as part of systems for treating oily water, the removal of oil from machine tool coolants and aqueous parts washers, and the processing of fat, oil, and grease in wastewater treatment facilities for the production of food. Oils, grease, and fats must be extracted using skimmers in industrial applications to comply with environmental discharge regulations before further processing. It may minimize water retention, odor, and unsightly surface scum by eliminating the top layer of oils. It should be observed that to extract condensed oil, all oil skimmers will accumulate a proportion of water with the oil, which will have to be decanted. Oil spill skimmers have a wide range of criteria to meet, such as buoyancy, the recovery rate of oil spillage, maneuverability, autonomous capacity, and many others to recover oil spills in any large body of water successfully. Buoyancy refers to the skimmer's ability to float in any water

body without sinking too far successfully. Without falling overboard, it must even tolerate small waves or currents along lakes, rivers, and oceans. The spillage recovery rate refers to the speed at which the skimmer can extract oil within a given timeframe. Maneuverability is the skimmer's ability to travel about on water rapidly and reliably while moving about oil spillages. Last but not least, autonomous functionality can help users ease their workload when handling oil spillages by having to monitor the oil spill skimmer themselves. To satisfy the needs of the consumers, these technological specifications somehow need to be built into oil spill skimmers.

## REVIEW ON OIL SPILL

### Causes of Oil Spill

Chemical pollution of saltwater happens as a result of motor oil spills overboard, collision-related fuel oil leaks, and spills from the shoreline that transport diesel fuel to fishing boats. In oil spill treatment, marine oil leaks are categorized as thick oil with a density of more than 10 mm and thinner

oil with a thickness of less than 10 mm. Besides, light oil with a thickness of less than 1 mm is known as oil film and, according to its presence on the water surface, can be divided into multiple levels.

### Effects of Oil Spills

Oil spills cause significant economic damage and affect public health. The number of living species would be degraded by oil on the sea and washed up oil on the beach for an extended period without being retrieved, causing harm to the fishing and aquaculture industries. Due to a lack of dissolved oxygen, oils that pollute the water cause fish to die in huge numbers. Oil sticking to the soil, rock embankments, and island banks, creating aesthetics, and causing foul odors, adds to the tourism industry's significant losses (Zhang et al. 2018). Fig. 1 shows the occurrence of significant oil spills around the world.

### Overview of Oil Spill Respond and Recovery Techniques

The modernized world needs speed in all areas. Therefore, the most critical thing is speed and fast work. Different devices and machinery are developed nowadays to achieve rapidity. In such a new age of globalization,

scaled-down businesses support our country's development differently.

Mechanical recovery is recognized as the most effective and environmentally sustainable procedure of all these approaches. It is also the first preferred approach for the rehabilitation of oil spill systems (Mirajkar et al. 2019). Therefore, as an essential aspect of the general oil spill response and preparedness system, connectivity to the mechanical recovery capacity by skimmer is necessary.

Chemical spills and oil slicks are listed as follows in three groups in the aquatic setting (Tuan Hoang et al. 2018):

Dispersion and solidifier are one of the methods that tackle oil spill issues in chemical techniques. Dispersant application's main objective is to decompose oil slicks into tiny droplets that can be immersed and dispersed quickly (Muizis 2013). They slow oil formation in water emulsions and are hazardous to marine life in general (Almeda et al. 2014). On the other hand, a solidifier possesses hydrophobic and oleophilic characteristics that attract oil while repelling water (Hum & Hamza 2016). High waves and water currents aid solidification by providing mixing strength to the oil and solidifiers.

There are also in-situ oil burning and biodegradation methods in the OSRR techniques. In situ oil burning is

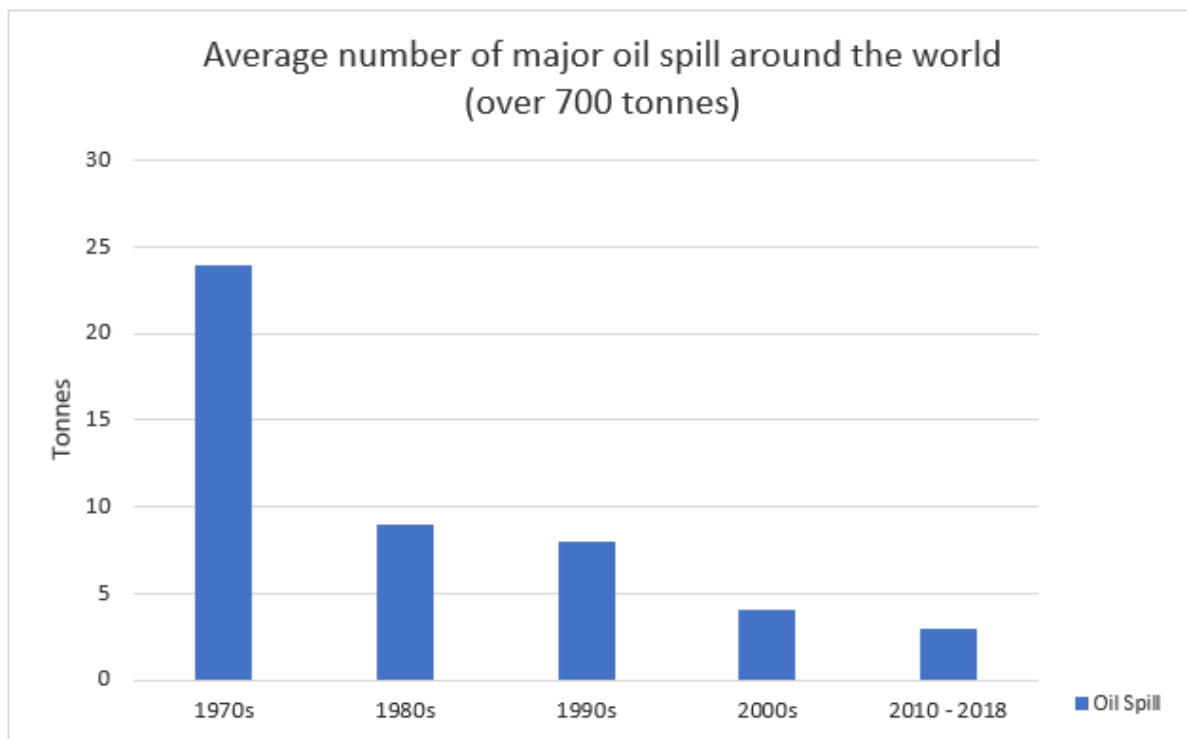


Fig. 1: The average number of significant oil spills around the world.



the most efficient process since, without any advanced equipment, the maximum concentrations of spilled oil can be eliminated. The critical drawback of burning is that it produces secondary emissions that create toxic by-products that can pose risks to human health and the environment. Furthermore, the goal of bioremediation is to promote the rate of natural biodegradation of oil without adversely affecting the atmosphere (Singh et al. 2020).

### Physical Methods

The physical and chemical characteristics of the oil remained unchanged despite the use of physical techniques to restrict and avoid the spread of the oil spill and oil slick. Many obstacles have been used to contain oil leaks, such as booms, skimmers, adsorbent fabrics, and oil slicks (Fingas 2016).

#### Boom

The boom was a standard system used to prevent oil spills and spreading slicks (Fritt-Rasmussen & Brandvik 2011). Nevertheless, the efficient operation of booms was impacted not only by the boom's structure but also by the characteristics of the waves, such as wind speed, amplitude, and height. They gather the oil in more significant layers to recover quickly and easily from the water's surface. They are effective safeguarding devices for the marine environment, rivers, and seas since they can readily reroute an oil spill's path to preserve delicate ecosystems (Pagnucco & Phillips 2018). Skimmers or other techniques aimed at removing impediments to oil flow could be employed to recover the oil spills and slick. Different kinds of booms such as fence and curtain booms were illustrated in Fig. 2 (Gong et al. 2014).

Unfortunately, because it directly violates the natural tendency of oil to scatter, break, and disperse under the influence of wind, waves, and tides, this method has a number of structural problems (ITOPF 2018). Therefore, even though

storage and extraction systems work within a few hours of the initial release, floating oil would appear to be encountered at a meager rate. The benefits of booms include being portable, limited storage space, corrosion resistance, immediate treatment, highly effective in calm waters (Hoang et al. 2018). In comparison, their key drawbacks were poor stability in the case of heavy winds and currents and low flexibility.

#### Skimmers

Skimmers are self-propelled machines that mechanically remove floating oils from the water surface (skimming). They are frequently employed in the physical recovery of oil spills and may be found in a range of equipment. They are commonly used in conjunction with booms and mainly consists of a reservoir tank for collection and settling of oil after removal (Fingas 2016). The major benefit of skimmers is that they can function in inclement weather and do not alter the oil's properties. The recovered oil might be refined or burned for further treatment. Skimmers shown in Fig. 3 might be classified as oleophilic skimmers, weir skimmers, elevating skimmers, submersion skimmers, suction/vacuum skimmers, and vortex/centrifugal skimmers (Kauble 2011).

#### Development of Oil Spill Skimmer

A boat-type oil skimmer has been innovated and researched to improve the oil skimmer in design and skimmer design requirements. The modification improves the oil skimmer design, including shaft size, sorbent material, oil scrapping design, scrapper placement speed, and scrapper material. Manivel & Sivakumar (2020) claimed that the efficiency of the new boat oil skimmer has slightly improved after the design modification.

A research was conducted to design and fabricate a belt-type oil skimmer. The belt-type oil skimmer is then tested for its efficiency by using various types of belt ma-



Fig. 2: The types of booms used to control the oil spill spread (Gong et al. 2014).

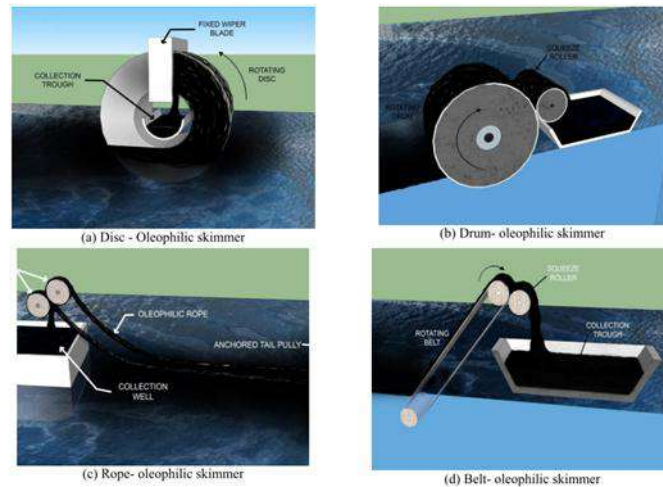


Fig. 3: Oleophilic Skimmers (Kuabile 2011).

terial. Patel (2013) concluded that belt-type oil skimmer significantly improved the oil recovery efficiency. The oleophilic belt was chosen as the best material to recover oil compared to steel, nylon, rubber, and polyurethane. However, Pawar et al. (2020) recommended polyurethane as the best material. Research by Widiaksana et al. (2018) analyzed the effectiveness of oil spill recovery using a disc-type oil skimmer. Based on the research done theoretically and experimentally, the increase in surface area of discs dipped in water increases the oil recovery significantly.

A more advanced oil skimmer was fabricated by Mathews et al. (2018), where a power source from solar was implemented. The oil skimmer robot has the ability to keep collecting oil for several weeks with the aid of a solar system with renewable energy. Recent research by Shirbhate et al. (2018) created an oil-skimming aqua robot to tackle the oil spill disaster. The robot helps to segregate the oil layer from the water and uses GPS to monitor the robot's location. Also, the ultrasonic sensor scans the level of oil collected in its storage.

All this fabrication and design research was done with minimal conscience of the user requirement of the Oil Spill Skimmer. It is due to difficulties for industrial engineers to analyze the user requirement. Only the aspects of technical requirements and designers'/researchers' opinions were considered while designing the oil spill skimmer. In conclusion, there is a need to consider user requirements and technical requirements to design and fabricate an Oil Spill Skimmer. The oil skimmer's maneuverability, however, was not specified as it is only stated that the oil skimmer could only float on water. There is no evidence of the oil

skimmer's maneuverability in the literature examined. A dynamic skimmer is a device that is either moved through the water or stationary, and the water and oil are moved by it (Pawar et al. 2020). Most skimmers are designed to be dynamic. As a result, an oil skimmer with portability and maneuverability attributes must be designed and manufactured.

### Multiple-Criteria Decision-Making (MCDM)

In manufacturing, there are several fundamental processes that need to be considered such as material selection, design development, performance analysis and after sales service. Concisely, the most crucial process that should not be ignored are design development and performance analysis. During design development stages, MCDM approach could be utilised (Renzi et al. 2017) whereas the precision functionality analysis could be used for performance evaluation (Abdullah et al. 2015). Due to the diverse and personalized functionality needed by end-users, decision-making in engineering design has drawn the interest of design engineers. The phases of the design process are affected by these personalized features. Many design criteria are now considered during concept exploration, model creation and selection, configuration design, and parametric design (Renzi et al. 2017). Multicriteria decision-making (MCDM) is a term for selecting the best option from a set of possibilities by weighing them against a set of parameters. When considering options, decision-makers should use multi-criteria decision-making approaches as scientific equipment. Researchers and engineers have suggested and implemented a variety of MCDA approaches to decision-making in engineering design. Choosing the right MCDA approach to

compare various options is crucial since different methods will generate different outcomes for the same problem (El Amine et al. 2014).

### **Application of MCDM**

#### ***Technique for Order of Preference by Similarity to Ideal Solution (TOPSIS)***

Anugraha et al. (2019) researched the best concept selection of dry-soybean machines using the TOPSIS method. The method successfully selected the best concept in which the defect rate is lowered to 6.5 percent, and the manual separating process is removed. Water consumption is reduced to 800 liters per 35,125 kg of tempe produced. A critical review done by El Amine et al. (2014) proved that TOPSIS was the approach that was more compliant with decision makers' preferences since the findings produced were very respectful of the decision makers' preferences after comparing several types of multi-criteria decision analysis (MCDA) by ranking alternatives. In the initial conceptual design phase for aircraft production, a method of assessing and selecting different alternative configurations based on devised standards using AHP, TOPSIS, and QDF was researched by Bae et al. (2017).

A hybrid Fuzzy TOPSIS and multi-objective particle swarm optimization (MOPSO) implementation of a multi-disciplinary product optimization was introduced by Renzi and Leali (2016) for solving issues related to the conceptual design of heel tips for women's shoes. In addition, unique parameters have been introduced within the MOPSO to improve solution precision and reduce the computational cost, such as the chaotic inertia weight. For the final selection method from the Pareto front, Jafaryeganah et al. (2020) conducted a comparative analysis using Weighted Sum, Weighted Product, TOPSIS, and ELECTRE for determining the evaluated rank of alternatives.

An article investigated seven widely used multi-criteria decision-making assisting approaches (weighed sum, weighted product, compromise programming, TOPSIS, quadratic mean, and ELECTRE I) (El Amine et al. 2016). Thus, the weighted product was determined to be the optimum multi-criteria decision-helping technique based on these criteria.

#### ***Analytical Network Process (ANP)***

A novel mixture of fuzzy decision-making trial and assessment laboratory (DEMATEL), undefined analytical network method (ANP), and fuzzy technique for order choice by similarity to ideal solution (TOPSIS) was used by Vinodh et al. (2016) in the analysis to improve the effectiveness of concept collection. Liu et al. (2021) published a paper to propose a realistic approach for dealing with pandemic circumstances through urban furniture design, utilizing an

integrated technique of Quality Function Deployment (QFD) and Analytic Network Process (ANP). The research focuses on the design selection of a product to select the best quality design of a wheelchair by using Analytic Network Process (ANP) as the decision-making method. Also, the Theory of Inventive Problem Solving (TRIZ) was used to solve several issues related to the market demand for wheelchairs (Hambali & Amira Farhana 2018).

The combination of the theory of innovative problem solving (TRIZ), morphological chart, and analytic network process (ANP) was used in the recent advanced design creation of a creep testing rig for a full-scale cross-arm (Sharaf et al. 2020). This technique is a rigorous concurrent engineering process for developing concepts, refining ideas, developing design methodologies, and selecting the best option. Asyraf et al. (2019) used similar hybridized approaches to create and choose the best design idea for product development based on product design criteria (PDS). By integrating the theory of innovative problem solving (TRIZ), morphological chart, and analytic network process (ANP) techniques, a study was conducted to analyze the framework of the conceptual design of a portable fire extinguisher constructed of carbon fiber-reinforced polymer composites. It displays the ability to generate ideas, create design methods, and choose the best design concept (Asyraf et al. 2020).

#### ***VlseKriterijumska Optimizacija I Kompromisno Resenje (VIKOR)***

In the presence of competing and non-commensurable (attributes of separate units) parameters, VIKOR is an MCDM approach that focuses on rating and choosing from a finite range of viable alternatives. It uses a multi-criteria rating index to determine how similar a solution is to the "ideal". Mardani et al. (2016) stated that as a consequence, the derived compromise solution is a realistic solution nearest to the positive ideal solution and the furthest from the negative ideal solution. A compromise is described as an agreement achieved by mutual compromises between the alternatives.

Research by Qi et al. (2020) identifies the best product idea that matches or exceeds most consumers' standards while still adhering to design requirements. In IR-VIKOR, customers' preferences for design attribute values, significance scores of design criteria, and features are integrated to find the best solutions for generating the rough evaluation index of each design alternative. Furthermore, in comparing the types of VIKOR methods, Chatterjee and Chakraborty (2016) found that fuzzy VIKOR is preferred to other VIKOR methods. Traditional VIKOR and fuzzy VIKOR and robust and updated VIKOR processes are found to behave similarly.

## Analytical Hierarchy Process (AHP)

The Analytical Hierarchy Method (AHP) is a decision-making tool developed by Saaty Thomas (1980) that aims to enhance the decision-making of engineers and researchers. In the analysis by Ayu Nariswari et al. (2019) in handling the stock of spare parts in the aircraft industry, the use of AHP can be seen. The findings indicate that AHP can lead to a highly informative, accurate, straightforward, rapid, and systematic classification model with an output comparable to traditional approaches. AHP has also been utilized by Du et al. (2020) to select the right remanufacturing of heavy-duty machine tools. The result indicates that the AHP classification model is more efficient and transparent than the current mathematical models.

Researchers have combined many approaches with AHP in their studies in recent years. (Diouf & Kwak 2018), for instance, incorporated Fuzzy Analytical Hierarchy Method (FAHP) and Data Envelopment Analysis (DEA) to rate and pick their company's best supplier. The research study found that other businesses facing similar challenges would adopt both the AHP and DEA systems. Also, Yazdi (2017) mentioned that the combination of fuzzy fault tree analysis (FFTA) and FAHP was added in a case study. The research aims to apply FAHP to improve the objectivity of experts' opinions and test them by FFTA for failure likelihood analysis.

AHP has also been used widely in ergonomics and has been reviewed by Abdul Aziz et al. (2018). The key aim of the study was to determine and verify the potential of work-related musculoskeletal disorders (WMSD) by using AHP to calculate the risk factor. In addition, the Technique for Order Preference by Similarity to Ideal Solution (TOPSIS) and AHP was paired with the aid of the Human Factor Analysis and Classification Scheme (HFACS) to classify human error causes in emergency departments (Hsieh et al. 2018). Besides, Nazim developed the AHP-SCOR Integrated Model (ASIM) to facilitate decision-making in the supply chain (Nazim & Yaacob 2017). They evaluated the best provider and picked it according to the parameters chosen.

Using the Analytical Hierarchy Process (AHP) system to analyze the development of a suitable wheelchair configuration, Ahmad et al. (2017) conducted research to improve the design of existing wheelchairs to reduce physical tiredness and promote older persons' independence or ability. A study by Liao and Chen (2018) suggested using the renowned benefits, opportunities, costs, and risks (BOCR) as an assessment factor and using the AHP decision model and sensitivity analysis to assess organizational results. Sensitivity analysis can determine the best solution to developing

criteria to understand the complicated relationships among competitive advantages.

## Advantages and Disadvantages of Multi-Criteria Decision-Making Method

According to Siksnylyte-Butkiene et al. (2020), the distinguished advantages and disadvantages of MCDM methods will help to establish which way is the most suitable for the assessment of design selection, technologies, and many more. Finding common MCDM approaches and characterizing their strengths and weaknesses is a crucial step in developing the research's framework. This process leads to a survey of users to ascertain which benefits and downsides are more prevalent for each methodology (Velasquez & Hester 2013). Table 1 shows the advantages and disadvantages of MCDM methods.

## Kansei Engineering

A literature review by Vieira et al. (2017) on Kansei Engineering (KE) claimed that it aims to define the feel-good aspect of the client in a product's design process. Ginting & Ali (2019) noted that the Kansei Engineering (KE) goals are to recognize human needs and preferences and provide mathematical and statistical attributes to relate technical requirements with responses. A comment in a study from Mele & Campana (2018) is that it is possible to create a successful interface between human and virtual design environments by integrating KE to incorporate both engineering specifications and consumer experience in product design. This technique is used to improve customer satisfaction by developing the product.

Hartono (2020) integrated the Kansei Engineering approach along with Kano and TRIZ in a study. By enhancing consumers' quality, imaginative ideas, and emotional satisfaction, the new approach was tested and effective. Also, the integration of KE with Kano and QFD can be seen in a study by Hartono et al. (2017) conducted to strengthen the computational structure of a logistics operation. The combined strategy effectively appreciates what can be understood and adopted by the service provider in optimizing the services offered while concentrating on prioritized options for limited capital. On top of that, in a surgical glove case report, Ginting & Ali, (2019) integrated KE and QFD. The study findings demonstrate that the integration of KE and QFD defines more acceptable technological goals for the technical characteristics used in the quality and quantity of a component.

The single semantic product of the CNC machine is difficult to express the shape features effectively, and therefore cannot effectively meet users' relatively vague semantic preferences. Thus, according to Chen et al. (2012), there is a need

Table 1: The advantages and disadvantages of the Multi-criteria Decision Making (MCDM) method.

Method	Advantages	Disadvantages	Source
AHP	<ul style="list-style-type: none"> <li>• One of the most often employed techniques and often combined with others. As compared to other MCDM systems, this approach is faster.</li> <li>• The approach has a comprehensible logic that is commonly used to answer energy policy/project selection questions, and it is also widely used for technology assessment and location selection.</li> <li>• In comparison to other approaches, the computing method is elementary.</li> <li>• Since the approach is based on a hierarchical system, it focuses more on each analysis parameter.</li> </ul>	<ul style="list-style-type: none"> <li>• Additional research is needed to confirm the findings, and different parameter hierarchies can affect the weight allocation differences.</li> <li>• When it comes to assigning weights, the more engineers involved, the more complicated the issue gets.</li> <li>• Interdependence among alternatives and goals may contribute to an erroneous outcome.</li> </ul>	(Kaya et al. 2018, Kumar et al. 2017, Siksnylyte et al. 2018, 2020)
TOP-SIS	<ul style="list-style-type: none"> <li>• TOPSIS is a very simple to compute and algorithmically organized approach that significantly simplifies implementing it.</li> <li>• The principle is represented in a straightforward mathematical structure that has logical and understandable logic.</li> <li>• Because of its simplicity, it is one of the most widely used MCDM techniques</li> <li>• In terms of the idea of being separated from optimal systems, it has a genuinely instinctive physical significance.</li> </ul>	<ul style="list-style-type: none"> <li>• TOPSIS, in its standard form, is deterministic and ignores ambiguity in weightings, making it easy to use but potentially unstable.</li> <li>• This approach is suitable for a challenge with a single source of information only.</li> <li>• It functions mainly on the principle of Euclidian distance and thereby ignores the distinction between negative and positive factors.</li> </ul>	(Abdulgader et al. 2018, Jato-Espino et al. 2014, Kumar 2018, Siksnylyte et al. 2018)
VIKOR	<ul style="list-style-type: none"> <li>• Removes the effect by calculating the combination between positive and negative ideal solutions.</li> <li>• In the measurement phase, the approach accepts the value variations.</li> <li>• adapted to respond to a variety of energy issues</li> </ul>	<ul style="list-style-type: none"> <li>• When a conflicting issue happens, it may be challenging to be dealt with.</li> <li>• When working with different types of data, modifications are needed because modeling a real-time model becomes difficult.</li> </ul>	(Gul et al. 2016, Liao et al. 2014, Liu et al. 2014, Siksnylyte et al. 2018)
ANP	<ul style="list-style-type: none"> <li>• The ANP method considers the feedback relationship and between model stages and the interconnections among components.</li> <li>• It shows how the criteria in the objectives or higher-level success criterion are interdependent and affect each other.</li> </ul>	<ul style="list-style-type: none"> <li>• A complicated mathematical process</li> <li>• In ANP, multiple pairwise comparison matrices are needed more than in AHP.</li> <li>• It can't be judged solely based on one aspect.</li> <li>• It is more time-intensive and more complex than the AHP.</li> </ul>	(Chou 2018, Jato-Espino et al. 2014, Wu et al. 2018, 2019)

to build a combination of product semantics corresponding to user semantics preferences and obtain the product features corresponding to this combination of semantics. Thus the Kansei Engineering approach is introduced. Kansei Engineering technology discusses how to transfer consumers' imagined feelings towards a product into the technology of its design elements to communicate product aesthetics concepts and images through the scientific analysis method. Also, it can be applied to almost all industrial design fields, including the design of heavy machines such as CNC machine tools (Chen et al. 2017).

Furthermore, until recently, the emotional aspects of machine tool design were overlooked. With the advancement in the industrial design of machine tools, it is essential to statistically and adequately comprehend the users' emotional expectations; thus, Kansei Engineering is implemented (Liu et al. 2013). Mental concepts of users are often challenging to identify and, consequently, a satisfactory product is difficult to design (Huang et al. 2012). In particular, designing injection molding machines (IMMs) often lacks user feedback and relies heavily on manufacturers' technical specifications and

imaginary targets. Technical specifications are frequently used to make decisions on which machine to buy or use. Although these technological characteristics can be assessed, critical machine needs, such as simplicity of use, safety, and robustness, are challenging to quantify and compare. As a result, Mondragón et al. (2005) use Kansei Engineering to demonstrate how the technique may measure the perception of those aspects.

**Combination of AHP and Kansei Engineering**

In recent years, researchers have thoroughly researched the adaptation of KE and AHP. The priority of emotional architecture in KE was studied by integrating the AHP process (Syaifoelida et al. 2018). In the user requirement aspect, the design of the car center stack was analyzed based on their emotional feelings, and the produced designs were evaluated using AHP to choose the best design. Besides, AHP and Kansei were used to investigate the interface architecture of electric cars (Wu & Kang 2020). Meanwhile, Impfo et al. (2018) constructed a drinking water filtering system using AHP, KE, QFD, and TRIZ. KE was combined with QFD to

achieve consumer specifications, whereas TRIZ was used to solve issues around technological requirements.

In deciding the technique for selecting the right music school, AHP and KE were also included. When used to create selection programs and evaluation frameworks for choosing music colleges, the variants of the Nagai method (5W1H), AHP, ISM, and GRA were tested (Sheu et al. 2016). Interface modeling using KE and AHP for mobile learning has been researched (Hadiana 2017). As a result, a mobile learning system interface prototype based on an emotionally dynamic and easy concept was launched to have a high effect on the interface and increase the accessibility of the mobile learning system. AHP and KE were introduced in the design of Jun Porcelain to reinvent the graphic style and improve the tradition (Chai et al. 2016). In promoting the business process in an organization, the application of a helpdesk plays a significant role. Therefore, Hadiana & Abdurrohman, (2018) analyzed clients' desires in terms of emotions using KE and AHP to optimize the new helpdesk framework. A research was conducted by Huda & Hadiana, (2020) to study consumer emotions against the existing helpdesk framework. The best alternative recommendations were selected using AHP to enhance the current helpdesks with the affected parameters.

Environmentally focused technologies such as oil spill skimmers have been created chiefly only through the efforts of engineers, as so few to none emerge from the skimmers' potential consumers. As customer perceptions of oil spill skimmers can shift from time to time, it is important to adjust this design technique, creating the need to integrate consumers into the design process. Kansei Engineering and Analytical Hierarchy Process (AHP) are the two commonly used techniques for integrating user requirements into engineering architecture. Nevertheless, in the design and development of technologies relating to products for environmental protection, the AHP, and Kansei Engineering strategy is somewhat lacking. The AHP and Kansei Engineering methodology can be extended to the design and manufacture of products for environmental protection.

## CONCLUSION

In conclusion, the fabrication of a portable oil spill skimmer lacks the involvement of user requirements. An oil spill is a disaster that could harm the environment and the ecosystem. Although there are several techniques to overcome the tragedy, the mechanical methods themselves have some limitations. Due to its limitation, a portable oil spill skimmer is a complementary technique that helps the boom and skimmer technique collect the oil residue. Thus, it eliminates the reset-up boom and skimmer, which consumes a lot of workforce and cost.

The development of conceptual designs starts with implementing the Kansei Engineering method to analyze the user requirement and technical specifications through human emotion and feelings. AHP has also grown in popularity as a tool for organizing, analyzing, and modeling complicated choices. As a result, AHP is used to pick the most refined Kansei Engineering-developed conceptual design. This article sought to explore Kansei Engineering and AHP's use in product design development to understand Kansei Engineering and decision issues that AHP might effectively address. The paper's goals were to summarise current literature on Kansei Engineering and AHP applications in the design development process and determine user and technical requirements using Kansei Engineering and choose the optimum conceptual design using AHP.

The study indicates that the fabrication of an oil skimmer was more concerned with technical specifications than with customer requirements. As a result, technical requirements cannot be directly compared to robustness, safety, or ease of use. Kansei Engineering can therefore be used to assess the robustness, safety, and ease of use of the system. There was also no argument or evidence that the oil spill skimmer could be maneuvered. The findings from the articles also show that there is a limitation in the design and development of technologies related to environmental protection goods and the AHP and Kansei Engineering applications.

## REFERENCES

- Abdul Aziz, F., Ghazali, Z., Mohd Jamil, M. J., Romli, A. and Nik Mohamed, N. M. Z. 2018. A Knowledge-Based Ergonomics Assessment System for WMSD prevention using AHP Methodology. Pleiades Publishing, Russia, pp. 161-173. [https://doi.org/10.1007/978-981-10-8788-2\\_16](https://doi.org/10.1007/978-981-10-8788-2_16)
- Abdulgader, F.S., Eid, R. and Rouyendegh, B.D. 2018. Development of decision support model for selecting a maintenance plan using a fuzzy MCDM approach: A theoretical framework. *Appl. Comput. Intell. Soft Comput.*, 2: 18. <https://doi.org/10.1155/2018/9346945>
- Abdullah, L., Jamaludin, Z., Maslan, M. N., Jamaludin, J., Halim, I., Rafan, N. A. and Chiew, T. H. 2015. Assessment on tracking performance of Cascade P/PI, NPID and NCasFF controller for precise positioning of XY table ballscrew drive system. *Procedia CIRP*, 26: 212–216. <https://doi.org/10.1016/J.PROCIR.2014.07.111>
- Ahmad, M.N., Maidin, N.A., Rahman, M.H.A. and Osman, M.H. 2017. Conceptual design selection of manual wheelchair for elderly by analytical hierarchy process (AHP) method: A case study. *Int. J. Appl. Eng. Res.*, 12(17): 6710-6719. <https://doi.org/10.1111/J.09739769>
- Almeda, R., Hyatt, C. and Buskey, E. J. 2014. Toxicity of dispersant Corexit 9500A and crude oil to marine microzooplankton. *Ecotoxicol. Environ. Saf.*, 106: 76–85. <https://doi.org/10.1016/j.ecoenv.2014.04.028>
- Anugraha, R.A., Darmawan, N.M. and Iqbal, M. 2019. Best concept selection for dry-soybean cracking machine process optimization using the TOPSIS method. *IOP Conf. Ser. Mater. Sci. Eng.*, 528(1): 2005. <https://doi.org/10.1088/1757-899X/528/1/012005>
- Asyraf, M. R. M., Ishak, M. R., Sapuan, S. M. and Yidris, N. 2019. Conceptual design of creep testing rig for full-scale cross arm using TRIZ-Morphological chart-analytic network process technique. *J. Mater. Res. Technol.*, 8(6): 5647-5658. <https://doi.org/10.1016/j.jmrt.2019.09.033>

- Asyraf, M.R.M., Rafidah, M., Ishak, M.R., Sapuan, S.M., Yidris, N., Ilyas, R.A. and Razman, M.R. 2020. Integration of TRIZ, morphological chart, and ANP method for the development of FRP composite portable fire extinguisher. *Polym. Compos.*, 41(7): 2917-2932. <https://doi.org/10.1002/pc.25587>
- Ayu Nariswari, N.P., Bamford, D. and Dehe, B. 2019. Testing an AHP model for aircraft spare parts. *Prod. Plan. Contr.*, 30(4):, 329-344. <https://doi.org/10.1080/09537287.2018.1555341>
- Bae, B.Y., Kim, S., Lee, J.W., van Nguyen, N. and Chung, B. C. 2017. Process of establishing design requirements and selecting alternative configurations for conceptual design of a VLA. *Chinese J. Aeronaut.*, 30(2), 738-751. <https://doi.org/10.1016/j.cja.2017.02.018>
- Bovio, E., Gnani, G., Prigione, V., Spina, F., Denaro, R., Yakimov, M., Calogero, R., Crisafi, F. and Varese, G. C. 2017. The culturable mycobiota of a Mediterranean marine site after an oil spill: Isolation, identification and potential application in bioremediation. *Sci. Total Environ.*, 576, 310-318. <https://doi.org/10.1016/j.scitotenv.2016.10.064>
- Chai, C., Li, D. and Bian, M. 2016. Research on Innovative Design of Jun Porcelain Culture Based on Kansei Features. *Proceedings - 2016 9th International Symposium on Computational Intelligence and Design, ISCID 2016*, 1, pp. 50-53. <https://doi.org/10.1109/ISCID.2016.1020>
- Chatterjee, P. and Chakraborty, S. 2016. A comparative analysis of the VIKOR method and its variants. *Decis. Sci. Lett.*, 5(4): 469-486. <https://doi.org/10.5267/j.dsl.2016.5.004>
- Chen, B., Tang, S., Pan, Z., Zhang, J. and Guo, D. 2012. Research on Kansei image in Kansei-based design system for CNC machine tools. *Proceedings - 4th International Conference on Computational and Information Sciences, ICCIS 2012*, 1220-1223. <https://doi.org/10.1109/ICCIS.2012.247>
- Chen, H.Y., Tu, J.C. and Wang, K.C. 2017. Research into the application of Kansei engineering to the modeling aesthetic design of a numerical control machine tool. *Int. J. Affect. Eng.*, 16(3): 191-202. <https://doi.org/10.5057/ijae.ijae-d-16-00042>
- Chou, C. 2018. Application of ANP to the selection of shipping registry: The case of Taiwanese maritime industry. *Int. J. Ind. Ergon.*, 67: 89-97. <https://doi.org/10.1016/j.ergon.2018.04.009>
- Diouf, M. and Kwak, C. 2018. Fuzzy AHP, DEA, and managerial analysis for supplier selection and development; From the perspective of open innovation. *Sustainability (Switzerland)*, 10(10): <https://doi.org/10.3390/su10103779>
- Du, Y., Zheng, Y., Wu, G. and Tang, Y. 2020. Decision-making method of heavy-duty machine tool remanufacturing based on AHP-entropy weight and extension theory. *J. Clean. Prod.*, 252: 119607. <https://doi.org/10.1016/j.jclepro.2019.119607>
- Ekperusi, A.O., Onyena, A.P., Akpudo, M.Y., Peter, C.C., Akpoduado, C.O. and Ekperusi, O.H. 2019. In-Situ Burning As An Oil Spill Control Measure and Its Effect on the Environment. *Society Of Petroleum Engineers - SPE Nigeria Annual International Conference and Exhibition 2019, NAIC 2019*. <https://doi.org/10.2118/198777-MS>
- El Amine, M., Pailhes, J. and Perry, N. 2014. A critical review of multi-criteria decision aid methods in conceptual design phases: Application to the development of a solar collector structure. *Procedia CIRP*, 21: 497-502. <https://doi.org/10.1016/j.procir.2014.03.134>
- El Amine, M., Pailhès, J. and Perry, N. 2016. Selection and use of a multi-criteria decision aiding method in the context of conceptual design with imprecise information: Application to a solar collector development. *Concurr. Eng. Res. Appl.*, 24(1): 35-47. <https://doi.org/10.1177/1063293X15613838>
- Fingas, M. 2013. *Review of Solidifiers : An Update 2013*. Spill Science. Springer, NY
- Fingas, M. 2016. *Oil Spill Science and Technology: Second Edition*. Springer, NY
- Fritt-Rasmussen, J. and Brandvik, P. J. 2011. Measuring ignitability for in situ burning of oil spills weathered under Arctic conditions: From laboratory studies to large-scale field experiments. *Mar. Pollut. Bull.*, 62(8): 1780-1785. <https://doi.org/10.1016/j.marpollbul.2011.05.020>
- Ginting, R. and Ali, A.Y. 2019. Improved Kansei Engineering with Quality Function Deployment Integration: A Comparative Case Study. *IOP Conf. Ser.: Mater. Sci. Eng.*, 505(1): 2092. <https://doi.org/10.1088/1757-899X/505/1/012092>
- Gong, Y., Zhao, X., Cai, Z., O'Reilly, S. E., Hao, X. and Zhao, D. 2014. A review of oil, dispersed oil and sediment interactions in the aquatic environment: Influence on the fate, transport, and remediation of oil spills. *Mar. Pollut. Bull.*, 79(1-2): 16-33. <https://doi.org/10.1016/j.marpollbul.2013.12.024>
- Gul, M., Celik, E., Aydin, N., Taskin Gumus, A. and Guneri, A. F. 2016. A state-of-the-art literature review of VIKOR and its fuzzy extensions on applications. *Appl. Soft Comput.*, 46: 60-89. <https://doi.org/10.1016/j.asoc.2016.04.040>
- Hadiana, A. 2017. Interface modeling for mobile learning using Kansei engineering and analytical hierarchy process. *Proceedings - 2017 International Conference on Computer, Control, Informatics, and Its Applications: Emerging Trends in Computational Science and Engineering, IC3INA 2017, 2018-Janua*, pp. 153-157. <https://doi.org/10.1109/IC3INA.2017.8251758>
- Hadiana, A. and Abdurrohman. 2018. Analysis of Customers' Emotional Preferences Using Kansei Engineering and AHP. *Proceedings - 2018 4th International Conference on Science and Technology, ICST 2018*, 1, pp. 1-5. <https://doi.org/10.1109/ICSTC.2018.8528675>
- Hambali, A. and Amira Farhana, M. T. 2018. Development of integrated analytic network process (ANP) and theory of inventive problem solving (Triz) in the conceptual design selection. *J. Eng. Sci. Technol. Rev.*, 13(9): 2716-2733.
- Hartono, M. 2020. The modified Kansei Engineering-based application for sustainable service design. *Int. J. Ind. Ergon.*, 79: 102985. <https://doi.org/10.1016/j.ergon.2020.102985>
- Hartono, M., Santoso, A. and Prayogo, D. N. 2017. How Kansei Engineering, Kano, and QFD can improve logistics services. *Int. J. Technol.*, 8(6): 1070-1081. <https://doi.org/10.14716/ijtech.v8i6.689>
- Hoang, P.H., Hoang, A.T., Chung, N.H., Dien, L.Q., Nguyen, X.P. and Pham, X.D. 2018. The efficient lignocellulose-based sorbent for oil spill treatment from polyurethane and agricultural residue of Vietnam. *Energy Sour. Part A: Recov. Utilis. Environ. Effects*, 14: 153. <https://doi.org/10.1080/15567036.2017.1415397>
- Hsieh, M., Wang, E.M., Lee, W., Li, L.W., Hsieh, C.Y, Tsai, W., Wang, C.P., Huang, J.L. and Liu, T.C. 2018. Application of HFACS, fuzzy TOPSIS, and AHP for identifying important human error factors in emergency departments in Taiwan. *International Int. J. Ind. Ergon.*, 67: 171-179. <https://doi.org/10.1016/j.ergon.2018.05.004>
- Huang, M.S., Tsai, H.C. and Lai, W.W. 2012. Kansei engineering applied to the form design of injection molding machines. *Open J. Appl. Sci.*, 02(03): 198-208. <https://doi.org/10.4236/ojapps.2012.23030>
- Huda, C.N. and Hadiana, A. 2020. Kansei Analysis using Analytical Hierarchy Process. *Proceedings of the International Conference on Business, Economic, Social Science, and Humanities – Economics, Business and Management Track (ICOBEST-EBM 2019)*, pp. 218-223. <https://doi.org/10.2991/aebmr.k.200108.050>
- Impho, W., Poonikom, K., Pannucharoenwong, N. and Echaroj, S. 2018. Application of the Integrated QFD technique in the Design of an Innovative Machine for Cleaning the Drinking Water Tank. *International Journal of Applied Engineering Research ISSN*, 13(2), 973-4562. <http://www.ripublication.com>
- ITOPF. 2018. *Promoting Effective Spill Response*. [http://www.itopf.com/fileadmin/data/Documents/Company\\_Lit/ITOPF\\_Handbook\\_2018.pdf](http://www.itopf.com/fileadmin/data/Documents/Company_Lit/ITOPF_Handbook_2018.pdf)
- Jafaryeganeh, H., Ventura, M. and Guedes Soares, C. 2020. Application of multi-criteria decision-making methods for selection of ship internal layout design from a Pareto optimal set. *Ocean Eng.*, 202(10): 107151. <https://doi.org/10.1016/j.oceaneng.2020.107151>

- Jato-Espino, D., Castillo-Lopez, E., Rodriguez-Hernandez, J. and Cante-ras-Jordana, J.C. 2014. A review of the application of multi-criteria decision-making methods in construction. *Autom. Constr.*, 45: 151-162. <https://doi.org/10.1016/j.autcon.2014.05.013>
- Kauble, C.A. 2011. Oil spill clean-up. science activities. *Class. Proj. Curriculum ideas*, 48(1), 9-12. <https://doi.org/10.1080/00368121.2010.504973>
- Kaya, ., Çolak, M. and Terzi, F. 2018. Use of MCDM techniques for energy policy and decision-making problems: A review. *Int. J. Energy Res.*, 42(7): 2344-2372. <https://doi.org/10.1002/er.4016>
- Kumar, A., Sah, B., Singh, A.R., Deng, Y., He, X., Kumar, P. and Bansal, R.C. 2017. A review of multi-criteria decision making (MCDM) towards sustainable renewable energy development. *Renew. Sustain. Energy Rev.*, 69(6): 596-609. <https://doi.org/10.1016/j.rser.2016.11.191>
- Kumar, G. 2018. A survey on multi-criteria decision-making recommendation system using sentiment analysis. *nt. J. Appl. Eng. Res.*, 13(15): 11724-11729. <http://www.ripublication.com>
- Liao, C.C. and Chen, C.C. 2018. Evaluating the performance of collaborative design systems using ANP sensitivity analysis. *Proceedings - 2018 33rd Youth Academic Annual Conference of Chinese Association of Automation, YAC 2018*, pp. 505-509. <https://doi.org/10.1109/YAC.2018.8406427>
- Liao, H., Xu, Z., Member, S. and Zeng, X.J. 2014. Hesitant fuzzy linguistic VIKOR method and its application in qualitative multiple criteria decision making. *IEEE. Trans. Fuzzy Sys.*, 23(5): 1343-1355
- Liu, H.C., You, J.X., Fan, X.J. and Chen, Y.Z. 2014. Site selection in waste management by the VIKOR method using linguistic assessment. *Applied Soft Computing Journal*, 21: 453-461. <https://doi.org/10.1016/j.asoc.2014.04.004>
- Liu, J., Kamarudin, K.M., Liu, Y. and Zou, J. 2021. Developing pandemic prevention and control by anp-qfd approach: A case study on urban furniture design in china communities. *Int. J. Environ. Res. Public Health.*, 18(5): 1-26. <https://doi.org/10.3390/ijerph18052653>
- Liu, X., Lei, T., Chen, T.J. and Wei, S.L. 2013. A study on the industrial design of machine tools based on the Kansei engineering methods. *Appl. Mech. Mater.*, 437: 914-917. <https://doi.org/10.4028/www.scientific.net/AMM.437.914>
- Manivel, R. and Sivakumar, R. 2020. Boat-type oil recovery skimmer. *Mater. Today Proceed.*, 21: 470-473. <https://doi.org/10.1016/j.matpr.2019.06.632>
- Mardani, A., Zavadskas, E., Govindan, K., Amat Senin, A. and Jusoh, A. 2016. VIKOR Technique: A Systematic Review of the State of the Art Literature on Methodologies and Applications. *Sustainability*, 8(1): 37. <https://doi.org/10.3390/su8010037>
- Mathews, N.J., Varghese, T.K., Zachariah, P. and Chirathalattu, N.A. 2018. Fabrication of solar-powered oil skimmer robot. *Int. Res. J. Eng. Technol.*, 5: 88-90.
- Mele, M. and Campana, G. 2018. Prediction of Kansei engineering features for bottle design by a Knowledge-Based System. *International Journal on Interactive Design and Manufacturing*, 12(4): 1201-1210. <https://doi.org/10.1007/s12008-018-0485-5>
- Michel, J. and Fingas, M. 2016. Oil spills: Causes, consequences, prevention, and countermeasures. In *Fossil Fuels: Current Status and Future Directions* (pp. 159-201). World Scientific Publishing Co. Pte. Ltd. [https://doi.org/10.1142/9789814699983\\_0007](https://doi.org/10.1142/9789814699983_0007)
- Mirajkar, A., Shinde, T., Saini, R., Nikam, V. and Verma, P. 2019. A Review Paper on Oil Spill Recovery System. *International Research Journal of Engineering and Technology*, 875: 875-878. [www.irjet.net](http://www.irjet.net)
- Mondragón, S., Company, P. and Vergara, M. 2005. Semantic Differential applied to the evaluation of machine tool design. *Int. J. Ind. Ergon.*, 35(11): 1021-1029. <https://doi.org/10.1016/j.ergon.2005.05.001>
- Muizis, A. 2013. Evaluation of the Methods for the Oil Spill Response in the Offshore Arctic Region. Bachelor Thesis, Helsinki Metropolia University of Applied Sciences, Finland, pp. 1-59.
- Nazim, R. and Yaacob, R.A.I.R. 2017. Criteria for supplier selection: An application of the AHP-SCOR integrated model (ASIM). *Int. J. Supply Chain Manag.*, 6(3): 284-290.
- Pagnucco, R. and Phillips, M.L. 2018. Comparative effectiveness of natural by-products and synthetic sorbents in oil spill booms. *J. Environ. Manage.*, 225: 10-16. <https://doi.org/10.1016/j.jenvman.2018.07.094>
- Patel, M. 2013. Design and efficiency comparison of various belt-type oil skimmers. *Int. J. Sci. Res.*, 4: 2-7.
- Pawar, S.H., Amit Kumar, S., Vishu, A., Yashodhan, P. and Mayuresh, P. 2020. Design and fabrication of oil collector. *Int. J. Prog. Res. Sci. Eng.*, 1: 11.
- Qi, J., Hu, J. and Peng, Y.H. 2020. Integrated rough VIKOR for customer-involved design concept evaluation combining with customers' preferences and designers' perceptions. *Adv. Eng. Inform.*, 46: 138. <https://doi.org/10.1016/j.aei.2020.101138>
- Renzi, C. and Leali, F. 2016. A multicriteria decision-making application to the conceptual design of mechanical components. *J. Multi-Criteria Decis. Anal.*, 23(3-4): 87-111. <https://doi.org/10.1002/mcda.1569>
- Renzi, C., Leali, F. and di Angelo, L. 2017. A review on decision-making methods in engineering design for the automotive industry. *Journal of Engineering Design*, 28(2): 118-143. <https://doi.org/10.1080/09544828.2016.1274720>
- Saaty Thomas, A.H. 1980. *The Analytical Hierarchy Process*.pdf. Priority Setting, Resource Allocation, MacGraw-Hill, New York International Book Company. <https://doi.org/10.1002/jqs.593>
- Sharaf, H.K., Ishak, M.R., Sapuan, S.M. and Yidris, N. 2020. Conceptual design of the cross-arm for the application in the transmission towers by using TRIZ–morphological chart–ANP methods. *J. Mater. Res. Technol.*, 9(4): 9182-9188. <https://doi.org/10.1016/j.jmrt.2020.05.129>
- Sheu, T., Chen, C., Hsu, J. and Masatake, N. 2016. The study on the strategies of choosing music schools from the viewpoint of Kansei engineering. *Themes Sci. Technol. Edu.*, 1: 45-49.
- Siksnyte, I., Zavadskas, E.K., Streimikiene, D. and Sharma, D. 2018. An overview of multi-criteria decision-making methods in dealing with sustainable energy development issues. *Energies*, 11(10): 754. <https://doi.org/10.3390/en1102754>
- Siksnyte-Butkiene, I., Zavadskas, E.K. and Streimikiene, D. 2020. Multi-criteria decision-making (MCDM) for the assessment of renewable energy technologies in a household: A review. *Energies*, 13(5). <https://doi.org/10.3390/en13051164>
- Singh, B., Bhardwaj, N., Arya, S. K. and Khatri, M. 2020. Environmental impacts of oil spills and their remediation by magnetic nanomaterials. *Environ. Nanotechnol. Monit. Manag.*, 14(119): 100305. <https://doi.org/10.1016/j.enmm.2020.100305>
- Syaifoelida, F., Hamdan, M. A. M. M., Eqwan, M. R. and Nazmi, I. 2018. An analysis to determine the priority emotional design in Kansei engineering by using the AHP approach in product development. *Int. J. Eng. Manag.*, 8(6): 151-156. <https://doi.org/10.31033/ijemr.8.6.14>
- Tuan Hoang, A., Viet Pham, V. and Nam Nguyen, D. 2018. A report of oil spill recovery technologies. *Int. J. Appl. Eng. Res.*, 13(7): 4915-4928. <http://www.ripublication.com>
- Velasquez, M. and Hester, P. 2013. An analysis of multi-criteria decision making methods. *Int. J. Oper. Res.*, 10(2): 56-66.
- Vieira, J., Osório, J.M.A., Mouta, S., Delgado, P., Portinha, A., Meireles, J.F. and Santos, J.A. 2017. Kansei engineering as a tool for the design of in-vehicle rubber keypads. *Appl. Ergo.*, 61: 1-11. <https://doi.org/10.1016/j.apergo.2016.12.019>
- Vinodh, S., Sai Balagi, T. S. and Patil, A. 2016. A hybrid MCDM approach for agile concept selection using fuzzy DEMATEL, fuzzy ANP and fuzzy TOPSIS. *J. Adv. Manuf. Technol.*, 83(9-12): 1979-1987. <https://doi.org/10.1007/s00170-015-7718-6>
- Widiaksana, N., Yudiana, A. A. and Nugroho, Y. S. 2018. Analysis of the effectiveness of oil spill recovery using disc-type oil skimmer at labo-



- ratory scale. *IOP Conf. Ser.: Earth Environ. Sci.*, 105(1): 2086. <https://doi.org/10.1088/1755-1315/105/1/012086>
- Wu, Y. and Kang, X. 2020. Establishment of an aggregation model associated with instrument interface design based on Kansei factors of electric vehicle drivers. *Math. Probl. Eng.*, 20: 620-641. <https://doi.org/10.1155/2020/8315641>
- Wu, Y., Zhang, B., Wu, C. Zhang, T. and Liu, F. 2019. Optimal site selection for parabolic trough concentrating solar power plant using extended PROMETHEE method: A case in China. *Renew. Energy*, 143: 1910-1927. <https://doi.org/10.1016/j.renene.2019.05.131>
- Wu, Y., Zhang, B., Xu, C. and Li, L. 2018. Site selection decision framework using fuzzy ANP-VIKOR for large commercial rooftop PV system based on sustainability perspective. *Sustain. Cities Soc.*, 40: 454-470. <https://doi.org/10.1016/j.scs.2018.04.024>
- Yazdi, M. 2017. Hybrid probabilistic risk assessment using fuzzy FTA and Fuzzy AHP in a process industry. *J. Fail. Anal. Prev.*, 17(4): 756-764. <https://doi.org/10.1007/s11668-017-0305-4>
- Zhang, B., Matchinski, E.J., Chen, B., Ye, X., Jing, L. and Lee, K. 2018. Marine oil spills-oil pollution, sources, and effects. In Sheppard, C. (ed), *World Seas: An Environmental Evaluation Volume III: Ecological Issues and Environmental Impacts*, Second Edition, Elsevier Ltd, Netherlands, pp. 391-406. <https://doi.org/10.1016/B978-0-12-805052-1.00024-3>





# A Review on Microalgae Biofuel Production and use in CI Engine Applications

S. R. Hariprakash and T. Prakash†

Department of Automobile Engineering, College of Engineering and Technology, SRM Institute of Science and Technology, Kattankulathur, Kancheepuram 603203, Tamil Nadu, India

†Corresponding author: T. Prakash; prakasht@srmist.edu.in

Nat. Env. & Poll. Tech.  
Website: [www.neptjournal.com](http://www.neptjournal.com)

Received: 10-11-2021

Revised: 18-12-2021

Accepted: 11-02-2022

## Key Words:

Algae cultivation  
Harvesting  
Drying  
Transesterification  
CI Engine  
Engine emissions

## ABSTRACT

Alternative fuel technology of third-generation biofuels in place of conventional fossil fuels is currently being witnessed at a global level. Due to its sustainability and environmental friendliness, in recent years more importance is being given to biodiesel in CI engine applications. Recent trends show that microalgae are promoted as a bio-fuel due to their inherent advantages of abundant availability of oil sources and faster growth rate with ease of cultivation. Particular species of algae such as *Chlorella*, *Botryococcus braunii*, and *Scenedesmus obliquus* are conventionally favored for biodiesel production as they have a prominent amount of lipids content. This review outlines the current state of experimental investigations on the use of different algae biodiesel blends with diesel for CI engines. Amongst the different algae-based biodiesel, the dual *Calophyllum Inophyllum* methyl ester blend (CIME20) with DEE demonstrated the maximum brake thermal efficiency (BTE) and better brake-specific fuel consumption (BSFC) of CI engines. In terms of emissions, the CO, UBHC, and smoke levels are significantly lower for algae blends in contrast to neat diesel.

## INTRODUCTION

Economic growth and development increase the energy demand. Recently global energy requirements are met by fast-depleting fossil fuels. Alternative fuels are particularly important to the transport sector as they address the problems of high demand rates and increasing costs. Furthermore, these fossil fuels emit a huge amount of hazardous substances into the atmosphere contaminating the fragile environment (Enamala et al. 2018). The use of renewable and sustainable energy sources of biofuels for energy production came into existence as a better replacement for conventional fossil fuels. Emissions from vehicles have increased drastically over the past decades (Baral et al. 2015). To achieve environmental and economic sustainability, fuel production must be renewable and capable of reducing CO<sub>2</sub>. In these circumstances, microalgae play a vital role in suppressing atmospheric CO<sub>2</sub> to O<sub>2</sub>, the primary contributor to global warming and other greenhouse gases (Saratale et al. 2017). Gaseous fuels, biodiesel, and alcohol-based fuels are the most common alternative fuels for IC engines. Most biofuels fall into one of three categories, namely I<sup>st</sup>, II<sup>nd</sup> and III<sup>rd</sup> generation biofuels.

## DIFFERENT GENERATIONS OF BIOFUELS

Fig. 1 shows various biodiesel feedstock classified by their generations. Land-based food crops produce first-generation

biofuels from cultivated crops known as wheat, barley, corn, and sugarcane produces bioethanol or butanol by fermentation of starch. Transesterification of feedstock like rapeseed, sunflower, palm, castor, and cooking oil (Prakash et al. 2018, Jeyakumar & Narayanasamy 2019) produces biodiesel. Second-generation fuels employ ligno cellulosic non-food biomass such as Jatropha, Mahua, Neem, Karanja, *Aegle marmelos*, Methyl ester from the tannery industry, Safflower, Mesua ferrea, and Rice husk in biodiesel production (Balasubramanian & Purushothaman 2019, Siluvaimuthu et al. 2019, Thiyagarajan et al. 2016, Dhananmurugan & Subramanian 2015, Singh et al. 2015, Kanthasamy et al. 2020, Vinukumar et al. 2017). I<sup>st</sup> and II<sup>nd</sup> generation biofuels with fossil fuels gaining research attention due to their significant benefits. Additionally, soybean, jatropha, canola, corn, and animal fats are being tested as fuels (Xin et al. 2011). Generations of such biofuels require an abundant amount of water and agricultural land for crop cultivation and biofuel production. Third-generation biofuel feedstock like algae, overcome these drawbacks as it does not interact with the food environment. However, the yield of algae biofuel necessarily stepped up to meet the higher demand.

## MICROALGAE AS BIOFUEL

Microalgae utilize sunlight and variant micronutrients from the environment for inherent growth (Ramachandra et al.

2013). Climate change legislation and governmental authorities are attempting to minimize greenhouse gases by opting for sustainable algae biofuels. Due to its lowest measure of emitted greenhouse gases, it has tremendous potential for alternative fuel technology. It is photosynthetic in nature without roots, stems, and leaves. Almost three lakhs species of algae are distributed and grown throughout the world in seawater, freshwater, and brackish water. Algae are classified into microalgae and macroalgae. Microalgae are single-celled organisms whereas macroalgae are multicellular organisms. Both kinds of algae can be effectively used in producing the byproducts of biodiesel and bioethanol. However, the yield of biodiesel through the transesterification process from microalgae is better whereas macroalgae are found to be superior in yield of bioethanol. As algae are carbon neutral, their use in biofuels does not result in any detrimental effects on the environment (Zaimes & Khanna 2013). Substances such as proteins, lipids, and carbohydrates are the main constituents of microalgae biomass. Biofuel production from microalgae is a promising field owing to its higher growth rates and potential to accommodate a superior amount of triglycerides. The composition of lipid content determines

the yield and quality of biodiesel produced (Ananthi et al. 2021).

## STRAIN SELECTION

Fig. 2 shows unique algae species utilized in methyl ester production. Algae cells are neutral lipids. High saturation and rapid accumulations of lipids in the cellular system at different phases of algae growth make them a potential diesel fuel substitute. Strain selection must be cared for, higher accumulation of lipids can lead to the formation of oxides in fuel injector lines during the process of combustion (Piloto-Rodríguez et al. 2017).

## PRODUCTION OF OIL AND METHYL ESTER (BIODIESEL)

### Algae Cultivation

Fig. 3 represents methyl ester production. For microalgae to grow, the temperature must be between 20°C and 30°C. The intensity of Sunlight is important for biofuel production (Alam et al. 2015). Algae cultivation is accomplished

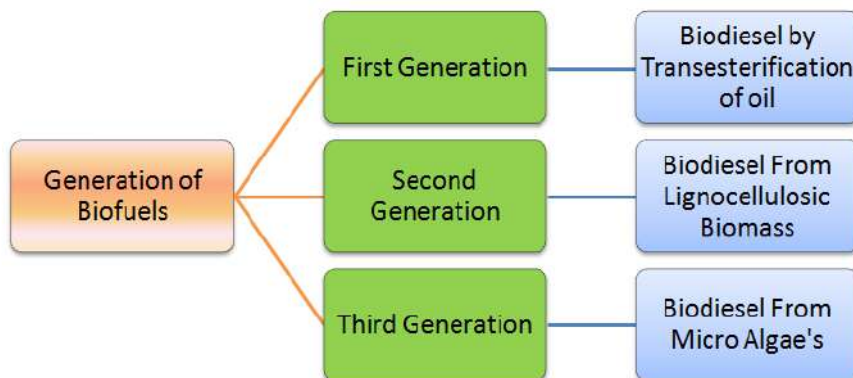


Fig. 1: Generation of biofuels.

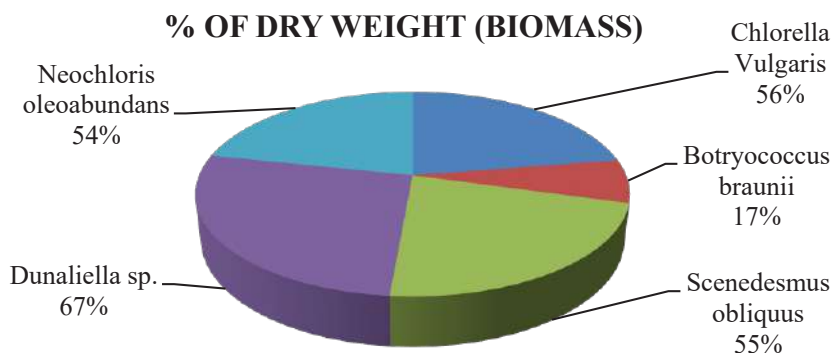


Fig. 2: Unique microalgae species for methyl ester production.

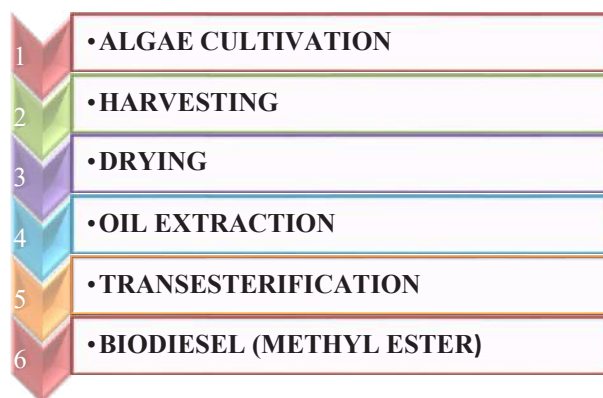


Fig. 3: Biodiesel production from algae.

with two different types of systems including open ponds (raceway) and closed reactors (photobioreactor). Commonly used reactors are Tubular PBR, Flat PBR, and Column PBR, where tubular PBR is less expensive and offers higher biomass productivity (Dragone et al. 2010). The tubular PBR gives superior pH, better temperature control, improved culture strain, finer combination, lesser evaporative losses, and superior cell densities. It is also relatively economical in terms of maintenance (Mata et al. 2010).

#### **Open Cultivation Systems**

The earliest type of farming involved a one-foot deep open cultivation system covering many acres that were exposed to natural sun rays. It can be made of concrete or simply excavated into the ground lined with plastic to prevent leakage and contamination (Duran et al. 2018). Nutrients (such as N and P) can be delivered directly by channeling water from water treatment or sewage treatment plants (Saleem & Moe 2014). The cost-effectiveness of the method adopted for manufacturing microalgae biomass is influenced by the algae strain used, local climatic conditions, cost of land, and availability of water. Open cultivation methods have two major drawbacks: first, their output is lower, and second, the environmental factors are more difficult to manage (Spolaore et al. 2006). Raceway-based pond biomass cultivation method tends to cover a total area of 440,000 m<sup>2</sup> (Andersson et al. 2014). Closed cultivation systems are more productive even though open culture systems are more economically viable due to issues such as H<sub>2</sub>O, temperature losses, vapor losses, and CO<sub>2</sub> dispersion into the environment resulting in environmental contamination issues (Ho et al. 2011).

#### **Closed Cultivation Systems**

Closed culture systems offer a monitored environment that effectively addresses contamination concerns. An open

culture method increases carbon dioxide fixation efficiency due to adequate mixing opportunities. However, as a result of its high infrastructure costs, the closed system technology is very expensive. This type of bioreactor is very effective, producing higher biomass concentrations (2–5 g.L<sup>-1</sup>) within two to four weeks with a greater surface area to vol. ratio than open cultivation systems (Wang et al. 2008, Min et al. 2011). Multilayer bioreactor is the most practical and cost-effective way to treat waste H<sub>2</sub>O from industrial and agricultural operations, both in terms of scaling up and nutrient removal (Chisti 2008). In terms of commercial production efficiency, the tubular photobioreactor is superior to other closed systems. A series of straight, clear plastic or glass tubes are used to gather solar energy with a diameter of less than 0.10 m, as penetration of sunrays is reduced in larger tubes. The tubes and a reservoir are used to circulate the microalgal broth (Rawat et al. 2011).

#### **Algae Harvesting**

In water, algae are frequently seen in a diluted form. Nearly 20-30% of the entire production cost is required for biomass recovery from dilute media. Flocculation, flotation, centrifugation, and filtration are the different harvesting procedures available. Filtration has proven good as it includes passing broth containing algal biomass through filters that collect algae biomass and allow the medium to flow through. A typical filtration procedure is best suited for harvesting algae biomass (>70µm) meanwhile for recovery of algae biomass (<30µm) ultra and microfiltration are technically viable alternatives to traditional filtration (Brennan & Owende 2010). Dewatering cannot be accomplished using a simple filtration approach (dead-end filtration) because of problems with back mixing. However, simple filters can be used in conjunction with centrifugation to improve separation (Harun et al. 2010).

## Drying

After the harvesting process, the dry solid concentration of biomass sludge is still modest. Moisture absorption of dewatered slurry is the final step in algae processing, with a moisture level of 12 to 15%. Algae slurry is dried or dehydrated at this point to achieve a stable state for future processing. Solar, convection, spray and freeze drying are some of the most common drying processes (Chen et al. 2015, Guldhe et al. 2014, Show et al. 2015, 2019).

### Solar Drying

Sun drying is the most cost-effective way of drying. It requires a prolonged drying period and might result in deterioration, fermentation, and spilling of the biomass. In as little as 3-5 h, closed sun drying machines can boost the ambient temperature from 35°C to 60°C.

### Convective Drying

Oven drying is a sort of hot air medium drying that is commonly used for convective drying. The minimum temperature range of this method is 40-55°C. However, the time required for removing the water content is about 12 h which is shorter than solar drying.

### Spray Drying

The spraying technique yields a dark green powder by means of hot gas drying, mostly air. It maintains more nutrients than convective-dried items, which lose 10–20 percent of their protein content.

### Freeze Drying

Freeze drying is the most popular method of conserving biomass as it preserves cell contents without damaging the cell wall. It involves the removal of bound water molecules by desorption. The time duration of different drying techniques is revealed in Fig. 4

## Oil Extraction from Algae Biomass

The most frequent methods of oil extraction include oil press,

solvent, supercritical fluid extraction, and ultrasound technology. Quick, scalable, and efficient extraction techniques are needed as they do not damage the extracted lipids.

### Expeller/Oil press

This technique is frequently used to extract oil from dry biomass. To make this procedure easier, it is necessary to dry the algae. A high-pressure approach is utilized to break down cells and squeeze off oil. It removes about 75% of the oil and requires no particular skills. Despite the prolonged extraction time, it's shown to be quite effective.

### Solvent Extraction

This technique is relatively inexpensive and is found to yield more amounts of algae oil. In this method, dried algae are treated with organic solvents such as benzene, cyclohexane, hexane, acetone, and chloroform. Though organic solvents are more soluble in organic solvents than water, they break the algal cell wall and extract oil from aqueous media. Amongst different solvents hexane has excellent extraction capacity and inexpensiveness.

### Supercritical Fluid Extraction

In this process of extraction, cells are ruptured using high pressure and temperature. This technique utilizes the treatment of liquefied CO<sub>2</sub> under pressure and heated to a temperature as it has both liquid and gas characteristics. However, it's found to be inadequate due to inter-sample interactions.

### Ultrasound Technique

This process involves creating high-intensity cavitation bubbles using ultrasonic waves. Shockwaves are generated when bubbles collapse crushing cell walls and expelling desirable chemicals. However, this type of extraction possesses higher interaction of solvents with lesser extraction time. Owing to its technical viability some sort of research must be done.

### Soxhlet Extraction Technique – Solvent Extraction

Fig. 5 illustrates the usage of a Soxhlet extractor to extract oil from algae biomass. The constructional arrangement consists of a round bottom flask, thimble, condenser, and

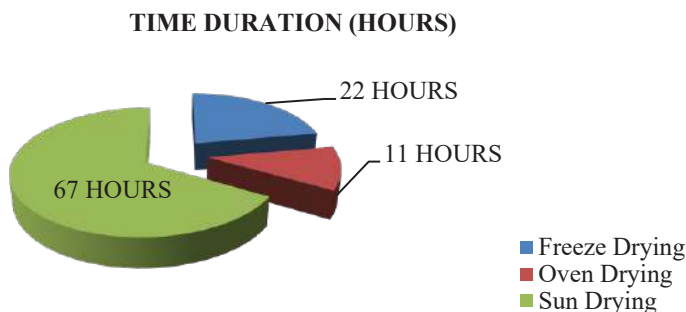


Fig. 4: Duration of drying.

extraction chamber. This apparatus uses a circular bottom flask that is filled with 300 mL of n-hexane, while the dry algae biomass is kept inside the thimble wall. The circular bottom flask is heated to 70°C with the help of the heating unit due to which the n-hexane gets vapourised and enters the condenser. Hexane vapor is condensed in the condenser and gets converted into warm hexane liquid. Once the dried algae biomass is in contact with the warm hexane solvent, oil is extracted from the biomass. The oil and warm hexane liquid are collected in the round bottom flask and the cycle is repeated. After the completion of cycles, the warm hexane liquid and algae oil are transported to a solvent extractor where they are separated.

### Determining Free Fatty Acid Percentage Of Algae Oil

Titration is used to assess the free fatty percentage of algae-based oil. A 0.1-0.5 mL of oil sample is taken and weighed using a conical flask. After weighing 50 mL of solvent mixture (95% ethanol and diethyl ether in 1:1 ratio) was added to the sample and is well mixed. Following the dissolving procedure, a burette was filled with 0.1 N potassium hydroxide (KOH) and the initial reading was recorded. Then the dissolved mixture is titrated by the vigorous swirling of the flask with a 1% of phenolphthalein indicator (Karmakar et al. 2017) until the solution turns pale pink. Finally, the end burette reading was observed. The formula described below determines the acid content of algal oil and the percentage of FFA was obtained by multiplying the acid value with the factor of 0.503.

Acid Value =

$$\frac{\text{Molecular weight of KOH} \times \text{Normality of KOH} \times \text{Volume of KOH solution used}}{\text{Weight of algae oil sample}}$$

Weight of algae oil sample

$$\% \text{ FFA} = 0.503 \times \text{Acid value}$$

### Transesterification Setup and Process

Before commencing this process, the obtained oil is checked for the percentage of FFA (Free Fatty Acid). Transesterification set-up is shown in Fig. 6. It is the most economical chemical process of converting the triglycerides in algae oil into methyl ester in the existence of a catalyst (Kubude et al. 2019). Transesterification is carried out by boiling 100 mL of *Chlorella vulgaris* algae oil in a round bottom flask. 0.95 gm of potassium hydroxide is mixed with 25 mL of methane solution. The prepared mixture is stirred at a temperature of 48-52°C for 30 min. After the stirring process, the mixture is transferred into the separator and left undisturbed to allow settling down at atmospheric temperature for 8-10 h by which the glycerol is separated at the bottom of the separator. The top surface of the biodiesel (methyl ester) is washed with water to minimize the pH value and remove the traces of acid (Emirbas & Demirbas 2011, Satputaley et al. 2018).

### Use of Algae in Ci Engines

The following section covers a comprehensive review of

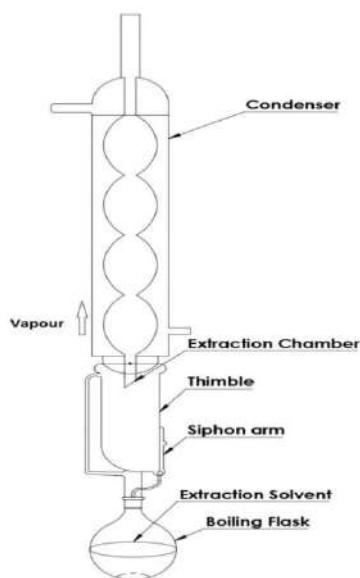


Fig. 5: Soxhlet extractor.

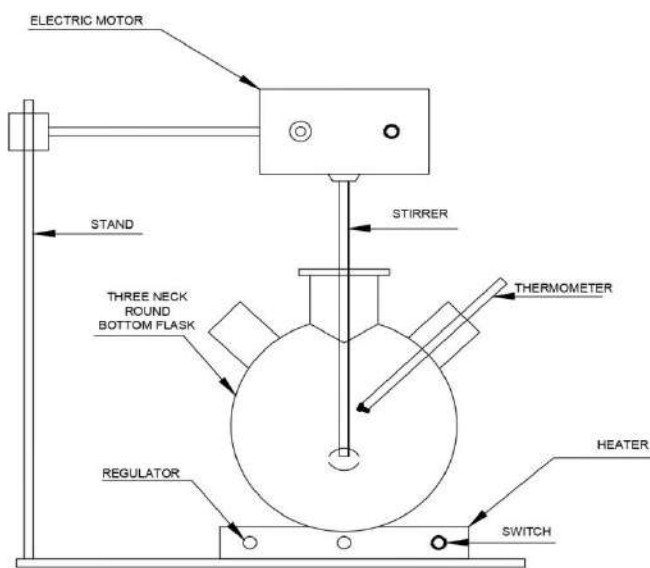


Fig. 6: Transesterification setup.

several research studies conducted by many researchers on various kinds of algae.

#### ***Chlorella vulgaris* as Neat Oil and Neat Biodiesel (B 100)**

The test fuels of *Chlorella vulgaris* oil and biodiesel were experimented with in one cylinder 4 stroke CI engine. BTE of neat oil and methyl ester was lowered and an increase in BSFC was observed for algae oil and methyl ester over diesel. Maximum pressure rise of algae oil and methyl ester were recorded as 63.26 bar and 58.5 bar respectively over diesel of 67.65 bar. However, no drastic variations were observed in Exhaust Gas Temperature (EGT) and NO<sub>x</sub> between diesel, neat algae oil, and biodiesel. CO, UBHC, and smoke were found to be lower. This was due to the existence of 10 to 12 percent of additional oxygen content in the oil and methyl ester (Satputaley et al. 2018).

#### ***Chlorella vulgaris* Oil With Low Viscous Turpentine Oil**

Three different test fuels (C90T10, C75T25, C50T50) along with neat diesel (D100) and neat *Chlorella vulgaris* oil (C100) were investigated experimentally to determine their performance characteristics in a single cylinder CI engine with a maximum power of 5.2 KW at 1500 rpm. After adding low-viscosity turpentine oil to *Chlorella vulgaris* oil, the BTE improved considerably. When *Chlorella vulgaris* oil was mixed with turpentine, there was a drastic increase in BSFC because of the low spray-forming characteristics of fuel in the combustion chamber (Karthikeyan et al. 2020a).

#### ***Chlorella vulgaris* as Methyl Ester**

The comparative performance of the CI engine with hydrogen induction technique of micro *Chlorella vulgaris* biodiesel with diesel was investigated experimentally in one cylinder 4 stroke CI engine with a rated output of 9KW at 3000 rpm. The test fuels were investigated for torque, power, and emissions such as CO, HC, and CO<sub>2</sub>. The experimental results showed that the addition of 10 LPM hydrogen to methyl ester (MCV20) increased the power and torque of the engine by 7.6% and 10.6%, respectively. A 6% reduction in BSFC was obtained. From an emission point of view, it was noted that the addition of 10 LPM of hydrogen to *Chlorella vulgaris*

methyl ester decreased CO, CO<sub>2</sub>, and HC by 13.7%, 6.8%, and 34.3%, respectively. However, the addition of hydrogen increased NO<sub>x</sub> emissions (Tayari et al. 2019).

A comparative study was carried out on *Chlorella vulgaris* methyl esters in the different blend ratios of (B30, B40, B50, and B60) with diesel in a CI engine at a rated power of 1500 rpm. The test fuels were investigated for BSFC, BTE, CO, CO<sub>2</sub>, UHC, and NO<sub>x</sub>. The experimental results showed that blending methyl ester blends with diesel showed a decrease in BTE with increased BSFC over diesel at all loading conditions. With higher NO<sub>x</sub> emissions, all biodiesel blends had lower CO, UHC, and smoke. However, blending higher ratios of methyl ester resulted in a poorer performance when compared to diesel. Hence, an optimum blend of methyl ester is necessary to enhance the performance of a CI engine (Mathimani et al. 2017).

#### ***Caulerpa racemosa* Algae**

Karthikeyan et al. (2020b) investigated the use of *Caulerpa racemosa* algae methyl ester with Bi<sub>2</sub>O<sub>3</sub> in a one-cylinder CI engine at a power rating of 1500 rpm. The test fuels were analyzed to examine the combustion, performance, and emission. The experimental outcome showed that the use of nano-additive with B20 improved the performance, lower CD and HRR were observed with Bi<sub>2</sub>O<sub>3</sub> supplemented blends than B20. From an emission perspective, it was observed that B20 with Bi<sub>2</sub>O<sub>3</sub> of 100 ppm gave lower CO (3%vol), HC (200 ppm), and smoke. Emissions of NO<sub>x</sub> were found to be higher due to the presence of oxygen at maximum load.

#### ***Scenedesmus obliquus* Algae**

In an experimental study conducted by (Elkelawy et al. 2020), the operational characteristics of a CI engine with a rated speed of 2200 rpm were investigated using the test fuels of *Scenedesmus obliquus* methyl ester blend B50 with three different proportions of n-pentane blends of 5%, 10%, and 15%. The experimental results showed that B50 with 15 mL.L<sup>-1</sup> n-pentane blends increased the BTE by 7.1% and decreased the BSFC by 6.4%. They observed that the

Table 1: Advantages and limitations of various extraction techniques.

Extraction methods	Advantages	Limitations	Reference
Oil Press	Easy to use	Longer extraction time	(Harun et al. 2010, Rajkumar et al. 2013)
Solvent extraction	Solvents are inexpensive	Solvent recovery is expensive and energy-intensive	(Harun et al. 2010, Rajkumar et al. 2013)
Supercritical fluid extraction	Absence of organic solvents and simple operation.	Found insufficient in the interaction between the samples	(Harun et al. 2010, Rajkumar et al. 2013)
Ultrasound technique	High interaction of solvents with less extraction time.	High power consumption	(Harun et al. 2010, Rajkumar et al. 2013)



Table 2: Comparison of performance and combustion characteristics.

Micro Algae Species	Performance parameters		Reference
	BTE	BSFC	
<i>Chlorella vulgaris</i>	Biodiesel and Algae Oil shows reduction in BTE of about 5.2% and 6.4% compared to diesel	Biodiesel and Algae Oil consumes more fuel to give the same power output	(Satputaley et al. 2018)
<i>Chlorella vulgaris</i>	-	BSFC improved by 6.6% with 10 LPM hydrogen gas for the blend B20	(Tayari et al. 2019)
<i>Chlorella vulgaris</i>	BTE diminished with increase in blends	Compared to diesel and other blended fuels BSFC of B60 was higher	(Mathimani et al. 2017)
<i>Caulerpa racemosa</i>	BTE decreased with blend B20 and nano additive	BSFC of blend B20 with 100 ppm was noted to be closer to the diesel	(Karthikeyan et al. 2020c)
<i>Scenedesmus obliquus</i>	BTE increased by 7.1% with 15 mL n-pentane blend	Decrease in BSFC of 6.4% is observed with 15mL n-pentane blend	(Elkelawy et al. 2020)
<i>Chlorella sp.</i>		BSFC of B30 methyl ester is 3.5% higher than diesel.	(Makareviciene et al. 2014)
<i>Calophyllum inophyllum</i> Algae	B20 with DEE improved BTE by 4.4% as compared to neat diesel	BFSC of a micro algal B20 blending with DEE is 3.76% lower than diesel	(Ranjithkumar et al. 2020)
<i>Spirulina</i>	BTE of B20 was found to be lower than diesel	BSFC of blend B20 was found to be 8.42% higher as compared to diesel.	(Krishaniaa et al. 2020)
<i>Spirulina</i>	BTE increased by 1.39% with a 30% butanol blend	The addition of butanol with methyl ester increases BSFC	(Rajak et al. 2019)
<i>Schizochytrium</i>	BTE of B20 was found to be compatible with the diesel	BSFC is found to be higher for all ratios (blends) with respect to diesel.	(Rajendra Prasad Reddy et al. 2020)
Micro Algae Species	Combustion parameters		Reference
	Cylinder Pressure	HRR (Heat Release Rate)	
<i>Chlorella vulgaris</i>	Diesel peak pressure increased by 4% and 14% as compared to algae oil and algae Biodiesel		(Satputaley et al. 2018)
<i>Chlorella vulgaris</i>			(Tayari et al. 2019)
<i>Chlorella vulgaris</i>			(Mathimani et al. 2017)
<i>Caulerpa racemosa</i>			(Karthikeyan et al. 2020a)
<i>Scenedesmus obliquus</i>	Higher cylinder pressure was found with the addition of pentane blends	An increase in HRR was found with the addition of pentane blends	(Elkelawy et al. 2020)
<i>Chlorella sp.</i>			(Makareviciene et al. 2014)
<i>Calophyllum inophyllum</i> Algae			(Ranjithkumar et al. 2020)
<i>Spirulina</i>	Cylinder pressure was found to be dropped with algae biodiesel as compared to diesel	HRR decreased with an impressed percentage of algae biodiesel blends	(Krishaniaa et al. 2020)
<i>Spirulina</i>	Cylinder pressure was increased by combining butanol with algal methyl ester and diesel (ternary blends)	The addition of butanol with algae methyl ester and diesel (ternary blends) increased the HRR	(Rajak et al. 2019)
<i>Schizochytrium</i>	B40 and B60 cylinder pressures were found to be higher than diesel		(Rajendra Prasad Reddy et al. 2020)

blending of n-pentane with methyl ester resulted in longer ignition delay, with high HRR and that cylinder pressure was higher. CO<sub>2</sub> and NO<sub>x</sub> were found to be increased for all pentane blends with reduced CO, HC, and O<sub>2</sub> emissions.

#### ***Chlorella sp.* Algae**

An attempt was made by (Makareviciene et al. 2014) to establish the performance and emission characteristics of *Chlorella sp.* methyl ester in a multi-cylinder CI engine at

Table 3: Comparison of Emission Characteristics

Micro Algae Species	Emission Parameters				Reference
	CO	UHC	Smoke	NO <sub>x</sub>	
<i>Chlorella vulgaris</i>	10 to 12% of excess oxygen level in methyl ester and algae oil results in reduced CO emissions	10 to 12% of excess oxygen level in methyl ester and algae oil results in reduced. UHC emissions	10 to 12% of excess oxygen level in methyl ester and algae oil results in reduced Smoke Opacity	At 5.15 kW brake power load, algae oil demonstrated the greatest reduction in NO <sub>x</sub> of 19 ppm	(Satputaley et al. 2018)
<i>Chlorella vulgaris</i>	CO emissions are reduced by 13.7% as a result of hydrogen enrichment.	UHC emissions are reduced by 34.3% as a result of hydrogen enrichment.		NO <sub>x</sub> emissions soared by 5.1 % when hydrogen was enriched	(Tayari et al. 2019)
<i>Chlorella vulgaris</i>	CO emissions fell as biodiesel content in blends increased	The percentage of biodiesel in blends reduced UHC emissions by 14.75%		There was no discernible difference in NO <sub>x</sub> emissions between diesel and mixed fuels	(Mathimani et al. 2017)
<i>Caulerpa racemosa</i>	Bi <sub>2</sub> O <sub>3</sub> and its blends have lower CO emissions than B20	Bi <sub>2</sub> O <sub>3</sub> and its compositions exhale less UHC than B20	Bi <sub>2</sub> O <sub>3</sub> and its constituents expel less Smoke than B20	NO <sub>x</sub> emissions for Bi <sub>2</sub> O <sub>3</sub> nano additions mixed fuel are higher than for B20	(Karthikeyan et al. 2020a)
<i>Scenedesmus obliquus</i>	Excess oxygen in methyl ester with pentane addition lowers CO emissions by 21.19%	Excess oxygen in methyl ester with pentane addition lowers UHC emissions by 9.82%		NO <sub>x</sub> emissions are raised owing to increased oxygen when pentane additives are used	(Elkelawy et al. 2020)
<i>Chlorella</i> sp.	CO reductions upto 10% were observed	Reduced UHC emissions by 5-25%		No drastic variations in NO <sub>x</sub> emissions were observed	(Makareviciene et al. 2014)
<i>Calophyllum inophyllum</i> Algae	B40 with DEE showed reduced CO emissions by 33% compared to diesel	B40 with DEE showed the lowest UHC emissions by 30.7% compared to diesel		Blend B60 had a 4.91(%) increase in NO <sub>x</sub> .	(Ranjithkumar et al. 2020)
<i>Spirulina</i>			B20 reduces smoke emissions by 18.33 %	With B20, NO <sub>x</sub> emissions are decreased by 10.66%	(Krishaniaa et al. 2020)
<i>Spirulina</i>				NO <sub>x</sub> emissions were raised owing to an increase in butanol blends	(Rajendra Prasad Reddy et al. 2020)
<i>Schizochytrium</i>	CO emissions from biodiesel compositions are higher compared to diesel	UHC emissions were decreased by increasing the amount of biodiesel in blends	Smoke emissions from biodiesel compositions are higher compared to diesel	No obvious variations in NO <sub>x</sub> emissions were found	(Rajak et al. 2019)

a maximum power of 1500 rpm. The empirical study on chlorella sp methyl ester B30 showed that it had an approximately 3.5 percent greater BSFC than natural petroleum diesel. When the engine was run on B30 methyl ester, there was no noticeable variation in the BSFC readings. Energy utilization of methyl ester was found to be 2.5 to 3 percent superior to diesel-fueled operation. A noticeable improvement in emission factor was seen. The blending of the methyl ester with mineral diesel reduced emissions of HC, CO, and

smoke by 75%, 25%, and 10% respectively as compared to diesel, meanwhile, NO<sub>x</sub> increases.

#### *Calophyllum inophyllum* Algae

The performance and emission characteristics of dual-blended biodiesel were examined in internal combustion (CI) engine with a power rating of 1500 rpm. Using vol. ratios of 20%, 40 %, and 60 %, methyl ester made from CIME and MAME was mixed with diesel fuel. Comparing (B40 and

B60), B20 with DEE showed a 4.4% higher improvement in BTE when compared to neat diesel. However, the BSFC of the B20 blend with DEE was 3.76% less than diesel. Meanwhile, B40 with DEE had the lowest HC and no variations in CO were observed. An increase in  $\text{NO}_x$  was observed when B60 (30 % CIME + 30% MAME) was blended with DEE (Ranjithkumar et al. 2020).

### *Spirulina* Algae

#### *Spirulina Methyl Ester*

Krishaniaa et al. (2020) experimentally investigated the performance and emission characteristics of spirulina algae methyl ester in a single-cylinder compression ignition engine at a power rating of 1500 rpm. The experimental results obtained showed that blending of *Spirulina* methyl ester B20 with diesel resulted in higher BSFC and lower BTE. EGT was raised as engine load increased due to better combustion quality. Smoke was reduced by 8.3% and a decrease in  $\text{CO}_2$  emission was observed for B20.  $\text{NO}_x$  emission decreased for biodiesel blends by 10.66 percent as a result of the lower combustion process of methyl ester.

#### *Spirulina Methyl Ester With Butanol Blend*

Rajak et al. (2019) analyzed the emission and performance characteristics with the use of *Spirulina* algae methyl ester with butanol in a one-cylinder CI engine that had a power rating of 1500 rpm. The MSB (40, 30 and 20 percent) n-butanol (10, 20 and 30 percent) blends were 50 percent with low sulphur diesel fuel in volume basis as B1 (LSD 50-MSB 40-nB 10), B2 (LSD 50- MSB 30-nB20) and B3 (LSD50-MSB20-nB30). The results of their experimental work revealed that the addition of 30% butanol to diesel-spirulina methyl ester blends improved the BTE with a high heat release rate and cylinder pressure. The BTE was noted to be 34.57% whereas for petroleum diesel it was found to be 33.18%. The authors noticed that an increase in n-butanol resulted in a corresponding increase in BSFC and relatively low smoke emissions. Contrarily, the  $\text{NO}_x$  emissions were found to be increased.

### *Schizochytrium* Algae

Rajendra Prasad Reddy et al. (2020) examined the combustion, performance, and emission behavior of *Schizochytrium*-diesel blends in a single cylinder CI engine that had a rated power of 3.7 KW at 1500 rpm. The test fuels of diesel and *Schizochytrium* with ratios of B0, B20, B40, and B60 were prepared and tested. Experimental results showed that the BTE of B20 was found to be similar (24.53%) to the BTE of fossil diesel (25.37%). However, the BSFC was higher with reduced BTE for all the blends which were because of its lower calorific value. The authors determined that there

was an improvement as the cylinder pressure was 65 bar for the B60 blend compared to the fossil diesel (63.1 bar) at full load. In addition, the ignition delay of methyl ester blends was reduced due to the presence of intrinsic oxygen and higher CN. On the contrary, they noted that CO and  $\text{NO}_x$  levels increased with the methyl ester blends. However, there was a decrease in UHC at all loads.

## CONCLUSION

The purpose of this review study is to provide an overview of algae oil production and its use in CI engine applications. Biodiesel production from microalgae involves identifying the algae species with high oil content and high growth rates, while the second is treating the selected algae with several processing steps. The main advantage of the algae species is that it is carbon neutral and does not release any harmful emissions into the environment. Techniques such as algae cultivation, harvesting, drying, and extraction have been discussed, however, the selection of suitable methods for obtaining biodiesel continues to be a challenge to the research community.

The importance of the photobioreactor in cultivating algae biomass has been highlighted. Open pond cultivation depends on weather conditions whereas the photobioreactor depends on  $\text{CO}_2$ , sunlight, and nutrients.

The combination of filtration with centrifugation gives better separation of biomass from the broth. The size factor of algae biomass plays a major role in selecting the suitable filtration technique. If algae strain is more than 70 $\mu\text{m}$  then conventional filtration is feasible. However, for the recovery of algae biomass, less than 30 $\mu\text{m}$  micro filtration and ultra-filtration are widely used.

Among various drying techniques, the freeze drying technique is most widely used as it retains the algae biomass without any damage to cell walls. It is observed that there is a threefold increase in the yield of oil derived from algae dried under natural sunlight in comparison with the oil produced using conventional methods. Dried algae biomass is subjected to extraction to yield oil and later transesterified to obtain biodiesel. Amongst different extraction techniques, the solvent extraction technique is relatively inexpensive and is found to be the best for obtaining more amount of algae oil.

The experimental investigations of different algae have been discussed. It is observed that there is a significant improvement in performance with the use of algae biodiesel. From the review of several experimental studies, it is seen that the addition of butanol and pentanol with methyl ester improves the BTE in contrast with BSFC. An increase in

algae methyl ester mix ratios results in poor performance with higher  $\text{NO}_x$ .

Adding 30 % butanol to the diesel-spirulina methyl ester blends improves the BTE to 34.57% with high HRR and cylinder pressure whereas for diesel it is found to be 33.18%. BTE of the dual fuel CI engine is found to be 31% for dual *Calophyllum inophyllum* methyl ester blend (B20) with Diethyl Ether and there is a drop in BSFC of 3.76% in comparison with diesel. This is because the high oxygen concentration of biodiesel might make it burn much more effectively. However, algae methyl ester blends without alcoholic blends are found to have lower BTE with higher BSFC. From the emissions aspect, it is observed that there is a decrease in CO, UHC, and smoke for all algae blends owing to the presence of oxygen sources in the range of 10 to 12 percent in methyl ester and algae oil. No extreme variations are observed in EGT and Nitrous oxide ( $\text{NO}_x$ ) emission between diesel and biodiesel.

Edible species such as *Spirulina* algae are gaining immense popularity of late in the food processing industry. It has however not been widely explored as a possible alternative fuel for CI engines. Only a limited number of research studies have been carried out on its use. The challenging knowledge gap to find the best alternatives to fossil fuels needs to be addressed in future research endeavors. Minor blending (B20) of methyl ester is identified to be the most effective way to improve CI engine performance.

## ABBREVIATIONS

BTE - Brake Thermal Efficiency  
 BSFC – Brake Specific Fuel Consumption  
 CO – Carbon Monoxide  
 UBHC – Unburned Hydrocarbon  
 $\text{NO}_x$  – Nitrous Oxide  
 HRR – Heat Release Rate  
 CP – In-Cylinder Pressure  
 EGT – Exhaust Gas Temperature

## REFERENCES

Alam, F., Mobin, S. and Chowdhury, H. 2015. Third Generation Biofuel from Algae. *Procedia Engineering*, 105: 763-768.  
 Ananthi, V., Raja, R., Carvalho, I. S., Brindhadevi, K., Pugazhendhi, A. and Arun, A. 2021. A realistic scenario on microalgae-based biodiesel production: Third generation biofuel. *Fuel*, 284: 118965.  
 Andersson, V., Broberg Viklund, S., Hackl, R., Karlsson, M. and Berntsson, T. 2014. Algae-based biofuel production is part of an industrial cluster. *Biom. Bioenergy*, 71: 113-124.  
 Balasubramanian, K. and Purushothaman, K. 2019. Effect of acetylene addition on performance, emission, and combustion characteristics of neem biodiesel and corn biodiesel-fueled CI engine. *J. Therm. Anal. Calorim.*, 138(2): 1405-1414.  
 Baral, S.S., Singh, K. and Sharma, P. 2015. The potential of sustainable

algal biofuel production using  $\text{CO}_2$  from the thermal power plant in India. *Renew. Sustain. Energy Rev.*, 49: 1061-1074.  
 Brennan, L. and Owende, P. 2010. Biofuels from microalgae: A review of technologies for production, processing, and extractions of biofuels and co-products. *Renew. Sustain. Energy Rev.*, 14(2): 557-577.  
 Chen, C.L., Chang, J.S. and Lee, D.J. 2015. Dewatering and drying methods for microalgae. *Dry. Technol.*, 33(4): 443-454.  
 Chisti, Y. 2008. Biodiesel from microalgae beats bioethanol. *Trends Biotechnol.*, 26(3): 126-131.  
 Dhanamurugan, A. and Subramanian, R. 2015. Emission and performance characteristics of a diesel engine operating diesel-bael (Aegle marmelos) biodiesel blends. *Nat. Environ. Pollut. Technol.*, 14(2): 331-336.  
 Dragone, G., Fernandes, B., Vicente, A. and Teixeira, J. 2010. Third-Generation Biofuels From Microalgae. In Méndez-Vilas, A. (ed), *Current Research, Technology and Education Topics in Applied Microbiology and Microbial Biotechnology*, Formatex Research Center, Badajoz, Spain, pp.1355-1366  
 Duran, S.K., Kumar, P. and Sandhu, S. S. 2018. A review on microalgae strains, cultivation, harvesting, biodiesel conversion, and engine implementation. *Biofuels*, 12(1): 91-102.  
 Elkelawy, M., Alm-Eldin Bastawissi, H., El Shenawy, E.A., Taha, M., Panchal, H. and Sadasivuni, K.K. 2020. Study of performance, combustion, and emissions parameters of DI-diesel engine fueled with algae biodiesel/diesel/n-pentane blends. *Energy Conv. Manag.*, 61: 100058.  
 Emirbas, A. and Demirbas, M. 2011. Importance of algae oil as a source of biodiesel. *Energy Conv. Manag.*, 52(1): 163-170.  
 Enamala, M.K., Enamala, S., Chavali, M., Donepudi, J., Yadavalli, R., Kolapalli, B. and Kuppam, C. 2018. Production of biofuels from microalgae: A review on cultivation, harvesting, lipid extraction, and numerous applications of microalgae. *Renew. Sustain. Energy Rev.*, 94: 49-68.  
 Guldhe, A., Singh, B., Rawat, I., Ramluckan, K. and Bux, F. 2014. Efficacy of drying and cell disruption techniques on lipid recovery from microalgae for biodiesel production. *Fuel*, 128: 46-52.  
 Harun, R., Singh, M., Forde, G.M. and Danquah, M.K. 2010. Bioprocess engineering of microalgae to produce a variety of consumer products. *Renew. Sustain. Energy Rev.*, 14(3): 1037-1047.  
 Ho, S.H., Chen, C.Y., Lee, D.J. and Chang, J.S. 2011. Perspectives on microalgal  $\text{CO}_2$ -emission mitigation systems: A review. *Biotechnol. Adv.*, 29(2): 189-198.  
 Jayakumar, N. and Narayanasamy, B. 2019. Effect of Basil antioxidant additive on the performance, combustion, and emission characteristics of used cooking oil biodiesel in CI engine. *J. Therm. Anal. Calorim.*, 140(1): 457-473.  
 Kanthasamy, P., Selvan, V.A.M. and Shanmugam, P. 2020. Investigation of the performance, emissions, and combustion characteristics of CRDI engine fueled with tallow methyl ester biodiesel blends with exhaust gas recirculation. *J. Therm. Anal. Calorim.*, 141(6): 2325-2333.  
 Karmakar, R., Kundu, K. and Rajor, A. 2017. Fuel properties and emission characteristics of biodiesel produced from unused algae grown in India. *Petrol. Sci.*, 15(2): 385-395.  
 Karthikeyan, S., Periyasamy, M. and Prathima, A. 2020a. Combustion analysis of a CI engine with *Caulerpa racemosa* algae biofuel with nano additives. *Mater. Today Proceed.*, 33: 3324-3329.  
 Karthikeyan, S., Periyasamy, M. and Prathima, A. 2020b. Performance characteristics of CI engine using *Chlorella vulgaris* microalgae oil as a pilot dual fuel blends. *Mater. Today Proceed.*, 33: 3277-3282.  
 Karthikeyan, S., Periyasamy, M., Prathima, A. and Ram Balaji, M. 2020c. Performance and exhaust emissions of a CI engine using  $\text{Bi}_2\text{O}_3$  nano blends as an alternate *Caulerpa racemosa* algae oil biofuel. *Mater. Today Proceed.*, 33: 3265-3270.  
 Krishania, N., Rajak, U., Nath Verma, T., Kumar Birru, A. and Pugazhendhi, A. 2020. Effect of microalgae, tire pyrolysis oil, and *Jatropha* biodiesel enriched with diesel fuel on performance and emission characteristics of CI engine. *Fuel*, 278: 118252.

- Kubude, V. C., Nwaigwe, K. N. and Dintwa, E. (2019). Production of biodiesel from microalgae via nanocatalyzed transesterification process: A review. *Mater. Sci. Energy Technol.*, 2(2): 216-225.
- Madhankumar, S., Stanley, M.J., Thiyagarajan, S., Geo, V.E., Karthickeyan, V. and Chen, Z. 2019. Effect of oxygen enrichment on CI engine behavior fueled with vegetable oil: an experimental study. *J. Therm. Anal. Calorim.*, 142(3): 1275-1286.
- Makareviciene, V., Lebedevas, S., Rapalis, P., Gumbyte, M., Skorupskaite, V. and Žaglinskis, J. 2014. Performance and emission characteristics of diesel fuel containing microalgae oil methyl esters. *Fuel*, 120: 233-239.
- Mata, T.M., Martins, A.A. and Caetano, N.S. 2010. Microalgae for biodiesel production and other applications: A review. *Renew. Sustain. Energy Rev.*, 14(1): 217-232.
- Mathimani, T., Senthil Kumar, T., Chandrasekar, M., Uma, L. and Prabaharan, D. 2017. Assessment of fuel properties, engine performance, and emission characteristics of outdoor grown marine *Chlorella vulgaris* BDUG 91771 biodiesel. *Renew. Energy*, 105: 637-646.
- Min, M., Wang, L., Li, Y., Mohr, M. J., Hu, B., Zhou, W. and Ruan, R. 2011. Cultivating *Chlorella* sp. in a Pilot-scale photobioreactor using centrate wastewater for microalgae biomass production and wastewater nutrient removal. *Appl. Biochem. Biotechnol.*, 165(1): 123-137.
- Piloto-Rodríguez, R., Sánchez-Borroto, Y., Melo-Espinosa, E. A. and Verhelst, S. 2017. Assessment of diesel engine performance when fueled with biodiesel from algae and microalgae: An overview. *Renew. Sustain. Energy Rev.*, 69: 833-842.
- Prakash, T., Geo, V.E., Martin, L.J. and Nagalingam, B. 2018. Improved cold flow properties and combustion analysis of high viscous castor oil and its biodiesel in a CI engine. *Nature Environ. Pollut. Technol.*, 7(4): 1183-1192.
- Rajak, U., Nashine, P. and Verma, T.N. 2019. Characteristics of microalgae *Spirulina* biodiesel with the impact of n-butanol addition on a CI engine. *Energy*, 189: 116311.
- Rajendra Prasad Reddy, B., Rana Prathap Reddy, N., Manne, B. and Srikanth, H.V. 2020. Performance, combustion, and emission characteristics of a diesel engine fuelled with *Schizochytrium* micro-algae biodiesel and its blends. *Int. J. Amb. Energy*, 16: 1-7.
- Rajendran, S. 2021. A comparative study of performance and emission characteristics of neat biodiesel operated diesel engine: a review. *J. Therm. Anal. Calorim.*, 146: 1015-1025.
- Rajkumar, R., Yaakob, Z. and Takriff, M.S. 2013. Potential of micro and macro algae for biofuel production: A brief review. *BioResources*, 9(1): 1606-1633.
- Ramachandra, T.V., Durga Madhab, M., Shilpi, S. and Joshi, N.V. 2013. Algal biofuel from urban wastewater in India: Scope and challenges. *Renew. Sustain. Energy Rev.*, 21: 767-777.
- Ranjithkumar, M., Karuppusamy, S., Lakshmanan, P., Ragulnath, D., Saravanan, K. and Rameshbabu, A.M. 2020. Study on diesel engine combustion parameters using *Calophyllum inophyllum* methyl ester and microalgae methyl ester with level addition of Di-Ethyl ether. *Mater. Today Proceed.*, 37: 3388-3392.
- Rawat, I., Ranjith Kumar, R., Mutanda, T. and Bux, F. 2011. Dual role of microalgae: Phytoremediation of domestic wastewater and biomass production for sustainable biofuels production. *Appl. Energy*, 88(10): 3411-3424.
- Saleem, M. and Moe, L.A. 2014. Multitrophic microbial interactions for eco- and agro-biotechnological processes: theory and practice. *Trends in Biotechnol.*, 32(10): 529-537.
- Saratale, R.G., Kuppam, C., Mudhoo, A., Saratale, G. D., Periyasamy, S., Zhen, G. and Kumar, G. 2017. Bioelectrochemical systems using microalgae: A concise research update. *Chemosphere*, 177: 35-43.
- Satputaley, S.S., Zodpe, D.B. and Deshpande, N.V. 2018. Performance, combustion, and exhaust emissions analysis of a diesel engine fuelled with algae oil and algae biodiesel. *Mater. Today Proceed.*, 5(11): 23022-23032.
- Show, K.Y., Lee, D.J. and Mujumdar, A.S. 2015. Advances and Challenges on Algae harvesting and drying. *Drying Technology*, 33(4), 386-394.
- Show, K.Y., Yan, Y.G. and Lee, D.J. 2019. Algal biomass harvesting and drying. *Biofuels from Algae*, 135-166.
- Siluvaimuthu, S., Thiyagarajan, S., Martin, L.J. and Nagalingam, B. (2019). Comparative analysis of premixed combustion and blending of alcohols with neem and wintergreen oil biofuel blends in CI engine. *Journal of Thermal Analysis and Calorimetry*, 140(4): 1945-1956.
- Singh, N., Kumar, H., Jha, M.K. and Sarma, A.K. 2015. Complete heat balance, performance, and emission evaluation of a CI engine fuelled with Mesua ferrea methyl and ethyl ester's blends with petrodiesel. *J. Therm. Anal. Calorim.* 122(2): 907-916.
- Spolaore, P., Joannis-Cassan, C., Duran, E. and Isambert, A. 2006. Commercial applications of microalgae. *J. Biosci. Bioeng.*, 101(2): 87-96.
- Tayari, S. and Abedi, R. 2019. Effect of *Chlorella vulgaris* methyl ester enriched with hydrogen on performance and emission characteristics of CI engine. *Fuel*, 256: 115906.
- Thiyagarajan, S., Geo, V.E., Martin, L.J. and Nagalingam, B. 2016. Effects of low carbon biofuel blends with *Karanja (Pongamia pinnata)* oil methyl ester in a single cylinder CI engine on CO<sub>2</sub> emission and other performance and emission characteristics. *Nat. Environ. Pollut. Technol.*, 15(4): 1249-1256.
- Vinukumar, K., Azhagurajan, A., Vettivel, S.C. and Vedaraman, N. 2017. Rice husk as nano additive in diesel-biodiesel fuel blends used in a diesel engine. *J. Therm. Anal. Calorim.*, 131(2): 1333-1343.
- Wang, B., Li, Y., Wu, N. and Lan, C.Q. 2008. CO<sub>2</sub> bio-mitigation using microalgae. *Appl. Microbiol. Biotechnol.*, 79(5): 707-718.
- Xin, L., Hong-Ying, H. and Yu-Ping, Z. 2011. Growth and lipid accumulation properties of a freshwater microalga *Scenedesmus* sp. under different cultivation temperatures. *Bioresour. Technol.*, 102(3): 3098-3102.
- Zaimes, G.G. and Khanna, V. 2013. Environmental sustainability of emerging algal biofuels: A comparative life cycle evaluation of algal biodiesel and renewable diesel. *Environ. Prog. Sustain. Energy*, 32(4): 926-936.





# Effect of Greening Trees on Thermal Comfort of the Pedestrian Streets in Hot Summer and Cold Winter Regions in China

L. S. Cao\*, H. Xu†\* and H. Li\*

\*School of Geography, Geomatics and Planning, Jiangsu Normal University, Xuzhou, China

†Corresponding author: H. Xu; 6020180133@jsnu.edu.cn

Nat. Env. & Poll. Tech.  
Website: [www.neptjournal.com](http://www.neptjournal.com)

Received: 26-11-2021

Revised: 24-01-2022

Accepted: 10-02-2022

## Key Words:

Thermal comfort  
Pedestrian street  
Green coverage  
ENVI-met

## ABSTRACT

The thermal environment problems of pedestrian streets space are becoming increasingly important with the growing rate of urbanization, especially in regions with hot summers and cold winters. Taking *Cinnamomum camphora* as an example, several urban design scenarios with dynamic setting parameters of streets orientation (N-S, E-W), aspect ratio (0.5, 1, 1.5, 2) are simulated by ENVI-met to analyze the impact of the green coverage on the thermal comfort of the street canyons in Shanghai. Results showed that: (1) green coverage has an impact on the thermal comfort of the street both in summer and winter and the significance of this effect is affected by the orientation and aspect ratio of the streets. (2) In summer, with the increase in aspect ratio, N-S orientation streets need more and more green coverage to bring a significant impact on thermal comfort, while E-W orientation streets only need 24 % green coverage. (3) In winter, with the increase in aspect ratio, N-S orientation streets also need more green coverage to significantly reduce thermal comfort. For E-W orientation, only when the aspect ratio is 1/2, the green coverage can effectively reduce the thermal comfort of the street. (4) The planting layout had no significant effect on the thermal comfort effect of trees. Based on the above conclusions, the greening strategy was proposed for pedestrian streets in the hot summer and cold winter region in China.

## INTRODUCTION

The thermal comfort of urban street space is related to people's comfortable experience of outdoor activities (Lee et al. 2018, Zhu et al. 2020). This is particularly evident in the pedestrian street space, because people are not just for traffic, but will stay, talk and hang out on foot, which will prolong people's stay time in the pedestrian street.

The thermal comfort of street space has been widely discussed by many scholars. Yahia & Johansson (2014) discussed the advantages and disadvantages of different urban design patterns in Damascus and argue that efficient use of vegetation positively affects the thermal environment. Deng et al. (2016) found that deep street canyons with higher aspect ratios reduce solar access and air temperature. In a study conducted by Rodriguez Algeciras et al. (2016), to achieve acceptable thermal comfort in the summer and winter seasons, the value for this design factor (aspect ratio) was suggested as 1 and 1.5. Achour-Younsi & Kharrat (2016) discussed the impact of the geometry of an urban street canyon on outdoor thermal comfort and found that the deepest streets are the most comfortable. Abdollahzadeh & Boloria (2021) evaluated the thermal performance of streets in residential zones of Liverpool, NSW, Australia, and found

that street canyon orientation is the most influential factor, followed by aspect ratio.

Landscape elements such as trees, waterscapes, and shading facilities play a positive effect on the regulation of thermal comfort (Soares et al. 2021, Zhao & Fong 2017). However, research mainly focuses on the influence of street space morphology (e.g., orientation, aspect ratio, sky view factor, and surface conditions) at the present stage, ignoring the role of streetscape (Li et al. 2020). The spatial morphology of the street is more stable and difficult to be changed, but the streetscape can be easily modified (Yang et al. 2018). Moreover, these studies mainly focus on the summer season, and there is a lack of studies that take into account both summer and winter. Therefore, the study of the influence of street landscapes on thermal comfort in different seasons should be taken seriously.

Table 1 shows the relationship between the values of PET and heat feeling. The thermal comfort model is divided into an eight-point scale by combining physiological parameters and environmental parameters. Based on the human body's energy balance, PET is matched to the human biometeorological evaluation of the thermal component in each different climate. According to the literature reviewed, although PET

is not proposed for the climate in China, it can still be an effective evaluation index for thermal comfort in China. In China's cold (Lai et al. 2014), hot summer and cold winter (Rupp et al. 2015), and hot summer and warm winter (Li et al. 2016) climate zone, PET has been proven to be applicable.

Shanghai is located in the hot summer and cold winter climate region in China. As the economic center of China, it has a wide variety of pedestrian streets. Tree planting patterns in pedestrian streets are more diverse, but the effect of trees on thermal comfort in pedestrian streets is unclear. In this study, we will use ENVI-met as a simulation tool to explore the impact of greening trees on the thermal comfort of pedestrian streets (Hu et al. 2021). The objectives of this study are to (1) explore the influence of green coverage on the thermal comfort of pedestrian streets in summer and winter under different street orientations and aspect ratio conditions. (2) Analyze the influence of planting layout on the thermal comfort effect of trees. (3) Propose the landscape greening strategy for pedestrian streets.

## MATERIALS AND METHODS

### Study Area

Shanghai is located in the east of China at a longitude between 120.5°E and 122.1°E and latitude between 30.4°N and 31.5°N. In summer, the average daytime air temperature is 26°C and the mean relative humidity is 77%. The mean wind speed is 3.2 m.s<sup>-1</sup> and the primary wind direction is southeast. In winter, the average daytime air temperature is 18°C and the mean relative humidity is 65%. The mean wind speed is 3.0 m.s<sup>-1</sup> and the primary wind direction is northwest. July and January are the hottest and coldest months respectively in Shanghai.

### Construction of Simulation Models

#### Tree model

Table 1: PET value and thermal perception.

PET(°C)	Human Subjective Comfort Feeling
<4	Very Cold
4-8	Cold
8-13	Cool
13-18	Slightly Cool
19-23	Neutral
23-29	Slightly Warm
29-35	Warm
35-41	Hot
>41	Very Hot

Leaf Area Index (LAI) can describe an area or a plant's overall degree of lushness (Cao et al. 2021). Changes in the LAI can contrast different degrees of greening. LAD is defined as the ratio of the total leaf area to the unit volume in different levels of the canopy. LAD can describe the leaf density and the distribution of a plant (Ng et al. 2012). Where the LAD is 0, it means the trunk is in this area.

$$LAI = \int_0^H LAD \cdot \Delta h \quad (1)$$

Where H (m), Height of the vegetation;  $\Delta h$  (m), Vertical Grid Size; LAI, Leaf Area Index; LAD (m<sup>2</sup>.m<sup>-3</sup>), Leaf Area Density

In this study, the evergreen tree species *Cinnamomum camphora* (L.) Presl., which is widely grown in Shanghai, was modeled. The tree's height of 10 m was ideal for the Shanghai street's urban design pattern. According to the measurement results of Gao et al. (2010), the LAI value of *Cinnamomum camphora* was set to 3.8 both in summer and winter. The vertical grid size was set to 1m and the LAD value (from top to bottom) of the model is calculated according to Eq. (1), as shown in Fig. 1. The remaining conditions adopt the default values of the system.

#### Street Model

The setting of the aspect ratio of streets refers to the actual size of Shanghai pedestrian streets and related architectural design guidelines (Abdollahzadeh & Biloria 2021). The width is set to 18 m, and the building models on both sides of the street are established according to four aspect ratios (0.5, 1, 1.5, 2) (Fig. 2). The length of the street is set to 60 m. The green coverage of streets was estimated by the ratio of the vertical projection area of the tree crown to the street area. Increase the green coverage with a gradient of 12% (4 trees) based on a blank street (Fig. 3). To simplify the experimental process, this study only modeled the streets in the east-west (E-W) and north-south (N-S) orientations.

#### Simulation by ENVI-Met

A model domain with a 60 × 60 × 30 grid version was applied in the simulations. The grid sizes for the site were set to be 2 m. In addition, 10 nesting grids were added around the model to improve simulation accuracy (Yang et al. 2020). The simulation was carried out on the 15th of July since this day is more or less in the middle of the three hottest months in summer, and the day 15th of January was studied to represent the winter season because it is in the middle of the three coldest months. The simulated period lasted from 9:00 local time (LT) in the morning until 16:00 LT in the afternoon including the time period with obvious sunshine. The main parameters used in the summer and winter simulations are shown in Table 2.



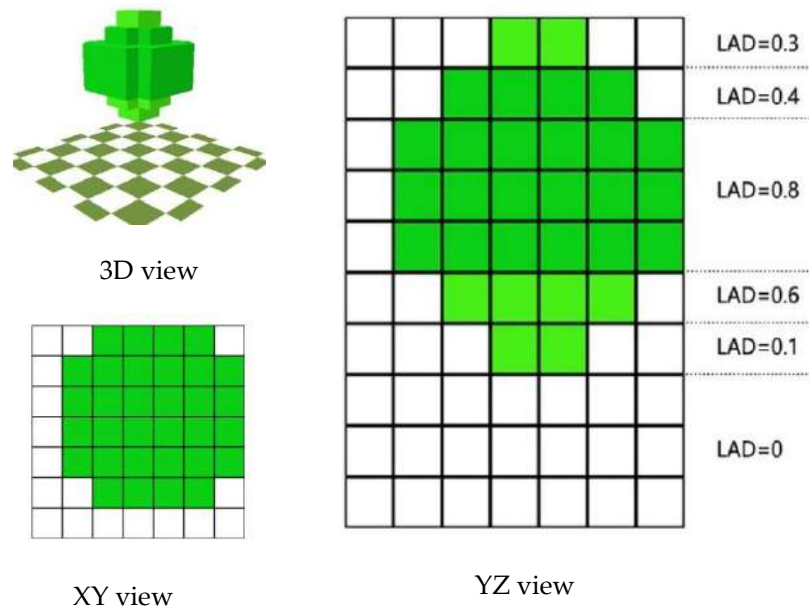


Fig. 1: Description of the tree model.

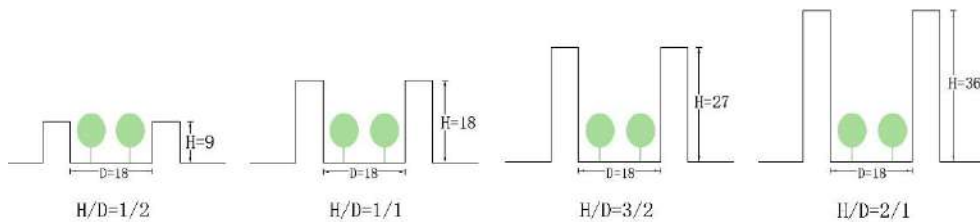


Fig. 2: Description of the aspect ratio of the street(m).

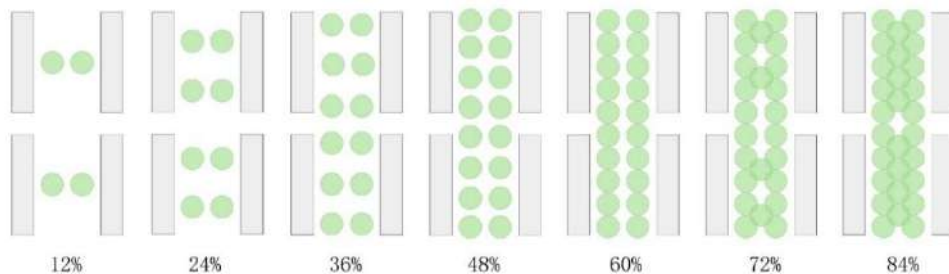


Fig. 3: Planting layout of the tree and its corresponding green coverage.

## RESULTS

### Effect of Green Coverage on PET in Summer

#### Characterization of PET

Fig. 4 shows the relationship between green coverage and the PET means (9:00-16:00) of the streets in summer. It can be found that as the green coverage increases, the PET values of the streets all tend to decrease, and this trend tends to level

off after the green coverage reaches 60%. The PET values of E-W orientation street are higher than that of N-S orientation street under the same green coverage, and the gap between the two increases with the increase of street aspect ratio.

With the increase of the aspect ratio, the influence of the green coverage on the PET becomes smaller, which is particularly obvious in the N-S orientation street. With the increase of green coverage, the standard deviation of

Table 2: Main parameters input in the ENVI-met.

Simulation Parameters	Summer	Winter
Day	15 July	15 Jan
Time	9:00-16:00	9:00-16:00
Roughness length	0.1	0.1
Simple forcing: air temperature (K)	Min 298 at 6:00; max 305 at 16:00	Min 276 at 6:00; max 282 at 16:00
Simple forcing: relative humidity (%)	Min 70 at 16:00; max 85 at 6:00	Min 60 at 16:00; max 75 at 6:00
Wind speed at 10 m above ground level (m.s <sup>-1</sup> )	3.2	3.0
Wind direction (°)	135	315
Cloud cover	0	0
Materials of buildings and roads	Default settings in ENVI-met	Default settings in ENVI-met
Clothing parameters	0.3	0.9
Body parameters	Default settings in Biomet	Default settings in Biomet

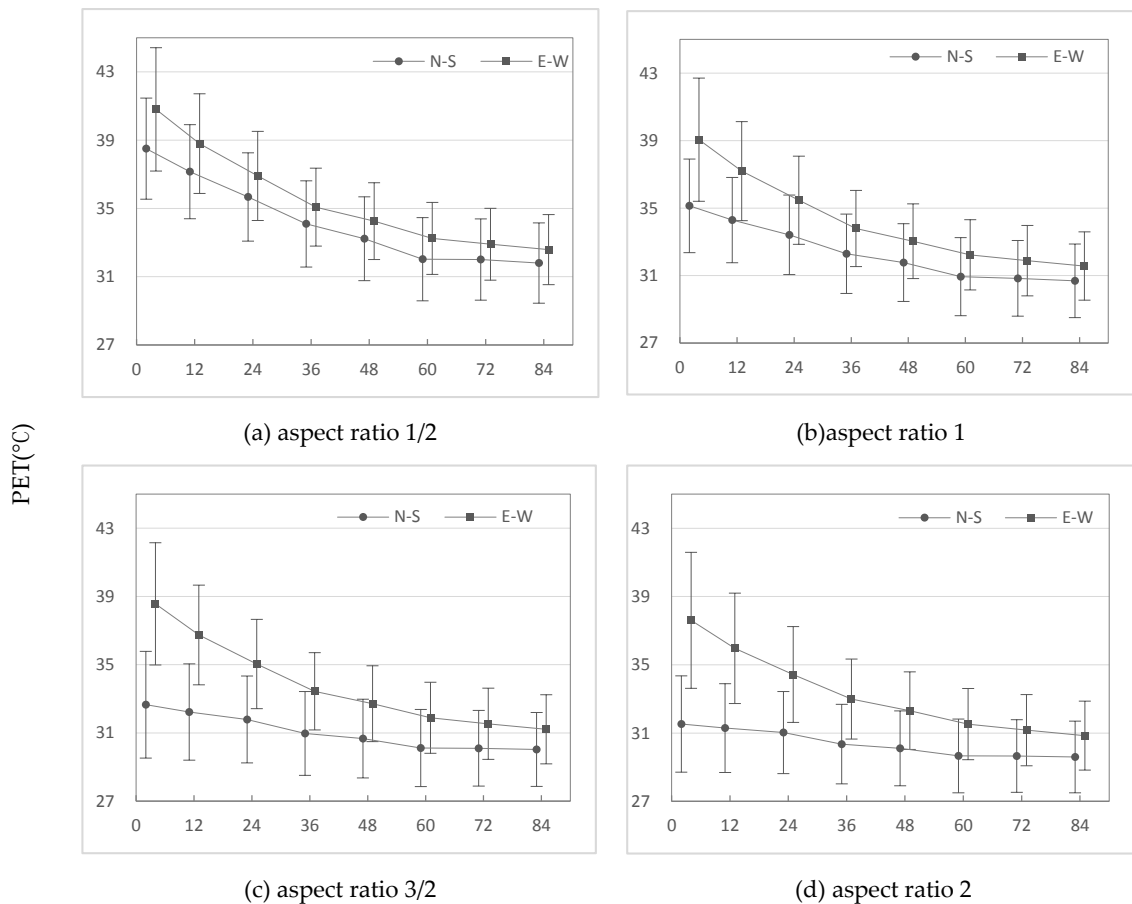


Fig. 4: Mean (9:00-16:00) and standard deviation of PET in summer.

PET values decreases, indicating that green coverage could stabilize thermal comfort in the daytime.

**Difference Analysis of PET Means**

The single-sample T-test method was used to analyze the differences in PET means between green streets and blank streets. The results are shown in Table 3. For the N-S orientation, with the increase in aspect ratio, more and more

green coverage is needed to significantly reduce the PET means of the street. For the E-W orientation, regardless of the aspect ratio, 24% green coverage can significantly reduce the PET mean of the street. It can be seen that green coverage has more influence on the thermal comfort of the E-W orientation streets.

### The Impact of Green Coverage on PET at Different Time Points

To analyze the difference in green coverage on PET at different time points, taking Table 1 as a standard, mark the greening coverage corresponding to the PET grade difference (relative to the blank street) at each time point. The results are shown in Figs. 5-6.

With the increase of aspect ratio, the time points that PET values have grade difference become less. Relatively speaking, the number of impacted time points in N-S orientation streets is less than in E-W

orientation streets, which is consistent with the previous results.

For the N-S orientation, when the aspect ratio is less than or equal to 1, almost all time points will be affected effectively. When the aspect ratio is 3/2, only the PET values at 10:00, 13:00, and 14:00 are effectively affected. And when the aspect ratio reaches 2, only the thermal comfort at 10:00 is upgraded. For the E-W orientation, regardless of the aspect ratio, the thermal comfort of most time points has been improved. As the aspect ratio increases, green coverage has little effect on thermal comfort between 11:00 and 13:00.

### Effect of Green Coverage on PET in Winter

#### Characterization of PET

Fig. 7 shows the relationship between green coverage and the PET means (9:00-16:00) of the street in winter. Although there is still a downward trend in the PET values with the increase of green coverage, this effect is relatively weaker

Table 3: The results of the single-sample T-test between green streets and blank streets.

Aspect ratio	Orientation	Green coverage						
		12%	24%	36%	48%	60%	72%	84%
1/2	N-S	.208	.017*	.002**	.001**	.000**	.000**	.000**
	E-W	.094	.004**	.000**	.000**	.000**	.000**	.000**
1/1	N-S	.376	.077	.011*	.004**	.001**	.001**	.001**
	E-W	.117	.006**	.000**	.000**	.000**	.000**	.000**
3/2	N-S	.683	.371	.095	.046*	.016*	.014*	.011*
	E-W	.121	.007**	.000**	.000**	.000**	.000**	.000**
2/1	N-S	.796	.570	.193	.108	.044*	.041*	.035*
	E-W	.193	.015*	.001**	.000**	.000**	.000**	.000**

Note: \* Significance at the 0.05 level. \*\* Significance at the 0.01 level. The same is below.

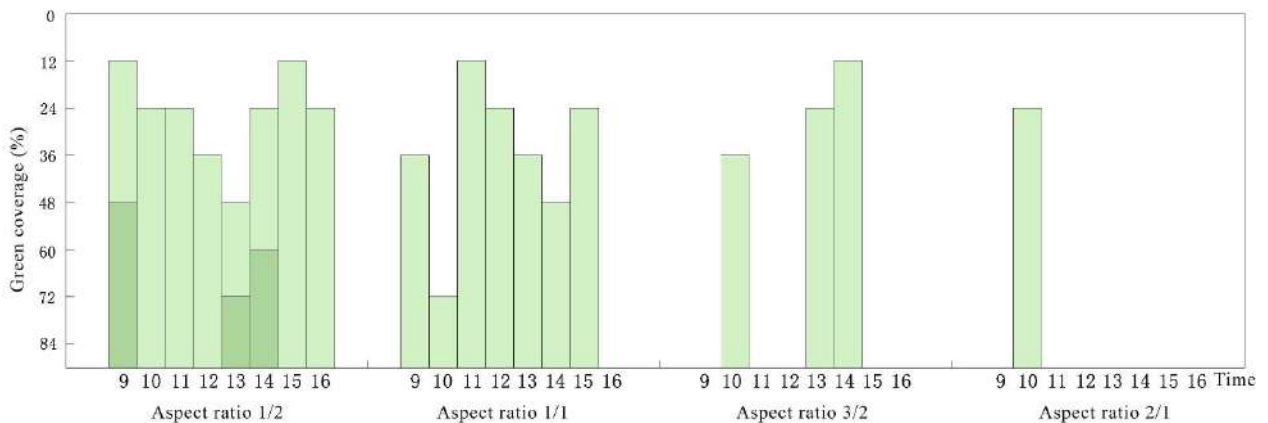


Fig. 5: The green coverage of N-S orientation streets when PET produces grade change.

Note: Light green: one-level difference; Dark green: two-level difference; Blank: no grade difference. The same is below.

than in summer and mainly affects the N-S orientation streets. Similarly, with the increase in aspect ratio, the impact of green coverage on thermal comfort is gradually weakened. For the E-W orientation, only when the aspect ratio is 1/2, the green coverage has an effective impact on the PET values. In addition, with the increase of green coverage, the standard deviation of PET values decreases. It can be seen that the green coverage also makes the thermal comfort of streets tend to be stable in winter.

**Difference Analysis of PET Means**

Table 4 shows the differences in PET means between green streets and blank streets. For the N-S orientation, when the aspect ratio is 1/2, starting with 24 % green coverage, the PET means can be significantly reduced. After the aspect ratio reaches 1, 36% green coverage is needed to make the PET mean decrease significantly. For the E-W orientation, only the street with an aspect ratio of 1/2 has a significant difference in PET mean starting from 24% green coverage. For streets with other aspect ratios, the green coverage does

not have a significant impact on the thermal comfort of the streets.

**The Impact of Green Coverage on PET at Different Time Points**

Fig.8-9 shows the greening coverage corresponding to the PET grade difference (relative to the blank street) at each time point. In contrast to summer, the green coverage of N-S orientation streets has a greater influence on thermal comfort than N-S orientation streets in winter. The thermal comfort of the majority of time points has decreased when the aspect ratio is 1/2. The green coverage no longer significantly affects thermal comfort after the aspect ratio reaches 1 except between 10:00 and 14:00.

**The Impact of Planting Layout Factors on PET**

Whether the planting layout of trees has an impact on their thermal comfort effect? To make clear it, we took the street with an aspect ratio of 1/2 and 36 % green coverage as an example and summarized four planting layouts based on on-

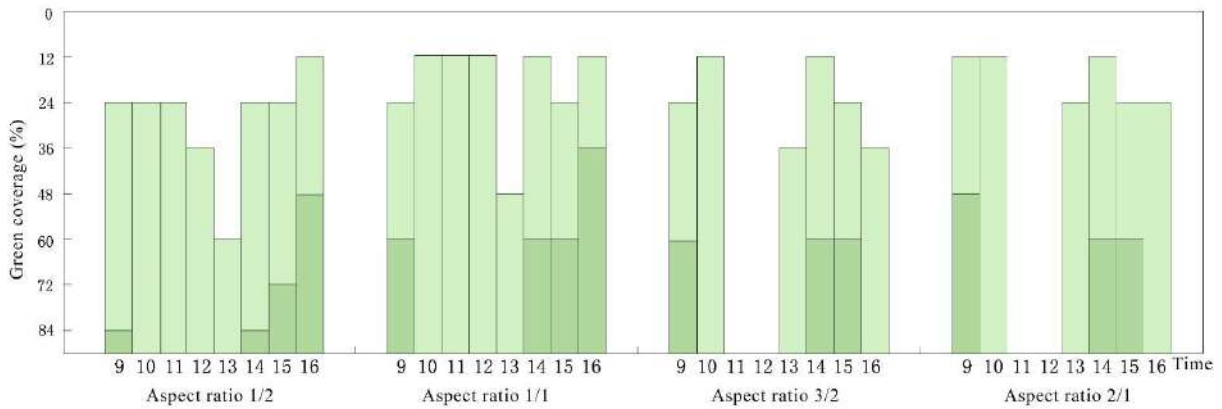


Fig. 6: The green coverage of E-W orientation streets when PET produces grade change.

Table 4: The results of the single-sample T-test between green streets and blank streets.

Aspect ratio	Orientation	Green coverage						
		12%	24%	36%	48%	60%	72%	84%
1/2	N-S	.061	.005**	.000**	.000**	.000**	.000**	.000**
	E-W	.278	.023*	.000**	.000**	.000**	.000**	.000**
1/1	N-S	.541	.151	.013*	.002**	.000**	.000**	.000**
	E-W	.451	.406	.493	.698	.587	.789	.891
3/2	N-S	.630	.205	.028*	.003**	.000**	.000**	.000**
	E-W	.530	.526	.742	.465	.277	.386	.439
2/1	N-S	.671	.239	.033*	.003**	.000**	.000**	.000**
	E-W	.570	.619	.877	.368	.191	.255	.292

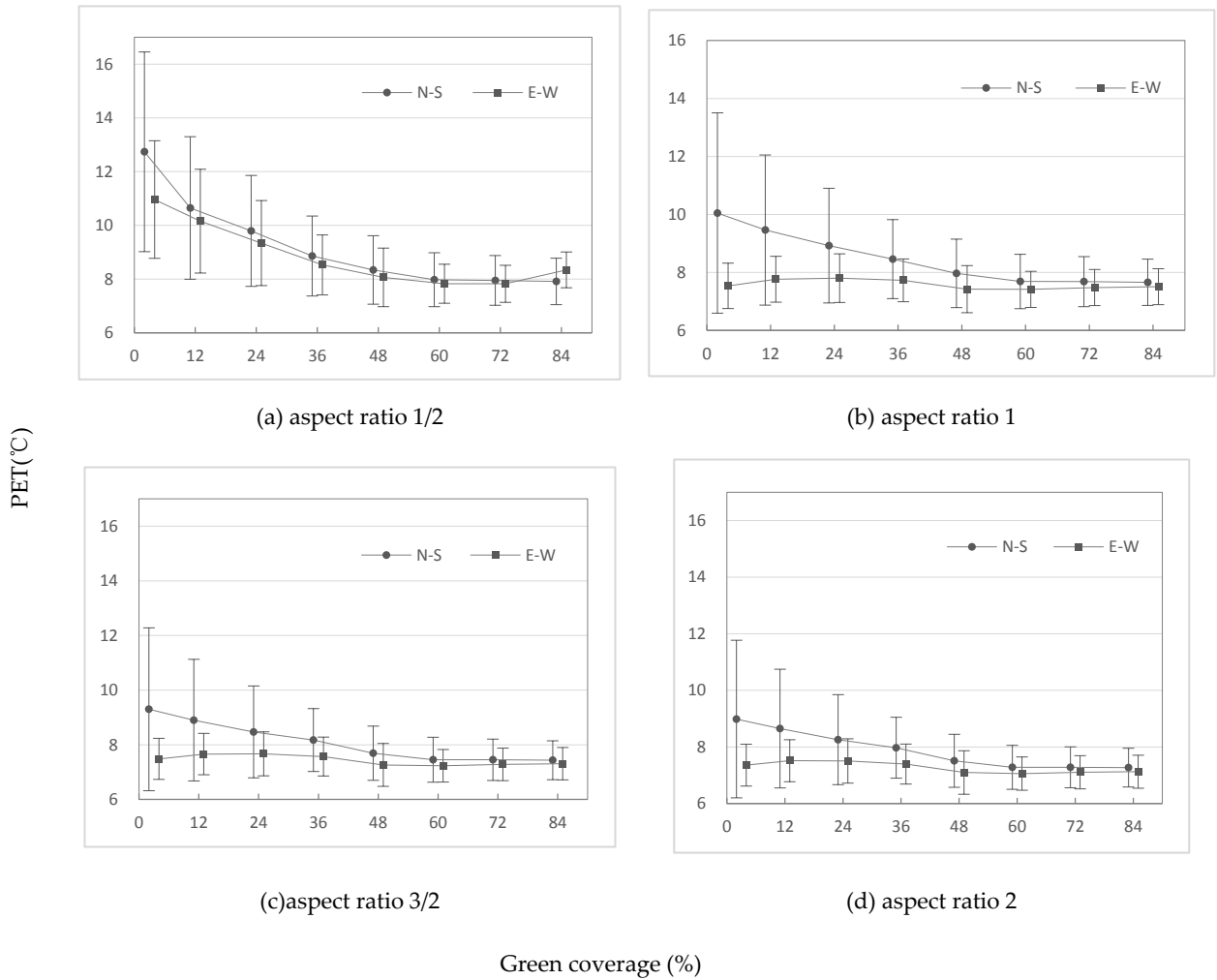


Fig. 7: Mean (9:00-16:00) and standard deviation of PET in winter.

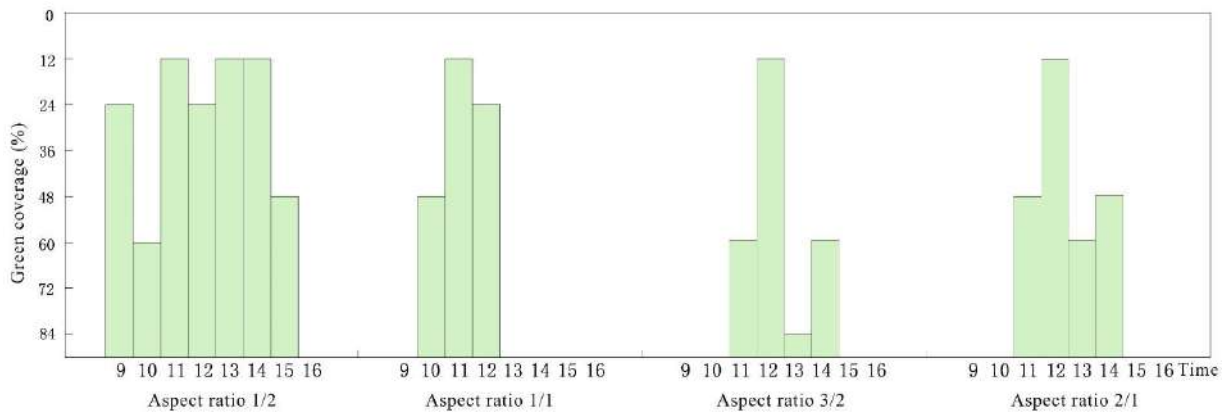


Fig. 8: The green coverage of N-S orientation streets when PET produces grade change.

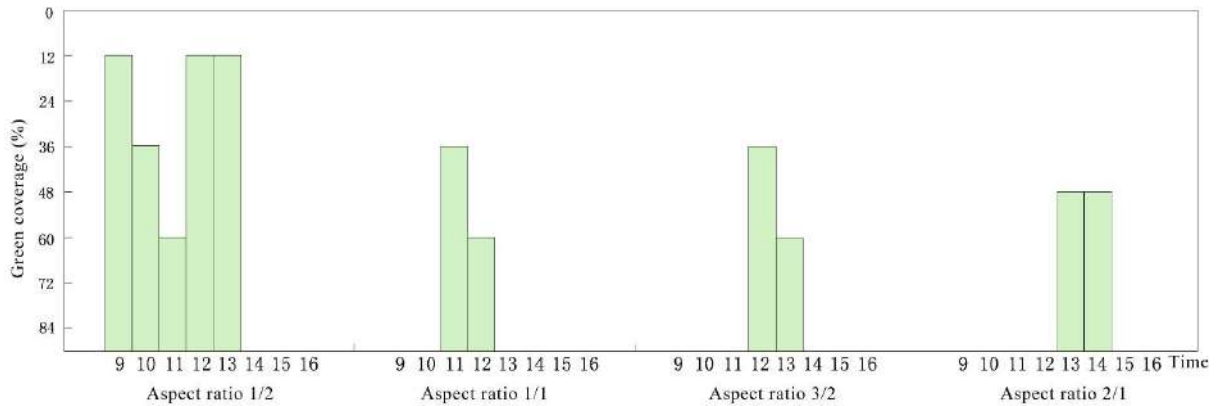


Fig. 9: The green coverage of E-W orientation streets when PET produces grade change.

site investigations on pedestrian streets (Fig. 10). The PET values of these four cases in different street orientations and seasons were simulated and calculated. Single-factor ANOVA analysis is used to analyze the difference in calculation results. The results are shown in Fig.11.

Fig. 11 shows that regardless of the street orientations and season, planting layouts cannot bring about significant differences in the thermal comfort effects of trees. For N-S orientation, in both summer and winter, the ‘two-group’ planting layout results in the highest PET values for the street, and the ‘two-row-middle’ planting layout results in the lowest PET values. For E-W orientation, in both summer and winter, the ‘two rows side planting layout can make the street more suitable. But it should be pointed out that these differences are not significant.

**DISCUSSION**

*Effect of Green Coverage on Thermal Comfort of Streets*

The study found that tree greening has a positive impact on

the thermal comfort of the street in summer, and a negative impact in winter. However, the significance of this effect is affected by the orientation and aspect ratio of the street.

In summer, tree greening has less influence on thermal comfort in N-S orientation streets than in E-W orientation streets. with the increase in aspect ratio, the N-S orientation streets need more and more green coverage is needed to significantly improve the thermal comfort of the street, while E-W orientation streets only need 24 % green coverage. For the N-S orientation, building shadows on both sides can affect the thermal comfort of the street. For the E-W orientation, only the shadows of the building on the south side can affect the thermal comfort of the street. This is the main reason why the N-S orientation streets can provide better thermal comfort (Srivanit & Jareemit 2020). However, more building shadows cover trees, which weakens the blocking effect of trees on light, resulting in a reduction in the plant’s regulation of thermal comfort(Zheng et al. 2020). That’s why the influence of trees in N-S orientation streets is weaker than that in E-W orientation streets. Similarly, with the increase

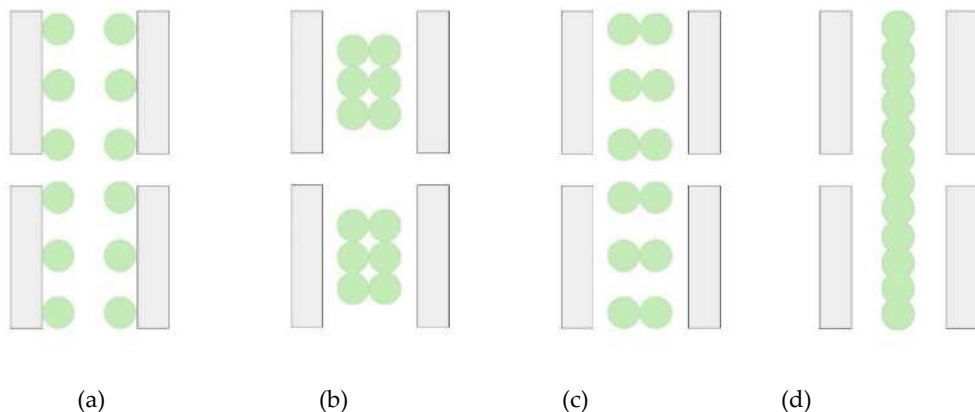


Fig. 10: Four planting layouts of trees: (a) two rows-side; (b) two groups; (c) two rows-middle; (d) one row-middle

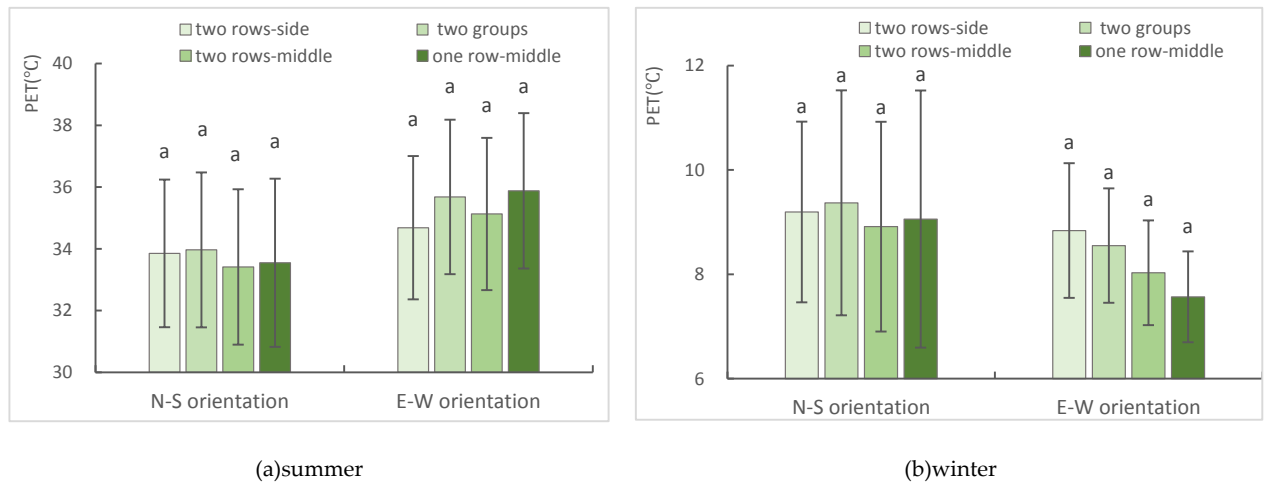


Fig. 11: Difference in thermal comfort effect of four planting layouts.

of the aspect ratio, the shadow range of buildings on both sides of N-S orientation streets expands, and more trees are covered by building shadows. Therefore, more trees are needed to effectively regulate the thermal comfort of the street. In contrast, the building shadow range on the E-W orientation streets changes little. No matter what the aspect ratio is, 24 % of the green coverage can effectively improve thermal comfort.

On the contrary, in winter, tree greening has a bigger influence on thermal comfort in N-S orientation streets than in E-W orientation streets. This is also because of the impact of building shadows on trees. In winter, the direct angle of sunlight becomes smaller, resulting in a larger shadow range of the building. The shadow of the building on the south side of E-W orientation streets easily covers the whole street. That's why for E-W orientation, green coverage can only effectively improve the thermal comfort of streets with an aspect ratio of 1/2. For S-W orientation, although the shadow range of buildings is also expanded in winter, the streets have sufficient light at noon (11:00-14:00), and trees can effectively reduce the thermal comfort of this time period.

In addition, the study found that the planting layout had no significant effect on the thermal comfort effect of trees. The shading effect of the canopy is the main reason trees regulate thermal comfort (Chen et al. 2021, Speak et al. 2021). However, different planting layouts will not have a significant impact on the shade range of trees under the condition of a certain number of trees. So there is no significant difference in the thermal comfort effect brought by different tree planting layouts.

### Greening Strategy for Pedestrian Streets

For the N-S orientation, to get a more suitable thermal

feeling in summer, the larger the aspect ratio of the street, the more trees need to be planted. The specific relationship between green coverage and aspect ratio can be referred to in Table 1. But inevitably, evergreen trees such as camphor trees also reduce the thermal comfort of streets in winter. Therefore, for the N-S orientation streets, planting deciduous trees is a more appropriate choice. This ensures that the thermal comfort of the streets in winter is not significantly reduced.

For the E-W orientation, in summer, when the green coverage reaches 24%, the thermal comfort of the street can be significantly improved. In winter, the green coverage has little effective impact on street thermal comfort (except for streets with an aspect ratio of 1/2). Therefore, for the sake of landscape effect, evergreen trees could be planted in E-W orientation streets.

In addition, the planting layout had no significant effect on the thermal comfort effect of trees. This suggests that we can design the planting layout of trees according to the landscape needs. At the same time, the green coverage of streets should be controlled by 60%.

### Limitations and Future Research

In this study, only one type of evergreen tree was considered, and the influence of tree morphology such as tree height, LAI, and crown shape on the results was not considered. Many studies have found that the morphological variables of trees have an important impact on their thermal comfort effect (Cao et al. 2020, Wai et al. 2021). Besides green trees, landscape elements such as shrubs, waterscape, and shading facilities can also influence thermal comfort (Liu et al. 2021), which can continue to be explored in future street thermal comfort studies.

## CONCLUSIONS

Taking Shanghai as an example, we used ENVI-met to simulate the impact of green coverage on the thermal comfort of pedestrian streets in summer and winter. Results showed that green coverage has an impact on the thermal comfort of the street both in summer and winter, and the significance of this effect is affected by the orientation and aspect ratio of the street. Overall, the PET value of the street decreases as the green cover increases. In summer, green coverage has more influence on thermal comfort in E-W orientation streets. With the increase in aspect ratio, N-S orientation streets need more and more green coverage to bring a significant impact on thermal comfort, while E-W orientation streets only need 24 % green coverage. Inversely, in winter, green coverage has a greater impact on thermal comfort in N-S orientation streets. With the increase in aspect ratio, N-S orientation streets need more green coverage to significantly reduce thermal comfort. For E-W orientation, only when the aspect ratio is 1/2, the green coverage can effectively reduce the thermal comfort of the street. The study also found that the planting layout had no significant effect on the thermal comfort effect of trees. Based on the above conclusions, the greening strategy was proposed for pedestrian streets in hot summer and cold winter regions in China.

## ACKNOWLEDGEMENTS

This research was funded by The Natural Science Foundation of the Jiangsu Higher Education Institutions of China (No. 21KJJD220002), The Ministry of Education, Humanities and Social Science Youth Fund Projects (No. 20YJC760112) and A Project Funded by the Priority Academic Program Development of Jiangsu Higher Education Institutions (PAPD).

## REFERENCES

- Abdollahzadeh, N. and Bilorina, N. 2021. Outdoor thermal comfort: Analyzing the impact of urban configurations on the thermal performance of street canyons in the humid subtropical climate of Sydney. *Frontiers of Architectural Research.*, 10 (2): 394-409.
- Achour-Younsi, S. and Kharrat, F. 2016. Outdoor Thermal Comfort: Impact of the geometry of an urban street canyon in a Mediterranean Subtropical Climate: Case Study Tunis, Tunisia. *Procedia - Social and Behavioral Sciences.*, 216: 689-700.
- Cao, L., Xu, H. and Li, H. 2020. Research on Residential Landscape Design Based on Microclimate Effect. *Construct. Sci. Technol.*, (22): 84-88.
- Cao, L., Xu, H. and Li, H. 2021. Numerical Simulation of the Influence of Landscape Plants on Human Thermal Comfort in Cold Season in Nanjing City. *J. Northwest Frest. Univ.*, 36(05): 238-245.
- Chen, T., Pan, H., Lu, M., Hang, J., Lam, C.K.C., Yuan, C. and Pearlmuter, D. 2021. Effects of tree plantings and aspect ratios on pedestrian visual and thermal comfort using scaled outdoor experiments. *Sci. Total Environ.*, 801: 149527.
- Deng, J., Wong, N.H. and Zheng, X. 2016. The study of the effects of building arrangement on microclimate and energy demand of CBD in Nanjing, China. *Procedia Eng.*, 169: 44-54.
- Gao, K., Qin, J. and Hu, Y. 2010. Correlation of leaf area index and morphological features for main evergreen broadleaf tree species in Shanghai City. *J. Central South Univ. Forest. Technol.*, 30 (10): 34-40.
- Hu, X., Yang, J., Feng, H. and Marvin, S. 2021. Verifying an ENVI-met simulation of the thermal environment of Yanzhong Square Park in Shanghai. *Urban for Urban Gree: 127384.*
- Lai, D., Guo, D., Hou, Y., Lin, C. and Chen, Q. 2014. Studies of outdoor thermal comfort in northern China. *Build Environ.*, 77: 110-118.
- Lee, S., Moon, H., Choi, Y. and Yoon, D.K. 2018. Analyzing Thermal Characteristics of Urban Streets Using a Thermal Imaging Camera: A Case Study on Commercial Streets in Seoul, Korea. *Sustainability-Basel.*, 10 (2).
- Li, G., Ren, Z. and Zhan, C. 2020. Sky View factor-based correlation of landscape morphology and the thermal environment of street canyons: A case study of Harbin, China. *Build Environ.*, 169: 106587.
- Li, K., Zhang, Y. and Zhao, L. 2016. Outdoor thermal comfort and activities in the urban residential community in a humid subtropical area of China. *Energy Build.*, 133: 498-511.
- Liu, S., Zhao, D.J., Xu, M. and Ahmadian, E. 2021. Effects of landscape patterns on the summer microclimate and human comfort in urban squares in China. *Sustain Cities Soc.*, 73: 103099.
- Ng, E., Chen, L., Wang, Y. and Yuan, C. 2012. A study on the cooling effects of greening in a high-density city: An experience from Hong Kong. *Build Environ.*, 47(1): 256-271.
- Rodriguez Algeciras, J.A., Gomez Consuegra, L. and Matzarakis, A. 2016. Spatial-temporal study on the effects of urban street configurations on human thermal comfort in the world heritage city of Camagüey-Cuba. *Build Environ.*, 101: 85-101.
- Rupp, R.F., Vásquez, N.G. and Lamberts, R. 2015. A review of human thermal comfort in the built environment. *Energy Build.*, 105: 178-205.
- Soares, R., Corvacho, H. and Alves, F. 2021. Summer thermal conditions in outdoor public spaces: A case study in a Mediterranean climate. *Sustainability*, 13(10): 5348.
- Speak, A., Montagnani, L., Wellstein, C. and Zerbe, S. 2021. Forehead temperatures as an indicator of outdoor thermal comfort and the influence of tree shade. *Urban Climate*, 39: 100965.
- Srivani, M. and Jareemit, D. 2020. Modeling the influences of layouts of residential townhouses and tree-planting patterns on outdoor thermal comfort in Bangkok suburbs. *J. Build. Eng.*, 30: 101262.
- Wai, K., Xiao, L. and Tan, T.Z. 2021. Improvement of the outdoor thermal comfort by water spraying in a high-density urban environment under the influence of a future (2050) climate. *Sustainability*, 13(14): 7811.
- Yahia, M.W. and Johansson, E. 2014. Landscape interventions in improving thermal comfort in the hot dry city of Damascus, Syria: The example of residential spaces with detached buildings. *Landsc. Urban Plan.*, 125: 1-16.
- Yang, S., Zhou, D., Wang, Y. and Li, P. 2020. Comparing the impact of multi-factor planning layouts in residential areas on summer thermal comfort based on the orthogonal design of experiments (ODOE). *Build Environ.*, 182: 107145.
- Yang, Y., Zhou, D., Gao, W., Zhang, Z., Chen, W. and Peng, W. 2018. Simulation on the impacts of the street tree pattern on built summer thermal comfort in a cold region of China. *Sustain Cities Soc.*, 37: 563-580.
- Zhao, T.F. and Fong, K.F. 2017. Characterization of different heat mitigation strategies in the landscape to fight against heat islands and improve thermal comfort in a hot-humid climate (Part I): Measurement and modeling. *Sustain. Cities Soc.*, 32: 523-531.
- Zheng, S., Guldmann, J., Liu, Z., Zhao, L., Wang, J. and Pan, X. 2020. Modeling of shade creation and radiation modification by four tree species in hot and humid areas: A case study of Guangzhou, China. *Urban Green.*, 47: 126545.
- Zhu, Z., Liang, J., Sun, C. and Han, Y. 2020. Summer outdoor thermal comfort in urban commercial pedestrian streets in severe cold regions of China. *Sustainability*, 12 (5): 151.





# A Review on Atmospheric Dispersion System for Air Pollutants Integrated with GIS in Urban Environment

Namrata\*† and N. D. Wagh\*\*

\*School of Applied Sciences, Amity University, Mumbai-410206, India

\*\*Department of Environment Science, School of Applied Sciences, Amity University, Mumbai-410206, India

†Corresponding author: Namrata; namrata.kislay@gmail.com

Nat. Env. & Poll. Tech.  
Website: [www.neptjournal.com](http://www.neptjournal.com)

Received: 28-11-2021  
Revised: 15-02-2022  
Accepted: 22-02-2022

## Key Words:

Air Pollution  
GIS  
Modelling  
Pollutant dispersion  
Turbulence

## ABSTRACT

The objective of this article is to present comprehensive findings and analysis of studies performed on air pollutant dispersion in urban environments. It captures India's rising environmental pollution due to urbanization, industrialization, and population growth. Dispersion of pollutants due to the wind in the lower Atmospheric Boundary Layer (ABL) is a major concern nowadays. The dispersion field around the buildings is a critical parameter to analyze and it primarily depends on the correct simulation of the wind flow structure. Therefore, studies performed on this in past years are being reviewed. Additionally, a brief review of different air dispersion models that are integrated with the Geographic Information System (GIS) has been studied in this article to assess the exposure. The results of these studies provide the urban air dispersion model aligning to three sub-models i.e., Emission, Weather Prediction, and Dispersion models. Various factors like wind speed, wind direction, cloud cover, traffic emission, disposal of waste, transportation, and others are considered. This study also captures the problems and risks being faced while creating a model, and its possible mitigation approaches.

## INTRODUCTION

Ambient air pollution is estimated to cause 7 million deaths per year (WHO 2018). Air pollution has been linked to a variety of health problems according to several epidemiological reports. Several studies since March 2020 have also revealed that COVID-19 development was substantially higher in cities or regions where certain air contaminants were detected at comparatively higher levels and are the main cause of traffic and industrial pollution (Domingo et al. 2020).

In 2010, the Central Pollution Control Board (CPCB) created the Comprehensive Environmental Pollution Index (CEPI), a system for measuring air, water, and soil pollution in the country's industrial clusters. In collaboration with the Ministry of Environment and Forestry, CPCB established 43 critically polluted CEPI-based industrial clusters after reviewing the environmental conditions in 88 industrial clusters across India (CPCB 2016). Contributions to vehicle emissions are primarily urban (on-road), but rural areas can also be affected by off-road agricultural sources (Guttikunda et al. 2014). Emissions of primary particulate from residential combustion sectors are more common in rural and low-income urban areas, where people depend more on traditional biomass for cooking and heating.

The 2014 Intergovernmental Panel on Climate Change (IPCC) reveals that the total emission of greenhouse gases from 1970 to 2010 increased by 78% from manufacturing processes and fossil fuel combustion. Since the 1970s, CO<sub>2</sub> emissions have more than doubled, and have risen by 40% since 2000. Even though CO<sub>2</sub> emissions remained stable from 2013 to 2016, they increased by 1.5% in 2017 and are continuing to rise, led by China, India, and the European countries (Anwar et al. 2020). Another major global concern is Polyaromatic Hydrocarbon (PAH) as it gets linked to PM<sub>2.5</sub> and ultrafine fractions of airborne particulates cause severe health risks (Mohanraj et al. 2011).

In urban areas, pollutant dissemination in the lower Atmospheric Boundary Layer (ABL) by the wind flows is a major concern. The dispersion of pollutants represents a very important environmental drawback with respect to human health. Depending on their chemical and physical properties (e.g., chemical structure, water solubility, etc.), these air pollutants may travel hundreds, even thousands of kilometers from their release worldwide.

To save human lives and reduce economic losses, computer models of air pollutant dispersion are being developed to explain and predict the result of such events and incidents.

The goal of the model-driven work represented during this paper is to develop a decision support system to cut back the impact of pollution caused by road traffic. Such a simulation coming up with a system consists of a comprehensive air-quality prediction model supported by data management, a mathematical model, and a friendly interface, integrated with GIS that uses spatial coordinates to explain the structure of urban areas, road networks, and waste product distribution within the atmosphere (Gualtieri & Tartaglia 1998). The use of a GIS integrated system is very common in research on a regional-local scale (Gulliver & Briggs 2011).

## ATMOSPHERIC BOUNDARY LAYER OVERVIEW

### Structure of Atmospheric boundary Layer and Turbulence

In meteorology, the lowest component of the atmosphere is the ABL, also known as the Planetary Boundary Layer (PBL), and its action is directly affected by its interaction with a planetary surface (Bonner et al. 2010). ABL can change both in space and time, depending on the orography. Also, it changes with surface cover, season, daytime, and weather (Gifford 1976). It experiences a daily cycle of changes in temperature, humidity, wind, and pollution variations in response to various fluxes in the air (Stull 2017).

Oke (1976) initially proposed a simple and two-layer model of the urban atmosphere, which recognizes the Urban Canopy Layer (UCL) and the Urban Boundary Layer (UBL) respectively. The first layer, called the Urban Canopy, consists of air in between the urban roughness elements (mainly building). The second layer, located directly above the first, is referred to as the urban boundary layer. This is the phenomenon that exists in local or mesoscale concepts (Oke 1976). A Roughness Sub-Layer (RSL) near the ground, also known as the Transition layer, and an Inertial Sub-Layer (ISL) above it make up this layer (Fisher et al. 2006).

The turbulence induces vertical mixing between horizontally moving air at one stage which is important in the dispersion of pollutants (Stull 2017). The ABL height is crucial in the dispersal of air pollution. The main environmental factors of urban turbulence are the roughness of the urban surface, buildings, trees, and other large structures (Roth 2000). There is a need of modelling the flow as a homogeneous flow essentially by well reproducing the turbulence profiles including the wind velocity profile (Cai et al. 2014). The relationship between wind speed and height is called the wind profile. It can be expressed as:

$$\frac{du}{dz} = \frac{u_*}{l} \quad \dots(1)$$

$u_*$  - the local friction velocity (proportional to the square root of the local Reynolds stress)

$l$  - the length scale (function of the state of the atmosphere and height)

Turbulent mixing in the atmosphere is induced by wind shear and buoyancy. Defining categories including radiation parameters, surface roughness, wind intensity, and cloud cover is an easy method for measuring turbulence parameters. Pasquill's commonly used approach describes six stability levels from the extremely unstable (6) to the relatively stable (1) based on wind direction, sunrise, and cloud cover (Turner 1997, Pasquill 1961) (Figs. 2 and 3).

**Fig. 2 & 3:** Pasquill stability class: unstable (1), slightly unstable (2), neutral (3), slightly stable (4), stable (5), and very stable (6) boundary layer. Neutral (3) class has been used for overcasting conditions and within one hour after sunrise/before sunset (Luna & Church 1972).

### Flow of Wind Around Buildings

Wind currents over buildings are inherently complicated, exhibiting a wide variety of physical phenomena such as

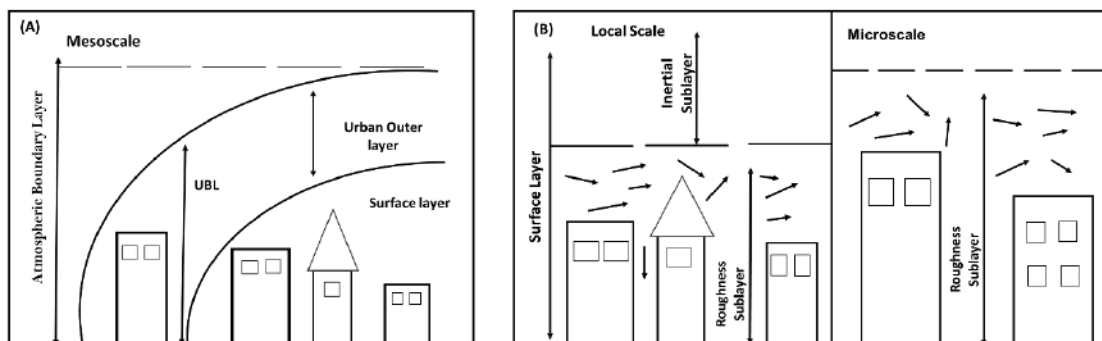


Fig. 1: Diagrammatic representation of the urban boundary-layer (A, B) (Adapted from Piringner et al. 2007).

high-pressure gradients, large low-speed fields, three-dimensional impacts, turbulent flow zones, and boundary layers (Deck 2005). It is obvious that proper modeling of pollutant dispersion within a group of buildings continues to be a very complex issue, as wind movement in a metropolitan environment can have significant effects on pollutant dispersion across buildings (Zhang et al. 2005). Moreover, the issue becomes more complicated due to the diversity and complexity of the mixture of emission sources, such as industries, automobiles, generators, domestic fuel combustion,

roadside dust, construction activities, etc. Therefore, a precise concentration forecast of contaminants released into the urban environment is needed to understand the mechanisms regulating the pollutants' dispersion (Tseng et al. 2006). Several methods along with GIS have been widely used to research the pollutant dispersion around urban buildings.

**GIS Overview**

A GIS is a computer application that captures, stores, analyzes, and displays data about locations on the Earth's

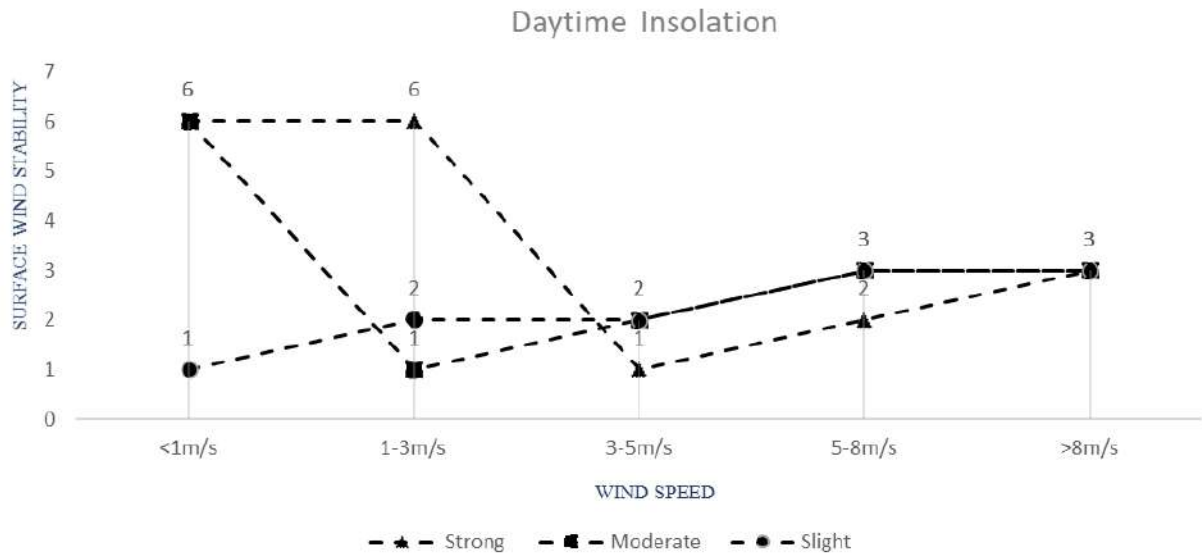


Fig. 2: Daytime insolation.

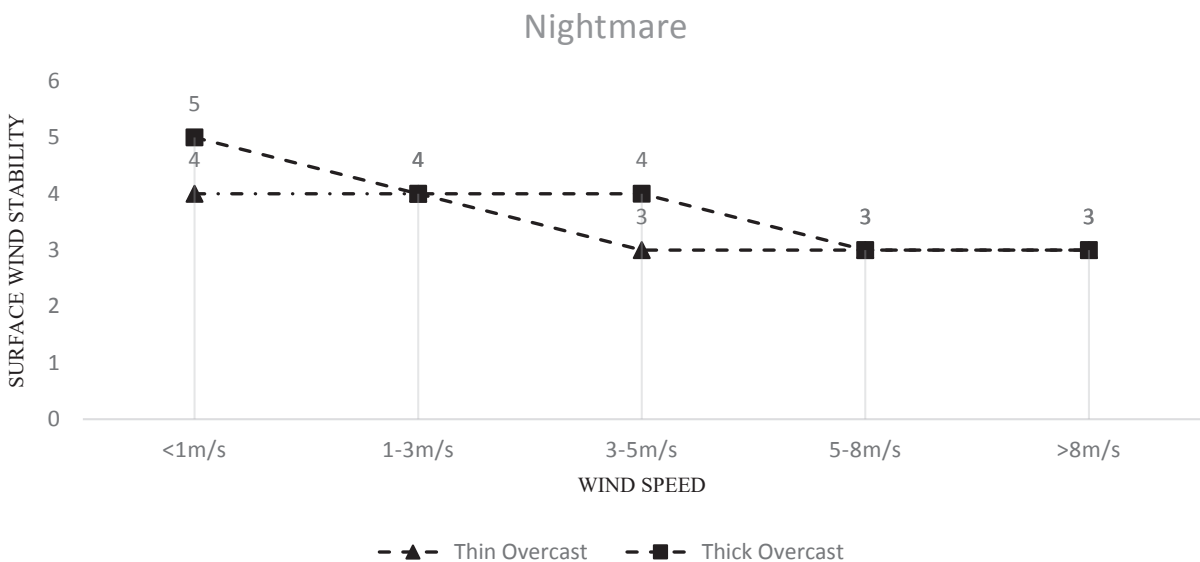


Fig. 3: Nightmare.

surface. It is a multi-layered approach to representing data from multiple sources and connecting spatial and non-spatial information. The analysis of spatial data and handling of massive spatial databases are the advantages of GIS over other information systems. There is a vast amount of data that can help deal with air pollution (Gualtieri & Tartaglia 1998).

## MODEL STRUCTURE

The GIS integrated air dispersion model consists of the whole database and mathematical models. These models work in a cascade manner that has different parameters. These can be used as an input for the emission model and its output in turn is necessary to stimulate pollution levels of the dispersion models. It consists of 3 different sub-models i.e., emission, weather prediction, and dispersion models (Gulliver & Briggs 2011). Each of the mandatory model components and related data is described, separately below.

### Emission Model

The emission model has been developed on the idea of the consequences shown by Joumard et al. (1992), Eggleston et al. (1991), and Tartaglia (1995). There are multiple sources of pollution in urban areas, where traffic, manufacturing industries, and the open burning of waste contribute significantly to it.

The emission model can calculate traffic-associated pollutants like - Carbon Monoxide (CO), Hydrocarbons

(HC), Nitrogen Oxides (NO<sub>x</sub>), and others. It represents the number of released pollutants and the activity associated with the release of pollutants. The formula is used to calculate total pollutant emission Q provided by traffic flow 'f' for N vehicular groups.

$$Q = \sum_{g=1}^N \frac{C_g}{100} \times E_g(V_m) \times f \quad \dots(2)$$

Where:

$C_g$  - the percentage of vehicles in category g in terms of vehicle feet.

$E_g$  -The emission factor due to road vehicles belonging to group g-traveling in the typical road and environmental conditions & is expressed as the mass of pollutant per unit length ( $m.L^{-1}$ ) as a function of the average travel speed  $V_m$  (Gualtieri & Tartaglia 1998).

Most emissions emitted by manufacturing industries are due to the use of fossil fuels, a major source of emissions from the manufacturing sector. Overall, the share of emissions during the period varies between 65% and 75%; and was found that carbon emissions represent nearly 70% of total fuel consumption emissions. The formula used to calculate the emission is as follows.

$$E_{gas} = A_{fuel} * C. V_{unit} * C. V_{fuel} * E. F_{gas} * GWP_{gas} \quad \dots(3)$$

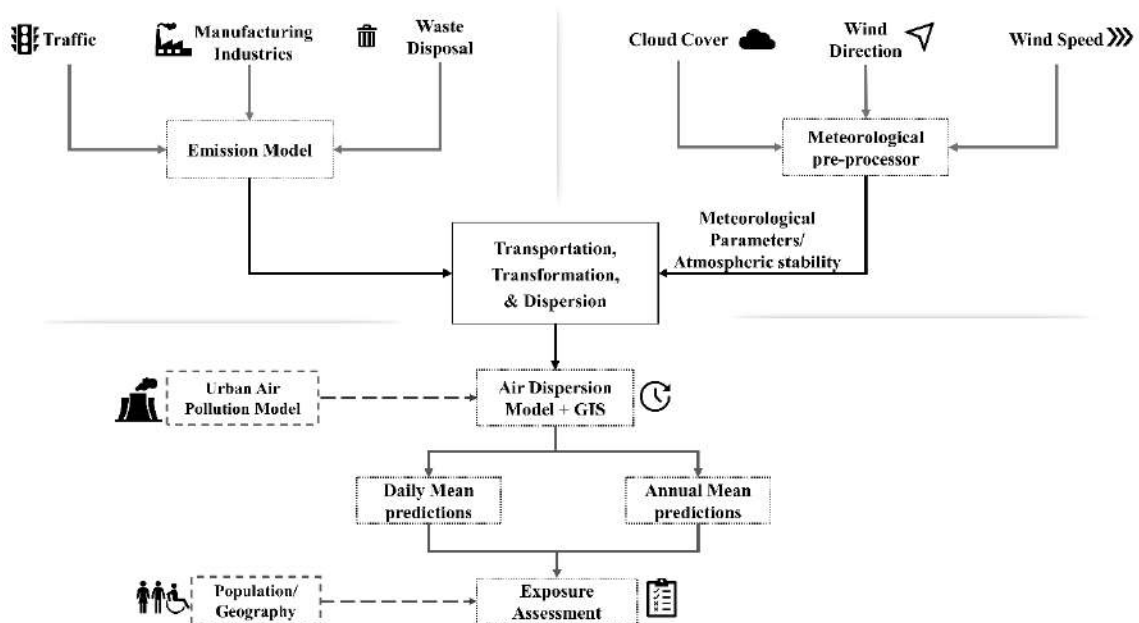


Fig. 4: The GIS-based dispersion model (based on Gulliver & Briggs 2011).

Where:

*E<sub>gas</sub>*: Emission of greenhouse gas(es) in a ton

*A<sub>fuel</sub>*: Activity data of fuel (in L.kg.ton<sup>-1</sup>)

*C*: *Vunit*: Conversion factor(s) to convert activity data to ton (please refer to Appendix 1)

*C.V.fuel*: Calorific value of fuel (a ton of energy in Tera Joule (TJ) per ton of fuel

*E.F<sub>gas</sub>*: Emission factor of GHG gas due to combustion of the fuel (a ton of gas.TJ<sup>-1</sup> (gas.TH<sup>-1</sup> of energy input)

*GWP<sub>gas</sub>*: Global warming potential of gas

Open burning of waste is a possible nonpoint source of emissions, causing major concern, particularly in urban areas, and pollutants that are released are Carbon monoxide, Particulate matter, Sulphur dioxide, Nitrogen oxide, etc. Waste produced depends on factors such as population, livelihood, season, way of life, topography, and industry. The equation used to estimate the emission of pollutants was given as shown below (NEERI 2010).

$$\text{Amount of Pollutant emitted (P)} = \text{SWB} \times \text{EF} \quad \dots(4)$$

Where:

P = Amount of pollutant emitted (Kg.day<sup>-1</sup>, g.day<sup>-1</sup>, or µg.day<sup>-1</sup>)

SWB = Solid Waste Burned (MT.day<sup>-1</sup>)

EF = Emission Factor (Kg.MT<sup>-1</sup>, g.MT<sup>-1</sup>, or µg.MT)

### Meteorological Pre-Processor and Weather Prediction Models

The weather forecast refers to the use of science and technology to estimate the future condition of the environment in relation to a specific area or location (pressure, temperature, etc) (Yerramilli et al. 2011). While various methods are available, quantitative weather forecasts are provided by numerical models alone. Such models employ a closed system of mathematical equations based on mass, momentum, and water vapor conservation, as well as the equation of state and thermodynamic energy for differential temperature. To solve these equations mathematically, the study area should

be formulated in a rectangular shape with an evenly spaced horizontal intersecting grid in the horizontal direction and appropriate vertical levels for numerical solution.

Due to limitations in mathematical formulation, numerical setup, and computing tools, the horizontal grid resolution is limited to a few miles. As the atmospheric model comprises dynamic and physical components, it is important for these processes such as planetary boundary layer, atmospheric radiation, convection, face physics, and cloud microphysics must be parameterized on a smaller scale.

Anomalies in weather forecasting and a rise in errors as prediction progress are caused by measurement errors, model grid interpolation, flaws in the presentation of physical processes, and mistakes due to numerical solution methods. Rapid developments in computational resources have resulted in the design and implementation of atmospheric models as suitable for real-time weather forecasts of different weather phenomena with scales from a few kilometers to thousands of kilometers. There are many weather prediction meteorological models available and the mainly used ones are the RAMS, MM5, and WRF (Yerramilli et al. 2011). The following is a summary of these models.

### Dispersion Model

Air pollution models are the only tool that quantifies the deterministic relationship between emissions and concentrations or depositions, including the effect of past and future scenarios and determining the efficiency of reduction strategies. Measurements of air pollution provide information on atmospheric concentrations and deposition at specific places and times, but they do not provide clear guidance on identifying the causes of the air quality issue. Transport, absorption, chemical transformation, and ground deposition all play a role in determining the atmospheric concentrations of substances. Atmospheric pollutants are carried over longer distances by large-scale atmospheric wind currents and then released into the atmosphere by small-scale turbulent

Table 1: List of different weather prediction models.

Model	Developer Name	Features	Function
RAMS	Colorado State University	Highly versatile numerical code	To simulate and forecast meteorological phenomena
MM5	Written in Fortran and developed at Penn State and NCAR	Non-hydrostatic, Terrain-following sigma-coordinate model	To simulate mesoscale atmospheric circulation (Grell et al. 1995) To predict weather forecasts and climate projections
WRF	National Centre for Atmospheric Research (NCAR)	The prognostic variables and completely compressible non-hydrostatic equations	

**Note.** RAMS: Regional Atmospheric Modelling System; MM5: Mesoscale Model; WRF- Weather Forecasting and Research

flows, where they mix with the environment. The turbulence dynamics and turbulent diffusion are commonly considered intractable, even under laboratory conditions (Yerramilli et al. 2011). The atmospheric dispersion is influenced by weather factors, as transport is driven by wind flows and dispersal by air stability, vertical mixing, and mesoscale winds. There is no general full formula describing the physical relationship between the atmospheric air emission concentrations and the meteorological causative factors and processes. Overall, modeling data reduces the expense of continuous monitoring over vast areas and over longer periods of time.

### Box Model

The mass-conservation principle is used in box models. The site is treated like a box that releases toxins and undergoes physical and chemical processes. It needs simple meteorology and emissions input, and it allows contaminants to flow into and out of the box. The inside of the box is not specified, and the air mass is handled as if it is well mixed with uniform concentrations (Holmes & Morawska 2006). This model, on the other hand, simulates the accumulation of contaminants inside the box after initial conditions are entered, but it does not include any details about the pollutants' local concentrations. For this reason, they are inappropriate for modeling particle concentrations in a local environment where concentrations and therefore particle dynamics are highly influenced.

Lettau (1970) proposed for the first time a simple urban air quality box model, in which the concentration decreases exponentially and reaches its balance value. It is calculated as:

$$c = b + \frac{ql}{uH} \quad \dots(5)$$

Where:

- c - Pollutant concentration in air living box
- b - Pollutant concentration in entering air
- q - Pollutant mass emission rate per unit area in the city
- l - Length of the box in direction of the wind
- u - Wind speed
- H - Mixing Height

### Gaussian Model

The Gaussian plume model is the air emission dispersion model most used. This fits well with the majority of field and laboratory evidence while there are frequent non-systemic variations from a Gaussian distribution. This model is commonly used in atmospheric dispersion modeling, es-

pecially for regulatory purposes, and is frequently "nested" in Lagrangian and Eulerian models (Leelossy 2014). Under steady-state conditions, these models are based on a vertical and horizontal Gaussian distribution of the plume (Zhang et al. 2000) And are described as follows:

$$C(x, y, z, h_e) = \frac{Q}{2\pi\sigma_y\sigma_z} \exp\left(-\frac{1}{2}\left(\frac{y}{\sigma_y}\right)^2\right) \left( \exp\left(-\frac{1}{2}\left(\frac{z-h_e}{\sigma_z}\right)^2\right) + \exp\left(-\frac{1}{2}\left(\frac{z+h_e}{\sigma_z}\right)^2\right) \right) \dots(6)$$

Where:

- C - Concentration level (ug.m<sup>-3</sup>, or as a ratio in fraction or ppm),
- x - Distance downwind from the source (m),
- y - Distance perpendicular from the source(m),
- z - Elevation of the destination point (m),
- h<sub>e</sub> - Elevation of the source (m),
- Q- Release rate of pollutant (mass emission rate – g.s<sup>-1</sup>, or volumetric flow rate -m<sup>3</sup>.s<sup>-1</sup>),
- u - Average wind speed (m.s<sup>-1</sup>),
- σ<sub>y</sub> and σ<sub>z</sub> - Diffusion parameters in the y and z directions (both in m)

The term  $\frac{Q}{(2\pi\sigma_y\sigma_z)}$  is the centreline concentration;  $\exp\left(-\frac{1}{2}\left(\frac{y}{\sigma_y}\right)^2\right)$  accounts for off-axis location;  $\exp\left(-\frac{1}{2}\left(\frac{z-h_e}{\sigma_z}\right)^2\right)$  accounts for the source elevation above the ground surface; and  $\exp\left(-\frac{1}{2}\left(\frac{z+h_e}{\sigma_z}\right)^2\right)$  treats the ground surface as a perfect reflector, absorbing none of the pollutants.

The plume width is determined by σ<sub>y</sub> and σ<sub>z</sub>, which are defined either by stability classes (Pasquill 1961, Gifford 1976) or travel time from the source.

Since plume models use constant approximations, they do not account for the time taken for the pollutant to migrate to the receptor, which is a significant limitation in terms of particle dispersion modeling (Yerramilli 2011). Although most Gaussian models still consider the diffusion and advection of contaminants, more Gifford advanced Gaussian models have recently been established that include physical processes such as deposition and rapid chemical reactions. Further disadvantages of the Gaussian approach include the fact that it is unable to model dispersion under low wind conditions or at locations close to the source, i.e., distances less than 100 m.

## Lagrangian Model

The formulation of air dispersion can vary significantly from one model to another. The Lagrangian and Eulerian solutions are the most known methods (Holmes & Morawska 2006). Lagrangian models are like box models and describe a region of air as a box containing an initial pollutant concentration (Leelosy 2014). This approach is focused on the estimation of wind trajectories and the transport of air parcels along the paths. In source-oriented models, trajectories are calculated over a period after the source releases an air parcel containing contaminants (forward trajectories from a fixed source) before it reaches the receptor location. The trajectories in receptor-oriented models are calculated backward in time from the arrival of an air parcel at a suitable receptor (backward trajectories from a fixed receptor). This model works well over flat terrain for both uniform and stationary conditions (Tsuang 2003) as well as for non-uniform and unstable media conditions for complex terrain (Jung et al. 2003). Meteorological data are used to measure the variance of wind velocity variations and the Lagrangian autocorrelation function. Because Lagrangian particle models measure diffusion characteristics by producing semi-random numbers, they are not limited to stability groups or sigma curves, as is the case with Gaussian dispersion models (Holmes & Morawska 2006).

## Eulerian Model

The 3-dimensional atmosphere in the Eulerian system is divided into horizontal and vertical grid cells. Each grid cell defines changes to the times and thus is called "grid models". This modeling has been adopted for ozone studies (Reynolds et al. 1973) and SO<sub>2</sub> studies (Shir & Shieh 1974) in urban areas. Reynolds' modeling experiments on the Los Angeles basin formed the basis for Model-UAM, the well-known Urban Air shed. This model was used by Holmes and Morawska (2006) to estimate long-distance transport and dispersion.

## Computational Fluid Dynamic Models

The Computational Fluid Dynamic (CFD) model forecasts the wind speed and pollutant concentration profiles in real

three-dimensional environments, enabling an analysis of gas dispersion effects of complex terrain (Tsuang 2003). These models provide complex fluid flow analysis based on mass and momentum conservation by solving Navier – Stokes's equation using three-dimensional finite differential and finite volume approaches (Lettau 1970). It is formulated as:

$$\frac{\partial \vec{v}}{\partial t} + (\vec{v}\nabla)\vec{v} = -\frac{1}{\rho}\nabla p - \vec{g} + \nu_T\nabla^2\vec{v} \quad \dots(7)$$

Where:

$\vec{v}$  is the wind field,

$\rho$  is the density,

$\nu_T$  is the eddy viscosity,

$p$  is the pressure,

$\vec{g}$  is the acceleration vector due to gravity

Given that CFD models are mostly used for complex geometry, explicit measuring up to a very small scale of turbulence requires a fine grid resolution that leads to very high computational costs. Subgrid-scale instability, though, also must be measured and assumed isotropic. Models of CFD street canyons are commonly used for forecasting air quality in industrial and urban areas (Yamada 2004). Different types of models are mentioned below:

Photochemical modeling, Particle models, Statistical models, Odor models, Deposition modules, and Plume Rise models are among the various modeling approaches available and described in Table 3.

## MAPPING RESULTS BASED ON GIS

Most GIS packages have many ways to quickly and efficiently view and show data in a map layer. They can zoom into and out on the map layer, highlight the features selected in the map layer by the selection, classify them based on certain criteria, and then display them in a variety of coded colors (Tippichai 2017).

## PROBLEMS AND CHALLENGES

- I. The format adopted by the GIS and by the atmospheric dispersion models are vector and tabulated text data respectively which is a serious problem (Teggi 2017)
- II. There are several problems with urban air pollution mapping. Because of the multiple emission sources and their uncontrolled dispersion processes in an urban setting, the air pollution levels usually differ over very short distances, often just a few tens of meters (Hewitt 1991).

Table 2: Different models and their examples.

Models	Examples
Box models	CPB, AURORA, and PBM
Gaussian models	HIWAY2, OSPM, CAR-FMI, CALINE4, CALPUFF, UK-ADMS AEROSOL, SCREEN3, and AERMOD
Lagrangian/ Eulerian Models	TAPM, GRAL, ARIA Regional
CFD models	ARIA Local, MICRO-CALGRID, MISKAM

Table 3: Different dispersion models.

Model	Function	Applicable	Examples
Photochemical models	Models that predict the changes in atmospheric pollutant concentrations using a series of mathematical equations and describe the physical and chemical processes of the atmosphere.	At a wide range of different spatial clusters from local to global.	Community Multi-scale Air Quality (CMAQ), WRF/Chem, Urban Airshed Model (UAM), Comprehensive Air quality Model with extensions (CAMx), etc.
Particle models	The source is simulated by releasing many particles throughout the fire. Each particle's trajectory is calculated, as well as a random component that simulates atmospheric turbulence. Instead of following the parameterized spatial distribution pattern, a particle cluster will extend into space according to atmospheric turbulence patterns.	The most effective way to simulate levels at any time, but restricted to single point sources with single chemical or sources that have essential components, such as toxins, which must be monitored accurately	HYSPLIT
Statistical models	The model focused on non-deterministic statistical data analysis of measured atmospheric concentrations, which do not clarify or predict the cause-and-effect relationship, or the relationship between pollution and environmental concentrations.	Techniques for forecasting air pollution patterns a few hours ahead of time so that the public can be alerted.	Chemical Mass Balance (CMB)model
Odor models	The model provides instant or semi-instantaneous algorithms for simulating concentrations, as odors are instantaneous for human sensations.	At Local scales	
Deposition modules	Computer module to measure the amount of plum deposited in the ground due to the phenomenon of dry and wet deposition.	At Local scales	
Plume rise models	Models typically assume stable conditions, which means wind speed, wind direction, and emission rates are all relatively constant.	Close to the source or for a limited period, with land use or topography restrictions	PRIME in HYSPLIT and AERMOD

III. In addition to inherent uncertainties related to the stochastic processes (for example turbulence) in the atmosphere, all models generate primarily two forms of uncertainties: (i) structural and (ii) parametric (Holmes et al. 2009). The use of unpredictable input values (e.g., wind speed and direction, number of emission factors, etc) for model calculations cause parametric uncertainty. These can be caused by the lack of significant data sets (e.g., local weather data), data inconsistencies (e.g., instrument calibration, measurement conditions instability), or lack of understanding of key parameters (e.g., emission factors) (Kumar et al. 2011). The determination of emission factors is one of the most important problems in the Emission model. As a result, emission inventory has certain limitations and uncertainties, when it is performed (Collet et al. 2012)

## CONCLUSION

The issue of air pollution needs to be addressed

systematically with an all-government approach that includes preparation for short, and long-term air quality management strategies. Some of the approaches to control this include the adoption of renewable power sources for public transport, industrial activities, and initiatives to minimize road traffic. Additional approaches include increasing taxes on fuel and car parking, levying congestion charges, developing free zones & cycling paths, use of solar lighting, and encouraging vegetation on the roadside. For long-term control, many of these updates will be motivated by improvements in the Numerical Air Prediction Model in operation.

## ACKNOWLEDGEMENTS

The writers share their great appreciation and heartfelt thanks to the readers for their constructive comments and valuable feedback that led to this article's development, completeness, and transparency.



### APPENDIX 1: CONVERSION FACTORS USED FOR DIFFERENT FUEL TYPES.

Description	Unit Conversion
Anthracite (raw coal)	1
Benzol	1
Briquettes and similar solid fuels manufactured from coal, n.e.c.	1
Briquettes, coal, coal dust	1
Briquettes, coke	1
Coal	1
Coal (under sized)	1
Coal ash	1
Coal bed Methane	1
Coal compressed (middling's)	1
Coal consumed	1
Coal for carbonisation	1
Coal gas	1
Coal gas, water gas, producer gas and similar gases, other than petroleum gases and other gaseous hydrocarbons; n.e.c	1
Coal rejects	1
Coal slack	1
Coal tar by-product	1
Coal tar crude	1
Coal tar Oil	1
Coal tar peat	1
Coal tar processed	1
Coal tar product	1
Coal tar, crude	1
Coal tar, pitch	1
Coal washed	1
Coal, not agglomerated, n.e.c.	1
Coke and semi-coke of coal, of lignite or of peat; retort carbon n.e.c	1
Coke breeze	1
Coke cp	1
Coke dust	1
Coke hard	1
Coke mixed	1
Coke peat	1
Coke seme	1
Coke soft	1
Diesel	0.837520938
Fuel oils n.e.c	0.9765625

Description	Unit Conversion
Fuel, aviation turbine	0.798722045
Furnace oil	0.000976563
Gas compressed natural	0.000711238
Gas oils	0.856164384
Gas, n.e.c	1
High speed diesel	0.826446281
Kerosene	0.798722045
Kerosene n.e.c	0.798722045
Kerosene type jet fuel	1
Light petroleum oil	0.862068966
Lignite briquettes	1
Lignite, agglomerated	1
Lignite, not agglomerated	1
Liquid or liquid gas fuel for lighter	1
Liquefied petroleum gas (LPG)	1
Liquified natural gas	0.000711238
Medium petroleum oil, n.e.c.	0.825082508
Motor spirit (gasoline), including aviation spirit n.e.c	0.734214391
Natural gas	1
Oil, coal tar	1
Other coal tar oil pitch products, n.e.c.	1
Other gaseous hydrocarbons	1
Other light petroleum oils and light oils obtained from bituminous minerals n.e.c	0.862068966
Other than petroleum gas	1
Peat, hard/medium	1
Peat, n.e.c.	1
Peat, other than hard/medium	1
Petrol / motor spirit/ gasoline	1
Petrol, diesel, oil, lubricants consumed	1
Petroleum coke	1
Petroleum coke calcined	1
Petroleum products obtained from bitumen n.e.c.	1
Pitch other than hard/medium	1
Pitch, hard/medium	1
Propane and butanes, liquefied, n.e.c.	1
Regasified liquefied natural gas	1
Shale Oil	1
Spirit type (gasoline type) jet fuel	0.8
Superior kerosene	0.778210117
Tar from Coal or Lignite	1
Water gas	1

Source: -CEEW

## REFERENCES

- Anwar, A., Younis, M. and Ullah, I. 2020. Impact of urbanization and economic growth on CO<sub>2</sub> emission: A case of Far East Asian countries. *Int. J. Environ. Res. Public Health*, 2020; 17: 2531. doi:10.3390/ijerph17072531.
- Bonner, C.S., Ashley, M.C.B., Cui, X., Feng, L., Gong, X., Lawrence, J.S., Luong-Van, D.M., Shang, Z., Storey, J.W.V., Wang, L., Yang, H., Zhou, X. and Zhu, Z. 2010. The thickness of the atmospheric boundary layer above dome A, Antarctica, during 2009. *Astronom. Soc. Pac.*, 122: 1122-1131. <https://doi.org/10.1086/656250>
- Cai, X., Huo, Q., Kang, L. and Song, Y. 2014. Equilibrium atmospheric boundary-layer flow: computational fluid dynamics simulation with balanced forces. *Bound. Layer Meteorol.*, 152: 349-366. DOI: 10.1007/s10546-014-9928-0
- CPCB 2016. Central Pollution Control Board, Environmental Assessment of Industrial Clusters. <https://cpcb.nic.in/comprehensive-environmental-pollution-index-cepi/>
- Collet, S., Kidokoro, T., Sonoda, Y., Lohman, K., Karamchandani, P., Chen, S.Y. and Minoura, H. Air quality impacts of motor vehicle emissions in the south coast air basin: Current versus more stringent control scenario. *Atmos. Environ.*, 47: 236-240. doi: 10.1016/j.atmosenv.2011.11.010.
- Deck, S. 2005. Zonal-detached-eddy simulation of the flow around a high-lift configuration. *AIAA J.*, 43(11): 2372-2384. <https://doi.org/10.2514/1.16810>
- Domingo JL, Marques M, Rovira J. Influence of airborne transmission of SARS-CoV-2 on COVID-19 pandemic. A review. *Environmental Research*. 188 (2020) 109861. <https://doi.org/10.1016/j.envres.2020.109861>.
- Eggleston, H.S., Gaudioso, D., Gorissen, N., Joumard, R., Rijkeboer, R.C., Sameres, Z. and Zierock, K.H. 1991. CORINAIR Working Group on Emission Factors for Calculating 1990 Emissions from Road Traffic. Vol. 1, Methodology and Emission Factors. Final Report, Contract n.B4/3045(91) IOPH, Directorate Generale XI. European Environmental Agency Task Force, Commission of European Communities, Bruxelles, Belgium.
- Fisher, B., Kukkonen, J., Piringer, M., Rotach, W. and Schatzmann, M. 2006. Meteorology applied to urban air pollution problems: Concept from COST 715. *Atmos. Chem. Phys.*, 6(2): 555-564. <https://doi.org/10.5194/acp-6-555-2006>.
- Gifford, F.A. 1976. Consequences of effluent releases. *Nucl. Safety*, 17(1): 68-86.
- Greenhouse Gases Emission Estimates from the Manufacturing Industries in India State level estimates: 2005 to 2013, Council on Energy, Environment and Water (CEEW).
- Grell, G. A., Dudhia, J. and Stauffer, D.R. 1995. A Description of the Fifth Generation PennState/ NCAR Mesoscale Model (MM5), NCAR Technical Note, 6-1995.
- Gualtieri, G. and Tartaglia, M. 1998. Predicting urban traffic air pollution: A GIS framework. *Transp. Res.*, Part D, 3(5): 329-336. [https://doi.org/10.1016/S1361-9209\(98\)00011-X](https://doi.org/10.1016/S1361-9209(98)00011-X)
- Gulliver, J. and Briggs, D. Stems-air: a simple GIS-based air pollution dispersion model for city-wide exposure assessment". *Sci. Total Environ.*, 409: 2419-2429. DOI: 10.1016/j.scitotenv.2011.03.004
- Guttikunda, S.K., Goel, R. and Pant, P. 2014. Nature of air pollution, emission sources, and management in the Indian cities. *Atmos. Environ.*, 95: 501-510. <https://doi.org/10.1016/j.atmosenv.2014.07.006>
- Hewitt, C.N. 1991. Spatial variations in nitrogen dioxide concentration in an urban area. *Atmos. Environ.*, 25B: 429-434. [https://doi.org/10.1016/0957-1272\(91\)90014-6](https://doi.org/10.1016/0957-1272(91)90014-6).
- Holmes, K.J., Graham, J.A., McKone, T. and Whipple, C. 2009. Regulatory models and the environment: practice, pitfalls, and prospects. *Risk Anal.*, 29: 159-170. doi: 10.1111/j.1539-6924.2008.01186.x.
- Holmes, N.S. and Morawska, L. 2006. A review of dispersion modeling and its application to the dispersion of particles: An overview of different dispersion models available. *Atmos Environ.*, 81: 40: 5902-5928. <https://doi.org/10.1016/j.atmosenv.2006.06.003>.
- Joumard, R., Hickmann, L., Nemerlin, J. and Hassel, D. 1992. Model of Exhaust and Noise Emissions and Fuel Consumption of Traffic in Urban Areas. INRETS, Lion-Bron, France. <https://doi.org/10.1155/2013/736285>
- Jung, Y.R., Park, W.G. and Park, O.H. 2003. Pollution dispersion analysis using the puff model with numerical flow field data. *Mech. Res. Commun.*, 30(4): 277-286. doi:10.1016/S0093-6413(03)00024-7
- Leelosy, J.M. 2014. Dispersion modeling of air pollutants in the atmosphere: A review. *Cent. Eur. J. Geosci.*, 6(3): 257-278. <https://doi.org/10.2478/s13533-012-0188-6>
- Kumar, P., Ketzler, M., Vardoulakis, S., Pirjola, L. and Britter, R. 2011. Dynamics and dispersion 826 modeling of nanoparticles from road traffic in the urban atmospheric environment - A review. *J. Aeros. Sci.*, 42(9): 580-603. doi: 10.1016/j.jaerosci.2011.06.001
- Lettau, H.H. 1970. The physical and meteorological basis for mathematical models of the urban diffusion process. *Proc. Symp. on Multiple-Source Urb. Diff. Mod.*, 86: 2-26
- Luna, R.E. and Church, H.W. 1972. A comparison of turbulence intensity and stability ratio measurements to Pasquill stability classes. *J. Appl. Meteorol.*, 11: 663-669. <https://www.jstor.org/stable/26175715>
- Mohanraj, R., Dhanakumar, S. and Solaraj, G. 2012. Polycyclic aromatic hydrocarbons bound to PM 2.5 in urban Coimbatore, India with emphasis on source apportionment. *Sci. World J.*, 98: 843. <https://doi.org/10.1100/2012/980843>.
- National Environmental Engineering Research Institute (NEERI). 2010. Air quality assessment, emissions inventory, and source apportionment studies. Mumbai. Central Pollution Control Board (CPCB), New Delhi.
- Oke, T.R. 1976. The distinction between canopy and boundary-layer urban heat islands. *Atmosphere*, 14: 268-277. <https://doi.org/10.1080/00046973.1976.9648422>
- Pasquill, F. 1961. The estimation of the dispersion of windborne material. *Meteorol. Mag.*, 90(1063): 33-40
- Piringer, M., Joffre, S., Baknalov, A., Christen, A., Deserti, M., De-Ridder, K., Emeis, S., Mestayer, P., Tombrou, M., Middleton, D., Baumann-Stanzer, K., Dandou, A., Karpinen, A. and Burzynski J. 2007. The surface energy balance and the mixing height in urban areas - activities and recommendations of COST-Action 715. *Boundary-Layer Meteorol.*, 124(1): 3-24. DOI: 10.1007/s10546-007-9170-0
- Reynolds, S., Roth, P. and Seinfeld, J. 1973. Mathematical modeling of photochemical air pollution. *Atm. Env.*, 7. [https://doi.org/10.1016/0004-6981\(73\)90214-X](https://doi.org/10.1016/0004-6981(73)90214-X).
- Roth, M. 2000. Review of atmospheric turbulence over cities. *Q. J. R. Meteorological Soc.* 126, 941-990.
- Shir, C.C. and Shieh, L.J. 1974. A generalized urban air pollution model and its application to the study of SO<sub>2</sub> distribution in the St. Louis Metropolitan area. *J. Appl. Met.*, 19: 185-204. DOI: <https://doi.org/10.1175/1520-0450-13.2.185>
- Stull, R. 2017. *Practical Meteorology: An Algebra-Based Survey of Atmospheric Science, Version 1.02b*. University of British Columbia, Vancouver, BC, Canada.
- Tartaglia, M. 1995. Relationship between polluting emissions and speed of road vehicles. *Rail. Eng.*, 5: 337-346
- Teggi, A. 2017. GIS-based atmospheric dispersion model for pollutants emitted by complex source areas. *Sci. Total Environ.*, 610-611: 175-190. doi: 10.1016/j.scitotenv.2017.07.196.
- Tippichai, A. 2017. Applications of GIS for analyzing air pollution from urban road traffic (Thai). *KKU Res. J.*, 10(4): 201.
- Tseng, Y.H., Meneveau, C. and Parlange, M.B. 2006. Modeling flow around bluff bodies and predicting urban dispersion using large-eddy simulation. *Environ. Sci. Technol.*, 40(8): 2653-2662. <https://doi.org/10.1021/es051708m>.

- Tsuang, B.J. 2003. Quantification on the source/receptor relationship of primary pollutants and secondary aerosols by a Gaussian plume trajectory model: Part I theory. *Atmos. Environ.*, 37(28): 3981-3991. [https://doi.org/10.1016/S1352-2310\(03\)00471-0](https://doi.org/10.1016/S1352-2310(03)00471-0).
- Turner, D.B. 1997. The long lifetime of the dispersion methods of Pasquill in U.S. regulatory air modeling, *J. Appl. Meteorol.*, 36: 1016-1020
- WHO 2018. World Health Organization releases new global air pollution data. <https://www.ccacoalition.org/en/news/world-health-organization-releases-new-global-air-pollution-data>
- Yamada, T. 2004. Merging CFD and atmospheric modeling capabilities to simulate airflows and dispersion in the urban area., *Comput. Fluid Dyn. J.*, 13: 329-341
- Yerramilli, A., Dodla, V.B.R. and Yerramilli, S. 2011. Air pollution, modeling, and GIS-based decision support systems for air quality risk assessment. *Eur. J. Oper. Res.*, 10(4): 220. DOI: 10.5772/22055.
- Zhang, A., Gao, C. and Zhang, L. 2005. Numerical simulation of the wind field around different building arrangements. *J. Wind Eng. Indus. Aerodyn.*, 93(12): 891-904. DOI: 10.1016/j.jweia.2005.09.001.
- Zhang, J., Hodgson, J. and Erkut, E. 2000. Using GIS to assess the risks of hazardous materials transport in networks. *Eur. J. Oper. Res.*, 121: 316-329. DOI: 10.1016/S0377-2217(99)00220-9.





# Air Pollution, Cardiovascular and Respiratory Admissions in Klang Valley, Malaysia - Finding the Effects

W. M. W. Rozita\*†, S. Zamtira\*, FI. Mohd\*\*, T. L. Mohd\*\*\*, I. A. Nurul\*, I. A. W. Muhammad\*\*\*\* and S. Mazrura\*\*\*\*

\*Institute for Medical Research, National Institute of Health, Ministry of Health, Setia Alam, Malaysia

\*\*Faculty of Medicine, Universiti Kebangsaan Malaysia, Kuala Lumpur, Malaysia

\*\*\*Faculty of Science Technology, Universiti Kebangsaan Malaysia, Selangor, Malaysia

\*\*\*\*Faculty of Health Sciences, Universiti Kebangsaan Malaysia, Kuala Lumpur, Malaysia

†Corresponding author: W.M.W. Rozita; rozita.wm@moh.gov.my

Nat. Env. & Poll. Tech.  
Website: [www.neptjournal.com](http://www.neptjournal.com)

Received: 19-08-2021

Revised: 10-11-2021

Accepted: 17-11-2021

## Key Words:

Air pollution  
Respiratory disorder  
Cardiovascular disorder  
Klang Valley

## ABSTRACT

This study aims to determine the association and risk of daily fluctuations of air pollution parameters in Klang Valley, Malaysia, with cardiovascular and respiratory admissions. The data on admissions and air pollution concentrations were obtained from various government agencies in Malaysia. The associations were estimated using a time series analysis of Poisson regression. The effects for every  $10\mu\text{m}^3$  increase in pollutants were reported as Relative Risk (RR).  $\text{SO}_2$  showed the highest association with immediate effects at lag 0 for all cardiovascular admissions followed by  $\text{NO}_2$ . Gaseous pollutants of  $\text{SO}_2$  and  $\text{NO}_2$  showed a higher risk among elderly more than 60 years old. Immediate effects were found in both genders, with higher risks observed in males.  $\text{NO}_2$  continues to be suggestively associated with all respiratory admissions. Children less than 9 years old presented a higher risk of  $\text{NO}_2$  at various lag times with the highest value at lag0, followed by  $\text{PM}_{10}$ . Stratified analysis showed an incremental risk of respiratory admissions for males exposed to  $\text{NO}_2$  compared to females. We found noteworthy associations for overall and age-specific admissions of cardiovascular and respiratory with the pollutants. Compared to particulates pollutant, gaseous pollutants showed a higher risk in both admissions.

## INTRODUCTION

Air pollution has been identified as one of the world's major environmental adverse health effects concerns (Mahiyuddin et al. 2013, Tajudin et al. 2019). Common air pollutants included particulate matters ( $\text{PM}_{10}$  and  $\text{PM}_{2.5}$ ), carbon monoxide (CO), ozone ( $\text{O}_3$ ), sulfur and sulfur dioxide ( $\text{SO}_2$ ), nitrogen oxides ( $\text{NO}_2$ ), heavy metals, pesticides, volatile organic compounds, acid gases, solvents, radiation and bioaerosols (Sentian et al. 2019). These undesirable materials come from anthropogenic sources such as mobile, stationary, agricultural, and natural (Usmani et al. 2020, Amato et al. 2019). These harmful materials may harm human and ecosystem health, and the built environment, and lead to economic loss (Li et al. 2016, Rovella et al. 2021). Many epidemiological studies in all parts of the world have shown significant associations between air pollution and human morbidity, including in multi-cities studies, mainly affecting respiratory and circulatory systems (Phosri et al. 2019, Slama et al. 2019).

Different studies in various parts of the world revealed that cerebrovascular admissions were suggestively associated with short-term effects of  $\text{NO}_2$  (Tajudin et al. 2019), particulate matter 10 micrometers or less in diameter ( $\text{PM}_{10}$ ) (Moolgavkar 2000),  $\text{O}_3$ , CO and particulate matter 2.5 micrometers or less in diameter ( $\text{PM}_{2.5}$ ) (Chan et al. 2006). In Malaysia, Mahiyuddin et al. (2013) conducted the first study on the health effects of air pollution using time series analysis to determine the association between air pollution and mortality in urban areas. Findings showed that  $\text{O}_3$ , CO, and  $\text{PM}_{10}$  were the pollutants that were found to be significantly associated with natural and respiratory mortality. This is also similar to what was reported by Tajudin et al. (2019).

Since the 1980's Malaysia faced frequent episodes of haze and most of them were the major episodes (Usmani et al. 2020). The sources could be either local or transboundary, such as forest fire from Indonesia (Sentian et al. 2019, Awang et al. 2000). Haze comprised high concentrations of  $\text{PM}_{10}$ , metal (Fe) ions, and zinc (Zn) together with gaseous (Usmani et al. 2020). The cost of medical care, especially inpatient

hospital care in Malaysia increases tremendously. The results from Hassan et al. (2000), showed that limited activity days contributed to about 79.3% of the health damage costs, followed by an asthma attack, which contributed 10.7%. Other less significant health effects were respiratory, hospital admission, emergency room visits, and chronic bronchitis which contributed to total health damage cost estimated at Ringgit Malaysia (RM) 129 million (RM36-RM258 range).

This study aimed to obtain the risk estimates of pollutants towards cardiovascular and respiratory admissions in Malaysia's most urbanized area. This study differs from other time series studies on admissions and air pollution because it utilizes data from all main public hospitals in the Klang Valley area.

## MATERIALS AND METHODS

### Air Quality and Meteorological Data

The air quality data from 1st January 2008 to 31st December 2010 were obtained from the Department of Environment, Malaysia (DOE). The air pollutant parameters utilized in this study were PM<sub>10</sub>, CO, SO<sub>2</sub>, NO<sub>2</sub> and O<sub>3</sub>. There were

52 continuous air quality monitoring stations (CAQMs) in Malaysia with six located in Klang Valley at Cheras, Kajang, Shah Alam, Klang, Gombak, and Petaling Jaya. The daily average for the pollutants was used to represent the daily concentration of pollutants concentrations for Klang Valley.

Data on meteorological parameters in Klang Valley were gained from two stations by Malaysia Meteorological Department. The data components were a daily 24 h average of temperature, relative humidity, and rainfall. Fig. 1 showed the locations of CAQMs and meteorological stations in Klang Valley.

### Study Area

Klang Valley is one of the most industrialized areas following fast urbanization and is a densely populated region (Hassan et al. 2000). It is the most susceptible region exposed to air pollution compared to other regions of the country (Rahman et al. 2015, Juneng et al. 2011). Situated with mountains in the east and the Straits of Malacca in the west, this basin provides a conducive environment for pollutants to mount up, particularly when the meteorological condition is stable. Klang Valley has a 2832 km<sup>2</sup> area with

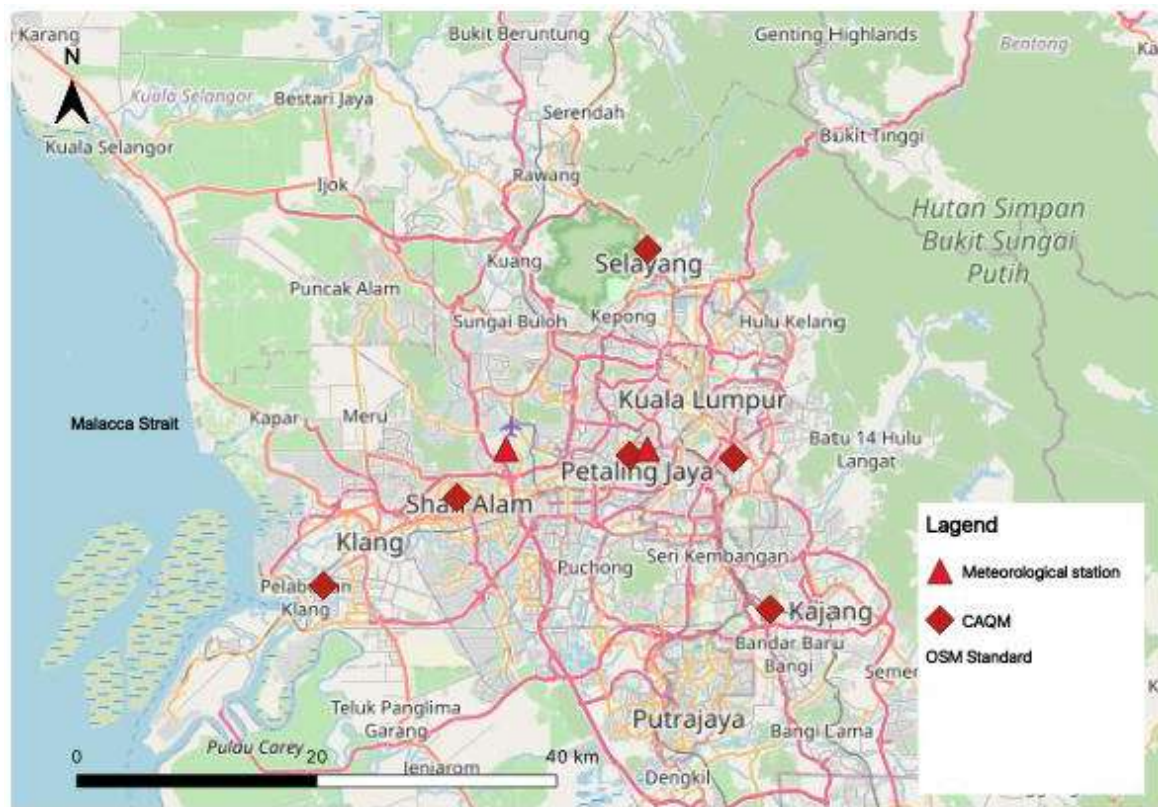


Fig. 1: Locations of continuous air quality monitoring stations (CAQMs) and meteorological stations in Klang Valley.

a total population of 7.9 million (UN World Urbanization Prospects 2021).

**Hospital Admissions Data**

Daily hospital admissions data between 1st January 2008 and 31st December 2010 was obtained from Health Informatics Centre, Ministry of Health’s (MOH) database. Nine public hospitals in Klang Valley were selected for this study. The date of the patient’s discharge from the hospital for which the diagnosis was classified according to the International Classification of Disease, Tenth Revision (ICD10) was assumed to be the date of disease diagnosis. The diseases selected for these studies were respiratory (J00-J99) and cardiovascular diseases (I00-I99). The data taken was anonymous.

**Modeling and Statistical Analysis**

Generalized Additive Model (GAM) with Poisson time series regression was applied to examine the short-term effects of daily air pollutants on cardiovascular and respiratory admissions. The time variable representing the day, ambient temperature, relative humidity, total rainfall, day of the week, and holiday coding were the covariates used in the models. The time variable of the day was used to control for systematic variations by time in the data. Natural spline smoothing functions were used to control for long-term trends and seasonality from the admissions or other time-varying covariates that could confound the estimates of risk between admissions and pollutants. This study follows a similar methodology as what was done by Mahiyuddin et al. (2013) and Wong et al. (2008). A partial autocorrelation function (PACF) plot of the residuals and the minimum Akaike Information Criterion (AIC) were used to assess the goodness of fit of the models. After examining the results of PACF and AIC, we applied 4 *dfs* per year smoothing for time and 2 *dfs* per year each for the continuous covariates.

The following equation of the log-linear model is given below:

$$\text{Log} [E(y)] = \beta_0 + \beta_1 X + \beta_2 Z_1 + \beta_3 Z_2 + \Sigma S(\gamma_i, df_i) \dots(1)$$

- E(y): Expected daily hospital admissions counts
- X: pollutants concentration
- Z<sub>1</sub>: days of the week,
- Z<sub>2</sub>: holiday indicator
- γ: time, temperature, rainfall, and relative humidity
- β: regression coefficients
- S: smoothing function using natural spline
- df: degree of freedom: 2 *dfs* for temperature, relative humidity, and rainfall; 4 *dfs* per year for time

We started the modeling process by fitting the single pollutant models for each pollutant to determine the effects of the pollutants. Later we run a sensitivity analysis to measure the consistency and robustness of the estimates. The results were presented as relative risk (RR) and excess risk (ER) The ER per 10ug/m3 of each pollutant increase was calculated as ER= (RR– 1)\*100. Effects of the pollutants on the current day (lag 0) to the previous five days (lag 5) were observed. We followed a similar methodology of sensitivity analysis done by Vichit-Vadakan et al. (2008) and Mahiyuddin et al. (2013).

**RESULTS AND DISCUSSIONS**

**Descriptive Statistics**

Table 1 showed the summary statistics of the hospital admissions. A total of 77,063 admissions for cardiovascular diseases and 98,869 for respiratory diseases were recorded from 1st January 2008 to 31st December 2010. There were on average, 70 admissions for cardiovascular diseases and

Table 1: Summary statistics of the daily hospital admissions (n) in Klang Valley.

Variables (n)	Mean	SD	Min	Max	Total
Cardiovascular cases	70	15.83	5	119	77063
Gender					
Male	43	10.67	13	76	47063
Female	28	7.39	11	53	30306
≥60 years old	30	7.47	8	52	33375
Respiratory cases	90	25.65	5	228	98869
Gender					
Male	50	13.92	16	114	54847
Female	41	13.44	12	119	44397
≤9 years old	87	27.27	22	234	95184

90 admissions per day for respiratory diseases. The average of male admissions was higher than females for both diseases. Forty-three percent of the cardiovascular admissions were among the 60 years old and above. Children aged less than 9 years old had the highest admissions (96%) due to respiratory diseases.

The daily average temperature in Klang Valley was 27.64°C, relative humidity 76%, and rainfall 8.65mm, indicating the tropical climate in Klang Valley. Daily average concentrations of all the pollutants were; 1066.92  $\mu\text{g.m}^{-3}$  for CO, 36.25  $\mu\text{g.m}^{-3}$  for O<sub>3</sub>, 8.82  $\mu\text{g.m}^{-3}$  for SO<sub>2</sub>, 42.52  $\mu\text{g.m}^{-3}$  for NO<sub>2</sub>, and 51.40  $\mu\text{g.m}^{-3}$  for PM<sub>10</sub>. (Table 2). The daily average of pollutants was compared with the ambient Malaysia air quality guideline (MAQG) in 2005 (Department of Environment 2015) together with the interim target 1 (IT-1) which was adopted by DOE in the year 2015, and WHO air quality guideline of the year 2005 (WHO AQG) (Amancio & Nascimento 2012).

The daily average of PM<sub>10</sub> was 51.40  $\pm$  15.93  $\mu\text{g.m}^{-3}$ , which exceeded the WHO air quality guideline. The maximum concentration of PM<sub>10</sub> was observed on 12th June 2009 with a concentration of 147.87  $\mu\text{g.m}^{-3}$  and did not exceed the MAQG 2005 and MAQG New IT-1 2015 but exceeded the WHO AQG 2005.

Fig. 2 displayed the trends of hospital admissions and air pollution concentrations together with a simple smoothing spline. Cardiovascular series showed a slightly increasing trend with seasonality fluctuations whilst respiratory series showed a clear increasing trend with a peak in 2009.

SO<sub>2</sub> fluctuated around a constant mean with clear seasonality with few days were found to exceed the WHO AQG 2005. NO<sub>2</sub> and CO declined slightly from 2008 to 2009 and started to increase in 2010 with clear seasonality. PM<sub>10</sub> recorded 16 days with concentrations of more than 100  $\mu\text{g.m}^{-3}$  in 2009 which were related to the haze episodes between

June to August. In contrast, O<sub>3</sub> showed a slight decreasing pattern from 2008 to 2010 (Fig. 3).

### Modeling

Tables 3 and 4 display the significant results from the single pollutant models at various lags models. The models range from lag0 to lag5 for cardiovascular and respiratory admissions at all ages together with age and gender-specific. The highest risk for cardiovascular was found with SO<sub>2</sub> (RR=1.048; 95%CI: 1.007-1.091) and followed by NO<sub>2</sub> (RR=1.021; 95%CI: 1.009-1.033) (Table 4). Both gaseous showed an immediate or acute effect at lag0. Among the elderly, similar pollutants were found to be associated with cardiovascular admissions. Higher RR was observed among the elderly for SO<sub>2</sub> (RR=1.065; 95%CI: 1.012-1.120) and NO<sub>2</sub> (RR=1.031; 95%CI: 1.016-1.046) at lag0. However, O<sub>3</sub> showed a delayed effect after 2 days of exposure (RR=1.014; 95%CI: 1.003-1.026). In gender-specific analysis, higher RR was found in males compared to females. NO<sub>2</sub> (RR=1.025; 95%CI: 1.012-1.039) and SO<sub>2</sub> (RR=1.069; 95%CI: 1.019-1.120) continue to show significant associations with immediate cardiovascular admissions (lag0) for males and NO<sub>2</sub> for females (RR=1.018; 95%CI: 1.002-1.034). Delayed effects of five days (lag5) for SO<sub>2</sub> (RR=1.063; 95%CI: 1.0073-1.120) and O<sub>3</sub> (RR=1.013; 95%CI: 1.001-1.026) were observed among females (Table 3).

In Table 4, NO<sub>2</sub> was the only pollutant associated with respiratory (RR=1.021; 95%CI 1.006-1.035:) at lag0. Among children less than 9 years old, NO<sub>2</sub> and PM<sub>10</sub> were associated with respiratory admissions at similar lags which were lag0, lag1, and lag2 days. NO<sub>2</sub> showed the highest risk of exposure at lag0 (RR=1.031; 95%CI: 1.014-1.048) and decreasing risks were observed as the lags increased. However, a different pattern was observed in PM<sub>10</sub>. Acute or immediate effect was observed at lag0 (RR=1.013;95%CI: 1.003-1.023) for PM<sub>10</sub>, started to decline at lag1 (RR=1.011;95%CI: 1.001-

Table 2: Summary statistics of daily concentration of pollutants and meteorological variables in Klang Valley.

Variables	Averaging Time	Mean $\pm$ SD	Min	Max	MAQG (2005)	MAQG New IT-1(2015)	WHO AQG 2005
Temperature (°C)		27.64 $\pm$ 1.21	23.6	30.90			
Humidity		76.06 $\pm$ 6.57	58	93.30			
Rainfall		8.65 $\pm$ 15.54	0.0	92.4			
CO [ $\mu\text{g.m}^{-3}$ ]	8 h	1066.92 $\pm$ 280.49	285.74	2363.12	10000	10000	11500
O <sub>3</sub> [ $\mu\text{g.m}^{-3}$ ]	8 h	36.25 $\pm$ 11.08	10.26	85.71	120	120	100
SO <sub>2</sub> [ $\mu\text{g.m}^{-3}$ ]	24 h	8.82 $\pm$ 2.57	2.70	33.86	105	105	20
NO <sub>2</sub> [ $\mu\text{g.m}^{-3}$ ]	24 h	42.52 $\pm$ 9.77	12.51	76.51	75	75	40
PM <sub>10</sub> [ $\mu\text{g.m}^{-3}$ ]	24 h	51.40 $\pm$ 15.93	18.95	147.87	150	150	50



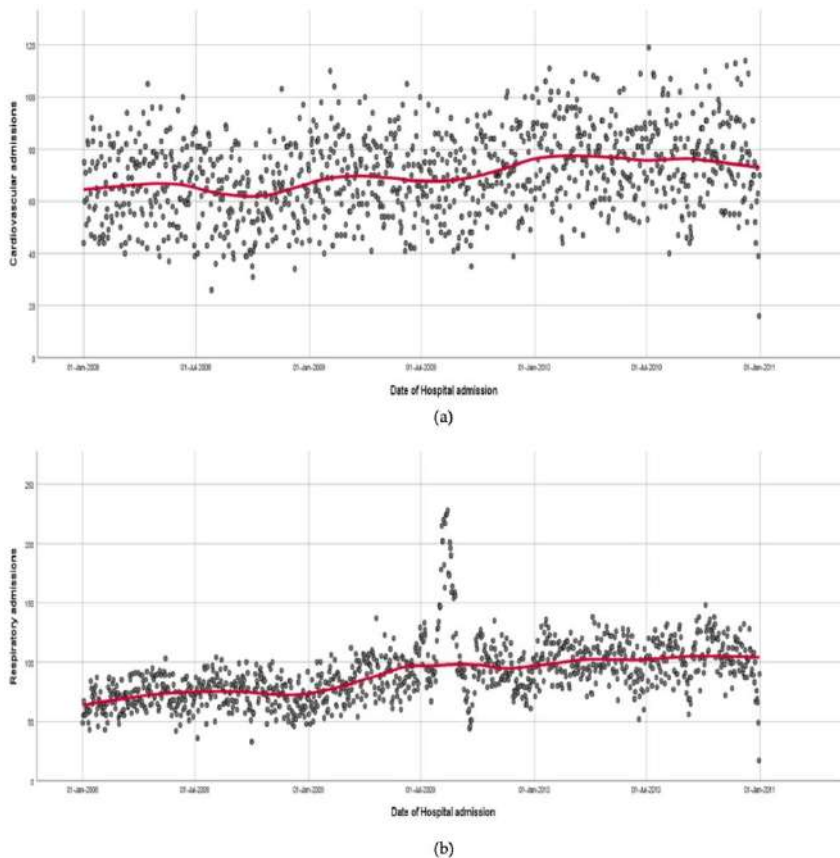


Fig. 2: The trend series of hospital admission in Klang Valley from 2008-2010.

1.021) and increased back at lag2 (RR=1.013; 95%CI: 1.003-1.022). Males continue to show higher risk compared to females. NO<sub>2</sub> was consistent immediately associated with males (RR=1.026;95%CI:1.012-1.041) and females (RR=1.019;95%CI: 1.001-1.037). PM<sub>10</sub> was also associated with females but at various delayed effects, while CO

was associated with males at immediate effect (RR=1.001; 95%CI: 1.0001-1.001).

NO<sub>2</sub> was chosen as the pollutant in the sensitivity analysis because it was consistently associated with cardiovascular and respiratory admissions. The sensitivity analysis was performed using alternative *dfs* for smoothing of time and

Table 3: Summary statistics of the daily cardiovascular hospital admissions (n) in Klang Valley.

Types of admissions	Pollutant	Lags	RR	Lower CI for RR	Upper CI for RR
CVD all ages	NO <sub>2</sub>	0	1.021	1.00935	1.032641
	SO <sub>2</sub>	0	1.048	1.007337	1.091443
CVD > 60 years old	NO <sub>2</sub>	0	1.031	1.016239	1.046112
	SO <sub>2</sub>	0	1.065	1.011632	1.120241
	Ozone	2	1.014	1.002755	1.026129
CVD (males)	NO <sub>2</sub>	0	1.025	1.011795	1.039375
	SO <sub>2</sub>	0	1.069	1.019726	1.120055
CVD (females)	NO <sub>2</sub>	0	1.018	1.002219	1.034269
	SO <sub>2</sub>	5	1.063	1.007391	1.120725
	Ozone	5	1.013	1.000757	1.025912

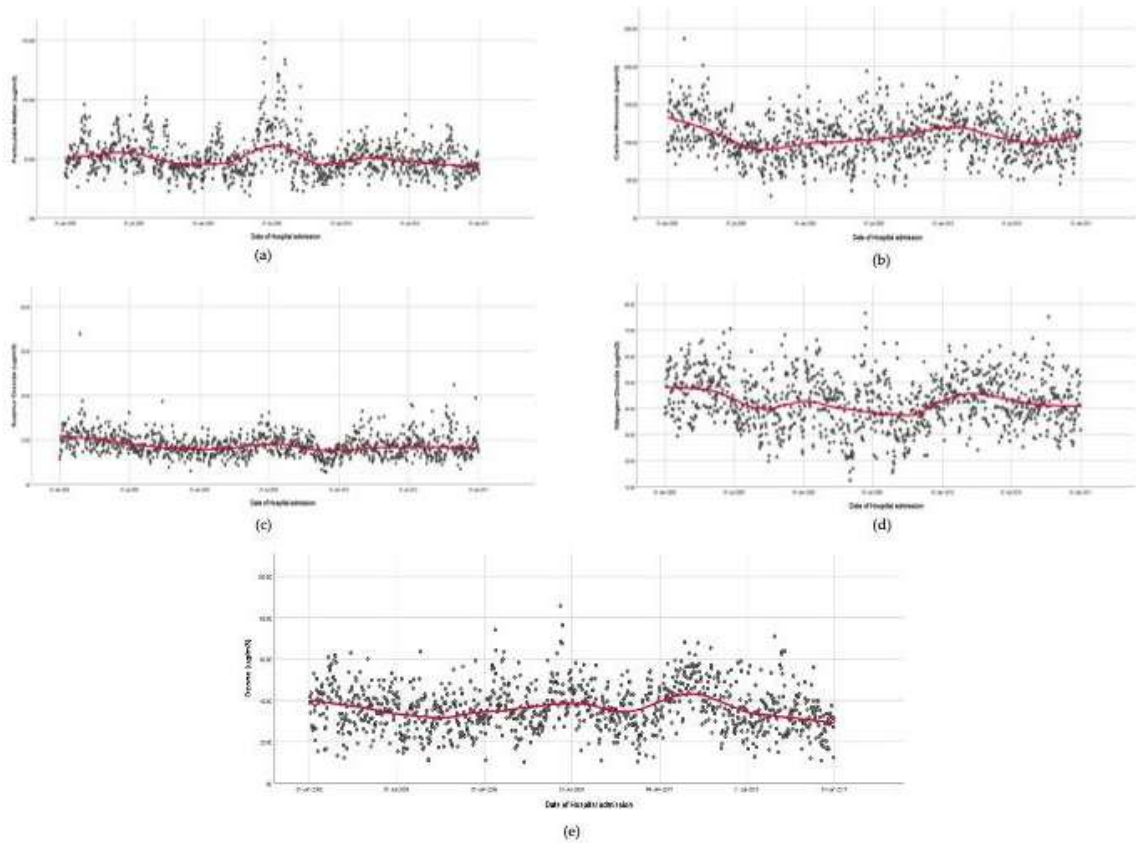


Fig. 3: Daily concentrations of pollutants in Klang Valley from 2008-2010.

Table 4: Summary statistics of the daily respiratory hospital admissions (n) in Klang Valley.

Types of admissions	Pollutant	Lags	RR	Lower CI for RR	Upper CI for RR
Respiratory all ages	NO <sub>2</sub>	0	1.021	1.006467	1.035246
Respiratory < 9 years old	NO <sub>2</sub>	0	1.031	1.013681	1.048208
		1	1.018	1.00096	1.034336
		2	1.018	1.001518	1.034099
	PM <sub>10</sub>	0	1.013	1.002759	1.022943
		1	1.011	1.001228	1.020908
		2	1.013	1.002817	1.022361
Respiratory (males)	NO <sub>2</sub>	0	1.026	1.011538	1.041365
		1	1.018	1.003517	1.032498
		5	1.015	1.011538	1.041365
Respiratory (females)	CO	0	1.001	1.000112	1.00111
	NO <sub>2</sub>	0	1.019	1.001158	1.036559
		1	1.010	1.000396	1.020393
		2	1.013	1.002749	1.022622
		3	1.013	1.002984	1.022808
5	1.012	1.002025	1.021832		

lag0. A change in the ER of >20% from the main analysis in the single pollutant model of NO<sub>2</sub> at various *dfs* was used to indicate the sensitivity of the data. Table 5 showed that the effects of NO<sub>2</sub> on cardiovascular and respiratory admissions were insensitive to the number of *df* specified. Therefore, we conclude that the effect estimates did not alter much even when we change the *df* for the smoothing of time. This suggests that the core model is relatively robust to model specification.

## DISCUSSION

Our results from the study demonstrated some important findings. Three pollutants were found to exceed the WHOAQG 2005 on certain days which were SO<sub>2</sub>, NO<sub>2</sub>, and PM<sub>10</sub>. There was an increasing trend of SO<sub>2</sub> in our study, with some values exceeding the WHOAQG 2005 but not exceeding MAQG 2005. The concentration of SO<sub>2</sub> exceeded the WHOAQG 2005 on the 23<sup>rd</sup> of February 2008 and the 28<sup>th</sup> of October 2010, with the value of 33.86 µg.m<sup>-3</sup> and 22.45 µg.m<sup>-3</sup>, respectively. However, the annual average concentrations of SO<sub>2</sub> are still far below the WHOAQG 2005 which were less than 10 µg.m<sup>-3</sup> for the study period. As for NO<sub>2</sub>, we found that there were in total 652 days of which the average concentrations exceeded the WHOAQG 2005 for which 230 days in the year 2008, 185 days in the year 2009, and 237 days in 2010. The number of days on which the concentrations exceeded the WHOAQG 2005 was more than 50% of the total number of days in a year.

Only gaseous pollutants were found to be associated with cardiovascular admission, which was highest in SO<sub>2</sub>, followed by NO<sub>2</sub> and O<sub>3</sub>. These associations were consistent in all types of cardiovascular admissions. Our results are

Table 5: Summary of sensitivity analysis.

Types of admissions	<i>df</i> for time	RR	ER [%]	%Change in ER Relative to Main Analysis [%]
Cardiovascular all ages	3	1.023	2.323	11.15
	4*	1.021	2.09	
	5	1.021	2.145	2.63
	6	1.022	2.226	6.51
	7	1.024	2.448	17.13
Respiratory all ages	3	1.023	2.320	11.54
	4*	1.021	2.08	
	5	1.017	1.658	20.29 <sup>a</sup>
	6	1.020	2.049	1.49
	7	1.023	2.259	8.61

consistent with the findings from Tajuddin et al. (2019) which showed a delayed effect for SO<sub>2</sub> at lag 4, but our study showed acute effects for SO<sub>2</sub> at lag0. In Thailand, Phosri et al (2019) revealed evidence of an association between SO<sub>2</sub> and hospital admissions with higher risks observed for cardiovascular disease. Similarly, epidemiological studies in Brazil (Amancio & Nascimento 2012) and China (Amsalu et al. 2019, Shen et al. 2020) have linked SO<sub>2</sub> to cardiovascular admissions and mortality, including hypertension, coronary heart disease, and stroke. The mechanisms underlying the development of circulatory disorders resulting from SO<sub>2</sub> exposure have not been thoroughly studied. However, the possible mechanism could be the activation of systemic vascular oxidative stress reaction (Miller 2020, Fiorito et al. 2018). Furthermore, an increase in plasma fibrinogen and inflammatory factors leads to increased blood viscosity and contributes to cardiovascular dysfunction (Peters et al. 2017).

NO<sub>2</sub>, PM<sub>10</sub>, and CO were the three pollutants that were significantly associated with respiratory admissions. We found that there were 496 days in which the concentrations of PM<sub>10</sub> exceeded the concentration of WHOAQG of 50 µg.m<sup>-3</sup>. The risks were higher among children less than 9 years old. NO<sub>2</sub> at high concentrations will highly affect those with respiratory diseases such as bronchitis and asthma (Kowalska et al. 2020, Carthy et al. 2021). Air pollution reduces the airway epithelium's defense mechanism by reducing barrier function, impairing host response against pathogens, and exaggerating inflammatory responses. The destruction of respiratory epithelium increased mucus production and bronchospasm (Huff et al. 2019).

Our study revealed that the elderly aged 60 years and above were at a higher risk for exposure to gaseous pollutants. This result is consistent with other findings from the tropical region (Yap et al. 2019, Chan et al. 2006). Chan et al. (2006) concluded that long-term exposure to NO<sub>2</sub>, O<sub>3</sub>, and PM<sub>2.5</sub> were significantly associated with increased blood pressure, total cholesterol, fasting glucose, HBA1c, IL-6, and neutrophils among elderly aged 65 years of age. However, in our study, we could not find any significant association between cardiovascular admissions with particulates, in our case PM<sub>10</sub>. We found that children are also vulnerable and susceptible to air pollution. The main reason is that children's organ development, such as the lungs, does not fully develop compared to adults. Children's physiology also has a higher respiratory rate; thus, they breathe faster than adults, exposing them to higher pollutant concentrations (Zhou et al. 2019).

Among the cardiovascular admissions, both genders were susceptible to gaseous pollutants compared to particulates.

The risk for males was only slightly higher compared to females. However, females showed significant risks to particulates at various lags in respiratory admissions, which was not observed among males. Furthermore, females showed significant associations with all pollutants except CO, making females more vulnerable to pollutants compared to males. Our findings tally with other findings from all over parts of the world (Zhang et al. 2015, Boezen et al. 2005). Butter (2006) in her article explained the reasons why females are more vulnerable to air pollution. Many environmental pollutants tend to bind to the body's receptors. Receptors for estrogens and androgens in the human body modulate toxic reactions in a gender-specific way. Besides we know that males have more relative fat mass, which allows them to give a larger distribution volume for chemical particles in the environment. However, females' bodies metabolize more quickly than males, resulting in higher toxicity.

Generally, we knew that the risk of having cardiovascular disease due to air pollution is relatively small compared to the effect of established cardiovascular risk factors associated with lifestyles such as smoking, obesity, and high blood pressure. Even though the risk is small, air pollution effects are considered a severe public health problem because a large number of people are exposed over their entire lifetime.

We compare our results from this study with Mahiyuddin et al. (2013), which was done in the same urbanized area of Klang Valley. Mahiyuddin et al. (2013) observed that only PM<sub>10</sub>, CO, O<sub>3</sub> and NO<sub>2</sub> were associated with mortality. However, the risks among mortality were found to be higher than the risk from this study with no acute effects at lag0 observed. This showed that the pollutants' effects on hospital admission were acute effects, which will lead to mortality after a few days of exposure.

Since the study was done in 2008-2010, we compared the concentrations of pollutants with the MAQG IT-1 for the year 2015, which was also far above the WHOAQG. Malaysia introduced the new ambient air quality standard to replace the old standard that had been used since 1989. The air pollutants concentration limit will be strengthened in stages until the year 2020. There are 3 interim targets set which include interim target 1 (IT-1) in 2015, interim target 2 (IT-2) in 2018, and the full implementation of the standard in 2020. Even with the current concentrations, the risks were still observed. Therefore, the current air quality standards might not be appropriate to protect public health in an urbanized area such as Klang Valley.

Separating the effects of one pollutant from the effects of others is often difficult. At the same time, not all members of the population are equally sensitive to such effects. Some subgroups such as the elderly, asthmatics children,

and people with heart diseases are more likely to be at risk from exposure to air pollution compared to others. Several epidemiological studies have shown that the individual effects of air pollution are normally rather small. However, the public health effect can be substantial. This also means that in general, everyone in the world is exposed to air pollution, but in varying degrees.

There are several limitations of the study that should be acknowledged. We used air pollutant data from fixed-site monitoring stations, as in all other similar time series studies, rather than measuring individual exposures. This causes measurement errors in the assessment of exposure, but these errors are generally random. Second, we assumed that all individuals in the study area were equally exposed to almost the same air pollutants at all times, which may not be accurate.

## CONCLUSION

This study found that NO<sub>2</sub>, CO, and PM<sub>10</sub> increased the risk of hospital admission for cardiovascular and respiratory diseases among the residents of Klang Valley, Malaysia. The elderly, children, and females have been identified as vulnerable sub-populations to air pollution. As the concerns about these health effects, regulations to reduce emissions of harmful air pollutants have been discussed and implemented at the international, regional, national, and local levels. Thus, there is a need for accurate evidence and comparable estimates between countries on the health effect of air pollution as a foundation for designing scientific and effective strategies to reduce these effects.

## ACKNOWLEDGMENTS

The authors would like to gratefully acknowledge the Director General of Health, MOH, and the Director of Institute for Medical Research (IMR), MOH, for the permission to publish this paper. We would like to thank the Health Informatics Center, MOH, Department of Environment (DOE), and Malaysia Meteorological Department (MMD), for providing the data. This research was funded by the National Institute of Health (NMRR-13-630-16667) and approved by Malaysia Medical Research and Ethics Committee (KKM/NIHSEC/800-2/2/2 Jld.3. P13-698).

## REFERENCES

- Amancio, C.T. and Nascimento, L.F.C. 2012. Association of sulfur dioxide exposure with circulatory system deaths in a medium-sized city in Brazil. *Brazil. J. Med. Biol. Res.*, 45:1080-1085
- Amato, F., Laib, M., Guignard, F. and Kanevski, M. 2019. Analysis of air pollution time series using complexity-invariant distance and information measures. *Phys A Stat Mech its Appl.*, 547.

- Amsalu, E., Guo, Y. and Li, H. 2019. Short-term effect of ambient sulfur dioxide (SO<sub>2</sub>) on cause-specific cardiovascular hospital admission in Beijing, China: A time series study. *Atmos. Environ.*, 208:74-81
- Awang, M.B., Jaafar, A.B. and Abdullah, A.M. 2000. Air quality in Malaysia: Impacts, management issues, and future challenges. *Respirology*, 5:183-196
- Boezen, H.M., Vonk, J.M. and Vander, Z.S.C. 2005. Susceptibility to air pollution in elderly males and females. *Eur. Respir. J.*, 25: 1018-1024
- Butter, E.M. 2006. Are women more vulnerable to environmental pollution? *J. Hum. Ecol.*, 20(3): 221-226
- Carthy, P., ÓDomhnaill, A. and O'Mahony, M. 2021. Local NO<sub>2</sub> concentrations and asthma among over-50s in Ireland: A microdata analysis. *Int. J. Epidemiol.*, 49: 1899-1908.
- Chan, C.C., Chuang, K.J. and Chien, L.C. 2000. Urban air pollution and emergency admissions for cerebrovascular diseases in Taipei, Taiwan. *Eur Heart J.*, 27:1238-1244.
- Department of Environment. 2015. New Malaysia Ambient Air Quality Standard. In: DOE. <https://www.doe.gov.my/portalv1/wp-content/uploads/2013/01/Air-Quality-Standard-BI.pdf>. Accessed on 4 April 2021.
- Fiorito, G., Vlaanderen, J. and Polidoro, S. 2018. Oxidative stress and inflammation mediate the effect of air pollution on cardio- and cerebrovascular disease: A prospective study in nonsmokers. *Environ. Mol. Mutagen.*, 59: 234-246.
- Hassan, M.N., Choo, W.Y. and Afroz, R. 2000. Estimation of health damage cost for 1997-haze episode in Malaysia using the Ostro model. In: Malaysian Science and Technology Congress (MSTC). Ipoh, Perak, Malaysia.
- Huff, R.D., Carlsten, C. and Hirota, J.A. 2019. An update on immunologic mechanisms in the respiratory mucosa in response to air pollutants. *J. Allergy Clin. Immunol.*, 143: 1989-2001.
- Juneng, L., Latif, M.T., and Tangang, F. 2011. Factors influencing the variations of PM10 aerosol dust in Klang Valley, Malaysia during the summer. *Atmos. Environ.*, 45: 4370-4378.
- Kowalska, M., Skrzypek, M., Kowalski, M. and Cyrus, J. 2020. Effect of NO<sub>x</sub> and NO<sub>2</sub> Concentration increase in ambient air to daily bronchitis and asthma exacerbation, Silesian Voivodeship in Poland. *Int. J. Environ. Res. Public Health*, 17: 754.
- Li, L., Lei, Y. and Pan, D. 2016. An economic evaluation of the air pollution effect on public health in China's 74 cities. *Springerplus*, 5: 402.
- Mahiyuddin, W.R.W., Sahani, M. and Aripin, R. 2013. Short-term effects of daily air pollution on mortality. *Atmos. Environ.*, 65: 69-79.
- Miller, M.R. 2020. Oxidative stress and the cardiovascular effects of air pollution. *Free Radic. Biol. Med.*, 151: 69-87.
- Moolgavkar, S.H. 2000. Air pollution and hospital admissions for diseases of the circulatory system in three U.S. Metropolitan areas. *J. Air Waste Manag Assoc.*, 50:1199-1206. <https://doi.org/10.1080/10473289.2000.10464162>
- Peters, S.A., Woodward, M. and Rumley, A. 2017. Plasma and blood viscosity in the prediction of cardiovascular disease and mortality in the Scottish heart health extended cohort study. *Eur. J. Prev. Cardiol.*, 24: 161-167.
- Phosri, A., Ueda, K. and Phung, V.L.H. 2019. Effects of ambient air pollution on daily hospital admissions for respiratory and cardiovascular diseases in Bangkok, Thailand. *Sci. Total Environ.*, 651: 1144-1153.
- Rahman, S.A., Hamzah, M.S. and Elias, M.S. 2015. A long-term study on characterization and source apportionment of particulate pollution in Klang Valley, Kuala Lumpur. *Aerosol Air Qual. Res.*, 15: 2291-2304.
- Rovella, N., Aly, N. and Comite, V. 2021. The environmental impact of air pollution on the built heritage of historic Cairo (Egypt). *Sci. Total Environ.*, 764: 142905.
- Sentian, J., Herman, F., Yih, C.Y. and Hian, W.J.C. 2019. Long-term air pollution trend analysis in Malaysia. *Int. J. Environ. Impacts. Manag. Mitig. Recover.*, 2: 309-324.
- Shen, S., Li, X. and Yuan, C. 2020. Association of short-term exposure to sulfur dioxide and hospitalization for ischemic and hemorrhagic stroke in Guangzhou, China. *BMC Publ. Health*, 20: 263.
- Slama, A., Iwiczki, A. and Woyniak, J. 2019. Impact of air pollution on hospital admissions with a focus on respiratory diseases: a time-series multi-city analysis. *Environ. Sci. Pollut. Res.*, 26: 16998-17009.
- Tajudin, M.A.B.A., Khan, M.F. and Mahiyuddin, W.R.W. 2019. Risk of concentrations of major air pollutants on the prevalence of cardiovascular and respiratory diseases in an urbanized area of Kuala Lumpur, Malaysia. *Ecotoxicol. Environ. Saf.*, 171: 290-300.
- UN World Urbanization Prospects - Population Division - United Nations. <https://population.un.org/wup/>. Accessed on 1 April 2021.
- Usmani, R.S.A., Saeed, A., Abdullahi, A.M. 2020. Air pollution and its health impacts in Malaysia: a review. *Air Qual Atmos Heal* 13:1093-1118. <https://doi.org/10.1007/s11869-020-00867-x>.
- Vichit-Vadakan, N., Vajanapoom, N. and Ostro, B. 2008. The public health and air pollution in Asia (PAPA) Project: Estimating the mortality effects of particulate matter in Bangkok, Thailand. *Environ. Health Perspect.*, 116: 1179-1182. <https://doi.org/10.1289/ehp.10849>
- WHO. 2019. Air Quality Guidelines: Global Update 2005. <http://www.who.int/airpollution/publications/aqg2005/en/>. Accessed on 4 April 2021.
- Yap, J., Ng, Y., Yeo and K.K. 2019. Particulate air pollution on cardiovascular mortality in the tropics: Impact on the elderly. *Environ. Heal. A Glob. Access. Sci. Source*, 18: 34. <https://doi.org/10.1186/s12940-019-0476-4>
- Zhang, Y., Wang, S.G. and Ma, Y.X. 2015. Association between ambient air pollution and hospital emergency admissions for respiratory and cardiovascular diseases in Beijing: A time series study. *Biomed. Environ. Sci.*, 28: 352-363.
- Zhou, H., Wang, T. and Zhou, F. 2019. Ambient air pollution and daily hospital admissions for respiratory disease in children in Guiyang, China. *Front. Pediat.*, 7: 1-9.





# Enhancement of Xanthan Biosynthesis Using Medicinal Herbs - A Novel Approach

B. S. Rajyaguru\*, A. Varma\*, A. C. Kharkwal\*† and J. Singh\*\*

\*Department of Microbiology, Amity Institute of Microbial Technology, Amity University, Noida-201313, India

\*\*Department of Global Regulatory Affairs, Danisco (India) Private Limited, Gurgaon-122002, India

†Corresponding author: A. C. Kharkwal; [ackharkwal@amity.edu](mailto:ackharkwal@amity.edu)

Nat. Env. & Poll. Tech.  
Website: [www.neptjournal.com](http://www.neptjournal.com)

Received: 06-01-2022

Revised: 20-02-2022

Accepted: 24-02-2022

## Key Words:

Herbs

Molasses

Polysaccharide

Xanthan

*Xanthomonas campestris*

## ABSTRACT

This study aimed to evaluate the potential of five medicinal herbs in the enhancement of xanthan gum production when used against indigenously isolated (from molasses, an agricultural waste) phytopathogen *Xanthomonas campestris* MW741556. Antibiotic susceptibility of five medicinal herbs (*Moringa oleifera*, *Bacopa monnieri*, *Glycyrrhiza glabra*, *Withania somnifera*, and *Arthrospira platensis*) against *X. campestris* culture was first checked. All five herbs exhibited a clear zone of inhibition against *X. campestris* during the investigation. Thereafter their effect on enhancing the xanthan gum production was studied using molasses enriched medium. The results of this experiment showed that all five herbs were capable of enhancing xanthan gum production significantly. Xanthan gum produced differed in viscosity and dried biomass. Among all, *A. platensis* and *M. oleifera* were found to be the most promising for xanthan gum production with higher viscosity. These results were further confirmed by the characterization of xanthan gum produced by five herbs using Fourier Transform Infrared Spectroscopy. Further, a multivariate approach using principal component analysis confirmed the variability among the herbs used. This versatility of these medicinal herbs opens the possibility of their utilization and application in various fields.

## INTRODUCTION

Xanthan is a polysaccharide, which is a widely used food additive produced by bacteria commonly known as *X. campestris* (Petri 2015). It acts as an effective thickening agent and stabilizer in largely consumed products produced by various industrial sectors like the food industry, cosmetics, pharmaceutical, textile, petroleum, etc. (Lopes et al. 2015, Petri 2015). Based on its non-toxic and non-sensitizing nature, it has been approved as a food additive by the States Food and Drug Administration (FDA) (Kennedy et al. 1984). In food industries, it is used as a suspending and thickening agent for butter, ice creams, chocolates, etc. (Infee Sharley & Priyadarshini 2015, Suput et al. 2015). Due to its easy pourability and ability to keep the dressing on the tops of the salad, it is widely used in salad dressings also (Abedinzadeh et al. 2016).

The bacterium, *X. campestris*, is gram-negative, and aerobic, hence needs oxygen for its growth and production of xanthan gum (Sarbatly & England 2016). The conventional ways of increasing the production of xanthan in industries by *Xanthomonas campestris* on the appropriate medium under optimal conditions include the addition of sucrose or glucose as a carbon source (Garcia-Ochoa et al. 2000, Lopes et al. 2015). However, these methods are relatively expensive and increase the cost of the product produced.

Researchers are more focused on exploring different waste residues which can be used as carbon sources. In addition, isolation of new strains to produce xanthan, which can metabolize different carbon sources (Bajic et al. 2014, 2015). This type of approach will not only encourage the reuse of the residual waste but will also reduce the production cost of the xanthan gum (Dos Santos et al. 2016, Ng et al. 2020).

In such a scenario, molasses, a waste byproduct of sugarcane can be an interesting option to use as a substrate for xanthan gum production, since it contains approximately 40% sucrose (Clarke 2003) hence a good source of carbon (Souw & Demain 1979) which enhances the growth of the *X. campestris* and therefore, resulting in xanthan gum production. Besides this, it is a renewable source and a by-product that is produced in large quantities during the processing of sugarcane juice. The present study also aims to evaluate the contribution of five different medicinal herbs in the production of xanthan gum along with their antibacterial effect against *Xanthomonas campestris* grown in molasses solution.

## MATERIALS AND METHODS

### Organism and Selection of Medicinal Plants

In this study, *in vitro* isolation of the bacterium was carried out, which was further identified as *Xanthomonas*

MW741556 using 16S\_rRNA by National Center for Biotechnology Information (NCBI). Five medicinal plants (Table 1) were selected for the study based on their antibacterial properties against phytopathogens like *X. campestris*.

### Inoculum for Antibiotic Susceptibility Test (AST)

The sub-cultured *X. campestris* strain was inoculated in a nutrient broth medium and incubated at 37°C for 24 h to obtain a fresh 24-hour culture. The culture was standardized according to the 0.5 McFarland Standard to obtain a standard inoculum size of  $1.5 \times 10^8$  CFU.mL<sup>-1</sup> (Magaldi et al. 2004). This standardized strain has been used as an inoculum for AST.

### Sample and Standard Drug Preparation for AST

For this, 5 medicinal herbs extracts have been dissolved in methanol in four concentrations of the sample as 100 µg.mL<sup>-1</sup>, and 250 µg.mL<sup>-1</sup>, 500 µg.mL<sup>-1</sup> and 1000 µg.mL<sup>-1</sup>. The standard antibiotic drug Kanamycin of concentration 30 µg.mL<sup>-1</sup> is also prepared which is used as a control in the experiments.

### Well, Diffusion-Inoculation and Incubation for AST

Five different plates containing Mueller-Hinton agar were prepared and swabbed with the standard inoculum of *X. campestris*. After inoculation, 5 wells of 10 mm were bored in each plate using a good borer. Each plate was inoculated with 4 different concentrations of each plant sample and 1 well using the standard drug Kanamycin. Post-inoculation, the plates were incubated at 37°C for 24 h in an upright position.

### Xanthan Gum Extraction

Xanthan gum production by *X.campestris* has been carried out using Molasses enriched growth media along with the addition of indigenous medicinal herbs as an additive and the effect of herbs on the quantity of the xanthan gum production was studied.

### Plant Extract Preparation for Xanthan Gum Production

Five different medicinal plants 1A, 2B, 3C, 4D, and 5E (Table 1) were shade dried for a period of ten days. Then the

dried plant material was grounded to a fine powder and was sieved (sieve 60 size) to obtain granules of the same size. 10 g of each sample was taken and solubilized using 10 ml of the respective solvents (distilled water and methanol) using a cyclomixer. These solubilized samples were then filtered thoroughly using a double-layered muslin cloth. This filtrate was then centrifuged at 4000 g for a period of 3 minutes. Post-centrifugation, the supernatant was collected and filtered using Whatman filter paper (No. 1). This filtrate was then heat sterilized using an autoclave at 121°C for 15 minutes and preserved in amber glass bottles.

### Media Preparation for Xanthan Gum Production

*X. campestris* was further inoculated in molasses-rich media for the production of xanthan gum. The medium (g/l) consisted of molasses (8%), KH<sub>2</sub>PO<sub>4</sub>, MgSO<sub>4</sub>, (NH<sub>4</sub>)<sub>2</sub>SO<sub>4</sub>, and CaCO<sub>3</sub>. Except for molasses, the remaining components of the media were autoclaved for sterilization whereas molasses was membrane filtered using a 0.45µm filter.

### Inoculum Preparation for Xanthan Gum Production

The previously prepared inoculum of *X. campestris* was inoculated in 50ml of production media and incubated at 30°C for 48hours under shaking conditions of 200 RPM. The grown cultures are either used directly for further tests or preserved at 4°C until further use. This microbial culture is used as a starter culture for further tests involving xanthan gum production.

### Xanthan Gum Production

The 48 hrs culture grown in the production media was added with 10% (v/v) of the respective plant extract. For the 5 herbs, 5 different media containing each specific plant extract is prepared in 5 replicates (50 mL production media with 5 g of respective herb extract). The pH of the media was maintained at 7. The inoculated media were incubated at 30°C for 48 hours under shaking conditions of 200 RPM.

### Xanthan Gum Recovery

Post-incubation, the cultures were subjected to pretreatment by heating using a water bath at 90 °C for 15 minutes and

Table 1: List of medicinal herbs used in study.

Sample	Common Name	Scientific Name	Family	Parts Used
A1	Moringa	<i>Moringa oleifera</i>	Moringaceae	Leaves
B2	Brahmi	<i>Bacopa monnieri</i>	Plantains	Leaves
C3	Yastimadhu	<i>Glycyrrhiza glabra</i>	Legumes	Roots
D4	Ashwagandha	<i>Withania somnifera</i>	Solanacea	Roots
E5	Spirulina	<i>Arthrospira platensis</i>	Phormidiaceae	Algae



then filtered using Whatman No. 1 filter paper. The filtrate was then added with 50% ice-cold isopropanol (2x volume of filtrate) to which 1% (w/v) of potassium chloride was also added to stimulate the process of precipitating the xanthan gum (Kawahara & Obata 1979, Stredansky & Conti 1999). The product was then dried in the oven at 45°C for 24 h. Freeze drying is carried out to obtain the dry weight of precipitated xanthan gum. The dried biomass of cells and xanthan gum production was weighed and compared. 1% of xanthan gum solution is prepared in water and analyzed for viscosity using Brookfield Viscometer at 25°C (Dogan et al. 2007).

### Spectroscopy of Fourier Transform Infrared (FTIR)

Samples of control and all five herbs producing xanthan were characterized using a Jasco Fourier Transform Infrared

Spectrometer. Fourier transforms infrared spectra generated by the absorption of electromagnetic radiation in the frequency range of 400 to 4000  $\text{cm}^{-1}$ . Graphs were drawn using Spectragryph 1.2.

### Statistical Analysis

The yield data of gum production, its viscosity, and dried biomass of control (*X. campestris*) and five medicinal herbs were obtained from 5 replicates. Results obtained were averaged and the standard deviation of all the averaged (mean) results has been evaluated. Further, the multivariate approach of Principal Component Analysis (PCA) was used to identify which concentrations and combinations of medicinal herbs are effectively producing xanthan gum. The analysis was performed using PAST (4.0) software.

Table 2: Inhibitory effect of varying concentrations of different medicinal herbs against *Xanthomonas Campestris* in the form of zone of inhibition (ZOI).

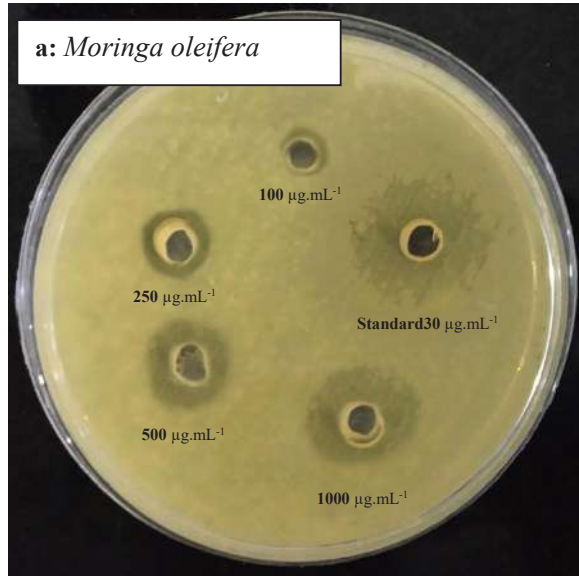
Name of the Sample	Concentration ( $\mu\text{g.mL}^{-1}$ )	Diameter of ZOI (mm)
<i>M. oleifera</i>	100	12
	250	14
	500	19
	1000	23
	Kanamycin- 30 $\mu\text{g.mL}^{-1}$	27
<i>B. monnieri</i>	100	11
	250	13
	500	16
	1000	21
	Kanamycin- 30 $\mu\text{g.mL}^{-1}$	29
<i>G. glabra</i>	100	11
	250	14
	500	17
	1000	19
	Kanamycin- 30 $\mu\text{g.mL}^{-1}$	28
<i>W. somnifera</i>	100	11
	250	13
	500	18
	1000	22
	Kanamycin- 30 $\mu\text{g.mL}^{-1}$	29
<i>A. platensis</i>	100	12
	250	15
	500	17
	1000	23
	Kanamycin- 30 $\mu\text{g.mL}^{-1}$	27

## RESULTS

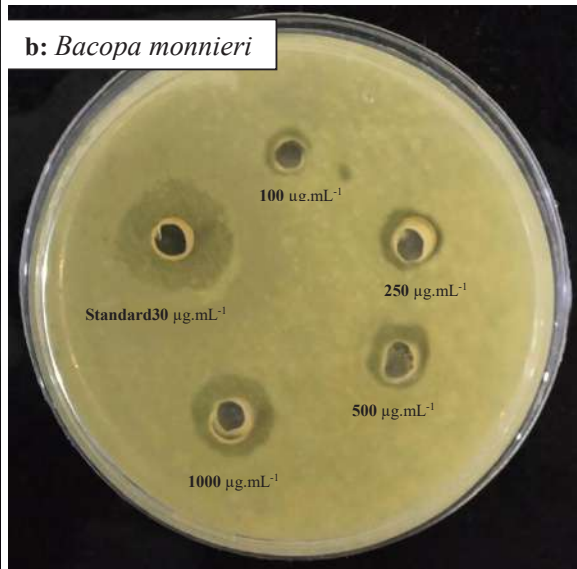
### Antibiotic Susceptibility Test (AST)

Antibiotic Susceptibility Test (AST) of five medicinal herbs was investigated for their effect on the growth of *X. campestris* by inhibition zone assay technique in-vitro conditions. In this study, post-incubation, the plates were observed for

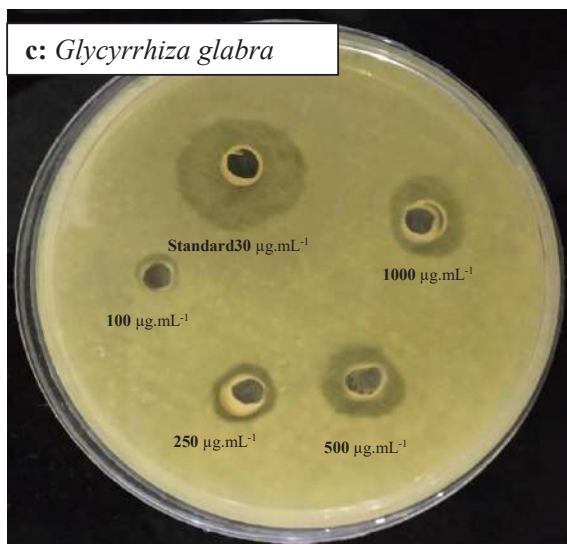
the zone of inhibition (ZOI) around the inoculated wells and the diameter of the zone is measured (Table 2). For this, growth is measured in different concentrations of methanol extract viz. 100  $\mu\text{g.mL}^{-1}$ , 250  $\mu\text{g.mL}^{-1}$ , 500  $\mu\text{g.mL}^{-1}$  and 1000  $\mu\text{g.mL}^{-1}$  and Kanamycin (30  $\mu\text{g.mL}^{-1}$ ) as a control (Table 2). *Moringa oleifera* produced ZOI of 23 mm, 19 mm, 14 mm, and 12 mm at concentrations of 1000  $\mu\text{g.mL}^{-1}$ , 500  $\mu\text{g.mL}^{-1}$ ,



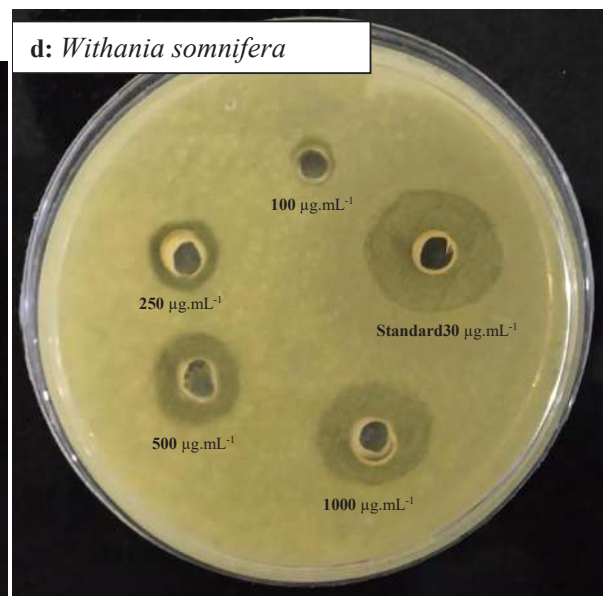
1(a)



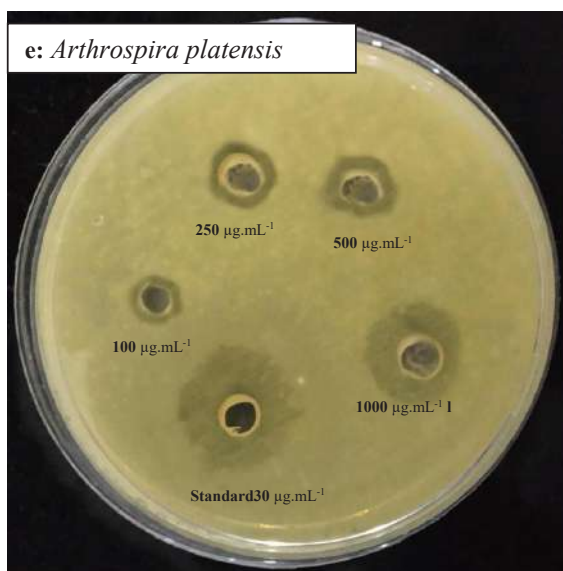
1(b)



1(c)



1(d)



1(e)

Fig 1. Antibacterial Study Test (AST) results of different herbs used in the study at dilution of  $30 \mu\text{g.mL}^{-1}$  (standard),  $100 \mu\text{g.mL}^{-1}$ ,  $250 \mu\text{g.mL}^{-1}$ ,  $500 \mu\text{g.mL}^{-1}$  and  $1000 \mu\text{g.mL}^{-1}$  dilutions (a) *Moringa oleifera* (b) *Bacopa monnieri* (c) *Glycyrrhiza glabra* (d) *Withania somnifera* (e) *Arthrospira platensis*.

$250 \mu\text{g.mL}^{-1}$ ,  $100 \mu\text{g.mL}^{-1}$  respectively and 27mm in control as shown in Fig. 1a. However, *Bacopa monnieri* produced ZOI of 21mm, 16mm, 13mm, and 11mm at concentrations of  $1000 \mu\text{g.mL}^{-1}$ ,  $500 \mu\text{g.mL}^{-1}$ ,  $250 \mu\text{g.mL}^{-1}$ ,  $100 \mu\text{g.mL}^{-1}$  respectively, and 29 mm in control (Fig. 1b). *Glycyrrhiza glabra* exhibited ZOI of 28mm in control, 19 mm, 17 mm, 14 mm, and 11mm at concentrations of  $1000 \mu\text{g.mL}^{-1}$ ,  $500 \mu\text{g.mL}^{-1}$ ,  $250 \mu\text{g.mL}^{-1}$ , and  $100 \mu\text{g.mL}^{-1}$  respectively (Fig. 1c). *Withania somnifera* exhibited ZOI of 29 mm in control, 22 mm, 18 mm, 13 mm, and 11mm at concentrations of  $1000 \mu\text{g.mL}^{-1}$ ,  $500 \mu\text{g.mL}^{-1}$ ,  $250 \mu\text{g.mL}^{-1}$ ,  $100 \mu\text{g.mL}^{-1}$  respectively (Fig. 1d). *Arthrospira platensis* produced ZOI of 23 mm, 17 mm, 15 mm and 12 mm at concentrations of  $1000 \mu\text{g.mL}^{-1}$ ,  $500 \mu\text{g.mL}^{-1}$ ,  $250 \mu\text{g.mL}^{-1}$ ,  $100 \mu\text{g.mL}^{-1}$  respectively, and 27mm in control (Fig. 1e). Results indicate that the ZOI of five plant extracts dissolved in methanol increased with an increase in concentration. However, the largest ZOI is reported in control of every sample.-

### Xanthan Gum Production

All the results were obtained in 5 replicates in preoptimized conditions of 48hours. However, the mean of these replicate readings was taken for the analysis of the results obtained. Experiments were conducted to observe the effect of five medicinal herbs on the production of xanthan gum, viscosity, and dried cell biomass per liter of the solution.

For this, five herbs namely *M. oleifera*, *B. monnieri*, *G. glabra*, *W. somnifera*, and *A. platensis* along with a control (without herb) were studied for 48hrs. Table 3 presents the results of the yield of xanthan gum (obtained by adding medicinal herbs as an additive) per liter of the solution. Among all the studied herbs, the maximum yield of xanthan gum was obtained by the stress of *A. platensis* ( $9.12 \text{ g.L}^{-1}$ ) followed by *M. oleifera* ( $8.66 \text{ g.L}^{-1}$ ). However, in control (without any herb) the xanthan yield was determined as  $7.41 \text{ g.L}^{-1}$ . The results show that the presence of the medicinal herbs used in the study enhanced the production of xanthan gum in *X. campestris*. The highest yield of xanthan is observed by the stress of *A. platensis* followed by *M. oleifera* after 48 h. A present study is a novel approach, in which we studied the effect of medicinal herbs on xanthan production when used against *X. campestris* as antibacterial agents. Our results demonstrated the significantly enhanced production of xanthan gum under the influence of these herbs.

In the present study, the highest viscosity of xanthan gum was observed by the stress of *A. platensis* ( $905 \text{ mPa.s}$ ) followed by *M. oleifera* ( $717.2 \text{ mPa.s}$ ), *G. glabra*,  $675.2 \text{ mPa.s}$ , *B. monnieri* ( $440.2 \text{ mPa.s}$ ) and the least by *W. somnifera* ( $485.2 \text{ mPa.s}$ ). However, in control, in which no herb was added, the viscosity of xanthan gum was determined as  $430.20 \text{ mPa.s}$  (Table 4).

Table 3: Effect of medicinal herbs on production of xanthan (g.L<sup>-1</sup>).

S. No.	<i>M. oleifera</i>	<i>B. monnieri</i>	<i>G. glabra</i>	<i>W. somnifera</i>	<i>A. platensis</i>	Control
	8.74	7.52	8.12	7.84	9.00	7.41
	8.62	7.56	8.18	7.76	9.20	7.37
	8.74	7.57	8.20	7.69	9.18	7.47
	8.63	7.60	8.16	7.81	9.14	7.34
	8.59	7.51	8.22	7.78	9.09	7.45
Mean	8.66±0.07	7.55±0.04	8.18±0.04	7.78±0.06	9.12±0.08	7.41±0.05

In the present study, dried biomass of *A. platensis* (4 g.L<sup>-1</sup>) was the maximum per liter of the solution as compared to other medicinal herbs used in the study. However, the dried biomass of control was observed as 3.18 g.L<sup>-1</sup>, which was found least in amount as compared to samples having herbs. However, dried biomass in samples of *M. oleifera*, *B. monnieri*, *G. glabra*, and *W. somnifera* was determined as 3.82 g.L<sup>-1</sup>, 3.42 g.L<sup>-1</sup>, 3.76 g.L<sup>-1</sup>, and 3.52 g.L<sup>-1</sup> respectively as shown in Table 5.

#### Spectroscopic Analysis using Fourier Transform Infrared (FTIR)

Fig. 2(a-e) represents the samples of xanthan gum from the medicinal herbs and Fig. 2f represents the control used in the study. By comparing the results, similar peaks (peaks in the range of 1550–1600 and 2700cm<sup>-1</sup>) were found to be present in all the samples (Fig. 2a-e) as observed in control confirming the formation of xanthan gum. By comparing the intensity of

the peaks, it is observed that some carbonyl double bonds, which can be from ketones, aldehydes, esters, or carboxyls may be present. A stretch in the range of 2700 cm<sup>-1</sup> to 2835 cm<sup>-1</sup> in control (Fig. 2f), *M.oleifera* (Fig. 2a), *B. monnieri* (Fig. 2b), *G. glabra* (Fig. 1c), *W. somnifera* (Fig. 2d) and *A. platensis* (Fig. 2e) attributes to –CH<sub>2</sub>, RC-OH groups. A sharp peak at 2430 cm<sup>-1</sup> is observed in Fig. 2d of *W. somnifera* indicating the P-H phosphine group. The absence of some of the peaks between the standard xanthan and plant additives explains the major structural changes caused by plants due to the influence of their bio-reducing phytochemical groups.

#### Principal Component Analysis (PCA)

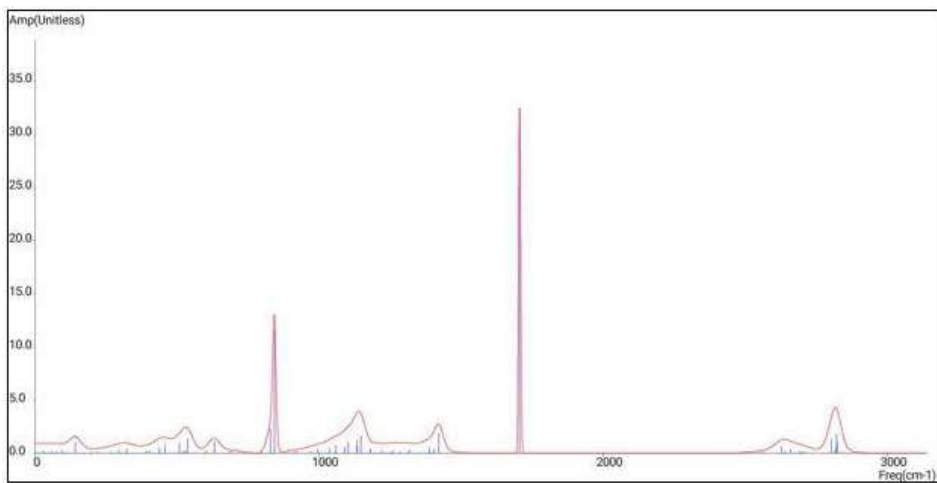
PCA analysis of the data matrix used 5 samples each of 5 herbs and control, which resulted in most of the data variance being explained by the first two principal components i.e., PC1 and PC2 (Fig. 3a-c). In Fig. 3a the first PC1 accounted for 43.73% of the total variance and the second PC 2 (name)

Table 4: Viscosity of xanthan gum produced under the stress of medicinal herbs (Pa.s).

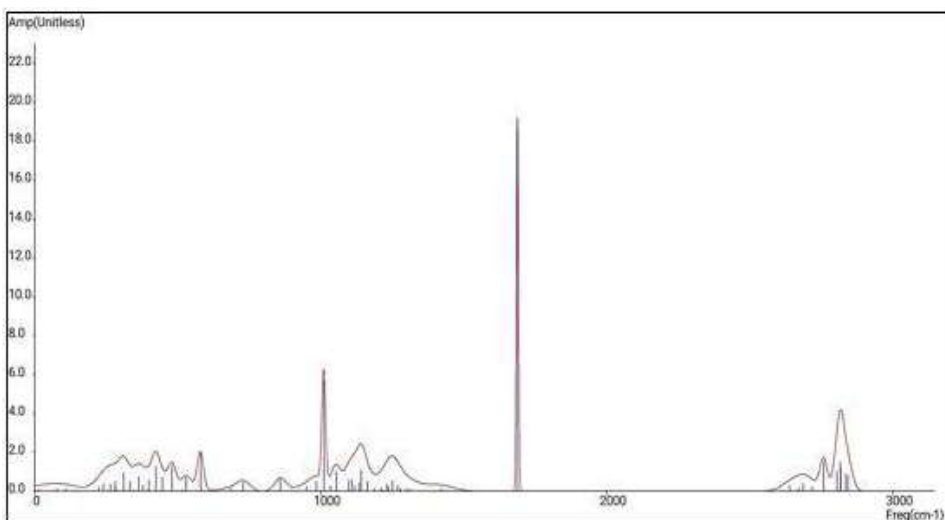
S.No.	<i>M. oleifera</i>	<i>B. monnieri</i>	<i>G. glabra</i>	<i>W. somnifera</i>	<i>A. platensis</i>	Control
	720	430	670	490	900	430
	714	444	675	484	910	427
	722	448	678	480	907	436
	718	452	673	487	905	424
	712	427	680	485	903	434
Mean	717±4.15	440±11.10	675±3.96	485±3.70	905±3.81	430±4.92

Table 5: Dried biomass produced after formation of xanthan by medicinal herbs (g.L<sup>-1</sup>).

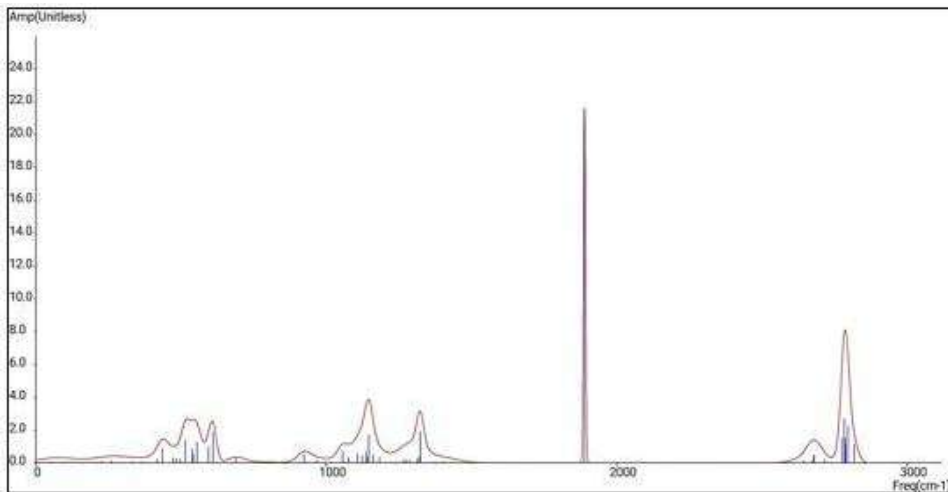
S.No.	<i>M. oleifera</i>	<i>B. monnieri</i>	<i>G. glabra</i>	<i>W. somnifera</i>	<i>A. platensis</i>	Control
	3.90	3.30	3.70	3.60	4.10	3.10
	3.70	3.50	3.80	3.50	3.90	3.10
	4.00	3.50	3.80	3.50	3.90	3.30
	3.80	3.60	3.70	3.60	4.10	3.20
	3.70	3.20	3.80	3.40	4.00	3.20
Mean	3.82±0.13	3.42±0.16	3.76±0.05	3.52±0.08	4.00±0.10	3.18±0.08



2(a)

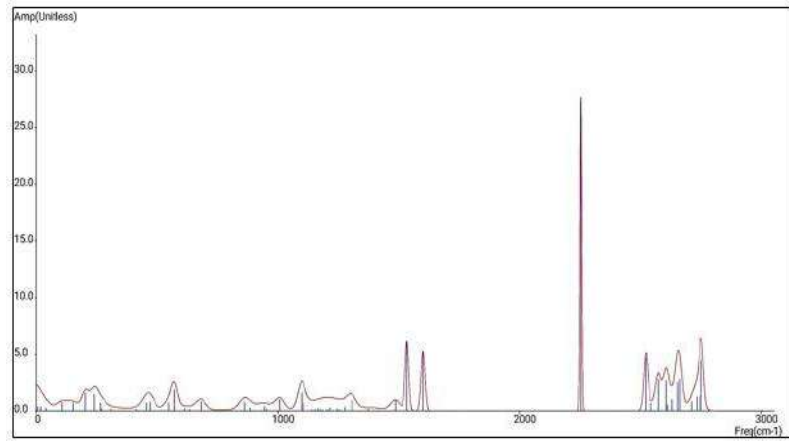


2(b)

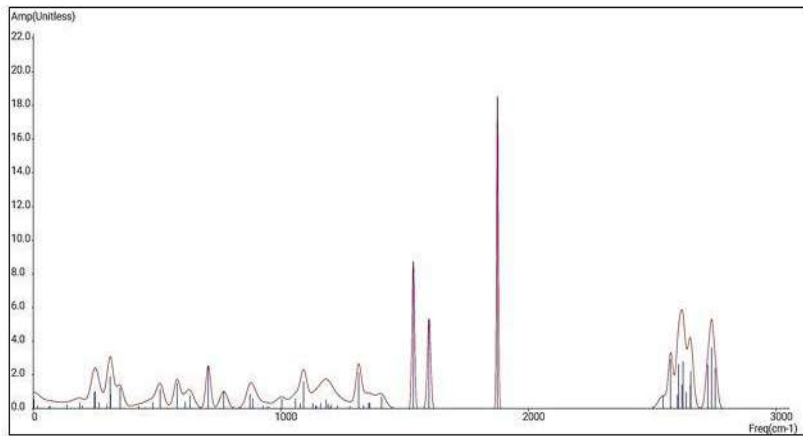


2(c)

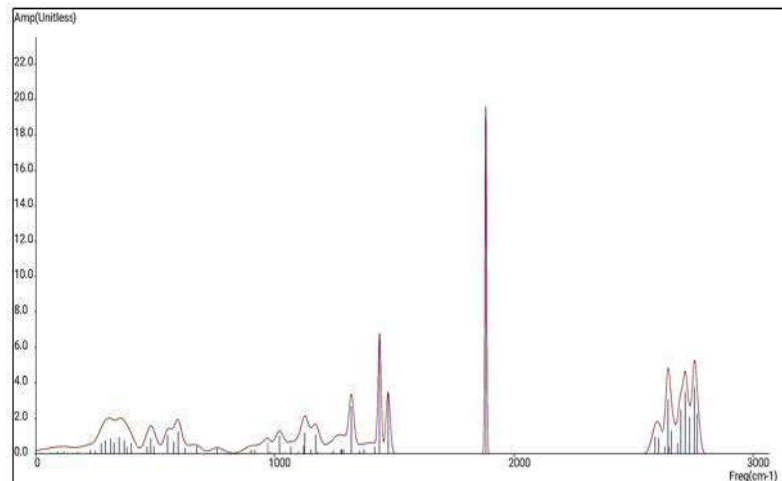
Fig. 2 cont....



2(d)



2(e)

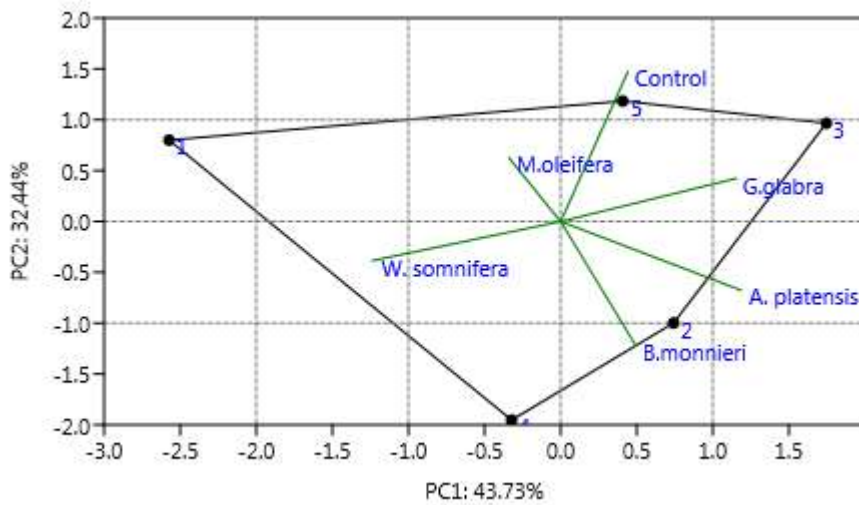


2(f)

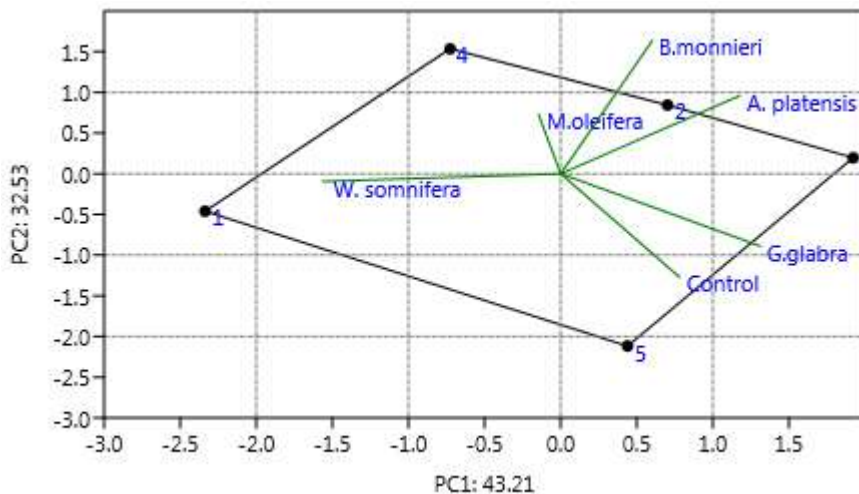
Fig. 2: FTIR spectra of xanthan gum produced with (a) *Moringa oleifera* (b) *Bacopa monnieri* (c) *Glycyrrhiza glabra* (d) *Withania somnifera* (e) *Arthrospira platensis* (f) Control (without any plant additive).

for 32.44%. As evident in Fig. 3a, *A. platensis* is the most important contributor to PC1 and Control is the most important contributor to PC2. *A. platensis* and *B. monnieri* are highly correlated whereas *W. somnifera* is almost unrelated to the rest of the two herbs in PC1. However, in PC2, all three variables are at almost equal angles, showing lesser correlation within them. *G. glabra* and *W. somnifera* fall in different clusters and show a negative correlation. Similarly, *M. oleifera* and *B. monnieri* are negatively correlated. *G. glabra* and *B. monnieri* are almost equally correlated to *A. platensis* as inferred from the vector angles of approx. 35°, whereas the vector angle of nearly 90° between the *A. platensis* and Control showed a very poor correlation in the responses.

Fig. 3b, explains the graphical representation of the effect of different herbs on the viscosity of xanthan gum production. Here also, PC1 (43.21%) and PC2 (32.53%) show most of the variability. Control, *G. glabra*, and *W. somnifera* fall under PC1. Control and *G. glabra* are highly correlated to each other. However, *A. platensis*, *B. monnieri* and *M. oleifera* are equally correlated to each other and fall under PC2. Here, *B. monnieri* was found to contribute the most. Dried biomass obtained is presented in Fig. 3c with PC1 (47.04%) and PC2 (29.45%) using PCA. In PC1, *A. platensis* is found to be the only contributor, the rest of all herbs including control falls under PC2. *B. monnieri* and *M. oleifera* are found to be highly correlated.



3(a)



3(b)

Fig. 3 cont....

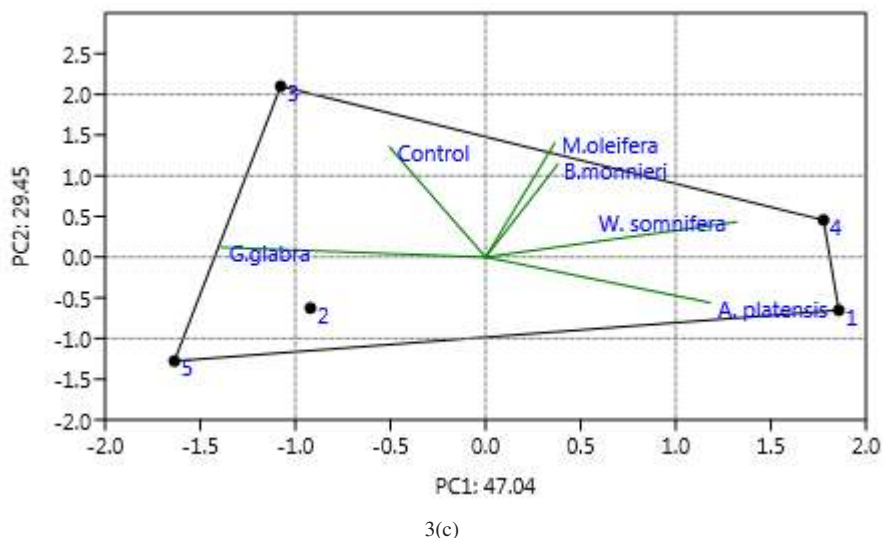


Fig. 3: Principal Component Analysis plot for (a) xanthan yield (b) viscosity of xanthan yield (c) dried biomass (only the first principal component, PC1, and the second principal component, PC2 are shown).

## DISCUSSION

Sharma & Mehta (2001) tested leaf extracts from *Prosopis juliflora*, *Allium sativum*, *Vitis quadrangularis*, *Curcuma longa*, *Occimum sanctum*, and *Eucalyptus citridosa* for their antibacterial potential against *X. campestris*. Sheikh et al. (Sheikh et al. 2012) also studied the antimicrobial potential of eleven aqueous leaf extracts on *Xanthomonas campestris*, *Agrobacterium rhizogenes* and *Aspergillus fumigatus* by the formation of a zone of inhibition (ZOI). Pandey et al. (2011) also reported the antibacterial activity of *R. graveolens* in alcohol and water extracts against many Gram-negative bacterial and plant pathogenic fungi.

Various authors reported the enhanced xanthan yield by a change in their substrate, source of carbon, pH and agitation rates, etc. Recent studies conducted by Mudoi et al. (2013) and Renata et al. (2018) compared the waste residual molasses and carbon sources like glucose, sucrose, lactose, galactose, and maltose for the xanthan production. Lopez et al. (2001) reported the use of agro-industrial wastes such as olive mill wastewaters and date juice by-products (Salah et al. 2010) as a carbon source for xanthan production. In another study, Mohan & Babitha (2010) studied the effect of time on xanthan production and reported the maximum xanthan production after 48 hours. Chavan & Baig (2016) reported maximum xanthan production at 96hrs, after that it started decreasing. A study demonstrated that gum production tends to increase with high pH conditions (De Mello et al. 2016). However, Rana & Raval (2019) demonstrated the effect of carbon sources and incubation states on the viscosity of xanthan yield. Roncevic et al. (2019) observed

the effect of different carbon sources (glucose, lactose, and starch) on the viscosity of xanthan yield and found the high quality of xanthan in terms of viscosity with glucose as compared to lactose and starch. In recent studies exopolysaccharides excreted by *A. platensis* under stress, conditions are determined and analyzed by Nagananthini et al. (2020). In the present study, the Elucidation of results shows that the addition of medicinal herbs not only exhibits antibacterial activity against *X. campestris* but also increases the yield of xanthan gum. These herbs are capable of creating stress when added during the stationary phase i.e. during 48 hrs. of incubation of culture in molasses medium, resulting in enhanced xanthan gum production. *A. platensis*, which is commonly known as *Spirulina* (filamentous, a gram-negative bacteria) was found most efficient, when used as an antibacterial drug against *X. campestris* and resulted in the highest yield of xanthan gum with maximum viscosity. Although, there could be many factors affecting the process which need to be further studied for a better understanding of the metabolism taking place.

## CONCLUSION

The present investigation established novel research on the dual benefits of five medicinal herbs against the *X.campestris*. The antibacterial nature of five medicinal plants not only inhibits the growth of *X.campestris* but also increases the production of xanthan gum (which is used commercially in the food and pharmaceutical industries mainly). Characterization using FTIR spectroscopy confirms the formation of xanthan gum by the five plants when compared with



the control. Results illustrated that *Moringa oleifera* and *Arthrospira platensis* are the most promising herbs for the production of xanthan along with their antibacterial potentials against *X. campestris*. In the future, this opens the prospects of these medicinal herbs exclusively against *X. campestris* as an eco-friendly and safe production of xanthan gum.

## ACKNOWLEDGEMENT

Great thanks to the Faculty of Microbiology, Amity Institute of Microbial Technology, Amity University, Noida for their continuous guidance and support. I would also like to thank Mr. Prasanth, Simbioen Labs, and Scientific Services for his support. Thanks to Dr. Anjana Kamra for her contribution to drafting. Special thanks to Mr. Girish Parikh (Ex- Managing Director, Zandu Pharmaceutical Works Ltd) for his inspiration.

## REFERENCES

- Abedinzadeh, S., Torbati, M. and Azadmard-Da-mirchi, S. 2016. Some qualitative and rheological properties of virgin olive oil-apple vinegar salad dressing stabilized with xanthan gum. *Adv. Pharma. Bull.*, 6(4): 597-606. <https://doi.org/10.15171/apb.2016.074>
- Bajic, B., Dodic, J. and Roncevic, Z. 2014. Biosynthesis of xanthan gum on wastewater from the confectionery industry. *Analecta*, 8(2): 13-17.3. <https://doi.org/10.14232/analecta.2014.2.13-17>
- Bajic, B., Roncevic, Z. and Puskas, V. 2015. White wine production effluents are used for the biotechnological production of xanthan. *J. Process. Energy Agric.*, 19(1): 52-55.
- Chavan, S. and Baig, M.M.V. 2016. Relationship of biomass and xanthan gum production by *Xanthomonas campestris*: optimization of parameters. *Brit. Biotechnol. J.*, 11(1): 1-8. <https://doi.org/10.9734/BBJ/2016/22431>
- Clarke, M.A. 2003. *Syrups Encyclopedia of Food Sciences and Nutrition*. Second edition. MacGraw Hill, USA
- De Mello, L.M., Borges, C.D. and de Oliveira, T.D. 2016. Structure of xanthan gum and cell ultrastructure at different times of alkali stress. *Brz. J. Microbiol.*, 47: 102-109. <https://doi.org/10.1016/j.bjm.2015.11.006>
- Lopes, B., De Monaco, M., Lessa, V.L. and Silva, B.M. 2015. Xanthan gum: properties, production conditions, quality, and economic perspective. *J. Food Nutri. Res.*, 54(7): 185-194.
- Dogan, M., Kayacier, A. and Erhan, I.C. 2007. Rheological characteristics of some food hydrocolloids processed with gamma irradiation. *Food Hydrocoll.*, 21: 392-396. <https://doi.org/10.1016/j.foodhyd.2006.04.010>
- Dos Santos, F.P., Antonio, M. and Oliveira, J. 2016. Bioconversion of agro-industrial wastes into xanthan gum. *Chem. Eng. Transac.*, 49: 145-150. <https://doi.org/10.3303/CET1649025>
- Garcia-Ochoa, F., Santos, V.E., Casas, J.A. and Gómez, E. 2000. Xanthan gum: Production, recovery, and properties. *Biotechnol. Adv.*, 18: 549-579. [https://doi.org/10.1016/S0734-9750\(00\)00050-1](https://doi.org/10.1016/S0734-9750(00)00050-1)
- Infee Sherley, K. and Priyadarshini, R.D. 2015. Review on the production of Xanthan gum in batch and continuous reactors. *Int. J. Chem. Tech. Res.* 8(2): 711-717.
- Kawahara, H. and Obata, H. 1998. Production of xanthan gum and ice-nucleating material from whey by *Xanthomonas campestris* pv.translucens. *Appl. Microb. Biotech.*, 49: 353-358. <https://doi.org/10.1007/s002530051181>
- Kennedy, J.F. and Bradshaw, I.J. 1984. Production, properties and applications of xanthan. *Progress Ind. Microbiol.*, 19: 319-371.
- Lopez, M.J., Moreno, J. and Ramos-Cormenzana, A. 2001. *Xanthomonas campestris* strain selection for xanthan production from olive mill wastewaters. *Water Res.*, 35: 1828-1830. [https://doi.org/10.1016/S0043-1354\(00\)00430-9](https://doi.org/10.1016/S0043-1354(00)00430-9)
- Magaldi, S., Mata-Essayag, S., De Capriles, C.H., Perez, C., Colella, M.T., Olaizola, C. and Ontiveros, Y. 2004. Well diffusion for antifungal susceptibility testing. *Int. J. Infect. Dis.*, 8(1): 39-45.
- Mohan, T.S. and Babitha, R. 2010. Influence of nutritional factors on xanthan production by *Xanthomonas malvacearum*. *Arch. App. Sci. Res.*, 2(6): 28-36.
- Mudoj, P., Bharali, P. and Konwar, B.K. 2013. Study on the effect of pH, temperature, and aeration on cellular growth and xanthan production by *Xanthomonas campestris* using waste residual molasses. *J. Bioprocess. Biotechnol.*, 3(2): 1000135.
- Nagananthini, G., Rajapriya, S. and Arivuvel, P.S. 2020. Extraction and optimization of extracellular polysaccharide production in *Spirulina platensis* MK 343101. *Int. J. Sci. Technol. Res.*, 9(4): 1-5.
- Ng, H.S., Kee, P.E. and Yim, H.S. 2020. Recent advances in the sustainable approaches for conversion and reutilization of food wastes valuable bioproducts. *Bioresour. Technol.*, 302: 12289. <https://doi.org/10.1016/j.biortech.2020.122889>
- Pandey, P., Mehta, A. and Hajra, S. 2011. Evaluation of the antimicrobial activity of *Rutagraveolens* stem extracts by disc diffusion method. *J. Phytol.*, 3(3): 92-95.
- Petri, D.F.S. 2015. Xanthan gum: A versatile biopolymer for biomedical and technological applications. *J. App. Polym. Sci.*, 132: 1-13. <https://doi.org/10.1002/app.42035>
- Rana, B.M. and Raval, A.A. 2019. Isolation, production, and characterization of the polysaccharide “xanthan gum” from *Xanthomonas* sp. *Int. J. Curr. Microbiol. App. Sci.*, 8(5): 1019-1030.
- Renata, A.T., Adriel, P.M. and Carlos, B. 2018. Impact of a carbon source and stress conditions on some properties of xanthan gum produced by *Xanthomonas campestris* pv. *Mangiferae indicae*. *Biocatal. Agric. Biotech.*, 15: 167-172. <https://doi.org/10.1016/j.bcab.2018.06.003>
- Roncevic, Z.Z., Zahovic, I.E. and Pajcin, I.S. 2019. Effect of carbon sources on xanthan production by *Xanthomonas* spp. Isolated from pepper leaves. *Food Feed Res.*, 46(1): 11-21. <https://doi.org/10.5937/FFR1901011R>
- Salah, R.B., Chaari, K. and Besbes, S. 2010. Optimization of xanthan gum production by palm date (*Phoenix dactylifera* L.) juice by-products using response surface methodology. *Food Chem.*, 121: 627-633.
- Sarbatly, R. and England, R. 2006. Review of xanthan gum production from unmodified starches by *Xanthomonas compressors* sp. *Enzyme Microbial. Tech.*, 39(2): 197-207. <https://doi.org/10.1016/j.foodchem.2009.12.077>
- Sharma, P. and Mehta, B.P. 2001. Antibacterial activity of plant extracts to phytopathogenic *Xanthomonas campestris* pv. *Campestris* causing black rot of cabbage. *J. Mycol. Pathol.*, 31: 111-112.
- Sheikh, M., Malik, A., Meghavanshi, M. and Mahmood, I. 2012. Studies on some plant extracts for their antimicrobial potential against certain pathogenic micro-organisms. *Am. J. Plant Sci.*, 3(2): 209-213. <https://doi.org/10.4236/ajps.2012.32025>
- Souw, P. and Demain, A.L. 1979. Nutritional studies on xanthan production by *Xanthomonas campestris* NRRL-B-1459. *Appl. Environ. Microbiol.*, 37: 118-119. <https://doi.org/10.1128/aem.37.6.1186-1192.1979>
- Stredansky, M. and Conti, E. 1999. Xanthan production by solid-state fermentation. *Process. Biochem.*, 34: 581-587. [https://doi.org/10.1016/S0032-9592\(98\)00131-9](https://doi.org/10.1016/S0032-9592(98)00131-9)
- Suput, D., Lazic, V., Popovic, S. and Hromis, N. 2015. Edible films and coatings –sources, properties, and application. *Food Feed Res.*, 42(1): 11-22. <https://doi.org/10.5937/FFR1501011S>





# Environmental Modelling of Ionic Mass Transfer Coefficient in a Unique Electrocoagulation Reactor

Safaa K. Hashim Al-Khalaf <sup>(\*\*)</sup>, Ahmed Samir Naje <sup>\*†</sup>, Zaid Abed Al-Ridah <sup>\*</sup> and Haider M. Zwain <sup>\*</sup>

<sup>\*</sup>Collage of Engineering, AL-Qasim Green University, Babylon 51031, Iraq

<sup>\*\*</sup>Faculty of Engineering, University of Kufa, Al-Najaf, Iraq

<sup>†</sup>Corresponding author: Ahmed Samir Naje: [ahmednamesamir@yahoo.com](mailto:ahmednamesamir@yahoo.com)

Nat. Env. & Poll. Tech.  
Website: [www.neptjournal.com](http://www.neptjournal.com)

Received: 18-02-2022

Revised: 21-03-2022

Accepted: 22-03-2022

## Key Words:

Rotating anode  
EC process  
Mass transfer  
CFD simulation  
Bland-Altman method

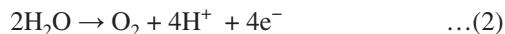
## ABSTRACT

Ionic mass transfer in a novel electrocoagulation reactor (ECR) using a rotating impeller anode is studied experimentally using the limiting current density method. The CFD simulation is also conducted for characterizing the novel electrocoagulation reactor (ECR) and validating the experimental study of ionic mass transfer. Variables included rotational speed and anode diameter. The Bland-Altman method was used to verify the accuracy of experimental and simulation results. Data for the condition  $11852 < Re < 58550$  and  $88 < Sc < 285$  were found to fit the equation for the largest diameter of 11.2 cm;  $Sh = 2.1Re^{0.93}Sc^{0.33}$ . Based on COD removal efficiency, optimal EC performance is realized at the largest anode diameter of 11.2 cm, confirming the enhancement of aluminum mass transfer by increasing the anode diameter. The experimental values of current density and mass transfer coefficient are validated by CFD simulation for all the rotational speeds and anode diameters. The accuracy is up to 95% for the experimental current densities compared with simulation values.

## INTRODUCTION

Electrochemically assisted coagulation involves in situ generations of coagulants through an electrode solution of a sacrificial anode, which is usually composed of iron or aluminum. The reactions in an electrocoagulation cell are summarized in Eqs. (1) to (3), with the oxidation of the metallic anode ( $M = Fe$  or  $Al$ ) and reduction of water as the main electrochemical reactions. In the reactions, oxidation occurs at the anode, and water reduction occurs through the electrocoagulation reactions (Chen 2004).

At the anode:



At the cathode:



Creating turbulence via an electrocoagulation (EC) reactor reduces the electrode inter-resistance drop (IR-drop) and improves the performance of the current using either a mixer with static or rotating electrodes. This trend may be alleviated by enhancing mass transfer towards increasing turbulence (Mollah et al. 2004). Mass transfer monitoring is essential for electrocoagulation reactors, which leads to mass transfer measurements (MTMs). The MTMs can be

conducted by employing several electrochemical reactor geometries, with three-dimensional porous electrodes and a parallel plate or rotating electrodes. The reactors often operate during partial or complete mass transfer control. This trend is due to the controlled rate of convection diffusion of the reactant from the surface of the electrode to the bulk of the solution. The EC technology that involves the control of mass transfer has numerous applications in different fields of study. The fields include electrosynthesis, photocatalysis, metal recovery, effluent treatment, and energy conversion and storage (Eisenberg et al. 1954, Ponce-de-Leon et al. 2007). In the EC process, the limiting current is an essential determinant for the analysis of rates of mass transfer. When the limiting current controls the EC system, the comparison of that system with other electrochemical systems can help in determining the hydrodynamic characteristics for better removal efficiencies of pollutants. The following equations are employed to determine the mass transfer behavior in the EC cell or reactor involving mass transfer coefficients ( $K_m$ ) for the anode oxidation, which are determined from the values of the limiting current Selman JR, Tobias CW. Mass-transfer measurements by the limiting-current technique (Adv et al. 1978, Burns & Jachuck 2005, Rong et al. 2007, Ibrahim et al. 2013, Abdel-Aziz et al. 2011, El-Shazly et al. 2013).

$$K_m = i_L/nFAC_b \quad \dots(4)$$

where  $i_l$  is the limiting current (A),  $F$  is Faraday's constant ( $96500 \text{ C.mol}^{-1}$ ),  $n$  is electron moles (3 for Al),  $A$  is the electrode surface area in  $\text{cm}^2$ , and  $C_b$  is the concentration of the bulk solution in  $\text{mol.cm}^{-3}$ .

Dimensionless numbers like the Reynolds number (Re), Schmidt number (Sc), and Sherwood number (Sh) are often used for different systems having rotating electrodes instead of superficial solution velocity and mass transfer coefficients. Below are the dimensionless numbers used:

$$\text{Sh} = K_m d/D, \quad \dots(5)$$

$$\text{Re} = \rho N d^2/\mu, \quad \dots(6)$$

$$\text{Sc} = \mu/\rho D, \quad \dots(7)$$

where  $D$ ,  $d$ ,  $N$ ,  $\mu$ , and  $\rho$  diffusion coefficient ( $\text{cm}^2.\text{s}^{-1}$ ), represent effective diameter (cm), rotational speed (rps), fluid viscosity ( $\text{g.cm}^{-1}.\text{s}^{-1}$ ) and fluid density ( $\text{g.cm}^{-3}$ ).

The experimental mass transfer data for a variety of ECR designs are correlated by using the dimensionless relationship (Rajeshwar & Ibanez 1997, Tamas et al. 2007):

$$\text{Sh} = b\text{Re}^a\text{Sc}^{0.33}, \quad \dots(8)$$

where  $a$  is the Reynolds number exponent, which is dimensionless and  $b$  is the mass transfer correlation constant.

Several studies have used hydrodynamic voltammetry to determine the correlations of the mass transfer by using the potential ranges and the limiting current. Under such conditions, the reaction is mass transfer controlled in electrochemical systems using rotating disc electrodes (Tamas et al. 2007, Ragnini et al. 2000, Lanza & Bertazzoli 2007) and rotating cylinder electrodes (Ponce-de-Leon et al. 2007, Grau & Bisang 2005, Grau & Bisang 2011). The main aims of this study are to investigate the mass transfer coefficients for a new model of EC reactor with rotating impeller anode at different rotational speeds and impeller diameters by experimental work and to validate by computational fluid dynamic (CFD) simulation to reveal the importance of mass transfer in electrocoagulation processes. The model and experiments focus on an EC process using a rotating electrode. The Bland-Altman statistical method has been used to verify the experimental results.

## MATERIALS AND METHODS

### Experimental Setup

Fig. 1 presents the experimental setup used for the novel electrocoagulation reactor. The volume of the stirred tank reactor was 10 liters, made from Perspex. The reactor came with a rotating shaft with a diameter of 32 mm, to sustain the impeller and sustain the rotational speed of the mounted electrode. The electrode is made of aluminum. The designed

rotational speed of the electrode varies from 75, 100, 150, 200, to 250 rpm. 10 impellers were used with a rotating anode and 10 rings as the cathode. In the design, the impeller consisted of 4 rods each with dimensions of 30 mm and 12 mm as the length and diameter, respectively. The dimensions of each ring were as 172 mm, 134 mm, and 12 mm, the outer diameter, internal diameter, and thickness, respectively. The rings were kept 30 mm apart and  $500 \text{ cm}^2$  as the active surface area of the reactor. Three baffles (equally spaced) were used in the reactor. Further details on experimental procedure and design can be found in previous work (Naje 2019). Table 1 enlightens the main properties of wastewater collected from a textile manufacturer in Babylon, Iraq.

### Computational Fluid Dynamics Modelling

The three-dimensional Solid Oxide Fuel Cell (SOFC) model built in commercial CFD software ANSYS 15.0 was used. The numerical model was completed to resemble the experimental setup used. The model considers all the complex electro-thermo-chemical characteristics by simulation of the complex processes in the SOFC operations. The working principle of the SOFC model is compatible with electrochemical reactions (Puthran 2011). Further details on the model and procedure for the model development are as under.

### The Model

The modeling strategy is detailed in the official manual of Ansys<sup>(R)</sup> (Eickhoff & Roeser 2009). The SOFC model numerically solves a set of partial differential equations (PDE) contained in SOFC theory. The PDE equations involve mass transfer via the flow channels, the fuel flow, the electrodes, and the chemical and electrochemical reactions that occur in the SOFC system (O'Hayre et al. 2006). The potential field in the conductive layers of the cell depends on the electrical model. The computational mesh generated for the model is shown in Fig. 2 (a and b).

### Computational Model Theory

The following cell phenomenon is required for the understanding and development of the SOFC (Singhal & Kendall 2003):

Table 1: Characteristics of textile wastewater.

Parameters	Values
Electrical conductivity [ $\mu\text{S.cm}^{-1}$ ]	1450
pH	4.52
Density [ $\text{g.cm}^{-3}$ ]	0.997
Absolute viscosity [ $\text{g.cm}^{-1}.\text{s}^{-1}$ ]	0.0089
COD [ $\text{mg.L}^{-1}$ ]	990

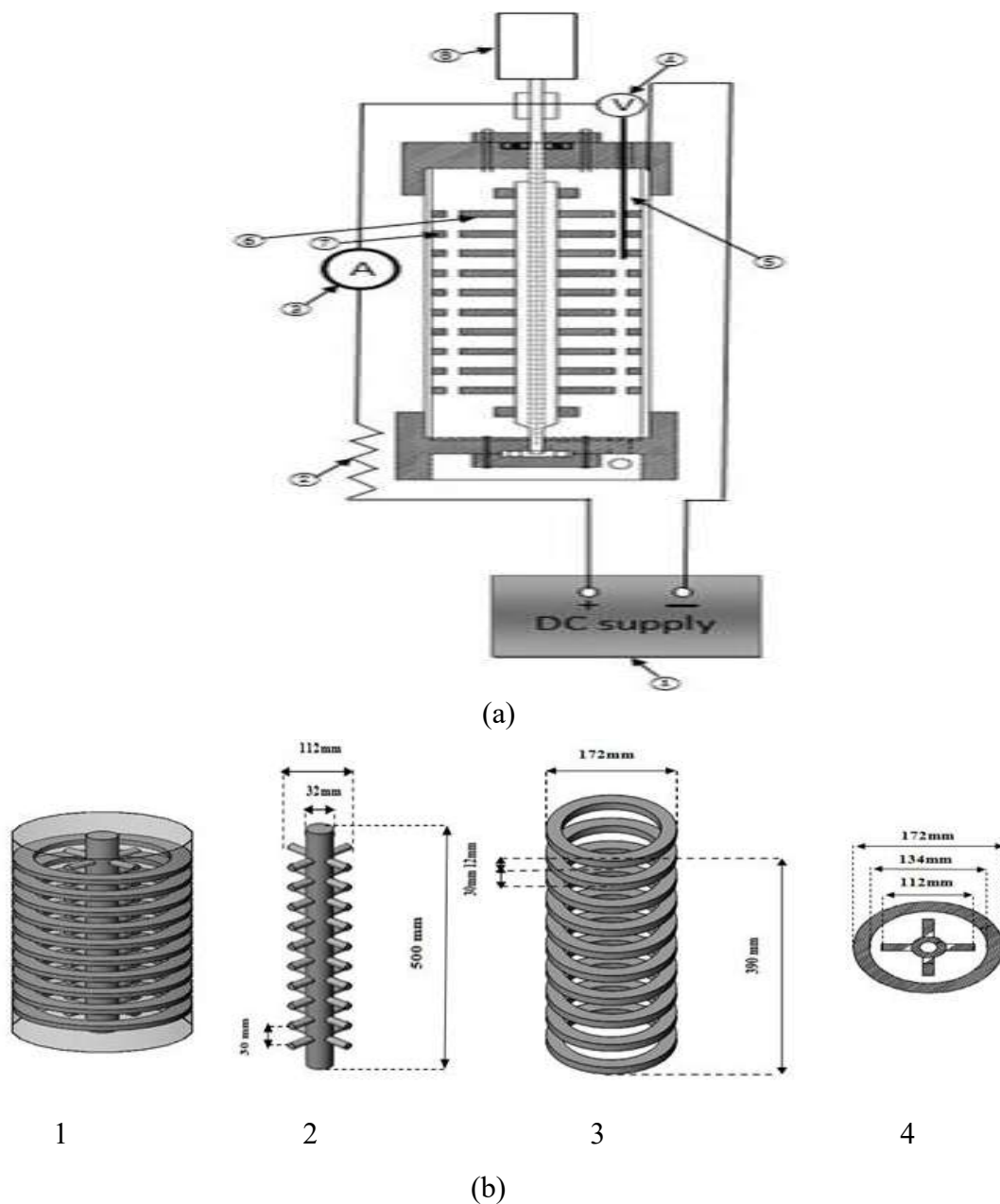


Fig. 1: (a). Schematic view of EC experimental setup (1) DC power supply; (2) variable resistance; (3) multirange ammeter; (4) voltmeter; (5) reference electrode; (6) rotating impellers anode; (7) rings of cathode; (8) variable speed motor. (b). Configurations of electrodes (1) anode and cathode; (2) impellers of the anode; (3) rings of the cathode; (4) top view of impellers anode and rings cathode.

1. The ions and electrons transfer, as well as the computation of the cell potential and the current obtained under current and potential field transport.
  2. The electrochemical reactions taking place at the electrodes.
  3. The mass transfer involving mass conservation and species conservation.
  4. The flow channels of the fluid (for both the non-porous and porous media).
- The conservation equations are used to solve this phenomenon using the finite volume technique in combination with an implicit discretization scheme. The following assumptions were made to solve these equations (Srinivasan 2006):

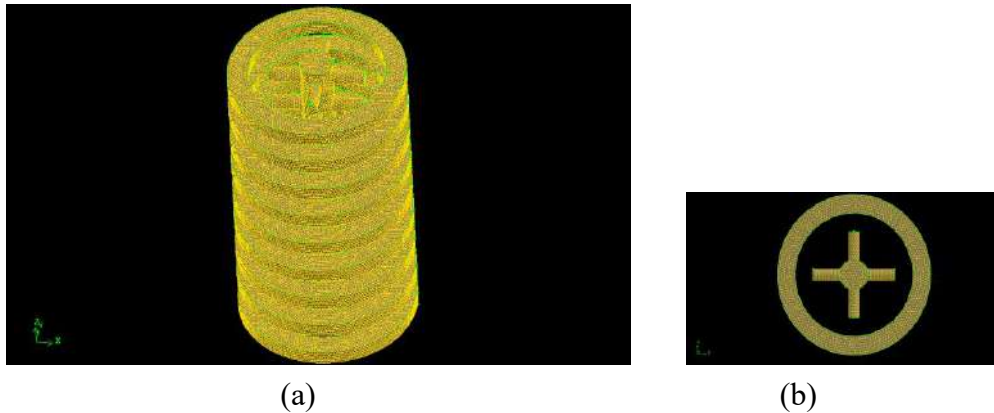


Fig. 2: Mesh structure representation of EC model with rotating anode (a) Whole geometry; (b) Top view of anode and cathode.

1. All the components exhibit similar thermal expansions, neglecting the effects of radiation heat transfer, and considering the single-cell model.
2. The reactions occur in a single step.
3. The principle of conservation of momentum for the model mass flow by zones in the cell operation is presented in Eq. 9.

$$\frac{\partial}{\partial t} \rho \vec{v} + \nabla \cdot \rho \vec{v} y_i = \nabla \cdot \mathbf{J}_i + S_{S,i} \quad \dots(9)$$

The effective binary diffusion coefficient is determined for the electrodes based on the tortuosity and porosity of the electrode matrix. The effective binary diffusion coefficient is given by Eq. 10.

$$D_{ij,eff} = \frac{\epsilon}{\tau} D_{ij} \quad \dots(10)$$

The principle of conservation of charge used for conductive regions is expressed as

$$\nabla \cdot \mathbf{i} = 0 \quad \dots(11)$$

Where,  $i$  is:

$$\mathbf{i} = -\sigma \nabla \phi \quad \dots(12)$$

The Laplace equation is employed as a governing principle to solve the species conservation equation.

$$\nabla \cdot \sigma \nabla \phi = 0 \quad \dots(13)$$

When the current is applied, there is a reduction in aluminum to  $\text{Al}^{3+}$  ions, flowing through the electrolyte. The release of electrons takes place through electrochemical reactions. These electrons flow through the current collector-connected external circuit. A potential difference is developed across two electrodes when electron transfer produces a current through the circuit. Nernst Equation was used to compute the output voltage of the cell (ANSYS Manual 15.0), and the

setting up of boundary conditions by electric potential value at the anode-impeller which means the reference potential of aluminum and the potential at the cathode-ring is varied. The single-cell structure temperature profile is demonstrated with the energy conservation equation in Eq.14.

$$\frac{\partial}{\partial t} \rho E + \nabla \cdot \vec{v} \rho E + p = \nabla \cdot (k_{eff} \nabla T - \sum_j h_j \mathbf{J}_j + \vec{\tau}_{eff} \cdot \vec{v}) + S_h \quad \dots(14)$$

Where  $S_h$  is the volumetric sink or source of energy and,

$$E = h - \frac{p}{\rho} + \frac{v^2}{2} \quad \dots(15)$$

And

$$h = \sum_j Y_j h_j \quad \dots(16)$$

The enthalpy flux terms are added to the energy equation accounting for the electrochemistry. The overall energy balance for the production of hydrogen and the corresponding enthalpy of formation is presented in Eq. 17 and 18, respectively.

$$\dot{Q}'' = h_{H_2}'' + h_{O_2}'' - h_{H_2O}'' - i \nabla V \quad \dots(17)$$

$$h_{H_2} = m_{H_2} \left[ \int_{T_{ref}}^T C_p dT + h_0 \right] \quad \dots(18)$$

The effects of electrode potential voltage are taken into account in the energy equation. The Butler-Volmer equation can be used to obtain the interface current density. Therefore, the rate of reaction could be written in terms of the exchange current density as follows:

$$i = i_{0,eff} \left[ e^{\frac{\alpha_a n \eta_{act,a} F}{RT}} - e^{-\frac{\alpha_c n \eta_{act,c} F}{RT}} \right] \quad \dots(19)$$

Where,

$$i_{0,eff} = i_{0,ref} \left( \frac{\chi_j}{\chi_{j,ref}} \right)^{\gamma_j} \dots(20)$$

The effective exchange current density is determined for the cathode side and the anode side. Considering the anode side:

$$i_{0,eff}^{anode} = i_{0,ref}^{anode} \left( \frac{\chi_{H_2}}{\chi_{H_2,ref}} \right)^{\gamma_{H_2}} \left( \frac{\chi_{H_2O}}{\chi_{H_2O,ref}} \right)^{\gamma_{H_2O}} \dots(21)$$

Considering the cathode side,

$$i_{0,eff}^{cathode} = i_{0,ref}^{cathode} \left( \frac{\chi_{O_2}}{\chi_{O_2,ref}} \right)^{\gamma_{O_2}} \dots(22)$$

Newton’s method can be used to solve the Butler-Volmer equation after the initial input of anode potential voltages. The values of current density are dependent on potential voltage. The production rate of the species helps to compute the concentration dependence of the species on the current-potential voltage characteristics of the cell are used to model the electrochemical reactions.

$$S = - \frac{ai}{nF} \dots(23)$$

To measure the source terms for the equations, the underlying electrochemistry in equation 23 can be used with the conventions and the inputs to the governing equations’ definition of basic initial parameters required. The initial current of the system determined from the applied potential voltage can be specified using the CFD module. The present simulation uses the initially specified potential voltage of the anode to find out the developed current of the system for each rotational speed and anode diameter.

**Boundary Conditions Simulation Setup**

The initial boundary conditions must be paired with the instance of the anode diameter. It is daunting to get the parameters required to set up a replica of the experimental setup. The available conditions and approximate values for the other parameters were used to develop the model. Anode rotational speeds are given as boundary conditions for the present model. The rotational speed is followed for the three impeller diameters of 9.2cm, 10.2cm, and 11.2cm. The operation was performed at atmospheric pressure, temperature room, and solution conductivity, density, and viscosity as mentioned in Table 1.

**RESULTS AND DISCUSSION**

**Experimental Outcomes**

The experimental results used in this study are from previous studies (Naje 2019). Results brought to light that the highest mass transfer coefficient was observed at the highest impeller anode diameter of 11.2 cm used. The Sherwood number estimated for different impeller diameters and the rotational speeds by plotting ( $Sh/Sc^{0.33}$ ) versus Reynolds number (Eq. 6), is exhibited in Fig. 3. The following correlations were obtained by fitting data at different impeller anode diameters:

If d = 0.092 m,  
 $Sh = 2.09 Re^{0.89} Sc^{0.33} \dots(25)$

If d = 0.102 cm,  
 $Sh = 2.1Re^{0.91} Sc^{0.33} \dots(26)$

If d = 0.112 cm,  
 $Sh = 2.1Re^{0.93} Sc^{0.33} \dots(27)$

If  $11852 < Re < 58550$  and  $88 < Sc < 285$ , 0.98 is the correlation coefficient.

It can be observed from the determined correlations that exponents of Re increase with an increase in anode diameter. The exponent values together with heading constant (b = 2.1) were greater than the previously reported values for rotating cylinder electrode ( $Sh = 0.079 Sc^{0.356} Re^{0.7}$ ) and rotating disk electrode ( $Sh = 0.01 Sc^{0.33} Re^{0.87}$ ), for turbulent flow. The value of the factors (a and b) are influenced by the geometric design of the electrode, indicating a higher mass transfer coefficient in comparison with the rotating disk or cylinder (Abdel-Aziz et al. 2011, Yanez-Varela et al. 2020).

**CFD Simulation Outcomes**

The flow physics and the various electrochemical reactions have been simulated from the CFD software. The various contours are plotted to analyze the changes happening in the electrochemical behavior inside the EC reactor with a rotating anode. The various rotational speeds for the three impeller anode diameters give information about their influence on the current density/intensity.

The contour of current density in Fig. 4 for 0.5V potential voltage, 150 rpm rotational speed, and 9.2cm anode diameter shows the maximum change happening in the place of the impeller’s anode. There is nominal change throughout excluding the impeller as is noticed in the EC reactor. In the case of potential voltage, as shown in Fig. 5. Maximum voltage was observed at the wall of the cathode rings, whereas minimum voltage in the impeller, and a medium voltage throughout as expected by the behavior of the electrochemical system (Ra-

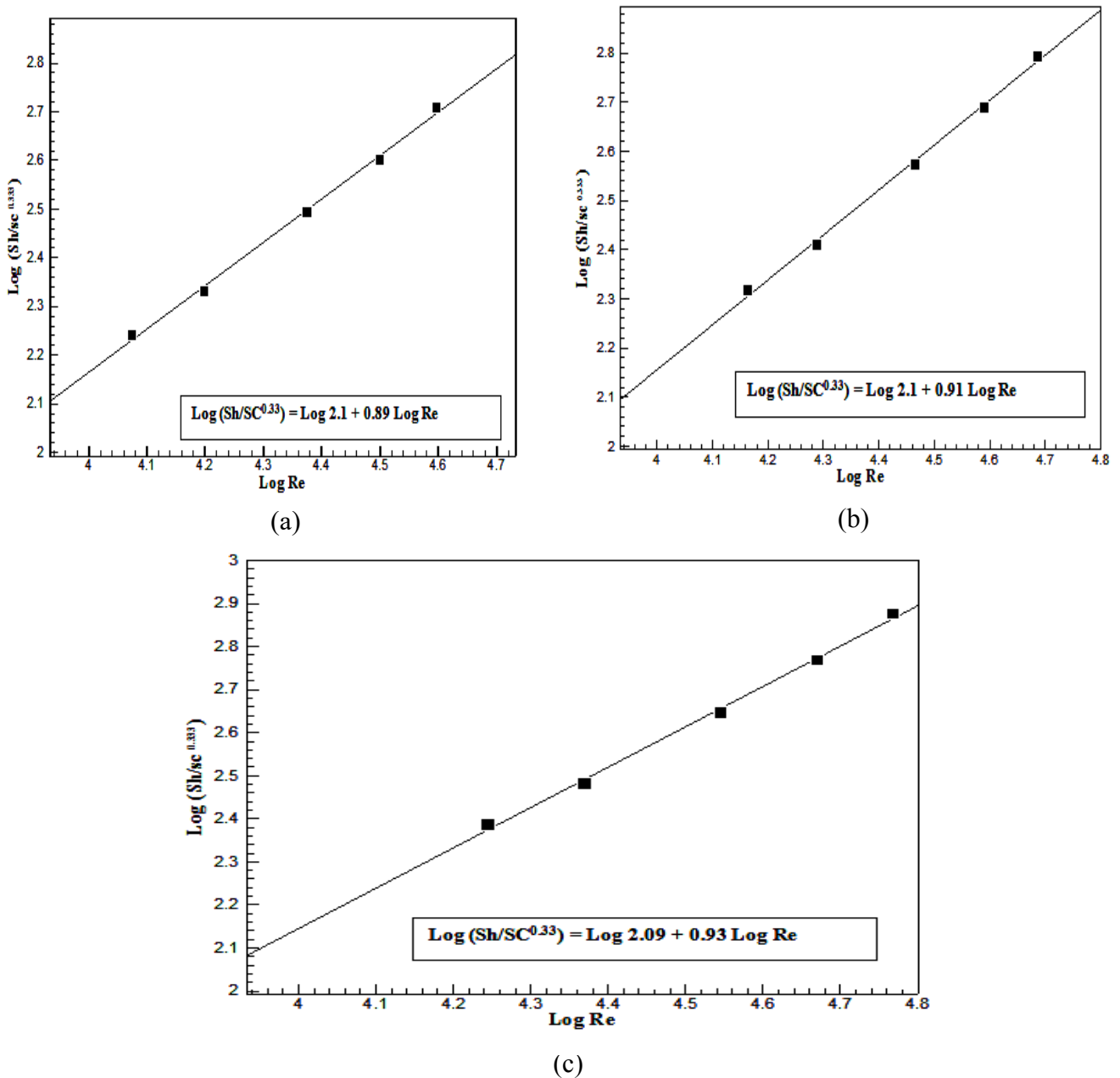


Fig. 3: Sherwood-Reynolds correlation for rotating impeller anode (a)  $d=9.20\text{cm}$ ; (b)  $d=10.20\text{cm}$ ; (c)  $d=11.20\text{cm}$ .

jeshwar & Ibanez 1997, Rodriguez et al. 2003, Yanez-Varela et al. 2020).

The relationship of current density versus potential voltage for an impeller diameter of 9.2cm follows an increasing trend, as shown in Fig. 6. The current intensity increases when the potential difference increases for the rotational speed of 75rpm, till a potential difference of 2500 mV is

reached. After that, it remains constant for any changes in potential difference. The nature of the curves for 100, 150, 200, and 250 rpm are the same starting 75rpm however begin at an expanding slope than the latter. The expanding of slope because of increment of limiting current with the increasing of anode rotational speed. For each rotational speed and anode diameter, CFD simulation values are



consistent with the experimental values. Fig. 7 explains the limiting current densities for each impeller anode diameter and rotational speed. The results show limiting current densities increased with increasing rotational speed and also the impeller's anode diameter. The results are presented in Fig. 5, 6, and 7, under the same potential voltage and increment of anode diameter or rotational speed. The current flow increases, resulting in the acceleration of the

EC reaction response. This behavior is perfect with the consequences of experimental results and former studies (González-Neria et al. 2021, Mora et al. 2016). The coefficient of mass transfer of ionic Al was enhanced by increasing the rotation speed and diameter of an anode, as shown in Fig. 8. The mass transfer coefficients obtained by CFD simulation are compatible with the experimental values.

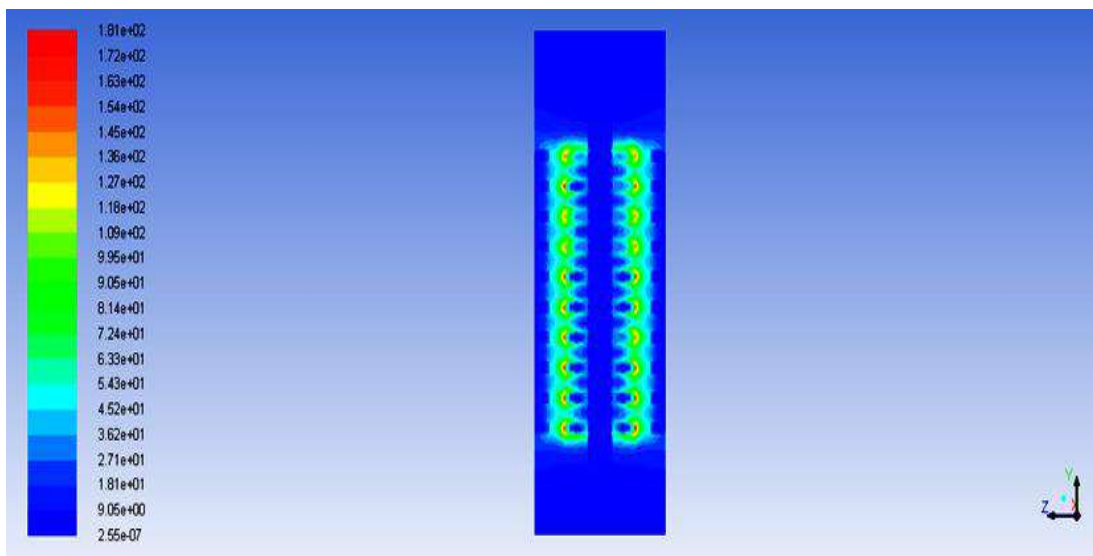


Fig. 4: Contours of current density ( $A.m^{-2}$ ) in case of potential voltage is 0.5V in case of rotating speed =150 rpm and anode diameter = 9.2cm at x=0 section.

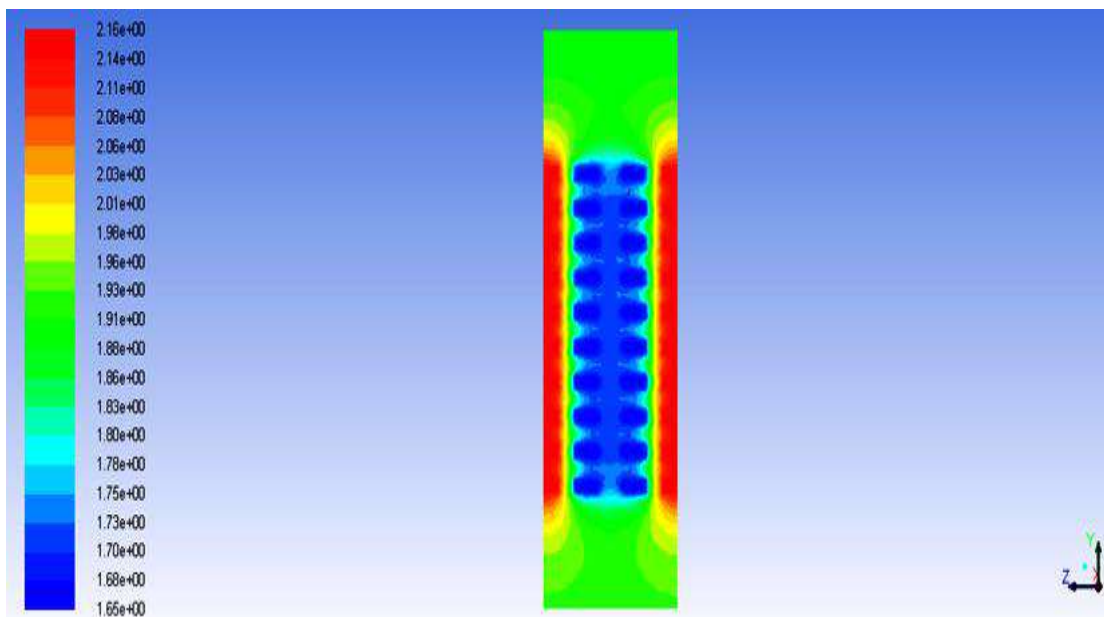


Fig. 5: Contours of potential voltage in case of rotating speed =150 rpm and anode diameter = 9.2cm at x=0 section.

## Outcomes Verification

A statistical method is employed to confirm the measured limiting current of experimental work with CFD simulation values for each impeller's anode diameter and rotational speed. The Bland–Altman method is one of the statistical methods utilized for this purpose (Mendez et al. 2018, Tesche et al. 2018).

The data were collected from the developed devices based on the comparison with data obtained from the simulation or

validated devices. This technique is based on the mean difference between the simulation and the developed instrument or system. The value of the mean difference will limit the acceptable area of the data that is generated by subtraction or addition of the standard deviation (SD) (González-Landaeta et al. 2008). This method will evaluate the parameters that affect the performance of the model design (device) in the zone of standard deviation limit as the acceptable area of the distribution of the measured data (Martínez-Delgadillo et al. 2013). Any design device is pronounced as good in

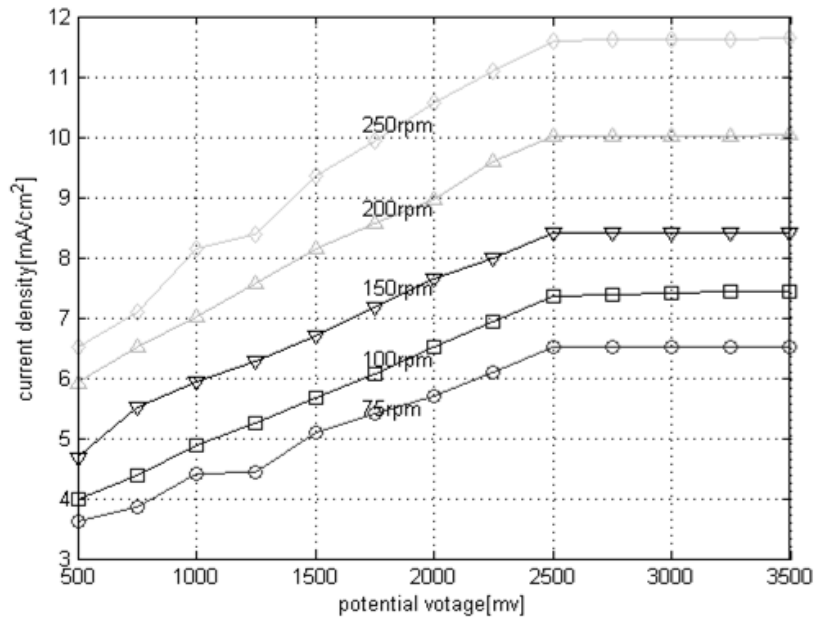


Fig. 6: Simulation current-potential voltage curves at an anode diameter of 9.20cm.

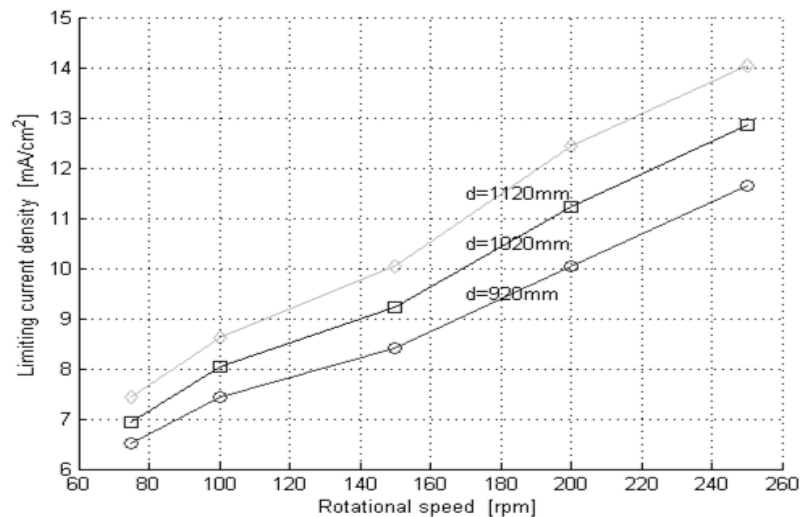


Fig. 7: Simulation limiting current density for different anode diameters.

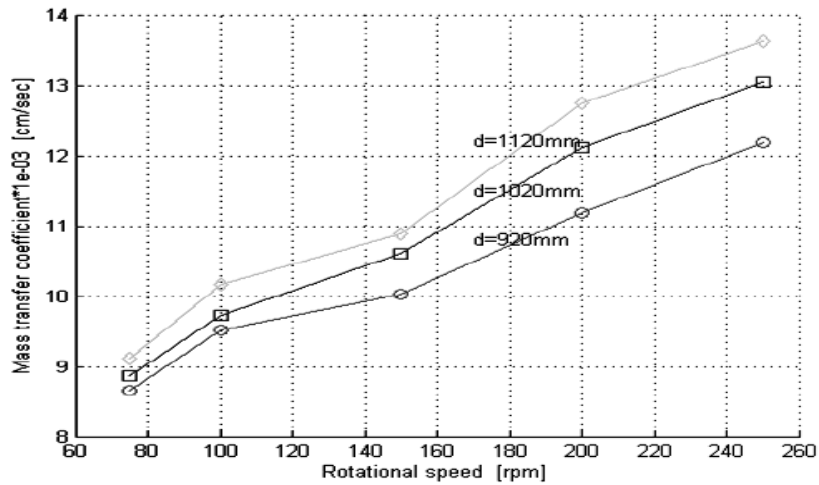
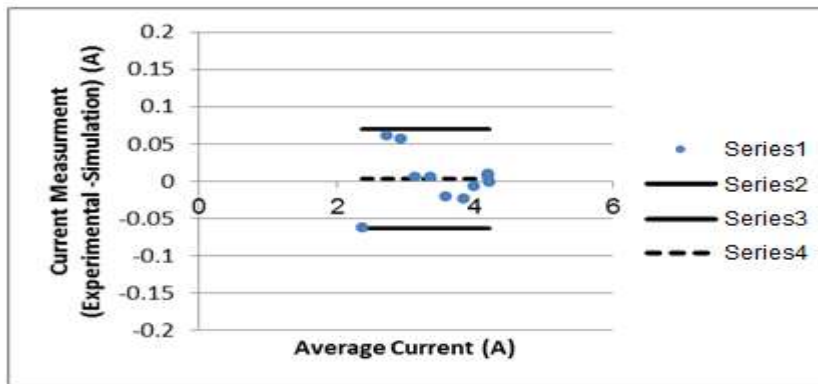


Fig. 8: Simulation mass transfer coefficient for different anode diameters.

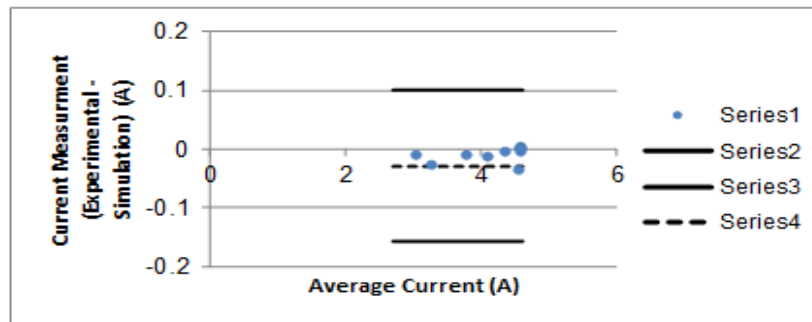
performance if any measured data should be more than 95% potentially measured the data and the error must be less than 5% whereby the error boundary limits are via mean ± 2×SD stated by (Su et al. 2014).

Three impellers anode diameters (9.2, 10.2, and 11.2cm) are considered in measuring current (A), and the rotational

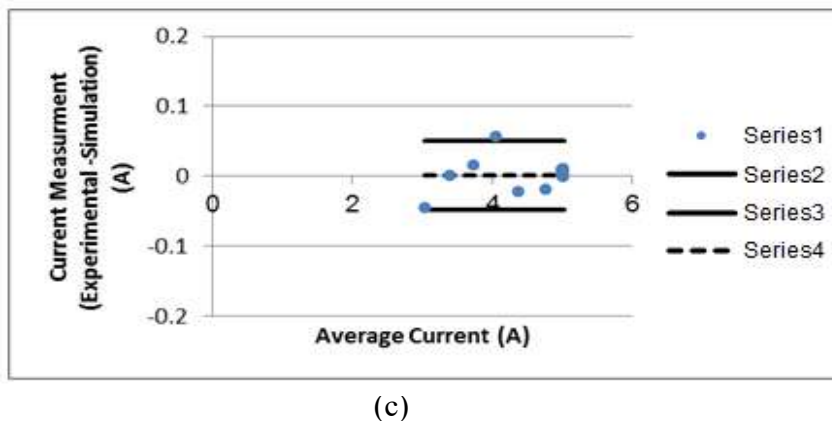
speeds are 75, 100, 150, 200, and 250rpm. Fig. 9 (a), (b), and (c) indicated the distribution measured zone via standard deviation error for each anode diameter at optimal rotational speed (150 rpm). From Figs. 5, 6, and 7, it is seen that most of the measured current values in the mean of the 2×SD as required and the accuracy of these values between the



(a)



(b)



(c)

Fig. 9: Measured current verification between experimental and simulation work at 150 rpm with impellers anode diameter: (a). 9.2cm; (b). 10.2cm; (c). 11.2cm.

experiment and the CFD simulation has achieved a good agreement up to 95% for each anode diameter at 150 rpm.

## CONCLUSIONS

The results show that increasing the impeller anode diameter and rotation speed increases the limiting current density. The results of the correlations using Reynolds and Sherwood numbers show that the optimum coefficient of mass transfer for experimental and simulated data is found at 11.2 cm of the impeller anode diameter. Where the correlation is as  $Sh = 2.1Re^{0.936} Sc^{0.33}$ . The current densities from CFD simulation show values close to that of the experimental data for all the anode diameters and rotation speeds employed. According to the Bland–Altman method, the accuracy is up to 95% for the experimental current density values.

## ACKNOWLEDGMENT

The authors thank Babylon Textile Plant, Iraq for supplying the textile wastewater. They also thank Al-Qasim Green University, Iraq for funding this research.

## REFERENCES

Abdel-Aziz, M., El-Shazly, A., Farag, H. and Sedahmed, G. 2011. Mass transfer behavior of rotating square cylinder electrochemical reactor in relation to wastewater treatment. *Energy Conv. Manag.*, 52: 2870-2875.

Burns, J. and Jachuck, R. 2005. Determination of liquid-solid mass transfer coefficients for a spinning disc reactor using a limiting current technique. *Int. J. Heat Mass Transf.*, 48: 2540-2547.

Chen, G. 2004. Electrochemical technologies in wastewater treatment. *Sep. Purif. Technol.*, 8:11-41.

Eickhoff, J. and Roeser, H.P. 2009. *Simulating Spacecraft Systems*. Springer, Cham.

Eisenberg, M., Tobias, C. and Wilke, C. 1954. Ionic mass transfer and concentration polarization at rotating electrodes. *J. Electrochem. Soc.*, 101: 306-320.

El-Shazly, A., Al-Zahrani, A. and Alhamed, Y. 2013. Kinetics and performance analysis of batch electrocoagulation unit used for the removal of a mixture of phosphate and nitrate ions from industrial effluents. *Int. J. Electrochem. Sci.*, 8: 3176-3185.

González-Neria, I., Yáñez-Varela, J.A., Martínez-Delgadillo, S.A., Rivadeneyra-Romero, G. and Alonzo-García, A. 2021. Analysis of the turbulent flow patterns generated in isotropic porous media composed of aligned or centered cylinders. *Int. J. Mech. Sci.*, 199: 106396.

Grau, J. and Bisang J. 2011. Mass-transfer studies at rotating cylinder electrodes with turbulence promoters. *Chem. Eng. Process Intensif.*, 50: 940-943.

Grau, J. and Bisang, J. 2005. Mass transfer studies at rotating cylinder electrodes of expanded metal. *J. Appl. Electrochem.*, 35: 285-291.

Ibrahim, D.S., Veerabahu, C., Palani, R., Devi, S. and Balasubramanian, N. 2013. Flow dynamics and mass transfer studies in a tubular electrochemical reactor with a mesh electrode. *Comp. Fluids*, 73: 97-103.

Lanza, M. and Bertazzoli, R. 2000. Removal of Zn (II) from chloride medium using a porous electrode: current penetration within the cathode. *J. Appl. Electrochem.*, 30: 61-70.

Martínez-Delgadillo, S.A., Gutiérrez-Torres, C. and Jiménez-Bernal J. 2013. Determination of the spatial distribution of the turbulent intensity and velocity field in an electrochemical reactor by CFD. *Int. J. Electrochem. Sci.*, 8: 274-289.

Mendez, V., Di Giuseppe, M. and Pasta, S. 2018. Comparison of hemodynamic and structural indices of ascending thoracic aortic aneurysm as predicted by 2-way FSI, CFD rigid wall simulation, and patient-specific displacement-based FEA. *Comp. Biol. Med.*, 100: 221-229.

Mollah, M.Y., Morkovsky, P., Gomes, J.A., Kesmez, M., Parga, J. and Cocke, D.L. 2004. Fundamentals, present and future perspectives of electrocoagulation. *J. Hazard. Mater.*, 114: 199-210.

Mora, M.M., Vergara, C.P., Leiva, M.A., Delgadillo, S.M. and Rosa-Dominguez, E.R. Life cycle assessment of carbon capture and utilization from ammonia process in Mexico. *J. Environ. Manag.*, 183: 998-1008.

Naje, A.S. 2019. Enhancement of ionic mass transfer coefficient using a unique electrocoagulation reactor with a rotating impeller anode. *Sep. Sci. Technol.*, 9: 1-10.

O'Hayre, R.P., Cha, S.W., Colella, W. and Prinz, F.B. 2006. *Fuel Cell Fundamentals*: John Wiley & Sons, New York.

Ponce-de-Leon, C., Low, C., Kear, G. and Walsh, F. 2007. Strategies for the determination of the convective-diffusion limiting current from steady-state linear sweep voltammetry. *J. Appl. Electrochem.*, 37: 1261-1270.

Puthran, S.L. 2011. 3-Dimensional Computational Fluid Dynamics Modeling of Solid Oxide Fuel Cell Using Different Fuels. DTIC Document.

- Ragnini, C.A., Di Iglia, R.A., Bizzo, W. and Bertazzoli, R. 2000. Recycled niobium felt as an efficient three-dimensional electrode for electrolytic metal ion removal. *Water Res.*, 34: 3269-3276.
- Rajeshwar, K. and Ibanez, J.G. 1997. *Environmental Electrochemistry: Fundamentals And Applications in Pollution Sensors and Abatement*: Academic Press, Cambridge, MA
- Rodriguez, M.G., Aguilar, R., Soto, G. and Martínez, S.A. 2003. Modeling an electrochemical process to remove Cr (VI) from rinse water in a stirred reactor. *J. Chem. Technol. Biotechnol.*, 78: 371-36.
- Rong, X., Haiyan, F., Peng, Z. and Heping, G. 2007. Measurement of enhanced mass transfer coefficient in the tube by limiting diffusion current technique. *Petrochem. Technol.*, 36: 712.
- Selman, J.R. and Tobias, C.W. 1978. Mass-transfer measurements by the limiting-current technique. *Adv. Chem. Eng.*, 10: 311-318.
- Singhal, S.C. and Kendall, K. 2003. *High-Temperature Solid Oxide Fuel Cells: Fundamentals, Design, and Applications*. Elsevier, Netherlands.
- Srinivasan, S. 2006. *Fuel Cells: From Fundamentals to Applications*. Springer Science & Business Media, Netherlands.
- Su, Y., Zhang, Y., Jin, Y., Yao, Y., Zhang, R. and Jiang, Y. 2014. The feasibility of the dicrotic augmentation index to replace the tidal augmentation index. *Information and Automation (ICIA), 2014 IEEE International Conference*, pp. 943-948.
- Tamas, A., Martagiu, R. and Minea, R. 2007. Experimental determination of mass transfer coefficients in dissolution processes. *Chem. Bull. Polit. Univ. Timisoara*, 52: 133-138.
- Tesche, C., De Cecco, C.N., Baumann, S., Renker, M., McLaurin, T.W., Duguay, T.M. and Schoepf, U.J. 2018. Coronary CT angiography-derived fractional flow reserve: machine learning algorithm versus computational fluid dynamics modeling. *Radiology*, 288(1): 64-72.
- Yanez-Varela, J.A., Alonzo-Garcia, A., Gonzalez-Neria, I., Mendoza-Escamilla, V., Rivadeneyra-Romero, G. and Martinez-Delgadillo, S.A. 2020. Experimental and numerical evaluation of the performance of the electrochemical reactor operated with static and dynamic electrodes in the reduction of hexavalent chromium. *Chem. Eng. J.*, 390: 124575.





# Preparation and Characterization of Hydrophobic Membranes and Their Seawater Desalination Performance Study by Direct Contact Membrane Distillation

Chitrakara Hegde<sup>†\*</sup> and Rahul Ribeiro<sup>\*\*</sup>

\*Department of Science, Alliance University, Anekal, Bangalore, 562106, India

\*\*Department of Mechanical Engineering, Alliance University, Anekal, Bangalore, 562106, India

<sup>†</sup>Corresponding author: Chitrakara Hegde; chitrakarahegde@gmail.com

Nat. Env. & Poll. Tech.  
Website: [www.neptjournal.com](http://www.neptjournal.com)

Received: 16-01-2022

Revised: 02-03-2022

Accepted: 11-03-2022

## Key Words:

Electrospinning

Membrane characterization

Direct contact membrane distillation

Seawater desalination

Performance study

## ABSTRACT

Hydrophobic membranes prepared using Poly (tetrafluoroethylene) (PTFE) along with Poly (1,4-phenylene ether ether-sulfone) and zinc oxide nanoparticle was used in membrane distillation. To examine seawater purification, prepared polymeric membranes were evaluated, tested, and used in a lab-scale direct contact membrane distillation arrangement. These membranes which are synthesized using the electrospinning method have good mechanical and thermal stability. To understand prepared membranes' desalination performance, the physicochemical properties of the seawater were analyzed before and after membrane distillation. The salt rejection remained at 99% and the highest energy efficiency of the system observed is 67.3%.

## INTRODUCTION

Most of the civilizations developed at the bank of rivers. As per chemosynthetic theory (Das et al. 2011), the evolution of life might have originated by a combination of different chemical substances with water as the platform. Though geographically 71% of water is there on earth, potable water for all is still a distant dream. For ages, mankind is trying to purify water in many ways like using heat energy, solar energy, disinfectant using copper pot, cloth, sand filtration, etc. The water purification process took a new dimension after the occurrence of the following events i. 1748, Abbe Nollet, work (Nollet 1748, Glater 1998) on water diffusion from dilute to concentrated solution ii. In 1959, Sidney Loeb and Srinivasa Sourirajan prepared the first asymmetric RO membrane from cellulose acetate for salt rejection (Loeb 1981) iii. 1980, Cadotte developed a new thin-film composite reverse osmosis membrane for single-pass seawater operation (Cadotte et al. 1980). It is noteworthy to know that many researchers are working to improve membrane desalination performance through membrane surface modification (Hegde et al. 2011).

Membrane distillation (MD) is an emerging technique for seawater desalination (Summers et al. 2012). MD is the

transportation of water, consisting of a porous hydrophobic membrane, separating two aqueous solutions of a non-volatile component maintained at different temperatures (Findley 1967). In MD, due to the temperature difference, liquid-vapor interfaces are formed on both sides of the hydrophobic membrane pores. When a vapor pressure difference is created between sides of each pore, evaporation takes place at the warm interface and, after vapor is transported through the pores, condensation takes place at the cold interface. Resulted water flux occurs through the membrane in the direction from warm to cold. MD process is an easy and much more efficient process compared to other distillation techniques. MD is one of the promising candidates for the treatment of water, river water, wastewater, and seawater because this operation can be run by solar, tidal, and geothermal energy; works at room pressure; has minimal fabrication cost; marginal fouling effect (Manna 2016, Ramos et al. 2021). As reported in the literature, efficient MD can be realized with a minimum LEP (liquid entry pressure) of 2.5 bar, porosity 80-90% (Schneider et al. 1988), pore size 0.1-1  $\mu\text{m}$ , contact angle  $< 90^\circ$  (Alkhudhiri et al. 2011, Ma & Hill 2011) and membrane thickness 2-700  $\mu\text{m}$  (Eyken et al. 2016). In DCMD (Direct Contact Membrane Distillation), where the feed solution is in direct contact with the hot membrane side

surface producing evaporation at the cold-membrane surface (Khayet et al. 2005). DCMD configuration is the simplest with much stable flux rate (Hsu et al. 2002, Drioli et al. 2015) but has some points of concern like high thermal polarization, sensitivity to feed concentration, and quality of distillate depending on the hydrophobic nature of the membrane (Feng et al. 2018). DCMD configuration was extensively studied by many research groups using PTFE material with different types of feed solutions and the same configuration was found useful in seawater desalination (Table 1).

DCMD is one of the oldest modules that can perform water purification without a cooling condenser for distillation and gives the best permeate flux with optimal operational conditions (Ashoor et al. 2016).

Table 1: DCMD module in various literature.

Reference	Configuration	Material type	Feed
(Feng et al. 2018)	DCMD	PTFE	Seawater
(Ding et al. 2003)	DCMD	PTFE	Pure water
(El-Abbassi et al. 2009)	DCMD	PTFE	Wastewater
(Sakai et al. 1988)	DCMD	PTFE	Mixed waste
(Martínez-Díez et al. 1999)	DCMD	PTFE	NaCl
(Phattaranawik et al. 2003)	DCMD	PTFE	Pure water
(Bhattacharya et al. 2014)	DCMD	PTFE	Simulated water
(Singh & Sirkar 2012)	DCMD	PTFE	Produced water
(Wijekoon et al. 2014)	DCMD	PTFE	Synthetic solution
(Hickenbottom & Cath 2014)	DCMD	PTFE	Hyper salty water
(Hwang et al. 2011)	DCMD	PTFE	NaCl
(Li et al. 2018)	DCMD	PTFE	NaCl
(Winter et al. 2017)	DCMD	PTFE	NaCl
(Damtie et al. 2018)	DCMD	PTFE	Wastewater
(Lyly et al. 2021)	DCMD	PTFE	Bovine serum albumin
(Zhao et al. 2017)	DCMD	-	Seawater
(Fadhil et al. 2019)	DCMD	-	Seawater
(Lee et al. 2015)	DCMD	-	Seawater
(Naidua et al. 2016)	DCMD	-	Seawater
(Duong et al. 2015)	DCMD	-	Seawater
(Shim et al. 2015)	DCMD	-	Seawater
(Rezazazemi 2018)	DCMD	-	Seawater
(Al-Obaidani et al. 2008)	DCMD	-	Seawater

## MATERIALS AND METHODS

### Materials and Sampling

PTFE (poly tetrafluoro ethylene) dispersion (60 wt%, 0.05 - 0.5  $\mu\text{m}$ ) and semitransparent beads of Poly (1,4-phenylene ether ether-sulfone) (PPEES), having a molecular weight of 35,000 and ZnO (average 50 nm size) were obtained from Sigma Aldrich. Reagent grade N-methyl pyrrolidone (NMP) was obtained from Merck-India and was used without any further purification.

For seawater desalination, raw water was collected from the Arabian Sea (Kasba Bengre, Mangalore, Karnataka, India, 12°53' 22.956'N 74°48' 56.844' E). Water was taken from under one and a half meters of seawater level and large particles were removed by filtration.

### Membrane Preparation

PPEES was taken in 12.5 ml NMP, the solution was stirred for 24 hours at 70 °C for completion of dissolution. With the temperature still at 70°C, different weight percentages of ZnO nanoparticles were dispersed over a period of 30 min, and then PTFE emulsion was added to the aforementioned solution while being constantly stirred for at least 3 h. This was followed by a 30-minute sonication. Solutions containing different weight % of PTFE and PPEES (90:10, 80:20, 70:30 and 60: 40) (Table 2) were prepared. For the making of composite membranes, the electrospinning unit consists of a high-voltage source, a syringe pump, and a stainless-steel collector. A 15 kV voltage is used during the electrospinning process, with a spinning distance of 15 cm and a fluid flow rate of 0.4 mL.h<sup>-1</sup>. After more than 4 electrospinning, the membrane was separated from the collector. The electro-spun membrane was sintered in a furnace at 320°C for 20 min. A schematic diagram of the electrospinning process of membrane preparation is represented in Fig. 1.

Table 2 provides a list of the membrane's fundamental characteristics. Here, PPEES was employed to make the sheet flexible, ZnO served as a possible antifouling, and PTFE provided hydrophobicity.

In Table 1, the porosity and pore size of the membrane were determined by Capillary Flow Porometer (model CFP EX. 1500, Porous Materials Inc., USA). Contact angle (CA) with seawater measurements was made by sessile drop method using a goniometer VCA- Optima (AST products Inc., MA, USA). All prepared membranes exhibit a contact angle of more than 90° giving good hydrophobicity which is one of the essential requirements for MD. It should be noted from Table 1 that porosity and contact angle are influenced by the concentration of PTFE and ZnO.



Table 2: Basic characteristics of the prepared membrane.

Membrane code	Thickness [ $\mu\text{m}$ ]	Membrane material			Pore size [ $\mu\text{m}$ ]	Porosity	CA	Reference
		PTFE	PPEES	ZnO				
PZP-1	$119 \pm 4 \mu\text{m}$	90%	1%	9%	0.2-1.0	75-80%	$120-123^\circ$	(Xiong et al. 2009, Greiner & Wendorff 2007, Hegde et al. 2015)
PZP-2	$119 \pm 4 \mu\text{m}$	80%	10%	10%	0.4-1.2	75-80%	$116-118^\circ$	
PZP-3	$119 \pm 4 \mu\text{m}$	70%	10%	20%	0.5-1.3	76-77%	$110-111^\circ$	
PZP-4	$119 \pm 4 \mu\text{m}$	90%	9%	1%	0.6-1.4	75-79%	$90-95^\circ$	

### Direct Contact Membrane Distillation (DCMD)

MD investigations were carried out using self-designed and fabricated flat sheet cross-flow DCMD equipment. All membrane modules, listed in Table 1 were tested for leakage before the DCMD experiment. The prepared membrane module was assembled in the DCMD system, 1 % NaCl solution at  $80^\circ\text{C}$  flowed through the side at a constant flow rate between  $400 - 900 \text{ mL}\cdot\text{min}^{-1}$ , and deionized water flowed through the tube side at room temperature. The conductivity of the distillate was monitored with a constant increasing sodium chloride flow rate. Collected distillate water does not show any increase in conductivity, confirming leak free membrane module.

The schematic experimental set-up is shown in Fig 2. The installation of DCMD consists of two water loops (feed and distillate) connected to five modules of the membrane with an inner diameter of 120 mm. Deionized water having low conductivity of less than  $1\mu\text{S}/\text{cm}$  was used as the cold flow. Distillate having TDS less than 100 ppm was collected as potable water. The inlet temperature of distillate was maintained at  $60-8^\circ\text{C}$  and the circulating cold water temperature was maintained at  $30^\circ\text{C}$ . At the end of each operation, the membrane module is cleaned by flushing with a 2 L solution

of 1% HCl and distilled water followed by a 2 L solution of 1% NaOH and distilled water. After repeated reproducibility tests the operating condition is summarized in Table 3. The schematic process is given in Fig. 2.

### Calculations

Using the following equation, the water vapor permeation flux was calculated using the water that permeated from the DCMD over time.

$$J_v = V \times \rho / A \times t$$

where  $J_v$  is water vapor permeation flux ( $\text{L}\cdot\text{m}^{-2}\cdot\text{h}^{-1}$ ),  $V$  is the volume of collected water (l),  $\rho$  is water density ( $\text{kg}\cdot\text{m}^{-3}$ ),

Table 3: Operational parameters and specifications for DCMD.

Operational Parameter	Specification
Warm water flow, five modules	Range [ $80 \text{ mL}\cdot\text{min}^{-1}$ ]
Cold water flow, five modules	Range [ $60 \text{ mL}\cdot\text{min}^{-1}$ ]
Distillate flow	$10-30 \text{ L}\cdot\text{h}^{-1}$
Warm water operation temperature	$60-80^\circ\text{C}$
Cold water operation temperature	$30^\circ\text{C}$
Max operating pressure	300 KPa

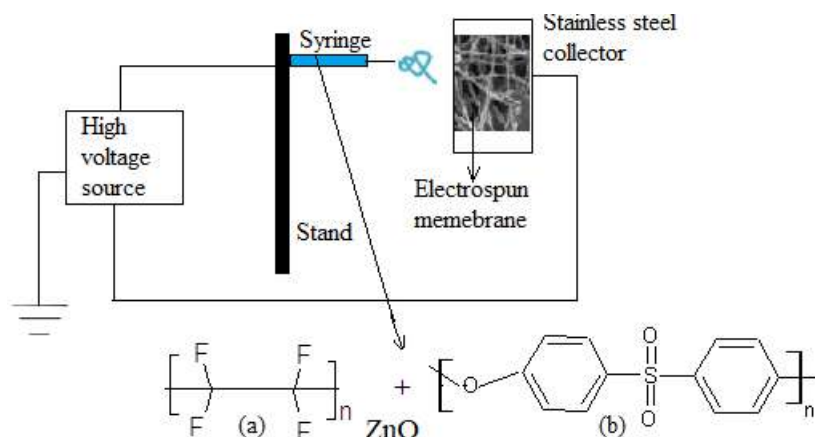


Fig. 1: Electrospinning process of membrane preparation (a = PTFE, b = PPEES) (Lalia et al. 2013).

A is the effective surface area of the membrane ( $m^2$ ), and t is water collected time (h).

The salt concentrations of the feed water and permeate water into and out of the DCMD module were measured by a conductivity meter (Model DDS 307, Germany). To calculate the salt rejection, the following equation was used

$$R (\%) = [1 - (C_p/C_f)] \times 100$$

Where 'R' is the salt rejection, 'C<sub>p</sub>' is the concentration of permeates solution and 'C<sub>f</sub>' is the concentration of the feed solution (Alkhudhiri et al 2011, Banat 2007).

## RESULTS AND DISCUSSION

### Membrane Characterization

Prepared membrane were characterized using different equipments.

### Spectral Characterization

To obtain detailed information about the formation of the membranes, FT-IR spectra of the membrane are recorded using Nicolet Avatar 330 FTIR (Thermo Corporation) spec-

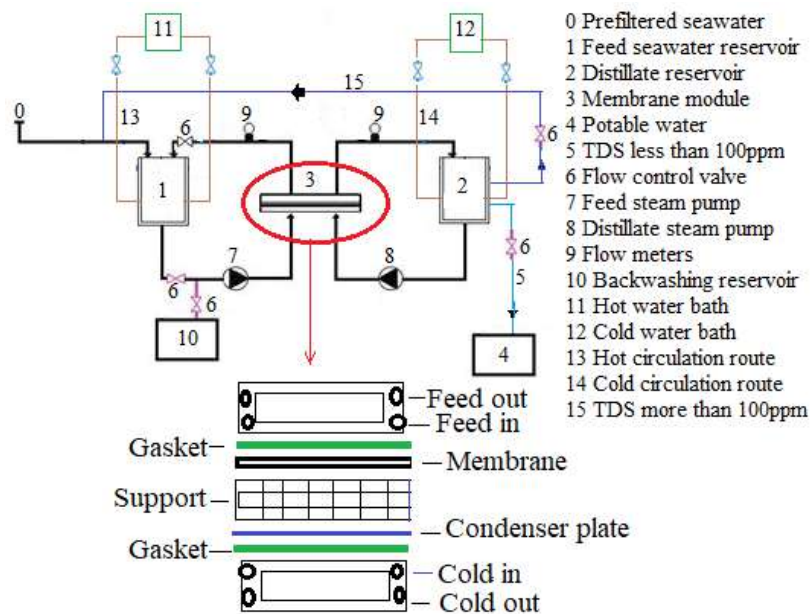


Fig. 2: Schematic DCMD process (Histov et al. 2017, Deshpande et al. 2017).

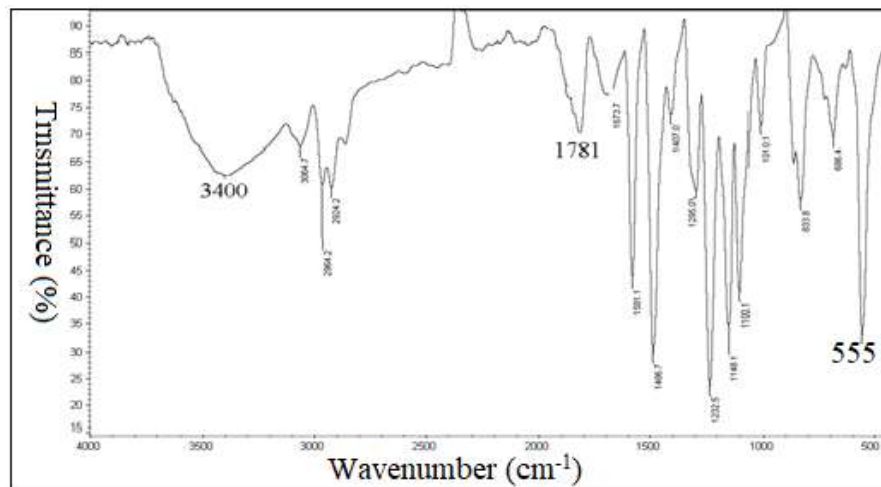


Fig. 3: IR spectrum of the PTFE-ZnO-PPEES membrane.

trometer. Fig.3 shows the IR spectrum of the PTFE -ZnO-PPEES membrane. Following stretching frequencies were observed; the carboxyl group was identified at  $1781\text{ cm}^{-1}$ ,  $3600\text{-}3200\text{ cm}^{-1}$  for O-H stretching vibrations along with characteristic group frequencies of C - F at  $630\text{ cm}^{-1}$ , peak at  $555\text{ cm}^{-1}$  for ZnO (Handore et al. 2014, Li et al. 2019)

### Mechanical and Thermal Study

The mechanical strength of the prepared membrane is associated with its degree of crystallinity and morphology. Membranes with poor mechanical properties may lead to early failure. The declination in mechanical strength in membranes could be due to reasons like cracks, tears, punctures, blisters stress. This paper mainly focuses on the variation of mechanical strength (young's modulus and elongation at break) and thermal properties of the membranes with respect to different times of DCMD operation (Collier et al. 2006, Ohagan 2008, Feng et al. 2016, Ranjbarzadeh-Dibazar et al. 2014). Membranes are subjected to 2 h DCMD operation (keeping cold temperature flow at  $30^{\circ}\text{C}$  and hot feed temperature at  $80^{\circ}\text{C}$ ) with intervals of 20 min after each interval membranes are removed from the module and tested for young's modulus, elongation at break, and thermal property. Instron 5569 machine (Instron, USA) was used to measure young's modulus and nominal elongation at the break of the membranes. Nominal elongation break is given by:

$$\frac{\text{Elongation of the membrane under DCMD operation} \times 100}{\text{Virgin membrane}}$$

The effect of desalination time on the membrane's thermal properties was investigated using Shimadzu DSC 60, Japan. For DSC analysis small piece of 5 mg of sample was placed into the crucible and the data analysis was recorded at an operating temperature of  $0^{\circ}\text{C}$  to a maximum of  $200^{\circ}\text{C}$  with a heating rate of  $10^{\circ}\text{C}\cdot\text{min}^{-1}$ . Figs. 4 and 5,

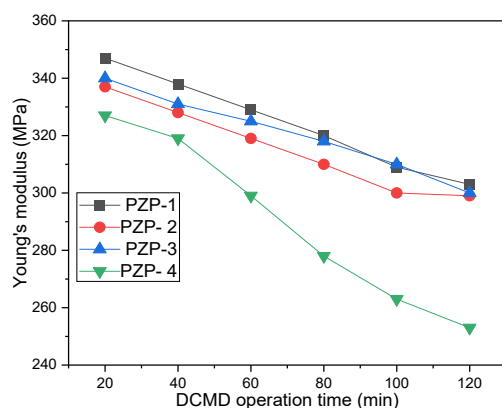


Fig. 4: Yong's modulus vs operation time.

show a decrease in young modulus and elongation break with an increase in operational temperature. The decline of the nominal elongation may be due to the chain breaking of membrane materials leading to the deterioration of the membrane layer and subsequently, weakening the interaction between polymer molecules making it easy to crack. The strong C-F bond in PTFE contributes to its remarkable thermal stability, yet this study shows that the melting point of the membrane falls between  $174$  and  $139^{\circ}\text{C}$ . (Fig 6). This might be explained by the membranes' surface deterioration in a high-temperature area. Among all prepared membranes, the PZP-1 membrane demonstrates the best mechanical and thermal stability.

### Morphology of the Membranes

The Morphology of the prepared membranes PZP-1 was studied using scanning electron microscopy (SEM). Fig.7, represents an SEM image of the membranes. The membrane's surface and cross-sectional images were recorded using Jeol JSM-84. The membrane was cryogenically fractured in liquid nitrogen and then sputtered with gold to get the membrane's image. Fig 7 (a) show evidence of linear nanofiber.

Fig 7 (b), and (c) were taken after a 6-h continuous desalination process, which exhibits stretched-apart nanofiber structure and pores deposited with other materials.

Table 4: LEP value of the prepared membranes.

Membrane code	LEP [KPa]
PZP-1	$578 \pm 3$
PZP-2	$498 \pm 3$
PZP-3	$398 \pm 3$
PZP-4	$297 \pm 3$

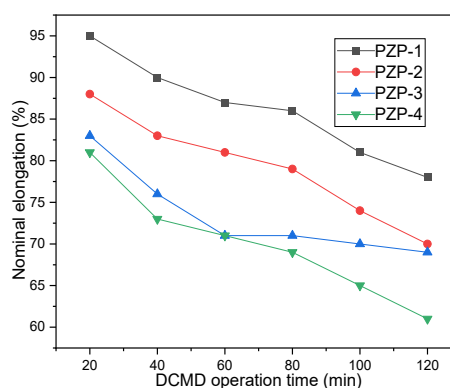


Fig. 5: Nominal elongation vs operation time.

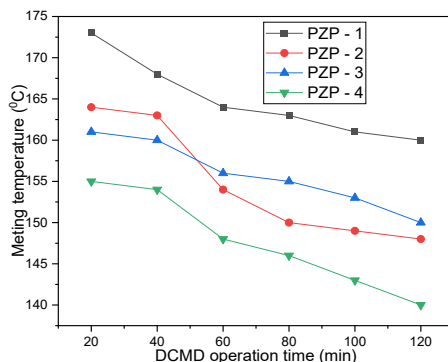


Fig. 6: Melting temperature of the membranes with different operational times.

### Liquid Entry Pressure (LEP)

It is fundamental for an MD process; the applied pressure should not exceed so that the feed solution may directly enter the membrane pores. LEP depends on the pore size, membrane hydrophobicity, contact angle, surface tension, presence of organic solutes, and material used for membrane preparation (Feng et al 2018). LEP Can be calculated using the Franken equation (Franken et al. 1987).

$$\Delta P = P_f - P_p = -2B\gamma \cos\theta / r_{\max}$$

Where  $\Delta P$  is LEP,  $P_f$  and  $P_p$  are the hydraulic pressure on the feed and permeate side,  $B$  is a geometric pore coefficient (it is equal to 1 assuming cylindrical pores),  $\gamma$  is liquid surface tension,  $\theta$  contact angle, and  $r_{\max}$  is the maximum pore

size. LEP values are summarized in Table 4. All prepared membranes show sufficiently good LEP value. A significant factor in raising LEP value is the concentration of ZnO and PTFE. This may be due to PZP-1 having a high contact angle and small pore size as given in Table 2.

### The DCMD Performance

After many repeated trials, the author concluded that prepared membrane PZP-1 showed good result with the self-designed, fabricated, lab scale DCMD module (Fig. 8). Table 5 exhibit the desalination performance of different membranes with the condition of cold circulation at 30°C and feed temperature 80°C. The energy efficiency (EE) of the process is obtained by the following equation

Table 5: Desalination performance of different membranes at cold temperature 30°C and hot feed temperature 80°C.

Parameter	Raw Sea-water	PZP-1		PZP-2		PZP-3		PZP-4		Instruments
		Distillate	R[%]	Distillate	R [%]	Distillate	R [%]	Distillate	R [%]	
Conductivity [ $\mu\text{S}\cdot\text{cm}^{-1}$ ]	55000	10-20	-	35-55	-	45-55	-	68-77	-	Model DDS 307, conductivity meter, Germany
TDS [ppm]	42600	20-30	99.9	300-400	99	425-475	99	496-515	98	HQ440 d TDS meter
Na <sup>+</sup> [ $\text{mg}\cdot\text{L}^{-1}$ ]	12000	0.8 -5	99.9	200-300	98-97	360-460	97-96	500-558	95	Flame photometer OFM 66 (Optima instruments)
K <sup>+</sup> [ $\text{mg}\cdot\text{L}^{-1}$ ]	2100	1-5	99.9	50-60	97	85-95	95	100-111	95-94	Flame photometer OFM 66 (Optima instruments)
Cl <sup>+</sup> [ $\text{mg}\cdot\text{L}^{-1}$ ]	18400	1-6	99.9	300-450	98-97	500-620	97-96	660-700	96	4500-Cl <sup>-</sup> -D potentiometric methods
SO <sub>4</sub> <sup>2-</sup> [ $\text{mg}\cdot\text{L}^{-1}$ ]	1900	1-4	99.9	75-95	96-95	100-130	94-93	175-195	90-89	ASTM D4130-15
Ca <sup>2+</sup> [ $\text{mg}\cdot\text{L}^{-1}$ ]	420	1-2	99.9	20-30	95-92	100-114	76-72	110-119	73-71	Flame photometer OFM 66 (Optima instruments)
Mg <sup>2+</sup> [ $\text{mg}\cdot\text{L}^{-1}$ ]	1200	1-3	99.9	150-200	87-83	95-105	92-91	120-135	90-88	Flame photometer OFM 66 (Optima instruments)
EE (%)	-	67.3 ± 3		64.2 ± 3		60.1 ± 3		57.6 ± 3		

$$EE(\%) = \frac{-\Delta H A}{F C_p (T_i - T_o)} 100$$

Where,  $N$  ( $\text{kg}\cdot\text{m}^{-2}\cdot\text{h}^{-1}$ ) is the water flux,  $\Delta H$  ( $\text{J}\cdot\text{kg}^{-1}$ ) is the enthalpy of evaporation,  $F$  ( $\text{kg}\cdot\text{s}^{-1}$ ) is the mass flow rate,  $A$  ( $\text{m}^2$ ) is the effective membrane surface area,  $C_p$  ( $\text{J}\cdot\text{kg}^{-1}\cdot^\circ\text{C}$ ), is the specific heat capacity of the feed solution,  $T_i$  and  $T_o$  are inlet and outlet bulk temperatures of the module in  $^\circ\text{C}$  respectively (Khayet 2013, Sabbah et al. 1999).

### Removal efficiency (R)

Removal efficiency (R) is calculated using the following equation.

$$R(\%) = \frac{\text{Concentrate of feed} - \text{Concentrate of permeate}}{\text{Concentrate of feed}} \times 100$$

Understanding Table 5, all the membranes demonstrated good salt removal efficiency with PZP-1 producing excellent performance. Salt rejection percentage agrees with previous studies (Drioli et al. 2015, Fard et al. 2015, Francis et al. 2014). Many instruments were used to determine the different components of the raw seawater and distillate (APHA 2005). PZP-1 membrane outperformed the PZP-4 membrane in terms of desalination performance, confirming previous studies in this regard (Yong et al. 2015, Hong & He 2012, Jafarzadeh et al. 2015, Liang et al. 2012). Notably, ZnO has a superb antifouling characteristic that might be influenced by the efficient membrane distillation process. Distillate flux ( $\text{L}\cdot\text{m}^{-2}\cdot\text{h}^{-1}$ ) of 6 h of desalination with PZP -1 is given in Fig. 9. Except for varying values at the beginning and conclusion, distillate flux has a nearly constant plateau at roughly  $25.6 \text{ L}\cdot\text{m}^{-2}\cdot\text{h}$  distillate flux.

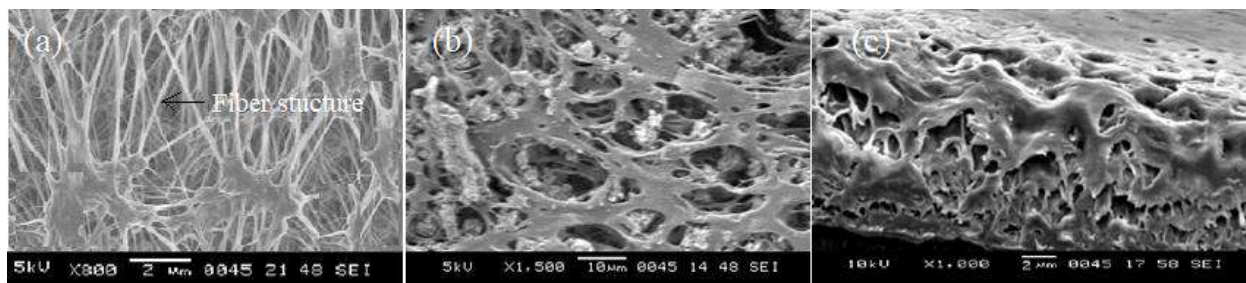


Fig. 7: SEM images of the prepared membrane (a) surface image of the membrane (b) surface image after desalination (c) cross-section image after desalination.



Fig. 8: Digital photograph of lab scale DCMD.

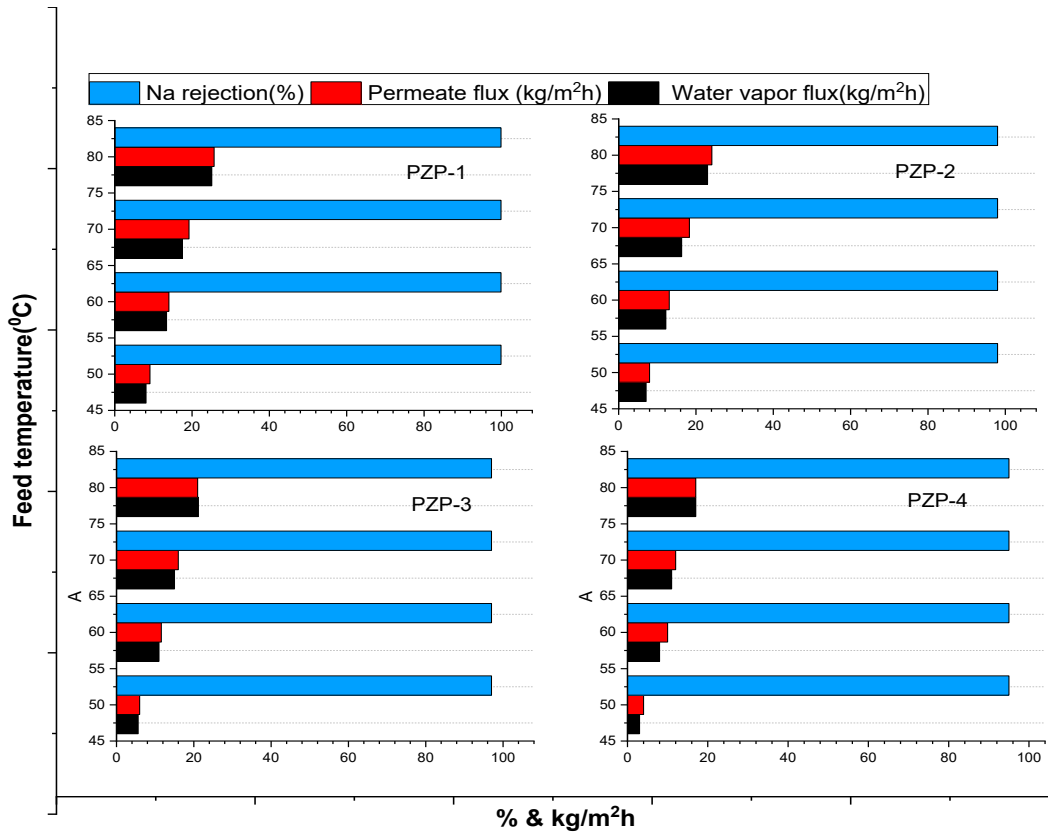


Fig. 10: Desalination performance of different membranes with feed temperature.

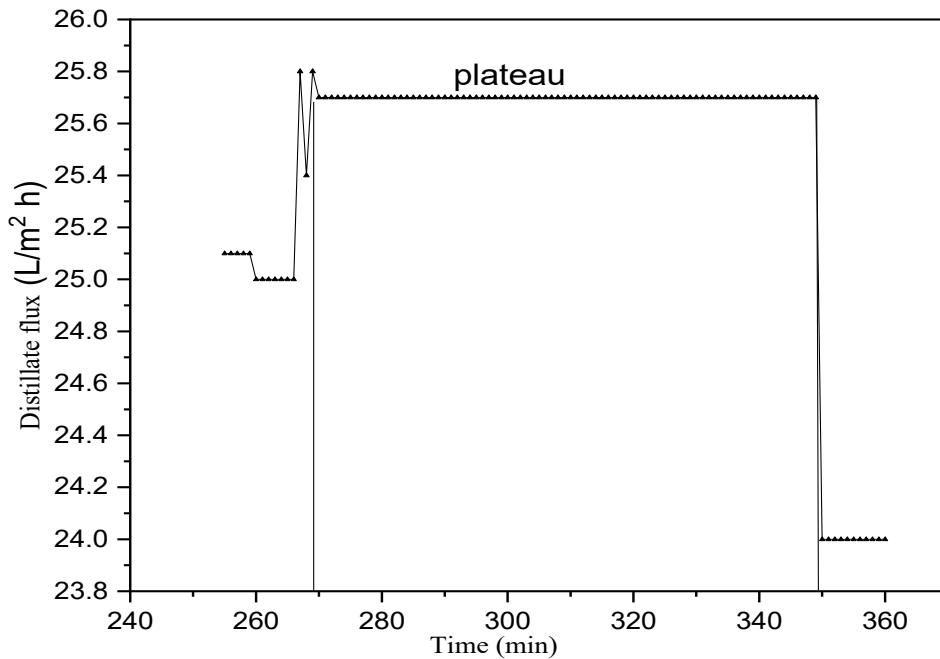


Fig. 9: 6-h Desalination process producing distillate flux with PZP-1.

From the water collected after distillation, water vapor flux (WTF) of the different prepared membranes was calculated for feed temperature at 50, 60, 70, and 80°C, maintaining a cold temperature at 30°C. Equation (1) is used to calculate WTF.

$$\text{WTF} = \frac{\text{vol. of water transferred(L)} \times \text{density of water} \left(\frac{\text{kg}}{\text{L}}\right)}{\text{membrane area}(\text{m}^2) \times \text{time}(\text{h})}$$

... 1

Experimentally, at cold (30°C) and feed hot temperature (80°C), PZP-1 gives the highest values for WTF, permeate flux, and sodium rejection percentage with 25.1 kg.m<sup>-2</sup>.h<sup>-1</sup>, 25.6 kg.m<sup>-2</sup>.h<sup>-1</sup>, and 99.9% respectively whereas, PZP-4 had only 17(WTF), 17.2 (permeate flux) and 95% (sodium rejection percentage) (Fig.10). Notably, all the prepared membranes depicted good salt rejection varying from 95-99.9%.

## CONCLUSION

In this research work, the desalination performance of a newly prepared membrane is evaluated using lab-scale DCMD equipment. Arabian Seawater from the southern part of India was collected for this purpose. Combining prepared membrane and DCMD resulted in a highly encouraging outcome for the reduction of various components of seawater. The elimination of ions like sodium, magnesium, and potassium, in the range of 90-99%, is the best aspect of the research effort. All prepared membranes revealed a significantly respectable EE percentage. The point of contention of this work is that the data obtained in the lab scale operating conditions may require further optimization of equipment and membrane modules to reflect reality on a pilot scale. Unlike the lab scale, in the pilot scale managing high flow rate, and temperature difference between cold and hot is difficult. Irrefutably to update our module for large-scale seawater desalination further redesigning may be required.

## REFERENCES

Alkudhri, A., Darwish, N. and Hilal, N. 2011. Membrane distillation: A comprehensive review. *Desalination*, 287: 2-18.

Al-Obaidani, S., Curcio, E., Macedonio, F., Profio, G.D., Al-Hinai, H. and Drioli, E. 2008. Potential of membrane distillation in seawater desalination: Thermal efficiency, sensitivity study, and cost estimation. *J. Memb. Sci.*, 323: 85-98.

APHA, AWWA, WEF. 2005. Standard methods for the examination of water and wastewater. in: Eaton, A.D., Clesceri, L.S., Rice, E.W. and Greenberg, A.E. (eds), Centennial Edition, American Public Health Association Publication, Washington DC, pp.66-125.

Ashoor, B. Mansour, S. Giwa, A. Dufour, V. and Hasan, S.W. 2016. Principles and applications of direct contact membrane distillation (DCMD): A comprehensive review. *Desalination*, 398: 222-246.

Banat, F. 2007. Desalination by a "compact SMADES" autonomous solar-powered membrane distillation unit. *Desalination*, 217: 29 - 37.

Bhattacharya, M., Dutta, S.K., Sikder, J. and Mandal, M.K. 2014. Computational and experimental study of chromium (VI) removal in direct contact membrane distillation. *J. Membr. Sci.*, 450: 447-456.

Cadotte, J.E., Petersen, R.J., Larson, R.E. and Erickson, E.E. 1980. A new thin-film composite seawater reverse osmosis membrane. *Desalination*, 32: 25-31.

Collier, A., Wang, H.J., Yuan, X.Z., Zhang, J.J. and Wilkinson, D.P. 2006. Degradation of polymer electrolyte membranes. *Int. J. Hydro. Energy*, 31: 1838-1854.

Damtie, M.M., Kim, B., Woo, Y.C. and Choi, J.S. 2018. Membrane distillation for industrial wastewater treatment: Studying the effects of membrane parameters on the wetting performance. *Chemosphere*, 206: 793-801.

Das, A., Sujith, P.P., Mourya, B.S., Biche, S.U. and Lokhabharathi, P.A. 2011. Chemosynthetic activity prevails in deep-sea sediments of the Central Indian Basin. *Extremophiles*, 15: 177 -189.

Deshpande, J., Nithyanandam, K. and Pitchumani, R. 2017. Analysis and design of direct contact membrane distillation. *J. Membr. Sci.*, 523: 301-316.

Ding, Z.R., Ma, R. and Fane, A.G. 2003. A new model for mass transfer in direct contact membrane distillation. *Desalination*, 151(3): 217-227.

Drioli, E., Ali, A. and Macedonio, F. 2015. Membrane distillation: Recent developments and perspectives. *Desalination*, 356: 56 - 84.

Duong, H.C., Cooper, P., Nelemans, B., Cath, T.Y. and Nghiem, L.D. 2015. Optimizing thermal efficiency of direct contact membrane distillation by brine recycling for small-scale seawater desalination. *Desalination*, 374: 1-9.

El-Abbassi, A., Hafidi, A., Garcia-Payo, M. C. and Khayet, M. 2009. The concentration of olive mill wastewater by membrane distillation for polyphenols recovery. *Desalination*, 245: 670-674.

Eykens, L., Hitsov, I., De Sitter, K., Dotremont, C., Pinoy, L., Nopens, I. and Van der Bruggen, B. 2016. Influence of membrane thickness and process conditions on direct contact membrane distillation at different salinities. *J. Membr. Sci.*, 498: 353-364.

Fadhil, S., Alsahy, Q.F., Makki, H.F., Figueroa, R., Marino, T., Criscuoli, A., Macedonio, F., Drioli, E., Giorno, L. and Figoli, A. 2019. Seawater desalination using PVDF-HFP membrane in DCMD process: Assessment of operating condition by response surface method. *Chem. Eng. Commun.*, 206: 237-246.

Fard, A.K., Manawi, Y.M., Rhadfi, T., Mahmoud, K. A., Khraisheh, M. and Benyahia, F. 2015. Synoptic analysis of direct contact membrane distillation performance in Qatar: A case study. *Desalination*, 360: 97 -107.

Feng, S., Zhong, Z., Wang, Y., Xing, W. and Drioli, E. 2018. Progress and perspectives in PTFE membrane: Preparation, modification, and applications. *J. Membr. Sci.*, 549: 332 - 349.

Feng, Y., Xiong, T., Xu, H., Li, C. and Hou, H. 2016. Polyamide-imide reinforced polytetrafluoroethylene nanofiber membranes with enhanced mechanical properties and thermal stabilities. *Mater. Lett.*, 182: 59-62.

Findley, M.E. 1967. Vaporization through the porous membrane: Process design and development. *Int. Eng. Chem.*, 6: 226-237.

Francis, L., Ghaffour, N., Alsaadi, A.S., Nunes, S.P. and Amy, G.L. 2014. Performance evaluation of the DCMD desalination process under bench scale and large-scale module operating conditions. *J. Membr. Sci.*, 455: 103-112.

Franken, A.C.M., Noltén, J.A.M., Mulder, M.H.V., Bargeman, D. and Smolders, C.A. 1987. Wetting criteria for the applicability membrane distillation. *J. Membr. Sci.*, 33: 315-328.

Glaser, J. 1998. The early history of reverse osmosis membrane development. *Desalination*, 117: 297-309.

Greiner, A. and Wendorff, J. H. 2007. Electrospinning: a fascinating method for the preparation of ultrathin fibers. *Angew. Chem.*, 46: 5670-5703.

Handore, K., Bhavsar, S., Horne, A., Chhattise, P., Mohite, K., Ambekar, J., Pande, N. and Chabukswar, V. 2014. Novel green route of synthesis of ZnO nanoparticles by using natural biodegradable polymer and its

- application as a catalyst for oxidation of Aldehydes. *J. Macromol. Sci. Part A*, 51: 941-947.
- Hegde, C., Padaki, M., Isloor, M.A., Wanichapichart, P. and Liangdeng, Y. 2011. Synthesis and desalination performance of Ar<sup>+</sup>-N<sup>+</sup> irradiated polysulfone based new NF membrane. *Desalination*, 265:153 -158.
- Hegde, C., Rao, S. and D'Souza, J. 2014. Synthesis of new composite polymer membrane from tapioca grains - polysulfone for desalination. *Desal. Water Treat.*, 52: 1-8.
- Hickenbottom, K.L. and Cath, T.Y. 2014. Sustainable operation of membrane distillation for enhancement of mineral recovery from hypersaline solutions. *J. Membr. Sci.*, 454: 426-435.
- Histov, I., Eykens, L., DeSchepper W., Desitter, K., Dotremont, C. and Nopens, I. 2017. Full-scale direct contact membrane distillation (DCMD) model including membrane compaction effects. *J. Membr. Sci.*, 534: 245-256.
- Hong, J.M. and He, Y. 2012. Effects of nano-sized zinc oxide on the performance of PVDF microfiltration membranes. *Desalination*, 302: 71-79.
- Hsu, S.T., Cheng, K.T. and Chiou, J.S. 2002. Seawater desalination by direct contact membrane distillation. *Desalination*, 143: 279 -287.
- Hwang, H.J., Gray, K.H.S., Zhang, J. and Moon, S. 2011. Direct contact membrane distillation (DCMD): Experimental study on the commercial PTFE membrane and modeling. *J. Membr. Sci.*, 371: 90-98.
- Jafarzadeh, Y., Yegani, R. and Sedaghat, M. 2015. Preparation, characterization, and fouling analysis of ZnO/polyethylene hybrid membranes for collagen separation. *Chem. Eng. Res. Des.*, 94: 417-427.
- Khayet, M. 2013. Solar desalination by membrane distillation: Dispersion in energy consumption analysis and water production costs: A review. *Desalination*, 308: 89 -101.
- Khayet, M., Matsuura, T., Mengual, J.I. and Qtaishat, M. 2005. Design of novel direct contact membrane distillation membranes. *Desalination*, 192: 105-111.
- Lalia, B. S., Kochkodan, V., Hashaikeh, R. and Hilal, N. 2013. A review on membrane fabrication: Structure, properties, and performance relationship. *Desalination*, 326: 77-95.
- Lee, J., Kim, Y., Kim, W. and Francis, L. 2015. Performance modeling of direct contact membrane distillation (DCMD) seawater desalination process using a commercial composite membrane. *J. Memb. Sci.*, 478: 85-95.
- Li, K., Zhang, Y., Xu, L., Zeng, F., Hou, D. and J. Wang, J. 2018. Optimizing stretching conditions in the fabrication of PTFE hollow fiber membrane for performance improvement in membrane distillation. *J. Memb. Sci.*, 550: 126-135.
- Li, M., Chen, F., Liu, C., Qian, J., Wu, Z. and Chen, Z. 2019. Electrospun fibrous PTFE supported ZnO for oil-water separation. *J. Inorganic Organon. Poly. Mater.*, 29: 1738 - 1745.
- Liang, S., Xiao, K., Mo, Y. and Huang, X. 2012. A novel ZnO nanoparticle blended polyvinylidene fluoride membrane for anti-irreversible fouling. *J. Membr. Sci.*, 394-395: 184-192.
- Loeb, S. 1981. The Loeb-Sourirajan membrane: How it came about. *Syn. Membr.*, 53: 1-9.
- Lyly, L.H.T., Ooi, B.S., Lim, W.J., Chang, Y.S., Derek, C.J.C. and Lim, J.K. 2021. Desalinating microalgal-rich water via thermo-responsive membrane distillation. *J. Environ. Chem. Eng.*, 9: 105897.
- Ma, M. and Hill, R.M. 2006. Superhydrophobic surfaces. *Curr. Opin. Coll. Interface Sci.*, 11: 193-202.
- Manna, P.P. 2016. Solar-driven flash vaporization membrane distillation for arsenic removal from groundwater: experimental investigation and analysis of performance parameters. *Chem. Eng. Process. Intensif.*, 99: 51-57.
- Martínez-Díez, L. and Vazquez-Gonzalez, M.I. 1999. Temperature and concentration polarization in membrane distillation of aqueous salt solutions. *Journal of Membrane Science*, 156(2): 265-273.
- Naidua, G., Jeonga, S., Vigneswaran, S., Jangc, E., Choib, Y. and Hwang, T. 2016. Fouling study on vacuum-enhanced direct contact membrane distillation for seawater desalination. *Desal. Water Treat.*, 57: 10042-10051.
- Nollet, A. 1748. *Lessons in Experimental Physics*. Guerin Brothers, Paris, France..
- OHagan, D. 2008. Understanding organofluorine chemistry. An introduction to the C-F bond. *Chem. Soc. Rev.*, 37: 308-319.
- Phattaranawik, J., Jiraratananon, R. and Fane, A.G. 2003. Effect of pore size distribution and air flux on mass transport in direct contact membrane distillation. *J. Membr. Sci.*, 215:75-85.
- Ramos, R.L., Martins, M.F., Lebron, Y.A.R., Moreira, V.R., Reis, B.G., Grossi, L.B. and Amaral, M. C.S. 2021. The membrane distillation process for phenolic compounds removal from surface water. *J. Environ. Chem. Eng.*, 9: 105588.
- Ranjbarzadeh-Dibazar, A., Shokrollahi, P., Barzin, J. and Rahimi, A. 2014. Lubricant facilitated thermo-mechanical stretching of PTFE and morphology of the resulting membranes. *J. Memb. Sci.*, 470: 458-469.
- Rezazakemi, M. 2018. CFD simulation of seawater purification using direct contact membrane desalination (DCMD) system. *Desalination*, 443: 323-332.
- Sabbah, R., Xu-wu, A., Chickos, J.S., Leitao, M.L.P., Roux, M.V. and Torres, L.A. 1999. Reference materials for calorimetry and differential thermal analysis. *Thermochim. Acta.*, 331: 93-204.
- Sakai, K., Koyano, T., Muroi, T. and Tamura, M. 1988. Effects of temperature and concentration polarization on water vapour permeability for blood in membrane distillation. *Chem. Eng. J.*, 38: B33-B39.
- Schneider, K., Holz, W. and Wollbeck, R. 1988. Membranes and modules for transmembrane distillation. *J. Membr. Sci.*, 39: 25-42.
- Shim, W.G., He, K., Gray, S. and Moon, I.S. 2015. Solar energy assisted direct contact membrane distillation (DCMD) process for seawater desalination. *Sep. Purif. Technol.*, 143: 94-104.
- Singh, D. and Sirkar, K.K. 2012. Desalination of brine and produced water by direct contact membrane distillation at high temperatures and pressures. *J. Membr. Sci.*, 389: 380-388.
- Summers, E.K., Arafat, H.A. and Lienhard, J.H. 2012. Energy efficiency comparison of single stage membrane distillation (MD) desalination cycles in different configurations. *Desalination*, 290: 54 - 66.
- Wijekoon, K.C., Hai, F.I., Kang, J., Price, W.E., Cath, T.Y. and Nghiem, L.D. 2014. Rejection, and fate of trace organic compounds (TrOCs) during membrane distillation. *J. Membr. Sci.*, 453: 636 - 642.
- Winter, D., Koschikowski, J., Gross, F., Maucher, D., Duver, D., Jositz, M., Mann, T. and Hagedorn, A. 2017. Comparative analysis of full-scale membrane distillation contactors - methods and modules. *J. Membr. Sci.*, 524: 758-771.
- Xiong, J. Huo, P. and Ko, F.K. 2009. Fabrication of ultrafine fibrous polytetrafluoroethylene porous membranes by electrospinning. *J. Mater. Res.*, 24: 2755-2761.
- Yong, H. E., Krishnamoorthy, K., Hyun, K. T. and Kim, S. J. 2015. Preparation of ZnO nanopaint for marine antifouling application. *J. Ind. Eng. Chem.*, 29: 39-42.
- Zhao, D., Zuo, J., Lu, K.J. and T.S. 2017. Chung, Fluorographite modified PVDF membranes for seawater desalination via direct contact membrane distillation. *Desalination*, 41: 119-126.





# Optimal Models for Plant Disease and Pest Detection Using UAV Image

Dashuang Liang, Wenping Liu<sup>†</sup> and Yugang Zhao

School of Information Science and Technology, Beijing Forestry University, Beijing, 100083, China

<sup>†</sup>Corresponding author: Wenping Liu; wendyl@vip.163.com

## Nat. Env. & Poll. Tech.

Website: [www.neptjournal.com](http://www.neptjournal.com)

Received: 25-12-2021

Revised: 09-02-2022

Accepted: 12-02-2022

### Key Words:

Anchor-free detector

Deep learning

Unmanned aerial vehicle

Automated machine learning

Pest detection

## ABSTRACT

The use of deep learning methods to detect plant diseases and pests based on UAV images is an important application of remote sensing technology in modern forestry. This paper uses a CenterNet-based object detection method to construct models for plant disease and pest detection. The accuracy of the models is influenced by parameter alpha, which is used to control the affine transformation in the preprocessing of CenterNet. First, different alphas are sampled for training and testing. Next, the least square method is used to fit the curve between alpha and accuracy measured by mAP (mean average precision). Finally, the equation of the curve is fitted as  $mAP = -0.22 * \alpha^2 + 0.32 * \alpha + 0.42$ . In comparison, an automated machine learning (AutoML) method is also conducted to automatically search for the best model. The experiments are done with 5,281 images as the training dataset, 1,319 images as the verification dataset, and 3,842 images as the test dataset. The results show that the best alpha value obtained by the least square method is 0.733, and the accuracy of the corresponding model is 0.536 in mAP@[.5, .95]. In contrast, the accuracy of the AutoML method model is higher with the model accuracy of 0.545 in mAP@[.5, .95]. However, the training time and training resource consumption of the AutoML method are about 3 times that of the least square method. Therefore, in practice, a trade-off should be made according to the accuracy requirements, resource consumption, and task urgency.

## INTRODUCTION

Plant diseases and insect pests seriously threaten the growth of forests and can be great impediments to forest health and forestry production (Zhang et al. 2010). Traditionally, the monitoring methods of forestry pests and diseases mainly consisted of field surveys. These manual scoring and counting through field surveys are expensive, and the monitoring methods have time lags and strong subjectivity. Moreover, in areas with dangerous terrain and restricted access, the surveyors are unable to discover plant diseases and insect pests in time (Chiu 1993). Therefore, it is necessary to detect plant diseases and insect pests more accurately and quickly, which will help to develop early treatment technologies and greatly reduce economic losses at the same time (Fuentes et al. 2017).

In the early 1970s, with the launch of the first remote sensing satellite, remote sensing images were used to monitor forestry diseases and pests (Gao et al. 2006, Lehmann et al. 2015). However, it is difficult to popularize and widely apply because of its inaccurate positioning accuracy, high cost, weather influence, and relatively long imaging cycle (Wu 2013). Fortunately, with the rapid development of unmanned aerial vehicle (UAV) technology and continuous improvement in its performance, UAV remote sensing has

many advantages such as low cost, high precision, simple operation, and flexibility (Tang 2014). At present, people have also begun to explore the application of UAV remote sensing image in monitoring forest diseases and insect pests, combined with traditional computer vision methods and image analysis technology. The application integrates a global positioning system and geographic information system to detect the distribution of pests and achieves good results (Tetila et al. 2020, Yuan & Hu 2016).

In addition, Hinton et al. (2016) proposed the concept of deep learning. Krizhevsky et al. (2012) first applied the convolutional neural network (CNN) to the ImageNet large-scale visual recognition challenge (ILSVRC). In the ILSVRC-2012 challenge, the trained deep CNN won first place in tasks of image classification and object detection, and the error rate was far lower than the other programs. Since then, deep learning has been rapidly applied to different research fields and has achieved great success in many fields, including image classification (Huang et al. 2016), object detection (Girshick 2015, Redmon et al. 2016), image segmentation (Chen et al. 2018, Lee & Park 2020) and so on.

In recent years, deep CNN are applied to the detection of plant disease severity and has been proven to be a good method. For example, Liu et al. (2018) proposed a new CNN

model based on Alexnet to identify four common apple leaf diseases. The overall accuracy of the model was 97.62%, and the parameters were reduced by 51,206,928 compared with the standard Alex net model. Xie et al. (2020) proposed a faster DR-IACNN model by introducing the concept-v1 module, concept-resnet-v2 module, and SE module. The results showed that the average detection accuracy of the detection model for the grape leaf disease dataset was 81.1% and the detection speed was 15.01 FPS. Wang et al. (2019) proposed a corn leaf disease segmentation method based on an improved fully convolution network (FCN). The method mainly included an encoding network and corresponding decoding network, as well as a pixel-level classifier behind the decoding network. This method had good segmentation performance and could accurately segment the diseased area of corn leaves.

Similar to computer vision tasks, the application of CNN in the research of plant diseases and insect pests can be roughly divided into classification networks, object detection networks, and segmentation networks according to their different tasks. The object detection network model not only gives the types of pests and diseases but also accurately finds out the location of the pests and diseases on the images. Object detection methods are further roughly divided into two categories, anchor-based object detection methods, and anchor-free object detection methods. For example, anchor-based object detection methods include the Faster RCNN series (Girshick 2015, Ren et al. 2017), YOLO series (Bochkovskiy et al. 2020, Redmon et al. 2016, 2017, 2018), SSD series (Jeong et al. 2017, Liu et al. 2016, Zhang et al. 2020), RFCN (Dai et al. 2016) and so on. All these methods rely on a set of predefined anchor boxes. Thus, to avoid the shortcomings brought by the pre-defined anchor box, people began to study the anchor-free object detection method. This method does not need to use anchors but adopts the idea of key point regression. First, some key points are defined to describe an object, and then each key point of the object is regressed. There are some classic methods, such as CornerNet (Law & Deng 2020), CenterNet (Zhou et al. 2019a), FCOS (Tian et al. 2020), and extreme (Zhou et al. 2019b), etc., all of which take object detection as a standard key point estimate problem.

In the above anchor-free object detection algorithms, CenterNet is a simple, fast, and accurate detector without any non-maximum suppression (NMS) as the post-processing method. In the training of the original CenterNet, a random affine transformation is done to each image to enrich the data, and the new object's boundary box is generated by clip operation, which is usually not correct. To make the boundary box generated by clip operation as accurate as possible,

Liang et al. (2021) only used a criterion that the proportion of the remaining objects should be at least 90% of the size of the original objects. Therefore, this study mainly focuses on identifying an optimal model based on parameter alpha, which is the parameter used to control the affine transformation in the preprocessing of CenterNet, to improve the accuracy of detecting plant diseases and pests. Both the least square method and an automated machine learning (AutoML) method are proposed to find an appropriate model for detecting plant diseases and pests.

## MATERIALS AND METHODS

### Study Area

The study area is located in Lingyuan City, Liaoning Province, Northeast China. Lingyuan City is located in the west of Liaoning Province, bordering Hebei Province and Inner Mongolia. The main vegetation is Chinese red pine (*Pinus tabulaeformis*) and scattered with some poplar. The pest dendroctonus (*Scolytidae*) has caused damage and tree death in the area.

Six sample plots that are being infected by plant diseases and pests were selected. They were named plot 1 to plot 6. Fig. 1 shows the detailed location and distribution of these plots on the map.

### Data Collection

The images of the UAV were taken in the study area from August 11 to August 12 during the growing season, which can better reflect the characteristics of plant growth. UAV took off from the center of six sample plots, and a batch of images was taken in each sample plot at different heights. The model of the UAV is four rotor DJI inspire2, equipped with DJI X5 professional camera, and the resolution of each image is 5280 × 3956 pixels.

### CenterNet Principles

For image I, after the full convolution network, three outputs will be generated. One is the feature map containing C (number of categories of the detection task) layers. Each feature map corresponds to one category. Each pixel on the feature map represents the score of the pixel belonging to the center of an object. Another layer represents the offset ( $x/S_x - x/S_{x_c}, y/S_y - y/S_{y_c}$ ), where (x, y) is the center of an object with class C on the input image, and ( $S_x, S_y$ ) is the horizon and vertical scale parameters of the input image to that of the output feature image, respectively. The number of this layer is 1, and each pixel on this layer represents the offset between the real center point position and center pixels on the feature map. The other layer represents the length and

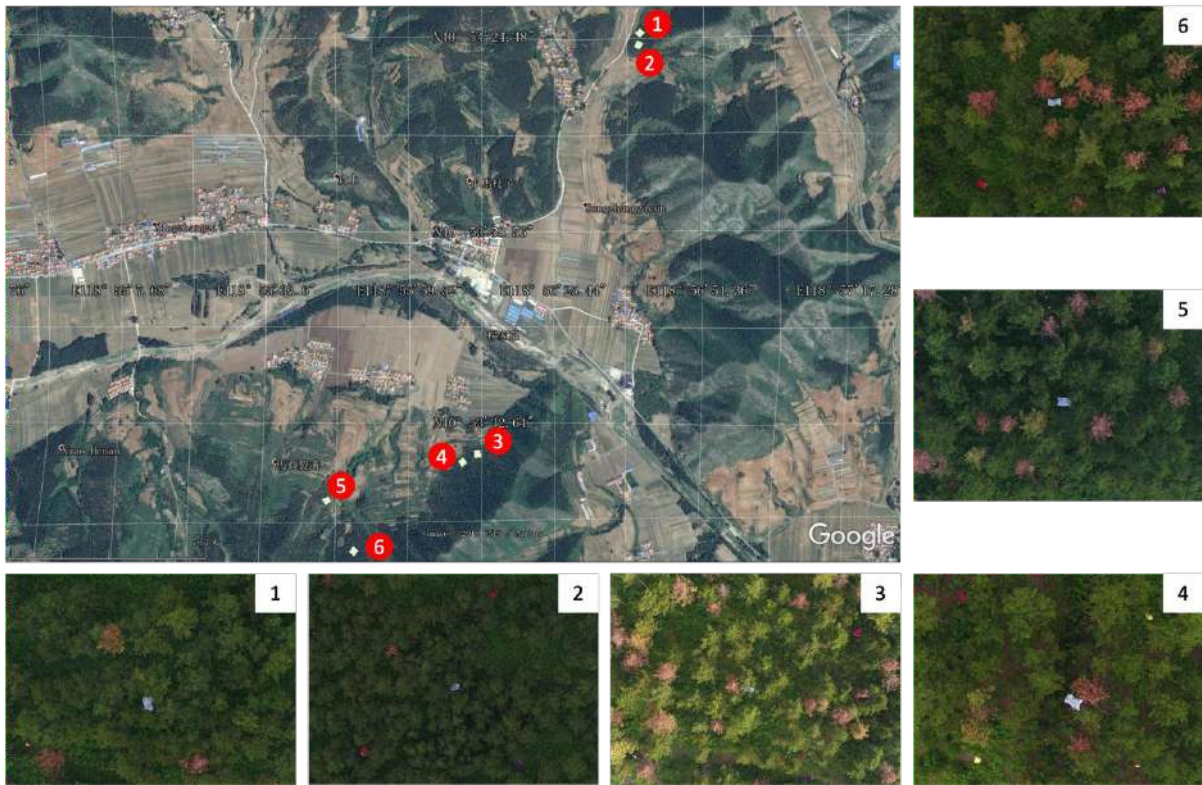


Fig. 1: The study area.

width of the boundary box of an object. Each pixel on this layer represents the length and width of the object's boundary box (box) corresponding to the point. The overall structure of CenterNet is shown in Fig. 2.

### Data Enhancement by Affine Transformation

In the original CenterNet, before sending the image to the network, an affine transformation of random center translation and scaling is made to the image. As a result, some objects on the image will be removed from the new image boundary, while some objects on the image will be retained in the new image, and other objects on the image will fall on the new image boundary, as shown in Fig. 3(b). For objects that fall on the boundary, the original CenterNet only recalculates the boundary box's coordinates of the remaining objects with a simple clip operation. The new boundary box of the remaining objects calculated by the clip operation is often inaccurate, as shown in Fig. 3(b), while Fig. 3(c) shows the ground truth of the boundary box of the remaining object.

For an object that remains in the new image after affine transformation to the original image, the ratio of the area of the new boundary box (boundary box created by clip operation) to the original boundary box (boundary box in

the original image) is defined as alpha. It is known that, for an object that falls on the new image's boundary after the affine transformation to an image, the larger the alpha ratio, the more accurate the new boundary box obtained by clip operation is. As the shapes of the plants' canopy are often approximate to circular, in most situations, with the growing of alpha, the remaining object's boundary box calculated by clip operation will be more accurate, as shown in Fig. 4.

### Optimal Parameter Search by Least Square Fitting

Alpha is a scale factor, and its value falls within the range of [0, 1]. To quickly obtain the appropriate value of alpha, the following strategies are adopted: after affine transformation, no constraints are made for the objects that are moved out of the image or the whole objects that are still within the image scope, while the alpha value is required to be greater than 0.5 to objects that fall on the image boundary, that is, the alpha value must be limited to the range of [0.5, 1] if some objects fall on the image boundary after an affine transformation.

To explore the relationship between alpha and the detection accuracy of diseased and pest plant detectors, different alpha values are selected to train models on the same training dataset and then tested on the same test dataset. Finally, the

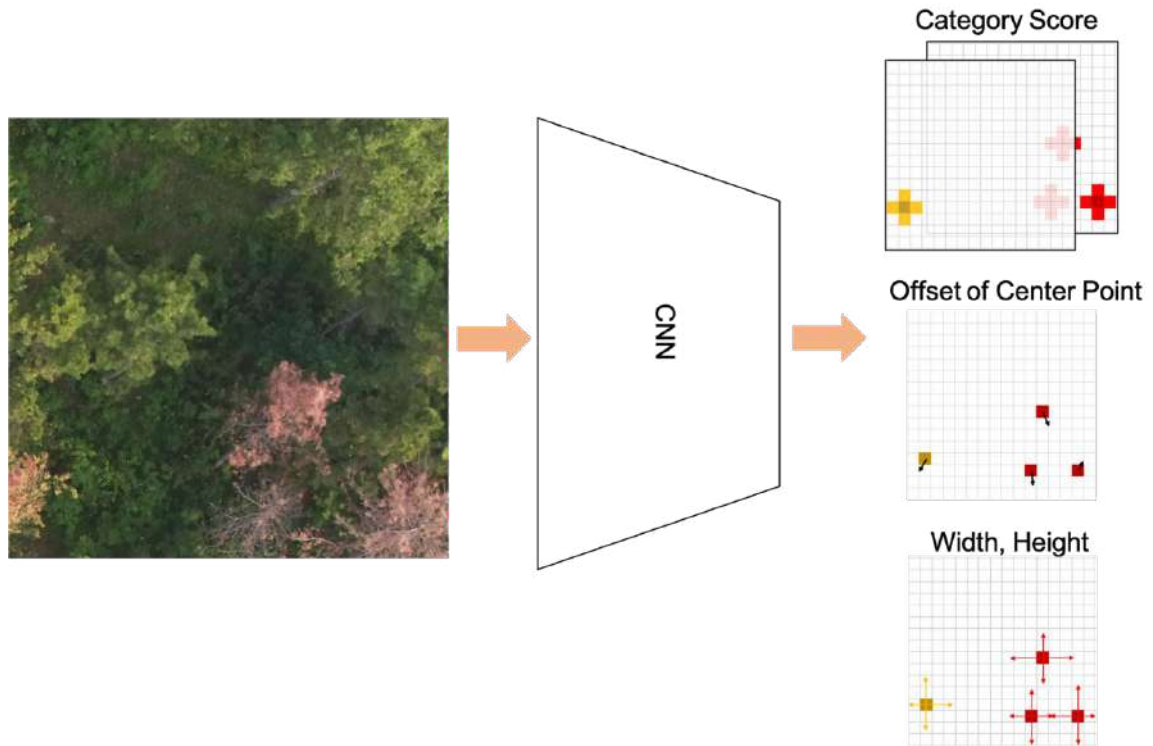


Fig. 2: Structure of Centernet network.

least square method is used to fit the curve between alpha value and object detection accuracy.

### AutoML Method for Optimal Model Search

In addition to the above-mentioned method to search for an optimal parameter, another AutoML method is also used to search for an optimal model automatically for the detection

of plant diseases and pests here. Following is the procedure:

Step 1. In the first epoch of training, the model trained from ImageNet is used as the initial model, and 9 different alphas values chosen from the interval of  $[0.5, 0.95]$  with a step of 0.05 are used to train the 9 models.

Step 2. In the next epoch of training, the best model among the 9 models obtained by the previous epoch is re-



Fig. 3: (a) Original image, (b) boundary box generated by clipping after random affine transformation, (c) the ground truth of the boundary box after an affine transformation.

garded as the pre-training model, and then different alpha values within [0.5, 0.95] with the step of 0.05 are chosen again to train another 9 different models.

Step 3. Repeat Step 2 until the last epoch is completed or the training is converged.

The general schematic diagram of the whole process is shown in Fig. 5:

## EXPERIMENTS

### Data Preparation

The size of the original image obtained by the UAV is  $5,280 \times 3,956$  pixels. Each original image will be cropped to smaller images with sizes between 1,000 and 2,000 pixels before training. This study only focuses on infected plants

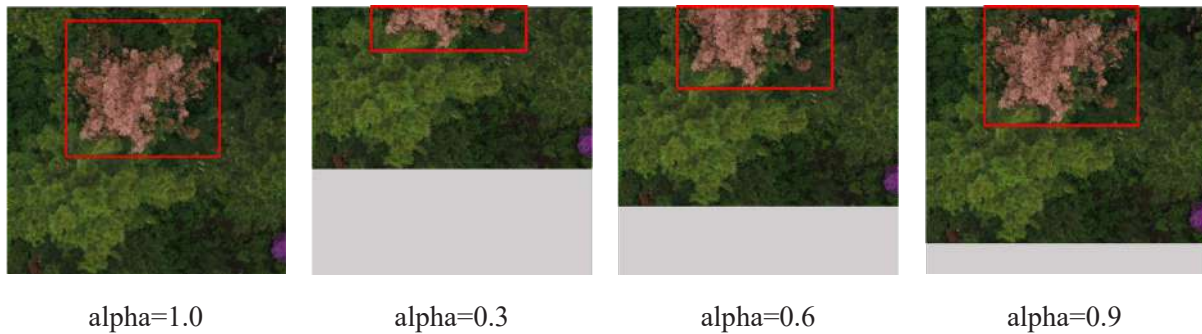


Fig. 4: Boundary box generated by clipping after random affine transformation with different alpha values.

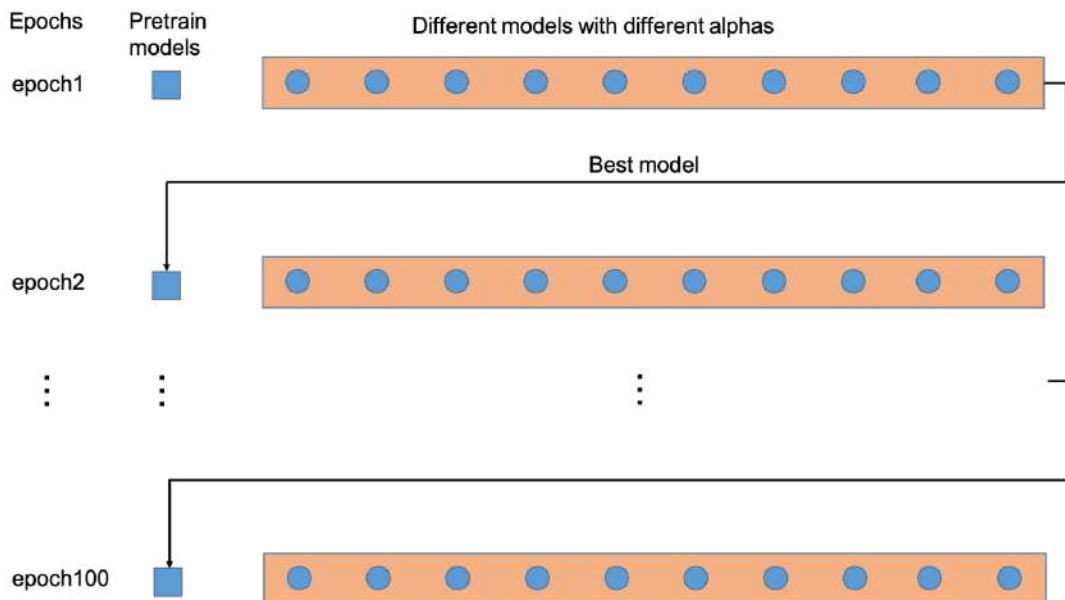


Fig. 5: Flow chart of AutoML method.

and dead plants, which are mainly yellow and red in the image. In the six sample plots, the images of sample plot 1, sample plot 3, sample plot 4, and sample plot 6 are divided into training and verification datasets, while the images of sample plot 2 and sample plot 5 are used as test datasets. Finally, the training and verification datasets contain 5,281 images and 1,319 images respectively, and the test dataset

contains 3,842 images. In all, the training dataset contains about 2,433 infected instances and 13,539 dead instances, while the testing dataset has 938 infected instances and 3,144 dead instances, respectively. Before training, to obtain as many samples as possible, more data are created through data enhancement methods such as flipping, random color, random rotation, and random clipping.

## Training

As Pytorch deep learning framework is one of the most famous and fastest deep learning frameworks, it is chosen to train the models on GPU machines in this experiment. In all these experiments, no matter how large the original image is, it will be scaled to a fixed size of 512 \* 512 through affine transformation, and then sent to the backbone of the CenterNet network. The backbone network is the classic resnet-101 structure. The training is carried out from 0 and is stopped after 100 epochs. The learning strategy is Adam's method. The detailed training super parameters are shown in Table 1.

## Test and Comparison

To evaluate the final test results, the official coco API (Lin & Dollar 2016) is used to calculate the accuracy of mAP, which is the average precision (AP) in multiple IOU thresholds ranging from 0.5 to 0.95 with the step of 0.05. It is simply defined as mAP@[.5, .95], which is used as the performance indicator in object detection tasks. IOU is calculated as follows:

$$IOU(A, B) = \frac{A \cap B}{A \cup B} \quad \dots(1)$$

where A represents the boundary box of ground truth, and B represents the predicted boundary box by the network.

The Average Precision (AP) is the area under the Precision-Recall curve for the detection task. As in the COCO Challenge, the AP is computed by averaging the precision over a set of spaced recall levels from 0 to 1 with steps of 0.01.

$$AP = \frac{1}{11} \sum_{r \in \{0, 0.1, \dots, 1\}} P_{interp}(r)$$

$$P_{interp}(r) = \max_{\tilde{r} \geq r} \tilde{p}(\tilde{r}) \quad \dots(2)$$

Where  $\tilde{p}(\tilde{r})$  is the measure precision at recall  $\tilde{r}$ ? AP (Average Precision) is a concept of integrating precision as recall varied from 0 to 1, and mAP is defined as the average of AP for all of the object classes.

Table 1: Parameters of network training.

Argument	Value
Mini-batch size	8
Num_epochs	100
Lr_policy	Multistep
Step value	40, 80
Initial learning rate	1.25e-4
Gamma	0.1

## RESULTS

### Results of Least Squares Parameter Fitting Parameter Model

In the interval of [0.5, 0.95], we take 0.05 as the step to obtain different alpha values while keeping other parameters unchanged. different models are trained on the same training data and then tested on the same test set. The detailed results are shown in Table 2:

As shown in Table 2, at the lower alpha levels, the object detection accuracy increases with the increase of alpha; when alpha increases to about 0.75, the value of mAP reaches the highest. After that, the mAP decreases with the increasing value of alpha, showing a U-shaped pattern (quadratic). Therefore, based on this observation, taking the alpha parameter as the independent variable and mAP as the dependent variable, an expression of a quadratic equation is established:  $mAP = a * \alpha^2 + b * \alpha + c$ .

Fitting the quadratic curve equation  $mAP = a * \alpha^2 + b * \alpha + c$  with the least square method, the result coefficients of a, b and c are -0.22, 0.32, and 0.42, respectively. Therefore, the expression of the curve is  $mAP = -0.22 * \alpha^2 + 0.32 * \alpha + 0.42$ , which is a bottom-up quadratic curve. In the range of [0.5, 0.95], the accuracy of mAP increases at the beginning and then decreases with the increase of alpha. When alpha reaches 0.733, the maximum value of the curve is 0.533. The overall curves are shown in Fig. 6. The red curve is the broken line connected by the original points, and the green curve is the least square fitting result of a one-dimensional quadratic equation curve.

### Results of different models

For comparison, the least squares method model trained with the alpha of 0.733, which is the maximum point of the quadratic curve, together with the model created by the AutoML method and some other standard object detection models such as Faster RCNN (Ren et al. 2017), SSD (Liu et al. 2016), CenterNet (Zhou et al. 2019a) are all tested on the same test dataset. The results of all these models are as follows in Table 3.

As can be seen from the table, the accuracy of the AutoML method model and the least square method model are 0.545 and 0.536, respectively. Among the anchor-based methods (Faster RCNN, SSD, and RetinaNet), RetinaNet attained the highest accuracy, reaching 0.480 in mAP@[.5, .95]. When compared with all the models, CenterNet (AutoML) reached the best accuracy of 0.545 in mAP@[.5, .95].

It also can be seen in Fig. 7 that in the early stage of training, the convergence speed of the AutoML method model is faster than that of the least square method model, and when

it goes to about the 20th epoch, the accuracy of the AutoML method model almost equals to convergent accuracy of least square method model.

## DISCUSSION

### Can Affine Transformation Operation be Replaced with Resize Operation

To verify the effect of the affine transformation operation on the model's accuracy, the affine transformation operation is replaced by a simple resizing operation in the training stage. Therefore, random translation and scaling affine transformation operation are removed in the preprocess of training, and all the original images are uniformly resized to 512 \* 512 pixels to train a CenterNet model. the accuracy of the experimental results can only reach 0.493 in mAP@[.5, .95]. It is lower than the original CenterNet's accuracy with

0.498 in mAP@[.5, .95]. This may be because the resizing operation uniformly scales all original images to a size of 512 \* 512 pixels, on the contrary, the operation of random affine transformation in the original CenterNet generates images of multiple different sizes (Fig. 8), which can enrich the richness of the training data. As a result, although resizing operation can produce a more accurate boundary box than that of the affine transformation operation, it is no better than the affine transformation operation in improving the detection model's accuracy.

### Analysis of the Relationship Between Alpha and Detection Accuracy

Generally, when the affine transformation is performed on the image, some plant objects may fall on the image boundary. The larger the alpha ratio, the more accurate the newly created boundary box of the remaining plants is. However, Fig. 6 indicates that in the experiment, the accuracy of ob-

Table 2: Object detection accuracy corresponding to different alphas.

alpha	0.50	0.55	0.60	0.65	0.70	0.75	0.80	0.85	0.90	0.95
mAP	0.522	0.526	0.528	0.530	0.533	0.534	0.533	0.529	0.528	0.522

Table 3: Detection results comparison using different frameworks and network architectures.

Method	backbone	mAP@[.5]	mAP@[.75]	mAP@[.5, .95]
Faster RCNN	ResNet-101	0.693	0.535	0.472
SSD	ResNet-101	0.573	0.489	0.451
RetinaNet	ResNet-101-FPN	0.724	0.546	0.480
CornerNet	Hourglass-104	0.722	0.559	0.491
CenterNet	ResNet-101	0.703	0.557	0.498
CenterNet (LSM)	ResNet-101	0.726	0.584	0.536
CenterNet (AutoML)	ResNet-101	0.737	0.603	0.545

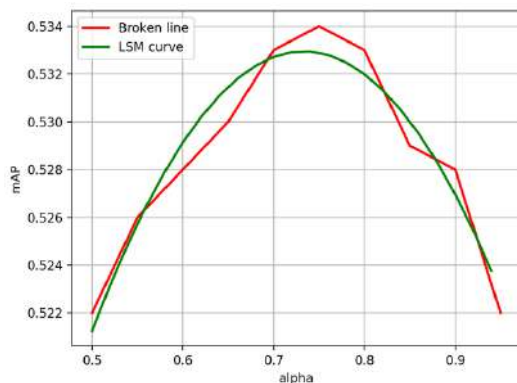


Fig. 6: Least square fitting curve and broken line connected by the original points.

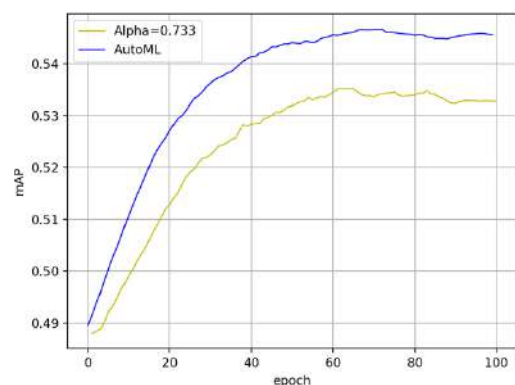


Fig. 7: Convergence curves of the least square fitting model with alpha=0.733 and AutoML model.

ject detection does not increase with the increase of alpha all the time, but actually increases at first and then begins to decrease. The reason is mainly that during the increase of alpha from 0.600 to 0.733, the new boundary box calculated by clip operation for the remaining plants becomes more accurate. As the alpha continues to increase, although the new boundary box obtained by the clip operation is more accurate, the training data's diversity begins to decrease. Nevertheless, the deep learning model needs to be driven by big data with high richness to get better accuracy. It can be seen from Fig. 6 that after the alpha increases to 0.733, the accuracy of the model begins to show a downward trend, which is mainly because the low data richness begins to play a greater impact on the model's accuracy from then on. On the whole, in the range of 0.5 to 0.95, alpha presents a univariate quadratic monotonic function to the accuracy of the model, and it makes the accuracy of the model increase at first and then begins to decrease.

#### Advantages and Disadvantages of Automl Method and Least Squares Method

In comparison to the least square method model, the AutoML model's accuracy is higher and it is an end-to-end training method without manual intervention, but the training time and training resources of the AutoML model are also higher. From the overall point of view, the final accuracy of the AutoML model is 0.545 in  $mAP@[.5, .95]$ , which is higher than the accuracy of 0.536 in  $mAP@[.5, .95]$  selected by the least square method. However, since the variables alpha and

$mAP@[.5, .95]$  conform to a quadratic equation of one variable, only 3 different alphas and  $mAP@[.5, .95]$  are needed to determine the equation expression. that is, the univariate quadratic equation can be determined only after 3 rounds of training and testing with different alphas. By contrast, when training the AutoML model, in each epoch 9 models need to be trained with 9 different alpha values from the parameter interval of [0.5, 0.95] with a step of 0.05. To sum up, though the AutoML method is an end-to-end method, the time cost and training resource cost of the AutoML method to find an optimal is about 3 times that of the least square method.

#### CONCLUSIONS

This article mainly proposed an AutoML method and a least square method for searching for an optimal model for detecting diseases and pest plants on the UAV image. The least square method finally fits an optimal alpha with the value of 0.733, and the accuracy of the corresponding model can reach 0.536 in  $mAP@[.5, .95]$ . The AutoML method uses the best model in the previous epoch as the initial model in each epoch, and the accuracy of the AutoML method is 0.545 in  $mAP@[.5, .95]$ , which is higher than that of the optimal model find by the least square method. However, the training duration and training resource consumption of the AutoML model is about 3 times that of the least square method model. Therefore, in the actual application, a trade-off can be made according to the accuracy requirements, resource consumption, and task duration.

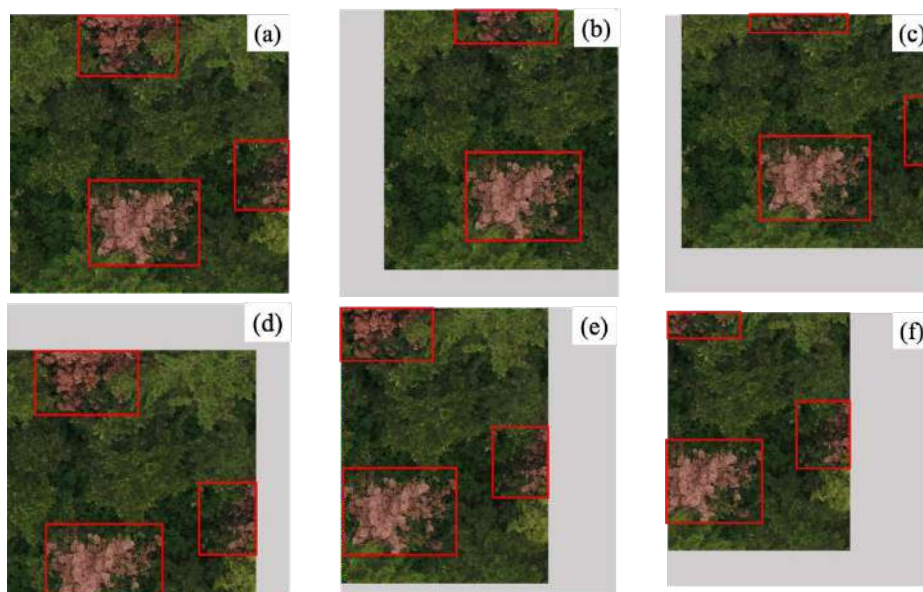


Fig. 8: (a) original image, (b), (c), (d), (e) and (f) images and boundary box labels generated by affine transformation operation.



## ACKNOWLEDGMENTS

The authors are very grateful to the Lingyuan Forestry Bureau for assisting in the data collection process.

## REFERENCES

- Bochkovskiy, A. Wang, C. and Liao, H. 2020. Yolov4: Optimal speed and accuracy of object detection. arXiv Preprint arXiv:2004.10934.
- Chen, L.C., Papandreou, G., Kokkinos, I., Murphy, K. and Yuille, A.L. 2018. Deeplab: Semantic image segmentation with deep convolutional nets, atrous convolution, and fully connected CRFS. *IEEE Trans. Pattern Anal. Mach. Intell.*, 40(4): 834-848.
- Chiu, S. F. 1993. Investigations on botanical insecticides in south China: An update. *Bot. Pest. Integr. Pest Manag.*, 19: 134-147.
- Dai, J.F. Li, Y., He, K.M. and Sun, J. 2016. R-FCN: Object detection via region-based fully convolutional networks. *Adv. Neural Inform. Process. Sys.*, 41: 379-387.
- Fuentes, Y., Kim, S.C. and Park, D. S. 2017. A robust deep-learning-based detector for real-time tomato plant diseases and pests recognition. *Sensors*, 17(9): 2022.
- Gao, Y., Liu, D., Zhang, F. and Yang, X. 2006. The application development of satellite remote sensing technology in the assessment of forest damage. *Chin. Agric. Sci. Bull.*, 22(2): 113-117.
- Girshick, R. 2015. Fast R-CNN. In: *Proceedings of the IEEE International Conference on Computer Vision*. pp. 1440-1448.
- Huang, G., Liu, Z., Laurens, V.D.M. and Weinberger, K.Q. 2017. Densely Connected Convolutional Networks. 2017 IEEE Conference on Computer Vision and Pattern Recognition (CVPR), Honolulu, HI, USA, pp. 2261-2269. <https://doi.org/10.1109/CVPR.2017.243>.
- Jeong, J., Park, H. and Kwak, N. 2017. Enhancement of SSD by concatenating feature maps for object detection. arXiv:1705.09587.
- Krizhevsky, A., Sutskever, I. and Hinton, G. E. 2012. Imagenet classification with deep convolutional neural networks. *Adv. Neural Inform. Process. Syst.*, 25: 1097-1105.
- Law, H. and Deng, J. 2020. Cornernet: Detecting objects as paired key points. *Int. J. Comp. Vision*, 128(3): 642-656.
- Lee, Y. and Park, J. 2020. Centermask: Real-time anchor-free instance segmentation. *Proceedings of the IEEE/CVF Conference On Computer Vision And Pattern Recognition*, Seattle, WA, pp. 13906-13915.
- Lehmann, J.R.K. Nieberding, F., Prinz, T. and Knoth, C. 2015. Analysis of unmanned aerial system-based cir images in forestry: A new perspective to monitor pest infestation levels. *Forests*, 6(3): 594-612.
- Liang, D., Liu, W., Zhao, L., Zong, S. and Luo, Y. 2021. An improved convolutional neural network for plant disease detection using unmanned aerial vehicle images. *Nature Environ. Pollut. Technol.*, 10: 386. <https://doi.org/10.35940/ijrte.F1110.038620>.
- Lin, T.Y. and Dollar, P. 2016. Ms coco API. <https://github.com/pdollar/coco>.
- Liu, B., Zhang, Y., He, D. and Li, Y. 2018. Identification of apple leaf diseases based on deep convolutional neural networks. *Symmetry*, 10(1): 11. <https://doi.org/10.3390/sym10010011>.
- Liu, W., Anguelov, D., Erhan, D., Szegedy, C., Reed, S., Fu, C.Y. and Berg, A.C. 2016. SSD: Single shot multibox detector. *Europ. Conf. Comput. Vision.*, 19: 21-37.
- Redmon, J., Divvala, S. Girshick, R. and Farhadi, A. 2016. You only look once: Unified, real-time object detection. 2016 IEEE Conference on Computer Vision and Pattern Recognition (CVPR), pp. 779-788. <https://doi.org/10.1109/CVPR.2016.91>.
- Redmon, J. and Farhadi, A. 2017. YOLO9000: Better, faster, stronger. 2016 IEEE Conference on Computer Vision and Pattern Recognition (CVPR), pp. 779-788. <https://doi.org/10.1109/CVPR.2016.91>.
- Redmon, J. and Farhadi, A. 2018. Yolov3: An incremental improvement. arXiv:1804.02767.
- Ren, S., He, K., Girshick, R. and Sun, J. 2017. Faster R-CNN: Towards real-time object detection with region proposal networks. *IEEE Trans. Pattern Anal. Mach. Intell.*, 39(6): 1137-1149.
- Tang, Y. 2014. Research on the vegetation identification method based on UAV image acquisition, Chengdu University of Technology, Chengdu, Sichuan.
- Tetila, E.C., Machado, B.B., Astolfi, G., de Souza Belete, N A. Amorim, W. P. Roel and A. R. Pistori, H. 2020. Detection and classification of soybean pests using deep learning with UAV images. *Computers and Electronics in Agriculture*, 179, 105836. <https://doi.org/10.1016/j.compag.2020.105836>.
- Tian, Z., Shen, C., Chen, H. and He, T. 2020. FCOS: Fully convolutional one-stage object detection, 2019 IEEE/CVF International Conference on Computer Vision (ICCV). arXiv:1904.01355.
- Wang, Z. Shi, Y. and Li, Y. 2019. Segmentation of corn leaf diseases based on improved fully convolutional neural network. *Computer Engineering and Applications*. 55(22): 127-132. (Abstract in English)
- Wu, Q. 2013. Research on bursaphelenchus xylophilus area detection based on remote sensing image. Anhui University, Hefei, Anhui.
- Xie, X., Ma, Y., Liu, B., He, J. and Wang, H. 2020. A deep-learning-based real-time detector for grape leaf diseases using improved convolutional neural networks. *Front. Plant Sci.*, 11: 751. <https://doi.org/10.3389/fpls.2020.00751>.
- Yuan, Y. and Hu, X. 2016. Random forest and objected-based classification for forest pest extraction from UAV aerial imagery. *The International Archives of the Photogrammetry, Remote Sensing and Spatial Information Sciences*, XLI-B1: 1093-1098.
- Zhang, S., Wen, L., Lei, Z. and Li, S.Z. 2020. Refinedet++: Single-shot refinement neural network for object detection. *IEEE Trans. Circ. Syst. Video Technol.*, 31(2): 674-687.
- Zhang, T. Zhang, X. Liu, H. and Pei, X. 2010. Application of remote sensing technology in monitoring forest diseases and pests. *Journal of Anhui Agricultural Sciences*, 38(21): 11604-11607.
- Zhou, X. Wang, D. and Krhenbühl, P. 2019a. Objects as points. arXiv:1904.07850.
- Zhou, X. Zhuo, J. and Krhenbühl, P. 2019b. Bottom-up object detection by grouping extreme and center points. arXiv:1901.08043.





# The Inherent Grave Consequences of Glacial Retreat

Shefali Arora

Department of Chemistry, University of Petroleum and Energy Studies, Dehradun-248007, Uttarakhand, India

†Corresponding author: Shefali Arora; shefali.arora@ddn.upes.ac.in

**Nat. Env. & Poll. Tech.**  
Website: [www.neptjournal.com](http://www.neptjournal.com)

Received: 29-11-2021  
Revised: 07-02-2022  
Accepted: 22-02-2022

## Key Words:

Glacier retreating  
Global warming  
Flora and fauna  
Tourism

## ABSTRACT

Glaciers are the protector of climate change. As glacier melting is a long-term process, it does not gain the same attention in comparison to other crises. The visible evidence of global warming is the glaciers. The main cause of glaciers melting is the rising temperature of the earth by CO<sub>2</sub> emission and ocean warming. Deforestation, burning fossil fuels, transportation, and other human activities raise the atmospheric concentration of CO<sub>2</sub> and other greenhouse gases (GHGs) which warm the planet and ultimately cause the glacier to melt. 90% of the earth's warmth is absorbed by the ocean and is responsible for the melting of marine glaciers. The main deglaciation consequences are sea-level rise which has contributed to rising sea level by 2.7cm since 1961. Glaciers are always been of substantial research as their long-term behavior is like a barometer to check the weather variability, change in flora and fauna, and economic activity. Deglaciation promises grave consequences for wildlife, plant, and the region's people and a frightening future. This paper showcase how glaciers are melting and hearts are frozen.

## INTRODUCTION

Currently, we are on the edge of a climate crisis, so a lot of work is to be done to control the present situation. Reducing the human carbon footprint and climate change solutions would be the main focus of society if they want to avail the nature's gift for long. Melting glaciers could create actual loss to the livelihoods of untold millions. The risks become too real in terms of unpredictable water supplies, increased extreme flooding, varying weather patterns, and changes in energy and food production. 10% of the earth's surface is covered by glaciers and 70% of the world's freshwater comes from it. The building of glaciers takes millennia and its size depends on the retaining capacity of ice glaciers throughout their lifespan. The main culprit of glaciers melting is human activity which in turn emits carbon dioxide and other greenhouse gases. It has been stated that glacial melting has accelerated over the past three decades. Per the study of 2019 satellite by the University of Zurich (Switzerland) and the World Wildlife Fund warns to evaporate over a third of all glaciers by 2100 and the loss of ice has already reached 335 billion tones/year. As soon as the glacier starts to break down, the glacier structure starts interacting with meltwater and seawater which increases the process of fast melting and retreat. The white surface of glaciers reflects the sun's rays which makes our current climate forbearing. As soon as the glacier melts, the dark surface of the glacier absorbs and releases heat and increases the earth's temperature. Glaciers

have snow with gases, dissolved chemicals, and particulates which were carried by atmospheric wind current, and this snow traps all the transported substances. Long-lived gases e.g. CO<sub>2</sub> and air bubbles accumulate over the months and years and preserve the current atmospheric conditions at the time of precipitation. The mountain glacier has a special place in the heart of people. Disappearance and fast retreat of glaciers directly impact the survival and livelihood of residents and also threaten the cultural importance of glaciers (Jurt et al. 2015). Glaciers are delicate like human beings and we humans are building instability into them. This review is focusing on the relationship between the environment and glacial retreating and how deglaciation affects the flora and fauna and tourism industry.

## GLACIERS RETREATING VS ENVIRONMENT

Direct and indirect human activity affects the climate and climate, in turn, affects the glacier retreating. Rapid increasing temperature potentially affects the natural and social system (IPCC 2014). Because of global warming, most of the world's mountain glaciers are decaying since 1950 and due to climate conditions, the glaciers are going to shrink even in the absence of future temperature rises (IPCC 2013). As glaciers are so sensitive to temperature swings and going with climate change. In the early 20th century glacial retreat (the position of a mountain glacier's terminus is farther up the valley than before) was found around the world at un-

paralleled rates. The reason for this massive glacier retreat was industrial revolution started around 1760. In this century various ice caps (a dome-shaped mass of glacier ice that spreads out in all directions) and ice shelves (a portion of an ice sheet that spreads out over the water) vanish together. Glaciers divulge clues about global warming. Within the past 200 years, 40% of CO<sub>2</sub> is enhanced in the atmosphere by human activity. Other gases e.g. methane are increased by a factor of 2 to 3 or more. Heat radiated from the surface of the earth is absorbed by these greenhouse gases and warms up the atmosphere slowly. These greenhouse gases are called heat-trapping gases and are responsible for the warm climate and glacier retreat in the past 50 years. Other causes such as the burning of fossil fuel and forests, increased dust,

farming, and soot from grazing also affect the glacier retreat. The Worlds Glacier Monitoring Services (WGMS) monitors changes worldwide in more than 100 alpine glaciers and out of 42 of those glaciers defines as climate references glaciers with records span of more than 30 years. NASA has shared an image of the melting Upsala Glacier which is the third-largest in the Southern Patagonian Icefield of Argentina and Chile. The image depicted that a large chunk of the Upsala Glacier (Fig. 1) breaks away due to the climate crisis. The glacier retreated more than 3 km Between 2001 and 2016. The image is shot by a fresh astronaut, Thomas Pesquet from International Space Station (ISS) (NASA Image 2021).

Ice is very white and the white color reflects the sunlight more, that's why large ice fields can govern the weather

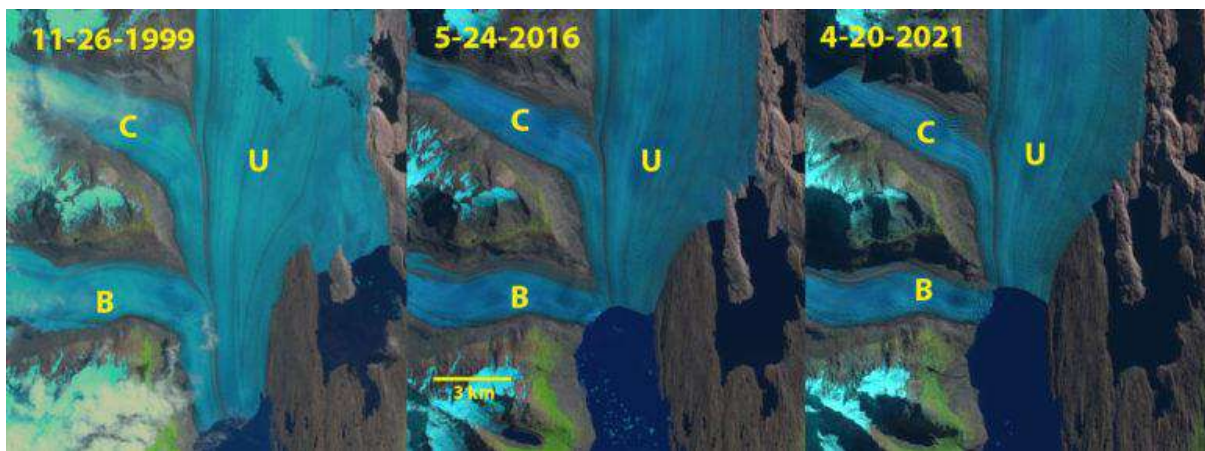


Fig. 1a. Upsala Glacier (U) in Landsat images from 1999, 2016, and 2021 illustrate both retreat and the separation from Bertacchi Glacier (B). Cono Glacier (C) is the next tributary to the north.

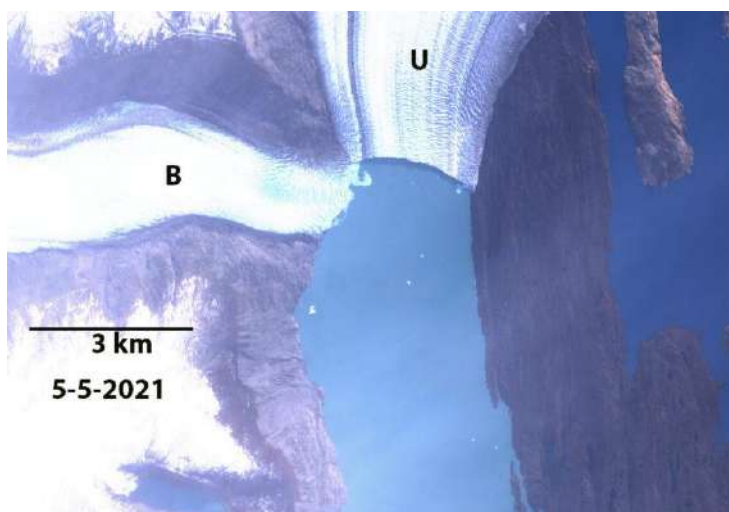


Fig. 1b. Sentinel image of terminus zone of Upsala and Bertacchi Glacier (Image, shared by NASA, was taken from the International Space Station on May 5, 2021).

patterns. Another factor is air temperature which is very high above the ice caps rather than its surface. The weather system is affected by wind patterns and can be dramatic around ice-covered land masses. International Panel on Climate change (IPCC) reported that more water flows to the seas from glaciers due to temperature rises which cause increased volume and warm ocean water. In the past hundred years, the global sea level has increased between 4 & 8 inches (10 & 20 cm). 25% (1% per year) of glaciers declined from 1975-2000 and during 2001-2005, this value dropped up to 10-15% (2 to 3 % per year) (Haeberli et al. 2007). It was estimated that by 2100, the reduction in alpine glaciers will be 4%-18% of its 2012 size (Matthias et al. 2012). During 1930-2012, a 30% reduction in the total area of the Blanca glaciers was studied in the Peruvian Andes of South America (Schauwecker et al. 2014). In the past 100 years, 85% of ice bodies have been reduced in the glacier area of Kilimanjaro National Park which was 11.40km<sup>2</sup> to 1.76km<sup>2</sup> from 1912 to 2011 (Cullen et al. 2013). Various meteorological conditions e.g. gale wind, heavy rain, fog, and strong sunlight is responsible for moraine (material left behind by the moving glacier) stability and influence glacial runoff. The climate change effect was reported by NASA Scientists because of the fast decay of ice sheets and increase global sea levels in a gigantic cavity of nearly 300 meters tall found at the bot-

tom of Thwaites Glacier in West Antarctica (Fig. 2). As per the NASA statement, Scientists found some gaps between bedrock and ice at Thwaites's bottom resulting in the flow in of ocean water and melting of the glacier from the bottom reported by Eric Rignot of the University of California, Irvine in the US. The cavity is very large and contained 14 billion tonnes of ice and mostly ice melted over the past three years (World's News 2019).

The Franz Joseph Glacier retreated 2.44 km during 1946-2008 with an annual retreat of nearly 39 km (Purdie 2013, Purdie et al. 2015). By 2100, the Franz Josef Glacier will be lost from 11 km to 6.4 km of its current length with a 62% reduction in the ice (Anderson et al. 2008). 70% of the world's tropical glaciers are found in Peru and by the 1970s, 40% of their surface area has been lost. The best example is the Patoruri glaciers in Peruvian Andes (Scott et al. 2007) reported that during 1991-2006, the Chacataya Glacier decreased by 80% in Bolivia and the glacier had completely disappeared by 2009.

Edson Ramirez, the local expert predicted the demise of an 18,000-year-old ice field namely Bolivia's 5,300 m high Chacaltaya glacier will disappear by 2015 but the last of the permanent snow disappeared in 2009 (Fig. 3). Alfredo Martinez of the neighborhood ski club Andino



Fig. 2: NASA scientists have discovered a gigantic cavity, almost 300 meters tall, growing at the bottom of the Thwaites Glacier in West Antarctica, indicating rapid decay of the ice sheet and acceleration in global sea levels due to climate change (AFP) (World's News 2019).

Boliviano wrote in a very tearful nostalgic message for the glacier “*Chacaltaya was my bride in white-now she’s dressed for a funeral*”. Another very good example of glacier retreat due to climate effect is the largest glacier in the Italian Alps, the Forni glacier which retreated 535m and annually retreats more than 30m. The Forni Glacier area had lost 0.51 km<sup>2</sup> by 2012 as compared to 2007 (Azzoni et al. 2017). During 1950-2000, the air temperature increased by 2.5°C and in the 1930s the regional rapid warming increased (Turner et al. 2017, Vaughan et al. 2003). Glacier recession and ice-shelf collapse have been observed due to the southward movement of annual mean air temperature by -9°C isotherm. Warming in the region of James Ross Island started around 600 years ago and rapidly increased over the last century. This situation of warming is uncommon (Mulvaney et al. 2012). So global warming is responsible for the disappearing, shrinking, and retreating of glaciers (Marzeion et al. 2014, Zemp et al. 2015, Roe et al. 2017).

### GLACIER RETREATING VS FLORA

Scientists revealed that facilitation and competition work together in the same ecosystem. So, competition alone is not the factor for studying criteria of species succession and coexistence (Callaway & Lawrence 1997, Losapio et al. 2015), especially in the mountain ecosystem. The role of species interaction and environment present geophysical focus is helpful to understanding the biotic pattern.

Ecological succession also depends upon the interactions with surroundings organisms, such as seed predators, herbivores, soil microbes, and pollinators. The retreat of glaciers disturbs the natural hazards, water availability, landscape configuration, and the world’s ecosystem, and ultimately great impact on society (Fell et al. 2017, Cauvy-Fraunie & Dangles 2019). Plants communities are very sensitive to the proglacial environments and ongoing glacier recession and sensitive to planning and projecting sustainable ecosystem management and biodiversity dynamics (Walker & Del Moral 2003, Erschbamer 2007). Losapio et al. (2021) studied the environmental condition, leaf traits, fine spatial scale, Spatio-temporal context, and species-to-species studies in various plant communities spanning 0 to 5000 years on average and collected the data after glacier retreat. Scientists found that 22% of plant species showed a response to glacier retreat non-linearly and with glacier extinction, the local species disappear. 66% of the species contribute to distribution patterns positively in soil carbon enrichment. In addition to 34% of the variance in plant communities is found in driving the Spatio-temporal dynamics. This study concluded that with the glacial retreat, the plant diversity first increases and more than a fifth of plant species considerably decreases and will lose with glacier disappearance. Coldwater temperature is the requirement for the survival of many aquatic flora and fauna species in the mountain environment. The loss of 4glaciers threatened various rare and endemic species that exist at their tolerance limits. Deglaciation affected



Fig. 3. A nostalgic look back at the demise of the world’s highest Chacaltaya glacier (Wilkin 2013).

plant succession and was investigated in Alaska-USA and Glacier Bay (Cooper 1923a, Cooper 1923b, Cooper 1923, Cooper 1939, Gurung et al. 2012). Three main vegetation types were reported at Glacier Bay: Spruce forest, willows alder thicket, and pioneer community. Soil development due to deglaciation is the major cause of this vegetation. Various factors such as temperature, availability of nutrients, length of growing seasons, and topography are affected the plant succession in de-glaciated soil. In East, Brogger Glacier scattered patches of vascular plants and Bryophytes are found in comparison to the older de-glaciated area where well-developed patterns of some bryophytes and vascular plants exist (Kleiden & Mooney 2000, Minami et al. 1996, Cannone et al. 2004). The four steps seen for the plant succession in the Alexander Fiord region are mass, graminoid forest, deciduous shrub moss, and evergreen dwarf-shrub moss (Jones & Henry 2003). As per the reporter of BBC, Victoria Gill, climate change destroy Antarctica's ancient moss bed. Every Antarctica summer, the lush green mosses come out from the ice in East Antarctica. Prof. Robinson has done a pilot study in 2003, with continuous monitoring in 2003 and 2008, and found that green moss beds had first turned dark red and then grey (means dying). He reported that the mosses

are severely stressed and the antioxidant and UV-Screening compounds and pigments were produced by the mosses to protect themselves (Victoria 2018) (Fig. 4).

### GLACIER RETREATING VS FAUNA

Glacier retreat impact is also seen in the extinction of animals that live on or near glaciers. Glaciers are the home of many unique organisms e.g. the entire life of the tiny ice worms spends on ice. Feeding on glacier algae and once in a while snatched up by hungry snow bunting. These worms disintegrate over 50C and their physiological adaptation to survive at 0°C remains unknown. The 3000 years old "epishelf lake" in the Northern hemisphere supported a rare ecosystem in which marine organisms lived in harmony with their freshwater brethren. It was quoted that 96% of this low-salinity habitat has been disappearing by 2002 (WWF Report 2016). Animals that are directly dependent on glaciers are also threatened. Small living sea birds (Kittitz murrelet) who depend on food, especially in areas where glacial meltwater enters the oceans are going to be extinct. The population of these birds is located in Alaska. Kittitz's murrelet is very unique and found its inmost association with



Fig. 4. Stressed Antarctic mosses turn from green to red as they produce compounds to protect themselves (Victoria 2018).

glaciers in danger. Deglaciation creates the disturbance of the bird's glacial habitat and decreases the availability of the fish which it eats. In 2001, Lynn Canal Conservation and Sitka Conservation society listed Kittitz's murrelet on the list of endangered species. By 2013, a landmark agreement called the federal listing proposal comes for the protection of 757 species including the Kittiltz's murrelet (Siegel 2009) (Fig. 5).

The sea level rises continuously by 0.2-0.4 mm per year due to glaciers retreating. A recent study of Alaska and the Patagonia Icefield confirmed the increase in the sea level by 0.375mm/year. A 1 m global sea level rise displaces 24 million people in Bangladesh, India, and Indonesia and overwhelms 80% of the Maldives. The Sunderban, the home of the world's largest tiger population, disappeared by the end of the 21st century due to rising sea levels. The primary factor is the tiger's ability to adapt as a result of Sunderban's anticipated sea level rise (WWF report 2010). By 2070, a 28 cm sea level rise will result in a 96% loss in the Sunderban's remaining tiger habitat. Keya Chatterjee, director of WWF-US reported that due to climate change the sea-ice of the polar bear and mangrove forest of the Bengal tiger, and various species of reptiles, fishes, birds, and mammals will effect. The rapid melting of the glacier causes the transport and mobilization of various organic and inorganic molecules with some pollutants (Fountain et al. 2012). In the mountain area of the Alps, the level of nickel and other heavy metals

increases due to the melting of rock glaciers which was a great threat to the ecosystem (Thies et al. 2007).

### GLACIAL RETREATING VS TOURISM

Various organizations and programs such as World Meteorological Organization and the United Nations Environment program give special focus on the impact of climate change on tourism (Hall et al. 2013, Wang 2015). The sustainable development, beauty, and quality of glacier tourism are greatly affected by global warming (Wang & Jiao 2012, Wang & Cao 2015, Wang & Zhou 2019). The shrinking and retreating of glaciers around the world have been proved by a time series analysis of glacier areas, lengths, volumes, and physical balance monitoring changes (IPCC 2013). Rocky Mountain, the Andes, and the Alps are the world's glacier tourist destinations that have lost 7000 km of ice from 1971-2010 (WGMS, 2012). Glacier tourism is a multimillion-dollar industry. Glacial retreat causes a change in surface morphology, thinning rates, and assessing hazards that create difficulty in the access of the glaciers. The impact of deglaciation on the economic earner was significant but only a few studies have been reported (Burki et al. 2005, Ritter et al. 2012). Another aspect of glacier retreating is to increase the interest in glacier tourism. In Norway, at Jostedalbreen, tourists take the effect of climate change as a catalyst, and the number of visitors increases (Aal & Høyer 2005). They take this as a last-time opportunity and their response is like a final



Fig. 5. The Kittiltz's murrelet is found only in Alaska and portions of the Russian Far East (Siegel 2009).





Fig. 6: Antarctica tourism is heating (Halpern 2020).

chance to tourism. So it can be said that “Tourists specifically look for disappearing landscape” (Lemelin et al. 2010). Tourists want to explore the location where distinct species, landscapes, or social heritages are going to vanish. In China, at Biashui Glacier No. 1, various tourism opportunities like glacier museums and telescope tours are developed to retain the disappearing resources as pristine as possible (Lemelin et al. 2012). The Canadian Rocky Mountains did a survey and found that the warmer temperature conditions increase the summer tourist season (Scott et al. 2016). Internationally, different measures are adopted to give momentum to glacier tourism, and in this direction, the ski industry is very proactive. In New Zealand, the ski-industry value is exceeding 1.4 million per year (Price 2010). In 2018-2019, 5000 people traveled to the Southern part of the Antarctica glacier (Fig. 6). It was a 53% jump from 2014-2015 as per the data of the International Association of Antarctic Tour Operators (IAATO) (Halpern 2020).

Now snowmaking technology is the main focus of the ski industry for increasing the economic value of the industry in

terms of monetary and environmental aspects (Hendrikx et al. 2012). Eijgelaar said, “*Glaciers are unlike endangered species and when they’re gone, they’re gone forever.*” The glacier was God’s great plow so enjoy every bit of the existence of the beauty of it.

## CONCLUSION

For controlling the glacier retreat there must be a collaboration between the scientific community and government policy. The gap between science and industry should be addressed. Important studies like surface morphology change, bed topography, remote sensing, hazard analysis, surface melting and increased debris studies, etc. are helpful to know the cause, process, and impact of glacier retreats and how safely they can be accessed (Brook & Winkler 2013). As our globe is under the new environmental pressure of glacial retreating which in turn affect very-very wrong with our ecosystem and disastrous consequence elsewhere. At last, we have to think about “*What happens when the roof of the world melts.*”

## REFERENCES

- Aal, C. and Høyer, K.G. 2005. Tourism and climate change adaptation: The Norwegian case. In: Hall, M. and Higham, J. (eds), *Tourism, Recreation, and Climate Change*. Channel View Publications, Clevedon, United Kingdom, pp. 209-221.
- Anderson, B. W. Lawson, W. and Owens I. 2008. Response of Franz Josef Glacier ka Roimata o Hine Hukatere to climate change. *Glob. Planet. Chang.*, 63(1): 23-30.
- Azzoni, R.S., Fugazza, D., Zennaro, M., Zucali, M., D'Agata, C., Maragno, D., Cernuschi, M., Zennaro, M. and Diolaiuti, G.A., 2017. Recent structural evolution of Forni glacier tongue (Ortles-Cevedale group, Central Italian Alps). *J. Maps*, 13(2): 870-878.
- Brook, M. and Winkler, S. 2013. Debris cover and surface melt at a temperate maritime alpine glacier: Franz Josef, New Zealand. *NZ J. Geol. Geophys.*, 56(1): 27-38.
- Burki, R., Elsasser, H., Abegg, B. and Koenig, U. 2005. Climate change and tourism in the Swiss Alps. In: M Hall J Higham editors. *Tourism, Recreation and Climate Change*. Clevedon, United Kingdom: Channel View Publications, pp. 155-163.
- Callaway, R.M. and Lawrence, W.R. 1997. Competition and facilitation: a synthetic approach to interactions in plant communities. *Ecology* 78: 1958-1965. doi: 10.1890/0012-9658(1997)078[1958:CAFASA]2.0.CO;2
- Cannone, N., Guglielmin, M. and Gerdol, R. 2004. Relationships between vegetation patterns and peri-glacial landforms in northwestern Svalbard. *Polar Biol.*, 27: 562.
- Cauvy-Fraunié, S. and Dangles, O. 2019. A global synthesis of biodiversity responses to glacier retreat. *Nat. Ecol. Evol.*, 3: 1675-1685. doi: 10.1038/s41559-019-1042-8.
- Cooper, W.S. 1923b. The recent ecological history of Glacier Bay, Alaska: II: The present vegetation cycle. *Ecology*, 4: 223.
- Cooper, W.S. 1923c. The recent ecological history of Glacier Bay, Alaska: III. Permanent quadrats at Glacier Bay: An initial report upon a long-period study, *Ecology*, 4, 355.
- Cooper, W.S. 1939. The fourth expedition to Glacier Bay, Alaska. *Ecology*: 20:130.
- Cooper, W.S. 1923a. The recent ecological history of Glacier Bay, Alaska: I: The interglacial forests of Glacier Bay. *Ecology*, 4: 93.
- Cullen, N.J., Sirguey, P., Molg, T., Kesar, G., Winkler, M. and Fitzsimons, S.J. 2013. A century of ice retreat on Kilimanjaro: The mapping reloaded. *Cryosphere*, 7(2): 419-431.
- Erschbamer, B. 2007. Winners and losers of climate change in a Central Alpine Glacier Foreland. *Arctic Antar. Alp. Res.*, 39: 237-244. [https://doi.org/10.1657/1523-0430\(2007\)39\[237:WALOCC\]2.0.CO;2](https://doi.org/10.1657/1523-0430(2007)39[237:WALOCC]2.0.CO;2)
- Fell, S.C., Carrivick, J.L. and Brown, L.E. 2017. The multitrophic effects of climate change and glacier retreat in mountain rivers. *Bioscience*, 67: 897-911. <https://doi.org/10.1093/biosci/bix107>.
- Fountain, A.G., Campbell, J.L., Schuur, E.A.G., Stammerjohn, S.E., Williams, M.W. and Ducklow, H.W. 2012. The disappearing cryosphere: impacts and ecosystem responses to rapid cryosphere loss. *Bioscience*, 62: 405-415.
- Gurung, J. and Bajracharya, R.M. 2012. Climate change and glacial retreat in the Himalaya: implications for soil and plant development. *Kathmandu Univ. J. Sci. Eng. Technol.*, 8(1): 153-163.
- Haerberli, W., Hoelzle, M., Paul, F. and Zemp, M. 2007. Integrated monitoring of mountain glaciers as key indicators of global climate change: The European Alps. *Ann. Glaciol.*, 46(1): 150-160.
- Hall, C.M., Scott, D. and Stefan, G. 2013. *Tourism and Climate Change: Impacts, Adaptation, and Mitigation*. Routledge, London.
- Halpern, A. 2020. What the Future of Polar Travel Looks Like. <https://www.cntraveler.com/story/how-the-coronavirus-could-impact-polar-travel>.
- Hendriks, J., Hreinsson, E., Clark, M. and Mullan, A.B. 2012. The potential impact of climate change on seasonal snow in New Zealand: Part 1-An analysis using 12 GCMs. *Theoret. Appl. Climatol.*, 110(4): 607-618. <http://dx.doi.org/10.1007/s00704-012-0711-1>.
- IPCC. 2013. *Climate Change 2013: The Physical Science Basis*. Contribution of Working Group I to the Fifth Assessment Report of the Intergovernmental Panel on Climate Change. Cambridge University Press, Cambridge and New York.
- IPCC. 2013. *Technical Summary, Climate Change 2013: The Physical Science Basis*. Contribution of Working Group I to the Fifth Assessment Report of the Intergovernmental Panel on Climate Change. Cambridge University Press, Cambridge and New York.
- IPCC. 2014. *Climate Change 2014: Impacts, Adaptation, and Vulnerability. Part B: Regional Aspects*. Contribution of Working Group II to the Fifth Assessment Report of the Intergovernmental Panel on Climate Change. Cambridge University Press, Cambridge and New York.
- Jones, G.A. and Henry, G.H.R. 2003. Primary plant succession on recently deglaciated terrain in the Canadian High Arctic. *J. Biogeogr.*, 30: 277.
- Jurt, C., Brugger, J.V., Dunbar, K.W., Milch, K. and Ben Orloveet, B. 2015. *Cultural Values of Glaciers*. Cambridge University Press, Cambridge and New York, pp. 90-106. <https://doi.org/10.1017/CBO9781107588653.006>.
- Kleiden, A. and Mooney, H.A. 2000. Global distribution of biodiversity inferred from climate constraints: results from a process-based modeling study, *Global Change Biology*, 6, 507.
- Lemelin, H., Dawson, J. and Stewart, E. 2012. *Last Chance Tourism: Adapting Tourism Opportunities in a Changing World*. Routledge, London, UK.
- Lemelin, H., Dawson, J., Stewart, E., Maher, P. and Jueck, M. 2010. Last-chance tourism: The boom, doom, and gloom of visiting vanishing destinations. *Curr. Issues Tour.*, 13(5): 477-493.
- Marzeion, B., Cogley, J.G., Richter, K. and Parkes, D. 2014. Attribution of global glacier mass loss to anthropogenic and natural causes. *Science*, 345: 919. doi: 10.1126/science.1254702.
- Matthias, H. 2012. *Glacier Melt and Runoff: from the Local to the Continental Scale*, General Information.
- Minami, Y., Kanda, H. and Masuzawa, T., 1996. The relationship between the distribution of bryophytes and soil conditions on deglaciated arctic terrain in Ny-Ålesund, *Polar Biology*, 9: 307.
- Mulvaney, R., Abram, N.J., Hindmarsh, R.C.A., Arrowsmith, C., Fleet, L., Triest, J., Sime, L.C., Alemayehu, O. and Foord, S. 2012. Recent Antarctic Peninsula warming relative to Holocene climate and ice-shelf history. *Nature*, 489(7414): 141-144.
- NASA image 2021. <https://gadgets.ndtv.com/science/news/nasa-releases-image-of-upsala-glacier-in-retreat-captured-from-iss-2445505>.
- Price, B.W. 2010. *Climate Change Adaptation and Mitigation in New Zealand Snow Tourism*. Industry Report, Ministry of Economic Development, The Tourism Strategy Group, School of Geography, Environment and Earth Sciences, Victoria University of Wellington, Wellington, New Zealand.
- Purdie H. 2013. *Glacier retreat and tourism: Insights from New Zealand*. *Mt. Res. Dev.*, 33(4): 463-472.
- Purdie, H., Gomez, C. and Espiner, S. 2015. Glacier recession and the changing rock fall hazard: Implications for glacier tourism. *NZ. Geogr.*, 71(3): 189-202.
- Ritter, F., Fiebig, M. and Muhar, A. 2012. Impacts of global warming on mountaineering: A classification of phenomena affecting the alpine trail network. *Mt. Res. Dev.*, 32(1): 4-15.
- Roe, G. H., Baker, M. B. and Herla, F. 2017. Centennial glacier retreat as categorical evidence of regional climate change. *Nat. Geosci.*, 10: 95-99. doi: 10.1038/ngeo2863.
- Schauwecker, S., Rohrer, M., Acuña, D., Cochachin, A., Davila, L., Frey, H., Giraldaz, C., Gomez, J., Huggel, C., Jacques-Coper, M., Loarte, E., Salzmann, N. and Vuille, M. 2014. Climate trends and glacier retreat in the Cordillera Blanca, Peru, revisited, *Glob. Planet. Chang.*, 119: 85-97.

- Scott, D., Hall, C.M. and S. Gössling, S. 2016. A review of the IPCC Fifth Assessment and implications for tourism sector climate resilience and decarbonization. *J. Sustain. Tour.*, 24(1): 8-30
- Scott, D., Jones, B. and Konopek, J. 2007. Implications of climate and environmental change for nature-based tourism in the Canadian Rocky Mountains: A case study of Waterton Lakes National Park. *Tour. Manag.*, 28(2): 570-579.
- Siegel, M. 2009. [https://www.biologicaldiversity.org/species/birds/Kit-tlitz\\_murrelet/index.html](https://www.biologicaldiversity.org/species/birds/Kit-tlitz_murrelet/index.html).
- Thies, H., Nickus, U., Mair, V., Tessadri, R., Tait, D., Thaler, B. and Psenner, R. 2007. Unexpected response of high alpine lake waters to climate warming. *Environ. Sci. Technol.*, 41: 7424-7429.
- Turner, J., Colwell, S.R., Marshall, G.J., Lachlan-Cope, T.A., Carelton, A.M., Jones, P.D., Lagun, V., Reid, P.A. and Iagovkina, S. Antarctic climate change during the last 50 years. 2005. *Int. J. Climatol.*, 25: 279-294.
- Vaughan, D.G., Marshall, G.J., Connelly, W.M., Parkinson, C., Mulvaney, R., Hodgson, D.A., King, J.C., Pudsey, C.J. and Turner, J. 2003 Recent rapid regional climate warming on the Antarctic Peninsula. *Clim. Change*, 60: 243-274.
- Victoria, G. 2010. <https://www.bbc.com/news/science-environment-45629395>.
- Walker, L.R. and Del Moral, R. 2003. *Primary Succession and Ecosystem Rehabilitation*. Cambridge University Press, Cambridge, UK.
- Wang, S.J. 2015. *Glacier Tourism Resources Spatial Development and Planning in China*. Science Press, Beijing.
- Wang, S.J. and Cao, W.H. 2015. Climate change perspectives in an Alpine area, Southwest China: a case analysis of local residents' views *Ecol. Indic.*, 53: s211-219.
- Wang, S.J. and Jiao, S.T. 2012. Adaptation models of mountain glacier tourism to climate change: a case study of Mt. Yulong Snow scenic area. *Sci. Cold Arid Reg.*, 4(5): 401-407.
- Wang, S.J. and Zhou, L.Y. 2019. Integrated impacts of climate change on glacier tourism, *Adv. Climate Change Res.*, 10(2): 71-79.
- WGMS, 2012. *Fluctuations of Glaciers 2005-2010*, World Glacier Monitoring Service, Zurich, Switzerland, 36. 10.5904/wgms-fog-2012-11.
- Wilkin, F. 2013. <https://www.weathertoski.co.uk/our-blog/going-going-gone/>.
- World's News. 2019. <https://www.hindustantimes.com/world-news/ice-melting-faster-in-antarctic-glacier-vast-hole-surprises-nasa-scientists/story-5O6EjNS5tYvsfHLveMscIO.html>.
- WWF Report. 2016. <https://wwf.awsassets.panda.org/downloads/glacierspaper.pdf>.
- WWF Reports. 2010. [https://wwf.panda.org/wwf\\_news/?186621/Climate-change-could-drown-out-Sundarbans-tigers---study](https://wwf.panda.org/wwf_news/?186621/Climate-change-could-drown-out-Sundarbans-tigers---study).
- Zemp, M., Frey, H., Gärtner-Roer, I., Nussbaumer, S. U., Hoelzle, M., Paul, F., Zemp, M., Frey, H., Gärtner-Roer, I., Nussbaumer, S.U., Hoelzle, M., Paul, F., Haeberli, W., Denzinger, F. Ahlstrøm, A.P., Anderson, B., Bajracharya, S., Baroni, C., Braun, L.N., Cáceres, B.E., Casassa, G., Cobos, G., Dávila, L.R., Granados, H.D. Demuth, M.N., Espizua, L., Fischer, A., Fujita, K., Gadek, B., Ghazanfar, A., Hagen, J.O., Holmlund, P., Karimi, N., Li, Z., Pelto, M., Pitte, P., Popovnin, V.V., Portocarrero, C.A., Prinz, R., Sangewar, C.V., Severskiy, I., Sigurdsson, O. Soruco, A., Usabaliyev, R., Vincent, C., 2015. Historically unprecedented global glacier decline in the early 21st century. *J. Glaciol.*, 61: 745-762. doi: 10.3189/2015JG15J017.





# Petroleum Hydrocarbon Degradation and Treatment of Automobile Service Station Wastewater by Halophilic Consortia Under Saline Conditions

Ramzi H. Amran\*(\*\*\*)†, Mamdoh T. Jamal\*, Arulazhagan Pugazhendi\*(\*\*), Mamdouh Al- Harbi\* and Saba Bowrji\*\*\*

\*Department of Marine Biology, Faculty of Marine Sciences, King Abdulaziz University, Jeddah-21589, Saudi Arabia

\*\*Center of Excellence in Environmental Studies, King Abdulaziz University, Jeddah-21589, Saudi Arabia

\*\*\*Department of Marine Biology and Fisheries, Faculty of Marine Sciences and Environments, Hodeidah University, Hodeidah, Yemen

†Corresponding author: Ramzi H. Amran; ramziamran06@gmail.com

## Nat. Env. & Poll. Tech.

Website: [www.neptjournal.com](http://www.neptjournal.com)

Received: 04-01-2022

Revised: 20-02-2022

Accepted: 24-02-2022

### Key Words:

Hydrocarbon degradation

Halophilic bacteria

Bioremediation

*Propionispira*

Automobile service station

Wastewater treatment

## ABSTRACT

The halophilic consortia were enriched from water samples of Abhor, Red Sea, Jeddah, Saudi Arabia for the degradation of phenanthrene, fluorene, hexadecane, pyrene, and treatment of automobile service station wastewater under saline conditions (4%). Complete degradation of phenanthrene and fluorene was recorded up to a concentration of 500 mg.L<sup>-1</sup> in 12 days, when the concentration was raised to 800 mg.L<sup>-1</sup>, the percentage of degradation of the two compounds was recorded by 84 and 90% within 14 days, while when the concentration increased to 1000 mg.L<sup>-1</sup>, a significant decline was recorded. Pyrene degradation was studied under saline conditions, where it recorded a degradation rate of 92 and 81% at a concentration of 50 and 100 mg.L<sup>-1</sup> in 10 and 12 days, respectively, while when increasing the concentration, a severe decrease in the percentage of degradation was recorded that reached 57 and 44% at concentration 200 and 300 mg.L<sup>-1</sup>, respectively. Hexadecane recorded complete degradation at a concentration of 0.5 and 1%, within 4 and 6 days, respectively, while at a concentration of 1.5%, the rate of deterioration was 88% in 10 days. Record 93% removal of COD in CSTR within 40<sup>th</sup> day, when treatment of automobile service station wastewater with halophilic bacterial consortia. The existing bacterial strains were classified as potentially responsible for petroleum hydrocarbon degradation and treatment of automobile service station wastewater such as *Ochrobactrum*, *Propionispira*, *Marteella*, *Bacillus*, *Marinobacter*, and *Azospira*. The present study recommends that the hydrophilic consortia can be used in the treatment of automobile service station wastewater under saline conditions.

## INTRODUCTION

Pollution by petroleum hydrocarbons is one of the most serious issues that occupy the world at the present time, as it is considered one of the most dangerous pollutants in the water and terrestrial environments (Isiodu et al. 2016, Logeshwaran et al. 2018, Imron et al. 2019, Khalid et al. 2021). During the past century, the production and transportation of the use of petroleum compounds witnessed great progress, as this led to more concerns towards both humans and the environment, as oil spills in the marine environment caused many devastating environmental problems (Ivshina et al. 2015, Pereira et al. 2019, Khalid et al. 2021).

Due to human activities in the environment, many toxic compounds and pollutants entered marine ecosystems, and this led to changes in the composition and life of these aquatic ecosystems (Chen et al. 2017). Pollution of the seas

with petroleum compounds occurs through oil spills, naturally or artificially, as natural spills occur through oil spills through volcanic processes and natural leaks from reservoirs in the depths of the oceans, synthetic spills, including many processes, including spills that occur during oil extraction and transportation, oil loading operations, and transportation accidents. These operations are among the main problems of pollution of the seas and oceans with hydrocarbons. As well as oil spills from oil transportation pipelines, vehicles, spills from sites, and drilling and exploration operations, in addition to wrong practices for the disposal of petroleum waste (Simister et al. 2013, Hewelke et al. 2018, Xu et al. 2018).

The automobile service station is considered one of the basic components in the service sector industry, as the most important environmental impacts that result from these services are the leakage of motor oils into the soil, as well as water used in washing and other wastes resulting from these

stations. This pollutant release leads to many problems in the soil such as loss of fertility, permeability, the ability of the soil to hold water, and other important biological properties of the soil.

At present, the interest of researchers and the world has become focused on finding renewable and environmentally friendly energy sources (Pereira et al. 2019). Crude oil is a complex compound (Xue et al. 2015), it contains thousands of different hydrocarbon compounds (Cheng et al. 2014) and due to the toxicity of these compounds for both humans and the environment. Bioremediation of hydrocarbon pollutants has been proposed as a promising solution to get rid of various environmental pollutants, in addition to the natural biodegradation operations that naturally occur in the polluted environment (Thapa et al. 2012, Ron & Rosenberg 2014).

Many previous studies and research have focused on the ability of single or combined bacterial strains, as these cannot biodegrade hydrocarbon pollutants in the presence of different concentrations of salt (Jamal & Pugazhendi 2018, 2021). The present study aims to determine the ability and efficiency to degrade the petroleum hydrocarbon compounds (Phenanthrene, Pyrene, Fluorene, and Hexadecane) by halophilic consortia, which was, enriched from the coast of Abhor, Jeddah, Saudi Arabia (SA) under 4% salty conditions.

The halophilic consortia were also used to treat the automobile service station wastewater under salty conditions and to define the existing bacterial strains that have the capability to degradation of hydrocarbons under these conditions.

## MATERIALS AND METHODS

### Sampling

Marine water samples were gathered from Abhor, Red Sea, Jeddah, SA. Samples were gathered in sterilized Schott glass bottles (250 ml) and transferred to the laboratory for further research experiments.

### Chemicals

Fluorene, phenanthrene, pyrene, and hexadecane were purchased from Sigma Aldrich<sup>®</sup> with a purity of 98-99%, while all chemicals and reagents used were purchased from Himedia<sup>®</sup>.

### Medium Composition

The medium used in this study was mineral salts medium (MSM), which was described by Liu et al. (1995), and this medium consists of the following mg/L: 435 K<sub>2</sub>HPO<sub>4</sub>, 85 NH<sub>4</sub>Cl, 170 KH<sub>2</sub>PO<sub>4</sub>, 27.5 CaCl<sub>2</sub>, 668 Na<sub>2</sub>HPO<sub>4</sub>·7H<sub>2</sub>O, 0.25 FeCl<sub>3</sub>·6H<sub>2</sub>O, 22.5 MgSO<sub>4</sub>·7H<sub>2</sub>O, as it was modified by adding up to 40 g/L of NaCl, and then it was sterilized by

autoclave (JSR, South Korea), at 121 °C for 15 min at 15 lbs. In this study, 4 compounds of petroleum hydrocarbons (Fluorene (FLU), Phenanthrene (PHE), Pyrene (PY), and Hexadecane (HXD)) were used, to evaluate the biodegradation capacity of a halophilic consortia that were enriched from in Abhor, Jeddah, SA. Different concentrations of stock solution were prepared for the petroleum hydrocarbon compounds used in this study and then stored in the refrigerator at 4 °C.

### Enrichment of Consortia

Samples were enriched after collection in mineral salts medium (MSM) in an Erlenmeyer flask (250 mL), with phenanthrene (PHE) compound as the sole carbon source, and incubated in an IKA™ orbital shaker at 150 rpm.

### Biodegradation of Petroleum Hydrocarbons

All biodegradation experiments of petroleum hydrocarbons were carried out using an experimental design. This design consisted of two controls (C1, C2) = (MSM + hydrocarbon as carbon source), and two test samples (T1, T2) = (MSM + hydrocarbon as carbon source + Bacterial Culture (BC)), where the degradation process was studied at 4% NaCl concentration under a saline condition in MSM.

All biodegradation experiments were performed in duplicate and then kept in IKA™ orbital shaker at 150 rpm at 30 °C. For the extraction of hydrocarbons remaining from the biodegradation process, ethyl acetate (C<sub>4</sub>H<sub>8</sub>O<sub>2</sub>) v/v, was utilized for the process of separating hydrocarbons from the media and the halophilic consortia in experimental flasks, in which the samples were filtered by anhydrous sodium sulfate to remove the aqueous phase. After extracting, the samples were condensed to 1 mL after the filtration process by a PTFE syringe filter (0.2 μm) in a vial for GCMS (Gas chromatography-mass spectrometry)/HPLC (High-Performance Liquid Chromatography) analysis. The extraction process was performed twice to ensure a high recovery of hydrocarbons.

### High-Performance Liquid Chromatography (HPLC) Analysis

Mineralization of PAHs (PHE-FLU-PY) was analyzed in HPLC (Agilent, USA). The mobile phase (acetonitrile-1mL.min<sup>-1</sup>) and stationary phase (C<sub>18</sub> column, Zorbax Eclipse plus) was used in HPLC for PAH degradation analysis. UV detector (254 nm) was utilized to disclose the PAHs present in the sample. Standards with high purity (>99%) were used to attain the linearity line for the calibration process.

**Gas Chromatography-Mass Spectrometry (GCMS) Analysis**

Hexadecane degradation by the consortia was analyzed in GCMS (Shimadzu, Japan). The temperature program for the analysis was used as detailed by Pugazhendi et al. (2017). Helium was utilized as the carrier gas with a flow rate of 1 mL.min<sup>-1</sup>. Hexadecane high pure grade obtained from sigma was used for standard graph calibration.

**Bioreactor Study**

A double casing acrylic bioreactor continuous stirred tank reactor (CSTR) with a total amplitude of about 10 L. About 7 L were utilized in the experiment, samples were collected from automobile service station wastewater (6.5 L), running the reactor under continuous stirring, and 0.5 L of halophilic consortia. The air pump was linked to preserving the oxygen standard in the reactor and the temp was also controlled at 30°C by the water circulation unit (temp controlled) under salty conditions (Fig.1). Organic loading rates were determined as 0.084, 0.112, and 0.168 kg COD / m<sup>3</sup>day. It was found that the improved OLR is 0.112 kg COD / m<sup>3</sup>day with Hydraulic Retention Time (HRT) for 15 days. The bioreactor study took about 40 days during which the analysis of chemical oxygen demand (COD), mixed liquor volatile suspended solids (MLVSS), and mixed liquor suspended solids (MLSS),

measurement was done according to the standard methods (APHA 2005).

**Phylogenetic Analysis**

Bacterial strains present in the consortia during the PAHs degradation and bioreactor study were analyzed using high throughput sequencing technique. The samples collected during biodegradation and operation of CSTR succumbed to DNA extraction (DNA Extraction Kit, Qiagen, Germany). Initial DNA was amplification was performed in PCR (Polymerase Chain Reaction) machine with universal primer (27F and 1492R). High throughput sequencing was executed with primers (515-532U and 909-928U) targeting the V4-V5 region in the 16S rRNA nucleotide sequence (Pugazhendi et al. 2017). The sequence obtained was analyzed in BLAST (Basic Local Alignment Search Tool) to recognize the bacterial strains.

**RESULTS AND DISCUSSION**

The biodegradation of petroleum hydrocarbons was studied by a halophilic bacterial consortia under salty conditions (40 g/L) of NaCl concentration, which was enriched from the coast of Abhor, Red Sea, Jeddah, SA, where degradation and treatment of automobile service station wastewater were used. An initial study of PHE degradation at 50 mg/L con-

Table 1: Degradation of polycyclic aromatic hydrocarbons at different concentrations under salty conditions (4%).

Petroleum Hydrocarbons	Concentration	Degradation [%]	Time (day)
Phenanthrene [mg.L <sup>-1</sup> ]	50	100	6
	100	100	7
	200	100	8
	500	100	12
	800	84	14
	1000	62	16
Fluorene [mg.L <sup>-1</sup> ]	50	100	6
	100	100	7
	200	100	8
	500	100	12
	800	90	14
	1000	71	16
Pyrene [mg.L <sup>-1</sup> ]	50	92	10
	100	81	12
	200	57	14
	300	44	16
Hexadecane [%]	0.5	100	4
	1	100	6
	1.5	88	10

centration in MSM confirmed the capability of the halophilic bacterial consortia to fully degrade PHE and FLU within 6 days see Table 1.

### Degradation of Various Petroleum Hydrocarbons

#### Phenanthrene (PHE) and Fluorene (FLU)

The biodegradation of PHE and FLU were studied by the halophilic consortia at various concentrations (50, 100, 200, 500, 800, and 1000 mg.L<sup>-1</sup>) under salty conditions. PHE and FLU were degraded at concentrations of 50, 100, 200, and 500 mg.L<sup>-1</sup> completely within 6, 7, 8, and 12 days, respectively as shown in Fig.1 & 2. When the PHE and FLU concentration was raised to 800 mg.L<sup>-1</sup> the proportion of degradation was about 84% and 90% within 14 days, respectively. In the concentration of 1000 mg.L<sup>-1</sup> for each of the two compounds, a significant decrease in the percentage of biodegradation was recorded, reaching about 62% for PHE and 71% for FLU within 16 days, where a diminution in the percentage of degradation and a raise in the time taken for degradation of these compounds were observed. Table 1 shows the concentrations and degradation rates of hydrocarbons and the days to degradation. The results revealed a high agreement with studies conducted by Jamal and Pugazhendi (2018, 2021) - a degradation of more than 92% of PHE and FLU to a concentration of 800 mg.L<sup>-1</sup> under salty conditions by halophilic consortia.

#### Pyrene

The biodegradation of PY by a halophilic consortia was studied under salty conditions. The degradation of PY was recorded at a concentration of 50 m.L<sup>-1</sup>, where the percentage of degradation was about 92% within 10 days as shown in Fig. 3. Whereas when the PY concentration augmentation was 100 mg.L<sup>-1</sup>, a degradation of about 81% was recorded within 12 days. When the concentration was raised to 200 and 300 mg.L<sup>-1</sup>, a degradation ratio of about 57% and 44% were recorded within 14 and 16 days, respectively. A severe decrease in the percent degradation was observed due to the suppression of the compound and its high toxicity, as it works to inhibit bacterial growth and stop biodegradation (Vaidya et al. 2017).

#### Hexadecane

The biodegradation of HXD was studied at a concentration of 0.5 and 1%, and complete degradation of HXD was registered within 4 and 6 days, respectively (Fig.4). When the HXD concentration was raised to 1.5%, the compound registered 88% degradation in 10 days by the halophilic bacterial consortia. Jamal and Pugazhendi (2021) recorded a complete degradation of hexadecane at different concentrations (0.5 and 1%), and at a concentration of 1.5%, the degradation rate reached 93% within 6 days under saline conditions (4%).

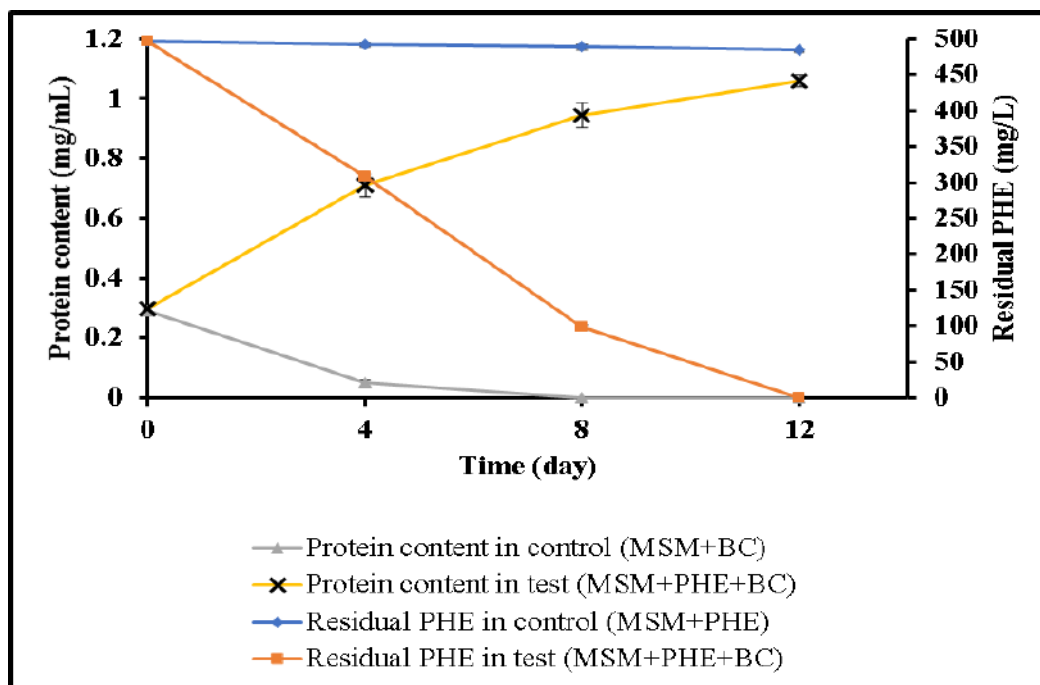


Fig. 1: Degradation of PHE at 500 ppm by the halophilic consortia under salty conditions (4%).



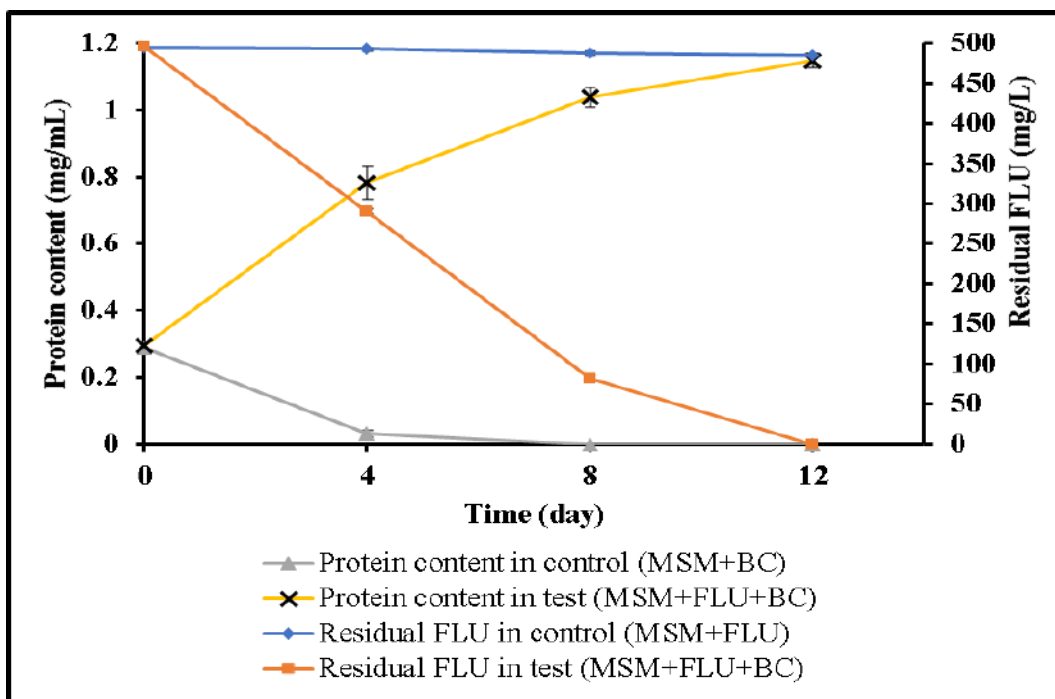


Fig. 2: Degradation of FLU at 500 ppm by the halophilic consortia under salty conditions (4%).

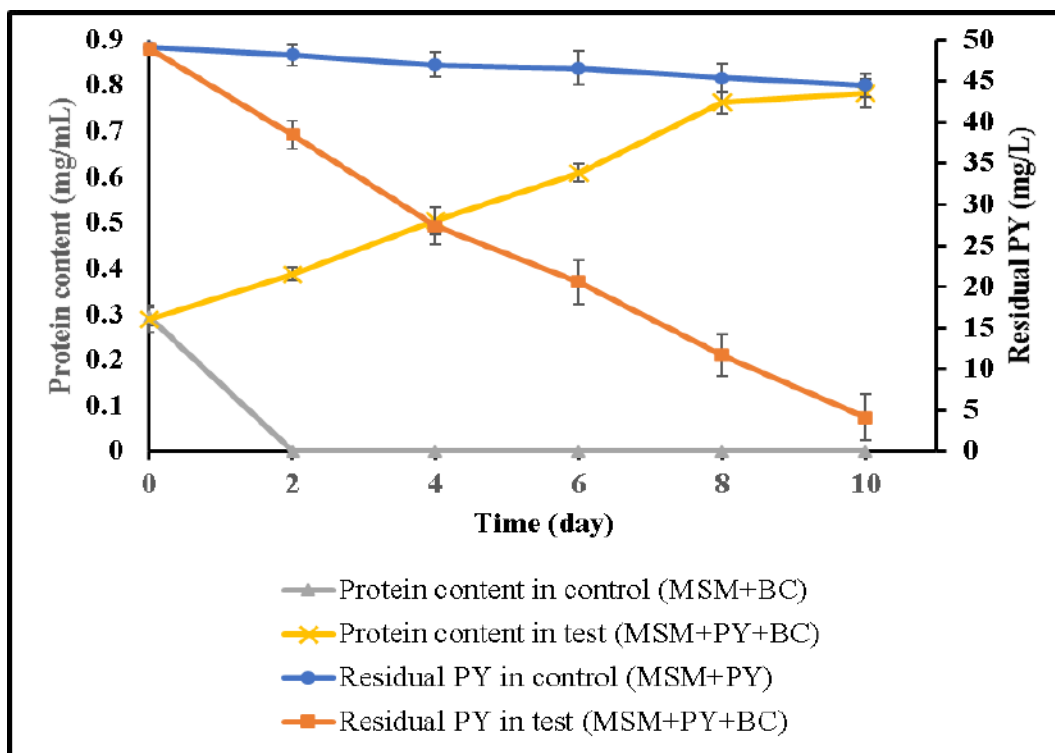


Fig. 3: Degradation of PY at 50 ppm by the halophilic consortia under saline conditions (4%).

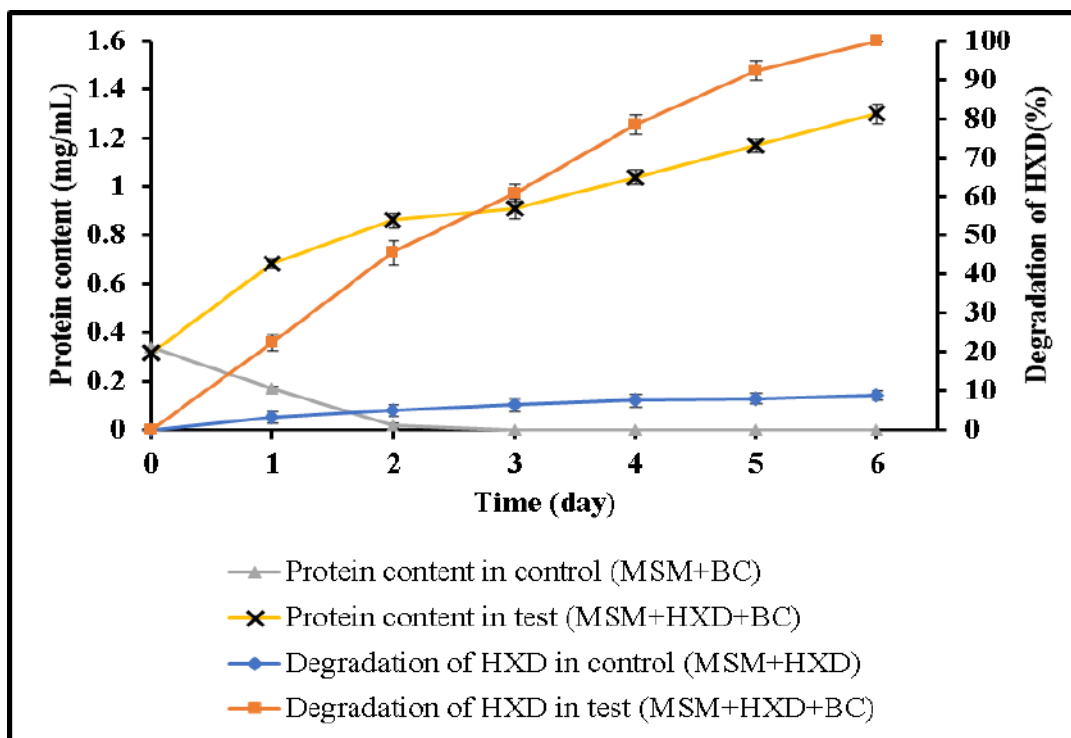


Fig. 4: Degradation of HXD at 1% concentration by the halophilic consortia under saline conditions (4%).

### Bacterial Society Analysis

Initial analysis of the bacterial communities detected the presence of different groups of bacteria and archae bacteria from the samples, as this consortia degraded the PHE and used it as the sole carbon source. Several bacterial strains found in the consortia were dominated by *Martellella*, *Microbacterium*, *Propionispira*, *Ochrobactrum*, *Azospira*, and *Gordonia*, in addition to the presence of a trace amount (1%) of different bacterial genera (*Bacillus*, *Rhodococcus*, *Mycobacterium*, *Fusobacteria*, *Aeromonas*, and *Flavobacterium*), which were present in the consortia during the biodegradation of PHE.

Interestingly, the bacterial consortia exhibited high growth when HXD was used as a carbon source and recorded different lineage of and dominated bacterial strains such as *Bacillus*, *Microbacterium*, *Martellella*, *Gordonia*, *Ochrobactrum*, and *Mycobacterium*. Through the aforementioned results, it was found that the presence of halophilic bacterial consortia has the potential to degrade the various hydrocarbons and the strains' occupation percent change instituted on the hydrocarbons used as the sole carbon source.

In the studied samples from CSTR, several bacterial strains were found in the reactor where *Martellella* was

dominated, followed by *Propionispira*, *Bacillus*, *Microbacterium*, *Mycobacterium*, *Ochrobactrum*, *Azospira*, *Pseudomonas* and *Gordonia*, in addition to a small number estimated at 0.5 of other bacterial strains such as *Rhodococcus*, *Sphingomonas*, *Fusobacteria*, *Pseudomonas*, *Sphingomonas*, *Flavobacterium*, *Stenotrophomonas*, and *Aeromonas*. Table 2 shows the percentage of bacterial strains that were dominant in this study. There are several studies revealed the efficiency of *Martellella* on the degradation of different PAHs that have proven its ability to degrade these compounds under saline conditions (Al Farraj et al. 2020, Chen et al. 2020, Li et al. 2020, Jamal & Pugazhendi 2021). Several studies have demonstrated the ability of several bacterial strains to degrade petroleum hydrocarbons, such as *Martellella*, *Bacillus*, *Ochrobactrum*, *Gordonia*, and *Marinobacter* under saline conditions (Adam 2016, Varjani 2017, Huang et al. 2019, Al-Mur et al. 2021).

### Treatment of Petroleum Hydrocarbon from Automobile Service Station Wastewater in the Bioreactor (CSTR)

In this study, a bioreactor (CSTR) was operated to treat automobile service station wastewater collected from Jeddah, SA by a halophilic consortium under saline conditions, which is

Table 2: The percentage of bacterial strains that were dominant in this study.

Petroleum Hydrocarbons	Bacterial strain	Percentage [%]
PHE	<i>Propionispira</i>	35.6
	<i>Martelevella</i>	28.5
	<i>Microbacterium</i>	15
	<i>Azospira</i>	10
	<i>Ochrobactrum</i>	6
	<i>Gordonia</i>	1.5
	<i>Bacillus, Rhodococcus, Mycobacterium, Fusobacteria, Aeromonas and Flavobacterium</i>	≤1
HXD	<i>Bacillus</i>	56
	<i>Martelevella</i>	26
	<i>Microbacterium</i>	12
	<i>Ochrobactrum</i>	4.4
	<i>Gordonia</i>	1.2
	<i>Mycobacterium</i>	0.34
CSTR	<i>Martelevella</i>	24.5
	<i>Propionispira</i>	21.4
	<i>Bacillus</i>	18.5
	<i>Microbacterium</i>	11.6
	<i>Ochrobactrum</i>	9.3
	<i>Mycobacterium</i>	5.2
	<i>Azospira</i>	4
	<i>Gordonia</i>	1.1
	<i>Pseudomonas</i>	1
	<i>Rhodococcus, Shingomonas, Fusobacteria, Pseudomonas, Shingomonas, Flavobacterium, Stenotrophomonas, and Aeromonas.</i>	≤0.5

prospective to be able to treat and degrade hydrocarbons in the wastewater. The reactor was operated at different organic loading rates (OLR) (0.168, 0.112, and 0.084 kg.m<sup>-3</sup>day), and the OLR was optimal (0.112 kg.m<sup>-3</sup> day), with a hydraulic retention time (HRT) of 15 days (Fig. 5). Maximal COD removal of 93% was recorded in CSTR on 40<sup>th</sup> day, while MLSS and MLVSS were maintained at 3.8 g.L<sup>-1</sup> and 3.2 g.L<sup>-1</sup> in the optimized conditions as shown in Fig.6. Al-Mur et al. (2021) in a study conducted on petroleum refinery wastewater treatment in CSTR, where COD removal recorded about 92%, this is consistent with the current study.

**CONCLUSIONS**

In this study, halophilic bacterial consortia enriched from Abhor, Red Sea, Jeddah, SA, showed its ability to degrade petroleum hydrocarbons under salty conditions (4%). Halophilic consortia’s ability to degrade PHE and FLU compounds is up to 92% up to 1000 mg.L<sup>-1</sup> effectively, while PY

degradation has a degradation rate of less than 70%, while HXD recorded a complete degradation at the concentration (0.5 and 1%), while at 1.5 % concentration the degradation recorded 88% under salty conditions. The CSTR study clearly demonstrated the efficiency and potential of the halophilic consortia in the treatment of automobile service station wastewater with about 93% removal of COD on the 40<sup>th</sup> day under salty conditions. Thus, the halophilic bacterial consortia are a promising candidate that we can employ in the treatment of automobile service station wastewater and the degradation of petroleum hydrocarbons in our various ecosystems.

**ACKNOWLEDGEMENTS**

The authors thank Prof. Iqbal Mohammad Ibrahim Ismail, Director, Center of Excellence in Environmental Studies, King Abdulaziz University, Jeddah, SA for his extensive support and encouragement during the research.

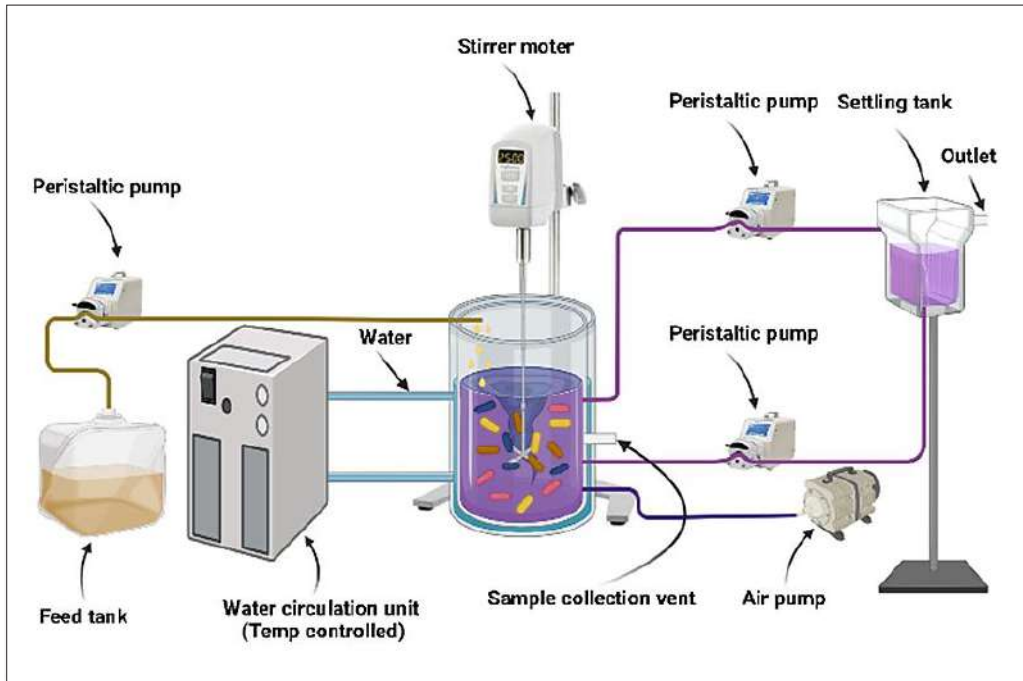


Fig. 5: Bioreactor (CSTR) design for the treatment of automobile service station wastewater by halophilic consortia.

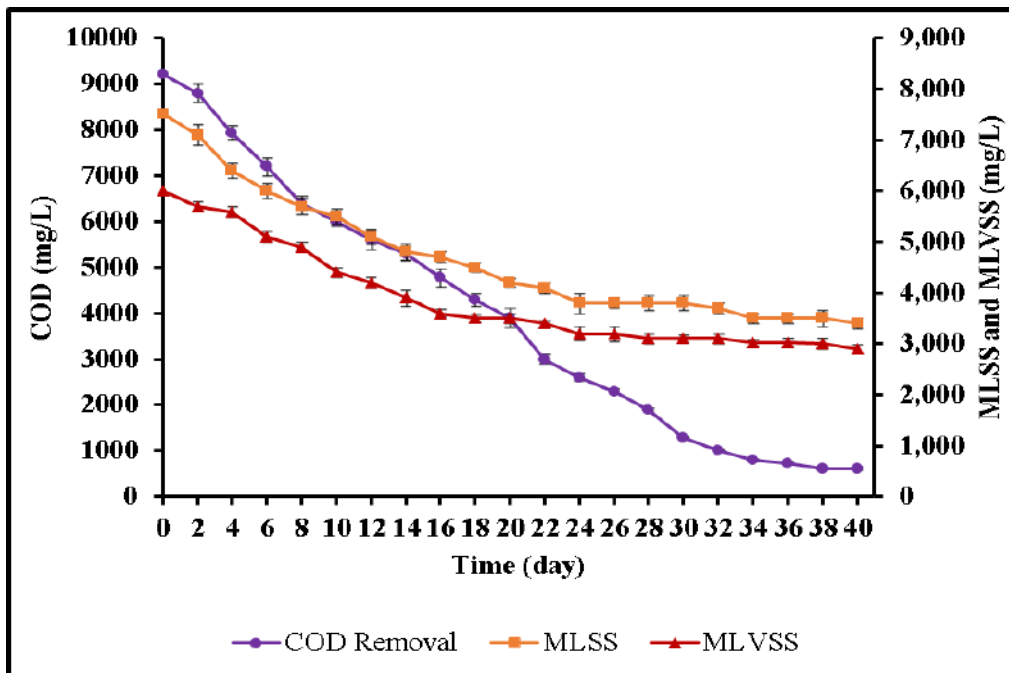


Fig. 6: Treatment of automobile service station wastewater in CSTR using halophilic bacterial consortia under saline conditions (4%).

## REFERENCES

- Adam, M. 2016. Biodegradation of marine crude oil pollution using a salt-tolerant bacterial consortium isolated from Bohai Bay, China. *Marine Pollut. Bull.*, 105(1): 43-50.
- Al-Mur, B.A., Pugazhendi, A. and Jamal, M.T. 2021. Application of integrated extremophilic (halo-alkalo-thermophilic) bacterial consortium in the degradation of petroleum hydrocarbons and treatment of petroleum refinery wastewater under extreme conditions. *J. Hazard Mater.*, 12: 5351.
- Al Farraj, D.A., Hadibarata, T., Yuniarto, A., Alkufeidy, R.M., Alshammari, M.K. and Syafiuddin, A. 2020. Exploring the potential of halotolerant bacteria for biodegradation of polycyclic aromatic hydrocarbon. *Bio-process Biosyst. Eng.*, 43(12): 2305-2314.
- APHA. 2005. Standard Methods for the Examination of Water and Wastewater. In Rice E.W., Baird, R.B., Eaton, A.D. and Clesceri, L.S. (eds) American Public Health Association/American Water Works Association/Water Environment Federation. 21st Edition, American Public Health Association, Washington.
- Chen, Q., Li, J., Liu, M., Sun, H. and Bao, M. 2017. Study on the biodegradation of crude oil by the free and immobilized bacterial consortium in the marine environment. *PLoS One*. 12(3): e0174445.
- Chen, X., Wang, W., Hu, H., Tang, H., Liu, Y., Xu, P., Lin, K. and Cui, C. 2020. Insights from comparative proteomic analysis into the degradation of phenanthrene and salt tolerance by the halophilic *Martellella* strain ad-3. *Ecotoxicology*, 1:1-12.
- Cheng, L., Shi, S., Li, Q., Chen, J., Zhang, H and Lu, Y. 2014. Progressive degradation of crude oil n-alkanes coupled to methane production under mesophilic and thermophilic conditions. *PLoS One*, 9(11): e113253.
- Hewelke, E., Szatyłowicz, J., Hewelke, P., Gnatowski, T. and Aghalarov, R. 2018. The impact of diesel oil pollution on the hydrophobicity and CO<sub>2</sub> effluxes of forest soils. *Water Air Soil Pollut.*, 229(2): 1-11.
- Huang, X., Wang, J., Ma, C., Ma, L. and Qiao, C. 2019. Diversity analysis of microbial communities and biodegradation performance of two halotolerant and thermotolerant bacillus licheniformis strains in oilfield-produced wastewater. *Int. Biodeter. Biodegrad.*, 137: 30-41.
- Imron, M.F., Kurniawan, S.B. and Titah, H.S. 2019. Potential of bacteria isolated from diesel-contaminated seawater in diesel biodegradation. *Environ. Technol. Innov.*, 14: 100368.
- Isiodu, G., Stanley, H., Ezebuoro, V. and Okerentugba, P. 2016. Role of plasmid-borne genes in the biodegradation of polycyclic aromatic hydrocarbons (PAHs) by a consortium of aerobic heterotrophic bacteria. *J. Petr. Environ. Biotech.*, 7(1): 264.
- Ivshina, I.B., Kuyukina, M.S., Krivoruchko, A.V., Elkin, A.A., Makarov, S.O., Cunningham, C.J., Peshkur, T.A., Atlas, R.M. and Philp, J.C. 2015. Oil spill problems and sustainable response strategies through new technologies. *Environ. Sci.: Process. Impacts*, 17(7): 1201-1219.
- Jamal, M.T. and Pugazhendi, A. 2018. Degradation of petroleum hydrocarbons and treatment of refinery wastewater under saline conditions by a halophilic bacterial consortium enriched from marine environment (red sea), Jeddah, Saudi Arabia. *3 Biotech.*, 8(6):1-10.
- Jamal, M.T. and Pugazhendi, A. 2021. Isolation and characterization of halophilic bacterial consortium from seagrass, Jeddah coast, for the degradation of petroleum hydrocarbons and treatment of hydrocarbons-contaminated boat fuel station wastewater. *Clean Technol. Environ. Policy*, 23(1): 77-88.
- Khalid, F.E., Lim, Z.S., Sabri, S., Gomez-Fuentes, C., Zulkharnain, A. and Ahmad, S.A. 2021. Bioremediation of diesel contaminated marine water by bacteria: A review and bibliometric analysis. *Journal of Marine Science and Engineering*, 9(2): 155.
- Li, X., Peng, D., Zhang, Y., Ju, D. and Guan, C. 2020. *Klebsiella* sp. Pd3, a phenanthrene (phe)-degrading strain with plant growth promoting properties enhances the pH degradation and stress tolerance in rice plants. *Ecotoxicol. Environ. Safety*, 201: 110804.
- Liu, Z., Jacobson, A.M., and Luthy, R.G. 1995. Biodegradation of naphthalene in aqueous nonionic surfactant systems. *Appl. Environ. Microbiol.*, 61(1): 145-151.
- Logeshwaran, P., Megharaj, M., Chadalavada, S., Bowman, M. and Naidu, R. 2018. Petroleum hydrocarbons (PH) in groundwater aquifers: An overview of environmental fate, toxicity, microbial degradation, and risk-based remediation approaches. *Environ. Technol. Innov.*, 10: 175-193.
- Pereira, E., Napp, A.P., Allebrandt, S., Barbosa, R., Reuwsaat, J., Lopes, W., Kmetzsch, L., Staats, C.C., Schrank, A. and Dallegre, A. 2019. Biodegradation of aliphatic and polycyclic aromatic hydrocarbons in seawater by autochthonous microorganisms. *Int. Biodeter. Biodegrad.*, 145: 104789.
- Pugazhendi, A., Qari, H., Basahi, J.M.A.B., Godon, J.J. and Dhavamani, J. 2017. Role of a halothermophilic bacterial consortium for the biodegradation of PAHs and the treatment of petroleum wastewater under extreme conditions. *Int. Biodeter. Biodegrad.*, 121: 44-54.
- Ron, E.Z. and Rosenberg, E. 2014. Enhanced bioremediation of oil spills in the sea. *Current Opinion in Biotechnology*, 27: 191-194.
- Simister, R., Taylor, M.W., Rogers, K.M., Schupp, P.J. and Deines, P. 2013. Temporal molecular and isotopic analysis of active bacterial communities in two New Zealand sponges. *FEMS Microbiol. Ecol.*, 85(1): 195-205.
- Thapa, B., Kc, A.K. and Ghimire, A. 2012. A review on bioremediation of petroleum hydrocarbon contaminants in soil. *Kathmandu Univ. J. Sci. Eng. Technol.*, 8(1): 164-170.
- Vaidya, S., Jain, K. and Madamwar, D. 2017. Metabolism of pyrene through the phthalic acid pathway by an enriched bacterial consortium composed of *Pseudomonas*, *Burkholderia*, and *Rhodococcus* (pbr). *3 Biotech.*, 7(1): 29.
- Varjani, S.J. 2017. Microbial degradation of petroleum hydrocarbons. *Bioresour. Technol.*, 223: 277-286.
- Xu, X., Liu, W., Tian, S., Wang, W., Qi, Q., Jiang, P., Gao, X., Li, F., Li, H. and Yu, H. 2018. Petroleum hydrocarbon-degrading bacteria for the remediation of oil pollution under aerobic conditions: A prospective analysis. *Front. Microbiol.*, 9: 2885.
- Xue, J., Yu, Y., Bai, Y., Wang, L. and Wu, Y. 2015. Marine oil-degrading microorganisms and biodegradation process of petroleum hydrocarbon in marine environments: A review. *Curr. Microbiol.*, 71(2): 220-228.





# Geoelectrical Sounding to Identify Sub-surface and Groundwater State at Village Banauli, Singrauli District, Madhya Pradesh, India

Dharmendra Kumar Singh† and Nawal Kishore

Department of Mining Engineering, Indian Institute of Technology, BHU, Varanasi-221005, India

†Corresponding author: Dharmendra Kumar Singh; dharmendramsiiit@gmail.com

Nat. Env. & Poll. Tech.  
Website: [www.neptjournal.com](http://www.neptjournal.com)

Received: 27-09-2021

Revised: 30-11-2021

Accepted: 24-12-2021

## Key Words:

Groundwater  
Geoelectrical sounding  
Village Banauli

## ABSTRACT

Electrical resistivity (Geoelectrical) methods are well-known and common techniques for investigating the groundwater potential zone. These methods are economically viable and have the highest resolving power compared with other geophysical methods. A total of fifteen Vertical electrical soundings were conducted in the village of Banauli, located in Singrauli district in Madhya Pradesh, India. Vertical electrical sounding was carried out using Schlumberger electrode configuration with the maximum current electrode (AB) spacing of 200 m and potential electrode (MN) spacing of 10 m. For interpretation of measured resistivity, the Partial curve matching technique was used to calculate the layer parameters (resistivity and thickness) and further depict the depth section of the profile. In this study, the maximum five-layer model is obtained, and most curves are of HAK types. The first layer has a mean resistivity value of 12.41  $\Omega$ m and a mean thickness of 0.94 m. The second layer has mean resistivity of 7.93  $\Omega$ m and a mean thickness of 4.79 m. The third layer has a mean thickness value of 10.55 m and a mean resistivity value of 16.54  $\Omega$ m. The fourth layer has a mean resistivity value of 20.17  $\Omega$ m and a mean thickness of 9.20 m, and finally, the fifth layer, the bedrock, has a higher mean resistivity value of 59.92  $\Omega$ m. Thus, the obtained results may be used for identifying the drilling site for the groundwater potential zone.

## INTRODUCTION

Groundwater is very important for industry, irrigation, and domestic purposes. Irrigation is the lifeline of agriculture in Arid and semi-arid regions. The demand for groundwater for irrigation is increasing day by day because of the induction of modern technology and the introduction of high-yielding varieties of seeds, pesticides, insecticides, chemical fertilizers, etc and due to the progress of the green revolution, the demand for groundwater in agriculture has increased a lot as compared to surface water (Gupta 2010). As a result, in some regions of India, water levels have declined significantly (CGWB 2009). Day by day decrease in the levels of groundwater has resulted in failure of bores holes, the drying up of dug wells and reduction in individual good yield, and an increase in power consumption (Gupta et al. 2021). Therefore, the availability and sustainability of safe groundwater are of great importance and demand and need a scientific action plan to ensure water security in the region. Groundwater is often developed without fully understanding its temporal and spatial formation and therefore in danger of its Overuse and pollution (Kumar et al. 2011). Therefore, groundwater management is key to the conflict in emerging water security problems. Knowing the depth of groundwater

is a very important element in many cases, such as hydrological research, including agricultural salinity management, storage characterization, chemical seepage movement, and water supply studies (Maiti et al. 2013).

Water levels are also dropping as a result of natural and man-made activities, particularly in dry and semi-arid regions. Vertical electrical sounding (VES) surveys are beneficial and cost-effective in understanding underlying lithology and delineating potential groundwater zones (Bayowa 2020, Adagunodo & Oladejo 2020). In groundwater studies, the Schlumberger array is found to be more appropriate and common (Zhody 1969, Karlik & Kaya 2001). Many researchers have successfully used the approach to tackle groundwater problems (Karanth 1991, Janardhana et al. 1996, Balasubramanian et al. 1985). In groundwater investigation, the electrical resistivity method is the most generally recognized and used frequently (Kehinde & Oyeyemi 2018, Gupta et al. 2012). Electric currents are transmitted through electrodes into the ground, and the resistivity of rock formations is measured. In the study of groundwater, electrical resistivity techniques have become more important in exploration due to their inexpensive cost, ease of use, and ability to distinguish between fresh and saltwater (Pal & Majumdar 2001, Majumdar & Pal 2005, Narayanpethkar et al. 2006).

## THE STUDY AREA

### Location

Banauli village is in the Singrauli Tehsil of Madhya Pradesh Singrauli district. It is 15 km from Singrauli, which is the district and sub-district headquarters of Banauli village. According to 2019 statistics, Banouli is the gram panchayat of Banauli village. The study area lies between latitude 24°1'0"N to 24°2'30"N and longitude 82°30'0"E to 82°32'0"E as shown in Fig.1. The settlement covers a total area of 251.83 hectares, and the population of Banauli is 1,233 people. In Banauli village, there are around 281 homes. Banauli village is a part of the Devsar assembly and Sidhi parliamentary constituencies.

### Geology and Hydrology

In Village Banauli and surrounding regions, Talchir and Barakar formations are dominated by arenaceous facies consisting mostly of medium to coarse and very coarse-grained white to light brown sandstones, and Grey shale, arenaceous shale, and carbonaceous shale are the most common types of shale found in coal seams (Yadav et al. 1993). The weathering of sandstone in the Barakar formation is high to moderately and poorly consolidated mostly at a depth of 65 m and even up to a depth of 100 m in certain areas (Yadav 1997). The major groundwater reservoirs in the area are sandstone and fractured shale. Groundwater is found in sandstone and shales under water table conditions and is transferred through the cleavage and bedding planes of shale and sandstones. Rainfall through direct percolation to the saturation zone in the village and adjacent region is the primary source of groundwater re-

charge. Due to the area's shallow soils, a large portion of the rainfall is lost as runoff. As a result, only a small proportion of rainfall reaches saturation and forms part of groundwater storage when evaporation losses are met.

## MATERIALS AND METHODS

Fifteen Vertical Electrical Soundings (VES) stations were occupied with Signal Stacking resistivity meter model SSR-MP1. The SSR-MP1 IGIS Microprocessor-based Signal Enhancement Resistivity Meter is a high-quality microprocessor-based data acquisition system with many unique characteristics. The instrument's design includes numerous modern digital circuitry techniques to make it a reliable geophysical tool that produces high-quality data valuable for mineral and groundwater exploration studies. The current electrode spacing on the Schlumberger electrode array ranged from 1 to 200 m. The data was plotted on bi-log papers and was then analyzed using partial curve matching. The parameters of the initial and final layers were then obtained using WinResist1D and Ipi2win software (Bobachev 2003). This study utilized a sounding technique for analyzing and recording data. The procedure was based on the data acquisition and processing techniques mentioned by Sunmonu et al. Finally, 2D geoelectric sections were generated based on the interpretation of layer parameters. The apparent resistivity ( $\rho_a$ ) is computed using the Schlumberger electrode configuration (Kearey & Brooks 1988).

$$\rho_a = \frac{\left(\frac{AB}{2}\right)^2 - \left(\frac{MN}{2}\right)^2}{MN} \times \frac{\Pi \Delta V}{I}$$

Where, AB = Current electrode spacing in meter

MN = Potential electrode spacing in meter

I = Current in ampere

$\Delta V$  = Potential difference in mV

On a log-log graph, apparent resistivity vs. half of the current electrode separation (AB/2) of fifteen Vertical Electrical Sounding indicates a 3-5 layered structure in the research region (Fig.2 ).

## RESULTS AND DISCUSSION

### Resistivity Curve Matching

Fifteen VES data were collected from various sites in the study area. The data was collected for quantitative analysis to determine the subsurface layering, surface layers, and thickness of the groundwater layer beneath the studied sites. The field resistivity data were interpreted using Winresist

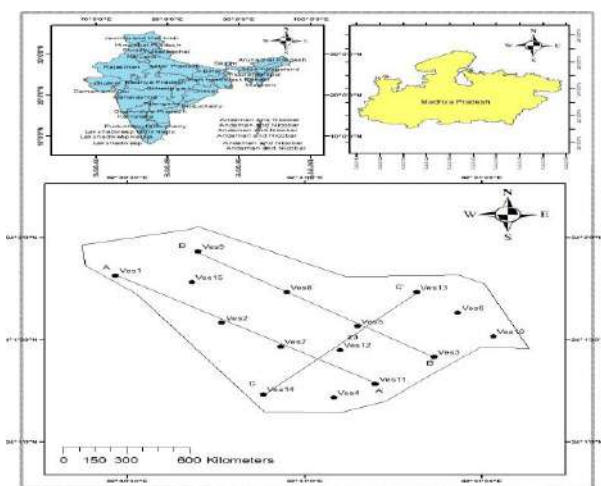


Fig.1: A map of the study area showing the location of VES points along traverses AA', BB', and CC' in Banauli village, Singrauli district, M.P., India.



and Ipi2win software. The model parameters were resolved with minimum (0.79) and maximum (3.4) RMS errors. Out of 15 VES station ,VES stations 1,2,4,5,7,9,10 and 12

shows five-layer earth section, VES stations 3,6,11,13 show four-layer earth section and VES stations 8,14,15 show 3-layer earth section.

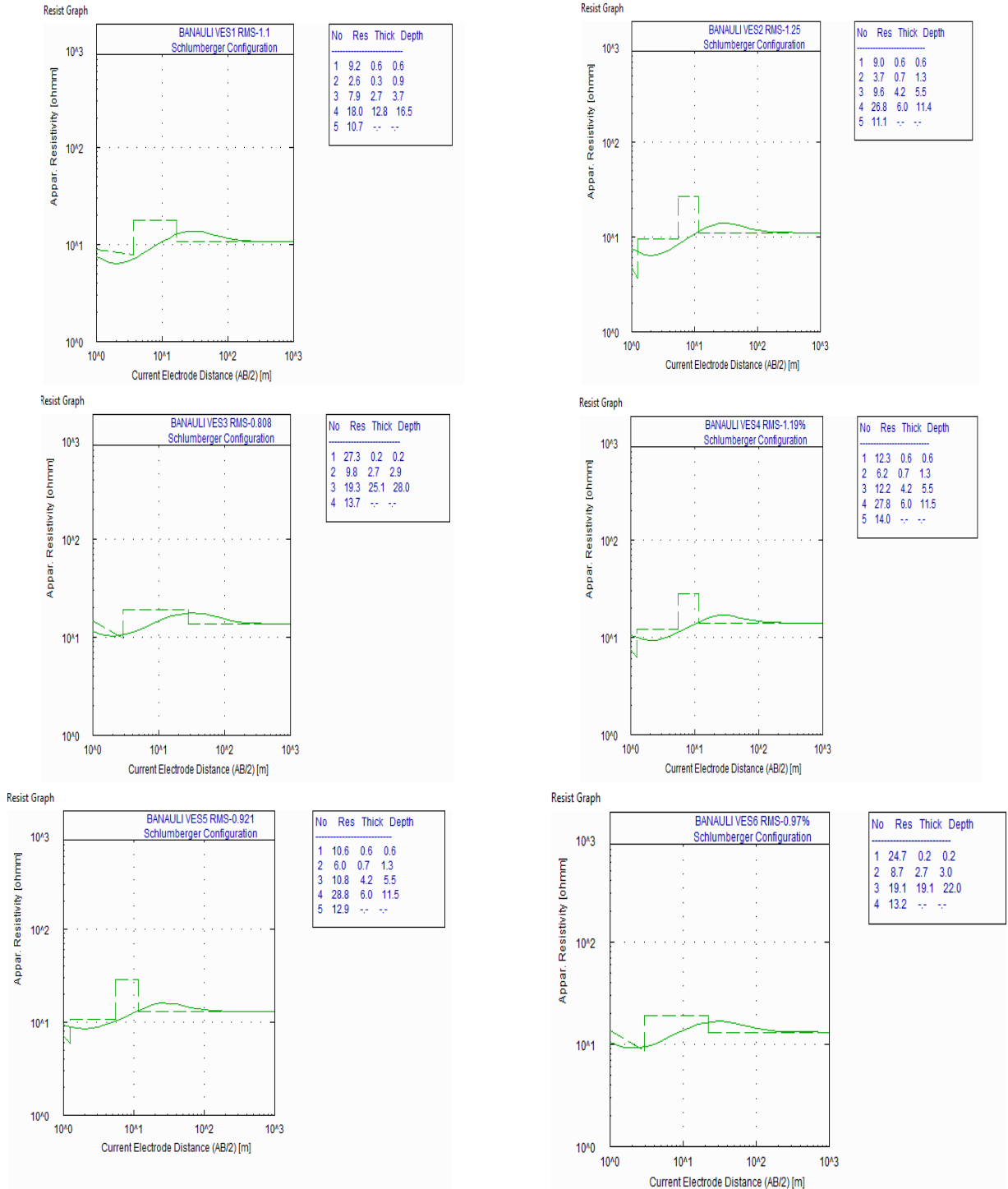


Fig. cont....

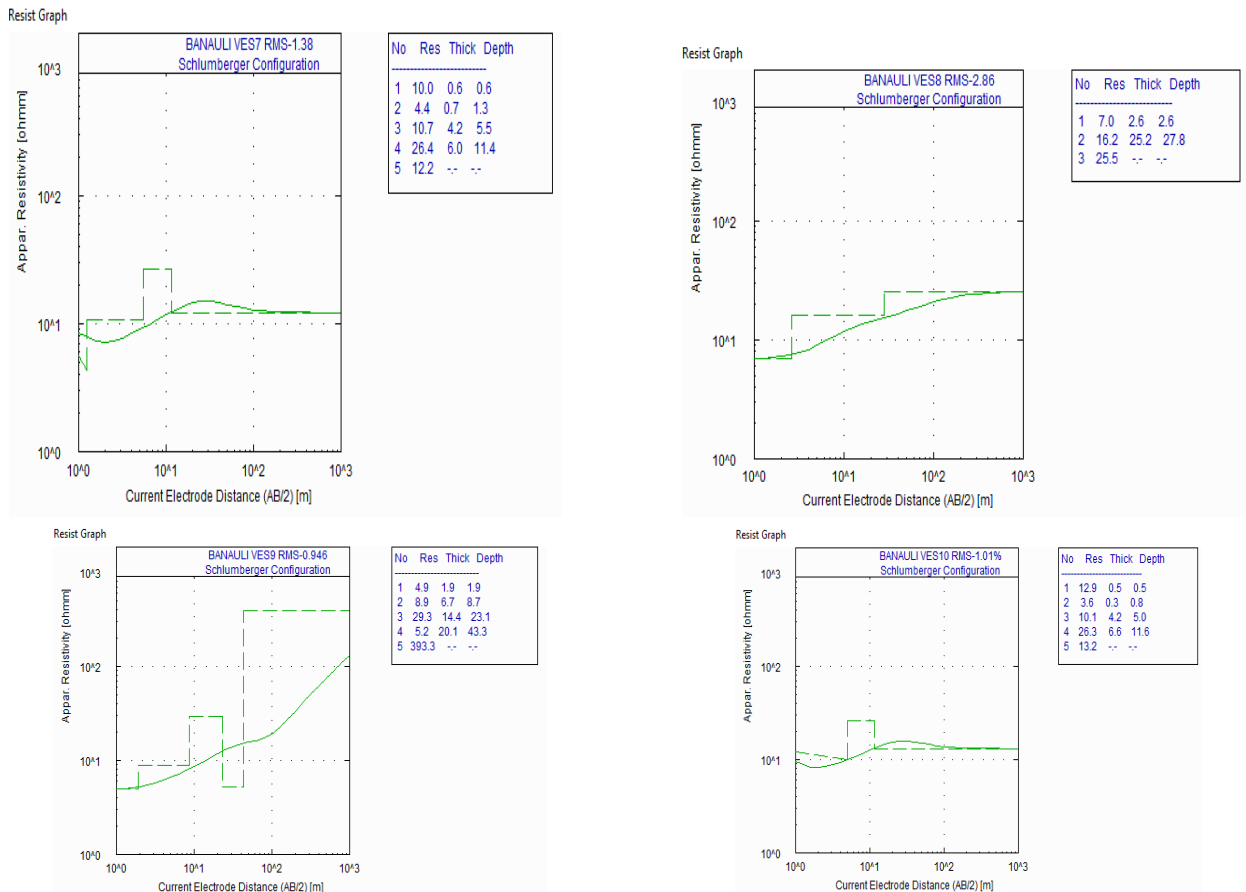


Fig. 2: Vertical electrical sounding curve of stations 1-15.

## Curve Types

Curve Types A, Q, H, K, and combinations of resistivity curves were produced (Table 1). The curve matching approach using four and five-layer master curves is used to understand these curves (Singh & Tripathi 2009). The following are the several fundamental types of curves:

1.  $\rho_1 > \rho_2 > \rho_3$  Q Type
2.  $\rho_1 > \rho_2 < \rho_3$  H Type
3.  $\rho_1 < \rho_2 > \rho_3$ . K Type
4.  $\rho_1 < \rho_2 < \rho_3$  A Type

If the model is established for more than three layers, a combination of the fundamental curves can be obtained. The following are examples of possible combinations:

1.  $\rho_1 > \rho_2 < \rho_3 < \rho_4$  Curve Type HA
2.  $\rho_1 > \rho_2 < \rho_3 > \rho_4$  Curve Type HK
3.  $\rho_1 < \rho_2 < \rho_3 < \rho_4$  Curve Type AA
4.  $\rho_1 < \rho_2 < \rho_3 > \rho_4$  Curve Type AK

5.  $\rho_1 < \rho_2 > \rho_3 < \rho_4$  Curve Type KH
6.  $\rho_1 < \rho_2 > \rho_3 > \rho_4$  Curve Type KQ
7.  $\rho_1 > \rho_2 > \rho_3 < \rho_4$  Curve Type QH
8.  $\rho_1 > \rho_2 > \rho_3 > \rho_4$  Curve Type QQ

In the research area, a Four to Five-layer Earth model is obtained, and the curve types are then determined; Table 1 shows the obtained resistivity as well as the thickness of each layer. Fig. 2 depicts a representative VES curve.

The first layer topsoil layer seemed to have a thickness of 0.20 m - 2.59 m and a resistivity of 4.88  $\Omega\text{m}$  – 27.29  $\Omega\text{m}$  Alluvial soil, red Sandy soil. The second layer has a thickness of 0.30m -25.2m and resistivity of 2.62  $\Omega\text{m}$ -16.2  $\Omega\text{m}$  which corresponds to subsoil to fine-grained sandstone. The third layer, Fine-grained sandstone, to fractured or weathered sandstone, has a resistivity of 7.903  $\Omega\text{m}$  to 29.2  $\Omega\text{m}$ ; this layer is most suitable for storage and movement of groundwater. The fourth layer has a thickness of 5.22 m to 20.14 m and resistivity of 5.19  $\Omega\text{m}$  to 28.78  $\Omega\text{m}$ . This layer corresponds to fine to medium-grained fractured or

Table 1: Interpretation results of VES 1 to 15.

VES point	$\rho_1[\Omega\text{m}]$	$\rho_2[\Omega\text{m}]$	$\rho_3[\Omega\text{m}]$	$\rho_4[\Omega\text{m}]$	$\rho_5[\Omega\text{m}]$	h1[m]	h2[m]	h3[m]	h4[m]	h5	RMS % Error	Curve type	Depth of Bedrock [m]
1	9.201	2.627	7.903	17.97	10.73	0.6188	0.3141	2.723	12.83		1.1	HAK	16.49
2	8.97	3.66	9.615	26.75	11.09	0.6	0.654	4.224	5.97		1.25	HAK	11.45
3	27.29	9.777	19.31	13.65		0.209	2.692	25.11			0.808	HK	28.01
4	12.26	6.203	12.15	27.84	14.04	0.6	0.654	4.23	5.97		1.19	HAK	11.57
5	10.63	5.962	10.78	28.78	12.92	0.6	0.654	4.228	5.97		0.921	HAK	11.45
6	24.71	8.71	19.12	13.15		0.2247	2.746	19.06			0.97	HK	22.03
7	9.96	4.358	10.65	26.42	12.23	0.6	0.654	4.223	5.97		1.38	HAK	11.45
8	6.96	16.2	25.5			2.59	25.2				2.86	A	27.8
9	4.931	8.931	29.29	5.199	393	1.933	6.746	14.45	20.14		0.946	AKH	43.27
10	12.95	3.639	10.12	26.28	13.16	0.512	0.3041	4.16	11.6		1.01	HAK	11.6
11	24.71	8.71	19.06	13.15		0.2247	2.746	19.06			0.97	HK	22.03
12	9.97	4.376	10.08	27.77	12.24	0.6011	0.6185	3.899	5.226		0.792	HAK	10.64
13	12.87	10.28	20.45	15.11		0.6	2.023	21.34			0.989	HK	23.96
14	4.88	12.7	21.3			2.14	14.1				3.4	A	16.2
15	5.9	12.9	22.9			2.11	11.8				2.55	A	13.9
Mini- mum	4.88	2.627	7.903	5.199	10.73	0.209	0.3041	2.723	5.226		0.792		10.64
Maxi- mum	27.29	16.2	29.29	28.78	393	2.59	25.2	25.11	20.14		3.4		43.27
Average	12.4128	7.93553333	16.54853333	20.17242	59.92625	0.94422	4.793713	10.55892	9.2095		1.40906667		18.79

weathered sandstone, so there is storage and movement of groundwater. The fifth last basement layer has a resistivity of 10.73  $\Omega\text{m}$  to 393  $\Omega\text{m}$ , which corresponds to medium to coarse-grained sandstone. The thickness and resistivity of VES cross-sections are correlated with the presence of geological features near the sounding stations. It is suggested to associate the weathered and fractured zone with the resistivity of 5.19  $\Omega\text{m}$  to 30  $\Omega\text{m}$  and thickness of 2.7 m to 25 m. This zone is saturated with groundwater and capable of storage and movement of groundwater.

### Geo-Electric Cross-Section

Three geoelectric cross-sections were created in the study area to analyze the subsurface features and understand the underlying aquifer bodies. AA' and BB' are the two profiles with four VES points each, and CC' is the third profile with three VES points. The profiles AA' and BB' are orientated in the NW-SE direction, while the profile CC' is oriented in the NE-SW direction.

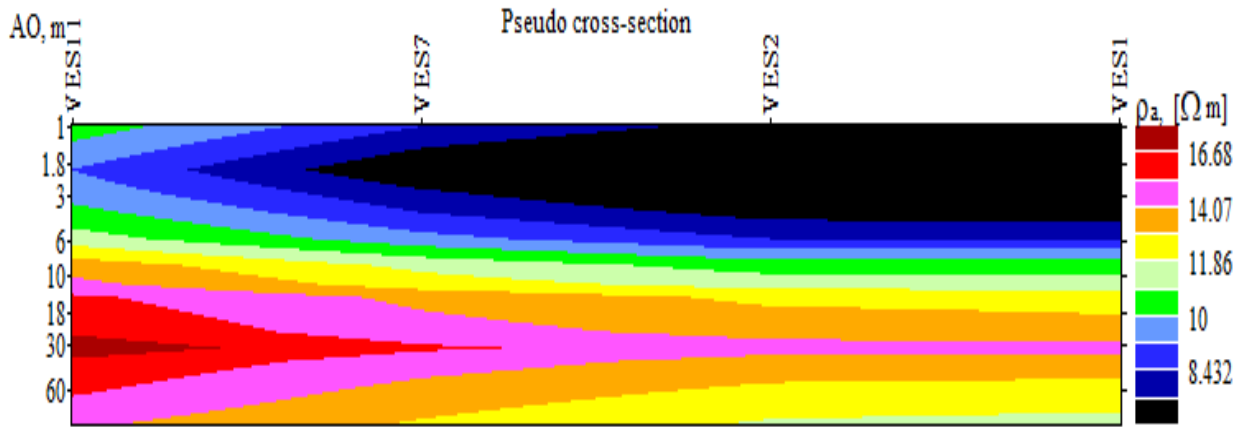
#### Profile AA'

Profile AA' covers the VES stations 1, 2, 7, and 11 trending in the NW-SE direction (Fig.3). A shallow low resistive layer (8.11 $\Omega\text{m}$  to 10 $\Omega\text{m}$ ) occurs beneath stations 1, 2, and 11 at

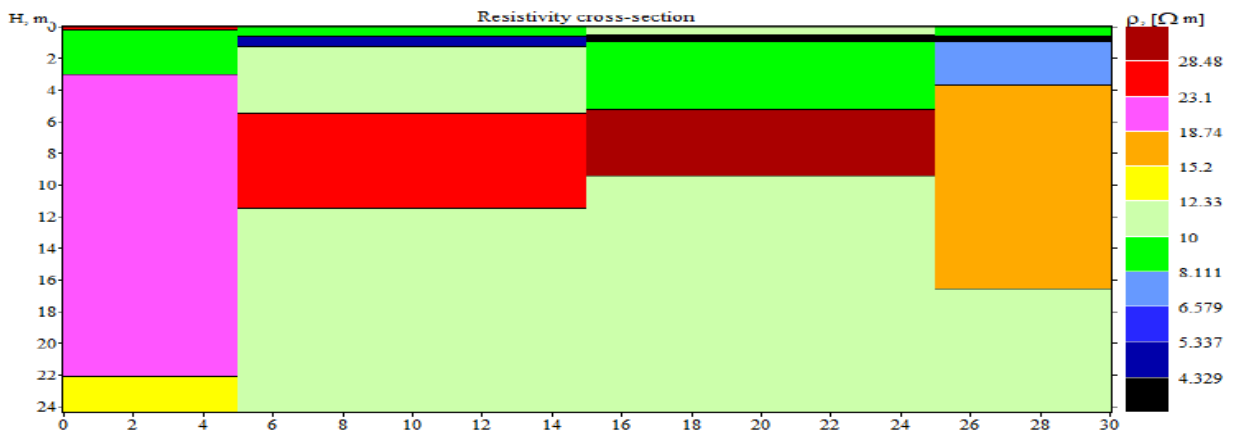
a depth of 0.5m to 3m. This effect is due to the presence of lithomarge clay, which may contain groundwater. A high resistive feature (23.1  $\Omega\text{m}$  to 28.48  $\Omega\text{m}$ ) was observed at VES7 at a depth of 6 m to 12 m and also high resistive feature was observed at VES2 of resistivity (28.48  $\Omega\text{m}$  to 390  $\Omega\text{m}$ ) at a depth of 5 m to 9 m. Beneath this high resistive formation, a low resistive formation up to a depth of penetration is observed having resistivity (10  $\Omega\text{m}$  to 16.2  $\Omega\text{m}$ ) and thickness (2 m to 14 m) at stations 1, 2, 7, and 11. This high resistive indicates hard and compact sandstone formation, and all these low resistive zones are likely to be a good potential zone for groundwater. Hence these sites are suitable for groundwater exploration.

#### Profile BB'

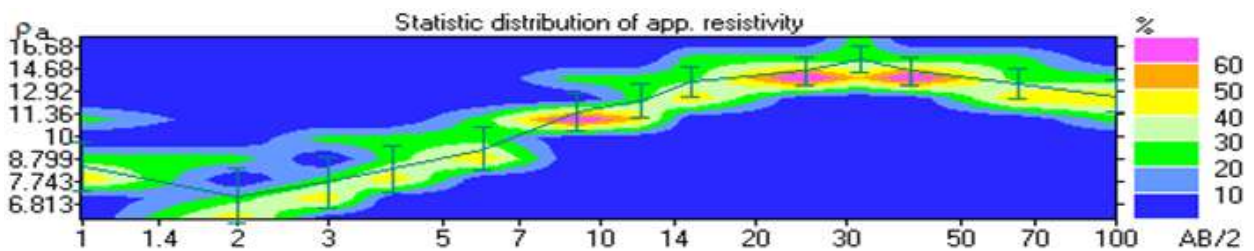
The profile BB' comprises VES stations 3,5,8, and 9 trending in the NW-SE direction (Fig.4). A shallow low resistive layer (7.19  $\Omega\text{m}$  to 10  $\Omega\text{m}$ ) and thickness (0-5m) were observed beneath stations 3 and 5. This low resistive layer is due to the presence of lithomarge clay, and there may be the presence of groundwater. Beneath this layer, a high resistive (19.31  $\Omega$  to 26.83  $\Omega\text{m}$ ) and thickness (10 m to 14 m) were observed at VES3 and VES5. Below this layer, a low resistive layer having resistivity(10  $\Omega\text{m}$  to 13.89  $\Omega\text{m}$ ) and at a depth of (10 m to 28 m) is observed at stations 3 and 5. A shallow



(a)



(b)



(c)

Fig. 3: (a) Pseudo cross-section,(b) Resistivity cross-section,(c) Statistic distribution of apparent resistivity.

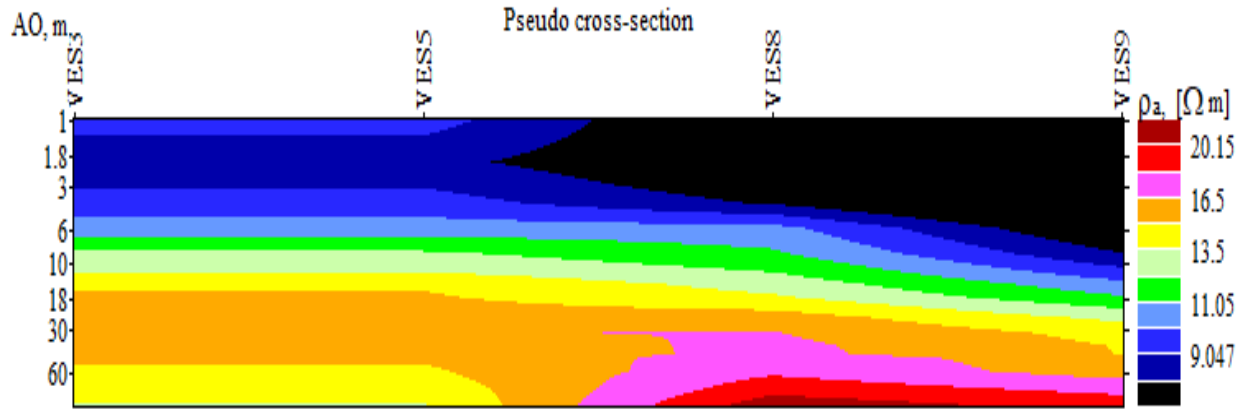
low resistive layer (3.7  $\Omega\text{m}$  to 7.19  $\Omega\text{m}$ ) and thickness (0-2.5m) are observed beneath stations 8 and 9. This effect is due to the presence of lithomarge clay, which may contain groundwater also. A high resistive layer (51.79  $\Omega\text{m}$  to 300  $\Omega\text{m}$ ) occurs as a basement layer at station 9. A conductive layer of resistivity (10  $\Omega\text{m}$  to 13.89  $\Omega\text{m}$ ) and thickness (5m

to 30m) occur at station eight, and a low resistivity layer (5.1  $\Omega\text{m}$  to 7.1  $\Omega\text{m}$ ) and thickness of 20 m occur at station 9. These all low resistive layers that are observed at stations 3,5,8, and 9 are likely to be a good potential zone for storage and movement of groundwater. Hence these sites are suitable for groundwater exploration.

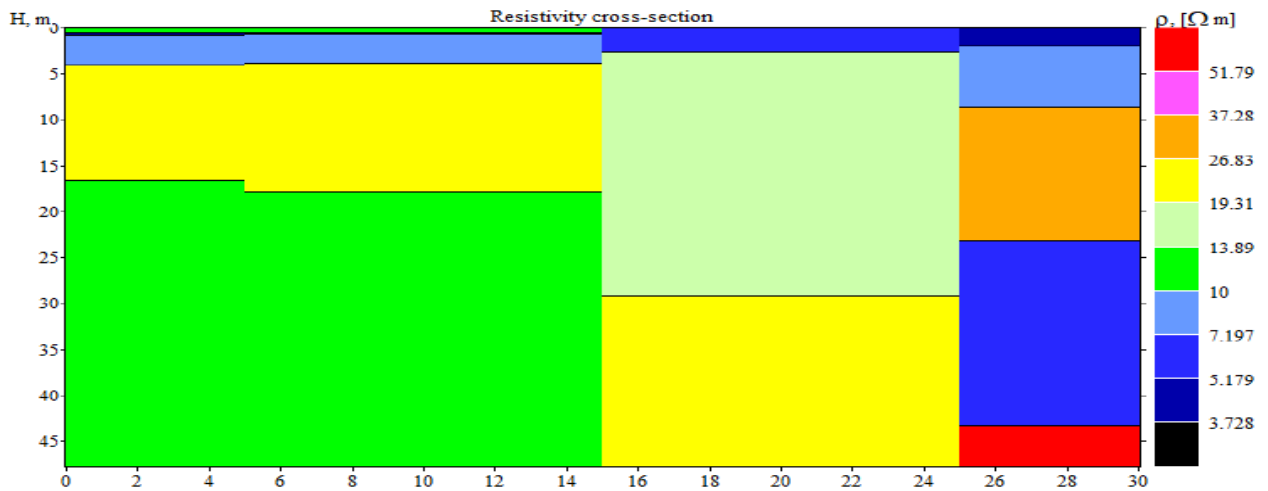
**Profile CC'**

The Profile CC' comprises VES stations 13,12 and 14 trending in the NE-SW direction (Fig. 5). A low resistive ( $1\Omega\text{m}$  to  $8.43\Omega\text{m}$ ) layer is characterized at the top surface all along with the profile, and the thickness of this low resistive layer is small at

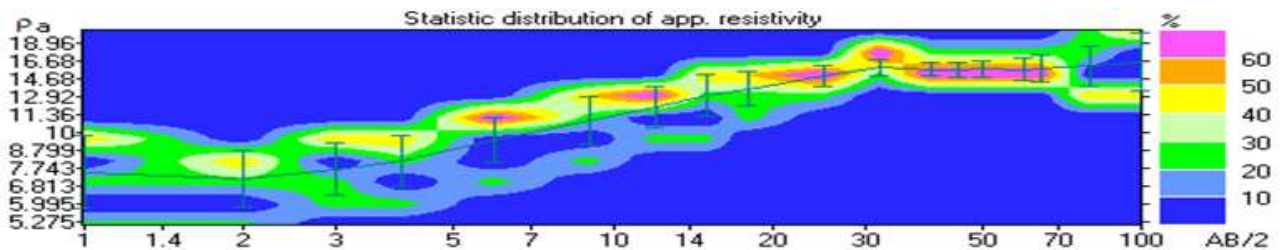
stations 13 and 14, and thickness is about 1m at VES station 14. This effect is due to the presence of clay in the soil. This layer may contain groundwater at station 14. A high resistive layer ( $26\Omega\text{m}$  to  $300\Omega\text{m}$ ) occurs at VES12 at a depth of 5 m to 10 m. This effect is due to the presence of Hard and compact sandstone. A low resistive layer ( $10\Omega\text{m}$  to  $13.89\Omega\text{m}$ ) of



(a)

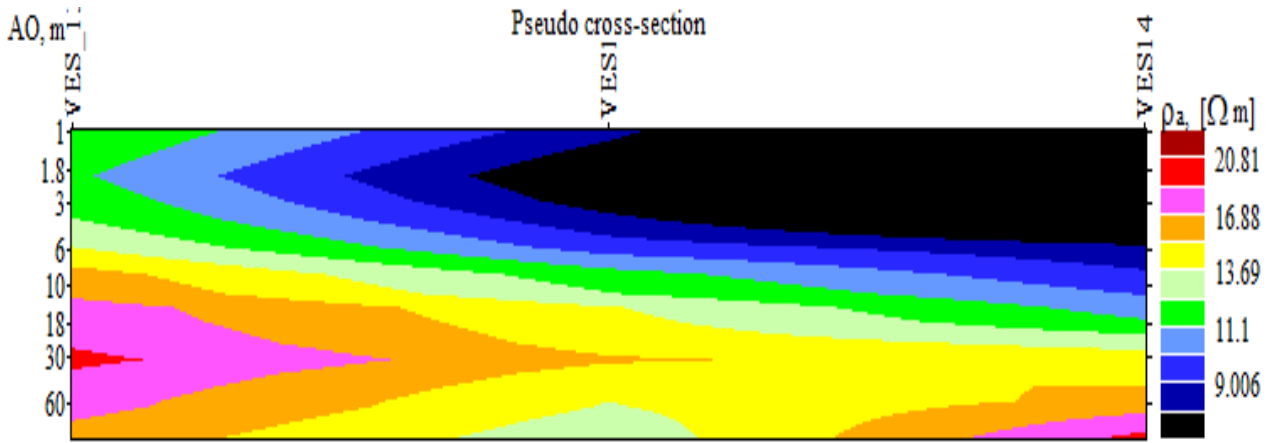


(b)

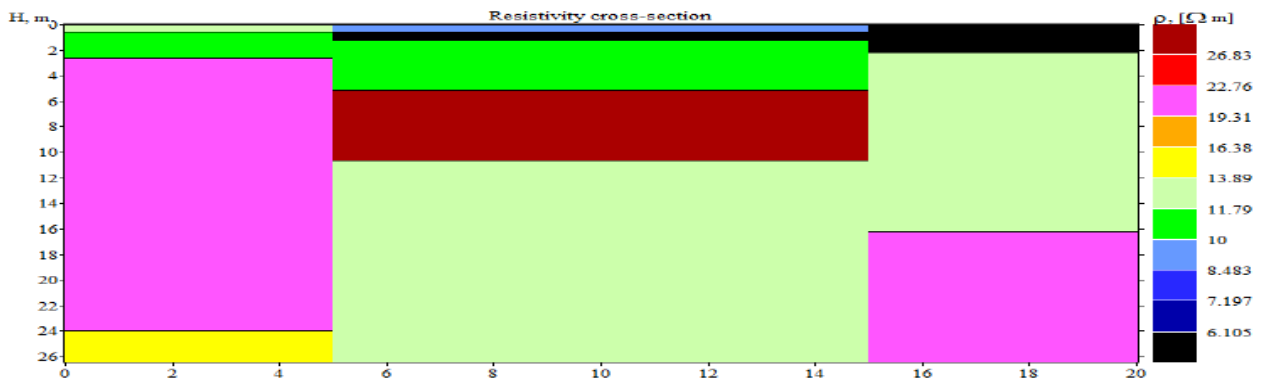


(c)

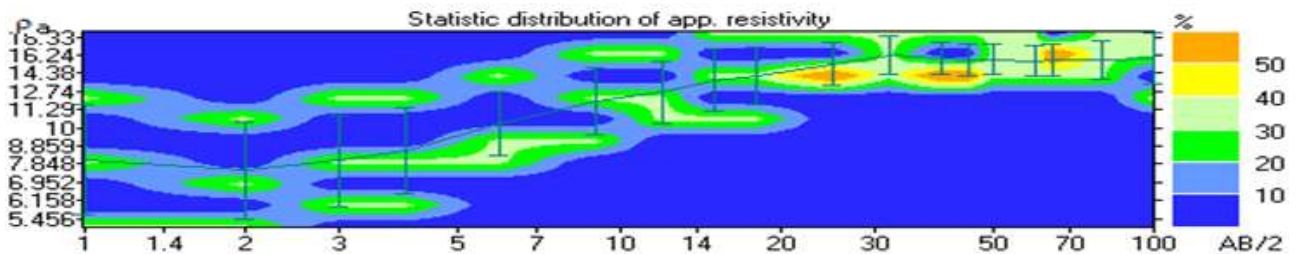
Fig.4: (a) Pseudo cross-section,(b) Resistivity cross-section,(c) Statistic distribution of apparent resistivity.



(a)



(b)



(c)

Fig.5: (a) Pseudo cross-section,(b) Resistivity cross-section,(c) Statistic distribution of apparent resistivity.

varying thickness occurs at stations 13, 12, and 14 at a depth of 0.5 m, 1 m, and 2 m, respectively. This low resistive layer is likely to be a potential zone for the storage and movement of groundwater. At a maximum depth of observation, a low resistive layer (11.79  $\Omega m$  -14  $\Omega m$ ) and thickness of 15 m occur at station 12, which is likely to be a potential zone for groundwater. Hence a low resistive layer at station 13, 12, and 14 are likely to be a good groundwater potential zone.

### CONCLUSION

Fifteen vertical electrical sounding data were acquired within the Village Banauli Singrauli district, in the eastern part of Madhya Pradesh, India, to delineate the resistivity and thickness of the geological formation and to assess the potential groundwater aquifer zones beneath the formation. Generally, good accumulation of groundwater occurs in

weathered/fractured geological formations, In the study area, it is found that the top layer which has low resistivity may contain groundwater, but its thickness is small. By observing the layered resistivity and thickness of all fifteen VES stations, it is found that VES stations 1,2,4,5,7,9,10, and 12 have five layered Earth sections, and VES stations 3,6,11, and 13 have four layered Earth sections while VES stations 8,14,15 have three-layered Earth sections. Correlating the resistivity and thickness obtained in 15 VES stations with known lithology of the study area, it is found that the third layer of fine-grained sandstone to fractured or weathered sandstone has a resistivity of 7.903 $\Omega$ m to 29.2 $\Omega$ m and mean thickness of 10.55m, this layer is potential groundwater aquifer zones. Thus, the vertical electrical sounding technique has proven to achieve success and is extremely effective within the study area for the identification and delineation of subsurface structures that are favorable for groundwater accumulation in the study area. The electrical resistivity survey method utilized in this project necessitates locating favorable dug well and boreholes in the area.

## ACKNOWLEDGMENTS

The authors are very thankful to the Department of Mining Engineering, Indian Institute of Technology, Banaras Hindu University, Varanasi, for providing technical support during the Research period. The authors are also thankful to Rohit, Dharendra, and Budhsen Sharma for their contribution to data acquisition in the study area.

## REFERENCES

- Adagunodo, T.A. and Oladejo, O.P. 2020. Geoelectrical variations in a residential area of Ojongbodu, Oyo, Southwestern Nigeria. *Nat. Environ. Pollut. Technol.*, 19(4): 1771-1774.
- Balasubramanian, A., Sharma, K.K. and SASTRI, J.V. 1985. Geoelectrical and hydrogeochemical evaluation of coastal aquifers of Tambraparni basin, Tamil Nadu. *Geophysical Research Bulletin*, 23(4): 203-209.
- Bayowa, O.G. 2020. Hydrolithological investigation for near-surface aquifers within Lekki Peninsula, Lagos, Southwestern Nigeria. *Nat. Environ. Pollut. Technol.*, 19(2): 511-520.
- Bobachev, A. 2003. Resistivity soundings interpretation. IPI2WIN: Version 3.0.1.a7.01.03. Moscow State University, Moscow, Russia.
- CGWB 2009. Ground Water Information, Jalgaon district, Maharashtra 1606/DBR/2009 19 p.
- Gupta, A., Vyas, R.K. and Gupta, A.B. 2021. Occurrence of acyclovir in the aquatic environment, its removal, and research perspectives: A review. *J. Water Process Eng.*, 39: 101855.
- Gupta, G., Erram, V.C. and Kumar, S. 2012. Temporal geoelectric behavior of dyke aquifers in northern Deccan volcanic province, India. *J. Earth Syst. Sci.*, 121(3): 723-732.
- Gupta, G., Kachate, N.R., Erram, V.C., Maiti, S. and Patil, S.N. 2010. Geoelectrical studies for delineating seawater intrusion in parts of Konkan coast, western Maharashtra. *Int. J. Environ. Earth Sci.*, 1(1): 62-79.
- Janardhana Raju, N., Reddy, T.V.K. and Nayudu, P.T. 1996. Electrical resistivity surveys for groundwater in the upper Gunjanaeru catchment, Cuddapah district, Andhra Pradesh. *J. Geol. Soc. India*, 47: 705-716.
- Karanth, K.R. 1991. Impact of human activities on the hydro-geological environment. *J. Geol. Soc. India*, 38: 195-206.
- Karlik, G. and Kaya, M.A. 2001. Investigation of groundwater contamination using electric and electromagnetic methods at an open waste-disposal site: a case study from Isparta, Turkey. *Environ. Geol.*, 40, 725-731.
- Kearey, P. and Brooks, M. 1988. *An Introduction to Geophysical Exploration*, ELBS, Blackwell Scientific Publication, Oxford, 296.
- Kehinde D. and Oyeyemi, E.A. 2018. Evaluation of groundwater pollution near municipal solid waste landfill site using ERI technique: A case study in southwestern Nigeria. *Nat. Environ. Pollut. Technol.*, 17(2): 453-458.
- Kumar, D., Thiagarajan, S. and Rai, S.N. 2011. Deciphering geothermal resources in the DeccanTrap region using electrical resistivity tomography technique. *J. Geol. Soc. India*, 78: 541-548.
- Maiti, S., Gupta, G., Erram, V. C. and Tiwari, R. K. 2013. Delineation of shallow resistivity structure around Malvan, Konkan region, Maharashtra by neural network inversion of vertical electrical sounding measurements. *Environ. Earth Sci.*, 68: 779-794. doi: 10.1007/s12665-012-1779-8.
- Mujumdar, R.K. and Pal, S.K. 2005. Geoelectric and borehole lithology studies for groundwater investigation in alluvial aquifers of Munger District, Bihar. *J. Geol. Soc. India*, 66(4): 463.
- Narayanpethkar, A.B., Vasanthi, A. and Mallick, K. 2006. Electrical resistivity technique for exploration and studies on the flow pattern of groundwater in the multi-aquifer system in the Basaltic Terrain of Adila Basin, Maharashtra. *J. Geol. Soc. India*, 35(3): 696-708.
- Pal, S.K. and Majumdar, R.K. 2001. Determination of groundwater potential zones using Isoresistivity maps in alluvial areas of Munger district, Bihar, India. *J. Earth Sci.*, 1(4): 16-26.
- Singh, V.B. and Tripathi, J.N. 2009. An investigation of groundwater condition using geoelectrical resistivity method: A case study from some parts of Kaushambi district (U.P.), India. *J. Spatial Hydrol.*, 9(2): 63
- Yadav, G.S. 1997. Impact of surface mining on groundwater table in the western part of Singrauli Coalfield, India: A study with resistivity measurements. *J. Sci. Res.*, 47: 49-71.
- Yadav, G.S., Kumar, R., Singh, P.N. and Singh, S.C. 1993. Geoelectrical soundings for aquifer characterization around Jayant Colony-Singrauli, Sidhi District, M.P. *J. Assoc. Expl. Geophys.*, 14: 123-131.
- Zhody, A.A.R. 1969. The use of Schlumberger and equatorial soundings on groundwater investigations near El Paso. *Texas Geophys.*, 34: 713-728.







# Investigation of Adsorption of Heavy Metal Ions on $C_3N_4$ Nanosheets by Batch and Microscopic Methods

C. K. Fu\*, Y. Fang\*, C. Y. Yang\*, C. G. Chen\* and L. X. Wang\*†

\*Department of Chemistry and Chemical Engineering, Shaoxing University, Zhejiang 312000, P. R. China

†Corresponding authors: Linxia Wang; wlxsyx@163.com

Nat. Env. & Poll. Tech.  
Website: [www.neptjournal.com](http://www.neptjournal.com)

Received: 17-11-2021

Revised: 16-02-2022

Accepted: 24-02-2022

## Key Words:

Heavy metals

$C_3N_4$

Adsorption

Nd(III)

Th(IV)

## ABSTRACT

This paper mainly studies the adsorption of  $C_3N_4$  on a series of heavy metals and focuses on the adsorption performance of  $C_3N_4$  on Nd and Th. The main conclusions are as follows: Through the use of the thermal stripping method and melamine as the raw material,  $C_3N_4$  was obtained at a lower cost, with superior adsorption performance. Through SEM-EDS, TEM, and other characterization analyses, the results show that  $C_3N_4$  has a clear multilayer sheet structure, and the surface of the material is more uniformly dispersed. The maximum adsorption capacity of  $C_3N_4$  for Th is  $86.6 \text{ mg}\cdot\text{g}^{-1}$ , and the maximum adsorption capacity for Nd is  $60.1 \text{ mg}\cdot\text{g}^{-1}$ . The kinetic model is also used for fitting, and the results showed that the kinetic of the adsorption was in line with the pseudo-second-order model, indicating that the adsorption was chemical interaction. After  $C_3N_4$  adsorbed heavy metal elements, it was characterized by SEM-EDS, TEM, UHRTEM, and AFM. The results showed that a variety of heavy metal ions can be adsorbed by  $C_3N_4$ , which proved that  $C_3N_4$  has good adsorption performance. Due to factors such as metal particle size, the adsorption of  $C_3N_4$  on heavy metal elements is different.

## INTRODUCTION

With the rapid development of economic globalization, the use of heavy metals by humans is increasing, which has led to an increasingly serious problem of heavy metal pollution. At present, the problem of heavy metal ions pollution is widespread in all regions of our country (Li et al. 2015), which has already caused a serious impact on the environment. In addition, heavy metal ions have the characteristics of concealment, long-term, and irreversibility (Li et al. 2014). There will be serious enrichment in the human body (Xu et al. 2016), so it can still cause huge health risks at low concentrations. Moreover, different heavy metal ions have different hazards to the human body. Excessive lead (Pb) content can easily lead to neurological disorders, induced anemia, and other diseases (Islam et al. 2014). Neodymium (Nd) and thorium (Th) two rare earth elements are low for a long time Dose exposure and intake will have adverse consequences for human health or metabolism in the body, and even cause lung and liver diseases (Ahmad et al. 2019, Talip et al. 2009). Moreover, the unreasonable exploitation of neodymium (Nd) and thorium (Th) will also lead to the destruction of the ecological environment, and cause problems such as the greenhouse effect and the acidification effect.

Therefore, finding a convenient, economical, and effective method to deal with heavy metal pollution has become one of the key areas of research by scientists in the world. To date, various technologies have been proposed and practiced, such as ion exchange, membrane filtration, chemical precipitation, adsorption, etc. Considering the removal efficiency of heavy metal ions and the convenience of operation, the adsorption method is favored by many researchers (Zheng et al. 2007). Its main mechanism is that when the fluid passes through the adsorbent, the molecules and ions in the fluid will accumulate on the adsorbent. Moreover, the adsorption method has the characteristics of green and environmental protection, which is simpler and more efficient than other methods. In recent years, new adsorbents have been continuously developed and applied, and the choice of adsorbents has increased year by year. Carbon nanomaterials are the most common type among them. Common carbon nanomaterials include activated carbon (Bali & Tlili 2019), fullerene (Aleksieva et al. 2016), and carbon nanomaterials. Nanotubes (Tian et al. 2012), graphene materials (Zhao et al. 2011), etc. The above-mentioned adsorbents have been widely reported as effective adsorbents (Liao et al. 2018), and because of its special properties,  $C_3N_4$  is widely used in photocatalysis, electrocatalysis, bioimaging, heavy metal adsorption, and other fields, and it is often used as a precursor to synthetic

composite materials. For example, Zheng et al. (2011) used a composite of  $C_3N_4$  and porous graphite to prepare high-efficiency electrocatalysts, which have better methanol tolerance and higher catalytic efficiency than current commercial products. Hu et al. (2020) also found that g-  $C_3N_4$  nanosheets have higher catalytic efficiency in the field of photoelectric catalysis. Compared with ordinary graphene materials, the ultra-thin g-  $C_3N_4$  nanosheets prepared by Zhang et al. (2013) enhanced the light responsiveness of the material in aqueous solutions, which makes g-  $C_3N_4$  also have greater application prospects in the field of bioimaging. Furthermore, Wang et al. (2017) found that g-  $C_3N_4$  under the synergistic effect of photocatalysis and adsorption can remove Cr(VI) more efficiently, with a degradation rate of 100% at low concentrations. Similarly, Shen et al. (2015) found that g-  $C_3N_4$  has a good adsorption effect on heavy metal elements such as Pb(II), Cu(II), Cd(II), Ni(II), and the adsorption kinetics all follow the pseudo-secondary model.

Based on the above facts and analysis, this thesis will study the following three aspects: First, use the thermal stripping method to prepare melamine into  $C_3N_4$ , and perform SEM-EDS and TEM characterization analysis on the prepared  $C_3N_4$ ; secondly, use the prepared  $C_3N_4$  Adsorbent, to study the adsorption effect and mechanism between  $C_3N_4$  and heavy metal ions, and determine its adsorption performance, optimize the experimental conditions; finally, the  $C_3N_4$  after adsorbing different heavy metal elements is characterized by SEM-EDS, TEM, UHRTEM and AFM, and other methods Process and analyze the adsorption of  $C_3N_4$  on different types of metals.

## MATERIALS AND METHODS

### Experimental Materials and Apparatus

Hydroxylamine hydrochloride, sulfamic acid, citric acid, disodium hydrogen phosphate, arsenazo III, and melamine were provided by Shanghai Aladdin Biochemical Science and Education Co., Ltd. Neodymium nitrate hexahydrate, thorium oxide, sodium hydroxide, and hydrochloric acid were provided by Shanghai Ling Feng Chemical Reagent Co., Ltd. The purity of the reagents is analytically pure, and the deionized water is self-made. The components of the buffer solution obtained are citric acid and disodium hydrogen phosphate, and the components of the reducing agent are hydroxylamine hydrochloride and sulfamic acid.

Electronic balance (AL204) and pH meter (Five Easy plus) are produced by Mettler-Toledo (Shanghai) Co., Ltd. The ultrasonic cleaner (KQ5200DA) is produced by Kunshan Ultrasonic Instrument Co., Ltd. UV-Vis spectrophotometer (SP-756P) is produced by Shanghai Spectrometer Co., Ltd.

And the vacuum drying oven (DZF-6020) is produced by Shanghai Jinghong Experimental Equipment Co., Ltd. The desktop low-temperature constant-temperature shaking shaker adopts the German IKA KS4000i control shaker. Use the muffle furnace (KSL-1700) produced by Hefei Kejing Material Technology Co., Ltd., And the micro-continuous adjustable pipette (7010101017) produced by Dalong Xingchuang Experimental Instrument (Beijing) Co., Ltd., experimental method

### Preparation of $C_3N_4$ Adsorbent

Prepare a dry and impurity-free alumina crucible, weigh 20g of melamine raw material into it with an electronic balance, spread the powder evenly in the crucible, and raise it to 520°C at a heating rate of 3°C.min<sup>-1</sup> in a muffle furnace. After baking for 3 hours, the temperature is reduced from 520°C to room temperature at a cooling rate of 3°C.min<sup>-1</sup> to complete the first thermal stripping treatment. Then put it into the muffle furnace, and repeat the above-mentioned roasting process, after the treatment is completed, take out the block-like light yellow powder  $C_3N_4$ . Transfer  $C_3N_4$  to an agate mortar and grind into a fine powder, bag it for later use.

### Static Adsorption Experiment

Take several 150 mL reaction flasks, use a pipette to accurately pipette the quantitative heavy metal ion standard solution into the reaction flask, add deionized water to make the total volume of the solution 100 mL, and adjust with 0.1 mol.L<sup>-1</sup> HCl and 0.1 mol.L<sup>-1</sup> NaOH respectively the pH of the solution is such that it has a pH gradient. After adding quantitative  $C_3N_4$ , use an ultrasonic cleaning machine for 30min ultrasonic treatment, and place it in a desktop low-temperature constant temperature shaking shaker for 24h after ultrasonication. Detect the influence of different pH on the adsorption of heavy metal ions. Choose several 150 mL reaction flasks. Accurately pipette the quantitative heavy metal ion standard solution into the reaction flask, add deionized water to make the solution volume 100 mL, and adjust the pH with 0.1 mol.L<sup>-1</sup> HCl and 0.1 mol.L<sup>-1</sup> NaOH respectively to make the pH value the same. Finally,  $C_3N_4$  adsorbents of different qualities were added respectively, and ultrasonic treatment was carried out with an ultrasonic cleaning machine for 30 min. After ultrasonication, they were placed in a desktop low-temperature constant-temperature shaking shaker for 24 h to detect the influence of different adsorbent qualities on the adsorption of heavy metal ions. Select several 150 mL reaction flasks, respectively pipette different heavy metal ion standard solutions into the reaction flasks, add deionized water to make the reaction system 100 mL, and adjust the pH with 0.1 mol.L<sup>-1</sup> HCl and 0.1 mol.L<sup>-1</sup>

NaOH, Make the pH the same. Add quantitative C<sub>3</sub>N<sub>4</sub>, use an ultrasonic cleaning machine for 30min ultrasonic treatment, and place it in a desktop low-temperature constant-temperature shaking shaker for 24 h after ultrasonication. After the oscillation is complete, take 1 mL of the above solution in a 25 mL colorimetric tube. The volume is adjusted to 25 mL, and the absorbance is measured with an SP-756P UV-visible spectrophotometer.

### Adsorption Experiment Data Processing

Calculate the adsorption capacity (q<sub>e</sub>) of different sets of data. The adsorption capacity refers to the concentration of heavy metal ions adsorbed per gram of adsorbent. Adsorption capacity: q<sub>e</sub>=m<sub>e</sub>/M where m<sub>e</sub>(mg) represents the mass of heavy metal ions adsorbed, and M (mg) represents the mass of adsorbent.

In kinetic equation research, the three kinetic fitting models used in this experiment are fitted (pseudo-first-level model fitting, pseudo-second-level model fitting, and Elovich model fitting). The kinetic model is fitted to the experimental data according to the following formula (Chen et al. 2021, Wu et al. 2021):

Pseudo first-level model fitting:  $\ln(q_e - q_t) = \ln q_e - k_1 t$

Pseudo secondary model fitting:  $t / q_t = 1 / (k_2 q_e^2) + t / q_e$

Elovich model fitting:  $q_t = 1/\beta \ln \alpha \beta + 1/\beta \cdot \ln t$

Where q<sub>e</sub> refers to the adsorption capacity (mg.g<sup>-1</sup>) of the adsorbent after reaching the adsorption equilibrium, and q<sub>t</sub> refers to the adsorption capacity of the adsorbate on the adsorbent at time t (mg.g<sup>-1</sup>);

The pseudo first-order kinetic adsorption rate constant is k<sub>1</sub> (1.min<sup>-1</sup>), k<sub>2</sub> (g.m<sup>-1</sup>.min<sup>-1</sup>) is the pseudo-second-order kinetic adsorption rate constant, α (g.m<sup>-1</sup>.min<sup>-1</sup>) and β (g.mg<sup>-1</sup>) represent respectively Initial adsorption rate constant and desorption rate constant.

### Characterization Method

In this study, JEOL, JSM-6360LV Scanning electron microscope-energy spectrum (SEM-EDS) was used for SEM characterization to analyze the morphological characteristics of the solid surface. The transmission electron microscope (TEM) can observe the finer structure of the sample, as well as the microstructure inside the material. After the team dispersed the samples evenly, they used the JEM-101 transmission electron microscope of JEOL for TEM characterization. The high-resolution transmission electron microscope (UHRTEM) can analyze the morphology, interface, and crystal defects of the material, and combine the morphology information with the structure information to analyze the material's particle size, growth orientation,

and other properties. The instrument model used to test UHRTEM: JEM-2100F high-resolution transmission electron microscope produced by JEOL. To analyze the surface roughness measurement, surface size, and statistical processing of pits and protrusions, this study used the Atomic force microscope (AFM) of the Brooker dimension icon for characterization.

## RESULTS AND DISCUSSION

In this study, the kinetic experimental conditions for Th(IV) were pH=3.0, adsorbent 40 mg, 200 mL 80 ppm Th solution, and Nd(III) kinetic experiment conditions were pH=5.5, adsorbent 80 mg, 200 mL 80 ppm Nd solution. Kinetic discussion, Fig. 1A shows the adsorption time curve of C<sub>3</sub>N<sub>4</sub> on Th(IV) and Nd(III). It can be seen from the figure that the adsorption effect of C<sub>3</sub>N<sub>4</sub> on Th(IV) and Nd(III) is obvious. As time increases, the amount of adsorption gradually increases. The adsorption rate is faster from 0 to 50 minutes, and the adsorption amount does not change much after 50 minutes, which tends to reach the adsorption equilibrium. The maximum adsorption capacity of C<sub>3</sub>N<sub>4</sub> for Th(IV) is 86mg.g<sup>-1</sup>, the maximum adsorption capacity for Nd(III) is 60 mg.g<sup>-1</sup>, and the adsorption equilibrium time is 50min. Fig. 1B shows the fitting of the pseudo-first-order model of C<sub>3</sub>N<sub>4</sub> adsorption of Th(IV) and Nd(III); Fig. 1C shows the fitting of the pseudo-second-order model of C<sub>3</sub>N<sub>4</sub> adsorption of Th(IV) and Nd(III); Fig. 1D shows the Elovich model fitting of C<sub>3</sub>N<sub>4</sub> adsorption of Th(IV) and Nd(III). It can be seen from the figure that the adsorption of Th(IV) and Nd(III) by C<sub>3</sub>N<sub>4</sub> is in line with the pseudo-second-order model fitting, indicating that the adsorption experiment is chemical adsorption.

### Scanning Electron Microscope Band Energy Spectrum (SEM-EDS) Analysis

Fig. 2 and Fig. 3A, B, C, and D respectively represent C<sub>3</sub>N<sub>4</sub> and its SEM-EDS images after adsorption of Nd, Th, Cd, and Co. It can be seen from the figure that the C<sub>3</sub>N<sub>4</sub> before the adsorption of heavy metal ions has an obvious multi-layer flake structure and a large number of defects, and the dispersion is relatively uniform. After the heavy metal ions are adsorbed, it can be seen that part of the defects on the C<sub>3</sub>N<sub>4</sub> surface is filled, and from the EDS spectrum, it can be seen that the four heavy metal elements are enriched in the defects on the C<sub>3</sub>N<sub>4</sub> surface. It can be inferred that the heavy metal ions are successfully adsorbed on the C<sub>3</sub>N<sub>4</sub> surface.

### Transmission Electron Microscopy (TEM) Analysis

Fig. 4A, B, C, and D are TEM images of C<sub>3</sub>N<sub>4</sub> under the transmission electron microscope and its adsorption of Cu, Pb, and Zn. It can be seen from the figure that there are a large

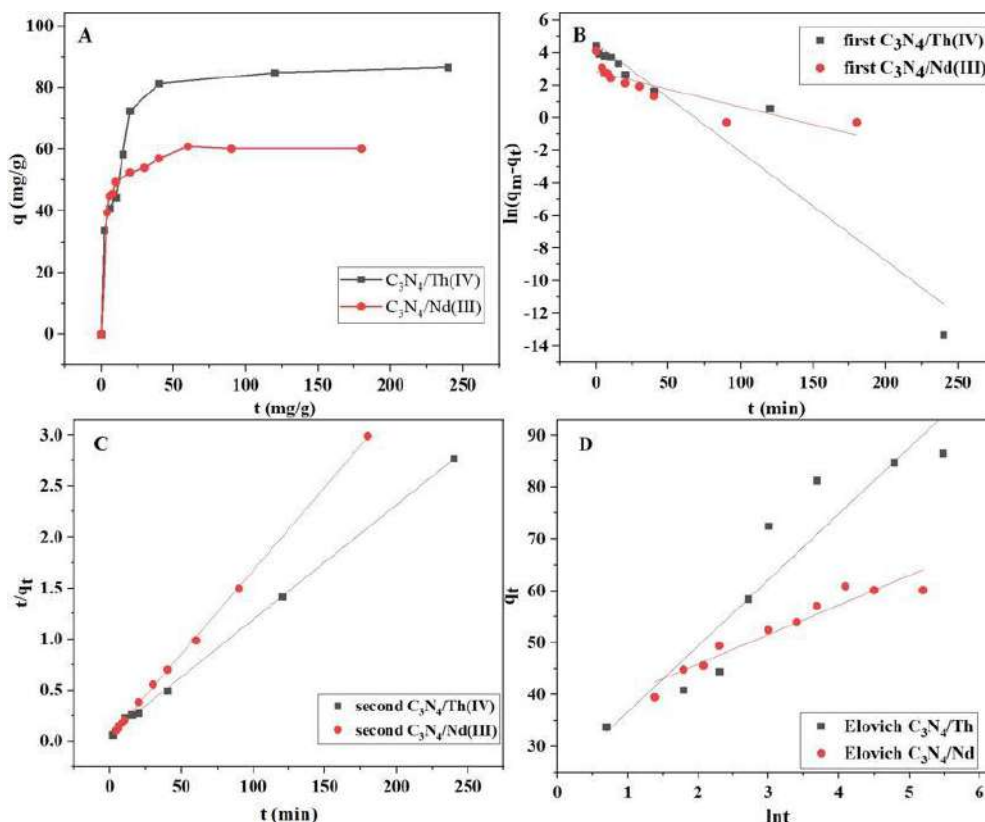


Fig. 1:  $C_3N_4$  adsorption time curve for Th(IV) and Nd(III) (A), pseudo-first-order model fitting (B), pseudo-second-order model fitting (C), Elovich model fitting (D).

number of defects in the adsorbent. After the heavy metal ions are adsorbed, a large amount of material accumulation can be seen on the surface defects of  $C_3N_4$ , and it can be inferred that the heavy metal elements have been adsorbed.

### High-Resolution Transmission Electron Microscope (UHRTEM) Analysis

Fig. 5 is the UHRTEM image of Cu(II) adsorbed by  $C_3N_4$ . According to the image obtained by high-resolution transmission electron microscope and energy spectrum analysis, it can be clearly observed from the characterization image that Cu(II) fills part of the defects, and it can be seen from the energy spectrum, Cu(II) is enriched in the defects of  $C_3N_4$  surface. so it can be inferred that Cu(II) is successfully adsorbed on the  $C_3N_4$  surface.

### Atomic Force Microscopy (AFM) Analysis

Fig. 6 A, B, C, and D are the AFM images of  $C_3N_4$  after adsorbing Nd, Th, Cd, and Co, respectively. It can be seen from the 3D diagram in Fig. 4-6 that  $C_3N_4$  has an obvious three-dimensional structure. In addition, in the 2D image, the

color depth can represent the height of the area, the darker area has a larger height, and the darker area has a smaller height. According to the above method, the three-dimensional structure of  $C_3N_4$  can also be observed. As shown in Fig. 4-6 A2 and C2, the height of  $C_3N_4$  is about 3.3nm, while Fig. 4-6 B2 and D2 show that the height of  $C_3N_4$  is about 1.6nm. This may be due to the partial overlap of  $C_3N_4$  in the A2 and C2 pictures, resulting in a large difference in local thickness.

### CONCLUSION

Based on the above analysis, this paper describes the preparation and characterization process of  $C_3N_4$ , and explores the adsorption performance of  $C_3N_4$  on heavy metals such as Nd, Th, Co, Cu, and focuses on the optimal pH, the amount of adsorbent, and reaction kinetics experiment was carried out. Finally, the adsorption effect of  $C_3N_4$  on a variety of heavy metals was analyzed through the characterization image. conclusion as below:

- (1) The adsorbent  $C_3N_4$  was prepared by thermally peeling melamine, and it was characterized by SEM-EDS, TEM, and other methods. The results showed that the material

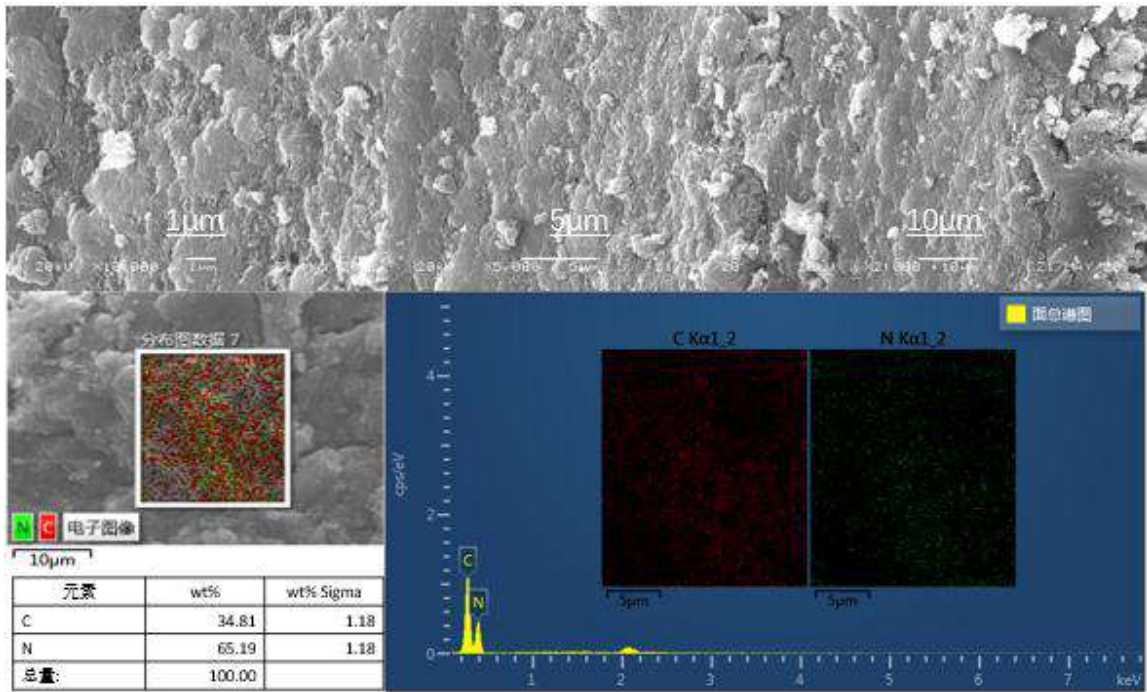


Fig. 2: SEM-EDS image of C<sub>3</sub>N<sub>4</sub>.

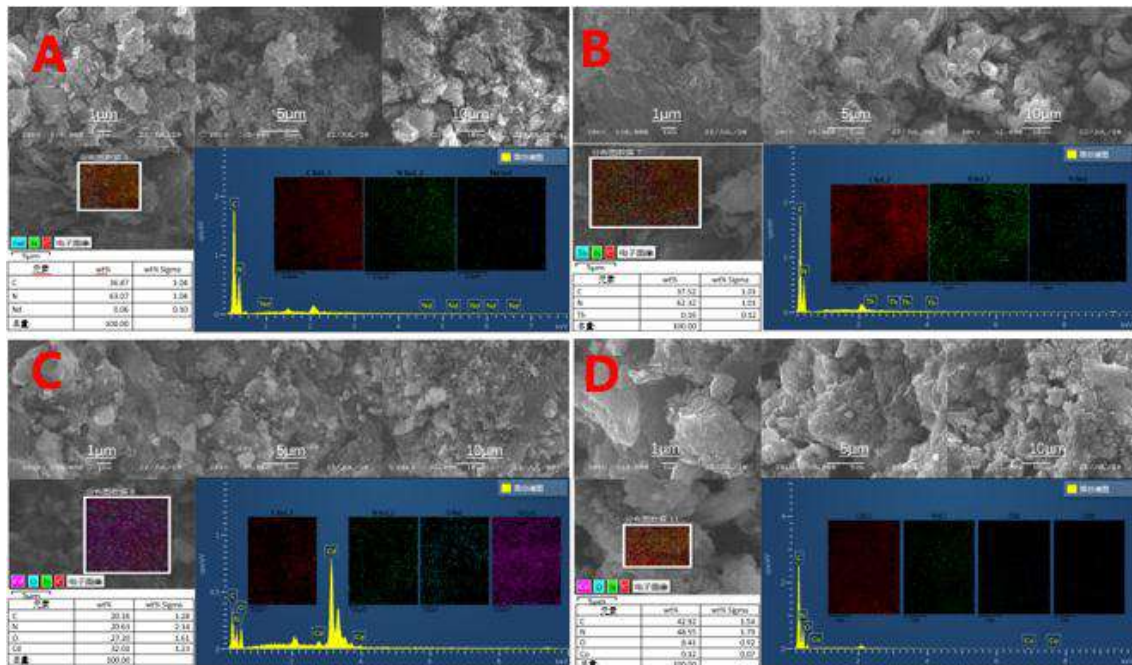


Fig. 3: SEM-EDS image of Nd adsorbed by C<sub>3</sub>N<sub>4</sub> (A), SEM-EDS image of Th adsorbed by C<sub>3</sub>N<sub>4</sub> (B), SEM-EDS image of Cd adsorbed by C<sub>3</sub>N<sub>4</sub> (C), SEM-EDS image of Co adsorbed by C<sub>3</sub>N<sub>4</sub> (D).

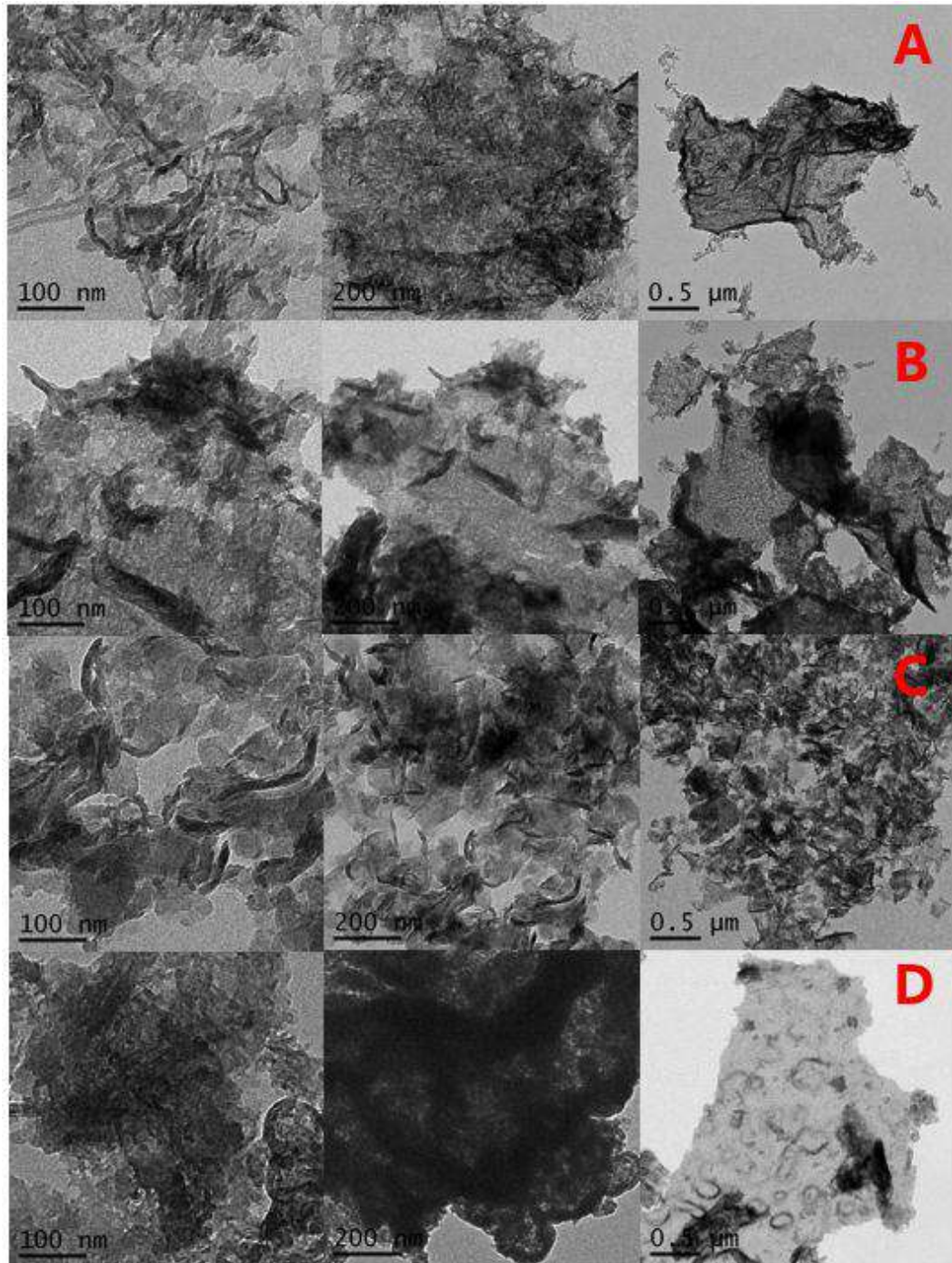


Fig. 4: TEM image of  $C_3N_4$  (A), TEM image of  $C_3N_4$  after adsorption of Cu (B), Pb (C), and Zn (D), respectively.

has a clear lamellar structure, the dispersion is relatively uniform, and the state of layered accumulation is not obvious.

(2) Using  $C_3N_4$  as the adsorbent, it adsorbed heavy metal

elements such as Nd, Th, Co, Cu, etc. And through SEM, TEM, UHRTEM, AFM, and other characterization methods. It is proven that  $C_3N_4$  has relatively good adsorption performance for heavy metal elements.

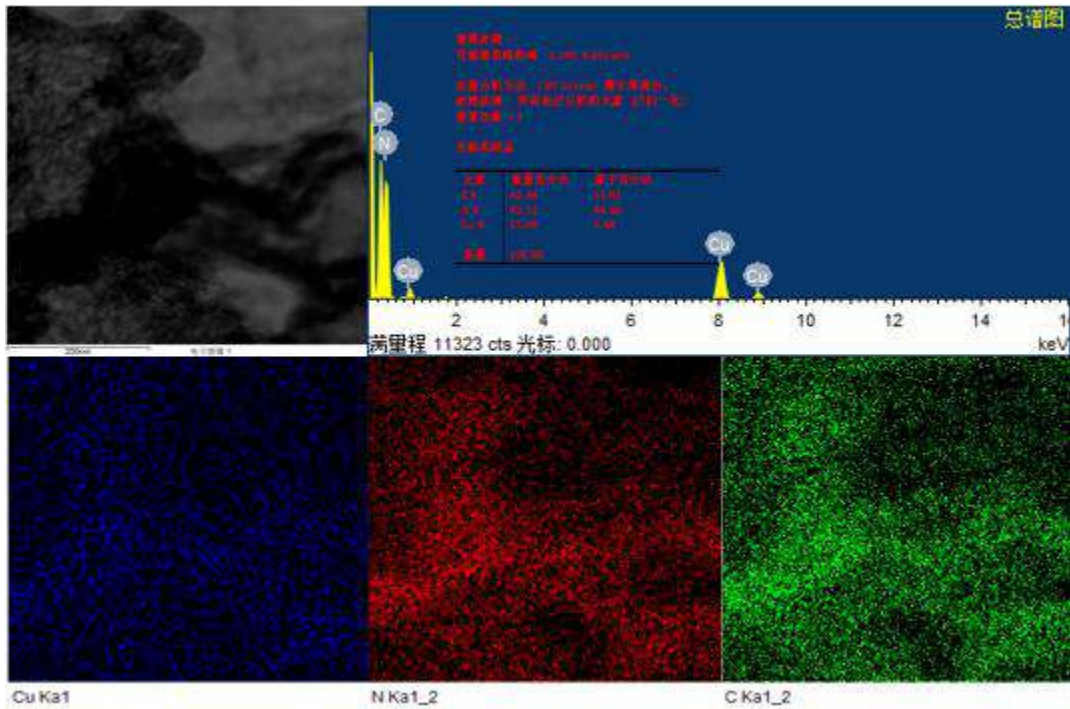


Fig. 5: UHRTEM image of Cu adsorbed by C<sub>3</sub>N<sub>4</sub>.

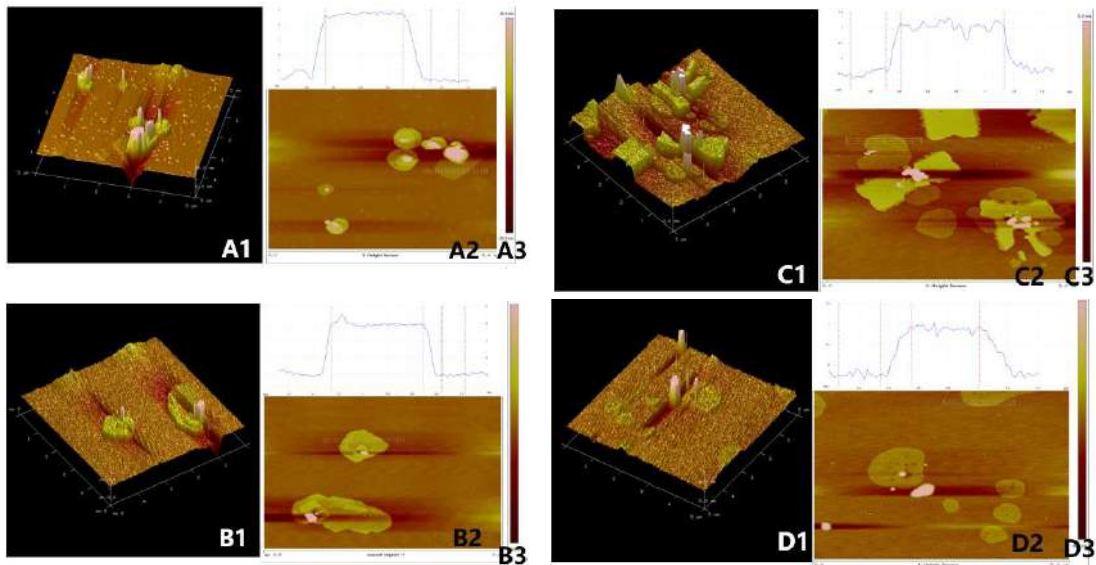


Fig. 6: AFM image after C<sub>3</sub>N<sub>4</sub> adsorbed Nd (A), AFM image after C<sub>3</sub>N<sub>4</sub> adsorbed Th (B), AFM image after C<sub>3</sub>N<sub>4</sub> adsorbed Cd (C), AFM image after C<sub>3</sub>N<sub>4</sub> adsorbed Co (D).

(3) Based on the C<sub>3</sub>N<sub>4</sub> adsorbent, the influencing factors such as pH, adsorbent dosage, and heavy metal ion concentration for the adsorption of Nd and Th are explored. Finally, combined with pH=5.5, adsorbent mass of 80 mg, and Nd solution concentration of 80

ppm, the adsorption experimental kinetics of the Nd element is explored. Similarly, under the conditions of pH=3, adsorbent mass equal to 40mg, and Th solution concentration of 40 ppm, Exploring the dynamics of Th element. The investigation results show that the kinetic

fitting of the adsorption experiment is in accordance with the pseudo-second-order model fitting, indicating that the adsorption experiment is chemical adsorption.

## REFERENCES

- Ahmad, Z.U., Yao, L., Wang, J., Gang, DD., Islam, F., Lian, Q. and Zappi, M.E. 2019. Neodymium embedded ordered mesoporous carbon (OMC) for enhanced adsorption of sunset yellow: Characterizations, adsorption study, and adsorption mechanism. *Chem. Eng. J.*, 359: 814-826.
- Alekseeva, O.V., Bagrovskaya, N.A. and Noskov, A.V. 2016. Sorption of heavy metal ions by fullerene and polystyrene/fullerene film compositions. *Prot. Met. Phys. Chem. Surf.*, 52(3): 443-447.
- Bali, M and Tlili, H. 2019. Removal of heavy metals from wastewater using infiltration-percolation process and adsorption on activated carbon. *Int. J. Environ. Sci. Technol. (IJEST)*, 16(1): 249-258.
- Chen, J., Wu, H., Xu, L., Li, M., Du, K. and Sheng G. 2021. New insights into colloidal GO, Cr (VI), and Fe (II) interaction by a combined batch, spectroscopic, and DFT calculation investigation. *J. Mol. Liq.*, 337: 116365.
- Hu, X., Peng, Q., Zhang, W., Ye, W. and Wang, H. 2020. Preparation of g-C<sub>3</sub>N<sub>4</sub> nanosheets photoelectrode and its photoelectrocatalytic activity for tetracycline degradation. *J. Mater. Eng.*, 48(12):82-89. (in Chinese)
- Islam, A., Ahmad, H., Zaidi, N. and Kumar, S. 2014. Graphene oxide sheets immobilized polystyrene for column preconcentration and sensitive determination of lead by flame atomic absorption spectrometry. *ACS Appl. Mater. Interfaces*, 6(15): 13257-13265.
- Li, H., Li, Y., Lee, M. K., Liu, Z. and Miao, C. 2015. Spatiotemporal analysis of heavy metal water pollution in transitional China. *Sustainability*, 7(7): 9067-9087.
- Li, Z., Ma, Z., van der Kuijp, T. J., Yuan, Z. and Huang, L. 2014. A review of soil heavy metal pollution from mines in China: pollution and health risk assessment. *Sci. Total Environ.* 468: 843-853.
- Liao, Q., Yan, S., Linghu, W., Zhu, Y., Shen, R., Ye, F., Feng, G., Dong, L., Asiri, A.M., Marwani, H.M., Xu, D., Wu, X. and Li, X. 2018. Impact of key geochemical parameters on the highly efficient sequestration of Pb (II) and Cd (II) in water using g-C<sub>3</sub>N<sub>4</sub> nanosheets. *J. Mol. Liq.*, 258: 40-47.
- Shen, C., Chen, C., Wen, T., Zhao, Z., Wang, X. and Xu, A. 2015. The superior adsorption capacity of g-C<sub>3</sub>N<sub>4</sub> for heavy metal ions from aqueous solutions. *J. Colloid Interface Sci.*, 456: 7-14
- Talip, Z., Eral, M. and Hiçsönmez, Ü. 2009. Adsorption of thorium from aqueous solutions by perlite. *J. Environ. Radioactiv.*, 100(2): 139-143.
- Tian, X., Li, T., Yang, K., Xu, Y., Lu, H. and Lin, D. 2012. Effect of humic acids on physicochemical property and Cd (II) sorption of multiwalled carbon nanotubes. *Chemosphere*, 89(11): 1316-1322.
- Wang, X., Liang, Y., An, W., Hu, J., Zhu, Y. and Cui, W. 2017. Removal of chromium (VI) by a self-regenerating and metal-free g-C<sub>3</sub>N<sub>4</sub>/graphene hydrogel system via the synergy of adsorption and photo-catalysis under visible light. *Appl. Catal. B: Environ.*, 219: 53-62.
- Wu, H., Chen, J., Xu, L., Guo, X., Fang, P., Du, K., Shen, C. and Sheng, G. 2021. Decorating nanoscale FeS<sub>2</sub> onto metal-organic framework for the decontamination performance and mechanism of Cr (VI) and Se (IV). *Colloids Surf. A: Phys. Eng. Aspects*, 625: 126887.
- Xu, J., Wang, H. and Liu, Y. 2016. Ecological risk assessment of heavy metals in soils surrounding oil waste disposal areas. *Environ. Monit. Assess.*, 188(2): 125.
- Zheng, W., Li, X.M., Yang, Q., Zeng, G.M., Shen, X., Zhang, Y. and Liu, J. 2007. Adsorption of Cd(II) and Cu(II) from aqueous solution by carbonate hydroxylapatite derived from eggshell waste. *J. Hazard. Mater.*, 147(1-2): 534-539
- Zhao, G., Li, J., Ren, X., Chen, C. and Wang, X. 2011. Few-layered graphene oxide nanosheets as superior sorbents for heavy metal ion pollution management. *Environ. Sci. Technol.*, 45(24): 10454-10462.
- Zheng, Y., Jiao, Y., Chen, J., Liu, J., Liang, J., Du, A., Zhang, W., Zhu, Z., Smith, S.C., Jaroniec, M., Lu, G.Q. and Qiao, S. Z. 2011. Nanoporous graphitic-C<sub>3</sub>N<sub>4</sub>@ carbon metal-free electrocatalysts for highly efficient oxygen reduction. *J. Am. Chem. Soc.*, 133(50): 20116-20119.
- Zhang, X., Xie, X., Wang, H., Zhang, J., Pan B. and Xie Y. 2013. Enhanced photoresponsive ultrathin graphitic-phase C<sub>3</sub>N<sub>4</sub> nanosheets for bioimaging. *J. Am. Chem. Soc.*, 135(1): 18-21.





# Ganga and Yamuna Rivers: Through the Lens of the National Green Tribunal

N. Siddiqui\*†, T. Faiyaz\*\* and V. S. Tari\*\*\*

\*CHRIST (Deemed to be University), Delhi-NCR, India

\*\*Rajiv Gandhi School of Intellectual Property Law, Indian Institute of Technology, Kharagpur, W. B., India

\*\*\*University of Mumbai, Sub-Centre, Ratnagiri, Maharashtra, India

†Corresponding author: N. Siddiqui; nabeela.siddiqui@res.christuniversity.in

**Nat. Env. & Poll. Tech.**  
Website: [www.neptjournal.com](http://www.neptjournal.com)

Received: 17-09-2021

Revised: 02-12-2021

Accepted: 18-12-2021

## Key Words:

Water quality  
NGT Act  
Ganga river  
Yamuna river

## ABSTRACT

Despite the country's extensive environmental jurisprudence and many historic rulings in which the courts have rescued worsening environmental situations, river (Ganga and Yamuna) water does not match the mandated minimum "bathing quality." Rivers like the Ganga and Yamuna, which flow through numerous states and towns, would be in a different situation. Without strict monitoring and enforcement of the measures, no action plan can work. Punishment of defaulters can serve as deterrence while also instilling fear in other non-compliant enterprises. In comparison to environmental legislation, the NGT Act allows for substantially harsher fines and penalties. River rejuvenation plans must be carefully monitored to ensure that they do not suffer the same fate. Making action plans will not improve river water quality unless they are implemented with sincerity and consistency, as well as continuous monitoring and severe enforcement.

## INTRODUCTION

The Ganga (Ganges) basin covers more than 1 million square kilometers and is made up of parts of India (roughly 80% of the basin area), Nepal, China, and Bangladesh. The key channel is 2,525 kilometers long, with altitudes ranging from 8,848 meters in the high Himalayas to sea level in India and Bangladesh's coastal deltas. The basin covers a fifth of India's total land area and is one of the most populous regions on Earth. The River Yamuna is the Ganga's main tributary. It starts at a height of 6,387 meters on the southwestern slopes of the Banderpooch peaks in the uppermost area of the Lower Himalaya in Uttarkashi, Uttarakhand State, and travels approximately 1,376 kilometers through Uttarakhand, Himachal Pradesh, Delhi, Haryana, and Uttar Pradesh until finally meeting the Ganges at Triveni Sangam, Prayagraj.

The Ganga Action Plan began cleaning the river Ganga in 1985 (GAP) and in 1993, the Yamuna Action Plan (YAP) was created. Sewerage/drain interception and diversion, sewage treatment plants (STPs), low-cost sanitation/community toilet complexes, and electric/improved wood crematoria were among the projects undertaken. The Central Government formed the National Ganga River Basin Body (NGRBA) in 2009 as an empowered planning, funding, monitoring, and coordinating authority for the Ganga River to achieve successful pollution abatement and river conservation through

a comprehensive strategy. On the 13th of May, 2015, the Cabinet approved the Namami Gange policy as a holistic strategy to rejuvenate the Ganga and all of its tributaries by combining current ongoing activities and preparing a clear action plan for the future (Xun et al. 2017). There is no special scheme for the rejuvenation of the river Yamuna since the Namami Gange policy encompasses all of the Ganga's tributaries, including the Yamuna, which is one of them. Since the mid-1980s, river cleaning campaigns have failed to either recover or replace our waterways (Xun et al. 2017).

## THE SCALES OF JUSTICE

The issue before the court in the famous case of M. C. Mehta Vs Union of India (AIR 1988 SC1037: (1987) 4 SCC463) in 1985 was that tanneries in Uttar Pradesh were discharging industrial effluents into the Ganga without treatment (M. C. Mehta vs. Union of India, n.d.). In light of this, the Supreme Court (SC) issued a slew of orders prohibiting tanneries from polluting the Ganga. The court also ordered that water and effluents be treated before being dumped into the Ganga (M.C. Mehta vs Union Of India & Ors on 12 January 1988, n.d.). The Supreme Court has ordered tanneries in and near the Ganga basin to install effluent treatment plants and emissions control systems. The Apex Court has set a six-month deadline for these directives to be implemented.

The Supreme Court invoked Article 48-A of the Constitution, which requires the state to protect and enhance the natural environment. Each citizen of India has a constitutional obligation under Article 51-A to conserve and conserve the natural environment (Hashim 2013). In this context, the court remembered the passage of the Water (Prevention and Control) Act 1974, the Environment (Protection) Act 1986, and the circumstances that led to the UN Conference on the Human Environment's proclamation in Stockholm in 1972 (Balaji 2008). The court received expert advice from a group of scientists on the construction of the sewage treatment system. To set up treatment plants, the annual turnover of the tanneries was taken into account. In *M.C. Mehta Vs Union of India*, the Supreme Court addressed the issue of riparian rights (AIR 1988, SC 1115). In another important decision of the High Court of Allahabad in *S. K. Garg Vs State of Uttar Pradesh* (AIR 1999, ALL 21), the important issue was about safe drinking water, as the Ganga and Yamuna rivers were polluted to the point that the water was unsafe to drink. The Supreme Court of India ordered the National Environmental Engineering Research Institute (NEERI) to prepare a study on the contamination caused by tanneries in the Eastern part of Calcutta, such as Tangra, Tiljala, Tapsia, and Pagla Danga, in *M.C. Mehta Vs Union of India* (1997(2) SCC 411) (*Eastern Book Company - Practical Lawyer*, n.d.). The study reported that there was a systemic lack of waste control and recycling and that none of the tanneries had a proper drainage system.

## DEVOLUTION OF THE PRINCIPLES

### Polluter Pays Principle

In the well-known case of *M. C. Mehta Vs Union of India* (AIR 1987 SC1086), the Supreme Court of India, when reviewing the extent of remedies available under Article 32 provided guidelines for human rights protection and broadening the horizons of Article 21 of the Constitution, held that the right to live implicitly includes the right to seek compensation for pollution victims (United Nations. Office of the High Commissioner for Human Rights 2013, Vilhena et al. 2013). The Polluter Pays Principle is the most critical of the three important concepts outlined in Section 20 of the NGT Act, 2010, namely, the "principles of sustainable growth, precautionary principle, and the polluter pays principle," under which the National Green Tribunal (NGT) determines the amount of punitive and monetary penalties and issues a reasoned warrant, verdict, or award (Dutta & Purohit 2015, Gill 2016, Rengarajan et al. 2018, The National Green Tribunal Act, 2010 2013).

Simply stated, it means that the harm caused by contamination should be mitigated by the person who caused the

damage and that the person who caused the damage should pay the whole cost (Polluter-Pays Principle n.d.). The core premise is to ensure that environmental costs are internalized while keeping the public interest and natural environment protection in mind, without risking long-term growth and future by imposing a fee on environmental breaches. In this sense, this admirable Principle must aid in the quantification and determination of criminal fines and costs, allowing for the calculation of compensation dependent on environmental breaches incurred by persons or businesses, as well as the establishment of maximum values for allowable discharges (Barrett et al. 2019, Beder 2013, Ebbesson 2009, Martin-Ortega et al. 2011). The idea of environmental justice is a noble philosophy that allows restitution for losses caused by emissions, and it is under this theory that the National Green Tribunal compensates for the destruction of the natural ecosystem (Choudhry et al. 2016, Gill 2016). The National Green Tribunal (NGT), in the case of *Samir Mehta vs Union of India and Others* (Before the National Green Tribunal, Principal Bench, New Delhi, O. A. No. 24 of 2011, Decided On: 23.08.2016), applied the Polluter Pays Principle and ordered the Respondent to compensate for the environmental harm.

This polluter pays principle takes its authority from the European Community environmental policy on waste management adopted in the year 1973 (Johnson & Corcelle 1995, Lister 1996, Lowe & Ward 2005, Mazzucco et al. 2020, Tanil 2021). The Court of Justice has unanimously decided that the owner of the property where waste is dumped is the owner of the waste as defined by the definition and therefore liable (Court of Justice, case C-365/97 Commission v. Italy, (1999) ECR I-7773). The member states, on the other hand, have the final say in deciding where these stations will be built (Kjellstrom et al. 2006). In the *H. Acid* case (1996 3 SCC 212 at 247), the Supreme Court established the polluter pays principle by invoking the principles of the European Community Treaty on Environment under Article 130 R(2), which allows the state to give mandatory directions under the provisions of the Environment Act. In the above case, the Supreme Court ordered the government to take appropriate action against polluting factories that generated extremely radioactive acidic waste (Lister 1996). As a result, the cost of penalties and fines was transferred from the government to the polluting companies. The polluter pays theory was upheld by the Supreme Court in this instance, stating that the polluter is responsible for the harm caused by environmental pollution (Polluter-Pays Principle n.d.).

In the case of *Manoj Mishra Vs Union of India and Others*, the NGT ordered the Civic and Municipal authorities of Delhi to levy property taxes on any home, which included

finer or compensation for the Yamuna River pollution abatement. In *Krishan Kant Singh vs National Ganga River Basin Authority* (2014), the NGT ordered the defaulting industrial unit to pay a fee of Rupees Five Crores to the concerned State Pollution Control Board based on the Polluter Pays Principle for performing remedial practices to ensure river safety in its judgment delivered on October 16, 2014. In another case, *R K Patel Vs Union of India*, the NGT ordered environmental compensation of Rupees Ten Lakhs to the aggrieved farmers in Vapi, Gujarat, due to hazardous waste contamination in a judgment issued on February 18, 2014.

### **The Doctrine of Public Trust**

The philosophy of public trust can be traced back to Roman law, and it is founded on the righteous idea that all natural resources are public property, with ownership rights vesting in humanity as a whole. According to Roman law, no one owns these properties solely (*res nullus*), but the common citizens of the society have vested ownership rights (*res communis*). The English common law, on the other hand, stipulated that the Sovereign retained possession, though restricted (Wehmeier 2021). The Crown was considered to be holding resources eligible for this use of confidence for the public's benefit. The Supreme Court of India enunciated this noble concept in *M.C. Mehta Vs Kamal Nath and Others* ((1997) I SCC388), which has served as the foundation for Indian environmental law (Balaji 2008). In yet another case (*M. C. Mehta Vs Union of India* (Span Motel cases), 1997(1) SCC388), the Supreme Court addressed the doctrine of public confidence in greater depth, reinforcing the people's right to natural capital (Sivaramakrishnan 2011). The noble ideal enshrined in this theory was that individuals in a society as a whole have the right to possession, as opposed to the principle of private ownership. Natural resources, according to the philosophy, are public land, and so the general public can benefit (Adler 2021).

### **ANALYZING THE FUNDAMENTALS OF THE ISSUE**

River Ganga is a symbol of Indian faith and tradition, and it is regarded as so pure that it has been dubbed the "elixir of life." For millions of devotees of Indian civilization, the holy water of the Ganga has the greatest religious significance (Victor 2017). The Ganga is the epitome of the Indian subcontinent's long-standing traditions, history, and civilizational ideals (Kumar 2017). The river Ganga has aided the development of Indian society, and it is properly regarded as the emblem of Indian culture, tradition, and faith, as well as its importance (Ahmed & Sinha 2014). For centuries, Ganga, the founder of righteousness and holiness, has become a constant source of purification of the inner as well as inner selves of humankind

(Sanghi 2013). Despite its physical, natural, cultural, and religious importance, the Ganga River ranks tenth among the world's most polluted rivers (Trivedi & Trivedi 2014). The Ganga has a total length of 2,525 kilometers and is significant in that it has influenced India's culture, personality, religious values, and economy, as well as being the world's fourth-largest river basin (Meena 2020). The Uttarakhand High Court, in a well-known judgment (Mohd. Salim v. State of Uttarakhand & Others, Writ Petition (PIL) No. 126 of 2014, decided on March 20, 2017), highlighted the importance of the Holy Rivers Ganga and Yamuna, holding that the rivers Ganges and Yamuna are worshipped by Hindus and are very sacred and revered.

The proliferation of pharmaceutical and other industries, as well as other practices such as dumping waste and other hazardous substances directly into river systems in urban areas, have harmed the ecosystem, climate, livelihood, and lifestyle of millions of people in many states where these rivers flow (Trivedi & Trivedi 2014). Rivers have long been important to human development around the world, and the Ganga river basin has made a significant contribution to the growth of the human population and, as a result, to rapid urbanization (Fig. 1). As a result, the towns and cities that the Ganges flows through, as well as thousands of villages, have become the primary source of pollutants because they spill their untreated or maltreated waste products, such as sewage and human and animal carcasses, totaling more than 6 billion liters, directly into the Ganges (Maji & Chaudhary 2019). This is compounded by the reality that many factory setups, mills, and tanneries drain untreated industrial sewage and wastewater directly into the Ganges, amounting to 260 million liters every day. In addition, according to a report by the Ministry of Water Resources, River Development, and Ganga Rejuvenation, 6 million tonnes of chemical fertilizers and 9000 tonnes of pesticides used in agricultural fields along the Ganga basin were dumped directly into the Ganga garbha (Dutta et al. 2020). As a result, the Central Pollution Control Board (CPCB) has come to the disturbing conclusion that the Ganga at Kanpur, Allahabad, and Varanasi has become one of the world's most polluted rivers. Thousands of people bathe in the Ganga River every day as part of their religious rituals. The National Green Tribunal (NGT) has issued timely health alerts about the dangers of bathing in the polluted Ganga and has directed that the health hazards be displayed along the Ganga's banks between Haridwar and Unnao (Ganga water is injurious to health! NGT says Holy river should carry warnings like cigarettes, 2018, 28).

### **RIVER POLLUTION AND ACTION PLANS**

The term pollutant is defined by the Environment (Protec-



Fig. 1: Sources of 'The Ganga' River Pollution.

tion) Act of 1986 as any harmful material contained in the environment that has the potential to harm the environment or ecosystem. The amount of waste caused by anthropogenic contaminants that enter the Ganga daily is unfathomable. However, the Central Pollution Control Board, which has been assigned the duty to report the quality of rivers since 1980, has provided estimations in a report in the year 2017, and as per the report, the situation is alarming. According to a more recent study titled "Biological Water Quality Assessment of the River Ganga (2017-18)" released in June 2018, water quality sampling was performed in the states of Uttarakhand, Uttar Pradesh, Bihar, and West Bengal, and the situation was found to be more troubling than ever. This report was later declassified by the CPCB as a result of a Supreme Court judgment mandating that all CPCB findings on the state of health, climate, and emissions be made public. The report concluded that different factors such as Biochemical Oxygen Demand (BOD), Chemical Oxygen Demand (COD), Dissolved Oxygen (DO), temperature, pH, total coliforms, fecal coliforms, and others influence the quality of water in a given region.

The 1986 Environment (Protection) Act regulates the regulation, mitigation, and abatement of water contamination. Section 17 of the Act also states that the government offices, by the Head of the Agency, are solely responsible for any breach of the legislation by the department. The Central Pollution Control Board recommended the establishment of the

Central Ganga Authority in 1981-1982 in its comprehensive report on Ganga pollution, and the Ganga Action Plan (GAP) was launched in 1985 with the primary goal of cleaning the Ganga (Xun et al. 2017). In the year 1985, the Government of India under the aegis of the Ministry of Environment and Forest (MoEF) as it then was called, launched Ganga Action Plan (GAP) Phase-1 to address and abate the increasing pollution of the river Ganga and the initiatives were taken to clean the Ganga. This proposal was later expanded to cover all other waterways, and the National River Conservation Plan (NRCP) was officially initiated in December 1996 to determine the extent of the contamination. As early as 1983, the urgency of the massive issue of river contamination was addressed in depth by U. N. Mahida.

The influx of vast amounts of untreated domestic and industrial wastes is the primary source of Ganga contamination. Since the factories in the area still lack adequate effluent and sewage treatment units, the people living along the Ganga basin, which number over 300 million, are the most affected (Sanghi 2013, Trivedi & Trivedi 2014, Xun et al. 2017). According to a 2015 World Bank study, domestic waste accounts for nearly 80% of the overall pollution in the Ganga, with just 15% coming from untreated agricultural waste and effluents. Despite successive governments investing thousands of crores of rupees in it, the Ganga Action Plan failed to meet its target, despite the government's lofty statements. And, as we can see today, the holy Ganga is

always filthy, as it has always been (Sinha & Prasad 2020). The River Boards Act was passed in 1956, and the River Boards were formed to provide advice to the government on river pollution management. The law has no impact since the Board's function in terms of water quality is purely advisory.

The Factories Act of 1948 (Great Britain 1948) contains provisions for the treatment of waters and effluents by factories. Sec. 12 of the Act is significant in that it requires industries to dispose of properly handled hazardous waste and effluents efficiently. It also gives the state government the authority to make any laws or arrangements necessary to reduce emissions. Non-observance or non-compliance with the requirements of Sec.12 and other laws made under the Act are subject to a general punishment under Sec. 92 of the Act. Untreated industrial effluents can contain extremely toxic chemical compounds. Toxic wastes pollute rivers as untreated sewage water is released into them (Great Britain 1948, MONAPPA2012, Panda 2012). Food manufacturing and the food goods industries contribute a significant amount of toxins. It is a reality that many large and medium-sized food manufacturing businesses lack adequate waste and effluent treatment facilities on their premises.

## **GANGA RIVER POLLUTION THROUGH THE LENS OF NGT ORDERS**

The National Green Tribunal (M.C. Mehta vs. Union of India, ORIGINAL APPLICATION NO. 200 OF 2014 (C.WRIT PETITION No.3727/1985) (M.A. No. 594/2017 &598/2017, Decided on 13.07.2017) has gone into great depth about the shortcomings in the implementation of GAP-I and GAP-II, citing supporting reports and evidence. It went on to say that it needs to find a path forward that is free of certain flaws and capable of achieving the goal of cleaning and rejuvenating the Ganga. The Indian Institute of Technology (IIT) Consortium, other technical experts, the stakeholders' consultative mechanism, the Tribunal's Principal Committee, and finally the Tribunal itself all agree that ad-hocism was a major factor in making GAP I and GAP II inefficient and unsuccessful.

The Ganga River Basin Management Plan (GRBMP) prepared by the seven IIT consortiums for National Ganga River Basin Authority (NGRBA) proposed a separate statute and constitutional mechanisms and further recommended the establishment of the National River Ganga Basin Management Commission (NRGBMC). It's pointless to handle either the hotspots or one or two parts of a city along the riverbank while allowing all the drains carrying mixed waste to flow into the river. Even where a Sewage Treatment Plant/ Common Effluent Treatment Plant (STP/CETP) is built to handle effluents or sewage, it connects to other larger drains

downstream, resulting in heavily contaminated treated water (Bharati et al., 2016; Smakhtin, 2006; Tchobanoglous et al., 1991). There must be a systemic solution that will assist in cleaning the whole section on a watershed basis rather than the specific location, which may be a highly polluting spot, but addressing it alone without taking any necessary measures for pollution prevention and control will be of little concern and would yield ineffective results (Agarwal & Agarwal, 2021; Singh et al., 2019).

The Tribunal would take a systematic approach rather than one that cannot withstand review in terms of technical, science, and application. The lessons learned in the past must be shared by all parties so that they do not make the same errors and waste public funds indiscriminately, avoiding waste of public funds on the one hand and increased emissions on the other. The tribunal also went into great depth on end-of-pipe disposal. The need of the hour is to disinfect the river as quickly as possible, and for that, care of the drains that enter the river and hold mixed effluents should take precedence (Agarwal & Agarwal, 2021; Singh et al., 2019). This is also consistent with the river basin approach, which treats the whole river basin, including tributaries and storm drains that enter the river, as a single organic body. The Tribunal had extensive discussions with all stakeholders, and the only sensible decision that emerged and is most reasonable is that drain-wise treatment should be used instead of city cleaning, particularly where cities include a variety of planned, unplanned, haphazard construction, and slum areas.

However, the river has stayed polluted, increasing emission levels such as heavy metals like arsenic, hexavalent chromium, fluoride, iron, and other sediment contaminants (Pandey et al. 2015). So, bearing in mind the magnitude of the issue and to expedite the cleaning operation, and measuring the urgency and significance of the task of cleaning Ganga, the National Democratic Alliance, which has been in power in the government since mid-May 2014, has launched a new program popularly known as the Namami Gange Programme (NGP). As a result, the government has urged the Ganga's five basin states to work together to revitalize the river. The project was expected to cost more than Rs. 20,000 crores, with a task deadline of 2019, which has now been pushed back to 2020. There are logistical issues with cleaning the Ganga, including a lack of proper coordination inside and across the different government ministries. On the 10th/18th December 2015, the court issued a comprehensive order in the case of 'Indian Council for Enviro Legal Action Vs National Ganga River Basin Authority (Original Application No. 10 of 2015), in which the demarcation of the floodplain, restricted consumer, and restriction of 100 meters from the center of the river was discussed and instructions were given (Gill 2016).

The National Green Tribunal in *Social Action for Forest and Environment (Safe) Vs Union of India & Ors.* (Original Application No. 87 of 2015, Decided on 02.03.2017), while considering different issues, including whether there is an immediate need for the full shutdown of camping activities in the River Ganga basin in the Rishikesh district (Original Application No. 87 of 2015, Decided on 02.03.2017). Since they were causing irreversible air and water contamination in the River Ganga and the surrounding regions, the court ruled that all operations would be carried out in compliance with the rules. In a 2017 order reprimanding the government, its functionaries, and other stakeholders, the National Green Tribunal stated emphatically that "... not a single drop of river Ganges has been cleaned thus far, and just wasting public resources." As a result, it is abundantly clear that a stringent, open, and accountable framework within the system is needed for the cleaning of the Ganga, as well as proper management of funds appropriately and productively.

### **YAMUNA RIVER POLLUTION THROUGH THE LENS OF NGT ORDERS**

River Yamuna flows south and east through the states of Uttarakhand, Haryana, Delhi (UT), and Uttar Pradesh, with major cities/towns along the known polluted stretch being Gautam Budh Nagar, Bulandshahar, Aligarh, Vrindavan, Mathura, Agra, Firozabad, Etawah, and Kalpi. Hamirpur and Prayagraj contribute to the contamination of the Yamuna River. On the banks of this Priority-1-polluted stretch of the Yamuna, there are 121 villages. The catchment area's waste and effluent are discharged into the River Yamuna by 35 drains, 18 of which are mixed and 17 of which are solely domestic. Sugar, Pulp & Paper, Distillery, Textile, Slaughterhouses, and other factories are very polluting (Rout 2017).

In Mathura, there is a textile industrial cluster with 30 Saari Washing & Printing Units at Site-A, UPSIDC, Industrial Area, Mathura. Around 20 are currently in operation, whereas the other 10 remain closed for various reasons. The installed capacity of CETP Mathura is 6.5 MLD, but due to the self-closure of industries, only 3.0 MLD is currently being used. The treated effluent is discharged in the urban drain (Ambakhar Drain), which eventually contributes to the river Yamuna and has been partly tapped and diverted to STP Trans-Yamuna. The objective of the Action Plans is to rejuvenate the quality of this priority -1 polluted stretch of River Yamuna to be fit for at least bathing purposes within 06 months from the date of action plan gets approved, as directed by Hon'ble National Green Tribunal vide its order dated 20th September 2018 passed in the original Application No 673/2018 in the matter of News Item Published In 'The

Hindu' Authored By Shri Jacob Koshy titled "More river stretches are now critically polluted".

Both water-polluting factories will be continuously regulated by three agencies: the UPPCB, the District Ganga Committee/Zila Paryavaran Samiti, and reputable third-party institutions. The District Ganga Committee/Zila Paryavaran Samiti will track GPIs periodically, and other industries will be tracked at random. CPCB and NMCG will both entrust Third Party Institutions with the burden of robust oversight. In addition, District Ganga Committees/Zila Paryavaran Samitis, with adequate Magisterial and Police assistance, will conduct a campaign to identify and close illicit factories existing in non-conforming areas. The National Green Tribunal directed that a Control Room be built in Agra with proper facilities and human resources for monitoring and coordinated reporting of numerous pollution sources.

The control room will be managed by the UP Pollution Control Board with the assistance of District Ganga Committees/Zila Paryavaran Samitis and will be supervised by the Commissioner of Agra. District Ganga Committees / Zila Paryavaran Samitis can hire JRFs/Monitoring Assistants on a contractual basis for monitoring purposes, with financial assistance from the District Ganga Committees/Zila Paryavaran Samitis. Educational/Technical Institutions and Colleges will also be known for their assistance in pollution source control and remediation. The Pollution Control Board will also develop the capacity for tracking pollution sources among students at such established institutions and colleges. The proposed surveillance would be carried out from the Control Room using a Web Portal to which field monitoring data would be submitted. The UP Pollution Control Board was suggested to create a Web Portal with access shared with District Ganga Committees/Zila Paryavaran Samitis for easier access to the portal.

### **COVID-19, THE LOCKDOWN, AND ITS EFFECTS ON THE RIVERS**

The spread of the novel coronavirus known as COVID-19 has resulted in unparalleled degrees of adversity. Around the same time, it is a cause for celebration because it has resulted in a reduction in air and water emissions. The self-cleaning property of the river improved during the nationwide lockdown period (Vinaya & Karthik 2021). Rivers have never been cleaner or clearer than they are right now. Rivers have a normal ability to clean themselves up by consuming massive quantities of oxygen, but the amount of garbage pumped into them regularly, whether commercial or otherwise, obstructs this mechanism, and they become unclean in the long run. According to a study by the Asian Development Research Institute (ADRI), approximately 70% of surface

water supplies were severely degraded beyond repair, with a total of 40 million liters of uncontrolled municipal pollution and wastewater entering rivers and other water bodies every day, just 37% of it is properly handled. The lockdown took just weeks to accomplish this feat of a cleaner Ganga and Yamuna, which governments have failed to achieve despite investing thousands of crores over decades. It is clear that the rivers have finally been able to breathe after such a long time of national shutdown, and the Ganga and Yamuna rivers have been healthier than ever before, with the water quality of these rivers exceeding expectations. This change can be credited to the nationwide lockdown imposed by Covid-19, as a result of which events such as tourism, fairs, swimming, and cloth washing near the ghats ceased, resulting in a poisonous load being removed from the river and the full cessation of untreated industrial waste discharge has improved the Ganga's water quality.

## CONCLUSION

Environmental conservation in India has largely failed, especially when it comes to rivers and urban water bodies. The cleaning of the Ganga and Yamuna rivers is a monumental challenge that necessitates top-down and bottom-up policies that include all stakeholders and leave no stone unturned. Cities discharge millions of gallons of untreated or partly treated wastewater into urban lakes and waterways to complete the hydrological cycle. As a result, India's waterways are heavily polluted and often eroded into foul-smelling streams, posing considerable ecological and health risks (Rout 2017). Using a bottom-up strategy will mean using a common collection of parameters to evaluate all stakeholders' success across the networks to identify compliance challenges that could emerge in the future rather than judging how they occurred previously. It would also make it easier to meet regulatory goals cost-effectively.

Many analysts have raised concerns about violations of environmental laws and regulations, especially about shortcomings and inconsistencies in environmental clearances provided by the Ministry of Environment and Forests (MoEF) and emission control systems (Panigrahi et al. 2012, Karpouzoglou 2011). Indian state authorities, especially the Ministry of Environment and Forests (MOEF) and the Central Pollution Control Board (CPCB), have publicly admitted that institutional frameworks and regulatory enforcement to protect the environment are inadequate (CPCB 2006, 2010, MoEF 2009). Although large-scale riverfront developments are encouraged across India as ecological restoration projects, the construction of iconic and aesthetic riverfronts takes precedence, and river restoration projects are largely unsuccessful in terms of ecological restoration (Desai 2012, Follmann 2015).

The accountable ministry would work to improve the phase-by-phase execution of these policies. There is also a pressing need to investigate why the government of India's numerous policies over the decades have failed to yield the desired results. Thousands of crores of rupees have been spent on various schemes to clean the Ganga and Yamuna rivers, but none of them have met their objectives. Furthermore, in addition to the continuing plans to clean the Ganga and Yamuna, these can be exacerbated with small-scale, phase and location-specific, low-cost, and long-term solutions. The Central Government, State Governments, and their respective agencies, as well as the Judiciary, must develop an integrated Ganga and Yamuna River management strategy (Tortajada 2014). This will necessitate a thorough knowledge of the Ganga and Yamuna basin's geography, history, ecology, policy, geology, anthropology, society, culture, and economy (Helmer & Hespanhol 1997).

The government's efforts would eventually be a civil-society initiative in which people's constructive participation is paramount. At various levels, such as policymaking, execution, supervision, and management of an integrated program to clean the Ganga and Yamuna, there should be active cooperation with and among different stakeholders such as politicians, scientists, civil society, and religious leaders. Climate change effects on the Ganga and Yamuna Rivers, as well as the environment around them, should be assessed. In brief, a holistic approach to urban river ecological rejuvenation is a pressing problem for India's long-term urban growth and environmental governance (Uberoi 2004). Environmental advocacy has stressed the natural integrity of waterways and the intimate river-city interactions, even though state actors do not see it that way.

## REFERENCES

- Adler, R. 2021. Natural resources and natural law part ii: the public trust doctrine. *Michigan J. Environ. Adm. Law.*, 10(1): 225. <https://doi.org/10.36640/mjeal.10.1.natural>.
- Agarwal, Y. and Agarwal, G.K. 2021. *Water an element of life: Price sensitivity and consumption by marginalized*. Bloomsbury Publishing, London, UK.
- Ahmed, B. and Sinha, RK. 2014. *Rivers for life: Proceedings of the International Symposium on River Biodiversity: Ganges-Brahmaputra-Meghna River System*. IUCN, Gland, Switzerland.
- Balaji, V. 2008. *Environment and Human Rights Law: An Indian Perspective*. In: Eberhard, C. (ed.), *Law, Land Use and the Environment: Afro-Indian Dialogues*. Institut français de Pondichéry, Pudducherry, India, pp. 527-549. <https://doi.org/10.4000/books.ifp.3954>
- Barrett, A., Lawlor, J. and Scott, S. 2019. *The Fiscal System and the Polluter Pays Principle: A Case Study of Ireland*. Routledge, London.
- Beder, S. 2013. *Environmental Principles and Policies: An Interdisciplinary Introduction*. Routledge, London.
- Bharati, L., Sharma, B.R. and Smakhtin, V. 2016. *The Ganges River Basin: Status and Challenges in Water, Environment, and Livelihoods*. Routledge, London.

- Choudhry, S., Khosla, M. and Mehta, P.B. 2016. *The Oxford Handbook of the Indian Constitution*. Oxford University Press, Oxford.
- Dutta, R. and Purohit, S. 2015. *Commentary on the National Green Tribunal Act, 2010*.
- Dutta, V., Dubey, D. and Kumar, S. 2020. Cleaning the river Ganga: Impact of lockdown on water quality and future implications on river rejuvenation strategies. *Sci. Total Environ.*, 743: 140756. <https://doi.org/10.1016/j.scitotenv.2020.140756>
- Eastern Book Company - Practical Lawyer. (n.d.). Retrieved July 9, 2021, from <https://www.ebc-india.com/lawyer/articles/718.htm>
- Ebbesson, J. 2009. *Environmental Law and Justice in Context*. Cambridge University Press, MA.
- Gill, G.N. 2016. *Environmental Justice in India: The National Green Tribunal*. Taylor & Francis, NJ.
- Great Britain. 1948. *The Factories Act, 1948*. Universal Law Publishing, Delhi, India.
- Hashim, N.B. 2013. Constitutional recognition of the right to a healthy environment: the way forward. *Proced. Soc. Behav. Sci.*, 105: 204-210. <https://doi.org/10.1016/j.sbspro.2013.11.021>.
- Helmer, R. and Hespanhol, I. 1997. *Water Pollution Control: A Guide to the Use of Water Quality Management Principles*. CRC Press, Boca Raton, Florida.
- Johnson, S. and Corcelle, G. 1995. *The Environmental Policy of the European Communities*. Springer, Cham.
- Kjellstrom, T., Lodh, M., McMichael, T., Ranmuthugala, G., Shrestha, R. and Kingsland, S. 2006. Air and Water Pollution: Burden and Strategies for Control. In Jamison, D.T., Breman, J.G., Measham, A.R., Alleyne, G., Claeson, M., Evans, D.B., Jha, P., Mills, A. and Musgrove, P. (eds), *Disease Control Priorities in Developing Countries*, 2nd edition, Oxford University Press, New York, pp.825-826
- Kumar, D. 2017. River Ganges: Historical, cultural, and socioeconomic attributes. *Aqua. Eco. Health Mgmt.*, 20(1-2): 8-20. <https://doi.org/10.1080/14634988.2017.1304129>
- Victor, M. 2017. *River of Life, River of Death: The Ganges and India's Future*. Oxford University Press., Oxford, p. 71.
- Lister, C. 1996. *European Union Environmental Law: A Guide for Industry*. John Wiley & Sons Incorporated, NJ.
- Lowe, P. and Ward, S. 2005. *British Environmental Policy and Europe: Politics and Policy in Transition*. Routledge, London.
- Maji, K.J. and Chaudhary, R. 2019. Principal component analysis for water quality assessment of the Ganga river in Uttar Pradesh, India. *Water Resour.*, 46(5): 789-806. <https://doi.org/10.1134/s0097807819050129>
- Martin-Ortega, J., Brouwer, R. and Aiking, H. 2011. Application of a value-based equivalency method to assess environmental damage compensation under the European environmental liability directive. *J. Environ. Manag.*, 92(6): 1461-1470.
- Mazzucco, W., Costantino, C., Restivo, V., Alba, D., Marotta, C., Tavormina, E., Cernigliaro, A., Macaluso, M., Cusimano, R., Grammauta, R., Tramuto, F., Scondotto, S. and Vitale, F. 2020. The management of health hazards related to municipal solid waste on fire in Europe: an environmental justice issue? *Int. J. Environ. Res. Pub. Health*, 17(18): 617. <https://doi.org/10.3390/ijerph17186617>
- M. C. Mehta vs. Union of India. (n.d.). Retrieved July 9, 2021, from <https://www.cla.auburn.edu/envirolitigators/litigation/ganga-pollution-case-mehta/m-c-mehta-vs-union-of-india/>
- M.C. Mehta vs Union Of India & Ors on 12 January 1988. (n.d.). Retrieved July 9, 2021, from <https://indiankanon.org/doc/59060/>
- Meena, R.P. 2020. *Indian And World Geography: Current Affairs Yearbook*. IAS Insights, Delhi, India
- Monappa, A. 2012. *Industrial Relations and Labour Laws*. Tata McGraw-Hill Education, NY.
- Panda, B. 2012. *Industrial Safety, Health Environment, and Security*. University Science Press (USP), Sausalito, CA, United States.
- Polluter-Pays Principle. (n.d.). Retrieved July 8, 2021, from <https://www.sciencedirect.com/topics/earth-and-planetary-sciences/polluter-pays-principle>
- Rengarajan, S., Palaniyappan, D., Ramachandran, P. and Ramachandran, R. 2018. National green tribunal of India-an observation from environmental judgments. *Environ. Sci. Pollut. Res. Int.*, 25(12): 11313-11318.
- Rout, C. 2017. Assessment of water quality: A case study of river Yamuna. *Int. J. Earth Sci. Eng.*, 10(2): 398-403. <https://doi.org/10.21276/ijee.2017.10.0239>
- Sanghi, R. 2013. *Our National River Ganga: Lifeline of Millions*. Springer Science & Business Media, NY. <https://doi.org/10.1007/978-3-319-00530-0>.
- Singh, A., Saha, D. and Tyagi, A. C. 2019. *Water Governance: Challenges and Prospects*. Springer.
- Sinha, R. K. and Prasad, K. 2020. Management of Water Quality and Biodiversity of the River Ganga. In: Gunawardena, E.R.N., Gopal, B. and Kotamaga, H. (eds.) *Ecosystems and Integrated Water Resources Management in South Asia* (pp. 104-132). <https://doi.org/10.4324/9781003157847-5>
- Sivaramakrishnan, K. 2011. Environment, law, and democracy in India. *J. Asian St.*, 70(4): 905-928. <https://doi.org/10.1017/S0021911811001719>
- Smakhtin, V.Y. and Anputhas, M. 2006. *An Assessment of Environmental Flow Requirements of Indian River Basins*. International Water Management Institute (IWMI), Delhi, India.
- Tanil, G. 2021. *Environmental Sustainability: Water and Waste Management Policy in the European Union and the Czech Republic*. Rowman & Littlefield, Lanham, Maryland, US.
- Vinaya, T. and Karthik K.V.M. 2021. COVID-19 Pandemic: Its Origin, Implications, and Effect of Lockdown on Environment. In Pasupuleti, D.S.R.M. and Nakkella, D.A.K (eds.), *Health, Hygiene, Sanitation and Environment at Pandemic Times*, Immortal Publication, Vijaywada, AP, India, pp. 187-201.
- The National Green Tribunal Act, 2010. 2013. Universal Law Publishing, Delhi, India.
- Tortajada, C. (ed.). 2014. *Water Quality Policy and Management in Asia*. Routledge, London.
- Trivedi, R.C. and Trivedi, R.C. 2014. Water Quality Challenges in Ganga Basin, India: In *Our National River Ganga* (pp. 189-210). [https://doi.org/10.1007/978-3-319-00530-0\\_7](https://doi.org/10.1007/978-3-319-00530-0_7)
- Uberoi, N.K. 2004. *Environmental Management*. Excel Books India, Kerala, India.
- United Nations. Office of the High Commissioner for Human Rights. 2013. *Realizing the Right to Development: Essays in Commemoration of 25 Years of the United Nations Declaration on the Right to Development*. United Nations Publications, New York.
- Vilhena, O., Baxi, U. and Viljoen, F. (eds.) 2013. *Transformative Constitutionalism: Comparing the Apex Courts of Brazil, India and South Africa*. Pretoria University Law Press (PULP), Pretoria, SA.
- Wehmeier, N. (ed). 2021. *Oxford Advanced Learner's Dictionary*. Oxford University Press, Oxford.
- Xun, W., James, W.R. and Oraorn, P. 2017. *Ganga Rejuvenation: Governance Challenges and Policy Options*. World Scientific Publishers, Singapore. <https://doi.org/10.1142/9715>





# Population Structure of *Thrips parvispinus* Karny (Thysanoptera: Thripidae) and Population Abundance of Predatory Insect on Red Chili (*Capsicum annum* L.) Treated with Imidacloprid Insecticide

I.W. Supartha<sup>†\*</sup>, A. Roifiq<sup>\*\*</sup>, I.W. Susila<sup>\*</sup>, I.M. Damriyasa<sup>\*\*\*</sup>, M. Tulung<sup>\*\*\*\*</sup>, I.K.W. Yudha<sup>\*\*\*\*\*</sup>,  
I.W.E.K. Utama<sup>\*\*\*\*\*</sup> and P. A. Wiradana<sup>\*\*\*\*\*</sup>

\*Laboratory of Integrated Pest Management (IPMLab), Faculty of Agriculture, Udayana University, Jln. PB. Sudirman Denpasar City (80231), Bali, Indonesia

\*\*Agroecotechnology Program, Faculty of Agriculture, Udayana University, Jln. PB. Sudirman Denpasar City (80231), Bali, Indonesia

\*\*\*Faculty of Veterinary Medicine, Udayana University, Jln. PB. Sudirman Denpasar City (80231), Bali, Indonesia

\*\*\*\*Faculty of Agriculture, Sam Ratulangi University, Jalan Bahu, Malalayang, Manado City, North Sulawesi, Indonesia

\*\*\*\*\*Doctoral Student of Agriculture Sciences, Land Agriculture Graduate Program, Faculty of Agriculture, Udayana University, Jln. PB. Sudirman Denpasar (80231), Bali, Indonesia

\*\*\*\*\*Study Program of Biology, Faculty of Health, Science and Technology, Universitas Dhyana Pura, Jln. Raya Padangluwih, North Kuta (80361), Badung, Bali, Indonesia

<sup>†</sup>Corresponding author: I. W. Supartha; yansupartha@yahoo.com

Nat. Env. & Poll. Tech.  
Website: [www.neptjournal.com](http://www.neptjournal.com)

Received: 27-10-2021  
Revised: 07-01-2022  
Accepted: 24-01-2022

## Key Words:

Population density  
*Capsicum annum*  
*Thrips parvispinus*  
Ecotoxicology  
Imidacloprid  
Insecticide contamination

## ABSTRACT

In Indonesia, the pest *Thrips parvispinus* Karny is a major problem for red chili plants. Most pest control techniques rely on synthetic pesticides, resulting in environmental degradation, the extinction of natural enemies, and the emergence and resilience of a variety of different pests. The aim of this study is to determine the impact of a 25% Imidacloprid insecticide on population density and the proportion of infestations and natural enemies in the field. A randomized block design with 5 treatments and 5 replications was utilized in this field investigation. Plant samples were collected in a "U-shaped" pattern. According to the findings, a 25% Imidacloprid pesticide had a significant influence on population density and *T. parvispinus* attack on red chili plants. Moderate damage was caused by *T. parvispinus*' infestation on red chili plants using 50-200 L.ha<sup>-1</sup> 25 % Imidacloprid pesticide. Furthermore, a 25 % Imidacloprid insecticide applied at a rate of 100 L.ha<sup>-1</sup> had a significant influence on the population variety and abundance of *T. parvispinus* natural enemies. A 25 % Imidacloprid insecticide dosage increase was shown to have a very strong relationship with a reduction in population density, the proportion of *T. parvispinus* assault, and the variety and quantity of natural enemies in red chili. Thus, a 25 % Imidacloprid insecticide at a rate of 100 L.ha<sup>-1</sup> proved successful in reducing *T. parvispinus* while remaining safe for natural enemies. Future pest control techniques must still be based on improved field data collection, such as data on pesticide contamination or other anthropogenic chemicals, which may also be used to estimate natural enemy population levels in the field.

## INTRODUCTION

Red chili (*Capsicum annum* L.) is one of the top national commodities generating public income and state foreign exchange in the non-oil and gas sector. Compared to its potential production of more than 20 tons.ha<sup>-1</sup>, the average red chili yield per farmer in 2015 was 8.65 tons.ha<sup>-1</sup> (BPS 2015). The infestation of *Thrips parvispinus* Karny in every growing season causes low red chili yield (Johari et al. 2016). These pests target red chili shoots, young leaves, and flowers

by inserting their stylets into the epidermal tissue, palisade tissue, and mesophyll cells to extract nutrients from the plant fluid (Merta et al. 2017). The brown-turned silvery spots are typical symptoms of a normal infestation on the foliage. Damage to the leaves can interfere with the photosynthesis process, resulting in a reduction in leaf photosynthesis rate (Gassmann 2004). Curling leaves and stunted terminal shoots are two more indications of this pest infestation (Tyagi et al. 2015).

Classical biological management utilizing imported exotic natural enemies has a long history of effectiveness in controlling target pest populations in many nations (Horrocks et al. 2020). Natural enemies from predatory groups may be employed to naturally control these pests (van Lenteren 2012, Duan et al. 2015, Barratt et al. 2018, Supartha et al. 2020). Natural enemies, for example, are reported to have had a significant part in at least a 50% decrease in pest infestation on certain agricultural fields, which contribute US\$13 billion in ecosystem benefits in the United States each year (Losey & Vaughan 2006).

However, if biological control measures fail to manage certain pests, further management methods, such as synthetic pesticides are required. In 2003-2005, Prabaningrum & Moekasan, (2008) reported the control activities on red chili planting in the West Bandung Regency, Indonesia with agrochemicals such as Imidacloprid insecticide. In Indonesia, rice farmers have been using imidacloprid pesticides since 1994 (Thorburn 2015). This pesticide is good and efficient against pests such as whitefly and aphids (Hartwig et al. 1991). According to Firmansyah et al. (2014), of five imidacloprid insecticide doses namely 3,200 g.ha<sup>-1</sup>, 1,600 g.ha<sup>-1</sup>, 800 g.ha<sup>-1</sup>, 400 g.ha<sup>-1</sup>, and 200 g.ha<sup>-1</sup>, the suggested amount for controlling brown leafhoppers was 800 g.ha<sup>-1</sup>. In another case, the imidacloprid pesticide was well-known for its effectiveness in suppressing the Silverleaf whitefly, *Bemisia tabaci* (Hemiptera: Aleyrodidae) (Setiawati et al. 2007). In addition to the pesticide Imidachloride, there is another insecticide with the active ingredient Fipronil 50 g.L<sup>-1</sup> that considerably lowers the dominance and diversity index of the yellow rice stem borer, *Scirpophaga incertulas* Walker (Lepidoptera: Pyralidae) and their abundance of parasitoids, especially at higher doses (Putra et al. 2017).

This field study aimed to assess the efficiency of 25% Imidacloprid insecticide in suppressing the population of thrips, as well as its effect on the population diversity and abundance of *T. parvispinus* on red chili (*Capsicum annum L.*). In terms of the use of synthetic pesticides that impact the balance of insects in agricultural landscapes, these results may be useful information, particularly for farmers and relevant authorities. Additionally, environmental and human health must be emphasized via the application of Integrated Pest Management.

## MATERIALS AND METHODS

### Study Area

This study was carried out in Kerta Village, Payangan District, Gianyar Regency, Bali Province, on a *T. parvispinus*-attacked red chili (Pilar variety) plantation owned by local farmers. The study site is located 850 meters above sea

level with temperatures ranging from 26 to 28°C and 77% humidity. Meanwhile, the laboratory-scale study was carried out at IPM Lab, Faculty of Agriculture, Udayana University, Denpasar-Bali.

### Research Design

This study used Randomized Block Design with five treatment doses of 25% Imidacloprid insecticide: 50 g/ha, 100 g.ha<sup>-1</sup>, 150 g.ha<sup>-1</sup>, and 200 g.ha<sup>-1</sup>, and the control (no insecticide) in five replications. The total land area is 1,440 m<sup>2</sup> with a bed area of 36 m<sup>2</sup>. The plant population per bed was 144 plants, with a spacing of 50 cm × 45 cm. The number of plants sampled per bed was ten with a "U" (U-shape) sampling technique. When the red chili plants were 4 weeks old after planting (wap) or 10 *T. parvispinus* nymphs were identified per plant, the 25% Imidacloprid pesticide was applied once a week for a total of ten applications using a high-pressure sprayer.

### Population Density

The population density of *T. parvispinus* was observed on three selected red chili blooms. *T. parvispinus* population density (PD) is determined using the following formula:

$$\text{Population density} = \frac{\text{number of individuals}}{\text{area (m}^2\text{)}}$$

### Percentage of Attack

The percentage of attack was determined using six leaves namely every two leaves from the bottom, middle, and top of the red chili plant. The percentage of attack (P) is calculated using the formula:

$$P = \frac{\text{number of affected leaves (a)}}{\text{total number of leaves observed (b)}}$$

### Diversity of Natural Enemies

Shannon-Weaver's natural enemy diversity formula (Price, 1984) :

$$H' = \sum Pi \log Pi = \sum \left( \frac{ni}{N} \log \frac{ni}{N} \right)$$

Where:

$H'$  = Diversity Index

$Pi$  =  $ni/N$  (the number of i-species individuals divided by the total number of individuals).

$ni$  = Number of i-species individuals

$N$  = Total number of individuals

The observation was performed by collecting specimens, documenting, and photographing the type and quantity of predators encountered in the field once a week for identification in the laboratory.

**Data Analysis**

ANOVA (SPSS 23.0, IBM, USA) was used to evaluate data on population density and the proportion of *T. parvispinus* assaults on plants, as well as the index of population diversity and predator abundance on red chili. If the treatment has a significant effect on the observed variables, the Least Significant Difference (LSD) test at a 5% level (P<0.05) will be conducted. Meanwhile, regression analysis was performed to investigate the relationship between demographic data and the proportion of infestations (MS Excel 2019, Microsoft Windows USA).

**RESULTS AND DISCUSSION**

**Population Density**

Based on the results, *T. parvispinus* population density decreased from 7 weeks after planting (wap) to 13 wap. This happened as a result of 25% Imidacloprid insecticide application in lowering *T. parvispinus* population density on red chili plants (Table 1). This is supported by Abdel Farag El-Shafie (2020) that pest population density may be

reduced by application-based control methods. The 25% Imidacloprid has a high effectiveness value for eliminating insects including aphids, peach aphids, armyworms, rice ear bugs, and brown leafhoppers, and is generally safe because of its minimal toxicity to mammals (Saharan et al. 2014). In addition to affecting the density of insect populations, exposure to imidacloprid for 35 days affects the physiology of crops and is easily concentrated on the shoots of vegetables which are generally used as a source of nutrition by several invasive pests in the field (Li et al. 2019).

The results are supported by Supartha et al. (2002) that pesticides with systemic and contact characteristics can impair the growth and development of insect larvae. The decrease in population density of *T. parvispinus* at the 10 to 13 Week after Planting (WAP) was assumed to be related to the physical traits (the developed plant tissue, a decrease in the food supply, and the appearance of red chili plants. Histological, physiological, and behavioral effects of exposure to low doses of the insecticide Imidacloprid were also investigated in *Drosophila melanogaster* and these findings indicate that oxidative stress is a key factor in the process of action of this insecticide by generating Ca<sup>2+</sup> fluxes that enter neurons and increase levels of relative oxygen species (ROS) in fly larvae brain (Martelli et al. 2020).

Table 1: The effect of 25% imidacloprid insecticide on population density of *T. parvispinus* in red chili plants.

Treatment Dose (g.ha <sup>-1</sup> )	Population density of <i>T. parvispinus</i> [m <sup>2</sup> ]									
	Week after planting (WAP)									
	4	5	6	7	8	9	10	11	12	13
200	14.9 a	14.6 a	13.1 a	11.8 a	11.7 a	11.3 a	10.2 a	8.4 a	6.6 a	4.3 a
150	15.0 a	14.6 a	14.1 a	12.2 ab	11.9 a	11.7 a	10.7 a	8.9 a	7.2 a	4.6 a
100	15.3 a	14.8 a	14.3 a	12.9 ab	12.4 ab	13.0 ab	12.1 b	9.7 ab	7.9 a	5.3 a
50	15.4 a	15.5 a	15.8 b	13.5 b	13.1 b	14.0 b	13.4 b	11.2 b	10.0 b	6.7 b
0	15.5 a	16.1a	16.1 b	17.2 c	19.1 c	23.1 c	20.0 c	17.3 c	13.0 c	8.6 c

Note: the numbers followed by the same letter in the same column show no significant difference in the *Least Significant Different* (LSD) Test at the 5% level (<0.05).

Table 2: The effect of 25% imidacloprid insecticide on percentage of attack index in red chili plants.

Treatment Dose (g/ha)	Week after planting (WAP)									
	4	5	6	7	8	9	10	11	12	13
200	15.7 a	16.0 a	15.7 a	12.9 a	11.0 a	10.3 a	9.3 a	6.5 a	6.2 a	4.4 a
150	15.9 a	16.2 a	16.4 a	14.1 ab	11.9 a	11.7 a	9.9 a	7.4 a	6.2 a	4.5 a
100	16.3 a	16.2 a	16.8 ab	15.0 b	14.1 b	14.5 b	11.6 b	10.0 b	7.4 ab	4.8 a
50	17.1 a	17.4 a	17.6 ab	15.8 b	14.7 b	15.6 b	12.8 b	11.6 b	8.1 b	5.3 a
0	17.5 a	17.6 a	19.1 b	21.0 c	21.9 c	25.9 c	22.5 c	17.3 c	12.9 c	8.7 b

Note: the numbers followed by the same letter in the same column show no significant difference in the *Least Significant Different* (LSD) Test at the 5% level (<0.05).

### Percentage of Attack Index

Based on the results of data analysis, the effect of 25% Imidacloprid insecticide on the percentage of attack was substantially different between the control and the treatment studied. From top to lowest, the percentage of attacks was 50 g.ha<sup>-1</sup>, 100 g.ha<sup>-1</sup>, 150 g.ha<sup>-1</sup>, and 200 g.ha<sup>-1</sup> (Table 2). The 25% Imidacloprid insecticide, used as a contact and systemic poison against *T. parvispinus*, has the potential to block the signal flow that would otherwise travel to the receiving neuron, making it impossible for the nerve to receive messages spontaneously. As a result, insects suffer paralysis leading to death (Wang et al. 2008, Khoa et al. 2018).

### Diversity of Natural Enemies Index

Based on the results, 25% Imidacloprid insecticide to the diversity of natural enemies at 50 g.ha<sup>-1</sup> to 150 g.ha<sup>-1</sup> doses were not significantly different from the control treatment. These results indicated that the insecticide had no significant effect on natural enemies, especially predatory insects. This can be seen in 50 g.ha<sup>-1</sup> and 150 g.ha<sup>-1</sup> doses that several types of predatory insects were still able to survive. However, not all types of natural enemies can survive at high doses, for example, at 200 g.ha<sup>-1</sup> doses, the predatory

insects significantly decreased compared to the control. This is presumably because several types of predatory insects exposed to the 25% Imidacloprid insecticide were unable to maintain the viability of the toxic nature at the highest concentration (Table 3). The 25% Imidacloprid insecticide can penetrate the bodies of insects by systemic and contact poisoning (Kreutzweiser et al. 2008).

### The Abundance of Natural Enemies

Based on the results, 25% Imidacloprid insecticide had a significant effect compared to the control, especially at 100 g.ha<sup>-1</sup>, 150 g.ha<sup>-1</sup>, and 200 g.ha<sup>-1</sup> (Table 4). The unwise use of synthetic insecticides (especially non-selective ones) can reduce the population of insect pests and can adversely affect the decrease in the abundance of natural enemy populations in fields (El-Wakeil et al. 2013, Gödel et al. 2020, Gesraha & Ebeid 2021).

### Relationship Between 25% Imidacloprid Insecticide Dose and Population Density and Percentage of Attack

The R<sup>2</sup> value of population density and percentage of attack was 0.6708 and 0.9137, respectively (Fig. 1). These results indicated a positive and very strong relationship between the 25% Imidacloprid Insecticide and population density as well

Table 3: The effect of 25% imidacloprid insecticide on diversity of natural enemies index in red chili plants.

Treatment Dose (g.ha <sup>-1</sup> )	Week after planting (WAP)									
	4	5	6	7	8	9	10	11	12	13
200	0.60 a	0.59 a	0.59 a	0.56 a	0.56 a	0.56 a	0.55 a	0.52 a	0.51 a	0.48 a
150	0.56 a	0.61 a	0.62 ab	0.64 ab	0.64 ab	0.64 ab	0.62 ab	0.60 ab	0.60 ab	0.58 a
100	0.57 a	0.61 a	0.63 ab	0.64 ab	0.66 b	0.67 b	0.65 ab	0.64 b	0.63 ab	0.60 a
50	0.60 a	0.65 a	0.65 ab	0.69 ab	0.70 b	0.68 b	0.68 b	0.70 b	0.65 b	0.61 a
0	0.59 a	0.66 a	0.69 b	0.73 b	0.73 b	0.74 b	0.72 b	0.71 b	0.64 b	0.61 a

Note: the numbers followed by the same letter in the same column show no significant difference in the Least Significant Different (LSD) Test at the 5% level (<0.05).

Table 4: The effect of 25% imidacloprid insecticide on abundance index of natural enemies in red chili plants.

Treatment Dose (g.ha <sup>-1</sup> )	Week after planting (WAP)									
	4	5	6	7	8	9	10	11	12	13
200	11,1 a	11,6 a	10,8 a	10,1 a	10,1 a	9,5 a	9,6 a	8,5 a	8,7 a	8,2 a
150	10,8 a	11,3 a	11,5 a	12,1 a	11,8 a	12,2 b	11,6 b	10,9 b	9,7 a	9,0 ab
100	10,8 a	11,4 a	12,1 ab	12,4 a	12,3 a	12,2 b	12,2 b	11,7 b	10,3ab	9,0 ab
50	12,3 a	12,9 a	13,8 ab	15,0 b	15,0 b	16,3 c	14,8 c	13,9 c	11,9bc	10,7 bc
0	11,9 a	13,3 a	15,0 b	15,4 b	16,1 b	16,9 c	16,3 c	15,4 c	12,4 c	11,2 c

Note: the numbers followed by the same letter in the same column show no significant difference in the Least Significant Different (LSD) Test at the 5% level (<0.05).

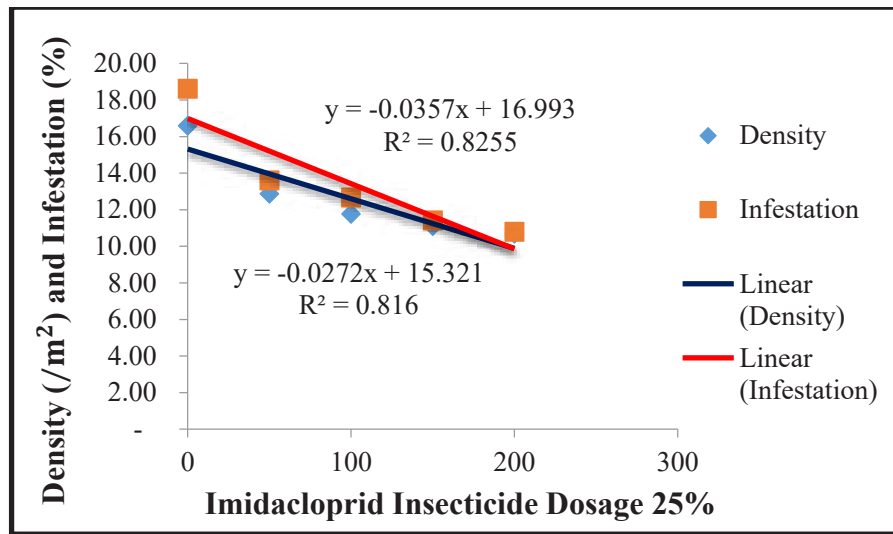


Fig. 1: Relationship between 25 % Imidacloprid insecticide dose with population density and percentage of attack.

as attack percentage. Thus, 25% Imidacloprid Insecticide was very effective in suppressing population density and the percentage of *T. parvispinus* attack on red chili plants.

The decrease in population density and the percentage of attacks was in line with the increase in the tested dose, meaning that the higher the dose applied, the lower the population density and the percentage of attacks. The population decrease was caused by the direct effect of the 25% Imidacloprid insecticide either by contact or systemically on the body of the insect (Sanchez-Bayo et al. 2013, Pisa et al. 2021). The 25% Imidacloprid insecticide had a strong influence on the types of insect pests in eating, grating, and

sucking (Ahmed et al. 2014). The way the insecticide works is very compatible with the behavior of *T. parvispinus* attacking leaves and flowers, namely by grinding and sucking the liquid from the leaves and flowers of red chili plants containing 25% Imidacloprid insecticide. This is supported by Summers et al. (2004) that the 25% Imidacloprid insecticide is effective in suppressing population density and the attack of aphids on red chili plants.

**Relationship Between 25% Imidacloprid Insecticide dose and the Diversity and Abundance of Natural Enemies**

The R<sup>2</sup> value of diversity and abundance of natural enemies

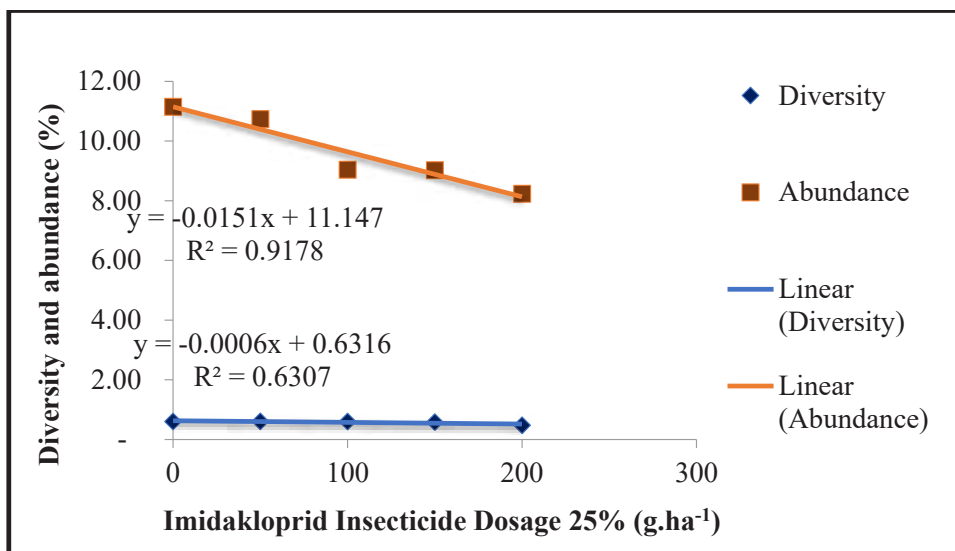


Fig. 2: The relationship between 25% Imidacloprid insecticide and the diversity and abundance of *T. parvispinus* natural enemies.

was 0.6307 and 0.9178, respectively (Fig. 2). These results indicated a positive and very strong relationship between the 25% Imidacloprid Insecticide and the diversity and abundance of natural enemies. An increase in the dose of 25% Imidacloprid insecticide significantly decreased the abundance of natural enemies in red chili plantations. The use of selective insecticides even at high doses can have a negative effect on decreasing the abundance of natural enemies (Xiao et al. 2016). Insecticides cause species shift phenomena, trophic level simplification, and pest resurgence (Yamamuro et al. 2019). The overall density of predators applied with insecticides was lower than in the control plots (Janssen & Rijn 2021).

## CONCLUSION

The 25% Imidacloprid insecticide had a significant effect on population density and the attack of *T. parvispinus* on red chili plants. The percentage of *T. parvispinus* attack on red chili plants with the 25% Imidacloprid insecticide at a dose (50-200 L.ha<sup>-1</sup>) was included in the "mild damage" category. 25% Imidacloprid insecticide had a significant effect on the diversity and abundance of natural enemies at a dose of 100 g.ha<sup>-1</sup>. An increase in the dose of 25% Imidacloprid insecticide showed a very strong relationship to the decrease in population density, the percentage of *T. parvispinus* attack, and the diversity and abundance of natural enemies in red chili (*Capsicum annum* L.). Thus, 100 L.ha<sup>-1</sup> 25% Imidacloprid insecticide was effective in controlling *T. parvispinus* and safe for natural enemies.

It is still necessary to conduct further research on the contamination of 25% Imidacloprid insecticide on heavy metals in horticultural crops and their impact on human health, to provide important information on human health and the agricultural environment.

## ACKNOWLEDGEMENT

This study was carried out with the assistance of the Integrated Pest Management Laboratory (IPMLAB) of the Faculty of Agriculture, Udayana University. The authors would like to thank the Head of the Laboratory for their assistance. The authors are grateful to local farmers who have given permission for field research.

## REFERENCES

- Abdel Farag El-Shafie, H. 2020. Integrated Insect Pest Management. Pests Control and Acarology, Intech Open.
- Ahmed, S., Nisar, M.S., Shakir, M.M., Imran, M. and Iqbal, K. 2014. Comparative efficacy of some neonicotinoids and traditional insecticides on sucking insect pests and their natural enemies on BT-121 cotton crop. *J. Anim. Plant Sci.*, 24: 660-663.
- Barratt, B.I.P., Moran, V.C., Bigler, F. and van Lenteren, J.C. 2018. The status of biological control and recommendations for improving uptake for the future. *BioControl*, 63: 155-167.
- BPS. 2015. Production of Large Chilies, Cayenne Peppers, and Shallots in 2014. Indonesia.
- Duan, J.J., Bauer, L.S., Abell, K.J., Ulyshen, M.D. and Van Driesche, R.G. 2015. Population dynamics of an invasive forest insect and associated natural enemies in the aftermath of invasion: Implications for biological control. *J. Appl. Ecol.*, 52: 1246-1254.
- El-Wakeil, N., Gaafar, N., Sallam, A. and Volkmar, C. 2013. Side Effects of Insecticides on Natural Enemies and Possibility of Their Integration in Plant Protection Strategies. *Insecticides - Development of Safer and More Effective Technologies*, InTech Open.
- Firmansyah, A.S., Ratna, E.S. and Rahmini, 2014. Imidacloprid Insecticide Efficacy and Its Implications for Increasing Brown Planthopper Populations in Three Rice Varieties. IPB University, Bogor, Indonesia.
- Gassmann, A.J. 2004. Effect of photosynthetic efficiency and water availability on tolerance of leaf removal in *Amaranthus hybridus*. *J. Ecol.*, 92: 882-892.
- Gesraha, M.A. and Ebeid, A.R. 2021. Impact of indoxacarb and sulfur formulation on aphid and three specific predators in Okra fields. *Bull. Natl. Res. Cent.*, 45: 10.
- Gödel, B., Lemic, D. and Bažok, R. 2020. Alternatives to synthetic insecticides in the control of the Colorado potato beetle (*Leptinotarsa decemlineata* Say) and their environmental benefits. *Agriculture*, 10: 1-27.
- Horrocks, K.J., Ward D. and Suckling D.M. 2020. Can natural enemies of current insect pests provide biotic resistance to future pests? *Agric. For. Entomol.*, 22: 20-29.
- Janssen, A. and Rijn, P.C.J. 2021. Pesticides do not significantly reduce arthropod pest densities in the presence of natural enemies. *Ecol. Lett.*, 13: 819.
- Johari, A., Herlinda, S., Irsan, C. and Pujiastuti, Y. 2016. The phenomenon of thrips (Thysanoptera) attack on chili plant (*Capsicum annum* L.). *Am. J. Agric. Biol. Sci.*, 11: 103-109.
- Khoa, D.B., Thang, B.X., Liem, N., Van, H.N. and Kristensen, M. 2018. Variation in susceptibility of eight insecticides in the brown planthopper *Nilaparvata lugens* in three regions of Vietnam 2015-2017. *PLoS One*, 13: e0204962.
- Kreutzweiser, D.P., Good, K.P., Chartr, D.T., Scarr, T.A. and Thompson D.G. 2008. Toxicity of the systemic insecticide, imidacloprid, to forest stream insects and microbial communities. *Bull. Environ. Contam. Toxicol.*, 80: 211-214.
- van Lenteren, J.C. 2012. The state of commercial augmentative biological control: plenty of natural enemies, but a frustrating lack of uptake. *BioControl*, 57: 1-20.
- Li, Y., Long, L., Ge, J., Li, H., Zhang, M., Wan, Q. and Yu, X. 2019. Effect of Imidacloprid uptake from contaminated soils on vegetable growth. *J. Agric. Food Chem.*, 67: 7232-7242.
- Losey, J.E. and Vaughan, M. 2006. The economic value of ecological services provided by insects. *Bioscience*. 56: 311-323.
- Martelli, F., Zhongyuan, Z., Wang, J., Wong, C.O., Karagas, N.E., Roessner, U., Rupasinghe, T., Venkatachalam, K., Perry, T., Bellen, H.J. and Batterham P. 2020. Low doses of the neonicotinoid insecticide imidacloprid induce ROS triggering neurological and metabolic impairments in *Drosophila*. *Proc. Natl. Acad. Sci.*, 117: 25840-25850.
- Merta, I.N.M., Darmiati, N.N. and Supartha, I.W. 2017. Population development and plant damage by *Thrips parvispinus* Karny (Hemiptera: Aphididae) on the phenology of chili in the three elevation levels in Bali. *J. Trop. Agroecotechnol.*, 6: 414-422.
- Pisa, L., Goulson D., Yang, E.C., Gibbons, D., Sánchez-Bayo, F., Mitchell, E., Aebi, A., van der Sluijs, J., MacQuarrie, C.J.K., Giorgio, C., Long, E.Y., McField, M., Bijleveld van Lexmond, M. and Bonmatin, J.M. 2021. An update of the Worldwide Integrated Assessment (WIA) on systemic insecticides - Part 2: Impacts on organisms and ecosystems. *Environ. Sci. Pollut. Res.*, 28: 11749-11797.

- Prabaningrum, L. and Moekasan, T. 2008. Vertical distribution pattern of *Thrips Parvispinus* Karny (Thysanoptera: Thripidae) on pepper plants. *J. Hortik.*, 18: 852-19.
- Putra, I., Gede, F.M., Supartha, I.W. and Widaningsih, D. 2017. The influence of fipronil 50 g/l against population abundance and parasitization level of egg parasitoid of yellow rice stem borer in Tabanan District. *E-J. Agroekotek. Trop.*, 6: 459-468.
- Saharan, V.K., Pinjari, D.V., Gogate, P.R. and Pandit, A.B. 2014. *Advanced Oxidation Technologies for Wastewater Treatment*. Elsevier, The Netherlands.
- Sanchez-Bayo F., A. H. and Gok K. 2013. Impact of Systemic Insecticides on Organisms and Ecosystems. *Insecticides - Development of Safer and More Effective Technologies*, InTech.
- Setiawati, W., Budiarto, B. and Soetiarso, T. 2007. Selectivity of several insecticides against whitefly pests (*Bemisia tabaci* Genn.) and predator *Menochilus Sexmaculatus* Fabr. *J. Hortik.*, 17: 819-21.
- Summers, C.G., Mitchell, J.P. and Stapleton, J.J. 2004. Management of aphid-borne viruses and *Bemisia argentifolii* (Homoptera: Aleyrodidae) in Zucchini squash by using UV reflective plastic and wheat straw Mulches. *Environ. Entomol.*, 33: 1447-1457.
- Supartha, I.W., Rauf, A. and Sosromarsono, S. 2002. Population dynamics and attacks of *Liriomyza huidobrensis* (Blanchard) (Diptera: Agromyzidae) in potato plantation. *J. Agric. Sci.*, 21: 117-122.
- Supartha, I.W., Yudha, I.K.W., Wiradana, P.A. and Susila, I.W. 2020. Response of parasitoids to invasive pest *Phenacoccus manihoti* Matile-Ferrero (Hemiptera: Pseudococcidae) on cassava crop in Bali, Indonesia. *J. Biol. Divers.*, 21: 610-623.
- Thorburn, C. 2015. The rise and demise of integrated pest management in rice in Indonesia. *Insects*, 6: 381-408.
- Tyagi, K., Kumar, V., Singha, D. and Chakraborty, R. 2015. Morphological and DNA barcoding evidence for invasive pest thrips, *Thrips parvispinus* (Thripidae: Thysanoptera), newly recorded from India. *J. Insect Sci.*, 15: 105.
- Wang, Y., Chen, J., Zhu, Y.C., Ma, C., Huang, Y. and Shen J. 2008. Susceptibility to neonicotinoids and risk of resistance development in the brown planthopper, *Nilaparvata lugens* (Stål) (Homoptera: Delphacidae). *Pest Manag. Sci.*, 11: 414.
- Xiao, D., Zhao, J., Guo, X., Chen, H., Qu, M., Zhai, W., Desneux, N., Biondi A., Zhang, F. and Wang, S. 2016. Sublethal effects of imidacloprid on the predatory seven-spot ladybird beetle *Coccinella septempunctata*. *Ecotoxicology*, 25: 1782-1793.
- Yamamuro, M., Komuro, T., Kamiya, H., Kato, T., Hasegawa, H. and Kamada, Y. 2019. Neonicotinoids disrupt aquatic food webs and decrease fishery yields. *Science*, 80: 366: 620-623.







# Identification of Dominant Air Pollutants Over Hyderabad Using Principal Component Analysis (PCA)

N. Vasudha\*† and P. Venkateswara Rao\*\*

\*Department of Mathematics, Vasavi College of Engineering, Hyderabad, India

\*\*Department of Physics, Vasavi College of Engineering, Hyderabad, India

†Corresponding author: N. Vasudha; dr.nvasudha@gmail.com

Nat. Env. & Poll. Tech.  
Website: [www.neptjournal.com](http://www.neptjournal.com)

Received: 02-11-2021

Revised: 16-12-2021

Accepted: 25-12-2021

## Key Words:

Air pollutants  
Principal component analysis  
Hyderabad

## ABSTRACT

The study aims to bring out the interdependence of the air pollutant components through Correlation and Principal Component Analysis (PCA) to identify the sources causing air pollution in Residential, Resident cum Industrial and Industrial areas of Hyderabad. For this purpose, daily data (from 1st January 2018 to 31st December 2020) of air pollutants recorded by Continuous Ambient Air Quality Monitoring Stations (CAAQMS) that includes 15 air pollution-causing components was collected from the Centre Pollution Control Board (CPCB) website. Data from Residential (Hyderabad Central University (HCU)), Residential and Industrial (ICRISAT-Patencheru), and purely Industrial (Pashmylaram) areas were analyzed and it was identified that 5 majorly contributed pollutants at HCU were due to residential activities however, 5 major pollutants at ICRISAT and Pashmylaram were due to vehicular traffic and industry emissions. The purpose of the study was to figure out the sources of air pollutants and their interdependency under different local conditions. The findings of the study may help the policymakers and authorities concerned to implement different strategies and take necessary steps to keep the pollution levels under control.

## INTRODUCTION

The rapid increase in urbanization and industrialization has been observed in many Indian cities over the last two decades. Hyderabad, Telangana State is one of the fast-growing and most urbanized, and industrialized cities in the country. It is located on the bank of the Musi River, covering 650 sq km at an altitude of 542 m above sea level. In recent years the city experienced striking development in many areas, especially in information technology, pharmaceuticals, and other industries. Many World-class companies like Google, Amazon, etc., started their business which leads to a remarkable expansion of the city in all directions. In this process, several residential communities were developed, High range and multi-stored buildings had come up and resulted in an exponential increase in transport vehicles. This growth has a greater impact on air pollution, and it is well known that air pollution has adverse effects on human health and also on the environment.

In nature, the air is an essential element that does not have any potential defending barrier that can be isolated therefore, there is a need to analyze the impact of pollutants on Global, National, and Local-scale, thereby measures can be taken to control the pollution at all levels (Cichowicz & Wielgosi ski 2015, Ménard et al. 2016, Vallero 2014).

World Health Organization (WHO) reported that the premature deaths of more than two million people each year are attributed to the effect of air pollution during the 21st century. According to the National Institutes of Health, industrial and photochemical smog are the two major forms of air pollution that can create health hazards.

Generally, pollutants found in urban areas are from short-range sources, which include vehicle exhaust, combustion, standby generators, construction, demolition, and kitchen exhaust (Cichowicz & Wielgosi ski 2015, Gurney et al. 2012, Lelieveld et al. 2015, Nemitz et al. 2002). Airborne particulate matter is a complex mixture of organic and inorganic substances, that stay for more time in the atmosphere; as a result, they can easily bypass the filters of the nose and throat of human beings, causing a great impact on health that includes chronic bronchitis, breathing issues heart problems and asthma.

Many studies have proved that industrial and vehicular emissions are the two major contributors to atmospheric pollution (Ajay Kumar et al. 2020, Ravindra et al. 2016, Zhang et al. 2019, Zhao et al. 2019, Singh et al. 2020).

The air quality over Hyderabad gradually declined due to industrial and transport sectors (Guttikunda et al. 2014). The source contribution of Particulate matter over Hyderabad was quantified, using a chemical mass balance receptor

model, and reported that more than 60 % of pollution was dominated by vehicular exhaust and road dust (Venkateswara et al. 2016). In this paper, an attempt was made to identify the dominant air pollutants in different areas of Hyderabad using PCA.

## MATERIALS AND METHODS

Over the past two decades, Hyderabad city has evolved into an IT hub hosting several Global software companies and is famous for several Pharmaceutical industries and others. The extensive network of public transport includes state-owned road transport, Multi-Modal Transport System, elevated Mono Rail transit system apart from private cabs, and three-wheeler autos. The increased economic activity coupled with the migration of the population has resulted in the outward expansion of the city and made industrial estates an integral part of the city.

The CPCB is operating 6 continuous ambient air quality monitoring stations (CAAQMS) [Bolarum; Sanathnagar; Zoo park; Hyderabad central university; ICRISAT; Pashamylaram] over Hyderabad. The details of the stations and their significance are mentioned in Table 1.

All the above CAAQM stations using sophisticated analyzers generate data instantly and facilitate online data dissemination of various parameters including Particulate Matter of size less than 10 microns and 2.5 microns (PM10, PM2.5), chemical pollutants (NO<sub>x</sub>, SO<sub>2</sub>, CO, O<sub>3</sub>, NH<sub>3</sub> VOCs) and meteorological parameters (Temperature, Relative Humidity, and Wind Speed). Our study includes air quality data taken from 3 stations out of the above six stations across Hyderabad. The aim behind choosing them was due to their proximity to the residential area (HCU) residential and Industrial area (ICRISAT) and Industrial area (Pashmylaram).

### Data Analysis

The daily air quality data for three years from January 2018 to December 2020 amounting to 1905 days was taken from the CPCB website for the aforesaid stations. Significant outliers were removed from the data before the analysis.

The details of pollutant components studied for the purpose are given in Table 2.

The pre-processed data of three stations (the residential area (HCU) residential and Industrial area (ICRISAT) and Industrial area (Pashmylaram), shown in Fig. 1 are correlated using Karl Pearson's Coefficient of correlation, and the results are reported in Table 3a, b and c respectively. From the correlation matrix, it is observed that most of the variables are moderate to highly correlated, they have been highlighted in bold.

Factor Analysis is a statistical technique used for dimension reduction of variables that are considered to be a linear combination of underlying factors. Initially, the data were tested for the suitability of factor analysis using KMO and Bartlett's Test. It was observed that KMO > 0.6 is a reasonable and acceptable value. Sig. <0.001 for Bartlett's test indicates the correlation matrix is significantly different from the identity matrix which is consistent that the matrix is factorable.

### Principal Component Analysis

The purpose of Principal component analysis is to account for the utmost portion of the variance with a minimum number of latest or composite variables called principal components. If  $X_1, X_2, \dots, X_k$  are variables required to represent the complete economy by removing overlapping the same can be accounted for by a small number  $p$  of the principal components. Replacing the initial  $k$  variables with  $p$  principal components the original data set consisting of  $n$  measurements of  $k$  variables thus reduces to an information set consisting of  $n$  measurements of  $p$  principal components. Algebraically principal components represent the linear combination of  $k$  variables  $X_1, X_2, \dots, X_k$  and a new coordinate system is obtained by rotating the original system with  $X_1, X_2, \dots, X_k$  is the new coordinate axes. The new axes represent the direction of maximum variability that gives rise to simple and precise covariances.

If  $X^t = [X_1, X_2, \dots, X_k]$  stands for transformed covariance matrix, then  $\lambda_1 \geq \lambda_2 \geq \dots \geq \lambda_k \geq 0$  are its eigenvalues.

Table 1: Details of Continuous Ambient Air Quality Monitoring Stations.

S.No.	Name of the station	Significance of station	Latitude [°N]	Longitude [°E]
1	Bollaram Industrial Area, Hyderabad-TSPCB	Industrial Residential Rural and Other Area	17.54	78.34
2	Central University, Hyderabad-TSPCB	Downstream of industrial area and sensitive zone	17.45	78.34
3	ICRISAT Patancheru, Hyderabad-TSPCB	Industrial Residential Rural and Other Area	17.51	78.27
4	IDA Pashamylaram, Hyderabad-TSPCB	Industrial Residential Rural and Other Area	17.53	78.18
5	Zoo Park, Hyderabad-TSPCB	Industrial Residential Rural and Other Area	17.34	78.45
6	Sanathnagar, Hyderabad-TSPCB	Centre of the city and Balanagar IDA	17.45	78.44

The principal components are generated using the linear combinations

$$Y_1 = a_1^t X = a_{11}X_1 + a_{12}X_2 + \dots + a_{1k}X_k$$

$$Y_2 = a_2^t X = a_{21}X_1 + a_{22}X_2 + \dots + a_{2k}X_k$$

$$Y_k = a_k^t X = a_{k1}X_1 + a_{k2}X_2 + \dots + a_{kk}X_k$$

Then  $\text{Var}(Y_i) = a_i^t \sum a_i$  for  $i = 1, 2, \dots, k$

and  $\text{Cov}(Y_i, Y_j) = a_i^t \sum a_j$  for  $i, j = 1, 2, \dots, k$

The uncorrelated linear combinations of  $Y_1, Y_2, \dots, Y_k$  generate principal components with the largest possible variances.

### RESULTS AND DISCUSSION

Principal Component Analysis using the Varimax method is applied for data reduction. The rotated component matrix of the 3 stations is consolidated in Table 4 and the resulting factors are summarized in Table 5.

From Table 5 three factors are extracted from 15 pollutant components at HCU, however, four factors each were extracted at other stations (ICRISAT and Pashmylaram). Eigenvalues at HCU amount to 68.4% of the variability whereas at ICRISAT and Pashmylaram amount to 74.049% and 67.486% respectively. The cumulative percentage of

variation is well preserved by rotation, however; the spread of variation is distributed evenly over the components.

The air pollution at HCU rose due to its proximity to the IT corridor. The major variability of 29.487% at HCU is contributed by Volatile organic compounds (VOCs), the most

Table 2: Details of air pollutants.

Air Pollutants	Abbreviation	Units of Measurements
Particulate Matter 2.5	PM 2.5	$\mu\text{g.m}^{-3}$
Particulate Matter 10	PM 10	$\mu\text{g.m}^{-3}$
Nitric Oxide	NOx	$\mu\text{g.m}^{-3}$
Ammonia	NH <sub>3</sub>	$\mu\text{g.m}^{-3}$
Sulfur Dioxide	SO <sub>2</sub>	$\mu\text{g.m}^{-3}$
Carbon Monoxide	CO	$\mu\text{g.m}^{-3}$
Ozone	O <sub>3</sub>	$\mu\text{g.m}^{-3}$
Benzene	Benzene	$\mu\text{g.m}^{-3}$
Toluene	Toluene	$\mu\text{g.m}^{-3}$
Relative Humidity	RH	%
Wind Speed	WS	Meter/sec [m.s <sup>-1</sup> ]
Wind Direction	WD	Degree [°]
Solar Radiation	SR	Watt/Meter <sup>2</sup> [W/m <sup>2</sup> ]
Ambient Temperature	AT	°C
Xylene	Xylene	$\mu\text{g.m}^{-3}$

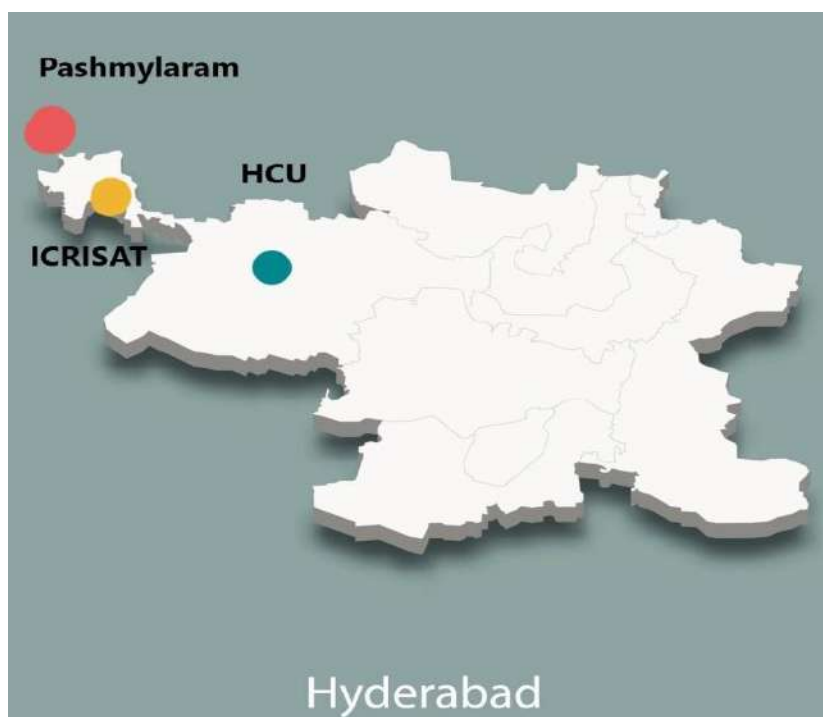


Fig.1: Selected CAAQMS stations based on their proximity to Residential, Residential & Industrial, and Industrial areas.

Table 3a: Correlation matrix of air pollutants at HCU.

	PM 2.5	PM 10	NOx	NH <sub>3</sub>	SO <sub>2</sub>	CO	O <sub>3</sub>	Benzene	Toluene	RH	WS	WD	SR	AT	Xylene
PM 2.5	1	<b>.911**</b>	<b>.683**</b>	<b>.513**</b>	<b>.493**</b>	<b>.536**</b>	<b>.538**</b>	<b>.553**</b>	<b>.477**</b>	<b>-.328**</b>	<b>-.428**</b>	<b>-.361**</b>	<b>.138**</b>	<b>-.132**</b>	<b>.451**</b>
PM 10		1	<b>.721**</b>	<b>.516**</b>	<b>.550**</b>	<b>.557**</b>	<b>.623**</b>	<b>.607**</b>	<b>.566**</b>	<b>-.561**</b>	<b>-.362**</b>	<b>-.321**</b>	<b>.316**</b>	<b>.083**</b>	<b>.517**</b>
NOx			1	<b>.584**</b>	<b>.513**</b>	<b>.575**</b>	<b>.390**</b>	<b>.676**</b>	<b>.630**</b>	<b>-.433**</b>	<b>-.440**</b>	<b>-.372**</b>	<b>.201**</b>	<b>-.021</b>	<b>.630**</b>
NH <sub>3</sub>				1	<b>.226**</b>	<b>.235**</b>	<b>.305**</b>	<b>.375**</b>	<b>.336**</b>	<b>-.301**</b>	<b>-.197**</b>	<b>-.352**</b>	<b>.074*</b>	<b>-.056</b>	<b>.337**</b>
SO <sub>2</sub>					1	<b>.287**</b>	<b>.404**</b>	<b>.526**</b>	<b>.525**</b>	<b>-.446**</b>	<b>-.240**</b>	<b>-.173**</b>	<b>.171**</b>	<b>-.020</b>	<b>.387**</b>
CO						1	<b>.580**</b>	<b>.518**</b>	<b>-.659**</b>	<b>-.080**</b>	<b>-.092**</b>	<b>.403**</b>	<b>.348**</b>	<b>.549**</b>	
O <sub>3</sub>							1	<b>.941**</b>	<b>-.481**</b>	<b>-.228**</b>	<b>-.043</b>	<b>.211**</b>	<b>.101**</b>	<b>.899**</b>	
Benzene								1	<b>-.486**</b>	<b>-.238**</b>	<b>-.066*</b>	<b>.227**</b>	<b>.131**</b>	<b>.838**</b>	
RH									1	<b>.062*</b>	<b>.111**</b>	<b>-.654**</b>	<b>-.573**</b>	<b>-.433**</b>	
WS										1	<b>.383**</b>	<b>-.059</b>	<b>.254**</b>	<b>-.128**</b>	
WD											1	<b>-.033</b>	<b>.121**</b>	<b>-.027</b>	
SR												1	<b>.538**</b>	<b>.228**</b>	
AT													1	<b>.192**</b>	
Xylene														1	

common pollutant found in urban residential areas (Mar et al. 2010). VOCs are derived from benzene and a sub-group of this family of compounds. The significance of VOCs is in lower solar radiation (SR) and also they are precursors of ozone O<sub>3</sub> which is justifiable by the highest variability

of ozone O<sub>3</sub> than that of ICRISAT and Pashmylaram. The variability of PM<sub>2.5</sub>, PM<sub>10</sub>, NOx, and NH<sub>3</sub> is 21.313% can be attributed to vehicular pollution.

PM 2.5, PM 10, NOx, NH<sub>3</sub>, and CO contribute to 33.587% of the variance at ICRISAT. Pollution generated

Table 3b: Correlation matrix of air pollutants at ICRISAT.

	PM 2.5	PM 10	NOx	NH <sub>3</sub>	SO <sub>2</sub>	CO	O <sub>3</sub>	Benzene	Toluene	RH	WS	WD	SR	AT	Xylene
PM 2.5	1	<b>.923**</b>	<b>.770**</b>	<b>.671**</b>	<b>.396**</b>	<b>.792**</b>	<b>.255**</b>	<b>.295**</b>	<b>.304**</b>	<b>-.292**</b>	<b>-.522**</b>	<b>-.666**</b>	<b>-.034</b>	<b>-.231**</b>	<b>.239**</b>
PM 10		1	<b>.787**</b>	<b>.676**</b>	<b>.489**</b>	<b>.781**</b>	<b>.340**</b>	<b>.314**</b>	<b>.309**</b>	<b>-.512**</b>	<b>-.465**</b>	<b>-.595**</b>	<b>.155**</b>	<b>-.107**</b>	<b>.270**</b>
NOx			1	<b>.617**</b>	<b>.385**</b>	<b>.806**</b>	<b>.154**</b>	<b>.359**</b>	<b>.393**</b>	<b>-.292**</b>	<b>-.519**</b>	<b>-.559**</b>	<b>.032</b>	<b>-.262**</b>	<b>.382**</b>
NH <sub>3</sub>				1	<b>.297**</b>	<b>.660**</b>	<b>.231**</b>	<b>.295**</b>	<b>.287**</b>	<b>-.353**</b>	<b>-.476**</b>	<b>-.553**</b>	<b>.048</b>	<b>-.259**</b>	<b>.264**</b>
SO <sub>2</sub>					1	<b>.273**</b>	<b>.326**</b>	<b>-.049</b>	<b>-.073*</b>	<b>-.356**</b>	<b>.158**</b>	<b>-.207**</b>	<b>.096**</b>	<b>.003</b>	<b>-.001</b>
CO						1	<b>.265**</b>	<b>.363**</b>	<b>.383**</b>	<b>-.351**</b>	<b>-.561**</b>	<b>-.598**</b>	<b>.019</b>	<b>-.397**</b>	<b>.439**</b>
O <sub>3</sub>							1	<b>.140**</b>	<b>.099**</b>	<b>-.537**</b>	<b>-.089**</b>	<b>-.271**</b>	<b>.359**</b>	<b>.026</b>	<b>.138**</b>
Benzene								1	<b>.849**</b>	<b>-.075*</b>	<b>-.461**</b>	<b>-.311**</b>	<b>.099**</b>	<b>-.139**</b>	<b>.549**</b>
Toluene									1	<b>-.063*</b>	<b>-.478**</b>	<b>-.321**</b>	<b>.088**</b>	<b>-.243**</b>	<b>.533**</b>
RH										1	<b>.201**</b>	<b>.291**</b>	<b>-.650**</b>	<b>-.050</b>	<b>-.034</b>
WS											1	<b>.584**</b>	<b>-.126**</b>	<b>.253**</b>	<b>-.353**</b>
WD												1	<b>-.015</b>	<b>.303**</b>	<b>-.149**</b>
SR													1	<b>.245**</b>	<b>.042</b>
AT														1	<b>-.131**</b>
Xylene															1

by vehicular traffic and industry emissions is the major contributor. Also being a residential area the second highest contributor to atmospheric pollution is VOCs amounting to 16.874% of the total variance. These large amounts of VOCs prohibit atmospheric ozone to decompose and the presence of a large amount of ozone contributes to 14.708% of the variance. It was observed that SO<sub>2</sub> has contributed 8.881% variance to the pollution. According to a report released by Telangana Pollution Control Board in 2019 (CBCP 2019), ICRISAT is housing many steel industries whose major air pollutants are Sulphur dioxide and Nitrogen oxides.

Pashmylaram is a hub of chemical and pharmaceutical industries. Major chemical pollutants released in the air are in the form of smog with air-borne particulate matter and Sulphur dioxide (Naidu et al., 2021). It is evident from particulate matter PM 2.5, PM 10, and So<sub>2</sub> contributed to 23.163% of the total variance. Air pollutants generated by pharmaceutical industries predominantly constitute VOCs consisting of sulfur dioxide, nitrogen oxide, etc. (Yaqub et al. 2012). It can be noted that the contribution of NH<sub>3</sub> and NOx is 9.328% to the variability.

Fig. 2 illustrates the box and whisker plot of various pollutants under the study at three different stations. It was observed from 2(b) and 2(h) of Box and whisker plots of NOx and Ambient temperature (AT) that the higher the AT

in ICRISAT and HCU lower is the NOx. This indicates that the concentrations of NOx have a strong negative correlation with ambient temperature. A similar observation was made by Chen et al. (2010). Fig.2 (c), (b), and (e) are Box and whiskers plots of NH<sub>3</sub>, CO, and NOx. Lower boxes of NH<sub>3</sub> at ICRISAT support lower production of CO and NOx, and higher boxes of NH<sub>3</sub> at HCU and Pashmylaram support higher production of CO and NOx. Industrial and traffic emissions are also important ammonia sources in urban areas (Ianniello 2010, Pandolfi 2012, Phan 2013). It was recently proved that Ammonia in the air plays a primary role in the formation of CO, SO<sub>2</sub>, and NOx (Behera & Sharma 2010, Updyke et al. 2012).

The destruction of atmospheric O<sub>3</sub> is done by the action of solar radiation (SR) on NOx to break it down to Nitrogen monoxide (NO) and atomic oxygen (O), This atomic oxygen synthesizes with molecular oxygen(O<sub>2</sub>) to form tropospheric ozone (O<sub>3</sub>), which in turn reacts with NO to form new NO<sub>2</sub> and O<sub>2</sub>, maintaining the concentrations of reagents and products in equilibrium (Yurdakul et al. 2013). Box and whisker plots corresponding to SR and O<sub>3</sub> are in agreement with the results of the aforesaid paper.

**CONCLUSIONS**

Interdependency of the air pollutants was very well brought

Table 3c: Correlation matrix of air pollutants at Pashmylaram.

	PM 2.5	PM 10	NOx	NH <sub>3</sub>	SO <sub>2</sub>	CO	O <sub>3</sub>	Ben- zene	Tolu- ene	RH	WS	WD	SR	AT	Xylene
PM 2.5	1	<b>.929**</b>	.398**	.147**	<b>.502**</b>	.458**	.458**	.303**	.339**	-.342**	<b>-.553**</b>	-.433**	-.116**	-.181**	.171**
PM 10		1	.424**	.177**	<b>.502**</b>	.434**	.409**	.337**	.401**	-.473**	<b>-.509**</b>	-.365**	.028	-.042	.234**
NOx			1	.088**	.330**	.219**	.139**	.113**	.159**	-.217**	-.162**	-.085**	-.111**	-.371**	.158**
NH <sub>3</sub>				1	.115**	.314**	.202**	.019	.141**	-.365**	.031	-.173**	.072*	.318**	.156**
SO <sub>2</sub>					1	.140**	.259**	.297**	.346**	-.256**	-.270**	-.315**	-.020	-.172**	.256**
CO						1	.437**	-.042	.008	-.385**	-.291**	-.230**	.027	.136**	-.043
O <sub>3</sub>							1	-.056	.067*	<b>-.683**</b>	-.187**	-.387**	.219**	.250**	.083**
Ben- zene								1	<b>.733**</b>	.017	-.205**	-.334**	-.024	-.048	.452**
Tolu- ene									1	-.173**	-.238**	-.417**	.096**	.152**	<b>.616**</b>
RH										1	.089**	.297**	<b>-.543**</b>	<b>-.543**</b>	-.199**
WS											1	.192**	.088**	.179**	-.105**
WD												1	-.064*	-.229**	-.322**
SR													1	<b>.586**</b>	.105**
AT														1	.214**
Xylene															1

\*\* Correlation is significant at the 0.01 level (2-tailed).

Table 4: Rotated Component Matrix of 3 Stations.

	Rotated Component Matrix											
	HCU			ICRISAT				Pashmylaram				
	Component			Component				Component				
	1	2	3	1	2	3	4	1	2	3	4	
PM 2.5	0.453	<b>0.745</b>	0.083	<b>0.891</b>	0.143	0.06	0.205	<b>0.886</b>	0.243	-0.121	0.139	
PM 10	0.503	<b>0.678</b>	0.322	<b>0.824</b>	0.179	0.276	0.307	<b>0.828</b>	0.302	-0.008	0.202	
NOx	0.601	<b>0.629</b>	0.087	<b>0.803</b>	0.298	0.04	0.215	0.325	0.112	-0.373	<b>0.654</b>	
NH3	0.216	<b>0.613</b>	0.099	<b>0.767</b>	0.146	0.135	0.067	0.034	0.076	0.326	<b>0.65</b>	
SO <sub>2</sub>	<b>0.468</b>	0.377	0.157	0.337	-0.098	0.199	<b>0.794</b>	<b>0.463</b>	0.382	-0.146	0.293	
CO	<b>0.637</b>	0.208	0.188	<b>0.849</b>	0.286	0.075	0.078	<b>0.619</b>	-0.205	0.206	0.268	
O <sub>3</sub>	0.5	0.218	0.579	0.193	0.087	<b>0.646</b>	0.229	<b>0.617</b>	-0.097	0.471	0.194	
Benzene	<b>0.934</b>	0.157	0.151	0.2	<b>0.878</b>	0.081	-0.117	0.126	<b>0.838</b>	-0.114	-0.083	
Toluene	<b>0.891</b>	0.128	0.156	0.238	<b>0.855</b>	0.04	-0.175	0.16	<b>0.89</b>	0.086	0.042	
RH	-0.36	-0.206	<b>-0.815</b>	-0.319	0.056	<b>-0.844</b>	-0.086	-0.438	-0.033	<b>-0.694</b>	-0.395	
WS	-0.124	<b>-0.641</b>	0.169	<b>-0.621</b>	-0.344	-0.139	0.513	<b>-0.703</b>	-0.157	0.159	0.297	
WD	0.125	<b>-0.771</b>	-0.022	<b>-0.787</b>	-0.076	-0.136	0.185	-0.419	<b>-0.452</b>	-0.282	0.011	
SR	0.086	0.092	<b>0.822</b>	-0.095	0.076	<b>0.882</b>	-0.104	-0.031	0.055	<b>0.748</b>	-0.015	
AT	0.071	-0.273	<b>0.824</b>	<b>-0.47</b>	-0.043	0.327	0.292	-0.12	0.1	<b>0.909</b>	-0.006	
Xylene	<b>0.917</b>	0.079	0.143	0.162	<b>0.795</b>	-0.012	0.104	-0.019	<b>0.764</b>	0.158	0.202	

Table 5: Summary of resulted factors.

Factors	HCU		ICRISAT		Pashmylaram	
	Components	% of Variance	Components	% of Variance	Components	% of Variance
1	SO <sub>2</sub> , CO, Benzene, Toluene, Xylene	29.487	PM 2.5, PM 10, NOx, NH <sub>3</sub> , CO, WS, WD, AT	33.587	PM 2.5, PM 10, SO <sub>2</sub> , CO, O <sub>3</sub> , WS	23.163
2	PM 2.5, PM 10, NOx, NH <sub>3</sub> , WS, WD	21.313	Benzene, Toluene, Xylene	16.874	Benzene, Toluene, Xylene, WD	17.912
3	O <sub>3</sub> , RH, SR, AT	17.602	O <sub>3</sub> , RH, SR	14.708	RH, SR, AT	17.084
4			SO <sub>2</sub>	8.881	NH <sub>3</sub> , NOx	9.328
		68.402		74.049		67.486

out in the correlation matrix and was grouped into various factors using PCA. The weightage of each group was carefully examined, and the major contributors were identified in the three different areas of Hyderabad. It was observed that VOCs were the dominant contributors in residential areas and particulate matter was significant in the areas where industries are located. Causes of various pollutants were well deciphered from the Box and whiskers plot emphasizing the role of meteorological parameters in pollution.

## ACKNOWLEDGMENTS

The authors acknowledge Telangana State and Central

Pollution Control Board for making the data available to users. The authors would like to thank the management of Vasavi College of Engineering, Hyderabad, India.

## REFERENCES

- Ajay Kumar, M.C., Vinay Kumar, P. and Venkateswara Rao, P. 2020. Temporal variations of PM<sub>2.5</sub> and PM<sub>10</sub> Concentration over Hyderabad. *Nat. Environ. Pollut. Technol.*, 19: 421-428.
- Behera, S.N. and Sharma, M. 2010. Investigating the potential role of ammonia in ion chemistry of fine particulate matter formation for an urban environment. *Sci. Total Environ.*, 408: 3569-3575.
- Chen, X., Xia, X.H. and Zhao, Y. 2010. Heavy metal concentrations in roadside soils and correlation with urban traffic in Beijing, China. *Hazard. Mater.*, 181: 640-646
- Cichowicz, R. and Wielgosiński, G. 2015a. Effect of meteorological con-

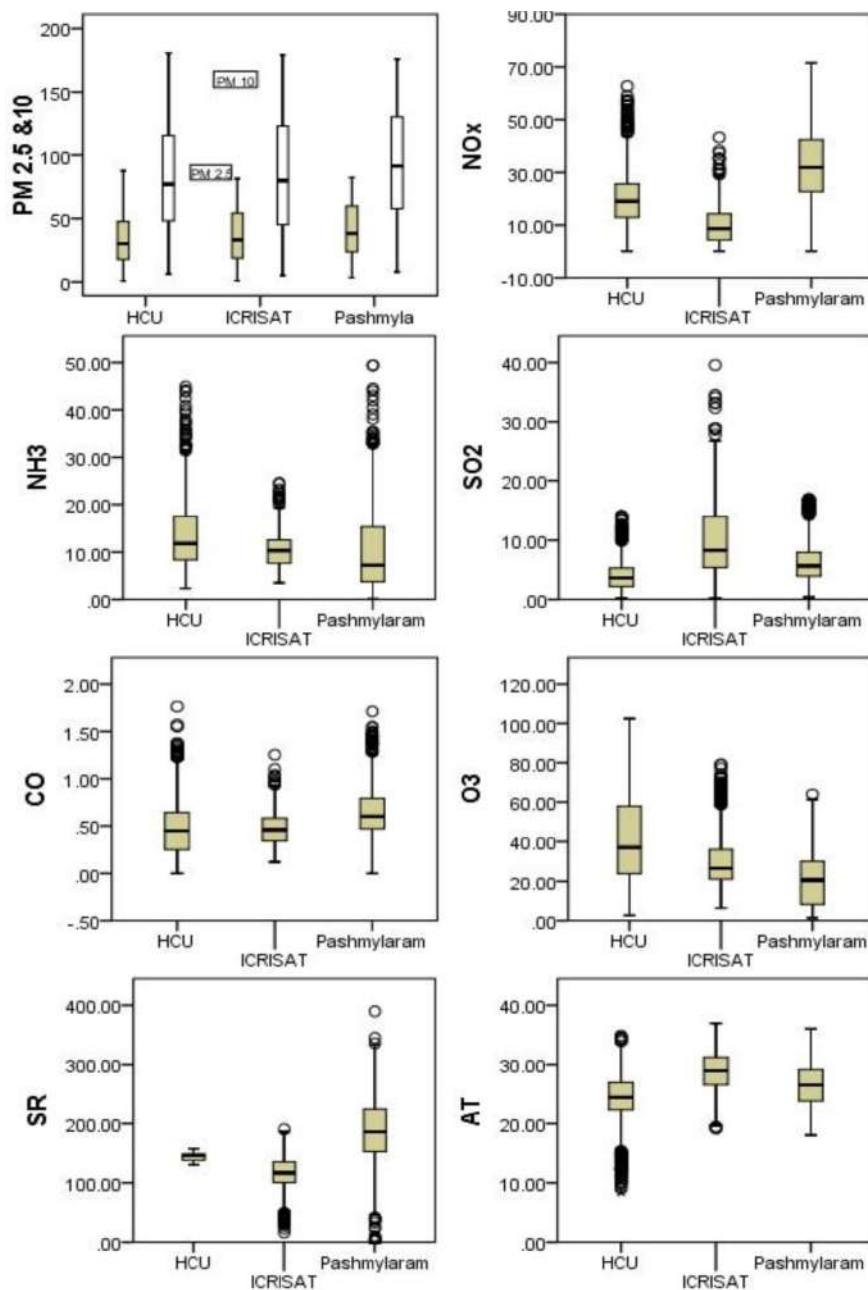


Fig. 2: Box and whisker plots of PM 2.5 & PM 10, NO<sub>x</sub>, NH<sub>3</sub>, SO<sub>2</sub>, CO, and O<sub>3</sub> at HCU, ICRISAT, and Pashmylaram in Hyderabad.

ditions and building location on CO<sub>2</sub> concentration in the university campus. *Ecol. Chem. Eng.*, 22(4): 513-525.

CPCB 2019. Action Plan for the restoration of environmental qualities with regard to the identified polluted industrial cluster of Patancheru-Bollaram; [https://cpcb.nic.in/industrial\\_pollution/New\\_Action\\_Plans/CEPI\\_Action%20PlanPatancheru-Bollaram.pdf](https://cpcb.nic.in/industrial_pollution/New_Action_Plans/CEPI_Action%20PlanPatancheru-Bollaram.pdf)

Gurney, K.R., Razlivanov, I., Song, Y., Zhou, Y., Benes, B. and Massih, M. A. 2012. Quantification of fossil fuel CO<sub>2</sub> emissions on the building/street scale for a large U.S. City. *Environ. Sci. Technol.*, 46(21): 12194-12202.

Guttikunda, S.K. and Ramani, V.K. 2014. Source emissions and health impacts of urban air pollution in Hyderabad, India. *Air Qual. Atmos. Health*, 7:195-207. doi.10.1007/s11869-013-0221

Ianniello, A. 2010. Occurrence of gas-phase ammonia in the area of Beijing (China). *Atmos. Chem. Phys.*, 10: 9487-9503.

Lelieveld, J., Evans, J.S., Fnais, M., Giannadaki, D. and Pozzer, A. 2015. The contribution of outdoor air pollution sources to premature mortality on a global scale. *Nature*, 525: 367-371.

Marć, M., Namieśnik, J. and Zabiegała, B. 2014. BTEX concentration

- levels in urban air in the area of the Tri-City agglomeration (Gdansk, Gdynia, Sopot), Poland. *Air Qual. Atmos. Health*, 7: 489-504
- Ménard, R., Deshaies-Jacques, M. and Gasset, N. 2016. A comparison of correlation-length estimation methods for the objective analysis of surface pollutants in the environment and climate change in Canada. *J. Air Waste Manag. Assoc.*, 66: 9,874-9,895.
- Naidu, R., Biswas, B., Ian, R., Julian Cribb, W., Singh, B.R.C., Nathanail, P., Coulon, F., Semple, K.T., Kevin C. J., Barclay, A. and Aitken, R.J.. 2021. Chemical pollution: A growing peril and potentially catastrophic risk to humanity. *Environ. Int.*, 156: <https://doi.org/10.1016/j.envint.2021.106616>.
- Nemitz, E., Hargreaves, K.J., McDonald, A.G., Dorsey, J.R. and Fowler, D. 2002. Micrometeorological measurements of the urban heat budget and CO<sub>2</sub> emissions on a city scale. *Environ. Sci. Technol.*, 36(14): 3139-3146.
- Pandolfi, M. 2012. Summer ammonia measurements in a densely populated Mediterranean city. *Atmos. Chem. Phys.*, 12: 7557-7575.
- Phan, N.T. 2013. Analysis of ammonia variation in the urban atmosphere. *Atmos. Environ.*, 65: 177-185.
- Ravindra, K., Sidhu, M.K., Mor, S., John, S. and Pyne, S. 2016. Air pollution in India: bridging the gap between science and policy. *J. Hazard. Toxic Radioact. Waste*, 20(4): A4015003.
- Singh, V., Biswal, A., Kesarkar, A.P., Mor, S. and Ravindra, K. 2020. High resolution vehicular PM<sub>10</sub> emissions over megacity Delhi: relative contributions of exhaust and non-exhaust sources. *Sci. Total Environ.*, 699: 134273.
- Updyke, K.M., Nguyen, T.B. and Nizkorodov, S.A. 2012. Formation of brown carbon via reactions of ammonia with secondary organic aerosols from biogenic and anthropogenic precursors. *Atmos. Environ.*, 63: 22-31.
- Vallero, D. 2014. *Fundamentals of Air Pollution*. Fifth edition. Elsevier Inc., & Academic Press, London.
- Venkateswara, R.K., Raveendhar, N. and Swamy, A.V.V.S. 2016. Status of air pollution in Hyderabad City, Telangana State. *Int. J. Innov. Sci. Eng. Technol.*, 5(4): 4769-4780.
- Yaqub, G., Hamid, A. and Iqbal, S. 2012. Pollutants generated from pharmaceutical processes and microwave-assisted synthesis as a possible solution for their reduction: A mini-review. *Nat. Environ. Pollut. Technol.*, 11(1): 29-36.
- Yurdakul, S., Civan, M. and Tuncel, G. 2013. Volatile organic compounds in suburban Ankara atmosphere, Turkey: Sources and variability. *Atmos. Res.*, 120-121: 298-311.
- Zhang, K., Zhao, C., Fan, H., Yang, Y. and Sun, Y. 2019. Toward understanding the differences of PM<sub>2.5</sub> characteristics among five China urban cities. *Asia-Pacific J. Atmos. Sci.*, 56: 493-502.
- Zhao, C., Wang, Y., Shi, X., Zhang, D., Wang, C., Jiang, J.H., Zhang, Q. and Fan, H. 2019. Estimating the contribution of local primary emissions to particulate pollution using high-density station observations. *J. Geophys. Res. Atmos.*, 124: 1648-1661.





# Impact of the Chemical Composition of Oil for Biodiesel Production to Reduce Environmental Pollution

K. A. Viraj Miyuranga, U. S. P. R. Arachchige†, D. Thilakarathne, R. A. Jayasinghe and N. A. Weerasekara

Department of Civil and Environmental Technology, Faculty of Technology, University of Sri Jayewardenepura, Homagama, Sri Lanka

†Corresponding authors: U.S.P.R. Arachchige; udara@sjp.ac.lk

Nat. Env. & Poll. Tech.  
Website: [www.neptjournal.com](http://www.neptjournal.com)

Received: 25-12-2021

Revised: 08-02-2022

Accepted: 10-02-2022

## Key Words:

Biodiesel

Chemical composition

Physical properties

Transesterification

Waste vegetable oil

## ABSTRACT

The primary motivation for researching biofuels is to meet the world's energy requirements. Demand for fossil fuels is rising significantly due to population expansion. Biodiesel is a promising renewable energy source that, if implemented effectively, has the potential to reduce the dependency on fossil fuels. Because biodiesel is a cleaner fuel that requires no engine modification, its implementation is not complicated. It can directly be used in diesel engines or as a blended diesel with fossil diesel. Seven different vegetable oils were utilized to replicate restaurant waste cooking oil in the laboratory to make biodiesel. The qualities of biodiesel produced were investigated and compared to determine how they vary depending on the chemical composition of the oil source. The physical appearance of biodiesel varies slightly depending on the oil source. Density, kinematic viscosity, flash point, and acid levels, on the other hand, are all within acceptable biodiesel criteria for all types of oil sources used.

## INTRODUCTION

The use of biofuel as a sustainable substitute for petroleum diesel is a timely vital solution to the inescapable global issues related to environmental pollution and fossil fuel. Implementing biofuel is considered crucial for both economic and ecological reasons, and has gained significant attention. Biodiesel is derived from lipids such as edible or non-edible oils reacting with alcohol with a catalyst (Ramos 2021). Biodiesel, which is considered clean and environmentally friendly, could be produced from edible oils such as coconut, palm, olive, and sunflower oil and non-edible oils such as rubber seed oil and algal oil using a process known as transesterification (Miyuranga et al. 2021). Waste cooking oil (WCO) is one of the promising sources of biodiesel production, which can be considered non-edible oil as it is the waste from the cooking process (Saydut et al. 2010).

WCO is a potentially problematic waste stream that requires proper management even though it is not currently happening in many countries. Nevertheless, WCO can be considered a promising alternative for producing biodiesel as it is a cheaper raw material with the handling of waste produced during the cooking process (Supple et al. 2002). Moreover, it reduces the need for agricultural lands for biodiesel-producing crops if produced from edible oil sources

(Enweremadu & Mbarawa 2009). However, the presence of water in the WCO accelerates the hydrolysis of triglycerides and eventually increases the free fatty acid (FFA) content of the oil (Kawentar & Budiman 2013).

FFA content of the WCO gradually increases with the frying attempts. As food particles and water consist in the WCO, the pretreatment step is necessary to prevent saponification during the biodiesel production process. It can be done by pre-filtering to remove food particles and sediments and heating to remove the moisture content of the WCO. Pretreated WCO reacts with alcohol in the presence of the catalyst around 60°C for 30 min to produce biodiesel. The primary transesterification reaction is given in Fig. 1.

## DIFFERENT OIL SOURCES

There are various oil sources available in the market as vegetable oil, such as Coconut oil, Palm oil, Corn oil, Sunflower oil, Olive oil, Canola, Soybean, etc. Edible vegetable oil is vital for our health as it maintains the balance of lipids, cholesterol, and lipoproteins that circulate in the blood. The application of non-edible oils to synthesize biodiesel is considered beneficial compared to edible oils to avoid the food crisis and make biodiesel a cost-effective process. However, WCO can be a potential source as it is a waste that will be

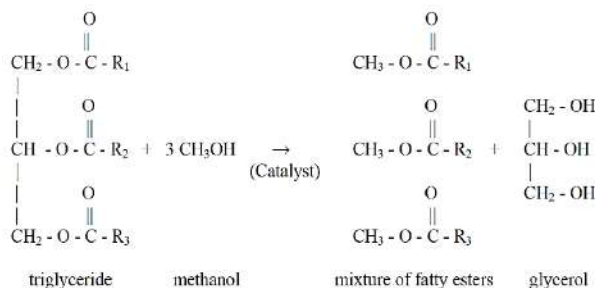


Fig. 1: A schematic representation of the Transesterification Reaction (Allah & Alexandru 2016).

discarded. Hence, the main aim of the study is to analyze the biodiesel production capability of waste cooking oil sources and the variation of the quality based on the chemical composition of the oil source.

Coconut oil mainly falls into two categories; Copra oil extracted from the dried kernel by mechanical milling, and virgin coconut oil extracted from the fresh kernel without applying high heat or chemical processing. Previous studies revealed that Lauric acid (Fig. 2) was the major Fatty acid (FA) present in coconut oil, comprising 45% of total FAs (Deen et al. 2020). Among edible oils, palm oil feedstock has the highest oil yield compared with other available oil sources (Zulqarnain et al. 2021). The primary fatty acid composition of palm oil is Palmitic acid (Fig. 3), while the major fatty acid of corn oil is regarded as Linoleic acid (Fig. 4) based on the experimental analysis (Ilkiliç et al. 2017). Similarly, the major fatty acid of sunflower oil is Linoleic acid, based on the experimental analysis (Ilkiliç et al. 2017). Biodiesel production from fresh Sunflower oil and biodiesel production from fresh olive oil has been previously studied (Sagiroglu et al, 2011, Mansourpoor 2012). The major fatty acid of olive oil is identified as Oleic acid (Fig.5) (International Olive oil Council 2003). Canola (*Brassica napus L.*) is high in

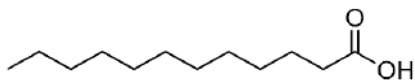


Fig. 2: Chemical structure of Lauric acid.

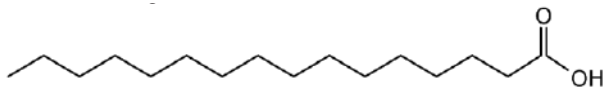


Fig. 3: Chemical structure of Palmitic acid.

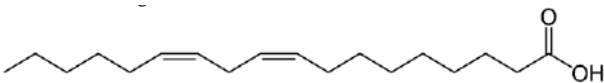


Fig. 4: Chemical structure of Linoleic acid

Oleic acid, which makes it competitive with other cooking oil (<https://catalog.extension.oregonstate.edu>). Multiple researchers have previously studied biodiesel production from fresh canola oil (Sagiroglu et al. 2011, Ge et al. 2017, Encinar et al. 2018). The major fatty acid of soybean oil is considered Linoleic acid based on the experimental analysis (Ilkiliç et al. 2017). In short, biodiesel has attracted much attention due to its various environmental benefits. However, the main challenges include its production cost and availability of suitable raw materials. Edible oil source as a raw material for biodiesel production is not encouraging due to demand for food, and the prices increase eventually. Therefore, waste cooking oil is considered one of the best alternative raw materials for biodiesel production.

Moreover, the productivity of the oil from the biomass crop and the oil content of the source are considered and given in Table 1. It is seen that the seed oil content of the corn is the highest among them, while coconut shows the lowest oil content of the seed. The oil productivity per hectare per year is most elevated in palm oil, around 5366 L oil per hectare.

## WASTE VEGETABLE OIL

Direct use of vegetable oil for biodiesel production has been continuously practiced worldwide to reduce environmental pollution and carbon emission. However, as a food crop, that concept is not a sustainable solution for a better future as part of the world will be struggling for their food sources. The waste cooking oil as a biodiesel source is promising. Waste cooking oil is considered an effective raw material due to its availability and cost-effectiveness. Different types of waste cooking oil have been previously tested for biodiesel production, such as waste canola oil (Hossain & Mazen 2010), waste olive oil (Mihankhah et al., 2016), etc. Multiple cooking oils are used by different restaurants and hotels. However, most of them have been already used for biodiesel preparation worldwide. Several research groups have tested the use of palm oil for biodiesel production as palm oil contributes to the majority of the market share in the vegetable oil market (Chozhavendhan et al. 2020, Ojiego et al. 2014). However, no research has been conducted to compare the properties of biodiesel from many different oil sources similar to this study. Therefore, it was identified as beneficial to compare the biodiesel production from WCO

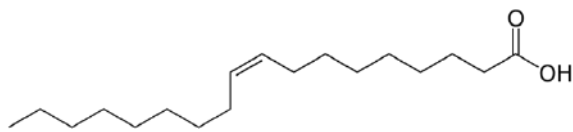


Fig. 5: Chemical structure of Oleic acid.

Table 1: Comparison of oil feedstocks.

Plant Source	Seed Oil Content [% oil w/w in biomass]	Oil Volumetric Productivity [L oil.ha*year <sup>-1</sup> ]
Coconut ( <i>Cocos nucifera</i> L.)	13 <sup>a</sup>	1350 <sup>b</sup>
Palm ( <i>Elaeisguineensis</i> )	36 <sup>c</sup>	5366 <sup>c</sup>
Corn/Maize ( <i>Zea mays</i> L.)	44 <sup>c</sup>	172 <sup>c</sup>
Sunflower ( <i>Helianthus annuus</i> L.)	40 <sup>c</sup>	1070 <sup>c</sup>
Olive ( <i>Olea europaea</i> L.)	15-30 <sup>d</sup>	360-700 <sup>e</sup>
Canola/Rapeseed ( <i>Brassica napus</i> L.)	41 <sup>c</sup>	974 <sup>c</sup>
Soybean ( <i>Glycine max</i> L.)	18 <sup>c</sup>	636 <sup>c</sup>

<sup>a</sup>(Agarwal 2017)

<sup>b</sup>(<https://www.gardeningplaces.com/articles/oil-crops-compared1.htm>)

<sup>c</sup>(Mondal et al. 2017)

<sup>d</sup>(Zeb & Murkovic 2011)

<sup>e</sup>(Russo et al. 2016)

and the properties' variations when the source of the oil and chemical composition changes.

## MATERIALS AND METHODS

### Materials

Here in this study, seven different oil sources such as coconut oil, Palm oil, corn oil, sunflower oil, olive oil, canola, and soybean are considered for biodiesel production. The properties of oil sources are analyzed in the laboratory and shown in Table 2. Kinematic viscosity, specific gravity, acid value, FFA%, and flash point, are considered the oil source's primary properties. WCO from seven different oil sources is generated at the laboratory by frying fresh marinated chicken for five frying attempts (Which means the same oil sample was heated for frying until the fifth batch of the chicken sample is fried). It was carried out in the laboratory to replicate the exact WCO generated by the restaurant. The produced WCO was filtered using a cloth filter to remove food particles and thereafter pre-heated to 110°C for 20 minutes to remove the moisture. For the biodiesel production experiments, the following reference quantities of reactants and catalysts were used: 100 ml of pre-treated Waste Cooking Oil (WCO), 20ml of methanol, and 1 w/w% of KOH based on the oil weight.

Table 2: Properties of vegetable oil.

Parameters	Types of Vegetable Oil						
	Coconut Oil	Palm Oil	Corn Oil	Sunflower Oil	Olive Oil	Canola Oil	Soybean Oil
Density [15°C, kg.m <sup>-3</sup> ]	0.9331	0.9120	0.9132	0.9040	0.9160	0.9130	0.9060
Kinematic Viscosity at (40°C, cSt)	27.71	38.86	33.51	33.22	36.08	35.67	28.66
Flash Point [°C]	309	270	300	312	310	320	318
FFA%	0.5640	0.9818	0.4208	0.9818	0.9818	0.7015	0.7015

### Transesterification

In the first step of the experiment, KOH was added to the methanol and stirred until all KOH dissolved. Then, 100 ml of pre-filtered and purified WCO was measured using a measuring cylinder and heated until 55-60°C. After reaching the desired temperature, the Methoxide mixture was added to the continuously mixed-heated oil, and the reaction was carried out for 30 minutes. After the reaction finished, the reaction mixture was allowed to settle until the biodiesel light layer was completely separated from the heavy glycerin layer. It took around three hours for the glycerin and biodiesel layers to separate. The biodiesel layer, known as Fatty Acid Methyl Ester (FAME), was separated by removing the glycerin layer. Afterward, the biodiesel was prepared for the washing procedure. For the washing process, 50% (related to the biodiesel volume) of warm distilled water was added to the biodiesel to extract contaminants.

The mix was allowed to separate, forming a top biodiesel layer and a bottom aqueous layer, due to differences in densities and immiscibility. After complete separation, the aqueous layer is removed, and the extraction process is repeated until the aqueous layer shows no contamination. The next step is the drying process, where heating the biodiesel sample to a

temperature range of 105-110°C. The biodiesel was heated for about 20 minutes until all the water evaporated and separated from the sample. A similar procedure is followed for seven different waste cooking oil samples. The produced biodiesel samples have color differences due to the source of the oil (Fig. 6).

### Analysis of Physical and Chemical Properties

The physical properties of the produced biodiesel were tested at the laboratory for flash point, density, kinematic viscosity, and acid value. The ASTM analysis method was followed by maintaining similar conditions for all samples. Three biodiesel samples from each oil source were produced to get the average value by minimizing human errors. The Cleveland open-cup flash point tester was used to analyze the oil samples and the biodiesel samples. Experiments were conducted in an open cup tester exposed to the air outside. While the temperature of the oil sample gradually raised, an ignition source is passed over the top to catch the flashes after a specific time. The temperature which initiates the flashes is recognized as the flashpoint of the substance. The redwood viscometer was used for the viscosity analysis of oil and biodiesel samples.

## RESULTS AND DISCUSSION

The physical properties of the seven different biodiesel

samples which were produced in the optimum conditions were measured in the university laboratory and shown in Table 3. These results are compared with the standard ASTM biodiesel properties.

### Density

Fuel density has a significant impact on engine performance and emissions. The density of a methyl ester is determined by its molecular mass, the content of free fatty acids, the amount of water present, and the temperature. Density increases when chain length decreases and the number of double bonds increases density; on the other hand, it can be reduced by having a lower density contaminant such as methanol. Polyunsaturated fatty acids are more polar, and dipole-dipole interactions are the interacting forces between these molecules. These interaction forces are more significant than the interactions of non-polar molecules, causing the distance between the molecules to be closer, and therefore the density increases.

In this study, Biodiesel densities were determined at a constant temperature of 15°C. However, according to the experimental results shown in Table 3, all samples were shown similar densities, which do not have many deviations according to the oil source. This is because the density of methanol and oil is close to the density of biodiesel produced. Furthermore, the densities of the biodiesels were within the acceptable ASTM D6751 standard range.



Fig. 6: Biodiesel generated by waste cooking oil samples from different oil sources.

Table 3: physical and chemical properties of produced biodiesel.

Parameters	Source of the Vegetable Oil used for WCO to produce biodiesel							ASTM D6751 Standard
	Coconut Oil	Palm Oil	Corn Oil	Sunflower Oil	Olive Oil	Canola Oil	Soybean Oil	
Density [15°C, kg.m <sup>-3</sup> ]	0.884	0.855	0.863	0.87	0.858	0.87	0.872	860-900
Kinematic Viscosity at (40°C, cSt)	3.84	5.32	5.94	5.61	5.53	5.35	5.11	1.9 - 6.0
Flash Point [°C]	109	188	180	174	178	118	178	>130
Total acid value (mg KOH.g <sup>-1</sup> )	0.2	0.5	0.48	0.5	0.42	0.42	0.42	<0.5
Yield [%]	95	94.1	88.1	90.4	86.5	90.6	91.8	

<sup>f</sup>(Lamichhane et al. 2020)

### Kinematic Viscosity

The viscosity is one of the most crucial fuel characteristics directly connected to the hydrocarbon chain's molecular structure and length. It is one of the contributing components that substantially impact the atomization of fuel having a length of 12 carbons. Because it is a medium-chain fatty acid, the interaction force between molecules is comparatively weaker, and lauric acid's viscosity is lower. The interaction forces between molecules are relatively substantial because it is a long-chain fatty acid; consequently, the viscosity of Linoleic acid is high. Oleic acid is an unsaturated fatty acid with a long chain. It exhibits a double bond from its carboxylic end (-COOH) after the 9th carbon and shows 18 carbon atoms inside its molecules. Since the contact forces between molecules are tremendous, oleic acid has a high viscosity, consisting of long-chain fatty acid.

As a result, coconut oil has a very low viscosity (27.71 cSt) in comparison to other oils, owing to the high concentration of lauric acid, a medium-chain fatty acid. This effect is visible in the biodiesel produced from each vegetable oil, containing fatty acids with slightly different fatty acid profiles than vegetable oils. Accordingly, biodiesel produced from coconut oil has a lower kinematic viscosity (3.84 cSt) than others.

Viscosity is affected by the double bond configuration; According to Refaat (2009), the *cis*-double-bond configuration has a lower viscosity than the *trans*-double-bond configuration. This is especially important when using

WCO as a feedstock for biodiesel, as they are often partially hydrogenated and have high trans fatty acid chain concentrations. Palm oil, corn oil, sunflower oil, olive oil, canola oil, and soybean oil contain varying amounts of long-chain fatty acids. Nevertheless, due to the length of the carbon chain, the kinematic viscosity of the biodiesel produced from these oils remained rather constant, ranging between 5.11 and 5.94 cSt. According to Sagiroglu et al. 2011, biodiesel derived from olive oil has lower un-saturation fatty acid content (84.45%) than biodiesel derived from canola oil (88.99%). Thus, olive oil has a higher kinematic viscosity than canola oil, as demonstrated by the experiment results in Table 3.

The unsaturation fatty acid content of biodiesel composite for corn oil (81.73%), sunflower oil (86.92%), and soybean oil (93.93%) was enhanced, according to Sagiroglu et al. (2011), Therefore, as the unsaturation level increases, the kinetic viscosity of these biodiesels is expected to decrease. According to the kinematic viscosity at 40°C in Table 3, as predicted, kinematic viscosity was lowered, such as 5.94, 5.61, and 5.11 cSt for corn oil, sunflower oil, and soybean oil, respectively. However, each biodiesel generated from all oils falls within the ASTM D6751 standard value range for biodiesel.

### Flashpoint

The flashpoint of a fuel is the temperature at which it begins to burn when it comes into contact with a heat source. Although the flashpoint has no direct effect on combustion,

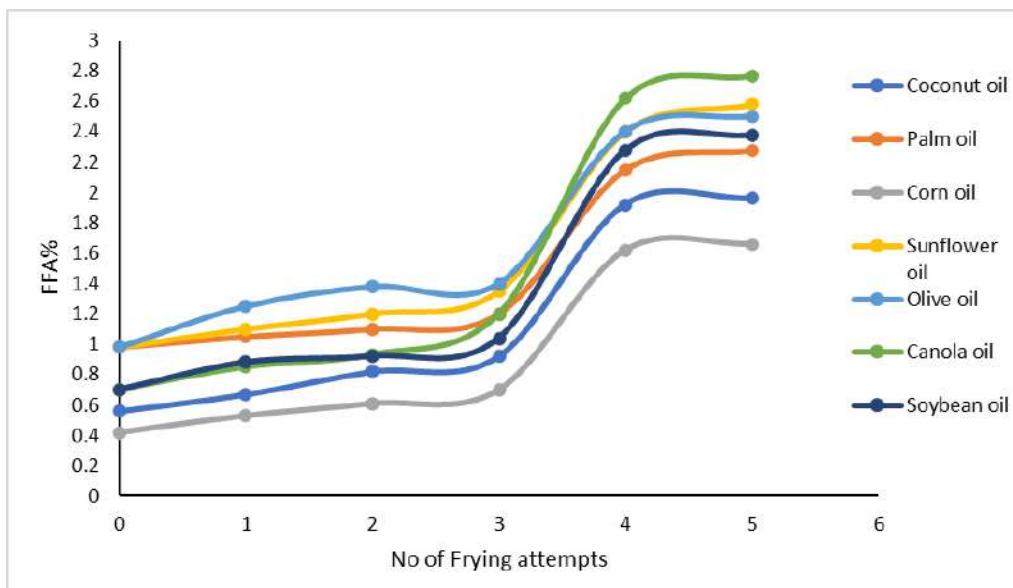


Fig. 7: FFA% change with the number of attempts fried for seven different vegetable oils.

it is critical for fuel transportation, storage, and handling. Numerous factors affect the flashpoint of biodiesel, one of which is the residual alcohol level (Thilakarathne et al. 2021). Additionally, the flashpoint is affected by the number of double bonds and carbon atoms. As the percentage of unsaturated fatty acids and polyunsaturated fatty acids increases, unsaturated bonds introduce bends into the molecule, thus preventing adjacent fatty acids from packing together. This causes the van der Waals forces to decrease. The lower the van der Waals force, the less energy is needed to evaporate the oil. Therefore, causes the flashpoint to drop.

Furthermore, as the length of the fatty acid's carbon chain in the oil increases, the flashpoint of the oil increases. This is because the intermolecular forces increase as the number of carbon increases. According to Table 2, the flashpoint of corn oil, sunflower oil, olive oil, canola oil, and soybean oil is high because they contain many long-chain fatty acids. On the other hand, Palmitic acid is a 16-carbon saturated fatty acid; however, palm oil showed the lowest flashpoint (270°C) since it contains a relatively small percentage of saturated fatty acids (47.9%) compared to coconut oil (86.3%) according to the previous experiments (Ganesan et al. 2013). The flashpoint of all vegetable oil methyl esters is much lower than their vegetable oil. According to Table 3, all biodiesel had lower flash points than their vegetable oil counterparts, with coconut oil having the lowest flashpoint for biodiesel (109°C). However, the flashpoint of biodiesel produced from all vegetable oils except coconut oil satisfies the ASTM D6751 standard. Contamination of biodiesel with methanol may cause it to fail to fulfill the regulatory criteria for a minimum flashpoint, as methanol reduces flashpoints. Methanol contamination is generally occurred by inadequate purification of the ester following the transesterification process. In addition, the wear problem is considered to be caused by a formic acid attack when methanol is utilized for transesterification, according to Demirba (2008).

### Acid Value

Acid value determination is a critical analysis for determining the quality of particular biodiesel. The acid value of the starting material (oil) can significantly affect the final product's FAME content. A variety of factors determines the acid value of biodiesel. On the one hand, it affects the type of feedstock used in biodiesel manufacturing and its refined degree. On the other hand, the acid value can be increased by raising the FFA content during the production process. Finally, the parameter indicates the amount of fuel that ages during storage due to the ester bond being hydrolyzed. High acid value fuel has been considered concerning engine corrosion and, more specifically, the production of deposits in the fuel injectors due to catalyzed polymerization of highly recycled fuel loops. However, FFA

as free carboxylic acids is less dangerous than strong mineral acids. Therefore, the maximum acid value for pure biodiesel is 0.5 mgKOH.g<sup>-1</sup> according to ASTM D6751 standard. As the FA is broken down into shorter chain acids, the acid value increases. When edible oil is exposed to atmospheric oxygen, moisture, and steam at elevated temperatures during frying conditions, a multitude of complex chemical reactions such as hydrolysis, oxidation, polymerization, lipid decomposition, and other thermal reactions is taken place, which causes the ester linkages of triacylglycerols to break down and that results in the formation of numerous undesirable compounds form FFA, monoacylglycerols, diacylglycerols, and glycerol. As a result, the FFA content of fried oils increases with the number of fried, as shown in Fig. 7. The acid value is twice as high as FFA%. High levels of FFA% can lead to increased viscosity, according to Aliasa.

### CONCLUSIONS

Fatty acid methyl ester (i.e., Biodiesel) was manufactured through different waste vegetable oils such as coconut oil, Palm oil, corn oil, sunflower oil, olive oil, canola, and soybean. As the raw material cost is high for biodiesel production, waste cooking oil is considered for the current experiment. According to the study, the number of frying attempts has a significant effect on the FFA% of the oil. However, the main idea was to compare the different waste cooking oil-based biodiesel properties. Under similar reaction conditions, various samples of Biodiesel were prepared and tested in accordance with ASTM standards. The sample's densities, specific gravity, kinematic viscosity, flash point, and acid value were reported. Even though there are slight variations of those variables, they can be negligible as all values follow the standard values. Therefore, the chemical composition, the major acid component of the oil source, does not affect the production of Biodiesel from WCO. Physical properties and appearance have slight variations due to the color and chemical composition of the oil source. However, all physical properties are following ASTM standards of Biodiesel.

### ACKNOWLEDGMENT

The authors express their gratitude to the AHEAD project (RIC-2) of the World Bank for the financial support provided for this study.

### REFERENCES

- Agarwal, R.K. 2017. Extraction processes of virgin coconut oil. *MOJ Food Process. Technol.*, 4(2): 87. <https://doi.org/10.15406/mojft.2017.04.00087>
- Aliasa, N.I., JayaKumara, J.K.A.L. and Zain, S.M. 2018. Characterization of Waste Cooking Oil for Biodiesel Production. *JurnalKejuruteraan*, SI 1(2), 79-83.

- Allah, F.U.M. and Alexandru, G. 2016. Waste cooking oil is a source of renewable fuel in Romania. *IOP Conf. Ser.: Mater. Sci. Eng.*, 147: 012133. <https://doi.org/10.1088/1757-899x/147/1/012133>
- Chozhavendhan, S., Vijay Pradhap Singh, M., Fransila, B., Praveen Kumar, R. and Karthiga Devi, G. 2020. A review on influencing parameters of biodiesel production and purification processes. *Curr. Res. Green Sustain. Chem.*, 1-2: 1-6. <https://doi.org/10.1016/j.crgsc.2020.04.002>
- Deen, A., Visvanathan, R., Wickramarachchi, D., Marikkar, N., Nammi, S., Jayawardana, B.C. and Liyanage, R. 2020. Chemical composition and health benefits of coconut oil: an overview. *J. Sci. Food Agric.*, 101(6): 2182-2193. <https://doi.org/10.1002/jsfa.10870>
- Demirbaş, A. 2008. *Biodiesel: A Realistic Fuel Alternative for Diesel Engines*. Springer, The Netherlands. <https://doi.org/10.1007/978-1-84628-995-8>
- Encinar, J., Pardal, A., Sánchez, N. and Nogales, S. 2018. Biodiesel by transesterification of rapeseed oil using ultrasound: A kinetic study of base-catalyzed reactions. *Energies*, 11(9): 2229. <https://doi.org/10.3390/en11092229>
- Enweremadu, C.C. and Mbarawa, M.M. 2009. Technical aspects of production and analysis of biodiesel from used cooking oil: A review. *Renew. Sustain. Energy Rev.*, 13(9): 2205-2224. <https://doi.org/10.1016/j.rser.2009.06.007>
- Ganesan, B., Brothersen, C. and McMahon, D.J. 2013. Fortification of foods with omega-3 polyunsaturated fatty acids. *Crit. Rev. Food Sci. Nutri.*, 54(1): 98-114. <https://doi.org/10.1080/10408398.2011.578221>
- Ge, J., Yoon, S. and Choi, N. 2017. Using canola oil biodiesel as an alternative fuel in diesel engines: A review. *Appl. Sci.*, 7(9): 881. <https://doi.org/10.3390/app7090881>
- Hossain, A. and Mazen, M. 2010. Effects of catalyst types and concentrations on biodiesel production from waste soybean oil biomass as renewable energy and environmental recycling process. *Austr. J. Crop Sci.*, 4(7): 550-555. <https://catalog.extension.oregonstate.edu>. <https://www.gardeningplaces.com/articles/oil-crops-compared1.htm>
- Ilkiliç C., Öner C. and Firat, M. 2017. Biodiesel fuel is obtained from sunflower oil as an alternative fuel for diesel engines. *E-J. Sci. Technol.*, 7(3): 141
- International Olive Oil Council. 2003. Trade standards applying to olive oil and olive pomace oil". COI/T.15/NC, no 3/Rev.1./5.December 2003. International Olive Oil Council, Madrid, Spain.
- Kawentar, W.A. and Budiman, A. 2013. "Synthesis of Biodiesel from Second-Used Cooking Oil". *Energy Procedia*, 32, 190-199. <https://doi.org/10.1016/j.egypro.2013.05.025>
- Lamichhane, G., Khadka, S., Adhikari, S., Koirala, N. and Poudyal, D.P. 2020. Biofuel production from waste cooking oils and its physicochemical properties in comparison to petrodiesel. *Nepal J. Biotechnol.*, 8(3): 87-94. <https://doi.org/10.3126/njb.v8i3.33661>
- Mansourpoor, M. 2012. Optimization of biodiesel production from sunflower oil using response surface methodology. *J. Chem. Eng. Process Technol.*, 03(05): 141. <https://doi.org/10.4172/2157-7048.1000141>
- Mihankhah, T., Delnavaz, M. and Khaligh, N.G. 2016. Eco-friendly biodiesel production from olive oil waste using solar energy. *Energy Sour. Part A: Recov. Utiliz. Environ. Eff.*, 38(24): 3668-3672. <https://doi.org/10.1080/15567036.2016.1167792>
- Miyuranga, K.A.V., Thilakarathne, D., Arachchige, U.S.P.R., Jayasinghe, R.A. and Weerasekara, N.A. 2021. Catalysts for biodiesel production: A review. *Asian J. Chem.*, 33(9): 1985-1999. <https://doi.org/10.14233/ajchem.2021.23332>
- Mondal, P., Kumari, P., Singh, J., Verma, S., Chaurasia, A. and Singh, P. 2017. Oil from Algae. In Mondal, P. and Dalai, A. (eds), *Sustainable Utilization of Natural Resources* (1st ed.). CRC Press, Florida, pp. 66-141.
- Ojiego, B., Onyia, O. and Abdulraman, F. 2014. Production of biodiesel from used vegetable oil. *Glob. J. Biol. Agric. Health Sci.*, 3(1): 278-282.
- Ramos, B. 2021. *Production of Biodiesel from Vegetable Oils*. Master of Science thesis, Royal Institute of Technology (KTH).
- Refaat, A. 2009. Correlation between the chemical structure of biodiesel and its physical properties. *Int. J. Environ. Sci. Technol.*, 6(4): 677-694. <https://doi.org/10.1007/bf03326109>
- Russo, C., Cappelletti, G., Nicoletti, G., Di Noia, A. and Michalopoulos, G. 2016. Comparison of European olive production systems. *Sustainability*, 8(8): 825. <https://doi.org/10.3390/su8080825>
- Sagiroglu, A., Selen, I., Ozcan, M., Paluzar, H. and Toprakiran, N. 2011. Comparison of biodiesel productivities of different vegetable oils by acidic catalysis. *Chem. Ind. Chem. Eng. Quat.*, 17(1): 53-58. <https://doi.org/10.2298/ciceq100114054s>
- Saydut, A., Kafadar, A., Tonbul, Y., Kaya, C., Aydin, F. and Hamamci, C. 2010. Comparison of the biodiesel quality produced from refined sunflower (*Helianthus Annuus L*) oil and waste cooking oil. *Energy Explor. Exploit.*, 28(6): 499-512. <https://doi.org/10.1260/0144-5987.28.6.499>
- Supple, B., Howard-Hildige, R., Gonzalez-Gomez, E. and Leahy, J. 2002. The effect of steam treating waste cooking oil on the yield of methyl ester. *J. Am. Oil Chem. Soc.*, 79(2): 175-178. <https://doi.org/10.1007/s11746-002-0454-1>
- Thilakarathne, D., Miyuranga, K.A.V., Arachchige, U.S.P.R., Weerasekara, N.A. and Jayasinghe, R.A. 2021. Production of biodiesel from waste cooking oil in laboratory scale: A review. *Int. J. Sci. Eng. Sci.*, 5(6): 28-34.
- Zeb, A. and Murkovic, M. 2011. Olive (*Olea europaea L.*) seeds, from chemistry to health benefits. *Nuts Seeds Health Dis. Prev.*, 61: 847-853. <https://doi.org/10.1016/b978-0-12-375688-6.10100-8>
- Zulqarnain, A.M., Yusoff, M.H.M., Nazir, M.H, Zahid, I., Ameen, M., Sher F., Floresyona D. and Nursanto E.B. 2021. A comprehensive review of oil extraction and biodiesel production technologies. *Sustainability*, 13(2): 788. <https://doi.org/10.3390/su13020788>







# Impact of Environmental Pollutants on Alzheimer's Disease: A Review

Yogyata Srivastava\*, Abhishek Chauhan\*\*†, S. B. Singh\*\*\* and Tanu Jindal\*\*

\*Amity Institute of Environment Science, Amity University, Noida, Uttar Pradesh, 201303, India

\*\*Amity Institute of Environmental Toxicology, Safety and Management (AIETSM), Amity University, Noida, Uttar Pradesh, 201303, India

\*\*\*Rajendra Institute of Medical Sciences (RIMS), Ranchi, Jharkhand, 834009, India

†Corresponding author: Abhishek Chauhan; akchauhan@amity.edu

Nat. Env. & Poll. Tech.  
Website: [www.neptjournal.com](http://www.neptjournal.com)

Received: 28-10-2021  
Revised: 17-01-2022  
Accepted: 08-02-2022

## Key Words:

Alzheimer's disease  
PM<sub>10</sub>  
PM<sub>2.5</sub>  
Nanoparticles  
Lipophilic vaporized toxicants

## ABSTRACT

Environmental pollution is one of the major concerns as it affects public health and is responsible for various neurological disorders too. Neurological disorders are governed by many different factors - they can be genetic, based on lifestyle, or environmental. In many recent studies, it has been observed that exposure to many environmental pollutants increases the risk of Alzheimer's disease (AD). Pollutants like PM<sub>10</sub>, PM<sub>2.5</sub>, and some other ultrafine nanoparticles, lipophilic vaporized toxicant (acrolein) can easily reach the brain by crossing the blood-brain barrier after it they can activate the innate immune responses inside the target site like neurons, astrocytes, and microglia by this way they can be neurotoxic. Human epidemiological evidence proves that there is a correlation between environmental pollutants and neurological disorders like dysfunction of mitochondrial, oxidative stress, disruption in the myelin sheath, the blood-brain barrier anatomy alterations, and endoplasmic reticulum stress which direct towards cognitive impairment with lower quality of lifestyle. The review article aims to culminate the correlation between the environmental factors and Alzheimer's disease, The different sources of pollution and their effect on various stages of human life, developmental neurotoxicity, and neurological disorders also have been discussed.

## INTRODUCTION

Alzheimer's disease is called elderly dementia as it is responsible for 60–70% of global cases. This debilitating is progressive, and it is an irreversible illness (McKhann et al. 2011) According to WHO it is a global public health issue. Environmental air pollutions are responsible for neurotoxicity related to development, and for the teratogenic effect. Eventually, it becomes a cause of mental retardance or just a reduction in IQ level, or both. The exact process of how pollution induces neurotoxicity is still unknown but it is clear that it interferes with an inflammatory pathway (Akt/GSK3 $\beta$ , Nrf2/NF-k, and MAPKs/PI3K), modulates the neurotransmitters, and affects the endogenous antioxidant defense system too (Iqbal et al. 2020). Etiologically the relation between AD and environmental pollution is still not clear but in pathology, it is heavily acknowledged (Mir et al. 2020). German physician Alois Alzheimer originally described Alzheimer's disease in 1907 (Prince et al. 2016). He conducted years of research on two patients who exhibited hallucinations, aggression, and cognitive problems. Since 1907, there has not been a single treatment available to change AD. A summary of its pathology, epidemiology, and

genetics is provided in this article. After it, further therapy opportunities and upcoming remedial approaches will be taken into account (Sharma et al. 2020). According to epidemiological proof, education and physical fitness can act as a safeguard but diseases like diabetes in middle age and hypertension too can increase the risk of Alzheimer's disease (Xu et al. 2015). Research showed that obesity increases the risk of Alzheimer's disease and dementia but recently this was challenged (Qizilbash et al. 2015). Vascular risk factors can increase the risk of AD by a "double-hit" of superimposed cerebrovascular injury. It can also be possible that if there is any vascular damage that can affect the progress of pathology of Alzheimer's disease directly (Van Norden et al. 2012)

## ENVIRONMENT POLLUTANTS RESPONSIBLE FOR ALZHEIMER'S DISEASE

Air pollutants especially particulate matters increase the risk of oxidative stress, and hypertension, resulting in dementia and cognitive decline (Peters et al. 2019) Lancet commission (Commissions from the Lancet journals) in 2017 included air pollution in the list of responsible factors for dementia

(Livingston et al. 2017). Various pieces of evidence (Listed in Table 1) prove that pollutants like ozone, NO<sub>2</sub>, and particulate matter are responsible to decrease cognitive strength and increase the case of dementia and Alzheimer's disease.

## MECHANISM OF EXPOSER AND EFFECT ON BRAIN HEALTH

As part of the mechanism of neurodegenerative illness, oxidative stress, inflammation, protein aggregation, and dysfunction in mitochondrial neurons all play a role (Genc et al. 2012) (Fig.1). A study on a dog was conducted in Mexico City (highly polluted). The dog was living in a highly polluted area for a long time. The study observed high brain inflammation (Calderon et al. 2002). The progression of oxidative stress involves the mechanisms of neurological disturbances and it can be caused by pollution (Calderon et al. 2002, Peters et al. 2006). Air pollution is a mixture of gasses and some other factors like PM<sub>10</sub> and PM<sub>2.5</sub> (Costa et al. 2017). PM<sub>2.5</sub> have the ability to translocate up to the alveolar region. From the alveolar region, it merges with the systemic circulation and finally reaches the brain (Costa et

al. 2019). The ultrafine particulate matter (UFPM), which has a size <100 nm is more harmful as because of its size it can easily enter into the systemic circulation. They can reach up to the brain via the olfactory bulb or the other way through the blood-brain barrier (Costa et al. 2017, Iqbal et al. 2018). After translocating across the CNS, they activate the innate immune responses, which activate microglia and increase lipid peroxidation. Because of it, patients suffer from neuroinflammation specifically in the cortex and hippocampus (Morris-Schaffer et al. 2019). The exact pathway of neurotoxicity induced by air pollution is still unknown; but, few studies suggest nanoparticles interference in the alteration of the amyloid-beta process and neuroinflammation (Oudin 2020).

## EVIDENCES ABOUT ALZHEIMER'S DISEASE AND POLLUTION

In other published studies including people (who took part in the third National Health and Nutrition Examination Survey; NHANES III; USA) aged 18 to 59, it was found that there was only a weak correlation between reaction time,

Table 1: Effect of pollutants on cognitive health.

Pollutants	Air Quality Standards			Summary	Reference
	India: Air Quality Standards		WHO: Ambient (outdoor) air pollution		
	Industrial, Residential, Rural, and Other Area	Ecologically Sensitive Area (notified by Central Government)	Industrial, Residential, Rural, and Other Area		
PM <sub>2.5</sub>	40 µg.m <sup>-3</sup> annual mean 60 µg.m <sup>-3</sup> 24-hour mean	40 µg.m <sup>-3</sup> annual mean 60 µg.m <sup>-3</sup> 24-hour mean	20 µg.m <sup>-3</sup> annual mean 50 µg.m <sup>-3</sup> 24-hour mean	The study suggested that the cognitive decline rate is higher in women who live in a polluted areas where the level of PM <sub>2.5</sub> is higher. In the long-term exposure rate of cognitive decline per 10 µg.m <sup>-3</sup> . No correlation could be found between one month, one to two months, or 2 or 5 years of exposure.	Weuve et al. (2012)
PM <sub>10</sub>	60 µg.m <sup>-3</sup> annual mean 100 µg.m <sup>-3</sup> 24-hour mean	60 µg.m <sup>-3</sup> annual mean 100 µg.m <sup>-3</sup> 24-hour mean	20 µg.m <sup>-3</sup> annual mean 50 µg.m <sup>-3</sup> 24-hour mean	The study was conducted on participants who did not move to London during the study. According to this study PM <sub>10</sub> exposure (with a 4-y lag) is linked with cognitive decline.	Tonne et al. (2014)
NO <sub>2</sub>	40 µg.m <sup>-3</sup> annual mean 80 µg.m <sup>-3</sup> 1-hour mean	30 µg.m <sup>-3</sup> annual mean 80 µg.m <sup>-3</sup> 1-hour mean	40 µg.m <sup>-3</sup> annual mean  200 µg.m <sup>-3</sup> 1-hour mean	An increased interquartile concentration of NO <sub>2</sub> is directly associated with dementia risk.	Chen et al. (2017)
O <sub>3</sub>	100 µg.mL <sup>-1</sup> per 8 hour 180 µg.m <sup>-1</sup> per hour	100 µg.mL <sup>-1</sup> per 8 hour 180 µg.m <sup>-1</sup> per hour	100 µg.m <sup>-3</sup> 8-hour mean	A study was conducted based on CDR-SB assessments and MMSE ( <i>p</i> <0.05). In this study, participants were exposed to the highest and medium O <sub>3</sub> as a result of cognitive decline triggered.	Cleary et al. (2018)

visual-motor coordination, and learning with an increment of annual Particulate Matter 10(PM<sub>10</sub>) levels. (cardiovascular risk factors, many markers of socioeconomic status, and ethnicity are adjusted.) (Chen & Schwartz 2009). Another study (in which N=780) was conducted on non-Hispanic black and white people in which the age group was 55 and older. It was observed that the older adults who were living in the areas where the concentrations of PM<sub>2.5</sub> were high, had an error rate 1.5 times higher than the people who were living in lower concentrations (Ailshire & Crimmins 2014). One more finding suggested that long-term exposure to pollution can cause Alzheimer's disease in elderly people

(Calderón-Garcidueñas et al. 2004). Small particles are more dangerous for cognitive performance than larger ones. It can be because they have more chances to reach the brain than larger ones as they have a smaller size (Zeng et al. 2010).

A postmortem study on a dog suggested that air pollution affects the brain by creating neurotoxicity and histological aberration, especially in the cortex region, histological damage can be easily marked. Neuroinflammation and neurodegeneration are also marked (Calderon-Garciduenas et al. 2003). In Alzheimer's disorder etiology, there are many other factors responsible like certain kinds of head injury, genetics aging, different environmental metabolites, and substances.

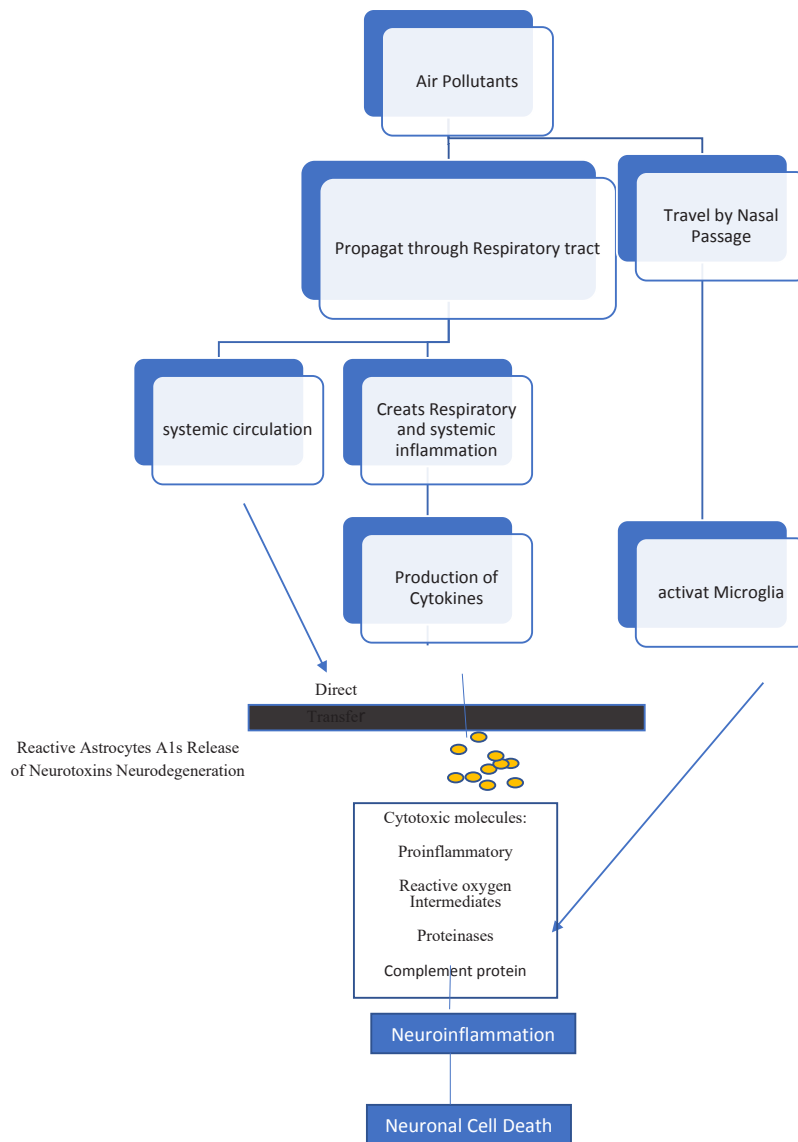


Fig. 1: Effect of air pollutants on brain.

(Coon et al. 2007, Calderon-Garciduenas et al. 2004, Guo et al. 2000). This fact is already known that AD is affected by genetic elements. AD is correlated with the APOE-E4 allele predominantly. Because the environmental element is still poorly understood, there is a connection between the delay in exposure to Alzheimer's disease and the onset of AD. However, due to the time delay between exposure and the role of environmental factors, their function in AD is not well known (Coon et al. 2007, Rahman et al. 2020).

Research indicates that genetic predisposition accounts for 70% of AD cases, whereas the remaining 30% are caused by lifestyle-related problems including obesity, hypertension, smoking, etc. (Ballard et al. 2011). All environmental pollutants and toxins are not responsible for Alzheimer's disease, neurotoxins found in the environment are responsible for neurological issues in elderly people (Baldi et al. 2003). However, research is needed in the field that environmental pollutants are alone responsible for the progress of AD or a combination of being responsible.

## EFFECT OF AIR POLLUTANTS ON THE PROGRESSION OF ALZHEIMER'S DISEASE

Due to metabolic imbalance oxidative stress generates and as a result free radicles accumulate in the body which leads to problems like neuroinflammation and neuropathology (Block & Calderón-Garcidueñas 2009). Many studies suggested that PM<sub>2.5</sub> and PM<sub>10</sub> play a very important role in AD and other neurodegenerative disorders causation. Metals such as nickel, lead, and gases like sulfur-di-oxide, carbon-mono oxide, and nitrogen oxide may play an important role in the production of ROS (reactive oxygen species) and can cause oxidative stress cerebrovascular damage, neuroinflammation, accumulation of A $\beta$ peptide which is a major contributor in the progression of to AD (Moulton & Yang 2012). It is reported that the brain of mice which was exposed to Ni (nickel) showed increased amyloid- $\beta$ 40 and amyloid- $\beta$ 42 these both are associated with Alzheimer's disease (Kim et al. 2012). A study on children conducted in Mexico City showed that when children get exposed to pollutants, a protein starts

depositing inside their body which is analogous to the protein found in the early stages of Alzheimer's disease (Calderon-Garciduenaset al. 2004). In another study, it is reported that 56% of children who were exposed to PM at a younger age had white matter lesions which can cause neurodegeneration and neuroinflammation in upcoming stages of life (Kim et al. 2012). Exposure to these particles can cause neuro-inflammation because of the activation of the sensor of the ROS pathogen (Calderón-Garcidueñas et al. 2012). Hippocampus is a commonly affected area in the brain that is affected by AD. Adult Wistar rats show heavy progressive neuro degradation when exposed to O<sub>3</sub>, In the inflammation process, it disrupts ROS, and minimizes hippocampus repair (Rivas-Arancibia et al. 2009). It is shown in a study that in humans and animals, the expression of neurodegenerative disease pathology-linked makers increases with the organic compound, PM<sub>10</sub>, gases, and PM<sub>2.5</sub> (Costa et al. 2017). Many epidemiological, experimental, observational, and clinical studies suggested that air pollution can cause the disease related to CNS and AD is one of them (Genc et al. 2012). Laboratory experiments have proved that many VOCs such as toluene, ketone, and benzene can perform biochemical and morphological changes in neurons eventually which can be a cause of AD. (Kukull et al. 1995). Results from chromatography and mass spectrometry show that AD patients have higher levels of VOCs than normal patients when compared to those without the disease (Tisch et al. 2013).

## NANOPARTICLES EXPOSURE TO ALZHEIMER'S DISEASE

Epidemiologically there is no study to correlate nanoparticles exposure to Alzheimer's disease, but according to experimental evidence, it is proved that NP has a role in neurological disorders. Recently, it was discovered in a study on mice that giving TiO<sub>2</sub>-NPs to them through their noses causes gliosis and oxidative stress. Other impacts include a decline in the number of neurons in the hippocampus that are connected to cognition and memory due to neuronal death (Ze et al. 2014). When male and female mice were

Table 2: Air pollutants Responsible for AD Progression.

Air pollutant	Dose	Sample size	Summary of the experiment	References
PM and O <sub>3</sub>	1mg.m <sup>-3</sup> Ni and NP were given through inhalation. Ozone exposure dose was 0.25 ppm.day <sup>-1</sup> up to 4h.	Male and Female mice were used Control n = 5 Exposed n = 11 male = 6 female = 5	Rapid doubling of amyloid- $\beta$ 40 affected the repairing system of the brain	Rivas-Arancibia et al. (2009), Kim et al. (2012)
VOCs	Exposed Occupationally	Male Wistar rats: g were chosen AD n = 193 Control n = 243	AD developed	Kukull et al. (1995)

Table 3: Some research pieces of evidence showing the change in cognitive behavior due to air pollution.

Title of the Study	Findings	References
Association between Traffic-Related Air Pollution in Schools and Cognitive Development in Primary School Children: A Prospective Cohort Study	The polluted area has seen a small cognitive development in school children as compared to the non-polluted area.	Sunyer et al. (2015)
Association of Traffic-Related Air Pollution with Children's Neurobehavioral Functions in Quanzhou, China	Children studying in schools in polluted areas had fewer marks in testing cognitive, sensory, motor, and psychomotor functions than those studying in non-polluted areas.	Wang et al. (2009)
Impact of short-term risk to ambient air pollution on cognitive performance and cognitive air pollution on human capital formation.	The conclusion was that PM <sub>10</sub> , PM <sub>2.5</sub> , and CO Exposure reduced the test scores of high school students in Israel.	Lavy et al. (2014)
Neurobehavioral performance in adolescents is inversely associated with traffic exposure.	The study suggested an opposite relationship between the ability to pay attention in a group of 606 teenagers and traffic contact.	Kicinski et al. (2015)
Longitudinal relationship between air pollution risk in school and cognitive development among schoolchildren over a period of 3.5 years.	A study found 3.5 years were between exposure to air pollution at longitudinal Association School and the development of cognitive health in school-going children.	Forns et al. (2017)
Traffic-related air pollution and cognitive function in a platoon of older men.	It was observed in the old people that ambient air pollution which was related to traffic is associated with the decline in cognitive functioning in older men.	Power et al. (2011)
Exposure to air pollution and cognitive decline in older women.	The study was about cognitive decline regarding the relationship between PM <sub>25</sub> and PM <sub>10</sub> .	Weuve et al. (2012)
Residential proximity to the nearest major roadway and cognitive function in community-dwelling seniors: results from the MOBILIZE Boston Study	The study cleared that people who live close to the road get a 34% more chance of scoring less in MMSE (the study population was ~ 77 years old). According to the study, the proximity of the road was directly linked to psychomotor speed, oral learning and memory, executive functioning, and language reduction.	Wellenius et al. (2012)
Living near major roads and the incidence of dementia, Parkinson's disease, and multiple sclerosis: a population-based cohort study	A large population-based study in which people living near the road were at a higher risk of dementia, but not Parkinson's disease.	Chen et al. (2017)
Components of air pollution and cognitive function in middle-aged and older adults in Los Angeles.	In a study of 1496 older healthy and middle-aged people that specific components in ambient air pollution are associated with low cognitive abilities.	Gatto et al. (2014)
Exposure to ambient air pollution and dementia events: a population-based platoon study	In a population-based study that involved residents in Ontario (Canada), 55–85-year-old authors studied the population. In which it was exposed to air pollution even at relatively low levels related to a high risk of insanity.	Chen et al. (2017)
Fine particulate matter air pollution and cognitive function among older adults in the US.	The study was on adults aged 50 ~ who were living in areas where PM <sub>2.5</sub> was higher. It was observed that they had a worse cognitive function, especially in concern of the relevant memory component.	Ailshire and Clarke (2014)

treated with nanoparticles of Al, Cu, and Ag multiple times various alterations like motor deterioration, sensory, and cognitive were recorded in their brain. (Sharma et al. 2009, Shanker Sharma & Sharma 2012). When mouse neuro-2a and human (SK-N-SH) neuroblastoma cells were exposed to silica nanoparticles, the A level of (intracellular) both cell lines increased, and the APP level increases with a decrease in NEP protein level. The whole process was mediated with the help of increased ROS production (Yang et al. 2014). In another study when Neuro 2a cells were treated with silver nano-particles, they exhibited the deposition of A $\beta$  plaques

and the expression of APP enhanced, but NEP and LPR1 expression was reduced which directly says that silver NPs alter the amyloidogenic pathway as a result of AD chances get increased (Huang et al. 2015)

## CONCLUSION

In the Progression of AD, environmental toxicant has an important role and are important for public health. But some chemical agents will be always in the limelight. Many inorganic and organic compounds have a direct or indirect link

with AD. but in the lack of direct evidence, all these things are just elusive. As there are other factors contributing to the genesis of AD, the neurotoxic chemical has to be further examined for its potential role in AD. Experimental research and data demonstrate the fact that there are potential risks associated with exposure to various environmental contaminants. These pollutants and oxidative stress production show a similar toxicity mechanism. Both of these represent typical neurodegenerative disease mechanisms. If oxidative stress is caused by the creation of ROS or antioxidant enzymes that disrupt a few proteins, such as  $\alpha$ -syn, A $\beta$ , and Tau. As a result, the cerebral cortex and hippocampus of AD patients lose neurons.

Due to these neurotoxins, oxidative stress generates which inhibits various enzymes in pathways that are involved in the accession of various noxious materials in many neural cells including A $\beta$ , byproducts of oxidative aberrant proteins, and DNA oxidation which can alter regulations (epigenetic/genetic). Chemicals related to AD exposure will continue in the future also as they are commercially in use and an essential service also but awareness can be one of the weapons against it. Research is also needed in the field of biomarkers related to this field so that early diagnosis can be possible. There is also a need for epidemiological study in this field.

## ACKNOWLEDGMENT

The work for this article was supported by the Council of Scientific & Industrial Research (CSIR), India for the CSIR-UGC-NET fellowship [award letter No. 09/915(0015)/2019-EMR-I]. The author is also thankful to Amity, Noida, UP, and India for all the necessary support.

## ABBREVIATIONS

**PM<sub>2.5</sub>**: Fine particles with a diameter of 2.5 microns ( $\mu$ m) or less

**NO<sub>2</sub>**: Nitrogen dioxide

**PM<sub>10</sub>**: Coarse particles with a diameter of 10  $\mu$ m or less

**PM**: Particulate matter

**AD**: Alzheimer's Disease

## REFERENCES

Ailshire, J.A. and Crimmins, E.M. 2014. Fine particulate matter air pollution and cognitive function among older US adults. *Am. J. Epidemiol.*, 180(4): 359-366.

Ailshire, J. A. and Clarke, P. 2015. Fine particulate matter air pollution and cognitive function among US older adults. *Journals of Gerontology Series B: Psychological Sciences and Social Sciences*, 70(2): 322-328.

Baldi, I., Lebaillly, P., Mohammed-Brahim, B., Letenneur, L., Dartigues, J. F. and Brochard, P. 2003. Neurodegenerative diseases and exposure to pesticides in the elderly. *American Journal of Epidemiology*, 157(5): 409-414.

Block, M. L. and Calderón-Garcidueñas, L. 2009. Air pollution: mechanisms of neuroinflammation and CNS disease. *Trends in Neurosciences*, 32(9): 506-516.

Ballard, C., Khan, Z., Clack, H. and Corbett, A. 2011. Nonpharmacological treatment of Alzheimer disease. *The Canadian Journal of Psychiatry*, 56(10): 589-595.

Calderón-Garcidueñas, L.N., Reed, W., Maronpot, R.R., Henriquez-Roldán, C., Delgado-Chavez, R., Calderón-Garcidueñas, A.N. and Swenberg, J.A. 2004. Brain inflammation and Alzheimer's-like pathology in individuals exposed to severe air pollution. *Toxicol. Pathol.*, 32(6): 650-658.

Calderon-Garcidueñas, L., Azzarelli, B., Acuna, H., Garcia, R., Gambling, T. M., Osnaya, N. and Rewcastle, B. 2002. Air pollution and brain damage. *Toxicologic Pathology*, 30(3): 373-389.

Calderón-Garcidueñas, L.N., Azzarelli, B., Acuna, H., Garcia, R., Gambling, T.M., Osnaya, N. and Rewcastle, B. 2002. Air pollution and brain damage. *Toxicol. Pathol.*, 30(3): 373-389.

Calderón-Garcidueñas, L., Kavanaugh, M., Block, M., D'Angiulli, A., Delgado-Chávez, R., Torres-Jardón, R. and Díaz, P. 2012. Neuroinflammation, hyperphosphorylated tau, diffuse amyloid plaques, and down-regulation of the cellular prion protein in air pollution exposed children and young adults. *Journal of Alzheimer's Disease*, 28(1): 93-107.

Calderón-Garcidueñas, L., Reed, W., Maronpot, R. R., Henriquez-Roldán, C., Delgado-Chavez, R., Calderón-Garcidueñas, A. and Swenberg, J. A. 2004. Brain inflammation and Alzheimer's-like pathology in individuals exposed to severe air pollution. *Toxicologic Pathology*, 32(6): 650-658.

Chen, J. C. and Schwartz, J. 2009. Neurobehavioral effects of ambient air pollution on cognitive performance in US adults. *Neurotoxicology*, 30(2): 231-239.

Chen, H., Kwong, J.C., Copes, R., Tu, K., Villeneuve, P.J., Van Donkelaar, A. and Burnett, R.T. 2017. Living near major roads and the incidence of dementia, Parkinson's disease, and multiple sclerosis: a population-based cohort study. *The Lancet*, 389(10070): 718-726.

Cleary, E.G., Cifuentes, M., Grinstein, G., Brugge, D. and Shea, T.B. 2018. Association of low-level ozone with cognitive decline in older adults. *J. Alzheimer's Dis.*, 61(1): 67-78.

Costa, L.G., Cole, T.B., Coburn, J., Chang, Y.C., Dao, K. and Roqué, P.J. 2017. Neurotoxicity of traffic-related air pollution. *Neurotoxicology*, 59: 133-139.

Costa, L.G., Cole, T.B., Dao, K., Chang, Y.C. and Garrick, J.M. 2019. Developmental impact of air pollution on brain function. *Neurochem. Int.*, 131: 104580.

Coon, K. D., Myers, A. J., Craig, D. W., Webster, J. A., Pearson, J. V., Lince, D. H. and Stephan, D. A. 2007. A high-density whole-genome association study reveals that APOE is the major susceptibility gene for sporadic late-onset Alzheimer's disease. *Journal of Clinical Psychiatry*, 68(4): 613.

Forns, J., Dadvand, P., Esnaola, M., Alvarez-Pedrerol, M., López-Vicente, M., Garcia-Esteban, R., Cirach, M., Basagaña, X., Guxens, M. and Sunyer, J. 2017. Longitudinal association between air pollution exposure at school and cognitive development in school children over a period of 3.5 years. *Environmental Research*, 159: 416-421.

Gatto, N. M., Henderson, V. W., Hodis, H. N., John, J. A. S., Lurmann, F., Chen, J. C. and Mack, W. J. 2014. Components of air pollution and cognitive function in middle-aged and older adults in Los Angeles. *Neurotoxicology*, 40: 1-7.

Guo, C., Wang, P., Zhong, M. L., Wang, T., Huang, X. S., Li, J. Y. and Wang, Z. Y. 2013. Deferoxamine inhibits iron induced hippocampal tau phosphorylation in the Alzheimer transgenic mouse brain. *Neurochemistry International*, 62(2): 165-172.

Huang, C. L., Hsiao, I. L., Lin, H. C., Wang, C. F., Huang, Y. J. and Chuang, C. Y. 2015. Silver nanoparticles affect on gene expression of inflammatory and neurodegenerative responses in mouse brain neural cells. *Environmental Research*, 136: 253-263.

- Kicinski, M., Vermeir, G., Van Larebeke, N., Den Hond, E., Schoeters, G., Bruckers, L. and Nawrot, T. S. 2015. Neurobehavioral performance in adolescents is inversely associated with traffic exposure. *Environment International*, 75: 136-143.
- Kim, S.H., Knight, E.M., Saunders, E.L., Cuevas, A.K., Popovech, M., Chen, L.C. and Gandy, S. 2012. Rapid doubling of Alzheimer's amyloid- $\beta$ 40 and 42 levels in brains of mice exposed to a nickel nanoparticle model of air pollution. *F1000Research*, 1.
- Kukull, W. A., Larson, E. B., Bowen, J. D., McCormick, W. C., Teri, L., Pfanschmidt, M. L. and van Belle, G. 1995. Solvent exposure as a risk factor for Alzheimer's disease: a case-control study. *American Journal of Epidemiology*, 141(11): 1059-1071.
- Lavy, V., Ebenstein, A. and Roth, S. 2014. The impact of short term exposure to ambient air pollution on cognitive performance and human capital formation (No. w20648). National Bureau of Economic Research.
- Myers, A. J., Gibbs, J. R., Webster, J. A., Rohrer, K., Zhao, A., Marlowe, L. and Hardy, J. 2007. A survey of genetic human cortical gene expression. *Nature Genetics*, 39(12): 1494-1499.
- Genc, S., Zadeoglulari, Z., Fuss, S. H. and Genc, K. 2012. The adverse effects of air pollution on the nervous system. *J. Toxicol.*, 2: 12
- Iqbal, A., Sharma, S., Sharma, K., Bhavsar, A., Hussain, I., Iqbal, M.K. and Kumar, R. 2018. Intranasally administered pitavastatin ameliorates pentylentetrazol-induced neuroinflammation, oxidative stress, and cognitive dysfunction. *Life Sci.*, 211: 172-181.
- Iqbal, A., Ahmed, M., Ahmad, S., Sahoo, C.R., Iqbal, M.K. and Haque, S. E. 2020. Environmental neurotoxic pollutants. *Environ. Sci. Pollut. Res.*, 11: 1-24.
- Livingston, G., Sommerlad, A., Orgeta, V., Costafreda, S.G., Huntley, J., Ames, D. and Mukadam, N. 2017. Dementia prevention, intervention, and care. *The Lancet*, 390(10113): 2673-2734.
- McKhann, G.M., Knopman, D.S., Chertkow, H., Hyman, B.T., Jack Jr, C.R., Kawas, C.H. and Phelps, C.H. 2011. The diagnosis of dementia due to Alzheimer's disease: recommendations from the National Institute on Aging Alzheimer's Association workgroups on diagnostic guidelines for Alzheimer's disease. *Alzheimer's Dementia*, 7(3): 263-269.
- Mir, R.H., Sawhney, G., Pottou, F.H., Madishetti, S., Jachak, S.M., Ahmed, Z. and Masoodi, M. H. 2020. Role of environmental pollutants in Alzheimer's disease: A review. *Environ. Sci. Pollut. Res.*, 54: 1-19.
- Morris-Schaffer, K., Merrill, A. K., Wong, C., Jew, K., Sobolewski, M. and Cory-Slechta, D. A. 2019. Limited developmental neurotoxicity from neonatal inhalation exposure to diesel exhaust particles in C57BL/6 mice. *Particle Fib. Toxicol.*, 16(1): 1-14.
- Moulton, P. V. and Yang, W. 2012. Air pollution, oxidative stress, and Alzheimer's disease. *Journal of Environmental and Public Health*, <https://doi.org/10.1155/2012/472751>
- Oudin, A. 2020. Short review: Air pollution, noise and lack of greenness as risk factors for Alzheimer's disease-epidemiologic and experimental evidence. *Neurochem. Int.*, 134: 104646.
- Peters, A., Veronesi, B., Calderón-Garcidueñas, L., Gehr, P., Chen, L. C., Geiser, M. and Schulz, H. 2006. Translocation and potential neurological effects of fine and ultrafine particles a critical update. *Particle Fiber Toxicol.*, 3(1), 1-13.
- Power, M. C., Weisskopf, M. G., Alexeeff, S. E., Coull, B. A., Spiro III, A. and Schwartz, J. 2011. Traffic-related air pollution and cognitive function in a cohort of older men. *Environmental Health Perspectives*, 119(5): 682-687.
- Prince, M. J., Comas-Herrera, A., Knapp, M., Guerchet, M. M. and Karagiannidou, M. 2016. World Alzheimer Report 2016-Improving healthcare for people living with dementia: Coverage, quality and costs now and in the future.
- Rahman, A., Schelbaum, E., Hoffman, K., Diaz, I., Hristov, H., Andrews, R. and Mosconi, L. 2020. Sex-driven modifiers of Alzheimer risk: a multimodality brain imaging study. *Neurology*, 95(2): e166-e178.
- Rivas-Arancibia, S., Guevara-Guzmán, R., López-Vidal, Y., Rodríguez-Martínez, E., Zanardo-Gomes, M., Angoa-Pérez, M. and Raisman-Vozari, R. 2010. Oxidative stress caused by ozone exposure induces loss of brain repair in the hippocampus of adult rats. *Toxicological Sciences*, 113(1): 187-197.
- Sharma, V. K., Mehta, V. and Singh, T. G. 2020. Alzheimer's disorder: epigenetic connection and associated risk factors. *Current Neuropharmacology*, 18(8): 740-753.
- Shanker Sharma, H. and Sharma, A. 2012. Neurotoxicity of engineered nanoparticles from metals. *CNS & Neurological Disorders-Drug Targets (Formerly Current Drug Targets-CNS & Neurological Disorders)*, 11(1): 65-80.
- Sunyer, J., Esnaola, M., Alvarez-Pedrerol, M., Forns, J., Rivas, I., López-Vicente, M. and Querol, X. 2015. Association between traffic-related air pollution in schools and cognitive development in primary school children: a prospective cohort study. *PLoS Medicine*, 12(3): e1001792.
- Tisch, U., Schlesinger, I., Ionescu, R., Nassar, M., Axelrod, N., Robertman, D. and Haick, H. 2013. Detection of Alzheimer's and Parkinson's disease from exhaled breath using nanomaterial-based sensors. *Nanomedicine*, 8(1): 43-56.
- Tonne, C., Elbaz, A., Beevers, S. and Singh-Manoux, A. 2014. Traffic-related air pollution in relation to cognitive function in older adults. *Epidemiology*, 25(5): 674.
- Van Norden, A.G., van Dijk, E.J., de Laat, K.F., Scheltens, P., OldeRikkert, M.G. and De Leeuw, F.E. 2012. Dementia: Alzheimer pathology and vascular factors: From mutually exclusive to interaction. *Biochim. Biophys. Acta Mol. Basis Dis.*, 1822(3): 340-349.
- Peters, R., Ee, N., Peters, J., Booth, A., Mudway, I. and Anstey, K.J. 2019. Air pollution and dementia: A systematic review. *J. Alzheimer's Dis.*, 70(s1): S145-S163.
- Wang, S., Zhang, J., Zeng, X., Zeng, Y., Wang, S. and Chen, S. 2009. Association of traffic-related air pollution with children's neurobehavioral functions in Quanzhou, China. *Environmental Health Perspectives*, 117(10): 1612-1618.
- Weuve, J., Puett, R. C., Schwartz, J., Yanosky, J. D., Laden, F. and Grodstein, F. 2012. Exposure to particulate air pollution and cognitive decline in older women. *Archives of Internal Medicine*, 172(3): 219-227.
- Qizilbash, N., Gregson, J., Johnson, M.E., Pearce, N., Douglas, I., Wing, K. and Pocock, S.J. 2015. BMI and risk of dementia in two million people over two decades: A retrospective cohort study. *The Lancet Diab. Endocrinol.*, 3(6): 431-436.
- Wellenius, G. A., Boyle, L. D., Coull, B. A., Milberg, W. P., Gryparis, A., Schwartz, J. and Lipsitz, L. A. 2012. Residential proximity to nearest major roadway and cognitive function in community-dwelling seniors: results from the MOBILIZE boston study. *Journal of the American Geriatrics Society*, 60(11): 2075-2080.
- Yang, X., Li, J., Chen, H., Ma, Q., Sui, X., Tian, S., Ying, M., Zhang, Q., Luo, Y., Zhuang, Z. and Liu, J. 2014. Uptake of silica nanoparticles: neurotoxicity and Alzheimer-like pathology in human SK-N-SH and mouse neuro2a neuroblastoma cells. *Toxicology Letters*, 229(1): 240-249.
- Zeng, Y., Gu, D., Purser, J., Hoening, H. and Christakis, N. 2010. Associations of environmental factors with elderly health and mortality in China. *Am. J. Pub. Health*, 100(2): 298-305.
- Ze, Y., Sheng, L., Zhao, X., Hong, J., Ze, X., Yu, X. and Hong, F. 2014. TiO<sub>2</sub> nanoparticles induced hippocampal neuroinflammation in mice. *PLoS One*, 9(3): e92230.







# Nitrous Oxide Emissions Generated in Coffee Cultivation: A Systematic Review

L. Quiñones-Huatangari\*†, F. H. Fernandez-Zarate\*\* and A. E. Huaccha-Castillo\*(\*\*\*)

\*Instituto de Ciencia de Datos, Universidad Nacional de Jaén, Cajamarca, Perú

\*\*Facultad de Ciencias Agrarias, Universidad Nacional Autónoma de Chota, Cajamarca, Perú

\*\*\*Ingeniería Forestal y Ambiental, Universidad Nacional de Jaén, Cajamarca, Perú

†Corresponding author: L. Quiñones-Huatangari; lenin.quinones@unj.edu.pe

## Nat. Env. & Poll. Tech.

Website: [www.neptjournal.com](http://www.neptjournal.com)

Received: 19-01-2022

Revised: 08-03-2022

Accepted: 10-03-2022

### Key Words:

Greenhouse effect

Climate change

Nitrous oxide emissions

*Coffea arabica*

## ABSTRACT

The objective of the research was to provide an overview of soil N<sub>2</sub>O emissions in coffee cropping systems; summarizing available field data on soil emissions and identifying controlling factors (fertilizer type, precipitation, temperature, altitude). A systematic search of Scopus, Science Direct, Springer, and Scielo for experimental-type studies was conducted from January 2000 to October 2021. Of the seventy manuscripts determined through the search strategy, eight studies met the inclusion criteria. Analysis of the included studies revealed that they were conducted in Ecuador, Costa Rica, and Nicaragua; the rainfall of the fields ranged from 910 mm to 2740 mm per year and the average temperature was 20.3°C. Coffee is planted under agroforestry systems and monocultures; in addition, the most abundant forest species in coffee agroforestry systems are leguminous plants of the Inga and Erythrina genus and 60% of the studies have been developed with the Catuai coffee variety. The pH and humidity of the soil where coffee plantations are developed range from 4.67 to 6.34 and 53.3 to 67.05% respectively. Finally, the fertilizers used are of chemical, organic, and chemical + polymer origin, at fertilization rates ranging from 66 to 400 kg.N.ha<sup>-1</sup>.yr<sup>-1</sup> and N<sub>2</sub>O emissions ranging from 0.2 to 12.8 kg.N.ha<sup>-1</sup>.yr<sup>-1</sup>. Overall, the present systematic review provides a scientific basis for evaluating N<sub>2</sub>O emissions generated in coffee crops.

## INTRODUCTION

Agriculture is responsible for 10 to 12% of total greenhouse gas (GHG) emissions, 52% of N<sub>2</sub>O, 18% of CO<sub>2</sub> and 84% of CH<sub>4</sub> (IPCC 2014), the increase in the atmospheric concentrations of these gases generates global warming (Guo et al. 2021). Coffee is the most traded tropical agricultural product worldwide, its cultivation thrives in more than 50 countries and covers an area of more than 11 million hectares (Davis et al. 2012, De Beenhouwer et al. 2015), due to population growth and increased demand for this product, GHG emissions from these agricultural ecosystems tend to continue to increase (Wang et al. 2021). The increase of coffee monoculture systems in Latin America has led to the application of a high rate of mineral fertilizers to improve the productivity and profitability of these plantations (Romero-Alvarado et al. 2002); however, the excessive use of these inputs by coffee growers generates several environmental problems (Capa et al. 2015), for example, eutrophication (Borbor-Cordova et al. 2006), reduction of soil microorganism biodiversity (De Beenhouwer et al. 2015), GHG emissions (Hergoualch et al. 2012, Hergoualch et al. 2008). Maintaining or increasing crop productivity while reducing GHG emissions is one of

the major challenges facing agriculture (Lesk et al. 2016).

N<sub>2</sub>O is a long-lived GHG in the atmosphere, whose global warming potential is 298 times that of CO<sub>2</sub> (Forster et al. 2007), is mainly emitted in agricultural soils fertilized with nitrogen (Recio et al. 2020) and is the substance that has the greatest effect on the destruction of stratospheric ozone (Ravishankara et al. 2009). Both nitrification and denitrification are considered to be the main biological processes leading to N<sub>2</sub>O emission in agroecosystems (Butterbach-Bahl et al. 2013, Recio et al. 2020). Nitrification generally occurs under aerobic conditions, while denitrification occurs under oxygen-deficient conditions, although the two processes often occur simultaneously when there is a close coexistence of oxic and anoxic conditions (Baggs & Philippot 2011, Hallin et al. 2018). These two processes are favored by the amount of soil water (water-filled pore space, WFPS) under saturation (40-60% WFPS) (Sanz-Cobena et al. 2017).

Different N<sub>2</sub>O emission reduction strategies have been established in nitrogen-fertilized agroecosystems (Sanz-Cobena et al. 2017), these include the synchronization of the N applied with the N demand of the crop, the use of water-saving irrigation systems to prevent N<sub>2</sub>O formation

through denitrification in water-saturated soils, and the use of water-saving irrigation systems to prevent the formation of  $N_2O$  through denitrification in water-saturated soils (Guardia et al. 2017) or application of nitrification inhibitors (NI) (Sanz-Cobena et al. 2016). The most commonly used INs are dicyandimide (DCD) and 3,4-dimethylpyrazole phosphate (DMPP) which have demonstrated a high potential to decrease nitrifying activity and consequently decrease  $N_2O$  emissions (Cayuela et al. 2017, Lam et al. 2018).

Systematic reviews (SR) is a useful and comprehensive technique to search, collect, select, evaluate and synthesize all the existing evidence on a specific problem, this method suggests key features, including the development of a thorough search and coding method, analysis-interpretation, and systematic reporting (Bai et al. 2022). Recently, several SR studies on GHG emissions have been reported (Gao et al. 2018, Guardia et al. 2017, Hu et al. 2020, Lynch 2019); however, there are no such studies focused on  $N_2O$  emissions in coffee cultivation. The objective of this SR was to provide an overview of soil  $N_2O$  emissions in coffee cropping systems; summarizing available field data on soil  $N_2O$  emissions and identifying  $N_2O$  control factors (fertilizer type, precipitation, temperature, altitude) as a basis for developing  $N_2O$  mitigation strategies.

## MATERIALS AND METHODS

### Search Strategy

The Preferred Reporting Items for Systematic Reviews and Meta-Analyses (PRISMA) guidelines were followed for the literature search and review (Moher et al. 2014). Duplicate articles were eliminated, then all titles and abstracts were evaluated following the inclusion and exclusion criteria to identify relevant research for the present review, after which full-text articles were reviewed to determine whether they met the inclusion criteria according to the research objective.

The databases used in the search for articles were Scopus, ScienceDirect, Springer, and Scielo. The keywords used were “nitrous oxide” and “coffee monoculture” or “nitrous oxide” and “coffee agroforestry systems” or “carbon footprint” and “coffee cultivation” or “óxido nitroso” y “café”. All original full-text articles in English or Spanish, published from January 2000 to October 2021, were considered for review. To increase the quality of the review, only peer-reviewed literature was examined and results published in the form of master’s theses, Ph.D. dissertations, and conference abstracts were excluded.

### Inclusion and Exclusion Criteria

Inclusion criteria for the selection of articles were a)

research studies conducted in the field; b) studies measuring cumulative emissions ( $kg \cdot ha^{-1}$ ) of  $N_2O$ ; c) means, standard deviations (or standard errors), and several replicates that were reported, and/or could be calculated; d) experimental duration, N application rate and management practices that were reported. All study designs had to correspond to primary studies, including randomized controlled trials, crossover, cohort, case-control, case reports, and case series.

The following criteria were used to exclude articles (a) studies with a secondary design, such as meta-analyses, systematic reviews, and narrative reviews; (b) non-experimental studies; (c) studies in which other greenhouse gases were estimated; (d) articles without full text available; (e) studies whose object of research is other than  $N_2O$  emissions in coffee crops; (f) opinion articles, commentaries, and editorials were not considered for inclusion.

## RESULTS AND DISCUSSION

### Selection of Research Articles

A total of 70 articles were identified across the four databases and 10 articles were excluded due to duplication. Of that number, 46 articles were excluded after the first review of the title and abstract as it was determined that they did not meet the inclusion criteria. Next, 14 articles were evaluated by reading the full text to certify that they met all inclusion and exclusion criteria. Finally, the total number of studies included in the present systematic review was eight (Fig. 1).

### Analysis of Included Studies

Table 1 shows the eight selected papers, indicating the country in which the study was carried out, as well as the precipitation, temperature, and altitude of the study areas.

Of the studies found, 75% were developed in Costa Rica, 12.5% in Ecuador, and the other 12.5% in Nicaragua. The range of precipitation reported in the RS goes from 910 mm to 2740  $mm \cdot yr^{-1}$ . Coffee is planted in areas with rainfall ranging from 750 mm to 3000 mm per year (Laderach et al. 2011). Precipitation is the climatic factor with the greatest impact on the decrease in coffee production (Rivera Silva et al. 2013), the reduction of rainfall in relation to the reduction of coffee productivity is estimated at 75-90% (Laderach et al. 2011).

The minimum temperature reported in the SR was 16°C, the maximum temperature was 24°C and the average temperature was 20.3°C. These values are within the optimal temperature range for coffee cultivation, which establishes the average temperature between 18 and 22°C and the maximum temperature of 30°C (Descroix & Snoeck 2009, Sarmiento-Soler et al. 2019), higher temperatures accelerate

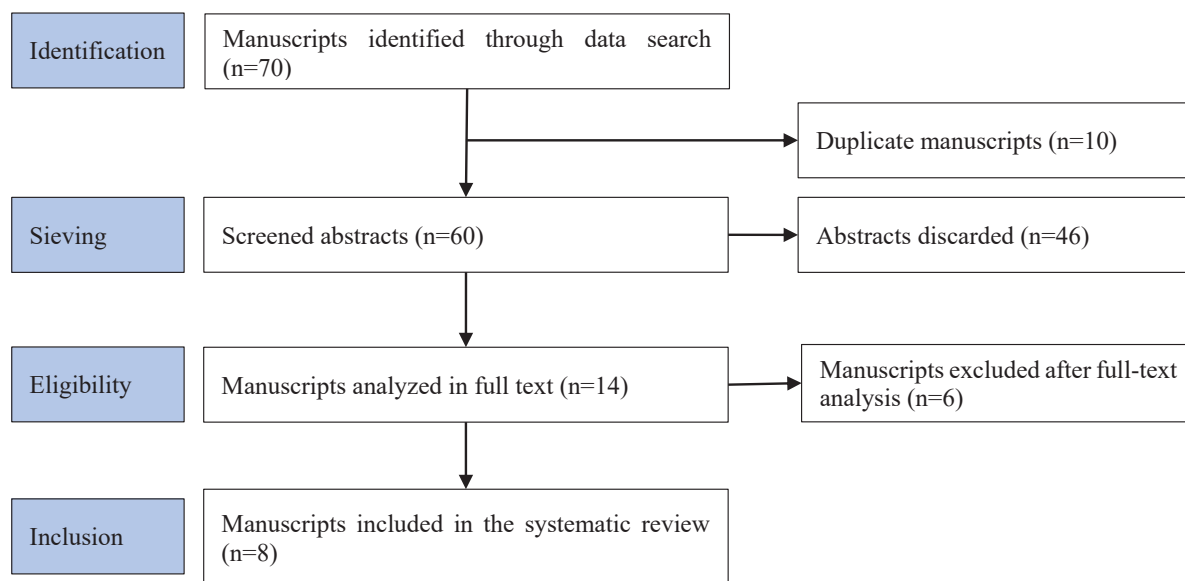


Fig. 1: Eligible item identification flowchart.

the development and maturation of the fruits and this leads to a decrease in the cup quality of the coffee, in addition, continuous exposure to high temperatures generates stress, which is manifested by slow growth and abnormalities such as yellowing of the leaves (Davis et al. 2012) similarly, in areas where the average annual temperature is below 17-18°C, growth also becomes slower (DaMatta & Ramalho 2006). Climatic characteristics influence the development and growth of coffee in different ways and at different stages of growth (Camargo 2010).

As for N<sub>2</sub>O emissions, they increase with increasing temperature; in general, there is a positive correlation between temperature and N<sub>2</sub>O emissions (Aguilera et al. 2013) the optimum range for nitrification is between 25

and 30°C, while denitrification can occur in a range between 4 and 60°C. In addition, the increase in temperature produces an increase in soil respiration, which leads to O<sub>2</sub> consumption and the appearance of anaerobiosis, which in turn favors denitrification (Ussiri & Lal 2012). In addition, the amount and distribution of precipitation influence soil N<sub>2</sub>O emissions (Du et al. 2006).

Table 2 details aspects such as the coffee cultivation system, associated forest species, variety, age, and the number of coffee plants per ha.

In the SR it was found that coffee is planted under agroforestry systems and monocultures, however, coffee has a variety of cultivation systems, from complex agroforestry,

Table 1: Climatic and location conditions in which the selected studies were carried out.

Author and year of publication	Country	Altitude (msnm)	Precipitation (mm)	Average temperature (°C)
Capa et al. (2015)	Ecuador	2100	910	18
Harmand (2007)	Costa Rica	600	2740	23
Hergoualc'h et al. (2008)	Costa Rica	1180	2300	21
Hergoualc'h et al. (2012)	Costa Rica	1180	2300	21
Montenegro (2019)	Costa Rica (Naranjo)	1200	2200	21
Montenegro (2019)	Costa Rica (San Marcos)	1650	2223	16
Montenegro (2020)	Costa Rica (Naranjo)	1200	2200	21
Montenegro (2020)	Costa Rica (San Marcos)	1650	2223	16
Noponen et al. (2012)	Costa Rica	685	2600	22
Noponen et al. (2012)	Nicaragua	445	1386	24

Table 2: Characteristics of the cultivation system installed in each selected studio.

Author and year of publication	Crop system	Associated forest species	<i>Coffea arabica</i> variety	Age of the coffee crop (years)	Number of coffee plants per ha
Capa et al. (2015)	Monoculture	-	Caturra	1	5000
Harmand (2007)	Agroforestry system	<i>Eucalyptus deglupta</i>	Costa Rica 95	14	5900
	Monoculture	-	Costa Rica 95	14	5900
Hergoualc'h et al. (2008)	Agroforestry system	<i>Inga densiflora</i>	Catuai	8	4722
	Monoculture	-	Catuai	8	5000
Hergoualc'h et al. (2012)	Agroforestry system	<i>Inga densiflora</i>	Catuai	7	4722
	Monoculture	-	Catuai	7	4722
Montenegro (2019)	Agroforestry system	<i>Inga</i> spp, <i>Erythrina</i> spp	Catuai	7	5848
	Agroforestry system	<i>Inga</i> spp, <i>Erythrina</i> spp	Catuai	15	5848
Montenegro (2020)	Agroforestry system	<i>Inga</i> spp, <i>Erythrina</i> spp	Catuai	7	5848
	Agroforestry system	<i>Inga</i> spp, <i>Erythrina</i> spp	Catuai	15	5848
Noponen et al. (2012)	Agroforestry system	<i>Erythrina poeppigina</i>	Caturra	9	5000
	Agroforestry system	<i>Inga laurina</i>	Pacas	9	4000

simulating secondary forests, to intensive monocultures (Perfecto et al. 2005), choosing a particular cropping system is a very important management decision because cropping systems will provide different benefits, e.g. nutrient regulation, pest control, microclimate regulation, pollination and productivity (Chain-Guadarrama et al. 2019, Padovan et al. 2018). Coffee planted under agroforestry systems may be affected, reducing its productivity (Franck et al. 2007, Vaast et al. 2006) however, it provides a variety of ecosystem services (Perfecto et al. 2005), on the other hand, coffee planted as a monoculture and using high fertilization rates can achieve high yields (DaMatta et al. 2018, Perfecto et al. 2005). The most abundant forest species in coffee agroforestry systems are leguminous plants of the genus *Inga* and *Erythrina* (Cannavo et al. 2011) emissions, such as the data found in this SR. If we talk about N<sub>2</sub>O emissions, these would increase in a coffee crop planted under an agroforestry system due to the higher amount of organic matter and water in the top layer of soil under the trees (Hergoualc'h et al. 2008, Verchot et al. 2006).

In the last decades, this variety has been replacing older varieties of coffee due to its productivity, especially in Central America, and in the last decades, the Catuai variety has been replacing older varieties of coffee (Hergoualc'h et al. 2008).

Table 3 shows the edaphic characteristics of the areas where the studies included in this SR were carried out. In the SR it was found that the pH and humidity of the soil where the coffee plantations are developed range from 4.67 to 6.34 and 53.3 to 67.05% respectively, these properties influence N<sub>2</sub>O emissions. N<sub>2</sub>O emissions are the product

of microbial processes that in turn are controlled by physical and chemical properties of the soil that influence the growth of microorganisms, among these properties are texture, availability of oxygen (O<sub>2</sub>), organic C, mineral N, moisture, and pH (Müller et al. 2014). Soil moisture has a considerable influence on N<sub>2</sub>O production, due to its relationship with the concentration of oxygen O<sub>2</sub> in the soil, the higher the water content, the lower the O<sub>2</sub> content in the soil pores, when the percentage of water-filled pores (WFPS) is between 50 and 70% and decreases to values below 50% or above 80%, the process of complete denitrification predominates, therefore, the reduction of N<sub>2</sub>O to N<sub>2</sub> is more

Table 3: Edaphic conditions in which the selected studies were conducted.

Author and year of publication	pH	Soil humidity [%]	Texture
Capa et al. (2015)	6.34	-	Clay loam
Harmand (2007)	6.2	53.3	Sandy
Harmand (2007)	6.1	53.3	Sandy
Hergoualc'h et al. (2008)	4.67	62.95	Clay
Hergoualc'h et al. (2008)	4.92	67.05	Clay
Hergoualc'h et al. (2012)	4.67	-	Clay
Hergoualc'h et al. (2012)	4.92	-	Clay
Montenegro (2019)	5	60	Clay loam
Montenegro (2019)	5	55	Clay
Montenegro (2020)	5	60	Clay loam
Montenegro (2020)	5	55	Clay
Noponen et al. (2012)	-	-	Clay
Noponen et al. (2012)	-	-	Sandy loam

Table 4: Nitrogen fertilization and calculated N<sub>2</sub>O emissions in selected studies.

Author and year of publication	Fertilizer type	Fertilization rate [kg.N.ha <sup>-1</sup> ]	Emissions N <sub>2</sub> O [kg.N.ha <sup>-1</sup> .yr <sup>-1</sup> ]
Capa et al. (2015)	Urea	200	2.90
	Urea	300	10.90
	Urea	400	12.80
	Control	0	1.30
Harmand (2007)	Ammonium nitrate	180	1.90
	Ammonium nitrate	180	1.90
Hergoualc'h et al. (2008)	Urea	250	5.80
	Urea	250	4.30
Hergoualc'h et al. (2012)	Urea	250	3.55
	Urea	250	2.32
Montenegro (2019)	Urea	0	0.63
	Urea	100	0.95
	Urea	225	0.95
	Urea	350	1.40
	Urea	0	0.63
	Urea	100	0.83
	Urea	225	1.00
	Urea	350	1.07
	Urea	350	1.07
Montenegro (2020)	Ammonium nitrate	250	1.00
	Calcium nitrate	250	0.94
	Polymer coated urea	250	0.87
	Urea	250	0.67
	Ammonium nitrate	250	0.65
	Calcium nitrate	250	0.60
	Polymer coated urea	250	0.65
	Urea	250	0.57
Noponen et al. (2012)	Moderate organic	66	0.20
	Intensive organic	248	1.56
	Conventional moderate	150	1.02
	Conventional intensive	287	1.87
	Moderate organic	140	0.37
	Intensive organic	346	1.83
	Conventional moderate	78	0.49
	Conventional intensive	157	0.95

important (Pilegaard 2013). In addition, denitrification and nitrification processes are affected by other soil physical and chemical parameters such as pH, temperature, and the presence of other species. Soil pH has been recognized as an important property controlling N<sub>2</sub>O emissions through its effect on soil microbial activity and diversity (Barton et al. 2013, Čuhel et al. 2010). At pH values close to 7 or basic,

N<sub>2</sub> production is favored over N<sub>2</sub>O emission (Šimek et al. 2002) which results in lower N<sub>2</sub>O emissions (García-Marco et al. 2016) than at acid pH.

In addition, texture influences N<sub>2</sub>O emissions, for example, in clay soils the number of macropores increases anaerobic zones, which leads to partial or total denitrification processes, resulting in higher N<sub>2</sub>O emissions from fine-text-

tured soils (Butterbach-Bahl et al. 2011). Table 4 details the type of nitrogen fertilizer used in the coffee crop, as well as the fertilization rate and N<sub>2</sub>O emissions of the crop.

In the SR it was found that the fertilizers used are of chemical, organic and chemical + polymer origin, at fertilization rates ranging from 66 to 400 kg N ha<sup>-1</sup> and N<sub>2</sub>O emissions ranging from 0.2 to 12.8 kg N ha<sup>-1</sup> yr<sup>-1</sup>, it has been observed that N<sub>2</sub>O emissions tend to increase as the fertilization rate does, as well as other studies, where they state that as the annual rate of N increases, so does the annual emissions of N<sub>2</sub>O in soils (Capa et al. 2015, Hergoualc'h et al. 2008, Noponen et al. 2012, Rahman et al. 2021) which are mainly due to nitrification and denitrification processes generated by high rates of nitrogen fertilization (Rochette et al. 2004). In addition to this factor, N<sub>2</sub>O emissions are due to environmental and agricultural factors, such as the presence of native mineral elements in the soil, soil moisture, temperature, type of tillage, and climatic conditions (Hergoualc'h et al. 2008).

## CONCLUSION

The systematic review included eight experimental studies that determined N<sub>2</sub>O emissions in coffee plantations, suggesting that this emission is directly proportional to the fertilization rate. The precise identification of the factors remains unclear. Further research is needed in this field to make recommendations to reduce N<sub>2</sub>O emissions.

## REFERENCES

- Aguilera, E., Lassaletta, L., Sanz-Cobena, A., Garnier, J. and Vallejo, A. 2013. The potential of organic fertilizers and water management to reduce N<sub>2</sub>O emissions in Mediterranean climate cropping systems. A review. *Agric. Ecosyst. Environ.*, 164: 32-52.
- Baggs, E. and Philippot, L. 2011. Nitrous Oxide Production in the Terrestrial Environment. Caister Academic Press, MA.
- Bai, Z.G., Bing, Q., Gong, R.R., Bai, R.H., Zhou, Y. and Yang, K.H. 2022. Evidence-based social science in China: The quality of social science systematic reviews and meta-analysis published from 2000 to 2019. *J. Clin. Epidemiol.*, 141: 132-140.
- Barton, L., Gleeson, D.B., Maccarone, L.D., Zúñiga, L.P. and Murphy, D.V. 2013. Is liming soil a strategy for mitigating nitrous oxide emissions from semi-arid soils? *Soil Biol. Biochem.*, 62: 28-35.
- Borbor-Cordova, M.J., Boyer, E.W., McDowell, W.H. and Hall, C.A. 2006. Nitrogen and phosphorus budgets for a tropical watershed impacted by agricultural land use: Guayas, Ecuador. *Biogeochemistry*, 79(1): 135-161.
- Butterbach-Bahl, K., Baggs, E.M., Dannenmann, M., Kiese, R. and Zechmeister-Boltenstern, S. 2013. Nitrous oxide emissions from soils: How well do we understand the processes and their controls? *Phil. Trans. Royal Soc. B Biol. Sci.*, 368(1621): 20130122.
- Butterbach-Bahl, K., Gundersen, P., Ambus, P., Augustin, J., Beier, C., Boeckx, P., Dannenmann, M., Sanchez Gimeno, B., Ibrom, A., Kiese, R., Kitzler, B., Rees, R. M., Smith, K.A., Stevens, C., Vesala, T. and Zechmeister-Boltenstern, S. 2011. Nitrogen Processes in Terrestrial Ecosystems. In Sutton, M., Howard, C.M., Erisman, J.W., Billen, G., Bleeker, A., Greenfelt, P., Grisen, V.H. and Grizzetti, B. (eds), The European Nitrogen Assessment: Sources, Effects and Policy Perspectives. Cambridge University Press (CUP), Cambridge, MA, pp. 99-125.
- Camargo, M.B.P. 2010. The impact of climatic variability and climate change on Arabic coffee crop in Brazil. *Bragantia*, 69: 239-247.
- Cannavo, P., Sansoulet, J., Harmand, J.M., Siles, P., Dreyer, E. and Vaast, P. 2011. Agroforestry associating coffee and *Inga densiflora* results in complementarity for water uptake and decreases deep drainage in Costa Rica. *Agric. Ecosyst. Environ.*, 140(1): 1-13.
- Capa, D., Pérez-Esteban, J. and Masaguer, A. 2015. The unsustainability of recommended fertilization rates for coffee monoculture due to high N<sub>2</sub>O emissions. *Agron. Sustain. Dev.*, 35(4): 1551-1559.
- Cayuela, M.L., Aguilera, E., Sanz-Cobena, A., Adams, D.C., Abalos, D., Barton, L., Ryals, R., Silver, W.L., Alfaro, M.A., Pappa, V.A., Smith, P., Garnier, J., Billen, G., Bouwman, L., Bondeau, A. and Lassaletta, L. 2017. Direct nitrous oxide emissions in Mediterranean climate cropping systems: Emission factors based on a meta-analysis of available measurement data. *Agric. Ecosyst. Environ.*, 238: 25-35.
- Chain-Guadarrama, A., Martínez-Salinas, A., Aristizábal, N. and Ricketts, T.H. 2019. Ecosystem services by birds and bees to coffee in a changing climate: A review of coffee berry borer control and pollination. *Agric. Ecosyst. Environ.*, 280: 53-67.
- uhel, J., Šimek, M., Laughlin, R. J., Bru, D., Chêneby, D., Watson, C. J. and Philippot, L. 2010. Insights into the effect of soil pH on N<sub>2</sub>O and N<sub>2</sub> emissions and denitrifier community size and activity. *Appl. Environ. Microbiol.*, 76(6): 1870-1878.
- DaMatta, F.M., Avila, R.T., Cardoso, A.A., Martins, S.C.V. and Ramalho, J.C. 2018. Physiological and agronomic performance of the coffee crop in the context of climate change and global warming: A review. *J. Agric. Food Chem.*, 66(21): 5264-5274.
- DaMatta, F.M. and Ramalho, J.D.C. 2006. Impacts of drought and temperature stress on coffee physiology and production: A review. *Braz. J. Plant Physiol.*, 18: 55-81.
- Davis, A.P., Gole, T.W., Baena, S. and Moat, J. 2012. The Impact of Climate Change on Indigenous Arabica Coffee (*Coffea arabica*): Predicting Future Trends and Identifying Priorities. *PLOS ONE*, 7(11): e47981.
- De Beenhouwer, M., Muleta, D., Peeters, B., Van Geel, M., Lievens, B. and Honnay, O. 2015. DNA pyrosequencing evidence for large diversity differences between natural and managed coffee mycorrhizal fungal communities. *Agron. Sustain. Dev.*, 35(1): 241-249.
- Descroix, F. and Snoeck, J. 2009. Environmental factors were suitable for coffee cultivation. Coffee: Growing, Processing, Sustainable Production. A Guidebook for Growers, Processors, Traders and Researchers, pp. 168-181.
- Du, R., Lu, D. and Wang, G. 2006. Diurnal, seasonal, and inter-annual variations of N<sub>2</sub>O fluxes from native semi-arid grassland soils of inner Mongolia. *Soil Biol. Biochem.*, 38(12): 3474-3482.
- Forster, P., Ramaswamy, V., Artaxo, P., Betts, R., Bernsten, T., Fahey, D.W., Haywood, J., Lean, J., Lowe, D.C., Myhre, G. and Nganga, J. 2007. Climate change 2007: The Physical Science Basis. Contribution of Working Group I to the Fourth Assessment Report of the Intergovernmental Panel on Climate Change. Chap. Changes in Atmospheric Constituents and Radiative Forcing. UK and New York, NY, USA.: Cambridge University Press, Cambridge.
- Franck, N., Vaast, P. and Dauzat, J. 2007. Coffee A Shade-Adapted Plant: Implications on Its Carbon Balance and Consequences on Coffee Yield and Quality in Agroforestry Systems. 21st International Conference on Coffee Science, Montpellier, France, 11-15 September 2006, 1023-1031.
- Gao, J., Kovats, S., Vardoulakis, S., Wilkinson, P., Woodward, A., Li, J., Gu, S., Liu, X., Wu, H., Wang, J., Song, X., Zhai, Y., Zhao, J. and Liu, Q. 2018. Public health co-benefits of greenhouse gas emissions reduction: A systematic review. *Sci. Total Environ.*, 627: 388-402.
- García-Marco, S., Abalos, D., Espejo, R., Vallejo, A. and Mariscal-Sancho, I. 2016. No-tillage and liming reduce greenhouse gas emissions from

- poorly drained agricultural soils in Mediterranean regions. *Sci. Total Environ.*, 56: 512-520.
- Guardia, G., Cangani, M.T., Andreu, G., Sanz-Cobena, A., García-Marco, S., Álvarez, J.M., Recio-Huetos, J. and Vallejo, A. 2017. Effect of inhibitors and fertigation strategies on GHG emissions, NO fluxes, and yield in irrigated maize. *Field Crops Res.*, 204: 135-145.
- Guo, L.-N., She, C., Kong, D.B., Yan, S.-L., Xu, Y.P., Khayatnezhad, M. and Gholinia, F. 2021. Prediction of the effects of climate change on hydro-electric generation, electricity demand, and emissions of greenhouse gases under climatic scenarios and optimized ANN model. *Energy Rep.*, 7: 5431-5445.
- Hallin, S., Philippot, L., Löffler, F.E., Sanford, R.A. and Jones, C.M. 2018. Genomics and Ecology of Novel N<sub>2</sub>O-Reducing Microorganisms. *Trends Microbiol.*, 26(1): 43-55.
- Harmand, J.M., Ávila, H., Dambrine, E., Skiba, U., de Miguel, S., Rrenderos, R.V. and Beer, J. 2007. Nitrogen dynamics and soil nitrate retention in a *Coffea arabica*-*Eucalyptus deglupta* agroforestry system in Southern Costa Rica. *Biogeochemistry*, 85(2): 125-139.
- Hergoualc'h, K., Blanchart, E., Skiba, U., Hénault, C. and Harmand, J.M. 2012. Changes in carbon stock and greenhouse gas balance in a coffee (*Coffea arabica*) monoculture versus an agroforestry system with *Inga densiflora*, in Costa Rica. *Agric. Ecosyst. Environ.*, 148: 102-110.
- Hergoualc'h, K., Skiba, U., Harmand, J.M. and Hénault, C. 2008. Fluxes of greenhouse gases from Andosols under coffee in monoculture or shaded by *Inga densiflora* in Costa Rica. *Biogeochemistry*, 89(3): 329.
- Hu, M., Sardans, J., Yang, X., Peñuelas, J. and Tong, C. 2020. Patterns and environmental drivers of greenhouse gas fluxes in the coastal wetlands of China: A systematic review and synthesis. *Environ. Res.*, 186: 109576.
- IPCC. 2014. Climate Change 2014-Mitigation of Climate Change: Working Group I Contribution to the Fourth Assessment Report of the IPCC. Cambridge University Press.
- Laderach, P., Lundy, M., Jarvis, A., Ramirez, J., Portilla, E. P., Schepp, K. and Eitzinger, A. 2011. Predicted Impact of Climate Change on Coffee Supply Chains. In Leal Filho, W. (ed.), *The Economic, Social and Political Elements of Climate Change*. Springer, Berlin, Heidelberg, pp. 703-723.
- Lam, S.K., Suter, H., Bai, M., Walker, C., Davies, R., Mosier, A.R. and Chen, D. 2018. Using urease and nitrification inhibitors to decrease ammonia and nitrous oxide emissions and improve productivity in a subtropical pasture. *Sci. Total Environ.*, 644: 1531-1535.
- Lesk, C., Rowhani, P. and Ramankutty, N. 2016. Influence of extreme weather disasters on global crop production. *Nature*, 529(7584): 84-87.
- Lynch, J. 2019. Availability of disaggregated greenhouse gas emissions from beef cattle production: A systematic review. *Environ. Impact Assess. Rev.*, 76: 69-78.
- Moher, D., Liberati, A., Tetzlaff, J., Altman, D.G. and Group, T.P. 2014. Reference items to publish systematic reviews and meta-analyses: the PRISMA declaration. *Rev. Espanola de Nutr. Hum. Diet.*, 18(3): 172-181.
- Montenegro, J. 2019. Respuesta polinómica de la emisión de óxido nitroso en plantaciones de café en Costa Rica. *Rev. de Ciencias Amb.*, 53(2): 1-24.
- Montenegro, J. 2020. Efecto de diferentes fuentes de nitrógeno en la emisión de óxido nitroso en plantaciones de café en Costa Rica. *Rev. de Ciencias Amb.*, 54(2): 111-130.
- Müller, C., Laughlin, R.J., Spott, O. and Rütting, T. 2014. Quantification of N<sub>2</sub>O emission pathways via a 15N tracing model. *Soil Biol. Biochem.*, 72: 44-54.
- Noponen, M.R.A., Edwards-Jones, G., Haggard, J.P., Soto, G., Attarzadeh, N. and Healey, J.R. 2012. Greenhouse gas emissions in coffee grown with differing input levels under conventional and organic management. *Agric. Ecosyst. Environ.*, 151: 6-15.
- Padovan, M.P., Brook, R.M., Barrios, M., Cruz-Castillo, J.B., Vilchez-Mendoza, S.J., Costa, A.N. and Rapidel, B. 2018. Water loss by transpiration and soil evaporation in coffee shaded by *Tabebuia rosea* Bertol and *Simarouba glauca* dc. compared to unshaded coffee in sub-optimal environmental conditions. *Agric. For. Meteorol.*, 248: 1-14.
- Perfecto, I., Vandermeer, J., Mas, A. and Pinto, L.S. 2005. Biodiversity, yield, and shade coffee certification. *Ecol. Econ.*, 54(4): 435-446.
- Pilegaard, K. 2013. Processes regulating nitric oxide emissions from soils. *Philosophical Trans. Royal Soc. B Biol. Sci.*, 368(1621): 20130126.
- Rahman, N., Richards, K.G., Harty, M.A., Watson, C.J., Carolan, R., Krol, D., Lanigan, G.J. and Forrester, P. J. 2021. Differing effects of increasing calcium ammonium nitrate, urea, and urea + NBPT fertilizer rates on nitrous oxide emission factors at six temperate grassland sites in Ireland. *Agric. Ecosyst. Environ.*, 313: 107382.
- Ravishankara, A.R., Daniel, J.S. and Portmann, R.W. 2009. Nitrous oxide (N<sub>2</sub>O): The dominant ozone-depleting substance emitted in the 21st century. *Science*, 326(5949): 123-125.
- Recio, J., Montoya, M., Ginés, C., Sanz-Cobena, A., Vallejo, A. and Alvarez, J.M. 2020. Joint mitigation of NH<sub>3</sub> and N<sub>2</sub>O emissions by using two synthetic inhibitors in an irrigated cropping soil. *Geoderma*, 373: 114423.
- Rivera Silva, M., del R., Nikolskii Gavrillov, I., Castillo Álvarez, M., Ordaz Chaparro, V.M., Díaz Padilla, G. and Guajardo Panes, R.A. 2013. Vulnerabilidad de la producción del café (*Coffea arabica* L.) al cambio climático global. *Terra Latinoamer.*, 31(4): 305-313.
- Rochette, P., Angers, D.A., Bélanger, G., Chantigny, M.H., Prévost, D. and Lévesque, G. 2004. Emissions of N<sub>2</sub>O from Alfalfa and soybean crops in Eastern Canada. *Soil Sci. Soc. Am. J.*, 68(2): 493-506.
- Romero-Alvarado, Y., Soto-Pinto, L., García-Barrios, L. and Barrera-Gaytán, J.F. 2002. Coffee yields and soil nutrients under the shades of *Inga* sp. Vs. Multiple species in Chiapas, Mexico. *Agrofor. Syst.*, 54(3): 215-224.
- Sanz-Cobena, A., Lassaletta, L., Aguilera, E., Prado, A. del, Garnier, J., Billen, G., Iglesias, A., Sánchez, B., Guardia, G., Abalos, D., Plaza-Bonilla, D., Puigdueta-Bartolomé, I., Moral, R., Galán, E., Arriaga, H., Merino, P., Infante-Amate, J., Meijide, A., Pardo, G. and Smith, P. 2017. Strategies for greenhouse gas emissions mitigation in Mediterranean agriculture: A review. *Agric. Ecosyst. Environ.*, 238: 5-24.
- Sanz-Cobena, Alberto, Abalos, D., Meijide, A., Sanchez-Martin, L. and Vallejo, A. 2016. Soil moisture determines the effectiveness of two urease inhibitors to decrease N<sub>2</sub>O emissions. *Mitig. Adapt. Strateg. Glob. Chang.*, 21(7): 1131-1144.
- Sarmiento-Soler, A., Vaast, P., Hoffmann, M.P., Rötter, R.P., Jassogne, L., van Asten, P.J.A. and Graefe, S. 2019. Water use of *Coffea arabica* in open versus shaded systems under smallholder's farm conditions in Eastern Uganda. *Agric. For. Meteorol.*, 26: 231-242.
- Šimek, M., Jiřová, L. and Hopkins, D.W. 2002. What is the so-called optimum pH for denitrification in soil? *Soil Biol. Biochem.*, 34(9): 1227-1234.
- Ussiri, D. and Lal, R. 2012. Soil Emission of Nitrous Oxide and its Mitigation. Springer Science & Business Media.
- Vaast, P., Bertrand, B., Perriot, J.J., Guyot, B. and Génard, M. 2006. Fruit thinning and shade improve bean characteristics and beverage quality of coffee (*Coffea arabica* L.) under optimal conditions. *J. Sci. Food Agric.*, 86(2): 197-204.
- Verchot, L.V., Hutabarat, L., Hairiah, K., Van Noordwijk, M. 2006. Nitrogen availability and soil N<sub>2</sub>O emissions following conversion of forests to coffee in southern Sumatra. *Glob. Biogeochem. Cyc.*, 20(4).
- Wang, H., Zheng, J., Fan, J., Zhang, F. and Huang, C. 2021. Grain yield and greenhouse gas emissions from maize and wheat fields under the plastic film and straw mulching: A meta-analysis. *Field Crops Res.*, 270: 108210.







# Elephant Habitat Suitability Analysis of Alipurduar District, West Bengal Using Geospatial Technology

Jonmenjoy Barman\*, Subhom Narjinary\*\*, Sankar Biswas\*\*\*, Brototi Biswas\*† and Ratnaprabha Jadhav\*\*\*\*

\*Department of Geography and RM, Mizoram University, Aizawl-796004, India

\*\*Department of Geography, ABN Seal College, Cooch Behar-736101, India

\*\*\*Department of Geography and Applied Geography, University of North Bengal, Darjeeling-734013, India

\*\*\*\*Department of Geography, SNDT Women's University, Pune, India

†Corresponding author: Brototi Biswas; brototibiswas@gmail.com

**Nat. Env. & Poll. Tech.**  
Website: [www.neptjournal.com](http://www.neptjournal.com)

Received: 10-11-2021

Revised: 07-02-2022

Accepted: 11-02-2022

## Key Words:

Geospatial technology  
Elephant habitat  
Habitat suitability  
Alipurduar

## ABSTRACT

In India's Tarai-Dooars region, elephants are the most common wildlife species. The man-wildlife conflict has arisen as a result of forest scarcity, forest fragmentation, global climate change, land use land cover change in the Dooars region, and encroachment into forest life. Although the Wildlife Protection Act of 1972 addressed the conservation of wild animals, the number of wild elephants in West Bengal was constantly changing. The goal of this project is to use geospatial technologies to determine wild elephant habitat suitability zones in West Bengal's Alipurduar area. The first stage in the conservation and management of wild elephants is to determine their habitat suitability. To assess the result, the various habitat suitability factors/parameters of wild elephants were integrated through weighted overlay analysis in the ArcGIS environment. The result shows that the central part of the district - the Buxa forest area, holds the largest suitable environment for elephant habitat. The rest of the study area can be categorized as a medium habitat suitable area excluding some settlements and built-up areas. The authors hope the result will help the proper management and conservation of wild elephants.

## INTRODUCTION

The keystone and iconic animal in the forest, the elephant, is an intelligent and herbivore sociable wild mammal that plays a crucial role in maintaining biodiversity and the environment (Puri et al. 2019, Mandal & Chatterjee 2020). South Asian elephant, being the largest terrestrial animal, is adapted in the Dooars' riverine flood plain. Dooars region hosts the largest elephant reserves in West Bengal (99.51 Km<sup>2</sup>). Alipurduar district is a tribal dominant district of West Bengal covering 31.54% of forest area including Buxa national park, Jaldapara national park, Buxa wildlife sanctuary, and Chilapata forest area. The Eastern Himalayan region is a biodiversity hotspot region of India (Huang et al. 2019). With increasing population pressure, the natural forests around the world are facing the brunt of anthropogenic activities spelling doom for flora and fauna. With the shrinkage of forest land and changes in land use land cover the bio-reserve of Alipurduar district has been facing man-animal conflict over the years. The study area has been facing the conversion of its natural forests into agricultural land, residential land, road, and industrial land. The development of GIS and remote sensing plays an important role in wildlife conservation, management, and

habitat suitability analysis over the world. The habitat suitability index was initially developed by Oldham et al. (2000) for evaluating habitat quantity and quality. Researchers such as Wennink et al. (2018) focused on the habitat suitability of golden jackals in the Netherlands. Catullo et al. (2008) discussed Asian mammals' analysis based on habitat suitability models. Snaith et al. (2002) had done moose habitat suitability analysis in Canada. Purify et al. (2019) worked on Waterbird habitat suitability on an urban coastal wetland in the Lantebung mangrove area. Debeljak et al. (2001) discussed red deer habitat suitability in South-central Slovenia. Khwairakpam et al. (2019) worked on Pengba fish habitat suitability in Loktak Lake and its river basin, Manipur.

Habitat Suitability Index is a numerical knowledge-based index ranging between 0 and 1. A value near 0 indicates unsuitable habitat and a value near 1 represents suitable habitat (Oldham et al. 2000). The purpose of the present study is to identify the habitat suitability index for wild elephants in the Alipurduar district of West Bengal. India has the largest encroachment into forest areas through railway tracks in the form of the Lumding-Guhawati track in Assam; Siliguri-Alipurduar tract in West Bengal; Coimbatore-Thrissur

track in Karnataka and Tamil Nadu, etc. (Roy & Sukumar 2017). A number of roadways also cross through the forest areas of the country. In the study area, NH-317 and SH-16 run through the Buxa forest, while NH-317 has divided the Jaldapara forest area. These hamper the free movement of wild animals and as such are a major problem for the study area. Owing to human encroachment into forest areas owing to the expansion of settlements, elephant encroachment into settlements and destruction of cropland has increased in the recent past triggering man-animal conflict. The present study is focused on habitat suitability zonation and man-elephant collision considering the parameters of land use land cover, NDVI, NDWI, distance to stream, distance to road, and distance to settlement and altitude.

### Elephant Habitat Preference in the Alipurduar District

Alipurduar district is situated in the foothills of the Siwalik Himalaya. The northern part of the district is hilly with a moderate slope. Elephants do not prefer high altitudes and steep slopes and extended winter with snowfall (Giannatos 2004). The study area is devoid of a steep slope and long-term snow cover, favoring elephant habitation. Generally, elephants prefer large forests with dense vegetation near water sources. They sometimes use forest corridors in search of food within the forest or any other nearby location. The forest variability within this district takes care of the fodder and camouflages their existence along with taking care of other needs. There are a lot of rivers flowing from Bhutan hills that go through this district serving as a water source for the elephants.

The study's key objective is to elucidate elephant habitat suitability evaluation. The current study investigates the relationship between the performance of the elephant habitat in the study area and the forest ecosystem in addition to other parameters. Thus favorable factors like terrain, climate, water availability, food availability, and forest cover along with other encouraging factors have made the Alipurduar district a preferable place for elephant habitat.

## MATERIALS AND METHODS

### Study Area

Alipurduar district is one of the newly formed districts of West Bengal, extending between 26°23'50"N to 26°51'56"N latitude and 89°2'58"E to 89°53'40"E longitude having an elevation ranging from 60m to 350m above mean sea level (Fig. 1). It is bounded by Bhutan in the North, Assam in the east, Jalpaiguri in the West, and Cooch Behar in the South. River Raidak, Sankosh, Torsa, Jayanti, Checko, Hollong, Gadadhar, Basra, Kalikhola, etc., flow through the Alipurduar district. The area is characterized by high rainfall (350-

650cm) and the forest comprises dry deciduous, moist deciduous, semi-evergreen, and evergreen types of Sal (*Shorea Robusta*) and its associated form of vegetation. Wild elephant (*Elephant maximus*), Gaur (*Bos gauras*), and one-horned Rhinoceros (*Rhinoceros unicornis*) are the most abundant species of Jaldapara, Buxa, and Chilapata forest area. The forest area of this district is fragmented and interspersed with tea gardens and villages. Since 1947 over 20% of the forest area has been converted into tea garden plantations and other anthropogenic activities of economic importance. People in the study area are mainly engaged in agriculture and tea gardens while industrial activities are almost absent. The population density in the study area varies from 300 per Km<sup>2</sup> to 500 per Km<sup>2</sup> as per the Census of India, 2011 which is more than the national average population density.

### Methodology

The present study was done by following steps: (1) Sentinel-2 satellite data was downloaded from the USGS portal (<https://earthexplorer.usgs.gov/>); (2) Road, settlement position, and stream shapefile were downloaded from (<https://extract.bbbike.org/>). (3) SRTM Digital elevation model (DEM) was downloaded from USGS portal (<https://earthexplorer.usgs.gov/>). All the imageries and shapefile were georeferenced in WGS-1984 UTM zone 45N. Landsat satellite imageries were analyzed in the ArcGIS environment for preparing the land use and land cover identification. The interactive supervised image classification system was used for land use land cover layer preparation and classified into seven subclasses as- water body, agricultural land, dense vegetation cover, grassland, settlement, sparse vegetation, and barren land. NDVI is a significant method for vegetation quantification, where a value near +1 indicates dense vegetation on the other hand value near -1 indicates a water body. NDVI was calculated from Sentinel -2 using band 4 and band 8 with the help of Pettorelli et al. (2005) by following equation (1)-

$$NDVI = \frac{(NIR - RED)}{(NIR + RED)} \quad \dots(1)$$

NDWI is another method to predict the moisture content of vegetation that reflects the possibility of a forest fire. NDWI values near +1 indicate much moisture content and value near -1 indicate low water content. NDWI was calculated from Sentinel 2 using band 4 and band 12 with the help of the McFeeters (1996) by the equation (2).

$$NDWI = \frac{(NIR - SWIR)}{(NIR + SWIR)} \quad \dots(2)$$

Distance to the road, distance to stream, and distance to settlement layers were prepared according to the Euclidean distance method in the ArcGIS environment (Fig. 2). Elevation was extracted from SRTM 1 (Fig. 2). All the thematic

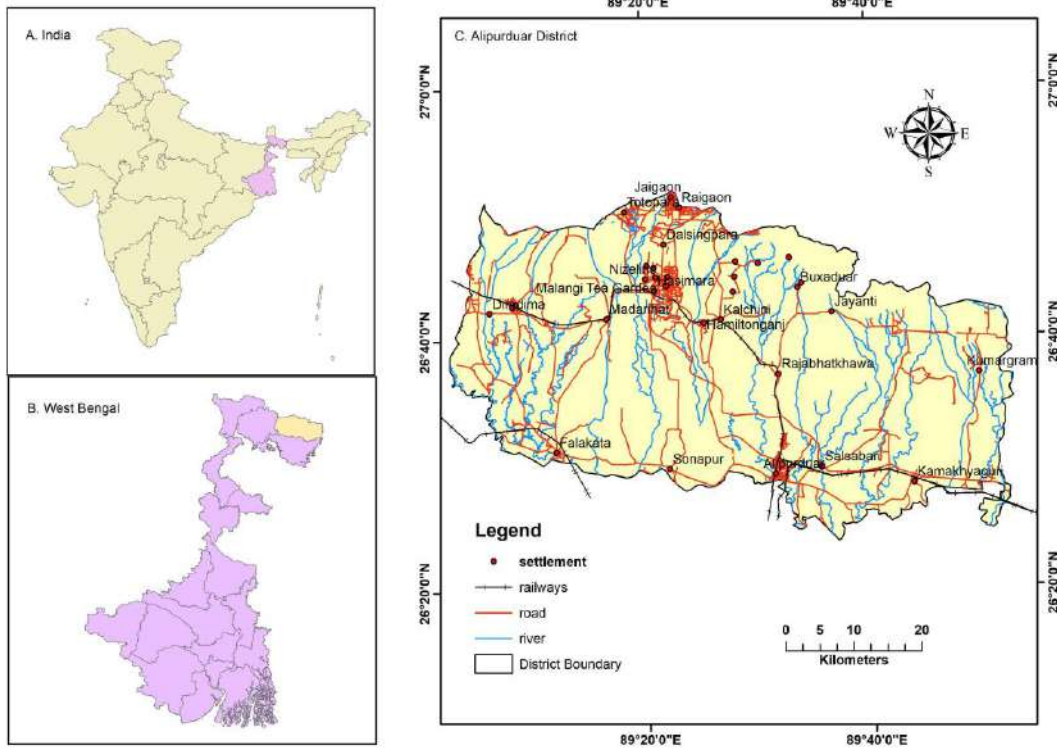


Fig. 1: Study area.

layers were then reclassified and suitable weights were given (Goparaju et al. 2017) using ArcGIS extension weighted overlay (Table 1).

The final habitat suitability map was categorized into three classes- highly suitable areas, medium suitable, and low suitable areas.

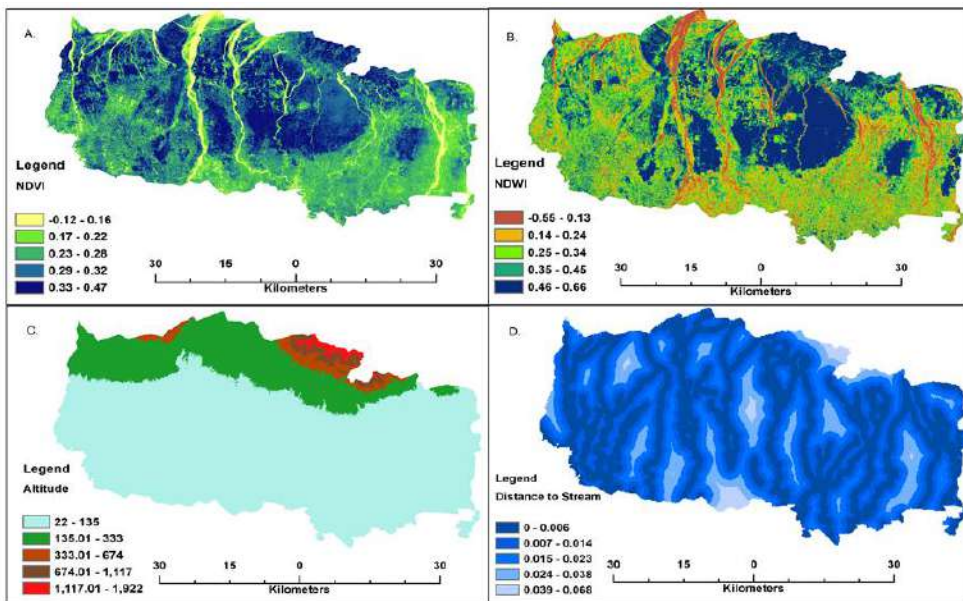


Fig. 2a: (A) NDVI (B) NDWI (C) Altitude (D) Distance from the stream.

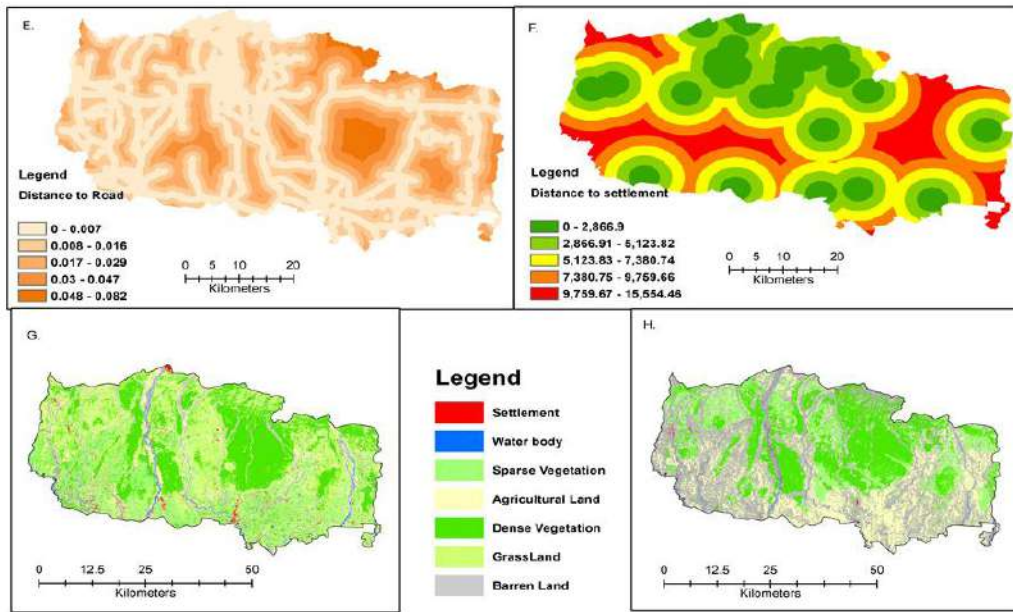


Fig. 2b: (E) Distance to road (F) Distance to settlement (G) LULC, 2020 (H.) LULC, 1990.

**RESULTS AND DISCUSSION**

Growth and reduction in a wildlife population are generally triggered by changes in population density and available resources. Forest areas help them hide, provide shelter, and fodder, and maintain their body metabolism. Forest fragmen-

tation and existing local vegetation impact the colonization of elephants in a variety of environments (Kumar et al. 2010). For Suitability zoning, all the conditioning thematic raster has been superimposed in a weighted overlay GIS environment and categorized into three high groups, medium, and low suitability (Fig. 3)

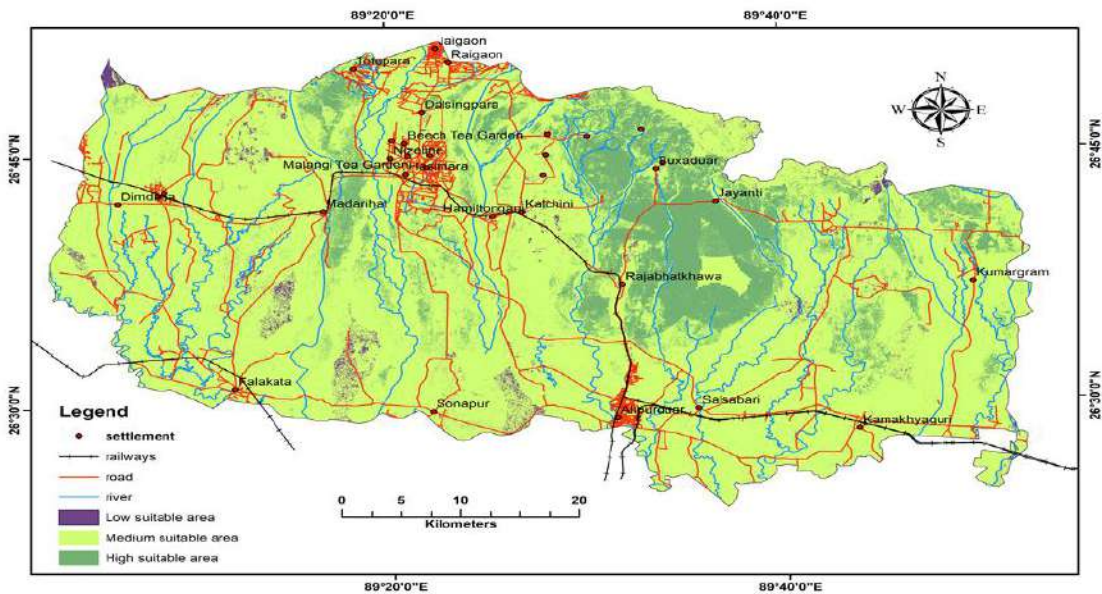


Fig. 3: Elephant habitat suitability zones.

Table 1: Weight of each parameter.

Parameters	Classes	Influence	Scale value
Distance to Road	0 to 0.007 m	5	1
	0.008 to 0.016 m		2
	0.017 to 0.029 m		3
	0.03 to 0.047 m		3
	0.048 to 0.082 m		5
Distance to Settlement	0 to 2866.9 m	15	1
	2866.91 to 5123.82 m		2
	5123.83 to 7380.74 m		3
	7380.75 to 9759.66 m		4
	9759.67 to 15554.46 m		5
Land use / Land cover	Water Body	25	3
	Agricultural Land		2
	Dense Vegetation Cover		7
	Grass Land		5
	Built-up Area		1
	Tea Garden		4
	Vacuum land		1
Distance to Stream	0 to 0.006 m	25	1
	0.007 to 0.014 m		2
	0.015 to 0.023 m		3
	0.024 to 0.038 m		4
	0.039 to 0.068 m		5
Altitude	22 to 135 m	5	2
	135.01 to 333 m		1
	333.01 to 674 m		1
	674.01 to 1117 m		1
	1117.01 to 1922 m		1
NDVI	-0.12 to 0.16	15	1
	0.17 to 0.22		2
	0.23 to 0.28		3
	0.29 to 0.32		4
	0.33 to 0.47		5
NDWI	-0.55 to 0.13	10	5
	0.14 to 0.24		3
	0.25 to 0.34		3
	0.35 to 0.45		1
	0.46 to 0.66		1

Wild elephant habitat suitability using weighted overlay geospatial technology in the Alipurduar district resulted in only 14.48 % of the area (Table 2) being under highly suitable area, 83.63 % area under medium suitable, and

only 1.89 % being under low suitability area (Fig. 4). Result reveals that most of the area comes under medium suitable conditions. Areas coming under highly suitable areas have been rapidly getting converted to medium suitable areas

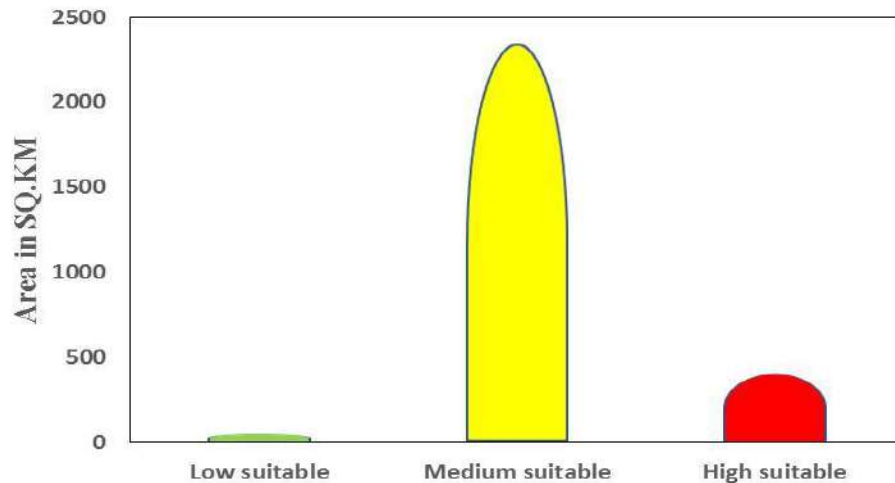


Fig. 4: Areal extension of suitability zones.

due to rapid deforestation, fragmentation of forest areas, encroachment, etc.

A Lorenz curve was done to assess the inequality of the number of elephants in north Bengal from the period 2002 to 2017 (Fig. 5). The man-elephant conflict has been an important issue for several decades in the Alipurduar district along with the entire Dooars region. Different analyses were performed to identify Man-elephant conflict management (Neupane et al. 2018). The management of Man-elephant conflict varies according to different social, financial, and environmental conditions. In the Alipurduar district, the human-elephant conflict has been increasing with every passing day. A comparative analysis of the land use between 1990 and 2020 (Fig. 2), revealed that settlement area has increased by 1.62%, thereby reducing dense vegetation areas by 11.4% during the same time. This change has spelled doom for the free movement and habitation of wild animals in the study area. During the same time, there has been a reduction in the number and areal extent of tea gardens which erstwhile played the role of an elephant corridor. Riverbank soil erosion is a major problem in the Dooars region. There has been a reduction of 22% in the water bodies of the study area due to riverbank erosion (Table 3).

Besides human interference, change in the natural environment is another important cause behind human-elephant conflict in this area. Elephants were mainly sighted by the

authors in two seasons in the study area - the winter season and the rainy season. Dooars region has wet deciduous natural vegetation that becomes leafless in the winter season creating a food crisis within the forest area forcing the elephants to come out of the forest towards localities. The rainy season is their breeding season, hence forcing them to come out of forests to local residential areas in search of food (Fig. 6). In the absence of any buffer zone between the forests and settlements, encroachment into settlements triggers man-elephant conflict. Many times such conflict results in loss of life on both sides. Damage to life, property, and crops has become a persistent problem in the study area owing to man-elephant conflict.

The study area lacks indigenous measures to curb the conflict. Mwamidi et al. (2012) mentioned the Taita community's indigenous knowledge to protect wildlife. After seeding they return home without looking back, believing that God Mlungu would protect their crop and restrain from harvesting the crops until the wild animals consume a substantial part. Su et al. (2020) also mentioned that the Bulang community of China protects Banyan trees believing that the species help them maintain their vitality and keeps them alive longer owing to their divinity. Certain communities have also used various agricultural-based deterrents, like chili, to curb the encroachment of elephants into settlements (Hedges & Gunaryadi 2010). The technique of combining often damaged crops with crops that are less appealing or palatable to elephants is another agriculture-based deterrent (Gross et al. 2016). The alternative crops, which include coriander, mint, ginger, onion, garlic, lemongrass, and citrus trees, can aid farmers economically by compensating for the reduced production of major crops (Shaffer et al. 2019). New research in Africa has shown promising results employing bio-acoustic

Table 2: Areal extension of suitability classes.

Suitability Classes	Area in SQ.KM	[%]
Low suitable	52.9664	1.89
Medium suitable	2344.736	83.63
High suitable	406.0052	14.48

measures/deterrents to prevent elephants, such as beehive fences, which also provide an additional economic benefit to pollinators and honey (King et al. 2017).

**CONCLUSION**

Among the districts of West Bengal state of India, Alipurduar

district ranks fourth in terms of forest cover (31.54%) closely followed by the districts of South 24 Parganas, Darjeeling and Kalimpong. Major forest areas in the district, such as the Buxa forest, Jaldapara forest, and Chilapata forest, have been dwindling and experiencing encroachment as a result of both natural (rivers) and anthropogenic (roads, railway

Table 3: Land use land cover changes (1990-2020).

Class name	Area in SQ.KM (1990)	Area in SQ.KM (2020)	Change [%]	Trend
Settlement	14.0286	59.5173	1.62	Increased
Grassland	182.159	49.1463	4.74	Decreased
Waterbody	15.7624	638.018	22.19	Increased
Dense vegetation	703.785	391.36	11.14	Decreased
Sparse vegetation	355.201	805.484	16.06	Increased
Vacuum land	980.949	693.369	10.26	Decreased
Agricultural land	551.811	166.813	13.73	Decreased

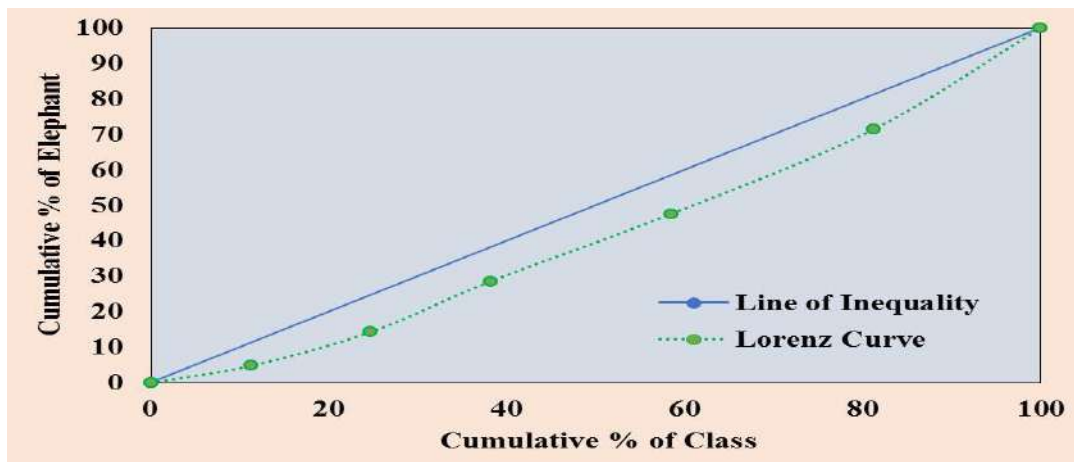


Fig. 5: Inequality of the number of elephants in North Bengal from the period 2002 to 2017.



Fig. 6: Elephant outing at night.

tracks, and settlement) causes. The study area has a high potential for elephant conservation as well as biodiversity management. It is the home to a host of tribal indigenous people. Ethnic knowledge plays a vital role in conserving and managing biodiversity and wildlife. Various management techniques like ensuring fodder for the animals in their natural habitat throughout the year, identification of alternative railway tracks outside the jungles, creation of buffer zones, expansion of ecological corridors, prevention of forest land encroachment, creation of biodiversity awareness among locals, development of various deterrents, etc along with promoting indigenous knowledge-based management techniques will help the reduction of man-animal conflict and support the protection and conservation of wild elephants.

## REFERENCES

- Catullo, G., Masi, M., Falcucci, A., Maiorano, L., Rondinini, C. and Boitani, L. 2008. A gap analysis of Southeast Asian mammals based on habitat suitability models. *Biol. Conserv.*, 141(11): 2730-2744.
- Debeljak, M., Džeroski, S., Jerina, K., Kobler, A. and Adami, M. 2001. Habitat suitability modeling for red deer (*Cervus elaphus* L.) in South-central Slovenia with classification trees. *Ecol. Model.*, 138(1-3): 321-330.
- Goparaju, L.N., Ahmad, F. and Sinha, D. 2017. Wildlife habitat suitability analysis around Madihan forest, Mirzapur district, Uttar Pradesh, India: A Geospatial approach. *Eurasian J. Forest Sci.*, 5(1): 13-28.
- Giannatos, G. 2004. Conservation action plan for the golden jackal *Canis aureus* L. Greece. *WWF Greece*, 47: 152
- Gross, E.M., McRobb, R., and Gross, J. 2016. Cultivating alternative crops reduces crop losses due to African elephants. *J. Pest. Sci.*, 89: 497-506. doi: 10.1007/s10340-015-0699-2
- Huang, C., Li, X., Khanal, L. and Jiang, X. 2019. Habitat suitability and connectivity inform a co-management policy of protected area networks for Asian elephants in China. *Peer. J.*, 7: e6791 DOI 10.7717/peerj.6791
- Hedges, S., and Gunaryadi, D. 2010. Reducing human-elephant conflict: Do chillies help deter elephants from entering crop fields? *Oryx* 44: 139-146. doi: 10.1017/S0030605309990093
- King, L.E., Lala, F., Nzumu, H., Mwambingu, E. and Douglas-Hamilton, I. 2017. Beehive fences as a multidimensional conflict-mitigation tool for farmers coexisting with elephants. *Conserv. Biol.* 31, 743-752. doi: 10.1111/cobi.12898
- Khwairakpam, E., Khosa, R., Gosain, A. and Nema, A. 2020. Habitat suitability analysis of Pengba fish in Loktak Lake and its river basin. *Ecologyhydrology*, 13(1): e2164.
- Kumar, M.A., Mudappa, D. and Raman, T.R.S. 2010. Asian elephant *Elphas maximus* habitat used and ranges in fragmented rainforest and plantations in the Anamalai Hills. *Trop. Conserv. Sci.*, 3(2): 143-158.
- Mwamidi, D., Nunow, A. and Mwasi, S.H. 2012. The use of indigenous knowledge in minimizing human-wildlife conflict: The case of Taita Community, Kenya. *Int. J. Curr. Res.*, 4(02): 026-030.
- Mandal, M. and Das Chatterjee, N. 2020. Elephant's habitat suitability assessment through geospatial quantification in Panchet forest division, West Bengal. *Ecofem. Climate Change*, 1(3): 127-140. <https://doi.org/10.1108/EFCC-05-2020-0012>
- McFeeters, S.K. 1996. The use of the normalized difference water index (NDWI) in the delineation of open water features. *Int. J. Remote Sens.*, 17(7): 1425-1432.
- Neupane, B., Budhathoki, S. and Khatiwoda, B. 2018. Human-elephant conflict and mitigation measures in Jhapa District, Nepal. *Journal of Forest and Livelihood*, 16(1): 103-112.
- Oldham, R.S., Keeble J., Swan, M.J.S. and Jeffcote M. 2000. Evaluating the suitability of habitat for the Great Crested Newt (*Triturus cristatus*). *Herpetol. J.*, 10(4): 143-155.
- Purify, A., Nurdin, N., Maulani, R.I. and Lanuru, M. 2019. Waterbird habitat suitability analysis in an urban coastal wetland (Case study: Lantebung mangrove ecotourism area). *IOP Conf. Series Earth Environ. Sci.*, 370(1): 012042.
- Puri, K., Yadav, V. and Joshi, R. 2019. functional role of elephants in maintaining forest ecosystem and biodiversity: Lessons from Northwestern elephant range in India. *Asian J. Environ. Ecol.*, 9(2): 1-8. <https://doi.org/10.9734/ajee/2019/v9i230091>
- Pettorelli, N., Vik, J.O., Mysterud, A., Gaillard, J. M., Tucker, C.J. and Stenseth, N.C. 2005. Using the satellite-derived NDVI to assess ecological responses to environmental change. *Trends Ecol. Evol.*, 20(9): 503-510.
- Roy, M. and Sukumar, R. 2017. Railways and wildlife: A case study of train-elephant collisions in Northern West Bengal, India. In Borda-de-Água, L., Barrientos, R., Beja, P. and Pereira H. (eds) *Railway Ecology*. Springer, Cham, pp. 1-10. [https://doi.org/10.1007/978-3-319-57496-7\\_10](https://doi.org/10.1007/978-3-319-57496-7_10)
- Shaffer, L.J., Khadka, K.K., Van Den Hoek, J. and Naithani K.J. 2019. Human-elephant conflict: A review of current management strategies and future directions. *Front. Ecol. Evol.* 6: 235. doi: 10.3389/fevo.2018.00235
- Snaithe, T. V., Beazley, K. F., MacKinnon, F. and Duinker, P. 2002. Preliminary habitat suitability analysis for moose in mainland Nova Scotia, Canada. *Alces*, 38: 73-88.
- Su, K., Ren, J., Qin, Y., Hou, Y. and Wen, Y. 2020. Efforts of indigenous knowledge in forest and wildlife conservation: A case study on Bulang People in Mangba Village in Yunnan Province, China. *Forests*, 11(11): 1178.
- Wennink, J., Lelieveld, G., de Knegt, H.J. and Klees, D. J. 2019. Habitat suitability analysis for the golden jackal (*Canis aureus*) in the Netherlands. *Lutra*, 62(1): 13-29.





# Potency of *Jatropha integerrima* Jacq., *Hibiscus rosa-sinensis* L. and *Ruellia tweediana* as Absorbants of Lead (Pb) in Air

Nella Yulia Sari<sup>\*(\*\*)</sup> and Fida Rachmadiarti<sup>†\*(\*\*)</sup>

\*Biology Study Program, Universitas Negeri Surabaya, Ketintang Street, Gayungan, Surabaya 60231, East Java, Indonesia

\*\*Department of Biology, Faculty of Mathematics and Natural Sciences, Universitas Negeri Surabaya, Ketintang Street, Gayungan, Surabaya 60231, East Java, Indonesia

†Corresponding author: Fida Rachmadiarti; fidarachmadiarti@unesa.ac.id

## Nat. Env. & Poll. Tech.

Website: [www.neptjournal.com](http://www.neptjournal.com)

Received: 20-01-2022

Revised: 08-03-2022

Accepted: 10-03-2022

### Key Words:

Chlorophyll content

*Hibiscus rosa-sinensis* L.

*Jatropha integerrima* Jacq.

*Ruellia tweediana*

Lead levels

## ABSTRACT

Air pollution is an atmospheric condition with high concentrations of toxic metals that exceed normal limits and are harmful to humans, animals or plants. *Jatropha integerrima* Jacq., *Hibiscus rosa-sinensis* L., and *Ruellia tweediana* have the potential to absorb (Pb) in the air. The aim of the study to analyze the levels of (Pb), chlorophyll, and the relationship between levels of (Pb) and chlorophyll in the three plant species at different locations. Samples were obtained from three locations with different traffic volumes Mayjend Yono Soewoyo street (100346.50 units/day), Dr. Soetomo street (58997.80 units/day), and Polisi Istimewa street (25692.50 units/day) Surabaya. Each sample was taken as many as 15 leaves at the third node. Leaf (Pb) measurements were carried out by dry ashing method using *Atomic Absorption Spectrophotometry* (AAS) and chlorophyll content was measured extraction method followed analysis by Spectrophotometer. Data levels (Pb) and chlorophyll were analyzed using two-way ANOVA followed by Duncan's test and correlation test with SPSS Statistics 26. The results showed that (1)Pb levels in the three plants from high to low *J. integerrima* ( $0.152 \pm 0.032 \text{ mg.L}^{-1}$ ); *H. rosa-sinensis* ( $0.042 \pm 0.008 \text{ mg.L}^{-1}$ ); and *R. tweediana* ( $0.007 \pm 0.006 \text{ mg.L}^{-1}$ ), (2)chlorophyll content of plant leaves from high to low *R. tweediana* ( $33.891 \pm 0.510 \text{ mg.L}^{-1}$ ); *H. rosa-sinensis* ( $28.499 \pm 0.32 \text{ mg.L}^{-1}$ ), and *J. integerrima* ( $10.597 \pm 1.697 \text{ mg.L}^{-1}$ ) high volume of vehicles followed by increasing levels of (Pb) and decreasing levels of chlorophyll, namely at Mayjend Yono Soewoyo street, Dr. Soetomo street, and Polisi Istimewa street, (3)there is a correlation between levels (Pb) and leaf chlorophyll content ( $0.524 > 0.381$ ). Can be concluded that *J. integerrima*, *H. rosa-sinensis*, and *R. tweediana* have the potential as absorbents (Pb) in the air.

## INTRODUCTION

The second largest city in Indonesia is Surabaya with a dense population. The population of Surabaya City in 2020 is 2.971.300 (Surabaya City Central Statistics Agency 2021). Population growth causes the number of motorized vehicles that support community activities to increase (Arifyananta 2015). Surabaya is included in the top five most congested cities in the world with a congestion value of 29.880/year (Irawan 2017). Traffic density in Surabaya on several roads is not the same.

Efforts to reduce pollutants in the air due to motor vehicle emissions are created parks on the edge or in the middle of the road. Plants can absorb lead (Pb) in the air through a passive absorption mechanism (Fascavetri et al. 2018, Gunarno 2014). Muzayanah et al. (2016) stated that lead (Pb) is a type of PM<sub>10</sub> pollutant which has a particle size

of less than 10  $\mu\text{m}$ . Lead (Pb) is particulate measuring  $\pm 2\text{m}$  and leaf stomata measuring  $10 \mu\text{m} \times 27 \mu\text{m}$  so that (Pb) can easily enter through leaf stomata (Sari et al. 2016). Heavy metals absorbed by leaves can affect the work of enzymes involved in the dark reactions of the photosynthesis process (Harianto 2018).

Lead (Pb) causes plants to have chlorosis, decreases chlorophyll biosynthesis processes, and damages plant cell walls. The decrease in chlorophyll is followed by an increase in (Pb) levels, this destroys chloroplasts. The average level (Pb) of several plant species is between 0.1-10 ppm with a toxicity limit of lead (Pb) in higher plants at 100 ppm (Inayah et al. 2010).

Leaf morphological characteristics such as smooth leaves, rough leaf surface, scaly, jagged edges, needle-like leaves, and sticky surfaces affect the ability to absorb (Pb)

in the air (Santoso 2013). Plants that have hairy leaves and rough surfaces absorb pollutants more optimally than smooth leaves and smooth surfaces (Rachmadiarti et al. 2019). The potential of plants to absorb pollutants in the air is also influenced by several environmental factors such as temperature, water content, light intensity, humidity, and wind speed.

*J.integerrima* plants have a shrub habit and elongated leaf morphology with tapered ends; *H.rosa-sinensis* plant has a shrub habitus and ovate leaf morphology; and *R.tweediana* have a herbaceous habitus and morphology of leaves is single, oppositely crossed, ends are rounded, the base is pointed, edges are serrated, the leaf is pinnate, and leaves are green. Based on previous research, plant leaves can absorb (Pb) in the air. This is evidenced when levels of (Pb) are high, and the chlorophyll content of leaves is low. From the results of previous research, further research is needed to determine the ability of the leaves of *J.integerrima*, *H.rosa-sinensis*, and *R.tweediana* plants to absorb (Pb) and their effect on chlorophyll content.

## MATERIALS AND METHODS

### Sample Collection

Sampling was carried out from polluted and unpolluted locations. The location is unpolluted on Bukit Darmo Golf and three roads in Surabaya City with an average daily volume of high, medium, and low-density levels (Fig. 1). Data on the average volume of vehicles passing at different densities were obtained from the Surabaya City Transportation Service 2020. The average daily volume of vehicles passing on Mayjend Yono Soewoyo street (100.346.50 units/day) high vehicle density; Dr.Soetomo Street (58997.80 units/day) medium vehicle density; and Polisi Istimewa street (25.692.50 units/day) low vehicle density category. Sampling leaves were carried out at each location, repetition was carried out 3 times by plotting at 09.00 WIB.

At each sampling location, physical and chemical environmental factors were measured before a sample was taken,

including soil temperature, air temperature, air humidity, soil moisture, soil pH, and light intensity. Samples were taken from as many as 15 leaves from the third node counted from the tip of each plant *J. integerrima*, *H.rosa-sinensis*, and *R.tweediana*. Each sample obtained was put in plastic and given a label. Leaf samples obtained were analyzed for lead (Pb) levels, chlorophyll, and leaf surface area measurements. Analysis test for lead (Pb) levels in samples was carried out at Chemical Physics Laboratory, Chemistry Department, FMIPA UNESA. Tests for the content of chlorophyll a, b, and total and surface area of leaf samples were carried out at Physiology Laboratory, Department of Biology, FMIPA UNESA.

### Analysis Leaf Surface Area

Measurement of leaf surface area using *leaf meter* ADC AM350 by placing the sample on the meter area. Measurement of leaf surface area by pressing the scanner button on the tool and moving it from base to tip. The scanner button is pressed again when the measurement has been made, the results can be viewed on the monitor and recorded.

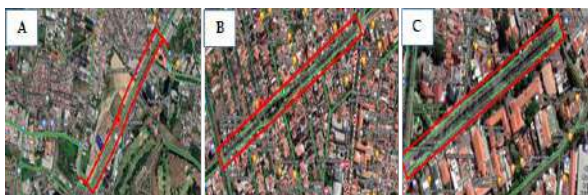
### Analysis of Chlorophyll Content

Testing the leaf chlorophyll content of each sample begins with calibration The Mapada V-1100D spectrophotometer uses 95% alcohol. The sample at each location was weighed as much as 1g, cut into small pieces, and crushed with a mortar pestle. Samples that have been finely added 100mL 95% alcohol and filtered through filter paper. The filtrate was then tested for chlorophyll content with wavelengths of 649 nm and 665 nm using the Mapada V-1100D Spectrophotometer. The value of chlorophyll content that appears on the screen is recorded and the chlorophyll content a, b, and the total is calculated using the Wintermasn and de Mots formula as follows (Rahayu et al. 2014):

$$\text{Chlorophyll a} = 13.7 \times \text{OD}_{665} - 5.76 \times \text{OD}_{649} \text{ (mg.L}^{-1}\text{)}$$

$$\text{Chlorophyll b} = 25.8 \times \text{OD}_{649} - 7.7 \times \text{OD}_{665} \text{ (mg.L}^{-1}\text{)}$$

$$\text{Total chlorophyll} = 20.0 \times \text{OD}_{649} + 6.1 \times \text{OD}_{665} \text{ (mg.L}^{-1}\text{)}$$



Note Notation A: Sampling on Mayjend Yono Soewoyo street, Notation B: Sampling on Dr. Soetomo street, Notation C: Sampling in Polisi Istimewa street.

Fig. 1: Sampling Locations (Google Maps, 2021)

## Analysis of Pb Content

**Sample preparation:** The analysis of accumulation levels (Pb) in the leaves was started by conducting sample preparation using the dry destruction method. *J.integerrima*; *H.rosa-sinensis*, and *R.tweediana* plant leaves were weighed as much as 2.5 g in a porcelain dish and roasted at 800°C for 3 h. The samples that have been kilned are put into a glass beaker, 1mL concentrated HNO<sub>3</sub> solution is added, and 10 mL aqua demin is added. The sample was stirred until dissolved and filtered, then analyzed by AAS (Atomic Absorption Spectrophotometry) PERKIN ELMER Analyst 100.

**Production standard metal solutions:** Preparation of standard solutions is done by making a standard solution of lead (Pb) as much as 100 ppm. Standard lead solution (Pb) was made from 100 ppm lead (Pb) mother liquor, then 10 mL was taken using a dropper and put into a 100 mL volumetric flask. The solution that has been put into a measuring flask is then diluted to the tera mark and homogenized. Metalworking solution (Pb) 10 ppm was prepared from standard solution (Pb) 100 ppm.

**Production calibration curves:** The calibration curve was made by making a standard solution (Pb). The standard solution was prepared by diluting solution (Pb) of 10 ppm to obtain a concentration between 0-3ppm. The standard solution then measured its absorption value using AAS PERKIN ELMER Analyst 100 with a hollow cathode (Pb) lamp.

**Sample measurement:** Measurement of leaf samples of each plant was carried out using the SNI method number 06-698945 of 2005 concerning Testing for Levels (Pb). Calculation of levels (Pb) contained in each sample of plant leaves *J.integerrima*; *H.rosa-sinensis* and *R.tweediana* use the following formula:

$$Cy' = \left( Cy \times \frac{V}{W} \right) \times 1000$$

Description:

Cy' = Pb levels absorbed in leaves ( $\mu\text{g}\cdot\text{g}^{-1}$ )

Cy = Measurable Pb levels in AAS ( $\text{mg}\cdot\text{L}^{-1}$ )

V = Volume of diluent solution (L)

W = Leaf biomass in the form of leaf dry weight (g)

1000 = Convert mg to  $\mu\text{g}\cdot\text{g}^{-1}$

## Data Analysis

Observational data in form of levels (Pb) and leaf chlorophyll were analyzed using statistical tests *Two Way* ANOVA with SPSS statistic 26 was conducted to see the effect of sampling location, plant species and interaction between the observation location and plant species on content (Pb). The analysis test was continued with Duncan's Test to see which plants

had the best potential to absorb lead (Pb) in the air. Leaf surface area data and environmental physicochemical factors were analyzed quantitatively descriptively. A correlation test using SPSS Statistics was carried out to see the relationship between (Pb) in the leaves of each plant and chlorophyll.

## RESULTS

Based on the results of testing the levels (Pb) in the leaves of *J.integerrima*; *H.rosa-sinensis* and *R.tweediana* in three different locations including Mayjend Yono Soewoyo street, Dr. Soetomo street, and Polisi Istimewa street showed different levels of (Pb). The highest (Pb) content was found in *J.integerrima*  $0.152\pm 0.032 \text{ mg}\cdot\text{L}^{-1}$  found on Mayjend Yono Soewoyo. The lowest leaf (Pb) levels were found in *R.tweediana*  $0.007\pm 0.006 \text{ mg}\cdot\text{L}^{-1}$  was found on Polisi Istimewa. The results from Duncan's test showed that there were differences in leaf (Pb) levels of each plant at each location (Table 1).

Testing of leaf chlorophyll content in *J.integerrima* plants; *H.rosa-sinensis*, and *R.tweediana* at three different locations including Mayjend Yono Soewoyo street, Dr. Soetomo street, and Polisi Istimewa street showed different results. The highest leaf chlorophyll content was found in *R.tweediana*  $33.891\pm 0.510 \text{ mg}\cdot\text{L}^{-1}$ . The lowest leaf chlorophyll content was found in *J.integerrima*, which was  $10.597\pm 1.697 \text{ mg}\cdot\text{L}^{-1}$ . The results of Duncan's test showed that there were differences in leaf chlorophyll levels in each plant at each location (Table 2).

Measurements of the leaf surface area of each plant at each sampling location showed different values. The results of the measurement of the highest leaf surface area were found in *R.tweediana* on Mayjend Yono Soewoyo ( $20.358\pm 0.490 \text{ cm}^2$ ). The lowest average leaf surface area was found in *J.integerrima* plants with a value of ( $15.612\pm 1.790 \text{ cm}^2$ ) which was located on Polisi Istimewa street (Table 3).

Table 1: Metal (Pb) Content of Leaves *J.integerrima*; *H.rosa-sinensis*, and *R.tweediana*.

Plant Type	Average Leaf (Pb) Content at Each Location [ $\text{mg}\cdot\text{L}^{-1}$ ]		
	1	2	3
<i>J.integerrima</i>	$0.152\pm 0.032\text{bB}$	$0.101\pm 0.031\text{bAB}$	$0.008\pm 0.001\text{bA}$
<i>H.rosa-sinensis</i>	$0.042\pm 0.008\text{abB}$	$0.014\pm 0.010\text{abAB}$	$0.125\pm 0.018\text{abA}$
<i>R.tweediana</i>	$0.061\pm 0.015\text{aB}$	$0.101\pm 0.070\text{aAB}$	$0.007\pm 0.006\text{aA}$

Notes: Notation: Numbers followed by different notations in rows and columns show significantly different results based on Duncan's Test with a test level of 0.05; 1= Mayjend Yono Soewoyo street (3 repetition points); 2= Dr. Soetomo street (3 repetition points); and 3= Polisi Istimewa Street (3 repetition points).

Physical and chemical environmental factors of each plant *J.integerrima*; *H.rosa-sinensis*, and *R.tweediana* at Mayjend Yono Soewoyo street, Dr. Soetomo street, and Polisi Istimewa street are not the same. Soil pH values range from 7-8; soil moisture 1-8(%Rh); soil temperature 26-29(°C); air humidity 32-60(%); air temperature 31-40(°C); and light intensity 3652-25044(Lux) (Table 4).

High levels of Pb in the plant, resulting a decrease in leaf chlorophyll content. The highest Pb levels in *J.integerrima*

on Mayjend Yono Soewoyo street ( $0.152\pm 0.032 \text{ mg.L}^{-1}$ ) had the lowest chlorophyll content ( $10.597\pm 1.697 \text{ mg.L}^{-1}$ ), while the lowest Pb levels were found in *R.tweediana* plants on Polisi Istimewa street ( $0.007\pm 0.006 \text{ mg.L}^{-1}$ ) had chlorophyll content ( $20.276\pm 0.478 \text{ mg.L}^{-1}$ ) (Table 5).

Plant surface types *J.integerrima*; *H.rosa-sinensis*, and *R.tweediana* are not the same. Different leaf types and leaf characteristics affect the absorbing metal (Pb) in the air (Table 6).

Table 2: Chlorophyll Content of Plant Leaves *J.integerrima*; *H.rosa-sinensis*, and *R.tweediana*.

Plant Type	Average Leaf Chlorophyll Levels at Each Location [ $\text{mg.L}^{-1}$ ]		
	1	2	3
<i>J.integerrima</i>	10.597±1.697aC	12.236±1.333aB	21.540±1.427aA
<i>H.rosa-sinensis</i>	28.499±0.321bC	24.262±0.456bB	14.869±0.975bA
<i>R.tweediana</i>	33.891±0.510cC	23.561±0.039cB	20.276±0.478cA

Notes: Notation: Numbers followed by different notations in rows and columns show significantly different results based on Duncan's Test with a test level of 0.05; 1= Mayjend Yono Soewoyo street (3 repetition points); 2= Dr. Soetomo street (3 repetition points); and 3= Polisi Istimewa street (3 repetition points).

Table 3: Leaf Surface Area of *J.integerrima*; *H.rosa-sinensis*, and *R.tweediana*.

Plant Type	Average Leaf Surface Area at Each Location ( $\text{cm}^2$ )		
	1	2	3
<i>J. integerrima</i>	16.526±0.589	16.319±0.442	15.612±1.790
<i>H. rosa-sinensis</i>	17.778±0.558	17.630±0.726	17.732±0.140
<i>R. tweediana</i>	20.358±0.490	19.640±0.180	20.111±0.366

Notes: 1= Mayjend Yono Soewoyo street (3 repetition points); 2= Dr. Soetomo street (3 repetition points); and 3= Polisi Istimewa street (3 repetition points).

Table 4: Environmental Chemical Physics Factors

Plant Type	Average Soil pH			Average Soil Moisture [%Rh]		
	1	2	3	1	2	3
<i>J. integerrima</i>	7.33±0.57	8.00±0.00	7.00±0.00	6.00±2.00	2.66±1.15	1.00±0.00
<i>H. rosa-sinensis</i>	7.00±0.00	8.00±0.00	7.66±0.57	8.33±0.57	4.66±0.57	1.00±0.00
<i>R. tweediana</i>	7.11±3.333	8.00±0.00	7.55±0.52	8.33±1.15	1.66±0.57	1.00±0.00
Plant Type	Average Air Humidity (%)			Average Air Temperature (°C)		
	1	2	3	1	2	3
<i>J. integerrima</i>	32.66±1.15	58.33±0.57	51.66±0.57	36.33±0.57	33.66±0.57	37.33±0.57
<i>H. rosa-sinensis</i>	60.00±1.00	60.00±0.00	50.66±0.57	31.00±2.00	33.00±0.00	35.00±0.00
<i>R. tweediana</i>	50.11±13.14	60.00±1.50	50.77±0.83	40.33±11.84	40.00±11.26	37.66±0.57
Plant Type	Average Soil Temperature (°C)			Average Light Intensity (Lux)		
	1	2	3	1	2	3
<i>J. integerrima</i>	26.66±0.57	27.00±0.00	29.33±0.57	10847.00±2555.36	3652.66±1177.06	6458.33±1189.94
<i>H. rosa-sinensis</i>	28.00±0.00	26.66±0.57	28.00±1.00	23200.00±769.08	7480.00±423.42	7689.00±1468.55
<i>R. tweediana</i>	28.3±0.57	27.66±0.57	29.33±2.08	25044.33±7289.70	15136.00±3270.56	15098.66±3678.690

Notes: 1= Mayjend Yono Soewoyo street (3 repetition points); 2= Dr. Soetomo street (3 repetition points); and 3= Polisi Istimewa street (3 repetition points).

Tests on Pb levels, leaf chlorophyll content, leaf surface area, and physical and chemical factors in the unpolluted environment at Bukit Darmo Golf Surabaya. *J.integerrima* plants showed the highest levels of Pb (0.025 mg.L<sup>-1</sup>); followed by *H.rosa-sinensis* (0.012 mg.L<sup>-1</sup>), and *R.tweediana* (0.008 mg.L<sup>-1</sup>). The highest leaf chlorophyll content was found in *R.tweediana* (13.309 mg.L<sup>-1</sup>), followed by *H.rosa-sinensis* (11.793 mg.L<sup>-1</sup>), and *J.integerrima* (11.679 mg.L<sup>-1</sup>). The highest leaf surface area was found in *R.tweediana* (20.69 cm<sup>2</sup>), followed by *H.rosa-sinensis* (16.75 cm<sup>2</sup>), and *J.integerrima* (15.66 cm<sup>2</sup>). Measurement of environmental physicochemical factors at Bukit Darmo Golf, Surabaya showed a different range of results for each plant. The soil pH value of the three plants is 7; soil moisture 1-1.89 (%Rh); Soil temperature 27-29(°C); humidity 70.22-70.89 (%), air temperature 29-30 (°C), and light intensity 5267.8-11465.1 (Lux) (Table 7).

**DISCUSSION**

Every year number of motorized vehicles continues to

increase. Population growth causes the number of motorized vehicles as community activity increases (Arifyananta 2015). Air pollution is a condition where there is a mixture of several harmful elements in the atmosphere that cause damage and reduce environmental quality (Abidin & Hasibuan 2019). The decline in environmental quality due to air pollution can harm living things (Fransiska 2016).

Lead (Pb) is one of the most common pollutants produced by motorized vehicles. Fossil-fueled motor vehicles are known to affect air quality as much as 79-97% of concentration (Pb) (Ruslinda et al. 2016). Metal (Pb) is dangerous metal; has bluish-gray color; with theatomic number 82; molecular weight of 207.2; density of 11.34 g.cm<sup>-3</sup>; and boiling point of 621.43°F (Kumar et al. 2020).

Plants can absorb pollutants (Pb) in the air and adapt in different ways. Efforts that are currently being developed in overcoming heavy metals in the air are using green plants. Phytoremediation is an air pollution control that is carried

Table 5: Relationship of Levels (Pb) and Leaf Chlorophyll Levels in Plants *Jatropha integerrima* Jacq., *Hibiscus rosa-sinensis* L., and *Ruellia tweediana*.

Sampling Location	Plant Type					
	<i>J.integerrima</i>		<i>H.rosa-sinensis</i>		<i>R.tweediana</i>	
	1	2	1	2	1	2
Mayjend Yono Soewoyo street	0.152±0.032	10.597±1.697	0.042±0.008	28.499±0.321	0.061±0.015	33.891±0.510
Dr. Soetomo street	0.101±0.031	12.236±1.333	0.014±0.010	24.262±0.456	0.101±0.070	23.561±0.039
Polisi Istimewa street	0.008±0.001	21.540±1.427	0.125±0.018	14.869±0.975	0.007±0.006	20.276±0.478

Notes: 1= Leaf Pb Content (mg/L); Leaf Chlorophyll Content (mg/L)

Table 6: Leaf surface type *J. integerrima*; *H. rosa-sinensis*, and *R. tweediana*.




Plant Type	Leaf Surface Type	Characteristic features	Picture
<i>J. integerrima</i>	Hispidus (Rough Trichomed Leaf Surface)	Single leaf, oval shape, finger bone, scattered.	
<i>H. rosa-sinensis</i>	Laevis (Slippery Leaf Surface)	The leaf blade is oval, the base is tapered, the edges are jagged, and the bones are fingered.	
<i>R. tweediana</i>	Villosus (Smooth and Tight Trichomed Leaf Surface)	Single leaf, crossed opposite, sole-shaped, rounded leaf tip, tapered leaf base, serrated leaf edge, and pinnate leaf spines.	

Table 7: Test results for metal content (Pb), leaf chlorophyll content, leaf surface area, and environmental physicochemical factors in *J. integerrima*; *H. rosa-sinensis*, and *R. tweediana* at Bukit Darmo Golf, Surabaya.

Plant Type	Leaf Pb [mg.L <sup>-1</sup> ]	Leaf Chlorophyll [mg.L <sup>-1</sup> ]	Leaf Surface Area [cm <sup>2</sup> ]
<i>J. integerrima</i>	0.025	11.679	15.66
<i>H. rosa-sinensis</i>	0.012	11.793	16.75
<i>R. tweediana</i>	0.008	13.309	20.69
Plant Type	Soil Moisture (%Rh)	Soil Temperature (°C)	Humidity (%)
<i>J. integerrima</i>	1.00	27	70.22
<i>H. rosa-sinensis</i>	1.89	28	70.89
<i>R. tweediana</i>	1.00	28	70.56
Plant Type	Soil pH	Air Temperature (°C)	Light Intensity (Lux)
<i>J. integerrima</i>	7	29	5267.8
<i>H. rosa-sinensis</i>	7	30	5856.0
<i>R. tweediana</i>	7	29	11465.1

out using cost-effective, energy-saving, and environmentally friendly technology (Rachmadiarti et al. 2021).

The highest (Pb) content was found in the *J.integerrima* plant obtained at Mayjend Yono Soewoyo (0.188 mg.L<sup>-1</sup>). The lowest levels of (Pb) in the leaf were found in *R.tweediana* obtained at Polisi Istimewa (0.002 mg.L<sup>-1</sup>). The level (Pb) at Bukit Darmo Golf from high to low is *J.integerrima* (0.025 mg.L<sup>-1</sup>); *H.rosa-sinensis* (0.012 mg.L<sup>-1</sup>), and *R.tweediana* (0.008 mg.L<sup>-1</sup>). Muzayanah et al. (2016) stated that metal (Pb) of the PM<sub>10</sub> group has particulates measuring ±2µm and leaf stomata 10µmx27µm so that (Pb) easily enters through leaf stomata (Sari et al. 2016). The test results show if *J.integerrima* potential to absorb (Pb) in the air.

The ability of *J.integerrima* to absorb (Pb) in the air is influenced by leaf morphology. *J.integerrima* leaves have an oval egg with 1-2 lobes in the lower half of the strands; base rounded, flat, or heart; and tapered tips (Sihalahi & Mustaqim 2021). *J.integerrima* is a shrub habitus plant with a height of 3m; has a single green leaf, oval in shape, leaf bones are fingered, the tip is tapered, and has a very thick trichome. Plant *J.integerrima* is considered the most effective in absorbing (Pb) because it has leaf morphology that supports and lines with previous studies. The results of Rachmadiarti's et al. (2019) that plants with thyme leaves and rough surfaces absorb pollutants more optimally than plants with smooth leaves and smooth surfaces.

Testing of total leaf chlorophyll content showed that the highest was found in *R.tweediana* (34,202 mg.L<sup>-1</sup>) obtained from Mayjend Yono Soewoyo. The lowest chlorophyll is found in *J.integerrima* (9.271 mg.L<sup>-1</sup>) at Mayjend Yono Soewoyo. Testing of chlorophyll content at Bukit Darmo Golf showed that the highest level was found in *R.tweediana*

(13.309 mg.L<sup>-1</sup>) and the lowest was found in *J.integerrima* (11.679 mg.L<sup>-1</sup>). *R.tweediana* is a herbaceous habitus plant with a height of 1-1.5m; tricot rod; single leaf, opposite solet shape, rounded tip, pointed base, toothed edge, and pinnate leaf bone. *R.tweediana* potential as metal (Pb) absorbent in the air. These results are in line with research by Fathia et al. (2015) plants that have the potential to absorb pollutants can accumulate lead in large quantities without causing a decrease in leaf chlorophyll and causing poisoning to plants. High levels of (Pb) in leaf tissue *J.integerrima* causes a decrease in leaf chlorophyll content. The test results are in line with Sari et al. (2016) and Rachmadiarti et al. (2019) who state that the increase in leaf chlorophyll levels is directly proportional to a decrease in pollution by (Pb), so that leaf chlorophyll levels can be used as identification of plant resistance to pollution in the air by (Pb).

Lead Pb in plants can inhibit photosynthesis, disrupt mineral nutrition and water balance, change hormonal status, and affect the structure and membrane permeability of plants (Hadi & Aziz 2015). Heavy metals will inhibit enzymes that play a role in the photosynthesis process of dark reactions (Harianto & Pohan 2018). Metals (Pb) can inhibit the absorption of cations such as Ca, Mg, K, Cu, Zn, and Fe through modification of membrane activity and permeability so that they cannot be absorbed and transported into the plant body is disrupted (chlorosis occurs) (Patra et al. 2011). Physiologically toxicity (Pb) inhibits chlorophyll biosynthesis in leaf chloroplasts.

Measurement of plant leaf surface area shows leaves *R.tweediana* on Mayjend Yono Soewoyo had the highest average rating (20,358 cm<sup>2</sup>) and plant leaves *J.integerrima* on Polisi Istimewa shows the lowest average value (15,612 cm<sup>2</sup>).

Measurement of the highest leaf surface area at Bukit Darmo Golf was found in *R.tweediana* (20.69 cm<sup>2</sup>), *H.rosa-sinensis* (16.75 cm<sup>2</sup>), and *J.integerrima* (15.66 cm<sup>2</sup>). The results of leaf surface area measurements are in line with research by Irma (2016) which states that levels of (Pb) can result in changes in leaf morphology covering the leaf surface; an arrangement of leaf veins, leaf base; leaf edge; leaf tips; and leaf color so that morphological changes result in a reduction in leaf surface area.

The entry of metal (Pb) in the network is influenced by physical and chemical environmental factors. The results of soil pH measurements showed values from 7-8. Research by Gultom and Lubis (2014) states that the optimal pH for absorbing (Pb) is 4 or in an acidic environment. Although the results of the research conducted showed that the environmental pH conditions were normal and not acidic, it was known that all types of plants were able to absorb pollutants (Pb) in the air.

The results of air humidity showed values between 32-60(%). Air humidity affects the opening of leaf stomata. High humidity values can cause leaf stomata to open wide so that pollutants can be absorbed more optimally. Humid environmental conditions also cause some pollutants in the air to bind water and then settle in plant bodies (Azzari et al. 2020).

Air temperature measurement shows a value of 31-40(°C). The temperature of each environment shows the optimal value. The results of research by Azizah & Rachmadiarti (2018) state that the optimal temperature in the environment is 30°C with a maximum level of 40°C. The optimal temperature in the environment has a positive impact because the leaf stomata will open and (Pb) in the air enters the plant tissue. The high temperature causes the concentration of (Pb) in the air to decrease because the high air temperature causes the concentration of pollutants in the air to become dilute (Winardi 2014).

Another physical and chemical factor that affects the absorption of (Pb) is soil moisture. Measurement of soil moisture shows the number 1-8 (%Rh). The high value of soil moisture results in disruption of the process of transpiration and absorption (Pb) in the air. The results of Dewanti's research (2012) state that high humidity values cause the transpiration rate to slow down due to the presence of water vapor.

The results of the measurement of light intensity ranged from 3652-25044 (Lux). A good light intensity ranges from ±32,000 lux, and a low light intensity value causes the photosynthesis process to not run optimally and the leaf stomata to close (Ibrahim & Hizqiyah 2013). Light intensity is a physical and chemical environmental factor that has influence the absorption of (Pb) in the air. The moderate or full

light intensity can affect the growth of a plant (Yuliantika & Sudarti 2021).

## CONCLUSION

The results of the research conducted can be concluded that the *J.integerrima*; *H.rosa-sinensis*, and *R.tweediana* have the potential to absorb pollutants (Pb) in the air. The level of (Pb) in the air is influenced by the amount of traffic density on Surabaya. The average levels (Pb) in plant leaves sequentially from high to low starting from *J.integerrima* (0.152±0.032 mg.L<sup>-1</sup>); *H.rosa-sinensis* (0.042±0.008 mg.L<sup>-1</sup>), and *R.tweediana* (0.007±0.006 mg.L<sup>-1</sup>). Levels (Pb) affect leaf chlorophyll levels. The highest chlorophyll content was found in *R.tweediana* (33,891±0.510 mg.L<sup>-1</sup>), *H.rosa-sinensis* (28,499±0.32 mg.L<sup>-1</sup>), and *J.integerrima* (10,597±1,697 mg.L<sup>-1</sup>). Based on the results of the study, it shows that if the average daily traffic volume is getting denser, it will be followed by high levels of (Pb) in the leaves, namely at Mayjend Yono Soewoyo, Dr. Soetomo, and Polisi Istimewa street. There is a correlation between the levels of (Pb) and chlorophyll (0.524>0.381). From these results, it can be concluded that *J.integerrima*, *H.rosa-sinensis*, and *R.tweediana* have the potential as absorbents (Pb) in the air.

## ACKNOWLEDGMENTS

Thanks to Mr. Dr. Tarzan Purnomo, M.Si., and Mrs. Dra. Herlina Fitrihidajati, M.Si. as a reviewer.

## REFERENCES

- Abidin, J. and Hasibuan, F.A. 2019. The Effect of Air Pollution on Health to Increase Public Understanding of the Dangers of Air Pollution. Paper presented in the Proceedings of the National Seminar on Physics, Riau IV University, Pekanbaru, 7 September.
- Arifiyananta, R.D. 2015. The Strategy of the Surabaya City Transportation Service to Reduce Highway Congestion in the City of Surabaya. Scientific articles. UNESA State Administration, Surabaya.
- Azizah, D.N. and Rachmadiarti, F. 2018. Potential of Daffodils (*Hymenocallis speciose*), Puring (*Codiaeum variegatum*), and Bintaro (*Cerbera manghas*) as Absorbents of Lead (Pb) in the Air. *J. Lentera Bio.*, 7(3): 195-202.
- Azzari, S.E., Muslim, B. and Riviwanto, M. 2020. Differences of Pb Absorption in different types of plants. *J. Independent Healthy*, 15(1): 140-148.
- Central Bureau of Statistics. 2021. Number of Population by Sex Per District Registration Result (Soul) 2018-2020. BPS City of Surabaya, Surabaya.
- Dewanti, D. 2012. Effect of Temperature on Plant Growth and Production. Essay. East Java "Veteran" National Development University. Not Published.
- Fascavetri, A., Rachmadiarti, F. and Bashri, A. 2018. Potential of Paris Lilies (*Cholorophytum comosum*), Japanese Jasmine (*Pseuderanthenum reticulatum*), and Deer Antlers (*Platyserium bifurcatum*) as Absorbents of Lead (Pb) in Air. *J. Lentera Bio.* 7(3): 188-194.
- Fathia, L.A.N., Baskara, M. and Sitawati. 2015. Analysis of the Ability of Bush Plants in the Median Road to Absorb Metal (Pb). *J. Plant Production.* 3(7): 528-534.

- Fransiska, N. 2016. Risk Analysis of Total Suspended Particulates (TSP) Exposure in Ambient Air on Public Health in PT Semen Padang Industrial Estate in 2016. Padang: Andalas University.
- Google. 2021. Google Maps: Map of Street Locations in the City of Surabaya in <http://maps.google.com/>
- Gultom, E.M., and Lubis, M.T. 2014. Application of activated carbon from oil palm shells with  $H_2PO_4$  activator for the absorption of heavy metals Cd and Pb. *J. Chem. Eng.*, 3(1): 5-10.
- Gunarno, M. 2014. Effect of Air Pollution on Leaf Area and Number of Leaf Stomata Rhoecol Discolor. Young Widyaishwara BPK Medan, Medan.
- Hadi, F. and Aziz, T. 2015. A mini-review on lead (Pb) toxicity in plants. *J. Biol. Life Sci.*, 6(2): 91-101.
- Harianto, V. and Pohan, S.D. 2018. Growth and physiological response of mustard plant (*Brassica rapa* var. *Parachinensis*) exposed to lead (Pb). *J. Biosci.*, 4(3): 154-160.
- Ibrahim, M and Hizqiyah, M. 2013. *Fundamentals of Plant Physiology*. Pelangi Press, Bandung.
- Inayah, S.N., Las, T. and Yunita, E. 2010. Content (Pb) in Angsana Leaves (*Pterocarpus indicus*) and Mini Elephant Grass (*Axonopus* sp.) on Protocol Tangerang City. *J. Valence*, 2(1): 340- 346.
- Irawan, D. 2017. Collaborative governance: Descriptive study of collaborative government processes in air pollution control in the city of Surabaya). *J. Pub. Policy Manag.*, 5(3): 1-12.
- Irma, W. 2016. Effect of lead (Pb) on the morphology of spinach (*Amaranthus tricolor* L.) leaves on a laboratory scale. *J. Appl. Sci. Technol.*, 9(2): 179-184.
- Kumar, A., Kumar, A., MMS, C.P., Chaturvedi, A.K., Shabnam, A.A., Subrahmanyam, G., Mondal, R., Gupta, D.K., Malyan, S.K., Kumar, S.S. and A. Khan, S., 2020. Lead toxicity: health hazards, influence on food chain, and sustainable remediation approaches. *International Journal of Environmental Research and Public Health*, 17(7): .2179.
- Muzayannah, A., Sudarto, P. and Yanuwadi, B. 2016. Effects of the green space proportion with a cumulative concentration of particulate matter 10 ( $PM_{10}$ ) in Surabaya-Indonesia. *J. Int. Chem. Tech. Res.*, 9(4): 431-436.
- Patra, R.C., Rautray, A.K. and Swarup, D. 2011. Oxidative stress in lead and cadmium toxicity and its amelioration. *Veter. Med. Int. J.*, 15: 616-672 doi: 10.4061/2011/457327.
- Rachmadiarti, F., Asri, M.T., Sari, N.Y., Sahani, K., Vatmawati, V.N. and Nafidiasri, F.A. 2021. The Potential of Tabebuia as Phytoremediator of Lead (Pb) in Atmosphere. *E3S Web Conf.*, 328:1-4.
- Rachmadiarti, F., Purnomo, T., Azizah, D.N. and Fascavitri, A. 2019. *Syzygium oleina* and *Wedelia trilobata* for Phytoremediation of Lead Pollution in the Atmosphere. *J. Nature Environ. Pollut. Technol.*, 18(1): 157-162.
- Rahayu, Y.S. and Yuliani, M. 2014. *Instructions for Practicum in Plant Physiology*. Surabaya State University, Surabaya.
- Ruslinda, Y., Gunawan, H., Goembira, F. and Wulandari, S. 2016. The Effect of the Number of Gasoline Fueled Vehicles on the Concentration of Lead (Pb) in Ambient Air on Jalan Raya Padang City. *National Seminar on Environmental Science and Technology II*. Padang: Unand Limau Manis Campus.
- Santoso, S.N. 2013. *Use of Plants as Air Pollution Reduction*. Institute Technology Sepuluh November, Surabaya.
- Sari, F.R., Purnomo, T. and Rachmadiarti, F. 2016. The ability of Betel Gading (*Epipremnum aureum*) Plant as Absorbent of Heavy Metal Lead (Pb) in Air. *J. Lentera Bio.*, 5(3): 116-124.
- Silalahi, M. and Mustaqim, W.A. 2021. *Seed Plants in Jakarta: Selected Non-Tree Species*. UKI Press, Jakarta.
- Surabaya City Transportation Service. 2020. *Traffic Performance Survey Report Phase I*. Surabaya City Government Transportation Service, Surabaya.
- Winardi, T.M. 2014. Effect of temperature and humidity on concentration (Pb) in Pontianak City Air. *J. Borneo Akcaya*, 1: 56-66.
- Yuliantika, M.M. and Sudarti, M.S. 2021. Effect of Light Intensity on Turmeric Plant Growth. *J. Phys. Appl. Res.*, 2(2): 52-57.





# Sustainable Production of Soybean (*Glycine max* L.) Crop Through Chemical Fertilizers and Organic Manures Along with the Improvement in Soil Health

R. R. Lohar\*† and C. P. Hase\*\*

\*Department of Environmental Science, B. G. College, Sangvi, Pune-411007, Maharashtra, India

\*\*Department of Botany, B. G. College, Sangvi, Pune-411007, Maharashtra, India

†Corresponding author: R. R. Lohar; rajaram.lohar@ritindia.edu

Nat. Env. & Poll. Tech.  
Website: [www.neptjournal.com](http://www.neptjournal.com)

Received: 17-11-2021

Revised: 21-01-2022

Accepted: 21-02-2022

## Key Words:

*Glycine max*  
Chemical fertilizers  
Organic manures  
Growth attributes  
Yield attributes  
Soil health

## ABSTRACT

A field experiment was carried out on the black cotton soil in the years 2018 and 2019 in the district of Sangli, Maharashtra, India to evaluate the sustainable agricultural practices for improving the growth and yield of the soybean (*Glycine max* L.) variety JS-335 along with the soil improvement. Twelve treatments were evaluated in a randomized block design with three replications. The results revealed that combined applications of chemical fertilizer (RDF-30:80:20:40) and organic manures (FYM and VCM) improved the growth attributes and seed yield as compared to control and other treatments along with a significant improvement in the soil health parameters. This agricultural practice emerged as a promising method for sustainable cultivation of soybean (C.V. JS-335) which improved the economic yield ( $\text{kg}\cdot\text{ha}^{-1}$ ), agronomic efficiency ( $\text{kg}\cdot\text{ha}^{-1}$ ), physiological efficiency ( $\text{kg}\cdot\text{ha}^{-1}$ ), partial factor productivity ( $\text{kg}\cdot\text{ha}^{-1}$ ), apparent recovery efficiency ( $\text{kg}\cdot\text{ha}^{-1}$ ) and sustainable yield index (0.80) with maximum return having cost: benefit ratio (1:3.8). The results found statistically significant and correlated having a positive relationship between yield and sustainability parameters.

## INTRODUCTION

Soybean (*Glycine max* L.) is often designated as the “Golden bean” which is one of the most economic, nutritious, and oil seed crops, rich in protein and carbohydrate (Patil et al. 2017). The food items like soy milk, sauce, paste, cake, paneer, soy flour, soy-namkeen, and soy flakes are prepared from soybean on a commercial scale which is exceptionally very popular among consumers. It is also added to bread, cereals, and meat products (Huang et al. 2014). Soybean protein is rich in lycin, different minerals, and vitamins like thiamine and riboflavin (Dass et al. 2018). Because of these nutrient qualities in soybean it is known as ‘vegetarian meat’ and described as a ‘miracle crop’. The area under soybean cultivation at the global level is 121.53 million hectares and production is 334.89 million tons. In India, the area under soybean cultivation is 11.72 million hectares with a production of 10.5 million tons (Anonymous 2014-15, ICAR). Leading states in the cultivation of soybean are Madhya Pradesh, Rajasthan, Maharashtra, and Andhra Pradesh. It was reported that the use of FYM and Vermicompost in soybean caused adequate expansion in plant development and seed yield in the two seasons (Ranjitha 2016). Javed & Panwar (2013) revealed that a mixture of organic and inorganic composts causes a significant rise in the yield of soybean.

To meet the global demand for soybean, the application of sustainable agricultural practices is a need of time. Considering all these realities, present investigation was undertaken to evaluate sustainable agricultural practices through applications of different fertilizers for improving the soil health, growth parameters and the yield attributes of the crop. The sustainability of agricultural practices was assessed based on sustainable parameters like economic yield, agronomic efficiency, physiological efficiency, partial factor productivity, apparent recovery efficiency, and sustainability yield index.

## MATERIALS AND METHODS

The present investigation was carried out on the black cotton soil in the Walwa-tehsil, Sangli district which is located in the western part of Maharashtra having latitude and longitude coordinators as 16.8676 and 74.5703 respectively. The average temperature is 25.4°C and the total annual rainfall is 580 mm. The experiment was designed with RBD including 12 different treatments of organic and chemical fertilizers for soybean variety JS-335. The whole experimental field was divided into three equal blocks and each block was again divided into twelve equal-sized plots measuring 2.5 m × 2.5 m to accommodate the treatments and control. A total of 36 plots were prepared and all the treatments were

randomly designed. The seeds as well as FYM, VCM, and RDF were procured from authentic and reliable sources. The twelve treatments were selected with three replications and each consisted of T1:75% RDF, T2:75% RDF + 25% FYM, T3:75% RDF + 25% VCM, T4: 100% RDF, T5: 100% RDF + 25% FYM, T6: 100% RDF + 25% VCM, T7: 125% RDF, T8: 125% RDF + 25% FYM, T9: 125% + 25% VCM, T10: 100% FYM, T11: 100%VCM, T12: absolute control (No fertilizer). The recommended dose of fertilizer (RDF-30:80:20:40, N:P:K:S), Farmyard Manure, Vermicompost.

The N, P, K, and other nutrients of organic manures were determined by official methods of analysis of AOAC international (AOAC 2005). N was estimated by the micro-Kjeldahl digestion method. Samples were digested with the nitric perchloric sulphuric acid mixture for the determination of P, K, Ca, and Mg. Phosphorus was determined by colorimeter using the vanadomolybdate method, K was determined using a flame photometer, and Ca and Mg were determined by the EDTA titration method.

### The Chemical Composition of Organic Manures

**Farmyard manure:** N-0.52%, P<sub>2</sub>O<sub>5</sub>-0.22%, K<sub>2</sub>O-0.54%, Na-0.08%, S-0.01%, Fe-1900 mg/kg, Zn-52mg/kg, B-2.1mg/kg, Mo-0.72 mg/kg, Cu-2mg/kg, Mn-6mg/kg

**Vermicompost:** N-0.54%, P<sub>2</sub>O<sub>5</sub>-0.023%, K<sub>2</sub>O-0.28%, Na- 0.12%, Fe- 1.1%, Zn-0.09%, Ca-0.003%, Mg-0.32%, Cu-0.003%, Mn-0.10%

The organic and inorganic fertilizers were applied to each plot according to the planned treatments. The whole amount of organic manures was applied on a dry weight basis basally during final land preparation. The organic manures were applied one month before sowing so that well decomposition of the organic manures would take place for the crop and thoroughly incorporated into the soil. The growth parameters, seed yield, biochemical analysis, and oil content in the seed were analyzed as and when required by using the random collection method of the samples. The experimental plot was ploughed in mid-November after the monsoon rains were over. The field was then harrowed and leveled properly. All stubbles were removed and the layout was done according to the experimental design. The seeds of soybean were treated with Rhizobium culture for the entire nutritional schedule as seed treatment before sowing the seeds except for the absolute control plot. The required chemical fertilizers were purchased from a fertilizer store by calculating the quantity as per the recommended dose of fertilizer applied to each plot. The seeds were sown directly into the plots by maintaining 10 cm plant to plant and 45 cm row to row spacing. The seeds were sown on 15<sup>th</sup> November for both consecutive seasons. The crop was irrigated after 15

to 20 days of interval. From time to time inter cultivation for weeding and other operations was carried out regularly. The second dose was given before the pod formation. The pods were harvested after the full maturity of the crop.

The observations on plant height were measured at 30, 45, 60, and 75 DAS using randomly selected ten plants from each treatment, and the average height was calculated. A total number of leaves per plant were measured at 30, 45, and 60 DAS using randomly selected ten plants from each treatment.

Yield attributes like number of immature pods per plant, number of mature pods per plant, number of seeds per pod, Seed index (100 seed weight), total seed yield (kg.ha<sup>-1</sup>), and stover yield (kg.ha<sup>-1</sup>) were analyzed from each treatment using randomly selected ten plants and the average was recorded in tables.

**Analysis of soil:** The soil samples (0-15cm) were collected from all the experimental plots at harvest. The samples were air dried and then sieved through a 2 mm sieve and stored in a polythene bag with labels. Soil samples were analyzed for available nitrogen, phosphorus, potassium, and organic carbon content. Available nitrogen was determined by the antacid potassium permanganate method (Subbiah & Asija 1956). Available phosphorus was determined by Olsen's method. The available potassium in soil extracts was analyzed using a flame photometer. The organic carbon was determined by Walkley-Black's (1934) chromic acid wet oxidation method.

### Analysis of Sustainability Parameters

Harvest index (%), economic yield (kg.ha<sup>-1</sup>), agronomic efficiency (kg.ha<sup>-1</sup>), physiological efficiency (kg.ha<sup>-1</sup>), partial factor productivity (kg.ha<sup>-1</sup>), apparent recovery efficiency (kg.ha<sup>-1</sup>), and Sustainability yield index were calculated by using following formulae.

$$i) \text{ Harvest index (\%)} = \frac{\text{Economic Yield (Kg/ha)}}{\text{Biological Yield (Kg/ha)}} \times 100$$

$$ii) \text{ Agronomic efficiency (AE)} = \frac{Y - Y_0}{F}$$

$$iii) \text{ Physiological Efficiency} = \frac{Y - Y_0}{U - U_0}$$

$$iv) \text{ Apparent recovery efficiency (RE)} = \frac{U - U_0}{F}$$

$$v) \text{ Partial Factor Productivity (PFP)} = \frac{Y}{F}$$

$$vi) \text{ Sustainable Yield Index} = (Y_m - SD) / Y_{max}$$

Where, Y-yield of a harvested portion of the crop with nutrient applied, Y<sub>0</sub>-Yield with no nutrient applied, F- Amount

of nutrient applied,  $U$ - Total nutrient uptake in above-ground crop biomass with nutrient applied,  $U_0$ - Nutrient uptake in above-ground crop biomass with no nutrient applied.  $Y_m$ -Mean yield, SD- Standard Deviation,  $Y_{max}$ -Maximum yield,  $W_2$ -Weight of the empty flask (g),  $W_1$ -Weight of empty Flask + Weight of oil (g),  $X$ =Weight of a sample taken for extraction

**Economics of soybean production:** The cost of soybean production for all the treatments was calculated depending on input cost and the average market price of soybean per quintal. Overall returns were determined by deducting the cost of production from gross income. The cost-to-benefit ratio was estimated by the proportion of the total cost and gross returns of a particular treatment.

**Statistical analysis:** The data were statistically analyzed for least significance difference (LSD) at a 5% probability level and coefficient of correlations by analysis of variance (ANOVA) using the data analysis tool pack of MS Excel (2013).

## RESULTS AND DISCUSSION

**Growth attributes:** The growth attributes such as plant height, number of leaves per plant, number of branches per plant, leaf area, dry weight, etc. contribute to the crop yield (Rana & Badiyala 2014). It was observed that all these parameters were positively influenced by the treatment

of different doses of organic manures like farmyard manure, vermicompost, and inorganic or chemical fertilizer like RDF. Plant height was increased in Soybean by all the treatments applied. The results recorded in Table 1 indicated that the application of RDF 125%+ Farmyard manure 25% and RDF 125% + Vermicompost 25% had shown a significant increase in plant height as compared to all other treatments and control. The results are statistically significant. The maximum plant height was recorded at 30, 45, 60, and 75 DAS in the combined application of RDF + FYM and RDF +VCM (Table 1). The plant height was increased with the advancement of age in all the stages of the crop growth because the growth process is irreversible (Patil & Udmale 2016). Thakur and Girothia (2010) and Saxena et al. (2013) also reported an increase in growth attributes like plant height, leaf number, leaf area, leaf area index, branch number, etc. ultimately increasing the productivity of soybean.

The number of leaves per plant was significantly increased with the combined applications of 125% RDF + farmyard manure 25% and 125% RDF + Vermicompost 25% (Table 1). It was 17.33 and 18.67, 36.67 and 37.00, 72.33 and 73.67 at 30 DAS and 60 DAS respectively. These treatments caused the highest increase in the

Table 1: Effect of fertilizer treatments on the growth attributes of soybean plants.

Fertilizer Treatment	Plant Height DAS(cm)				No. of leaves per plant DAS			Plant dry weight (g)			Nodule Count per plant		Nodule fresh weight (g)		Nodule dry weight (g)	
	30	45	60	75	30	45	60	30	45	60	30	45	30	45	30	45
T1	20.0	32.7	39.7	42.3	9.0	26.3	41.3	2.5	8.5	16.6	8.8	18.5	0.3	0.4	0.1	0.4
T2	20.6	38.3	53.3	57.4	10.3	18.3	44.3	2.5	11.0	17.4	11.4	38.2	0.3	0.4	0.1	0.4
T3	21.3	40.0	54.7	58.7	11.7	19.0	45.0	2.6	11.8	17.6	11.7	31.7	0.3	0.4	0.1	0.4
T4	22.3	42.3	58.0	61.7	10.1	26.7	45.3	2.6	13.5	18.3	10.4	31.3	0.3	0.4	0.1	0.4
T5	25.3	43.0	60.3	65.3	12.3	34.3	48.7	2.8	14.7	18.8	11.8	26.9	0.3	0.4	0.1	0.5
T6	26.4	43.7	61.3	67.4	13.0	34.7	48.3	2.9	14.8	19.0	12.0	27.3	0.3	0.4	0.1	0.6
T7	23.3	45.3	59.7	62.2	13.3	33.7	50.7	2.8	16.5	21.2	16.3	43.1	0.3	0.4	0.1	0.5
T8	28.3	47.7	67.0	69.8	17.3	36.7	72.3	3.2	17.8	23.4	19.3	35.9	0.3	0.4	0.1	0.5
T9	28.7	48.3	68.7	69.7	18.7	37.0	73.7	3.3	18.0	23.5	20.1	36.0	0.3	0.4	0.1	0.5
T10	18.3	30.3	32.0	38.2	9.7	24.3	40.3	2.5	7.5	17.9	9.8	34.0	0.2	0.4	0.1	0.3
T11	19.3	32.3	33.0	39.3	10.0	25.7	41.0	2.5	7.9	18.0	10.0	34.5	0.2	0.4	0.1	0.3
T12	14.0	22.7	28.0	38.0	7.7	14.3	36.0	2.1	6.6	13.2	8.3	20.7	0.2	0.3	0.1	0.3
LSD (0.05)	8.06	13.95	28.67	26.69	7.04	15.19	26.31	0.62	8.61	5.28	8.68	14.64	.07	0.03	0.030	0.18
SE±	1.09	1.88	3.87	3.60	0.95	2.05	3.55	0.08	1.16	0.71	1.17	2.05	0.00	0.00	0.004	0.02
CV%	15.66	15.50	24.06	20.84	25.66	23.66	23.55	10.39	29.93	12.33	30.27	20.22	11.47	3.7	17.51	19.31

Note: LSD-Least Significant Difference at  $p=0.05$ , SE±: Standard Error of the Mean, CV%: Coefficient of Variation

number of leaves per plant as compared to the remaining treatments and control. The leaves are the main photosynthetic organ of every plant, hence increase in the number of leaves increases the photosynthetic area and chlorophyll content. The increase in plant height and number of leaves per plant leads to an increase in yield (Thakur & Girothia 2010, Devi et al. 2011, Kumar et al. 2016).

It was reported that there was an increase in plant dry weight in soybean for different treatments (Table 1) but it was revealed that the combined treatments of RDF + FYM and RDF + VCM emerged as superior treatments causing an increase in dry weight of plant as compared to other treatments used and control. The increase in dry weight of soybean was recorded at 30, 45, and 60 DAS. The increase was by 3.15 g and 3.25 g, 17.83g, 18.00 g, 23.35 g, and 23.45 g at 30, 45, and 60 DAS respectively. All the results are statistically significant and the finding of the present investigation was supported by Jagmeet et al. (2015).

In leguminous plants like soybean number of nodules on the roots of each plant is a very important factor in growth attributes. The root nodules fix atmospheric nitrogen symbiotically and provide it to the host plant. The nitrogen supplied by root nodule bacteria contributes significantly and plays a vital role in plant growth (Chaturvedi et al. 2010). In the present study, all the treatments of chemical and organic fertilizers have significantly induced an increase in the number of nodules per plant (Table 1). Due to the application of 125% RDF + 25% FYM and 125% RDF + VCM 25%. The increase was by 19.33, 20.10, 35.90, and 36.00 respectively. This has directly influenced the various growth attributes like plant height, number of leaves per plant, etc.

The fertilizer treatments of RDF 125% + FYM 25% and RDF 125% + VCM 25% caused a positive increase in the fresh and dry weight of nodules in soybean (Table 1). Nodule fresh weight was 0.32 g, 0.33 g, 0.42 g, and 0.43 g at 30, 45, and 60 DAS. Which was much better than control and other treatments? The nodule dry weight recorded was 0.099, 0.098, 0.48, and 0.48 g at 30, 45, and 60 DAS with both treatments. Similar results were reported by Billore et al. (2009) and Singh et al. (2010). They claimed that the combined application of synthetic and organic fertilizers increase positively soil condition as well as enhanced the activity of nodulation resulting in improved vegetative growth of the treated plant as compared to control. Further, they reported that such type of fertilizer application to plants increases their metabolic activities and causes improvement in various growth parameters. In the present study sulfur present

in the RDF is an integral component of the nitrogenase enzyme playing a key role in nitrogen fixation. This may be the probable reason for the increase in the number of nodules per plant, the fresh and dry weight of nodules in soybean treated with RDF + FYM and RDF + VCM (Najar et al. 2011). The additional probable reasons for the improvement of growth attributes and nodule number, dry and fresh weight of nodule may be due to the different types of enzymes and growth-promoting factors secreted by earthworms in vermicompost.

**Yield and yield attribute:** The results shown on this parameter in Table 2 indicated that a maximum number of pods per plant were recorded in the treatments of combined applications of RDF + FYM and RDF + VCM as compared to all other treatments and control. The highest number of pods per plant observed in soybean was 64.80 and 65.27 respectively in both the treatments. Similar results were observed by Rana et al. (2018) with combined treatments of organic and chemical fertilizers for the increase in the growth of the number of pods per plant. As recorded in Table 2 highest number of filled pods was also recorded in the treatments of combined applications of RDF + FYM and RDF + VCM. The maximum number of filled pods per plant recorded in both treatments was between 55 and 56. Both the parameters studied have greatly contributed to an increase in economic yield over control and remaining treatments (Singh & Rai 2004). The results recorded in Table 2 clearly showed that the highest results on this parameter were recorded in the combined treatments T8 and T9 i.e. RDF + FYM and RDF + VCM. The significant values are 2.83 and 2.90 seeds per pod respectively. The increase in the number of seeds per pod has a direct relation with enhanced seed yield or economic yield. All the above parameters mentioned have a direct relationship with economic yield in soybean (Suryawanshi et al. 2006). Similar to the increase in economic yield stover yield was also very high in both the treatments T8 (3184.47 kg.ha<sup>-1</sup>) and T9 (3210.28 kg.ha<sup>-1</sup>). It is seen that among these two better treatments of combined fertilizers T9 which is RDF + VCM was superior to T8 (RDF + FYM) and slightly better over T8 (Khutate et al. 2005).

Biological yield is a very important aspect of the cultivation of legume crops like soybean. The results recorded on this parameter in Table 2 indicates that the biological yield was also highest in the treatments of T8 and T9 in which combined application of RDF + FYM and RDF + VCM was followed for the soybean crop. The recorded values were 5669.64 kg.ha<sup>-1</sup> and 5720.61

Table 2: Effect of fertilizer treatments on yield and yield attributes of Soybean.

Fertilizer treatment	Season 2018/2019							
	No. of Pods per plant	No. of filled Pods per plant	No. of Seeds per Pod	Stover Yield (kg.ha <sup>-1</sup> )	Biological Yield [Kg.ha <sup>-1</sup> ]	Harvest Index [%]	Seed Index [%]	Economic Yield (kg.ha <sup>-1</sup> )
T1	50.7	40.0	2.6	2,057.5	3,478.1	40.8	13.3	1,420.6
T2	52.3	44.3	2.6	2,184.3	3,814.4	42.7	14.1	1,630.1
T3	53.0	44.9	2.6	2,208.0	3,853.1	42.7	14.3	1,645.0
T4	51.9	45.3	2.6	2,674.5	4,384.6	39.0	15.1	1,710.1
T5	55.1	70.8	2.6	2,884.0	4,962.3	41.9	14.7	2,078.3
T6	55.9	70.9	2.7	2,910.2	5,020.3	42.0	18.9	2,110.1
T7	56.9	47.9	2.6	3,085.3	5,275.3	41.5	15.1	2,190.0
T8	64.8	55.3	2.8	<b>3,184.5</b>	<b>5,669.6</b>	<b>43.8</b>	<b>15.8</b>	<b>2,485.2</b>
T9	65.3	56.0	2.9	<b>3,210.3</b>	5,720.6	43.9	16.1	2,510.3
T10	48.3	39.7	2.3	2,028.7	3,536.8	42.6	12.2	1,508.1
T11	48.8	40.3	2.3	2,082.0	3,592.1	42.0	12.7	1,510.1
T12	40.6	33.3	2.3	1,228.4	2,439.0	49.6	11.8	1,210.6
LSD (0.05)	12.76	25.58	0.42	1080.28	1948.98	3.05	4.06	887.36
SE±	1.72	3.45	.057	146.06	263.51	0.41	0.55	119.97
CV%	10.44	22.72	7.35	18.69	19.49	3.25	12.36	21.04

Note: LSD-Least Significant Difference at p=0.05, SE±: Standard Error of the Mean, CV%: Coefficient of Variation

kg.ha<sup>-1</sup> respectively. When the effect of both treatments on biological yield is compared the treatment T9 (RDF + VCM) had shown better results than T8 (Devi et al. 2011). The results on the harvest index showed the same trend as that of the seed index. The treatments of RDF + FYM and RDF + VCM had shown almost similar values (43.83% and 43.88%). Amongst all the yield attributes harvest index is the most reliable indicator of crop profitability and economic returns in general. The profitability of any crop when it is cultivated is judged through the values of the harvest index.

As it is the ratio of  $\left( \frac{\text{Economic Yield (Kg/ha)}}{\text{Biological Yield (Kg/ha)}} \right) \times 100$

These results are in conformity with the findings of Shweta et al. (2014). The results on the seed index revealed that the superior treatments T8 and T9 were almost at par (15.84% and 16.05%). Both treatments were equally influenced by the results of the seed index (Bandopadhyay et al. 2010).

**Soil health:** Soil health was significantly improved by the application of RDF + FYM and RDF + VCM (Table: 3). The contents of different soil nutrients and organic carbon were increased due to the application of a combination of fertilizers in T8 and T9 as compared to the control and other treatments. The increase in organic

carbon was very high in T8 and T9 treatment (5.63 g.kg<sup>-1</sup> and 5.67 g.kg<sup>-1</sup>) as compared to control (3.90 g.kg<sup>-1</sup>). Organic carbon plays a major role in the improvement of soil fertility and soil health. It has a direct effect on the increase in seed yield and seed quality in soybean. As soybean is a nodule crop fixing nitrogen symbiotically, effectively helps in the improvement of soil health and fertility. Similar results were recorded by several researchers Navale et al. (2003), Kundu et al. (2008), and Muneshwar et al. (2008). They claimed that the application of FYM and vermicompost resulted in higher content of N, P, K, and seed yield as well as oil content in soybean. The chemical or synthetic fertilizer if applied alone causes soil pollution and desertification of soil but the application of vermicompost and FYM as well as Nano-compost help to improve soil fertility, physico-chemical properties of soil, and biological properties such as soil enzymes, soil microflora, etc. are improved having with great effect on yield and yield quality of various crops (Naderi & Danes 2013).

**Sustainability parameters:** The application of organic fertilizers along with chemical fertilizers is an effective method for the sustainable cultivation of different crops (Table 4). The organic fertilizers showed a significant effect on economic yield, agronomic efficiency, physiological efficiency, partial factor productivity, apparent recovery, and

Table 3: Effects of fertilizer treatments on organic carbon and available nutrients in the soil before sowing and after harvesting in soybean (Pooled over 2 years).

Fertilizer Treatments	Before sowing					After harvest				
	N (kg.ha <sup>-1</sup> )	P <sub>2</sub> O <sub>5</sub> (kg.ha <sup>-1</sup> )	K <sub>2</sub> O	S	OC (g.kg <sup>-1</sup> )	N (kg.ha <sup>-1</sup> )	P <sub>2</sub> O <sub>5</sub>	K <sub>2</sub> O	S	OC (g.kg <sup>-1</sup> )
T1	182.7	13.4	164.2	16.9	4.1	214.3	17.8	165.3	17.3	4.2
T2	198.4	17.4	179.3	15.9	4.4	221.6	21.3	182.2	16.7	4.5
T3	200.8	17.9	180.8	16.8	4.4	223.4	21.8	183.1	17.0	4.5
T4	215.1	22.6	176.7	23.9	4.8	220.7	27.8	178.1	24.1	4.9
T5	230.4	18.3	181.2	24.8	5.2	232.3	22.1	183.8	25.7	5.4
T6	232.3	18.9	181.8	25.8	5.2	234.2	22.3	184.2	26.0	5.4
T7	255.2	21.2	182.7	26.7	5.4	258.9	23.3	186.5	27.6	5.5
T8	262.1	22.8	190.8	31.1	5.5	266.7	24.4	193.3	31.9	5.6
T9	265.0	23.0	190.9	30.4	5.6	267.4	24.7	194.0	31.8	5.7
T10	204.3	17.2	152.3	16.8	4.0	218.3	19.3	155.2	17.1	4.0
T11	205.4	17.4	152.8	16.8	4.0	219.2	19.7	156.1	17.1	4.1
T12	172.3	10.1	109.0	13.1	3.9	175.1	12.4	109.3	13.2	3.9
LSD(0.05)	62.74	6.72	30.06	13.0	1.41	45.17	6.26	30.24	13.60	1.48
SE±	8.48	0.90	4.06	1.76	0.19	6.10	0.84	4.08	1.83	0.20
CV (%)	12.60	15.79	7.66	26.1	13.24	8.64	12.6	7.60	26.58	13.59

Note: LSD-Least Significant Difference at p=0.05, SE±: Standard Error of the Mean, CV%: Coefficient of Variation

Table 4: Effect of fertilizer treatments on agronomic efficiency, physiological efficiency, partial factor productivity, apparent recovery efficiency, sustainable yield index in soybean.

Fertilizer treatments	Agronomic Efficiency (AE) (kg.kg <sup>-1</sup> )	Physiological Efficiency (PE) (kg.kg <sup>-1</sup> )	Partial Factor Productivity (PFP) (kg.kg <sup>-1</sup> )	Apparent Recovery Efficiency (RE) (kg.kg <sup>-1</sup> )	Sustainable Yield Index (SYI)
T1	7.0	5.5	47.4	1.3	0.4
T2	14.0	8.8	54.3	1.6	0.5
T3	14.5	8.9	54.8	1.6	0.5
T4	16.6	5.7	57.0	2.9	0.5
T5	28.9	9.0	69.3	3.2	0.7
T6	30.0	9.3	70.3	3.2	0.7
T7	32.6	8.2	73.0	4.0	0.7
T8	42.5	10.4	82.8	4.1	0.8
T9	43.3	10.5	83.7	4.1	0.8
T10	9.9	9.3	50.3	0.4	0.4
T11	10.0	9.1	50.3	0.4	0.4
T12	-	-	-	-	0.3
LSD(0.05)	36.31	14.8	29.57	3.17	0.3794
SE±	4.26	2.001	3.99	0.42	0.04
CV (%)	-	-	21.04	-	29.74

Note: LSD-Least Significant Difference at p=0.05, SE±: Standard Error of the Mean, CV%: Coefficient of Variation

sustainable yield index. All these sustainable parameters were highly improved due to the applications of chemical fertilizers along with FYM and vermicompost. The nutrient combination treatments of 125% RDF + FYM and 125% RDF + VCM emerged as the best sustainable treatments for the improvement of yield, yield parameters, growth parameters along with improvement in soil health.

**Economics of the soybean cultivation using different fertilizers treatments:** The economics of soybean cultivation was greatly influenced by the different treatments of fertilizers used (Table 5). It was seen from the data that a significant increase in seed yield (2510.3 kg.ha<sup>-1</sup>) was obtained for soybean variety JS-335 due to the treatment of T9 followed by T8. The maximum net return of Rs. 36,333.72 per hectare was achieved by these treatments. The cost-benefit ratio was 1: 3.8 followed by T8.

**Correlation and regression analysis:** The correlation coefficient between applied nutrients (kg.ha<sup>-1</sup>) to the soil and accumulation of organic carbon (g.kg<sup>-1</sup>), agronomic efficiency (kg.ha<sup>-1</sup>), and economic yield (kg.ha<sup>-1</sup>) were significantly and positively correlated ( $r = 0.97$  &  $r = 0.99$ ) respectively and there is a linear relationship between these variables. It all reflects the immediate effect of applied compost and VCM which has a direct influence on financial returns from the cultivation of soybean.

**Multiple regression analysis:** The multiple regression model employed to see the relationship between five independent variables ( $x_1$  to  $x_5$ ) and one dependent variable  $Y$  is given below.

Relationship between Yield of crop and Sustainability parameters

Regression equation:

$$Y = b_0 + b_1x_1 + b_2x_2 + b_3x_3 + b_4x_4 + b_5x_5 + e$$

Where,

$Y$  = Economic yield (kg.ha<sup>-1</sup>)

$b_0$  = Intercept value

$x_1$  = Agronomic efficiency (kg.ha<sup>-1</sup>)

$x_2$  = Physiological efficiency (kg.ha<sup>-1</sup>)

$x_3$  = Partial factor productivity (kg.ha<sup>-1</sup>)

$x_4$  = Apparent recovery (kg.ha<sup>-1</sup>)

$x_5$  = Organic carbon (g.kg<sup>-1</sup>)

The value of multiple  $R$  (0.99) and  $R^2$  (0.99) is positive (0.99) indicating that there is a positive correlation between Economic yield and the observed values of Agronomic efficiency, Physiological efficiency, Partial factor productivity, and apparent recovery which also indicates the regression model fits the observed data. A positive coefficient indicates that as the value of the independent variables increases the mean value of economic yield increases. A low p-value (<0.05) and correspondent t-stat of independent variables indicate a highly significant increase in the economic yield. The changes in these independent variables are related to changes in the response variable indicating the results are highly significant.

## CONCLUSION

It was reported that cultivation of soybean variety JS-335

Table 5: Economics of different fertilizer treatments for the cultivation of soybean variety JS-335 (Pooled for two years).

Fertilizer Treatment	Economic Yield (kg.ha <sup>-1</sup> )	Gross Income (Rs.ha <sup>-1</sup> )	Expenditure (Rs.ha <sup>-1</sup> )	Net Income (Rs.ha <sup>-1</sup> )	C:B ratio
T1	1,420.6	78,130.3	28,104.4	50,025.8	1:02.8
T2	1,630.1	89,655.5	31,458.1	58,197.4	1:02.9
T3	1,645.0	90,477.2	31,746.4	58,730.8	1:02.9
T4	1,710.1	94,053.9	32,432.4	61,621.5	1:02.9
T5	2,078.3	114,303.8	35,719.9	78,583.8	1:03.2
T6	2,110.1	116,054.4	35,168.0	80,886.4	1:03.3
T7	2,190.0	120,452.2	35,427.1	85,025.1	1:03.4
T8	2,485.2	136,684.4	36,941.7	99,742.6	1:03.7
T9	2,510.3	138,068.2	36,333.7	101,734.4	1:03.8
T10	1,508.1	82,945.5	26,756.6	56,188.9	1:03.1
T11	1,510.1	83,054.4	25,954.5	57,099.9	1:03.2
T12	1,210.6	66,581.9	25,412.9	41,169.0	1:02.6

\* Average market rate of soybean Rs. 5500/q, \*\*Total expenditure cost includes the expenditure from land preparation to the harvesting of turmeric.

showed promising results with the application of chemical fertilizers such as RDF and organic manures like FYM and vermicompost. There was significant improvement with these treatments in growth and yield attributes. Improvement in the yield attributes is directly related to the market price of soybean. The integrated application of chemical fertilizer + FYM and chemical fertilizer + vermicompost was found to be highly effective to improve soil health and productivity through improved sustainability attributes like agronomic efficiency, partial factor productivity, and sustainable yield index. The cost-benefit ratio of these treatments was comparatively higher indicating that such treatments may be recommended to the farmers for the sustainable cultivation of soybean.

## ACKNOWLEDGEMENT

The authors gratefully acknowledge the help rendered by Mr. Dipak A. Kapurkar, Lab. I/C Sushilanand Agro Polyclinic, Islampur District Sangli for various types of analyses. Similarly, the field facilities provided by the farmers for the cultivation of soybean is duly acknowledged. We are also thankful to our mentor Prof. Dr. K. N. Dhumal, Department of Botany, SPPU Pune. We duly thank Dr. Mrs. S. S. Kulkarni, Director, RIT, Rajaramnagar for providing the research opportunity.

## REFERENCES

- Anonymous 2014-15. Director's Report and Summary Tables of Experiments 201-15, All India coordinated research project on soybean, ICAR-Directorate of Soybean Research, Indore, India, pp-329.
- AOAC 2005. Official Methods of Analysis. Association of Official Analytical Chemists International. 18 edition. AOAC Press, Arlington, VA USA.
- Billore, S.D., Vyas, A.K. and Joshi, O.P. 2009. Effect of integrated nutrient management in soybean (*Glycine max* L.) and Pigeon pea (*Cajanus cajan* L.) intercropping on productivity, energy budgeting, and competition functions. *J. Food Leg.*, 22(2): 124-6.
- Bandopadhyay, K.K., Misra, A.K., Ghosh, P.K. and Hati, K.M. 2010. Effect of integrated use of farmyard manure and chemical fertilizers on soil physical properties and productivity of soybean. *Soil Till. Res.*, 110: 115-125.
- Chaturvedi, S., Chandel, A.S., Dhyani, A.S. and Singh, A.P. 2010. Productivity, profitability, and quality of soybean (*Glycine max*) and residual soil fertility as influenced by integrated nutrient management. *Indian J. Agro.*, 55(2): 133-7.
- Dass, A., Dey, D., Lal, S.K. and Ranjanna, G.A. 2018. Tank mix insecticide and herbicide application effects on weeds, insect-pest menace, and soybean productivity in the semi-arid northern plain of India. *Leg. Res.*, 42(3): 385-391.
- Devi, K.N., Abhay, K.V., Maibam, S.S. and Naorem, G.S. 2011. Effect of bioregulators on growth, yield, and chemical constituents of soybean (*Glycine max*). *J. Agric. Sci.*, 3(4): 151-159.
- Huang, M., Wanga, Q., Zhang and Mand Zhu, Q. 2014. Prediction of color and moisture content for vegetable soybean during drying using hyperspectral imaging technology. *J. Food Eng.*, 128: 24-30.
- Jagmeet, K., Ram, H., Gill, B.S. and Jasdeep, K. 2015. Agronomic performance and economic analysis of soybean (*Glycine max*) in relation to growth regulating substances in Punjab, India *Leg. Res.*, 38(5): 603-608.
- Javed, S. and Panwar, A. 2013. Effect of biofertilizer, vermicompost, and chemical fertilizer on different biochemical parameters of *Glycine max* and *Vigna mungo*. *Recent Res. Sci. Technol.*, 5: 40-44.
- Kumar, T., Samaiya, R.K., Singh, Y., Dwivedi, S.K. and Meena, K.C. 2016. Effect of foliar parameters of soybean (*Glycine max* L.) Merill. *Int. J. Agric. Sci.*, 8: 133-138.
- Kundu, S., Bhattacharya, R., Ved, P. and Gupta, H.S. 2008. Carbon sequestration potential of Inceptisols under long-term soybean-wheat rotation in sub-temperate rain-fed agro-ecosystem of North-west Himalayas. *J. Indian Soc. Soil Sci.*, 56(4): 423-429.
- Khutate, N.G., Mendhe, S.N., Dongarkar, K.P., Dadhe, N.N. and Gavande, V.H. 2005. Effect of nutrient management treatments on growth and yield of soybean. *J. Soils Crops*, 15(2): 411-414.
- Muneshwar, S.M., Singh, M. and Kumrawat, B. 2008. Influence of nutrient supply system on the productivity of soybean-wheat and soil fertility of vertisols of Madhya Pradesh. *J. Indian Soc. Soil Sci.*, 56(4): 436-41.
- Naderi, M.R. and Danes, A. 2013. Nano fertilizers and their roles in sustainable agriculture. *Int. J. Agric. Crop Sci.*, 5(19): 2229-2232.
- Najar, G.R., Singh, S.R., Akhtar, F.H. and Hakeem, S.A. 2011. Influence of sulfur level on yield, uptake, and quality of soybean (*Glycine max*) under temperate conditions of Kashmir. *Indian J. Agric. Sci.*, 81(4): 340-3.
- Navale, K.B., Gaikwad, C.B. and Tamboli, B.D. 2003. Effect of integrated nutrient management on yield, nutrient availability, and uptake of nutrients by soybean. *J. Maha. Agric. Univ.*, 25(1): 105-107.
- Patil, H.M. and Udmale, K.B. 2016. Response of different organic inputs on growth and yield of soybean on Inceptisol. *Scholarly. J. Agric. Sci.*, 6(5): 139-144.
- Patil, V., Meti, S., Mansur, C.P., Rajashekhara, E., Itagi, P. and Hadimani, H.P. 2017. Nutritional studies on vegetable soybean (*Glycine max* Merrill). In the Northern dry zone of Karnataka, India. *Int. J. Curr. Microbiol. Appl. Sci.*, 6(12): 5364-5374.
- Rana, R. and Badiyala, D. 2014. Effect of integrated nutrient management on seed yield quality and nutrient uptake of soybean *Glycine max* under mid hill conditions of Himachal Pradesh. *J. Agric.*, 59(1): 641-645.
- Rana, D.S., Dass, A., Rajanna, G.A. and Choudhary, A.K. 2018. Fertilizer phosphorus solubility affects Indian mustard maize and wheat-soybean cropping systems productivity. *Agron. J.*, 110(6): 2608-2618.
- Ranjitha, B.M. 2016. Effects of soil test-based INM practices on the performance of chili (*Capsicum annuum* L.) M. Sc. Thesis, University of Horticultural Sciences, Bagalkot.
- Singh, R. and Rai, R.K. 2004. Yield attributes, yield, and quality of soybean (*Glycine max*) are influenced by integrated nutrient management. *Indian J. Agro.*, 49(4): 271-274.
- Saxena, S.C., Nainwal, R.C. and Joshi, A. 2013. Optimization of nutritional levels for newly released soybean (*Glycine max* (L) Merrill) varieties in mollisols of Uttarakhand. *Soybean Res.*, 11(2): 43-54.
- Singh, G., Aggarwal, N. and Kumar, V. 2010. Integrated nutrient management in lentils with organic manures, chemical fertilizers, and biofertilizers. *J. Food Leg.*, 23(2): 149-51.
- Suryawanshi, S.B., Lad, N.G., Suryawanshi, V.P., Shaikh, A.K. and Adsul, P.B. 2006. The combined effect of organic and inorganic fertilization on yield attributes and yield of soybean (*Glycine max* L.). *J. Soils Crops*, 16: 145-147.
- Subbiah, B. V. and Asija, G. L. 1956. A rapid procedure for the estimation of available nitrogen in soils. *Cure Science*, 25,254-260.
- Shweta, G., Jain, M.P. and Atul, G. 2014. Effect of nitrogen and plant growth regulators on soybean under sown conditions. *Soybean Res.*, 12: 184-187.
- Thakur, H.S. and Girothia, O.P. 2010. Response of soybean (*Glycine max* L.) and chickpea (*Cicer arietinum*) cropping sequence to phosphorus nutrition. *Soybean Res.*, 8:13-19.
- Walkeley, A and Black I. A., 1934. Method for determining soil organic carbon matter, a proposed modification of the chromic acid titration method. *Soil Science*, 37(1): 29-38.





# Water Sustainability Concept of Hindu Javanese Community Settlements Toward Global Climate Change Resilience in the Indonesia Mountainous Area

Fauzan Ali Ikhsan<sup>\*(\*\*)</sup>†, Bambang Setioko<sup>\*\*\*</sup> and Atiek Suprapti<sup>\*\*\*</sup>

\*Doctoral Program of Architecture and Urban Science, Diponegoro University, Semarang, Indonesia

\*\*URDC Laboratory, Architecture Program, Sebelas Maret University, Surakarta, Indonesia

\*\*\*Architecture and Urban Science, Diponegoro University, Semarang, Indonesia

†Corresponding author: Fauzan Ali Ikhsan; fauzan@ft.uns.ac.id

Nat. Env. & Poll. Tech.  
Website: [www.neptjournal.com](http://www.neptjournal.com)

Received: 05-02-2022

Revised: 20-03-2022

Accepted: 22-03-2022

## Key Words:

Hindu Javanese community  
Water sustainability  
Mountainous area  
Cetho temple  
Climate change

## ABSTRACT

Traditional settlements in the mountains are most vulnerable to climate change impacts. The threat of water sustainability to support the life of a traditional residential area is one of the climate change challenges that must be faced. This research aims to explore the local wisdom of the Hindu Javanese community in regulating the landscape of its settlements to maintain water sustainability now. This research methodology used a qualitative approach. This study took place in a traditional settlement of the Hindu Javanese community in the Cetho Temple area. The Cetho Temple area is one of the traces of the remnants of the Majapahit kingdom civilization on Mount Lawu, which was built in the 15th century. Data collection techniques are conducted by direct observation and interviews of several purposively selected informants in the study area. Data analysis is done by analyzing data into physical data and socio-cultural data spatial analysis. The two groups of data were analyzed to obtain a complete picture of the strategy of the Javanese Hindu community to regulate water sustainability in residential areas. The research result shows that The Hindu Javanese community built its settlements concerning local topographic and hydrological conditions in maintaining water sustainability. The Mountain – Springs – Settlement - Farm field relationship forms an environmental ecosystem that is always balanced. In addition to maintaining physical water continuity, the Javanese Hindu community has a spiritual tradition to maintain the spirit of its people to maintain water continuity. The Hindu Javanese community in the Cetho Temple area can align settlements and nature through this local wisdom. This research in the future is expected to be useful as a reference for water management in traditional settlements in the mountains and planning for structuring settlement areas in the mountains.

## INTRODUCTION

In recent decades, climate change has impacted the environment and human life. Threats from the impacts of climate change-related to food security, water availability for living needs, and socioeconomic dynamics in a settlement landscape (Aktürk & Dastgerdi 2021, Dastgerdi et al. 2020). Although two-thirds of the planet is covered in water, some parts of the Earth experience water scarcity. The World Economic Forum's Global Risk Report 2019 ranked the water crisis as one of the top global risks. The threat of this water crisis is caused by the disruption of natural ecosystem balance, minimal water infrastructure investment, and uneven water distribution (Reig Paul 2020). Water has led to conflicts in various regions of the world, such as conflicts in Iran and Iraq over the Euphrates and Tigris reservoirs, water conflicts in Africa (Yemen, Mali), water crises in Guatemala, Honduras, and El Salvador (Gleick et al. 2020).

Water is essential for the sustainability of human life and the environment. Human needs for water are not only biological needs but also social, economic, and religious aspects. In the tradition of various human cultural backgrounds, water is a sacred object. Major religious traditions such as Muslims, Christians, Hindus, Buddhists, and various other local beliefs view water as one of the elements of purification in carrying out religious rituals (Bryan 2017).

The water sustainability concept is defined as managing water resources while considering water availability for future generations. Water sustainability management can be achieved through a multidisciplinary approach to various fields, namely environmental, economic, sociocultural, and engineering (Mendes et al. 2021). Traditional settlements are known to have the ability to adapt to various natural challenges. They organize their environment according to the values of local wisdom derived from the experience of

interaction with the natural environment (Wei et al. 2021). These local wisdom values respond to adapting to natural conditions and available resources (Velázquez-Rosas et al. 2018). Water resources and geographical conditions affect the design of a settlement (Omer 2016).

Ancient civilizations have shown that traditional settlements have had local wisdom in managing water. For example, People in the mountainous region of Kathmandu-Nepal have a water management method called Hiti (Selvaraj et al. 2021). The Dai Village-Yunnan settlement has an ecological concept that combines four settlement components, namely water-forest-field-village (Wang & Chiou 2019). Floating settlement system in Vietnam (Nguyen 2022). Water conservation culture in Egypt and Greece (Ahmed et al. 2020). Drainage system integrated with trenches in settlements in Chengkan village China (Bi et al. 2021). Water tank utilization system for agriculture and settlement in Sri Lanka (Kamani Sylva & Aruna Sylva 2021). Method of capturing rainwater and filling the aquifer layer with pond management in Bengal-India (Roy 2010). Terracing land management methods to prevent erosion and store water to maintain the land's fertility rate sustainably and using the rain harvesting method in managing water in settlements (Gravagnuolo & Varotto 2021, Taji et al. 2021, Zhou et al. 2018).

However, today mountain ecosystems with high slope characteristics tend to experience more complex impacts of climate change. One of the impacts is changes in the hydrological cycle caused by changes in precipitation patterns in the Earth's atmosphere. Changes in the hydrological cycle cause changes in the balance of regional ecosystems, including agricultural productivity and the livelihoods of the region's population (Bhagawati et al. 2017). The topographic conditions of mountains with high and steep slopes have challenges in managing heavy environmental ecosystems (Tarolli & Straffelini 2020). The topographic conditions of a residential area also affect groundwater conditions (Nagamani et al. 2021).

Land-use changes in the mountains have disrupted the balance of water catchment, runoff, and decreased groundwater supply. Expanding the residential and agricultural areas causes forest areas as catchment areas to decrease (Baruah 2020, Ketjulan et al. 2019). The expansion of residential and agricultural areas poses the risk of drought in the dry season and flooding in the rainy season (Muis 2019). Land-use changes in the mountains can also disrupt groundwater flow (Fan & Xiao 2020). Research on water sustainability in traditional settlements in the mountains has a strategic role. When viewed from the distribution of the world's population, one-tenth of the world's population lives in mountainous regions (Liu et al. 2019). Learning traditional

water sustainability knowledge is beneficial for dealing with water crises in other residential areas (Dayaratne 2018, Kamani Sylva & Aruna Sylva 2021, Roy 2010).

This settlement relies on springs for the needs of life and agricultural cultivation. The settlement of the Hindu Javanese community in the Cetho Temple area is one of the traditional settlements that still survive on the western slopes of Mount Lawu, Indonesia. In 2007, Cetho Temple was designated as one of the cultural landscape heritage by the Indonesian government.

However, since it was developed into a tourist area, there has been an increase in tourist activity. Tourist activity affects the increasing water consumption in the region. Based on studies of various existing tourist areas, the impact of tourism on an area will impact increasing water consumption. Globally, there is expected to be a 92% increase in water consumption between 2010 and 2050 (Shen 2020).

That's why it's important to do this research on the water sustainability concept in Hindu Javanese community settlements which aims to uncover the community's best practices in maintaining water sustainability until now. The study is focused on the characteristics of residential space that have a relationship with the position of agricultural land and socio-cultural activities.

## MATERIALS AND METHODS

### Research Design

This research methodology uses a qualitative approach. The research was conducted on the settlement of the Hindu Javanese community. The location of this settlement is fused with the Cetho Temple complex. The settlement of the Hindu Javanese community in the Cetho Temple area is one of the traditional settlements that still survive on the western slopes of Mount Lawu. This area is included in the administrative area of Cetho Village, Karanganyar, Indonesia.

### Description of Area Study

The Hindu Javanese settlement location is at an altitude of 1413 m above sea level and is located on the western slope of Mount Lawu. The region has the characteristics of a humid tropical climate with an average rainfall of 1,817mm per year. The highest rainfall occurs in January, while the lowest rainfall is June-October. The air temperature ranges from 24 -34 C. The type of soil in Cetho Village is brown Andosol which comes from a young volcano. The soil conditions are relatively fertile. The contour condition of the soil varies with a slope of about 10-40 percent. Pine and fir trees dominate the vegetation in the forest area of Mount Lawu. Agricultural land around residential areas is cultivated for horticultural

crops such as carrots, onions, and corn. The research was conducted for one year. The duration of study for one year aims to see the phenomena that occur in the rainy and dry seasons. Fig. 1. Shows the study area map of Cetho village, Karanganyar, Indonesia.

### The Instruments

Data collection techniques are conducted by direct observation and interviews of several purposively selected informants in the study area. The observation area is a residential area located in the Cetho Temple area. The object was a landscape of settlements formed in the Cetho Temple area. Landscape settlements in the form of residential areas and agricultural cultivation areas. Interviews with several key informants obtained socio-cultural data. The selection of informants was conducted purposively, a member of the Hindu Javanese community who has the knowledge to explain phenomena related to water conservation in the village of Cetho.

### Data Analysis Techniques

Data analysis is organized into physical spatial data and socio-cultural data. The two data groups were then dialogized and interpreted to obtain a complete picture of regulating water sustainability in the settlements of Hindu Javanese communities.

## RESULTS

**History of Hindu Javanese Community Settlements in Cetho Temple Area:** According to historical records, the settlement of the Hindu Javanese community on the western slope of Mount Lawu was initiated by the construction of

a *Mandala* (education center) and hermits who deliberately resigned from the crowd to get closer to *Hyang Widhi* (God). This phenomenon is indicated by considering the selection of locations located on remote mountain slopes. During the Majapahit kingdom, many Mandalas were built on mountain slopes that were considered sacred. In 1451 AD, around the *Mandala* was built a temple by followers of the last Majapahit King (Brawijaya). This temple came to be known as the Cetho Temple. Based on information obtained from various sources, Hindu Javanese community settlements in the Cetho Temple area began to appear in 1885. Over time, the population grew to form a Hindu community known until now. Fig. 2. shows a typical village of a Hindu Javanese settlement.

**The Spatial Arrangement of Settlements to Maintain Water Sustainability:** This settlement is divided into three zones based on the type of activity: Cetho Temple zone for worship, settlement zone, and moorland zone / agricultural field. The Temple Zone position is at a higher place than the settlement zone. Following the Hindu teachings embraced by the people in Cetho village, the place of worship is sacred and must be placed in the highest position on the east. This illustration can be seen in Fig. 3.

In the beginning, *Pundisari* springs are the oldest springs source of water needs in the Cetho Temple area. *Pundisari* spring is just east of Cetho Temple. The existence of *Pundisari* springs cannot be separated from the existence of the Cetho Temple. The water component is part of the needs of religious rituals in the Temple. After the settlements around Cetho Temple appeared, *Pundisari* springs began to be used for various needs. Water is used to meet the needs of settlements and agricultural areas.



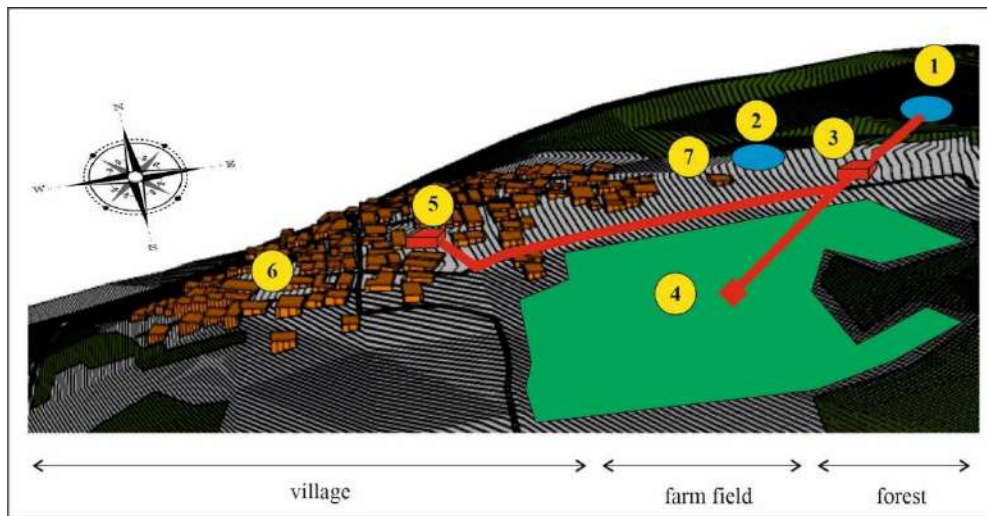
Source: Google Earth edited by author.

Fig. 1: Study area map of Cetho Village, Karanganyar, Indonesia.



Source: Author.

Fig. 2: Typical village of Hindu Javanese settlement



Source: Author

Fig. 3: The spatial layout of Cetho Village, 1 is *Sendang Macan* springs, 2 is *Pundisari* springs, 3 is water distribution station, 4 is farm field, 5 is *Kalibaku*, 6 is houses, and 7 is Cetho Temple.

In ancient times, air from *Pundisari* springs was distributed to settlements using water pipes made of bamboo stems connected one by one. Water is distributed to several water reservoirs located within the settlement. This shelter is called *Kalibaku*. To drain water from *Pundisari* springs to *Kalibaku* using the principle of gravity. The water will continue to flow downwards as long as the end of the drain is not closed. Once known as PVC water pipes (a type of water pipe that uses Polyvinyl chloride material), the community in Cetho village replaced bamboo water pipes with water pipes. The concept of water distribution using the principle of *Kalibaku* is a traditional way of Hindu Javanese communities in Cetho Temple areas to regulate water use in residential areas.

The houses of the first-generation residents in Cetho Village generally do not have bathroom facilities. *Kalibaku* becomes the center of activities to take clean water and bath-washing activities. *Kalibaku* is also used for traditional ceremonial facilities related to the life cycle (rite of passage). Such as the ceremony of bathing a baby and the ceremony of bathing the citizens who died. Along with the development of culture, bathing, cooking, and washing activities have shifted to their respective homes. However, the existence of *Kalibaku* as a water reservoir is still maintained. *Kalibaku* water is still used to take water for traditional ceremonies.

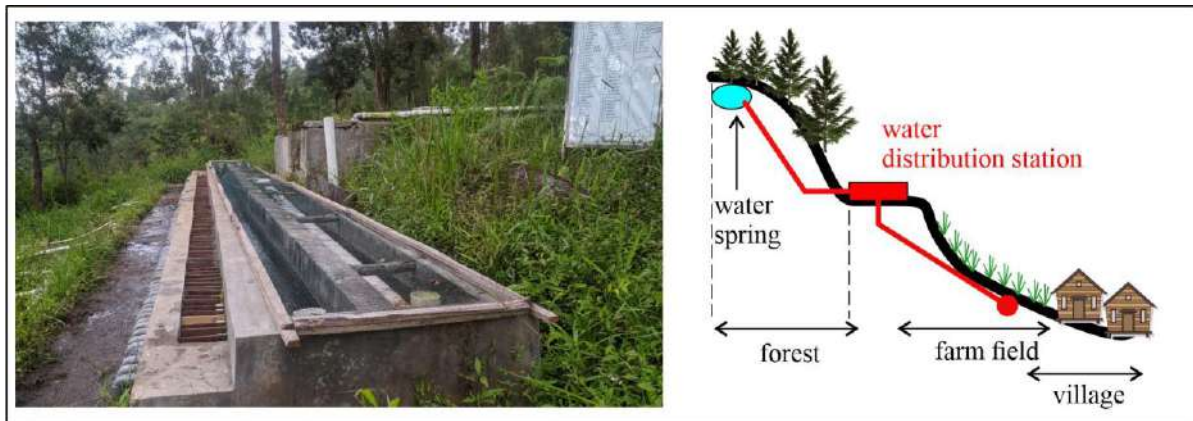
The larger population and increasing tourism activities in the temple area lead to increased water needs. The discharge

of *Pundisari* springs is not enough. Residents take a new spring from *Sendang Macan*. The location of the *Sendang Macan* springs is further away from the settlement but has a more extensive discharge. Water flows from the *Sendang Macan* springs with one main water pipe to the water distribution station. The water distribution station will divide the water into each resident's home, and farm fields use 0.5-inch PVC water pipes. Each resident has a private pipeline to the water distribution station. The number of pipes owned is arranged through a mutual consensus to distribute water evenly. The water distribution system utilizes the force of gravity, so no mechanical machine is needed to push water from the water distribution station to the residential area. This illustration of the water distribution station can be seen in Fig. 4.

**Water Retention Pond to Control Flooding and Irrigate Farm field:** The majority of Javanese Hindu community settlements are on the mountain's slopes with a slope of

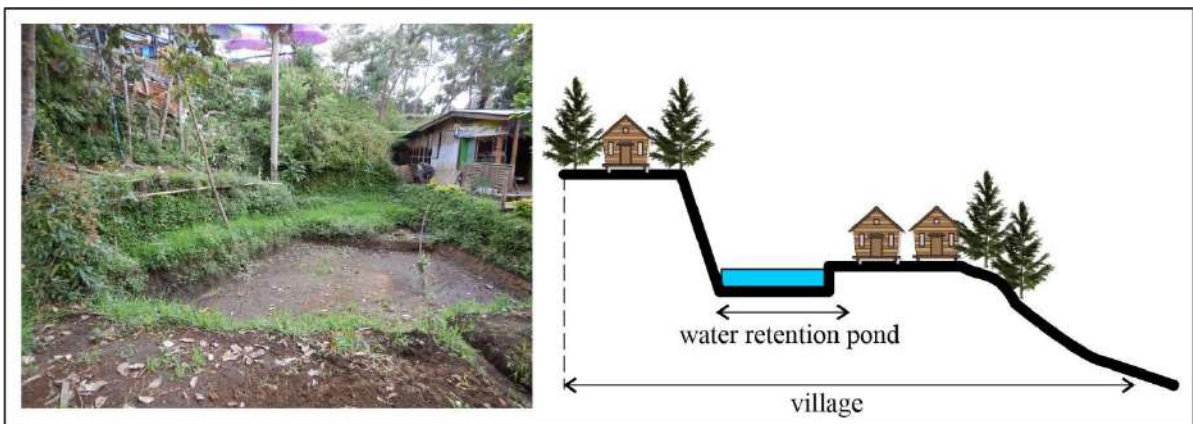
10-40%. During the rainy season, surface water will flow from the top of the mountain to the residential area. Locals regulate the pattern of rainwater flow by making water ponds around the house. This water pond has many functions, first, slowing the flow of rainwater from the top of the mountain to the settlement; second, maximizing the rainwater catchment area to support the stability of groundwater production; third can be used to irrigate agricultural land. Fig. 5. shows a water retention pond.

**Water Catcher to Support Water Supply on Farm Field:** Residents in the Cetho Temple area are very efficient in utilizing water. Rainwater and residual water use from the bathroom are used to irrigate farmland. Rainwater and residual water use from the bathroom are accommodated in a water collection place equipped with PVC water pipes. This water pipe flows to their farm field area located under the residential area. Water is flowed by utilizing the force of



Source: Author

Fig. 4: Water distribution station.



Source: Author

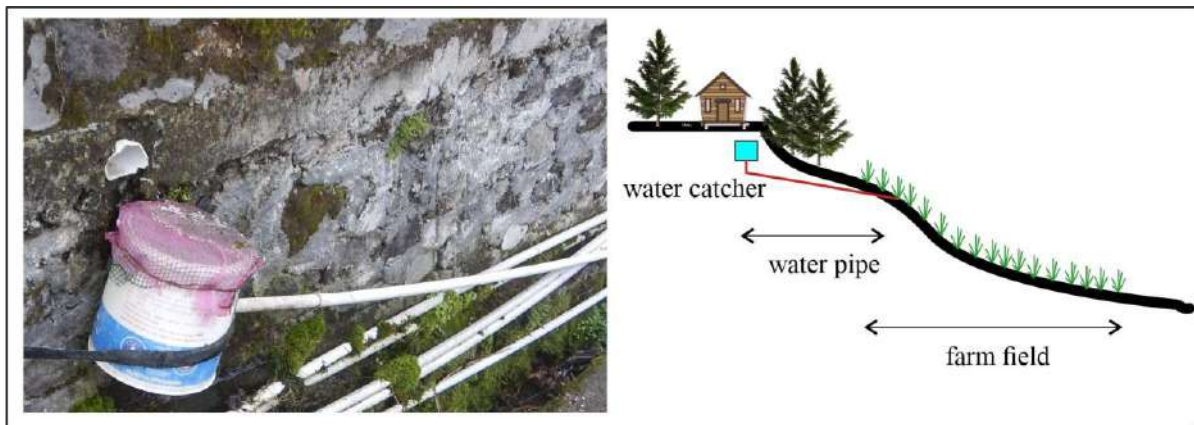
Fig. 5: Water retention pond.

gravity. Illustrations of the water catcher can be seen in Fig. 6.

**Mountain Belt to Control Water Movement and Soil Erosion:** The agricultural area around the Cetho Temple has a slope of land between 10-40 percent and relatively high rainfall. Farmers make a *sabuk gunung* (mountain belt) to control water movement when high intensity. A Mountain belt is a land engineering pattern on sloping areas by following the contours of cutting mountain slopes. This pattern visually looks like the shape of a belt or belt that circles the body of a mountain. The benefits of mountain belt systems are to slow water movement down and reduce erosion of agricultural soil surfaces. The mountain belt system will increase the water's suction power into the soil so that the water does not go down directly. This illustration of the mountain belt at the farm field can be seen in Fig. 7.

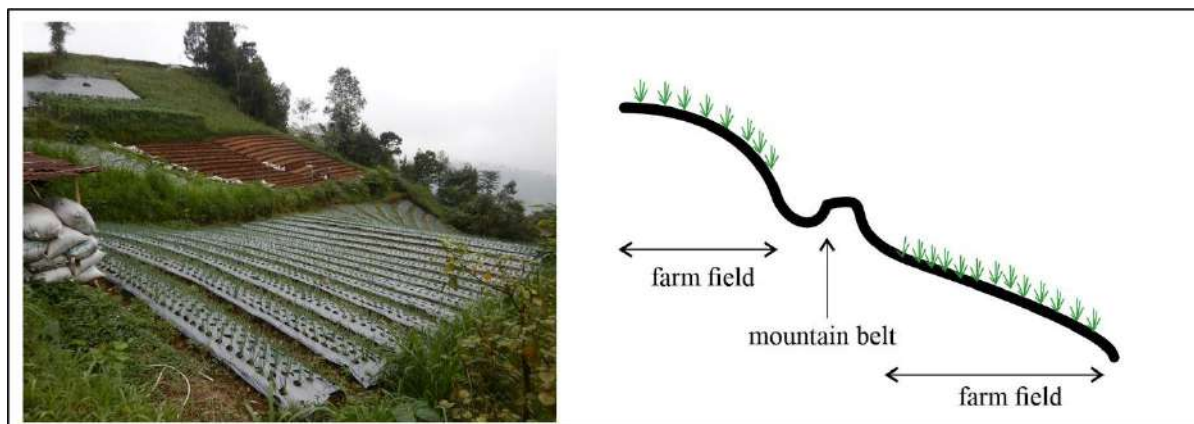
**Dawuhan Ritual Tradition as a Spirit to Maintain Water Sustainability:** The water source for the Hindu Javanese

community in the Cetho Temple area is a sacred place. In addition to being used for living needs, the water serves as a complement to worship rituals. The *Dawuhan* ritual is a form of traditional Hindu Javanese community ceremony to honor the source of the springs. The *Dawuhan* ritual is carried out for generations by the Javanese Hindu community around Cetho Temple. This ceremony is carried out regularly every Saturday *kliwon* month of *Sura* (Javanese calendar). This ceremony was attended by all residents in the Cetho Temple area. The meaning of this ceremony is an expression of gratitude to God for having been given springs that can be used for living needs such as drinking, cooking, and agricultural cultivation. Through *Dawuhan* rituals, the Hindu community in the Cetho Temple area wants to *meruwat* (rearrange the cosmological aura) of existing springs. The springs that have been performed at the ceremony will have an excellent cosmological aura, thus providing adequate



Source: Author

Fig. 6: Water catcher



Source: Author

Fig. 7: Mountain belt at farm field

water needs for all citizens. By carrying out this ceremony, it is expected that the lives of citizens will always get blessings and tranquility. Fig. 8. shows the *Dawuhan* ceremony in the Cetho Temple area.

The location of the ceremony is centered in front of the *Pundisari* spring building. Before carrying out *Dawuhan* rituals, people in Cetho village will carry out activities to clean the springs and check the distribution channels of water flowing throughout the settlement area. By the time *Dawuhan* day arrives, the series of *Dawuhan* ceremonies begin with the leadership of local stakeholders (*Mangku*). The ceremony began in the afternoon. Residents come to the location together using traditional clothes. The *Dawuhan* ceremony begins by placing offerings on the *Meru* building in the complex of *Pundisari* springs. A set of offerings in the form of *tumpeng* grilled packages (rice, roasted chicken, fruit, flowers). Then a prayer procession led by stakeholders followed by people sitting on mats with parallel configurations facing east. The ritual process lasts approximately 2.5 hours, ending with a blessing (giving holy water to all ceremony participants). Holy water is believed to be the essence of life for the well-being and salvation of humanity. The last stage of this ceremony is the *kembul bujono* (eating offerings that have been prayed together). This activity is a traditional way for the Hindu Javanese community to maintain nature passed down through generations. Rituals can remind all community members to manage water resources wisely every year.

## DISCUSSION

The Javanese Hindu community in the Cetho Temple area still maintains local wisdom in maintaining water sustainability in

their residential areas. They build their settlements regarding topographic and hydrological conditions to form a unique settlement pattern. The characteristics of mountain settlement space are closely related to agricultural land and sociocultural activities (Cillis et al. 2020, Zheng et al. 2021). There are three known mountain settlement structures; agglomeration, belt, and dispersion (Xu et al. 2021). The settlement of the Hindu Javanese community in the Cetho Temple area is a type of agglomeration settlement.

If traced further, the spatial layout of the village of Cetho is formed by the interaction of four main elements, namely the Mountain – Springs – Settlement - Farm field. This settlement is on the western slope of Mount Lawu. The top is the protected forest area. In this protected forest area, there is a *Sendang Macan* spring that becomes a source of water for the living needs and agricultural activities of the Hindu Javanese community in the village of Cetho. The Mountain-Spring-Settlement-Farm field is an inseparable ecosystem. Settlements and farm fields cannot live if there are no springs. Meanwhile, the springs will be lost if the surrounding residents cannot care for the forest. To care for this ecosystem, the Javanese Hindu community in the Cetho temple area strives to maintain the balance of nature both physically and spiritually. Arranging settlement landscaping, making water retention ponds, water use efficiency, and mountain belts are the embodiment of physically caring for the ecosystem. At the same time, the *Dawuhan* ritual ceremony is an embodiment to care for the ecosystem spiritually. This action cannot be separated from the background of Hindu teachings embraced by the community in the Cetho Temple area. Hindu teachings have always taught man always to maintain a balance of relations with God, relationships with fellow human beings, and relationships with nature.



Source: Solotrtrust documentation (Solotrtrust 2022)

Fig. 8: Illustration of the *Dawuhan* ceremony in the Cetho Temple area.

## CONCLUSION

In maintaining water sustainability, the Javanese Hindu community built a local mechanism that regulates the cycle for the needs of life and the process of agricultural land production. The relationship between the Mountains-Springs-Settlements-Farm field relationship forms an organic environmental ecosystem that is always balanced. In addition to maintaining physical water continuity, the Javanese Hindu community has a spiritual tradition of *Dawuhan* to maintain the spirit of its people in maintaining water sustainability. This understanding is in line with the Hindu teachings embraced by this community. In carrying out life must always maintain the relationship between Man-God, Man-Man, and Man-Nature to create a harmonious life. This research shows that traditional settlement arrangements built with local values can maintain water sustainability. This knowledge can be an additional reference in building a sustainable development theory in traditional settlements in mountainous areas.

## ACKNOWLEDGMENT

The author thanked the Research Institutions and Community Service of Sebelas Maret University for its research funding assistance. The authors also thank the Doctoral Program of Architecture and Urban Science at Diponegoro University for its research and education facilities.

## REFERENCES

- Ahmed, A.T., Gohary, F., Tzanakakis, V.A. and Angelakis, A.N. 2020. Egyptian and greek water cultures and hydro-technologies in ancient times. *Sustainability (Switzerland)*, 12(22): 1-26. <https://doi.org/10.3390/su12229760>
- Aktürk, G. and Dastgerdi, A.S. 2021. Cultural Landscapes under the threat of climate change: A systematic study of barriers to resilience. *Sustainability*, 13(17): 9974. <https://doi.org/10.3390/su13179974>
- Baruah, P. 2020. Potential of urban wetlands for ecotourism development: A case of deepor beel, Guwahati. *Nat. Environ. Pollut. Technol.*, 19(2): 611-625. <https://doi.org/10.46488/NEPT.2020.V19I02.016>
- Bhagawati, R., Bhagawati, K., Jini, D., Alone, R.A., Singh, R., Chandra, A., Makdoh, B., Sen, A. and Shukla, K. K. 2017. Review on climate change and its impact on agriculture of Arunachal Pradesh in the Northeastern Himalayan region of India. *Nat. Environ. Pollut. Technol.*, 16(2): 535-539. [www.neptjournal.com](http://www.neptjournal.com)
- Bi, Z., Chen, C., Li, Y. and Cheng, P. 2021. Analysis of the human settlement environment of Huizhou ancient villages based on the heritage of ancient roads: A case study of Chengkan Village. *E3S Web of Conf.*, 237: 4025. <https://doi.org/10.1051/e3sconf/202123704025>
- Bryan, M. 2017. Valuing sacred tribal waters within the prior appropriation. *Nat. Resour. J.*, 57(1): 139-181. <https://digitalrepository.unm.edu/nrj/vol57/iss1/6%0AThis>
- Cillis, G., Statuto, D. and Picuno, P. 2020. Vernacular farm buildings and rural landscape: A geospatial approach for their integrated management. *Sustainability (Switzerland)*, 12(1): 1004 <https://doi.org/10.3390/su12010004>
- Dastgerdi, A.S., Sargolini, M., Allred, S.B., Chatrchyan, A. and Luca, G.D. 2020. Climate change and sustaining heritage resources: A framework for boosting cultural and natural heritage conservation in central Italy. *Climate*, 8(2): 26. <https://doi.org/10.3390/cli8020026>
- Dayaratne, R. 2018. Toward sustainable development: Lessons from vernacular settlements of Sri Lanka. *Front. Arch. Res.*, 7(3): 334-346. <https://doi.org/10.1016/j.foar.2018.04.002>
- Fan, M. and Xiao, Y. 2020. Impacts of the grain for Green Program on the spatial pattern of land uses and ecosystem services in mountainous settlements in southwest China. *Glob. Ecology Conserv.*, 21(59): e00806. <https://doi.org/10.1016/j.gecco.2019.e00806>
- Gleick, P., Iceland, C. and Trivedi, A. 2020. Ending conflicts over water: Solutions to water and security challenges. *World Resour.*, 81: 19001 Institute. <https://doi.org/10.46830/wriprt.19.00081>
- Gravagnuolo, A. and Varotto, M. 2021. Terraced landscapes regeneration in the perspective of the circular economy. *Sustainability (Switzerland)*, 13(8): 1-20. <https://doi.org/10.3390/su13084347>
- Kamani Sylva, K.K. and Aruna Sylva, K.K.L. 2021. Sustainable City Planning and Management Strategies in Vernacular Settlement Patterns in Sri Lanka: Sustainability in the Built Environment in the 21st Century -Lessons Learned from India and the Region, *Environmental Science and Engineering*. Springer International Publishing, Cham. [https://doi.org/10.1007/978-3-030-61891-9\\_9](https://doi.org/10.1007/978-3-030-61891-9_9)
- Ketjulan, R., Imran, Z., Boer, M. and Siregar, V. P. 2019. Estimation of water carrying capacity for settlement activities in small Islands: A case study of small Islands of north Tiworo district, Muna sub-district, Indonesia. *Nat. Environ. Pollut. Technol.*, 18(2): 435-443. [www.neptjournal.com](http://www.neptjournal.com)
- Liu, Y., Fan, P., Yue, W., Huang, J., Li, D. and Tian, Z. 2019. Assessing polycentric urban development in mountainous cities: The case of Chongqing metropolitan area, China. *Sustainability (Switzerland)*, 11(10): 790. <https://doi.org/10.3390/su11102790>
- Mendes, J.P., Ferreira, D.H.L. and Sugahara, C.R. 2021. Periurban Settlements: A Discussion on Water Sustainability Indicators: Smart Innovation, Systems, and Technologies. Volume. 233. Springer International Publishing, NY. [https://doi.org/10.1007/978-3-030-75680-2\\_12](https://doi.org/10.1007/978-3-030-75680-2_12)
- Muis, B.A. 2019. Impact of land use change on the hydrological response of Krueang Aceh watershed in Aceh Province, Indonesia. *Nat. Environ. Pollut. Technol.*, 18(4): 1275-1281. [www.neptjournal.com](http://www.neptjournal.com)
- Nagamani, K., Batvari, P.D., Packialakshmi, S. and Reddy, C.S.K. 2021. Groundwater recharge planning using field survey for Talupula Mandal in Anantapur District, Andhra Pradesh, India. *Nat. Environ. Pollut. Technol.*, 20(5): 1981-1987. <https://doi.org/https://doi.org/10.46488/NEPT.2021.v20i05.014>
- Nguyen, T.T.T. 2022. Architectural design guideline for sustainable floating houses and floating settlements in Vietnam: Lecture Notes in Civil Engineering. Volume 158. Springer, Singapore. [https://doi.org/10.1007/978-981-16-2256-4\\_28](https://doi.org/10.1007/978-981-16-2256-4_28)
- Omer, A. 2016. The correlation of water with settlement and transportation network: A case study of Turkey. *J. Environ. Eng. Landsc. Manag.*, 24(3): 200-209. <https://doi.org/http://dx.doi.org/10.3846/16486897.2016.1179198>
- Reig Paul, S.C. 2020. Achieving Abundance : Understanding the Cost of a Sustainable Water Future. Working Paper (Issue January). [www.wri.org/publication/achieving-abundance](http://www.wri.org/publication/achieving-abundance)
- Roy, M. 2010. Managing the village-level open-access water resources in a region facing rapidly declining water availability. *Environ. Develop. Sustain.*, 12(6): 999-1012. <https://doi.org/10.1007/s10668-010-9237-9>
- Selvaraj, T., Yadav, A., Bahuguna, H., Drewnowski, J. and Ganesapillai, M. 2021. Ancient settlements-atavistic solutions for present water supply and drainage problems engendered by urbanism. *Environ. Develop. Sustain.*, 23(5): 8076-8088. <https://doi.org/10.1007/s10668-020-00954-0>
- Shen, Y.F. 2020. Measurement of tourism industry-ecological environment coupling degree and management and control measures for tourism environment: A case study of Henan Province, China. *Nat. Environ. Pollut. Technol.*, 19(2): 857-864. <https://doi.org/10.46488/NEPT.2020.V19I02.045>



- Solotruster. 2022. Month of Suro, Hundreds of Hindus in Ceto Hamlet Perform Dawuhan Traditional Ceremony. <https://solotruster.com/read/21790/Bulan-Suro-Ratusan-Umat-Hindu-Dusun-Ceto-Lakukan-Upacara-Adat-Dawuhan>
- Taji, S.G., Saraf, V.R. and Regulwar, D.G. 2021. Smart Rain Water Harvesting for Smart Cities: Studies In Systems, Decision, and Control. Volume 308). Springer International Publishing, Singapore. [https://doi.org/10.1007/978-3-030-53149-2\\_5](https://doi.org/10.1007/978-3-030-53149-2_5)
- Tarolli, P. and Straffelini, E. 2020. Agriculture in hilly and mountainous landscapes: Threats, monitoring and sustainable management. *Geogr. Sustain.*, 1(1): 70-76. <https://doi.org/10.1016/j.geosus.2020.03.003>
- Velázquez-Rosas, N., Silva-Rivera, E., Ruiz-Guerra, B., Armenta-Montero, S. and González, J.T. 2018. Traditional ecological knowledge as a tool for biocultural landscape restoration in northern Veracruz, Mexico: A case study in El Tajín region. *Ecol. Soc.*, 23(3): 306. <https://doi.org/10.5751/ES-10294-230306>
- Wang, H.F. and Chiou, S.C. 2019. Study on the sustainable development of human settlement space environment in traditional villages. *Sustainability (Switzerland)*, 11(15): 1-22. <https://doi.org/10.3390/su11154186>
- Wei, D., Wang, Z. and Zhang, B. 2021. Traditional village landscape integration based on social network analysis: A case study of the Yuan River Basin in South-Western China. *Sustainability*, 13(23): 13319. <https://doi.org/10.3390/su132313319>
- Xu, J., Yang, M., Lu, Z., Liu, D. and Wu, Y. 2021. Quality analysis on spatial planning pattern of rural area in southern Shaanxi, China. *Sustainability (Switzerland)*, 13(22): 668. <https://doi.org/10.3390/su132212668>
- Zheng, X., Wu, J. and Deng, H. 2021. Spatial distribution and land use of traditional villages in southwest China. *Sustainability (Switzerland)*, 13(11): 326. <https://doi.org/10.3390/su13116326>
- Zhou, Z., Jia, Z., Wang, N. and Fang, M. 2018. Sustainable mountain village construction adapted to livelihood, topography, and hydrology: A case of Dong villages in Southeast Guizhou, China. *Sustainability (Switzerland)*, 10(12): 619. <https://doi.org/10.3390/su10124619>





# Coated Controlled-Release Fertilizers: Potential Solution for Sustainable Agriculture

P. Negi\*†, R. Thakur\*, K. Manral\*, K. Tomar\*, B. S. Rawat\*, B. Ramola\* and Waseem Ahmad\*

\*School of Applied & Life Sciences (SALS), Uttarakhand University, Dehradun, Uttarakhand, 248007, India

†Corresponding author: Poonam Negi; hodchemistry@uttarakhanduniversity.ac.in

Nat. Env. & Poll. Tech.  
Website: [www.neptjournal.com](http://www.neptjournal.com)

Received: 12-12-2021

Revised: 10-02-2022

Accepted: 22-02-2022

### Key Words:

Controlled release fertilizer  
Sustainable agriculture  
Coatings

## ABSTRACT

The use of fertilizer in the agricultural field is essential for plant growth but an excess amount of pure chemical contents in fertilizers becomes harmful to every living being. To reduce this chemical exposure, the use of materials coated with Controlled Release Fertilizers (CRFs) are being used. The coating of materials outside the fertilizer does not allow the chemicals to spread completely within one application of fertilizer but its spread can be extended as will be done in 2-3 applications of fertilizer. The features of the undercoating material are thus vital to attain this delayed or slow release of the nutrients present in the fertilizer. The longevity of CRFs depends upon the width of the material coating surrounding the fertilizer, temperature, and moisture. The review focuses on the consequences of conventional fertilizers, the need to control the release of fertilizers and types of coatings used, and their application in sustainable agriculture.

## INTRODUCTION

The steady increase in population growth and food demand and the continuous reduction in cultivated land per capita induce steady intensification of fertilizer application worldwide (Shaviv 2001). For the cultivation of a healthy plant, it is necessary to provide nutrients and water from time to time. For this, fertilizers are being used in almost every part of the world. The nutrients in fertilizer act as plant building blocks, allowing the crop to grow to its full potential while remaining healthy and disease-free. Fertilizers are significant for the harvest development, yield, maintenance quality parameters, and the well-being of the soil when applied in ideal suggested doses or judiciously. Fertilizers improve the supplement status and nature of soil by enhancing it with supplements that it needs. Crop plants require nitrogen, phosphorous, and potassium to maintain the typical physiological capacity of the cell (Lawrencina et al. 2021). The absence of nitrogen brings about poor development, yet the abundant utilization of nitrogen brings about delayed maturity and low quality of the leaf. Concentrated Fertilizer application causes genuine ecological issues, like eutrophication of waters, loss of biodiversity, unnatural weather change, stratospheric ozone exhaustion, reduction in soil fertility, and destruction of microorganisms and friendly insects. Certain fertilizers additionally contain substantial metals, overabundance utilization of which drives fertilizers to enter the natural way of life by means of retention from the soil. Consequently, fertilization

prompts water, soil, and air contamination (Paraskar et al. 2010, Ravisankar & Poongothai 2007)

The excessive use of synthetic fertilizers has adversely affected the ecosystem (Patil et al. 2007, Nandini et al. 2009). Although the plant extracts nutrients from the soil, low nutrient content in the soil affects plant growth and thus leads to low cultivation. Every plant requires a specific amount of nutrients, and the remainder is wasted and released directly into the environment (Pandey 2018). A plant uses only 30-40% of the fertilizer sprayed on it and the rest of the fertilizer (60-70%) gets exposed to the environment in the form of the following factors:

**Nitrogen leaching:** In most cultivated land, under the ordinary, aerated environment, nitrate is the major form of 'N' used by plants. Nitrogen is oxidized to nitrate by various microbial activities taking place in the soil. As an outcome, comparatively high doses of the applied Nitrogen may leach from the root of the plant into the surface and groundwater. Increased concentration of nitrate is related to methemoglobinemia in infants, gastric cancer, and other diseases such as goiter, birth defects, and heart disease (Barker & Sawyer 2005).

**Volatilization of ammonia:** Surface-applied ammonium and urea fertilizers are a probable cause of ammonia volatilization, predominantly causing calcareous and alkaline soils due to which soil is unable to sustain the growth of crops. The  $\text{NH}_3$  released may be oxidized and transformed into nitric acid ( $\text{HNO}_3$ ), which, in coupling with sulfuric acid ( $\text{H}_2\text{SO}_4$ )

(from industrial activities), forms acid rain. Thus, causes severe damage to the vegetation and eco-system respectively (Scheppers & Fox 1986).

**Eutrophication:** The excessive amount of nutrients gets washed off into water streams like ponds and rivers nearby. This causes eutrophication due to which the water body is overly enriched with minerals and nutrients which persuade extreme growth of algae. This results in depletion of dissolved oxygen in the water body and forms algal bloom and a great rise of phytoplankton in the water body thereby affecting the aquatic life harshly (Shaviv & Mikkelson 1993).

This exposure of remaining fertilizer directly into the environment causes hazardous effects leading to global warming as the chemical components in the fertilizer mix with other greenhouse gases present in the environment (Karibasappa et al. 2009).

## CONTROL-RELEASE FERTILIZERS

Despite upgrades in the acts of supplement application, the utilization efficiency (UE) of fundamental components, for example, N and P are not satisfactory, bringing about an expansion of ecological issues. The utilization of controlled-release fertilizers (CRFs) has a promising future in contributing in an amazing way to improving the management of supplement application thereby diminishing altogether natural dangers while keeping up high harvest yields of good quality. Controlled-release fertilizers are normally coated with organic or inorganic materials which control the rate, pattern, and release of plant nutrients into the soil. Polymer-covered urea best represents CRFs (Du et al. 2006, Loper & Shober 2012). The release of nutrients in these fertilizers is due to semi-permeable coating or other chemical means by hydrolysis of water-soluble compounds (Trenkel 2010).

### Need for Controlled-Release Fertilizer

Nutrient fertilization plays a vital character in upholding soil lushness and refining crop yield and quality. Specific nutrient organization of crops is a foremost challenge worldwide as it relies primarily on chemical fertilizers (Zulfiqar et al. 2019). To overcome the ill effects of common fertilizer a new technology aroused known as controlled release fertilizer. The Nano-science provided a new method to develop a new coated fertilizer that was less hazardous compared to the common fertilizer. Nanotechnology deals with nanomaterials (NMs) which have at least one dimension ranging from 1 to 100 nm (He et al. 2018). The nano-particles of the fertilizer are made in the combination with coatings of organic/inorganic elements. Nano-science is solitary of the utmost significant study and expansion frontlines in

the present science. The usage of Nanoparticles has several benefits because of their exclusive structure and corporal properties. Due to their minor mass, nanoparticles display unique chemical, physical and electrical properties that are diverse from those of majority resources, and could be used to make innovative and better compounds. So, nanoparticles have emerged as the most promising class of modified particles being highly attractive because of their biodegradable and hydrophilic nature which is being exploited in a lot of applications (Hasaneen et al. 2014).

Also, the conventionally coated granules of fertilizers contain a small amount of active material coated with a polymer or other substances due to which the amount of total needful nutrient or active content which comes in contact with the soil and thereby to plant gets reduced significantly. The aforesaid limitation led to the formulation of nanoparticles which offer a large area of active component to be in contact with the plant and hence help in better and controlled release characters of the nutrients (Pereira et al. 2015). Nano fertilizers are nanomaterials that are both nutrients themselves (micro-nutrients or macro-nutrients) or otherwise act as transferors for the nutrients. Nano-fertilizers could equally be advanced by coating nutrients into the nanomaterials. They recover entire crop production and superiority with developed nutrient use efficiency (NUE) however dropping the rate of fabrication and therefore, subsidizing agrarian sustainability (Usman et al. 2020).

The nano-fertilizers are categorized into four clusters: macronutrient nano fertilizers, micronutrient nano fertilizers, nano material-enhanced fertilizers plant growth-stimulating nanomaterials (Marchiol et al. 2020).

All the CRFs must contain three norms: A smaller quantity i.e. lesser than 15% of the nutrients must be out in 24 hrs, Less than 75% ought to be free in one month (28 days), Minimum of 75% has to be free by the specified release interval (42–358 days) (Wei et al. 2020).

CRFs grab more attention than traditional fertilizers because the frequent discharge of Nitrogen from CRFs certifies adequate nutrient supply for plant uptake during the growing season of crops and prevents all the problems being caused to the environment (Wei et al. 2018). CRFs are entirely used for refining soil productivity. Yet, the stability of micronutrients such as Fe, Zn, Cu, and Mn in the soil is also very essential (Li et al. 2017). In total approx. 16 nutrients are very necessary for the plants out of which 13 are frequently taken up by the soil. Nitrogen (N), phosphorus (P), and potassium (K) are categorized as primary nutrients as they are mandatory in larger quantities (Tripathi et al. 2020). K, Ca, and Mg in soil emerge from the disintegration of bedrock and minerals that hold these elements (Cole et al.

2016). Nano fertilizers have facilitated the establishment of these essential nutrients in the soil based on the slow release. This steady release encourages the improved distribution of nutrients to the plants which promotes early germination and high nutritional content (Lateef et al. 2016). CRFs have been mostly considered under altered temperature and soil moisture systems (Nardi et al. 2018).

## FERTILIZER WITH EXTERNAL COATINGS

Currently, diverse polymeric and non-polymeric resources have been verified for controlled-release fertilizer coatings (Naz & Sulaiman 2016). In general, the preparation of CRFs, needs a support material, such as natural polymers chitosan, cellulose, alginate, starch, synthetic polymers polydopamine-graft-PAA, polydopamine-co-N, N-dimethyl amino ethyl polymethacrylate, etc. (Qi et al. 2020). To enhance the CRFs, coatings are being developed as outer covering on the fertilizer. The diffusion of nutrients happens at a considerably gentler rate than the normal fertilizer. This is for the reason that the layer becomes the physical fence which inhibits the transportation of nutrients present inside the coating. It was also found that the CRFs, containing functional groups like hydroxyl, phosphate, or amino groups contain the empathy for metal cations consisting of microelements which result in the formation of metal complexes. This creates the tie of micronutrient cations to bio-based constituents by biosorption. Such types of fertilizers would result in greater bioavailability and reduced nutrient discharge to the soil. The usage of normal constituents as fertilizer coverings causes lesser ecological contamination and killing energy, therefore, the obtained products are even called environment-friendly fertilizers.

Biodegradability is an essential characteristic when bearing in mind the various environmental concerns, and is a perilous asset for the application of fertilizer coating (Cui et al. 2020).

## Types of Coating

Controlled release fertilizers are mainly prepared by the coatings including the least solvable elements like Sulphur, polymers, or grouping of both (Products which consist the mixture of sulfur-coating as well as polymer-coating to occur. Usually, such products comprise urea, covered using a layer of sulfur, which is in turn coated with a layer of polymer. Respectively, every coating layer is normally fewer than the standard thickness for the discrete procedures.) These coatings release the urea when they come in contact with water or moisture. Of all materials, natural polymers and their derivatives have fascinated more consideration due to the benefits of low cost, non-toxicity, easy accessibility, biodegradability, and modifiability (Qi et al. 2020).

Controlled release fertilizers are mainly prepared by the coatings including the least solvable elements like Sulphur, polymers, or grouping of both Products which consists of the mixture of sulfur-coating as well as polymer-coating too occur. Usually, such products comprise urea, covered using a layer of sulfur, which is in turn coated with a layer of polymer. Every coating layer is normally lesser than the standard thickness for the discrete procedures. These coatings release the urea when they come in contact with water or moisture. Of all materials, natural polymers and their derivatives have attracted more consideration due to the benefits of low-cost, non-toxicity, easy accessibility, biodegradability, and modifiability (Qi et al. 2020).

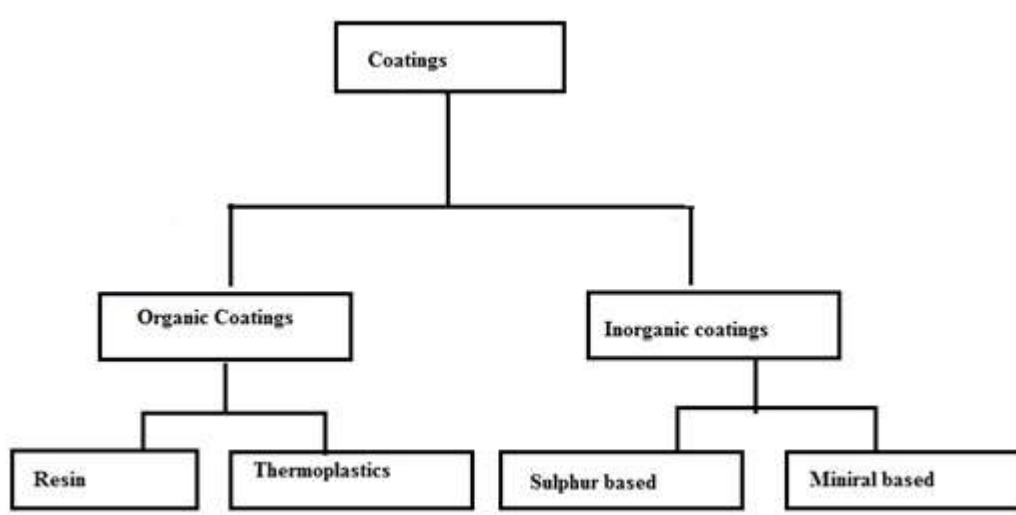


Fig.1: Types of coating.

## Organic Coatings

The naturally occurring coated materials are being specified as organic coatings. It includes **Chitosan**: Naturally ample, nontoxic and biodegradable, and biocompatible, minus immunogenic, much extremely less toxicity level, and insoluble in water with high swelling capacity (Pandey et al. 2019).

**Starch**: Easily altered material, low-cost, non-toxic, and biodegradable.

**Cellulose**: Renewable, degradable, and film-establishing ability.

**Agricultural residues**: Copiously available, economically effective, biodegradable, and renewable.

**Lignin**: cost-effective, freely available from plant sources and its derivatives (Chen et al. 2018).

**Thermoplastics**: (Polymer Coated urea (PCU) is established as a substitute for SCU to recover the restrictions of sulfur-coated urea. The sollicitation of a polymer-film coated fertilizer can raise the nutrient utilization efficiency (NUE) and diminish various environmental contaminations, and polymer latex is an environmentally responsive coating material with an encouraging future (An et al. 2017). Certain biodegradable polymers are being used as the coating material for normal fertilizer but super absorbent polymers are the theme of major emphasis due to their outstanding water absorption & retaining capabilities as CRFs in agronomy applications (Ni et al. 2011). These super absorbent polymers are frequently applied in the form of gel beads, which have low mechanical strength for fighting exterior forces (Zhou et al. 2018).

All coated materials have been established using numerous polymers from non-environmentally degradable polymers (like polyolefin, polyurethane (PU), polysulfonate, etc.) to degradable polymers (like polysaccharides, aliphatic polyesters, etc.) (Mikula et al. 2019). Although the non-degradable polymers are currently in more experimental cases, considerable attention is being shifted to the degradable polymers, to evade tainting of the environment caused by the gathering of coated materials (Ye et al. 2019).

**Polyurethane**: PU is normally applied as a covering material for the manufacture of film-coated fertilizers. PU generally has a great asset due to the tough polar force and hydrogen bond among the urethane bonds (Dai et al. 2020). PU coated fertilizers are economical, decomposable & environment friendly which makes them a high potential coated fertilizer (Liu et al. 2018).

**Polyacrylate**: A study was carried out to investigate the interface between PA coating on CRFs and soil in wheat-rice rotation fields Liang et al. 2019. Although the use of PA as

a coating on CRF is widely used the effects of PA coating on the soil becomes a serious concern. But according to this study, scientists confirmed that the PA coatings were decomposable and eco-friendly in the field of wheat & rice when used as CRFs. This study involves the formation of PA by polymerization of MMA (monomer). They concluded that the erosion of coating happened in both wheat & rice land. This changes the surface appearance & micro-morphologies because the soil and microbes might abide by the surface of PA coating (Liang et al. 2019).

## Inorganic Coatings

The coated substances that do not occur naturally and are synthesized artificially are considered inorganic coatings.

**Sulfur-based inorganic coating**: One of the firstly invented Controlled Release Fertilizers was prepared by coating Sulphur on it. The sulfur coating is one of the historical coating materials as it's economical and is a substrate for all the soil microbes which are chemoautotrophs and uses sulfur in generating sulphuric acid which dissolves insoluble phosphate existing in the soil. (Cui et al. 2020). sulfur coatings on CRFs are subtle to topsoil assets, and the nutrient discharge from SCU is extremely flexible. Because of all such aspects, the usage of sulfur in coating for SRFs had reduced courtesy of polymeric coatings (Irfan et al. 2018).

**Mineral-based inorganic coating**: These are the naturally occurring inorganic solids like Zeolite which consist of a crystalline structure and a definite chemical composition. Zeolite is used widely as coated mineral CRF because it is cost-effective and its inherent cation exchange property treats efficiently the control of the release rate of nutrients. zeolite-based CRF proves to be the best in strength and structural stability. As compared to other coated CRFs, zeolite CRF with an acyclic polymer binder can control the release of nitrogen by 54% (Dubey & Mailapalli 2019).

## FACTORS AFFECTING CRFS

The important factors which affect the release of CRF include temperature pH and size coating thickness. The availability of nutrients in the soil influences the release mechanism of nutrients from CRF. The shape of fertilizer is another important factor on which the release rate of CRF depends. Only granulated fertilizers are used for the coating process to produce controlled-release fertilizers. As it is difficult to coat the irregular granules uniformly and which can affect their releasing efficiency (Salman & Handslow 2006). The release rate of CRF also depends on the properties of the soil. pH, moisture content, temperature soil composition, and microbial activity. (Fan & Li 2010) An increase in tem-

perature increases the rate of release of nutrients from CRF as the temperature has increased the solubility of nutrients in the soil increases (Du et al. 2006).

The pH of the medium has a significant effect on the release of nutrients of CRFs. pH in the acidic range (2-5) decreases the swelling capacity and thus reduces the rate of release, while pH in the alkaline range (>pH 9) increases the swelling capacity (Salimi et al. 2020).

## ADVANTAGES OF CONTROL RELEASE FERTILIZERS

- **Excellent plant development:** CRFs provide the plant with balanced nutrient value according to its needs throughout the entire growing season of that particular plant. This ensures the optimal development and highest quality yields (Franca et al. 2019).
- **The number of applications of fertilizer reduced:** A slow release of nutrients is observed in CRFs, so the nutrient release is according to a rate that matches plant uptake. This minimizes the no. of fertilizer application required in growth season (Keeney & Follett 1991).
- **Environment friendly:** Any product being used in agriculture should firstly be eco-friendly so that nature does not suffer from it. The coatings being applied on CRFs are biodegradable and thus, it is environment friendly since it doesn't cause any harm to the surrounding environment.
- CRFs empower standard dosing of supplements in a non-stop way, which suggests that there's no need to fertilize many times. The issue of misfortunes of supplements and root loss caused by increased concentration of salts is reduced (Franca et al. 2019).
- Unlike conventional fertilizers in CRF fertilizers, a solitary application is adequate and the components are discharged all through the developing season (Lubkowski 2016).
- The application of sulfur-coated urea decreases the soil pH which is considered to be useful for the bioavailability of nutrients (Liu & Hanlon 2012).
- **Saves labor and time:** Approx. a single application of CRF is enough for covering the crop's nutritional requirement throughout its growing season. This in turn saves labor, and time and is highly cost-effective.

## LIMITATIONS OF CONTROLLED-RELEASE FERTILIZERS

Despite several advantages of controlled-release fertilizers over conventional fertilizers, CRF has not always been con-

sidered to be the best fertilizers. The use of sulfur-coated urea in high concentrations can increase soil acidity. While there are problems associated with the degradation of polymer coated control release fertilizers which can lead to another environmental problem. Another problem associated with CRF is the continuous release of nutrients even in the absence of crops in the field as a result of the tailing effect (Shaviv 2001).

The lack of a standardized procedure to determine the release rate of nutrients in a promising way is one of the major limitations of CRFs. Furthermore, the Manufacturing cost of control-release fertilizers is much higher in comparison with conventional fertilizers (Trenkel 2010).

## CONCLUSION

Fertilizers, whether inorganic or organic foundations, will be endlessly used to proliferate and withstand the overall crop production to fulfill the ever-increasing demand of the rising population worldwide. So, owing to the very high demand for fertilizer, environmental health has been one of the most important issues because the Ineffective use of fertilizer has caused severe environmental hitches and unsustainable growth of agricultural science. The use of Nano-fertilizers with coating with biodegradable elements is worth using. It protects nature from various traditional fertilizer issues like leaching, and denitrification, and is even labor/time saving enhances productivity, and provides resistance to abiotic stresses.

Various research is being carried out to notice the future aspects of CRFs. Several technologies for rising CRFs are progressing, transitioning from sulfur-coating to polymer-coating technologies. Through the advancement in nanotechnology, upcoming CRFs may need to assimilate these technologies for enhancing controlled-release features. Also, scientists are developing new techniques by using natural coating material to come up with different types of coated CRFs that are harmless to the environment. The new coated CRFs match up with the plant nutrient uptake in the entire season of plant cultivation within the single application of fertilizer. This instead makes the CRFs cost-effective and environment friendly.

Certain measures can be taken to draw attention to the use of CRFs like a better evaluation of estimated benefits, achievement of improved technologies to produce more competent and cost-effective CRFs, etc. New studies on CRFs would take agricultural science to a new better level.

## REFERENCES

- An, D., Liu, B., Yang, L., Wang, T.J. and Kan, C. 2017. Fabrication of graphene oxide/polymer latex composite film coated on  $\text{KNO}_3$  fertilizer to extend its release duration. *Chem. Engg. J.*, 311: 318-325.

- Barker, D.W. and Sawyer, J.E. 2005. Nitrogen application to soybean at early reproductive development. *Agronomy J.*, 97(2): 615-619.
- Chen, J., Lü, S., Zhang, Z., Zhao, X., Li, X., Ning, P. and Liu, M. 2018. Environmentally friendly fertilizers: A review of materials used and their effects on the environment. *Sci. Total Environ.*, 613-614: 829-839.
- Cole, J.C., Smith, M.W., Penn., C.J., Cheary, B.S. and Conaghan, K.J. 2016. Nitrogen, phosphorus, calcium, and magnesium applied individually or as a slow release or controlled release fertilizer increase growth and yield and affect macronutrient and micronutrient concentration and content of field-grown tomato plants. *Sci. Horti.*, 211: 420-430.
- Cui, Y., Xiang, Y., Xu, Y., Wei, J., Zhang, Z., Li, L. and Li, J. 2020. Poly-acrylic acid grafted natural rubber for multi-coated slow-release compound fertilizer: preparation, properties, and slow-release characteristics. *Int. J. Biol. Macromol.*, 146: 540-548.
- Dai, C., Yang, L., Xie, J. and Wang, T.J. 2020. Nutrient diffusion control of fertilizer granules coated with a gradient hydrophobic film. *Coll. Surf. A Physiochem. Eng. Asp.*, 588: 124361.
- Du, C., Zhou, J. and Shaviv, A. 2006. Release characteristics of nutrients from polymer-coated compound controlled release fertilizers. *J. Polym. Environ.*, 14 (3): 223-230.
- Dubey, A. and Mailapalli, D.R. 2019. Zeolite coated urea fertilizer using different binders: fabrication, material properties, and nitrogen release studies. *Environ. Technol. Innov.*, 16: 100452.
- Franca, R.D.G., Pinheiro, H.M., Loosdrecht, M.C.M.V. and Lourenço, N.D. 2019. Stability of aerobic granules during long-term bioreactor operation. *Biotechnol. Adv.*, 36: 228-246.
- Hasaneen, M.N.A., Abdel-Aziz, H.M.M., El-Bialy, D.M.A. and Omer, A.M. 2014. Preparation of chitosan nanoparticles for loading with NPK fertilizer. *Afri. J. Biotechnol.*, 13: 31.
- He, X., Deng, H. and Hwang, H. 2019. The current application of nanotechnology in food and agriculture. *J. Food Drug Anal.*, 27: 1-21.
- Irfan, S.A., Razali, R., KuShaari, K., Mansor, N., Azeem, B. and Ford Versypt, A.N. 2018. A review of mathematical modeling and simulation of controlled-release fertilizers. *J. Controlled Release.*, 271: 45-54.
- Karibasappa, H., Aravinda, H.B. and Manjappa, S. 2009. A study on eutrophication level in hosur town lakes. *Nat. Environ. Pollut. Technol.*, 8(2): 297-300.
- Keeney, D.R. and Follett, R.F. 1991. Managing nitrogen for groundwater quality and farm profitability: Overview and introduction. In: Follett, R.F. et al. (eds.) *Managing Nitrogen for Ground Water Quality and Farm Profitability*. SSSA, Madison, WI, pp. 1-7
- Lateef, A., Nazir, R., Jamil, N., Alam, S., Shah, R., Khan, M.N. and Saleem, M. 2016. Synthesis and characterization of zeolite-based nanocomposite: An environment-friendly slow release fertilizer. *Microporous Mesoporous Mater.*, 232: 174-183.
- Lawrencía, D., Wang, S.K., Low, D.Y.S., Goh., B.H. and Goh, J.K. 2021. Controlled release fertilizers: A review on coating materials and mechanism of release. *Plants*, 10: 238-263.
- Li, X., Lei, Z., Qu, J., Li, Z., Zhou, X. and Zhang, Q. 2017. Synthesizing Slow-Release Fertilizers via mechano-chemical processing for potentially recycling the waste ferrous sulfate from titanium dioxide production. *J. Environ. Manage.* 86: 120-126.
- Liang, D., Du, C., Ma, F., Shen, Y., Wu, K. and Zhou, J. 2019. Interaction between polyacrylate coatings used in controlled-release fertilizers and soils in wheat-rice rotation fields. *Agric. Ecosyst. Environ.*, 286: 106650.
- Liu, G.D. and Hanlon, E. 2012. Soil pH range for optimum commercial vegetable production. HS1207. Gainesville: University of Florida Institute of Food and Agricultural Sciences. 2012 <http://edis.ifas.ufl.edu/hs1207>
- Liu, J., Yang, Y., Gao, B., Li, Y.C. and Xie, J. 2018. Bio-based elastic polyurethane for controlled-release urea fertilizer: Fabrication, properties, swelling, and nitrogen release characteristics. *J.Clean. Prod.*, 209: 528-537.
- Loper, S. and Shober, A.L. 2012. *Soils & fertilizers for master gardeners: glossary of soil and fertilizer terms*. SL 277. Gainesville: University of Florida Institute of Food and Agricultural Sciences. <http://edis.ifas.ufl.edu/mg457>.
- Lubkowski, K. 2016. Environmental impact of fertilizer use and slow release of mineral nutrients as a response to this challenge. *Pol. J. Chem. Technol.*, 18(1): 72-79.
- Marchiol, L., Iafisco, M., Fellet, G. and Adamiano, A. 2020. Nanotechnology supports the next agricultural revolution: perspectives on the enhancement of nutrient use efficiency. *Adv. Agron.*, 161: 27-116.
- Mikula, K., Izydorczyk, G., Skrzypczak, D., Mironiuk, M., Moustakas, K., Witek-Krowiak, A. and Chojnacka, K. 2019. Controlled Release Micronutrient Fertilizers for precision agriculture – A Review. *Sci. Total Environ.*, 712: 136365.
- Nandini, N., Anupama, B. S. and Pavithra, S. 2009. Natural farming in harmony with the sustainable ecosystem. *Nat. Environ. Pollut. Technol.*, 8(4): 785-788.
- Nardi, P., Neri, U., Di Matteo, G., Trinchera, A., Napoli, R., Farina, R. and Benedetti, A. 2018. Nitrogen is a release from slow-release fertilizers in soils with different microbial activities. *Pedosphere*, 28(2): 332-340.
- Naz, M.Y. and Sulaiman, S.A. 2016. Slow release coating remedy for nitrogen loss from conventional urea: A Review. *J. Controlled Release*, 225: 109-120.
- Ni, B., Liu, M., Lü, S., Xie, L. and Wang, Y. 2011. Environmentally friendly slow-release nitrogen fertilizer. *J. Agric. and Food Chem.*, 59: 10169-10175.
- Pandey, G. 2018. Challenges and prospects of agri-nanotechnology for sustainable agriculture in India. *Env. Tech. Inn.*, 11: 299-307.
- Pandey, S.P., Shukla, T., Dhote, V.K., Mishra, D.K., Maheshwari, R. and Tekade, R.K. 2019. Use of polymers in controlled release of active agents. *fundamentals of drug delivery*. pp.113-172.
- Paraskar, D.R., Nanoty, V.D. and Musaddiq, M. 2010. Study of root nodulation efficiency of different rhizobium strains found in different regions of Akola district and developing *Rhizobia*-based biofertilizer. *Nat. Environ. Pollut. Technol.*, 9(1): 123-127.
- Patil, S. S., Kengar, S. B. and Sathe, T. V. 2007. New vermicast model for sustainable agriculture in India. *Nat. Environ. Pollut. Technol.*, 6(2): 281-284.
- Pereira, E.I., Giroto, A.S., Bortolin, A., Yamamoto, C.F., Marconcini, J.M., de Campos Bernardi, A.C. and Ribeiro, C. 2015. Perspectives in nanocomposites for the slow and controlled release of agrochemicals: fertilizers and pesticides. In *Nanotechnologies in Food and Agriculture*. Springer, Cham., 241-265.
- Qi, T., Lü, S., Zhang, S.F., Bai, X., Chen, J., Huang, M. and Liu, M. 2020. Zein Coated porous carboxy methyl starch fertilizer for iron promoting and phosphate sustainable release. *J. Clean. Prod.*, 258.
- Ravisankar, N and. Poongothai, S. 2007. Spatial analysis of groundwater quality in the tsunami-affected coastal areas of Tamilnadu, India. *Nat. Environ. Pollut. Technol.*, 6(4): 583-588.
- Salimi, M., Motamedi, E., Motesharezedeh, B., Hosseini, H.M. and Alikhani, H.A. 2020. Starch-g-poly (acrylic acid-co-acryl amide) composites reinforced with natural char nanoparticles toward environmentally benign slow-release urea fertilizers. *J. Environ. Chem. Eng.*, 2020, 8: 103765.
- Salman, J.P.K.S.A.D. and Handslow M.J. (eds.) 2006. *Handbook of Powder Technology Granulation*. Elsevier Publication, The Netherlands.
- Schepers, J.S. and Fox, R.H. 1989. Estimation of N Budgets, for Crops. In Follett, R.W. (eds.) *Nitrogen Management and Ground Water Protection*. Elsevier Science Publisher, Amsterdam. pp 221-246.
- Shaviv, A. 2001. Advances in controlled-release fertilizers. *Adv. Agron.*, 71: 1-49.
- Shaviv, A. and Mikkelsen, R.L. 1993. Controlled release fertilizer to increase the efficiency of nutrient use and minimize environmental degradation: A review. *Fert. Res.*, 35: 1-12.



- Trenkel, M.E. 2010. Slow- and controlled-release and stabilized fertilizers: an option for enhancing nutrient use efficiency in agriculture. *Int. Fert. Ind. Assoc.*, 11: 201.
- Tripathi, S., Srivastava, P., Devi, R.S. and Bhadouria, R. 2020. Influence of synthetic fertilizers and pesticides on soil health and soil microbiology. *Agrochem. Detect. Treat. Remed.*, 2020; pp. 25-54.
- Usman, M., Farooq, M., Wakeel, A., Nawaz, A., Cheema, S.A., Rehman, H.U. and Sanauallah, M. 2020. Nanotechnology in agriculture: Current status, challenges, and future opportunities. *Sci. Total Environ.*, 721: 137778.
- Wei, H., Chen, Z., Xing, Z., Zhou, L., Liu, Q., Zhang, Z. and Zhang, H. 2018. Effects of slow or controlled release fertilizer types and fertilization modes on yield and quality of rice. *J. Integr. Agric.*, 17(10): 2222-2234.
- Wei, X., Chen, J., Gao, B. and Wang, Z. 2020. Role of controlled and slow-release fertilizers in fruit crop nutrition. *Fruit Crops.*, 555-566.
- Fan, X.H. and Li, Y.C. 2010. Nitrogen release from slow-release fertilizers as affected by soil type and temperature. *Soil Sci. Soc. Am. J.*, 74(5): 1635-1641.
- Ye, H.M., Li, H.F., Wang, C.S., Yang, J., Huang, G., Meng, X. and Zhou, Q. 2019. Degradable polyester/urea inclusion complex applied as a facile and environment-friendly strategy for slow-release fertilizer: Performance and mechanism. *Chem. Engg. J.*, 381: 122704.
- Zhou, T., Wang, Y., Huang, S. and Zhao, Y. 2018. Synthesis of composite hydrogels from inorganic-organic hybrids based on leftover rice for environment-friendly controlled-release urea fertilizers. *Sci. Total Environ.*, 615: 422-430.
- Zulfiqar, F., Navarro, M., Ashraf, M., Akram, N.A. and Munné Bosch, S. 2019. Nano-fertilizer use for sustainable agriculture: Advantages and limitations. *Plant Sci.*, 289.





# Estimation of Indoor Radon Concentration in Some Houses in Al-Shatra District, Dhi-Qar Governorate, Iraq

A. A. Elewee<sup>\*(\*\*)</sup> and M. Sh. Aswood<sup>\*†</sup>

\*Department of Physics, College of Education, University of Al-Qadisiyah, Al-Diwaniyah, Iraq

\*\*Ministry of Education, Directorate General of Dhi-Qar Education, Shatra Education Department, Iraq

†Corresponding author: M. Sh. Aswood; murtadhababylon@gmail.com

Nat. Env. & Poll. Tech.  
Website: [www.neptjournal.com](http://www.neptjournal.com)

Received: 12-02-2022

Revised: 24-03-2022

Accepted: 26-03-2022

## Key Words:

Indoor radon  
CR-39  
Effective dose  
Lung cancer  
Al-Shatra

## ABSTRACT

Radon is present in houses and everywhere and causes lung cancer, heart problems, and respiratory infections in those who breathe it. Indoor Radon levels were tested for two months in 65 houses in the Al-Shatra, Dhi-Qar Governorate, Iraq, using solid-state nuclear track detectors CR-39. The results obtained indicate that the concentration rates varied clearly, as the lowest concentration was 20.805 Bq/m<sup>3</sup> in Al-Moalmen, while the highest concentration was 114.431 Bq/m<sup>3</sup> in AL-Shaala, with an average of 63.391±22.73 Bq/m<sup>3</sup>. The annual effective inhalation has varied between 0.524 mSv/y and 2.886 mSv/y with a mean of 1.598 mSv/y. On the other hand, the average lung dose was 2.529 nGy/h. All the results indicate the radon gas levels are within the permissible limits compared to the recommended by American Environmental Protection Agency EPA, which are set at 148 Bq/m<sup>3</sup>, and the inhalation dosage is less than ICRP recommended action limit of 3 mSv/y.

## INTRODUCTION

Natural sources of radioactivity in the environment are known as naturally occurring radioactive materials (NORM) and are classified as cosmic and terrestrial in origin. NORM is naturally found in the environment. NORM is present in varying amounts in rocks, soil, water, vegetables, air, building materials, and the human body itself. The specific levels of radioactivity in various soils are related to the nature of the parent rock (Ramsiya et al. 2017).

The radionuclides emit alpha particles, beta particles and gamma rays. It can be ingested or inhaled into the body, enters the lungs, and has an impact on the cells of the lungs, the cases of lung cancer, or it enters the human bloodstream and damages blood cells, causing leukemia (Showard & Aswood 2019). Radon is a noble radioactive gas that is produced when the natural uranium chain decomposes. It is colorless, odorless, and tasteless, and it is imperceptible to the human senses. It consists of three isotopes: Radon (<sup>222</sup>Rn), Thoron (<sup>220</sup>Rn), and Actinon (<sup>219</sup>Rn) (Tawfiq et al. 2015, Bineng et al. 2020). The main contribution to inhalation exposure comes from the short half-life decay products of radon. It may infiltrate houses through cracks and pores in floor tiles, as well as through soil through building materials such as sand, cement, and other components (Kadhim et al. 2022, Fahiminia et al. 2016). The

internal focus of Radon may depend on the parent elements connecting the dwellings as well as the interior designs (Mehra et al. 2017, Aswood et al. 2019). Radon has been identified as a risk factor for lung cancer because it breaks down into radioactive particles that can get stuck in the lungs (Rashid 2014). There are many studies have shown that (5 to 20%) of lung cancer deaths can be attributed to breathing air containing radon and its daughters, and Indoor Radon concentration measurements in nations to create baseline data on natural radiation levels (Farid 2016, Tawfiq et al. 2015, Fahiminia et al. 2016). Studies have confirmed that exposure to radon gas and its daughters the risk of developing bronchial epithelial cells, the cause of lung cancer (Tawfiq et al. 2015, Kaur et al. 2018). Exposure to Radon and its components contributes to more than 50% of the total radiation dose received by humans from natural sources (Aswood et al. 2018, Salih et al. 2019). The goal of the present study is to measure the Indoor Radon in 65 homes in the Al-Shatra, Dhi-Qar Governorate, Iraq using CR-39 detectors as well as their related lung doses.

## MATERIALS AND METHODS

### Study Area

Indoor Radon was carried out in 65 dwellings in the city of Al-Shatra and located approximately 40 km the North of Na-

siriyah. It is located from 46°11'34" to 46°8'42" N latitude and 31°23' 5" to 31°26'16" E longitude. The governorate is divided into five administrative divisions: Nasiriyah, the center of the governorate, Al Shatra, Suq Al-Shuyoukh, Al-Rifai, and Al-Jabayish. The area of Al Shatra is estimated at 384 km<sup>2</sup>, and its population according to the 2014 census is 254 thousand people (Rashid 2014). The city is located on one of the two branches of the Gharraf river, which descends from the Tigris river, in the middle Euphrates region in southern Iraq.

### CR-39

A passive method using CR-39 track detectors based on the SSNTD technique was employed for the assessment of radon concentration in some regions in Al Shatra city. Detectors (CR-39) of the thickness (500 μm) and size 1.5×1.5 cm<sup>2</sup> were exposed to the indoor environment of a dwelling for a known period of two months.

### Collected Samples

Sixty five dwellings in Al Shatra city, Dhi-Qar governorate were selected for the Radon study. The choice of houses was random. The majority of the houses were built of concrete with plastered walls with a proper ventilation system. The detectors were placed at a height of about 1.5 m from the ground is the level of breathing. Detectors were placed in different rooms on the ground floor of the dwelling. After that, the reagents from houses were collected and prepared for etching using a sodium hydroxide solution NaOH with a density of 6.25 mol/L at a temperature of 70° C for 6 hours, and then washed with distilled water (Aswood et al. 2019). The number of tracks was calculated using an optical microscope with a magnification capacity of 400X.

### Calculation

Measurement of Radon-222 concentrations ( $C_{Rn}$ ) in the air was calculated according to equation 1 as suggested by (Karim et al. 2017).

$$\rho\left(\frac{tr}{cm^2}\right) = \frac{N_t}{A} \quad \dots (1)$$

$\rho$ : the track density (track/mm<sup>2</sup>),  $N_t$ : the average number of tracks on the CR -39 detector, A: area of view field visible under the microscope.

Radon concentration has been calculated in samples using the following equation 2 (Showard & Aswood 2019).

$$C_{Rn}\left(\frac{Bq}{m^3}\right) = \frac{\rho}{K \times t} \quad \dots (2)$$

Where,  $C_{Rn}$ : Radon concentration, t: The storage time

60 days, K: The calibration factor of CR-39, the calibration factor K is 0.02607 Track.cm<sup>-2</sup> /Bq.m<sup>-3</sup> day. This factor is determined using the equation below which is a function of tube parameters:

$$K=0.25r\left(2\cos\theta_c - \frac{r}{r_\alpha}\right) \quad \dots(3)$$

Where, r: is tube radius and equals 1.75cm,  $\theta_c$  is the critical angle of CR-39 detectors and  $\theta_c = 35^\circ$ , and  $r_\alpha$  is alpha particle range in air ( $r_\alpha = 4.15$  cm) (Ramsiya et al. 2017).

The annual effective dose was calculated by equation 4 (Obaed & Aswood 2020b).

$$AED\ (m\ Sv/y) = C_{Rn} \leftarrow F \leftarrow H \leftarrow T \leftarrow D \quad \dots(4)$$

where (F) is the equilibrium factor and it is equal to (0.4), (H) is the occupancy factor which is equal to (0.8), (T) is the time in hours in one year, ( $T=8760\ h.y^{-1}$ ), and (D) is the dose conversion factor which is equal to  $[9 \leftarrow 10^{-6}\ (m.Sv) / (Bq.h.m^{-3})]$  (Obaed & Aswood 2020b).

When calculating the dosage rate to the lungs, the air volume in the lungs by equation 5 (Abbady et al. 2004).

$$Dose\ rate\ to\ lung,\ D\ lung = 0.04 \leftarrow C_{Rn} \quad \dots(5)$$

## RESULTS AND DISCUSSION

Indoor radon has been measured in 65 houses by CR-39, Shatra, Dhi-Qar Governorate-Iraq. The results showed the highest concentration of  $114.431 \pm 37.46\ Bq.m^{-3}$  in AL-Shaala, while the lowest concentration of Radon  $20,805 \pm 5.67\ Bq.m^{-3}$  was in the AL-Moalmen, with an average was  $63.246 \pm 22.8\ Bq.m^{-3}$ , as presented in Table 1. The high concentration is attributed to the war in 1991 and 2003. In addition, the dwellings are quite old and cramped, with no good ventilation. On the other hand, the results have been compared with the worldwide concentration limit of  $148\ Bq.m^{-3}$  set by the International Commission on Radiological Protection (ICRP 1993). The annual effective inhalation has varied between  $0.524\ mSv.y^{-1}$  and  $2.886\ mSv.y^{-1}$  with a mean of  $1.598\ mSv.y^{-1}$ . On the other hand, the average lung dose was 2.529. The inhalation dosage levels indicate within the permissible limits compared to the recommended ICRP of 3 mSv/y.

From Fig.1, the average concentration of Radon for the ten states has been indicated as the highest average in Besan ( $91.26\ Bq.m^{-3}$ ) and the lowest concentration was in AL-Fattahia ( $43.78\ Bq.m^{-3}$ ). The variance of the average concentration for ten states depends on different areas of the houses and different construction of the building of the house as well as the effect of the war, especially for the state of Besan. The annual effective doses of Besan are higher than the ICRP standard (Khalid et al. 2014). The increase in the effective annual dose depends on the building materials used,

Table 1: Indoor Radon concentration, annual effective dose (AED), and dose lung ( $D_{lung}$ ) for Al-Shatra city in Thi-Qar Governorate, Iraq.

Sample code	Location	Concentration (Bq.m <sup>-3</sup> )	Annual effective dose (AED) msv.y <sup>-1</sup>	$D_{lung}$ (nGy.h <sup>-1</sup> )
S 1	AL-Moalmen	106.86 ± 13.4	2.69	4.27
S 2		74.71 ± 12.29	1.88	2.98
S 3		59.587 ± 10.4	1.508	2.38
S 4		79.44 ± 17.54	2.004	3.17
S 5		28.37 ± 9.45	0.715	1.13
S 6		20.805 ± 5.67	0.524	0.83
S 7		74.71 ± 36.49	1.884	2.98
S 8		34.045 ± 7.565	0.859	1.36
S 9		60.525 ± 22.053	1.526	2.423
average		59.89 ± 14.98	1.509	2.39
S 10	AL-Fattahia	43.503 ± 20.371	1.097	1.74
S 11		47.285 ± 18.914	1.193	1.89
S 12		45.394 ± 21.482	1.145	1.81
S 13		79.44 ± 35.435	2.004	3.17
S 14		33.10 ± 24.751	0.835	1.32
S 15		39.72 ± 15.131	1.002	1.58
S 16		29.317 ± 13.001	0.739	1.17
S 17		46.34 ± 20.48	1.169	1.85
S 18		25.534 ± 8.511	0.644	1.02
S 19	48.231 ± 17.667	1.216	1.92	
average		43.78 ± 19.57	1.10	1.75
S 20	AL-Shomali	22.697 ± 4.633	0.572	0.90
S 21		27.425 ± 11.543	0.691	1.09
S 22		41.611 ± 19.927	1.049	1.66
S 23		65.254 ± 26.898	1.646	2.61
S 24		93.625 ± 29.741	2.362	3.74
S 25		83.223 ± 24.588	2.099	3.32
S 26		75.657 ± 18.914	1.908	3.02
S 27		77.548 ± 31.021	1.956	3.10
S 28		73.765 ± 29.545	1.861	2.95
average		62.31 ± 21.86	1.57	2.49
S 29	AL-Shortah	81.331 ± 38.808	2.051	3.25
S 30		46.34 ± 25.534	1.169	1.85
S 31		66.20 ± 24.295	1.67	2.64
S 32		86.06 ± 24.823	2.171	3.44
S 33		69.037 ± 29.921	1.741	2.76
S 34		66.20 ± 27.733	1.67	2.64
S 35		65.254 ± 18.652	1.646	2.61
S 36		43.502 ± 12.828	1.097	1.74
S 37		69.983 ± 22.057	1.765	2.79

Table cont....

Sample code	Location	Concentration (Bq.m <sup>-3</sup> )	Annual effective dose (AED) msv.y <sup>-1</sup>	D <sub>lung</sub> (nGy.h <sup>-1</sup> )
average		65.98 ± 24.69	1.66	2.63
S 38	AL-Zhour	69.983 ± 24.369	1.765	2.79
S 39		43.502 ± 29.362	1.097	1.74
S 40		23.642 ± 6.344	0.596	0.94
S 41		43.502 ± 7.565	1.097	1.74
S 42		61.471 ± 18.556	1.55	2.45
S 43		63.363 ± 26.765	1.598	2.53
S 44		59.58 ± 22.399	1.503	2.38
average		52.14 ± 19.33	1.31	2.08
S 45	AL-Shaala	45.394 ± 22.697	1.145	1.81
S 46		94.571 ± 39.221	2.385	3.78
S 47		114.431 ± 37.46	2.886	4.57
S 48		44.448 ± 41.016	1.121	1.77
S 49		49.177 ± 16.811	1.24	1.96
S 50		52.014 ± 12.147	1.3122	2.08
S 51		71.874 ± 25.092	1.813	2.87
average		67.410 ± 27.77	1.70	2.69
S 52	Besan	51.068 ± 20.371	1.288	2.04
S 53		99.30 ± 43.595	2.505	3.97
S 54		105.92 ± 32.978	2.672	4.23
S 55		108.757 ± 35.195	2.743	4.35
average		91.26 ± 33.03	2.30	3.65
S 56	AL-Hawi	61.471 ± 24.751	1.55	2.45
S 57	AL-Badaa	88.897 ± 30.848	2.242	3.55
S 58		82.277 ± 30.513	2.0757	3.29
S 59		65.254 ± 32.883	1.646	2.61
S 60		104.974 ± 33.953	2.648	4.19
average		85.35 ± 32.04	2.15	3.41
S 61	AL-Khalsah	102.137 ± 24.222	2.576	4.08
S 62		70.928 ± 19.496	1.789	2.83
S 63		34.991 ± 10.402	0.882	1.39
S 64		97.408 ± 33.582	2.457	3.89
S 65		69.037 ± 27.749	1.741	2.76
average		74.90 ± 23.09	1.89	2.99
Total Average		63.246 ± 22.806	1.59	2.52

the nature of the soil, and improper aeration. On the other hand, the lung dose value ( $D_{lung}$ ) varies from 3.65 (nGy.h<sup>-1</sup>) to 1.75 (nGy/h<sup>-1</sup>) as shown in Fig. 2. These results depend on the concentrations of radon.

The results have been compared with different studies in the world as presented in Table 2. The comparisons have

been showing the results from Iraq (Hilla), India, Germany, Iran, and Saudi Arabia were lower than those in the present study. Whilst, the previous studies of Iraq (Baghdad, Kurdistan) have been highest than the present study, as shown in Table 3, and the difference in concentration is due to the nature of the land, as well as ventilation and temperature,

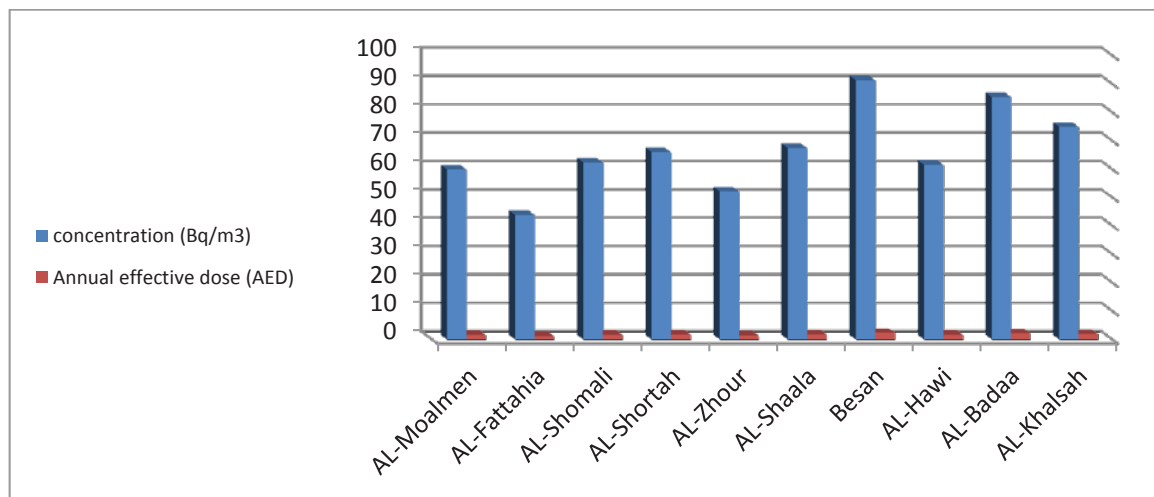


Fig. 1: Average Indoor Radon concentration and annual effective dose (AED) with different states.

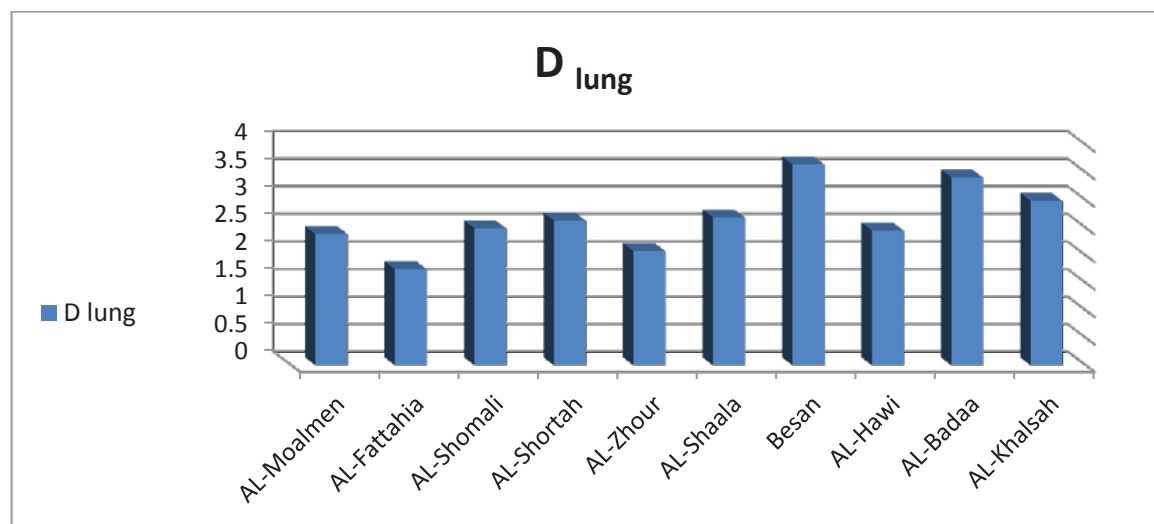


Fig. 2: Dose lung ( $D_{lung}$ ) with different states.

and that Indoor Radon concentrations range within the safe levels.

## CONCLUSION

Indoor Radon concentrations have been measured in some houses in the city of Al- Shatra, Dhi-Qar Governorate, Iraq for 65 houses by the CR-39 nuclear track detector. The variance results have been found in different houses in the city of Al- Shatra. The concentration of radon was higher in some houses than recommended by American Environmental Protection Agency. The highest concentration of radon attributes

to wars in 1991 and 2003. On the other hand, the different building materials, ventilation, pressure, and temperature are the main reason for the variance in radon concentration. The average annual effective dose was within the ICRP standard. The results indicate that Indoor Radon levels are within the permissible limits compared to the recommended by the American Environmental Protection Agency.

## ACKNOWLEDGEMENT

I would like to thank the people who live in the houses that were chosen for helping me to put the reagents.

Table 2: Comparison of Indoor Radon concentrations of the present study with other studies in the world.

Region	Concentration (Bq.m <sup>-3</sup> )	Annual effective dose	References
Baghdad, Iraq	123.8652	2.958	Salim and Ebrahiem (2019)
Baghdad, Iraq	116.78	2.95	Tawfiq et al. (2015)
Hilla, Iraq	4.18 ± 1.1	0.11±0.01	Obaed and Aswood (2020a)
Kurdistan, Iraq	143.7±46.1	3.62±1.16	Ismail and Jaafar (2010)
Saudi Arabia	36.2 ± 1.21	0.61 ± 0.18	Farid (2016)
Iran	55.1 ± 59.3	1.39 ±1.49	Hassanand et al. (02019)
German	55.9	2.2	Abbadly et al. (2004)
India	25.52	0.64	Kadhim et al. (2022)
Dhi-Qar, Iraq	63.246 ± 22.806	1.59	Present study

## REFERENCES

- Abbadly, A., Abbadly, A.G. and Michel, R. 2004. Indoor radon measurement with the Lucas cell technique. *Appl. Radiat. Isotop.*, 61(6): 1469-1475.
- Aswood, M.S., Jaafar, M.S. and Salih, N.F. 2018. Determination of radon and heavy metals in soil samples from Seberang Perai, Malaysia. *Pollut. Res.*, 37(3): 646-651.
- Aswood, M.S., Salih, A.A. and Al Musawi, M.S.A. 2019. Long-lived gamma-ray measurement in soil samples collected from the city center of Al-Diwaniyah, Iraq. *J. Phys. Conf. Ser.*, 1234(1): 012003- 012011.
- Bineng, G.S., Tokonami, S., Hosoda, M., Siaka, T., Flore, Y., Issa, H. and Bouba, O. 2020. The importance of direct progeny measurements for correct estimation of effective dose due to radon and thoron. *Front. Pub. Health*, 8(17): 1-12.
- Fahiminia, M., Fard, R.F., Ardani, R., Naddafi, K., Hassanvand, M.S. and Mohammadbeigi, A. 2016. Indoor radon measurements in residential dwellings in Qom, Iran. *Int. J. Radiat. Res.*, 14(4): 331.
- Farid, S.M. 2016. Indoor radon in dwellings of Jeddah city, Saudi Arabia and its correlations with the radium and radon exhalation rates from the soil. *Indoor Built Environ.*, 25(1): 269-278.
- Hassanvand, H., Birjandi, M., Amiri, A., Hassanvand, M.S. and Kamarehie, B. 2019. Investigation of indoor radon concentration in dwellings of Aleshtar (western part of Iran) and estimation of the annual effective dose from radon exposure. *Int. J. Radiat. Res.*, 17(4): 659-666.
- International Commission on Radiological Protection (ICRP). 1993. *Against Radon-222 at house and work*. Annual ICRP Pergamon, 23(1-2): 48.
- Ismail, A.H. and Jaafar, M.S. 2010. Indoor Radon Concentration and Its Health Risks in Selected Locations in Iraqi Kurdistan Using CR-39 NTDs. *IEEE Int. Conf. Bioinform. Biomed. Eng.*, 11: 1-8.
- Kadhim, S.A., Harjan, A.H., Alhous, S.F. and AL-Khafaji, Q.S. 2022. Study of the difference between uranium concentrations in blood samples of healthy, newly infected women who took chemotherapy in Iraq, Najaf. *AIP Conf. Proceed.*, 2386(1): 080004-080012.
- Karim, M.S., Mohammed, A.H. and Abbas, A.A. 2017. Measurements of uranium concentrations in human blood in some of the regions of Baghdad Governorate. *Ibn AL-Haitham J. Pure Appl. Sci.*, 23(2): 25-32.
- Kaur, M., Kumar, A., Mehra, R. and Mishra, R. 2018. Dose assessment from exposure to radon, thoron, and their progeny concentrations in the dwellings of the sub-mountainous region of Jammu & Kashmir, India. *J. Radioanal. Nucl. Chem.*, 315(1): 75-88.
- Khalid, N., Majid, A. A., Yahaya, R. and Yasir, M. S. 2014. Radiological risk of building materials using homemade airtight radon chamber. *AIP Conf. Proceed.*, 1584(1): 207-210.
- Mehra, R., Jakhu, R. and Mittal, H.M. 2017. Assessment of lung dose from indoor 222Rn and 220Rn exposure in the Jalandhar and Kapurthala districts of Punjab, India. *Indoor Built Environ.*, 26(9): 1305-1310.
- Obaed, H.K. and Aswood, M.S. 2020a. Indoor radon levels estimation in dwellings of Hillah, Iraq using Cr-39 detectors. *Pollut. Res.*, 39(3): 520-524.
- Obaed, H.K. and Aswood, M.S. 2020b. Estimated U, Rn, and Po concentrations in smokers' blood samples collected from Babylon, Iraq. *IOP Conf. Ser. Mater. Sci. Eng.*, 928(7): 072043- 072055.
- Ramsiya, M. Joseph, A. and Jojo, P.J. 2017. Estimation of indoor radon and thoron in dwellings of Palakkad, Kerala, India using solid state nuclear track detectors. *J. Radiat. Res. Appl. Sci.*, 10(3): 269-272.
- Rashid, J.M. 2014. Determination of indoor radon concentration in Thi-Qar province houses by using CR-39 SSNTD. *Univ. Thi-Qar J. Sci.*, 4(4): 175-180.
- Salih, N.F., Aswood, M.S. and Hamzawi, A.A. 2019. Effect of porosity on evaluation of radon concentration in soil samples collected from Sulaymania governorate, Iraq. *J. Phys.: Conf. Ser.*, 1234(1): 012024- 012035.
- Salim, D.A. and Ebrahiem, S.A. 2019. Measurement of radon concentration in College of Education, Ibn Al-Haitham buildings using Rad-7 and CR-39 detector. *Energy Proced.*, 157: 918-925.
- Showard, A.F. and Aswood, M.S. 2020. Effect of gender and occupations on uranium concentration in human blood and soil samples collected from Babylon, Iraq. *Pol. J. Med. Phys. Eng.*, 26(3): 143-148.
- Tawfiq, N.F., Rasheed, N.O. and Aziz, A.A. 2015. Measurement of indoor radon concentration in various dwellings of Baghdad Iraq. *Int. J. Phys.*, 3(5): 202-207.





# Effective Mixer Design an Important Factor In SSCR Systems for Reduction of NO<sub>x</sub> from Exhaust of Diesel Engines

M. K. Yadav† and A. K. Srivastava

Department of Mechanical Engineering, University of Petroleum and Energy Studies, Bidhauri Campus, Dehradun-248007, Uttarakhand, India

†Corresponding author: M. K. Yadav; mkyadav80@rediffmail.com, ddn@upes.ac.in

Nat. Env. & Poll. Tech.  
Website: [www.neptjournal.com](http://www.neptjournal.com)

Received: 20-12-2021

Revised: 24-01-2022

Accepted: 11-02-2022

## Key Words:

Diesel engines

SSCR

Mixer design

Uniform ammonia flow

Ammonia slip

NO<sub>x</sub>

## ABSTRACT

In recent decades, the environment has been seriously polluted by the hazardous exhaust components of diesel engines. The international community, which is dedicated to preserving the harmony between nature and humanity, has taken this seriously and imposed strict regulations on Diesel engine manufacturers regarding the quantity of exhaust components from Diesel engines that may apply to the standards of EURO-VI. The SCR technology attempted to reduce the problem somewhat, but the associated problems of solid particle formation on the pipe walls, ammonia slip, and incomplete NO<sub>x</sub> reduction led to the development of new technology - solid selective catalytic reduction. The use of solid ammonium salt for ammonia generation has shown better results in NO<sub>x</sub> reduction and reduction of solid particle formation compared to SCR. However, it was not possible to fully resolve the ammonia slip issue. A uniform flow rate of ammonia through the SCR catalyst can reduce NO<sub>x</sub> efficiently. In this paper, the role of mixer design in achieving a uniform flow rate of ammonia is investigated in detail. The results show that an optimized mixer design leads to efficient reduction of NO<sub>x</sub> and thus reduces ammonia slip to a great extent. When the mixer is placed near the ammonia injection point, the most homogeneous ammonia distribution is achieved for flow through the SCR catalyst.

## INTRODUCTION

The rapidly increasing demand for vehicles has badly affected the environment. Exhaust emissions of diesel engines contain extremely poisonous unburned hydrocarbons, carbon dioxide, carbon monoxide, particulate matter, sulfur dioxide, and oxides of nitrogen. Society is struggling with the adverse effects of exhaust emission components of diesel engines (Erickson et al. 2020). The removal of nitrogen oxides from the exhaust is the most difficult task.

Fig. 1 shows the exact distribution of the exhaust gas components of diesel engines which contain nitrogen, oxygen, carbon dioxide, carbon monoxide, particulate matter, unburnt hydrocarbons, and oxides of nitrogen. Due to the harmful effects of nitrogen oxides on human health, it is proposed in EURO-VI to limit NO<sub>x</sub> emissions to 0.4 kg.KWh<sup>-1</sup> in a steady state and 0.46 kg.kWh<sup>-1</sup> in the transient state (Williams & Minjares 2016).

Exhaust gas recirculation (EGR), Lean NO<sub>x</sub> trap (LNT), and selective catalytic reduction (SCR) are some of the technologies previously adopted by engine manufacturers (Praveena & Martin 2018) but could not increase the reduction efficiency by more than 75%. Selective catalytic reaction

(SCR) can reduce upto 90% of NO<sub>x</sub> with a suitable filter design and catalyst. But ammonia slip, freezing of diesel exhaust fluid (DEF) at low temperature, and nozzle clogging due to cyanuric acid formation reduce the NO<sub>x</sub> reduction performance of SCR. Latha et al. (2019) reviewed various after-treatment technologies for NO<sub>x</sub> reduction and found SCR to be the most promising technology for meeting EURO-VI emission standards. Major problems observed with SCR were ammonia slip and solid deposit formation. The authors investigated that catalyst deactivation can reduce ammonia slip by placing an oxidation catalyst after SCR (Latha et al. 2019).

## CONSTRUCTION OF SCR

The use of appropriate filters with suitable catalysts can improve the NO<sub>x</sub> reduction performance of catalytic converters without affecting fuel consumption and engine power (Zhang et al. 2018). The use of filters reduces the particle size of soot and at the same time reduces more than 90% of fine dust particles (Mamakos et al. 2013).

Correct positioning of various filters is an important factor in achieving the optimum amount of ammonia for NO<sub>x</sub>

## Percentage of exhaust components

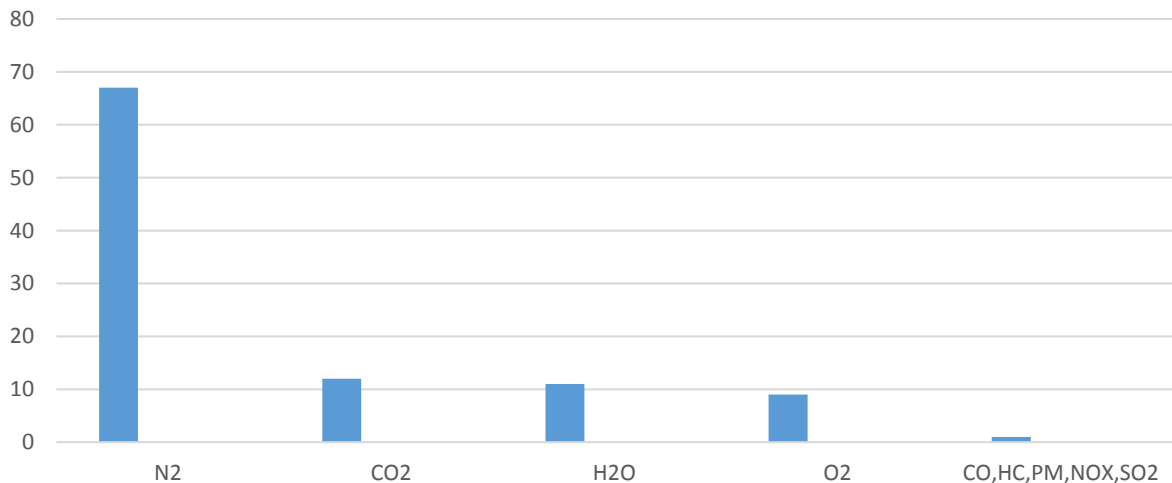


Fig. 1: Diesel engine exhaust composition (Reşitoğlu et al. 2015).

reduction. DOC helps in the oxidation of hydrocarbons and carbon monoxide thus reducing their toxicity. DPF reduces the size of soot particles and periodic active regeneration burns the carbon particles from the filter thus making the exhaust carbon-free. SCR reduces the oxides of nitrogen into nitrogen in presence of a suitable catalyst.

### DIESEL OXIDATION CATALYST (DOC)

17% unused oxygen from diesel engine exhaust can be used to oxidize hydrocarbons and carbon monoxide. These reactions take place in the presence of a catalyst (DOC) which increases the rate of reaction. DOC is placed before the DPF to take advantage of the temperature rise in DOC (Kurien et al. 2018). It has been studied that for every 1% oxidation of carbon monoxide, the exhaust gas temperature increases by 90°C, which supports the combustion of carbon particles

in the DPF (Reşitoğlu et al. 2015). DOC is a honeycomb structure of a platinum or palladium substrate surrounded by a catalyst such as V<sub>2</sub>O<sub>5</sub> or TiO<sub>2</sub>. It helps in the passive regeneration of soot particles in DPF (Wang et al. 2012). The production of NO<sub>2</sub> during oxidation leads to increased efficiency of SCR.

### DIESEL PARTICULATE FILTER (DPF)

DPF uses a ceramic substrate in the form of a honeycomb structure. Its purpose is to trap carbon particles and burn them periodically to prevent their emission into the atmosphere. The soot remains in the filter until active or passive regeneration occurs. Passive regeneration occurs at 275°C to 360°C and active regeneration occurs at 600°C. Active regeneration takes place when the filter is clogged. Fresh fuel is allowed to inject into the exhaust pipe to increase the

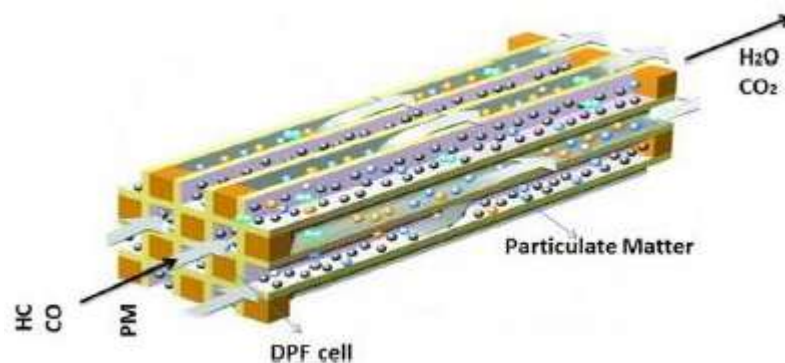


Fig. 2: Trapping of carbon particles in DPF (Mohankumar & Senthilkumar 2017a).

temperature to oxidize the accumulated soot. Plasma-assisted burner type DPF ensures the reduced particle size of soot (Wang et al. 2012)

Fig. 2 shows a schematic diagram of a DPF filter. It contains four openings. Exhaust gases from DOC enter through two openings, flow through the cells where carbon particles are trapped and are then discharged through opposite openings.

Vehicles with catalytic DPF and urea SCR reduced particulates with 99.9% and 90% efficiency, respectively. The Plasma assisted burner type DPF effectively reduces particulate matter over the entire size range. Lee et al. (2015) experimentally calculated the particle number size distribution for diesel engine exhaust gases with the FMPS rapid particle size measuring device TSI 3091. They concluded that an effective particle number size can be achieved with the help of plasma-assisted burner type DPF. Mohankumar & Senthilkumar (2017a) reviewed the various technologies for removing particulate matter. He concluded that the use of a suitable regeneration method, an electrostatic precipitator, a particulate filter and a multi-hole nozzle with high injection pressure can greatly reduce particulate matter (Mohankumar & Senthilkumar 2017b). Martinovic et al. (2020) mixed the soot oxidation catalyst with the SSCR catalyst and investigated that the soot temperature can be reduced by 150°C with a significant increase in NO<sub>x</sub> reduction efficiency of the SCR catalyst. It could happen due to the optimized mass ratio of the catalyst resulting in a rapid SCR reaction (Martinovic et al. 2020).

## DIESEL EXHAUST FLUID (DEF)

Because of its unpleasant odor, aqueous urea is used instead of ammonia, which, after decomposing to ammonia, reacts with NO<sub>x</sub> in the presence of the catalyst SCR and reduces a considerable amount of NO<sub>x</sub>. This aqueous urea solution, containing 32.5% urea and 67.5% deionized water, is called DEF. Spraying of DEF in the combustion chamber reduces the risk of deposits due to increased surface area, better mixing, and evaporation (Hasan Shahariar & Lim 2018). The turbulence and bounce created by the high wall temperature increase the mixing length, which helps to reduce the deposition of urea from the exhaust pipe (Hasan Shahariar et al. 2019). The aqueous urea is injected into the SCR tank using a nozzle. But the problem is that the tank has a low ammonia capacity (Qu et al. 2014a). Freezing of DEF at temperatures below -11°C is another big issue, which requires an integrated electric heater in the tank of DEF (Kurien & Srivastava 2018). DEF produces cyanuric acid and some other acids that lead to blockage of the urea nozzle, reduce the activity of the catalyst and thus reduce NO<sub>x</sub> efficiency (Zhang et al. 20116).

Chan et al. (2015) investigated a predictive approach by a nonlinear model to efficiently control injection timing and DEF dosing rate. A model with an NMPC approach for SCR control was simulated and the results showed a reduction in ammonia slip and an increase in NO<sub>x</sub> reduction efficiency (Chen & Wang 2015).

## SELECTIVE CATALYTIC REACTION (SCR)

It is a honeycomb structure of porous ceramic materials surrounded by catalytic components such as V<sub>2</sub>O<sub>5</sub> or TiO<sub>2</sub>. Here NO<sub>x</sub> combines with ammonia and is reduced to nitrogen. Zeolites of copper and iron are widely used catalysts in SCR out of which copper zeolite gives better results in NO<sub>x</sub> reduction due to its higher ammonia storage capacity, thermal stability, and reduced ammonia slip (Guan et al. 2014). Manganese-based catalysts are used in some applications, but they have lower NO<sub>x</sub> reduction efficiency at low temperatures (Li et al. 2017). NO<sub>x</sub> reduction efficiency acts as a performance indicator of SCR.

NO<sub>x</sub> conversion =  $[1 - (\text{NO}_x \text{ out} / \text{NO}_x \text{ in})] \times 100\%$  (Peng et al. 2015)

Ammonia slip occurs when either too much ammonia is produced that cannot react with the catalyst due to low temperature or when the catalyst has degraded (Latha et al. 2019). Torp et al. (2021) developed a mathematical model for the design of a reaction that combines two layers of ammonia slip catalyst. Chemical kinetics and N<sub>2</sub>O formation were observed in a high-flow reactor. The authors concluded that mixing SCR catalyst with oxidation catalyst results in less ammonia slip and high NO<sub>x</sub> reduction efficiency (Torp et al. 2021). Baleta et al. (2017) investigated that by designing the DeNO<sub>x</sub> system for uniform ammonia production, optimized ammonia slip can be achieved. A mathematical model was created to analyze the chemical reactions that occur during the movement of exhaust gases from the catalytic converter. Ammonia slip, NO<sub>x</sub> reduction, and droplet formation were also taken into account. For the simulation, the CFD code AVL FIRE was used. The authors concluded that the optimized droplet size and injection direction can reduce ammonia slip and increase the NO<sub>x</sub> reduction efficiency of SCR catalyst (Baleta et al. 2017). Hebbar et al. (2014) reviewed the various technologies used to reduce NO<sub>x</sub> from diesel engine exhaust gases. They discussed the advantages and disadvantages of the technologies used and concluded that EGR, LNT, and SCR do not meet the EURO-VI emission standards and hence new technologies are required to seek better emission control (Hebbar 2014). Qi et al. (2016) examined the parameters that influence the reduction of NO<sub>x</sub> by SCR. They discussed the effects of urea's ammonia storage capacity, the reaction mechanism involved, the urea dosing

system, and the types of catalysts used for reducing NO<sub>x</sub> in SCR. They concluded that SCR can be effective in reducing NO<sub>x</sub> through the use of an efficient control system (Qi et al. 2016). Chatterjee et al. (2017) discussed the optimal design of DOC, DPF, and SCR to reduce the maximum amount of NO<sub>x</sub> from the exhaust pipe. The authors briefly discussed the control of ammonia slip with an ammonia slip catalyst. FTIR was used to analyze the composition of exhaust gases (Chatterjee et al. 2017). Zhang et al. (2016) suggested that the SCR catalyst should be used in two homogeneous cells, assuming identical reactions in each cell. Optimal control of urea injection has been suggested for minimal ammonia slip. A dynamic algorithm was developed to calculate the SCR load. The authors concluded that an optimal SCR system size ratio leads to minimized ammonia slip (Zhang et al. 2016). Blending diesel with hydrogen can reduce the NO<sub>x</sub> by 70% when the optimum crank angle remains 43.2° (Lamas & Rodriguez 2017).

### SOLID SELECTIVE CATALYTIC REACTION (SSCR)

SCR is one of the best technologies used by diesel engine manufacturers to meet the emission standards of EURO-VI. However, it has some limitations that reduce the NO<sub>x</sub> reduction efficiency of SCR. The problems associated with it are listed in Table 1

Table 1 shows the problems faced by engine manufacturers when using SCR. These problems affect the performance of the catalyst and thus limit the efficiency of NO<sub>x</sub> reduction.

The solutions to most of the above-mentioned problems related to SCR lie in new technology, Solid selective catalytic reaction (SSCR). In SSCR, we use solid ammonium salt to produce ammonia. Kim et al. (2014) investigated that low-temperature urea freezing and deposition of solid particles on pipe walls were severe problems for SCR systems. They used solid urea and ammonium carbonate to generate ammonia as a substitute for aqueous urea. When comparing ammonium carbonate and urea in solid form, they found that the problem of solid particle formation occurs when using solid urea and is eliminated when using ammonium carbonate (Kim et al. 2014). Ammonia is directly injected with help of a nozzle into the exhaust pipe just before SCR. It eliminates the freezing problem of DEF, the early deactivation of the catalyst, and thus increases the NO<sub>x</sub> reduction efficiency of SCR. Due to the shorter mixing time and low decomposition temperature of the ammonium salt, the problem of nozzle blockage is also eliminated (Zhang et al. 2018). Another

Table 1: Problems associated with SCR.

S. No.	Problems associated with the use of SCR.
1	Deposition of solid particles on the pipe walls.
2	Freezing of DEF below -11°C.
3	Limited available volume for catalyst.
4	Undesirable ammonia slip.
5	The formation of a uniform mixture in SCR is quite difficult.
6	DEF needs to be filled frequently before the fuel tank gets empty.

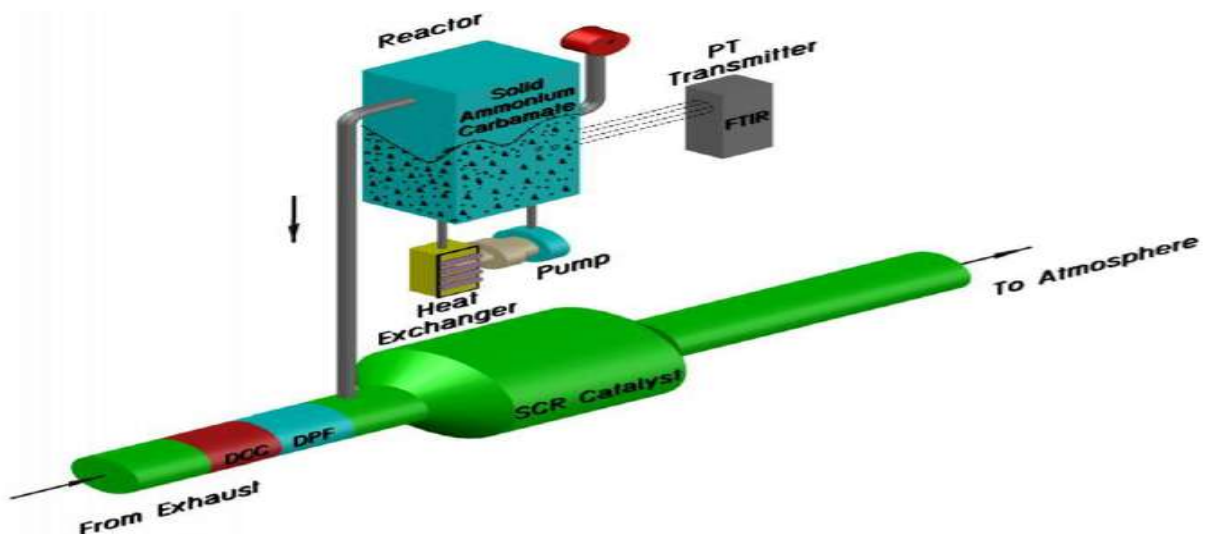


Fig. 3: Schematic diagram of SSCR system (Yadav & Srivastava 2021).

advantage of using solid ammonium salt for ammonia production is the better mixing of ammonia with exhaust gases (Krüger et al. 2003). Using the use of solid SCR increases the efficiency of NO<sub>x</sub> reduction, but at the same time power required for heating, and the salt also increases (Kim et al. 2014). Integrated hybrid systems can reduce ammonia slip and increase NO<sub>x</sub> reduction efficiency to a great extent (Guan et al. 2014).

Fig. 3 shows the arrangement of filters and accessories used in an SSCR system. It includes a DOC to oxidize hydrocarbons and carbon monoxide, a DPF to trap carbon particles, a tank containing solid ammonium carbamate, a heat exchanger, a pump, and an SCR catalyst. To reduce ammonia slip, an ammonia slip catalyst (ASC) is used after SCR.

Woo et al. (2021) investigated that insufficient heat transfer is a major challenge in the design of an ammonium carbamate pyrolysis reactor. They proposed a numerical model describing the sublimation phase of ammonium carbamate. The modeling also considered the effect of the collapse of ammonium carbamate and its sinking downward due to gravity. The program CFD at ANSYS FLUENT 19.2 was used for the analysis. The authors concluded that the prediction of the spatial temperature distribution is a herculean task since it depends on the internal structure of ammonium carbamate and the phenomena of collapse in the reactor (Woo et al. 2021).

Several parameters affecting the NO<sub>x</sub> reduction performance of SSCR have been studied. Some of these parameters are listed in Table 2

Table 2 contains most of the parameters of the SSCR system that affect performance. When these parameters are optimized, the best results can be achieved in meeting the EURO-VI emission standards.

Qu et al. (2014b) studied different parameters of the influence of SSCR ammonia spray using AVL FIRE 3D software when mixing ammonia and NO<sub>x</sub> in SCR catalyst. They concluded that better mixing, higher exhaust flow, and high temperature, resulting in less ammonia slip, can be optimized by the correct positioning of the nozzle (Qu et al. 2014c). The flow rate of exhaust through the nozzle depends upon the opening time of the nozzle, frequency, and back pressure. Using the nozzle opening control on the MOTOTRON platform using MATLAB achieves an effective flow rate (Qu et al. 2014a, 2014b, 2014c).

Guardiola et al. (2020) investigated that the problem of cross-sensitivity of NO<sub>x</sub> sensors can be reduced by estimating the ammonia slip and NO<sub>x</sub> reduction efficiency of SCR catalyst, and then passing this information to the control unit. SCR load plays an important role in reducing ammonia

slip. This load estimation can be done by preparing a model related to NO<sub>x</sub> reduction and mass conservation between the SCR inlet and outlet. Using the Kalman filter, the authors developed an algorithm to estimate ammonia slip along with SCR constraints. The authors concluded that SCR load is an important factor in the estimation of ammonia slip (Guardiola et al. 2020). The efficient nozzle design results in a longer mixing time and an even flow of ammonia through the SCR catalyst, reducing ammonia slip (Qian et al. 2019).

## ROLE OF EFFECTIVE MIXER DESIGN IN ACHIEVING THE BEST SSCR PERFORMANCE

It is investigated that a mixer must be included in the SSCR system for achieving the uniform flow of ammonia while moving through the SCR catalyst. A compact system can be designed for SSCR to achieve the best NO<sub>x</sub> reduction efficiency by using mixers and reducing the length of the chamber (Tan et al. 2018). Use of a mixer, near the urea injection point results in a uniform flow rate of ammonia through the SCR catalyst which increases the NO<sub>x</sub> conversion efficiency of SCR (Tian et al. 2015, Wardana et al. 2019). The commonly used mixers in the SSCR system are-

- (i) Line mixer
- (ii) Swirl mixer
- (iii) Combination of line and swirl mixer

Mehdi et al. (2019) investigated that the combination of linear and swirl mixer gives the lowest ammonia slip and the highest NO<sub>x</sub> reduction efficiency due to the uniformity of ammonia and temperature distribution. For this purpose, the authors created a mathematical and optimized the data by

Table 2: Parameters affecting SSCR performance.

S.No.	Parameters influencing SSCR performance
1.	Position of ammonia injector
2.	Number of holes in ammonia injector
3.	Mixing length
4.	Uniformity of ammonia flow while moving through SCR catalyst
5.	Design of mixer for uniformity of ammonia flow
6.	Mass flow rate
7.	Temperature at SCR
8.	Pressure at SCR
9.	Flow rate
10.	Mixing time of ammonia with SCR
11.	Storage capacity of SCR catalyst
12.	Engine speed

simulation after analyzing CFD (Mehdi et al. 2019). Birkhold et al. (2007) investigated the evaporation phenomena and urea droplet decomposition at different exhaust gas temperatures (Birkhold et al. 2007).

Tayamon & Wigren (2016) proved that NO<sub>x</sub> emissions from diesel engines can be controlled with a good control model. Using a recursive prediction error method, the authors created a model and used it to design a controller with 17 parameters. They concluded that the designed control model can help to keep the ammonia flow uniform, and thus increase the NO<sub>x</sub> reduction efficiency (Tayamon & Wigren 2016).

Li et al. (2017) conducted a bench test on high-performance diesel engines using solid metal ammine salt and proved that the proper design of the SCR chamber can increase the DeNO<sub>x</sub> efficiency of the catalyst. For the same injection parameters, the SSCR system was found to be 24.6% more efficient in NO<sub>x</sub> reduction than the SCR system (Li et al. 2017). Phaily et al. (2014) experimented to determine the suitability of the Cardierite/Pt catalyst. The authors conducted tests with different loads and different induction rates of ammonia. Then, a simulation was performed on AVL FIRE to validate the results. The authors, finally concluded that the ammonia induction rate of 0.6 kg/hr gives optimum results for NO<sub>x</sub> conversion efficiency. (Phaily et al. 2014). In 2015, Xin Mei Yuan et al. reviewed the previous literature regarding SSCR performance and interpreted that proper mixer design for uniform ammonia flow, modeling, calibration, and various control strategies result in lower ammonia slip and better NO<sub>x</sub> performance of SCR catalyst (Yuan et al. 2015). Jeong et al. (2005) investigated that a small distance between the catalyst inlet and the engine exhaust leads to insufficient evaporation and thermolysis. A higher thermolysis rate and good mixing of ammonia and exhaust gases can lead to better NO<sub>x</sub> reduction efficiency and lower ammonia slip.

Fig. 4 shows the arrangement of the mixer in the SSCR system. Ammonia generated due to the decomposition of ammonium carbamate enters the exhaust pipe with help of an ammonia nozzle. Here the flow of ammonia remains tur-

bulent. To obtain uniform ammonia flow, a mixer is placed after the nozzle and before the SCR catalyst. For oxidizing unused ammonia, an ammonia slip catalyst is used.

Kurien & Srivastava (2019) investigated various exhaust after-treatment systems. The authors proposed a fixed reducing agent for ammonia formation to avoid the problems associated with SCR systems. They suggested that effective control of ammonia flow can be used with an optimized mixer design to reduce the problem of reduced NO<sub>x</sub> reduction efficiency (Kurien & Srivastava 2019). Zhang et al. (2016) reviewed the available literature on SSCR technology and its advantages over SCR. They found that SSCR has higher NO<sub>x</sub> conversion efficiency, high ammonia density, and decomposition of salt occurs at low temperatures. Proper mixing of ammonia and exhaust gases and optimized flow rate of ammonia through SCR catalyst can lead to improved NO<sub>x</sub> reduction efficiency (Qu et al. 2014b). Ma et al. (2019) prepared a model explaining chemical kinetics and the flow field. They used this model to simulate a copper zeolite scripted system, specifying the boundary conditions of temperature, exhaust pressure, and mass flow rate through a bench test. They investigated the NO<sub>x</sub> reduction efficiency using an orthogonal experimental design, where the effect of nozzle injection angle and flow rate of ammonia was determined. It was concluded that fixed injection angle and chamber design for a uniform flow rate of ammonia through SCR catalyst can increase NO<sub>x</sub> reduction efficiency (Ma et al. 2019).

The use of layers of perforated plates of SCR catalyst results in a uniform flow of ammonia thus increasing NO<sub>x</sub> reduction efficiency but at the same time, a little pressure drop is observed during the process (Wardana et al. 2019). Koc et al. (2018) explored that an even ammonia flow can be achieved with an optimally designed mixer. A model based on the concept of the Eulerian-Lagrangian approach was created and the results were validated by CFD analysis using the HEEL software (Koc et al. 2018). Solid particle formation on exhaust pipe walls is greatly reduced by maintaining the uniform flow of ammonia through the SCR catalyst. The use

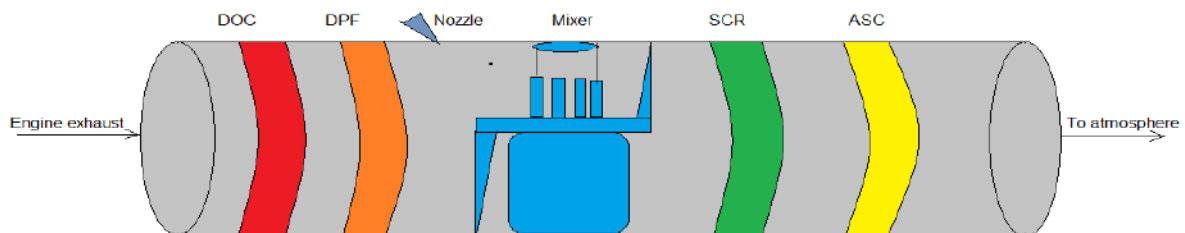


Fig. 4: Schematic diagram of SSCR with mixer.

of a mixer gives good results in direction of the achievement of uniform flow (Wang et al. 2021).

## CONCLUSION

SSCR technology has very quickly reached EURO-VI emission standards for Diesel Engines. The uniformity of the ammonia stream is an important factor in achieving the better formation of droplets and evaporation as it moves through the SCR catalyst. The aim of obtaining a better ammonia flow can be achieved using a suitable mixer. Line mixer, swirl mixer, and combination of line and swirl mixer are widely used in SCR systems. But the combination of line and swirl mixer gives the best results in terms of efficient SCR performance. Several techniques have been discussed in this article to obtain a uniform ammonia flow. Finally, it can be concluded that the use of a combination of line and swirl mixer gives the best urea conversion due to the lower residence time of the droplets. The use of these mixers makes it possible to obtain an even distribution of flow and temperature. The uniform temperature distribution results in better catalyst performance and less deposit formation. The study provides sufficient information for researchers working on the reduction of NO<sub>x</sub> emission from the exhaust of diesel engines. The reduction of ammonia slip by using a suitable mixer will certainly help diesel engine manufacturers in achieving stringent emission norms.

## REFERENCES

- Baleta, J., Matija, M., Milan, V., Klaus, P., Jin, W. and Neven, D. 2017. Numerical analysis of ammonia homogenization for selective catalytic reduction application. *J. Environ. Manag.*, 203: 1047-1061.
- Birkhold, F., Ulrich, M. and Wassermann, P. 2007. Modeling and simulation of the injection of urea-water-solution for automotive SCR DeNO<sub>x</sub> -Systems. *Applied Catalysis B: Environmental*, 70(1-4): 119-127.
- Chatterjee, S., Mojghan, N. and Jianquan, L. 2017. Heavy duty diesel engine emission control to meet BS VI regulations. *SAE Tech. Pap.*, 20: 17.85
- Chen, P. and Wang, J. 2015. nonlinear model predictive control of integrated diesel engine and selective catalytic reduction system for simultaneous fuel economy improvement and emissions reduction. *J. Dyn. Sys. Meas. Contr. Trans. ASME*, 37(8): 1-13.
- Erickson, L.E., Greg, L.N., Michael, J.H. and Wang, Z. 2020. Nitrogen oxides and ozone in urban air: A review of 50 plus years of progress. *Environ. Prog. Sustain. Energy*, 6: 1-9.
- Guan, B., Reggie, Z., He, L. and Zhen, H. 2014. Review of state-of-the-art technologies of selective catalytic reduction of NO<sub>x</sub> from diesel engine exhaust. *Appl. Therm. Eng.*, 66(1-2): 395-414.
- Guardiola, C., Benjamin, P., Pau, B. and Javier, M. 2020. Model-based ammonia slip observation for SCR control and diagnosis. *IEEE/ASME Trans. Mechatr.*, 25(3): 1346-1353.
- Hasan Shahariar, G.M., Hyun, J. and Ocktaeck, L. 2019. Analysis of the spray wall impingement of urea-water solution for automotive SCR De-NO<sub>x</sub> systems. *Energy Proced.*, 158: 1936-1941.
- Hasan Shahariar, G.M., Lim, O.T., Hasa, T. and Ock Taeck, L. 2018. Investigation of urea aqueous solution injection, droplet breakup, and urea decomposition of selective catalytic reduction systems. *J. Mech. Sci. Technol.*, 32(7): 3473-3481. doi: 10.1007/s12206-018-0651-5.
- Hebbar, G.S. 2014. NO<sub>x</sub> from diesel engine emission and control strategies: A review. *Int. J. Mech. Eng. Rob. Res* 3(4): 471-482.
- Jeong, S.J., Lee, S.J., Kim, W.S. and Lee, C. 2005. Simulation on the optimum shape and location of urea injector for urea-SCR system of heavy-duty diesel engine to prevent NH<sub>3</sub> slip. *SAE Technical Paper*, (01-388620052005).
- Kim, H., Cheon, Y., Junho, L. and Hoyeol, L. 2014. A study on the solid ammonium SCR system for control of diesel NO<sub>x</sub> emissions. *SAE Tech. Pap.*, 6: 11.
- Koc, S., Tetsuo, N., Nobuyuki, S., Kazuhiro, N., Taiki, M., Shotaro, U. and Daisaku, H. 2018. Design exploration study of exhaust system mixer for emission performance. *Int. J. Automot. Eng.*, 9(4): 202-207.
- Krüger, B., Michael, P.N. and Volker, S. 2003. A compact solid SCR system. *Appl. Therm. Eng.*, 64: 14-17.
- Kurien, C. and Srivastava, A.K. 2018. Geometrical modeling and analysis of automotive oxidation catalysis system for compliance with environmental emission norms. *Nat. Environ Pollut. Technol.*, 17(4): 1207-1212.
- Kurien, C. and Srivastava, A.K. 2019. Solid reductant-based selective catalytic reduction system for exhaust emission control of compression ignition engines. *Nat. Environ Pollut. Technol.*, 18(3): 969-973.
- Kurien, C., Srivastava, A.K., Gagan, A., Shivam, S., Vivek, S. and Vaibhav, T. 2018. Application of selective catalytic reduction system for exhaust emission control of compression ignition engines. *Nat. Environ Pollut. Technol.*, 1: 11-22.
- Lamas, M.I. and Rodriguez, C.G. 2017. A numerical model to analyze NO<sub>x</sub> reduction by ammonia injection in diesel-hydrogen engines. *Int. J. Hydro Energy*, 42(41): 26132-26141.
- Latha, H.S., Prakash, K.V., Veerangouda, M., Devanand, M. and Ramappa, K.T. 2019. A review on SCR system for NO<sub>x</sub> reduction in the diesel engine." *Int. J. Curr. Microbiol. Appl. Sci.*, 8(04): 1553-59.
- Lee, S.H., Kwak, J.H., Lee, S.Y. and Lee, J.H. 2015. On-road chasing and laboratory measurements of exhaust particle emissions of diesel vehicles equipped with aftertreatment technologies (DPF, urea-SCR). *Int. J. Auto. Tech.*, 16(4): 551-559.
- Li, J., Ge, Y., He, C., Tan, J., Peng, Zihang. And Li, Z. 2017. The application of solid selective catalytic reduction on a heavy-duty diesel engine. *SAE Tech Paper*, 10: 17.
- Li, J., Shi, Y. and Meng, X. A review on selective catalytic reduction of NO<sub>x</sub>. *SAE Tech Paper*, 11: 20.
- Ma, Q., Zhang, D. and Gan, X. 2019. Simulation of the flow field and the chemical reaction coupling of selective catalytic reduction (SCR) system using an orthogonal experiment. *PLOS ONE*. 2019;14(7):e0216138. doi: 10.1371/journal.pone.0216138
- Mamakos, A., Martini, G. and Manfredi, U. 2013. Assessment of the legislated particle number measurement procedure for euro 5 and euro 6 compliant diesel passenger cars under-regulated and unregulated conditions. *J Aerosol. Sci.*, 55: 31-47. doi: 10.1016/j.jaerosci.2012.07.012.
- Martinovic, F., Andana, T., Piumetti, M., Armandi, M., Bonelli, B. and Deorsola, F.A. 2020. Simultaneous improvement of ammonia-mediated NO<sub>x</sub> SCR and soot oxidation for enhanced SCR-on-filter application. *Appl. Cat. A*, 10: 596. doi: 10.1016/j.apcata.2020.117538.
- Mehdi, G., Zhou, S., Zhu, Y., Shah, A. and Chand K. 2019. Numerical investigation of SCR mixer design optimization for improved performance. *Processes*, 7(3): 168. doi: 10.3390/pr7030168.
- Mohankumar S and Senthilkumar P. 2017b. Particulate matter formation and its control methodologies for diesel engine: A comprehensive review. *Renew. Sustain. Energy. Rev.*, 80: 1227-38. doi: 10.1016/j.rser.2017.05.133.
- Mohankumar, S. and Senthilkumar, P. 2017a. Particulate matter formation and its control methodologies for diesel engine: A comprehensive review. *Renew. Sustain. Energy. Rev.*, 80: 1227-1238. doi: 10.1016/j.rser.2017.05.133.
- Peng, Y., Li, J., Si, W., Luo, J., Wang, Y. and Fu, J. 2015. Deactivation and regeneration of a commercial SCR catalyst: comparison with alkali

- metals and arsenic. *Appl. Cat. B.*, 168-169: 195-202. doi: 10.1016/j.apcatb.2014.12.005.
- Phaily, A., Kumar, M., Sreekala, S.J. and Padmanabha, M. 2014. The experimental and simulation study of selective catalytic reduction system in a single cylinder diesel engine using NH<sub>3</sub> as a reducing agent. *Int. J. Chem. Eng.*, 2: 14.
- Praveena, V. and Martin, M.L.J. 2018. A review of various after-treatment techniques to reduce NO<sub>x</sub> emissions in a CI engine. *J Energy Inst.*, 91(5): 704-720. doi: 10.1016/j.joei.2017.05.010.
- Qi, Z., Li, S. and Guo, X. 2016. Development, application, and direction of development of urea-SCR. *Int. J. Multimed. Ubiq. Eng.*, 11(6): 131-142. doi: 10.14257/ijmue.2016.11.6.12.
- Qian, F., Ma, D., Zhu, N., Li, P. and Xu, X. 2019. Research on optimization design of SCR nozzle for national VI heavy-duty diesel engine. *Catalysts*, 9(5): 452. doi: 10.3390/catal9050452.
- Qu, D.W., Liu, S.H., Fan, L.Y. and Ma, J.Y. 2014. 2014a. Nozzle opening time's impact on flow characteristics of SSCR. *Appl. Mech. Mater.*, 50: 718-721. doi: 10.4028/www.scientific.net/AMM.644-650.718.
- Qu, D.W., Zhang, K., Fan, L.Y. and Gao, H.B. 2014b. Simulation study for mixing characteristics of NH<sub>3</sub> and automobile exhaust in the SSCR system. *Appl. Mech. Mater.*, 596: 755-759. doi: 10.4028/www.scientific.net/AMM.596.755.
- Qu, D.W., Zhang, K., Fan, L.Y. and Gao, H.B. 2014c. Simulation study for mixing characteristics of NH<sub>3</sub> and automobile exhaust in the SSCR system. *Appl. Mech. Mater.*, 596: 755-59. doi: 10.4028/www.scientific.net/AMM.596.755.
- Re ito lu, .A., Altini ik, K. and Keskin, A. 2015. The pollutant emissions from diesel-engine vehicles and exhaust after-treatment systems. *Clean Technol. Environ. Policy*, 17(1): 15-27. doi: 10.1007/s10098-014-0793-9.
- Tan, L., Feng, P., Yang, S., Guo, Y., Liu, S. and Li, Z. 2018. CFD studies on the effects of SCR mixers on the performance of urea conversion and mixing of the reducing agent. *Chem. Eng. Process Intensif.*, 123: 82-88. doi: 10.1016/j.cep.2017.11.003.
- Tayamon, S and Wigren, T. 2016. Control of selective catalytic reduction systems using feedback linearization. *Asian J. Control*, 8(3): 802-816. doi: 10.1002/asjc.1164.
- Tian, X., Xiao, Y., Zhou, P., Zhang, W., Chu, Z. and Zheng, W. 2015. Study on the mixing performance of static mixers in selective catalytic reduction (SCR) systems. *J. Mar. Eng. Technol.*, 14(2): 57-60. doi: 10.1080/20464177.2015.1096615.
- Torp, T.K., Hansen, B.B., Vennestrøm, P.N.R, Janssens, T.V.W., Jensen, A.D., Klint, B., Brun, H. and Peter, N.R. 2021. Modeling and optimization of multi-functional ammonia slip catalysts for diesel exhaust after-treatment. *Emission Control Sci. Technol.*, 7(1): 7-25. doi: 10.1007/s40825-020-00183-x.
- Wang, M., Liu, X., Bao, J., Li, Z. and Hu, J. V. 2021. Simulation study on prediction of urea crystallization of a diesel engine integrated after-treatment device. *ACS Omega*, 6(10): 6747-56. doi: 10.1021/ACS omega.0c05785, PMID 33748588.
- Wang, X., Westerdahl, D., Hu, J., Wu, Y., Yin, H. and Pan, X. 2012. On-road diesel vehicle emission factors for nitrogen oxides and black carbon in two Chinese cities. *Atmos. Environ.*, 46: 45-55. doi: 10.1016/j.atmosenv.2011.10.033.
- Wardana, A., Khristamto, M., Hyun, J. and Lim, O. 2019. A study of urea injection timing to predict the NO<sub>x</sub> conversion in SCR systems. *Energy Proced.*, 158(2018): 1942-1948.
- Williams, M. and Minjares, R. 2016. Report: A technical summary of Euro 6/VI vehicle emission standards. *Int. Council Clean Transp.*, 6: 1-12.
- Woo, S.H., Noh, J.H., Raza, H. and Kim, H. 2021. Numerical modeling of sublimation of ammonium carbamate applied to supply system of Nox reductant. *Energies*, 214(13): 1-11. doi: 10.3390/en14133795.
- Yadav, M.K. and Srivastava, A.K. 2021. Solid selective catalytic reduction: A promising approach towards reduction of NO X emission from the exhaust of CI engines. *NEPT*, 20(4): 1-8. doi: 10.46488/NEPT.2021.v20i04.031.
- Yuan, X., Liu, H. and Gao, Y. 2015. Diesel engine SCR control: Current development and future challenges. *Emission Control Sci. Technol.*, 1(2): 121-133. doi: 10.1007/s40825-015-0013-z.
- Zhang, H., Wang, J. and Wang, Y.Y. 2016. Optimal dosing and sizing optimization for a ground-vehicle diesel-engine two-cell selective catalytic reduction system. *IEEE Trans. Veh. Technol.*, 65(6): 4740-4751. doi: 10.1109/TVT.2015.2476760.
- Zhang, Y., Lou, D., Tan, P. and Hu, Z. 2018. Experimental study on the particulate matter and nitrogenous compounds from diesel engines retrofitted with DOC+CDPF+SCR. *Atmos. Environ.*, 177: 45-53. doi: 10.1016/j.atmosenv.2018.01.010.





# Production and Characterization of Nano-Chitosan from Blood Clamshell (*Anadara granosa*) by Ionic Gelation

A. Ma'ruf \*† and S. Hartati\*

\*Chemical Engineering Department of Universitas Muhammadiyah Purwokerto Jl. K.H. Ahmad Dahlan, Dukuh Waluh, Kembaran, Purwokerto, 53182, Indonesia

†Corresponding author: A. Ma'ruf; anwarump@yahoo.com

## Nat. Env. & Poll. Tech.

Website: [www.neptjournal.com](http://www.neptjournal.com)

Received: 17-01-2022

Revised: 01-02-2022

Accepted: 10-03-2022

## Key Words:

Nano-chitosan  
Blood clamshell  
Ionic gelation

## ABSTRACT

Nano-chitosan can be produced from blood clams (*Anadara granosa*) because they contain 14-35% of chitin. The production of nano-chitosan can be conducted by a bottom-up process using sodium tripolyphosphate (Na-TPP). The aims of this study are to produce nano-chitosan from blood clamshell and to study the factor affecting the particle size of nano-chitosan such as the ratio of chitosan to Na-TPP solution (v/v) and rotation speed of the centrifuge. The research shows that The chitin content on blood clamshell is 25.42%. The yield of chitosan from chitin is about 80.92%. The degree of deacetylation of chitin from blood clamshell reaches 63.18%. The effect of the ratio of chitosan to Na-TPP solution (R) and the rotation speed of centrifuge (N) on the particlesize of nano-chitosan can be expressed by equation  $dp = 0.12 (R)^{0.714} (N)^{0.99}$ .

## INTRODUCTION

Blood Clam (*Anadara granosa*) is one of the Indonesian traditional food obtained from rivers. The use of blood clams as food leaves waste in the form of the clamshell. Therefore, it is necessary to study the utilization of clamshell waste so that it is not polluting the environment. Several studies have been carried out on the utilization of clamshell waste in various fields.

Clamshells can be used as the raw material of amorphous calcium phosphate (CPP-ACP) paste as teeth remineralization material (Asmawati et al. 2018). The clamshells can be used as filler on polyester resin particle boards due to the high calcium carbonate content in the clamshells (Ginting et al. 2017). One of the potential uses of the clamshell is the manufacture of nano chitosan (Avadi et al. 2010, Zhao et al. 2011, Patiño-Ruiz et al. 2020).

There are two methods to produce nano-chitosan from blood clamshells. The first method is the top-down method. In this method, chitosan is milled from a micrometer particle size to obtain a nanometer particle size (Rochima et al. 2017). The second method is the bottom-up method, where nanoparticles are formed due to assembly between macromolecules from the solutions (Nugraheni et al. 2019).

This research will examine the process of production of nano-chitosan from blood clamshells using the ionic gelation method. The ionic gelation method is a bottom-up meth-

od. Furthermore, this study will examine the effect of the ratio of chitosan to Na-TPP solution (v/v), and the rotation speed of the centrifuge on the diameter of the particle size of nano-chitosan formed.

## MATERIALS AND METHODS

### Materials

Blood clamshell (*Anadara granosa*) was obtained from the local market at Banyumas Regency, sodium hydroxide (NaOH), hydrochloric acid (HCl), sodium tripolyphosphate (Na-TPP), and acetic acid (CH<sub>3</sub>COOH) were obtained from Merck.

### Clamshell Preparation

Blood clamshells were washed using running water to clean the remaining dirt. The next stage was drying under the sun until they were completely dry. Then the blood clamshells were crushed until they become smaller in size. They were then milled using high-energy milling (HEM) to produce a fine powder. The blood clamshell powder was then sieved using a 100 mesh sieve.

### Chitosan Preparation

There were several steps carried out for the isolation of chitosan from blood clamshells, including the deproteinization stage, demineralization stage, and deacetylation stage.

**Deproteinization Stage:** The blood clamshell powder was weighed to 100 g and put into a glass beaker. Then, 3.5% (w/v) NaOH solution was added in a ratio of 1:10 (w/v). Then heated at 70°C for 2 h with stirring. In the next stage, the mixture was filtered and washed using aqua dest until a neutral pH. The solid obtained was dried in an oven at 60°C to obtain a constant weight.

**Demineralization Stage:** The powder resulting from the deproteinization stage was put into a glass beaker flask, and 1N HCl was added in a ratio of 1:10 (w/v). The mixture was put at room 30°C for immersion, then heated at 75°C for 1 h with stirring. In the next stage, the mixture was filtered and washed using aqua dest until a neutral pH. The solid obtained was dried in an oven at a temperature of 60°C to obtain a constant weight. Then, as a result, chitin product was obtained from blood clamshells.

**Deacetylation Stage:** The chitin powder obtained from the demineralization stage was weighed to 10 g, put into a third glass beaker, and then heated at a temperature of 90°C for 3 h with stirring. In the next stage, the mixture was filtered and washed using aqua dest until a neutral pH. The solid obtained was dried in an oven at a temperature of 60°C to obtain a constant weight. The next step was to weigh the chitosan from the blood clamshell powder obtained.

#### Preparation of Nano Chitosan Using Ionic Gelation Method

The amount of 1% chitosan solution was made in acetic acid solution. The solution was added with 1% Na-TPP solution with a variation of the ratio of chitosan to Na-TPP solution 1:1; 2:1; 3:1; 4:1; 5:1 with a rotation speed of centrifuge of 500; 600; 700; 800 and 900 rpm. The stirring was done for 1 h. The nano chitosan obtained was in the form of a dispersed solid.

#### Determination of Physical Characteristics of Nano-chitosan

**FTIR Spectroscopy:** The degree of chitosan deacetylation was determined using the Fourier Transform Infrared (FTIR) spectrophotometer analysis. In the analysis of the FTIR spectrophotometer, the chitosan sample obtained was then inserted into the sample container, and its infrared absorption spectrum was recorded at a wavenumber of 4000-400 cm<sup>-1</sup>. The chitosan obtained was tested using FTIR spectroscopy, and the resulting peak was compared with the peak of commercial chitosan. Based on the peak obtained, the degree of deacetylation was calculated by comparing the absorbance of the wavelength of the amide group (1650-1500) cm<sup>-1</sup> (A1655) with the absorbance of the wavelength of the amine group (3750-3000) cm<sup>-1</sup>. The chitosan deacetylation degree

was calculated using Equation (1) (Antonino et al. 2017).

$$DD = 100 - \left( \frac{A_{1655}/A_{3450}}{1.33} \right) \times 100 \quad \dots(1)$$

Where A1655 is an amine group and A3450 is a hydroxyl group.

**Particle Size of Nano-Chitosan:** The Particle size of nano-chitosan was analyzed using a particle size analyzer (PSA).

## RESULTS AND DISCUSSION

### Blood Clamshell Preparation

Blood Clamshell (*Anadara granosa*) could be used as chitosan because they contain 14-35% chitin (Salsabila et al. 2022). The preparation of raw materials included washing, drying, crushing, milling, and sieving. This stage aimed to expand the surface of the blood clamshell, as shown in Fig.1. The larger the surface area of the shells produced, the easier it was for the blood clamshell powder to react during the isolation process. This was due to the increased reaction rate with increasing surface area and increased quality of the resulting product.

### Chitosan Isolation

**Deproteinization Stage:** The deproteinization stage is the process of removing the protein contained in chitin in the shell of blood clams. Deproteinization can be done by adding chemical reactions such as sodium hydroxide (NaOH) (Antonino et al. 2017). Deproteinization using chemical reagents causes random cleavage of the acetyl group of chitin, resulting in a high degree of deacetylation. The sample used is 1:10 (w/v). After the blood clamshells were washed, dried, crushed, milled, and sieved, the blood clamshell powder was weighed 100 g and dissolved in 1000 mL NaOH with a concentration of 3.5%. Then stirred and heated for 2 h at a temperature of 70°C (kept constant). It was then cooled, and the blood clamshell powder was filtered through filter paper. The residue was filtered and neutralized using aqua dest to a neutral pH and then dried in an oven at 60°C for 1 h. The sample weight was obtained after weighing 88.68 g. Fig. 2 shows the blood clamshell after the deproteinization process. According to Percot et al. (2003), the protein content on clamshell contains amino acids, acidic amino acids corresponding to aspartic and glutamic acids, basic amino acids represented by lysine, histidine, and arginine, and nonpolar amino acids especially proline, alanine, valine, isoleucine, and leucine.

**Demineralization Stage:** The demineralization stage is

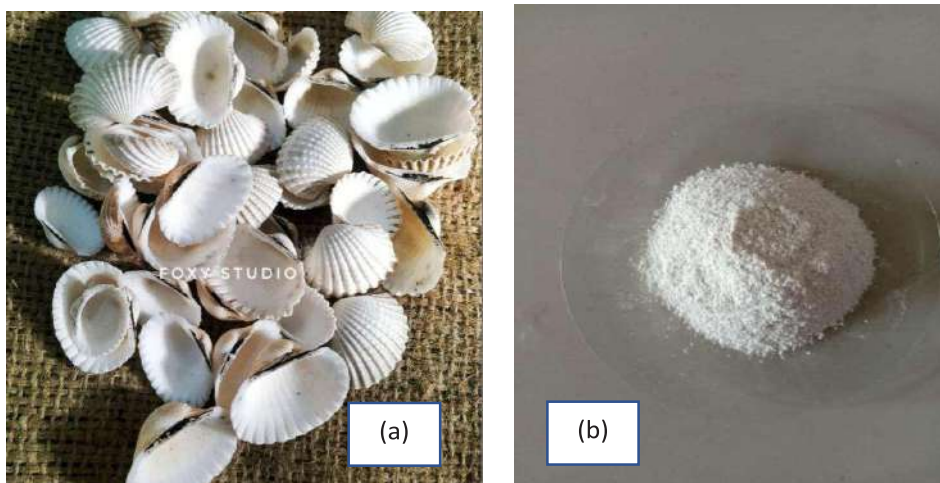
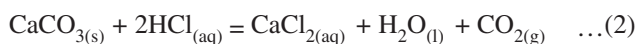


Fig. 1: Blood clamshell: (a) raw material; (b) clamshell powder.

the stage of removing minerals from chitin. The minerals contained in the shells of blood clams are  $\text{Ca}_3(\text{PO}_4)_2(\text{s})$  and  $\text{CaCO}_3(\text{s})$ . Demineralization can be done by adding chemical reactions such as hydrochloric acid (HCl). The use of HCl is carried out to dissolve  $\text{Ca}^{2+}$  ions in the form of  $\text{CaCO}_3(\text{s})$  to produce water-soluble  $\text{CaCl}_2(\text{aq})$  with  $\text{CO}_2$  gas and water as byproducts.  $\text{CaCO}_3(\text{s})$  in blood clamshell powder will react with HCl to form bubbles that indicate  $\text{CO}_2$  gas. The reaction is shown in Equation (2).



Meanwhile,  $\text{Ca}_3(\text{PO}_4)_2(\text{s})$  will react to HCl according to the product  $\text{CaCl}_2$  and  $\text{H}_3\text{PO}_4$  which is soluble in water. The reaction is shown in Equation (3).



Fig. 2: Blood clamshell powder after deproteinization process.

Heating in the demineralization process was carried out to accelerate the process of mineral destruction. In addition, stirring was needed to avoid the overflow of  $\text{CO}_2$  gas during the demineralization process. This mixture was then stirred using a magnetic stirrer for 2 h at  $75^\circ\text{C}$ . Furthermore, the resulting residue was washed until the pH was neutral. This washing was carried out to dissolve  $\text{CaCl}_2(\text{aq})$  and  $\text{H}_3\text{PO}_4(\text{aq})$ , which were soluble in water. After the blood clamshells passed through the deproteinization process, the sample weight was obtained in powder, weigh and the results were 88.68 g from 100 g of the initial sample before being isolated. Next, 1 N HCL was added in a ratio of 1:10 (w/v). Then it was stirred and heated at  $75^\circ\text{C}$  for 2 h (kept constant). The residue was filtered and neutralized using aqua dest to a neutral pH. Then the sample (residue) was put into an oven for 1 hour at  $60^\circ\text{C}$ . Then the sample was weighed, and the result was 25.42 g. It can be concluded that the chitin content on blood clamshells is 25.42%.

**Deacetylation:** The deacetylation process is the process of removing the acetyl group by adding an alkaline solution. The alkaline solution used was Sodium Hydroxide or (NaOH). The severance of the acetyl group in the chitin of blood clamshells was carried out through a deacetylation process using 65% NaOH at  $90^\circ\text{C}$  for 30 minutes. The precipitate (residue) obtained was washed and dried to a neutral pH. Blood clamshell chitosan produced was a grayish-white powder, while commercial chitosan had a yellowish flat shape, as shown in Fig. 3. The yield of chitosan from blood clamshells obtained after drying was 80.92%.

Fig. 4 shows the FTIR spectra of chitosan from blood clamshells and commercial chitosan. Two peaks have high intensity, namely at wavelengths 1419.61 and  $3356.14 \text{ cm}^{-1}$ .

<sup>1</sup>. The wavelength of  $1419.61\text{ cm}^{-1}$  corresponds to the C-H side-chain bending  $-\text{CH}_2\text{OH}$  (Varma & Vasudevan 2020). While the wavelength of  $3356.14\text{ cm}^{-1}$  shows amino groups (Ali & Gherissi 2017). The degree of deacetylation of blood clamshell reaches 63.18%, while commercial chitosan reaches 73.35%. Varma and Vasudevan (2020) on the process of chitosan isolation from horse mussel (*M. modiolus*), the degree of deacetylation only reaches 57.43%.

### Nano-Chitosan Production Using Ionic Gelation Method

The production of nano-chitosan using the ionic gelation method was conducted by making a solution of chitosan. The amount of 1% chitosan solution was made in acetic

acid solution. The chitosan solution was then reacted with 1% Na-TPP solution with a variation of the ratio of chitosan to Na-TPP solution (v/v). The mixture was then stirred at various speeds for 1 hour. The nano chitosan obtained was in the form of a dispersed solid. The particle size of nano-chitosan was then measured by a particle size analyzer (PSA). Fig. 5 shows the schematic reaction of chitosan and sodium triphosphate (Madni et al. 2017).

### Effect of Ratio of Chitosan to Na-TPP Solution

Fig. 6 shows the particle size of nano-chitosan at the various ratio of chitosan to Na-TPP solution at the rotation speed of 700 rpm. The greater the ratio of the chitosan solution, the larger the nano size of the chitosan formed. The approxima-

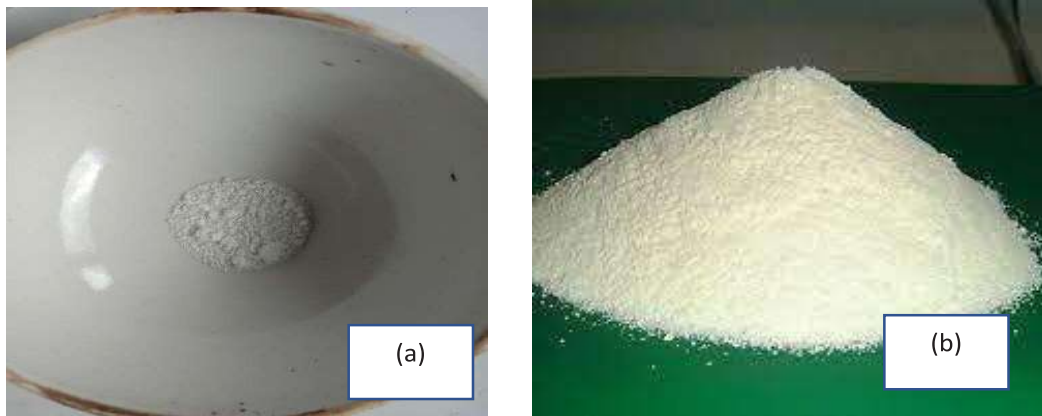


Fig. 3: Chitosan: (a) From blood clamshell; (b) commercial chitosan.

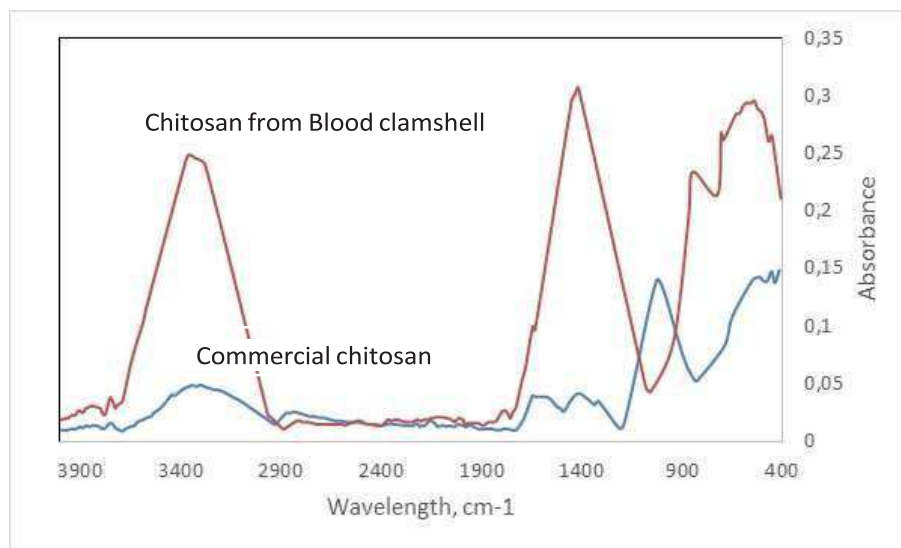


Fig. 4: FTIR spectra of chitosan from blood clamshell and commercial chitosan.

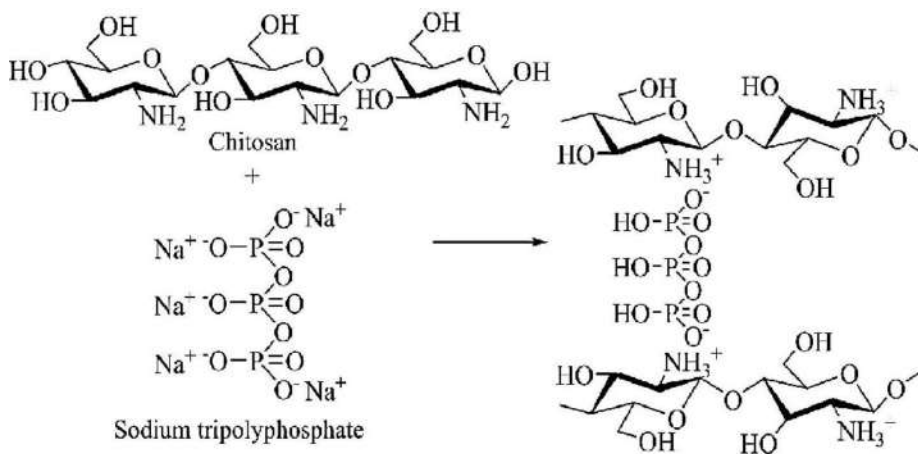


Fig. 5: schematic reaction of chitosan and sodium triphosphate.

tion equation can be expressed by equation (4).

$$dp = 95.55 (R) - 68.142 \quad \dots(4)$$

Where  $dp$  is the particle size of nano-chitosan (nm) and  $R$  is the ratio of chitosan to Na-TPP solution (v/v).

**Effect of Rotation Speed**

Fig. 7 shows the particle size of nano-chitosan at the speed rotation of centrifuge at the ratio of chitosan to Na-TPP solution of 5 v/v. The greater of speed rotation, the size of the nano chitosan formed tends to be greater. The approximation equation can be expressed by equation (5).

$$dp = 61.94 (N) - 3.6344 \quad \dots(5)$$

Where  $dp$  is the particle size of nano-chitosan (nm) and  $N$  is the speed rotation of the centrifuge.

The effect of the ratio of chitosan to Na-TPP solution ( $R$ ) and the rotation speed of centrifuge ( $N$ ) on particle size of nano-chitosan can be expressed by equation (6).

$$dp = 0.12 (R)^{0.714} (N)^{0.99} \quad \dots(6)$$

**CONCLUSION**

Nano-chitosan can be produced from blood clamshell with the ionic gelation method by using sodium triphosphate. The chitin content on blood clamshell is 25.42%. The yield of chitosan from chitin is about 80.92%. The degree of

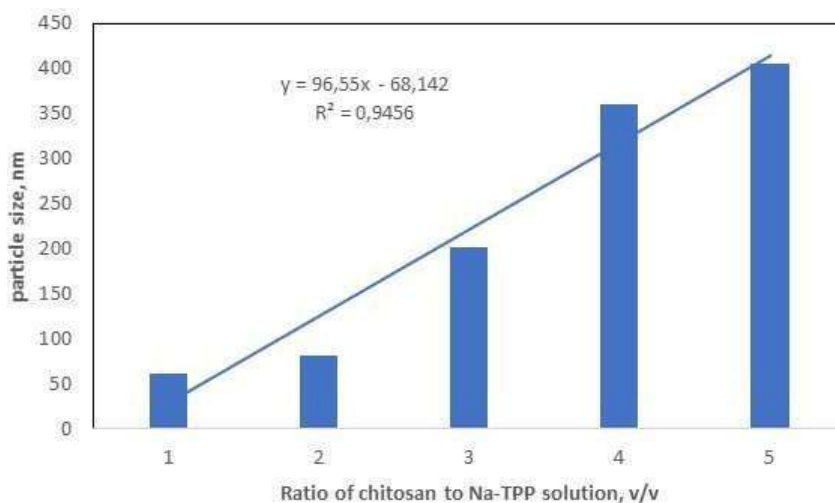


Fig. 6: Particle size of nano-chitosan at various ratio chitosan to Na-TPP solution (v/v).

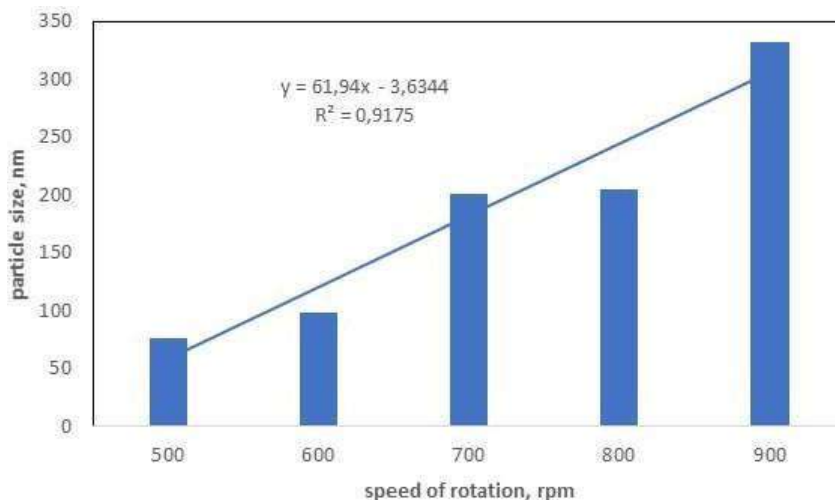


Fig. 7: Particle size of nano-chitosan at various speed rotations of the centrifuge

deacetylation of chitin from blood clamshell reaches 63.18%. The effect of the ratio of chitosan to Na-TPP solution (R) and the rotation speed of centrifuge (N) on the particle size of nano-chitosan can be expressed by equation  $dp = 0.12 (R)^{0.714} (N)^{0.99}$ .

## REFERENCES

- Ali, M. and Gherissi, A. 2017. Synthesis and characterization of the composite material PVA/Chitosan/5% sorbitol with different ratios of chitosan. *Int. J. of Mech. Mechat. Eng.*, 17(2): 15-28.
- Antonino, R.S.C.M.D.Q., Fook, B.R.P.L., Lima, V.A.O.L., Rached, R.I.F., Lima, E.P.N., Lima, R.J.S., Covas, C.A.P. and Fook, M.V.L. 2017. Preparation and characterization of chitosan obtained from shells of shrimp (*Litopenaeus vannamei* Boone). *Mar. Drugs*, 15(5): 1-12.
- Asmawati, A., Thalib, B., Thalib, A.M., Reni, D.S. and Hasyim, R. 2018. Comparison of blood clam (*Anadara granosa*) shell paste, shrimp (*Litopenaeus vannamei*) shell paste, and casein phosphopeptide-amorphous calcium phosphate (CPP-ACP) paste as teeth remineralization material. *J. Dent. Sci.*, 3(3): 162-165.
- Avadi, M.R., Sadeghi, A.M.M., Mohammadpour, N., Abedin, S., Atyabi, F., Dinarvand, R. and Rafiee-Tehrani, M. 2010. Preparation and characterization of insulin nanoparticles using chitosan and Arabic gum with ionic gelation method. *Nanomed.: Nanotech., Biol. Med.*, 6(1): 58-63.
- Ginting, M.H.S., Lubis, M., Suwito, F. and Tanujaya, B. 2017. Effect of clam shell powder (*Anadara granosa*) composition on physical and mechanical properties of polyester resin particle board products. *Asian J. Chem.*, 29(1): 81-85.
- Madni, A., Kashif, P.M., Nazir, I., Tahir, N., Rehman, M., Khan, M.I., Rahim, M.A. and Jabar, A. 2017. Drug-Polymer Interaction Studies of Cytarabine Loaded Chitosan Nanoparticles. *J. Chem. Soc. Pak.*, 39(6): 1045-1054.
- Nugraheni, P.S., Soeriyadi, A.H., Ustadi, S.W.B. and Budhijanto, W. 2019. Comparison of formulation methods to produce nano-chitosan as an inhibitor agent for bacterial growth. *J. of Eng. Technol. Sci.*, 51(3): 431-442.
- Patiño-Ruiz, D., Marrugo, L., Reyes, N., Acevedo-Morante, M. and Herrera, A. 2020. Ionotropic Gelation Synthesis of Chitosan-Alginate Nanodisks for Delivery System and in Vitro Assessment of Prostate Cancer Cytotoxicity. *Int. J. of Polymer Sci.*, 2020: 1-10.
- Percot, A., Viton, C. and Domard, A. 2003. Characterization of shrimp shell deproteinization. *Biomacromolecules*, 4(5): 1380-1385.
- Rochima, E., Azhari, S.Y., Pratama, R.I., Panatarani, C. and Joni, I.M. 2017. Preparation and characterization of nano chitosan from crab shell waste by a beads-milling method. *IOP Conf. Ser.: Mater. Sci. Eng.*, 193.
- Salsabila, C., Wahyuningsih, C., Fitriana, D.A., Asih, R.S., Ferniah, R.S. and Nida, K. 2022. Semi-manual processing of blood clamps wastes into Chitosan powder. *Int. J. Res. Comm. Serv.*, 3(1): 8-12.
- Varma, R. and Vasudevan, S. 2020. Extraction, characterization, and antimicrobial activity of chitosan from horse mussel modiolus. *ACS Omega*, 5(32): 20224-20230.
- Zhao, L.M., Shi, L.E., Zhang, Z.L., Chen, J.M., Shi, D.D., Yang, J. and Tang, Z.X. 2011. Preparation and Application of Chitosan Nanoparticles and Nanofibers. *Brazil. J. Chem. Eng.*, 28(03): 353-362.



# Health Impact Assessment of Air Pollution in India During COVID-19 Lockdown by Using Satellite Remote Sensing and Deep Learning

Sudhir Kumar Chaturvedi

School of Engineering, University of Petroleum and Energy Studies (UPES), Bidholi Energy Acres, Dehradun-248007, India

†Corresponding author: Sudhir Kumar Chaturvedi; [sudhir.chaturvedi@ddn.upes.ac.in](mailto:sudhir.chaturvedi@ddn.upes.ac.in)

Nat. Env. & Poll. Tech.  
Website: [www.neptjournal.com](http://www.neptjournal.com)

Received: 26-11-2021

Revised: 23-02-2022

Accepted: 24-02-2022

## Key Words:

COVID-19

Deep learning

Air quality assessment

Air pollution

Remote sensing

Health impact assessment

## ABSTRACT

Air pollution produces major environmental health problems with a vast number of entropies that can affect healthy, sustainable environments across the globe. Millions of people are dying prematurely each year as a direct cause of poor air quality. According to recent studies, living within 50 meters of any significant road can increase the risk of lung cancer by up to 10%. World Health Organization declares that approximately 3.7 million people died worldwide in 2012 due to outdoor air pollution. In this analysis, we analyzed air pollutants that were released into the air from a wide range of sources, such as motor vehicles, industrial combustion processes, etc. We analyzed the Sentinel-5 precursor data, which provides time series data on a multitude of trace gaseous compounds such as CO, NO<sub>2</sub>, SO<sub>2</sub>, O<sub>3</sub>, PM<sub>10</sub>, PM<sub>2.5</sub> aerosols, etc. with efficient statistics and special resolution. For better comparison, we have trained our statistical atmospheric data with deep learning methodology and analyzed them to obtain a reference for air quality in India. This study describes the scientific aspects and probable atmospheric composition entropy due to pollution. We also presented the overall operational product outcomes and emissions from the energy sectors, which involves the advancement of data analysis in a particular coordinate system.

## INTRODUCTION

COVID-19 was first detected in the Wuhan district of China in December 2019 as per the official report. And after that, this virus kept on spreading all around the world rapidly and it changes the global lifestyle and economy, and a lot more things (Garg et al. 2020). As per reports, the first detected COVID-19 infected person was found in the Kerala district of India on 20<sup>th</sup> January 2020 and the person's travel history had been disclosed which showed that he came from China. And after this, Kerala became the first state of India to have numerous COVID-19 positive cases by community spreading. And till now more than ten lakh COVID-19 positive cases have been detected in India (Suresh et al. 2020). The highest and lowest instances due to COVID-19 have been reported in Maharashtra and Mizoram, respectively. In this regard, a 21-day national Curfew/Lockdown was declared by the central government. As per the announcement of the Lockdown in India, all the Academic institutes, industries, markets, all people, and regional places were shut down until the next announcement. The results after the step were taken by the Government of India ended in fewer numbers of deaths reported in India so much as compared to other countries, and less air pollution in India, especially in Noida

next to New Delhi. The air pollution over Northern India has recently recorded a 20-year-low at this period of this entire year (Weblink 2). Fig. 1 exhibits the AEROSOL OPTICAL DEPTH immersion degree in India between 2016 and 2020. Fig. 1 is first created using gathered info set by MODIS (Moderate Resolution Imaging and AURA) that actions dimension distribution and optical depth of surrounding aerosol Across the world on an hourly basis.

The drop in concentration degree of aerosol optical depth (AOD) was projected after just a week of low individual pursuits. The exhibited images are accumulated in NASA Earth Observatory, showing AOD dimensions over the region of Kolkata, Noida, Kanpur, and Chandigarh of India during the time scale of January 31<sup>st</sup> to July 17<sup>st</sup> from 2016 to 2020 (Garg et al. 2020). Furthermore, the past (sixth) anomaly image in Fig. 1, shows that the AOD average in 2020 compared to 2016-2019 (average). It can be observed that black, and brown pixels, tan pixels, and pale yellowish areas reveal high, lower, and little to no aerosol concentrations (Fig. 1). aerosol is among the critical pollutants characterized by domestic and worldwide agencies, associated with mobility and mortality (Garg et al. 2020, Liu et al. 2020, Hadibasyir et al. 2020). In this analysis, the variants of AOD that were collected from

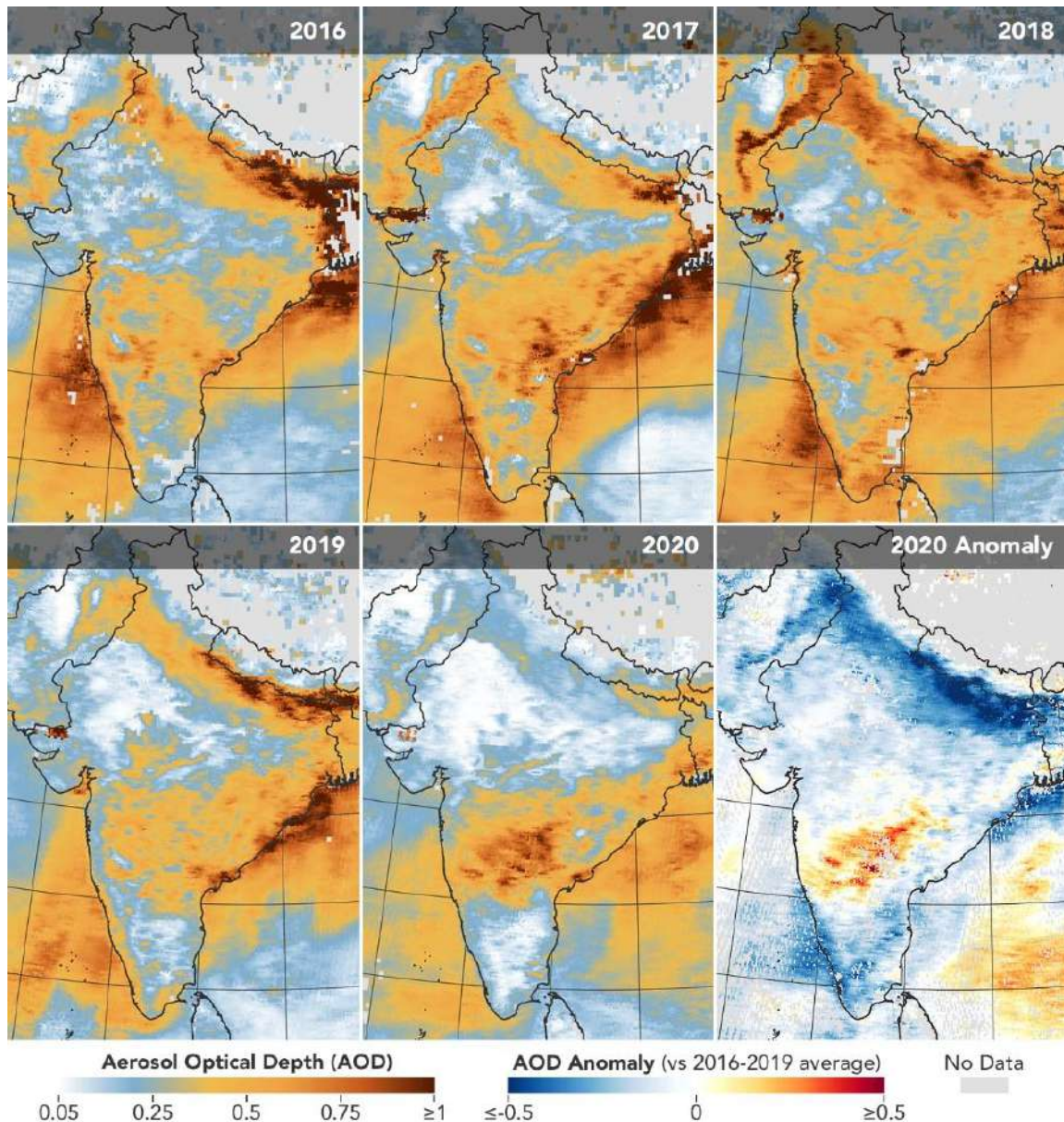


Fig. 1: Sequence of aerosol optical thickness concentration (month-Terra/Modis) in India from the period March 31 to April 5 in 2016, 2017, 2018, 2019, and 2020 (NASA 2020).

the satellite (Sentinel-5P) had been used to signify that a noticeable gap in the amount of aerosol that is at its lowest in twenty years thanks to COVID-19 lock-downs (Weblink 2). The outcome indicates that the spreading coronavirus is thought to be a blessing in disguise. The present status of air quality could be momentary; however, there is a rather great opportunity for us (scientists/researchers/students/humans) to learn/understand from related lock-down activities about how best to minimize the concentration level of air

pollutants (Suresh et al. 2020). Recent events over the past few months have shown results on molecular scales across the globe about an increase in biodegradable aerosol and its environmental effects. However, further research is needed to fully comprehend the open questions based on the interdisciplinary and complex nature of aerosols characterized by their connection to human health. To increase the assessment of mortality due to air pollution, the following conclusions are drawn from epidemiological, global modeling research,



aerosol, and health issues: (1) overall health effects because of specific biotic elements. Their origin can be described from Preliminary studies. The various compound composition/characterization and degradation of biotic components have to be researched. (2) Epidemiological cohort studies are highly essential, particularly in Asian and African countries where aerosol or bioaerosol and its vulnerability established scientific tests have yet to be effortlessly launched. (3) No-Observed-Adverse-Effect Level (NOAEL) or Lowest-Observed-Adverse-Effect Level (LOAEL)-expense devices must know the integration of private vulnerability in the duration of assessments; also (4) the association of lung surfactants and aerosol components will need to be learned. Similar remarks can be implemented to other COVID-19 affected states, as of April 18, 2020, “ there are 2284018 infected people along with 156140 claimed deaths from COVID-19 around the world. This viewpoint shows evidence of major changes in the atmosphere quality of their Indian location throughout the government lockdown intended to lessen the COVID-19 impacts (Mandal et al. 2019, Cheval et al. 2019, Hepburn et al. 2020, Timmermann et al. 2020). The massive reduction in aerosol focus during quarantine and the publication of the coronavirus may, paradoxically, have reduced the percentage of deaths throughout the period by significantly lowering the percentage of fatalities attributable to deterioration of air quality, as stated by the results and discussion.

The coronavirus outbreak will cause a dreadful crisis that will affect the entire world (COVID-19). Based on the escalating rate of COVID-19 episodes around the world, the WHO proclaimed COVID-19 a worldwide pandemic on March 11, 2020. The governments of numerous nations then placed their states on lockdown at the end of March in preparation for a containment strategy. As of 1 June 2020, 374,229 confirmed deaths worldwide and more than 6.2 million COVID-19 cases were reported from 215 states (WHO 2020, Behar et al. 2020, Chamola et al. 2020). Around January 30, 2020, Kerala, a state in India, reported having the country’s first confirmed case of COVID-19. Later, it spread to other parts of the country, and on March 4, 2020, 22 new states were officially recognized. The first COVID-19-related death in the nation was recorded on March 12, 2020 (Weblink 1): The President requested a fourteen-hour curfew on March 22, 2020, from all taxpayers around the country due to the rising number of COVID-19 scenarios. In response, India’s government declares a total national emergency for 21 consecutive days, starting at midnight on March 2–4, 2020. The government required Indian residents to closely adhere to the social distancing measures as a preventive strategy to manage the worsening of the pandemic in the nation (Kumar et al. 2020). All public meeting places, including restaurants,

movie theatres, schools, shopping centers, and educational institutions, were closed during the statewide lockdown. To avoid congestion, it was requested that employees and students work from home. All forms of transportation, including highway, railroad, and air travel, were restricted from receiving essential services. Additionally, not all industrial and manufacturing operations were stopped (Tang et al. 2020). Because everyone was asked to stay indoors during the lockdown, save from those providing basic services, the COVID-19 outbreak resulted in deserted and empty streets. The comprehensive lockdown has affected the economy of the United States; however, it also caused some dramatic mitigation in air pollution because of limited transport and economic activities (Chang et al. 2020, Shao et al. 2020). In the current study, we analyzed the variant in air quality data around four different towns in India (particularly, Kolkata, Noida, Kanpur, and Chandigarh) during the lockdown (i.e. January 31<sup>st</sup> to July 17<sup>th</sup>) of the COVID-19 pandemic.

### Air Pollutant Validation from Remote Sensing Data

To verify the pollutants from satellite images, this analysis used the actual data of pollutant (NO<sub>2</sub>) emission quantified from the thirty-eight monitoring stations found in Delhi from where we get the data for the Noida area. The daily mean of NO<sub>2</sub> emission calculated by these stations from January 1, 2020, to April 20, 2020, which expressively depicts both the pre-lockdown and throughout the lock-down period, may indicate that air contamination is higher in some places (Huang et al. 2020). The outcomes demonstrated before the lock-down, the level of NO<sub>2</sub> emission in Noida continues to be around 25 µg.m<sup>-3</sup>

Nevertheless, since the lock-down was declared in India, the level of NO<sub>2</sub> emission showed a dramatic decline. In Noida and its surrounding areas, the actual amount of NO<sub>2</sub> emission throughout the lock-down phase remains 5 to 15 µg.m<sup>-3</sup>. Even the outcomes explain that ahead of the lock-down phase, the amount of NO<sub>2</sub> yet it faced a massive reduction with the beginning of the lockdown in India. The analysis suggests that NO<sub>2</sub> emission remains low during the comprehensive lockdown at Mumbai. Thus, these statistics confirmed that the lockdown in India has imperatively enhanced environmental quality. Also, it confirmed the precision of all the information generated as a result of satellite images (Wei et al. 2020, Zhao et al. 2020, Jing et al. 2020).

### MATERIALS AND METHODS

The data from four different Indian cities, including Noida, Kolkata, Chandigarh, and Kanpur, which are located in the western, northern, and eastern regions of India, respectively, have been evaluated to review the impact of lock-

down on air quality. The Central Pollution Control Board (CPCB) collected the air quality data for three stations in Delhi, and one channel in each of Kolkata, Chandigarh, and Kanpur during the time period from 1) March 1, 2020, through April 15, 2020. Additionally, the high population density of major cities and the large number of people employed there contribute to the heavy traffic on the roads. In cities like Delhi and Noida, daily traffic and industrial emissions are both major contributors to air pollution. In contrast to Delhi and Mumbai, Kolkata, Chandigarh, and Kanpur have a low population index. Although many of India's best crops are grown in Kolkata, Chandigarh, and Kanpur, these cities are among the most polluted in the country as a result. Table 1 lists all the information on the channels that were selected from each city. These channels were selected because they accurately depict and compensate both metropolitan areas.

## RESULTS AND DISCUSSION

India's national lockdown, implemented in preparation for March 25, 2020, has greatly improved the country's air quality. We present statistics on the investigation of air quality in four different places, at varying stages. In the case of Noida, the average daily value of PM10, PM 2.5, and both NO<sub>2</sub> and SO<sub>2</sub> may be seen to have significantly decreased. However, during the post-lockdown phase, the O<sub>3</sub> concentration increased. Fig. (2–5) compares the mean air pollution concentration in the pre- and post-lockdown stages. The results show that during the lockdown, the air quality in the cities improved to a healthy level. The fact that NO<sub>2</sub>, SO<sub>2</sub>, PM10, and PM2.5 levels have all significantly decreased, along with PM10 and PM2.5, is an indication of a healthy

environment. Because of insufficient data sources, a few pollutants are not there in the output. The level of particle matter is typically found to be alarmingly high in Noida and Delhi. However, the lockdown turns out to be beneficial for nature to restore itself.

Fig. 2 of the aforementioned curves show that there were dangerously high levels of pollutants in the air over the Noida area before the lockdown, particularly PM2.5. When the density of particle matter in the air exceeds 60, it becomes detrimental, but in the Noida area, the level was over 200, which was dangerous for human health. However, as nature began to recover itself following the lockdown, the density of contaminants significantly decreased.

Well throughout the lockdown period the pollutants in the atmosphere over the Bidhan Nagar area in Kolkata (Fig.3) became less dense. The density of pollutants in Kolkata is far less than in Noida, Delhi, or Mumbai but still, it was above the danger level. But the lockdown also made the environment considerably cleaner and healthier than it had been.

In Fig.4 the air quality graph of Kanpur has been shown, where, also a positive sign can be seen for air quality. Because fewer fuels are used in the automotive, railroad, and even industrial sectors, all emissions are decreased. During the lockout, nature completely cleaned up the gaseous industrial wastes.

Well in Fig. 5 we can see that the particulate matter in the atmosphere of Chandigarh city throughout the lockdown was fluctuating because of the usage of the private vehicle. Since all industries were shut down during the lockdown, other pollutants like carbon monoxide, sulfur dioxide, nitrogen dioxide, and ozone were all naturally cleaned up.

Table 1: The Air quality levels and health impacts (PM2.5) (Source: CPCB - India Central Pollution Control Board).

AQI	Air Pollution Level	Health Implications	Cautionary Statement (for PM2.5)
0-50	Good	Air quality is considered to be satisfactory, and air pollution poses a minimum risk factor	None
51-100	Moderate	Air quality is acceptable; but, for some pollutants, there may be a moderate health concern for a very minimum number of people who are unusually sensitive to air pollution.	Active infants or children and adults, and people with respiratory disease, should limit prolonged outdoor exertion.
101-150	Unhealthy for Sensitive Groups	People from sensitive groups may experience health effects. The public is not likely to be affected.	Active children and adults, and people with respiratory disease, must limit prolonged outdoor exertion.
151-200	Unhealthy	Everyone may begin to experience health effects; members of sensitive groups may experience more serious health effects	Active children and adults, and people with respiratory disease, should avoid prolonged outdoor exertion; everyone else, especially children, should limit prolonged outdoor exertion
201-300	Very Unhealthy	Health warnings for emergency conditions. The entire population is more likely to be affected.	Active children and adults, and people with respiratory disease, must avoid all outdoor exertion; everyone else, especially children, should limit outdoor exertion.
300+	Hazardous	Everyone may experience more serious health effects.	Everyone should avoid all outdoor exertion

The restrictions placed on commercial, industrial, and transportation-related activities during the post-lockdown period have significantly reduced the major air pollutants (PM<sub>10</sub>, PM<sub>2.5</sub>, SO<sub>2</sub>, and NO<sub>2</sub>). In general, compared to the time before the lockdown, PM<sub>10</sub> and PM<sub>2.5</sub> levels decreased by an average of 55% and 49.34%, respectively. Since transportation accounts for 60% of Noida's NO<sub>2</sub> emissions,

transportation limitations caused NO<sub>2</sub> levels to drop by over 70% throughout the lockdown. However, a minimal decrease of 25 percent at SO<sub>2</sub> levels throughout the post-lockdown phase were noticed since the principal source of SO<sub>2</sub> in Noida are electrical power plants that remained operational during the lockdown span. Noticeably, O<sub>3</sub> immersion climbed by 37.35% in the post-lockdown period due to various rea-

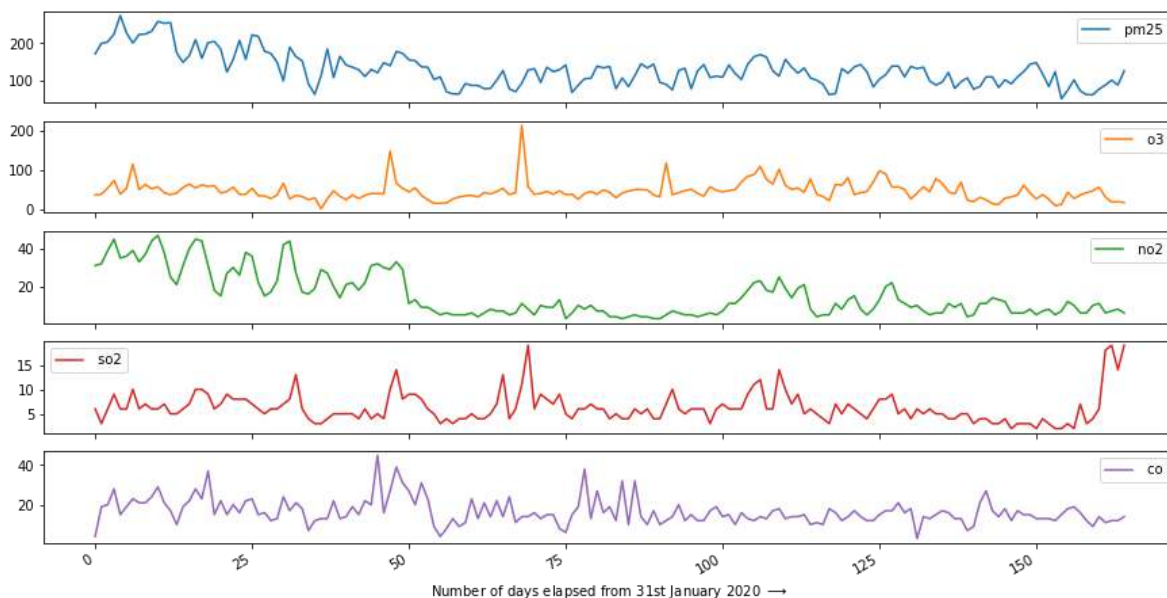


Fig. 2: Air quality graph of different pollutants in sector 1 Noida during the lockdown.

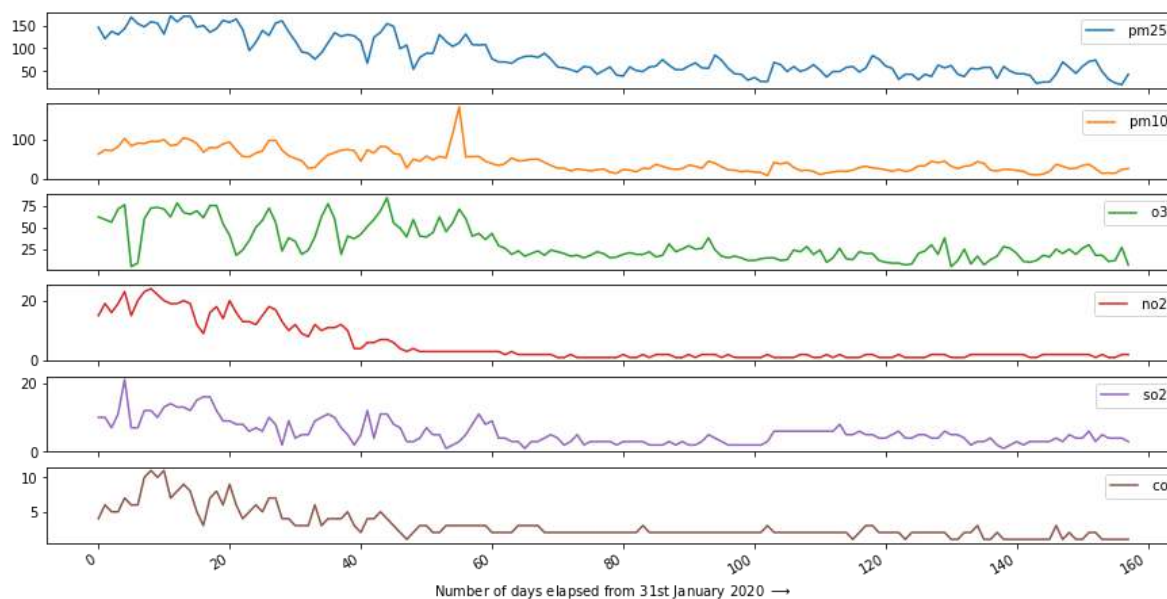


Fig. 3: Reduced air pollution levels at Bidhan Nagar, Kolkata during the lockdown.

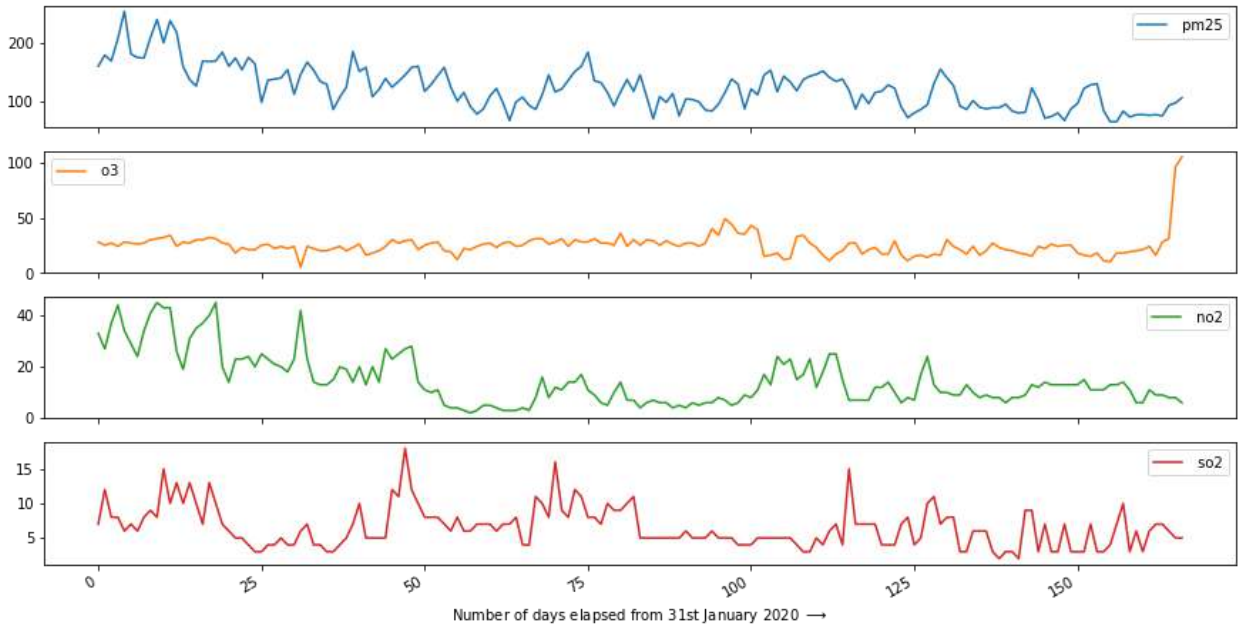


Fig. 4: Air quality graph of Nehru Nagar, Kanpur during the lockdown.

sons. The decrease in  $\text{NO}_2$  levels minimize  $\text{O}_3$  ingestion, which ends in increment at  $\text{O}_3$  levels; Consequently, once summer arrived, the temperature began to rise, going from a minimum and maximum of  $15^\circ\text{C}$  and  $27^\circ\text{C}$  on March 1 to  $24^\circ\text{C}$  and  $40^\circ\text{C}$  on April 15, 2020. This has caused an increase

in  $\text{O}_3$  dosages. All vital air pollutants (excluding  $\text{O}_3$ ) have been reduced throughout the lockdown phase. The focus of essential pollutants (i.e.  $\text{PM}_{10}$ ,  $\text{PM}_{2.5}$ , both  $\text{SO}_2$  and  $\text{O}_3$ ) has shown a growing trend during the post-lockdown stage. During the lockdown, the daily average  $\text{NO}_2$  and  $\text{SO}_2$  levels

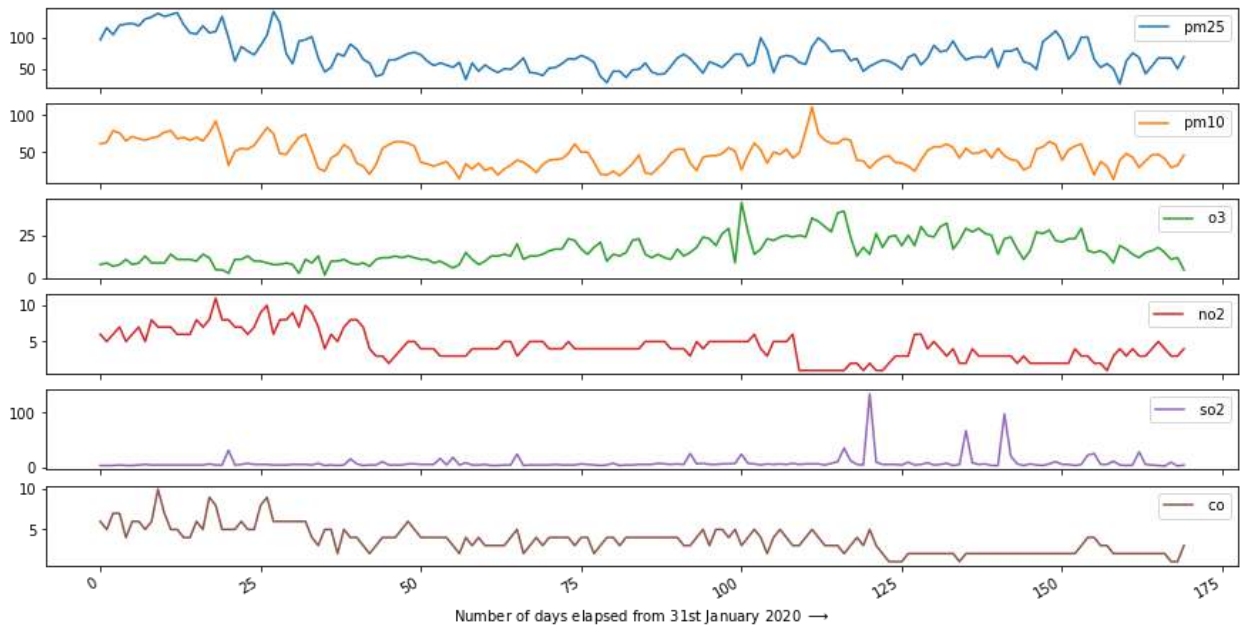


Fig. 5: Air pollutants curve throughout the lockdown period of Chandigarh during the lockdown.

mostly remained below the NAAQS standard value. Nevertheless, during the post-lockdown period, the PM<sub>10</sub> and PM<sub>2.5</sub> concentrations were higher than the NAAQS benchmark value. When compared to the Noida area, it may be observed that Kolkata, Chandigarh, and Kanpur are still among the top SO<sub>2</sub> metropolises. The majority of this pollution is caused by the largest coal-fired power plants located in these cities. All pollutants (besides NO<sub>2</sub>) demonstrate higher mean immersion levels throughout the post-lockdown phase, as compared to the pre-lockdown stage. Although NO<sub>2</sub> levels in Kolkata, Chandigarh, and Kanpur decreased by only 13% during the lockdown, it was much less than in the Noida area. The concentration of PM<sub>10</sub>, PM<sub>2.5</sub>, SO<sub>2</sub>, and O<sub>3</sub> has significantly increased in Kolkata, Chandigarh, and Kanpur during the lockdown.

## CONCLUSION

Globally, COVID-19 has a significant impact on both men's and women's lifestyles. This exposed a remarkable viewpoint on both domestic and foreign transportation. On the other hand, lockdown slows the economic circles on the Earth. The research disclosed that the level of nitrogen dioxide emission was reduced. This impact is significantly clearer in Noida, Kolkata, along with individual cities in Gujarat. Additionally, India's use of electricity has decreased in March 2020. However, the Indian electrical power generation facility has the potential to emit a significant amount of nitrogen dioxide. Lockdown has also affected ship transportation, in addition. The study found that the level of nitrogen dioxide along the Indian Ocean's maritime route has decreased. Additionally, the study verified these results at numerous monitoring stations for the local environment in Noida. The examination confirmed that the lockdown has proved to be a boon for the quality of air in India. These results give new insights into government officials, academicians, research workers, and contamination control governments. Although COVID-19 poses a serious threat to both the general public's health and security as well as the global economy, it has shown to have a good impact on the environment as pollution is declining and the ground is gradually regenerating itself. The present study successfully analyzed the effect of a complete national lockdown since March 25, 2020, on-air quality of leading Indian cities: Delhi, Mumbai, Kolkata, Chandigarh, and Kanpur. A significant reduction in the concentration of PM<sub>10</sub>, PM<sub>2.5</sub>, and NO<sub>2</sub> had been detected for Delhi and Mumbai during the lockdown span. But, O<sub>3</sub> focus had been raised throughout lockdown, which could be attributed to less consumption of O<sub>3</sub> at titration because of a decrease in NO<sub>2</sub> emission. Overall significant advancement in the atmosphere grade of Delhi and Mumbai was discovered throughout the lock-

down phase compared to the pre-lockdown phase, exactly the equal period of 20-19. Nevertheless, Kolkata, Chandigarh, and Kanpur have not shown much decrease in smog due to operational coal-based power plants. The preliminary investigation of air quality information in current research indicates the COVID-19 pandemic may be regarded as a 'boon in disguise,' where air quality is advancing and also the ground is reviving itself. This reduction in air pollution because of managed emission of significant air pollutants can significantly reduce several wellness problems like respiratory difficulties and cardiovascular disease such as asthma, early death, etc. This constructive impact of lockdown on atmosphere pollution can offer confidence to the authorities and government that the implementation of strict quality air coverages and energy control plans may dramatically improve environmental and human wellness.

## ACKNOWLEDGEMENT

The authors would like to thank UPES Dehradun for facilitating the space to carry out the research work. Corresponding author thanks Mr. Saikat Banerjee and Sourav Basu, Mr. Subhrangshu Adhikary of CubicX India for the great support in terms of the data processing and analysis

## REFERENCES

- Behar, J.A., Chengyu, L., Kenta, T., Valentina, D.A., Corino, J.S., Marco, A.F.P. and Walter, K. 2020. Remote health monitoring in the time of COVID-19. *arXiv*, 8: 537.
- Chamola, V., Vikas, H., Vatsal, G. and Mohsen, G. 2020. A comprehensive review of the COVID-19 pandemic and the Role of IoT, Drones, AI, Blockchain, and 5G in managing its impact. *IEEE Access* 8: 90225-90265.
- Chang, Y., Hsin-Ta, C., Satheesh, A., Yo-Ping, H., Yi-Ting, T. and Kuan-Ming, L. 2020. An LSTM-based aggregated model for air pollution forecasting. *Atmos. Pollut. Res.*, 6: 55-72
- Cheval, S., Cristian, M., Adamescu, T., Georgiadis, M., Hermegger, A., Piticar, R. and David, L. 2019. Observed and potential impacts of the COVID-19 pandemic on the environment. *Int. J. Environ. Res. Pub. Health*, 17(11): 4140.
- Garg, V., Shiv, P.A. and Prakash, C. 2020. Changes in turbidity along Ganga River using Sentinel-2 satellite data during lockdown associated with COVID-19. *Geom. Nat. Hazards Risk*, 11(1): 1175-1195.
- Hadibasyir, H., Zaky, S., Samsu, R. and Dewi, R.S. 2020. Comparison of land surface temperature during and before the emergence of Covid-19 using modis imagery in Wuhan City, China. *Geografi*, 34(1): 202.
- Hepburn, C., Brian, O., Nicholas, S., Joseph, S. and Dimitri, Z. Will COVID-19 fiscal recovery packages accelerate or retard progress on climate change? *Oxford Rev. Econ. Policy*, 36: 220.
- Huang, L., Qiuzhi, P. and Xueqin, Y. 2020. Change detection in multitemporal high spatial resolution remote-sensing images based on saliency detection and spatial intuitionistic Fuzzy C-Means clustering. *J. Spectr.*, 19: 20.
- Jing, F., Akshansa, C., Ramesh, P.S. and Prasanjit, D. 2020. Changes in atmospheric, meteorological, and ocean parameters associated with the 12 January 2020 Taal volcanic eruption. *Rem. Sens.*, 12(6): 1026.

- Kumar, A., Kriti, S., Harvinder, S., Sagar, G., Nagriya, S., Singh, G. and Rajkumar, B. 2020. A drone-based networked system and methods for combating coronavirus disease (COVID-19) pandemic. arXiv, 069: 43
- Liu, Q., Dexuan, S., Wei, L., Paul, H., Luyao, Z., Ruizhi, H. and Hai, L. 2020. Spatiotemporal patterns of COVID-19 impact human activities and the environment in Mainland China using nighttime light and air quality data. *Rem. Sens.*, 12(10): 1576.
- Mandal, A., Ratul, R., Debrup, G., Dhaliwal, S.S., Toor, A.S., Sarbartha, M. and Atin, M. 2019. COVID-19 pandemic: Sudden restoration in global environmental quality and its impact on climate change. *Enerar Xiv*, 11: 1-12
- Shao, Z., Lin, D., Deren, L., Orhan, A., Md, H. and Congmin, L. 2020. Exploring the relationship between urbanization and ecological environment using remote sensing images and statistical data: A case study in the Yangtze River Delta, China. *Sustainability*, 12(14): 5620.
- Suresh, A., Diksha, C., Amina, O., Neha, B., Aswin, S., Jais, J. and Nezha, M. 2020. Diagnostic comparison of changes in air quality over China before and during the COVID-19 pandemic. *Res.Square*, 30: 482.
- Tang, C., Evan, K., Paleologos, C., Vitone, Y., Jiang-Shan, L., Ning-Jun, J. and Yong-Feng, D. 2020. Environmental Geotechnics: Challenges and opportunities in the post-COVID-19 world. *Environ. Geotech.*, 1: 11-21.
- Timmermann, A., Sun-Seon, L., Jung-Eun, C., Eui-Seok, C. and June-Yi, L. 2020. COVID-19-related drop in anthropogenic aerosol emissions in China and corresponding cloud and climate effects. *Sci. Rep.*, 11: 16852.
- Wei, X., Ni-Bin, C., Kaixu, B. and Wei, G. 2020. Satellite remote sensing of aerosol optical depth: advances, challenges, and perspectives. *Crit. Rev. Environ. Sci. Technol.*, 50(16): 1640-1725.
- Zhao, J., Yanfei, Z., Xin, H., Lifei, W. and Liangpei, Z. 2020. A robust spectral-spatial approach to identifying heterogeneous crops using remote sensing imagery with high spectral and spatial resolutions. *Rem. Sens Environ.*, 239: 111605.
- Weblink1 : <https://www.nrdc.org/experts/vijay-limaye/report-air-pollution-major-driver-ill-health-worldwide>
- Weblink 2: <https://airquality.gsfc.nasa.gov/>



# Aeropalynology of *Parthenium hysterophorus* L. in Relation to Meteorological Parameters from Srinagar Valley of Garhwal Himalaya, Uttarakhand

Shikha Arya\*, Prabhawati Tiwari \*†, Alok Sagar Gautam\*\* and Manish Sharma\*\*\*

\*Department of Botany & Microbiology, HNB Garhwal University, Srinagar (Garhwal)-246174, Uttarakhand, India

\*\*Department of Physics, HNB Garhwal University, Srinagar (Garhwal)-246174, Uttarakhand, India

\*\*\*School of Science and Technology, Hingiri Zee University, Dehradun-248197, Uttarakhand, India

†Corresponding author: P. Tiwari; ptiwari29@rediffmail.com

Nat. Env. & Poll. Tech.  
Website: [www.neptjournal.com](http://www.neptjournal.com)

Received: 03-01-2022

Revised: 08-03-2022

Accepted: 11-03-2022

## Key Words:

*Parthenium hysterophorus*

Aeroallergens

Pollen grains

Rotarod sampler

Meteorological parameters

Back trajectory analysis

## ABSTRACT

*Parthenium hysterophorus* (congress grass) is a harmful weed and its pollen grains are important allergens. Due to its minute size and allergenic activity, this particular type of pollen is selected for the study. The aeropalynological survey was conducted for the year 2019 at Chauras Campus, Hemvati Nandan Bahuguna Garhwal University, Srinagar, Uttarakhand. It is located on the right bank of the Alaknanda river (30°13'35.81"N & 78°48'11.05"E; 560 m amsl). A Rotarod sampler was used for air sampling. The maximum pollen count was observed in July. To evaluate the correlation matrix in R software, correlations (Pearson's and Spearman's) between pollen count and meteorological parameters have been calculated. Back trajectory analysis has also been done using NOAA HYSPLIT MODEL.

## INTRODUCTION

Pollen grains are one of the important biological materials that are ubiquitous and inhaled by humans. The main purpose of pollen grains is to bring about fertilization but these also cause allergies. (Nair et al. 1986, Leuscher et al. 2000, Shukla & Shukla 2010). In several studies, pollen grains from different plants have been reported as aeroallergens (Subiza et al. 1994, Mari et al. 1996, Asturias et al. 2002).

*Parthenium hysterophorus* L. commonly known as congress grass is designated as a major allergenic plant by many workers from different parts of the world (Sohi et al. 1979, Wedner et al. 1989, Handa et al. 2001, Wiesner et al. 2007). Taxonomically, the plant is categorized under the family Asteraceae and was introduced in India along with food grains (Kohli & Rani 1994). The flowering period of *P. hysterophorus* is almost throughout the year (Nayar et al. 1990). Studies have shown the harmful effect of *P. hysterophorus* pollen on human beings, animals, crops, etc. (Khosla & Sobti 1981, Gupta et al. 1995, Yadav et al. 2010, Sharma et al. 2013). The meteorological parameters influence the dispersion and transport of pollen grains (Cour et al. 1999, Galán et al. 2000, Gioulekas et al. 2004) and play an important role in the pollen concentration in air (Piotrowska 2006, Iglesias et al. 2007).

The present work aims to find out the concentration of *P. hysterophorus* pollen and the effect of meteorological factors on pollen concentration in the area. Back-trajectory analysis helps to locate the origin of airborne biological particles at any selected sampling point. The HYSPLIT model is used in the present study to investigate airborne pollen concentrations. It has been used earlier by many workers (Cecchi et al. 2007, Mahura et al. 2007). It is highly effective in studies emphasizing defining the pathway and possible long-range transport of air pollutants (Sa'nchez-Ccoyllo et al. 2006, Davis et al. 2010). The main objective of the back-trajectory analysis was to establish the relationship between the movements of air mass and pollen counts of *P. hysterophorus* pollen counts in the valley Srinagar of Garhwal Himalaya.

## MATERIALS AND METHODS

### Study Area

The study was conducted at Chauras Campus Hemvati Nandan Bahuguna Garhwal University (Fig. 1). It is located on the right bank of Alaknanda. The coordinates for the sampling sites were latitude 30.226522 and longitude 78.803177 with an elevation of 560 m amsl. The study site has forests with broad leaves and dry scrubs. In the research

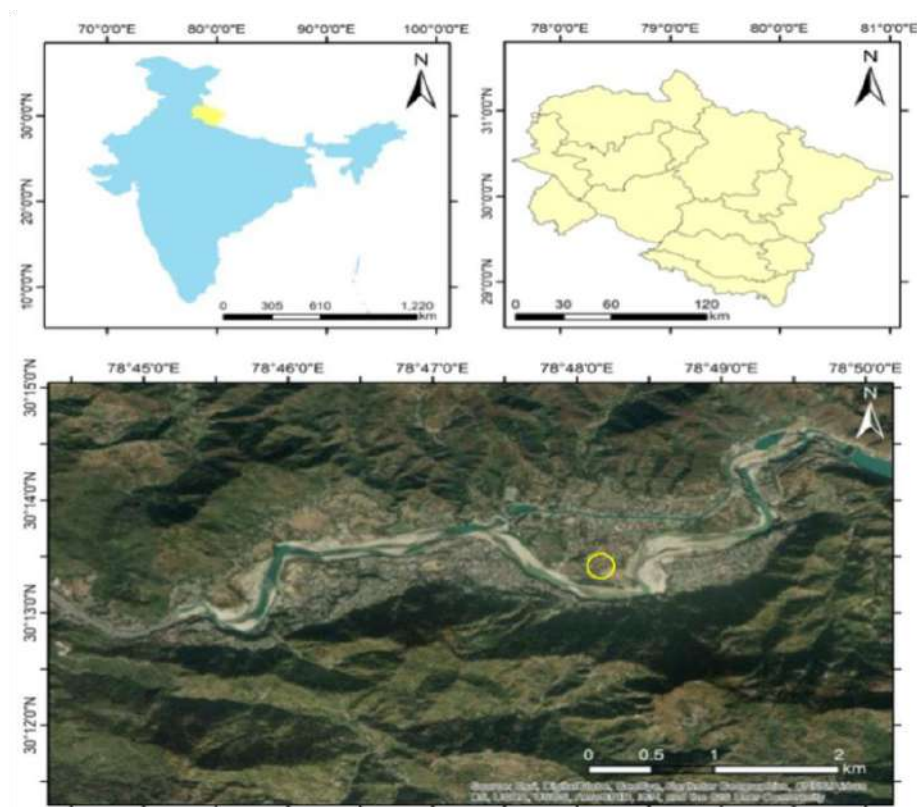


Fig. 1: Location map (yellow colored circle indicating sampling location at Chauras, Srinagar (Garhwal)).

region, *Parthenium* is an abundant weed that grows with other species like *Cannabis sativa*, *Erigeron*, *Lantana camara*, *Murraya koenigii*, and *Solanum* spp.

### Sampling Technique

Aerobiological sampling was carried out by Digital Rotorod pollen and Air particle collector for one year from January 2019 to December 2019. Glass slides smeared with glycerin jelly were exposed and changed after each hour of sampling. The slides were then examined under a microscope and the total number of pollen was counted by the continuous sweep method as suggested by Mandrioli et al. (1998).

Fresh pollen samples were taken directly from the plants for preparation of reference slides. The samples were then acetolyzed by the standard method (Erdtman 1960). The pollen was studied properly at the magnification of 400X under the Light microscope (Magnus Pro 3.7) and matched with the air sample. SEM image is taken with Scanning Electron Microscope Model JSM-6610 LV-JEOL, Japan. A customizable Davis Vantage Pro2 Automatic Weather Station (AWS) was used to extract Meteorological parameters like temperature, humidity, wind speed, and rainfall. The AWS

data was analyzed by Special Weather Link (version 6.0.3) as well as Aroldis Software. Correlations were calculated using Hmsc (version 4.4) package for the evaluation of the correlation matrix in R software as suggested by Feng et al. (2019), Gautam et al. (2020), and Liu et al. (2020). Air Mass Back trajectory analysis is carried out using National Oceanic and Atmospheric Administration (NOAA) HYSPLIT MODEL.

## RESULTS

### Plant and Pollen Description

The plant is annual, much branched and grows luxuriantly all around the year (Fig. 2 a). It reaches up to about 1.5 m or long. Each plant has several capitula. Each capitulum has several florets of which only five are female and the rest are male. The flowering occurs from July to November. Although heavy flowering occurs in the rainy season, the plant continues to flower and fruit till the environmental conditions favor it. The life cycle of *P. hysterophorus* is usually 9-10 months but can extend beyond it. *P. hysterophorus* is seed propagated. New plants grow as soon as the seed disperses. The plant can be seen in the fruiting, flowering, and vegeta-



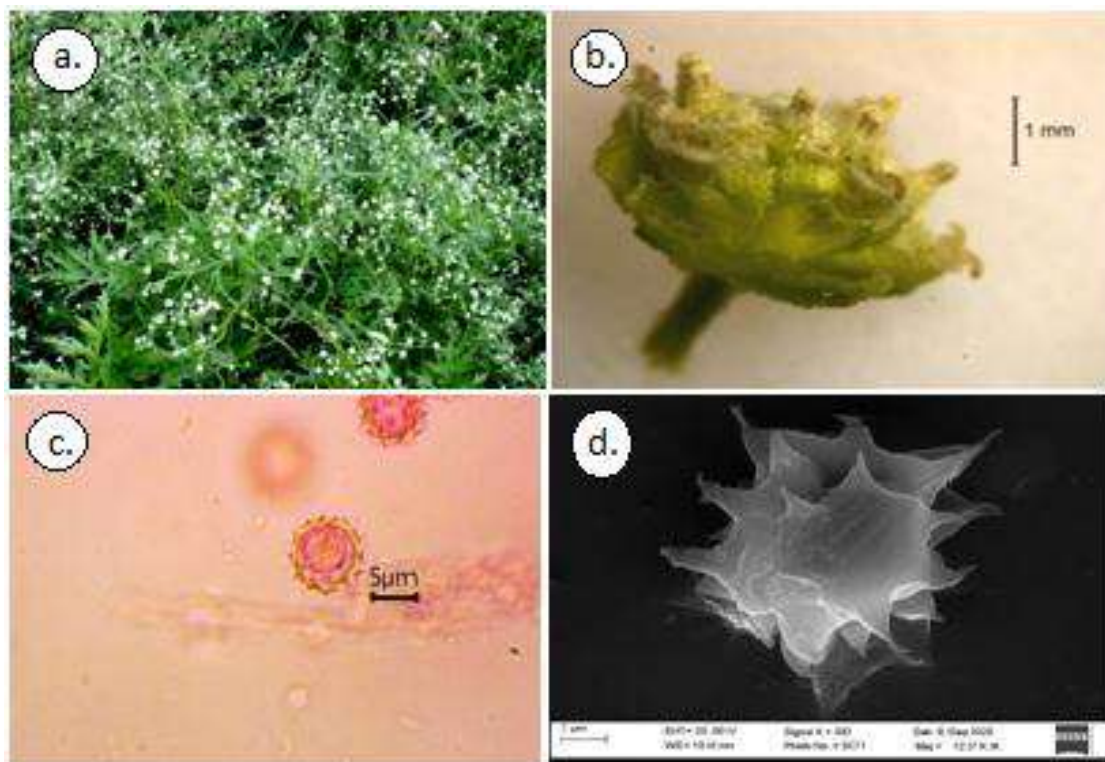


Fig 2: a. Plant habit (Lax panicle) b. Inflorescence (Single capitulum or head) c. Pollen grain (LM) d. SEM image of grain.

tive phase simultaneously. In a study in our laboratory, we germinated *P. hysterophorus* seeds and observed 38% seeds germination rate.

The inflorescence is the capitulum (head) on a lax panicle, white (Fig. 2 b). Each capitulum has ray and disc florets. Five ray florets are located at its periphery. These are narrowly ovate with puberulous bracts, white, ligulate, truncate, and zygomorphic with a well-developed female part. The ovary is unilocular with a basal ovule. The ovule is attached to the style with two arms. The remaining flowers of the capitulum are disc florets which are actinomorphic and white. The Corolla of the disc florets form a tube towards the base ends in a four-lobed apex. Stamens are four, epipetalous, and are fused near the base of the flower. Anthers are basifixed and ditheous. The pistil present in the disc floret is non-functional.

The Amb of the pollen is circular with three zonal colpi having a length of  $\sim 2.78 \mu\text{m}$ . The grain is radially symmetrical (Fig. 2 c, d). The shape class of the pollen is spheroidal with a 100 P/E ratio and the size of the pollen is minute ranging from  $14.80 \pm 1.92 \times 14.11 \pm 0.48 \mu\text{m}$ , the surface of the grain is spinulate with pointed spines of  $< 3 \mu\text{m}$  length. The exine width of the pollen grain is very thin ( $\sim 0.93 \mu$ ).

### Aerpalynological Analysis

*P. hysterophorus* pollen was collected from January 2019 to December 2019. The daily data have been converted accordingly. It was observed that the pollen number was at its peak in July with a total of 29.07% of the pollen count

Table 1: Pollen concentration per month (in percentage).

Month	Pollen concentration (%)
January	2.62
February	2.16
March	3.44
April	3.97
May	2.30
June	7.10
July	29.07
August	24.59
September	11.17
October	7.69
November	4.31
December	2.57

followed by August with 24.59%. The Main Pollen Season (MPS) can be estimated as July- August for *P. hysterothorus*. February was having a minimum of 2.16% pollen during the whole month (Table 1). The presence and distribution of pollen are throughout the year. The sudden increase in pollen concentration can be seen in July and August (Table 1). The monthly concentration of the *P. hysterothorus* pollen along with meteorological parameters is shown in the graphs below (Fig. 3).

### Correlation Analysis

It has been observed that there is some relation between the pollen count and the meteorological factors. To find out the relationship between pollen count and metrological parameters Spearman's and Pearson's correlation is calculated (Table 2). Analyzing Pearson's correlation shows a positive significant correlation between pollen count and rainfall ( $p < 0.05$ ). The correlation is non-significant by analyzing Spearman's correlation.

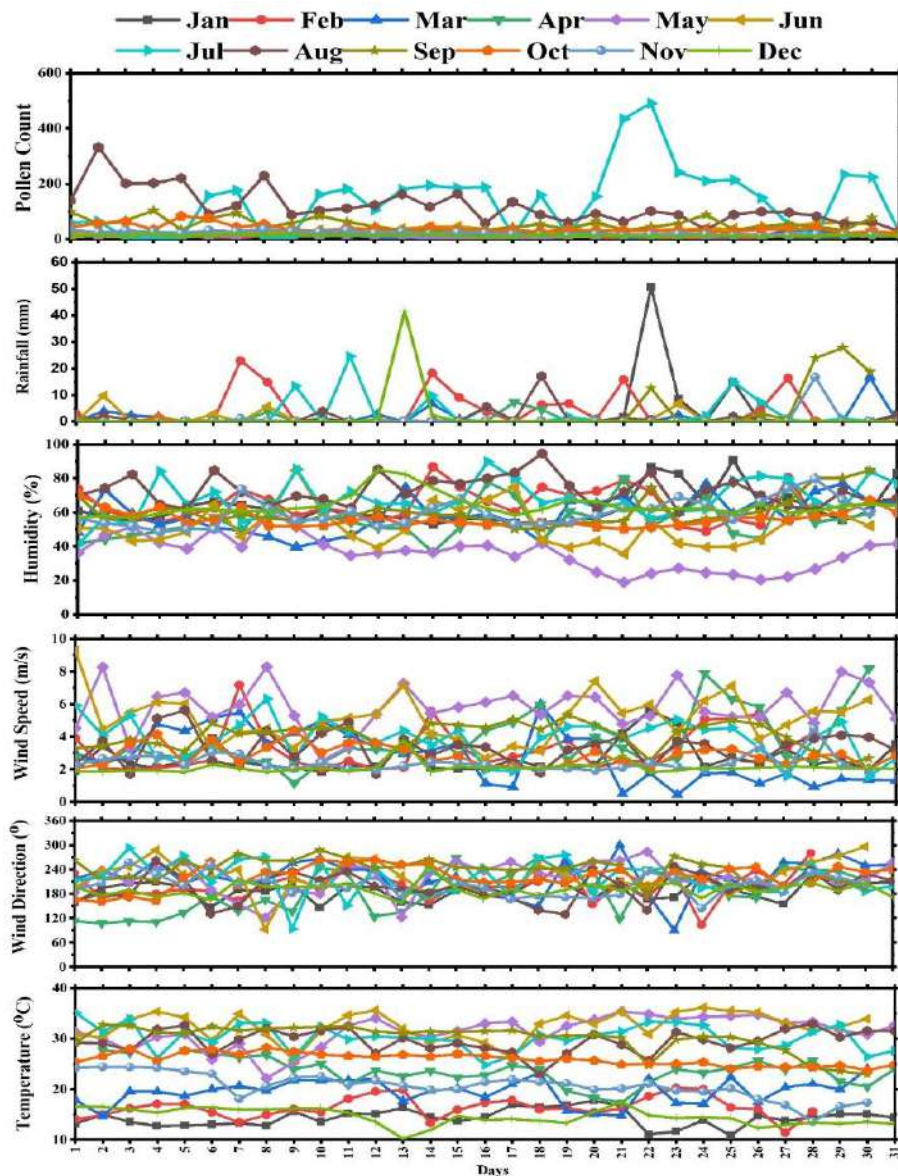


Fig 3: The monthly concentration of *P. hysterothorus* pollen grain along with meteorological parameters.

### Back-Trajectory Analysis

Back- trajectory analysis has been carried out using NOVA HYSPLIT MODEL (Stein et al. 2015) on the height of 1000m above ground level (Fig. 4). The trajectory presented here is for a single pollen episode, 31<sup>st</sup> July; at 2 pm (highest pollen concentration). The diurnal variation shows a peak at 2 pm. The trajectory indicates that the movement of air mass is from the sampling site (Uttarakhand) to Eastern India, then turn south from the Bay of Bengal. This path shows that with air mass, the pollen from *P. hysterophorus* can travel along and can cause allergic diseases to the individuals living in these areas.

### DISCUSSION

*P. hysterophorus* is a noxious weed and its pollen is known for causing dermatitis (Gunaseelan 1987, Towers & Subba Rao 1992, Morin et al. 2009) and is sensitive to rhinitis patients (Rao et al. 1985). A novel hydroxyproline-rich glycoprotein is identified as the major allergen in *P. hysterophorus* pollen by Gupta et al. (1996). Kumar et al. 2012 were the first who studied to immunologically characterize patients with *P. hysterophorus* sensitive atopic dermatitis.

The plant *P. hysterophorus* blooms throughout the year. Each plant has several capitula. Each capitulum has 5 female ray florets and numerous male disc florets. Four anthers are present in the disc florets. Each anther lobe produces a large number of pollen grains. Nayar et al. (1990) reported that *P. hysterophorus* produces 1.7 million pollen per plant.

By analyzing the meteorological data has been observed that despite heavy rains total number of *P. hysterophorus* pollen was highest in July. These findings are quite similar to some previous studies on *P. hysterophorus* pollen incidence in the aerospora. The frequency of *P. hysterophorus* pollen has been observed highest from June to August by Seetharamaiah et al. (1981) from Bangalore. Tilak & Patil (1983) also observed the maximum pollen count in July. Lalita and Ashok (2018) reported that this plant can produce flowers at any time of the year, but flowering occurs commonly in

the rainy season. Additionally, we discovered that 38% of *P. hysterophorus* seeds germinated in the lab. It suggests that it germinates and grows generously when there is the highest level of air humidity. This might be the cause of the high pollen grain count in July.

*P. hysterophorus* is an invasive alien plant species and grow abundantly in the bare lands, roadsides, barren places, and dumping sites of the Srinagar valley (Rawat et al. 2017). Although the pollen from the plant has mainly entemophilous characters it still contributes a prominent amount of pollen in the atmosphere, thus, it can be called anemophilous as well and categorized as amphiphilic.

The back trajectory analysis suggested the travel path of the airborne pollen grain along with the air parcels. Similar studies were conducted earlier by Satch et al. (2007).

### CONCLUSION

The present study leads us to the conclusion that though there is some relation between the meteorological factors and the pollen counts, the flowering season of plants is also important. It can also be concluded that the ornamentation on the surface of *P. hysterophorus* pollen is also responsible for allergies. As the surface has fine spines on it, these spines can irritate the skin, nasal cavity, or throat when inhaled with air. July is considered the main pollen season as the number was maximum during this month. The track of the air mass shows the possible areas in which pollen can find and can cause allergies.

### ACKNOWLEDGEMENTS

The authors acknowledge the Head, Department of Botany and Microbiology, HNB Garhwal University, Srinagar (Garhwal), Uttarakhand for providing facilities to conduct the study. The authors are also thankful to the Department of Physics, HNB Garhwal University, Srinagar (Garhwal), and the Department of Physics, School of Basic Sciences, Bahra University, Shimla, Himachal Pradesh, India for their assistance in trajectory analysis and for providing

Table 2: Correlation between pollen count and meteorological parameters.

Met parameters	Pearson's correlation		Spearman correlation	
	R-value	P value	R-value	P value
Temperature	0.399	0	0.153	2.660
Humidity	0.240	0.001	0.172	3.420
Wind speed	0.090	0.002	0.159	0.865
Wind direction	0.070	0.001	0.174	0.181
Rainfall	0.015	0.396	0.047	0.782

NOAA HYSPLIT MODEL  
Backward trajectory ending at 1400 UTC 31 Jul 19  
GDAS Meteorological Data

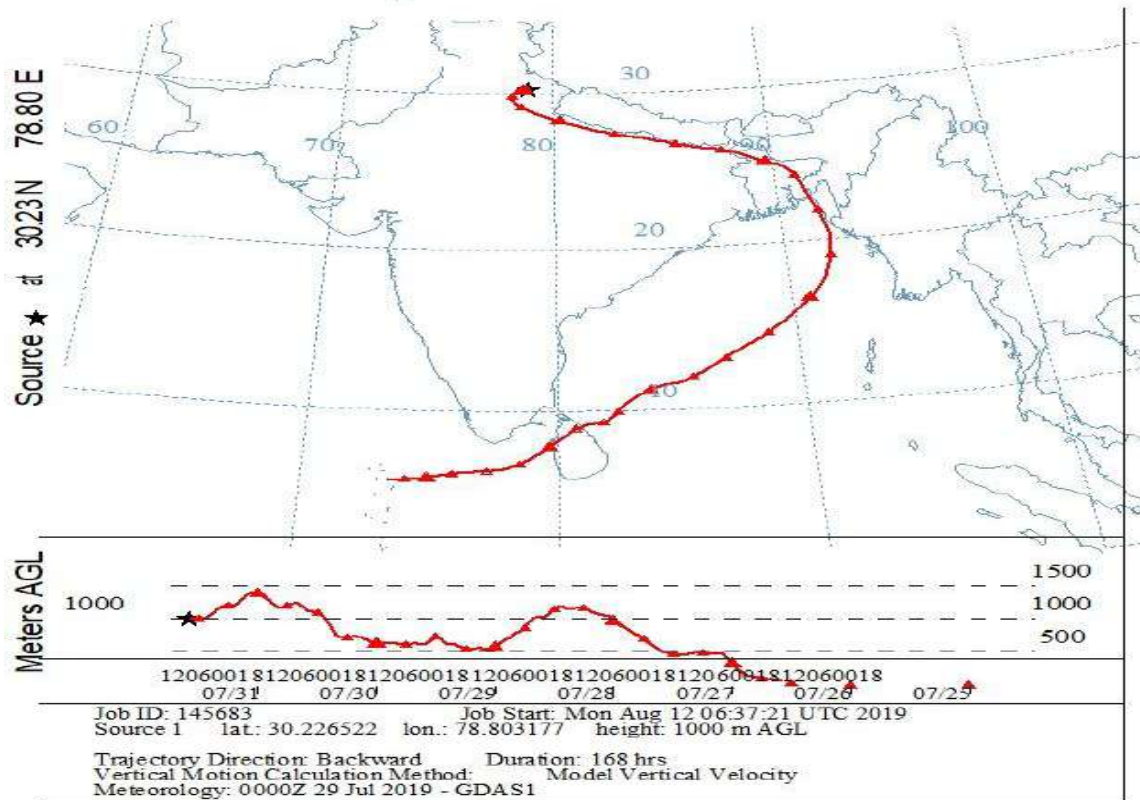


Fig 4: Back trajectory analysis.

meteorological data. SA is grateful to the University Grants Commission (UGC), New Delhi for granting a fellowship during the study period.

## REFERENCES

- Asturias, J.A., Ibarrola, I., Bartolome, B., Ojeda, I., Malet, A. and Martinez, A. 2002. Purification and characterization of Pla a 1, a major allergen from *Platanus acerifolia* pollen. *Allergy*, 57(3): 221-227.
- Cecchi, L., Malaspina, T.T. and Albertini, R. 2007. The contribution of long-distance transport to the presence of *Ambrosia* pollen in central northern Italy. *Aerobiologia*, 23: 145-151.
- Cour, P., Zheng, Z., Duzer, D., Calleja, M. and Yao, Z. 1999. Vegetational and climatic significance of modern pollen rain in northwestern Tibet. *Rev. Paleobot. Palynol.*, 104: 183-204.
- Davis, R.E., Normile, C.P., Sitka, L., Hondula, D.M., Knight, D.B., Gawtry, S.P. and Stenger, P.J. 2010. A comparison of trajectory and air mass approaches to examine ozone variability. *Atmos. Environ.*, 44(1): 64-74.
- Erdtman, G. 1960. Acetolysis method, A revised description. *Sven. Bot. Tidskr.* 54: 561-564.
- Feng, W., Zhu, Q., Zhuang, J. and Yu, S. 2019. An expert recommendation algorithm based on Pearson correlation coefficient and FP-growth. *Cluster Computing*, 22: 7401-7412.
- Galán, C., Alcázar, P., Cariñanos, P., Garcia, H. and Domínguez-Vilches, E. 2000. Meteorological factors affecting daily *Urticaceae* pollen counts in southwest Spain. *Int. J. Biometeorol.*, 43(4): 191-195.
- Gautam, A.S., Joshi, A., Kumar, S., Shinde, M., Singh, K. and Nautiyal, A. 2020. Variation of atmosphere parameters and dependent nature of Covid-19 pandemic in India during the lockdown period. *Journal of Critical Review*, 7(19): 2445-2453.
- Gioulekas, D., Balafoutis, C., Damialis, A., Papakosta, D., Gioulekas, G. and Patakas, D. 2004. Fifteen years' record of airborne allergenic pollen and meteorological parameters in Thessaloniki, Greece. *Int. J. Biometeorol.*, 48:128-136.
- Gunaseelan V. N. 1987. *Parthenium* is addictive to cattle manure in biogas production. *Biol. waste*, 21:195-202.
- Gupta, N., Martin, B.M., Metcalfe, D.D., and Rao, P.S. 1996. Identification of a novel hydroxyproline-rich glycoprotein as the major allergen in *Parthenium* pollen. *J. Allergy Clin. Immunol.*, 98(5): 903-912.
- Gupta, N., Sriramarao, P., Kori, R. and Rao, P.S. 1995. Immunochemical characterization of rapid and slowly released allergens from the pollen

- of *Parthenium hysterophorus*. Int. Arch. Allergy Immunol., 107(4): 557-565.
- Handa, S., Sahoo, B. and Sharma, V.K. 2001. Oral hyposensitization in patients with contact dermatitis from *Parthenium hysterophorus*. Contact Derm., 44: 279-282.
- Iglesias, I., Rodriguez-Rajo, F.J. and Mendez, J. 2007. The behavior of *Platanus hispanica* pollen, an important spring aeroallergen in northwestern Spain. J. Investig. Allergol Clin. Immunol., 17(3), 145-156.
- Khosla, S.N. and Sobti, S.N. 1981. Effective control of *Parthenium hysterophorus* L. Pesticides, 15(4): 18-19.
- Kohli, R.K. and Rani, D. 1994. *Parthenium hysterophorus*: A review. Res. Bull. Sci. Punjab Univ., 44: 105-109.
- Kumar, S., Khandpu, S., Rao, D.N., Wahaab, S., and Khanna, N. 2012. Immunological Response to *Parthenium hysterophorus* in Indian Patients with *Parthenium* Sensitive Atopic Dermatitis. Immunological Investigations, Informa Healthcare, USA, Inc. pp. 75-8.
- Lalita, R. and Kumar, A. 2018. Review on a weed *Parthenium hysterophorus* (L.). Int. J. Curr. Res. Rev., 10(17): 23-32.
- Leuscher, R.M., Christen H., Jordan P. and Vonthein R. 2000. 30 years of studies of grass pollen in Basel (Switzerland). Aerobiologia, 16: 381-391.
- Liu, Y., Mu, Y., Chen, K., Li, Y. and Gou, J. 2020. Daily activity feature selection in smart homes based on Pearson correlation coefficient. Neural Processing Letters, 51(2): 1771-1787.
- Mahura, A.G., Korsholm, U.S. and Baklanov, A.A. 2007. Elevated birch pollen episodes in Denmark: Contributions from remote sources. Aerobiologia, 23: 171.
- Mandrioli, P., Comtois, P. and Levizzani, V. 1998. Methods in Aerobiology. Pitagora Editrice Bologna, Italy.
- Mari, A., Di Felice, G., Afferni, C., Barletta, B., Tinghino, R., Sallusto, F. and Pini, C. 1996. Assessment of skin prick test and serum-specific IgE detection in the diagnosis of Cupressaceae pollinosis. J. Allergy Clin. Immunol., 98: 21-31.
- Morin, L., Reid, A. M., Sims-Chilton, N. M., Buckley, Y. M., Dhileepan, K., Hastwell, G. T., Nordblom T.L. and Raghu, S. 2009. Review of approaches to evaluate the effectiveness of weed biological control agents. Biol. Control, 51(1): 1-15.
- Nair, P.K.K., Joshi, A.P. and Gangal, S.V. 1986. Airborne Pollen, Spores and Other plant materials of India a survey. Publ. C.S.I.R. Centre of Biochemicals, Delhi and National Botanical Research Institute, Lucknow, India. p. 224.
- Nayar, J., Kumar, A. and Ramanujam, C. K. G. 1990. Monitoring of *Parthenium* pollen in the atmosphere of Hyderabad and its environs. J. Indian Inst. Sci., 70: 435-439.
- Piotrowska, K. 2006. The effect of meteorological factors on the start of the grass pollen season in Lubin in the years 2001-2004. Acta Agrobot., 59(1): 365-372.
- Rao, M., Prakash O. and Subba rao P.V. 1985. Reaginic allergy to *Parthenium* pollen: evaluation by skin test and RAST. Clin. Allergy, 15: 449-454.
- Rawat, D.S., Ballabha, R., Suri, S., Tiwari, J.K. and Tiwari, P. 2017. Photo restoration in the debris dumping sites of a hydroelectric power project: A case study from Srinagar (Garhwal), Western Himalaya, India. Environ. Conserv. J., 18(3): 189-197.
- Sa ́nchez-Ccoyollo, O.R., Ynoue, R.Y., Martins, L.D. and de Fátima Andrade, M. 2006. Impacts of ozone precursor limitation and meteorological variables on ozone concentration in Sao Paulo, Brazil. Atmos. Environ., 40, 552-562.
- Satch, A., Smith, M., Skjoth, A. and Brandt, J. 2007. Examining Ambrosia pollen episodes at Poznan (Poland) using back-trajectory analysis. Int. J. Biometeorol., 51: 275-286.
- Seetharamaiah, M.A., Viswanath, B. and Subba Rao, P.V. 1981. Atmospheric survey of pollen of *Parthenium hysterophorus*. Ann. Allergy, 47: 192-196.
- Sharma, V.K., Verma, P. and Maharaja, K. 2013. *Parthenium* dermatitis. Photochem. Photobiol. Sci., 12(1): 85-94.
- Shukla, S. and Shukla, R.V. 2010. A quantitative survey of pollen flora in the atmosphere of Korba- Chattisgarh, India. Int. J. Bot., 6(4): 449-455.
- Sohi, A.S., Tiwari, V.D., Lonker, A., Rangachar, S.K. and Nagasampagi, B.A. 1979. Allergic nature of *Parthenium hysterophorus*. Cont. Derm., 5: 133.
- Stein, A., Draxler, R., Rolph, G., Stunder, B., Cohen, M. and Ngan, F. 2015. NOAA's HYSPLIT atmospheric transport and dispersion modeling system. Bull. Amer. Meteor. Soc., 11: 545
- Subiza, J., Cabrera, M., Valdivieso, R., Subiza, J.L., Jerez, M., Jimenez, J.A., Narganes, M.J. and Subiza, E. 1994. Seasonal asthma caused by airborne Platanus pollen. Clin. Exp. Allergy, (24)12: 1123-1129.
- Tilak, S.T. and Patil, B.Y. 1983. The status of *Parthenium* pollen as aeroallergen. J. Bio. Res., 3:12-15.
- Towers, G.H.N. and Subba Rao, P.V. 1992. Impact of the pan-tropical weed, *Parthenium hysterophorus* L. on human affairs. In Proceedings of the First International Weed Control Congress, Weed Science Society of Victoria Melbourne, pp. 134-138.
- Wedner, H.J., Wilson, P. and Lewis, W.H. 1989. Allergic reactivity to *Parthenium hysterophorus* pollen: An ELISA study of 582 sera from the United States Gulf Coast. J. Allergy Clin. Immunol., 84(2): 263-271.
- Wiesner, M., Tessema, T., Hoffmann, A., Wilfried, P., Buttner, C., Mewis, I. and Ulrichs, C. 2007. Impact of the Pan-Tropical Weed *Parthenium hysterophorus* L. on Human Health in Ethiopia. Institute of Horticultural Science, Urban Horticulture, Berlin, Germany.
- Yadav, N., Saha, P. and Jabeen, S. 2010. Effect of methanolic extract of *Parthenium hysterophorus* L. on hematological parameters in Wistar albino rat. Bioscan. Int. J. Life Sci., 2: 357-363.





# Modeling Surface Water Quality and Nutrient Correlation with Sediment Oxygen Demand at Dam Water Reservoirs

N. N. Abdulqader<sup>(\*\*)</sup>†, B. S. İşgör<sup>(\*\*)</sup>, A. N. Genç<sup>\*\*\*</sup>, Enver Güler<sup>(\*\*)</sup> and Vahide Cansu Seymenoğlu<sup>\*\*\*\*</sup>

\*Department of Chemical Engineering, Atılım University, Kızılcaşar Mahallesi, 1184. Cad No: 13, 06830 Incek, Golbasi Ankara, Turkey

\*\*Graduate School of Natural and Applied Sciences, Atılım University, Kızılcaşar Mahallesi, 1184. Cad No: 13, 06830 Incek, Golbasi Ankara, Turkey

\*\*\*Department of Civil Engineering, TED University, Ziya Gökalp, Caddesi No: 48 06420, Kolej, Çankaya Ankara, Turkey

\*\*\*\*Directorate of Environmental Protection and Water Basins Division, Directorate of Laboratories Division, Yenimahalle, Ankara, Turkey

†Corresponding author: N. N. Abdulqader; noornabeel513@gmail.com

Nat. Env. & Poll. Tech.  
Website: [www.neptjournal.com](http://www.neptjournal.com)

Received: 09-06-2022

Revised: 07-07-2022

Accepted: 14-07-2022

## Key Words:

Water quality  
Sediment oxygen demand  
Reservoirs  
Simulation model  
WASP8

## ABSTRACT

The work presented here is a model approach based on WASP8 (Water analysis simulation program) a water quality model simulated to represent contaminants at the surface and bottom sediments of Kurtboğazı dam reservoir in Ankara city. However, our water quality output variables: are temperature, nitrate, total phosphorus, total Kjeldahl nitrogen, dissolved oxygen, Chlorophyll a, and ammonia. To ensure the model represents the actual case at the reservoir, the results from the simulation model were calibrated using actual data from the Kurtboğazı dam site, the calibration utilizes statistical techniques. The first method was the goodness-of-fit, R<sup>2</sup> between model variables and field data, and the results were in the range of 0.86 to 1.0 indicating excellent linear association. The second technique was the RE, the values of which obtained were less than 1, elaborating acceptable results. The dam reservoir Kurtboğazı had been affected by the negative impact arising from dissolved oxygen depletion in the hypolimnetic layer during stratification periods and that had been well documented. However, the processes of oxygen consumption at the sediment-water interface are still difficult to grasp conceptually and mainly linked to sediment oxygen depletion and the phenomena of sediment oxygen demand SOD. The novelty of this research work is the development of a quality model to predict the reactions of state variables that are occurring at the water body and how they interact with each other and their influence on the overall quality status of the Kurtboğazı reservoir, and the crucial factors influencing the depletion of oxygen at the water column; secondly, the effect of anoxic condition on the benthic flux and the impact of anoxia condition on the ratio of nitrogen to phosphorus ratio at the reservoir. It was evident from the results of calibration that the model successfully simulated the correlation of the parameters influencing the anoxic condition, and benthic flux and ratio shift from nitrogen-limited during the summer to phosphorus-limited at the beginning of winter.

## INTRODUCTION

Due to the problem of growing population, many countries in the world are either suffering water shortages (Simon & Hashemi 2018) or will eventually face this issue in the future, to make matters more complicated anthropogenic activities accelerate water resources depletion on a global scale, and there is an increasing emphasis on improving the quality of aquatic ecosystems, and monitoring surface waters have highlighted the need-to-know what factors cause the environmental deterioration (Ozmen et al. 2006), in Turkey, Ankara is considered to be the largest city in the Anatolia

region and the second-largest city, with a population of over four million people (TUIK 2008), and there are several dam resources that feed water supply to the city: Çubuk-II, Bayındır, Kurtboğazı, Çamlıdere, Eğrekkaya, and Akba (Tozsın et al. 2015, Magara 1997). Therefore, it is expected that in the coming years there is a decline in the water quality widespread around the world and on a global scale (Kendirli et al. 2009, Kernan & Allott 1999).

Due to the lack of water resources, it has become more difficult to supply sufficient high-quality drinking water to the Ankara metropolitan area (Patil et al. 2008) and the

application of technologies and strategies are the available solutions for treating polluted water resources. However, it is worth mentioning that adopting precautionary measures against the pollution of water resources is by far a more efficient and sustainable long-term solution. Water quality management often involves large capital investment. Managers must have means of evaluating and estimating different scenarios, this is where modeling is used to predict various impacts of alternatives on the whole system.

Water Quality Analysis Simulation Program (WASP) is a dynamic segment-based or compartment-modeling program for aquatic systems (Wang et al. 2018), including both the water column and the underlying benthos, which aids the interpretation and prediction of different water quality responses to anthropogenic and natural phenomena regarding quality and pollution control. The software is flexible and capable of simulating a wide range of pollutants in 1, 2, or 3 dimensions and examples are: the estimation of pollution load for the Taipu River (Bilal et al. 2009); total maximum daily load analysis (TMDL) for nutrients in the Neuse River Estuary, North Carolina (Wool et al. 2003a, 2003b); phytoplankton in St. Louis Bay, Mississippi (Camacho et al. 2014); impacts of climate change on water quality of Chungju Lake-South Korea (Park et al. 2013); dissolved oxygen in the Danshui and Chungkang Rivers, Taiwan (Chen et al. 2012); dissolved oxygen depletion in diverted floodwaters of the Elbe River, Germany (Lindenschmidt et al. 2009); eutrophication control in the Keban Dam Reservoir, Turkey (Soyupak et al. 1997). One of the most crucial factors that dominating the aquatic ecosystem's health is oxygen, therefore, it is of paramount importance to predict oxygen levels at lakes and reservoirs as part of an integrated water management system, reaeration from the atmosphere plays a vital role to replenish the DO levels in any water surface system, however, this must counter inflowing waters that transport organic matter into a reservoir, this matter will settle in the sediments along with dead plants and algae. When this material decomposes both chemical oxidation and biological respiration exert a significant oxygen demand on the water column (USGS Science 2020), known as biochemical oxygen demand BOD, and on the sediments, known as sediment oxygen demand SOD (Julie & Lindenschmidt 2017, Panagiotaki & Dimitrios 2015, Papastergiadou et al. 2009, Parlak 2007). Another important fact to consider is the depletion of dissolved oxygen due to the degradation of organic matter in the sediment, eventually, this will cause a release of metals such as iron and manganese, also, nutrients in the form of nitrogen and phosphorus (William 2002) into the water column, therefore DO depletion may also cause the release of toxic substances and anoxic conditions combined with the release of toxic substances can lead to severe water quality problems (Tufford & Hank 1999).

Sediment oxygen demand SOD (Li et al. 2021, Mbongowo et al. 2018) is the process impacted on a wide scale by the concentrations of materials in the sediments and overlying water column, nutrient release from the sediment due to mineralization diagenesis of organic materials in bottom sediments, which ultimately contributes to eutrophication and hypoxia (Testa et al. 2013).

Organic matter that settles into the sediments is subjected to several physical and biogeochemical processes (Miroslaw & Piotra 2014, Moltke et al. 2017). Benthic deposits have been known for a long time to cause depletion of oxygen concentration in natural waterways. Microbes consume oxygen when they break down organic matter. Bioturbation is a process in which benthic organisms modify the sediments. Organic matter decomposes and oxidizes, transforming nutrients and releasing them back into the water column. Within a few millimeters to centimeters of the water-sediment interface, sediment oxygen levels drop from bottom water concentrations to near zero, resulting in significant gradients. As oxygen is utilized to fuel the breakdown of organic matter, these gradients contribute to diffusion into the sediments, imposing a sediment oxygen demand (SOD) on the water column. Models of diagenetic processes predicting the effects of SOD on water quality have been difficult to assemble due to the lack of standard methods to accurately measure, quantify, and predict SOD, it is worth mentioning that several factors affect the SOD rate: such as sediment age, surface area, depth of deposit, temperature, water velocity, and chemical and biological differences (Quirós 2004).

With the considerable rise in pollution levels, populations, and the misconduct of natural resources (Ray et al. 2016) it is now of significant importance and a basic fundamental necessity to innovate methods and systems to sustain and minimize the impact of pollution and contamination to the water bodies, by the use of continuous monitoring systems. In this paper a simulation program system, WASP8 utilized in a novel manner to formulate a water quality simulation model that is a replica of conditions and status at the Kurtboğazi dam reservoir site. Water quality models can be effective tools to simulate and predict pollutant transport in the water environment and contribute to saving the cost of labor and materials for a large number of chemical experiments to some degree. Moreover, it is inaccessible for on-site experiments in some cases due to special environmental pollution issues and in the cases of specially protected areas. However, the model developed in this work was calibrated on actual data from the site. The model further investigated the depletion of oxygen and the related phenomena of sediment oxygen demand and the factors affecting this condition and how it is related to benthic flux and the nitrogen-to-phosphorus ratio. The simulated model developed and presented in this



research paper is monitoring and evaluation as it provides a base and know-how support for the sustainability of natural resources.

## MATERIALS AND METHODS

### Characteristics of the Study Area

Kurtboğazı Dam takes its name from the lake on which it was set, situated northwest of Ankara, coordinates at north latitude:  $40^{\circ}16'$  &  $40^{\circ}28'$  and between  $32^{\circ}37'$  &  $32^{\circ}46'$  at the east longitude, with a maximum depth of 32 m. Kurtboğazı was constructed as an earth-filled dam with a catchment of approximately  $331 \text{ km}^2$ . Its basin is smaller than the Sakarya basin, however, the construction of this dam was completed in 1967 and today it is used to supply drinking water to Ankara province. The dam basin and surrounding locations are affected by terrestrial climate; therefore, it is hot and dry in summer; cold, and moderately rainy in summer and winter, respectively (Altin et al. 2010). Meteorological Stations alongside the Kurtboğazı dam basin registered from 1988 to 2006 an average of 30.3 mm in summer, and 35 mm in autumn (Altin et al. 2010). The Basin of the dam has alluvium, hillside, Pliocene sediment, and andesite. Hillside debris covers the andesite formed mainly by rocks. The andesite in this region shows a massive structure and has been subjected to tectonic activity over a long period (Altin et al. 2010). Kurtboğazı dam reservoir is subjected to the growth of cyanobacteria (Turkish Water Pollution Control Regulation. 2004) that results in algae blooms and deteriorates water quality since it contains toxic materials resulting in, taste and odor problems in water occur and those threaten public health (Kali & Güngör 2020).

According to the information we obtained from the General Directorate of Ankara Water and Sewerage Administration -ASKI two main streams are feeding the Kurtboğazı Dam, the first is the Kurt Stream the second stream is known by the name Pazar Stream (Tozsın et al. 2015), (Fig. 1). Due to the importance of the Kurtboğazı dam reservoir as a source of water supply to Ankara city, the General Directorate of State Hydraulic Works-DSI along with the General Directorate of Ankara Water and Sewerage Administration -ASKI had launched many programs and special conservation plans to monitor the water quality of Kurtboğazı reservoir: to protect, improve and ensure sustainable use for it, this was eventually achieved by the distribution of five monitoring stations: K1, K2, K3, K4 and K5 of Kurtboğazı (Fig. 1) (ASKI 2021), two of the sampling points are built on the constantly flowing Pazar stream of the name K4 and K5, and sampling point K1 station was set just before entrance of water into the Ivedik Drinking Water treatment plant to observe water quality of the dam reservoir. The remaining stations K2 & K3

were distributed along the Kurtboğazı dam but I was not able to get the exact locations for the stations from ASKI. Therefore I resorted to the method of approximating their location based on available references and information. According to ASKI, the water samples are taken from the stations on weekly basis but they also have daily measurements. Some tests are performed at the site others are preserved in special conditions to be later delivered to ASKI laboratories for accurate and thorough testing.

Moreover, the available data from ASKI is presented in the appendix, it was also the basis for the calibration where the results are presented in (Table2) for the calibration between model results and the data provided from ASKI collected by stations (K1, K2 ...).

### Reservoir Water Quality Model

The WASP can be thought of as a dynamic compartment-modeling program for aquatic systems, including both the water column and the underlying benthos. The basic program simulates the following processes that change over time: dispersion, point, and diffuse mass loading, advection-dispersion, and boundary exchange (Stolarska & Kempa 2021).

An important issue is that when simulating a quality model you can decide upon the degree of the complexity you choose the model to carry, this implies to increasing the number of state variables means an increase in model complexity. However, for this work, the aim was to establish a sediment oxygen demand SOD model to correlate the different factors and variables that are influencing the oxygen level in the reservoir. To meet the objective of our work the first major step was to establish the water quality simulation model then followed by the SOD model.

The simulation program WASP8 can assess one, two, and three-dimensional systems as well as several types of pollutants. It can be used to examine various water quality issues in a variety of water bodies, including rivers, streams, coastal waters, ponds, estuaries, lakes, and reservoirs. The compartmentalization concept underpins this paradigm. A mass balance equation is presented for each equation. Rapid and full mixing occurs within each compartment. The program model depends on the principle of mass conservation when solving equations, and these equations represent the three primary types of water quality processes: loading; transformation; and conveyance. There are also biological, physical and chemical transformations that play a substantial influence on concentration variability along the water body that manifest in the form of dispersion; advection-dispersion and kinetic transformation (Ranjith et al. 2019).

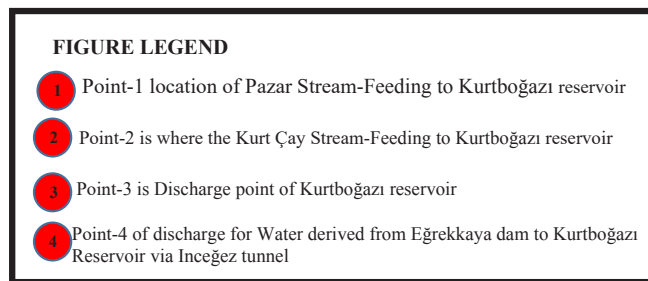
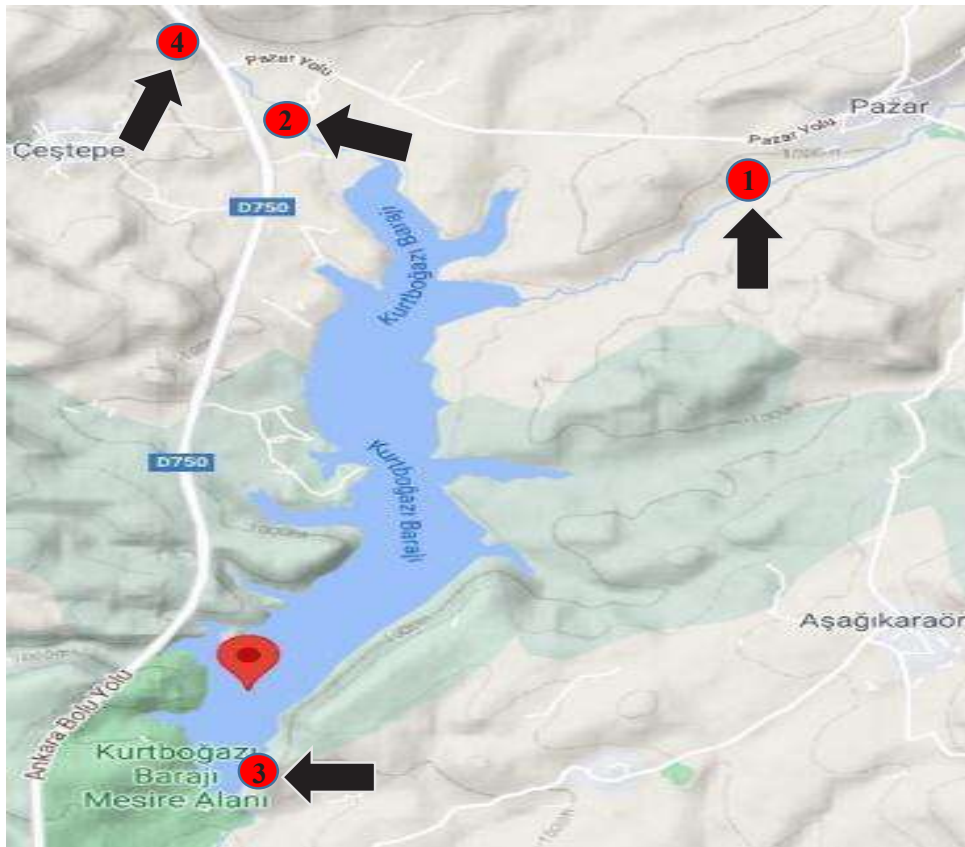


Fig. 1: Google map 2021. [Location of study area Kurtboğazi dam reservoir], Ankara Turkey, 40°16' 10.92" N, 32°42'2.16" E, Google Earth.

Table 1: Dimensions of segments.

Segment Name	Length of segment (L)	Width of segment (W)	Area (m <sup>2</sup> )= L.W	Volume (m <sup>3</sup> ) = L.W.depth
1	1136	845	959920	31677360
2	874	816	713184	24248256
3	904	714	645456	20654592
4	1020	670	683400	22552200
5	1224	641	784584	26675856
6	918	568	521424	17206992
7	1064	787	837368	29307880
8	758	685	519230	18173050

Table 2: Model result for state variables at segments 1, 2, and 8 with statistical tests for calibrating simulated results.

State Variable	Segment Number	May 2019	July 2019	Sept. 2019	Nov. 2019	Dec. 2019	R <sup>2</sup>	Root mean square error RMSE	Mean absolute % error MAPE	Relative error RE
Temperature °C	1	15	18.7	15.4	13.6	13	0.93	4.3	<88	0.34
	2	17.7	19.1	15.1	13.2	13.1	0.96	4.1	<72	0.32
	8	12.8	17	15.8	11.6	11	0.91	2.5	<40	0.2
Nitrate (mg.L <sup>-1</sup> )	1	250	242	26	63	60	0.97	35.4	<86	<b>1.86</b>
	2	525	521	189	60	56	1	129	<33	<b>1.52</b>
	8	545	543	376	73	62	0.96	80	<23	<b>1.78</b>
Dissolved Oxygen (mg.L <sup>-1</sup> )	1	8	8	8.1	8.7	8.5	0.86	1.7	<22	0.17
	2	9.8	9.7	9.2	8.6	8.7	0.97	1.2	<20	0.1
	8	8.3	8.2	8.5	8.9	9	0.93	0.9	<15	0.19
Chlorophyll a (µg.L <sup>-1</sup> )	1	1.67	1.7	1.76	1.85	1.83	0.97	0.4	<31	0.29
	2	1.87	2.05	2.07	2.11	2.13	0.98	0.6	<24	0.11
	8	0.49	0.51	0.53	0.53	0.54	0.92	1.4	<66	0.69
CBOD (mg.L <sup>-1</sup> )	1	2.09	2.5	2.56	2.93	2.98	0.97	0.24	<12	0.06
	2	2.1	2.42	2.68	2.7	2.6	0.96	0.2	<12	0.09
	8	2.14	2.4	2.7	2.8	2.8	0.98	0.7	<40	0.23
Ammonium (mg.L <sup>-1</sup> )	1	220	231	316.7	337	340	0.98	113.2	<30	0.04
	2	180	195	243	303	304	0.96	13.9	<15	0.05
	8	196.9	196.9	200.5	213	304	1	48.6	<24	0.11
Total Phosphorus (mg.L <sup>-1</sup> )	1	0.83	0.8	1	0.9	2.95	0.99	0.3	<80	0.45
	2	41	40	38	18.9	16.8	0.93	19.3	<58	0.42
	8	56	50	41	30.1	16.4	0.95	16	<40	0.3
Total Kjeldahl nitrogen (NH <sub>3</sub> /NH <sub>4</sub> )	1	159	168	221	372	410	0.98	47.6	<18	0.08
	2	177	181	199	380	400	0.88	112.6	<63	0.26
	8	149	156	209	380	384	0.99	11.3	<11	0.04

(Table 2) also displays the calibration result between model and field measurements for the state variables. Using statistical tests as shown in the last four columns:

1. R<sup>2</sup> is a goodness-of-fit measure for linear regression models
2. RMSE is the Root mean square error between the measured and model result
3. MAPE is the Mean absolute percentage error between the measured and model result

Conservation of mass forms the basic fundamental foundation of the Water Quality Analysis Simulation Program WASP theory. The simplest form of writing the mass would be Input system + production= out of the system. A lake or river can be considered a tank reactor and based on that idea the mass balance equation is (Wool et al. 2017):

$$Q_0 \cdot C_A + r_A \cdot V = Q \cdot C_A + \frac{dnA}{dt} \quad \dots(1)$$

From eq. 1, the Q<sub>0</sub> = Inflow (L<sup>3</sup> T<sup>-1</sup>), Q<sub>A</sub> = Outflow (L<sup>3</sup> T<sup>-1</sup>), at the left side of the equation it refers to C<sub>A</sub> = concentration of (A) inflow (M L<sup>-3</sup>), Q<sub>A</sub>C<sub>A</sub> = concentration of (A) in outflow (M L<sup>-3</sup>), r<sub>A</sub> = rate at which substances are produced,

$V = \text{volume (L}^3) \frac{dnA}{dt}$  = the number of moles of a substance A.

From the point of temporal and spatial input to the point of export and mass conservation in space and time, the model controls and assesses every component of water quality, when temporal and spatial fluctuations in constituent concentration are taken into consideration, a finite-difference equation is used for each segment, and, the finite difference form of the equation of mass balance is deduced for a 1D reach for ease of application, the concentration is computed for each segment. The initial value for each segment at time zero is the final concentration calculated from the previous segment. The dissolved components in a body of water represent the three primary categories of water quality processes as shown below (Wool et al. 2017):

$$\frac{\partial(AC)}{\partial t} = \frac{\partial}{\partial x} \left( -u_x AC + E_x A \frac{\partial C}{\partial x} \right) + A (S_L + S_B) + A S_K \quad \dots(2)$$

Where C is the concentration of water quality ( $\text{g.m}^{-3}$ ), t is time in (day),  $U_x$  is the longitudinal velocity ( $\text{m.day}^{-1}$ ),  $E_x$  is the longitudinal diffusion coefficient ( $\text{m}^2.\text{day}^{-1}$ ),  $S_L$  is diffusion loading rate ( $\text{g.m}^{-3} \text{day}^{-1}$ ),  $S_B$  is boundary loading rate including upstream, downstream, benthic, atmospheric ( $\text{g.m}^{-3}.\text{day}^{-1}$ ),  $S_k$  = transformation term (total kinetic transformation rate; positive is a source, negative sink, ( $\text{g.m}^{-3}.\text{day}^{-1}$ ) for variable i in a segment) and A is cross-sectional area ( $\text{m}^2$ ). Eq. 2 emphasizes that any mass enters a system must, by conservation of mass, either accumulate within the system or exit the system also Completely Mixed Flow Reactors (CMFRs) which means control volumes for which spatially uniform properties may be assumed (Wool et al. 2017):

$$\text{Accumulation} = S \text{ imports} - S \text{ exports} + S \text{ sources} - S \text{ sinks} \quad \dots(3)$$

There are many processes of physical and chemical perspective affecting the available dissolved oxygen in the water body and thus, eventually controlling the dynamic environment for the aquatic system, this involves phytoplankton, nutrients, Biochemical oxygen demand, and dissolved oxygen (Ranjith et al. 2019):

$$\frac{\partial c_b}{\partial t} = K_a (c_{sat} + c_6) - k_d \left( \frac{c_6}{k_{BOD} + c_6} \right) c_1 - \frac{SOD}{D} + G_{P1} \left[ \frac{32}{12} + 4(1 - P_{NH3}) \right] c_4 - \frac{32}{12} k_{1R} c_4 \quad \dots(4)$$

Where,  $C_6 = \text{DO (mg.L}^{-1})$ ,  $C_5 = \text{CBOD (mg.L}^{-1})$ ,  $C_{sat}$  = saturated concentration of DO ( $\text{mg.L}^{-1}$ ),  $C_1 = \text{ammonia-ni-$

$\text{trogen (mg N L}^{-1})$ ,  $k_d = \text{de-oxygenation rate (day}^{-1})$ ,  $k_{BOD} = \text{half-saturation constant for dissolved oxygen DO. D = depth of water (m), SOD = sediment oxygen demand (mg.m}^{-2}.\text{day}^{-1})$ ,  $P_{NH3} = \text{preference for ammonia term, } k_a = \text{re-aeration rate (day}^{-1})$ ,  $G_{p1} = \text{phytoplankton growth rate (day}^{-1})$ ,  $C_4 = \text{the phytoplankton biomass in carbon units (mg.C.L}^{-1})$ , and  $k_{1R} = \text{phytoplankton respiration rate (day}^{-1})$  (Ranjith et al. 2019).

However, the increase of anaerobic reactions in the underlying sediments and aerobic respiratory processes in the water column will lead to a decrease in DO. On the other hand, Phytoplankton growth, and re-aeration result in an increase in DO and sediment oxygen demand, but the respiration of phytoplankton and oxidation of CBOD result in loss and decrease of DO. In the WASP8 model, the State variable interactions in advanced eutrophication include: Phyto is phytoplankton as carbon,  $\text{NO}_3$  refers to nitrate,  $\text{NH}_4$  is ammonium,  $\text{PO}_4$  is ortho phosphorus, CBOD is carbonaceous biochemical oxygen demand, DO is dissolved oxygen ON is organic nitrogen, OP is organic phosphorous, DOM is dissolved organic matter, SS is inorganic suspended solids (Ranjith et al. 2019) and (Wool et al. 2017).

Based on eq. 4, it can be arranged in the following form (Ranjith et al. 2019):

$$\frac{\partial c_5}{\partial t} = a_{OC} k_{1d} c_4 - k_d \left( \frac{c_6}{k_{BOD} + c_6} \right) c_5 - \frac{V_{s3}(1-F_{d5})}{D} c_5 - 3 k_{2d} + (K_{NO3} + c_6) c_2 \quad \dots(5)$$

Where  $a_{oc} = \text{oxygen to carbon ratio} = 32/12 \text{ (mg O}_2 \text{ mg}^{-1}\text{C}^{-1})$ ,  $k_{1d} = \text{phytoplankton death rate (day}^{-1})$ ,  $k_d = \text{CBOD deoxygenation rate (day}^{-1})$ ,  $k_{2d} = \text{denitrification rate (day}^{-1})$ ,  $K_{NO3} = \text{half saturation constant for oxygen limitation for denitrification (mgN.L}^{-1})$ ,  $F_{d5} = \text{dissolved fraction of CBOD}$ ,  $V_{s3} = \text{settling velocity of organic matters (m.day}^{-1})$  and  $c_2 = \text{nitrate nitrogen (mg.L}^{-1})$ .

There is an important point to clarify regarding BOD measurements that may be affected by the decay of algal carbon and algal respiration. Thus, this requires corrective measures taken toward the internally computed value in the model and also given by (Ranjith et al. 2019):

$$\text{BOD}_5 = c_5(1 - e^{-k_{abot}}) + \frac{32}{12} c_1(1 - e^{-5k_{nbot}}) + a_{OC} c_4(1 - e^{-5k_{1R}}) \quad \dots(6)$$

Where  $c_5 = \text{the internally computed CBOD (mg.L}^{-1})$ ,  $C_1 = \text{the internally computed NH}_3, \text{ (mg.L}^{-1})$ ,  $C_4 = \text{the phytoplankton biomass represented as carbon units (mg.L}^{-1})$ ,  $a_{oc}$

= the oxygen to carbon ratio = 32/12 (mgO<sub>2</sub>.mg<sup>-1</sup>.C<sup>-1</sup>), k<sub>dbot</sub> = deoxygenation constant rate (day<sup>-1</sup>), k<sub>nbot</sub> = nitrification constant rate (day<sup>-1</sup>) and k<sub>1R</sub> = the algal respiration rate at 20°C (day<sup>-1</sup>)

Phytoplankton phosphorus in eq. 6 the term c<sub>4</sub> represents the dissolved inorganic phosphorus which is taken up, stored, and converted to biomass during the growing phase of the phytoplankton (William 2002). Will be re-written to include the mass of phytoplankton after it undergoes respiration and death (Ranjith et al. 2019):

$$\frac{\partial(c_4 a_{pC})}{\partial t} = \left(G_{p1} D_{p1} - D_{p1} - \frac{V_{s4}}{D}\right) a_{pC} c_4 \dots(7)$$

Where a<sub>pc</sub> is phosphorus to carbon ratio (mg P.mg<sup>-1</sup>.C<sup>-1</sup>), G<sub>p1</sub> = phytoplankton growth rate (day<sup>-1</sup>), D<sub>p1</sub> = phytoplankton death rate (day<sup>-1</sup>), V<sub>s4</sub> = phytoplankton settling velocity (m.day<sup>-1</sup>), a<sub>pc</sub> = Biomass in (mg) converted to both non-living inorganic ant of inorganic and organic matter. There is a connection between inorganic and organic phosphorus via a sorption-desorption mechanism, non-predatory mortality, and endogenous respiration return phosphorus to particulate organic form. Organic phosphorus is converted to dissolve inorganic phosphorus at a temperature-dependent mineralization rate. Non-living organic phosphorus must be decomposed by bacteria or mineralized into inorganic phosphorus before phytoplankton may use it, eq. 7 becomes (Ranjith et al. 2019):

$$\begin{aligned} \frac{\partial(c_3)}{\partial t} &= \left([a_{pc} D_{p1} (1 - f_0 p)]c_4 \right. \\ &\left. - k_{83} \left(\frac{c_4}{K_{mPc} + c_4}\right) c_8 - G_{p1} a_{pc} C_4 \right) \dots(8) \end{aligned}$$

Where c<sub>3</sub> = phosphate phosphorus (mg.L<sup>-1</sup>), c<sub>8</sub> = organic phosphorus (mg.L<sup>-1</sup>), f<sub>op</sub> = phytoplankton recycled to the organic phosphorus, f<sub>d8</sub> = fraction dissolved organic phosphorus, k<sub>83</sub> = mineralization of dissolved organic phosphorus (day<sup>-1</sup>), K<sub>mPc</sub> = the half saturation constant for phytoplankton (mg.CL<sup>-1</sup>) and V<sub>s3</sub> = organic matter settling velocity (m.day<sup>-1</sup>).

However, in many research papers, ammonia is preferred in the form of ammonia nitrogen. The phytoplankton nitrogen is gained during growth and lost during death. The settling velocity V<sub>s4</sub> = settling velocity (m.day<sup>-1</sup>) and a<sub>nc</sub> refers to the fact that for every mg of phytoplankton carbon consumed or lost there is an equivalent of nitrogen being generated so, there is nitrogen to carbon ratio = 0.25 mgN.mg<sup>-1</sup>.C<sup>-1</sup> as shown in eq. 9 below (Ranjith et al. 2019):

$$\frac{\partial(c_4 a_{nc})}{\partial t} = \left(G_{p1} - D_{p1} - \frac{V_{s4}}{D}\right) c_4 a_{nc} \dots(9)$$

The process of respiration for the phytoplankton may use a fraction of nitrogen at the cell denoted by f<sub>on</sub> is organic, while (1-f<sub>on</sub>) is in the inorganic form of ammonia nitrogen. For the phytoplankton to be able to use nitrogen the latter must undergo a process of mineralization or what is known as decomposition by bacteria. Organic nitrogen (c<sub>7</sub>) is acquired by phytoplankton death and dissipated by mineralization and settling, on the other hand, ammonia nitrogen (c<sub>1</sub>) is acquired through the process of phytoplankton mortality and dissipated by nitrification & phytoplankton growth nitrate-nitrogen (c<sub>2</sub>) is gained via nitrification and lost through phytoplankton growth and de-nitrification, eq. 10 below the display (c<sub>7</sub>) or organic nitrogen, while (c<sub>1</sub>) refers to ammonia nitrogen and (c<sub>2</sub>) is nitrate nitrogen, (Ranjith et al. 2019):

$$\begin{aligned} \frac{\partial(c_7)}{\partial t} &= D_{p1} (a_{nc} f_{on}) c_4 - K_{71} \left(\frac{c_4}{k_{mPc} + c_4}\right) \\ &- \left(\frac{V_{s3}(1-f_{d7})}{D}\right) c_7 \dots(10) \end{aligned}$$

The equation for (c<sub>1</sub>), and (c<sub>7</sub>) shall be presented below in eq.11 and eq.12 (Ranjith et al. 2019):

$$\begin{aligned} \frac{\partial(c_1)}{\partial t} &= D_{p1} a_{nc} (1-f_{on}) c_4 - K_{71} \left(\frac{c_4}{k_{mPc} + c_4}\right) c_7 \\ &- k_{12} \partial \left(\frac{c_6}{k_{nit} + c_6}\right) c_1 - G_{p1} a_{nc} p_{NH3} c_4 \dots(11) \end{aligned}$$

$$\begin{aligned} \frac{\partial(c_2)}{\partial t} &= k_{12} \partial \left(\frac{c_6}{k_{nit} + c_6}\right) c_1 - G_{p1} a_{nc} \\ &p_{NH3} c_4 - k_{2D} D \left(\frac{k_{NO3}}{k_{NO3} + c_6}\right) c_2 \dots(12) \end{aligned}$$

Where (c<sub>7</sub>)= organic nitrogen (mg.L<sup>-1</sup>), (c<sub>1</sub>)= ammonia nitrogen (mg.L<sup>-1</sup>), (c<sub>2</sub>) = nitrate nitrogen (mg.L<sup>-1</sup>), f<sub>on</sub> =dead phytoplankton recycled ON, k<sub>71</sub> = The ON mineralization rate (Day<sup>-1</sup>), f<sub>d7</sub> = Fraction of dissolved organic nitrogen, kmN = Michaelis value for ammonia preference (µgN.L<sup>-1</sup>), k<sub>mPc</sub> = half saturation constant for phytoplankton limitation of phosphorous recycle (mgC.L<sup>-1</sup>), K<sub>NO3</sub> = half saturation constant of oxygen de-nitrification (mgO<sub>2</sub>.L<sup>-1</sup>), k<sub>12</sub> = nitrification rate (day<sup>-1</sup>) and k<sub>2D</sub> =

Denitrification rate (day<sup>-1</sup>). The WASP8 model also takes into account the temperature effect for all first-order reactions in the model by eq. 13.

$$K(T) = k(20) \Theta^{T-20} \quad \dots(13)$$

Where  $K(T)$  = the reaction rate ( $\text{day}^{-1}$ ) at temperature  $T$  ( $^{\circ}\text{C}$ ) and  $\theta$  = the temperature coefficient for the reaction.

### Modeling Kurtboğazi Reservoir

According to the information obtained from the ASKI report, field data was collected at specific locations at the monitoring stations in the Kurtbogazi dam (ASKI 2021), and physico-chemical properties of water at the stations were provided by ASKI: K1, K2, K3, K4, and K5. This data was for one year which included the surface and sediment analysis at some stations. According to ASKI, the sampling frequency was weekly, and the method of sampling was according to Standard Methods for the Examination of Water and Wastewater (ASKI 2021). The simulation program WASP8 is generally based on the principle of mass conservation as viewed in eq. 2. This principle requires that the mass constituent being investigated must be accounted for, and the model traces each water quality constituent from the point of spatial and temporal input to its final point of export, conserving mass in space and time. To accomplish this task, there are important input data that must be defined by the user: Simulation and output control, model segmentation, advective portraying the transfer of matter and initial concentrations (Ray et al. 1996), boundary concentrations, waste loads, kinetic parameters, and constants. The simulation model will be tracking the movement and transformation of environmental parameters that are involved in the interaction of the Kurtboğazi reservoir. These parameters are Biological oxygen demand BOD (Kali & Güngör 2020) which measures the potential of water to deplete the oxygen. In other words it's the amount of dissolved oxygen needed by aerobic biological organisms in a body of water to break down organic material present in as total kjeldahl nitrogen (TKN) is essential for living organisms to function and excess amount of these nutrients cause eutrophication and oxygen depletion; total phosphorus (TP) levels provides reliable information on the water body quality and trophic state; nitrate ( $\text{NO}_3$ ) if the water body has exceeded nitrate this will eventually cause eutrophications and plant bloom, this large amount of plant growth depletes oxygen from the water and negatively affecting aquatic life; phytoplankton (Chlorophyll a) monitoring chlorophyll levels is a direct way of tracking algal growth and insuring it does not exceed permissible levels and lead to algae bloom; dissolved oxygen (DO) it is a key factor to determine the health state of a water body; ammonium ( $\text{NH}_4$ ) are monitored as increased concentrations of ammonium can enhance the growth of algae and aquatic plants the bacteria can also convert high ammonium to nitrate ( $\text{NO}_3$ ) in the process of nitrification, which lowers dissolved oxygen. There are

also other data requirements to be entered before running the model, for example, the weather parameters in the form of air temperature, dew point, wind speed, and solar radiation, (Ankara Çabuk Turkey Weather History 2020).

As explained earlier the model is a set of expanded control volumes, or "segments," that together represent the physical configuration of the water body. These segments are provided to help users interpret and predict water quality responses to natural phenomena and man-made pollution for various pollution management decisions since WASP is a dynamic compartment where individual compartments can interact with each other and undergo dynamic remodeling for aquatic systems, including both the water column and the underlying benthos (Ambrose 2017 and ). The Kurtboğazi reservoir is divided into 8 segments (Fig. 2) for the surface layer. However, these segments will have a subsurface layer below them as part of the water column. Also, there is the surface benthic and subsurface benthic that make up the sediment bed. The total number of segments will be 16. For each segment surface and subsurface, water dimensions with areas and volumes are given in (Table 1). The same concept was also applied to sediment beds for surface and subsurface benthic, based on the segment division in (Fig. 2). The dimensions were derived in length and width and the last two columns are for the area and volume of each segment, as listed in (Table 1). These dimensions are required to be entered into the model as part of the input procedure.

### Execution of Model and Development of Results

Our selected simulation period for this work is from 1/1/2019 to 1/1/2020, the reason for selecting this date is because the available data that was sent from ASKI was at this time frame, according to the municipality of Ankara Water and Sewerage Administration –ASKI (2021), Altin et al. (2010), and Tozsin et al. (2015) there are two inlet points to Kurtboğazi reservoir as shown in (Fig. 1), known as Kurt and Pazar. These will represent segment 1 and segment 2 in the model respectively. The discharge point from Kurtboğazi is the Dam point which corresponds to segment 8 in the model. The reason for selecting these specific segments is because they correspond to effective location points such as inlet and outlet points at the reservoir. As for the remaining observation stations, they correspond to other segment numbers as presented in (Fig. 2). Observation stations K1, K2, K3, K4, and K5 represent segment 8, segment 7, segment 5, segment 2, and segment 1 respectively. However, our work will focus on segments 1, 2, and 8 as mentioned earlier.

The adopted mathematical modeling approach was subjected to a thorough calibration before its use for determining the sediment oxygen demand, with this intention. The results

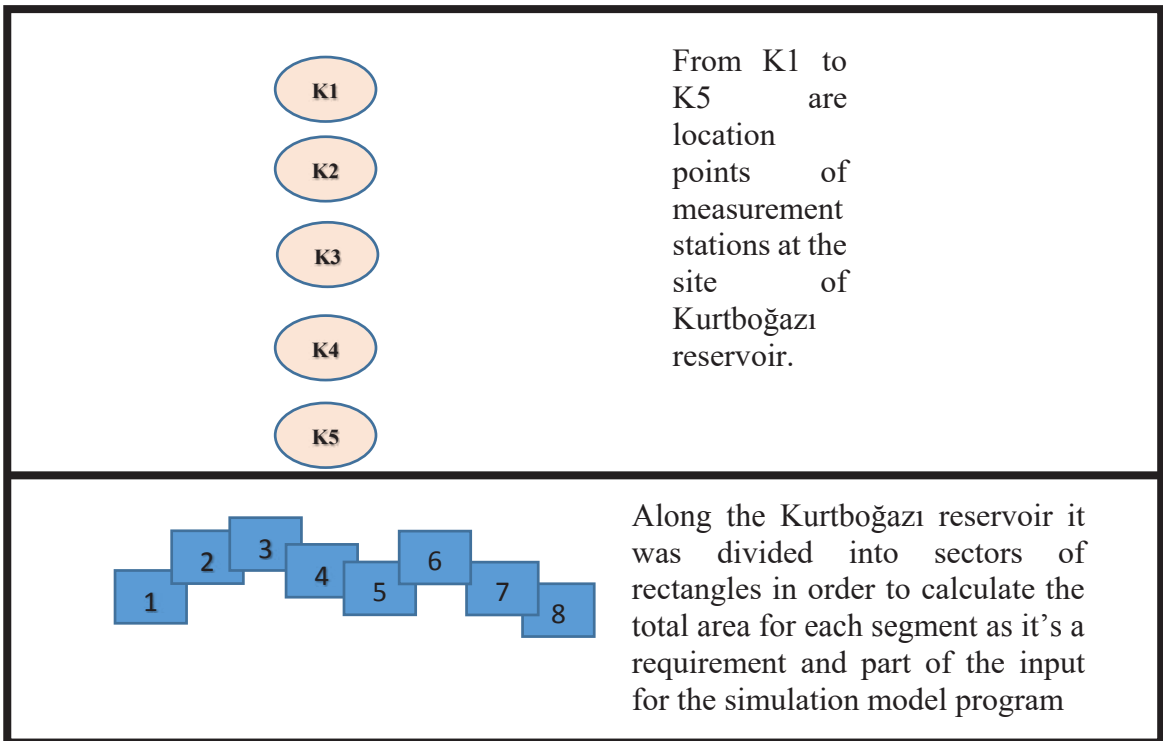
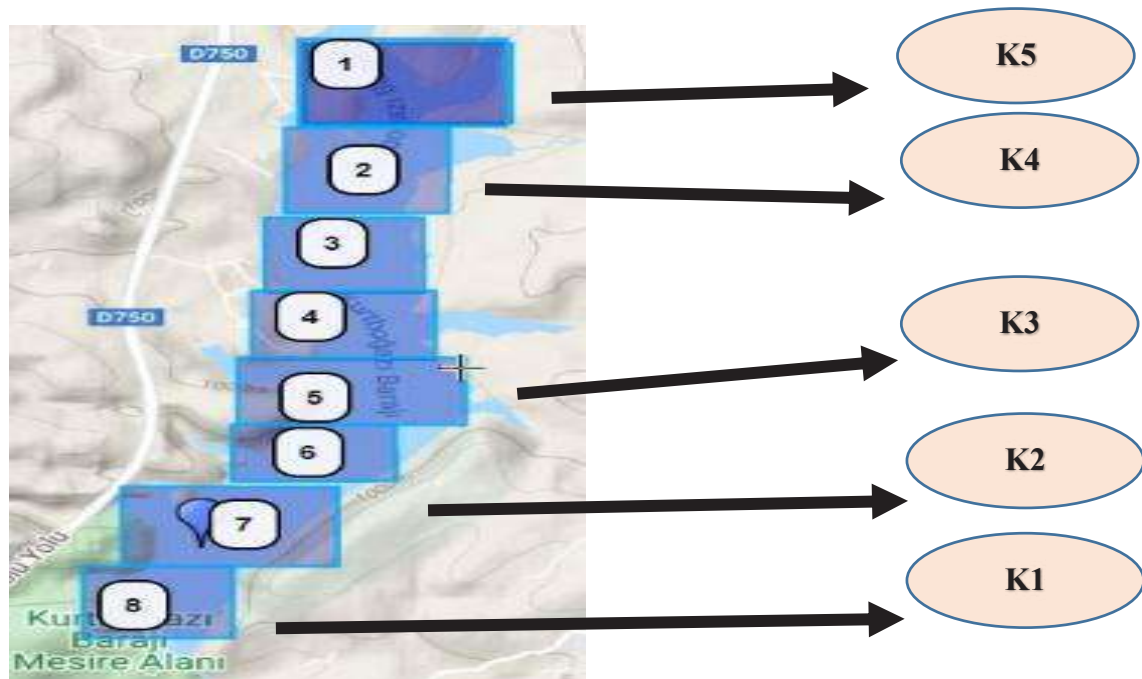


Fig. 2: Google map of Kurtboğazi reservoir with segments, Ankara Turkey, 40°16'10.92" N, 32°42'2.16" E, Google Earth, date accessed 1/3/2021, google.com/maps.

obtained from a series of calibration runs were compared with prescribed sets of field measurements. The purpose of executing calibration trials for specified periods was to find a suitable combination of numerical values for the model parameters and hence to obtain an acceptable match between model predictions and field data. The results of calibration were checked using statistical tools such as constrained regression analysis and the root mean of the square error will be presented in the results section. The calibration parameters based on total phosphorus, total Kjeldahl nitrogen, CBOD, and dissolved oxygen that was used are presented in (Table 2). However, it's important to point out that calibration is not limited to the above-mentioned parameters, it may include other state variables depending on the existing conditions of the water to be simulated.

### Modeling Sediment Oxygen Demand (SOD)

After calibration of the model, the work will focus on the simulation of the sediment oxygen demand SOD model,

as it's the rate at which dissolved oxygen is removed from the water column in surface water bodies due to the decomposition of organic matter in the bottom sediments, and it includes both the respiration rates of benthic communities and the chemical oxidation of reduced substances in the sediment. Since there is no available data on laboratory tests for the sediment at the Kurtboğazı reservoir we model the SOD then for the calibration of the result an equation was used by Sharma (2012), Sediment oxygen demand SOD is the rate at which dissolved oxygen is removed from the water column in surface water bodies due to the decomposition of inhibited organic matter at sediment, and it includes both the respiration rates of benthic communities and the chemical oxidation of reduced substances in the sediment, several factors affect the SOD rate, such as sediment age, surface area, depth of deposit, temperature, water velocity, and chemical and biological differences (Chen & Lung 2012) and (Fig. 3) is a conceptual drawing of the SOD and at sediment and water column. Since there are no available

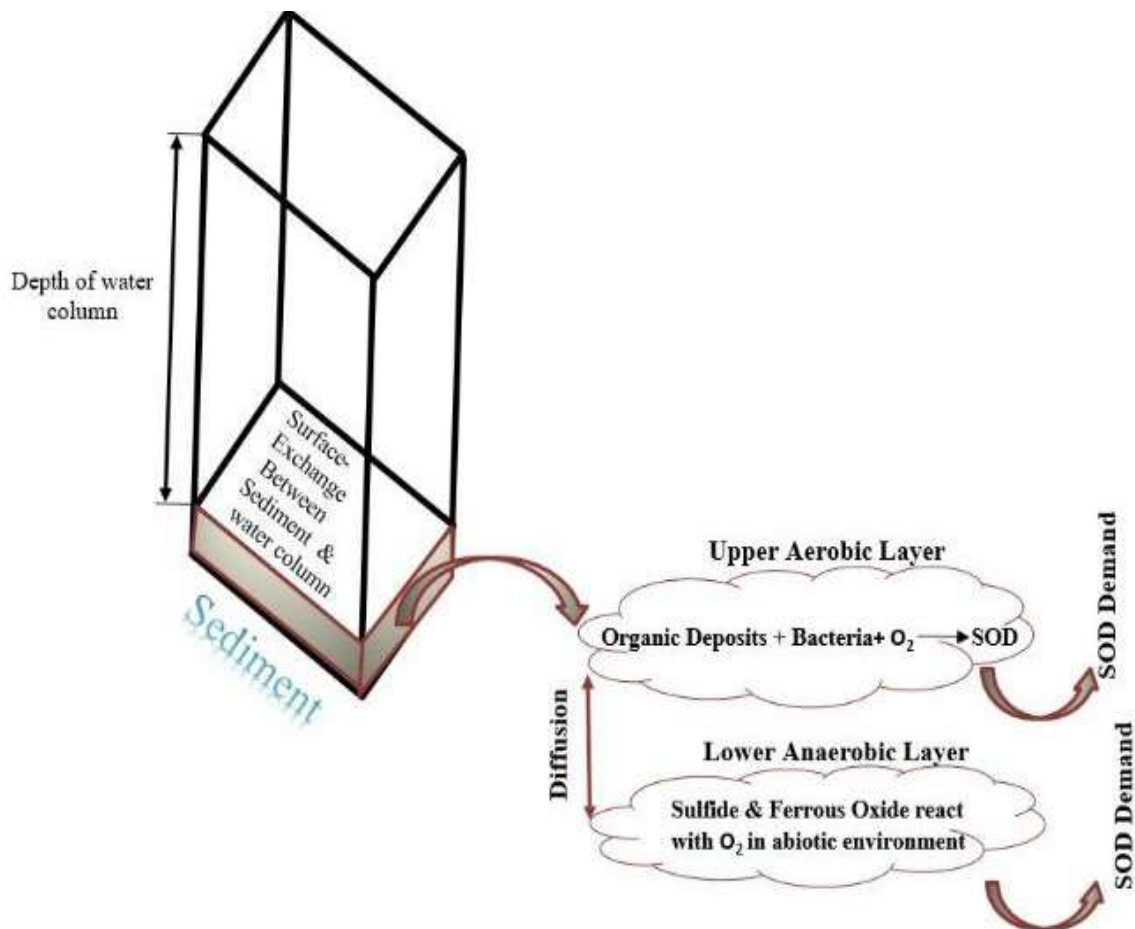


Fig. 3: Conceptual drawing of sediment oxygen demand between sediment and water column at Kurtboğazı dam reservoir.



data of laboratory tests for the sediment at the Kurtboğazi reservoir we are going to first model the SOD using the calibrated water quality model developed in this work then for the calibration of the result alternative steps are to be taken which will be explained in the following paragraphs, according to (Sharma 2012) the sediment oxygen demand could be calculated from the Total organic carbon (TOC) using the equation 14 (Sharma 2012).

$$\text{SOD (g m}^{-2} \text{ day}^{-1}) = 0.0302 \cdot \text{TOC} + 0.0845 \quad \dots(14)$$

Using the result from our model for TOC and applying it to eq. 14 and the results of segments 1, 2, and are given in (Table 3).

**RESULTS**

**Kurtboğazi Dam Reservoir Simulation Model**

The novelty of this work is to do with the fact that this simulation tool has not been used before for the Kurtboğazi reservoir water quality monitoring program, in general. This study focuses on anoxic and oxygen depletion due to stratification (Mahmud 2009) and sediment oxygen demand which increase in the summertime.

However, of the utmost important point to be emphasized at this stage is the difficulty I endured in the process of acquiring the data from the official institute in Turkey regarding one year of Kurtboğazi reservoir field data, obtained from the observation stations controlled by ASKI, for that I had to undergo a complex, lengthy and very exhausting process, having said that I consider myself lucky to even be able to obtain these data, and, in defense for the forthcoming situation regarding the limited availability of field data, there may be two directions of arguments: the first was initially confirmed by the ASKI official institute that in the last five years, the conventional data has been consistent, and no unusual or out-of-date data has been observed. Several additional parameters were employed in the model’s calibration process, and the findings are shown in (Table 2). The results

provided excellent variance in the dependent variable with readily available field data.

Once the model was executed, it was subjected to a thorough calibration before its use for determining the sediment oxygen demand. With this intention, the results obtained from a series of calibration runs were compared with prescribed sets of field measurements. The results of calibration were then checked using statistical tools as presented in (Table 2) of the model. Results starting from May to the end of the year 2019 included all the state variables: temperature, nitrate, dissolved oxygen, total phosphorus, chlorophyll-a, total Kjeldahl nitrogen, CBOD, and ammonium at segments 1, 2, and 8. The last four columns are applying the statistical analysis methods to check the accuracy of model results with actual measured data from the site, the first method used is R squared R<sup>2</sup> which is a statistical measure of how close the data are to the fitted regression line between measured field data and the model result and from (Table 2) our range for the state variables is between 0.86 and 1.0 according to (Moriassi et al. 2007), higher values indicating less error variance and are acceptable, inspection of (Table 2) Root mean square error RMSE is the root mean square error of approximation its absolute measure of fit, our range result for RMSE from 0.2 to 129 according to (Mielke & Berry 2001, U.S. EPA 2003) and (Burger et al. 2008) RMSE has no clear interpretation or related measures, and therefore calibration of our model will not be based on these techniques, the column of mean absolute percentage error MAPE resulting to be a very large value even though the model appears to fit the data well, this is because MAPE divides the absolute error by the actual data when the values are at times closer to 0 can greatly inflate the result of MAPE. The last column of (Table 2) is the relative error RE between simulated and measured data. RE are all less than 1 which indicates good results according to Haze-winkel (2001). Except for the Nitrate which is: 1.86, 1.52, and 1.78 for segments 1, 2, and 8 respectively. So, another test was performed only on this data of nitrate to ensure the model results are performing well since the R<sup>2</sup> for Nitrate

Table 3: SOD result from simulation of model with SOD from the equation at segments 1, 2 and 8.

	Month	DOC-Mod-el	SOD-from Equa-tion	SOD-from Model		Month	DOC-Model	SOD-from Equation	SOD-from Model		Month	DOC-Model	SOD-from Equa-tion	SOD-from Model
Segment 1	July	0.94	0.11	0.52	Segment 2	July	1.1	0.12	0.5	Segment 8	July	1	0.11	0.48
	Aug.	0.96	0.11	0.42		Aug.	1.1	0.12	0.46		Aug.	1.09	0.12	0.47
	Sept.	1.18	0.12	0.4		Sept.	1.26	0.12	0.39		Sept.	1.17	0.12	0.41
	Oct.	1.24	0.12	0.39		Oct.	1.24	0.12	0.39		Oct.	1.22	0.12	0.38
	Nov.	1.24	0.12	0.39		Nov.	1.24	0.12	0.38		Nov.	1.26	0.12	0.36

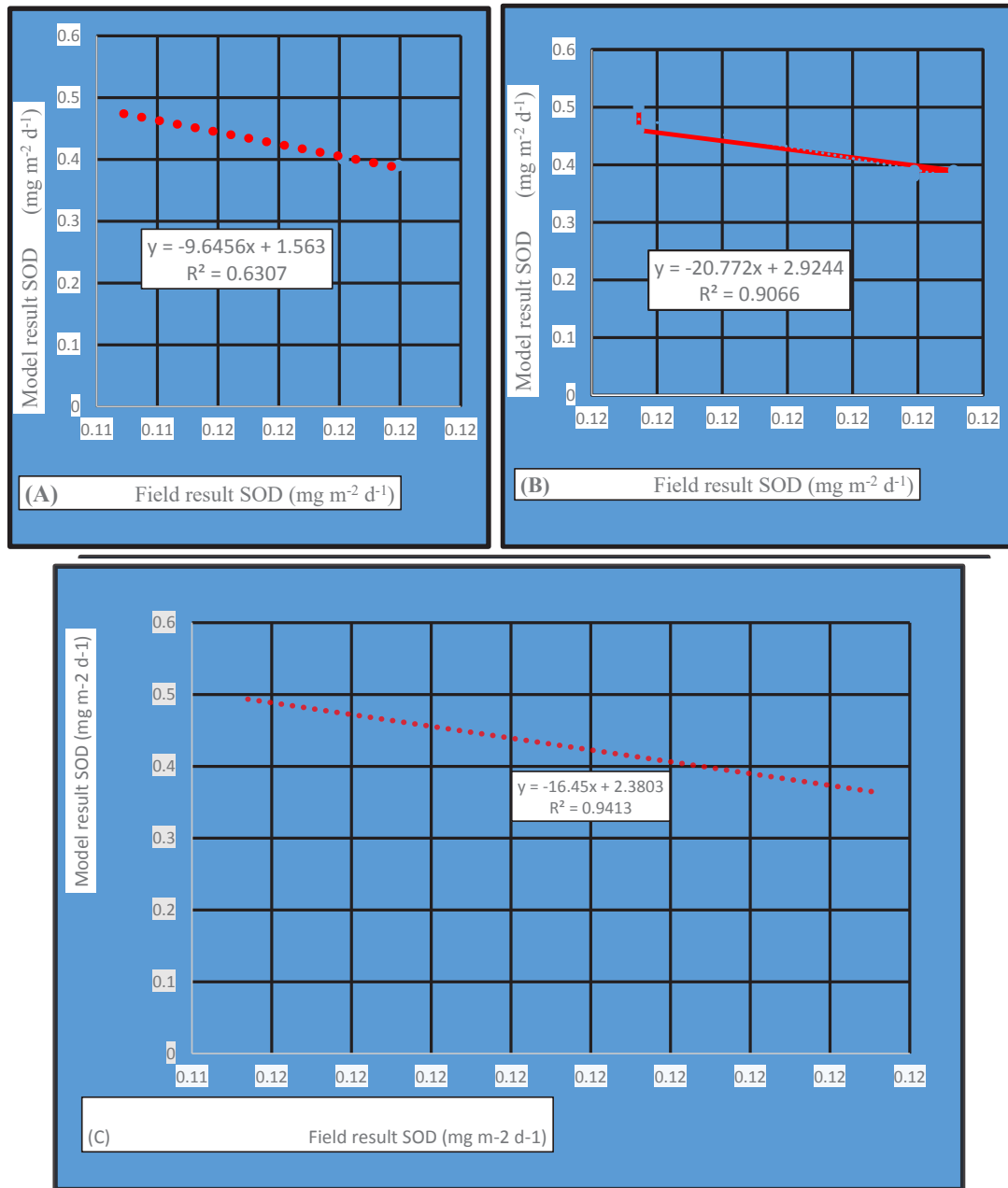


Fig. 4: Statistical test  $R^2$  for SOD model and SOD equation. (A)  $R^2 = 0.63$  calibration result for segment 1, (B)  $R^2 = 0.91$  calibration result for segment 2, (C)  $R^2 = 0.94$  calibration result for segment 8.

results is high. The results of NSE for the state variable of nitrate were 0.9, 0.84, and 0.92 for segment 1, segment 2, and segment 8 respectively, according to Moriasi, 2007 NSE  $> 0.75$  is very good.

In (Table 2) of the model, the result starting from May to the end of the year 2019 for the state variables include temperature, nitrate, dissolved oxygen, total phosphorus, chlo-

rophyll-a, total Kjeldahl nitrogen, CBOD, and ammonium at segments 1, 2, and 8. The last four columns are used to show the results of calibrating the model results with actual data obtained from the site. By applying statistical techniques, we can determine the accuracy and apply the statistical analysis methods to check the accuracy of model results with actual measured data from the site. The first method used is R

squared ( $R^2$ ). Our range for the state variables is between 0.86 and 1.0 and the second test from (Table 2) was the Root mean square error (RMSE), which is the root mean square error of approximation. The last column of (Table 2) is the relative error RE between simulated and measured data, RE is all less than 1 except for the Nitrate which is: 1.86, 1.52, and 1.78 for segments 1, 2, and 8 respectively. So, another test was performed only on this data of Nitrate to ensure the model results are performing well since the  $R^2$  for Nitrate results is high. The results of NSE for the state variable of nitrate were 0.9, 0.84, and 0.92 for segment 1, segment 2, and segment 8 respectively. The simulation process of the Kurtboğazı dam reservoir does not require daily input to the WASP8 system. As mentioned before, there are certain requirements of input data as part of the configuration pattern to build the system representing the actual state case and circumstances for Kurtboğazı reservoir. In addition to this, the user may have an allowance of daily prediction outcomes from the simulation model of different state variables depending on the initial purpose of the model.

### Sediment Oxygen Demand SOD

Since there is no available data for sediment oxygen demand SOD at the site, we need to ensure that our model result is representative of SO. At the site we used an equation from Sharma (2012) (eq. 11). The results are presented in (Table 3) for segments 1, 2, and 8 respectively, and displayed in (Fig. 4). However, the next step would be the calibration of results using  $R^2$  and RE to compare the SOD model and SOD from the equation with results in (Table 4) and (Fig. 5).

The model successfully simulated the sediment oxygen demand and the results which display high values for  $R^2$ . For segment 1, the  $R^2=0.63$ , segment 2 the  $R^2=0.91$ , and for segment 8 the  $R^2=0.94$ . The reason that  $R^2$  is much lower

in segment 1 than in the other locations could be because segment 1 is the inlet point arriving from the Inceğez tunnel to Kurtboğazı reservoir and there could be unaccounted nutrients that are entering the reservoir and causing the different SOD values. According to Santhi et al. (2001) and Van et al. (2003) values of  $R^2$  greater than 0.5 are considered acceptable.

### Internal Nutrient Loading

The model also simulated other phenomena occurring at sediment that contributed to increased levels of SOD at segment 8 or the measuring station at site K1. An overall dissolved oxygen deficiency at the water column, as in internal phosphorus from anoxic sediments, affected water column nutrient concentrations and ratios of total nitrogen over total phosphorus or TN: TP at the reservoir, in that perspective another parameter  $PO_4$  flux to the water column in ( $mg\ P.m^{-2}.day^{-1}$ ) would increase the internal loading release and thus decrease DO at the reservoir. Nutrient flux rates from the sediment represent the net result of various microbiological, chemical, and hydrodynamic processes. This cycle coincides with the development of anoxia in the overlying water. Phosphorus release involves the development of anoxia in the water column, resulting in the creation of reducing conditions in the sediments, with associated changes in the iron-phosphorus complexes, in an oxidizing environment. Iron is in the insoluble ferrous form and the formation of iron in the soluble ferric form with the release of bound phosphorus is usually marked by the development of anoxia condition. These results are in line with previous results (Dunalska et al. 2004) all the ratios of TN: TP is based on the model result presented in (Table 5). Internal Phosphorus from anoxic sediments affected water column nutrient (Elçİl et al. 2008) concentrations and ratios of total nitrogen to total

Table 4: Statistical tests of  $R^2$  and RE used to describe accuracy between the SOD model and SOD equation.

Diagenesis Model	Segment	R square	RE relative error
Sediment oxygen demand SOD	Segment 1	0.63	0.73
	Segment 2	0.91	0.71
	Segment 8	0.94	0.61

Table 5: Ratio of total nitrogen to total phosphorus simulated by the model at segment 8.

Month	TN	TP	Ratio=TN:TP ratio	Note
7	156	50	3	Ratio<9 N limited
8	209	41	5	Ratio<9 N limited
9	380	30.1	13	<9 Ratio <22
11	384	16.4	23	Ratio> 22 P limited

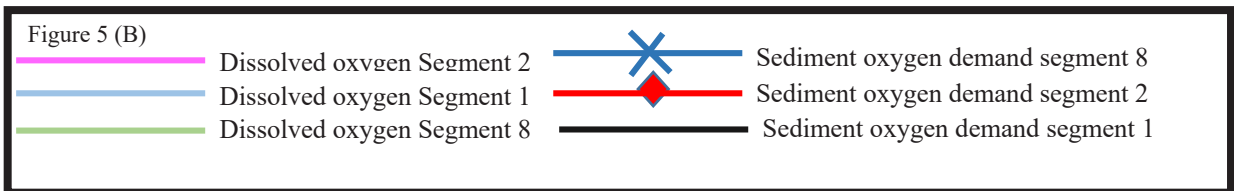
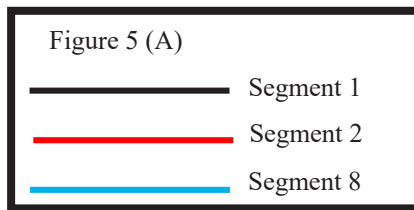
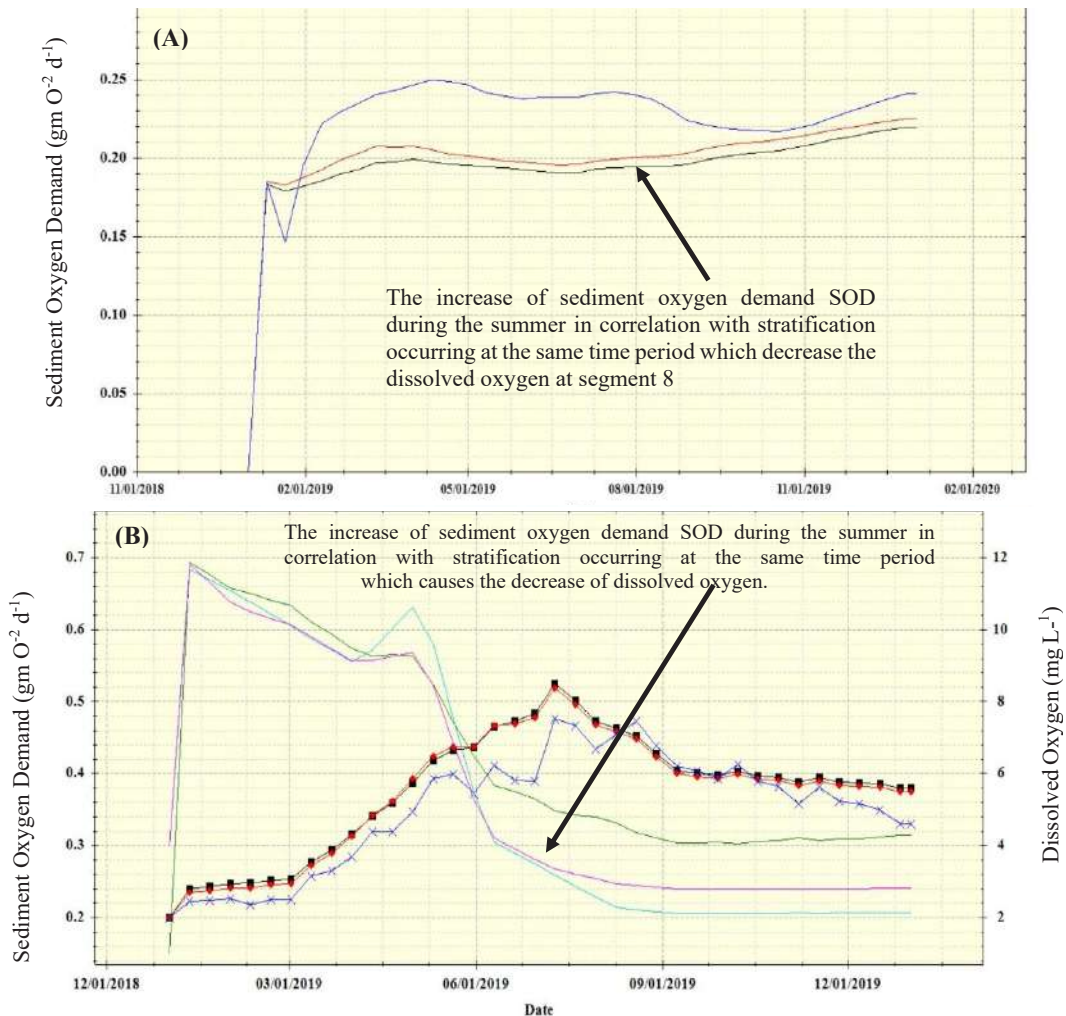


Fig. 5: SOD from the model at Kurtboğazı dam for the segments 1,2 and 8. (A) display the SOD of segment 8 being higher than in segment 1 and 2 specifically in the summer time with an increase of SOD due to stratification. (B) significantly show highest SOD cause lowest values in dissolved oxygen at water column

phosphorus or ratio of TN: TP at the reservoir (Benoit et al. 2006) and (Nikolai & Dzialowski 2014): If TN: TP ratio > 22 indicates Phosphorus limitation. TN: TP ratio <9 indicates Nitrogen limitation and if  $9 < \text{TN: TP ratio} < 22$ , it indicates P and N co limitation. As the temperature disparity between the warmer layer above and the cooler layer below increases in the late summer, the thermocline, a layer of water more frequently observed in a big body of water, decreases.

### Model Validation

Calibration always trains the model for certain hydrological conditions, which are those resembled by the observed data. When used in so-called “out of sample settings,” i.e., hydrological conditions that differ considerably from those referred to in calibration, the model may offer less desirable results in terms of what resulted from calibration. This is a key practical issue that may have a detrimental influence on the reliability of engineering design, because of the uncertainty that affects hydrological models, validation is always important in model simulation design. After calibration and before utilizing it in reality, the literature has proposed more extensive validation techniques, such as cross-validation applications. This type of testing is known as validation. The word validation is often used in hydrology and environmental modeling to describe a technique for examining the performance of simulation and/or forecasting models. In the scientific environment, the word validation has a broader definition that includes any method that aims to test a procedure’s capacity to fulfill a certain scope. In other words, it’s the degree needed for the model’s intended purpose or application, and this is achieved by determining the representative output of our simulation model. This is achieved by tracing the intermediate results and comparing them with observed outcomes. This method involves investigating the intermediate interaction between key variables in the system. In our case, the dissolved oxygen and sediment oxygen demand is selected as it has a high influence on the overall system. By utilizing the correlation coefficient we trace the correlation of SOD DO, temperature,

and chlorophyll a with other state variables and compare with the outcome, to reach this notion Pearson’s coefficient was used to measure validity, its correlation is widely used to validate the strength of an existing linear relationship between variables, and it assesses the linear relationship between quantitative variables (Zhuhua et al. 2019, Ernst et al. 2009). Pearson’s correlation coefficient is a way of determining if two variables have a close relationship, it is defined as the quotient of the covariance and the standard deviation of two variables as shown (Table 6) shows the outcomes of the calculations, the segment that was selected is segment 8, the reason for this choice is due to the fact segment 8 represents the discharge point from the reservoir and according to site field data it’s the critical point where the seasonal stratification and oxygen depletion occurs seasonally. The sediment oxygen demand has a high correlation with dissolved oxygen, temperature total phosphorus, and nitrate, and this result is confirmed by many studies earlier that nutrients can increase eutrophication and later on increase SOD (Mackenthun et al. 1999, Micelis et al. 2005, Belo et al. 2008, Rong et al. 2016). Dissolved oxygen is correlated with a SOD of 0.77 and temperature of 0.79 this is in accordance with previous studies (Lantrip et al. 1987, Hupfer & Lewandowski 2008, Sharma 2012, Wei-Bo et al. 2012, Akomeah & Lindenschmidt 2017). The DO and the nutrients’ total phosphorus (0.66), and nitrate (0.65), have a moderate association. Previous studies supported this finding (Lindenschmidt et al. 2009, Rong et al. 2016, Bierlein et al. 2016, Julie & Lindenschmidt 2017), as given in (Table 6) there is also a weak correlation between dissolved oxygen and chlorophyll 0.28 (Chen et al. 2019) and a high correlation between dissolved oxygen and sediment oxygen demand 0.77 while the CBOD and dissolved oxygen are negatively highly correlated -0.70 (Oskar et al. 2020), which is often observed the inverse strong relation between CBOD and dissolved oxygen (Chowdhury et al. 2014, Lindenschmidt et al. 2017, Chai & Draxler 2014). Our model was validated based on the concept of using Pearson’s correlation coefficient and the

Table 6: Application of Pearson correlation to variables at segment 8.

State variables	Sediment oxygen demand	Dissolved oxygen
Dissolved oxygen	0.77	
Temperature	0.89	0.79
Total Phosphorus	0.89	0.66
NO <sub>3</sub>	0.96	0.65
CBOD	-0.68	-0.70
Chlorophyll a	-0.7	-0.28
Sediment oxygen demand		0.77

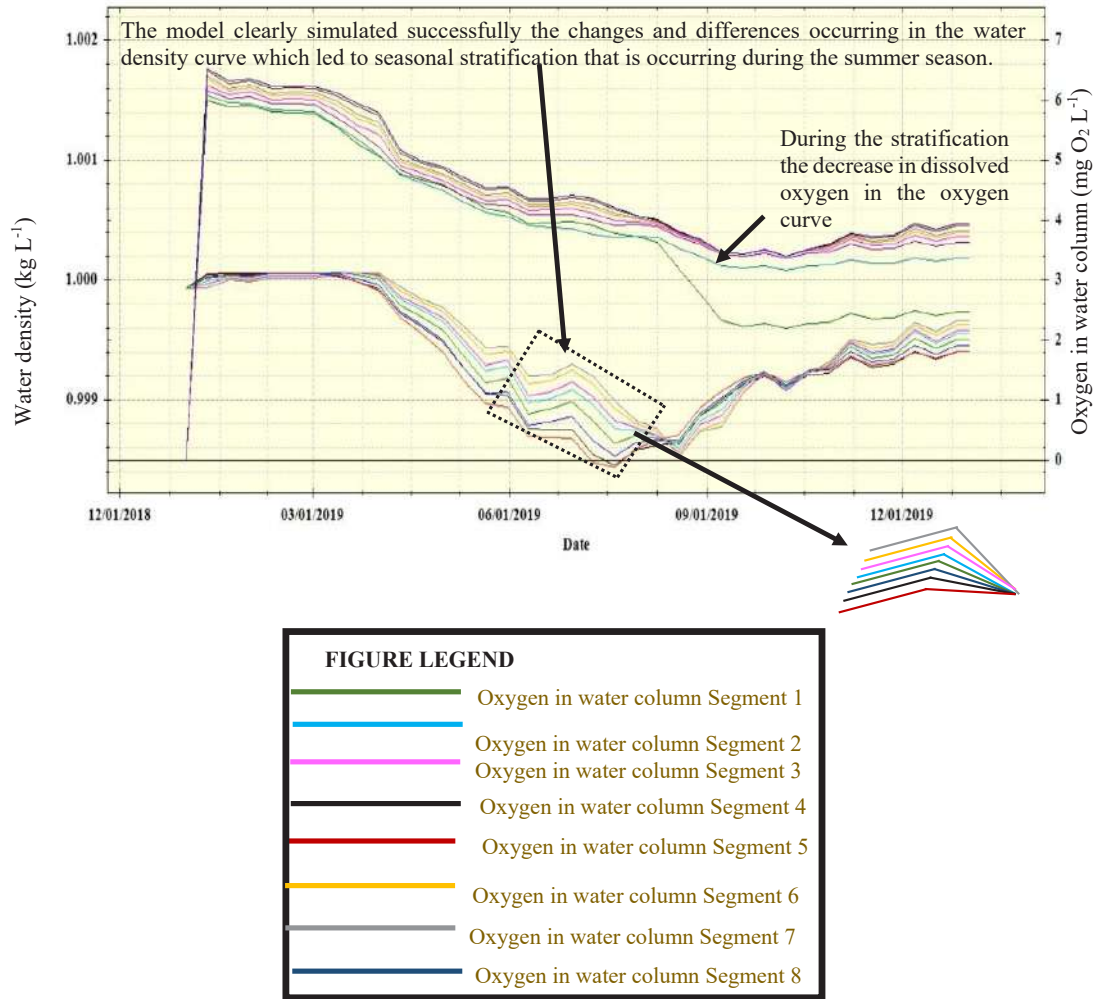


Fig. 6: Water density and dissolved oxygen level in the water column along with the dissolved oxygen for all 8 segments.

state variables in the model, which we checked and validated with previous research.

## DISCUSSION

As stratification is a process of generating thermal layers in a reservoir or a lake in summertime, the water temperatures at the upper layer become warmer while the bottom layer is colder. This leads to an increase in the differences in the temperatures between the upper layer and bottom layer. In the case of temperature differences, it results in differences in densities, thus resulting in thermal stratification (Mahmoud 2009, Şebnem 2008), the recurrence was successfully simulated by our model as presented in (Fig. 6). According to previous research (Chen et al. 2019, Jin et al. 2006, 1998, Pan et al. 2009, Schlezinger 2010, Testa et al. 2013, Haan

et al. 1995). From the simulation result of our model and by examining (Fig. 7), we conclude that with increasing total phosphorus and peak maximum value of total phosphorus; water temperature; Nitrate; dissolved oxygen corresponded to the highest SOD value.

Mineralization of nitrogen includes the processes by which organic compounds are decomposed and converted to ammonium and nitrate. The formation of complex nitrogen compounds occurs due to their assimilation and immobilization. The major nitrogen-related processes that occur in the aquatic environment are ammonification, nitrification, and denitrification.

The model simulated is shown in (Fig. 8). At observation station K1 or segment 8 in the model, the impact of anoxic conditions on the SOD and fluxes for ammonium, nitrate, and

phosphorus is shown in graph 8 (A) of nitrate benthic flow and the negative sign indicates the movement of nitrate from the water column to sediment in summer at station K1 or segment 8 for the same graph 8 (B) PO<sub>4</sub> benthic flux displayed a seasonal cycle with elevated fluxes in the spring and summer and reduced fluxes in the fall. Reaching a minimum in the winter, this cycle coincides with the development of anoxia in the overlying water. Finally, the examination of graph 8 (C) displaying the dissolved inorganic phosphorus benthic flux,

shows an increased movement of available phosphorus from sediment to the water column as anoxic conditions rise in summer and ammonium benthic flux variability is observed in spring and summer. On the whole, the reduction in flux to sediment in summer reflects a temperature or biological community dependency.

Our model displays (Table 5) the TN: TP ratio shift from N limited during the summer to P limited at the beginning of winter, and the results are in accordance with previous

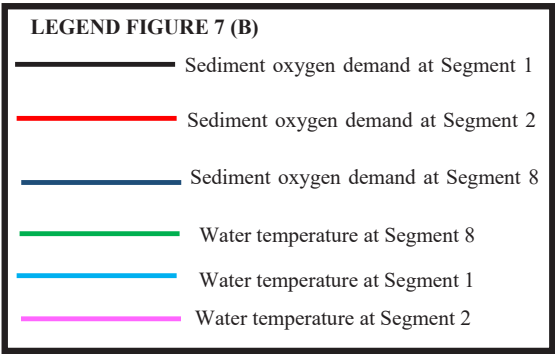
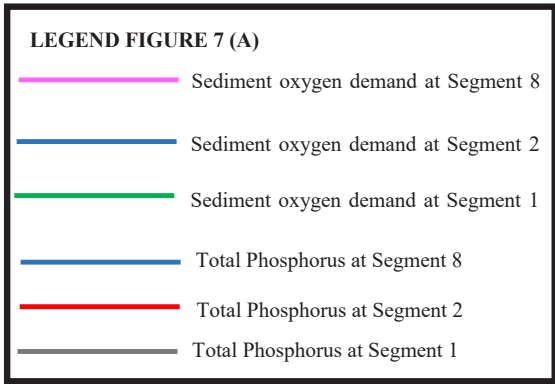
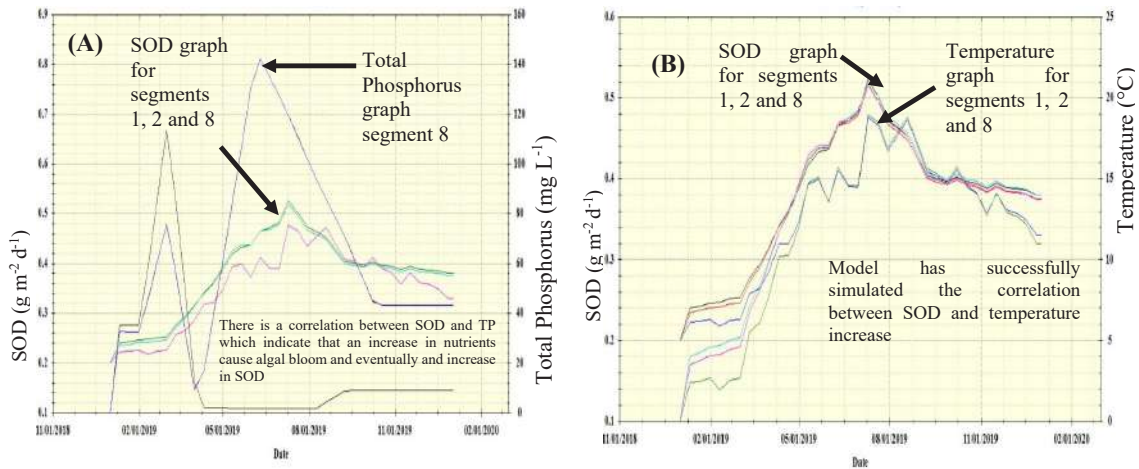


Fig. 7: The state variables that influence the sediment oxygen demand according to our model simulation result.

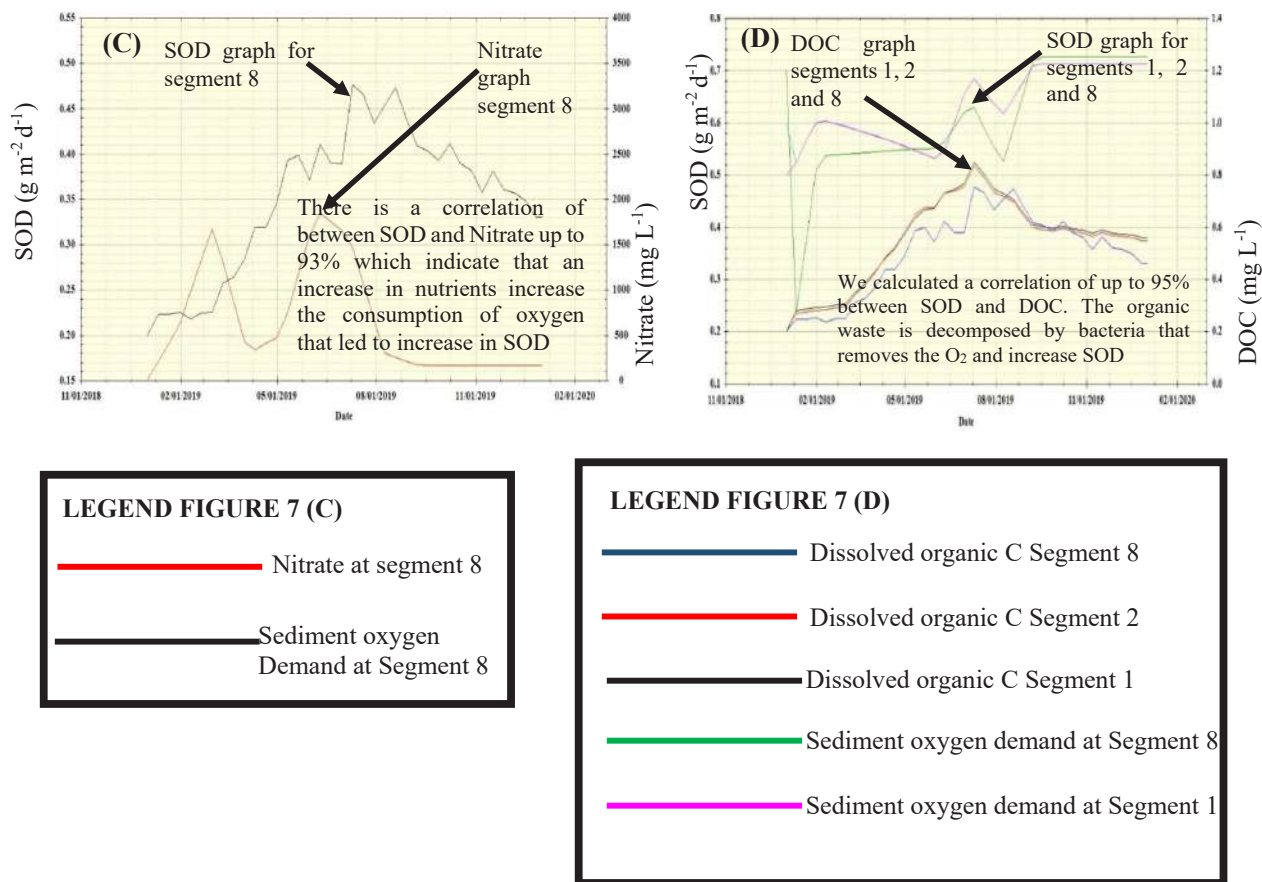


Fig. 7: (continue) the state variables that influence the sediment oxygen demand according to our model simulation result.

research (Jensen & Anderson 1992 & Rahman et al. 2008). Internal P can build up in the hypolimnion and help to lower TN: TP ratios and potentially create N limiting conditions in the epilimnion, this was confirmed by previous studies that have similarly shown that internal Phosphorus loading can play an important role in late season P concentrations and algal blooms (Bierlein et al. 2016, Coppens et al. 2020). The increase of N<sub>2</sub> gas in the water column during the stratification phase, which explains why the N was limited for the TN: TPN ratio at that time, can be seen as another significant signal from the results of the simulated model by examining the denitrification flux from sediment in (Fig. 9). Finally, the curve in (Fig. 10) explores the DO probability for segment 8, showing in detail that dissolved oxygen below 2 (mg.L<sup>-1</sup>) was only less than 3 percent of the time during the anoxic period and this is in alignment and accordance with field results from ASKI (2021)

## CONCLUSION

- As a valuable numerical tool for numerical modeling

of river water quality and temperature evolution, a full hydrodynamic and water quality model has been developed to estimate complicated temporal relationship situations in each of the physical processes that exist in real-life environments. Kinetic equations, for example, are physical processes, to this end, tributaries, abstractions, and heat fluxes are provided to simulate the yearly change in water depth, discharge, and temperature. A finite difference method was used to solve the resultant system of equations volume composition that promotes consistent and conservative performance solutions across all flow regimes.

- The suggested model may correctly and reliably depict the reality of the interactions between hydrodynamics and quality parameters after it is thoroughly calibrated and validated, as a result, the integrated model can estimate water quality in a variety of settings, this tool may be valuable to the entities delivering this service since it will allow them to decrease and accurately identify the placement of the quality measurement stations.



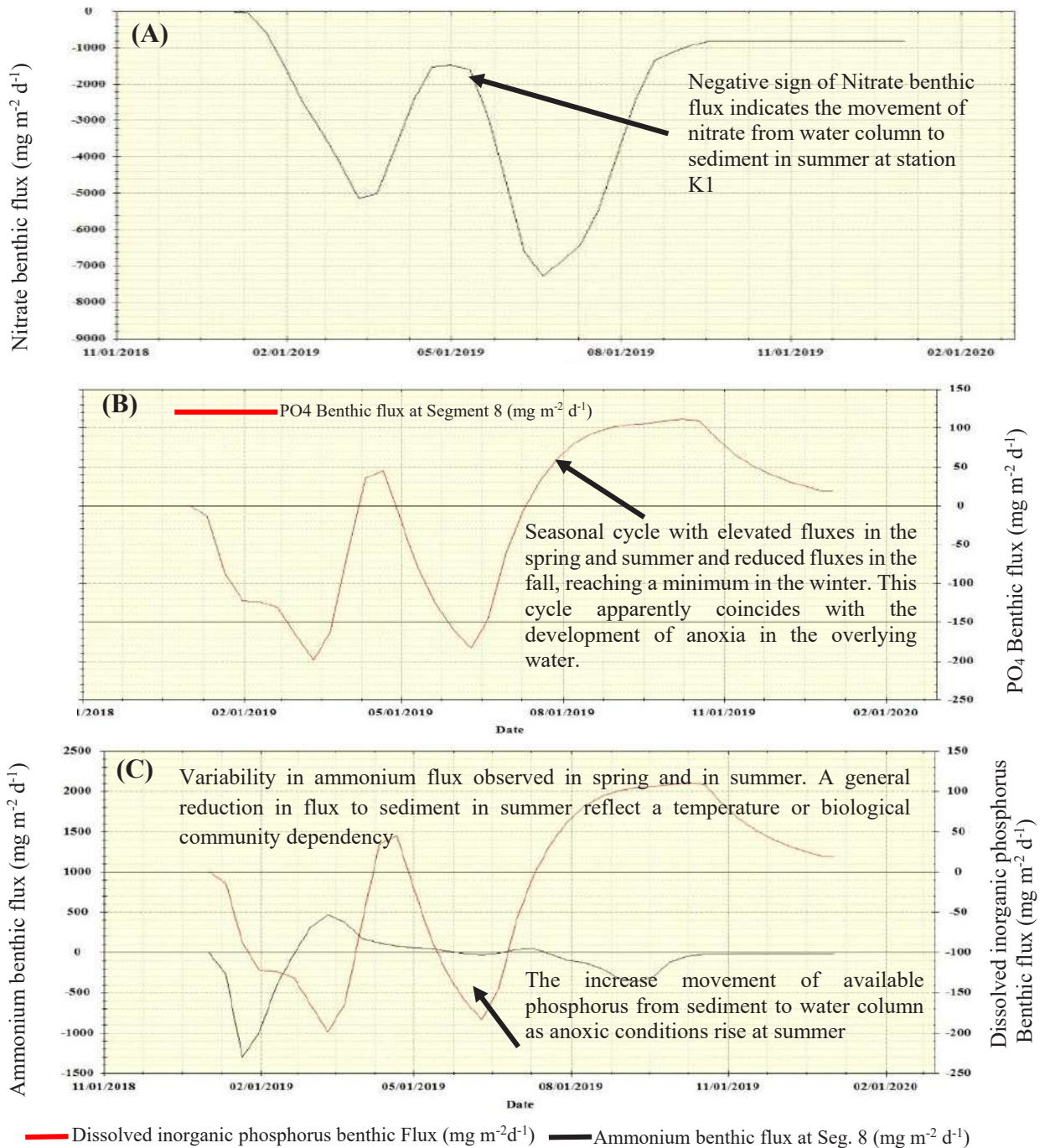


Fig. 8: The effect of anoxic conditions on the SOD and fluxes for ammonium, nitrate, and phosphorus at observation station K1 or segment 8 in the model.

- The effect of anoxic conditions on nitrate benthic flux causes the movement of nitrate from the water column to sediments in summer at station K1 or segment 8, regarding the PO<sub>4</sub> benthic flux at seasonal cycle with elevated fluxes in the spring and summer and reduced fluxes in the fall, reaching a minimum in the winter. This cycle coincides with the development of anoxia in the overlying water.
- As for the effect of anoxic conditions on inorganic phosphorus benthic flux, it increases the movement

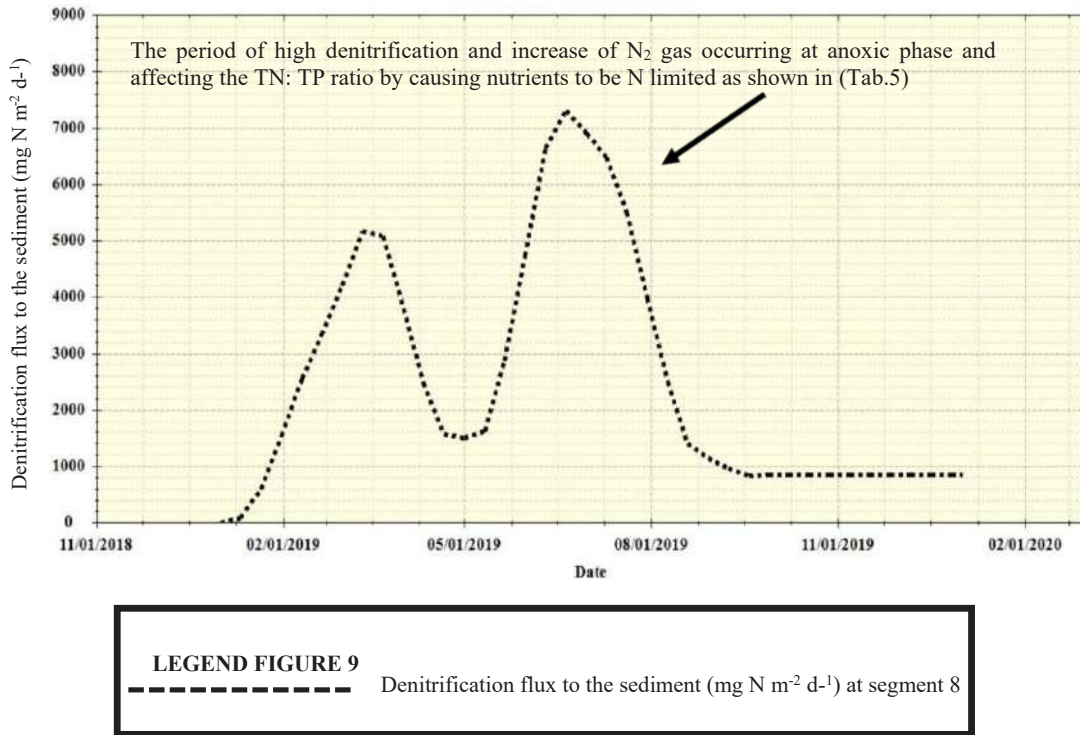


Fig. 9: Denitrification flux at anoxic phase from sediment to water column at segment 8.

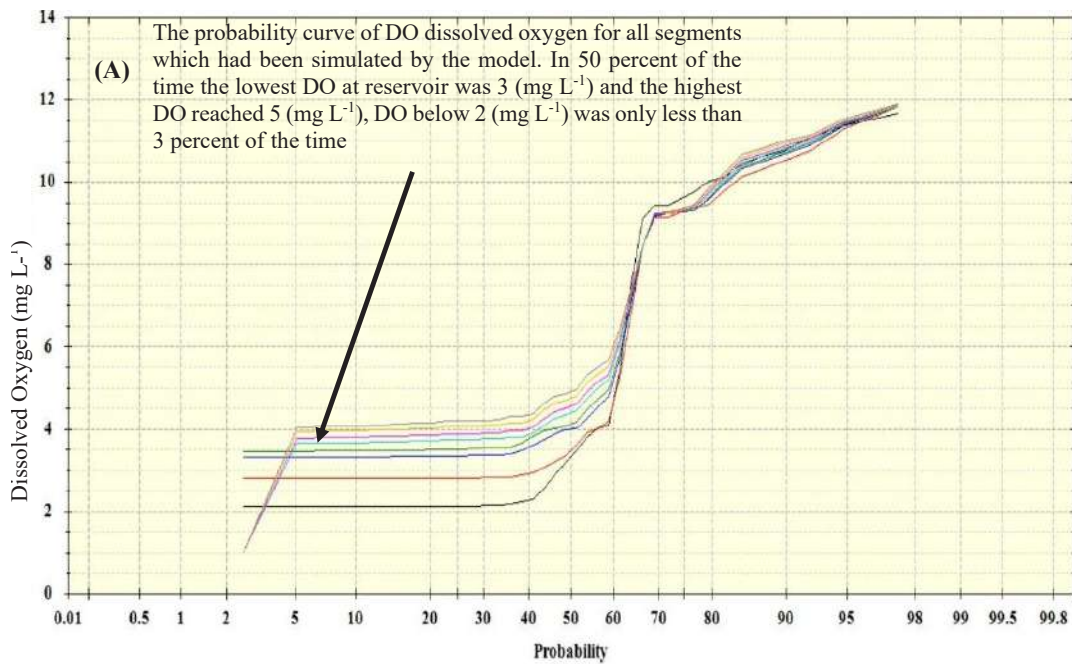


Fig. cont....

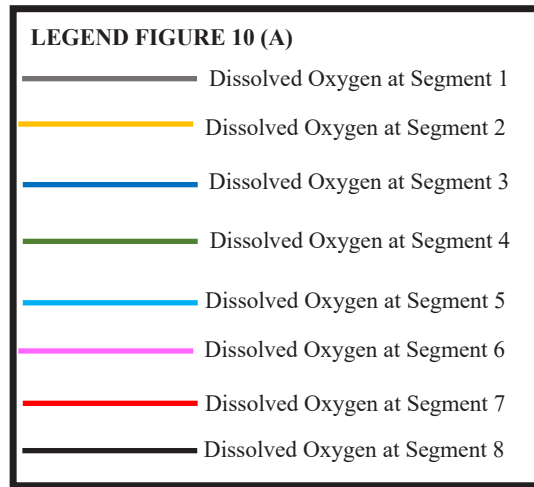


Fig. 10 A: Probability curve and simulated model result for dissolved oxygen for all segments of the model.

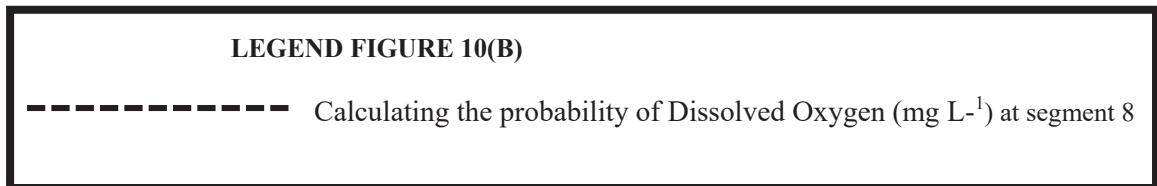
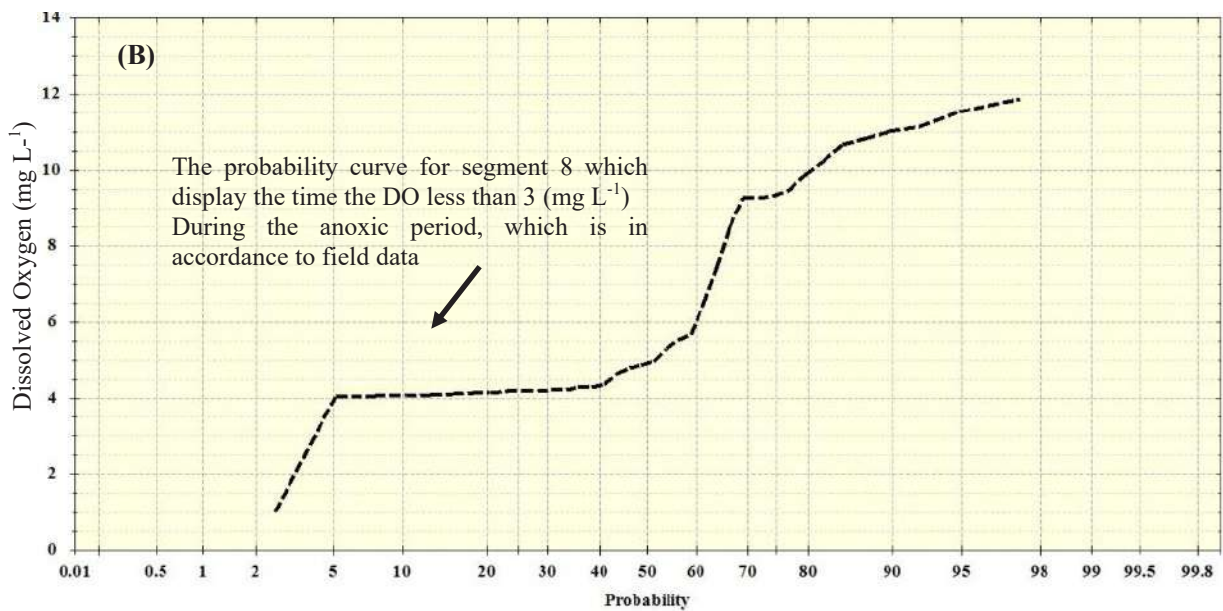


Fig. 10 B: Probability curve and simulated model result for dissolved oxygen for all segments of the model.

of available phosphorus from sediment to the water column as anoxic conditions rise in summer and ammonium benthic flux variability is observed in spring and summer. A general reduction in flux to sediment in summer reflects a temperature or biological community dependency - the period of high denitrification and increase of N<sub>2</sub> gas occurring at an anoxic phase and affecting the TN: TP ratio by causing nutrients to be limited as simulated by the model.

- In segment 8, there is a positive association between SOD and dissolved organic carbon, total phosphorus, temperature, and nitrate, which is evidenced by the anoxic situation and oxygen depletion that took place over the summer.
- The probability curve of DO dissolved oxygen for all segments had been stimulated by the model. 50 %, of the time the lowest DO at the reservoir, was 3 (mg.L<sup>-1</sup>) and the highest DO reach 5 (mg.L<sup>-1</sup>), dissolved oxygen below 2 (mg.L<sup>-1</sup>) was only less than 3 percent of the time.
- Our model was further validated using the Pearson correlation coefficient with results that were in accordance with previous research and model work, which confirmed the validity of our model results.

## REFERENCES

- Akomeah, E. and Lindenschmidt, K. 2017. Seasonal variation in sediment oxygen demand in a northern chained river-lake system. *Water*, 9: 254-300.
- Altin, A., Bakir, F. and Özölçer, I. 2010. The evaluation of Kurtboğazi Dam (Ankara, Turkey) from Hydro-Geochemical and Environmental Aspects. *Water Res. Manag.*, 24: 747-759.
- Ambrose, B. 2017. WASP8 Stream Transport - Model Theory and User's Guide. U.S. Environmental Protection Agency Office of Research and Development, Washington, DC.
- Ankara Çabuk, Turkey weather history, 2020 November 10, Wunderground, Retrieved from Wunderground history monthly LTAC, Çubuk, Turkey Weather History | Weather (wunderground.com).
- Ankara Water and Sewerage Administration (ASKI). 2021. Available at <http://www.aski.gov.tr/>. Accessed on April 3, 2021.
- Belo, L. 2008. Measurement of the Sediment Oxygen Demand in Selected Stations of the Pasig River Using a Bench Scale Benthic Respirometer. Master's Thesis Presented to the Faculty of the Engineering Graduate School, Department of Chemical Engineering, and University, Philippines.
- Benoit, P., Alfonso, M. and Yves, G. 2006. Modeling of dissolved oxygen levels in the bottom waters of the Lower St. Lawrence Estuary. *Sci. Marine Chem.*, 102: 13-32.
- Bierlein, K., Maryam, R., Scott, S., Lee, B. and John, L. 2016. Increased sediment oxygen flux in lakes and reservoirs: The impact of hypolimnion oxygenation. *Water Resour. Res.*, 53: 4876-4890
- Bilal, Q., Avais, M., Ijaz, M. and Khan, J.A. 2009. Prevalence and chemotherapy of *Balantidium coli* in cattle in the River Ravi region. *Vet. Parasitol.* 163: 15-17.
- Burger, D., David, P. and Conrad, A. 2008. Modeling the relative importance of internal and external nutrient loads on water column nutrient concentrations and phytoplankton biomass in a shallow lake, ecological modeling, *Sci. Dir.*, 211: 411-423.
- Camacho, A., Martin, J., Watson, B. and Stribling, L. 2014. Modeling the factors controlling phytoplankton in the St. Louis Bay Estuary, Mississippi, and evaluating estuarine responses to nutrient load modifications. *J. Environ. Eng.*, 54: 818.
- Chai, T. and Draxler, R. 2014. Root mean square error (RMSE) or mean absolute error (MAE)? Arguments against avoiding RMSE in the literature, *Geosci. Model Develop.* 7: 1247-1250.
- Chen, C. and Lung, W. 2012. Technical challenges with BOD/DO modeling of rivers in Taiwan. *J. Hydro. Environ.* 11: 33-46.
- Chen, W., Wen-Cheng, L. and Li-Ting, H. 2012. Measurement of sediment oxygen demand for modeling the dissolved oxygen distribution in a lake. *Inter. J. Physic. Sci.*, 7: 5036-5048.
- Chen, L., Changchun, H., Ronghua, M. and Yuxin, M. 2019. Can the watershed non-point source phosphorus flux amount be reflected by lake sediment? *Ecol. Indic.*, 102: 118-130.
- Chowdhury, A., Khairul, H. and Kaosar, A. 2014. The use of an aeration system to prevent thermal stratification of water bodies: Ponds, lakes, and water supply reservoirs. *Appl. Ecol. Environ. Sci.*, 2: 1-7.
- Coppens, J., Dennis, T., Erik J. and Meryem, B. 2020. The impact of climate change on a Mediterranean shallow lake: insights based on catchment and lake modeling. *Reg. Environ. Change*, 14: 56.
- Dunalska, J., Górniak, D. and Teodorowicz, M. 2004. Seasonal distribution of dissolved and particulate organic carbon in the water column of a Meromictic Lake. *Pol. J. Environ.*, 13: 375-379.
- El I, . 2008. Effects of Thermal Stratification and Mixing on Reservoir Water Quality. Springer, Singapore. DOI 10.1007/s10201-008-0240-x
- Ernst, M. and Jennifer, O. 2009. Development and application of a WASP model on a large Texas reservoir to assess eutrophication control. *Lake Reserv. Manag.*, 25: 136-148.
- Google map, Earth google, 2021 March 5, Retrieved from Google Earth Map, Turkey, /[www.google.com/maps/@36.2089,43.98383,726m/data](http://www.google.com/maps/@36.2089,43.98383,726m/data)
- Guildford, S. and Hecky, R. 2000. Total nitrogen, total phosphorus, and nutrient limitation in lakes and oceans: is there a common relationship? *Limnol. Oceanogr.* 45: 1213-1223.
- Haan, C., Aured, B. and Prabhu, S. 1995. Statistical procedure for evaluating Hydrologic/water quality models. *Am. Soc. Agric. Eng.*, 38: 725-733.
- Hazewinkel, M. 2001. Theory of Errors. Springer, Singapore.
- Hupfer, M. and Lewandowski, J. 2008. Oxygen controls the phosphorus release from lakes sediments, a long-lasting paradigm in limnology. *Int. Rev. Hydrobiol.*, 93: 415-432.
- Jensen, H. and Andersen, F. 1992. Importance of temperature, nitrate, and pH for phosphate release from aerobic sediments of four shallow, eutrophic lakes. *Limnol. Oceanogr.*, 37: 577-589.
- Jin, X., James, K., Lung, W., D.P. and Tisdale, S. 1998. Assessing Lake Okeechobee eutrophication with water quality models. *J. Water Resour. Plan Manag.*, 124: 22-30.
- Jin, X., Wan, S. and Pang, Y. 2006. Phosphorus fractions and the effect of pH on the phosphorus release of the sediments from different trophic areas in Taihu Lake, China. *Environ. Pollut.*, 139: 288-295.
- Julie, A. and Lindenschmidt, K. 2017. Modeling dissolved oxygen/sediment oxygen demand under the ice in a shallow eutrophic Prairie reservoir. *Water J.*, 9: 3-16.
- Kali, N. and Güngör, M. 2020. Usage and effects of algaeicide in Kurtboğazi Dam Lake, Turkish. *J. Water Sci. Manag.*, 4: 162-177.
- Kendirli, B., Çakmak, B. and Gökalp, Z. 2009. Assessment of water quality management in Turkey. *Int. Water Resour. Assoc.*, 30: 446-455.
- Kernan, M. and Allott, T. 1999. Spatial variability of Nitrate concentration

- in Lakes in Snowdonia lakes in North Wales. *Hydrol. Earth Syst. Sci.*, 3: 395-408.
- Lantrip, M., Robert, M., Summers, D.J., Phelan, R. and William, A. 1987. Sediment/Water-Column Flux of Nutrients and Oxygen in the Tidal Patuxent River and Estuary, Maryland. Department of the interior, U.S. Geological Survey, Reston, Virginia.
- Li, N., Huang, T., Chang, Z and Li, K. 2021. Effects of benthic hydraulics on sediment oxygen demand in a canyon-shaped deep drinking water reservoir: Experimental and modeling study. *J. Environ. Sci.*, 102: 226-234.
- Lindenschmidt, K., Pech, I. and Baborowski, M. 2009. Environmental Risk of Dissolved Oxygen Depletion of Diverted Flood Waters in River Polder Systems-A Quasi-2D Flood Modelling Approach. *Sci. Environ.*, 407: 1598-1612.
- Mackenthun, A. and Heinz, S. 1995. Effect of Flow Velocity on Sediment Oxygen Demand: Experimental Results, University of Minnesota St. Anthony falls hydraulic laboratory. Project Report No. 371. Saint Paul, Minnesota, United States.
- Magara, Y. 1997. Classification of water quality standards. *Water Qual. Std.*, 1: 11.
- Mahmud Achmad 2009. Stratification in Reservoirs and Lakes 2009. Factors causing stratification. Academia Journal paper. E:\HD2\FromBigHDD706\Dissertation\Summary-MSWord\Wr-Summary\Stratification.doc
- Mbongowo, J., Richard, M. and Comfort, W. 2018. Water quality modeling and sensitivity analysis using Water Quality Analysis Simulation Program (WASP) in the Shenandoah River watershed. *Phys. Geogr.*, 15: 252-269. <https://doi.org/10.1080/02723646.2018.1507339>
- Micelis, C. and Dennis, D. 2005. Sediment Oxygen Demand in Lake Ewauna and the Klamath River, Oregon. Scientific Investigations, U.S. Department of the Interior Geological Survey, Reston, Virginia.
- Mielke, P. and Berry, K. 2001. Permutation Methods: A Distance Function Approach. Springer, N.Y.
- Mirolaw, S. and Piotra, O. 2014. Seasonal changes of nitrogen and phosphorus concentration in SUPRAŚL River. *J. Ecol. Eng.*, 15: 26-31.
- Moltke, L., Stiig, M., Katherine, R., Eva, F. and Hans, H. 2017. How well does chlorophyll explain the seasonal variation in phytoplankton activity? *Estuaries and Coasts*, 40: 1263-1275.
- Moore, D., Notz, S. and Flinger, W. 2013. The Basic Practice of Statistics. Freeman and Company, NY.
- Moriasi, D., Jeff, A. and Michael, W. 2007. Model evaluation guidelines for systematic quantification of accuracy in watershed simulations. *Am. Soc. Agric. Biol. Eng.*, 50: 885-890.
- Nikolai, S. and Dzialowski, A.R. 2014. Effects of internal phosphorus loading on nutrient limitation in a eutrophic reservoir. *Limnologia*, 49: 33-41.
- Oskar, S., Filstrup, C., Tasevska, O. and Brauns, M. 2020. Chlorophyll a relationship with nutrients and temperature, and predictions for lakes across perialpine and Balkan mountain regions. *Inland Waters*, 41: 4204. Doi: 10.1080/20442041.
- Ozmen, M., Abbas, G., Zerhra, K. and Elif, G. 2006. Monitoring the Effects of Water Pollution on Cyprinus Carpio Karakaya Dam Lake, Turkey. *Ecotoxicology*, 15: 157-169.
- Panagiotaki, P. and Dimitrios, V. 2015. Assessment of nutrients and heavy metals in the surface sediments of the artificial lake water reservoir Karla Thessaly Greece. *Environ. Earth Sci.*, 73: 4483-4493.
- Pan, B., Jun, W., Liang, X. and Hong-Zhu, W. 2009. Factors influencing chlorophyll concentration in the Yangtze- connected lakes. *Fresenius Environ. Bullet.*, 18: 1894-1900.
- Papastergiadou, E., Kagalou, I., Stefanidis, K., Retalis A. and Leonardos I. 2009. Effects of anthropogenic influences on the trophic state, land uses and aquatic vegetation in a shallow Mediterranean lake: implications for restoration. *Water Resour. Manag.* 10: 56-89. DOI: 10.1007/s11269-009-9453-y
- Park, J. and Kim, A. 2013. Assessment of future climate change impact on water quality of Chungju Lake, South Korea, Using WASP coupled with SWAT. *Water Resource. Assoc.*, 49: 1225-123814.
- Parlak, M., Dıngsoy, Y. and Seyrek K. 2007. Determination of Erosion Risk According to Corine Methodology. A Case study, International Congress River Basin Management, DSI, Antalya.
- Patil, J., Sarangi, A., Singh, O., Singh, A. and Ahmad, T. 2008. Development of a GIS interface for estimation of runoff from watersheds. *Water Resour. Manag.*, 22: 1221-1238.
- Quirós, R. 2004. The relationship between nitrate and ammonia concentrations in the pelagic zone of lakes. *Limnologia*, 22: 37-50.
- Rahman, S. and Hossain, F. 2008. Spatial assessment of water quality in peripheral rivers of Dhaka City for optimal relocation of water intake point. *Water Resour. Manag.*, 22: 377-39.
- Ranjith, S., Anand, S., Dhungana, S. and Kumar K. 2019. Water quality model for streams: A Review. *J. Environ. Protect.*, 10: 1612-1648.
- Ray, W., Wen, S., Ching-Ho, C. and Shu L. 1996. Simulation model for investigating the effect of reservoir operation on water quality. *Environ. Sci.*, 11: 143-150.
- Rong, N., Shan, B. and Wang, C. 2016. Determination of sediment oxygen demand in the Ziya River Watershed, China: Based on Laboratory Core Incubation and Microelectrode Measurements. *Int. J. Environ. Res. Pub. Health*, 13: 232-240.
- Roy, K., Rudra, N., Pravin, A. and Rahul B. 2016. Further studies on validation of predictive QSAR models. *Chemo. Metrics Intellig. Lab. Sys.*, 152: 18-33.
- Santhi, C., Arnold, J., Williams, R., Dugas S. and Hauck L. 2001. Validation of SWAT model on a large river basin with point and nonpoint sources. *J. Am. Water Resour. Assoc.* 37: 1169-1188.
- Sharma, K. 2012. Factors Affecting Sediment Oxygen Demand of The Athabasca River Sediment Under Ice Cover. University of Alberta, Civil and Environmental Engineering. Edmonton, Alberta.
- Schlezingner, D. 2010. Merrimack River Sediment Nutrient Regeneration 2009 Sampling Season- Technical Report, The School For Marine Science And Technology.
- Simon, P. and Hashemi, M. 2018. Ocean Modelling for Resource Characterization, Fundamentals of Ocean Renew. Energy, <https://doi.org/10.1016/B978-0-12-810448-4.00008-2>.
- Soyupak, S., Mukhallalati, L., Yemien, D., Bayar A. and Yurteri C. 1997. Evaluation of eutrophication control strategies for the Keban Dam reservoir. *Ecological Modelling*, 97: 99-110.
- Stolarska, Z. and Kempa, M. 2021. Modeling and monitoring of hydrodynamics and surface water quality in the Sulejów Dam Reservoir, Poland. *Water*, 13: 296-300.
- Testa, M., Damian, C., Dominic M., Walter R., Jeffrey C., Cornwell W. and Michael K. 2013. Sediment flux modeling: Simulating nitrogen, phosphorus, and silica cycles. *Estuarine, Coastal and Shelf Science*, 131: 245-263.
- Tozsin G., Bakir F., Acar C. and Koç E. 2015. Evaluation of water quality for the Kurtbo azı dam outlet and the streams feeding the dam in Ankara Turkey, World Academy of Science, Engineering, and Techno. Inter. J. of Geo. & Envi. Eng., 9: 11-17.
- Tufford, D. and Hank, N. 1999. Spatial and temporal hydrodynamic and water quality modeling analysis of a large reservoir in South Carolina. *Ecol. Model*, 114: 137-173.
- Turkish Statistical Institute (TUIK). 2021. Population recording system with the address. Available at [http://www.tuik.gov.tr/VeriBilgi.do?tb\\_id=39&ust\\_id=11](http://www.tuik.gov.tr/VeriBilgi.do?tb_id=39&ust_id=11). Accessed on April 10, 2021.
- Turkish Water Pollution Control Regulation. 2004. Official Journal, 687: 18-76. Retrieved from Bacteria and E. coli in water, Bacteria and E. coli in Water (usgs.gov).
- U.S. EPA. 2003. Technical Support Document for the Clear Skies Act 2003: air quality modeling analyses. Environmental Protection Agency,

- Office of Air Quality Planning and Standards, Emissions Analysis and Monitoring Division, Research Triangle Park, NC.
- USGS Science for a changing world, Water science school, 2020 December 10, Water Science School.
- Van, L., Arnold, M. and Garbrecht, J. 2003. Hydrologic simulation on agricultural watersheds: Choosing between two models. *Trans. ASAE*, 46: 1539-1551.
- Wei-Bo, C., Wen-Cheng, L. and Li-Ting, H. 2012. Measurement of sediment oxygen demand for modeling the dissolved oxygen distribution in a subalpine lake. *Int. J. Phys. Sci.*, 7: 5036-5048.
- William, W. 2002. Phosphorus balance models for Eucha and Spavinaw reservoirs: City of Tulsa and Tulsa Metropolitan Utility Authority. McKinney & Stringer P.C., Oklahoma.
- Wool, T.A., Davie, S.R. and Rodriguez, H.N. 2003a. Development of a three-dimensional hydrodynamic and water quality model to support the total maximum daily load decision process for the Neuse River Estuary, North Carolina. *American Society of Civil Engineers. J. Water Resource. Plan. Manag.*, 129: 295-306.
- Wool, T., Ambrose, L., Martin, J. and Comer, E. 2003b. *Water Quality Analysis and Simulation Program (WASP)*. Version 6.0, <http://www.epa.gov/athens/wwqtsc/html/wasp.html>. Accessed Feb 2021.
- Wool, T., Ambrose, R., Martin, J. and Comer, E. 2017. *Supplement to Water Analysis Simulation Program User Documentation WASP sediment diagenesis: Model Theory and User's Guide*. U.S. Environmental Protection, Agency, Washington DC.
- Wang, X., Jie, J., Tingli, S., Zhiyao, Z., Jiping, X. and Li, W. 2018. A fusion water quality soft-sensing method based on WASP model and its application in water eutrophication evaluation, *Hindawi, J. Chem.*, 16: 841.
- Zhuhua, H., Yiran, Z., Yaochi, Z., Mingshan, X., Jiezhao, Z., Zhigang, T. and Juntao, L. 2019. Water quality prediction method based on the deep LSTM network considering correlation in smart mariculture. *Sensors*. 11: 420. Doi: 10.3390/s19061420.



# Genotoxic Effects of Rice-Agrochemicals on *Channa punctatus* (Bloch) and *Cyprinus carpio* (Linnaeus) Using Micronucleus Assay and Alkaline Single Cell Gel Electrophoresis

M. Kaur\*, A. Bhatnagar\*†, O. Dhillon\* and A. S. Yadav\*

\*Department of Zoology, Kurukshetra University, Kurukshetra-136119, India

†Corresponding author: Anita Bhatnagar; anitabhatnagar@gmail.com

Nat. Env. & Poll. Tech.  
Website: [www.neptjournal.com](http://www.neptjournal.com)

Received: 16-01-2022  
Revised: 08-03-2022  
Accepted: 11-03-2022

## Key Words:

Agrochemicals  
DNA damage  
Genotoxicity  
Micronucleus assay  
Rice-cum-fish culture

## ABSTRACT

Rice-cum-fish culture is a cost-effective practice for marginal farmers but the major constraint is the indiscriminate use of agrochemicals. Present work was designed to assess the genotoxic effects of rice agrochemicals in *Channa punctatus* (Experiment 1 CP1 to CP3) and *Cyprinus carpio* (Experiment 2 CC1 to CC3); using micronucleus, chromosome aberration, and single cell gel electrophoresis/Comet assay. Two experiments with three treatments (CP1/CC1: without pesticide; CP2/CC2: recommended doses; CP3/CC3: farmers' dose) were maintained in triplicates. The presence of tail DNA and micronuclei depicted significant DNA damage ( $P < 0.05$ ) in all the treated fish. The mean percent frequency of MN showed significant ( $P < 0.05$ ) differences with respect to the initial. The chromosomal aberrations and mean frequencies of tail DNA (%) were significantly abundant in CP3 and CC3 indicating high a genotoxic effect. Keeping in view the low genotoxic effects, treatment of CP2 and CC2 with recommended doses of pesticides may be disseminated to farmers.

## INTRODUCTION

Rice is crucial to worldwide food security serving as the principal ingredient in the everyday diets of around three billion individuals. Rice is the main food crop on the planet with upgraded varieties developed globally in a wide range of biological conditions and water systems (Tsuruta et al. 2011). Coordinated paddy cum fish cultivation can assume a significant part in contributing food, pay, and sustenance to the farmers and tackling their economic problems. However, the major constraint of this aspect is the indiscriminate and extensive use of pesticides. Farmers have become progressively dependent on exorbitant pesticides that may ultimately subvert the efficiency of agro-biological systems and influence the environment. Pesticide deposits deteriorate aquatic waters and are harmful to non-target life forms, thus making their way through the food chain undermining the environmental equilibrium and biodiversity.

Farmers are quite unconcerned about the environmental drawbacks of pesticides. The agrochemicals used in rice fields may be toxic to stocked fish tending to build up residues in fish tissue due to stability in the environment causing genotoxicity and oxidative stress. Genotoxicity is the ability of the agrochemicals (xenobiotics) to impair genetic information contained in the cell. Micronuclei are

shaped during the telophase of mitosis or meiosis while reconstructing the nuclear envelope around the daughter cell's chromosomes (Udroiu 2006). Genotoxic effects of pesticides (chlorpyrifos, imidacloprid, pretilachlor, cartap hydrochloride, lambdacyhalothrin) applied in rice fields can be evaluated through different biomarkers like evaluation of structural modifications in chromosomes, sister chromatid exchanges, micronucleus frequency, DNA adducts and breaks (Bombail et al. 2001). Among these biomarkers, comet, micronucleus, and chromosome aberration assays are simple, reliable, and less time-consuming. Chromosomal aberrations are the abnormalities of chromosomes such as end-to-end joining, stickiness and clumping, attenuation, chromatid break, acentric fragment, pycnosis, despiralization of chromosomes, erosion of chromatid material; occur during the cell division due to physical, chemical or physiological factors. Comet assay is independent of chromosome number and does not require pre-treatment with chemicals like mitotic inhibitors. Therefore, it is the most frequent and recommended method to detect DNA damage in organisms including fishes. Owing to the importance of integrated fish culture, the present attempt was executed to assess the genotoxic effect of pesticide exposure on *Channa punctatus* and *Cyprinus carpio* in paddy-cum-fish culture.

## MATERIALS AND METHODS

The suitable quality confirmation strategies for the preparation of samples, handling, and protection were done as per US EPA protocols without causing any damage to the test organism. All chemicals utilized were of scientific grade from Himedia, India.

### Experimental Design, Seedling Transplantation, Stocking and Harvesting

Pusa Basmati 1121, a rice assortment of the 120-day term was utilized for the present study. Twenty days old rice seedlings were transplanted in rows, roughly 25-30 cm apart. Fish refugees were filled with water and stocking (1 fish 3 m<sup>2</sup>) of *C. punctatus* (15.50±0.40 g) and *C. carpio* (13±0.47 g) was done on the 25<sup>th</sup> day after transplanting the seedlings in respective experiments (Table 1). The experimental design and the use of agrochemicals were similar to Bhatnagar et al. (2021). Fish harvesting was done after a culture period of 85 days, 10 days before paddy harvesting. All treatment ponds were fertilized using urea and zinc sulfate monohydrate while pesticides and insecticides were sprayed uniquely in CP1-CP3 and CC1-CC3. Agrochemical exposure to treatment CP2 and CC2 was done with recommended doses, whereas in CP3 and CC3 dosage was according to farmers (they used these agrochemicals two to three times randomly to control paddy pests). To elucidate the genotoxic effect of paddy

agrochemicals on fish in paddy fields micronucleus, chromosome aberration, and comet assays have been evaluated in the present studies.

### Evaluation of Genotoxicity

The cell viability and count of the peripheral blood were checked utilizing a trypan blue dye exclusion test and hemocytometer to ensure enough number of live cells preceding the comet and micronuclei assay. The samples with 90% or more viability and a cell count of a minimum of 10<sup>6</sup> cells mL<sup>-1</sup> proceeded for the tests.

### Micronuclei test (Fenech et al. 2004)

A thin smear of collected blood samples was made on methanol-treated glass slides and air-dried overnight in sterilized conditions at room temperature. Fixed slides were stained with 2% Giemsa after air drying and were observed under Olympus CX-41 trinocular microscope at 40/100X magnification. Image acquisition of representative peculiarities just as control cells was finished with the assistance of Olympus Digital Camera (C-7070 Wide Zoom) for future records and study. Micronuclei frequency was determined as follows:

$$\% \text{ Micronuclei (MN)} = \frac{\text{Number of cells containing MN}}{\text{Total number of cells counted}} \times 100$$

Table 1: Experimental design and agrochemicals (fertilizers, pesticides, insecticides, and weedicide) used in paddy fields.

Experimental design for the first experiment				
CP1	CP2		CP3	
Paddy field with <i>Channa punctatus</i> , No pesticide	Paddy field with <i>Channa punctatus</i> , Recommended dose		Paddy field with <i>Channa punctatus</i> , Farmers' dose	
Experimental design for the Second experiment				
CC1	CC2		CC3	
Paddy field with <i>Cyprinus carpio</i> , No pesticide	Paddy field with <i>Cyprinus carpio</i> , Recommended dose		Paddy field with <i>Cyprinus carpio</i> , Farmers' dose	
S. No.	Agrochemicals (Fertilizers and Pesticides)			Recommended doses/Acre
	Commercial Name	Chemical Composition	Nature	
1.	Eifit 50 EC	Pretilachlor 50% EC	Herbicide	500 g
2.	Urea	46% Nitrogen	Fertilizer	40 kg
3.	Zinc sulfate monohydrate	Zinc 33% and Sulphur 15%	Fertilizer	10 kg
4.	Clorguard 20 EC	Chlorpyriphos 20% EC	Insecticide	1 Litre
5.	Padan	Cartap Hydrochloride 4% EC	Pesticide	5 kg
6.	Bravo TM 5000	Lambdacyhalothrin 5%EC	Insectide	25 kg
7.	Pulsor®	Thifluzamide	Insecticide	250 mL
8.	Parrymida	Imidacloprid 17.8 %	Insecticide	150 mL



### Chromosome Aberration Assay (Galloway 2000)

At the termination of the experimental period, five fish were randomly chosen from each treatment, and processed for chromosomal aberration assay for evaluating the effect of pesticide on fish chromosomes. Kidney tissue was extracted after injecting the test fish with 0.05% Colchicine. The tissue suspension was prepared in saline solution and fixed in chilled Carnoy's fixative. The cell suspension was centrifuged, fixed repetitively, and finally, the cells of the pellet were suspended in a small amount of fixative. One / or two drops of this suspension were then dropped from a height of about 2 feet on a clean, grease-free slide, held in a slightly slanting position. The air-dried slides were stained with 4% Giemsa and scanned thoroughly under Olympus CX 41 trinocular microscope for well-spread metaphase plates. The selected plates were photographed by using Olympus C-7070 wide zoom camera at a magnification of 1000X. The frequency of chromosomal aberrations was scored. A standard control procedure was employed to determine the various types of chromosomal aberrations.

### Single-Cell Gel Electrophoresis (SCGE)/Comet Assay (Tice et al. 2000)

0.2 mL blood was diluted with 0.5 ml PBS and coated gently on 0.5 mL of histopaque (Sigma) density gradients. Slides were prepared using 10,000 cells in 20  $\mu$ l PBS mixed with 80  $\mu$ l of 0.5% low melting point agarose (LMPA).

The DMSO (Dimethyl sulfoxide) was added to the lysing solution to prevent radical-induced DNA damage. Before electrophoresis, the slides were incubated in alkaline (pH>13) electrophoretic buffer for 30 minutes. Electrophoresis of microgels was done at 18V (0.7-1.0  $Vcm^{-1}$ ) for 20 minutes and the current was maintained at 300 mA (milliamperes) by raising or lowering the buffer level in the tank. This process was carried out in very dim light and at 4°C. Slides were then dehydrated in absolute methanol for 5-10 min.

After the completion of neutralization, slides were kept on an aluminum tray and allowed to dry completely in an incubator at 50°C for 30 min. The staining solution (75  $\mu$ l Ethidium bromide) was poured in 4-5 small, equally spaced droplets over the slides in such a way that it completely and uniformly covered the slides. This entire technique was performed under faint light to keep away from the photolysis and artefactual DNA harm. For comet visualization, two slides per sample and 50 comets per slide were scored. LUCIA Comet Assay™ image analysis software installed in Olympus Trinocular fluorescent research microscope CX-41 (having specific filters) attached with CCD camera at 10X objective was used in the present study. Visual scoring of comet cells (at least 100) was done by categorizing them into 4 classes and giving them scores of 1-4. For visualization of DNA damage, analysis was performed using the above-said image analysis system. It computed the integrated intensity profile for each cell, estimated the comet cell components, head, and tail, and evaluated the percentage of DNA in the comet head and tail, tail length, tail moment and tail inertia, etc.

### Statistical Analysis

Analysis of variance (ANOVA) followed by Duncan's multiple range test (Duncan 1955) for all the experiments was used to determine the significant variation between the different treatments. Statistical significance was settled at a probability value of  $P < 0.05$ . All statistics were performed using SPSS Version 18.0 for Windows. LUCIA Comet Assay software was used for visual scoring of the comet cells.

## RESULTS

### Induction of Micronucleus (MN) or Micronuclei Frequency

The results of micronucleus (MN) analysis in erythrocyte of *C. punctatus* and *C. carpio* reared in different treatments are summarized in Table 2 and Fig.1. There was

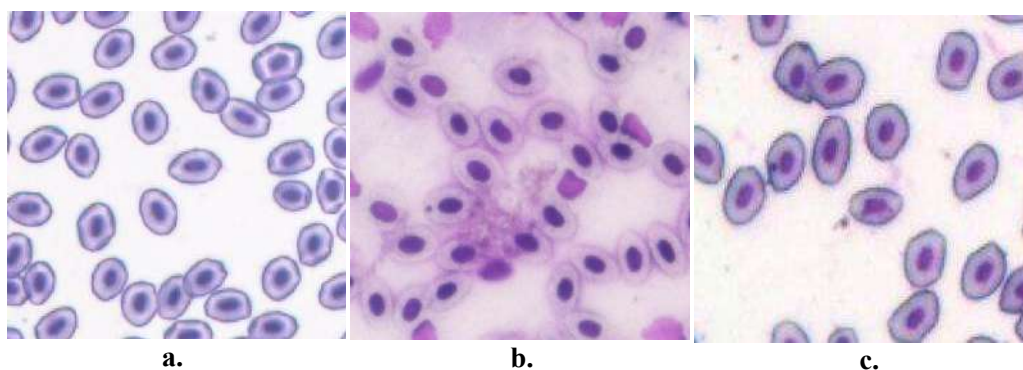


Fig. 1: Micronuclei in blood cells of fish stocked in treatments CP1-3 and CC1-3 in paddy fields on exposure to agrochemicals (a. Control, b. and c. micronuclei due to pesticide exposure).

significant induction of MN in the erythrocyte of fish due to exposure to different doses of agrochemicals applied in treatments CP1-CP3 and CC1-CC3. Maximum doses of pesticides used in treatment CP3 induced MN frequency of 2.6% in blood erythrocytes of fish which was significantly higher ( $P < 0.05$ ) as compared to MN frequency of 0.94% in treatment CP2 in which recommended doses of pesticides were used and minimum frequency was observed in treatment CP1 where no agrochemicals were used. The mean percent frequency of MN in CC1 ( $0.436 \pm 0.098$ ), CC2 ( $1.23 \pm 0.072$ ), and CC3 ( $2.46 \pm 0.027$ ) showed significant differences at a 0.05 level with respect to the control group. The result further depicted that the frequency of micronuclei increased with an increase in the dosage of pesticides.

### Chromosome Aberration

Somatic metaphase depicted that the diploid number of chromosomes in *C. punctatus* and *C. carpio* was 32 ( $2n=32$ ) and 100 ( $2n=100$ ), respectively. The aberrations in the diploid chromosome are stickiness, clumping, end-to-end joining (non-homologous association), chromosome gap, and precocious separation (Fig. 2). Results depicted that the chromosomal aberrations were higher in CP3 and CC3 where the fish were stocked in paddy fields with paddy agrochemicals as used by farmers.

Pycnosis (P) was characterized by differential staining of chromosomal portions due to more condensation in some regions due to the failure of other regions to condense properly. Pycnosis was observed in CP3 and CC3. If the centromere of chromatids of chromosomes got separated precociously then the count of chromosomes was equal to 4X.

Precocious separation (PS) was not accompanied by spindle apparatus and was observed in CP2, CP3, CC2, and CC3. The centromeric region of a chromosome got elongated and did not stain properly forming a centromeric gap. Chromatid break and gap (CG) were observed in CP2, CP3, CC2, and CC3. In a few metaphase plates of treated specimens, some chromosomes were extraordinarily small, their arms seemed thicker and smaller. This may be due to hypercoiling or hyper-condensation, giving a stubby appearance to chromosomes. Such stubbed arms (SA) were observed in CP3, CC2, and CC3. A single or two chromosomal breaks yielded an acentric fragment (AF) which was observed in CP2, CP3, and CC3. Chromatin material was eroded due to pesticide application. Erosion of chromatin material (EC) was encountered only in CP3 and CC3. Stickiness among a few chromosomal ends or clumping of all the chromosomes was observed as a result of severe effects in certain cells due to DNA depolymerization. Stickiness and clumping (SC) were encountered in all the treatments. A disturbance in the condensation of chromosomes at some sites resulted in the thinning of chromatids as attenuation (A) and was observed in CP2, CP3, CC2, and CC3. End-to-end joining was found in all the treatments whereas uncoiling the metaphasic chromosomes as Despiralization (DS) was observed only in CP3 and CC3.

### DNA Damage (Comet Assay)

DNA damage was measured as head area, head DNA (%), tail area, tail length, tail moment, % tail DNA, olive moment, integral intensity, and head radius (Table 3). Fig. 3 indicates an increase in the size of the comet tail from Type 0 (undamaged

Table 2: Frequency of micronuclei in blood cells of *Channa punctatus* and *Cyprinus carpio* at different treatments in paddy cum fish culture fields.

Treatments	Initial	CP1/CC1 (No pesticide)	CP2/CC2 (Recommended dose)	CP3/CC3 (Farmers' dose)
Number of examined blood cells	1000	1000	1000	1000
<i>Channa punctatus</i>				
MN (Mean $\pm$ S.E.)	$3.33 \pm 0.694^C$	$5.33 \pm 0.720^C$	$9.43 \pm 0.981^B$	$26.00 \pm 1.240^A$
% MN frequency (Mean $\pm$ S.E.)	$0.33 \pm 0.069^C$	$0.53 \pm 0.072^C$	$0.94 \pm 0.098^B$	$2.6 \pm 0.124^A$
<i>Cyprinus carpio</i>				
MN (Mean $\pm$ S.E.)	$4.33 \pm 0.347^C$	$4.66 \pm 0.981^C$	$12.33 \pm 0.720^B$	$24.66 \pm 0.027^A$
% MN frequency (Mean $\pm$ S.E.)	$0.43 \pm 0.034^C$	$0.46 \pm 0.0981^C$	$1.23 \pm 0.072^B$	$2.46 \pm 0.027^A$

All values are Mean  $\pm$  S.E. of the mean.

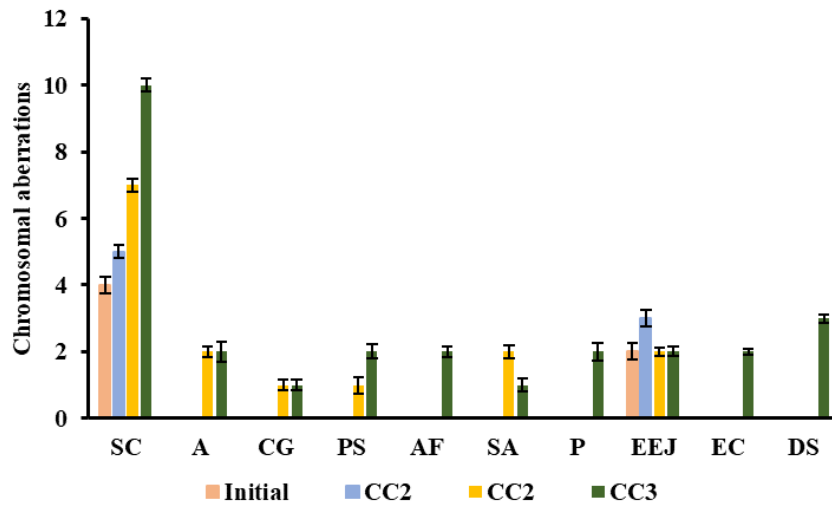
Means with different letters in the same columns are significantly ( $P < 0.05$ ) different. (Duncan's Multiple Range test)

nuclei) to Type 4 (damaged nuclei) comet. A general analysis of comet type showed that frequency of comet type '0' was high in fish of CP1/CC1(control), frequency of comet Type 1 and 2 were high in CP2/CC2; whereas Type 3 and 4 comet were high in CP3/CC3 where agrochemicals were sprayed three times during experimental period indicating that size of comet increased with increase in the dose of agrochemicals. The values when compared with the initial control depicted more damage in treatment groups. Results revealed that fish reared in CP3/CC3 have maximum DNA

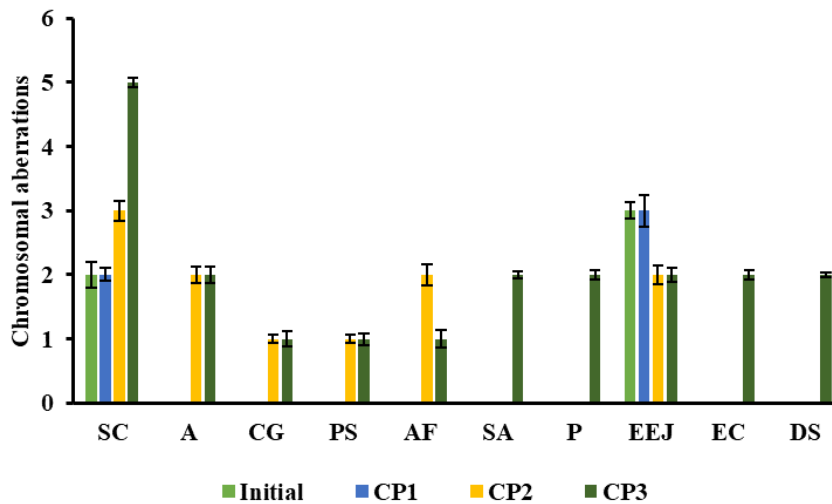
damage as compared to fish stocked in treatment CP2/CC2 where recommended doses of agrochemicals were used.

**DISCUSSION**

In the present study, various agrochemicals were used to combat the pest in the paddy fields, and the same piece of land was utilized for the integrated culture of *Channa punctatus* and *Cyprinus carpio*. Although the agrochemicals within recommended dose enhance paddy production (Bhatnagar



A



B

Fig. 2: Chromosomal aberration in the kidney cells per 125 metaphases in A) *Channa punctatus* and B) *Cyprinus carpio* stocked in paddy fields after 85 days (SC = Stickiness, A = Attenuated Chromosome, CG= Chromatid break, and Gap, PS = Precocious separation, AF = Acentric Fragments, SA= Stubbed arms, P= Pycnosis, EEJ = End to End joining, EC= Erosion of chromatid materials, DS= Despiralization of chromosomes.

Table 3: Assessment of genetic damage in erythrocytes of *Channa punctatus* and *Cyprinus carpio* reared in paddy fields after 85 days of different treatments.

Parameters	Treatments (Mean±S.E.)			
	Initial/Control	CP1/CC1 (No pesticide)	CP2/CC2 (Recommended dose)	CP3/CC3 (Farmers' dose)
<i>Channa punctatus</i>				
Head Area ( $\mu\text{m}^2$ )	1461.56±35.18 <sup>B</sup>	2289.58±633.38 <sup>B</sup>	2801.52±725.18 <sup>A</sup>	781.58±164.08 <sup>C</sup>
Head DNA(%)	95.46±0.65 <sup>AB</sup>	97.18±0.32 <sup>A</sup>	91.70±1.76 <sup>AB</sup>	84.42±2.76 <sup>B</sup>
Tail Area( $\mu\text{m}^2$ )	141.63±24.62 <sup>C</sup>	250.08±91.71 <sup>B</sup>	287.18±104.43 <sup>A</sup>	261.82±41.85 <sup>AB</sup>
Tail length( $\mu\text{m}$ )	2.00±0.71 <sup>B</sup>	2.66±0.86 <sup>AB</sup>	2.94±1.12 <sup>AB</sup>	3.47±0.92 <sup>A</sup>
Tail moment	0.21±0.009 <sup>AB</sup>	0.10±0.04 <sup>B</sup>	0.91±0.33 <sup>AB</sup>	1.11±0.34 <sup>A</sup>
Tail DNA(%)	4.53±0.21 <sup>B</sup>	2.82±0.326 <sup>C</sup>	8.30±0.76 <sup>AB</sup>	15.57±0.79 <sup>A</sup>
Olive moment	0.54±0.12 <sup>AB</sup>	0.42±0.13 <sup>B</sup>	1.36±0.37 <sup>AB</sup>	1.78±0.39 <sup>A</sup>
<i>Cyprinus carpio</i>				
Head Area ( $\mu\text{m}^2$ )	578.47±51.33 <sup>B</sup>	1047.72±79.44 <sup>AB</sup>	927.42±206.42 <sup>AB</sup>	1859.31± 499.19 <sup>A</sup>
Head DNA (%)	95.44±0.72 <sup>A</sup>	97.40±0.51 <sup>A</sup>	88.35±3.58 <sup>B</sup>	83.64±1.38 <sup>C</sup>
Tail Area( $\mu\text{m}^2$ )	58.32±10.22 <sup>C</sup>	122.28±19.67 <sup>B</sup>	218.04±38.51 <sup>AB</sup>	346.51±45.56 <sup>A</sup>
Tail length ( $\mu\text{m}$ )	1.01±0.22 <sup>B</sup>	2.77±0.64 <sup>AB</sup>	2.34±1.06 <sup>AB</sup>	5.42±1.30 <sup>A</sup>
Tail moment	0.33±0.20 <sup>B</sup>	0.15±0.05 <sup>AB</sup>	0.77±0.37 <sup>AB</sup>	2.06±0.45 <sup>A</sup>
Tail DNA (%)	2.59±0.516 <sup>B</sup>	4.55±0.89 <sup>AB</sup>	11.64±3.58 <sup>AB</sup>	16.35±1.38 <sup>A</sup>
Olive moment	0.397±0.11 <sup>B</sup>	0.43±0.07 <sup>AB</sup>	1.35±0.42 <sup>AB</sup>	2.58±0.28 <sup>A</sup>

All values are Mean ± S.E. of the mean.

Means with different letters in the same rows are significantly ( $P < 0.05$ ) different.

(Duncan's Multiple Range test)

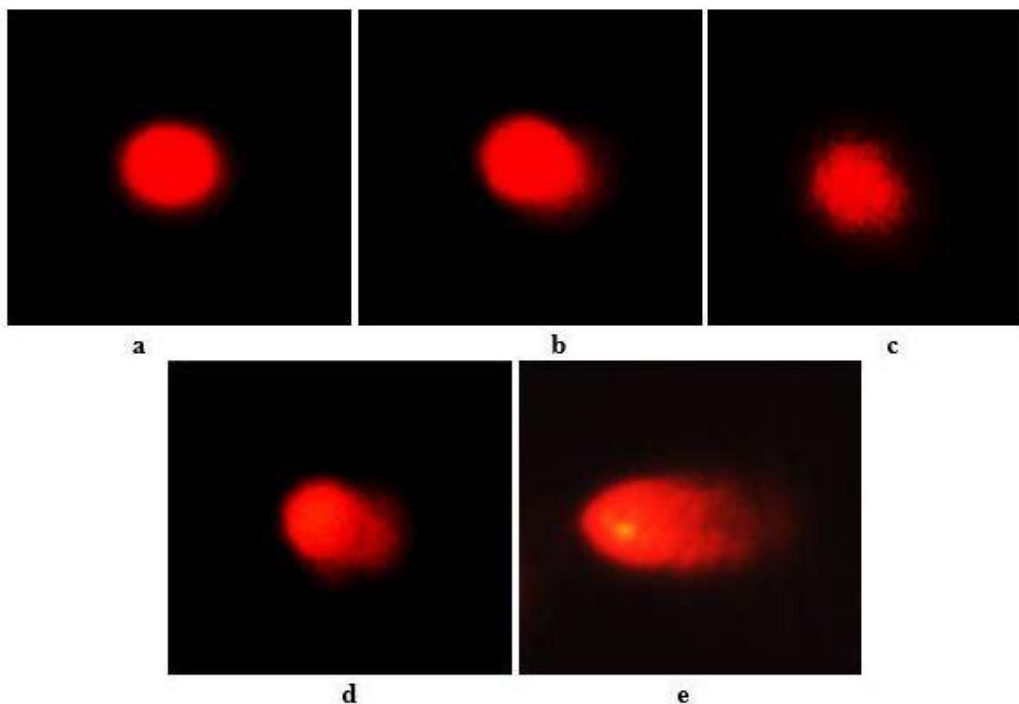


Fig. 3: Blood cells showing various types of comets (100X) a. Type 0 comet, b. Type 1 comet, c. Type 2 comet, d. Type 3 comet, e. Type 4 comet

et al. 2021) yet their presence causes a genotoxic effect on the organisms. In the present study, *C. Carpio* and *C. punctatus* were employed for analyzing the genotoxic effect in terms of micronucleus, chromosomal aberration, and comet assay in fish tissue due to the agrochemicals present in the paddy fields. Xenobiotics initiate DNA damage by causing strand breaks or by implication through the formation of reactive oxygen species (ROS) which at that point harms the DNA by shaping adducts and lesions (Marnett 2000). DNA repair mechanism, which attempts to mend the damaged section, can do so to a specific limit, beyond which DNA harm can persevere, as injuries or mis-repaired DNA, prompting mutagenesis and carcinogenesis (Moustacchi 2000). The dependable genotoxicity endpoints which are utilized for screening the genotoxicity of such xenobiotics are the micronuclei (MN) test, chromosomal aberrations, and the single-cell gel electrophoresis (comet assay). The MN test is essentially used to check the clastogenicity of a specific compound, while the comet test is utilized to check the impact of the compound on the respectability of DNA (Bolognesi & Cirillo 2014). The acquired aftereffects of the current investigation may likewise be valuable to alleviate contaminant impacts at a whole lot initial stage.

The outcome of the micronucleus assay uncovered that recurrence of micronuclei was fundamentally higher in fish erythrocyte stocked in the rice fields for 85 days in CP3 and CC3, where the amount of the agrochemicals used by the farmers was three times more than the recommended dose (CP2 and CC2) affirming the impact of agrochemical on genetic material. Micronuclei are particles comprising acentric sections of chromosomes or whole chromosomes which fall behind at the anaphase phase of cell division. After telophase, these parts may not be retained in the nuclei of daughter cells and structure single or various micronuclei in the cytoplasm. Consequently, micronuclei contain either chromosome part or the entire chromosome. MN recurrence in freshwater species was shown to be a delicate biomarker to distinguish genotoxic damage incited by pesticides (Clasen et al. 2018) and herbicides (Nwani et al. 2013) permitting to recognition of contaminant concentration gradients. The pertinence of occasional effect in the enlistment of chromosomal effect in the acceptance of chromosomal damage was additionally distinguished (Ergene et al. 2007). The outcomes have announced that these synthetic substances repress cell division by impeding protein synthesis and in this way forming micronuclei (Çavaş & Ergene-Gözükara 2005). The results of the present study are supported by Bhatnagar et al. (2016) where the presence of CPF (Chlorpyrifos) increased the micronuclei frequency in a time- and dose-dependent manner. Erythrocytes with two nuclei are formed during aberrant cell division as a result of cytokinesis block (Çavaş

& Ergene-Gözükara 2005). The formation of eight-shaped erythrocytes, considered to be remnants of the mitotic spindle, is also used as a cytotoxicity marker because it reflects a failure in erythropoiesis (Baršienė et al. 2014). The results obtained in from this study data suggest that the presence of agrochemicals affected fish erythrocytes more significantly ( $P < 0.05$ ) than the control.

Chromosome aberrations such as centromeric gap, attenuation, pycnosis, stickiness and clumping, erosion of chromatid material, and end-to-end joining in chromosomes were recorded maximum in CP3 and CC3 in comparison to CP2, CC2, CP1, and CC1. Different types of chemicals have been reported to be responsible for the production of various types of aberrations in the structure or number of chromosomes. By studying the comparative karyology after exposing the organisms to any chemical or physical agent, the clastogenic properties can be detected. In fish cytogenetic techniques have been applied widely as the most robust and consistent assay for genotoxicity assessment. The present study depicted that somatic metaphase has revealed that the diploid number of chromosomes in *C. carpio* was 100 ( $2n=100$ ). The aberrations in diploid chromosome number in *C. carpio* have been found to be stickiness, clumping, end-to-end joining (non-homologous association), chromatid gap, precocious separation, etc. frequency of each type of aberration were higher in CC3 where the fish were stocked in rice fields with rice agrochemicals as used by farmers. For *C. punctatus*, somatic metaphase depicted that the diploid number of chromosomes is 32 ( $2n=32$ ). The aberrations in diploid chromosome number in *C. punctatus* are stickiness, clumping, end-to-end joining (non-homologous association), chromosome gap, precocious separation, etc. The results depicted that the chromosomal aberrations were higher in CP3 in *C. punctatus* also. These results are in agreement with Rishi and Grewal (1995).

Organophosphates are ubiquitous environmental contaminants owing to their extended utilization in the fields. However, these are neurotoxic inhibiting acetylcholinesterase activity with subsequent disruption of nervous functions, thus interfering with various metabolic and physiological activities (Jokanović 2018). Imidacloprid is a neurotoxic chemical, which is utilized successfully against sucking insect pests of rice and diverse crops around the world. In any case, by its methodical nature, imidacloprid moves effectively between plant tissue and from the roots to the soil underneath and water in the field. The average amount of pesticides applied by the farmers is nearly twice or thrice as high as the upper dosage recommended by the distributing companies. There is a decline in the number of freshwater fish with the use of these chemicals. Furthermore, farmers shower their harvests in the wake of seeing bugs or weeds in the field notwithstand-

ing preventive splashing, especially in the more remote areas. The greater part is utilizing high fertilizer rates and applying an enormous concentration than required.

Structural and numerical modifications in chromosomes result from abnormalities in DNA duplication during the 'S' phase. The physiological changes that appeared in the fish are not just a reaction to low pesticide levels yet, in addition, give a comprehension of contaminations in organic terms and show a model for vertebrate toxicity. The present study's observations are similar to the studies by Saxena and Chaudhari (2010), Yadav et al. (2010), and Ahmed et al. (2015). All these studies are concerned about genotoxic effects in fishes when exposed to specific chemicals/pesticides/herbicides at specific doses under laboratory conditions. The present investigation revealed that chromosomal abnormalities were higher in CP2, CP3, and CC2, CC3 as compared to CP1/CC1. The number of aberrations was high in CP3 and CC3 where farmers used the agrochemicals 2-3 times the recommended dose. The numerical values of aberrations were comparatively less in CP2 and CC2 only once recommended doses of pesticides were used and were lowered in CP1 and CC1 where no pesticide treatment was given supporting the fact that these agrochemicals can cause chromosome aberrations.

The SCGE or Comet assay, recognize DNA strand breaks and alkali labile locales by estimating the movement of DNA from immobilized nuclear DNA and helpful procedure for environmental contamination bio-monitoring. It is a fast and delicate technique to quantify DNA lesions. Kumaravel and Jha (2006) revealed that parts of broken DNA just as loosened up DNA move towards the anode delivering the tail of the comet.

The fragmented DNA tends to move unreservedly during the electrophoresis, whereas the relaxed DNA loops are hauled out of the nuclear head. The tail length determines the distance relocated by DNA with the smallest one moving the farthest, the tail length is predominately directed (Kumaravel & Jha 2006) by the size of the DNA fragments generated during the alkaline unwinding step of the Comet Assay. Kilemade et al. (2004) revealed that % tail DNA is a mainstream and reasonable boundary that estimates the level of DNA that has moved from the head. Pandey et al. (2018) confirmed that profenofos (PFF) have genotoxic, mutagenic effects and are exceptionally harmful to *C. punctatus*. PFF causes biomagnification in the tissues of the test organisms and is neurotoxic for the hindrance of cerebrum and gill AChE in the fish (Rao et al. 2003). In the present studies, comet assay was performed after 85 days only and no such time-dependent response could be quantified. However, in CP2 and CC2 the spray of agrochemicals at recommended doses was done only once at lower and recommended doses

whereas in CP3 and CC3 the spray was done thrice (as suggested by the farmers) supporting the results that there might be a time-dependent decrease in DNA damage due to DNA repair as revealed by the size of the comet in CP1 and CC1. Stocking fish in rice fields reduces pest infestation and thus if not eliminates the need for the application of agrochemicals, reduces the quantity supporting the results of the present study.

The presence of micronuclei and tail DNA (%) is profoundly associated with one another and may happen in a portion subordinate and additionally time-subordinate way. The MN test and comet can, in this manner, be dependably used to evaluate the genotoxicity of agrochemicals in paddy cum fish culture. The current investigation recommends restricting the utilization of agrochemicals in rural practices to keep away from the possible defilement of nearby water bodies. Agrochemicals applied in rice fields may cause adverse effects that are specific to the toxicant and damage the organism without causing any observable changes. Keeping in view the low genotoxic effects in CP2 and CC2 (with recommended doses of pesticides) may be disseminated to farmers for economic benefits with paddy cum fish culture.

## ACKNOWLEDGEMENT

The authors are grateful to the Chairperson, Department of Zoology, and authorities of Kurukshetra University, Kurukshetra for providing the essential facilities to conduct the investigation.

## REFERENCES

- Ahmed, M.K., Habibullah-Al-Mamun, M., Islam, M.M., Akter, M.S. and Khan, M.S. 2015. Toxicological assessment of arsenic-induced hematological alterations and chromosomal aberrations in tilapia *Oreochromis mossambicus*. Hum. Ecol. Risk Assess., 21(1): 146-156.
- Baršienė, J., Butrimavičienė, L., Grygiel, W., Lang, T., Michailovas, A. and Jackūnas, T. 2014. Environmental genotoxicity and cytotoxicity in flounder (*Platichthys flesus*), herring (*Clupea harengus*), and Atlantic cod (*Gadus morhua*) from chemical munitions dumping zones in the southern Baltic Sea. Mar. Environ. Res., 96: 56-67.
- Bhatnagar, A., Kaur, M., Dhillon, O. and Yadav, A.S. 2021. Paddy cum fish culture: Growth performance of *Channa punctatus*, paddy yield, and economics. J. Appl. Nat. Sci., 13(1):145-156.
- Bolognes, C. and Cirillo, S. 2014. Genotoxicity biomarkers in aquatic bioindicators. Curr. Zool., 60(2): 273-284.
- Bombail, V., Aw, D., Gordon, E. and Batty, J. 2001. Application of the comet and micronucleus assays to butterfish (*Pholis gunnellus*) erythrocytes from the Firth of Forth, Scotland. Chemosphere, 44(3): 383-392.
- Çavaş, T. and Ergene-Gözükara, S. 2005. Induction of micronuclei and nuclear abnormalities in *Oreochromis niloticus* following exposure to petroleum refinery and chromium processing plant effluents. Aquat. Toxicol., 74(3): 264-271.
- Clasen, B., Loro, V.L., Murussi, C.R., Tiecher, T.L., Moraes, B. and Zanella, R. 2018. Bioaccumulation and oxidative stress caused by pesticides in *Cyprinus carpio* reared in a rice-fish system. Sci. Total. Environ., 626: 737-743.

- Duncan, D.B. 1955. Multiple range and multiple F-tests. *Biometrics*, 11:1-42.
- Ergene, S., Çelik, A., Çavaş, T. and Kaya, F. 2007. Genotoxic biomonitoring study of the population residing in pesticide-contaminated regions in Göksu Delta: micronucleus, chromosomal aberrations, and sister chromatid exchanges. *Environ. Int.*, 33(7): 877-885.
- Fenech, M., Chang, W.P., Kirsch-Volders, M., Holland, N., Banassi, S. and Zeiger, E. 2003. Human micronucleus project: detailed description of the scoring criteria for the cytokinesis-block micronucleus assay using human lymphocyte cultures. *Mut. Res.* 534 (1-3):65-75.
- Galloway, S.M. 2000. Cytotoxicity and chromosome aberrations in vitro: experience in the industry and the case for an upper limit on toxicity in the aberration assay. *Environ. Mol. Mutagen.*, 35(3): 191-201.
- Jokanović, M. 2018. Neurotoxic effects of organophosphorus pesticides and possible association with neurodegenerative diseases in man: A review. *Toxicology*, 410:125-131.
- Kilmeade, M.F., Hartl, M.G., Sheehan, D., Mothersill, C., van Pelt, F.N., O'Halloran, J. and O'Brien, N.M. 2004. Genotoxicity of field collected inter-tidal sediments from Cork Harbor, Ireland, to juvenile turbot (*Scophthalmus maximus* L.) as measured by the comet assay. *Environ. Mol. Mutagen.*, 44(1): 56-64.
- Kumaravel, T.S. and Jha, A.N. 2006. Reliable comet assay measurements for detecting DNA damage induced by ionizing radiation and chemicals. *Mutat. Res. Genet. Toxicol. Environ. Mutagen.*, 605(1-2): 7-16.
- Marnett, L.J. 2000. Oxyradicals and DNA damage. *Carcinogenesis*. 21(3):361-370.
- Mustache, E. 2000. DNA damage and repair: Consequences on dose-responses. *Mutat. Res. Genet. Toxicol. Environ. Mutagen.*, 464(1): 35-40.
- Nwani, C.D., Nagpure, N.S., Kumar, R., Kushwaha, B. and Lara, W.S. 2013. DNA damage and oxidative stress modulatory effects of glyphosate-based herbicide in freshwater fish, *Channa punctatus*. *Environ. Toxicol. Pharmacol.*, 36(2): 539-547.
- Pandey, A.K., Nagpure, N.S. and Trivedi, S.P. 2018. Genotoxicity assessment of pesticide profenofos in freshwater fish *Channa punctatus* (Bloch) using comet assay and random amplified polymorphic DNA (RAPD). *Chemosphere*. 211:316-323.
- Rao, J.V., Rani, C.H.S., Kavitha, P., Rao, R.N. and Madhavendra, S.S. 2003. Toxicity of chlorpyrifos to the fish *Oreochromis mossambicus*. *Bull. Environ. Contam. Toxicol.*, 70(5): 985-992.
- Rishi, K.K. and Grewal, S. 1995. Chromosome aberration test for the insecticide, dichlorvos, on fish chromosomes. *Mutat. Res.*, 344(1-2): 1-4.
- Saxena, K.K. and Chaudhari, R. 2010. Study of chromosomal abnormalities in *Channa punctatus* exposed to fenvalerate. *J. Appl. Nat. Sci.*, 2(1): 70-73.
- Tice, R.R., Agurell, E., Anderson, D., Burlinson, B., Hartmann, A., Kobayashi, H., Miyamae, Y., Rojas, E., Ryu, J.C. and Sasaki, Y.F. 2000. Single cell gel/comet assay: Guidelines for in vitro and in vivo genetic toxicology testing. *Environ. Mol. Mutagen.*, 35(3): 206-221.
- Tsuruta, T., Yamaguchi, M., Abe, S.I. and Iguchi, K.I. 2011. Effect of fish in rice-fish culture on the rice yield. *Fish. Sci.*, 77(1): 95-106.
- Udroiu, I. 2006. The micronucleus test in piscine erythrocytes. *Aquat. Toxicol.*, 79(2): 201-204.
- Yadav, A.S., Bhatnagar, A. and Kaur, M. 2013. Aberrations in the chromosomes of *Cirrhinus mrigala* (Hamilton) upon exposure to butachlor. *Int J. Technol.*, 7(21): 858-865.







# Sustainable Nano-Bioremediation Approaches for the Treatment of Polluted Soils

Irrinki Hemalatha\*, Dakamari Harika\* and Manoj Kumar Karnena\*\*†

\*Department of Mathematics, DADI Institute of Engineering and Technology, Visakhapatnam, India

\*\*Department of Environmental Science, GITAM Institute of Science, GITAM (Deemed to be) University, Visakhapatnam, India

†Corresponding author: Manoj Kumar Karnena; manojkumarenviro@gmail.com

Nat. Env. & Poll. Tech.  
Website: [www.neptjournal.com](http://www.neptjournal.com)

Received: 22-01-2022

Revised: 01-03-2022

Accepted: 11-03-2022

## Key Words:

Nano-bioremediation  
Polluted soil  
Toxic pollutants  
Remediation  
Nanotechnology

## ABSTRACT

Due to the widespread adoption of conventional approaches for the remediation of contaminated soils, these techniques have become more well-known in the literature. However, these methods have both advantages and disadvantages. Integrating traditional degradation technologies with Nano-technology might be the right solution for removing toxicants from the environment to overcome these problems. Nano bioremediation is a new technique that has gained prominence in recent years among many researchers worldwide. These techniques aim to remove the contaminants' concentration and minimize their impacts on the environment. The integrated approaches benefit bioremediation and nanotechnology to remove the pollutants more efficiently within less time in an eco-friendly manner than individual processes. The current review provides insights into nanotechnology and different kinds of nanomaterials that have been reported in eliminating pollutants from the environment. Further, the mechanism and challenges with nano bioremediation were explained in detail.

## INTRODUCTION

Nanotechnology in recent years has been gaining much prominence among many researchers owing to its advantages in allied fields of science. Feynman introduced nanotechnology concepts in 1952, and these technologies have become one of the top research areas in science and technology (Yadav et al. 2017). Rapid modernization and industrialization increased the unsustainable pollution load on the environment (Singh et al. 2020). Noxious pollutants in the background are growing at an alarming rate and degrading the quality of the ecosystem, which leads to the deterioration of human health. In India, increasing pollution is the third most global trend, as reported by the outlook of Global Agenda 2015 (Councils 2015, Vara & Karnena 2021); thus, many research groups have proposed many techniques for remediating the contaminated site with pollutants in a larger scale. Nevertheless, these methods have certain limitations and have not gained much importance in their widespread application as they are expensive in operation, and maintenance, require high energy, etc. The application of nanotechnology was increased in several sectors of our day-to-day life over the last few decades, moreover, in environmental remediation. The existing literature on nanotechnology clearly shows that it will enhance the capacities of remediation technologies and many challenges competently (Chauhan et al. 2022). In recent

times, remediation technologies with sustainability have gained much importance. It mainly focuses on reducing the toxic pollutant concentrations to safe levels without adding additional environmental impacts. Recent advancements are combined with these technologies to form a single system, which can be a proper solution to remediate the contaminant site economically within a lesser period in an efficient manner. Amongst the restoration methods, bioremediation is one such method that is competent and useful in remediating contaminated sites in an eco-friendly and economical way. Microorganisms are used in bioremediation techniques to remove the pollutants in soils and water (Galdames et al. 2020, Ramezani et al. 2021, Singh et al. 2020). Over the physicochemical methods, bioremediation has several advantages like cost-effectiveness, specificity, minimal energy requirement, etc. These methods have disadvantages, i.e., degrading the toxic compounds or recalcitrant chemicals in the soils takes months to a year. These technologies are limited if the contaminated sites have excess concentrations of harmful pollutants (Kahraman et al. 2022, Konni et al. 2021); However, integrating these methods with other methods might be an excellent solution to overcome these problems. Nano-bioremediation is a distinctive method that has gained prominence among several researchers in recent years; Nano-remediation has the added advantages of nanotechnology in combination with the benefits of bioremediation methods.

The current review provides insights into nanotechnology and different types of nanomaterials that have been reported in eliminating pollutants from the environment, followed by a detailed account of techniques in nano-bioremediation and their applications.

## DEFINITION OF NANOTECHNOLOGY AND NANOPARTICLES

The utilization of nanoparticles might be seen in all the science fields, for instance, agriculture, textiles, medicines, engineering, etc. “National Nanotechnology Initiative (NNI) of USA defined nanotechnology as the understanding and controlling matter at dimensions between approximately 1–100 nanometres, where unique phenomena enable novel nanotechnology applications.” Nanotechnology includes measuring, imaging, modeling, and manipulating the matter at the nanoscale (Fig. 1). In recent years, the utilization of nanotechnology in removing pollutants from the environment gained much attention from many researchers due to the size of the particles having high surface-volume ratios; due to these salient features, it gained flexibility for the application in both ex-situ and in-situ conditions.

These technologies generally deal with the nanoparticles having a dimension/range of 1-100 nm, and these particles form functionalized network systems that might be used to perform a function; thus, these features enabled these tech-

nological applications to be more suitable in the different scientific fields like purification of water, medicinal, packing industries, etc. The nano-sized particles might be developed in various shapes like spherical, rods, triangular, cubes, etc., and based on their forms (Fig 2), these particles are called “nanospheres, nano-rods”, etc. (Wu et al. 2016); nanomaterials structures can be arranged based on their dimensions; most of the nanomaterials are with zero-dimensional (e.g. Fullerenes); one-dimensional (e.g. nanowires); or two-dimensional (e.g. nanodisks) (Darwesh et al. 2021).

## SYNTHESIS OF NANOPARTICLES AND THEIR CHARACTERIZATION

Nanoparticle synthesis is done by two approaches that are “top-down and bottom-up”. In the top-down approach, larger particles are broken down into nanoscale-sized particles with the help of ball milling, laser ablation techniques, etc. In contrast, smaller atoms are mongrelized in the bottom-up approach and form congregates further. These substances will form nanoparticles (Karnena et al. 2020). Chemical reduction, co-precipitation, etc., are examples of the bottom-up approach method. The nanoparticle synthesis methods might be classified as “physical, chemical and biological methods”. Fig. 3 depicts the different processes for the synthesis of nanoparticles that fall into “physical, chemical and biological methods”. After synthesizing nanoparticles, there is a need

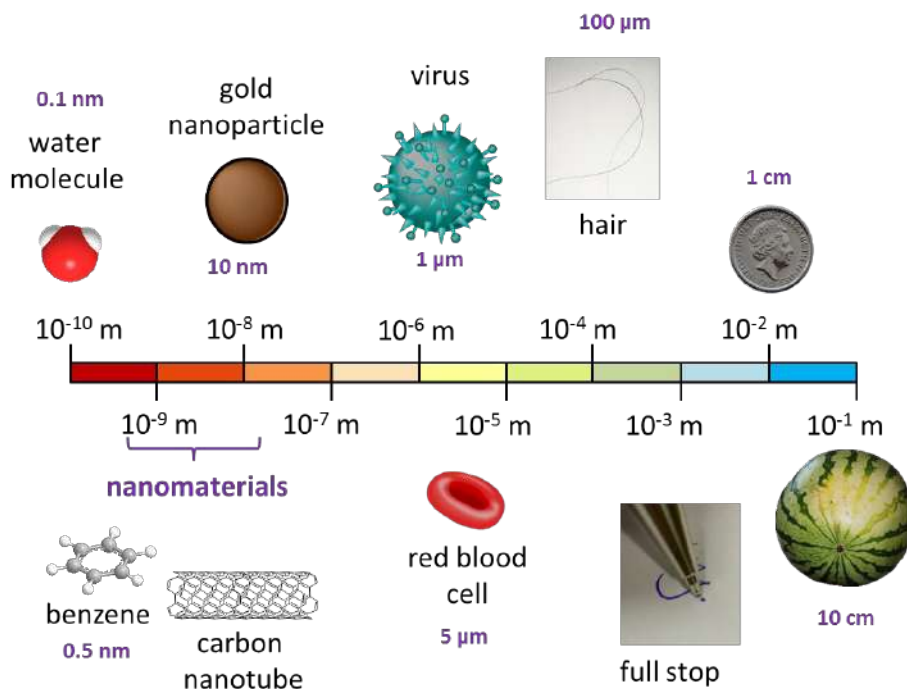


Fig 1: Nanotechnology and Nanoscale science.

to identify their physiology, morphology nature, etc. The nanoparticle characterization might be done via numerous instrumental techniques (Souza et al. 2020, Zhou et al. 2022, Singh et al. 2020).

**ENVIRONMENTAL REMEDIATION**

Novel technologies are required to decrease environmental pollutants as pollution loads are alarming. Even though other technologies are available for remediating the pollutants, nanotechnology becomes more prominent as it has

more significant advantages than the other technologies in removing the contaminants with greater efficacy in a lesser duration of time, which is more economically viable. The different types of nanomaterials were utilized to remove the pollutants from the environmental systems; The nanomaterials are classified as “nanofibers, nanoshells, nanoclusters, nanotubes nanocomposites” based on their composition and size. Nanomaterials showed their efficiency in removing the noxious pollutants from the soil, water, and sediments. Nanofibers eliminated the toxic impurities and showed their efficiency in treatment (Fig. 4). Qi et al. (2014) reported

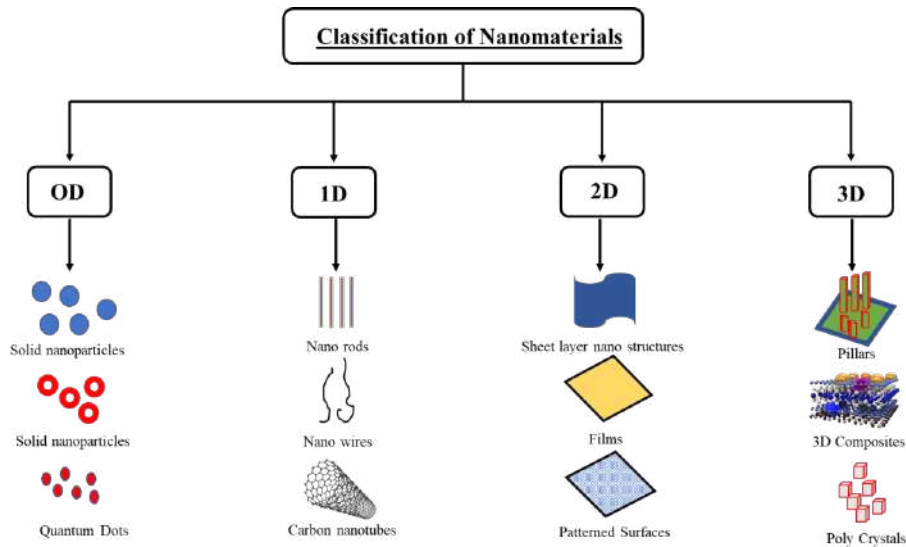


Fig 2: Nanomaterials based on the Size.

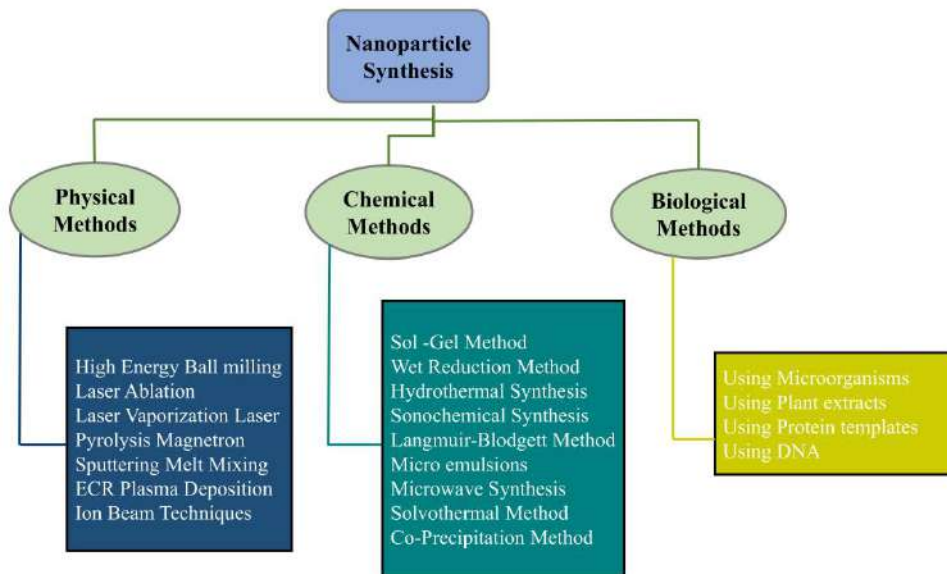


Fig. 3: Process used for nanoparticle synthesis (Redrawn with permission from Singh et al. 2020).

that electrospun nanofibres made up of nylon 6 removed the estrogen from the aqueous medium. It can be used for seven more cycles for removing the other pollutants. Barrocas et al. (2017) reported that nanofibers made up of titanium could degrade the phenols up to 96%. Nanoshells are spherical and have a dielectric core with thin metallic shells; primarily, silver nanoshells are utilized to degrade the organic dye in industrial effluents. Nano-based materials like nanocomposites and nanoclusters also showed their efficacy in treating environmental pollutants. Hussain et al. (2017) reported that nanocomposites degraded the nonylphenols with 96.2% efficiency with a dosage of  $40 \text{ mg.L}^{-1}$  in 2 h. Sarkar et al. (2018) reported that nanocomposites or nanostructures made of graphite/silica have greater efficacy in eliminating heavy metals. For the remediation of noxious pollutants, nanoparticles are significant as they can be used in both ex-situ and in-situ conditions; In the ex-situ remediation, soil and water that are contaminated with hazardous pollutants are brought to the remediating units and remediated with the nanoparticles to remove its toxicity; In contrast, in situ remediations, the nanomaterials are introduced directly to the sites or injected to PRBs (Permeable reactive barriers) of the contaminated sites or as it treats the toxicants and eliminates them from the areas (Qian et al. 2020). Zero valent iron oxide nanomaterials have shown more extraordinary abilities to reduce pollutants and effectively remediate the soil and groundwater via direct or PRBs injection (Oh et al. 2001). For instance, zerovalent iron of nanoscale was injected into

the soils of metal fabrications in Czech Republic industrial areas; It achieved more than 50% removal efficiencies in treating the sites contaminated with the ethylenes and chlorides within 180 days (Raja & Husen 2020, Shahi et al. 2021). Ahn et al. (2016), reported that the aquifers polluted with trichloroethylene are treated with the zerovalent iron nanoparticles and achieved removal efficiencies up to 96 % without releasing any secondary pollutants like chlorinated compounds; and found that these nanoparticles can be utilized many times after five months (Singh et al. 2020).

Sakulchaicharoen et al. (2010) found that nanoparticles have a greater tendency to accumulate, which may lead to fast oxidation. To overcome this problem, the nanoparticles must be coated with stabilizers which increase the stability and reduce the accumulation of nanoparticles; Coating the surfaces of the nanoparticles increases the adsorption capacities and reduce nanoparticle accumulation. Rashid et al. (2017) showed that nanoparticles coated with humic acid would remove the phosphate content efficiently from the water. Ekka et al. (2019) reported that silica nanoparticles coated with titanium degrade the safranin dyes up to 93 % within optimal conditions. Guo et al. (2016) showed that gold nanoparticles could be used for six cycles in removing pollutants from the environment with an efficacy of 90%. Table 1 shows the nanomaterials that have been widely utilized for eliminating contaminants.

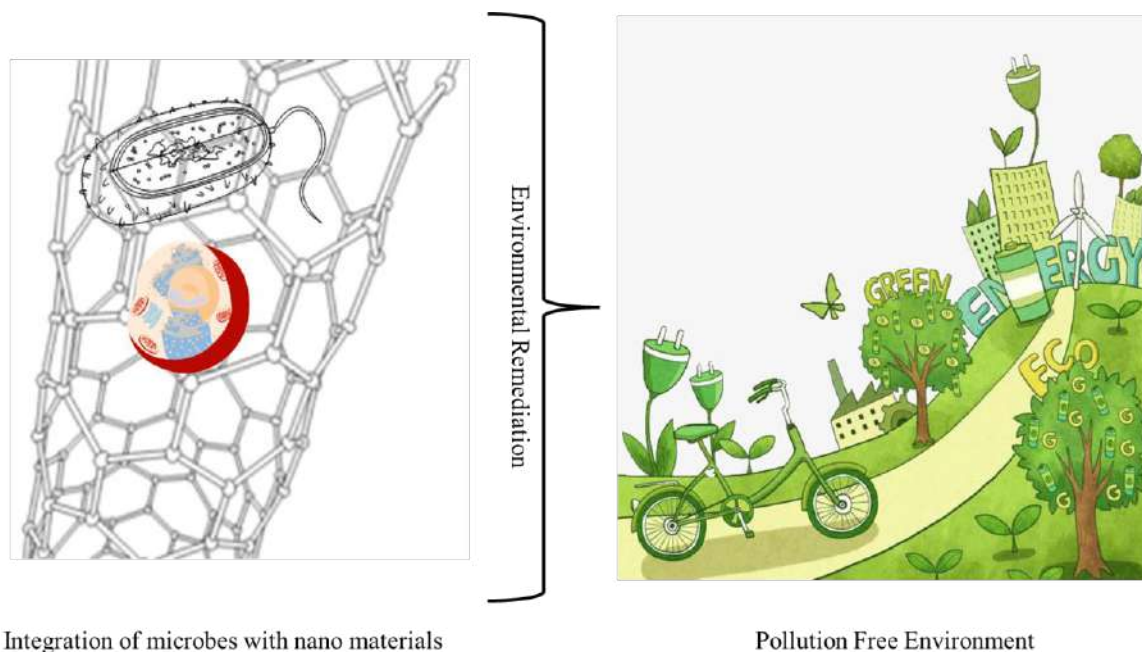


Fig. 4: Integration of microbes with nanomaterials for environmental remediation.

## NANOBIOREMEDIATION

Nanobioremediation is a combined technology comprised of nanotechnology and bioremediation; this integration helps remediate the pollutants with greater efficacy in a lesser time

in an eco-friendly manner. Drawbacks of the individual technologies for the treatment of contaminants can be overcome by these integrated approaches to achieve better results in remediation. For example, combining zerovalent iron oxide nanoparticles with the strains of the microbes remediated

Table 1: Some widely used nanomaterials for removing pollutants (Singh et al. 2020).

S.no	Nanoparticles used	Pollutant	Observations	References
1.	Activated Carbon	Copper and sulfates	The hydrophilicity of activated carbon nanoparticles increased by the surface area of nanoparticles and enhanced the removal efficiencies.	Hosseini et al. (2018)
2.	Aluminum	Arsenate	At optimum pH and temperatures, aluminum nanoparticles adsorb arsenate efficiently.	Prabhakar and Samadder (2018)
3.	Caesium oxide	Cadmium, Lead, Hexavalent Chromium	These nanoparticles effectively remove the heavy metal ions at pH 5-7.	Contreras et al. (2015)
4.	Copper oxide	Arsenic	The copper oxide nanoparticles adsorbed arsenic metal ions from the aqueous solutions and proved that these nanoparticles could be applied for potential applications.	Reddy et al. (2013)
5.	Hematite	Carbatrol	Adsorption efficacy increased with time; 90% of removal was observed after 120 minutes.	Rajendran and Sen (2018)
6.	Iron/Nickel (Bimetallic)	Tetracycline	During aging, the efficacy of bimetallic nanoparticles is decreased in degrading the tetracycline with time. The aging product in these experiments is magnetite/maghemite.	Dong et al. (2018)
7.	Maghemite-PC-MAs	Polyaromatic Aromatic Hydrocarbons and metal toxicants	Removal efficiencies were found to be more significant, 85%.	Guo et al. (2016)
8.	Manganese oxide	Estradiol	Estrogens in the soil were removed with an efficacy of 88% with these nanoparticles; a decrease in the velocity of injecting nanoparticles into the contaminated soils enhanced the degradation capacities.	Han et al. (2017)
9.	Modified Cetyltrimethylammonium bromide	Hexavalent Chromium	Iron-modified Cetyltrimethylammonium bromide nanoparticles removed hexavalent chromium efficiently.	Elfeky et al. (2017)
10.	Palladium	Pentachlorobiphenyl	PCBs in the soils were removed by the palladium nanoparticles doped with the CO <sub>2</sub> fluid (supercritical) at 200 atm.	Wang and Chiu (2009)
11.	Polystyrene	Estrone	Nanoparticles of polystyrene were low compared to nanofiltration, and removal efficiency was only 40%.	Akanyeti et al. (2017)
12.	Silver doped graphene oxide	Phenols, Atrazines, Bis-phenols	The silver-doped graphene oxide nanoparticles degraded the toxic organic compound under visible light during photocatalytic degradation, promoted oxidative degradation, and reduced contaminants.	Bhunja and Jana (2014)
13.	Titanium dioxide	Cadmium	Cadmium severely affects the lungs are removed effectively by titanium dioxide nanoparticles.	Zand et al. (2020)
14.	Titanium oxide	Endocrine-disrupting hormones	It was observed that the titanium oxide nanoparticles degrade the Endocrine-disrupting hormones; however, the larger size of the EDC particles are not degraded fastly.	Czech and Rubinowska (2013)
15.	Zero Valent Iron	Copper, Lead, Antimony	These experiments observed the selective removal efficacy of metals like copper, antimony, and lead in the soils.	Boente et al. (2018)
16.	Zerovalent iron	Lead	Plumbism is a disease caused by lead, and the zero-valent nanoparticles remove these contaminants.	Cao et al. (2018)
17.	Zerovalent iron	Cadmium	Cadmium severely affects the lungs are removed effectively by zero-valent nanoparticles.	Cao et al. (2018)
18.	Zinc oxide	Benzophenones	Endocrine-disrupting hormones (benzophenones) are degraded efficiently by zinc oxide nanoparticles.	Rajesha et al. (2017)

the pollutants more efficiently, and Iron oxide nanoparticles obliterated the aliphatic hydrocarbons.

### Mechanism of Nanobioremediation

The characteristics of the nanomaterials lead to enhancing the degradation of the contaminants in the soil. Due to their larger surface areas, the nanomaterials react faster with pollutants. The particle size of the nanomaterials allowed these materials to enter into the pores of the sediments in the soil, enhancing the contact with the contaminants-the nanoparticles exhibit Brownian movements due to gravity. The flow of the ground might be sufficient to transport the particles. Nanoparticles remain in the soil and facilitate the in-situ treatment. Once the nanoparticles contact the pollutant, they degrade them by various mechanisms. The microbial integration with the nanoparticles enables the adsorption and degradation of the contaminants at a greater level. The enzymes of the microbes even dissolve the pollutants to make them available to the nanoparticles for degradation. Figure 5 depicts the pictorial representation of the pollutant degradation in the contaminated soil.

Further from the literature, it is understood that chlorinated aliphatic hydrocarbons are removed by Koenig et al. 2016 by integrating technologies and maintaining appropriate dosages; further suggesting that the minerals can produce zerovalent nanomaterials utilized for the remediation. Polybrominated diphenyl ethers are degraded by the species of Sphingomonas and zerovalent iron oxide nanoparticles consisting of a reductive oxidative approach. Kim et al. (2012) reported that zerovalent iron oxide nanoparticles lessened the polybrominated diphenyl ethers to lower degree compounds (less toxic). The by-products released during this process

will further degrade the microbes more easily. Zerovalent iron oxide nanoparticles consisting of alginate beads under normal conditions removed the hexavalent chromium up to 91 %. The alginate beads removed the chromium when they were used in column experiments in comparison to the free beads; this may be attributed to the increase of column size enhanced the reactive sites; nevertheless, in real-time applications, the removal efficiencies of the hexavalent chromium decreased due to the presence of colloidal particles. The authors suggested that iron nanoparticles degraded the plumes of the ammunition and might be an effective option to treat these toxicants and enhance the argumentation process. Compared to the individual approach for remediating the integration process, i.e., zerovalent iron oxide with white-rot fungi was more effective.

Hydrogen liberated during the by-product degradations will donate electrons to the microbes responsible for the biotransformation of toxicants; the reasons to produce hydrogen gas and donate electrons to the microbes for the degradation were reported by several researchers in detail (Liu et al. 2005, Zhu et al. 2019). Xiu et al. (2010), showed that chlorinated compounds could be reduced by using zerovalent iron oxide nanoparticles with greater efficacy with integrating bacteria that use cathode depolarization. The nanoparticles that are nano metallic (Carboxymethylcellulose doped palladium/iron oxide) combined with species of Sphingomonas for the reduction of hexachloride hexanes revealed that the nanoparticles are stabilized with the carboxymethylcellulose and produced some bio stimulatory effects on the microbial growth. Shin & Cha (2008) reported that the microbial cells' bio stimulatory effects are mainly due to the iron nanoparticles; other zerovalent iron oxide nanoparticles enhance

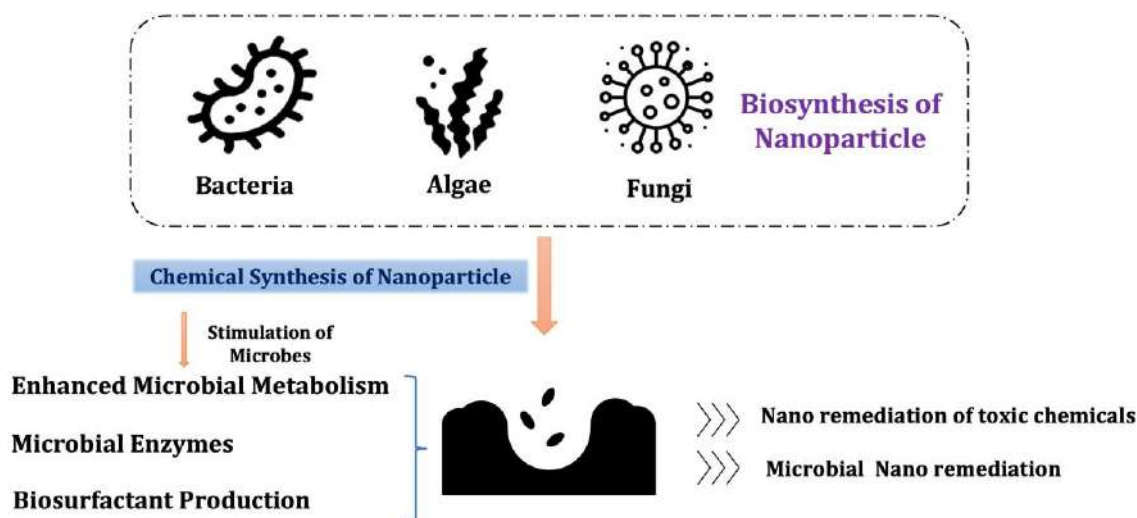


Fig. 5: Mechanisms of Nano-bioremediation in treating polluted soils.

the microbial reductions even at fluctuating temperatures; however, this may be disadvantageous in the case of nitrate reduction.

According to the literature available (Li et al. 2010), nanoparticle toxicity for microbes is extensively researched. The dosage plays a vital role in the integrated system to degrade the toxicants. Koenig et al. (2016) said that during the degradation of chlorinated aliphatic hydrocarbons by the zerovalent iron oxide nanoparticles, the bacterial cells become lethal. In contrast, the nanoparticles positively impacted the organochlorine respiring bacteria with a high dosage. The disadvantage of the toxicity of nanoparticles to microbial cells might be decreased by modifying nanoparticles via coating of nanoparticles, entrapment, or stabilization. Comparing the bactericidal effects of nanoparticles zerovalent iron oxide with polystyrene/poly aspartate and NOM (natural organic matter) with zerovalent iron oxide, it was found that modification of surfaces of nanoparticles reduced the toxicity with a dosage of  $500 \text{ mg.L}^{-1}$  (Li et al. 2010). An et al. 2010 stated that the improvement of iron oxide nanoparticles reduced nanoparticles' toxicity to microbes modified by the chitosan or sodium oleate during the nitrate reduction. Phenrat et al. (2009) said that nanoparticle oxidation is done with the aging of nanoparticles. To avoid directly contacting the microbes' cells, coating the nanoparticles will enhance the Dehalococoides genes responsible for the dichlorination and improve the reduction capacities of trichloroethane (Xiu et al. 2010).

Le et al. (2015) used an integrated approach (integration of *B. xenovorans* and Iron/Palladium nanoparticles) to degrade the chlorinated poly biphenyls and found these methods are cost-effective; further reported that the toxicity of nanoparticles to the E.Coli during the degradation is chlorinated poly biphenyls is very low and not lethal to cells of the bacteria. Němeček et al. (2016) reported that zerovalent iron oxide nanoparticles consisting of microbes injected into the contaminated sites having hexavalent chromium degraded the heavy metal with the efficacy of 99%; Furthermore, microbes are oxidized by the iron nanoparticles and enhanced the degradation rate and decreased utilization of the nanoparticles dosage.

Integration MCNTs ("Multi-walled carbon nanotubes") with bioremediation techniques reduced the toxicants at a greater level. Yan et al. (2013) immobilized the strains of *Shewanella oneidensis* with beads of alginate made up of calcium doped with nanotubes and reduced the hexavalent chromium to trivalent chromium; further, the study revealed that integrated methods degraded the toxicants rapidly in comparison to the individual process; this may be attributed to the transfer of electrons by the carbon nanotubes. Pang et al. 2011 used *Pseudomonas aeruginosa* to reduce

hexavalent chromium; immobilized the strains of microbes in the matrix of carbon nanotubes and alginates of sodium polyvinyl alcohols. The study revealed that the microbial cells immobilized by the modified carbon nanotubes reduced the hexavalent chromium nine-time effectively compared to pristine nanoparticles.

Chidambaram et al. 2010 conducted a study by integrating the Palladium nanoparticles *Clostridium pasteurianum* by the in-situ synthesis, the bacterial cells reduced the Palladium (II) ions to the Palladium nanoparticles, and these nanoparticles are retained in the cells of the bacteria to bio-palladium nanoparticles; the biobased palladium nanoparticles reduced the hexavalent chromium to trivalent chromium. Adikesavan & Nilanjana 2016 conducted a study on magnesium oxide nanoparticles integrated with the yeast candida species for treating the aqueous medium of Cefdinir and revealed that bio-based nanoparticles take lesser time for degrading the contaminants than individual microbial cells; the permeability of microbial cells enhanced, and pollutants are trapped by the cells of microbes and enhanced the degradation rate in comparison to particular treatment methods. Table 2 shows the various nano-bioremediation ways that have been widely used to treat pollutants.

Singh et al. 2020 stated that nano bioremediation had been applied to treat toxicants in two ways: first is the sequential technique in which the contaminants are first treated with the nanoparticles and later subjected to microbes for further degradation; second methods are combined method wherein the pollutants are treated with microbial and nanoparticles at the same time. Bokare et al. (2012), advanced a hybrid sequential approach with palladium/iron nanoparticles to degrade triclosan, an anti-agent used in cosmetics. In the first stage under the anaerobic conditions,  $5 \text{ mg/L}$  of triclosan toxicants are remediated with the Palladium/Iron oxide nanoparticles to dechlorinate the triclosan to phenoxy phenol; later, the nanoparticles are removed from the integrated system and subjected to oxidation with the help of enzyme laccase obtained from the *Trametes Versicolor* which act as a redox mediator; the study revealed that triclosan could completely be transformed into non-toxic substances via the redox process. Kim et al. 2012 conducted similar investigations and degraded the polybrominated diphenyl ethers using zerovalent iron oxide nanoparticles integrated with the *Sphingomonas* bacterial species. He et al. 2009 reported sequential treatment methods for the pentachloro biphenyls with zerovalent nanoparticles with aerobic bacteria. Xiu et al. (2010) conducted a study with zerovalent iron oxide nanoparticles and microorganisms to remediate trichloroethane. Similarly, two different experiments were conducted under similar conditions, i.e., one with zerovalent iron oxide and the

Table 2: Treatment of noxious pollutants by nano-bioremediation (Singh et al., 2020).

S.no	Type of nanoparticle	Biological Agent	Family of Microbe	Toxicants removed	References
1.	CNTs	<i>Shewanella oneidensis</i>	Shewanellaceae	Hexavalent Chromium	Yan et al. (2013)
2.	Electrospun nano-fibers	<i>Lysinibacillus</i>	Bacillaceae	Nickel	San et al. (2018)
3.	Electrospun nano-fibers	<i>Lysinibacillus</i>	Bacillaceae	Chromium	San et al. (2018)
4.	Iron oxide	Species of <i>Sphingomonas</i>	Sphingomonadaceae	Carbazole	Li et al. (2013)
5.	Iron oxide	<i>Pseudomonas delafieldii</i>	Pseudomonadaceae	Dibenzothiophene	Shan et al. (2003)
6.	Iron oxide	Species of <i>Sphingomonas</i>	Sphingomonadaceae	Carbazole	Wang et al. (2007)
7.	Palladium	<i>Clostridium pasteurianum</i>	Clostridiaceae	Hexavalent Chromium	Chidambaram et al. (2010)
8.	Palladium	<i>Sphingomonas wittichii</i>	Sphingomonadaceae	Tetrachlorodibenzo-p-disney	Bokare et al. (2012)
9.	Palladium	<i>Burkholderia xenovorans</i>	Burkholderiaceae	PCBs	Le et al. (2015)
10.	Zerovalent iron	<i>Dehalococcoides</i>	Dehalococcoidaceae	Trichloroethane	Xiu et al. (2010)
11.	Zerovalent iron	Species of <i>Paracoccus</i>	Rhodobacteraceae	Nitrates	Liu et al. (2014)
12.	Zerovalent iron al-ginate	<i>Acinetobacter junii</i>	Moraxellaceae	Hexavalent Chromium	Ravikumar et al. (2016)

other with species of *Dehalococcoides* individually (Singh et al. 2020). Even though many instances are available in the literature about nano-bioremediation, there is still a need to conduct many studies to move them from the bench-scale experiments to the industrial sectors to commercialize them.

### Challenges with Nanobioremediation

During the in-situ remediation, the reactive compounds might harm the microorganisms and prevent degradation. The cost and the production of the nanoparticles on a larger scale are difficult. Further, the nanoparticles during the degradation might even react with the non-target compounds and form a cluster in the soils and stop the reactions and enzymes synthesis by the microbes. In the in-situ remediation, some nanoparticle inhibits the reactions and prevents nanoparticle dispersing of nanoparticles in the contaminated sites, reducing their effectiveness. The coating of nanoparticles can overcome this problem, but this process might add more costs to the treatment. Even such designs might affect the interactions of nanoparticles with the microbes and even causes toxicity to the cells of the microbes. Continued research on the area using nanoparticles might affect the people, wildlife, and plants near it. Thus, there is a need for conducting more research on these topics to overcome these problems.

### CONCLUSIONS

Nano bioremediation was more promising and advantageous than conventional technologies currently used to remediate the toxicants present in contaminated soils. However, there is a paucity in the literature to gain in-depth knowledge about

these technologies; thus, there is a need to conduct more studies on these integrated methods to bring more actions to develop and implement these technologies to full scale; furtherly the effect of environmental conditions on the nano bioremediation are also needed to understand these methods.

### REFERENCES

- Adikesavan, S. and Nilanjana, D. 2016. Degradation of cefdinir by Cida Sp. SMN 04 and MgO nanoparticles-An integrated (Nano-Bio) approach. *Environ. Prog. Sustain. Energy.*, 35(3): 706-714.
- Akanyeti, I., Kraft, A. and Ferrari, M.C. 2017. Hybrid polystyrene nanoparticle-ultrafiltration system for hormone removal from water. *J. Water Process. Eng.*, 17: 102-109.
- An, Y., Li, T., Jin, Z., Dong, M., Xia, H. and Wang, X. 2010. Effect of bimetallic and polymer-coated Fe nanoparticles on biological denitrification. *Bioresour. Technol.*, 101(24): 9825-9828.
- Barrocas, B., Entradas, T.J., Nunes, C.D. and Monteiro, O.C. 2017. Titanate nanofibers sensitized with ZnS and Ag2S nanoparticles as novel photocatalysts for phenol removal. *Appl. Catal. B.* 218: 709-720.
- Bhunia, S.K. and Jana, N.R. 2014. Reduced graphene oxide-silver nanoparticle composite as visible light photocatalyst for degradation of colorless endocrine disruptors. *ACS Appl. Mater. Interfaces.*, 6(22): 20085-20092.
- Boente, C., Sierra, C., Martínez-Blanco, D., Menéndez-Aguado, J. M. and Gallego, J. R. 2018. Nanoscale zero-valent iron-assisted soil washing for the removal of potentially toxic elements. *J. Hazard. Mater.*, 350: 55-65.
- Bokare, V., Murugesan, K., Kim, J.H., Kim, E.J. and Chang, Y.S. 2012. Integrated hybrid treatment for the remediation of 2, 3, 7, 8-tetrachlorodibenzo-p-dioxin. *Sci. Total Environ.*, 435: 563-566.
- Cao, Y., Zhang, S., Zhong, Q., Wang, G., Xu, X., Li, T. and Li, Y. 2018. Feasibility of nanoscale zero-valent iron to enhance the removal efficiencies of heavy metals from polluted soils by organic acids. *Ecotoxicology and Environmental Safety*, 162, 464-473.
- Chauhan, G., González-González, R.B. and Iqbal, H.M. 2022. Bioremediation and decontamination potentials of metallic nanoparticles loaded nanohybrid matrices—A review. *Environ. Res.*, 204: 112407.



- Chidambaram, D., Hennebel, T., Taghavi, S., Mast, J., Boon, N., Verstraete, W and Fitts, J.P. 2010. Concomitant microbial generation of palladium nanoparticles and hydrogen to immobilize chromate. *Environ. Sci. Technol.*, 44(19): 7635-7640.
- Contreras, A. R., Casals, E., Puentes, V., Komilis, D., Sánchez, A. and Font, X. 2015. Use of cerium oxide (CeO<sub>2</sub>) nanoparticles for the adsorption of dissolved cadmium (II), lead (II), and chromium (VI) at two different pHs in single and multi-component systems. *Glob. Nest J.*, 17(3): 536-543.
- Councils, G. A. 2015. Outlook on the Global Agenda 2015. In World Economic Forum.
- Czech, B. and Rubinowska, K. 2013. TiO<sub>2</sub>-assisted photocatalytic degradation of diclofenac, metoprolol, and estrone chloramphenicol as endocrine disruptors in water. *Adsorption*, 19(2): 619-630.
- Darwesh, O., Shalapy, M., Abo-Zeid, A. and Mahmoud, Y. 2021. Nano-Bioremediation of Municipal Wastewater Using Myco-Synthesized Iron Nanoparticles. *Egypt. J. Chem.*, 64(5): 8-9.
- Ekka, B., Sahu, M.K., Patel, R.K. and Dash, P. 2019. Titania coated silica nanocomposite prepared via encapsulation method for the degradation of Safranin-O dye from aqueous solution: Optimization using statistical design. *Water Resour. Ind.*, 22: 100071.
- Elfeky, S. A., Mahmoud, S. E. and Youssef, A. F. 2017. Applications of CTAB modified magnetic nanoparticles for removal of chromium (VI) from contaminated water. *J. Adv. Res.*, 8(4), 435-443.
- Galdames, A., Ruiz-Rubio, L., Orueta, M., Sánchez-Arzalluz, M. and Vilas-Vilela, J.L. 2020. Zero-valent iron nanoparticles for soil and groundwater remediation. *Int. J. Environ. Res. Public Health.*, 17(16), 5817.
- Guo, P., Tang, L., Tang, J., Zeng, G., Huang, B., Dong, H. and Tan, S. 2016. Catalytic reduction-adsorption for removal of p-nitrophenol and its conversion p-aminophenol from water by gold nanoparticles supported on oxidized mesoporous carbon. *J. Colloid Interface Sci.*, 469, 78-85.
- Han, B., Zhang, M. and Zhao, D. 2017. In-situ degradation of soil-sorbed 17 $\beta$ -estradiol using carboxymethyl cellulose stabilized manganese oxide nanoparticles: Column studies. *Environ. Pollut.*, 223, 238-246.
- He, N., Li, P., Zhou, Y., Fan, S. and Ren, W. 2009. Degradation of pentachlorobiphenyl by a sequential treatment using Pd-coated iron and an aerobic bacterium (H1). *Chemosphere*, 76(11), 1491-1497.
- Hosseini, S. M., Amini, S. H., Khodabakhshi, A. R., Bagheripour, E. and Van der Bruggen, B. 2018. Activated carbon nanoparticles entrapped mixed matrix polyethersulfone-based nanofiltration membrane for sulfate and copper removal from water. *J. Taiwan Inst Chem Eng.*, 82, 169-178.
- Huang, Y., Fulton, A. N. and Keller, A. A. 2016. Simultaneous removal of PAHs and metal contaminants from water using magnetic nanoparticle adsorbents. *Sci. Total Environ.*, 571, 1029-1036.
- Hussain, I., Li, M., Zhang, Y., Li, Y., Huang, S., Du, X. and Anwar, N. 2017. Insights into the mechanism of persulfate activation with nZVI/BC nanocomposite for the degradation of nonylphenol. *Chem. Eng. J.*, 311, 163-172.
- Kahraman, B. F., Altin, A. and Ozdogan, N. 2022. Remediation of Pb-diesel fuel co-contaminated soil using nano/bioprocess: subsequent use of nanoscale zero-valent iron and bioremediation approaches. *Environ. Sci. Pollut. Res.*, 1-15.
- Karnena, M. K., Konni, M. and Saritha, V. 2020. Nano-catalysis process for treatment of industrial wastewater. In *Handbook of Research on Emerging Developments and Environmental Impacts of Ecological Chemistry* (pp. 229-251). IGI Global.
- Kim, Y.M., Murugesan, K., Chang, Y.Y., Kim, E.J. and Chang, Y.S. 2012. Degradation of polybrominated diphenyl ethers by sequential treatment with nanoscale zero-valent iron and aerobic biodegradation. *J. Chem. Technol. Biotechnol.*, 87(2): 216-224.
- Koenig, J. C., Boparai, H.K., Lee, M.J., O'Carroll, D. M., Barnes, R.J. and Manefield, M. J. 2016. Particles and enzymes: combining nanoscale zero-valent iron and organochlorine respiring bacteria for the detoxification of chloroethane mixtures. *J. Hazard. Mater.*, 308: 106-112.
- Konni, M., Mukkamala, S.B., Srikanth Vemuri, R.S.S. and Karnena, M.K. 2021. Sustainable Approaches for the Treatment of Industrial Wastewater Using Metal-Organic Frame Works. In *Water Safety, Security and Sustainability*, Springer, Cham, pp. 463-493.
- Le, T.T., Nguyen, K.H., Jeon, J.R., Francis, A.J. and Chang, Y. S. 2015. Nano/biotreated of polychlorinated biphenyls with an evaluation of comparative toxicity. *J. Hazard. Mater.*, 287: 335-341.
- Li, Y., Du, X., Wu, C., Liu, X., Wang, X. and Xu, P. 2013. An efficient magnetically modified microbial cell biocomposite for carbazole biodegradation. *Nanoscale Res. Lett.*, 8(1): 1-5.
- Li, Z., Greden, K., Alvarez, P.J., Gregory, K.B. and Lowry, G.V. 2010. Adsorbed polymer and NOM limit adhesion and toxicity of nanoscale zerovalent iron to E. coli. *Environ. Sci. Technol.*, 44(9): 3462-3467.
- Liu, Y., Majetich, S. A., Tilton, R.D., Sholl, D. S. and Lowry, G.V. 2005. TCE dechlorination rates, pathways, and efficiency of nanoscale iron particles with different properties. *Environ. Sci. Technol.*, 39(5): 1338-1345.
- Němeček, J., Pokorný, P., Lhotský, O., Knytl, V., Najmanová, P., Steinová, J. and Cajthaml, T. 2016. Combined nano-biotechnology for in-situ remediation of mixed contamination of groundwater by hexavalent chromium and chlorinated solvents mineralization by zerovalent iron and mixed anaerobic cultures. *Environ. Sci. Technol.*, 35(21): 4341-4346.
- Pang, Y., Zeng, G. M., Tang, L., Zhang, Y., Liu, Y.Y., Lei, X.X. and Liu, C. 2011. Cr (VI) reduction by *Pseudomonas aeruginosa* immobilized in a polyvinyl alcohol/sodium alginate matrix containing multi-walled carbon nanotubes. *Bioresour. Technol.*, 102(22): 10733-10736.
- Phenrat, T., Long, T., Lowry, G.V. and Veronesi, B. 2009. Partial oxidation ("aging") and surface modification decrease the toxicity of nanosized zerovalent iron. *Environ. Sci. Technol.*, 43(1): 195-200.
- Prabhakar, R. and Samadder, S.R. 2018. Low cost and easy synthesis of aluminum oxide nanoparticles for arsenite removal from groundwater: a complete batch study. *J. Mol. Liq.*, 250: 192-201.
- Qi, F. F., Cao, Y., Wang, M., Rong, F. and Xu, Q. 2014. Nylon 6 electrospun nanofibers mat as an effective sorbent for the removal of estrogens: kinetic and thermodynamic studies. *Nanoscale Res. Lett.*, 9(1): 1-10.
- Qian, Y., Qin, C., Chen, M. and Lin, S. 2020. Nanotechnology in soil remediation- applications vs. implications. *Ecotoxicol. Environ.*, 201: 110815.
- Raja, M. A. and Husen, A. 2020. Role of Nanomaterials in Soil and Water Quality Management. In Husen, A. and Jawaid, M. (eds), *Nanomaterials for Agriculture and Forestry Applications*. Elsevier, The Netherlands, pp. 491-503.
- Rajendran, K. and Sen, S. 2018. Adsorptive removal of carbamazepine using biosynthesized hematite nanoparticles. *Environ. Nanotechnol. Monit. Manag.*, 9: 122-127.
- Rajेशha, J.B., Ramasami, A.K., Nagaraju, G. and Balakrishna, G.R. 2017. photochemical elimination of endocrine disrupting chemical (EDC) by ZnO nanoparticles, synthesized by gel combustion. *Water Environ. Res.*, 89(5): 396-405.
- Ramezani, M., Rad, F.A., Ghahari, S., Ghahari, S. and Ramezani, M. 2021. Nano-bioremediation application for environmental contamination by microorganisms. In *Microbial Rejuvenation of Polluted Environment*. Springer, Singapore. pp. 349-378.
- Ravikumar, K.V.G., Kumar, D., Kumar, G., Mrudula, P., Natarajan, C. and Mukherjee, A. 2016. Enhanced Cr (VI) removal by nanoscale zerovalent iron-immobilized alginate beads in the presence of a biofilm in a continuous-flow reactor. *Ind. Eng. Chem. Res.*, 55(20): 5973-5982.
- Reddy, K.J., McDonald, K. J. and King, H. 2013. A novel arsenic removal process for water using cupric oxide nanoparticles. *J. Coll. Interface Sci.*, 397: 96-102.
- Sakulchaicharoen, N., O'Carroll, D.M. and Herrera, J. E. 2010. Enhanced stability and dechlorination activity of pre-synthesis stabilized nanoscale FePd particles. *J. Contam. Hydrol.*, 118(3-4): 117-127.

- San Keskin, N.O., Celebioglu, A., Sarioglu, O.F., Uyar, T. and Tekinay, T. 2018. Encapsulation of living bacteria in electrospun cyclodextrin ultrathin fibers for bioremediation of heavy metals and reactive dye from wastewater. *Colloids and Surfaces B: Biointerfaces*, 161: 169-176.
- Sarkar, B., Mandal, S., Tsang, Y.F., Kumar, P., Kim, K.H. and Ok, Y.S. 2018. Designer carbon nanotubes for contaminant removal in water and wastewater: A critical review. *Sci. Total Environ.*, 612: 561-581.
- Shahi, M.P., Kumari, P., Mahobiya, D. and Shahi, S.K. 2021. Nano-bioremediation of environmental contaminants: applications, challenges, and prospects. *Bioremed. Environ. Sustain.*, 71: 83-98.
- Shan, G., Xing, J., Zhang, H. and Liu, H. 2005. Biodesulfurization of dibenzothiophene by microbial cells coated with magnetite nanoparticles. *Appl. Environ. Microbiol.*, 71(8): 4497-4502.
- Shin, K.H. and Cha, D.K. 2008. Microbial reduction of nitrate in the presence of nanoscale zero-valent iron. *Chemosphere*, 72(2): 257-262.
- Singh, R., Behera, M. and Kumar, S. 2020. Nano-bioremediation: An innovative remediation technology for treatment and management of contaminated sites. In Bhargava, R.N., and Saxena, G. (eds), *Bioremediation of industrial waste for environmental safety*. Springer, Singapore, pp. 165-182.
- Souza, L.R.R., Pomarolli, L.C. and da Veiga, M.A.M.S. 2020. From classic methodologies to the application of nanomaterials for soil remediation: an integrated view of methods for decontamination of toxic metal (OID) *Environ. Sci. Pollut. Res.*, 27(10): 10205-10227.
- Vara, S. and Karnena, M.K. 2020. Fungal enzymatic degradation of industrial effluents—A review. *Curr. Res. Environ. Appl. Mycol.*, 10(1): 417-442.
- Wang, J.S. and Chiu, K. 2009. Destruction of pentachlorobiphenyl in soil by supercritical CO<sub>2</sub> extraction coupled with polymer-stabilized palladium nanoparticles. *Chemosphere*, 75(5): 629-633.
- Wang, X., Gai, Z., Yu, B., Feng, J., Xu, C., Yuan, Y. and Xu, P. 2007. Degradation of carbazole by microbial cells immobilized in magnetic gellan gum gel beads. *Appl. Environ. Microbiol.*, 73(20): 6421-6428.
- Wu, Z., Yang, S. and Wu, W. 2016. Shape control of inorganic nanoparticles from solution. *Nanoscale*, 8(3): 1237-1259.
- Xiu, Z.M., Gregory, K.B., Lowry, G.V. and Alvarez, P.J. 2010. Effect of bare and coated nanoscale zerovalent iron on *tceA* and *vcrA* gene expression in *Dehalococcoides* spp. *Environ. Sci. Technol.*, 44(19): 7647-7651.
- Yadav, K.K., Singh, J.K., Gupta, N. and Kumar, V.J. 2017. A review of nanobioremediation technologies for environmental cleanup: a novel biological approach. *J. Mater. Environ. Sci.*, 8(2): 740-757.
- Yan, F.F., Wu, C., Cheng, Y.Y., He, Y.R., Li, W.W. and Yu, H.Q. 2013. Carbon nanotubes promote Cr (VI) reduction by alginate-immobilized *Shewanella oneidensis* MR-1. *Biochem. Eng. J.*, 77: 183-189.
- Zand, A. D., Mikaeili Tabrizi, A. and Vaezi Heir, A. 2020. Application of titanium dioxide nanoparticles to promote phytoremediation of Cd-polluted soil: contribution of PGPR inoculation. *Bioremed. J.*, 24(2-3): 171-189.
- Zhou, Y., Kumar, M., Sarsaiya, S., Sirohi, R., Awasthi, S. K., Sindhu, R. and Awasthi, M. K. 2022. Challenges and opportunities in bioremediation of micro-nano plastics: A review. *Sci. Total Environ.*, 802: 149823.
- Zhu, Y., Xu, F., Liu, Q., Chen, M., Liu, X., Wang, Y. and Zhang, L. 2019. Nanomaterials and plants: Positive effects, toxicity and the remediation of metal and metalloid pollution in soil. *Sci. Total Environ.*, 662: 414-421.



# Comparison of As(III) Adsorption by Nanomagnetic Fe<sub>3</sub>O<sub>4</sub>, Activated Carbon and Modified Activated Carbon

J. Zhang<sup>†</sup>, L. Xia, R. Han and W. Wei

School of Environmental Sciences and Engineering, Dalian Maritime University, Dalian 116026, PR China

<sup>†</sup>Corresponding author: J. Zhang; zhangjin7986@163.com

Nat. Env. & Poll. Tech.  
Website: [www.neptjournal.com](http://www.neptjournal.com)

Received: 28-02-2022  
Revised: 30-03-2022  
Accepted: 06-04-2022

## Key Words:

Nanomagnetic Fe<sub>3</sub>O<sub>4</sub>  
Modified adsorbent  
Activated carbon  
Adsorption  
Arsenic pollution

## ABSTRACT

As a kind of new material, nanomagnetic Fe<sub>3</sub>O<sub>4</sub> (NMF) has many advantages in water and wastewater treatment. In this paper, the adsorption characteristic for arsenic(III) (As) by NMF was studied, and the adsorption was compared with the traditional adsorbent of activated carbon (AC) and modified activated carbon (MAC). The results showed that the NMF had high adsorption performance for As, and the adsorption performance of modified activated carbon and activated carbon were far lower than that of magnetic nanomagnetic Fe<sub>3</sub>O<sub>4</sub>. The adsorption capacity for As with NMF, MAC, and AC was 0.189 mg.g<sup>-1</sup>, 0.023 mg.g<sup>-1</sup> and 0.013 mg.g<sup>-1</sup> in 0.25 mg.L<sup>-1</sup> As solution, respectively. The adsorption rate for As was different from the three adsorbents. For NMF, it needs only 10 minutes to reach an adsorption balance, while the time to balance was 20 minutes for MAC and more than 120 minutes for AC. The adsorption for As by the three adsorbents all conform to Langmuir adsorption isotherm, and the adsorption kinetics for As by the three adsorbents were in accordance with the pseudo-second-order kinetics model. The adsorption efficiency of MAC and AC was lower than nanomagnetic Fe<sub>3</sub>O<sub>4</sub>. The nanomagnetic Fe<sub>3</sub>O<sub>4</sub> was an effective adsorbent for arsenic.

## INTRODUCTION

As one of the most abundant elements, arsenic (As) is widely distributed in nature. By estimate, the annual total global arsenic emissions to the environment are as high as 22,100 tons, and the total amount of arsenic flow into the water environment is about 110 thousand tons (Varga et al. 2017, Zheng et al. 2017). The arsenic in water has mainly come from one of the emissions of agricultural and industrial wastewater, which contains excessive pesticides, herbicides, and wood preservatives, and the second was the deposition of arsenic in the atmosphere. The combustion of arsenic-bearing coal and crude oil can make a lot of arsenic-containing compound particles enter the atmospheric environment in form of dust and then enter surface water by means of sedimentation, and the dissolution of natural minerals (Jerome et al. 2015). With the development of industry and agriculture, the total annual discharge of industrial wastewater increased over decades, and the amount of arsenic entering the environment increased (Hu et al. 2019, Sun et al. 2016).

Arsenic and its compounds are carcinogenic materials to humans and other species and are considered environmental virulence metals together with cadmium, lead, mercury, and chromium (Shen et al. 2017). IARC (International Agency for Research on Cancer) and CDC (Centers for Disease Control)

identified arsenic as the first carcinogenic substance. At the same time, due to its genetic toxicity, arsenic was considered a priority control pollutant by WHO (World Health Organization) (Pari & Jalaludeen 2011, El-Moselhy et al. 2017, Kukucka et al. 2016). It had been documented that when the content of arsenic in a human body is 0.01-0.052g, it would lead to arsenic poisoning, and when the content reached 0.06-0.2g, it would lead the person to death (Zeng et al. 2017, Nandre et al. 2017, Mukherjee et al. 2017). Documents showed that many people died from arsenic poisoning and hundreds of millions of people were being at serious risk from As in many countries throughout the world, such as China, India, Vietnam, Bangladesh, etc. (Itziar et al. 2004). The removal of arsenic from water and wastewater has become the focus problem in many countries (Egbosiuba et al. 2020, Ding et al. 2017, Molinari & Argurio 2017).

Adsorption technology of activated carbon has been deemed one of the most popular technologies for pollution removal in water and wastewater treatment (Orlando et al. 2020, Kiran et al. 2020, García-Mateos et al. 2015). However, there are still many drawbacks in the adsorption of activated carbon for heavy metals, such as low selectivity, low adsorption capacity, etc. In recent years, some modification methods have been proposed to improve the adsorption

capacity and selectivity of activated carbon. For example, Yang et al. modified the ACF with nitration treatment, heat treatment, and heat treatment after nitration, and they showed that the modification changed the surface physical and chemical properties of the ACF samples, and increased the adsorption capacity of ACF (Yang et al. 2016). Shafeeyan et al. studied the surface modification of activated carbon with gaseous ammonia and showed that the adsorption capacity of activated carbon for carbon dioxide increased with the introduction of basic nitrogen functionalities into the carbon surface (Shafeeyan et al. 2010). Palomo et al. produced more condensed nitrogen structures (such as pyridinic and pyrrolic structures) in the activated carbons by oxidation and reduction treatment (Palomo et al. 2017). Jaramillo et al. showed the treatment of activated carbon with ozone combined with heat treatment could control the acidic-basic character and the strength of the carbon surface, and the treatment with ozone yielded acidic carbons, carbon dioxide, and steam activations (Jaramillo et al. 2010). Macías-García et al. modified the porous texture and superficial groups of a commercial activated carbon through chemical and thermal treatment and showed high adsorption and electro adsorption for Cu(II) ion (Macías-García et al. 2017); Chiang and Juang had shown that the surface modifications of activated carbon could improve the adsorption for carbon dioxide in general (Chiang & Juang 2017).

With the development of adsorption technology, nanometer materials have been studied widely in water and wastewater treatment (Bao et al. 2016, Sun et al. 2017). As a new nanometer material, magnetic  $\text{Fe}_3\text{O}_4$  has been studied in water pollution treatment extensively and has received some good results (Song et al. 2015, Uheida et al. 2006, Zavareh et al. 2017, Mhamme & Samaka 2018).

To facilitate the development of adsorption technology in heavy metal removal in the environment, a comparison study of adsorption characteristics of conventional adsorbent of AC (activated carbon), MAC (modified activated carbon), and new material of nanomagnetic  $\text{Fe}_3\text{O}_4$  for arsenic has been carried out.

## MATERIALS AND METHODS

### Experimental Materials

**The preparation of nanomagnetic  $\text{Fe}_3\text{O}_4$ :** Nanomagnetic  $\text{Fe}_3\text{O}_4$  ( $\text{Fe}_3\text{O}_4$  or NMF) was prepared by the method of hydrothermal synthesis (Legod & Waal 2007). Ferrous precursor ( $\text{FeSO}_4 \cdot 7\text{H}_2\text{O}$ , 10g) and ferric chlorite ( $\text{FeCl}_3 \cdot 7\text{H}_2\text{O}$ , 20g) were dissolved in 1500ml of distilled water. To the filtered solution, 150ml of 25%  $\text{NH}_4\text{OH}$  solution was added to raise the pH to about 11-12. After aging for about 20h at room

temperature, the precipitate formed collected by filtering, washed with 500ml of distilled water, and then allowed to dry at room temperature.

**The preparation of AC:** The activated carbon was coconut shell granular activated carbon and the particle size was 25cm-50cm in diameter. After soaking in pure water for about 8-10h and washing repeatedly with deionized water, the activated carbon was dried to constant weight for over 24h at 105°C.

**The preparation of MAC:** The modification of activated carbon was performed under neutral conditions. The activated carbon (100 g) was immersed in a solution of potassium permanganate ( $0.1\text{mol}\cdot\text{L}^{-1}$ , 500mL) and stirred slowly with a constant temperature oscillator for 10h, then the activated carbon was separated and washed repeatedly with deionized water to no color, and dried to constant weight for 24 h at 105°C.

**The preparation for arsenic solution:** The arsenic(III) (As) was purchased from Beijing Wanjia Biotechnology co. LTD.  $1000\text{mg}\cdot\text{L}^{-1}$  of As(III) reserve solution was prepared with deionized water and diluted to a certain concentration when used.

All chemicals in the study were of analytical grade.

### Adsorption Experiments Method

Adsorption experiments were performed at room temperature ( $20\pm 1^\circ\text{C}$ ), and the pH of the water was 6.7. The adsorbent (NMF/MAC/AC) was put into 250 mL of water (containing As(III)) and shaken on a magnetic stirrer (50 RPM) for 180 min. Then the solution was filtered with a  $0.45\mu\text{m}$  membrane filter and the amount of arsenic adsorbed was analyzed.

### Analysis Method

The concentration of arsenic in water was analyzed by atomic fluorescence spectrometry. 1.0ml mixed solution of ascorbic acid and thiourea (10%) was added into 0.1mL water sample and stirred to blend, and then 2% of the hydrochloric acid was added to 10mL, stand still for 60min and then the content of arsenic was analyzed with non-dispersive atomic fluorescence photometer (PF6-2).

## RESULTS AND DISCUSSION

### Adsorption for Arsenic by NMF, AC and MAC

The study of adsorption capability for As by NMF, AC, and MAC was conducted in 250mL water with initial concentrations of  $0.25\text{mg}\cdot\text{L}^{-1}$ ,  $0.50\text{mg}\cdot\text{L}^{-1}$ ,  $0.75\text{mg}\cdot\text{L}^{-1}$ , and  $1.00\text{mg}\cdot\text{L}^{-1}$ , respectively. respectively. The dosage of NMF was 0.10 g, 0.31 g, and 0.62 g, and the dosage of AC and

MAC was controlled at 5 g, 10 g, and 15 g in 250 mL. The adsorption results with the three adsorbents were shown in Fig. 1, and Fig. 3.

It could be seen that the adsorbent of NMF, AC, and MAC had different adsorption capacities for As. The NMF showed high removal efficiency for As though at a low dosage. The removal rate for As could reach 75-85%, 80-90%, and 90-100% at a dosage of NMF was 0.10 g, 0.31 g, and 0.62 g, respectively. While the removal rate for As by adsorption with

the traditional adsorbent of AC was very low, and the removal rate was only 20-30%, 50-70%, and 80-90% at dosages of 5 g, 10 g, and 15 g. On the other hand, with MAC, the removal rate increased to 70-80%, 80-90%, and 80-100% at dosages of 5 g, 10 g, and 15 g. The results also showed that the adsorption of arsenic on NMF was very fast, and the adsorption could reach equilibrium in less than 10 min. The adsorption rate on AC was slow, and the arsenic removal rate increased slowly in 180 min. While the adsorption rate on MAC increased

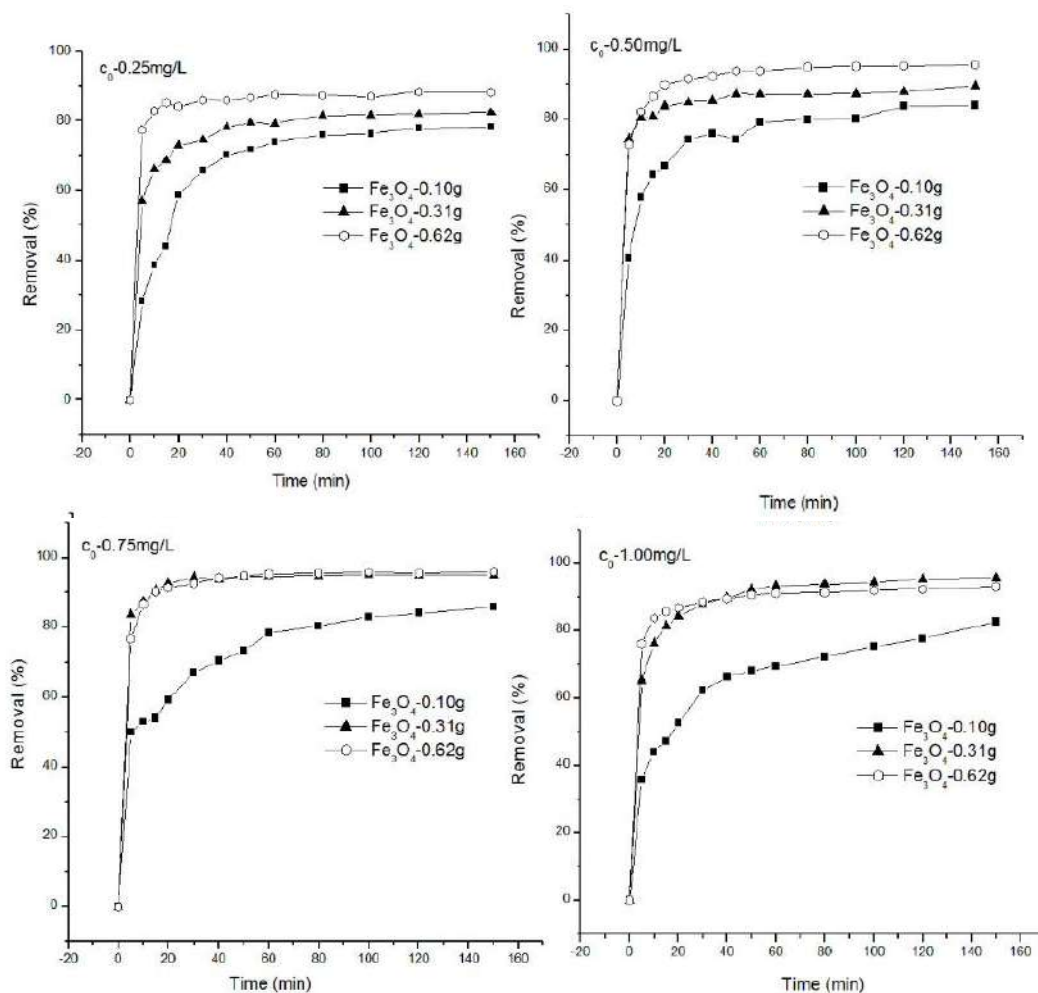


Fig.1: The adsorption for As with NMF.

Table 1: The kinetic parameters of adsorption for As.

	The first-order kinetics model				The second-order kinetics model		
	$q_t$ (mg.g <sup>-1</sup> )	$q_e$ (mg.g <sup>-1</sup> )	$k_1$ (min <sup>-1</sup> )	R <sup>2</sup>	$q_e$ (mg.g <sup>-1</sup> )	$k_2$ (g.mg.min <sup>-1</sup> )	R <sup>2</sup>
AC	0.013	0.004	0.011	0.671	0.016	0.718	0.996
MAC	0.023	0.012	0.023	0.959	0.024	4.330	0.997
NMF	0.189	0.027	0.042	0.812	0.191	6.947	0.962

Table 2: Parameters of Langmuir Equation and Freundlich Equation.

Langmuir model				Freundlich model		
	$a$	$K_L$	$R^2$	$n$	$K_F$	$R^2$
AC	0.062	1.781	0.961	0.487	0.036	0.821
MAC	0.085	3.518	0.983	0.413	0.062	0.677
Fe <sub>3</sub> O <sub>4</sub>	2.262	4.557	0.993	0.472	1.758	0.818

significantly, and the adsorption reached balance in 20-30 min. As a new adsorption material, nanomagnetic Fe<sub>3</sub>O<sub>4</sub> has a better adsorption effect for arsenic. The traditional material of activated carbon has little adsorption efficiency for As. The adsorption capacity of AC for arsenic was improved to a great extent by the modification of activated carbon.

### The study of Adsorption Kinetics and Isotherms

The adsorption kinetics study: The experiment was conducted in 250mL water with an initial concentration of arsenic of 0.25mg.L<sup>-1</sup>. The dosage of AC, MAC, and NMF was 5.0g,

5.0g, and 0.10g respectively. The adsorption amount at different times was analyzed according to equation (1), and the adsorption capacity results were shown in Fig 4.

$$q_t = \frac{V(C_{0i} - C_i)}{m} \quad \dots(1)$$

In which,  $q_t$  was the adsorption amount (mg.g<sup>-1</sup>);  $V$  was the volume of the water (L);  $C_{0i}$  was the initial concentration of As (mg.L<sup>-1</sup>), and  $C_i$  was the concentration of As at the time of  $t$ ;  $m$  was the mass of the adsorbent (g).

The adsorption amount for As with Fe<sub>3</sub>O<sub>4</sub> was much higher than that of MAC, and AC. The adsorption for As

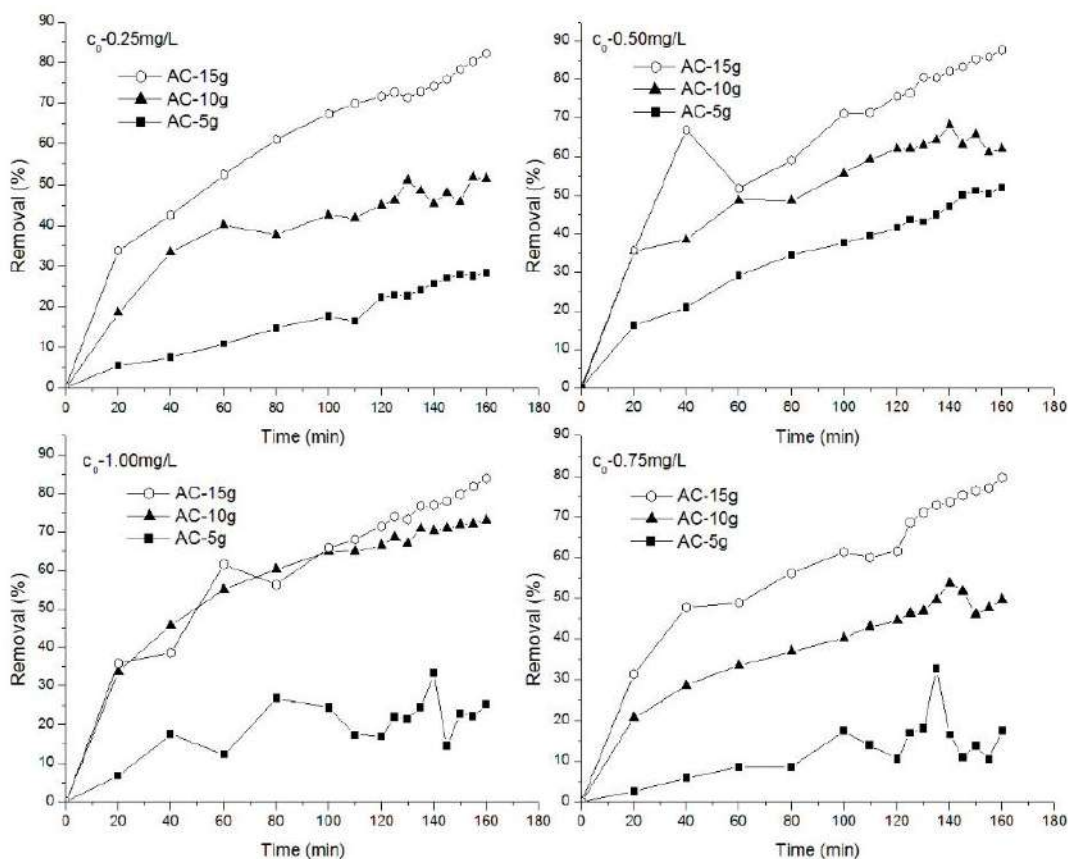


Fig.2: The adsorption for As with AC.

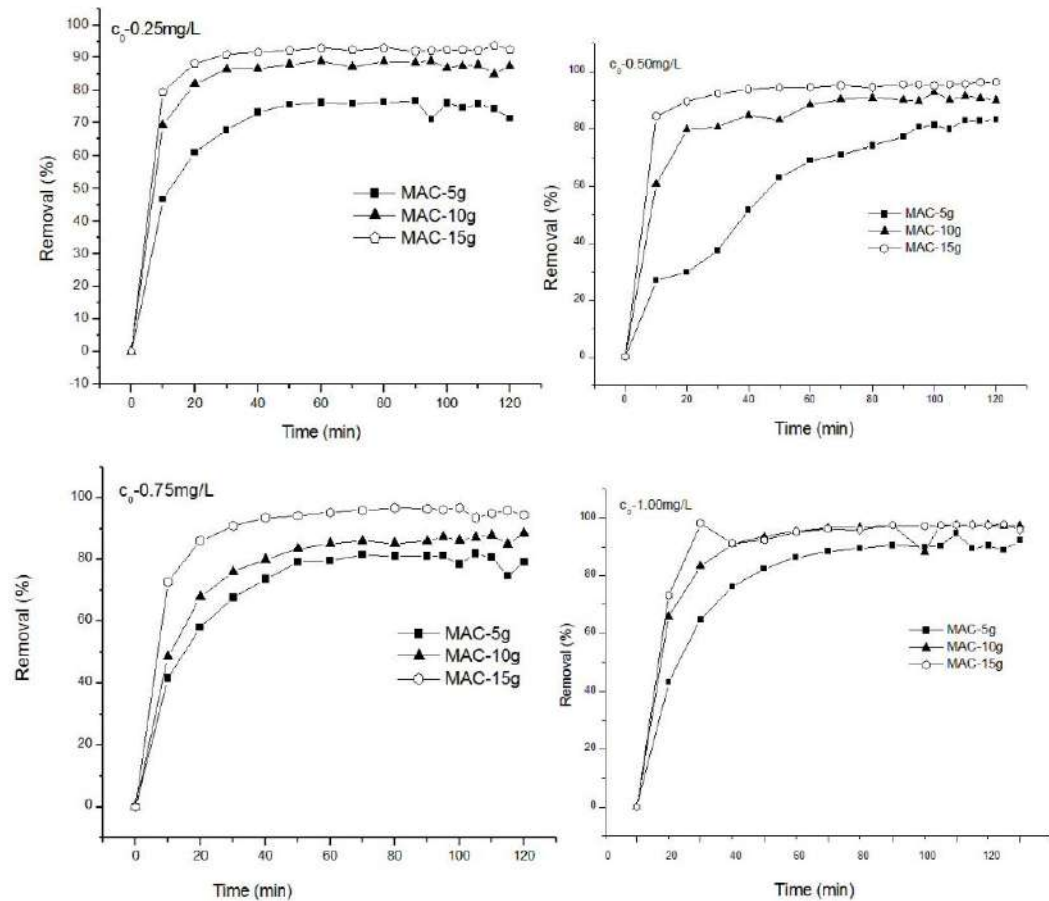


Fig.3: The adsorption for As with MAC.

with NMF reached equilibrium in about 10 min, while for MAC and AC, it needs more than 30 min.

The adsorption kinetics was fitted with a pseudo-first-order kinetics model and pseudo-second-order kinetics model according to equations (2) and (3) (Alvarez-Torrellas et al. 2016, Bao et al. 2017, Zhang et al. 2017), and the fitted results were shown in Table 1.

$$\ln(q_{e1} - q_t) = \ln q_{e1} - k_1 t \quad \dots(2)$$

$$\frac{t}{q_t} = \frac{1}{k_2 q_{e2}^2} + \frac{t}{q_{e2}} \quad \dots(3)$$

In which:  $q_t$  was the adsorption capacity at the contact time  $t$ ,  $q_{e2}$  was the equilibrium adsorption capacity calculated by pseudo first and second order kinetics model, and  $k_2$  was the rate constant of the pseudo-first and second order kinetics model respectively;  $R^2$  was simulated correlation coefficient.

The results in Table 1 showed that the  $R^2$  of the pseudo-second-order kinetics model of the three adsorbents was

superior to the first-order kinetics model, which indicated that the adsorption of As on the three adsorbents conforms to the pseudo-second-order kinetics model. The adsorption for As

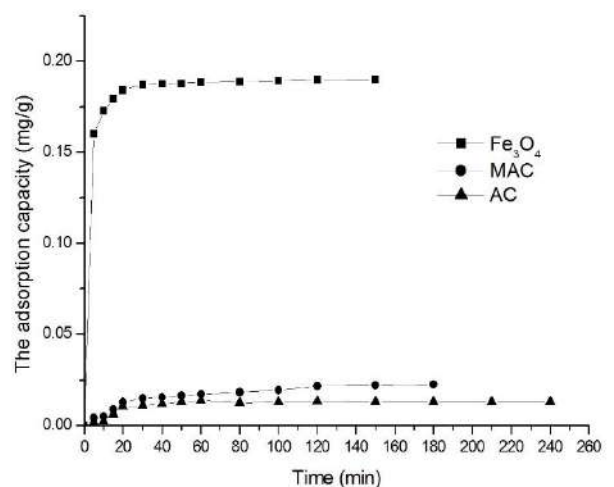


Fig. 4: Adsorption capacity with AC/MAC/NMF.

with AC, MAC, and NMF could be fitted by the pseudo-second-order kinetics model very well (Fig. 5). The rate constant with NMF was all higher than that with AC and MAC.

#### Adsorption isotherms for As with NMF, AC, and MAC:

The adsorption isotherms for As with the three kinds of adsorbents were analyzed in 250mL water with an initial concentration of As of 0.2 mg.L<sup>-1</sup>, 0.3 mg.L<sup>-1</sup>, 0.4 mg.L<sup>-1</sup>, 0.5 mg.L<sup>-1</sup>, 0.6 mg.L<sup>-1</sup>, 1.0 mg.L<sup>-1</sup>, 1.2 mg.L<sup>-1</sup>, 1.5 mg.L<sup>-1</sup>, 2.0 mg.L<sup>-1</sup>, 3.0 mg.L<sup>-1</sup> and 5.0 mg.L<sup>-1</sup>. The dosage of NMF, AC, and MAC was 0.1 g, 5.0 g, and 5.0 g respectively, and the adsorption time was 120 min. The equilibrium adsorption

capacity was calculated according to equation (1) and the results were shown in Fig. 6.

As a whole, the adsorption equilibrium capacity of As increased with the increase of the initial concentration of As. The NMF exhibited high adsorption capacity for As. The adsorption efficiency of NMF is significantly higher than that of MAC, and the efficiency of MAC is a little higher than that of AC. When the concentration of As is low, the equilibrium adsorption capacity increased rapidly with the increase of As concentration. With the increase of As concentration, more and more adsorption sites on the adsorbents' surface

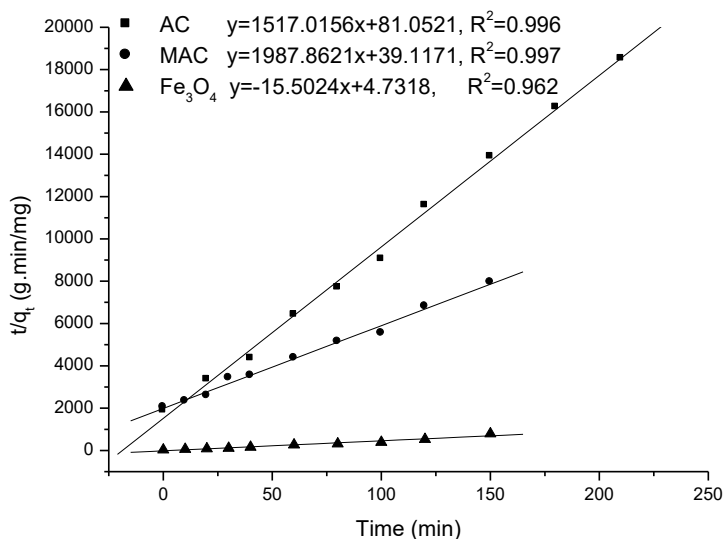


Fig. 5: The simulation results of the pseudo-second-order model.

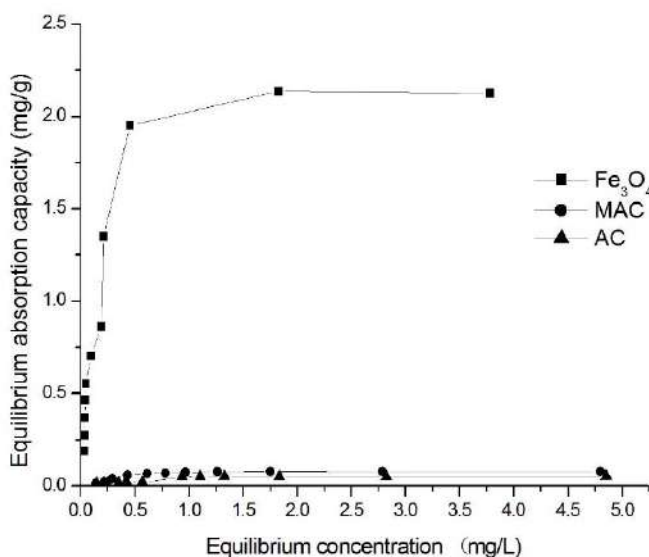


Fig. 6: Adsorption equilibrium for As with NMF, AC and MAC.



were occupied and thus reduced the adsorption capacity, and finally, the adsorption was saturated.

The adsorption equilibrium results were fitted with Langmuir adsorption isotherm (equation (4)) and Freundlich adsorption isotherm (equation (5)) (Pojananukij et al. 2017), and the results were shown in Table 2.

$$q_c = \frac{aK_L C_e}{1 + K_L C_e} \quad \dots(4)$$

$$q_c = K_F C_e^n \quad \dots(5)$$

In which,  $q_c$  (mg.g<sup>-1</sup>) was the equilibrium adsorption,  $C_e$  (mg.L<sup>-1</sup>) was the equilibrium concentration;  $a$  (mg.g<sup>-1</sup>) represent the maximum adsorption in the Langmuir model,  $K_L$ ,  $K_F$  and  $n$  were adsorption constants respectively,  $R^2$  was the simulated correlation coefficient.

The results in Table 2 showed that the adsorption for As with the three adsorbents expresses the same characteristics, and the adsorption could be better described with the Langmuir equation (Fig.7). The result in Fig. 7 also showed that the adsorption capacity for As by NMF was much higher than that of MAC, and the MAC was higher than that of AC.

### The Analysis of Surface Characteristics of NMF, AC and MAC

The groups on the surface of the adsorbent affect the properties of the adsorbent (Tom & Andreas 2017, Niu et al. 2017, Mines et al. 2017). Fig. 8 showed the FT-IR spectrum results of the three adsorbents of NMF, AC, and MAC. For AC, there was a weak absorption peak at 2,920 cm<sup>-1</sup>, which was the stretching vibration of the -CH<sub>2</sub> or -CH<sub>3</sub> bond on

the surface of alkanes; the strong absorption peak appears at 1,594 cm<sup>-1</sup>, which could be the stretching vibration of -C=O and -C=C bond, or the bending of the -HN group; the bending vibration of -OH contribute the adsorption peak of 1,436 cm<sup>-1</sup>; the peak at 1,170 cm<sup>-1</sup> could be attributed to the stretching vibration of -C-O-C- or the -C-O stretching vibration of the chain acid anhydride. The peak at 1,031 cm<sup>-1</sup> was caused by the stretching vibration of -C-O. At around 749 cm<sup>-1</sup>, it was caused by the outward vibration bending of -NH. The peak near 603 cm<sup>-1</sup> was caused by rocking of -NH (Ribeiro et al. 2015).

For MAC, the absorption peak at 3,526 cm<sup>-1</sup> was the single bridge stretching vibration of the alcohol -OH group, at 3,445 cm<sup>-1</sup> was the stretching vibration of the primary amine -HN group, and at 1,629 cm<sup>-1</sup> was the in-plane bending vibration of the alcohol -OH group. It could be seen that the modification changed the functional groups on the surface of activated carbon greatly, and the hydroxyl groups of alcohols or phenols on the surface of the modified activated carbon increased. The increase of the acidic oxygen-containing groups will adsorb more  $\pi$  electrons existing in a graphite state on the surface of the activated carbon, which makes the surface of the activated carbon carry more positive charges and have a stronger adsorption effect on the electro-negative arsenic ions. Therefore, the removal efficiency for As with modified activated carbon was much better than that of activated carbon.

For NMF, the adsorption peaks appear in 3,122 cm<sup>-1</sup>, 3,031 cm<sup>-1</sup>, 2,003 cm<sup>-1</sup>, 1,761 cm<sup>-1</sup>, 1,398 cm<sup>-1</sup>, 1,074 cm<sup>-1</sup>, 989 cm<sup>-1</sup> and 593 cm<sup>-1</sup>. The absorption peaks were caused by the stretching vibration of -OH, symmetrical stretching vibration of -C≡C, the stretching vibration of aldehyde -C=O or stretching vibration of lipid -C=O, stretching vibration of -C-N or primary inward bending vibration of -OH or stretch-

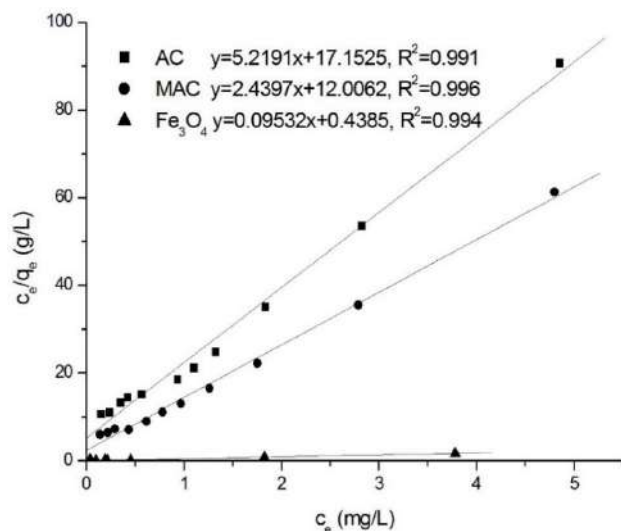


Fig.7: The simulation results of the Langmuir equation.

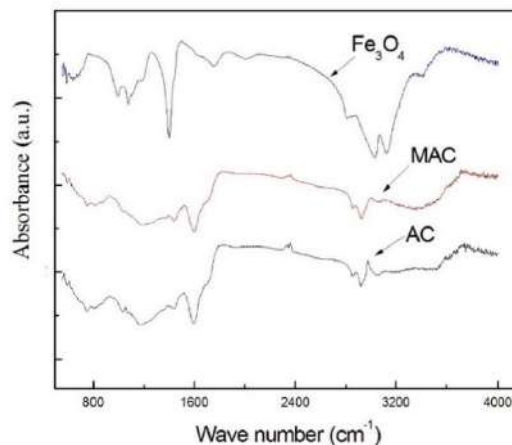


Fig. 8: FT-IR spectra.

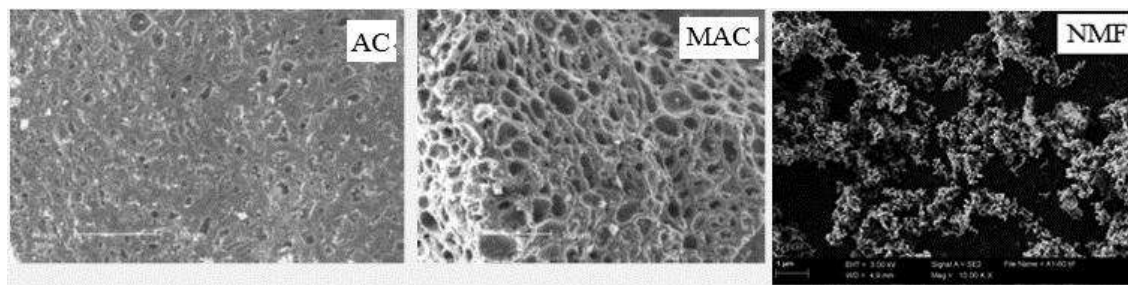


Fig. 9: SEM micrographs of NMF, AC and MAC.

ing vibration of R-NO<sub>2</sub>, the stretching vibration of C-O-C or the stretching vibration of C-O, the outward shaking of -NH<sub>2</sub>. The oxygen-containing functional groups on the surface of NMF enhanced the adsorption capacity. The surface groups impact the adsorption ability, and NMF showed high adsorption ability for As than AC and MAC.

The surface morphology of SEM of the three adsorbents (Fig.9) showed that the surface of AC was much smoother, and there were a few irregular pores with little mesopore and macro-pore on the surface of AC. While the surface of MAC was much rough, more macropore and mesopore could be seen. The modification process improved the surface pore characteristics and increased the adsorption capacity of activated carbon. The NMF was composed of uniform particles with particle sizes less than 50 nm, the particles were connected by a chain. This kind of chain structure of nanoparticles was conducive to the adsorption and aggregation of heavy metal ions to the surface.

## CONCLUSIONS

The adsorption efficiency for arsenic by conventional adsorbent of activated carbon-modified activated carbon and new adsorbent of magnetic nano Fe<sub>3</sub>O<sub>4</sub> was compared in the batch experiment. The results showed that the new nanomagnetic Fe<sub>3</sub>O<sub>4</sub> had excellent adsorption properties for As. Though the modification with potassium permanganate improved the surface pore structure and improved the adsorption ability of activated carbon, the adsorption efficiency for As with MAC was still low. When the As concentration was 2.5 mg.L<sup>-1</sup>, the maximum adsorption capacity for As with NMF could reach 2.262 mg.g<sup>-1</sup> with a dosage of 0.1 g NMF in 250 mL, while for MAC and AC, the maximum adsorption was only 0.0853 mg.g<sup>-1</sup> and 0.0623 mg.g<sup>-1</sup> with a dosage of 5g MAC and AC in 250 mL. The adsorption rate for As with NMF, MAC, and AC were different obviously. For NMF, it needs only 10-20 min to reach adsorption equilibrium, while for MAC and AC, the adsorption needs 100 min to reach equilibrium. The adsorption for As with the three adsorbents of NMF, AC, and

MAC followed the pseudo-second-order kinetics model and Langmuir isotherm model all.

## ACKNOWLEDGEMENT

The authors thank the support of the “science and technology project of Dalian (No.2015E11SF063)”, “the Fundamental research funds for the central universities” (No. 3132016327)”, and “the Sub-project of Central Sharing Funds for using sea area (No.2013-348-7)”.

## REFERENCES

- Alvarez-Torrellas, S., Munoz, M., Zazo, J.A., Casas, J.A. and García, J. 2016. Synthesis of high surface area carbon adsorbents prepared from pine sawdust-Onopordum acanthium L. for nonsteroidal anti-inflammatory drugs adsorption. *J. Environ. Manage.*, 183: 294-305.
- Bao, S., Tang, L., Li, K., Ning, P., Peng, J., Guo, H., Zhu, T. and Liu, Y. 2016. Highly selective removal of Zn(II) ion from hot-dip galvanizing pickling waste with amino-functionalized Fe<sub>3</sub>O<sub>4</sub>@SiO<sub>2</sub>magnetic nano-adsorbent. *J. Coll. Interface Sci.*, 462:235-242.
- Bao, S., Li, K., Ning, P., Peng, J., Jin, X. and Tang, L. 2017. Highly effective removal of mercury and lead ions from wastewater by mercapto amine-functionalized silica-coated magnetic nano-adsorbents: Behaviours and mechanisms. *Appl. Surf. Sci.*, 393:457-466.
- Chiang, Y.C. and Juang, R.S. 2017. Surface modifications of carbonaceous materials for carbon dioxide adsorption: A review. *J. Taiwan Inst. Chem. E*, 71: 214-234.
- Ding, Z., Fu, F., Cheng, Z., Lu, J. and Tang, B. 2017. Novel mesoporous FeAl bimetal oxides for As(III) removal: Performance and mechanism. *Chemosphere*, 169: 297-307.
- El-Moselhy, M.M., Ates, A. and Celebi, A. 2017. Synthesis and characterization of hybrid iron oxide silicates for selective removal of arsenic oxyanions from contaminated water. *J. Colloid Interf. Sci.*, 488: 335-347.
- Egbosubi T.C., Abdulkareem A.S., Kovo A.S., Afolabi E.A. and Tijani J.O. 2020. Enhanced adsorption of As(V) and Mn(VII) from industrial wastewater using multi-walled carbon nanotubes and carboxylated multi-walled carbon nanotubes. *Chemosphere*, 254: 26780.
- García-Mateos, F.J., Ruiz-Rosas, R., Marqués, M.D., Cotoruelo, L.M., Rodríguez-Mirasol, J. and Cordero, T. 2015. Removal of paracetamol on biomass-derived activated carbon: modeling the fixed bed breakthrough curves using batch adsorption experiments. *Chem. Eng. J.*, 279: 18-30.
- Hu, W., Tian, J., Zang, N., Gao, Y. and Chen, L. 2019. Study of the development and performance of centralized wastewater treatment plants in Chinese industrial parks. *J. Clean. Prod.*, 214: 939-951.
- Itziar, A., Javier, H.A. and Carlos, G. 2004. Plants against the global epidemic of arsenic poisoning. *Environ. Int.*, 30: 949-951.

- Jaramillo J., Álvarez P.M. and Gómez-Serrano V. 2010. Preparation and ozone-surface modification of activated carbon. Thermal stability of oxygen surface groups. *Appl. Surf. Sci.*, 256: 5232-5236.
- Jerome, N., Subhamoy, B., Amit, K.K., Jishnu, A., Debankur, C., Monica, I., Debendra, N.M., Basem, S. and Debashis, C. 2015. Assessment of toxic metals in groundwater and saliva in an arsenic affected area of West Bengal, India: A pilot scale study. *Environ. Res.*, 142: 328-336.
- Kukucka, M., Kukucka, N. and Habuda-Stanic M. 2016. Water reclamation during drinking water treatments using polyamide nanofiltration membranes on a pilot scale. *Environ. Sci. Pollut. Res.*, 23(18): 17919-17927.
- Kiran, P.S., Dharmveer, Y., Harshala, P., Sumit, S. and Shobha, S. 2020. Evaluation of techniques for the remediation of antibiotic-contaminated water using activated carbon. *Mol. Syst. Des. Eng.*, 5(4): 743-756.
- Legod M.A. and Waal D. 2007. The preparation of magnetite, goethite, hematite, and maghemite of pigment quality from mill-scale iron waste. *Dyes Pigments*, 74: 161-168.
- Macías-García, A., Corzo, M.G., Domínguez, M.A., Franco, M.A. and Naharro J.M. 2017. Study of the adsorption and electro-adsorption process of Cu (II) ions within thermally and chemically modified activated carbon. *J. Hazard. Mater.*, 328: 46-55.
- Mines, P.D., Thirion, D., Uthuppu, B., Hwang, Y., Jakobsen, M.H., Andersen, H.R. and Yavuz C.T. 2017. Covalent organic polymer functionalization of activated carbon surfaces through acyl chloride for environmental clean-up. *Chem. Eng. J.*, 309: 766-771.
- Molinari, R. and Argurio, P. 2017. Arsenic removal from water by coupling photocatalysis and complexation-ultrafiltration processes: A preliminary study. *Water Res.*, 109: 327-336.
- Mukherjee, A., Kundu, M., Basu, B., Sinha, B., Chatterjee, M., Bairagya, M.D., Singh, U.K. and Sarkar, S. 2017. Arsenic load in rice ecosystem and its mitigation through deficit irrigation. *J. Environ. Manage.*, 197: 89-95.
- Mhamme, A.A. and Samaka I.A.S. 2018. Bentonite coated with magnetite Fe<sub>3</sub>O<sub>4</sub> nanoparticles as a novel adsorbent for copper ( ) ions removal from water/wastewater. *Environ. Technol. Inno.*, 10: 162-174.
- Nandre, V.S., Bachate, S.P., Salunkhe, R.C., Bagade, A.V., Shouche Y.S. and Kodam, K.M. 2017. Enhanced detoxification of arsenic under carbon starvation: new insight into microbial arsenic physiology. *Curr. Microbiol.*, 74(5):614-622.
- Niu, Q., Luo, J., Xia, Y., Sun, S. and Chen, Q. 2017. Surface modification of bio-char by dielectric barrier discharge plasma for Hg<sup>0</sup> removal. *Fuel Process. Technol.*, 156: 310-316.
- Orlando, G.R., Audrey, V., Hugo, O.V., Claire, G., Yves, A. and Olivier, L. 2020. Impact of the saturation level on the electrochemical regeneration of activated carbon in a single sequential reactor. *Carbon*, 163: 265-275.
- Pari, L. and Jalaludeen, M. 2011. Protective role of sinapic acid against arsenic-Induced toxicity in rats. *Chem.-Biol. Interact.*, 194: 40-47.
- Palomo, J., Ternero-Hidalgo, J.J., Rosas, J.M., Rodríguez-Mirasol, J. and Cordero, T. 2017. Selective nitrogen functionalization of phosphorus-containing activated carbons. *Fuel Process. Technol.*, 156: 438-445.
- Pojananukij, N., Wantala, K., Neramittagapong, S., Lin, C., Tanangteerpong, D. and Neramittagapong, A. 2017. Improvement of As(III) removal with diatomite overlay nanoscale zero-valent iron (nZVI-D): Adsorption isotherm and adsorption kinetic studies. *Water Sci. Tech. W. Sup.*, 17 (1): 212-220.
- Ribeiro, R.F.L., Soares, V.C., Costa, L.M. and Nascentes C.C. 2015. Production of activated carbon from biodiesel solid residues: an alternative for hazardous metal sorption from aqueous solution. *J. Environ. Manage.*, 162: 123-131.
- Shafeeyan, M.S., Daud, W.M.A.W., Houshmand, A. and Shamiri, A. 2010. A review on surface modification of activated carbon for carbon dioxide adsorption. *J. Anal. Appl. Pyrol.*, 89: 141-151.
- Song, H.J., You, S., Jia, X.H. and Yang, J. 2015. MoS<sub>2</sub> nanosheets decorated with magnetic Fe<sub>3</sub>O<sub>4</sub> nanoparticles and their ultrafast adsorption for wastewater treatment. *Ceram. Int.*, 41(10): 13896-13902.
- Sun, Y., Chen, Z., Wu, G., Wu, Q., Zhang, F., Niu, Z. and Hu, H.Y. 2016. Characteristics of water quality of municipal wastewater treatment plants in China: implications for resources utilization and management. *J. Clean. Prod.*, 131:1-9.
- Sun, T., Zhao, Z., Liang, Z., Liu, J., Shi, W. and Cui, F. 2017. Efficient As(III) removal by magnetic CuO-Fe<sub>3</sub>O<sub>4</sub> nanoparticles through photo-oxidation and adsorption under light irradiation. *J. Colloid Interf. Sci.*, 495(1): 168-177.
- Shen, L., Jiang, X., Chen, Z., Fu, D., Li, Q., Ouyang, T. and Wang, Y. 2017. Chemical reactive features of novel amino acids intercalated layered double hydroxides in As(III) and As(V) adsorption. *Chemosphere*, 176: 57-66.
- Tom, J. and Andreas, H.A. 2017. The influence of carbon-oxygen surface functional groups of carbon electrodes on the electrochemical reduction of hemoglobin. *Carbon*, 112: 230-237.
- Uheida, A., Salazar-Alvarez, G., Bjorkman, E., Yu, Z. and Muhammed, M. 2006. Fe<sub>3</sub>O<sub>4</sub> and γ-Fe<sub>2</sub>O<sub>3</sub> nanoparticles for the adsorption of Co<sup>2+</sup> from aqueous solution. *J. Coll. Interf. Sci.*, 298: 501-507.
- Varga, A., Raucsik, B. and Szakmany, G. 2017. Origin of natural arsenic and antimony contents in the Permian to lower triassic siliciclastic rocks of the western Mecsek mountains, SW Hungary. *Carpath. J. Earth Env.*, 12(1): 5-12.
- Yang, S., Li, L., Xiao, T., Zheng, D. and Zhang Y. 2016. Role of surface chemistry in modified ACF (activated carbon fiber)-catalyzed peroxy monosulfate oxidation. *Appl. Surf. Sci.*, 383: 142-150.
- Zavareh, S., Behrouzi, Z. and Avanes, A. 2017. Cu( ) bonded chitosan/Fe<sub>3</sub>O<sub>4</sub> nanocomposite as a new biosorbent for efficient and selective removal of phosphate. *Int. J. Biol. Macromol.*, 101: 40-50.
- Zeng, C., Gonzalez-Alvarez A., Orenstein, E., Field, J.A., Shadman, F. and Sierra-Alvarez, R. 2017. Ecotoxicity assessment of ionic As(III), As(V), In(III), and Ga(III) species potentially released from novel III-V semiconductor materials. *Ecotox. Environ. Safe*, 140: 30-36.
- Zhang, L., Liu, Y., Wang, S., Liu, B. and Peng J. 2017. The removal of sodium dodecyl benzene sulfonate by activated carbon modified with quaternary ammonium from aqueous solution. *J. Porous Mater.*, 24: 65-73.
- Zheng, L., Liu, Z., Yan, Z., Yi, X., Zhang, J., Zhang, Y., Zheng X. and Zhu, Y. 2017. Deriving water quality criteria for trivalent and pentavalent arsenic. *Sci. Total Environ.*, 587-588: 68-74.





# An Assessment of Future Predictions of Rainfall Using GCM Projections in the Western Ghats Region of India

Shilpa A. Veerabhadranavar\*†<sup>ORCID</sup> and B. Venkatesh\*\*<sup>ORCID</sup>

National Institute of Hydrology, Hard Rock Regional Centre, Visvesvaraya Nagar, Belagavi, Karnataka 590019, India

†Corresponding author: Shilpa A. Veerabhadranavar; shilpaveer56@gmail.com

Nat. Env. & Poll. Tech.  
Website: [www.neptjournal.com](http://www.neptjournal.com)

Received: 11-02-2022

Revised: 03-04-2022

Accepted: 10-04-2022

## Key Words:

Predictions of rainfall  
GCM projections  
Western Ghats  
Global circulation model

## ABSTRACT

The present study has been taken up to quantify the possible impacts of climate change on the climate variables using the outputs of the global climate model dataset over the Sagar and Kokkarne catchments. The baseline period considered is 30 years (1991-2020), and the daily rainfall dataset is used. The rainfall dataset for the future period is derived from five selected GCMs (Global Circulation Model) datasets under the (Representative Concentration Pathway) RCP 4.5 scenario for the period (2021-2050). The mean, standard deviation, and coefficient of variation of yearly rainfall are determined to check the rainfall variability using statistical analysis. The ensemble rainfall mean values of the five GCMs suggest that the uncertainty in the projected results is reduced by considering the cluster of GCMs. The minimum rainfall for the future period has shown an increasing trend (42.3 % 10.5 %) whereas maximum rainfall has shown decreasing trend (52.44 %, 15.28 %) for Sagar and Kokkarne catchments respectively. The future predicted results show that the percentage change in Ensemble mean annual rainfall for the period 2021-2050 with reference to rainfall data of the baseline period (1991-2020) is depicting an increasing trend of 2.52 % and 4.12 % for Sagar and Kokkarne catchments respectively. Monsoon arrival is earlier in the Kokkarne catchment as compared to the Sagar catchment. The highest positive percentage change in mean annual rainfall of 24.89 %, 10.25 % is projected by MPI-ESM-LR GCM, and the Highest negative percentage change in mean annual rainfall of -28.49 %, -9.19 % is projected by ACCESS1.0 GCM for Sagar and Kokkarne catchments respectively. This analysis will provide useful information for water resources planning engineers, research scientists, and farmers to assess the water availability in the region and create storage if essential.

## INTRODUCTION

Climate change has posed threat to development all over the world. Climate change is projected to induce a reduction in the availability of surface water in the future (Pachauri et al. 2014). Climate change caused by humans is believed to be the greatest threat to the earth and the environmental system. According to the IPCC, humans are responsible for more than half of the average temperature increase between 1951 and 2010 (Pachauri et al. 2014). The temperature rises, although not as noticeable as changes found in the hydrological process but will result in global warming. The water cycle and land ecosystem processes are changing as a result of global warming.

The temperature rises and rainfall variation, which are considered to be the main component of the climate system, can have a negative impact on agriculture, forestry, economy, human health, and well-being (Kotir 2011, Mahato 2014, Thornton et al. 2014). According to future climate estimates, moist and mid-latitude regions will be going to witness an increase in rainfall frequency, whilst the sub-tropical, dry zone would be facing the opposite climatic situation. Rainfall variability is directly linked to the occurrence of events of floods and droughts. Floods will cause the overflow of water over the land surface, on the other hand, droughts can reduce the amount of water available, in the sources such as lakes and dams. Due to human overpopulation and their activities, the demand for water usage is increasing (Cassils 2004, Wang et al. 2018). Rainfall pattern trends have a significant impact on smallholder farmers, due to their reliance on water resources from natural sources for agricultural production and community sustenance, Particularly the farmers who are relying on rain-fed agriculture will be the hardest hit.

## <sup>ORCID</sup> OCID details of the authors:

S. A. Veerabhadranavar:

<https://orcid.org/0000-0002-1566-1640>

B. Venkatesh: <https://orcid.org/0000-0002-9352-5230>

With its complicated geographical characteristics, Various parts of India suffer from natural disasters, such as floods and long dry seasons (Pareek & Trivedi 2011, Rasul 2015), and climate variations are becoming more common as a result of climate change (Jolly et al. 2015), putting Indian geographical region at risk. High rainfall magnitude can be assessed in terms of water availability, agricultural development, food security, and the economics of the country. The amount of water available is determined by rainfall rates (García-Ruiz et al. 2011, Sharma 2000) and the land-use changes in the region. Historical climate fluctuation should be evaluated to anticipate future climate variations and manage the available water resources for agriculture and other purposes in the best possible way and be ready with contingency plans as there is always uncertainty associated with the rainfall received in the catchment. Hence the primary goal of this research is to identify rainfall changes during the future period of (2021-2050) with reference to the baseline period of (1991-2020). This will encourage the development of ecologically friendly, long-term technologies and innovation for self-sufficiency in agriculture and food security.

## STUDY AREA

The study area under consideration is composed of two river catchments, Sagar catchment, and Kokkarne catchments, belonging to Varada river and Seetha river respectively. Both the Varada river and Seetha river originate in the Western ghats of India in Karnataka (Fig. 1).

## MATERIALS AND METHODS

The various steps followed in the present study are as follows:

1. IMD gridded rainfall data for the baseline period (1991-2020) of Sagar catchment and Kokkarne catchment is used in the present study.
2. The rainfall dataset is obtained from the following five selected global climate models (GCMs) (Table 1) under the RCP 4.5 scenario for the future period of (2021-2050) which is downscaled for the South Asia region.
3. The downscaled rainfall dataset is further bias-corrected, and then statistical factors are used to investigate the variation in distribution across the study area. The rainfall dataset acquired for the catchments is statistically analyzed to see whether there are any significant

differences in the rainfall dataset. Also included are the graphs demonstrating the percentage change in rainfall statistical parameters for the study period of 2021-2050, as well as graphs depicting the effect of bias correction in the raw GCM dataset. The mean, median, standard deviation, kurtosis, skewness, minimum, maximum, and range are all used in this study to calculate the metric.

4. The standard deviation is a measure of dispersion. A low number implies that the data is clustered closely around the mean. A large number implies that the dataset is widely distributed on both sides of the mean. A high standard deviation denotes large year-to-year fluctuations, whereas a low standard deviation denotes smaller fluctuations. In other words, high-standard-deviation rainfall is deemed to be more volatile than low-standard-deviation rainfall.
5. The skewness and kurtosis are calculated to see if the annual rainfall dataset followed a normal distribution. Skewness is a metric for symmetry, or more specifically, the lack of it. If the dataset appears the same to the left and right of the center point, it is considered to be symmetric. A normal distribution has zero skewness, and any symmetric dataset should have skewness close to zero. Negative skewness values indicate that the dataset is skewed to the left, whereas positive skewness values show that the dataset is biased to the right. Kurtosis is a metric for how peaked or flat a dataset is in comparison to a normal distribution. To put it another way, a dataset with a high kurtosis has a noticeable peak near the mean, a rapid drop, and heavy tails. The low kurtosis dataset features a flat top near the mean instead of a high peak. The kurtosis of the standard normal distribution is zero. A peaked distribution has positive kurtosis, while a flat distribution has negative kurtosis.

## RESULTS AND DISCUSSION

### Statistical Analysis of Climate Projections for the Near Future (2021-2050)

The GCM model projecting the lowest mean annual rainfall for the Sagar catchment is the ACCESS1.0 GCM model, with a corresponding lowest mean value of 1271.29 mm, according to Table 2. The corresponding dataset is skewed right, with the standard deviation correlating the lowest annual rainfall

Table 1: List of CMIP5 GCMs used in the present study. (Source: <http://cccr.tropmet.res.in>)

GCM code	1	2	3	4	5
GCMs	ACCESS1.0	CNRM-CM5	GFDL-CM3	MPI-ESM-LR	NorESM1-M
Horizontal grid spacing (lon x lat)	1.875 x 1.25	1.4 x 1.4	2.5 x 2.0	1.9 x 1.9	x 1.9

being 414.83 mm. However, the maximum annual rainfall projected by the MPI-ESM-LR GCM model has a standard deviation of 472.05 mm, indicating that the maximum rainfall is greatly distributed or that the maximum rainfall pattern in the MPI-ESM-LR GCM model is inconsistent, as indicated by the highest range value. This conclusion is supported once more by the coefficient of variation statistics. The larger CV value signifies larger dispersion (Thangjai et al. 2020, Yosboonruang et al. 2019). The variation in CV values implies that the rainfall in the study area is highly variable.

For the period under consideration, the ACCESS1.0 GCM model projects the lowest and highest mean annual rainfall of 3555.61 mm, and 6197.29 mm respectively, and the corresponding standard deviation of 1244.91 mm for the Kokkarne catchment, as shown in Table 3. The ACCESS1.0 GCM model rainfall dataset is skewed to the right side. The high standard deviation figure is directly linked to the wide range of rainfall. The difference between the maximum and minimum annual rainfall is represented by the rainfall range. The standard deviation and range represent the unpredictability of annual rainfall and thus how dependable the rainfall is in terms of persistence.

Table 2 and Table 3 show that, except for the ACCESS1.0 GCM model, the coefficient of variation for all global

circulation models is lower for both catchments, indicating smaller variability from the mean, and comparable observations are made for the rainfall data projected by this GCM. The low coefficient of variability reported for the aforementioned global circulation models indicates that they are more reliable than the ACCESS1.0 GCM model in terms of rainfall. The CV indicates the degree of precision with which the treatments are compared and is a good indicator of the reliability of the experiment. It is also stated that the larger the CV value, the poorer the reliability of the experiment.

The mean annual rainfall of 1822.47 mm and the associated standard deviation of 200.67 mm is expected for the Sagar catchment, whereas the mean annual rainfall of 4076.94 mm and the related standard deviation of 447.96 mm is projected for the Kokkarne catchment. The highest median rainfall values are projected for the Sagar and Kokkarne catchments, with 2277.05 and 4463.12 mm (as projected by the MPI-ESM-LR GCM model) respectively. Tables 2 and 3 show that rainfall datasets for both catchments are positively skewed as projected by the ACCESS1.0 GCM model, CNRM-CM5 GCM model, GFDL-CM3 GCM model, and negatively skewed as projected by the MPI-ESM-LR GCM model, NORESM1-M GCM model.

Table 2: Statistical summary of annual rainfall over Sagar catchment.

GCM	ACCESS1.0	CNRM-CM5	GFDL-CM3	MPI-ESM-LR	NorESM1-M	Ensemble
Mean [mm]	1271.29	1541.47	2106.05	2220.15	1973.36	1822.47
Min [mm]	480.51	965.93	1200.46	1372.94	832.98	1442.61
Max [mm]	2238.05	2302.34	2982.49	3008.17	2942.97	2153.71
Median [mm]	1218.49	1492.66	2011.40	2277.05	1961.86	1831.21
Std Dev [mm]	414.83	342.75	420.86	472.05	413.02	200.67
CV [%]	32.63	22.24	19.98	21.26	20.93	11.01
Kurtosis [mm]	-0.42	-0.29	-0.07	-0.90	1.20	-0.62
Skewness [mm]	0.17	0.47	0.32	-0.20	-0.12	-0.12

Table 3: Statistical summary of annual rainfall over Kokkarne catchment.

GCM	ACCESS1.0	CNRM-CM5	GFDL-CM3	MPI-ESM-LR	NorESM1-M	Ensemble
Mean [mm]	3555.61	4202.54	4285.76	4317.04	4023.73	4076.94
Min [mm]	1483.08	2580.02	2547.21	2568.25	1588.61	3161.08
Max [mm]	6197.29	5813.67	5912.52	5843.10	5778.03	5191.50
Median [mm]	3366.61	4008.59	4127.59	4463.12	4169.99	4076.55
Std Dev [mm]	1244.91	839.03	826.27	927.43	856.34	447.96
CV (%)	35.01	19.96	19.28	21.48	21.28	10.99
Kurtosis [mm]	-0.59	-0.69	-0.70	-0.96	1.03	0.40
Skewness [mm]	0.29	0.23	0.14	-0.18	-0.42	-0.07

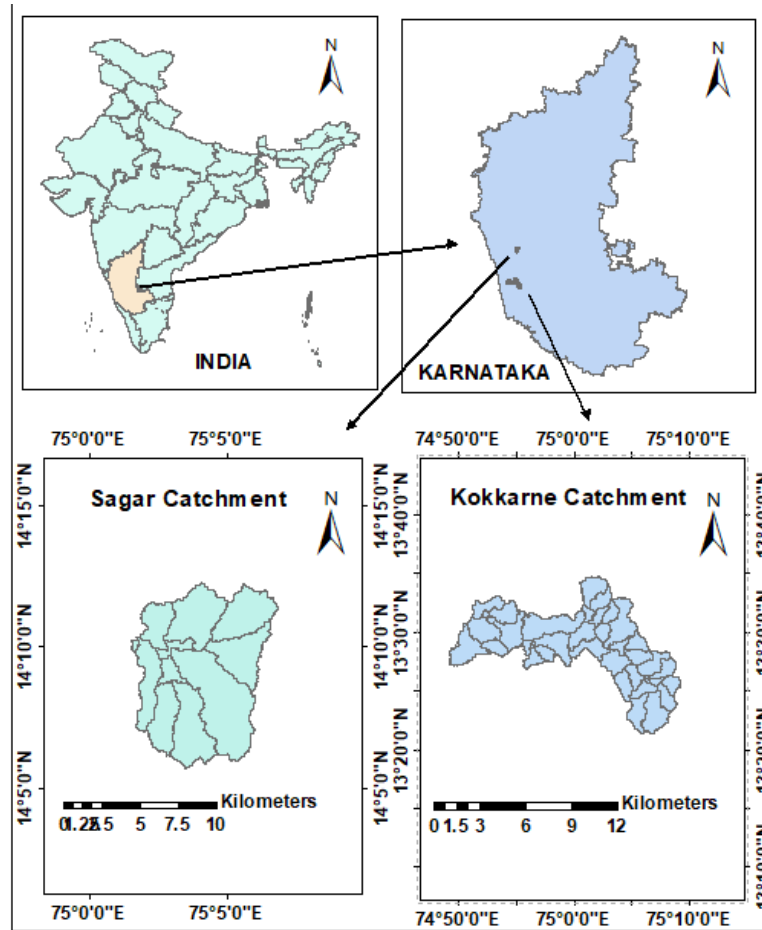


Fig. 1: Study areas (Sagar and Kokkarne catchments).

The standard deviation is one way of summarizing the spread of a probability distribution. It has to do with the level of uncertainty involved in projecting the value of a random variable. High levels indicate a greater degree of uncertainty than low values. Tables 2 and 3 clearly showed that the standard deviation values of the Kokkarne catchment are higher than the standard deviation values of the Sagar catchment. Because of the relationship between the standard deviation and the mean values, the deviation from the normal distribution cannot be ignored. This is backed up by the coefficients of variation of rainfall dataset projected by GCM models under consideration, which range from 19-33 and 19-36 for the Sagar and Kokkarne catchments, respectively. This demonstrates that rainfall values in the Kokkarne catchment are significantly different from the rainfall of the Sagar catchment. The fact that the CV values are so high indicates that the rainfall is highly unpredictable and unreliable, which can be ascribed to the length of the dataset set used or the quality of the dataset.

The smaller the coefficient of variation of rainfall dataset projected in a GCM, the lower the variability and the more reliable the projected rainfall of that particular GCM model. Tables 2 and 3 show that the rainfall variability projected by the GFDL-CM3 GCM model for both the catchments is the lowest of all the GCMs and so can be considered reliable.

According to the findings of statistical analysis tests, there are substantial discrepancies in the statistical characteristics of the rainfall dataset for the Sagar and Kokkarne catchments over the research period.

#### Evaluation of Climate Projections for the Near Future (2021–2050)

Fig. 3 also shows that rainfall in both the catchments is underestimated throughout the monsoon season. It can be seen that rainfall in the monsoon season is indicating delayed commencement of the monsoon season for Sagar catchment and a slightly early start of monsoon season in Kokkarne catchment.



The bias correction method is unable to rectify the beginning of monsoon as projected by many GCMs, and this may be the case for subsequent seasons when analyzing future estimates. The so-called climate change may be to blame for the change in rainfall season. This kind of natural variability in the precipitation trends being underestimated by the GCMs is also

reported by (Mahmood et al. 2018, Pervez & Henebry 2014, Singh et al. 2019, Tolika et al. 2006, Van Haren et al. 2013) During the winter season, underestimation of rainfall datasets may be seen in both catchments as a modest corrective shift in the quantity of rainfall received compared to the rainfall dataset of the baseline period (1991-2020).

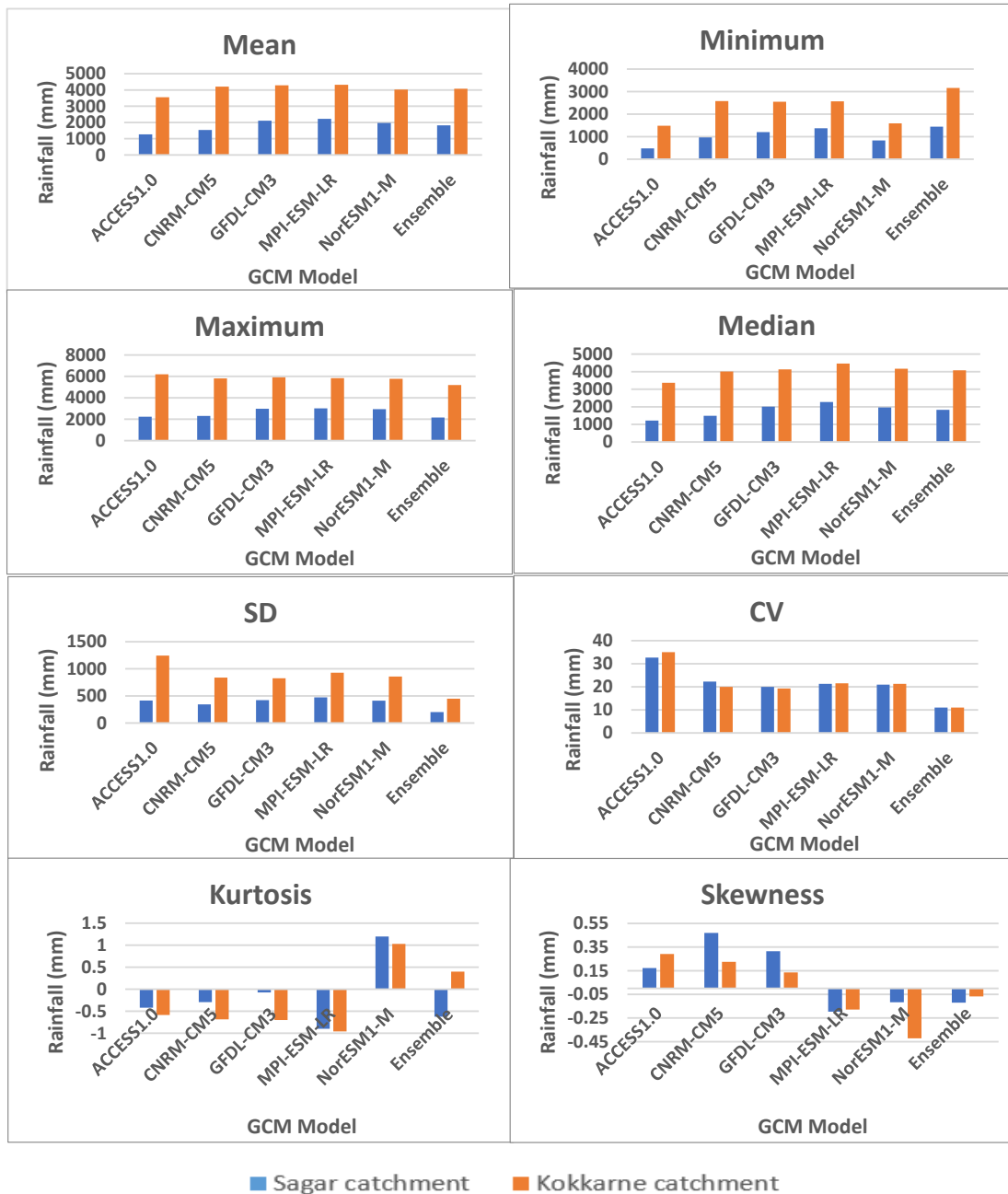


Fig. 2: Parameters of statistical analysis of rainfall dataset  
 Note: Std. Dev= standard deviation, CV=Coefficient of variation

Nevertheless, there are considerable sources of uncertainties in the results, related mainly to the climate model projections' ability to describe the probability of occurrence of extreme events. Further, due to the nature of extreme events, there is only a limited dataset available and the inherent natural or internal variability adds uncertainty to the analysis of the results. GCM bias might also be blamed for the uncertainties (Fig. 3). For locations with the GCM dataset, bias correction approaches can be employed in climate change studies. Using an ensemble of climate projections, as in this work, can provide an estimate of the internal variability uncertainty of the GCM model. The choice of the bias-correction method, on the other hand, influences the total uncertainty in the outcome, and the method should only be adopted after a thorough examination of other options. To deal with significant biases, such as those due to erroneous timing and location of stationary synoptic scale rainfall fields like the monsoon, improvements in climate model post-processing approaches are still needed. There have been advancements in analyzing the influence of climate change at the regional scale, but further methods for reducing the uncertainties associated with GCM datasets and scaling procedures need to be investigated.

### Seasonal Uncertainty

Table 4 shows the absolute difference in mean monthly rainfall between the GCM projections and the mean monthly rainfall in the baseline scenario for the Sagar catchment. The Ensemble mean of all the projections show an increase in rainfall contribution during monsoon (+4.59%), Post monsoon (+17.91%) winter (+1.52%) whereas a decrease in rainfall contribution during summer (-47.41%) is projected. The rainfall data values for the baseline period (1991-2020), as shown in Fig. 4 and Table 4, are significantly low in the monsoon, post-monsoon, and winter seasons, and high in the summer season which can be attributed to the effect produced by climate change. When compared to the reference dataset,

all GCMs are unanimously depicting decreasing trend in the percentage contribution during the summer season for the future period (2021-2020).

The Ensemble mean of all the projections shows an increase in rainfall contribution during monsoon (+4.69 %) and summer (+16 %), and a decrease in rainfall contribution during Post monsoon (-6.39 %), winter (-50.76 %) for the Kokkarne catchment. As shown in Fig. 4 and Table 5, the observed rainfall data values are comparatively low in monsoon and summer seasons, and substantially high in post-monsoon and winter seasons, which can be attributed to the effect of climate change. In comparison to the reference rainfall dataset for the baseline period, the overall percentage contribution to the winter season for the future period (2021-2020) is decreasing as projected by all the GCMs under consideration.

This kind of seasonal variation in precipitation in different regions has also been reported by (Cheung et al. 2008, Gedefaw et al. 2018, Hussain & Lee 2013) The weather system being different in a different season of a year is the prime factor leading to seasonal variation in precipitation as reported by (Arora et al. 2006).

### GCM Uncertainty

Uncertainties are inherent in any modeling system, and proper assessment of uncertainties is a major research task. Although uncertainties cannot be eliminated, evaluating and comprehending their impact on model prediction is critical (Rupa & Mujumdar 2019). Though the climate models for the research region are carefully chosen, the measurement of uncertainty in climate change impacts on climatic variables such as rainfall and temperature is required because GCM simulations are mostly based on initial boundary conditions. Rainfall and temperature are the most important input variables in hydrological modeling, hence uncertainty in these variables is important in climate change effect studies on streamflow.

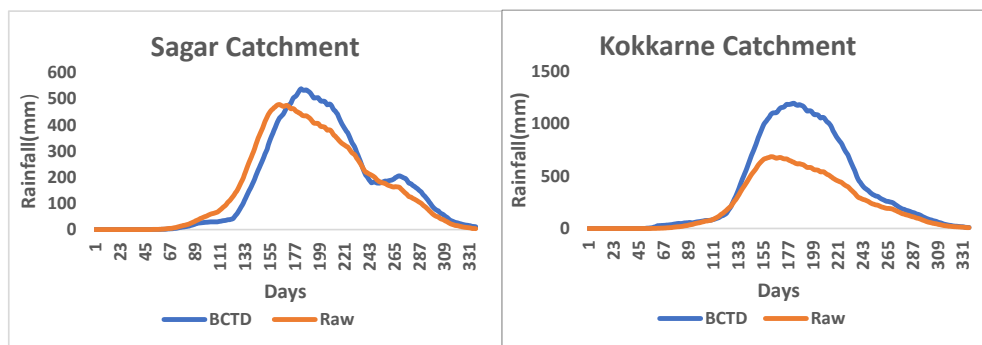


Fig. 3: Mean annual rainfall cycle over the future period (2021-2050) using a 30-day moving average of the Sagar and Kokkarne catchments.

The model uncertainty in climate change impact on the mean percentage change of mean, minimum and maximum annual rainfall in the Sagar catchment (Table 6) for RCP 4.5 indicate an increasing trend (+2.52%), an increasing trend (+42.30 %), and a decreasing trend (-52.44%) with respect to the corresponding mean, minimum and maximum annual rainfall of baseline period (1991-2020) respectively. reduction in maximum rainfall falls in line with a research report by (Al-Ansari et al. 2014, Modarres et al. 2018, Rana et al. 2014).

In the case of the Kokkarne catchment, the model uncertainty in climate change impact on the mean percentage change of mean, minimum and maximum annual rainfall (Table 7) for RCP 4.5 shows an increasing trend (+4.12 %), an increasing trend (10.50 %) and a decreasing trend (-15.28 %) with respect to the mean, minimum and maximum annual rainfall of baseline period (1991-2020) respectively. It is worth noting that most of the estimates show a decrease in mean annual rainfall when compared to the rainfall data of the baseline period of 1777.69 mm for the Sagar catchment. However, most predictions show

a rise in mean annual rainfall for the baseline period of 3915.61 mm for the Kokkarne catchment.

**CONCLUSIONS**

The current study examines the impact of global climate change on rainfall datasets from the Sagar and Kokkarne catchments from 2021 to 2050 (a 30-year period). The present statistical analysis of the rainfall dataset provides a clear picture of variations in the rainfall dataset with respect to various statistical parameters. The mean, standard deviation, and coefficient of variation of the annual rainfall dataset are calculated to check the rainfall variability. The rainfall pattern is observed to be slightly scattered based on the computed results. The purpose of this research is to determine the rainfall variability and GCM uncertainty in the projected rainfall data of the present studied areas.

Following conclusions can be made from the present study.

Table 4: Percentage changes of rainfall in near future bias corrected dataset (2021–2050) over the monsoon months as compared to baseline dataset (1991–2020) for Sagar catchment.

Season	Monsoon	Post-monsoon	Winter	Summer
Ensemble	16.64(4.59)	17.29(17.91)	0.07(1.52)	-18.86(-47.41)
ACCESS1.0	-105.73(-29.14)	-15.39(-15.94)	2.4(51.95)	-19.97(-50.2)
CNRM-CM5	-53.77(-14.82)	23.42(24.25)	-2.13(-46.1)	-20.52(-51.58)
GFDL-CM3	83.01(22.88)	20.32(21.04)	-1.63(-35.28)	-13.14(-33.03)
MPI-ESM-LR	110.75(30.52)	39.35(40.75)	0.33(7.14)	-26.74(-67.22)
NorESM1-M	48.94(13.49)	18.74(19.41)	1.4(30.3)	-13.92(-34.99)

Note: Values in the parentheses represent the relative change from IMD data for the baseline period (1991-2020).

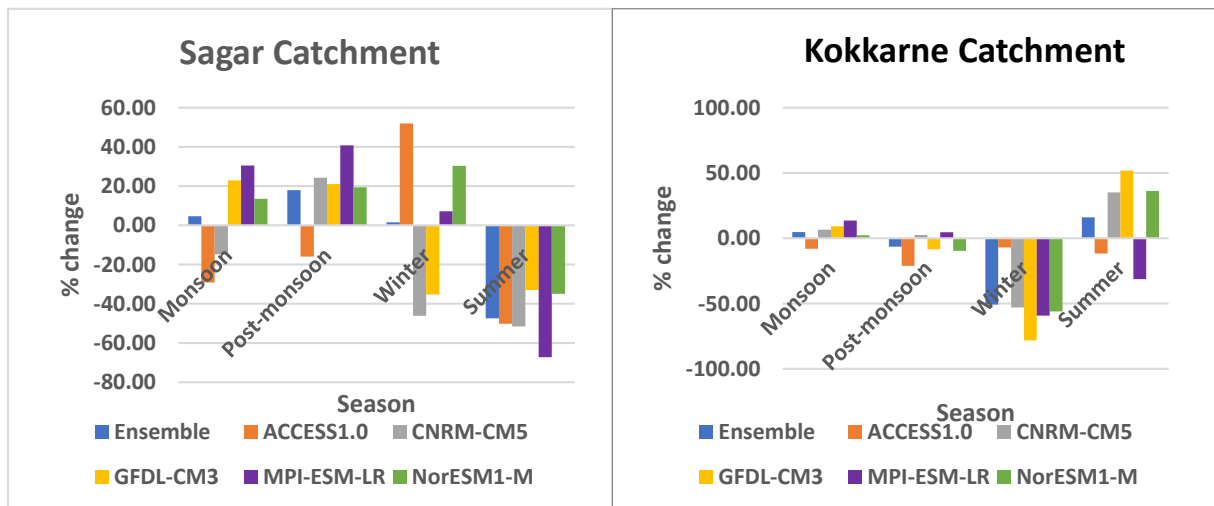


Fig. 4: Percentage changes of rainfall in near future bias corrected dataset (2021–2050) over the monsoon months as compared to the baseline dataset (1991–2020).

1. The mean annual rainfall in the Kokkarne catchment is more than Sagar catchment by 123.70 %.
2. Although the standard deviation values of ensemble rainfall data of Kokkarne catchment are higher than that of Sagar catchment, the coefficient of variation value of Kokkarne catchment is lower than that of Sagar catchment. This essentially means that the ensemble rainfall dataset of the Kokkarne catchment has lesser variability.
3. According to the RCP 4.5 scenario, by 2050, mean annual rainfall is expected to be highly variable, with an increasing trend in rainfall for the Sagar catchment (+2.52 %) and Kokkarne catchment (+4.12%).
4. The mean annual rainfall data of the Sagar catchment is slightly more negatively skewed than the rainfall data of the Kokkarne catchment.
5. It is preferable to use the ensemble mean for subsequent analysis since it reduces the standard deviation and coefficient of variation, making the rainfall data more dependable.
6. The raw rainfall data from both the catchments are underestimated. The underestimation of the case of the Kokkarne catchment is more than that of the Sagar catchment.
7. Ensemble means rainfall data of GCMs used in this analysis predict that monsoon rainfall from 2021 to 2050 in both

Table 5: Percentage changes of rainfall in the near future bias corrected dataset (2021–2050) over the monsoon months as compared to baseline dataset (1991–2020) for Kokkarne catchment.

Season	Monsoon	Post-monsoon	Winter	Summer
Ensemble	39.87(4.69)	-9.64(-6.39)	-3.34(-50.76)	10.38(16)
ACCESS1.0	-68.01(-8)	-31.97(-21.18)	-0.46(-6.99)	-7.55(-11.64)
CNRM-CM5	55.38(6.52)	3.83(2.54)	-3.49(-53.04)	22.74(35.06)
GFDL-CM3	77.53(9.12)	-12.61(-8.35)	-5.15(-78.27)	33.55(51.73)
MPI-ESM-LR	115.02(13.53)	6.97(4.62)	-3.9(-59.27)	-20.3(-31.3)
NorESM1-M	19.41(2.28)	-14.43(-9.56)	-3.69(-56.08)	23.47(36.19)

Note: Values in the parentheses represent the relative change from IMD data for the baseline period (1991–2020).

Table 6: Percentage changes in the mean, minimum and maximum annual rainfall (mm) over the study area for Sagar catchment during 2021–2050 with reference to the baseline period of 1991–2020.

GCM	Mean	Minimum	Maximum
ACCESS1.0	-506.41 (-28.49)	-533.26 (-52.6)	-2290.62 (-50.58)
CNRM-CM5	-236.22 (-13.29)	328.36 (18.47)	442.46 (24.89)
GFDL-CM3	328.36 (18.47)	186.69 (18.42)	-1546.17 (-34.14)
MPI-ESM-LR	442.46 (24.89)	359.17 (35.43)	-1520.5 (-33.58)
NorESM1-M	195.66 (11.01)	-180.78 (-17.83)	-1585.69 (-35.01)
Ensemble	44.78 (2.52)	428.84 (42.3)	-2374.96 (-52.44)

Note: Values in the parentheses represent the relative change from IMD data for the baseline period (1991–2020).

Table 7: Percentage changes in the mean, minimum and maximum annual rainfall (mm) over the study area for Kokkarne catchment during 2021–2050 with reference to the baseline period of 1991–2020.

GCM model	Mean	Minimum	Maximum
ACCESS1.0	-360 (-9.19)	-1377.55 (-48.16)	69.56 (1.14)
CNRM-CM5	286.93 (7.33)	-280.61 (-9.81)	-314.06 (-5.13)
GFDL-CM3	370.15 (9.45)	-313.42 (-10.96)	-215.21 (-3.51)
MPI-ESM-LR	401.43 (10.25)	-292.38 (-10.22)	-284.63 (-4.65)
NorESM1-M	108.12 (2.76)	-1272.02 (-44.47)	-349.7 (-5.71)
Ensemble	161.33 (4.12)	300.46 (10.5)	-936.23 (-15.28)

Note: Values in the parentheses represent the relative change from IMD data for the baseline period (1991–2020).

the catchments will be higher than monsoon rainfall data of the baseline period (1991-2020).

8. For Sagar and Kokkarne catchments, GFDL-CM3 GCM with the lowest CV of 19.98, 19.28 is projecting 2106.05 mm, 4285.76 mm of mean annual rainfall which is more than the ensemble mean annual rainfall by 15.56 %, 5.12 % respectively.
9. For Sagar and Kokkarne catchments, ACCESS1.0 GCM with the highest CV of 32.63, 35.01 is projecting 1271.29 mm, 3555.61 mm of mean annual rainfall which is less than the ensemble mean annual rainfall by 30.24 %, 12.78 % respectively.

To prove the conjecture of the scientists, more than one statistical procedure is required to measure changes in hydrological datasets such as rainfall. This endeavor is a little step in that direction.

## ACKNOWLEDGMENTS

The authors thank the Indian Institute of Tropical Meteorology (IITM), Pune for making CORDEX-SA data available. The authors also gratefully acknowledge the climate data provided by the India Meteorological Department, New Delhi. The authors acknowledge gratefully the National Institute of Hydrology, Belagavi, Karnataka, India for helping to acquire all the data used in this study.

## REFERENCES

- Al-Ansari, N., Abdellatif, M., Ezeelden, M., Ali, S.S. and Knutsson, S. 2014. Climate change and future long-term trends of rainfall in the North-Eastern part of Iraq. *J. Civil Eng. Arch.*, 8(6): 790-805.
- Arora, M., Singh, P., Goel, N. and Singh, R. 2006. Spatial distribution and seasonal variability of rainfall in a mountainous basin in the Himalayan region. *Water Resour. Manag.*, 20(4): 489-508.
- Cassils, J.A. 2004. Overpopulation, sustainable development, and security: Developing an integrated strategy. *Popul. Environ.*, 25(3): 171-194.
- Cheung, W.H., Senay, G.B. and Singh, A. 2008. Trends and spatial distribution of annual and seasonal rainfall in Ethiopia. *Int. J. Climatol. J. Royal Meteorol. Soc.*, 28(13): 1723-1734.
- García-Ruiz, J.M., López-Moreno, J.I., Vicente-Serrano, S.M., Lasanta-Martínez, T. and Beguería, S. 2011. Mediterranean water resources in a global change scenario. *Earth Sci. Revi.*, 105(3-4): 121-139.
- Gedefaw, M., Yan, D., Wang, H., Qin, T., Girma, A., Abiyu, A. and Batsuren, D. 2018. Innovative trend analysis of annual and seasonal rainfall variability in Amhara regional state, Ethiopia. *Atmosphere*, 9(9): 326.
- Hussain, M.S. and Lee, S. 2013. The regional and seasonal variability of extreme precipitation trends in Pakistan. *Asia-Pacific J. Atmos. Sci.*, 49(4): 421-441.
- Jolly, W.M., Cochrane, M.A., Freeborn, P.H., Holden, Z.A., Brown, T.J., Williamson, G.J. and Bowman, D.M. 2015. Climate-induced variations in global wildfire danger from 1979 to 2013. *Nat. Comm.*, 6(1): 1-11.
- Kotir, J.H. 2011. Climate change and variability in Sub-Saharan Africa: A review of current and future trends and impacts on agriculture and food security. *Environ. Develop. Sustain.*, 13(3): 587-605.
- Mahato, A. 2014. Climate change and its impact on agriculture. *Int. J. Sci. Res. Publ.*, 4(4): 1-6.
- Mahmood, R., Jia, S., Tripathi, N.K. and Shrestha, S. 2018. Precipitation extended linear scaling method for correcting GCM precipitation and its evaluation and implication in the transboundary Jhelum River basin. *Atmosphere*, 9(5): 160.
- Modarres, R., Ghadami, M., Naderi, S. and Naderi, M. 2018. Future extreme rainfall change projections in the north of Iran. *Meteorol. Appl.*, 25(1): 40-48.
- Pachauri, R.K., Allen, M.R., Barros, V.R., Broome, J., Cramer, W., Christ, R., Church, J.A., Clarke, L., Dahe, Q. and Dasgupta, P. 2014. Climate change 2014: Synthesis report. Contribution of Working Groups I, II, and III to the Fifth Assessment Report of the Intergovernmental Panel on Climate Change. IPCC, Geneva, Switzerland.
- Pareek, A. and Trivedi, P. 2011. Cultural values and indigenous knowledge of climate change and disaster prediction in Rajasthan, India. *Indian J. Trad. Knowledge*, 10(1): 183-189.
- Pervez, M.S. and Henebry, G.M. 2014. Projections of the Ganges-Brahmaputra precipitation: Downscaled from GCM predictors. *J. Hydrol.*, 517: 120-134.
- Rana, A., Foster, K., Bosshard, T., Olsson, J. and Bengtsson, L. 2014. Impact of climate change on rainfall over Mumbai using distribution-based scaling of global climate model projections. *J. Hydrol., Reg. Stud.*, 1: 5. <https://doi.org/10.1016/j.ejrh.2014.06.005>
- Rasul, G. 2015. Water for growth and development in the Ganges, Brahmaputra, and Meghna basins: An economic perspective. *Int. J. River Basin Manag.*, 13(3): 387-400.
- Rupa, R.C. and Mujumdar, P. 2019. Hydrologic impacts of climate change: Quant. Uncertain., 85(1): 77-94.
- Sharma, A. 2000. Seasonal to interannual rainfall probabilistic forecasts for improved water supply management: Part 1 - A strategy for system predictor identification. *J. Hydrol.*, 239(1-4): 232-239.
- Singh, V., Jain, S.K. and Singh, P.K. 2019. Inter-comparisons and applicability of CMIP5 GCMs, RCMs, and statistically downscaled NEX-GDDP based precipitation in India. *Sci. Tot. Environ.*, 697: 134163.
- Thangjai, W., Niwitpong, S.A. and Niwitpong, S. 2020. Confidence intervals for the common coefficient of variation of rainfall in Thailand. *Peer J.*, 8: e10004.
- Thornton, P.K., Ericksen, P.J., Herrero, M. and Challinor, A.J. 2014. Climate variability and vulnerability to climate change: A review. *Glob. Change Biol.*, 20(11): 3313-3328.
- Tolika, K., Maheras, P., Flocas, H.A. and Arseni Papadimitriou, A. 2006. An evaluation of a general circulation model (GCM) and the NCEP-NCAR reanalysis data for winter precipitation in Greece. *Int. J. Climatol. J. Royal Meteorol. Soc.*, 26(7): 935-955.
- Van Haren, R., van Oldenborgh, G.J., Lenderink, G., Collins, M. and Hazeleger, W. 2013. SST and circulation trend biases cause an underestimation of European precipitation trends. *Climate Dyn.*, 40(1): 1-20.
- Wang, Y., Wan, T. and Tortajada, C. 2018. Water demand framework and water development: The case of China. *Water*, 10(12): 1860.
- Yosboonruang, N., Niwitpong, S. and Niwitpong, S. 2019. Measuring the dispersion of rainfall using Bayesian confidence intervals for a coefficient of variation of delta-lognormal distribution: A study from Thailand. *Peer J.*, 7: e7344.





# Recent Advances in Electrocatalytic Nitrogen Reduction to Produce Ammonia Under Ambient Conditions

Feifei Wang\*, Jinlu Guo\*\*, Yufei Quan\*, Sumin Wang\*† and Qiguan Wang\*

\*Shaanxi Key Laboratory of Photoelectric Functional Materials and Devices, School of Materials and Chemical Engineering, Xi'an Technological University, Xi'an 710021, People's Republic of China

\*\*Shaanxi Guobin Health Technology Co. Ltd., Xi'an 710018, People's Republic of China

†Corresponding author: Sumin Wang; [suminwang@163.com](mailto:suminwang@163.com)

Nat. Env. & Poll. Tech.  
Website: [www.neptjournal.com](http://www.neptjournal.com)

Received: 08-03-2022

Revised: 04-04-2022

Accepted: 22-05-2022

## Key Words:

Nitrogen reduction  
Electrocatalysis  
Ammonia synthesis  
Catalytic mechanism  
Metal-based electrocatalysts

## ABSTRACT

Ammonia (NH<sub>3</sub>) is one of the most widely used chemicals in industry and agriculture, which is very important to the global economy. At present, the Haber Bosch process is adopted for ammonia synthesis in industry. The experimental temperature and pressure used in this process are relatively high, the process energy consumption is high, the one-way conversion of the hydrogen is low, and a large amount of carbon dioxide is discharged into the atmosphere, causing pollution to the environment. To solve its shortcomings, researchers began a new exploration. Electrocatalytic nitrogen reduction (NRR), as a clean and sustainable method of ammonia synthesis, has attracted extensive attention. However, the low activity and selectivity of electrocatalysts are one of the important challenges. Therefore, the search for cost-effective electrocatalysts has become one of the research hotspots of electrochemical ammonia synthesis. For enhancing the catalytic performance and selective performance of catalysts, scientists have carried out a lot of research on electrochemical nitrogen fixation catalysts. In this review article, electrolytic experimental devices, common ammonia detection research methods, and the electrocatalytic NRR mechanism are summarized, and then the research progress in electrocatalysts (precious metals, transition metals, and non-precious metals) is summarized. Then, the research progress of metal-based electrocatalysts is introduced, and the relevant theoretical calculations are given. The discussion of different catalytic systems provides ideas for the development and improvement of subsequent NRR electrocatalysts.

## INTRODUCTION

Ammonia (NH<sub>3</sub>) is widely used in several industries, such as chemical fertilizer, fiber, dye, explosive resin, and hydrogen carrier. At present, the output of ammonia is increasing year by year (Chen et al. 2018). 78% of the air is composed of N<sub>2</sub>. Combined with the nitrogen cycle in the environment, there is great interest in the conversion of N<sub>2</sub> to NH<sub>3</sub>. Fig. 1 shows numerous processes of the nitrogen cycle and nitrogen fixation in nature. However, N<sub>2</sub> has stable chemical properties and strong N≡N triple bond energy, so most chemical reactions cannot be carried out directly. Although some prokaryotes can convert atmospheric N<sub>2</sub> into nitrogen by biological nitrogen fixation in nature, the nitrogen fixed by this method is far from meeting the needs of human production and life (Ren et al. 2021, Qi et al. 2021, Ma et al. 2020). In industry, the Haber Bosch process with harsh reaction conditions, high energy consumption, and harm to the environment are still used to obtain ammonia (Hou et al. 2020, Li et al. 2020, Foster et al. 2018, Montoya et al. 2015). The resulting energy consumption is relatively

high (Kibsgaard et al. 2017, Rz et al. 2019). At the same time, the raw materials of the Haber Bosch process need pure hydrogen that does not exist in nature. It is mainly produced by the decomposition of fossil energy (such as natural gas). The natural gas consumed in this process is 3%-5% of the total natural gas consumption in the world. The production of a large number of CO<sub>2</sub> by-products will further aggravate the global greenhouse effect (Dg et al. 2022, Meng et al. 2020). Therefore, to overcome the limitations of harsh conditions and large environmental pollution of Haber Bosch process equipment, it is necessary to develop an environmentally friendly and low energy consumption ammonia production process (Spatzal et al. 2011, Lancaster et al. 2013). Among many ammonia synthesis methods, electrocatalytic nitrogen reduction reaction has the advantages of easy experimental conditions and less environmental pollution (Shipman et al. 2017, Zhu et al. 2020).

In the electrochemical NRR process, catalysts are the key to ammonia synthesis. However, the low reactivity and

selectivity of electrocatalysts are a significant challenge. Therefore, the search for cost-effective electrocatalysts has become one of the research hotspots of electrochemical ammonia synthesis (Zhu et al. 2020). At present, researchers have concluded through theoretical simulations and experimental studies that metal-based catalysts (transition metals, precious metals, and non-precious metals) can achieve the electrochemical NRR (Xu et al. 2020, Chen et al. 2021). Noble metal catalysts have excellent catalytic performance due to their strong binding energy, excellent electrical conductivity, and abundant active polycrystalline surface, and are widely used in electrochemical reactions. In recent years, precious metal catalysts with diverse active sites have been extensively investigated. Meanwhile, non-precious metal catalysts are abundant and inexpensive on earth and have broad application prospects (Yu et al. 2021). In recent years, non-noble metals, especially transient metal compounds were used as electrode materials for electrocatalytic reactions because of their low cost, rich content, and easily regulated catalytic properties (Wang et al. 2018). In this paper, different systems of NRR catalysts (precious metal catalysts and non-precious metal catalysts) are comprehensively reviewed to provide some useful enlightenment for improving the performance of NRR catalysts in the future (Zhao et al. 2019).

In this paper, the catalytic reaction mechanism of NRR, several electrolysis experimental devices for nitrogen reduction synthesis of  $\text{NH}_3$ , and different  $\text{NH}_3$  detection methods are introduced. On this basis, the latest progress of catalysts in electrocatalytic reactors is reviewed. The research progress of precious metal-based catalysts and non-precious metal transient metal-based catalysts is summarized. Then it is hoped that the research results of this paper can provide useful guidance for the rational design of electrocatalysts for ammonia synthesis, stimulate people's interest in the new research field of ammonia synthesis, and accelerate the green industrialization process of ammonia synthesis.

## THE DEVICE OF ELECTROCATALYTIC AMMONIA SYNTHESIS

The electrochemical cell structure is very important for the electrochemical process of  $\text{N}_2$  conversion to  $\text{NH}_3$ . Electrochemical experimental equipment is generally composed of the following parts: electrolytic cell electrolyte working electrode opposite electrode reference electrode gas pipeline and electrochemical workstation. According to the type and distribution of electrodes and electrolytes, electrolytic cells can be divided into back-to-back type, polymer electrolyte

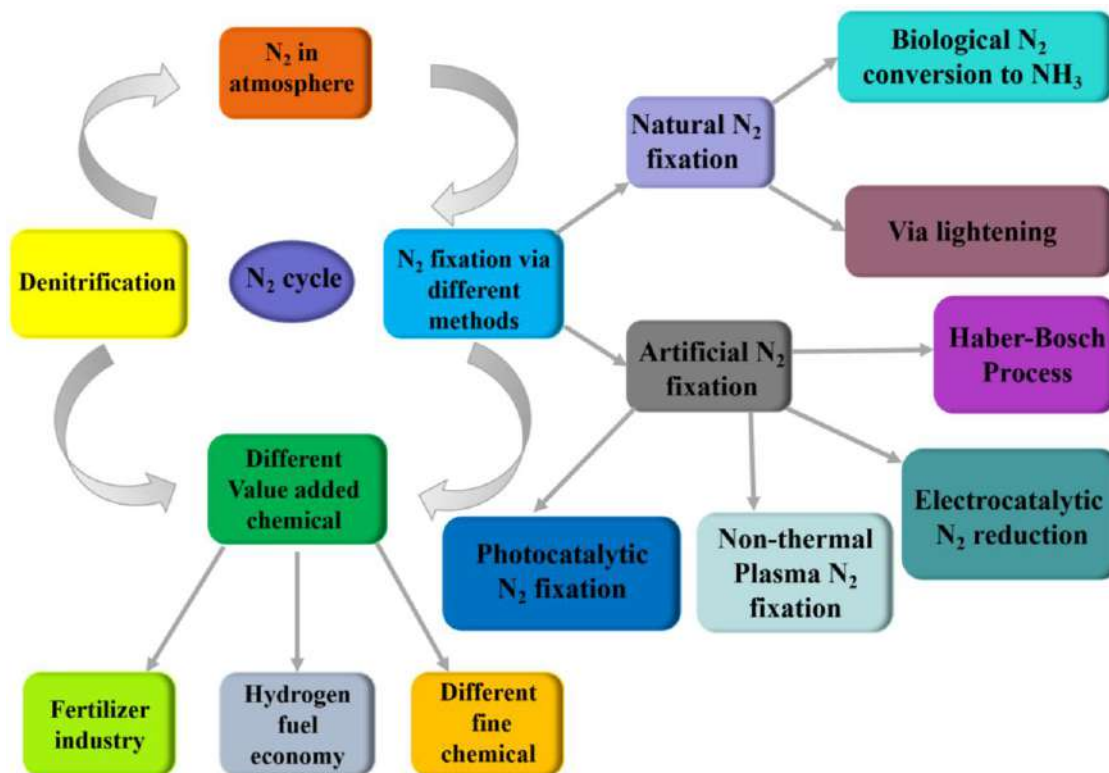


Fig. 1: The numerous processes of the nitrogen cycle and nitrogen fixation in nature.



membrane type, H-type, and single cell type. Among them, single-cell and H-type electrolyzers have been widely used in recent studies (Rostamikia et al. 2019). As shown in Fig. 2a, the cathode and anode of a back-to-back cell are injected with nitrogen and water respectively, the exchange membrane separates the two electrodes. As shown in Fig. 2b, a PEM cell differs from a back-to-back cell in that the electrolyte is injected into the anode, and the protons of the cathode are provided by electrolytic water. In Fig. 2c single-chamber cell, ammonia is oxidized at the anode due to simultaneous cathodic and anodic reactions in the same electrolyte, mak-

ing the determination of ammonia inaccurate. H-type cells (Fig. 2d-f) are widely used in the laboratory under current experimental conditions, where the negative and positive reactions are divided with a Nafion membrane in a separate electrolyte. Therefore, in the testing process of ammonia content, ammonia cross-contamination cannot be ignored.

## NRR PRODUCT DETECTION

The commonly used methods for NRR product detection include colorimetry (including Spectrophotometry with

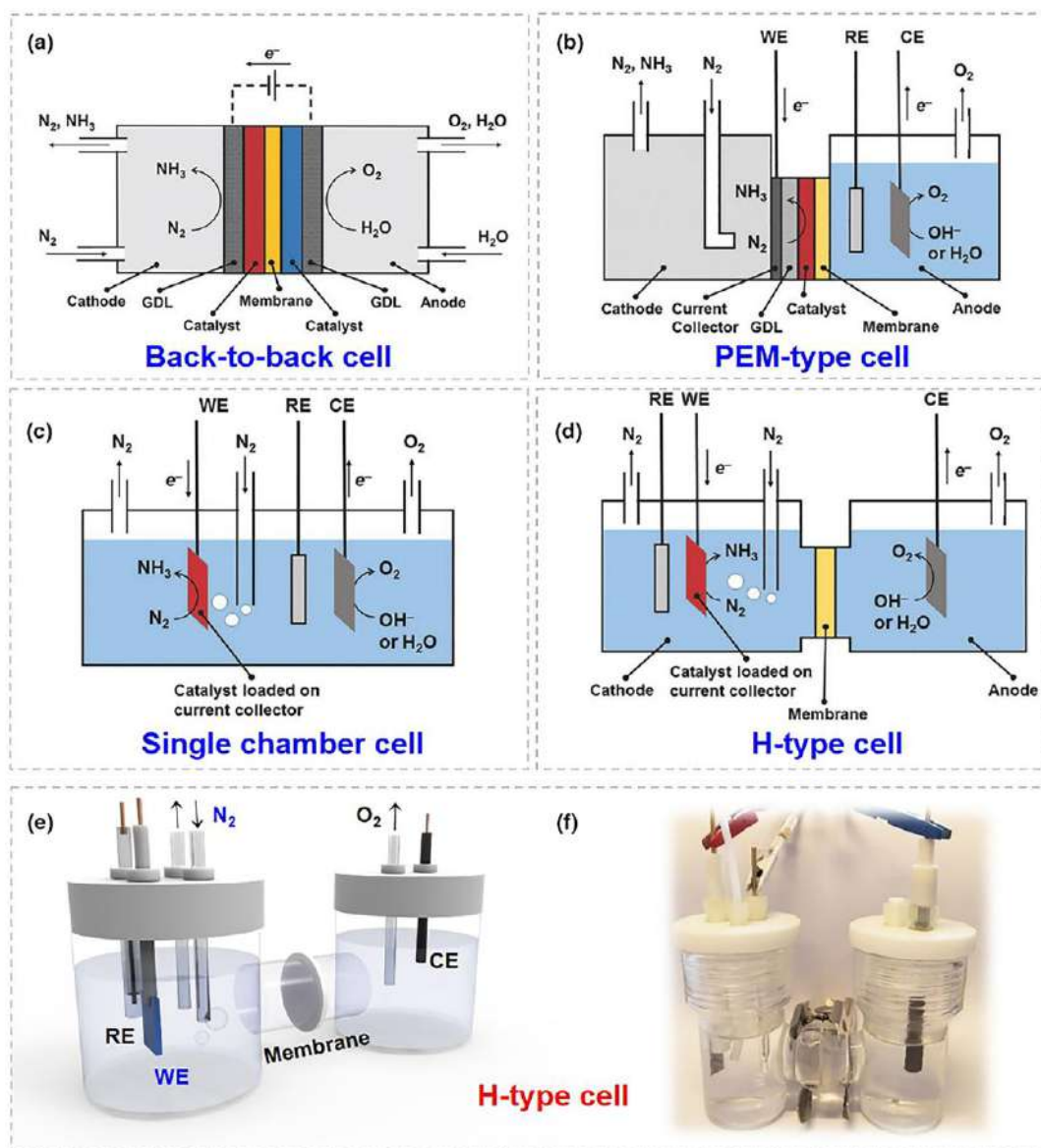


Fig. 2: Diagram of different electrochemical battery devices. Reproduced from Ref. (Rostamikia et al. 2019). (e-f) Installation diagram and photos of H-type electrolytic cell in the experiment (Wan et al. 2019).

Nessler's reagent colorimetric method and salicylic acid-hypochlorite spectrophotometry), ion-chromatography,  $^{15}\text{N}$  isotope labeling-nuclear magnetic resonance NMR method and so on.

The spectrophotometric method uses iodide ions and mercury ions to coordinate with  $\text{NH}_4^+$  under strongly alkaline conditions. The characteristic peaks of the complex can be found at 420 nm, and the concentration of  $\text{NH}_4^+$  can be reflected by the intensity of the absorption peak. The detection range of  $\text{NH}_4^+$  is 0.025-5.0  $\text{mg}\cdot\text{L}^{-1}$ . Salicylic acid-hypochlorite spectrophotometry is in an alkaline medium,  $\text{NH}_4^+$  in turn with the salicylate, hypochlorite ion, and sodium nitroferrocyanide (nitropuna) reaction to produce blue compounds. The characteristic absorption peak was at 664 nm, and the range of  $\text{NH}_4^+$  detected by this method was 0.01-1.0  $\text{mg}\cdot\text{L}^{-1}$  (Zhou & Boyd 2019).

Ion chromatography is also widely used in the detection of  $\text{NH}_4^+$ , with a detection range of 0.02-40  $\text{mg}\cdot\text{L}^{-1}$ . The experiment has high reproducibility, high sensitivity, and a short detection time. However, when using ion chromatography to determine the content of  $\text{NH}_4^+$ , it is noteworthy that the close position of  $\text{NH}_4^+$  and  $\text{Na}^+$  ion peak results in a low separation degree. If the content of  $\text{Na}^+$  ions in the electrolyte is too high, the concentration of  $\text{NH}_4^+$  cannot be accurately determined (Thomas et al. 2002, LeDuy & Samson 1982).

To obtain relatively reliable results, in addition to colorimetry and ion chromatography,  $^{15}\text{N}$  isotope-nuclear magnetic resonance NMR was used to verify the experimental results (Hodgetts et al. 2020). The source of ammonia formation can be traced directly through isotope calibration to determine catalyst activity. The detection range is 5-10  $\mu\text{mol}\cdot\text{L}^{-1}$ . The results of  $^{15}\text{N}$  isotope-nuclear magnetic resonance (NMR) should be similar to those of colorimetry or ion chromatography, and the ammonia yield of the catalyst should be determined by mutual verification of various detection results.

## REACTION MECHANISMS OF NRR

The reaction mechanism of NRR is very complex and mainly depends on the catalytic surface and application potential. The reaction principle of electrocatalytic NRR ammonia synthesis is shown in Fig. 3a. As can be seen from Fig. 3b, according to kinetics, there is a gap of 10.8 eV energy gap between the highest occupied molecular orbital (HOMO) and the lowest occupied molecular orbital (LUMO) in nitrogen molecules (Zheng et al. 2019). The sorption and activation hydrogenation process of nitrogen is the most critical step. The sorption and activation process of nitrogen mainly includes a dissociative pathway, associative pathway (alternative pathway, distal pathway), enzymatic pathway, and Mars-van Krevelen (MvK) pathway, as shown in Fig. 3c (Zheng et al. 2019). The first three are more common, and

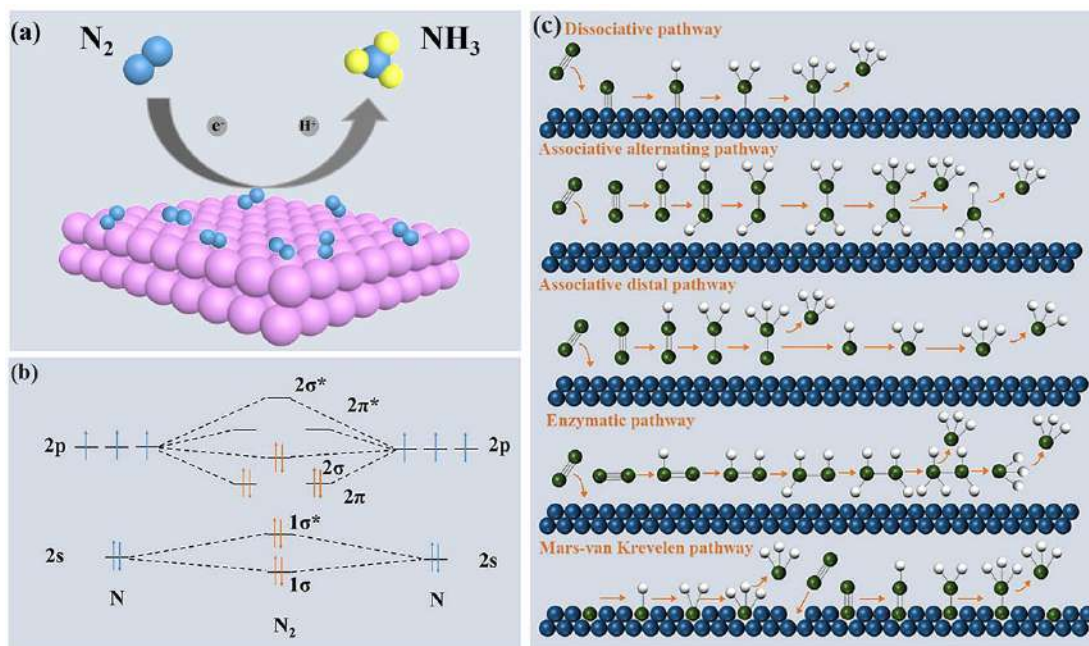


Fig. 3: Diagrammatic sketch of (a) NRR electrocatalysis and mechanisms. (b) Graphs of N orbitals and  $\text{N}_2$  orbitals. (c) Reaction pathway of catalyst for nitrogen reduction (Adapted from Ref. (Zheng et al. 2019)).

the detailed process is shown in Fig. 3c. The dissociative mechanism process is that  $N_2$  is first dissociated into N atoms adsorbed on the surface, each N atom is hydrogenated to form  $NH_3$  and desorbed from the surface to complete the catalytic process, and the H-B process belongs to the dissociative mechanism. In the associative mechanism (distal pathway),  $N_2$  is adsorbed on the surface in molecular form, and the chemical bond connection between the two nitrogen atoms is maintained. Hydrogenation first occurs on the nitrogen atom far from the surface. After hydrogenation, the N-N bond breaks, a molecule of  $NH_3$  is removed from the outside, and the inner N atom begins hydrogenation to form a molecule of  $NH_3$  and then desorbs from the surface. The preliminary process of the associative mechanism (alternative pathway) is similar to the distal pathway mechanism, but in the alternative pathway mechanism, two nitrogen atoms carry out the hydrotreating process alternately, the hydrogenated nitrogen atoms are the first to form  $NH_3$  and desorb from the surface, and the remaining nitrogen atoms continue the hydrogenation process. In the two association mechanisms, with the progress of hydrogenation, the chemical bond between two N atoms will weaken, and the fracture of the N-N bond is relatively easy. Therefore, compared with the dissociative mechanism, the associative mechanism consumes less energy and is easier to carry out. When the catalyst type, structure, and reaction conditions are different, the reaction process experienced by nitrogen reduction to synthesize ammonia is also different, and the application mechanism needs to be analyzed in detail.

In addition, there are two mechanisms: the enzymatic pathway and Mvk. The former mainly occurs in the nitrogen reduction reaction of nitrogenase. In this mechanism,  $N_2$  is still adsorbed in the form of molecules, but the two N atoms are not far from each other and are adsorbed on the surface side by side (Niu et al. 2021). The hydrogen process is the same as the alternative pathway mechanism. The Mvk mechanism appears more often in the catalytic process of transient metal nitrides (Abghoui & Skúlason 2017).

## ELECTROCATALYSTS FOR NRR

### Noble Metal-based Catalyst

At present, precious metal materials such as Pt, Rh, Au, Ru, Pd, Ag, and Ir Noble (Li et al. 2021) have been widely studied as catalysts for NRR because of their abundant surface active sites, unfilled d-electron orbitals, and superior conductivity. As mentioned earlier, precious metal materials have excellent HER properties and form fierce competition with nitrogen reduction reactions. Therefore, reasonable improvement and hybridization can improve its selectivity and yield. In recent years, many scholars have done a lot of research on

precious metal catalysts including (Au catalyst, Ru catalyst, Rh, and Pd catalysts). Experiments have shown that precious metal catalysts have obvious catalytic effects on NRR. This article uses the Au catalyst as an example to introduce the utilization of precious metal catalysts in nitrogen reduction reaction (NRR) and the performance achieved.

Gold (Au) is considered an ideal nuclear reactor material because, for the unfilled electron orbital, the reactant is easy to be adsorbed on the surface, has appropriate strength, and is conducive to the formation of intermediate “active compounds”. It can be obtained from Fig. 4a, the average particle size of Au nanoclusters in the  $TiO_2$  lattice is 0.5 nm. Fig. 4b shows that the use of this catalyst greatly improves the ammonia yield, and its  $NH_3$  yield can reach  $21.4 \mu g h^{-1} mg^{-1}$ . The electrolysis experiments of three different catalysts showed that TA-reduced Au/ $TiO_2$  (TA-Au/ $TiO_2$ ) showed the best nitrogen reduction performance compared with sodium borohydride reduction Au/ $TiO_2$  and Photoreduction Au/ $TiO_2$  (Fig. 4c). As shown in Fig. 4d, to investigate the stability of the nitrogen reduction performance of the catalyst TA-reduced Au/ $TiO_2$ , 10 electrolysis cycle experiments were carried out. It was found that there was no obvious change in the  $NH_3$  yield and Faradaic efficiency. In addition, nitrogen reduction was also applied at the same potential and different temperatures. In recent years, many researchers have found that the Faraday efficiency of Au in nitrogen reduction reaction needs to be improved, and have carried out a lot of research on it. Xue et al. have successfully loaded Au and Ni nanoparticles on an N-doped C supporter (Xue et al. 2019). HAADF-STEM (Fig. 4e) test was carried out on the catalyst. The results showed that an N-doped C supporter with gold nanoparticles was deposited on adjacent Ni particles. As shown in Fig. 4f, electrolytic experiments were conducted on several catalysts with different Au contents. Through comparison, it was found that the Faraday efficiency of Au<sub>6</sub>Ni was the highest among the catalysts, reaching 67.8% at -0.14 V (vs. RHE). Fig. 4g shows that the turnover rate (TOF) of the nitrogen reduction reaction on the Au catalyst continuously increases with the decrease of the Au content, which is similar to the electron enrichment of the Au component. By summarizing the previous density functional theory (DFT) calculation and experimental results and combined with the standard free energy spectrum of nitrogen reduction (Fig. 4g) in this work, we obtained the association mechanism on Au, in which the decomposition of adsorbed nitrogen ( $*N_2$ ) into  $*NNH$  is the rate-limiting step. As can be seen from Fig. 4i, the electron interaction between Au and Ni makes the electrons in Ni particles can be absorbed by Au, which is beneficial to the adsorption and dissociation of  $N_2$ . Therefore, higher Faraday efficiency of image pairs is obtained.

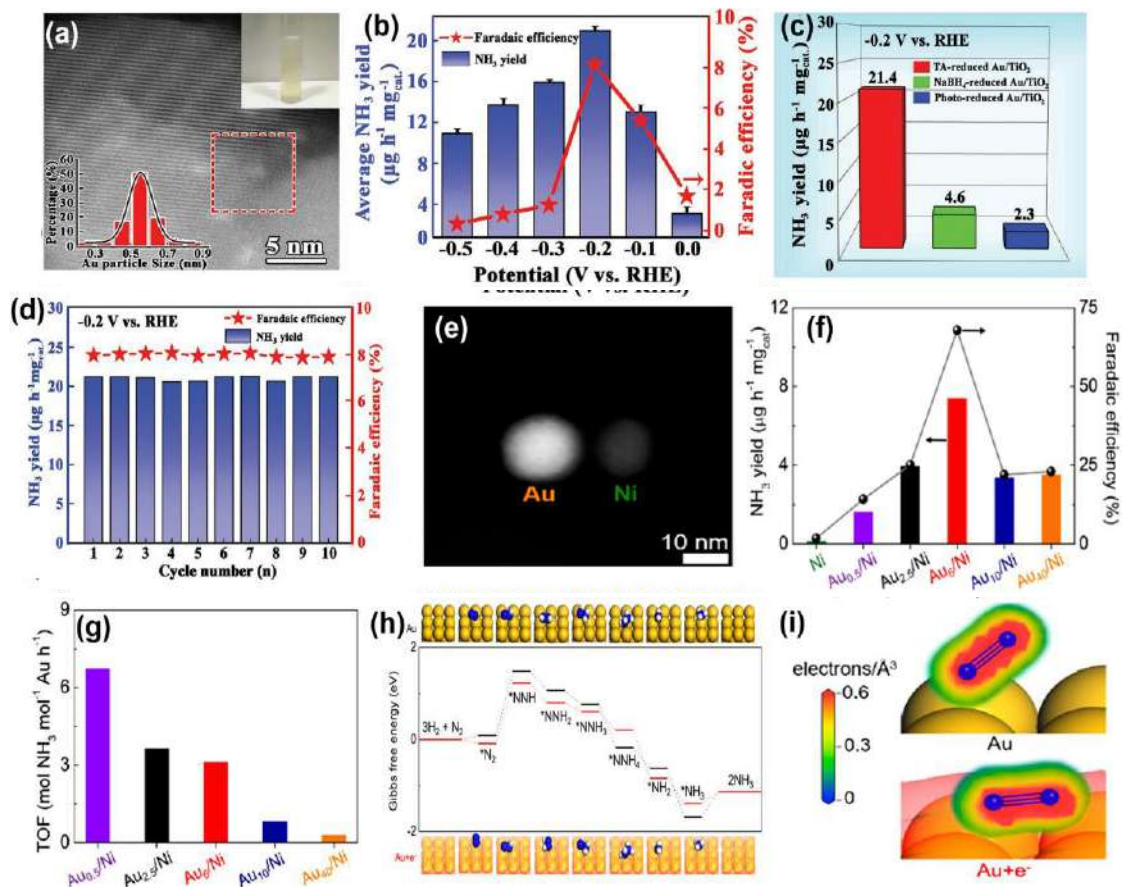


Fig. 4: (a) HAADF-STEM image of the TA-Au/TiO<sub>2</sub> (the picture of TA-Au/TiO<sub>2</sub> floated in the water, and the diameter distribution of Au). (b) Variation diagram of ammonia production rate and Faradaic efficiency. (c) Variation chart of the ammonia production rate of different catalysts. (d) Variation diagram of ammonia production rate and Faradaic efficiency of catalysts with different Au contents. (e) HAADF-TEM image. (f) Ammonia production rate and Faradaic efficiency of catalysts with different Au contents. (g) TOF values of the ammonia production rate based on the Au content. (h) The energy spectrum of nitrogen reduction. (i) The electron density map of N<sub>2</sub> adsorption was obtained by calculation. Reproduced with permission from Ref. (Shi et al. 2017). (Xue et al. 2019).

### Non-precious Transient Metal-based Catalyst

Precious metal catalysts usually have low ignition temperatures and high efficiency. Its catalytic efficiency is unmatched by other catalysts at low temperatures, but due to limited resources and high prices, it cannot be applied on a large scale (Zhang et al. 2018). Therefore, many scholars have shifted their research focus to non-precious transient metals as substitutes. Compared with noble metal catalysts, non-precious metal transient metals have the advantages of cheap and easy availability, abundant resources, and relatively good catalytic activity. Therefore, they are widely used as ideal electrocatalysts. At present, there are many kinds of transient element materials, mainly including their phosphides (Chu et al. 2019), chalcogenides (Zhang et al. 2018), borides (Yu et al. 2019), oxides (Yao et al. 2019), nitrides (Liu et al. 2020), metal single atoms (Guo et al. 2020), and carbides (Yang et al. 2020) have been widely

studied as valid electrocatalysts for the nitrogen reduction reaction.

Experiments have shown that non-precious transient metal-based catalysts have obvious catalytic effects on NRR. This article uses Fe-based electrocatalysts as an example to introduce the application of precious metal catalysts in NRR and the performance achieved. Fig. 5a is a schematic diagram of single-atom Fe supported on an n-doped carbon framework. In 0.1 M PBS, the electrolysis experiment of ISAS-Fe/NC catalyst shows that its ammonia production rate can reach 62.9  $\mu\text{g}\cdot\text{h}^{-1}\cdot\text{mg}_{\text{cat}}^{-1}$  and Faraday efficiency can reach 18.6%. Fig. 5b depicts the variation of current density and Faraday efficiency, implying that the catalyst has a FE of  $18.6 \pm 0.8\%$  at the highest NH<sub>3</sub> production rate. To explore the nitrogen reduction property of the ISAS-Fe/NC catalyst, we studied its three possible reactions, including the distal pathway, the alternative pathway, and enzymatic mechanisms (Liu et al.

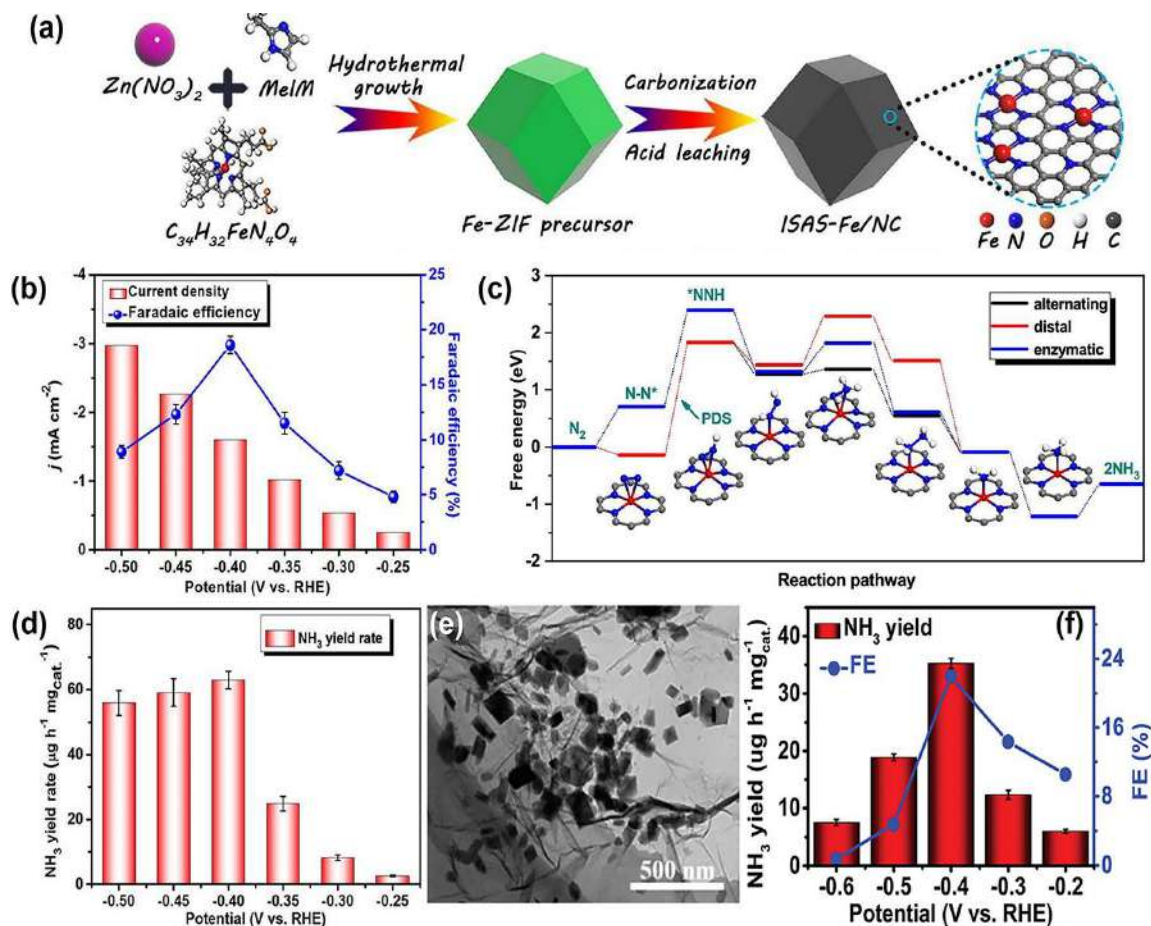


Fig. 5: (a) Composite diagram of ISAS-Fe/NC. Reproduced with permission from Ref. (Lü et al. 2019). (b) Variation diagram of current density and Faraday efficiency. (c) The calculation shows that nesting is the most stable of the three reaction mechanisms (d) Variation diagram of  $\text{NH}_3$  yield and different potentials. (e) TEM images of  $\text{FeP}_2$ -rGO. (f) Ammonia yields and Faraday efficiency of  $\text{FeP}_2$ -rGO/CP. Reproduced with permission from Ref. (Zhu et al. 2020).

2018). As shown in Fig. 5c, the first hydrogenation step is a potential determining step. Compared with distal and alternative PDS (1.98 eV), the PDS of the enzymatic mechanism (1.69 eV) is lower, indicating that the enzymatic mechanism of ISAS-Fe/NC catalyst in nitrogen reduction is better (Zhao et al. 2017). Fig. 5d shows the variation of ammonia yield under different potentials. Under this catalyst, the  $\text{NH}_3$  yield is  $62.9 \pm 2.7 \mu\text{g}\cdot\text{h}^{-1}\cdot\text{mg}_{\text{cat}}^{-1}$ . From the TEM image of  $\text{FeP}_2$ -rGO in Fig. 5e, it can be seen that  $\text{FeP}_2$  nanoparticles have been successfully loaded on rGO. Fig. 5f depicts the variation of ammonia yield and Faraday efficiency at different potentials after electrolysis of the  $\text{FeP}_2$ -rGO/CP catalyst.  $\text{FeP}_2$ -rGO/CP has significant nitrogen reduction activity, the  $\text{NH}_3$  yield is  $7.06 \mu\text{g}\cdot\text{h}^{-1}\cdot\text{cm}^{-2}$ , and the FE value is 21.99%.

## CONCLUSIONS AND PERSPECTIVES

At present, the development of low-cost and high-activity

catalysts is the key to optimizing the NRR process. To enhance the efficiency of the NRR process and promote the industrialization of electrocatalytic ammonia synthesis, the following aspects need to be considered.

- (1) Combine theory with experiment. Through the calculation of adsorption activation energy and reaction thermodynamic energy barrier, the overpotential and corresponding speed-limiting steps required to drive the reaction can be obtained, which plays a major role in revealing the catalytic mechanism and guiding the development of catalysts.
- (2) Enhance the catalytic activity of existing material systems. Material design and regulation strategies are applied to improve NRR reaction activity, such as lattice defect regulation strategies such as doping and vacancy construction, as well as surface and interface design such as morphology and size regulation to raise the active

points of the reaction, improve the adsorption performance of materials to nitrogen molecules, tuning the electron structure of catalysts, accelerate  $N\equiv N$  fracture, and regulate the adsorption and desorption performance of intermediates in the reaction process.

## ACKNOWLEDGMENT

This work was financially supported by the National Natural Science Foundation of China (Grant No. 21772152) and; the Shaanxi Provincial Education Department Program (No. 18JK0384).

## REFERENCES

- Abghoui, Y. and E Skúlason. 2017. Onset potentials for different reaction mechanisms of nitrogen activation to ammonia on transition metal nitride electro-catalysts. *Catal. Today*, 286(15): 69-77.
- Chen, J.G., Crooks, R.M., Seefeldt, L.C., Bren, K.L., Bullock, R.M. and Darensbourg, M.Y. 2018. Beyond fossil fuel-driven nitrogen transformations. *Science*, 360(91): 6611.
- Chen, R., Chen, D. and Xiao, Y. 2021. Theoretical scanning of bimetallic alloy for designing efficient  $N_2$  electroreduction catalyst. *Mater. Today Energy*, 20: 100684.
- Chu, K., Liu, Y.P., Li, Y.B., Zhang, H. and Tian, Y. 2019. Efficient electrocatalytic  $N_2$  reduction on CoO quantum dots. *J. Mater. Chem. A*, 7: 4389-4394.
- Dg, A., Sw, A., Jx, B., Wz, A. and Dw, A. 2022. Defect and interface engineering for electrochemical nitrogen reduction reaction under ambient conditions. *J. Energy Chem.*, 65: 448-468.
- Foster, S.L., Bakovic, S., Duda, R.D., Maheshwari, S. and Greenlee, L.F. 2018. Catalysts for nitrogen reduction to ammonia. *Nature Catal.*, 1(7): 490-500.
- Guo, C.Y., Liu, X.J., Gao, L.F., Kuang, X., Ren, X., Ma, X.J., Zhao, M.Z., Yang, H., Sun, X. and Wei, Q. 2020. Fe-doped  $Ni_2P$  nanosheets with a porous structure for electroreduction of nitrogen to ammonia under ambient conditions. *Appl. Catal. B Environ.*, 263: 118296.
- Hou, J., Yang, M. and Zhang, J. 2020. Recent advances in catalysts, electrolytes, and electrode engineering for the nitrogen reduction reaction under ambient conditions. *Nanoscale*, 12(13): 6900-6920.
- Hodgetts, R.Y., Kiryutin, A.S., Nichols, P., Du, H.L., Bakker, J.M., Macfarlane, D.R. and Simonov, A.N. 2020. Refining universal procedures for ammonium quantification via rapid  $^1H$  NMR analysis for dinitrogen reduction studies. *ACS Energy Lett.*, 5: 736-741.
- Kibsgaard, J., Nørskov, J.K., Cargnello, M., Lin, J.C., Schwalbe, J.A., Jaramillo, T.F., McEnaney, J.M. and Singh, Aayush, R. 2017. Ammonia synthesis from  $N_2$  and  $H_2O$  using a lithium cycling electrification strategy at atmospheric pressure. *Energy Environ. Sci.*, 10(7): 1621-1630.
- Li, K., Liu, Y.Q., Cui, B., Sima, D and Zheng, Z. 2020. Nitrogen reduction to ammonia at ambient conditions using hydrochar prepared from cigarette filters as a catalyst. *Int. J. Hydro. Energy*, 45(41): 20875-20882.
- Lancaster, K.M., Hu, Y.L., Bergmann, U., Ribbe, M.W. and DeBeer, S. 2013. X-ray spectroscopic observation of an interstitial carbide in NifEN-bound FeMoco precursor. *J. Am. Chem. Soc.*, 135: 610-612.
- Zhou, L. and Boyd, C.E. 2016. Comparison of Nessler, phenate, salicylate, and ion selective electrode procedures for determination of total ammonia nitrogen in aquaculture. *Aquaculture*, 450: 187-193.
- LeDuy, A. and Samson, R. 1982. Testing of an ammonia ion selective electrode for ammonia nitrogen measurement in the methanogenic sludge. *Biotechnol. Lett.*, 4: 303-306.
- Li, J., Wei, F., Dong, C., Wang, Z., Xiu, Z. and X Han. 2021. Recent progress of inorganic metal-based catalysts in the electrocatalytic synthesis of ammonia. *Mater. Today Energy*, 21: 100766.
- Liu, J., Liang, T.X., Wang, F., Lai, W.S. and Liu, Y.J. 2020. Enhancing of nitrogen reduction reaction to ammonia through  $CoB_4$ -embedded graphene: a theoretical investigation. *J. Hydro. Energy*, 45: 9555-9563.
- Lü, F., Zhao, S.Z., Guo, R.J., He, J., Peng, X.Y., Bao, H.H., Fu, J.T., Han, L.L., Qi, G.C. and Luo, J. 2019. Nitrogen-coordinated single Fe sites for efficient electrocatalytic  $N_2$  fixation in neutral media. *Nano Energy*, 61: 420-427.
- Liu, J.C., Ma, X.L., Li, Y., Wang, Y.G., Xiao, H. and Li, J. 2018. Heterogeneous  $Fe_3$  single-cluster catalyst for ammonia synthesis via an associative mechanism. *Nature Commun.*, 9: 1610.
- Ma, B., Zhao, H., Li, T., Liu, Q., and X Sun. 2020. Iron-group electrocatalysts for ambient nitrogen reduction reaction in aqueous media. *Nano Res.*, 14(3): 1-15.
- Montoya, J.H., Tsai, C., Vojvodic, A. and Nørskov, J.K. 2015. The challenge of electrochemical ammonia synthesis: a new perspective on the role of nitrogen scaling relations. *Chem. Sustain.*, 8(13): 2180-6.
- Meng, S.L., Li, X.B., Tung, C.H. and Wu, L.Z. 2020. Nitrogenase-inspired artificial photosynthetic nitrogen fixation. *Chemistry*, 7(6): 1431-1450.
- Niu, L., An, L., Wang, X. and Sun, Z. 2021. Effect on electrochemical reduction of nitrogen to ammonia under ambient conditions: Challenges and opportunities for chemical fuels. *J. Energy Chem.*, 61: 304-318.
- Qi, S., Fan, Y., Zhao, L., Li, W. and Zhao, M. 2021. Two-dimensional transition metal borides as highly efficient  $n_2$  fixation catalysts. *Appl. Surf. Sci.*, 536: 147742.
- Ren, Y., Yu, C.X Tan, H.H. and Qiu, J. 2021. Strategies to suppress hydrogen evolution for highly selective electrocatalytic nitrogen reduction: challenges and perspectives. *Energy Environ. Sci.*, 14: 1176-1193.
- Zhao, R.B., Xie, H.G., Chang, L., Zhang, X.X., Zhu, X.J., Tong, X., Wang T., Luo, Y.L., Wei, P.P., Wang, Z.M. and Sun, X.P. 2019. Recent progress in electrochemical ammonia synthesis under ambient conditions. *Energy Chem.*, 1(2): 100011-100011.
- Rostamikia, G., Maheshwari, S. and Janik, M.J. 2019. Elementary kinetics of nitrogen electroreduction to ammonia on late transition metals. *Catal. Sci. Technol.*, 9(1): 174-181.
- Spatzal, T., Aksoyoglu, M., Zhang, L.M., Andrade, S.L.A., Schleicher, E., Weber, S., Rees, D.C. and Einsle, O. 2011. Evidence for interstitial carbon in nitrogenase FeMo cofactor. *Science*, 334: 940.
- Shipman, M.A. and Symes, M.D. 2017. Recent progress towards the electrosynthesis of ammonia from sustainable resources. *Catal. Today*, 286: 57-68.
- Shi, M.M., Bao, D., Wulan, B.R., Li, Y.H., Zhang, Y.F., Yan, J.M. and Jiang, Q. 2017. Au sub nanoclusters on  $TiO_2$  toward highly efficient and selective electrocatalyst for  $N_2$  conversion to  $nh_3$  at ambient conditions. *Adv. Mater.*, 9(17): 1606550.
- Thomas, D.H., Rey, M. and Jackson, P.E. 2002. Determination of inorganic cations and ammonium in environmental waters by ion chromatography with a high-capacity cation-exchange column. *J. Chromatogr. A*, 956 (1-2): 181-186.
- Wang, Z.Q., Li, Y.H., Yu, H.J., Xu, Y., Xue, H.R., Li, X.N., Wang, H.J. and Wang, L. 2018. Ambient electrochemical synthesis of ammonia from nitrogen and water catalyzed by flower-like gold microstructures. *Chemistry*, 11(19): 3480-3485.
- Wan, Y., Xu, J. and Lv, R. 2019. Heterogeneous electrocatalysts are designed for nitrogen reduction reactions under ambient conditions. *Mater. Today*, 27: 69-90.
- Xu, X.S., Tian, X.J., Sun, B.T., Liang, Z.Q., Cui, H.Z., Tian, J. and Shao, M.H. 2020. 1 T-phase molybdenum sulfide nanodots enable efficient electrocatalytic nitrogen fixation under ambient conditions. *Appl. Catal. B Environ.*, 272(5): 118984.
- Xue, Z.H., Zhang, S.N., Lin, Y.X., Su, H. and Chen, J.S. 2019. Electrochemical reduction of  $N_2$  into  $NH_3$  by donor-acceptor couples of ni

- and Au nanoparticles with a 67.8% faradaic efficiency. *J. Am. Chem. Soc.*, 141(38):14976-14980.
- Yu, H., Wang, Z., Tian, W., Dai, Z., Xu, Y., Li, X., Wang, L. and Wang, H. 2021. Boosting electrochemical nitrogen fixation by mesoporous Rh film with boron and sulfur co-doping. *Mater. Today Energy*, 20: 100681.
- Yu, G.S., Guo, H.R., Liu, S.H., Chen, L., Alshehri, A.A., Alzahrani, K.A., Hao, F. and Li, T.S. 2019. Cr<sub>3</sub>C<sub>2</sub> nanoparticle-embedded carbon nanofiber for the artificial synthesis of NH<sub>3</sub> through N<sub>2</sub> fixation under ambient conditions. *ACS Appl. Mater. Interf.*, 11: 35764-35769.
- Yao, X., Chen, Z.W., Wang, Y.R., Lang, X.Y., Gao, W., Zhu, Y.F. and Jiang, Q. 2019. Activated basal planes of WS<sub>2</sub> by intrinsic defects as catalysts for the electrocatalytic nitrogen reduction reaction. *J. Mater. Chem. A*, 7: 25961-25968.
- Yang, T., Song, T.T., Zhou, J., Wang, S.J., Chi, D.Z., Shen, L., Yang, M. and Feng, Y.P. 2020. High-throughput screening of transition metal single atom catalysts anchored on molybdenum disulfide for nitrogen fixation. *Nano Energy*, 68: 104304.
- Zhu, X.J., Mou, S.Y., Peng, Q.L., Liu, Q., Luo, Y.L., Chen, G., Gao, S.Y. and Sun, X.P. 2020. Aqueous electrocatalytic N<sub>2</sub> reduction for ambient NH<sub>3</sub> synthesis: Recent advances in catalyst development and performance improvement. *J. Mater. Chem. A*, 8: 1545-1556.
- Zhu, X.J., Zhao, J.X., Ji, L., Wu, T.W., Wang, T., Gao, S.Y., Alshehri, A.A., Alzahrani, K.A., Luo, Y.L., Xiang, Y.M., Zheng, B.Z. and Sun, X.P. 2020. FeOOH quantum dots decorated graphene sheet: an efficient electrocatalyst for ambient N<sub>2</sub> reduction. *Nano Res.*, 13: 209-214.
- Zhao, Y.X., Shi, R., Bian, X.A.N., Zhou, C., Zhao, Y.F., Zhang, S., Wu, F., Waterhouse, G.I.N., Wu, L.Z., Tung, C.H. and Zhang, T.R. 2019. Ammonia detection methods in photocatalytic and electrocatalytic experiments: how to improve the reliability of NH<sub>3</sub> production rates? *Adv. Sci.*, 6: 1802109.
- Zheng, G., Yan, J. and Yu, G. 2019. Nitrogen reduction reaction. *Small Methods*, 3(6): 1900070.
- Zhang, Y., Qiu, W.B., Ma, Y.J., Luo, Y.L., Tian, Z.Q., Cui, G.W., Xie, F.Y., Chen, L., Li, T.S. and Sun, X.P. 2018. High-performance electrohydrogenation of N<sub>2</sub> to NH<sub>3</sub> catalyzed by multicelled hollow Cr<sub>2</sub>O<sub>3</sub> microspheres under ambient conditions. *ACS Catal.*, 8(9): 8540-8544.
- Zhang, L., Ji, X.Q., Ren, X., Luo, Y.L., Shi, X.F., Asiri, A.M., Zheng, B.Z. and Sun, X.P. 2018. Efficient electrochemical N<sub>2</sub> reduction to NH<sub>3</sub> on Mo nanosheets array under ambient conditions. *ACS Sustain. Chem. Eng.*, 6(8): 9550-9554.
- Zhao, J. and Chen, Z. 2017. Single Mo atom supported on defective boron nitride monolayer as an efficient electrocatalyst for nitrogen fixation: A computational study. *J. Am. Chem. Soc.*, 139: 12480-12487.
- Zhu, X., Wu, T., Ji, L., Liu, Q., Luo, Y., Cui, G., Xiang, Y.M., Zhang, Y.N., Zheng, B.Z. and Sun, X.P. 2020. Unusual electrochemical N<sub>2</sub> reduction activity in an earth-abundant iron catalyst via phosphorous modulation. *Chem. Commun.*, 56: 731-734.







# Research on the Governance of Rural Environmental Pollution in Heilongjiang Province Based on the Environmental Kuznets Curve

Yanwei Yang\*, Weiguo Sun\*\*† and Chi Li\*

\*School of Civil Engineering, Northeast Forestry University, Harbin 150040, China

\*\*School of Marxism, Northeast Forestry University, Harbin 150040, China

†Corresponding author: Weiguo Sun; [davisun7811@163.com](mailto:davisun7811@163.com)

Nat. Env. & Poll. Tech.  
Website: [www.neptjournal.com](http://www.neptjournal.com)

Received: 02-04-2022

Revised: 09-05-2022

Accepted: 16-05-2022

## Key Words:

Rural environmental pollution  
Governance  
Economic growth  
Environmental Kuznets curve

## ABSTRACT

At present, the effective management of the rural environment has drawn the attention of the entire global community. Heilongjiang Province majors in agriculture and animal husbandry resources. Compared with urban environmental pollution, the pollution caused by agriculture and animal husbandry has a strong impact on the use of agricultural elements and environmental constraints. At the same time, it has the characteristics of high governance cost, high governance difficulty, and difficulty in being monitored. In this study, the environmental Kuznets curve is used to verify the relationship between rural environmental pollution and economic growth in Heilongjiang Province, and a linear regression model is designed to verify time series data and indicators. The results show that the phenomenon of rural water pollution has become common in Heilongjiang Province, the discharge of rural environmental pollutants has exceeded the safe discharge limit value, and the pollution degree of the rural environment in Heilongjiang Province has exceeded the safety warning value at least, and it is very necessary for its treatment. This study enriches the research methods and content of the performance evaluation of rural environmental governance in my country helps to objectively evaluate the governance issues of the rural environment in Heilongjiang Province, and can be a functional area of grain production that is highly dependent on resources and environmental constraints of the same kind in my country. Rural environmental governance provides a universal reference.

## INTRODUCTION

Heilongjiang Province is a large agricultural and animal husbandry province in China. Its arable land area and grain output are ranked first in the country. The development level of planting and animal husbandry is relatively high. However, in rural areas, the extensive growth mode has increased environmental pollution and severely imbalanced rural ecosystems. and restricted the development of the rural economy in Heilongjiang. While rural environmental pollution damages the rural ecological environment, it also has an impact on the health of rural residents, and contaminated agricultural products will further reduce the quality of life of urban residents. Therefore, only by fully understanding the characteristics and hazards of rural environmental pollution and exploring its causes can we propose targeted measures for the treatment of rural environmental pollution. Agricultural environmental pollution in Heilongjiang mainly includes agricultural chemical fertilizers, pesticide use, livestock and poultry breeding, plastic film pollution, soil erosion, forest vegetation loss, etc. Among them, chemical fertilizers and pesticides are important factors that cause soil compaction,

reduced regeneration effects, and toxic pollution of agricultural products. It is also the main source of the deteriorating water quality of rivers and lakes.

The current health problems caused by environmental pollution are becoming more and more obvious, such as asthma (Choi et al. 2017), lung cancer (Wang et al. 2016), and mental illness (Roberts et al. 2019). At present, there is more and more research on the problems caused by environmental pollution in academia. For example, studies on the deterioration of water quality have predicted the trade-off between urban models and the production of ecosystem services: scenario analysis of alternatives to rapid urbanization area sprawl (Shoemaker et al. 2019), the impact of different media on constructed wetlands for rural domestic sewage treatment (Lu et al. 2016), the long-term impact of human factors on non-point source pollution in the upper reaches of the Yangtze River (Ding et al. 2019), rural watershed management (Ding et al. 2019), sustainable agricultural intensification practices and rural food security (Yahaya et al. 2018) and other studies. Research on pollution trends includes the changes in gas-phase air pollutants in New York State (Civerolo et al.

2017) and the temporal and spatial trends of ground-level ozone concentration and indicators in France from 1999 to 2012 (Sicard et al. 2016). Research on health risk assessment includes urban acoustic environment Quality evaluation (Di et al. 2018), the use of targeted ecological pharmacovigilance interventions to control antibiotic pollution in rural aquatic environments (Wang et al. 2019), the feasibility study of candidate reference materials for PM<sub>2.5</sub> ions (Emma et al. 2018), Chinese residents Assessment of total environmental exposure of heavy metals (Zhao et al. 2019), Chinese motor vehicle emissions in 2006 and 2010 (Tang et al. 2016), etc. The research on the problems caused by environmental pollution has gradually matured, but there is a lack of research on the problems of environmental pollution control in Chinese rural areas.

Therefore, this study analyzes in detail the current situation of rural environmental pollution in Heilongjiang in the past ten years, based on the environmental Kuznets curve, to study the problems of rural environmental pollution control in Heilongjiang, and points out the current problems in the rural environmental pollution control in Heilongjiang. This study has certain reference values for future rural environmental governance.

## MATERIALS AND METHODS

Rural environmental pollution in Heilongjiang is mainly divided into the pollution of agricultural production, pollution of rural life, pollution of sewage, and pollution from urban to rural areas. Rural environmental pollution in Heilongjiang has an “inverted U-shaped” relationship with the level of regional economic development, that is, when the level of economic development is relatively low, the rural environmental pollution is relatively low. With the continuous development of the economy, environmental pollution continues to deteriorate. The peak, that is, after the per capita GDP reaches a certain level, the rural environmental pollution will gradually improve with the improvement of the level of economic development. Therefore, based on the environmental Kuznets curve, this paper studies the rural environmental pollution control in Heilongjiang Province.

### Environmental Kuznets Curve

The Environmental Kuznets Curve (EKC) describes Heilongjiang as follows: rural environmental pollution in Heilongjiang has an “inverted U-shaped” with the level of regional economic development, that is, when the economic development level is relatively low, the rural environmental pollution is relatively low. As the economy continues to develop, environmental pollution continues to deteriorate. When it reaches a certain peak, that is, when the per capita

GDP reaches a certain level, rural environmental pollution will gradually improve with the improvement of economic development.

The theoretical reference of this study is to use this hypothesis to verify the relationship between rural environmental pollution and economic growth in Heilongjiang. The verification model is designed as follows:

$$N = \beta_0 + \beta_1 Pergdp + \beta_2 Pergdp^2 + \varepsilon \quad \dots(1)$$

$$P = \beta_0 + \beta_1 Pergdp + \beta_2 Pergdp^2 + \eta \quad \dots(2)$$

In this model,  $N$ , and  $P$  respectively represent the total nitrogen emissions and total phosphorus emissions of rural environmental pollution in Heilongjiang in  $y$  year and represent the per capita GDP of Heilongjiang in a certain year. Compared with total GDP, per capita GDP can more clearly reflect the real effect of environmental pollution on the level of economic development.  $\beta_0$ ,  $\beta_1$ , and  $\beta_2$  are the coefficient values in the model,  $\varepsilon$  and  $\eta$  are denoted as random error terms respectively. The verification results of the model can be divided into the following situations:

- (a) When  $\beta_1 \neq 0$ ,  $\beta_2 = 0$ , there is a linear relationship between economic growth and environmental pollution;
- (b) When  $\beta_1 < 0$ ,  $\beta_2 > 0$  there is an “inverted U-shaped” relationship between economic growth and environmental pollution; the inflection point of per capita GDP at this time is  $Pergdp^* = -\beta_1 / (2 * \beta_2)$ ;
- (c) When  $\beta_1 > 0$ ,  $\beta_2 < 0$ , there is a “U-shaped” relationship between economic growth and environmental pollution.

### Eco-environmental Factors of Governance Under the Framework of Environmental Kuznets Curve Analysis

Heilongjiang is a large ecological environment province with abundant natural resources. For rural environmental pollution control, the introduction of the ecological environment is quite important. Therefore, add the concept of ecological environment to the EKC curve, including environmental tolerance thresholds and safety warning lines. The pollutant discharge corresponding to the environmental tolerance threshold refers to the maximum amount of pollution that the ecological environment can withstand. Once the pollution exceeds this upper limit of pollution, the pollution is irreversible. No matter how the economy repairs the environment, the environment cannot be restored. The discharge of pollutants corresponding to the safety cordon refers to the discharge of a pollutant that has had a certain impact on the environment and must be treated in time. It is the limit value

of the safe discharge of pollution at this point. If there is a timely “response” to environmental pollution, the damaged environment can still be repaired.

As shown in Fig. 1, within a certain period of time, points A, B, and C are the inflection points of three different “inverted U-shaped” curves and the pollutant emissions at the inflection points (that is the maximum pollutant emissions of the EKC curve). They are  $P_A$ ,  $P_B$ , and  $P_C$ . The point where the environmental tolerance threshold line intersects the vertical axis is  $P_1$ , and the point where the safety pollution warning line intersects the vertical axis is  $P_2$ . Pollutant emissions  $P_A < P_2 < P_B < P_1 < P_C$ .

Definition of pollution level: assuming that other conditions remain unchanged, the EKC curve with the inflection point A is called the level-A pollution level curve, indicating that the pollution is at a relatively low level and has not reached the safety pollution warning line, which is an ideal state. The curve with the inflection point B is called the EKC curve of level B. The pollution at the inflection point is between the warning line and the threshold line. Economic growth has caused a bad impact on the environment, but the damaged environment can be repaired. The EKC curve with the inflection point C is called the level-C curve. It exceeds the environmental tolerance threshold. The pollution generated around inflection point C is irreparable to the environment. If the pollution level is on the curve of B or C, active control measures should be taken.

Rural water pollution has become more common in Heilongjiang, and the discharge of rural environmental pollutants has exceeded the safe discharge limit. This study roughly judges that the curve of the relationship between rural environmental pollution and economic growth in Heilongjiang must not be the curve of level-A in Fig. 6, but level B or level C. The level of pollution at the turning point has at least exceeded the safety warning value.

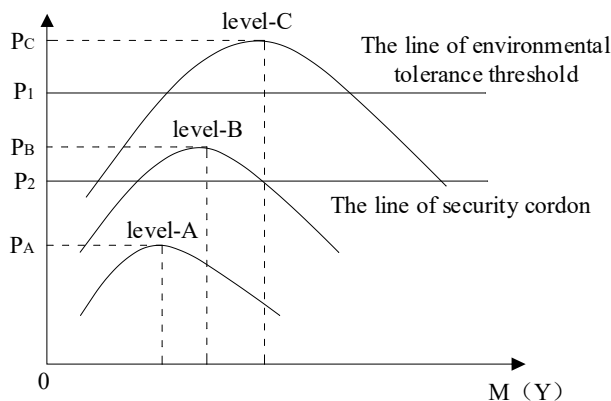


Fig. 1: The inflection point behind the threshold line and the safety guard line.

### Theoretical Analysis of Governance Function Under the Framework of Environmental Kuznets Curve Analysis

Assuming that there is only one family in the economy and there are no externalities, the Pareto optimal of the individual family is the Pareto optimal of the whole society. The family utility function expression is as follows:

$$U=U(C, P) \quad (3)$$

In the above formula, household consumption is  $C$ , and consumption  $C$  will produce pollution as  $P$ .  $U_C > 0$  and  $U_P < 0$ , respectively, indicate that the utility of the household increases with the increase in consumption, and decreases with the increase in pollution. There are two ways to reduce pollution, one is to directly reduce consumption and thus reduce the amount of pollution, and the other is to control the amount of pollution. When pollution is treated, the number of resources required to be input is  $E$ , assuming that the amount of pollution  $P$  is positively correlated with the amount of consumption  $C$  and the amount of governance resource input  $E$ , respectively, the pollution is a function of  $C$  and  $E$ , and the expression is as follows:

$$P=P(C, E) \quad (4)$$

In the above formula,  $PC < 0$  and  $PE < 0$ , respectively, mean that pollution increases with the increase in consumption and decreases with the increase of the input of treatment resources. Assuming that the household income is constant, the income can be consumed and governed, and the relative cost of consumption and governance is standardized to 1, then there is the following formula:

$$M=C+E \quad (5)$$

In the above formula,  $M$  is the total household income. Assuming that the utility function:

$$U=C-zP \quad (6)$$

In the above formula,  $z$  is a constant greater than zero, representing the marginal utility loss of pollution. Suppose that the pollution function is formula (7), and it is assumed that unit 1 of consumption will produce unit 1 of pollution,  $C$  is the total pollution amount before treatment, and the pollution treatment function adopts the form of the  $C$ - $D$  function.

$$P=C-C^\alpha E^\beta \quad (7)$$

The family's behavioral choice equation is the maximum utility of  $M$  under certain conditions, namely:

$$\text{Max}U=C-zP \quad (8)$$

$$P=C-C^\alpha E^\beta \quad (9)$$

$$M=C+E \quad (10)$$

When  $z=1$ ,  $C^* = \frac{\alpha}{\alpha+\beta}M$ ,  $E^* = \frac{\beta}{\alpha+\beta}M$

$$P^*(M) = \frac{\alpha}{\alpha+\beta}M - \left(\frac{\alpha}{\alpha+\beta}\right)^\alpha \left(\frac{\alpha}{\alpha+\beta}\right)^\beta M^{\alpha+\beta} \tag{11}$$

$$\frac{\partial P^*(M)}{\partial M} = \frac{\alpha}{\alpha+\beta} - (\alpha+\beta) \left(\frac{\alpha}{\alpha+\beta}\right)^\alpha \left(\frac{\alpha}{\alpha+\beta}\right)^\beta M^{\alpha+\beta-1} \tag{12}$$

When  $\alpha+\beta=1$ , formula (12) is a constant, and  $P$  and  $M$  are linear relations.

When  $\alpha+\beta \neq 1$ , the derivative of formula (12):

$$\frac{\partial^2 P^*(M)}{\partial M^2} = -(\alpha+\beta-1) (\alpha+\beta) \left(\frac{\alpha}{\alpha+\beta}\right)^\alpha \left(\frac{\alpha}{\alpha+\beta}\right)^\beta M^{\alpha+\beta-2} \tag{13}$$

When  $\alpha+\beta < 1$ , the scale benefit of pollution treatment is diminishing, and the second derivative value is greater than 0, so  $P$  and  $M$  have a U-shaped relationship.

When  $\alpha+\beta > 1$ , the scale benefit of pollution treatment increases, and the second derivative value is less than 0, so  $P$  and  $M$  are in an inverted U-shaped relationship. That is, the shape described by the EKC curve.

The same can be proved, when  $z \neq 1$ , still only when the scale benefit of pollution control increases,  $P$  and  $M$  show an inverted U-shaped relationship.

## RESULTS

In the research on the relationship between rural environmental pollution and economic growth in Heilongjiang Province, the time series data of rural environmental pollution in Heilongjiang Province from 2011 to 2020 in the “China Statistical Yearbook” was used. GDP per capita is calculated at the constant price of the initial calculation year to remove the price factor.

Table 1: Gross national product and population in Heilongjiang (2011-2020).

Years	2011	2012	2013	2014	2015	2016	2017	2018	2019	2020
GDP (RMB 100 million)	6201.45	7065.00	8314.37	8587.00	10368.60	12582.00	13691.58	14382.93	15039.38	15083.67
Population (10,000)	3823.12	3824.37	3825.76	3826.43	3833.17	3834.75	3834.89	3835.09	3835.76	3812.17

Table 2: Variable name unit and descriptive statistical analysis.

Variable	Symbol	Unit	Average value	Standard deviation	Minimum	Maximum
Total nitrogen	N	10,000 tons	26.8381	4.2977	21.3452	28.4657
Total phosphorus	P	10,000 tons	2.7160	0.4431	2.3742	2.9372
GDP per capita	Pergdp	Yuan/person	2.9071	0.8653	1.6221	3.9567

## Model Estimation Result Analysis

According to the linear regression method and test, the relationship between the total nitrogen emission index and total phosphorus emission index of rural environmental pollution in Heilongjiang and the per capita GDP were used for the regression test. The results are shown in Table 3.

It can be seen from Table 3 that when the dependent variable is the total nitrogen emission of rural environmental pollution, the value of Adj-R2 is 0.8847, indicating that the explanatory power of total nitrogen in this model is 88.47%. It shows that in this model, the explanatory power of total nitrogen is 88.47%. The F value is large, and the model generally passes the 1% level of a significance test, which shows that the combined effect of the primary and square terms of the per capita GDP factor on total nitrogen emissions is significant. The first coefficient of per capita income is greater than zero, and the quadratic coefficient is less than zero, indicating that the relationship between total nitrogen emissions and per capita GDP presents an “inverted U-shaped” within a certain period of time, and an inflection point has appeared.

At the same time, when the dependent variable is the total phosphorus emission of rural environmental pollution, the value of Adj-R2 is 0.8567, indicating that the explanatory power of total phosphorus in this model is 85.67%. The F value is large, and the model generally passes the 1% level of a significance test, which shows that the combined effect of the primary and square terms of the per capita GDP factor on total phosphorus emissions is significant. The primary coefficient of per capita income is greater than zero, and the secondary coefficient is less than zero, indicating that the relationship between total phosphorus emissions and per capita GDP presents an “inverted U-shaped” within a certain period of time, and an inflection point has appeared.

### The Factual Inference of Governance Under the Framework of Environmental Kuznets Curve Analysis

In view of the fact that there are many factors affecting rural environmental pollution, the corresponding treatment measures are also complicated. This section takes farmland fertilizers as an example to analyze the impact of treatment measures on the environmental Kuznets curve reflecting the relationship between farmland fertilizers and rural environmental pollution and economic growth. First, verify whether there is an environmental Kuznets curve between farmland chemical fertilizers and rural environmental pollution and economic growth.

(1) Verification of the curve of rural environmental pollution and economic growth caused by farmland chemical fertilizers

Using the theoretical analysis framework to verify the relationship between the environmental Kuznets curve and the economic growth of the rural environmental pollution caused by farmland fertilizers in Heilongjiang. The model to be verified is:

$$FN = \beta_0 + \beta_1 Pergdp + \beta_2 Pergdp^2 + \varepsilon \quad (14)$$

$$FP = \beta_0 + \beta_1 Pergdp + \beta_2 Pergdp^2 + \eta \quad (15)$$

Among them, *FN* and *FP* respectively represent the total nitrogen emissions and total phosphorus emissions of rural environmental pollution caused by farmland fertilizers in

Heilongjiang. *Pergdp* represents the per capita GDP value of Heilongjiang. After calculation, the meaning of each variable and descriptive statistical analysis are shown in Table 4. The estimated results of the model are shown in Table 5.

It can be seen from table 5 that when the dependent variable is the total nitrogen emission of rural environmental pollution caused by farmland chemical fertilizers, the value of Adj-R2 is 0.8241, which means that in this model, the explanatory power of nitrogen emissions is 82.41%. The F value is relatively low. The model generally passes the 1% level of a significance test, which shows that the combined effect of the primary and square terms of the per capita GDP factor on fertilizer nitrogen emissions from farmland is significant. The first coefficient of per capita income is greater than zero, and the quadratic coefficient is less than zero, indicating that the relationship between total nitrogen emissions and per capita GDP presents an "inverted U-shaped" within a certain period of time, and an inflection point has appeared.

At the same time, when the dependent variable is the total phosphorus emission of rural environmental pollution caused by farmland chemical fertilizers, the value of Adj-R2 is 0.7465, indicating that the explanatory power of nitrogen emissions in this model is 74.65%. The F value is larger, the model is Overall, it has passed the 1% level of a significance test, which shows that the combined effect of the primary and square terms of per capita GDP factor on farmland fertilizer nitrogen emissions is significant. The first coefficient

Table 3: Model estimation results.

Variable	N	P
Pergdp	23.47*** (10.47)	2.14*** (12.35)
Pergdp <sup>2</sup>	-0.00047*** (-9.51)	-0.000051*** (-8.79)
Constant	276639.9*** (27.64)	37063.72*** (39.41)
Adj-R <sup>2</sup>	0.8847	0.8567
F	93.17***	82.34***
Prob(F)	0.0000	0.0000

Note: \*\*\* means passing the 1% level of significance test; parentheses are T values.

Table 4: Variable name unit and descriptive statistical analysis.

Variable	Symbol	Unit	Average value	Standard deviation	Minimum	Maximum
Nitrogen emissions from farmland fertilizers	FN	10,000 tons	57.8435	3.2076	35.3351	78.4879
Phosphorus emissions from farmland fertilizers	FP	10,000 tons	37.7261	1.2561	28.3632	54.9271
GDP per capita	Pergdp	Yuan/person	2.9071	0.8653	1.6221	3.9567

Table 5: Model estimation results.

Variable	FN	FP
Pergdp	19.23*** (9.49)	0.84*** (9.35)
Pergdp <sup>2</sup>	-0.00034*** (-8.47)	-0.000018*** (-6.71)
Constant	18675.9*** (25.73)	7869.75*** (35.40)
Adj-R <sup>2</sup>	0.8241	0.7465
F	73.77***	51.34***
Prob(F)	0.0000	0.0000

Note: \*\*\* means passing the 1% level of significance test; parentheses are T values.

of per capita income is greater than zero, and the quadratic coefficient is less than zero, indicating that the relationship between total nitrogen emissions and per capita GDP presents an “inverted U-shaped” within a certain period of time, and an inflection point has appeared.

## DISCUSSION

Through the above analysis, we can know that some achievements have been made in the control of rural environmental pollution in Heilongjiang Province, but there are still five problems. They are the main body of environmental governance, residents' environmental awareness, grassroots environmental protection agencies, environmental supervision, and legal systems.

### Problems in the Main Body of Rural Environmental Governance

Public economics believes that the non-competitive and non-exclusive characteristics of public products determine that a competitive market cannot provide sufficient public products. The supply of public goods by the private sector cannot be compensated through the market. Therefore, letting private individuals provide public products is bound to be a serious shortage of output, and it is impossible to meet the requirements for the effective allocation of resources.

The government is the main body of governance, and other public organizations are less involved, so the governance methods are relatively traditional. Although there are environmental protection departments at the provincial and county levels, they are subordinate to the government. As a quasi-public good, the environment is non-exclusive. Excessive consumption by some people will inevitably affect the use of others. However, the government attaches greater importance to economic development. Environmental

pollution control is difficult to produce large economic benefits within a certain period of time.

It is difficult for law enforcement agencies to achieve good results in solving practical problems, and lack of voluntary and equal cooperation in all aspects. Corresponding to this is that the operation of traditional enterprises is relatively traditional. The disadvantage is that there is a fluke mentality when responding to government inspections. The equipment used is aging, and pollution cannot be monitored in real-time. The governance body lacks a long-term environmental governance and supervision mechanism. According to the author's investigation, after the establishment of environmental protection facilities and environmental protection projects in some areas, there is no special person to supervise and manage the normal operation of the project. The basic government has financial difficulties and lacks operating funds. Some facilities, in the end, became a decoration, which not only failed to achieve the effect of improving the rural environment, but wasted a lot of investment funds.

### Problems in the Environmental Protection Awareness of Rural Residents

With the construction of new rural areas, the living standards in rural areas are getting higher and higher, but rural lifestyles have not undergone fundamental changes. Heilongjiang's rural areas are remote, scattered, and the villages and towns are not centralized. It is difficult to train and publicize environmental protection in rural areas. The literacy and comprehensive quality of the residents are not high, they are unclear about the importance of environmental hazards, excessively chasing economic benefits, and ignoring potential environmental pollution.

Some rural cadres do not have a good understanding of environmental protection. Some cadres believe that the vast rural area and loose residential living make it difficult to carry

out proper environmental protection publicity and education, and it is difficult to build a new environmental protection system. Therefore, to pursue political achievements, blindly construct and introduce some polluting enterprises with serious pollution, and do not pay attention to the improvement of environmental protection infrastructure.

In many places, the construction and operation of sewage treatment plants and supporting pipeline networks have the phenomenon of focusing on cities and towns. At present, there is no township sewage treatment plant in some rural areas. The rural garbage collection, transfer, and harmless disposal systems are not sound, and almost 76% of rural domestic garbage has not been collected.

### Problems in Rural Grassroots Environmental Protection Agencies

According to investigations, each township in the province is only equipped with part-time environmental protection personnel, and the counties and districts have not yet set up township environmental protection offices, so they cannot effectively deal with the increasingly heavy rural environmental problems. The existing rural environmental protection agencies do not have a fixed model. Each township environmental protection agency is set up in one sentence. The organization, personnel, funding, establishment, and responsibilities are not unified, and there is a lack of unified rules and regulations, and supervision procedures, which are also to a certain extent. Affected the work of grassroots environmental protection agencies.

If a township environmental protection station is established, the staff can live in the countryside for a long time, publicize policies, laws, and regulations to key polluters, and carry out various forms of publicity and education activities to cultivate farmers' environmental awareness.

At present, the main body of environmental governance in my country is the government. Due to geographical limitations, rural areas have the characteristics of vastness, dispersion, and complex pollution. The government cannot centrally manage the rural environment, which leads to insufficient administrative efforts.

### Problems in Forces of Rural Environmental Supervision

The effects of environmental supervision, monitoring, and emergency response cannot meet the current increasing demands for environmental supervision. According to investigations, in most areas of the province, the three aspects of team building, equipment, and business premises of environmental supervision agencies have failed to meet the requirements of the national environmental supervision effect construction level one standard. Most of the construction

of environmental monitoring effects in all districts did not meet the requirements of the national third-level standards.

Taking Shuangyashan City in Heilongjiang as an example, the staffing of the Environmental Monitoring Center Station, monitoring funding, and monitoring housing did not meet the second-level national environmental monitoring station construction standards in the central region. Baoqing County in Shuangyashan City has serious shortages of environmental protection personnel and funding guarantees. There are 33 people, 19 of whom are self-raised and self-financed. Self-raised funds reach 925,000 yuan, and there is an annual law enforcement funding gap of 300,000 yuan.

### Problems in the Legal System of Rural Environmental Governance

There are not many administrative laws that regulate the administrative relationship between agriculture and the rural economy in Heilongjiang.

Some existing separate laws for the protection of the rural environment and resources can no longer meet the needs of rural environmental protection development. The rural cadres and the masses have strong policy awareness and weak legal awareness, resulting in many laws and regulations being policy-oriented in the process of rural implementation. The principle, practice, and flexibility of policies have replaced the compulsory and normative nature of laws and regulations. It has caused numerous obstacles to the construction of the rule of law in the rural market economy.

### REFERENCES

- Choi, H., Tabashidze, N. and Rossner, P. 2017. Altered vulnerability to asthma at various levels of ambient Benzo[a] Pyrene by CTLA4, STAT4, and CYP2E1 polymorphisms. *Environ. Pollut.*, 231: 1134-1144.
- Civerolo, Kevin L., Rattigan, Oliver V. and Felton, H. 2017. Changes in gas-phase air pollutants across New York State, USA. *Aero. Air Qual. Res.*, 17(1): 147-166.
- Di, H.L., Xingpeng, L. and Zhang, J. 2018. Estimation of the quality of an urban acoustic environment based on traffic noise evaluation models. *Appl. Acoustics*, 141: 115-124.
- Ding, X. and Liu, L. 2019. Long-term effects of anthropogenic factors on nonpoint source pollution in the upper reaches of the Yangtze River. *Sustainability*, 11(8): 2246
- Emma, G., Snell, J. and Charoud-Got, J. 2018. Feasibility study of a candidate reference material for ions in PM2.5: does commutability matter also for inorganic matrices? *Analytical and Bioanal. Chem.*, 410(23): 6001-6008.
- Lu, S., Zhang, X. and Wang, J. 2016. Impacts of different media on constructed wetlands for rural household sewage treatment. *J. Clean. Prod.*, 127: 325-330.
- Roberts, S., Arseneault, L. and Barratt, B. 2019. Exploration of NO2 and PM2.5 air pollution and mental health problems using high-resolution data in London-based children from a UK longitudinal cohort study. *Psych. Res.*, 272: 8-17.
- Shoemaker, D.A., BenDor, T.K. and Meentemeyer, R.K. 2019. Anticipating trade-offs between urban patterns and ecosystem service production:

- Scenario analyses of sprawl alternatives for a rapidly urbanizing region. *Comp. Environ. Urban Syst.*, 74: 114-125.
- Sicard, P., Serra, R. and Rossello, P. 2016. Spatiotemporal trends in ground-level ozone concentrations and metrics in France over the time period 1999-2012. *Environ. Res.*, 149: 122-144.
- Tang, G., Chao, N. and Wang, Y. 2016. Vehicular emissions in China in 2006 and 2010. *J. Environ. Sci.*, 48: 179-192.
- Wang, J., Zhang, M. and Liu, J. 2019. Using a targeted ecopharma co-vigilance intervention to control antibiotic pollution in a rural aquatic environment. *Sci. Tot. Environ.*, 696: 134007.
- Wang, L., Yu, C. and Liu, Y. 2016. Lung cancer mortality trends in China from 1988 to 2013: New challenges and opportunities for the government. *Int. J. Environ. Res. Pub. Health*, 13(11): 1052.
- Xin, Z., Ye, L. and Zhang, C. 2019. Application of export coefficient model and QUAL2K for water environmental management in a rural watershed. *Sustainability*, 11(21): 6022.
- Yahaya, I., Pokharel, K.P. and Alidu, A. 2018. Sustainable agricultural intensification practices and rural food security. The case of Northwestern Ghana. *Brit. Food J.*, 120(2): 468-482.
- Zhao, X., Li, Z. and Wang, D. 2019. Assessment of residents' total environmental exposure to heavy metals in China. *Sci. Rep.*, 9: 16386.





# Response Surface Optimization of Culture Conditions of *Microcystis* sp. to Enhance its Biomass Production and Explore its Potential as Antimicrobials

R. Kanimozhi\*, D. Arvind Prasath\*†, R. Dhandapani\*\* and Santhosh Sigamani\*\*

\*Medical Microbiology Laboratory, Department of Microbiology, School of Biosciences, Periyar University, Salem-636011, India

\*\*Fermentation Technology Laboratory, Department of Microbiology, School of Biosciences, Periyar University, Salem-636011, India

†Corresponding author: D. Arvind Prasath; [prasanthvi@periyaruniversity.ac.in](mailto:prasanthvi@periyaruniversity.ac.in)

Nat. Env. & Poll. Tech.  
Website: [www.neptjournal.com](http://www.neptjournal.com)

Received: 11-02-2022

Revised: 23-03-2022

Accepted: 07-04-2022

## Key Words:

Antioxidant  
Antimicrobial  
*Microcystis* sp.  
Optimization  
Biomass

## ABSTRACT

The menace of drug-resistant bacteria is an issue of global concern. The growth mechanism of the algae *Microcystis* sp. encompasses the capacity to upset bacterial pathogens, and this approach is explored in the study. *Microcystis* sp. biomass harnessing was optimized via DoE-RSM (Design of Experiment-Response Surface Methodology), and further, the in vitro antimicrobial abilities to counter the drug-tolerant microbes were considered. This investigation aimed to increase the biomass output via optimization of essential components of the media parameter like  $\text{NaNO}_3$ ,  $\text{K}_2\text{HPO}_4$ , and  $\text{MgSO}_4$  as the variables. A maximal biomass yield of  $262 \text{ mg.L}^{-1}$  was accomplished within the optimized conditions and the *Microcystis* sp. displayed notable antimicrobial action against *Staphylococcus aureus* and *Pseudomonas aeruginosa*. Hence the *Microcystis* sp. could be an ideal biocontrol agent to mitigate the drug-tolerant microbes. A partial sequencing was performed, and gene sequences were subject to BLAST at NCBI, and the microbial isolate was identified as *Microcystis aeruginosa*, and the accession number was also procured for this sequence submission as MT792731.1.

## INTRODUCTION

The photosynthetic and eukaryote microalgae flourish widely in the aquatic setting, irrespective of freshwater, marine, or polluted waters (Manner et al. 2017). Microalgae are acknowledged mostly as a sustainable resource that could be exploited and harnessed as bio-refineries to generate metabolites for food industries, nutraceuticals, and biomass has been extensively explored as a substrate in biofuel production (Pandey et al. 2019, Manikandan et al. 2021). Recent research publications have recognized microalgae as a potential source of bioremediation (Rempel et al. 2021). Many microalgae possess metabolites that can be used as antioxidants and antimicrobials (Elshobary et al. 2020, Falaise et al. 2016, Alsenani et al. 2020). Microalgae metabolites can be exploited using their biomass for the advance of unique antimicrobial agents, owing to their natural potency to mitigate other microorganisms found in the aquatic environment (Kim et al. 2012, Chanda et al. 2019).

Biofilms are complex matrix-network-structure generated by bacteria to counter various factors like antimicrobials, and stress signals and to augment their pathogenicity. The establishment of biofilm is the key attribute of pathogenic bacteria

encompassing multi-drug-resistant (MDR) and instigated  $1/3^{\text{rd}}$  of all biofilm-sourced infections occurring in humans (Manner et al. 2017). In this context, the US National Institutes of Health (NIH) have been befuddled by the appearance of MDR bacterial strains on a global level apprehension. *Staphylococcus aureus* and *Pseudomonas aeruginosa* are prominent bacteria thriving exclusively in biofilms, posing serious health risks and spreading infectious diseases to people in hospitals (Kannappan et al. 2017, Prabha et al. 2022). Researchers are trying to dwell deeper by exploring the antibiofilm amalgams from an assortment of resources like plants, mushrooms, nanoparticles, micro-macro algae, and other plant produces (Wang et al. 2020, Bin et al. 2012, Qzturk et al. 2020, Carneiro et al. 2017, Malaikozhundan et al. 2016). Furthermore, it was extensively reported in the literature that cyanobacteria (*Spirulina platensis* and *Oscillatoria subuliformis*) and microalgae (*Spirulina platensis*) could mitigate the MDR-bacteria (Boutin et al. 2019). Hence, bearing these actualities, this study attempted to isolate algae from freshwater and explore its potential in vitro as an antioxidant and antimicrobial against pathogenic bacteria which could cause severe drug-tolerant infections in humans.

## MATERIALS AND METHODS

### Sample Assemblage and Procurement of Microalgae

Algae comprising aquatic samples were gathered in sterile glass vials from dissimilar and diverse locations of the Nangavalli lake (11.75°N 77.88°E), Salem District, Tamil Nadu, India. The samples were transported to the lab and introduced to sterilized BG11-broth (Hi-Media, Mumbai, India) and nurtured at 28±2°C with the lighting of 54-67µmol photons.m<sup>-2</sup>.s<sup>-1</sup> by cool white 40 W fluorescent tubes, for a fortnight. After cultivation, algae were plated and isolated for identification and further inoculated in fresh BG11 broth medium for cultivation for 2 weeks; subsequently, the culture was centrifuged at 10,000 rpm, to collect the biomass, freeze-dried, and stored until further use (Koutra et al. 2019).

### Optimization Cyanobacteria Cultivation

The *Microcystis* sp. was cultivated using BG11-broth media to optimize biomass production (Yang et al. 2015, Ma et al. 2020). The key influences of RSM were used to enhance the interactions of three unlike factors at contrasting levels. The highest yield of biomass was attained by using the Box-Behnken design (BBD) of the RSM. The investigational design was articulated with 17 experimental runs. Table 1 describes the experimental parameters of NaNO<sub>3</sub> (100-1000 mg.L<sup>-1</sup>), K<sub>2</sub>HPO<sub>4</sub> (50-200 mg.L<sup>-1</sup>), and MgSO<sub>4</sub> (100-1000 mg.L<sup>-1</sup>) as the factors. The R<sup>2</sup> and ANOVA of the *Microcystis* biomass harnessed were considered as the response. The general arrangement of equation (1) is

$$Y = \beta_0 \sum \beta_i X_i + \sum \beta_i X_i \beta_{ij} + \sum X_i X_j \quad \dots(1)$$

Where, Y is the predicted response, β<sub>0</sub>, β<sub>i</sub>, and β<sub>ij</sub> are constant regression coefficients of the BBD model, and X<sub>i</sub> and X<sub>j</sub> stand for autonomous factors (Kanimozhi et al. 2021).

### Biomass Extraction

After the cultivation, biomass was gathered and dried for 5 days at 40°C- a measured quantity of biomass was suspended in a buffer and was sonicated via an ultra sonicator. The extracted batches were centrifuged at 7000 rpm for 10 min and then dried, the resultant pellets were used for in vitro antioxidant and antibiofilm activity (Tao et al. 2020).

### In Vitro Antimicrobial Action of *Microcystis* sp. Against Pathogenic Strains

The antimicrobial inhibitory action of the extracts (20-250 µg.well<sup>-1</sup>) was arrived at as per the procedure described by Frassinetti et al. (2020). *Staphylococcus aureus* and *Pseudomonas aeruginosa* were incubated at 37°C for 24 h in 200 µL of trypticase soy broth (TSB) placed in 96-well-plates. After 24 h, the 96-well-plates were washed thrice with PBS,

and dried and stained with 0.1% crystal violet for 20min. The microtitre plate was washed in sterile PBS and allowed to dry at 60°C for 1 h. The biofilm formation in the plate was assessed by introducing 30% acetic acid exposed for 15 min and the OD (optical density) was measured at 595nm using a plate reader (Bazargani & Rohloff 2016).

The % inhibition was premeditated by the formula,

$$\text{Inhibition (\%)} = [\text{Control OD} - \text{Test OD} / \text{Control OD}] \times 100$$

### Thin Layer Chromatography

Various fractions of biomass extract were scrutinized via thin-layer chromatographic (TLC) plate-silica gel coated to quantify with diverse solvent systems. The chromatograms were visualized under white light, and the spots were measured for RF values. The homologous restriction factor (hRf) of the diverse spots was calculated (Venkatesh et al. 2017).

## RESULTS AND DISCUSSION

### Evaluating the Significant Nutrient Factors for Biomass Production Using Box-Behnken Design

The *Microcystis* sp. biomass output has to be maximized to bring down the production cost and procure a maximal quantity of the extract for scaled-up applications. Hence due to the requirement to optimize the media factors to extend

Table 1: RSM design to optimize the media components.

Run	A: NaNO <sub>3</sub> [mg.L <sup>-1</sup> ]	B: K <sub>2</sub> HPO [mg.L <sup>-1</sup> ]	C: MgSO <sub>4</sub> [mg.L <sup>-1</sup> ]	Biomass [g.L <sup>-1</sup> ]
1	100	200	550	1.88
2	550	125	550	2.29
3	1000	200	550	2.49
4	550	125	550	2.29
5	550	125	550	2.29
6	100	125	100	1.99
7	1000	125	1000	2.4
8	1000	50	550	2.38
9	100	50	550	1.65
10	550	125	550	1.88
11	550	200	1000	1.5
12	550	50	100	1.66
13	550	50	1000	1.65
14	550	200	100	2.14
15	100	125	1000	1.8
16	550	125	550	2.34
17	1000	125	100	2.62

the overall yield, it was decided to conduct 17 experimental runs for the media components NaNO<sub>3</sub> (100-1000 mg.L<sup>-1</sup>), K<sub>2</sub>HPO<sub>4</sub> (50-200 mg.L<sup>-1</sup>), and MgSO<sub>4</sub> (100-1000 mg.L<sup>-1</sup>). The factors' optimal range arrived at 1000 mg.L<sup>-1</sup> for NaNO<sub>3</sub>, 125mg.L<sup>-1</sup> for K<sub>2</sub>HPO<sub>4</sub>, and 100mg.L<sup>-1</sup> for MgSO<sub>4</sub>, a maximal biomass yield of 2.62 g.L<sup>-1</sup> was achieved. An independent run was carried out to validate the optimized concentration of the three media components.

The ANOVA results projected the factor A-NaNO<sub>3</sub> as the most influencing and significant variable among the 3 variables [based on the F-values and P-values (37.67 and 0.0005) significant at P 0.01 (99 percentile)], followed by B-MgSO<sub>4</sub> (6.41, 0.039) significant at P 0.05 (95 percentile). The influence of C-KH<sub>2</sub>PO<sub>4</sub> impactfully interacted with that of MgSO<sub>4</sub> (BC) (significant at P 0.05). The interaction of NaNO<sub>3</sub>, KH<sub>2</sub>PO<sub>4</sub>, and MgSO<sub>4</sub> (A<sup>2</sup>, B<sup>2</sup> and C<sup>2</sup>) was significant, but A<sup>2</sup> and C<sup>2</sup> were at P 0.05, while B<sup>2</sup> was at P 0.01. The interaction of AB (NaNO<sub>3</sub>-KH<sub>2</sub>PO<sub>4</sub>) and AC (NaNO<sub>3</sub>-MgSO<sub>4</sub>) was significant at the 91 percentile (Table 2).

The role of F-values and P-values to glen the prominent factors in RSM has been explored extensively in the literature via ANOVA in DoE-RSM to design a model for optimization of parameters for *Microcystis aeruginosa* (Kirrolia et al. 2014, El-Mekkawi et al. 2020). A Quadratic equation output for the optimized condition was derived from RSM (eq. 2)

$$\text{Biomass} = 2.218 + (0.32125*A) + (0.08375*B) + (-0.1325*C) + (-0.03*AB) + (-0.0075*AC) + (-0.1575*BC) + (0.1735*A^2) + (-0.2915*B^2) + (-0.189*C^2) \dots(2)$$

From the above equation, it can be elucidated that both NaNO<sub>3</sub> and KH<sub>2</sub>PO<sub>4</sub> had a positive impact on the biomass

yield, whereas MgSO<sub>4</sub>, the interaction of NaNO<sub>3</sub> with KH<sub>2</sub>PO<sub>4</sub> (AC), the interaction of NaNO<sub>3</sub> with MgSO<sub>4</sub> (AC), and interaction of KH<sub>2</sub>PO<sub>4</sub> with MgSO<sub>4</sub> (BC) had slightly negative impact on the yield, irrespective of their overall significant probabilistic values. A<sup>2</sup> also had a positive impact contrary to B<sup>2</sup> and C<sup>2</sup> biomass yield (Srinivasan et al. 2019, Tao et al. 2020).

The half-normal plot of predicted versus actual (Fig. 1) showed good congruity and correlation between the two, implying that the design was sound and can be replicated or

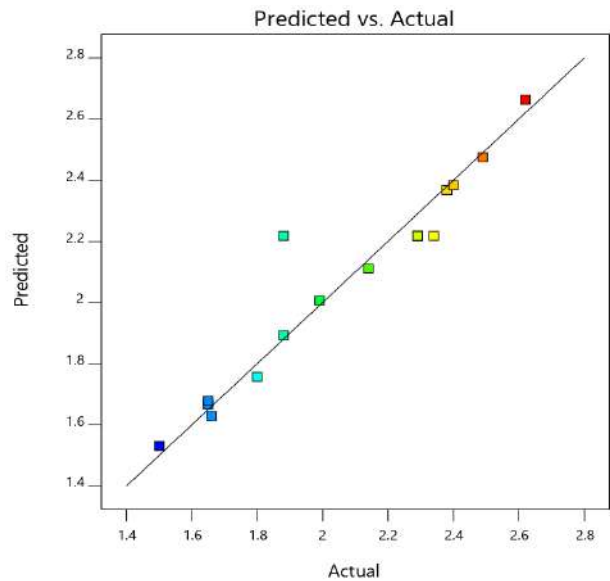


Fig. 1: Half-Normal plot of predicted with actual biomass values.

Table 2: ANOVA of the Quadratic model.

Source	Sum of Squares	df	Mean Square	F-value	p-value	
Model	1.75	9	0.1945	8.88	0.0044	significant
A-NaNO <sub>3</sub>	0.8256	1	0.8256	37.67	0.0005	
B-K <sub>2</sub> HPO <sub>4</sub>	0.0561	1	0.0561	2.56	0.1536	
C-MgSO <sub>4</sub>	0.1405	1	0.1405	6.41	0.0391	
AB	0.0036	1	0.0036	0.1643	0.6974	
AC	0.0002	1	0.0002	0.0103	0.9221	
BC	0.0992	1	0.0992	4.53	0.0709	
A <sup>2</sup>	0.1267	1	0.1267	5.78	0.0471	
B <sup>2</sup>	0.3578	1	0.3578	16.33	0.0049	
C <sup>2</sup>	0.1504	1	0.1504	6.86	0.0344	
Residual	0.1534	7	0.0219			
Lack of Fit	0.0087	3	0.0029	0.0804	0.9672	not significant
Pure Error	0.1447	4	0.0362			
Cor Total	1.90	16				

scaled up using the optimal conditions obtained at the end of the 17 experimental runs. The 3D plot figure (Fig. 2a) shows the interaction of A with B and can be used to compare at varying concentrations of  $\text{NaNO}_3$  and  $\text{KH}_2\text{PO}_4$ ; the contour plots were saddle-point output with a slight inclination towards rising-ridge more towards  $\text{KH}_2\text{PO}_4$  interaction with  $\text{NaNO}_3$  denoting the need for tweaking the concentration range of  $\text{KH}_2\text{PO}_4$ . Akin to the previous figure, the 3D plot figure (Fig. 2b) also has a saddle-point with a rising ridge at the  $\text{NaNO}_3$  axis, implying the need to configure the  $\text{MgSO}_4$

dosage range. Fig. 2c has a mound-type contour, which is the desired outcome, and the interactive influence of  $\text{KH}_2\text{PO}_4$  and  $\text{MgSO}_4$  dosage concentration had an impactful influence on the biomass yield. Aboim et al. (2019) explored the optimization of illuminated light intensity and  $\text{NaNO}_3$  concentration for 4 cyanobacteria (including *Microcystis aeruginosa*) to enhance biomass production, where their results elucidated the importance of nitrogen source to gain a notable increase in biomass yield (Aboim et al. 2019, Kanimozhi et al. 2021).

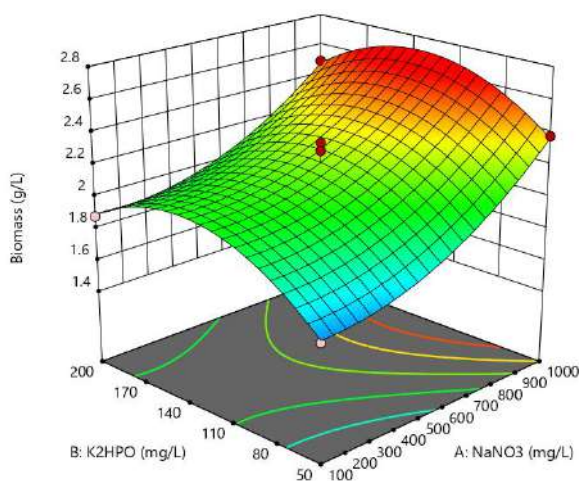


Fig. 2a: 3D contour-plot of  $\text{NaNO}_3$  and  $\text{KH}_2\text{PO}_4$  dose concentrations on the biomass yield.

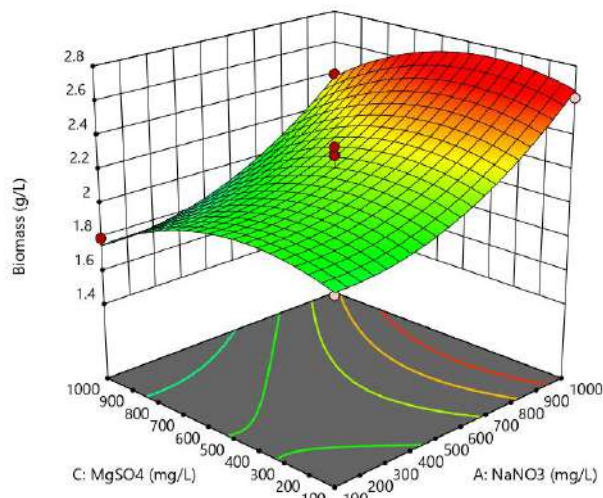


Fig. 2b: 3D contour-plot of  $\text{NaNO}_3$ ,  $\text{MgSO}_4$  dose concentrations on the biomass yield.

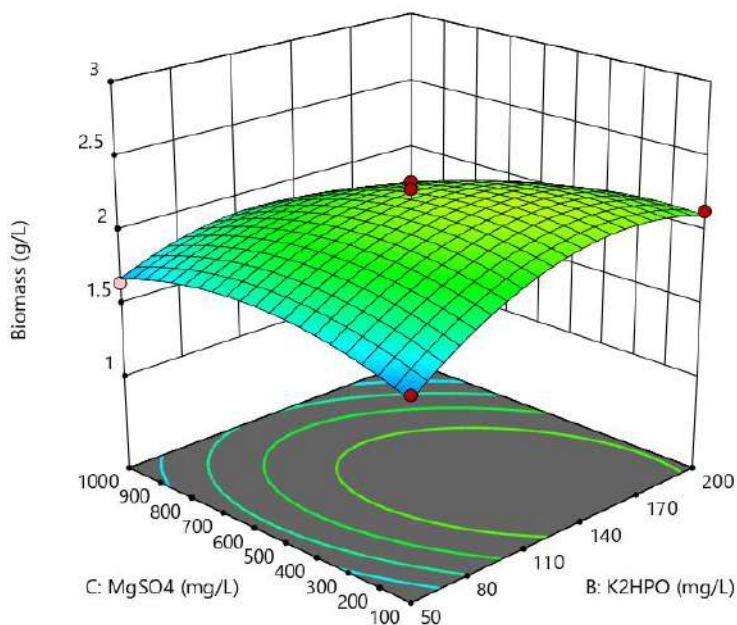


Fig. 2c: 3D contour-plot of  $\text{KH}_2\text{PO}_4$  and  $\text{MgSO}_4$  dose concentrations on the biomass yield.

### Sequential Solvent Extraction of *Microcystis* Antimicrobials

The efficiency of two potent extracts of *Microcystis* sp. was tested against biofilm-forming bacteria. For estimating the minimum biofilm concentration, two controls (positive and negative) were used. Phenol serves as a positive control, and 10% DMSO serves as a negative control. Both extracts were highly effective against *S. aureus*, *E. coli*, and *B. cereus* at low concentrations compared to *P. aeruginosa*. The anti-biofilm results performed in different concentrations of two extracts revealed higher inhibition against *S. aureus* and *B. cereus* at low concentrations of 50-75  $\mu\text{g}\cdot\text{well}^{-1}$ . If the optical density value was less than 0.1, it showed 90% of biofilm inhibition.

In the chloroform extract, more inhibition of less than 0.1 optical density was recorded against *S. aureus* and *B. cereus* at the concentration of 125  $\mu\text{g}\cdot 200\ \mu\text{L}^{-1}$ , whereas at 100  $\mu\text{g}$  was observed against *E. coli*. The biofilm formed by *P. aeruginosa* could not be reduced to 0.1 O.D value even at the highest concentration in 250  $\mu\text{g}\cdot\text{well}^{-1}$  (0.203 O.D), and positive control with 100  $\mu\text{g}\cdot\text{mL}^{-1}$  was effective in biofilm removal with optical density ranging from 0.17 to 0.83 (Table 3a).

In the hexane extract, more inhibition of less than 0.1 optical density was recorded against *S. aureus* at 225  $\mu\text{g}\cdot 200\ \mu\text{L}^{-1}$  and *E. coli* at the concentration of 250  $\mu\text{g}\cdot 200\ \mu\text{L}^{-1}$ . The biofilm formed by *P. aeruginosa* could not be reduced to a 0.1 O.D value even at the highest concentration of 250  $\mu\text{g}\cdot\text{well}^{-1}$  (0.402 O.D), and positive control with 100  $\mu\text{g}\cdot\text{mL}^{-1}$

was effective in biofilm removal with optical density ranging from 0.22 to 1.27 (Table 3b).

The extraction of *Microcystis* sp., by two non-polar (Hexane, Chloroform), two mid polar (Ethyl acetate, Acetone), and two polar (Methanol, Ethanol) solvents gave a yield of approximately 10-40 mg. The crude extracts were stored at 4°C for further use (Venkatesh et al. 2017).

#### The Anti-Biofilm-Forming Activity of the Extracts

All the extracts were tested against the biofilm-forming bacteria using an ELISA titer plate, and it was found that chloroform and hexane extracts were potent against these two bacteria (*Bacillus* sp., *Pseudomonas* sp.) (Fig 3a). Different concentration of the potent crude was tested against the two biofilm-forming bacteria. The absorbance was taken, and it was found that after the biofilm was formed, the titre plate was turbid with a higher absorbance value. Upon adding the extracts and the following treatment, the absorbance slowly decreased with an increasing dose of extract. The adherent cells were removed by the tested crude extracts showing the ability of compounds to alleviate the formation of the film on the surface after treatment with the different concentrations of the potent chloroform extracts and hexane extracts against bacterial pathogens. The treated wells were washed with deionized water, and their absorbance was taken at 570  $\text{nm}^{-1}$ . The biofilm formation gradually decreased with an increase in potent extract concentration (Fig. 3b).

Alsenani et al. (2020) explored three microalgae, *Isochrysis galbana*, *Scenedesmus* sp. NT8c, and *Chlorella* sp.

Table 3a. Effect of varying concentrations of chloroform extracts on bacterial biofilm formation.

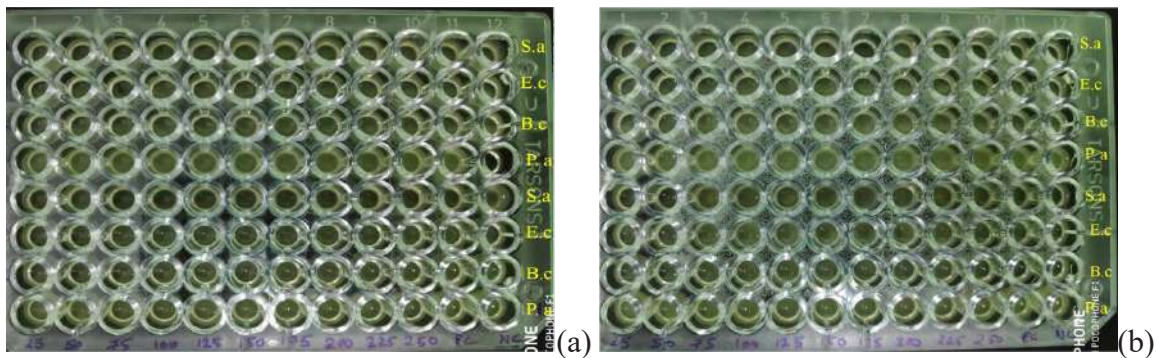
Name of Bacteria	The concentration of the chloroform extracts in $\mu\text{g}/\text{well}$										PC	NC
	20	50	75	100	125	150	175	200	225	250		
<i>E. coli</i>	0.12	0.20	0.17	0.12	0.07	0.03	0.04	0.03	0.04	0.03	0.17	1.19
<i>B. subtilis</i>	0.40	0.19	0.13	0.06	0.07	0.06	0.05	0.04	0.02	0.01	0.23	1.16
<i>P. aeruginosa</i>	0.26	0.18	0.13	0.11	0.09	0.06	0.05	0.06	0.05	0.05	0.24	1.20
<i>P. aeruginosa</i>	1.10	1.08	1.04	0.88	0.7	0.48	0.38	0.34	0.24	0.23	0.83	1.15

PC- Positive control (phenol- 100 $\mu\text{g}/\text{ml}$ ), NC- Negative control (10% DMSO) \*mean of two replicates performed (n=2)

Table 3b. Effect of varying concentrations of hexane extracts on bacterial biofilm formation.

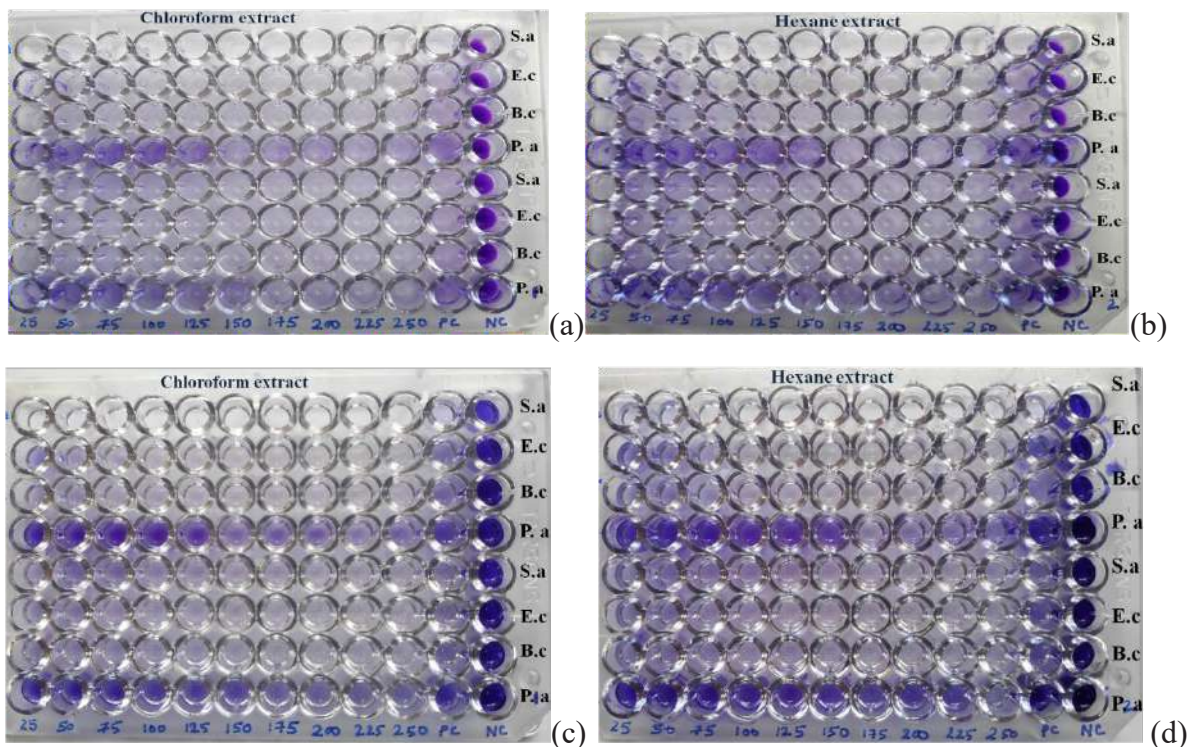
Name of Bacteria	The concentration of the chloroform extracts in $\mu\text{g}/\text{well}$										PC	NC
	20	50	75	100	125	150	175	200	225	250		
<i>E. coli</i>	0.31	0.34	0.21	0.21	0.14	0.13	0.13	0.12	0.10	0.07	0.22	1.28
<i>B. subtilis</i>	0.61	0.41	0.30	0.21	0.18	0.16	0.13	0.12	0.11	0.10	0.58	1.26
<i>B. subtilis</i>	0.43	0.40	0.30	0.22	0.19	0.17	0.16	0.16	0.15	0.11	0.29	1.27
<i>P. aeruginosa</i>	1.24	1.25	1.22	1.13	1.11	0.91	0.68	0.60	0.56	0.402	1.27	1.28

PC- Positive control (phenol- 100 $\mu\text{g}\cdot\text{mL}^{-1}$ ), NC- Negative control (10% DMSO) \*mean of two replicates performed (n=2)



[(a) Chloroform extract (b) Hexane extract (concentration: 25-250  $\mu\text{g/ml}$ ); S.a- *Staphylococcus aureus*, E.c-*Escherichia coli*, B.c-*Bacillus subtilis*, P.a- *Pseudomonas aeruginosa*, PC- positive control and NC- negative control.]

Fig. 3a: Growth of bacteria in 96 well microtiter plates (Tryptone soy broth) after 24 h incubation.



(96 well microtiter plates (a,b) Removal of biofilm after treating with extracts (c,d) Biofilm dissolution upon adding 30% acetic acid; S.a-*Staphylococcus aureus*, E.c-*Escherichia coli*, B.c-*Bacillus cereus*, P.a-*Pseudomonas aeruginosa*, PC- positive control and NC- negative control.)

Fig. 3b: Antibiofilm activity of *Microcystis* sp. potent extracts against pathogenic bacteria.

FN1 for their antimicrobial activity, and the result showed all three species performing well (inhibitory action) against gram-positive bacteria *S. aureus*. A comprehensive review of the antimicrobial Compounds from Microalgae to mitigate Human Pathogens by Falaise et al. (2016) provides ample examples of the antimicrobial action of microalgal extracts (Alsenani et al. 2020, Falaise et al. 2016, Abazari et al. 2013).

### Thin Layer Chromatography of the Potent Solvent Extract

The TLC analysis of the potent chlorophyll extract showed a total of five visible bands on the aluminum-coated sheets (Fig. 4). The separation was tested by Hexane: Ethyl acetate solvent system and different ratios of solvent were tested to

find the best ratio (4:1) and (3.5:1.5) for separation of all the compounds. The RF value of the separated bands was calculated for (4:1) and found to be 0.282 for band 1, 0.564 for band 2, 0.667 for band 3, 0.743 for band 4, and 0.820 for band 5. The RF value of the separated bands was calculated for (3.5:1.5) and found to be 0.3 for band 1, 0.7 for band 2, 0.8 for band 3, 0.875 for band 4, and 0.975 for band 5. The microalgal extract has been elucidated via TLC (Fig. 4).

A review article on the “Microalgae Biomolecules Extraction, Separation and Purification Methods” by Corrêa et al. (2021) emphasizes the role of TLC as an appropriate

technique with the least cost implications to find the basic components of microbial extracts (Corrêa et al. 2021).

### Sequence Submission and Procurement of Accession Number from NCBI

A partial sequence of the isolate involved in this current study was performed, and the gene sequences were subject to BLAST at NCBI to detect matches with existing reference sequences in the database, and a phylogenetic tree was constructed (Fig 5). Accession number was also procured for this sequence submission - MT792731.1 (<https://www.ncbi>).

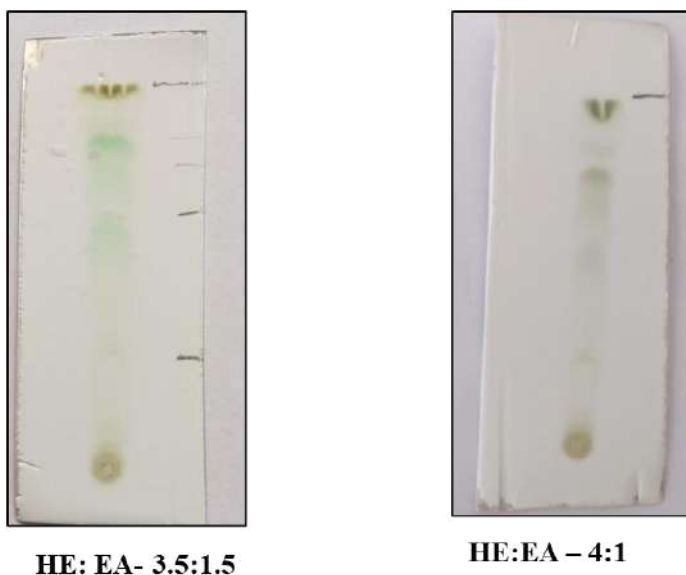


Fig. 4: Thin layer chromatography of Chloroform extract of *Microcystis* sp., [Hexane: Ethyl Acetate] a) 3.5:1.5 b) 4:1

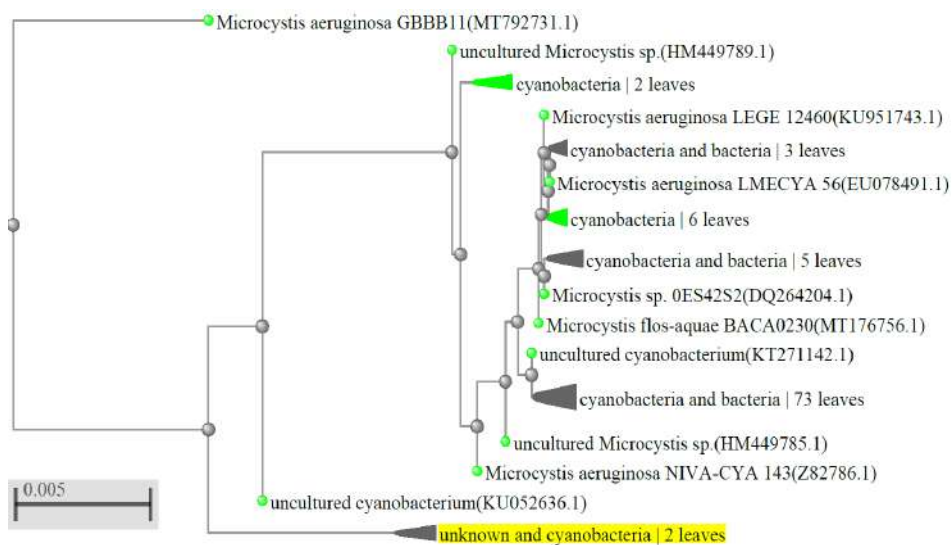


Fig. 5: Phylogenetic tree with NCBI accession number of *Microcystis* sp.

nlm.nih.gov/nucore/MT792731.1). The microalga has been identified as *Microcystis aeruginosa*.

## CONCLUSION

After being isolated from freshwater, *Microcystis* sp. was previously shown to have antibacterial properties. When its solvent extract was tested for antimicrobial activity against *Staphylococcus aureus* and *Pseudomonas aeruginosa*, it was found to be effective against both. This study validates the purpose of *Microcystis aeruginosa* to produce effective antimicrobials that could control microbial pathogens via its biomass extracts. To further explore the feasibility of this concept in a scaled-up operation, it is paramount that the biomass yield has to be maximized, and hence the media factors like  $\text{NaNO}_3$ ,  $\text{K}_2\text{HPO}_4$ , and  $\text{MgSO}_4$  were optimized via RSM-DoE to maximize the biomass yield.

## ACKNOWLEDGMENTS

The authors are thankful to Periyar University and the Department of Microbiology and all those who had encouraged and played a part in the fulfillment of this paper.

## REFERENCES

- Abazari, M., Zarrini, G. and Rasooli, I. 2013. Antimicrobial potentials of *Leptolyngbya* sp. and its synergistic effects with antibiotics. *Jundishapur J. Microbiol.*, 6: e6536.
- Aboim, J.B., Oliveira, D.T., Mescouto, V.A., Dos Reis, A.S., da Rocha Filho, G.N., Santos, A.V., Xavier, L.P., Santos, A.S., Gonçalves, E.C. and do Nascimento, L. 2019. Optimization of light intensity and  $\text{NaNO}_3$  concentration in amazon cyanobacteria cultivation to produce biodiesel. *Molecules*, 24: 2326.
- Alsenani, F., Tupally, K.R., Chua, E.T., Eltanahy, E., Alsufyani, H., Parekh, H.S. and Schenk, P.M. 2020. Evaluation of microalgae and cyanobacteria as potential sources of antimicrobial compounds. *Saudi Pharmaceut. J.*, 28:1834-1841.
- Bazargani, M. and Rohloff, J. 2016. Antibiofilm activity of essential oils and plant extracts against *Staphylococcus aureus* and *Escherichia coli* biofilms. *Food Control*, 61: 156-164.
- Bin, L., Wei, L., Xiaohong, C., Mei, J. and Mingsheng, D. 2012. In vitro antibiofilm activity of the melanin from *Auricularia auricula*, an edible jelly mushroom. *Ann. Microb.*, 62: 1523-1530.
- Boutin, R., Munnier, E., Renaudeau, N., Girardot, M., Pinault, M., Chevalier, S., Chourpa, I., Clément-Larosière, B., Imbert, C. and Boudesocque-Delaye, L. 2019. *Spirulina platensis* sustainable lipid extracts in alginate-based nanocarriers: An algal approach against biofilms. *Algal Res.*, 37: 160-168.
- Carneiro, R.F., Lima Jr, P.H.P., Chaves, R.P., Pereira, R., Pereira, A.L., Vasconcelos, M.A., Pinheiro, U., Teixeira, E.H., Nagano, C.S. and Sampaio, A.H. 2017. Isolation, biochemical characterization and antibiofilm effect of a lectin from the marine sponge *Aplysina lactuca*. *Int. J. Biol. Macromol.*, 99: 213-222.
- Chanda, M., Merghoub, N. and Arroussi, H. 2019. Microalgae polysaccharides: the new sustainable bioactive products for the development of plant biostimulants. *World J. Microbiol. Biotechnol.*, 35: 177.
- Corrêa, P.S., Morais Jr, W.G., Martins, A.A., Caetano, N.S. and Mata, T.M. 2021. Microalgae biomolecules: Extraction, separation and purification methods. *Processes*, 9: 10.
- El-Mekkawi, S.A., El-Ibiari, N.N., El-Arady, O.A., Abdelmonem, N.M., Elahwany, A.H., Abadir, M.F. and Ismail, I.M. 2020. Optimization of cultivation conditions for *Microcystis aeruginosa* for biodiesel production using response surface methodology. *Bull. Natl. Res. Cent.*, 44: 6.
- Elshobary, M.E., El-Shenody, R.A., Ashour, M., Zabed, H.M. and Qi, X. 2020. Antimicrobial and antioxidant characterization of bioactive components from *Chlorococcum minutum*. *Food Biosci.*, 35: 100567.
- Falaise, C., François, C., Travers, M.A., Morga, B., Haure, J., Tremblay, R., Turcotte, F., Pasetto, P., Gastineau, R., Hardivillier, Y., Leignel, V. and Mouget, J.L. 2016. Antimicrobial compounds from eukaryotic microalgae against human pathogens and diseases in aquaculture. *Marine Drugs*, 14: 159.
- Frassinetti, S., Gabriele, M., Moccia, E., Longo, V. and Di Gioia, D. 2020. Antimicrobial and antibiofilm activity of *Cannabis sativa* L. seeds extracts against *Staphylococcus aureus* and growth effects on probiotic *Lactobacillus* sp. *LWT Food Sci. Technol.*, 124: 109149.
- Kannappan, A., Gowrishankar, S., Srinivasan, R., Pandian, S.K. and Ravi, A.V. 2017. Antibiofilm activity of *Vetiveria zizanioides* root extract against methicillin-resistant *Staphylococcus aureus*. *Microb. Path.*, 110: 313-324.
- Kanimozhi, R., Arvind Prasad, D., Dhandapani, R. and Santhosh, S. 2021. Optimization of *Chlorella* culture conditions with response surface methodology to increase biomass. *Nat. Environ. Pollut. Technol.*, 20(5): 2111-2116.
- Kim, W., Park, J.M., Gim, G.H., Jeong, S.H., Kang, C.M., Kim, D.J. and Kim, S.W. 2012. Optimization of culture conditions and comparison of biomass productivity of three green algae. *Bioprocess Biosyst. Eng.*, 35(1): 19-27.
- Kirrolia, A., Bishnoi, N.R. and Singh, R. 2014. Response surface methodology as a decision-making tool for optimization of culture conditions of green microalgae *Chlorella* spp. for biodiesel production. *Ann. Microbiol.*, 64: 1133-1147.
- Koutra, E., Kopsahelis, A., Maltezou, M., Grammatikopoulos, G. and Kornaros, M. 2019. Effect of organic carbon and nutrient supplementation on the digestate-grown microalga *Parachlorella kessleri*. *Bioresour. Technol.*, 294: 122232.
- Ma, C., Yu, H., Gao, Y., Xu, W., Xu, T., Wang, L. and Xu, J. 2020. Operation parameters optimization of a hybrid dead-end/cross-flow forward osmosis system for microalgae dewatering by response surface methodology. *Process Safety Environ. Prot.*, 143: 14-24.
- Malaikozhundan, B., Vaseeharan, B., Vijayakumar, S., Sudhakaran, R., Gobi, N. and Shanthini, G. 2016. Antibacterial and antibiofilm assessment of *Momordica charantia* fruit extract coated silver nanoparticle. *Biocatal. Agric. Biotechnol.*, 8: 189-196.
- Manikandan, A., Suresh Babu, P., Shyamalagowri, S., Kamaraj, M., Muthukumar, P. and Aravind, J. 2021. The emerging role of microalgae in heavy metal bioremediation. *J. Basic Microbiol.*, 12: 93. doi:10.1002/jobm.202100363
- Manner, S., Goeres, D.M., Skogman, M., Vuorela, P. and Fallarero, A. 2017. Prevention of *Staphylococcus aureus* biofilm formation by antibiotics in 96-Microtiter well plates and drip flow reactors: Critical factors influencing outcomes. *Sci. Rep.*, 7: 43854.
- Pandey, A., Srivastava, S. and Kumar, S. 2019. Isolation screening and comprehensive characterization of candidate microalgae for biofuel feedstock production and dairy effluent treatment: A sustainable approach. *Biore-sour. Technol.*, 293: 121998.
- Prabha, S., Vijay, A.K., Paul, R.R. and George, B. 2022. Cyanobacterial biorefinery: Towards economic feasibility through the maximum valorization of biomass. *Sci. Tot. Environ.*, 152795.
- Qzturk, B.Y., Gürsu, B.Y. and Da, . 2020. Antibiofilm and antimicrobial activities of green synthesized silver nanoparticles using marine red algae *Gelidium corneum*. *Process Biochem.*, 89: 208-219.
- Rempel, A., Gutkoski, J.P., Nazari, M.T., Biolchi, G.N., Cavanhi, V., Treichel, H. and Colla, L.M. 2021. Current advances in microalgae-based



- bioremediation and other technologies for emerging contaminants treatment. *Sci. Total Environ.*, 772: 144918.
- Srinivasan, P., Selvankumar, T., Kamala-Kannan, S., Mythili. R., Sengottaiyan, A., Govarthanam, M., Senthilkumar, B. and Selvam, K. 2019. Production and purification of laccase by *Bacillus* sp. using millet husks and its pesticide degradation application. *3 Biotech*, 9: 396.
- Tao, S., Wang, S., Song, L and Gan, N. 2020. Understanding the differences in the growth and toxin production of anatoxin-producing *Cuspidothrix issatschenkoi* cultured with inorganic and organic N sources from a new perspective: carbon/nitrogen metabolic balance. *Toxins*, 12: 724.
- Venkatesh, U., Javarasetty, C. and Murari, S.K. 2017. Purification and fractional analysis of a methanolic extract of *Wedelia trilobata* possessing apoptotic and anti-leukemic activity. *Afr. J. Tradit. Compl. Altern. Med.*, 14: 167-174.
- Wang, E., Li, Y., Lubamba Maguy, B., Lou, Z., Wang, H., Zhao, W. and Chen, X. 2020. Separation and enrichment of phenolics improved the antibiofilm and antibacterial activity of the fractions from *Citrus medica* L. var. *sarcodactylis* in vitro and tofu. *Food Chem.*, 294: 533-538.
- Yang, C.C., Wen, R., Shen, C. and Yao, DJ. 2015. Using a microfluidic gradient generator to characterize BG-11 medium for the growth of cyanobacteria *Synechococcus elongatus* PCC7942. *Micromachines*, 6: 1755-1767.





# Optimization of Influential Parameters for the Degradation of Metronidazole Contained in Aquaculture Effluent via Sonocatalytic Process: Kinetics and Mechanism

O.H. Aremu\*†, C.O. Akintayo\*, S.M. Nelana\*\*, M.J. Klink\*\* and O.S. Ayanda\*

\*Department of Industrial Chemistry, Federal University Oye-Ekiti, PMB 373, Oye-Ekiti, Nigeria

\*\*Department of Chemistry, Vaal University of Technology, Vanderbijlpark, South Africa

†Corresponding author: O.H. Aremu; omololaaremu21@gmail.com

Nat. Env. & Poll. Tech.  
Website: [www.neptjournal.com](http://www.neptjournal.com)

Received: 04-04-2022

Revised: 20-05-2022

Accepted: 22-05-2022

## Key Words:

Ultrasound

Sonocatalytic process

Aquaculture effluent

Metronidazole

Advanced oxidation process

## ABSTRACT

This study examined the synthesis of a viable catalyst for the degradation of metronidazole contained in aquaculture effluent. Zinc oxide nanoparticles (n-ZnO) were synthesized via the precipitation method and calcined at 500°C in a muffle furnace to enhance the degradability properties. The morphology showed a hexagonal structure with an average particle size of 71.48 nm and the elemental composition showed a higher weight percent of 59.15% for zinc and 21.65% for oxygen. The FTIR confirms the vibrational characteristic mode of the Zn-O band at 427.21cm<sup>-1</sup>. The XRD showed a good crystallinity and the BET surface area was 8.58 m<sup>2</sup>.g<sup>-1</sup> which showed that the n-ZnO possesses more active sites that can remove pollutants from wastewater. However, no studies have been done on the removal of MNZ in aquaculture effluent. The kinetics followed pseudo-second-order kinetics and the Langmuir-Hinshelwood model best fit the degradation process with R<sup>2</sup>, K<sub>c</sub>, and K<sub>LH</sub> values of 0.96781, 1.486 × 10<sup>-1</sup> mg. Lmin<sup>-1</sup> and 8.790 × 10<sup>-2</sup> (L.mg<sup>-1</sup>). Under the influential parameters, the percentage COD removal achieved for MNZ in aquaculture effluent was 62.6%, 89.8%, and 98.5% of MNZ at 20% ultrasonic amplitude, 5 mL 2% H<sub>2</sub>O<sub>2</sub> and 0.02g n-ZnO within 60 min sonication time for US only, US/n-ZnO and US/n-ZnO/H<sub>2</sub>O<sub>2</sub> systems. Hence, MNZ contained in aquaculture effluent can best be degraded with the synergetic effect of the US/n-ZnO/H<sub>2</sub>O<sub>2</sub> system.

## INTRODUCTION

Pharmaceuticals and personal care products are evolving aquatic pollutants that are on the increase in the environment due to their active use (Calamari et al. 2003). The stored-up pharmaceuticals in the aquatic environment find their way via wastewater treatment plants, sewage sludge, pharmaceutical industries, and households (Petrie et al. 2015) as a result of extreme applications by humans (Felis et al. 2020). Almost 95% of pharmaceuticals are discharged from the body into the environment which has a toxic impact on the ecosystem (Habibi et al. 2018, Jury et al. 2010). Generally, antibiotics are used as feed condiments, growth promoters (Manyi-Loh et al. 2018), and therapeutics in the production of livestock and aquatic animals (Landers et al. 2012).

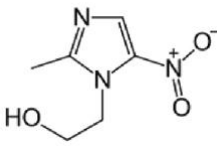
Metronidazole (MNZ) is one of the antibiotics consumed for the treatment of infections. It belongs to the class of compound nitroimidazole, it is used to treat infections caused by bacteria and protozoa. It is active against *Trichomonas vaginalis* and *Balantidium coli* (Das & Dhua 2014). The high solubility and stability of metronidazole in water have

led to its availability in the environment, non-biodegradability, and contribution to environmental pollution as a result of its excessive use (Yang et al. 2019). The buildup of metronidazole in the body is capable of leading to cancer and mutations which invariably promotes toxic substances in the body system and when metabolism takes place, the environment becomes toxic (Cunningham 2004). Table 1 shows the properties of metronidazole.

The solubility of MNZ has made it difficult to be removed from the aquatic environment via conventional treatment and activated carbon (Forouzesh et al. 2018). Advanced oxidation processes (AOPs) are innovative technologically in the treatment of wastewater through the generation of hydroxyl radicals that are capable of removing organic contaminants. AOPs have been integrated using ozonation, photocatalysis (Balarak et al. 2019), sono-Fenton, and electrochemical oxidation in the removal of MNZ in the aquatic environment.

Ultrasound is one of the advanced oxidation processes (AOPs) and is a technique that employs the generation of hydroxyl radicals that attacks the pollutants and mineralize to

Table 1: Properties of Metronidazole.

Structure	
Physical State	Crystalline solid powder
Molecular formulae	C <sub>6</sub> H <sub>9</sub> N <sub>3</sub> O <sub>3</sub>
Class	Nitroimidazole
Molecular weight	171.15 g.mol <sup>-1</sup>
Boiling point	405.4°C
Melting point	158-160°C
Synonyms	Flagyl
Color	White to pale yellow
Solubility	1g in 100 mL of water @ 20°C
Stability	Stable in air

CO<sub>2</sub> and H<sub>2</sub>O. Hydroxyl radicals (OH<sup>•</sup>) are powerful oxidants that do not produce secondary pollutants. Acoustic cavitation is the mechanism that ultrasound operates on; it involves the production of cavitation bubbles through sound energy at increased temperature and pressure which leads to the invention of active chemical oxidants (Ayanda et al. 2021).

Among all metal oxide catalysts, ZnO nanoparticles have proven to be as good catalysts due to their photocatalytic capacity, non-toxic nature, antimicrobial properties, the enlarged band gap of 3.37 eV, increased binding energy of 60 meV, easy synthesis, piezo and pyro-electric properties (Bian et al. 2017) have increased its wider applications. Different methods have been explored in the synthesis of zinc oxide nanoparticles, methods such as ultrasound, hydrothermal, green synthesis, electrochemical, precipitation, microwave, sol-gel, and chemical vapor deposition (Aremu et al. 2021). Studies have shown that there are fewer reports on the removal of metronidazole in aquaculture effluent using ultrasound, ultrasound/ H<sub>2</sub>O<sub>2</sub>, ultrasound/ZnO, and ultrasound/ZnO/ H<sub>2</sub>O<sub>2</sub> systems.

Hence, the objective of this research is to synthesize a non-toxic ZnO nanoparticle calcined at 500°C, characterize, and optimize the influential parameters on the degradation of metronidazole contained in aquaculture effluent via sonocatalytic process, and study the kinetics and mechanism

## MATERIALS AND METHODS

### Chemicals and Reagents

Metronidazole (MNZ) of 97% purity, ZnCl<sub>2</sub>, NaOH, and H<sub>2</sub>O<sub>2</sub> were purchased from Sigma Aldrich, USA. A 50 mg.L<sup>-1</sup>

of MNZ solution was prepared for the stock solution. Various working solutions were prepared from the stock solution. A pH meter (PHS-3C) was used to regulate the MNZ solution contained in the wastewater by adding 0.05M HCl or 0.05M NaOH solutions.

### Synthesis of n-ZnO

A 20 g of ZnCl<sub>2</sub> was weighed into 100 mL of de-ionized water in a 250 mL beaker. It was continuously stirred at a temperature of 90°C for 20 min with a magnetic stirrer. 50 mL of the ZnCl<sub>2</sub> solution was added to 0.6 M NaOH solution. The resultant mixture was filtered with a Whatman filter paper and washed thrice with deionized water to obtain the ZnO nanoparticles. The filtered sample was oven dried for 24 h at 75°C, calcined for 2 h in a muffle furnace at 500°C, and crushed to obtain fine ZnO nanoparticles.

### Characterization of n-ZnO

The morphology of the ZnO nanoparticles was examined using a scanning electron microscope (SEM; Phenon type Model: Pro X) and transmission electron microscope (TEM; Tecnai G<sup>2</sup> 20) at 100 nm. The elemental composition of the n-ZnO was quantitatively determined by electron dispersive spectroscopy (EDS), the crystallinity was investigated with X-ray diffraction (Siemens D8 Advance Bruker XRD) with CuK<sub>α</sub> radiation, the functional group was investigated with Fourier Transform Infrared Spectroscopy (FTIR; Perkin Elmer Spectrum Two<sup>TM</sup> Spectrometer) and the Brunauer Emmett and Teller (BET) surface area was investigated by a Tristar 3000 analyzer with N<sub>2</sub> adsorption at -196°C.

## Removal of MNZ

The removal of MNZ was investigated with ultrasound (US), US/n-ZnO, and a combined US/n-ZnO/H<sub>2</sub>O<sub>2</sub> system, respectively. At the end of the removal process, samples were taken and analyzed with a UV-visible spectrophotometer at a wavelength of 320 nm.

### Ultrasound

**Influence of ultrasonic amplitude and sonication time on the removal of MNZ:** Using different ultrasonic amplitudes (20-100%) and an ultrasonic frequency of 20 kHz, 50 mL of a 50 mg.L<sup>-1</sup> MNZ aqueous solution was processed in a 200 mL reactor for 20 to 60 minutes.

**Influence of H<sub>2</sub>O<sub>2</sub> concentration and sonication time on the removal of MNZ:** 5 mL of 1%, 2%, and 4% of H<sub>2</sub>O<sub>2</sub> were added in a 50 mL MNZ solution at varying sonication times (20-60 min), 60 % ultrasonic amplitude, and a frequency of 20 kHz.

**Influence of initial concentration of MNZ and sonication time on the removal of MNZ:** The influence of varying concentrations (3.125 mg.L<sup>-1</sup>-50 mg.L<sup>-1</sup>) was examined at sonication times (20-60 min), 60 % ultrasonic amplitude, and a frequency of 20 kHz.

**Influence of pH and sonication time on the removal of MNZ:** The influence of varying pH (2-10) was examined at sonication times (20-60 min), 60% amplitude, and a frequency of 20 kHz.

### Ultrasound/n-ZnO

**Influence of ultrasonic amplitude and sonication time on the removal of MNZ:** A 0.02 g of n-ZnO was added to 50 mL of 50 mg.L<sup>-1</sup> MNZ aqueous solution, sonicated at varying sonication times (20-60 min) and a frequency of 20 kHz.

**Influence of nanodosage and sonication time on the removal of MNZ:** 50 mL of 50 mg.L<sup>-1</sup> MNZ aqueous solution with the addition of 0.02–0.10 g of ZnO nanoparticles in a 200 mL reactor at an ultrasonic amplitude of 60% and ultrasonic frequency of 20 kHz within 20-60 mins.

**Influence of initial concentration and sonication time on the removal of MNZ:** A 0.06 g of n-ZnO was added to each of the varying concentrations of 50 mL of 50 mg.L<sup>-1</sup> MNZ aqueous solution at varying sonication times (20-60 min), 60% ultrasonic amplitude, and a frequency of 20 kHz.

**Influence of pH and sonication time on the removal of MNZ:** A 0.06 g of n-ZnO was added to each of the varying pH of 50 mL of 50 mg.L<sup>-1</sup> MNZ aqueous solution, sonicated at varying sonication times (20-60 min), 60% ultrasonic amplitude and a frequency of 20 kHz.

**Influence of H<sub>2</sub>O<sub>2</sub> concentration and sonication time on the removal of MNZ:** A 0.06 g of n-ZnO was added to each of the varying H<sub>2</sub>O<sub>2</sub> concentrations of 50 mL of 50 mg.L<sup>-1</sup> MNZ aqueous solution at varying sonication times (20-60 min), 60% ultrasonic amplitude, and a frequency of 20 kHz.

### Ultrasound/n-ZnO/H<sub>2</sub>O<sub>2</sub>

**Influence of ultrasonic amplitude and sonication time on the removal of MNZ:** A 0.06 g of n-ZnO and 5 mL of 1% H<sub>2</sub>O<sub>2</sub> were added to each of the varying amplitudes of 50 mL of 50 mg/L MNZ aqueous solution, sonicated at varying sonication times (20-60 min) and a frequency of 20 kHz.

**Influence of nanodosage and sonication time on the removal of MNZ:** 5 mL of 1% H<sub>2</sub>O<sub>2</sub> and each of 0.02-1.0 g of n-ZnO were added to 50 mL of 50 mg.L<sup>-1</sup> MNZ aqueous solution, sonicated at varying sonication time (20-60 min), 40% ultrasonic amplitude, and a frequency of 20 kHz.

**Influence of initial concentration of MNZ and sonication time on the removal of MNZ:** A 0.08 g of n-ZnO and 5 mL of 1% H<sub>2</sub>O<sub>2</sub> were added to 50 mL of each of the varying concentrations, sonicated at varying sonication times (20-60 min), 40% ultrasonic amplitude, and a frequency of 20 kHz.

**Influence of pH and sonication time on the removal of MNZ:** A 0.08 g of n-ZnO and 5 mL of 1% H<sub>2</sub>O<sub>2</sub> were added to 50mL of 50 mg.L<sup>-1</sup> MNZ aqueous solution, sonicated at varying sonication times (20-60 min), 40% ultrasonic amplitude and a frequency of 20 kHz. The percentage removal of MNZ was calculated using Eq. (1)

$$\% \text{ Degradation} = \frac{(MNZ)_0 - (MNZ)_e}{(MNZ)_0} \times 100 \quad \dots(1)$$

Where MNZ<sub>0</sub> and MNZ<sub>e</sub> are the initial and final concentrations of MNZ respectively.

**Application of influential parameters to aquaculture effluent:** The influential parameters such as the dosage of ZnO nanoparticles, sonication time, ultrasonic amplitude, H<sub>2</sub>O<sub>2</sub> concentration, and ultrasonic frequency were introduced to aquaculture effluent. A 50 mL of the aquaculture effluent was spiked with MNZ.

## RESULTS AND DISCUSSION

### Characterization

The SEM and TEM analyses of the calcined (500°C) ZnO nanoparticles formed from 0.6 M NaOH at 20.0 kx magnification, scaled at 2 μm, and shot at 100 nm are presented in Figs. 1a and 2a respectively. It was observed that more prominent pores with multiple hexagonal structures in mass were depicted (Mallika et al. 2015). The EDS spectrum of the synthesized n-ZnO calcined at 500°C

formed in 0.6 M NaOH are in proportion  $17.93 \pm 4.9\text{wt}\%$  C,  $21.65 \pm 7.2\text{wt}\%$  O,  $1.27 \pm 0.4\text{wt}\%$  Cl, and  $59.15 \pm 11.3\text{wt}\%$  Zn is shown in Fig. 1b. The result showed that as the Cl decreases, the percentage of Zn increases which indicates that ZnO nanoparticles were synthesized. The presence of Cl was due to the precursor used during synthesis. The particle size distribution of ZnO nanoparticles was examined by subjecting the TEM micrographs to image J software to measure the diameter of particles and this is presented in Fig. 2b. The result showed that the average particle size was 71.48 nm. The plots of  $\text{N}_2$  adsorption-desorption isotherm and Barret-Joyner-Halenda (BJH) pore size distribution of ZnO nanoparticles formed in 0.6 M NaOH, calcined at  $500^\circ\text{C}$  are presented in Fig. 3a and 3b. The result shows that surface area, pore volume, and pore size were  $8.5808\text{ m}^2 \cdot \text{g}^{-1}$ ,  $0.038\text{ cm}^3 \cdot \text{g}^{-1}$ , and  $164.177\text{ \AA}^0$  (Kołodziejczak-Radzimska et al. 2012). The hysteresis loop resembles type IV which is in line with the IUPAC classification (Ismail et al. 2018).

The FTIR spectrum of ZnO nanoparticles calcined at  $500^\circ\text{C}$  indicates an absorption band at  $467.21\text{ cm}^{-1}$  which corresponds to the vibrational mode of the Zn-O bond (Zak et al. 2011) as shown in Fig 4.

The X-ray diffractograms shown in Fig. 5 depict the hexagonal nature of ZnO nanoparticles as a result of its complete crystallinity with the highest peak at (101) plane which corresponds to the report of Saif-Aldin et al. (2020). The average crystallite size was calculated using the Debye Scherrer equation in Eq. 2

$$D = K\lambda / (\beta \cos \Theta) \quad \dots(2)$$

Where D is the crystallite size in nm, K is a constant (0.9),  $\lambda$  is the wavelength ( $1.54060\text{ \AA}^0$ ),  $\Theta$  is the Bragg's angle and  $\beta$  is the Full Width at Half Maximum (FWHM). The average crystallite size of the annealed ZnO nanoparticles at  $500^\circ\text{C}$  was 72.01 nm (Kayani et al. 2015) which corresponds to the particle size obtained from the TEM micrograph analysis.

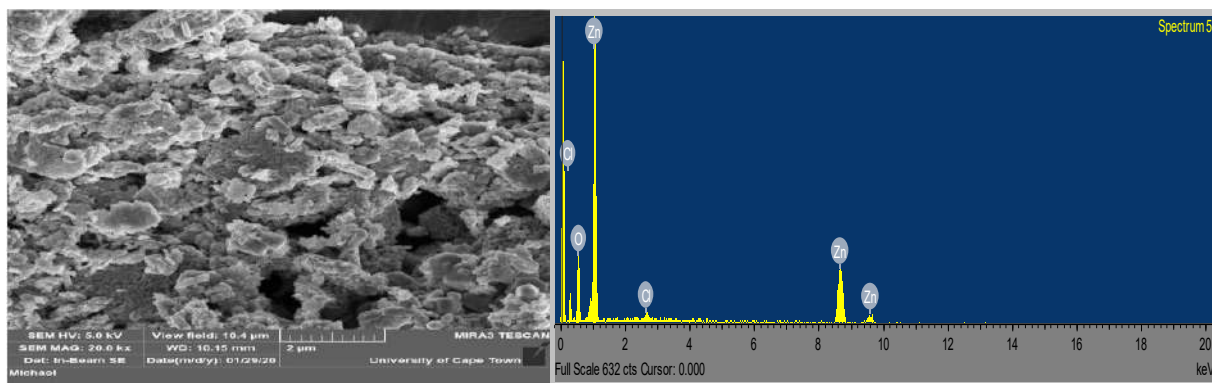


Fig. 1 (a) and (b): SEM-EDS of the ZnO calcined at  $500^\circ\text{C}$  formed in 0.6M NaOH.

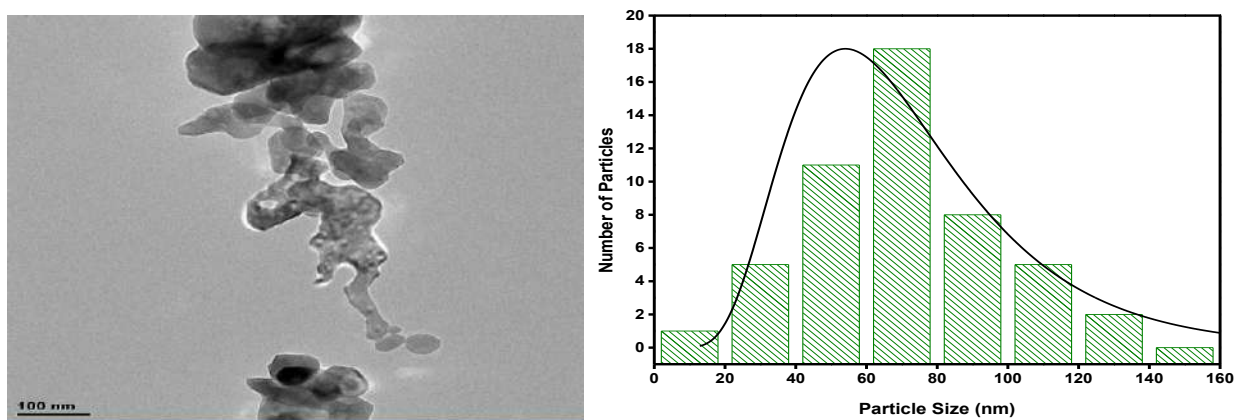


Fig. 2: TEM micrographs (a) and particle size distribution (b) of the calcined ZnO nanoparticles at  $500^\circ\text{C}$ .

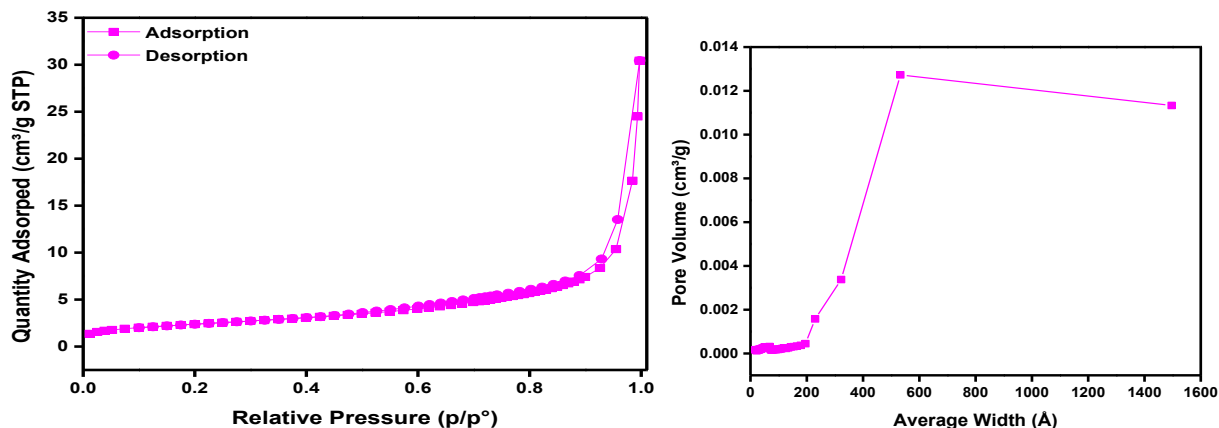


Fig 3: N<sub>2</sub> adsorption-desorption isotherm (a) and Barret-Joyner-Halenda (BJH) pore size (b) distribution of n-ZnO calcined at 500°C.

## Removal of MNZ

**Influence of ultrasonic amplitude and sonication time on the removal of MNZ:** Fig. 6 showed that the maximum degradation of MNZ was achieved at 60% ultrasonic ampli-

tude with values 30.3%, 33.3%, 36.7%, 38.3%, and 41.2% within 20-60 min sonication time. It was observed that the degradation of MNZ increases as sonication time increases. From the data presented, ultrasound alone is not sufficient for MNZ degradation. A 60% ultrasonic amplitude was kept constant for further experiments.

**Influence of H<sub>2</sub>O<sub>2</sub> concentration and sonication time on MNZ degradation:** The maximum removal of MNZ was achieved at a higher concentration of H<sub>2</sub>O<sub>2</sub> (4%) with percentage degradation of 83.5%, 85.6%, 87.4%, 88.5%, and 89.8% within 20-60 min sonication time in Fig. 7. This implies that increase in H<sub>2</sub>O<sub>2</sub> concentration is dependent on MNZ removal as more hydroxyl radicals were available to remove MNZ.

**Influence of initial concentration and sonication time on MNZ degradation:** The result in Fig. 8 shows that as the concentration of MNZ reduces, the degradation rate in-

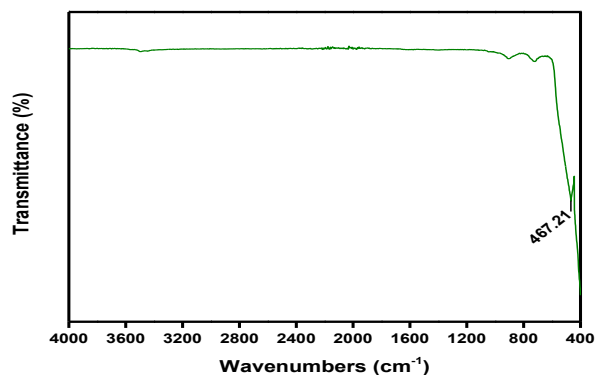


Fig. 4: The FTIR spectrum of ZnO nanoparticles calcined at 500°C.

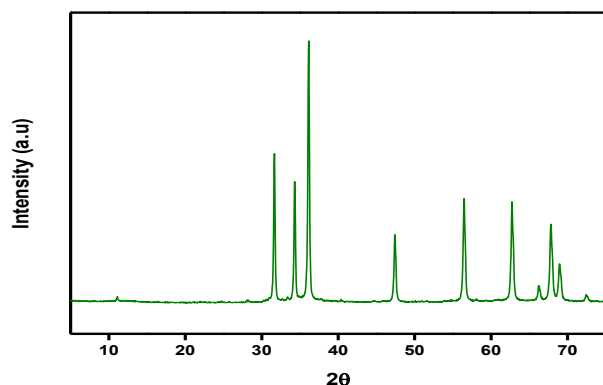


Fig. 5: The XRD of ZnO nanoparticles calcined at 500°C.

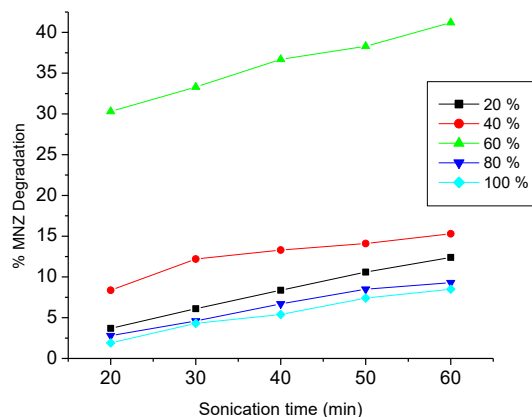


Fig. 6: Influence of ultrasonic amplitude and sonication time on MNZ removal.

creases. The maximum degradation of MNZ was achieved at  $3.125 \text{ mg.L}^{-1}$  within 20-60 min sonication time and 60% ultrasonic amplitude with percentage degradation of 58.8%, 61.1%, 62.2%, 64.1%, and 65.6%. This implies that better degradation of MNZ can be achieved at lower concentrations and this may be due to the flooding of more MNZ molecules in solution that is capable of reducing the reactive species in the ultrasonic reactor (Cordero et al. 2007). In the same vein, the kinetic studies follow a pseudo-second-order reaction which is shown in Fig. 9.

#### Influence of pH and sonication time on MNZ removal:

The pH of a solution has an effect on the ionization of contaminants and the charges on the surface of adsorbents. The result in Fig. 10 showed that the maximum removal was achieved at an acidic medium. This implies that the availability of more protons at higher pH to attack the pollutants will increase the degradation rate. The percentage removal

achieved were 67.4%, 68.5%, 69.5%, 70.6% and 71.7% at pH 2 (Hemati Borji et al. 2010).

#### Ultrasound/n-ZnO

#### Influence of ultrasonic amplitude and sonication time on MNZ removal:

A  $0.02 \text{ g n-ZnO}$  was added to  $50 \text{ mg.L}^{-1}$  MNZ solution and sonicated within 20-60 min at varying ultrasonic amplitude (20-100%). Fig. 11 shows that the maximum removal was achieved at 60% ultrasonic amplitude. The percentage removal achieved was 42%, 44.9%, 46.2%, 48%, and 50.9% which is higher than that of the US alone. This implies that more active sites were available from the catalyst to mineralize pollutants and also the OH radicals produced from ultrasound have led to a major increase in the removal process (Qiao et al. 2018). A 60% ultrasonic amplitude was kept constant for further experiments.

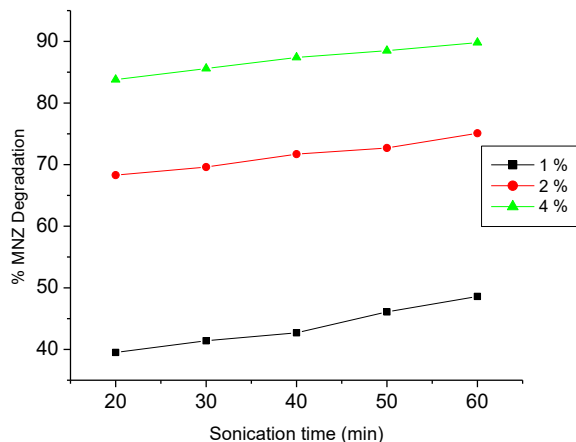


Fig. 7: Influence of  $\text{H}_2\text{O}_2$  concentration and sonication time on MNZ removal.

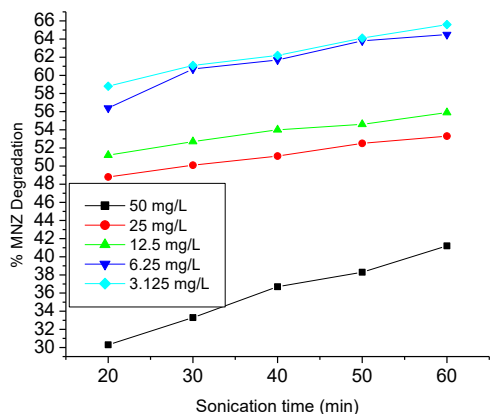


Fig. 8: Influence of initial concentration and sonication time on MNZ degradation.

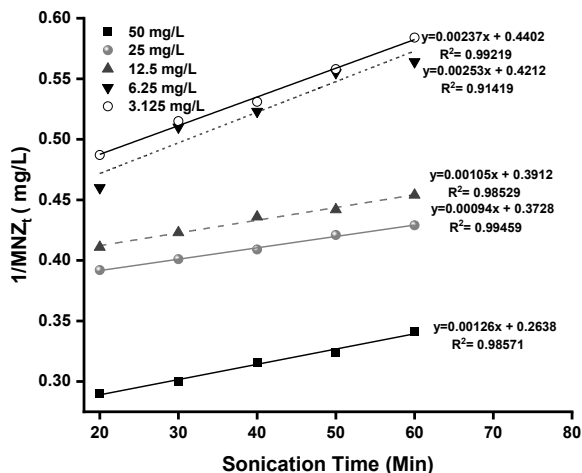


Fig. 9: Plot of  $1/(\text{MNZ}_t)$  and sonication time for pseudo-second-order kinetic model.

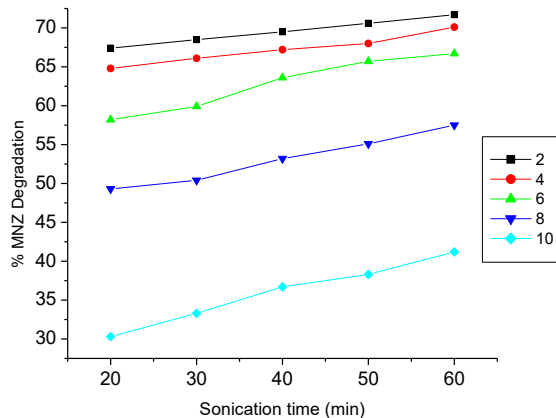


Fig. 10: Influence of pH and sonication time on MNZ degradation.



**Influence of nanodosage and sonication time on MNZ removal:** The result in Fig. 12 showed that a higher quantity of n-ZnO is not dependent on MNZ removal. The maximum MNZ removal achieved at 0.02g n-ZnO was 50.9% within 60 min sonication time. It was observed that as the quantity of n-ZnO increases, the removal of MNZ decreases which may be a result of insufficient surface area due to the agglomeration nature of n-ZnO (El Bouraie & Ibrahim 2020). Increasing n-ZnO in MNZ removal showed that the active sites are saturated and so there was no room for attacking pollutants. A 0.02g n-ZnO was kept constant for further experiments.

**Influence of initial concentration and sonication time on MNZ removal:** The maximum percentage removal shown in Fig. 13 follows the trend 68.2%, 70.6%, 71.9%, 73.7% and 75.1% at 3.125 mg.L<sup>-1</sup> within 20-60 min. Increasing the concentration of MNZ may lead to saturation of active sites of the adsorbent thereby reducing the degradation efficiency

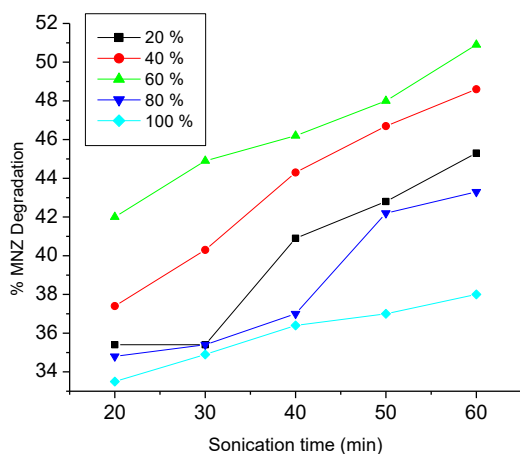


Fig. 11: Influence of ultrasonic amplitude and sonication time on MNZ removal.

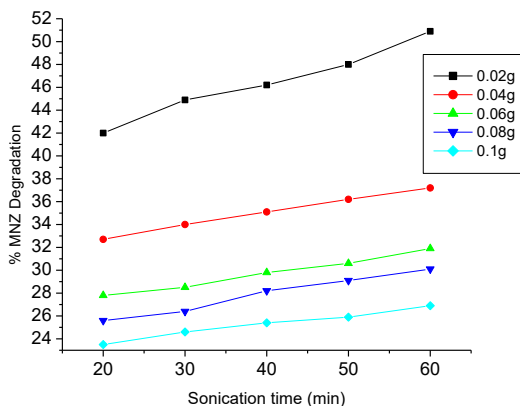


Fig. 12: Influence of nanodosage and sonication time on MNZ removal.

(Moussavi et al. 2013). The synergetic effect of US/n-ZnO is a viable technique for removing MNZ in an aqueous solution. In the same vein, the kinetic studies follow a pseudo-second-order reaction which is shown in Fig. 14.

**Influence of pH and sonication time on MNZ removal:** The initial pH of MNZ was 9.2. The maximum removal of MNZ was achieved at pH 2 with a percentage degradation of 79.5% within 60 min in Fig. 15. The combination of the protons from the adsorbate and the active sites of n-ZnO has improved the degradation rate from 71.9-79.5% within 20-60 min (El-Kemary et al. 2010).

**Influence of H<sub>2</sub>O<sub>2</sub> concentration and sonication time on MNZ removal:** The result in Fig. 16 showed that the maximum removal of MNZ achieved at 2% H<sub>2</sub>O<sub>2</sub> was 94% within 60 min. It was observed that the removal of MNZ increases with time. Increasing the concentration of H<sub>2</sub>O<sub>2</sub> may disrupt the removal process.

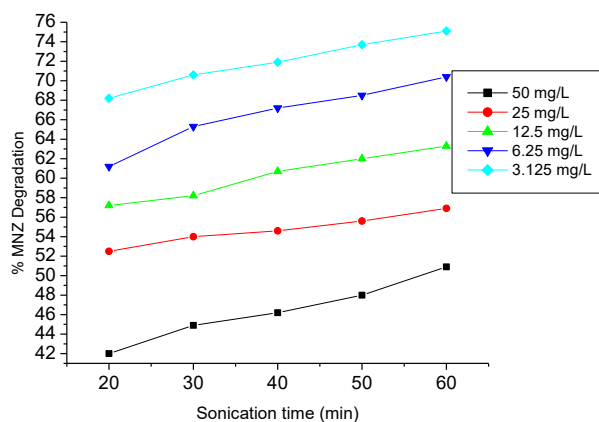


Fig. 13: Influence of initial concentration and sonication time on MNZ removal.

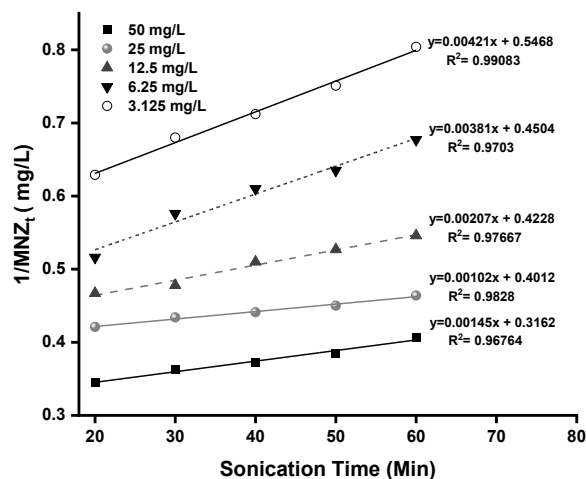


Fig. 14: Plot of  $1/(MNZ_t)$  and sonication time for pseudo-second-order kinetic model.

## US/n-ZnO/ H<sub>2</sub>O<sub>2</sub>

**Influence of ultrasonic amplitude and sonication time on MNZ removal:** A 5 mL of 2% H<sub>2</sub>O<sub>2</sub>, 0.02 g n-ZnO were added to 50 mg.L<sup>-1</sup> MNZ solution within 20-60 min sonication time. The result in Fig. 17 showed that the removal of MNZ increases with time from 63.8%-69.3% within 60 min at 20% ultrasonic amplitude. Increasing ultrasonic amplitude led to a decrease in the removal rate. This implies that amplitude is not dependent on MNZ removal. The synergetic influence of US/n-ZnO/ H<sub>2</sub>O<sub>2</sub> on the removal of MNZ yielded a better removal when compared to US/n-ZnO and US alone. A 20% amplitude was kept constant for further experiments.

**Influence of nanodosage and sonication time on MNZ removal:** A 0.02-0.1 g n-ZnO were investigated with US/n-ZnO/ H<sub>2</sub>O<sub>2</sub> system in 50 mg.L<sup>-1</sup> MNZ solution with 5 mL 2% H<sub>2</sub>O<sub>2</sub> at 20% ultrasonic amplitude. The result in Fig. 18 showed that the maximum removal of 69.3% was achieved at 0.02 g n-ZnO within 60 min. this implies that the removal

of MNZ increases with time and increasing the amount of n-ZnO may lead to saturation of active sites of the adsorbent (Sharifpour et al. 2018). A 0.02 g n-ZnO was kept constant for further experiments.

**Influence of pH and sonication time on MNZ removal:** The result in Fig. 19 showed that the removal of MNZ favors the basic medium (pH10) as more OH radicals will be available for the mineralization of MNZ (Malakootian et al. 2019). It was also observed that the removal of MNZ increases with time from 63.8-69.3% within 60 min sonication time.

**Influence of initial concentration and sonication time on MNZ removal:** The result in Fig. 20 showed that the removal of MNZ increases with decreasing concentration of MNZ. The maximum removal of MNZ was achieved at 3.125 mg.L<sup>-1</sup> within 20-60 min. the percentage removal increases from 81.1%-88%. This implies that at lower concentrations of MNZ, excess OH radicals are available for the removal process (Ayanda et al. 2021).

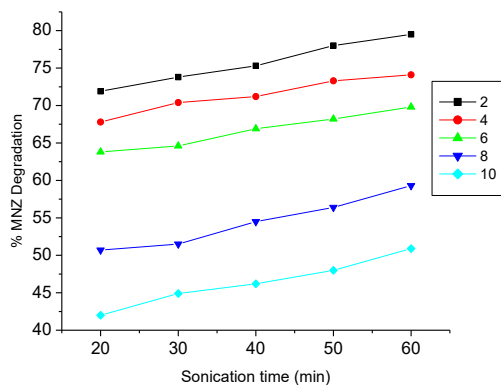


Fig. 15: Influence of pH and sonication time on MNZ removal.

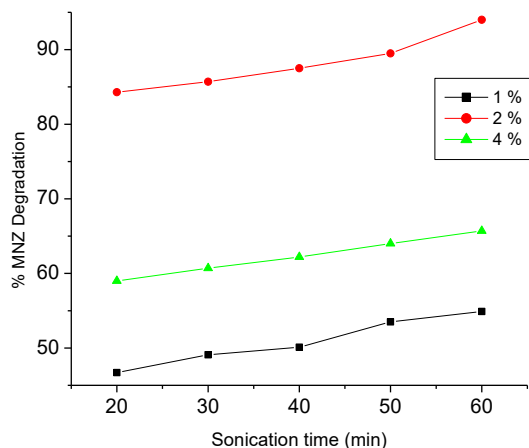


Fig. 16: Influence of H<sub>2</sub>O<sub>2</sub> concentration and sonication time on MNZ removal.

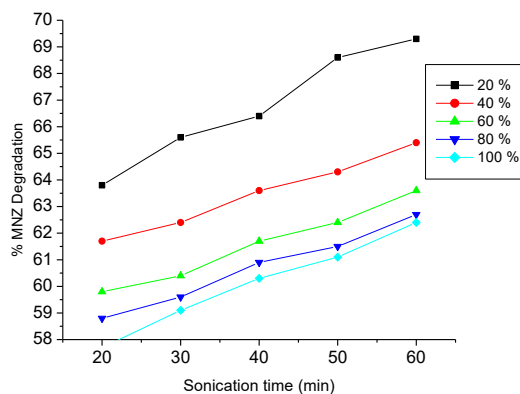


Fig. 17: Influence of H<sub>2</sub>O<sub>2</sub> concentration and sonication time on MNZ removal.

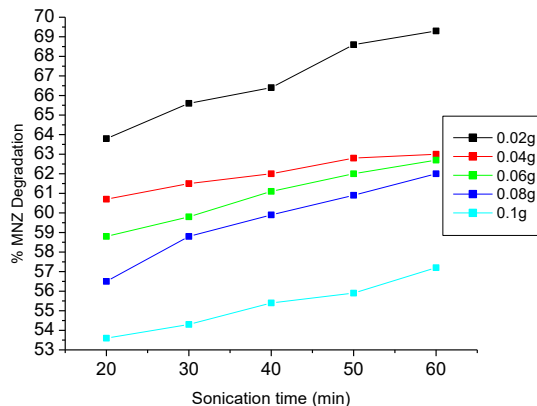


Fig. 18: Influence of nanodosage and sonication time on MNZ removal.

From the experimental data above, the influence of initial concentration was subjected to a pseudo-second-order kinetic model presented in Eq. (3)

$$\frac{1}{MNZ_t} = K_{obs}t \quad \dots(3)$$

Where  $MNZ_t$  is the final concentration of MNZ solution ( $mg.L^{-1}$ ),  $K_{obs}$  is the observed rate of degradation and  $t$  is the time. The plot of  $1/MNZ_t$  and sonication time is shown in Fig. 21 with  $K_{obs}$  values from the slope.

The mechanism of degradation of MNZ was investigated by subjecting the experimental data to Langmuir-Hinshelwood (L-H) model shown in Eq. (4)

$$\frac{1}{K_{obs}} = \frac{1}{K_c K_{LH}} + \frac{1}{K_c} MNZ_0 \quad \dots(4)$$

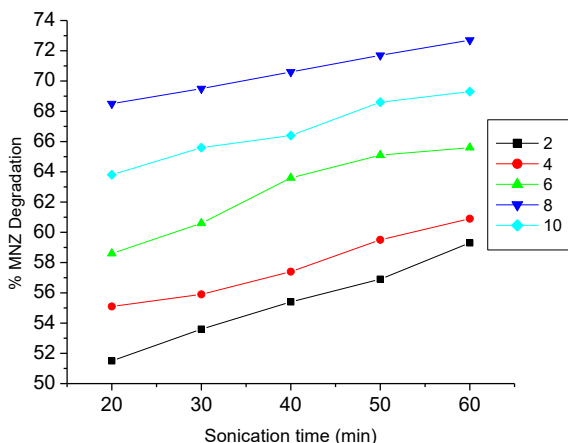


Fig. 19: Influence of pH and sonication time on MNZ removal.

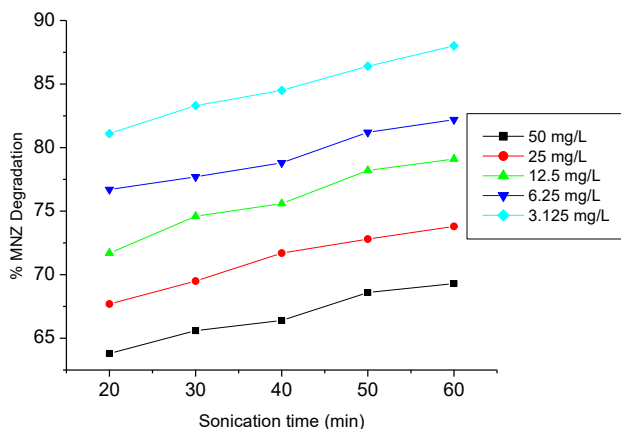


Fig. 20: Influence of initial concentration and sonication time on MNZ removal.

Where  $K_{obs}$  is the rate constant ( $min^{-1}$ ),  $K_c$  is the surface rate of reaction constant ( $mg.Lmin^{-1}$ ) and  $K_{LH}$  is the L-H adsorption equilibrium constant ( $L.mg^{-1}$ ). The plot of L-H kinetic and  $R^2$  values is shown in Fig. 22 with  $K_c$  and  $K_{LH}$  values of  $1.486 \times 10^{-1}$  ( $mg.Lmin^{-1}$ ) and  $8.790 \times 10^{-2}$  ( $L.mg^{-1}$ ).

**Proposed Reaction Mechanism for MNZ**

**US only**

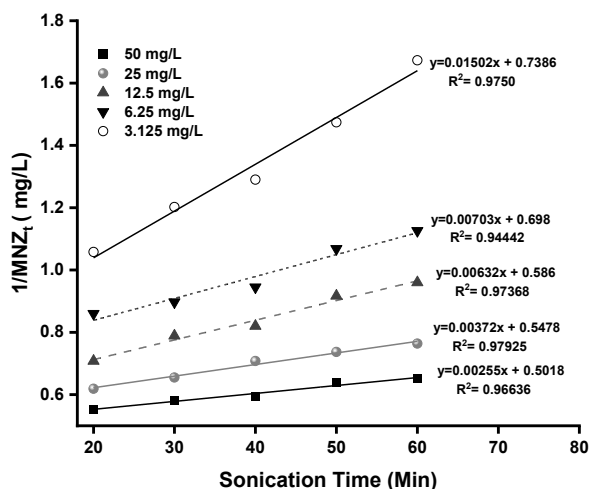


Fig. 21: Plot of  $1/MNZ_t$  and sonication time for pseudo-second-order kinetic model.

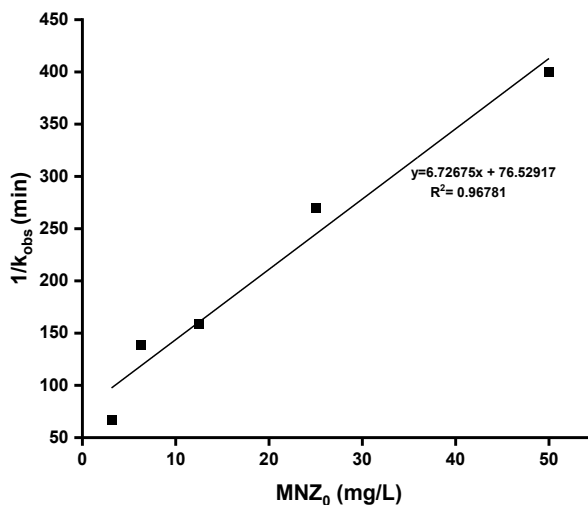
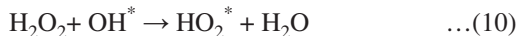


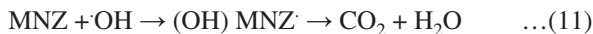
Fig. 22: L-H kinetic plot of MNZ removal.

## US/H<sub>2</sub>O<sub>2</sub>

H<sub>2</sub>O<sub>2</sub> was decomposed to form reactive radicals in equations (8-10)



## US/n-ZnO/H<sub>2</sub>O



## Degradation of MNZ Contained in Aquaculture Effluent

The experimental conditions such as 20% amplitude, 5 mL 2% H<sub>2</sub>O<sub>2</sub>, 0.02g n-ZnO, and 60 min sonication time were applied for MNZ degradation in aquaculture effluent. The percentage of COD removal achieved for MNZ in aquaculture effluent was 62.6%, 89.8%, and 98.5% for US only, US/n-ZnO and US/n-ZnO/H<sub>2</sub>O<sub>2</sub> systems and is shown in Fig. 23.

## CONCLUSION AND RECOMMENDATIONS

In this study, a stable and effective metal oxide nanoparticle with good antibacterial properties was synthesized and calcined at 500°C. The synthesized n-ZnO depicts a hexagonal structure with an average particle size of 71.48 nm. At 500°C, an absorption peak for the Zn-O bond was observed at 467.21 cm<sup>-1</sup>, and a well-crystalline zincite was achieved with a surface area of 8.58 m<sup>2</sup>.g<sup>-1</sup> which indicates that n-ZnO is a promising catalyst that is viable for removing antibiotics from wastewater. MNZ-formulated aquaculture

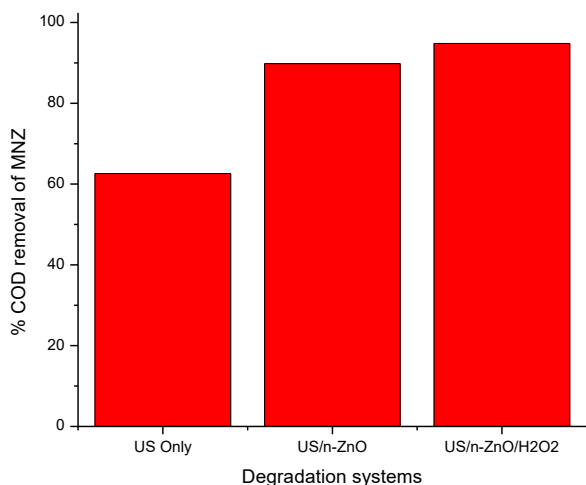


Fig. 23: Degradation efficiency by COD removal of MNZ from aquaculture effluent using US only, US/n-ZnO, and US/n-ZnO/H<sub>2</sub>O<sub>2</sub> systems.

effluent was subjected to US only, US/n-ZnO, and US/n-ZnO/H<sub>2</sub>O<sub>2</sub> systems. With the introduction of 0.02 g n-ZnO, 5 mL of 2% H<sub>2</sub>O<sub>2</sub>, 20% ultrasonic amplitude and 50 mg.L<sup>-1</sup> MNZ aqueous solution, the percentage COD removal followed the trend 62.6%, 89.8% and 98.5% for US only, US/n-ZnO and US/n-ZnO/H<sub>2</sub>O<sub>2</sub> systems. The available active sites of n-ZnO and the hydroxyl radicals generated from H<sub>2</sub>O<sub>2</sub> and that of the sonicator have improved the degradation efficiency. Pseudo-second-order kinetic best fit the degradation process of MNZ and the mechanism of degradation followed the Langmuir-Hinshelwood model. The discharge of metronidazole contained in aquaculture effluent can best be removed by subjecting the effluent to US/n-ZnO/H<sub>2</sub>O<sub>2</sub> system. Other advanced oxidation processes can be explored for further studies.

## REFERENCES

- Aremu, O.H., Akintayo, C.O., Naidoo, E.B., Nelana, S.M. and Ayanda, O.S. 2021. Synthesis and applications of zinc oxide nanoparticles-A review. *Int. J. Environ. Sci. Technol.*, 16: 1-20.
- Ayanda, O.S. Aremu, O.H. Akintayo, C.O. Sodeinde, K.O, Igboama, W.N. Osegbe, E.O. Nelana, S.M. (2021). Sonocatalytic degradation of amoxicillin from aquaculture effluent by zinc oxide nanoparticles. *Environ. Nanotechnol. Monit. Manag.*, 16: 100513.
- Balarak, D., Igwegbe, C.A. and Onyechi, P.C. 2019. Photocatalytic degradation of metronidazole using BIOD-MWCNT composites: Synthesis, characterization and operational parameters. *Sigma Journal of Engineering and Natural Sciences*, 37(4): 1235-1249.
- Bian, D., Guo, Y. and Zao, Y., 2017. Influence of zinc oxide on corrosion resistance of alumina-based chemically bonded ceramic coatings. *Russ. J. Appl. Chem.*, 89: 2091-2094.
- Calamari, D., Zuccato, E., Castiglioni, S., Bagnati, R. and Fanelli, R. 2003. Strategic survey of therapeutic drugs in the rivers Po and Lambro in Northern Italy. *Environ. Sci. Technol.*, 37: 1241-1248.
- Cordero, T., Chovelon, J.M., Duchamp, C., Ferronato, C. and Matos, J. 2007. Surface nano-aggregation and photocatalytic activity of TiO<sub>2</sub> on H-type activated carbons. *Appl. Catal. B*, 73: 227-235.
- Cunningham, V.L. 2004. Special Characteristics of Pharmaceuticals Related to Environmental Fate. In *Pharmaceuticals in the Environment*. Springer Berlin Heidelberg, Berlin, Germany, pp. 13-34.
- Das, J. and Dhua, M. 2014. UV-Spectrophotometric assay method development and validation of metronidazole in bulk and tablet formulation. *Journal of Pharm Sci Tech*, 3(2): 106-109.
- El-Kemary, M., El-Shamy, H. and El-Mehasseb, I. 2010. Photocatalytic degradation of ciprofloxacin drug in water using ZnO nanoparticles. *J. Lumin.*, 130(12): 2327-2331.
- Felis, E., Kalka, J., Sochacki, A., Kowalska, K., Bajkacz, S., harnisz, M. and Korzeniewska, E. 2020. Antimicrobial pharmaceuticals in the aquatic environment-Occurrence and environmental implications. *Europ. J. Pharma.*, 886: 172813.
- Forouzes, M., Ebadi, A. and Aghaeinejad-Meybodi, A. 2018. Degradation of metronidazole antibiotic in an aqueous medium using activated carbon as a persulfate activator. *Sep. Purif. Technol.*, 16: 1-31.
- Habibi, A., Belaroui, L.S., Bengueddach, A., Galindo, A.L. Díaz, C.I.S. and Peña, A. 2018 Adsorption of metronidazole and spiramycin by an Algerian palygorskite. Effect of modification with tin. *Micropor. Mesopor. Mater.*, 268: 293-302.
- Hemati Borji, S., Nabizadeh, R., Mahvi, A.H. and Javadi, A.H. 2010. Photocatalytic degradation of phenol in aqueous solutions by

- Fe (III)-doped TiO<sub>2</sub>/ UV process. *Iran. J. Health Environ.*, 3: 369-380.
- Hu, Y., Wang, G., Huang, M., Lin, K., Yi, Y., Fang, Z., Li, P. and Wang, K. 2017. Enhanced degradation of metronidazole by heterogeneous sono-Fenton reaction coupled ultrasound using Fe<sub>3</sub>O<sub>4</sub> magnetic nanoparticles. *Environ. Technol.*, 11: 1-22.
- Ismail, M.A., Taha, K.K., Modwi, A. and Khezami, L. 2018. ZnO nanoparticles: Surface and x-ray profile analysis. *J. Ovonic Res.*, 14(5): 381-393.
- Jury, K.L., Vancov, T., Stuetz, R.M. and Khan, S.J. 2010. Antibiotic resistance dissemination and sewage treatment plants. *Curr. Res. Technol. Educ. Top. Appl. Microbiol. Microbial Biotechnol.*, 2: 509-510.
- Kayani, Z.N., Saleemi, F. and Batool, I. 2015. Effect of calcination temperature on the properties of ZnO NPs. *Appl. Phys. A*, 119(2): 713-720.
- Kołodziejczak-Radzimska, A., Markiewicz, E. and Jesionowski, T. 2012. Structural characterization of ZnO particles obtained by the emulsion precipitation method. *J. Nanostruct.*, 3: 1-9.
- Landers, T.F., Cohen, B., Wittum, T.E. and Larson, E.L. 2012. A review of antibiotic use in food animals: perspective, policy, and potential. *Pub. Health Rep.*, 127(1): 4-22.
- Ma, H., Williams, P.L. and Diamond, S.A. 2013. Ecotoxicity of manufactured ZnO nanoparticles-a review. *Environ. Pollut.*, 172: 76-85.
- Malakootian, M., Olama, N. and Dehghani, M. 2019. Photocatalytic degradation of metronidazole from aquatic solution by TiO<sub>2</sub> doped Fe<sup>3+</sup> nano-photocatalyst. *Int. J. Environ. Sci. Technol.*, 16(8): 4275-4284.
- Mallika, N.A., Reddy, A.R. and Reddy, K.V. 2015. Annealing effects on the structural and optical properties of ZnO NPs with PVA and CA as chelating agents. *J. Adv. Ceramics*, 4(2): 123-129.
- Manyi-Loh, C., Mamphweli, S., Meyer, E. and Okoh, A. 2018. Antibiotic use in agriculture and its consequential resistance in environmental sources: potential public health implications. *Molecules*, 23(4): 795.
- Moussavi, G., Alahabadi, A., Yaghmaeian, K. and Eskandari, M. 2013. Preparation, characterization, and adsorption potential of the NH<sub>4</sub>Cl-induced activated carbon for the removal of amoxicillin antibiotic from wastewater. *Chemical Engineering Journal*, 217: 119-128.
- Petrie, B., Barden, R. and Kasprzyk-Hordern, B. 2015. A review on emerging contaminants in wastewaters and the environment: current knowledge, understudied areas, and recommendations for future monitoring. *Water Res.*, 72: 3-27.
- Qiao, J., Zhang, H., Li, G., Li, S., Qu, Z., Zhang, M., Wang, J. and Song, Y. 2018. Fabrication of a novel Z-scheme SrTiO<sub>3</sub>/Ag<sub>2</sub>S/CoWO<sub>4</sub> composite and its application in sonocatalytic degradation of tetracyclines. *Sep. Purif. Technol.*, 211: 843-856.
- Saif-Aldin, K., Al-Hariri, S. and Ali-Nizam, A. 2020. Zinc oxide nanoparticles synthesis without organic solvents with ultrasonic wave assistance. *Chem. Res. J.*, 5(3): 6-13.
- Sharifpour, E., Khafri, H.Z., Ghaedi, M., Asfaram, A. and Jannesar, R. 2018. Isotherms and kinetic study of ultrasound-assisted adsorption of malachite green and Pb<sup>2+</sup> ions from aqueous samples by copper sulfide nanorods loaded on activated carbon: experimental design optimization. *Ultrason. Sonochem.*, 40: 373-382.
- Yang, Z., Lai, A., Chen, H., Yan, Y., Yang, Y., Zhang, W. and Wan, L. 2019. Degradation of metronidazole by dielectric barrier discharge in an aqueous solution. *Front. Environ. Sci. Eng.*, 13(3): 1-9.
- Zak, A.K., Abd Majid, W.H., Wang, H. Z., Yousefi, R., Golsheikh, A.M. and Ren, Z. F. 2013. Sonochemical synthesis of hierarchical ZnO nanostructures. *Ultrason. Sonochem.*, 20(1): 395-400.





# Effect of High Temperature on Reproductive Phase of Plants: A Review

S. Talwar, K. Bamel<sup>†</sup>, Prabhavathi and A. Mal

Department of Botany, Shivaji College, University of Delhi, Delhi, India

<sup>†</sup>Corresponding author: K. Bamel; kbamel@yahoo.in

Nat. Env. & Poll. Tech.  
Website: [www.neptjournal.com](http://www.neptjournal.com)

Received: 24-01-2022

Revised: 22-03-2022

Accepted: 07-04-2022

## Key Words:

Climate change

Reproductive phase of plants

Temperature stress

Heat stress

## ABSTRACT

Climate change is a universal challenge that threatens the very existence of life on planet Earth. One of the most sensitive areas to climate change is agriculture. Climate change affects precipitation, cyclones, clouds, temperature, humidity, and CO<sub>2</sub> levels. All these factors affect plant productivity which poses another grave concern in feeding the ever-increasing population. The productivity in terms of crop yield is reduced due to a direct correlation between phenology and climate change. The reproductive organs of a plant and other parameters that define good fertility of a species are all affected by the increasing temperatures during their vegetative and reproductive phases of growth and development. Thus, this review is an attempt to understand the effect of climate change on the reproductive structures of plants and discuss the short-term and long-term adaptations in plants and agriculture as mitigation measures to combat the significant yield loss in developing countries.

## INTRODUCTION

Climate change is a grave concern impacting the production of various crops worldwide. One of the important components of global climate change is an increase in the Earth's near-surface temperature. Unusually dry and hot climatic conditions have been linked with a lessening of several tree species around the world. Physiological stress associated with fluctuation in temperature poses a serious threat to biodiversity by causing alteration in reproductive processes and plant-pollinator associations (Talwar et al. 2015, Rawat 2015).

The process of sexual reproduction contributes a dominant role in the life-cycle of plants and it is prone to any turmoil in the environment (Müller et al. 2016). The yield of the crop is an important parameter for human survival. Stakeholders are using various methods and techniques based from satellite remote sensing (Bamel et al. 2022) to mathematical modeling (Rani et al. 2022) to forecast the yield of crops. Agronomists use all available information related to nutrient, irrigation, and climatic requirement for their crops to enhance productivity. Seed production depends on vegetative as well as reproductive development. During the transition from the vegetative to a reproductive state of a plant, the environmental conditions usually affect photosynthetic efficiency, development of canopy, interception of solar radiation, and initiation of fruiting. An increase in the temperature of just a few degrees can considerably affect the yield of the crop (Thuzar et al. 2010).

Several morphological, physiological, developmental, and molecular responses of the reproductive structures may vary under climatic stresses (Gray & Brady 2016). The shift in the flowering period is a result of temperature variation and inconsistency in precipitation. The reproductive period and the reproductive structures are more susceptible to temperature stress than the development of vegetative organs, which eventually affect the crop yield (Snider & Oosterhuis 2011). According to Foolad (2005), high temperature negatively affects the various reproductive processes such as pollen viability, germination of pollen grains, growth of pollen tube, positions of stigma and style, pollen-pistil interaction, fertilization, and post-fertilization processes, such as the growth of the pro-embryo, endosperm and zygote.

Every crop shows optimal vegetative and reproductive growth at its own threshold temperature (Hatfield et al. 2011, Zinn et al. 2010). When the temperature overshoots the threshold range of crops, its vegetative and reproductive growth such as flowering, fruit set, fruit ripening, and seed germination are gravely affected and have an economic impact on agriculture (Christensen & Christensen 2007). The progamic phase, which extends from pollination to fertilization, is one of the most crucial phases and is extremely vulnerable to high temperatures (Hebbar et al. 2020).

To fulfill the food demand of the increasing population, it is mandatory to elucidate and strengthen the mechanisms that regulate pollination, leading to enhanced yield. The authors attempt to search the available literature that highlights the

significance of temperature stability for the sustenance of the usual reproductive systems of plants and how the slightest variation from the optimum affects the process. Suitable studies were screened to understand the stress impact on different plant organs that are important for the reproductive phase and adaptations of plants, if any, to combat or overcome it and complete their life cycle normally. This in-depth analysis led the investigators to give a comprehensive perspective and address the knowledge gaps by defining the future scope of research in the study area which is one of the most important concerns of humanity in today's changing environmental scenario. If change is inevitable then mankind has the challenge to slow it by curtailing the responsible factors or else find alternatives that can sustain life amid the changes.

## EFFECT ON PRE-ZYGOTIC REPRODUCTIVE PHASE

### Flower

Flower and its various constituent parts are very sensitive to the temperature both structurally and functionally as was observed in rice (Takeoka et al. 1991) and *Brassica* (Morrison & Stewart 2002). Depending upon the plant species temperature stress shifts the flowering either way. Most often higher than optimum temperatures are perceived as stress by the plant and in response, the flowering is preponed. In cowpea, the higher temperature at night is more detrimental in comparison to higher day temperature, which results in enhanced floral abscission (Mutters & Hall 1992).

Cubillos and Hughes (2016) investigated the impacts of elevated carbon-di-oxide on the floral traits of the three economically important crops tomato, pepper, and zucchini. The elevated CO<sub>2</sub> treatment did not affect flower longevity in any of these three species, it did not affect flowering in tomatoes, but less number of flowers were produced in pepper, whereas in zucchini more male flowers than female flowers were developed. At elevated CO<sub>2</sub>, fewer pollen grains and reduced nectar secretion have been observed in zucchini whereas no such difference was observed in tomato.

### Pollen

Various studies have revealed that the growth and development of male gametophytes are extremely sensitive to heat (Hedhly et al. 2009, Hedhly 2011, Zinn et al. 2010). Increased temperature affects the pollen grains in terms of number and viability. The viability of the pollen grains is a prerequisite for successful sexual plant reproduction. The quality of pollen grains is assessed on their viability over a period after dehiscence. The duration of pollen viability affects the reproductive success of a species. Due to the temperature stress collapse, desiccated, empty, and small-sized

pollen grains with reduced viability are formed in chickpeas (Devasirvatham et al. 2013). Pollen viability is affected by heat stress in several plants such as common bean (Gross & Kigel 1994, Prasad et al. 2003), cowpea (Warrag & Hall 1984), peanut (Boote et al. 2005), cotton (Song et al. 2015), flax (Cross et al. 2003), pepper (Erickson & Markhart 2002), rice (Endo et al. 2009), and tomato (Pressman et al. 2002).

Reduced pollen vigor has been reported in *Brassica* and *Petunia* when pollen grains were exposed to 45-60°C for 12 h (Rao et al. 1992). In *Glycine max*, when plants were exposed to 38°C during the day, the number of pollen grains was reduced (30-50%) and when exposed to 30°C at night, the viability of the pollen grains was also decreased (Koti et al. 2005). Similarly, in *Arachis hypogea* when kept under elevated temperature (44°C), the viability of the pollen grains was reduced (Prasad et al. 2003).

Temperature above 35°C caused the development of sterile pollen grains and thus affected the pollination and fertilization of rice. Higher temperatures inhibited the germinated pollen tubes to reach the embryo sac, affecting the fertility of the spikelet and crop yield (Shi et al. 2018). In cotton, exposure to 39°C, reduced pollen germination to 40% (Burke et al. 2004). Similarly, pollen viability and pollen tube elongation were reduced above 32°C and 29°C respectively (Kakani et al. 2005). In different potato varieties, pollen germination and crop yield were decreased between 30 to 70%, when the pollen grains were exposed to 30°C for up to 30 minutes although the seed set was less affected (Pallais et al. 1988).

In sorghum, the pollen grains showed the enhanced accumulation of reactive oxygen species (ROS) when the plants were exposed to high temperatures. The pollen membrane was damaged and pollen grains were small and deformed which eventually resulted in a reduced seed set (Djanaguiraman et al. 2018). Similarly, heat stress resulted in pollen sterility, lowering the seed set and crop yield in maize (Wang et al. 2019), kidney bean (Prasad et al. 2003), and chickpea (Kaushal et al. 2013).

### Pistil

During the pollination process, pollen grains fall on the receptive stigma, and in response to the stigmatic fluid pollen grains adhere to the surface and it is soon followed by hydration and germination. By penetrating the transmitting tissue of style through stigma pollen tube reach the ovule and discharges all its contents into the embryo sac to facilitate fertilization (Hiscock & Allen 2008, Losada & Herrero 2012). The compatibility between pollen and stigma is also required for effective fertilization. If the pollen grain is compatible, all post-pollination events (fertilization, fruit, and seed set)



proceed normally, but if the pollen is incompatible, the pistil effectively arrests one or more of the post-pollination events, thus preventing fertilization. The most distinct response of the stigma to incompatible pollen is the development of a callose plug which appears at the tip of the pollen tube, thereby preventing its further growth (Bhojwani et al. 2015).

The stigmatic receptivity and ovule degeneration are important parameters that control the interaction of male and female reproductive phases and have significant consequences on pollination. These processes are temperature-dependent (Cerović et al. 2000, Lora et al. 2011). Elevated temperature reduced the period of stigma receptivity, ovule life span, and style abscission from the ovary, whereas low-temperature exposure had opposite effects (Montalt et al. 2019, Estornell et al. 2016). Heat stress-induced stigma enlargement because of elongation of stigmatic papillae and reduce the adherence of pollen grains to stigma (Katano et al. 2020). It also shortened the filament length. These observations indicated that the decrease in pollen attachment to stigma might be partially due to short stamen which might increase the distance between stigma and anthers.

The receptivity of the stigma was strongly controlled by the elevated temperature and it significantly decreased the pollen germination as well as the number of pollen tubes growing on the stigma in citrus (Montalt et al. 2019). High temperature significantly influenced the processes of ovule degeneration and the style of abscission. In canola, high temperature also shortened the period of stigma-nectar secretion, affecting pollinator-based pollination efficiency (Chabert et al. 2018). Wang et al. (2021) studied the effects of heat stress on pistils and concluded that high temperatures affect the development of female gametophyte, pollen-pistil interactions, fertilization, and post-zygotic development and suggest more molecular studies to understand the regulatory mechanism involved in the female gametophyte development.

### **Pollen-Pistil Interaction**

Pollen-pistil interaction involves a series of reactions between the male gametophyte and sporophytic tissue of the stigma and style. These interactions result in the generation of appropriate physical and chemical signals which elicit the required responses in pollen or pistil. Pollination, pollen adhesion, pollen hydration, pollen germination, growth of pollen on the stigma, growth of pollen tube through the style, and entry of pollen tube into the ovule are sequential major events of this interaction. Any deviation prevents fertilization and as a result fruit and seed set. This is the most delicate period in the life span of the plants as various processes are involved during this short period of time (Hedhly et al. 2009, Zinn et al. 2010).

Several works have shown the impact of high temperature during the initial phases of pollen-pistil interaction. High temperature has been shown to affect stigmatic receptivity in peach (Carpenedo et al. 2020), cherimoya (Lora et al. 2011), ovule degeneration in plum, sweet, and sour cherry cultivars (Beppu et al. 2001, Cerović et al. 2000, Postweiler et al. 1985). In coconut, high temperature (33°C) induced the nectar secretion before the stigma became receptive and at the time of pollination, the stigma was dry. This significantly affected the pollination, fertilization, and seed set (Hebbar et al. 2020).

### **BIOCHEMICAL AND MOLECULAR CHANGES ASSOCIATED WITH HIGH TEMPERATURE**

Physiological and biochemical processes such as oxygen requirement during seed imbibition are severely affected by elevated temperature (Nascimento et al. 2008). Saini (1997) reported that malfunctioning of gametophytic development is also due to the stress-induced reduction in sugar delivery to reproductive tissues. Later, Snider et al. (2009) showed a significant decline in the amount of soluble carbohydrates and ATP content in the pistil of cotton when the plant was exposed (38°C/20°C) for a week before flowering, resulting in a reduction in the number of ovules and fertilization efficiency. Similarly, Li et al. (2015) observed that sugar starvation is the major cause of the failure of fertilization in rice because of the high temperature. It is due to the presence of acid invertase enzymes as invertase hydrolyzes sucrose into hexose which supports the pollen tube growth (Goetz et al. 2017). Under heat stress, the activity of the invertase enzyme was significantly decreased and thus restricted the hexose sugar supply. Similarly, the pistils of cotton flowers also showed less amount of carbohydrate reserves (particularly sucrose) and ATP production under the effect of moderately high temperatures, and thus there is a decline in photosynthesis because of the heat stress (Snider et al. 2011). Providing the exogenous acid invertase increased the amount of carbohydrates content as well as increased the spikelet fertility in Rice (Jiang et al. 2020). The interaction between sugars and hormones is also indicated by Kumar et al. (2021) whereas Jagadish et al. (2021) have reviewed the carbon dynamics and suggested not to draw a general conclusion about the role of sugars in crop reproduction.

### **FUTURE SCOPE AND PERSPECTIVE**

Though the rise in temperatures has detrimental effects on almost all physiological and developmental processes, it becomes an even more serious concern if the impacted stage is reproduction. The ultimate toll is taken by the quality (nutrient content) and quantity (yield) of the products like in

food crops. Since plants respond to multiple abiotic factors, a multidisciplinary understanding needs to be developed keeping in mind the interaction of different factors like the fluctuating temperature, and increasing CO<sub>2</sub> and nitrogen levels in the atmosphere.

'Omics' approach, targeting heat stress in plants in general and crop plants in specific, is the need of the hour. To mitigate the impact of rising temperatures new stress-tolerant species should be identified. The correlation between the genotypic and phenotypic studies will help in screening the appropriate genotype that can thrive well in the changing environment. The varieties may be selected from the existing gene pool based on their flexibility in flowering and anthesis time or their morphological feature that confer their tolerance to heat stress. The potential stress-tolerant germplasm may then be screened for specific genes that confer better adaptability to the changing scenario. Susceptible genotypes may be targeted for improvement by introducing the tolerant traits using the techniques of genetic engineering.

More work at the molecular level may elucidate the effect of the increase in air temperature on the floral tissue temperature. Extensive studies focusing on membrane fluidity, cytoskeleton, chromatin structural modifications, changes in enzyme activities, and signaling cascades are necessary. The information about changes in the plant and floral transcriptome due to high-temperature stress will pave way for focused adaptation and mitigation strategies. Another approach may be to use epigenetics to generate modified resilient genotypes with potential tolerance to the environmental stresses that are a threat to their normal growth and development. A better understanding of heat stress-induced biomolecules like osmoprotectants, heat shock proteins, free radical scavengers, membrane ionic transporters, and transcription factors may come to the rescue of plant biologists to develop effective mitigation strategies.

## REFERENCES

- Bamel, K., Bamel, J.S., Rani, N., Pathak, S.K., Gahlot, S. and Singh, R.N. 2022. Crop yield prediction using satellite remote sensing-based methods. *Int J. Botany Stud.*, 7(2): 35-40
- Beppu, K., Suehara, T. and Kataoka, I. 2001. Embryo sac development and fruit set of "Satohnishiki" sweet cherry as affected by temperature, GA3, and paclobutrazol. *J. Jpn. Soc. Hortic. Sci.*, 70: 157-162. <https://doi.org/10.2503/jjshs.70.157>
- Bhojwani, S.S., Bhatnagar, S.P. and Dantu, P.K. 2015. *The Embryology of Angiosperms*. Sixth Edition. Vikas Publishing House Pvt Ltd., New Delhi, India.
- Boote, K.J., Allen, L.H., Prasad, P.V.V., Baker, J.T., Gesch, R.W., Snyder, A.M., Pan, D. and Thomas, J.M.G. 2005. Elevated temperature and CO<sub>2</sub> impact on pollination, reproductive growth, and yield of several globally important crops. *J. Agric. Meteorol.*, 60: 469-474.
- Burke, J.J., Velten, J. and Oliver, M.J. 2004. In vitro analysis of cotton pollen germination. *J. Agron.*, 96:359-368. <http://dx.doi.org/10.2134/agronj2004.0359>
- Carpeneo, S., Bassols, M.D.C., Raseira, M., Franzone, R.C., Byrne, D.H. and Silva, J.B.D. 2020. Stigmatic receptivity of peach flowers submitted to heat stress. *Acta. Sci. Agron.*, 42, <https://doi.org/10.4025/actasciagron.v42i1.42450>
- Cerović, R., Ružić, Đ., and Mičić, N. 2000. Viability of plum ovules at different temperatures. *Ann. Appl. Biol.*, 137: 53-59. <https://doi.org/10.1111/j.1744-7348.2000.tb00056.x>
- Chabert, S., Lemoine, T., Cagnato, M.R. and Morison, N. 2018. Flower age expressed in thermal time: is nectar secretion synchronous with pistil receptivity in oilseed rape (*Brassica napus* L.)? *Environ. Exp. Bot.*, 155: 628-640
- Christensen, J.H. and Christensen, O.B. 2007. A summary of the PRU-DENCE model projections of changes in European climate by the end of this century. *Clim. Change.*, 81: 7-30. <http://dx.doi.org/10.1007/s10584-006-9210-7>
- Cross, R.H., McKay, S.A.B., Mchughen, A.G., and Bonham Smith P.C. 2003. Heat stress effects on reproduction and seed set in *Linum usitatissimum* L. (flax). *Plant Cell Environ.*, 26: 1013-1020.
- Cubillos, S.L. and Hughes, L. 2016. Effects of elevated carbon dioxide (CO<sub>2</sub>) on flowering traits of three horticultural plant species. *Aust. J. Crop. Sci.*, 10(11):1523-1528. doi: 10.21475/ajcs.2016.10.11.PNE46
- Devasirvatham, V., Gaur, P.M., Mallikarjuna, N., Raju, T.N., Trethowan, R.M. and Tan, D.K. 2013. Reproductive biology of chickpea response to heat stress in the field is associated with the performance in controlled environments. *Field Crops Res.*, 142: 9-19.
- Djanaguiraman, M., Perumal, R., Jagadish, S.V.K., Ciampitti, I.A., Welti, R. and Prasad, P.V.V. 2018. Sensitivity of sorghum pollen and pistil to high-temperature stress. *Plant Cell Environ.*, 41: 1065-1082.
- Endo, M., Tsuchiya, T., Hamada, K., Kawamura, S., Yano, K., Ohshima, M., Higashitani, A., Watanabe, M. and Kawagishi-Kobayashi, M. 2009. High temperatures cause male sterility in rice plants with transcriptional alterations during pollen development. *Plant Cell Physiol.*, 50: 1911-1922.
- Erickson, A.N. and Markhart, A.H. 2002. Flower developmental stage and organ sensitivity of bell pepper (*Capsicum annuum* L.) to elevated temperature. *Plant Cell Environ.*, 25: 123-130.
- Estornell, L.H., Gómez, M.D., Pérez-Amador, M.A., Talón, M. and Tadeo, F.R. 2016. Secondary abscission zones: Understanding the molecular mechanisms triggering styler abscission in citrus. *Acta. Hortic.*, 1119: 65-72. <https://doi.org/10.17660/ActaHortic.2016.1119.9>
- Foolad, M.R. 2005. Breeding for Abiotic Stress Tolerances in Tomato. In Ashraf, M. and Harris P.J.C. (eds.), *Abiotic Stresses: Plant Resistance Through Breeding and Molecular Approaches*, The Haworth Press, New York, pp.613-684
- Goetz, M., Guivarch, A., Hirsche, J., Bauerfeind, M.A., González, M.C., Hyun, T.K., Eom, S.H., Chriqui, D., Engelke, T., Großkinsky, D.K. and Roitsch, T. 2017. Metabolic control of tobacco pollination by sugars and invertases. *Plant Physiol.*, 173(2): 984-997. <doi.org/10.1104/pp.16.01601>
- Gray, S.B., and Brady, S.M. 2016. Plant developmental responses to climate change. *Dev. Biol.*, 419(1): 64-77.
- Gross, Y. and Kigel, J. 1994. Differential sensitivity to high temperature of stages in the reproductive development of common bean (*Phaseolus vulgaris* L.). *Field Crops Res.*, 36: 201-212.
- Hatfield, J.L., Boote, K.J., Kimball, B.A., Ziska, L.H., Izaurralde, R.C., Ort, D., Thomson, A. and Wolfe, D. 2011. Climate impacts on agriculture: Implications for crop production. *J. Agron.*, 103: 351-370. <http://dx.doi.org/10.2134/agronj2010.0303>
- Hebbar, K.B., Neethu, P., Sukumar, P.A., Sujithra, M., Santhosh, A., Ramesh, S.V., Niral, V., Hareesh, G.S., Nameer, P.O. and Prasad, P.V.V. 2020. Understanding physiology and impacts of high-temperature stress on

- the progamic phase of coconut (*Cocos nucifera* L.). *Plants*, 9: 1651-1670. doi:10.3390/plants9121651
- Hedhly, A. 2011. Sensitivity of flowering plant gametophytes to temperature fluctuations. *Environ. Exp. Bot.*, 74(1): 9-16. DOI: 10.1016/j.envexpbot.2011.03.016
- Hedhly, A., Hormaza, J.I. and Herrero, M. 2009. Global warming and sexual plant reproduction. *Trends Plant Sci.*, 14(1):30-36. doi: 10.1016/j.tplants.2008.11.001 PMID: 19062328
- Hiscock, S.J. and Allen, A.M. 2008. Diverse cell signaling pathways regulate pollen-stigma interactions: The search for consensus. *New Phytol.*, 179(2): 286-317. DOI: 10.1111/j.1469-8137.2008.02457.
- Jagadish, S.V., Way, D.A. and Sharkey, T.D. 2021. Scaling plant responses to high temperature from cell to ecosystem. *Plant Cell Environ.*, 44(7): 1987-1991. Doi: 10.1111/pce.14082, 44, 7. doi.org/10.1111/pce.14082
- Jiang, N., Pinghui, Y., Weimeng, F., Guangyan, L., Baohua, F., Tingting, C., Hubo, L., Longxing, T. and Guanfu, F. 2020. Acid invertase confers heat tolerance in rice plants by maintaining the energy homeostasis of spikelets. *Plant Cell Environ.*, 43(5): 1273-1287.
- Kakani, V.G., Reddy, K.R., Koti, S., Wallace, T.P., Prasad, P.V.V., Reddy, V.R. and Zhao, D. 2005. Differences *in vitro* pollen germination and pollen tube growth of cotton cultivars in response to high temperature. *Ann. Bot.*, 96: 59-67. <http://dx.doi.org/10.1093/aob/mci149>
- Katano, K., Oi, T. and Suzuki, N. 2020. Failure of pollen attachment to the stigma triggers elongation of stigmatic papillae in *Arabidopsis thaliana*. *Front. Plant Sci.*, 11: 989-1000. doi.org/10.3389/fpls.2020.00989
- Kaushal, N., Awasthi, R., Gupta, K., Gaur, P.M., Siddique, K.H.M. and Nayyar, H. 2013. Heat-stress-induced reproductive failures in chickpea (*Cicer arietinum*) are associated with impaired sucrose metabolism in leaves and anthers. *Funct. Plant Biol.*, 40:1334-1349.
- Koti, S., Reddy, K.R., Reddy, V.R., Kakani, V.G. and Zhao, D. 2005. Interactive effects of carbon dioxide, temperature, and ultraviolet-B radiation on soybean (*Glycine max* L.) flower and pollen morphology, pollen production, germination, and tube lengths. *J. Exp. Bot.*, 56: 725-736.
- Kumar, S., Thakur, M., Mitra, R., Basu, S. and Anand, A. 2021. Sugar metabolism during pre- and post-fertilization events in plants under high-temperature stress. *Plant Cell Rep.*, 1: 1-19. <https://doi.org/10.1007/s00299-021-02795-1>
- Li, X., Lawas, L.M., Malo, R., Glaubitz, U., Erban, A., Mauleon, R., Heuer, S., Zuther, E., Kopka, J., Hinch, D.K. and Jagadish, K.S. 2015. Metabolic and transcriptomic signatures of rice floral organs reveal sugar starvation as a factor in reproductive failure under heat and drought stress. *Plant Cell Environ.*, 38(10): 2171-2192. doi.org/10.1111/pce.12545
- Lora, J., Herrero, M. and Hormaza, J.I. 2011. Stigmatic receptivity in a dichogamous early divergent angiosperm species, *Annona cherimola* (Annonaceae): Influence of temperature and humidity. *Am. J. Bot.*, 98: 265-274. <https://doi.org/10.3732/ajb.1000185>
- Losada, J.M. and Herrero, M. 2012. Arabinogalactan-protein secretion is associated with the acquisition of stigmatic receptivity in the apple flower. *Ann. Bot.*, 110(3): 573-584. DOI:10.1093/aob/mcs116
- Montal, R., Cuenca, J., Vives, M.C., Navarro, L., Ollitrault, P. and Aleza, P. 2019. Influence of temperature on the progamic phase in Citrus. *Environ. Exp. Bot.*, 166: 103806 doi: <https://doi.org/10.1016/j.envexpbot.2019.103806>
- Morrison, M.J. and Stewart, D.W. 2002. Heat stress during flowering in summer Brassica. *Crop Sci.*, 42(3): 797-803.
- Müller, F., Xu, J., Kristensen, L., Wolters-Arts, M., de Groot, P.F., Jansma, S.Y., Mariani, C., Park, S. and Rieu, I. 2016. High-temperature-induced defects in tomato (*Solanum lycopersicum*) anther and pollen development are associated with reduced expression of B-class floral patterning genes. *PLoS One*, 11(12): e0167614. doi.org/10.1371/journal.pone.0167614.
- Mutters, R.G. and Hall, A.E. 1992. Reproductive responses of cowpea to high temperature during different night periods. *Crop Sci.*, 32(1): 202-206.
- Nascimento, W.M., Vieira, J.V., Silva, G.O., Reitsma, K.R. and Cantliffe, D.J. 2008. Carrot seed germination at high temperature: Effect of genotype and association with ethylene production. *Hort. Sci.*, 43(5):1538-1543.
- Pallais, N., Mulcahy, D., Fong, N., Falcon, R. and Schmiediche, P. 1988. The Relationship Between Potato Pollen and True Seed: Effects of High Temperature and Pollen Size. In: Cresti, M., Gori, P. and Pacini, E. (eds.), *Sexual Reproduction in Higher Plants*. Springer, Berlin, Heidelberg, pp. 13-45. [https://doi.org/10.1007/978-3-642-73271-3\\_45](https://doi.org/10.1007/978-3-642-73271-3_45)
- Postweiler, K., Stösser, R. and Anvari, S.F. 1985. The effect of different temperatures on the viability of ovules in cherries. *Sci. Hortic.*, 25: 235-239. [https://doi.org/10.1016/0304-4238\(85\)90120-7](https://doi.org/10.1016/0304-4238(85)90120-7).
- Prasad, P.V.V., Boote, K.J., Allen L.H. and Thomas, J.M.G. 2003. Super-optimal temperatures are detrimental to peanut (*Arachis hypogaea* L.) reproductive processes and yield both ambient and elevated carbon dioxide. *Glob. Change Biol.*, 9: 1775-1787.
- Pressman, E., Peet, M.M. and Pharr, D.M. 2002. The effect of heat stress on tomato pollen characteristics is associated with changes in carbohydrate concentration in the developing anthers. *Ann. Bot.*, 90: 631-636.
- Rani, N., Bamel, K., Shukla, A. and Singh, N. 2022. Analysis of five mathematical models for crop yield prediction. *South Asian J. Exp. Biol.* 12(1): 46-54
- Rao, G.U., Jain, A. and Shivanna, K.R. 1992. Effects of high temperature stress on *Brassica* pollen: viability, germination and ability to set fruits and seeds. *Ann. Bot.*, 68:193-198
- Rawat, B.R. 2015. Reproductive success of angiosperms in response to climate: An assessment. In: Kapoor, R., Kaur, I., and Koul, I.K. (eds.), *Plant Reproductive Biology and Conservation*. International Publishing House Pvt. Ltd., New Delhi, pp. 401-423.
- Saini, H.S. 1997. Effects of water stress on male gametophyte development in plants. *Sex. Plant Repro.*, 10: 67-73.
- Shi, W., Li, X., Schmidt, R.C., Struik, P.C., Yin, X. and Jagadish, S.V.K. 2018. Pollen germination and *in vivo* fertilization in response to high temperature during flowering in hybrid and inbred rice. *Plant Cell Environ.*, 41: 1287-1297.
- Snider, J.L. and Oosterhuis, D.M. 2011. How do timing, duration, and severity of heat stress influence pollen-pistil interactions angiosperms? *Plant Signal. Behav.*, 6(7): 930-933. doi.org/10.4161/psb.6.7.15315
- Snider, J.L., Oosterhuis, D.M. and Kawakami, E.M. 2011. Diurnal pollen tube growth is slowed by high temperature in field-grown *Gossypium hirsutum* pistils. *J. Plant. Physiol.*, 168(5): 441-448. doi.org/10.1016/j.jplph.2010.08.003
- Snider, J.L., Oosterhuis, D.M., Skulman, B.W. and Kawakami, E.M. 2009. Heat stress induced limitations to reproductive success in *Gossypium hirsutum*. *Physiol. Plant*, 137(2): 125-138. <https://doi.org/10.1111/j.1399-3054.2009.01266.x>
- Song, G., Wang, M., Zeng, B., Zhang, J., Jiang, C., Hu, Q., Geng, G. and Tang, C. 2015. Anther response to high-temperature stress during development and pollen thermotolerance heterosis as revealed by pollen tube growth and *in vitro* pollen vigor analysis in upland cotton. *Planta*, 24: 1271-1285.
- Takeoka, Y., Hiroi, K., Kitano, H. and Wada, T. 1991. Pistil hyperplasia in rice spikelets is affected by heat stress. *Sex. Plant Reprod.*, 4(1): 39-43.
- Talwar, S., Tayal, P., Kumar, S., Bamel, K. and Prabhavathi, V. 2015. Climate Change: A Threat to Biodiversity. Proceedings of National Conference on Climate Change: Impacts, Adaptation, Mitigation Scenario and Future challenges in Indian Perspective, 2-3 March 2015, New Delhi, Department of Botany, Deen Dayal Upadhyaya College, Delhi, pp. 84-93.

- Thuzar, M., Puteh, A.B., Abdullah, N.A.P., Mohd-Lassim, M.B. and Kamaruzaman, J. 2010. The effects of temperature stress on the quality and yield of soya bean (*Glycine max* L.) Merrill. *J. Agric. Sci.*, 2(1): 172-179.
- Wang, Y., Impa, S.M., Sunkar, R. and Jagadish, S.K. 2021. The neglected other half-role of the pistil in plant heat stress responses. *Plant Cell Environ.*, 44(7): 2200-2210
- Wang, Y., Tao, H., Tian, B., Sheng, D., Xu, C., Zhou, H., Huang, S. and Wang, P. 2019. Flowering dynamics, pollen, and pistil contribution to grain yield in response to high temperature during maize flowering. *Environ. Exp. Bot.*, 158: 80-88.
- Warrag, M.O.A. and Hall, A.E. 1984. Reproductive responses of cowpea (*Vigna unguiculata* (L.) Walp) to heat stress. II Responses to night air temperature. *Field Crops Res.*, 8: 17-33.
- Zinn, K.E., Ozdemir, M.T. and Harper, J.F. 2010. Temperature stress and plant sexual reproduction: uncovering the weakest links. *J. Exp. Bot.*, 61(7): 1959-1968. doi: 10.1093/jxb/erq053 PMID: 20351019



# Application of a Two-Level Full Factorial Design for the Synthesis of Composite Bioplastics from Durian Seed Flour and Yellow Konjac Flour Incorporating Ethanolic Extract of *Syzygium myrtifolium* Leaves and its Characterization

N.D. Permatasari<sup>(\*\*)</sup>†, J.E. Witoyo<sup>\*\*\*</sup>, M. Masruri<sup>\*\*\*\*</sup>, S.S. Yuwono<sup>\*\*</sup> and S.B. Widjanarko<sup>\*\*\*\*</sup>

\*Department of Food Technology, Politeknik Tonggak Equator, Jl. Fatimah No 1-2, Pontianak, 78243, Indonesia

\*\*Department of Food Science and Biotechnology, Faculty of Agricultural Technology, Universitas Brawijaya, Jalan Veteran, Malang, 65141, Indonesia

\*\*\*Alumnus of Department of Agroindustrial Technology, Faculty of Agricultural Technology, Universitas Brawijaya, Jalan Veteran, Malang, 65141, Indonesia

\*\*\*\*Department of Chemistry, Faculty of Mathematics and Natural Science, Universitas Brawijaya, Jalan Veteran, Malang, 65141, Indonesia

\*\*\*\*\*Porang Research Center, Universitas Brawijaya, Jalan Veteran, Malang, 65141, Indonesia

†Corresponding author: Nelsy Dian Permatasari; nelsypolteq@gmail.com

## Nat. Env. & Poll. Tech.

Website: [www.neptjournal.com](http://www.neptjournal.com)

Received: 12-04-2022

Revised: 25-05-2022

Accepted: 29-05-2022

## Key Words:

Bioplastics

Durian seed

*Amorphophallus muelleri*

Physical characteristics

*Syzygium myrtifolium*

## ABSTRACT

Increasing environmental problems related to synthetic plastics for food packaging encourage the creation of more environmentally friendly plastics from Indonesia's local natural resources, such as durian seed, yellow konjac, and *Syzygium myrtifolium* leaves, which are abundant in nature. The purpose of the study was to evaluate the effect of the durian seed flour (DSF) mass, yellow konjac flour (YKF) mass, and the concentration of ethanolic extract of *S. myrtifolium* leaves (5-25%) on the tensile strength, elongation, and inhibition zone area of composite bioplastics. The two-level full factorial design was conducted for this experiment with 3 independent factors: DSF mass (0.5-1 g), YKF mass (0.5-1 g), and the concentration of ethanolic extract of *S. myrtifolium* leaves (5-25% b/v), and 3 responses were observed: tensile strength, elongation, and inhibition zone area. The physicochemical characteristics were then used to further describe the best combination. The results showed that the DSF mass had only affected tensile strength, whereas the YKF mass had affected tensile strength and elongation of composite bioplastics. Meanwhile, the concentration of ethanolic extract of *S. myrtifolium* leaves only affects the inhibition zone area. The best combination was found in the DSF mass of 0.5 g, YKF mass of 1 g, and the concentration of ethanolic extract of *S. myrtifolium* leaves of 25%, with the tensile strength of 3.30 MPa, elongation of 50.00%, and inhibition zone area of 15.33 mm. Moreover, these combinations also had a thickness of 0.115 mm, modulus young of 0.066 MPa, density of 1.37 g.cm<sup>-3</sup>, moisture content of 17.14%, and water solubility of 76.91%.

## INTRODUCTION

Synthetic plastics have posed significant problems and challenges to the world today. It produces over 400 Mt per year globally and takes a long time to decompose. Synthetic plastics have unfriendly environmental properties that pollute humans indirectly (Fahim et al. 2021). Thus, environmentally friendly plastics are needed to reduce the impact of synthetic plastics. Generally, eco-friendly plastics are made from renewable materials such as starch (Thakur et al. 2019) or whole flour (Retnowati et al. 2015). Durian seed is an exotic natural resource that is relatively abundant and underutilization in Indonesia as the by-product of durian

fruit. The production of durian seeds as a bioproduct is approximately 233960.4 tons, according to data published by the BPS-Statistics Indonesia 2020 (BPS-Statistics Indonesia 2020). For further applications, durian seeds can be transformed into durian seed flour (DSF).

DSF contains high starch, gum, trace elements, and minerals (Leemud et al. 2020). Starch, gums, proteins, and lipids are constituent components in manufacturing eco-friendly plastics (Thakur et al. 2019, Permatasari et al. 2021). Our previous study reported the DSF had a starch content of 41.42%, a protein content of 6.26%, a fat content of 0.57%, a carbohydrate content of 80.61%, and a low fiber of 0.85%

(Permatasari et al. 2022), so it is promising as a source of bioplastics materials. Previously, the bioplastic production from DSF has been carried out and reported by Retnowati et al. (2015). However, Retnowati and her team found that bioplastics of DSF in individual composition had undesirable characteristics such as low modulus young, tensile strength, and elongation. Furthermore, in our preliminary study, the utilization of DSF alone as raw material could not form bioplastics properly. Thus, to improve its characteristics, it is necessary to substitute it with other ingredients, such as yellow konjac flour (YKF).

YKF is a product of processing yellow konjac (*Amorphophallus muelleri*) tubers through a dry method (Witoyo et al. 2020, 2021). It contains glucomannan, a type of polysaccharide with diverse food and non-food application (Zhang et al. 2014). Glucomannan is one of the biopolymer-based packaging film materials which attracts attention because it is classified as a safe, edible, and renewable polysaccharide (Zhang & Rhim 2022). Kurt and Kahyaoglu (2014) reported that it succeeded in making bioplastics from sahleplu glucomannan. Another study reported that the substitution of konjac glucomannan in biofilms from keratin could produce biofilms with better tensile strength and modulus young than those made from pure keratin (Strnad et al. 2019). To improve the anti-bacterial properties of the bioplastics produced, ethanol extract from *S. myrtifolium* leaves is added. Ahmad et al. (2021) reported that the ethanolic extract of *S. myrtifolium* leaves could inhibit bacterial growth of *A. baumannii*, *B. cereus*, *E. coli*, *K. pneumoniae*, *P. aeruginosa*, and *S. aureus* in vitro study. However, no one has applied ethanol extract from *S. myrtifolium* leaves to produce bioplastics as natural anti-bacterial agents.

Two-level full factorial is a recently introduced method used to study the interaction of various parameters during the process. Two-level factorial design helps determine significant independent variables that affect the dependent variable with few data compared with the conventional one factor (Lim et al. 2018). However, this approach is still rarely used to synthesize composite bioplastics and evaluate the effect of the independent factors on the specific responses of composite bioplastics. Thus, this study uses a two-level full factorial design to synthesize bioplastics from DSF and YKF incorporated with ethanolic extract of *Syzygium myrtifolium* and evaluated their effect on the mechanical properties and inhibition zone area of composite bioplastics.

## MATERIAL AND METHODS

### Materials

Durian seed flour (DSF) used in this study was obtained from our previous study (Permatasari et al. 2022), with the

characteristics as follows: starch content of 41.42%, amylopectin content of 21.79%, the protein content of 6.26%, the fat content of 0.57%, the carbohydrate content of 80.61%, and fiber of 0.85%. *S. myrtifolium* was obtained from the center of flowers and ornamental plants, Sidomulyo, Batu, and identified in *Materia Medica*, Batu, East Java, Indonesia. Yellow konjac flour (YKF) was obtained from the previous study (Witoyo et al. 2021) and used further purified using ethanol 3 times, then powdered using the roller mill (locally made), which contained glucomannan content of 81% d.b and a viscosity of 11000 mPa.s. All chemical reagents were purchased in analytical grade from Merck in Germany through the Chemical and Food Biochemistry Laboratory in Universitas Brawijaya.

### Extraction of *Syzygium myrtifolium*

The extraction of *S. myrtifolium* is followed by methods described by Ahmad et al. (2022) with minor modifications. Briefly, the fresh red leaves of *S. myrtifolium* were selected, cleaned, and blended into small pieces. Then, mixed and agitated (120 rpm) with 96% of ethanol for 48 h at room temperature, evaporated, and dried using a rotary evaporator at 60°C until the paste of the extracts was obtained. For further applications, the paste extracts were stored in a dark bottle (5°C in refrigeration condition).

### Synthesis of Composite Bioplastics

The production of composite bioplastics adopts Kurt and Kahyaoglu (2014) and Nasution and Wulandari (2021) methods, with the total of solid on bioplastics blends being 1.5% b/v. Briefly, DSF (0.5 or 1 g) was mixed with distilled water (100 mL) and stirred until the temperature reached 75 °C. Then, the YKF (0.5 or 1 ram) and 5 mL of ethanol extract of *S. myrtifolium* leaves (5% or 25% b/v) were mixed in the DSF solution until homogenized, respectively. After that, 5 mL of glycerol was added to the mixture solution, stirred, heated until fully gelatinized, and stood for 10 min. Then, the composite bioplastic solution was poured into a petri dish with a 14 cm diameter, followed by drying at 50°C for 48 h. After drying, the opaque composite bioplastic was input into a desiccator for stabilization and stored for further analysis.

#### Determined Bioplastic Characteristics

The elongation and tensile strength of composite bioplastics were measured using the ASTM- Methods D-638 (Umiyati et al. 2020). Before the measurement, the composite bioplastics were incubated at 28°C for 2 days in the humidity-controlled chamber. The anti-bacterial of bioplastics was evaluated using methods adopted by Wang et al. (2019). *E. coli* bacteria suspensions ( $10^5$  CFU.mL<sup>-1</sup>) were subsequently inoculated and cultured on agar media in Petri dishes. Then,

the bioplastic was cut in diameter of 10 mm, placed on a petri dish, and incubated for 12 h at 37°C. The diameter of the inhibition zone area was measured and recorded. The best composite bioplastic was further characterization, like thickness (Oluwasina et al. 2017), density (Salgado et al. 2010), moisture content (Oluwasina et al. 2017), water solubility (Rhim et al. 2007), and microstructure (Retnowati et al. 2015). The characterization was conducted in duplicate.

### Experimental Design and Statistical Analysis

Eight experiments ( $2^3 = 8$ ) were conducted to evaluate three independent factors at two levels (Lim et al. 2018). The independent factors used in the study were durian seed flour mass (Latter known as DSF mass), yellow konjac flour (Latter known as YKF mass), and the concentration of ethanolic extract of *S. myrtifolium* leaves. The response data, namely tensile strength, elongation, and inhibition zone area, were analyzed using Design Expert Ver. 13 (trial version, Stat-Ease, Inc., Minneapolis, MN, USA). The design experiment of bioplastics synthesis is listed in Table 1.

Table 1: The design experiment of composite bioplastics synthesis.

No.	DSF mass [g]	YKF mass [g]	The concentration of ethanolic extract of <i>S. myrtifolium</i> leaves [%]
1	1.0	1.0	5.0
2	0.5	1.0	5.0
3	1.0	0.5	5.0
4	0.5	0.5	5.0
5	0.5	1.0	25.0
6	1.0	0.5	25.0
7	1.0	1.0	25.0
8	0.5	0.5	25.0

Table 2: The characteristics of composite bioplastics.

No.	Independent Factor			Response		
	DSF mass [g]	YKF mass [g]	The concentration of ethanolic extract of <i>S. myrtifolium</i> leaves [%]	Tensile Strength [MPa]	Elongation [%]	Inhibition Zone Area [mm]
1	1.0	1.0	5.0	3.40	46.67	12.85
2	0.5	1.0	5.0	3.60	50.00	7.92
3	1.0	0.5	5.0	2.20	40.00	11.92
4	0.5	0.5	5.0	2.80	43.33	7.93
5	0.5	1.0	25.0	3.30	50.00	15.33
6	1.0	0.5	25.0	2.00	30.00	14.88
7	1.0	1.0	25.0	3.00	46.67	15.08
8	0.5	0.5	25.0	3.00	43.33	13.57

## RESULTS AND DISCUSSION

### The Tensile Strength

The tensile strength of composite bioplastic was 2.0 to 3.6 MPa, as listed in Table 2. This result is in the range of tensile strength data reported by Retnowati et al. (2015), which is 1.07 to 5.31 MPa in durian seed flour (DSF)–jack seed fruit (JSF) bioplastics. Based on the statistical analysis in Table 3, the tensile strength of composite bioplastics was affected by the DSF mass and YKF mass. The Pareto chart for tensile strength of composite bioplastics, as presented in Fig. 1A, showed that the YKF mass had a higher t-value, followed by the DSF mass and the concentration of ethanolic extract of *S. myrtifolium* leaves. It indicates that the YKF mass had a dominant effect on the tensile strength of composite bioplastics. Kalaydzhiev et al. (2019) stated that the higher t-value observed on the Pareto graph indicates the dominant factor's effect on a specific response. Fig. 1B shows the individual percentage contribution of each independent factor on the tensile strength of composite bioplastic. For tensile

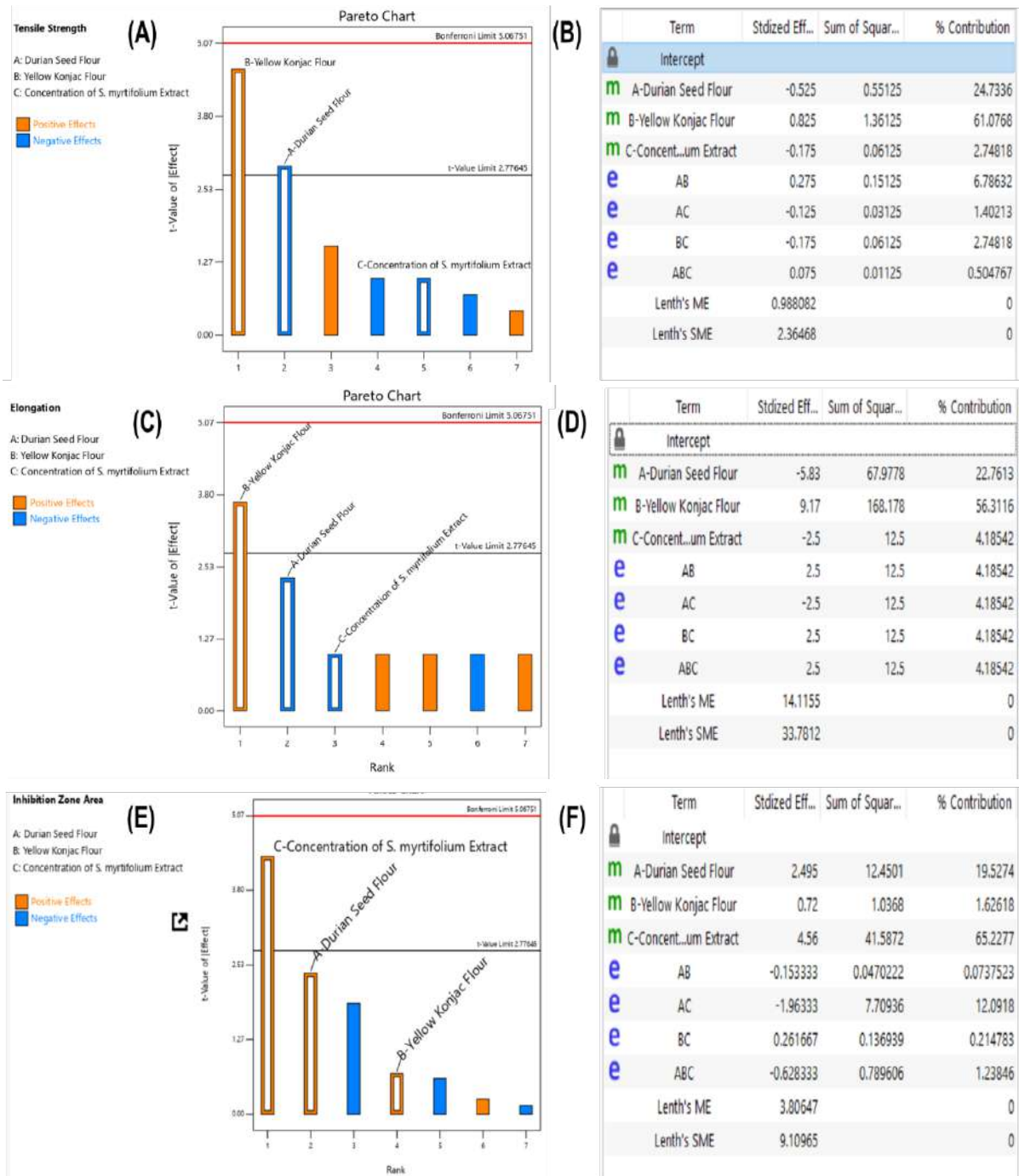


Fig. 1: Pareto chart for tensile strength (A), elongation (C), and inhibition zone area (E) of composite bioplastics, and percentage contribution chart for tensile strength (B), elongation (D), and inhibition zone area (F) on composite bioplastics.

strength response, the YKF mass had the highest percentage of contribution of 61.08%, followed by DSF mass and concentration of ethanolic extract of *S. myrtifolium* leaves with a contribution of 24.73% and 2.75%, respectively. The interaction also contributed between factors of 0.5 to 6.98%.

As a result, YKF mass is more critical than DSF mass, and the concentration of ethanolic extract of *S. myrtifolium* leaves, has a more significant impact on tensile strength, as evidenced by a higher percentage contribution to change measured variable.



Fig. 1A and Table 3 showed that the DSF mass had a significantly negative effect on the tensile strength. The increasing DSF mass from 0.5 to 1.0 g significantly decreased the tensile strength of composite bioplastics, as depicted in Fig. 2A. The decrease in tensile strength was due to the high amylopectin content in our DSF samples, which is 21.79% compared to amylose (19.64%), which contributed in composite bioplastics. Woggum et al. (2014) reported that the amylose content of starch contributes to film strength and the branched structure of amylopectin, leading to lower mechanical properties in films. However, this result was in line with Retnowati et al. (2015), who reported that the increase in the DSF ratio significantly affected the decrease in tensile strength. In addition, the Pareto chart (Fig. 1A) and Table 3 showed that the YKF mass had a significantly positive effect on the tensile strength. The tensile strength of composite bioplastic was significantly improved with increasing YKF mass, as presented in Fig. 2B. It is most likely due to the intermolecular interactions of glucomannan macromolecules in YKF, which can maintain bioplastics' compactness and stability and prevent brittleness. Moreover, the interaction of glucomannan in YKF with polymers in DSF (such as starch, gum, protein, and fat) and the plasticizer through hydrogen

bonding might contribute to the increased tensile strength of composite bioplastics. Fahrullah et al. (2020) reported that adding polysaccharides, namely konjac flour, at high concentrations increased tensile strength and prevented the brittleness of whey-based edible films. Ma et al. (2021) stated that the increased tensile strength in film-based chitosan with the addition of konjac glucomannan (KGM) is caused by their hydrogen bonding interaction. Furthermore, the concentration of ethanolic extract from *S. myrtifolium* leaves had an insignificantly negative effect on tensile strength, as presented in Fig. 1A, Fig. 2C, and Table 3.

### The Elongation

The elongation of composite bioplastic was 30.00 to 50.00%, as listed in Table 2. This result had higher elongation than data reported by Retnowati et al. (2015), which is 29.26 to 44.11 % in durian seed flour (DSF)– jack seed fruit (JSF) bioplastics. Based on the statistical analysis in Table 3, the elongation of composite bioplastics was only affected by YKF mass. Pareto chart for elongation of composite bioplastics, as presented in Fig. 1C, showed that the YKF mass had a higher t- value, followed by DSF mass and the concentration of ethanolic extract of *S. myrtifolium* leaves.

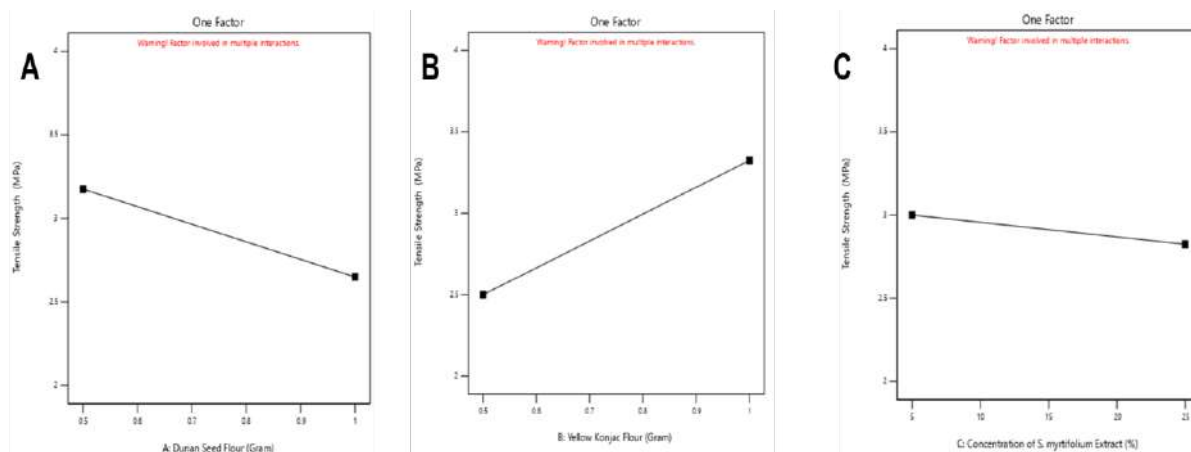


Fig 2: Effect of DSF mass (A), YKF mass (B), and the concentration of ethanolic extract of *S. myrtifolium* leaves (C) on the tensile strength of composite bioplastics.

Table 3: Coefficient estimates and significance analysis of composite bioplastics responses.

Factor	Coefficient estimates		
	Tensile Strength	Elongation	Inhibition Zone Area
Intercept	2.9125	43.75	12.43
DSF mass	-0.2625 <sup>s</sup>	-2.915 <sup>ns</sup>	1.25 <sup>ns</sup>
YKF mass	0.4125 <sup>s</sup>	4.585 <sup>s</sup>	0.3600 <sup>ns</sup>
The concentration of ethanolic extract of <i>S. myrtifolium</i> leaves	-0.0875 <sup>ns</sup>	-1.25 <sup>ns</sup>	2.28 <sup>s</sup>

Remarks: s: significant, and ns: not significant

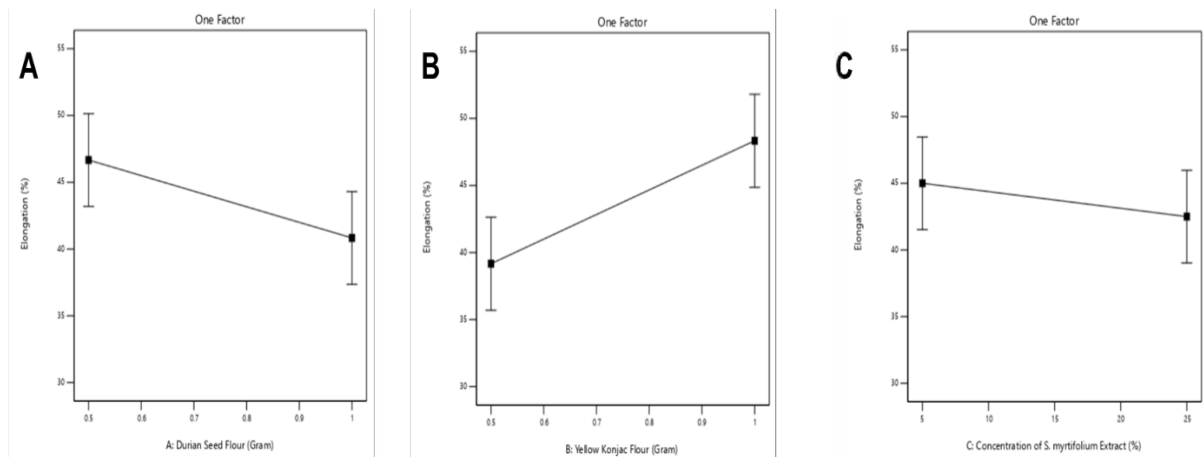


Fig 3: Effect of DSF mass (A), YKF mass (B), and the concentration of ethanolic extract of *S. myrtifolium* leaves (C) on the elongation of composite bioplastics.

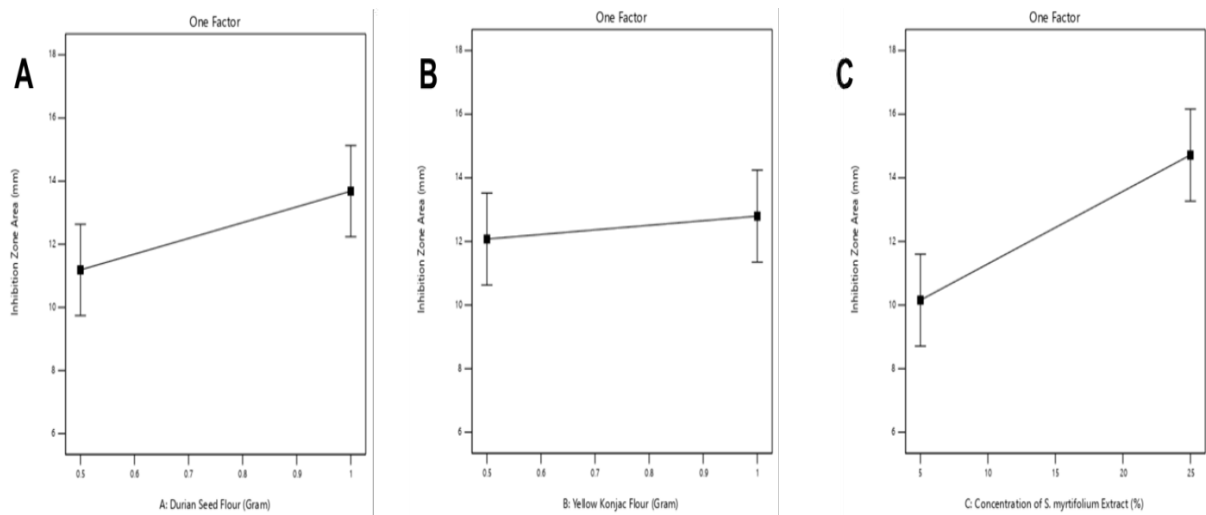


Fig. 4: Effect of DSF mass (A), YKF mass (B), and the concentration of ethanolic extract of *S. myrtifolium* leaves (C) on the inhibition zone area of composite bioplastics.

It indicates that the YKF mass had a dominant effect on the elongation of composite bioplastics. Kalaydzhev et al. (2019) that the higher t-value observed on the Pareto graph indicates the dominant factor effect on a specific response. Fig. 1D shows the individual percentage contribution of each independent factor to the elongation of composite bioplastic. The YKF mass had the highest effect on the elongation with a contribution of 51.31%, followed by DSF mass and concentration of ethanolic extract of *S. myrtifolium* leaves with a contribution of 22.76% and 4.18%, respectively. The interaction also had a contribution between factors was 4.19% in all factor interactions. As a result, YKF mass is more critical than DSF mass, and the concentration of ethanolic extract of *S. myrtifolium* leaves, has a more significant impact on

elongation, as evidenced by a higher percentage contribution to change measured variable.

Fig. 1C and Table 3 showed that the DSF mass had an insignificantly negative effect on elongation. The increase of DSF mass from 0.5 to 1.0 g tends to decrease the elongation of composite bioplastics, as depicted in Fig. 3A. This result was in line with the Retnowati et al. (2015), who reported that the increase in the DSF ratio significantly affected the decrease in elongation. In addition, the Pareto chart (Fig. 1C) and Table 3 showed that the YKF mass had a significantly positive effect on elongation. The elongation of composite bioplastic was significantly improved with increasing YKF mass, as presented in Fig. 3B. It might be due to the glucomannan intermolecular interaction in YKF, which affects

the elasticity and matrix strength of composite bioplastics. Additionally, the interaction of glucomannan in YKF with polymers in DSF (such as starch, gum, protein, and fat) and the plasticizer through hydrogen bonding might contribute to the increasing elongation of composite bioplastics. Fahrul-lah et al. (2020) stated that the increase in the elongation of whey-based edible films with the addition of konjac flour was caused by the polysaccharide content in konjac flour. Ma et al. (2021) stated that adding konjac glucomannan (KGM) improved film-based chitosan's elongation, probably the interaction hydrogen bonding of chitosan – KGM in molecular stages. The concentration of ethanolic extract from *S. myrtifolium* leaves had an insignificantly negative effect on elongation, as presented in Fig. 1C, Fig. 3C, and Table 3.

### The Inhibition Zone Area

The inhibition zone area of composite bioplastic was 7.92 to 15.33 mm, as listed in Table 2. This result was reported in the range of previous work by Yuniarni et al. (2020) (9.00 to 10.37 mm). Based on the statistical analysis in Table 3, the inhibition zone area of composite bioplastics was only affected by the concentration of ethanolic extract of *S. myrtifolium* leaves. The Pareto chart for the inhibition zone area of composite bioplastics, as presented in Fig. 1E, showed that the concentration of ethanolic extract of *S. myrtifolium* leaves had a higher t- value, followed by DSF mass and YKF mass. It indicates that the concentration of ethanolic extract of *S. myrtifolium* leaves had a dominant effect on the inhibition zone area of composite bioplastics. Kalaydzhiev et al. (2019) that the higher t-value observed on the Pareto graph indicates the dominant factor effect on a specific response. Fig. 1F shows the individual percentage contribution of each independent factor to the inhibition zone area of composite bioplastic. The concentration of ethanolic

extract of *S. myrtifolium* leaves had the highest effect on the inhibition zone area with a contribution of 65.23%, followed by DSF mass and YKF mass with a contribution of 19.53% and 1.63%, respectively. The interaction also contributed between factors of 0.07 to 1.23%. It indicates that the highest contribution of independent factors reflects a dominant effect on the specific response in bioplastic composites. As a result, the concentration of ethanolic extract of *S. myrtifolium* leaves is more critical than YKF mass and DSF mass, it has a more significant impact on the inhibition zone area, as evidenced by a higher percentage contribution to change measured variable.

Fig. 1E and Table 3 showed that the DSF mass had an insignificantly positive effect on the inhibition zone area. The increase of DSF mass from 0.5 to 1.0 g tends to increase the inhibition zone area of composite bioplastics, as depicted in Fig. 4A. In addition, the Pareto chart (Fig. 1F) and Table 3 showed that the YKF mass had an insignificantly positive effect on the inhibition zone area, as presented in Fig. 4B. Moreover, the concentration of ethanolic extract of *S. myrtifolium* leaves had a significantly positive effect on the inhibition zone area, as illustrated in Fig. 1E and Table 3. The increase in the concentration of ethanolic extract of *S. myrtifolium* leaves from 5.0 to 25%, increase the inhibition zone area of composite bioplastics, as depicted in Fig. 4C. Yuniarni et al. (2020) reported that the ethanol extract of *S. myrtifolium* could inhibit the growth of *E. coli* with inhibition diameter zones of 9.00, 9.30, and 10.37 mm at concentrations of ethanol extract of *S. myrtifolium* of 6, 12.5, and 12.5% in the *in-vitro* study, respectively. Ahmad et al. (2022) also reported that the ethanol extract of *S. myrtifolium* showed potent inhibitory activity against *E. coli* with a minimum inhibitory concentration of 0.63 mg mL<sup>-1</sup> in the *in-vitro* study. Chemical compounds in ethanolic

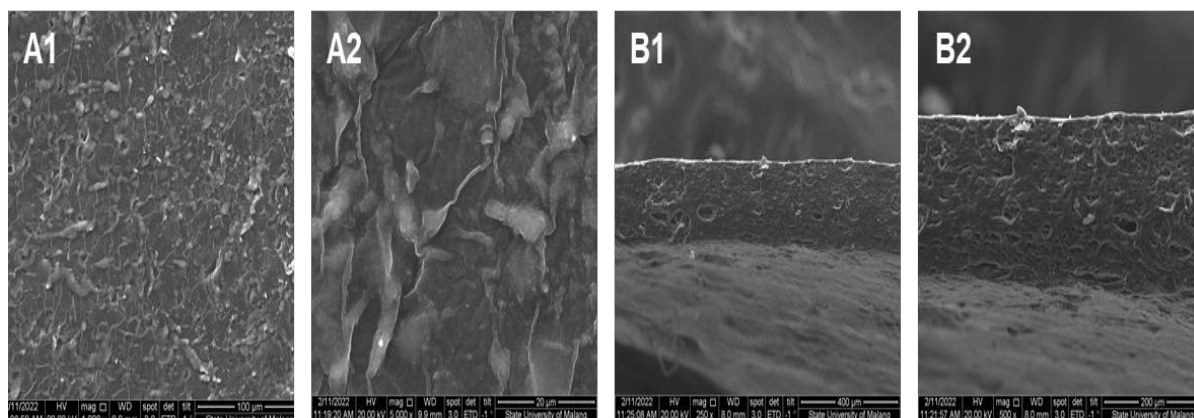


Fig. 5: The microstructure of the surface composite bioplastics in 1000x (A1), 5000x (A2) magnifications, and cross-section in 250x (B1), and 500x (B2) magnifications.

extract of *S. myrtifolium* leaves that act as an anti-bacterial are auraptinol, calopiptin, quercetin-3-o--L-arabinopyranoside, and quercetin-3-o--D-glucuronide (based on LC-MS screening analysis and data not shown). Tan et al. (2017) reported that crude extracts of the roots of *Prangos hulussii* that contain auraptinol compounds had anti-bacterial activity to inhibit the growth of g-positive and g-negative bacteria. Jaisinghani (2017) reported that the quercetin compound had anti-bacterial properties in *E. coli* NCIM2065 with a minimum inhibitory concentration (MIC) of 400 mcg.mL<sup>-1</sup> and minimum bactericidal concentration (MBC) of >500 mcg.mL<sup>-1</sup>. Elansary et al. (2020) reported that the quercetin and quercetin 3-glucuronide had moderate anti-bacterial activities on *B. cereus*, *P. aeruginosa*, *L. monocytogenes*, *E. coli*, *M. flavus* and *S. aureus* in the *in-vitro* study.

### Determination of the Best Treatment of Composite Bioplastics

The criteria were used to determine the best treatment of composite bioplastics: the DSF mass, YKF mass, and the concentration of ethanolic extract of *S. myrtifolium* leaves were set in the range, the tensile strength, elongation, and the inhibition zone area were set in maximize. Based on the criteria, the best treatment was found at the 0.5 g of DSF mass, 1 g of YKF mass, and 25% of the concentration of ethanolic extract of *S. myrtifolium* leaves, with the tensile strength of 3.30 MPa, elongation of 50.00%, and inhibition zone area of 15.33 mm. Additionally, further characterization showed that the best composite bioplastics had a thickness of 0.115 mm, modulus young of 0.066 MPa, density of 1.37 g.cm<sup>-3</sup>, moisture content of 17.14%, and water solubility of 76.91%.

### Microstructure

The surface and cross-section microstructure of the best composite bioplastics were presented in Fig. 5. Fig. 5 A1 and A2 revealed that the composite bioplastics had some starch granules, which means that the starch was not fully gelatinized during the film formation process. Moreover, the irregularities can be seen on the surface and cross-section of the composite bioplastics (Fig. 5 A-B). It could be due to the presence of many polymer molecules in the matrix of the composite bioplastics, such as starch, protein, lipid, and cellulose (Retnowati et al. 2015). In addition, the cross-section (Fig. 5 B1-B2) of the composite bioplastics also shows the presence of ungelatinized starch granules, as reported by Wu et al. (2009). Durian flour contains many amylopectins, which can cause flour not to dissolve in the film (Garcia-Hernandez et al. 2017). In our DSF used in this study, the amylopectin was 21.79%. Furthermore, the uniformity of the film's surface could reveal its mechanical properties.

The film matrix's uniformity will improve the polymer's integrity and improve the film's mechanical properties (Dias et al. 2010). The uneven and irregular surface of the bioplastic composites confirms the low tensile strength (Table 2) and low modulus young (0.066 MPa).

### CONCLUSION

The effect of the DSF mass, YKF mass, and concentration of ethanolic extract of *S. myrtifolium* leaves on composite bioplastics were successfully investigated using a two-level full factorial design. The YKF and DSF mass significantly affected the tensile strength of bioplastic composites. In addition, the YKF mass also had a significant effect on the elongation, and the concentration of the ethanolic extract of *S. myrtifolium* leaves only had a significant effect on the inhibition zone area. The best treatment was found at the 0.5 g of DSF mass, 1 g of YKF mass, and 25% of the concentration of ethanolic extract of *S. myrtifolium* leaves, with the tensile strength of 3.30 MPa, elongation of 50.00%, and inhibition zone area of 15.33 mm. Moreover, these conditions also had 0.115 mm of thickness, 0.066 MPa of modulus young, 1.37 g.cm<sup>-3</sup> of density, 17.14% of moisture content, and 76.91% of water solubility.

### ACKNOWLEDGEMENTS

Thank the Politeknik Tonggak Equator Foundation in Pontianak, Indonesia, for funding this research.

### REFERENCES

- Ahmad, M.A., Lim, Y.H., Chan, Y.S., Hsu, C.Y., Wu, T.Y. and Sit, N.W. 2021. Chemical composition, antioxidant, antimicrobial, and antiviral activities of the leaf extracts of *Syzygium myrtifolium*. *Acta Pharm.*, 72(2): 600-650
- BPS-Statistics Indonesia. 2020. Statistical Yearbook of Indonesia 2020. BPS, Jakarta.
- Dias, A.B., Müller, C.M.O., Larotonda, F.D.S. and Laurindo, J.B. 2010. Biodegradable films based on rice starch and rice flour. *J. Cereal Sci.*, 51(2): 213-219.
- Elansary, H.O., Szopa, A., Kubica, P., Ekiert, H., Al-Mana, F.A. and Al-Yafarsi, M.A. 2020. Antioxidant and biological activities of *Acacia saligna* and *Lawsonia inermis* natural populations. *Plants*, 9(7): 908
- Fahim, I., Mohsen, O. and Elkayaly, D. 2021. Production of fuel from plastic waste: A feasible business. *Polymers*, 13(6): 915
- Fahrullah, F., Radiati, L.E., Purwadi. and Rosyidi, D. 2020. The physical characteristics of the whey-based edible film added with konjac. *Curr. Res. Nutr. Food Sci.*, 8(1): 333-339.
- Jaisinghani, R.N. 2017. Antibacterial properties of quercetin. *Microbiol. Res.*, 8(1): 13-14.
- Kalaydzhev, H., Brandão, T.R.S., Ivanova, P., Silva, C.L.M. and Chalova, V.I. 2019. A two-step factorial design for optimization of protein extraction from industrial rapeseed meal after ethanol-assisted reduction of antinutrients. *Int. Food Res. J.*, 26(4): 1155-1163.
- Kurt, A. and Kahyaoglu, T. 2014. Characterization of a new biodegradable edible film made from salep glucomannan. *Carbohydr. Polym.*, 104: 50-58.

- Leemud, P., Karrila, S., Kaewmanee, T. and Karrila, T. 2020. Functional and physicochemical properties of Durian seed flour blended with cassava starch. *J. Food Meas. Charact.*, 14(1) : 388-400.
- Lim, M.W.S., Tan, K.M., Chew, L.Y., Kong, K.W. and Yan, S.W. 2018. Application of two-level full factorial design for the extraction of fucoxanthin and antioxidant activities from *Sargassum siliquosum* and *Sargassum polycystum*. *J. Aquat. Food Prod. Technol.*, 27(4): 446-463.
- Ma, S., Zheng, Y., Zhou, R. and Ma, M. 2021. Characterization of chitosan films incorporated with different substances of konjac glucomannan, cassava starch, maltodextrin, and gelatin, and application in Mongolian cheese packaging. *Coatings*, 11(1): 84.
- Nasution, H. and Wulandari, G. 2021. The effect of betel (*Piper betle*) leaf extract as an antimicrobial agent on characteristics of bioplastic based on sago starch. *IOP Conf. Ser. Mater. Sci. Eng.*, 1122(1): 012098.
- Oluwasina, O.O, Falola, T., Wahab, O.J. and Idahagbon, N.B. 2017. Enhancement of physical and mechanical properties of *Dioscorea dumetorum* starch films with dialdehyde starch solution. *Starch Stärke*, 70(3-4): 1700148.
- Permatasari, N.D., Witoyo, J.E., Ni' maturohmah, E., Masruri, M., Yuwono, S.S. and Widjanarko, S.B. 2021. Potential of Durian Seed (*Durio zibenthinus* Murr.) Flour as the Source of Eco-Friendly Plastics Materials : A Mini-Review. *Proceeding of International Conference on Agriculture and Applied Sciences (ICoAAS) 2021*. Lampung, Indonesia.
- Permatasari, N. D., Witoyo, J. E., Masruri, M., Yuwono, S. S. and Widjanarko, S. B. 2022. Nutritional and structural properties of durian seed (*Durio zibenthinus* Murr.) flour originated from West Kalimantan, Indonesia. *IOP Conf. Ser. Earth Environ. Sci.*, 1012(1): 012038.
- Retnowati, D.S., Ratnawati, R. and Purbasari, A. 2015. A biodegradable film from jackfruit (*Artocarpus heterophyllus*) and durian (*Durio zibenthinus*) seed flours. *Sci. Study Res. Chem. Chem. Eng.*, 16(4): 395-404.
- Rhim, J.W., Lee, J.H. and Ng, P.K.W. 2007. Mechanical and barrier properties of biodegradable soy protein isolate-based films coated with polylactic acid. *LWT*, 40(2): 232-238.
- Salgado, P.R., Molina Ortiz, S.E., Petruccielli, S. and Mauri, A.N. 2010. Biodegradable sunflower protein films are naturally activated with antioxidant compounds. *Food Hydrocoll.*, 24(5): 525-533.
- Strnad, S., Oberhollenzer, Z., Sauperl, O., Kreze, T. and Zemljic, L.F. 2019. Modifying properties of feather keratin bioplastic films using konjac glucomannan. *Cellul. Chem. Technol.*, 53(9): 1017-1027.
- Tan, N., Yazıcı-Tütüni, S., Bilgin, M., Tan, E. and Miski, M. 2017. Antibacterial activities of pyrenylated coumarins from the roots of *Prangos hulusii*. *Molecules*, 22(7): 1-8.
- Thakur, R., Pristijono, P., Scarlett, C. J., Bowyer, M., Singh, S.P. and Vuong, Q.V. 2019. Starch-based films: major factors affecting their properties. *Int. J. Biol. Macromol.*, 132: 1079-1089.
- Umiyati, R., Millati, R., Ariyanto, T. and Hidayat, C. 2020. *Calophyllum inophyllum* extracts as a natural enhancer for improving the physical properties of bioplastics and natural antimicrobial. *Biodiversitas*, 21(7): 1794-1802.
- Wang, L., Mu, R. J., Li, Y., Lin, L., Lin, Z. and Pang, J. 2019. Characterization and antibacterial activity evaluation of curcumin-loaded konjac glucomannan and zein nanofibril films. *LWT*, 113: 108293.
- Witoyo, J.E., Ni' maturohmah, E., Argo, B.D., Yuwono, S.S. and Widjanarko, S.B. 2020. Polishing effect on the physicochemical properties of porang flour using a centrifugal grinder. *IOP Conf. Ser. Earth Environ. Sci.*, 475(1): 012026.
- Witoyo, J.E., Argo, B.D., Yuwono, S.S. and Widjanarko, S.B. 2021. A pilot plant scale of yellow konjac (*Amorphophallus muelleri* Blume) flour production by a centrifugal mill using response surface methodology. *Potr. S. J. F. Sci.*, 15(1): 199-209.
- Woggum, T., Sirivongpaisal, P. and Wittaya, T. 2014. Properties and characteristics of dual-modified rice starch-based biodegradable films. *Int. J. Biol. Macromol.*, 67: 490-502.
- Yuniarni, U., Sukandar, E. and Fidrianny, I. 2020. Antibacterial activity of several Indonesian plant extracts and a combination of antibiotics with *Syzygium malaccense* extract as the most active substance. *Int. J. Pharm. Sci. Res.*, 11(3) : 3300-3308.
- Zhang, C., Chen, J. Da. and Yang, F. Q. 2014. Konjac glucomannan, a promising polysaccharide for OGDSS. *Carbohydr. Polym.*, 104(1): 175-181.
- Zhang, W. and Rhim, J.W. 2022. Recent progress in konjac glucomannan-based active food packaging films and property enhancement strategies. *Food Hydrocoll.*, 128: 107572.





# Community Level Physiological Profiling of Microbial Communities Influencing Mine Spoil Genesis in Chronosequence Coal Mine Overburden Spoil

P. Agrawal, A. Agrawal and A. K. Patel†

Department of Biotechnology and Bioinformatics, Sambalpur University, Jyoti Vihar, Burla-768 019, Odisha, India

†Corresponding author: A. K. Patel; amiya\_gene@yahoo.com

Nat. Env. & Poll. Tech.  
Website: [www.neptjournal.com](http://www.neptjournal.com)

Received: 18-02-2022

Revised: 30-03-2022

Accepted: 07-04-2022

## Key Words:

CLPP

Microbial community structure

Substrate utilization

Coal mine spoil

## ABSTRACT

Ecological restoration through mine spoil genesis should be dogmatic and the strategies involved a holistic approach, which emphasizes the role of microbial community composition that varies in accordance with the physiological and nutritional status of mine spoil profiles. This is because the patterns observed aboveground is being driven by the belowground diversity and processes. Thus, the relationship between microbial community structure and mine spoil genesis in chronosequence coal mine spoil has attracted considerable research attention. The occurrence of higher microbial diversity and difficulties in culturing microbes necessitate the use of a culture-independent approach through community-level physiological profiling based on the patterns of carbon source utilization using BIOLOG Ecoplate and thereby the functional diversity of microbial communities in different age series coal mine spoil was determined. The average well-color development exhibited an increasing trend with a minimum in OB0 (0.0640) and a maximum in OB15 (0.5060) over time. The patterns of substrate utilization (carbohydrates, carboxylic and ketonic acids, amino acids, polymers, amines, and amides) reflect the shift in microbial community composition in different age series coal mine spoil over time. Gradual increase in species richness and Shannon diversity index with the increase in age of mine spoil substantiated relatively higher microbial diversity reflecting the sign of mine spoil genesis. Principal component analysis and redundancy analysis based on the differential patterns of substrate utilization discriminate different age series coal mine spoil into independent clusters, which evaluated the broad-scale patterns of microbial community dynamics influencing the pace and progress of mine spoil genesis.

## INTRODUCTION

Mining activities result in disturbances in the landscape associated with a huge generation of mine spoil representing disequibrated geomorphic systems, altering the microenvironment of soil microorganisms and thereby disrupting the functional stability of microbial communities (Wang et al. 2009). Ecological restoration through mine spoil genesis should be dogmatic and the strategies involved a holistic approach (Rath et al. 2010), which not only involves periodic assessment of mine spoil using microbial ecological indicators but also recovery of a degraded ecosystem with acceleration to continue as productive and sustainable ecosystem (Gasch et al. 2014). The shift in microbial communities precedes the alternations in vegetational patterns, and soil physico-chemical and microbiological properties reflect the early signs of environmental stress and ecological evolution induced by anthropogenic activities (Dangi et al. 2012). Besides, the concept of biodiversity describes spatial diversity including its link to biodiversity, and landscape ecology has emerged as the functional determinant of ecosys-

tem processes. Ecological restoration following mine spoil genesis not only depends on mining methods, height and slope of mine overburden, nature of mine spoil, and geo-climatic conditions but also the shift in microbial community composition, resilience against ecological extremities, and microbial amelioration in coal mine spoil (Muknopadhyay et al. 2013).

Mining subsidence followed by the gradual establishment of vegetation cover exhibits a distinct influence on molecular ecological networks of microbial communities (Luo et al. 2020), which subsequently adapted to changes in distribution and activity in response to an interactive relationship with ecological processes (de Quadros et al. 2016). Being sensitive indicators of ecological restoration, mine spoil genesis focuses on the shift in microbial community composition and their relationships (Pascual et al. 2000, Harris 2003). Criteria for mine spoil genesis primarily focus on the microbial ecology of soil subsystems including microbial community dynamics, because the patterns observed aboveground are being driven by belowground diversity and processes (Kelly et al. 2003). Though the restoration of mine spoil is relatively longer, it

is a prerequisite to explore the shift in microbial community composition using sensitive soil quality biomarkers. The chronosequence study associated with the space-for-time substitutions influencing microbial community dynamics can be reliably used to assess the pace and progress of mine spoil genesis that occur between the temporally linked sites over multiple time scales (Walker et al. 2010). Microbiological properties including microbial biomass pool, enzyme activities, microbial community composition, species richness, relative distribution, and abundance of microbial communities are reliably used for monitoring mine spoil genesis (Ngugi et al. 2020).

Microbial community structure acts as an ecologically relevant endpoint and is realistically utilized for impact assessment associated with anthropogenic disturbances, which influence microbial communities at multiple spatial extents linked to environmental heterogeneity. Microbial community structure is the driving force for organic matter decomposition and nutrient turnover that regulate its size and activity (Zeller et al. 2001). The shift in microbial community composition occurs even though microbial community size remains unchanged, which reflects the role of microbial communities as a sensitive indicator of disturbances compared to measures of either microbial processes or overall community size (Veresoglou et al. 2011). Several studies explored the shift in microbial community structure along the time gradient of post-mining restoration (Li et al. 2019, Liu et al. 2019).

The approach used to detect the adaptive variations in microbial community structure in response to ecological processes caused by mining activities can be analyzed through community-level physiological profiling (CLPP). Being metabolically heterogeneous with diverse microbial metabolic pathways (Scheffer & Schachtschabel 2010), it is imperative to determine metabolic profiles for analyzing the functional diversity of microbial communities (Haferburg & Kothe 2012, Lenart-Boroń & Wolny-Koladka 2015) in chronosequence coal mine overburden spoil through community level physiological profiling using 'BILOG system' (Frąc et al. 2012, Rutgers et al. 2016). CLPP involves direct inoculation of environmental samples in BILOG™ ecoplate and resulting responses of NADH produced via cellular respiration that reduces tetrazolium dye to colored formazan at different time intervals of incubation provide information about functional adaptations of mixed microbial communities (Garland 1997), cell viability (Winding 1994), a measure of functional diversity (Zak et al. 1994) and overall microbial community fingerprints based on the patterns of substrate utilization (Kennedy & Gewin, 1997, Winding & Hendriksen 1997). The diversity of responses based on average well color development is a function of both richness and evenness

among wells (Zak et al. 1994, Lehman et al. 1995), which determines the shift in microbial community structure and functional diversity (Frąc et al. 2012), which reveal the sign of mine spoil genesis and ecological restoration.

The forest soil with well-defined microbial communities was taken as a reference to interpret the shift in microbial community structure. The study was designed to determine the shift in microbial community structure and their functional status in chronosequence coal mine overburden spoil, which reveal the importance of metabolic diversity driving succession through microbial community dynamics that deepen the understanding of microbial interactions with mining ecosystems over time ideal for microbial ecology studies.

## MATERIALS AND METHODS

### Study Site

The present study was carried out in the Basundhara (west) open cast colliery, Ib valley area of Mahanadi Coalfields Limited (MCL) located in the revenue district of Sundargarh, Odisha, India (22°03'58"-20°04'11" north latitude and 83°42'46"-83°44'45" east longitude). Topologically, the area is hilly and sloppy (244 m above sea level) to plateau. The thickness of native top soils in the site varies from 0.15 m to 0.30 m (average: 0.22 m). The study area experiences a semi-arid climate with an annual rainfall of 1483 mm yr<sup>-1</sup>, an average temperature of 26°C, and 58.58% relative humidity. Tropical dry deciduous forest is considered to be the natural vegetation of the study site and broadly the climate is dry, hot, and arid. The open cast coal mining activities in the study site lead to the formation of different age series coal mine spoil overburdens and grouped according to their inception (Fresh mine spoil: OB0, 3 yr: OB3, 6 yr: OB6, 9 yr: OB9, 12 yr: OB12 and 15 yr: OB15).

### Mine Spoil Sampling

Each overburden was divided into 5 blocks, and from each block, five soil samples were collected from 0-15 cm depth by digging pits (15×15×15) cm<sup>3</sup> size. Samples collected from each block were referred to as 'sub-samples' and were mixed to form a 'composite sample' obtained from each overburden. A similar strategy was adapted for sampling from different age series of coal mine overburden along with forest soil (NF), which was used as a reference. Composite samples were homogenized, sieved (0.2 mm), and stored at 4°C until analyzed.

### Microbial Enumeration

Microbial enumeration of the different age series coal mine overburden spoil was performed following standard microbi-



ological approaches through serial dilution ( $10^{-10}$  fold) and spread plate technique. The azotobacter count (AZB) was enumerated using azotobacter mannitol agar. The arthrobacter count (ARB) was determined using the arthrobacter medium. The rhizobial population (RZB) was estimated using yeast extract mannitol agar. The heterotrophic aerobic bacterial count (HAB) was enumerated using nutrient agar. The sulfate-reducing bacterial count (SRB) was estimated using the sulfate-reducing medium. Besides, the actinomycetes count (ACT) was determined using starch-casein agar supplemented with streptomycin and griseofulvin. The yeast population (YES) in different mine spoil samples was estimated using potato sucrose agar. The fungal count (FUN) was estimated using rose bengal agar supplemented with streptomycin.

### BIOLOG<sup>TM</sup> Ecoplate

Community level physiological profiling was performed using BIOLOG<sup>TM</sup> Ecoplate with 31 carbon sources (C1 – C31) along with control well in triplicates. Mine spoil sample (5 g) was suspended in 50 mM PBS (pH 6.5 to 7) and incubated for 1 h. After shaking, the flask was kept undisturbed for 30 mins and 150  $\mu$ L of supernatant was transferred to BIOLOG<sup>TM</sup> Ecoplate and incubated at 45°C. Five substrates such as (i) carbohydrates, (ii) carboxylic and ketonic acids, (iii) amino acids, (iv) polymers, and (v) amines and amides have been selected (Weber & Legge 2009). The time between sampling and inoculation should be minimized to reduce cell death. Substrate utilization rate was indicated by the reduction of tetrazolium dye that changes its color from colorless to purple was quantified (Konopka et al. 1998), if a single source was used by inoculated microbes (Lehman et al. 1995, Islam et al. 2011). Absorbance was taken at 590 nm using BIOLOG<sup>TM</sup> Microstation (Thermo Fischer Scientific Inc, USA) at different time intervals of incubation (24 h, 48 h, 72 h, and 96 h).

### Average Well Color Development (AWCD)

Overall color development in BIOLOG<sup>TM</sup> Ecoplate was expressed in terms of the average well color development (Garland & Mills 1991, Gomez et al. 2004), which was derived from the mean difference among the absorbance values of 31 response wells containing sole carbon source against control. The microbial response was expressed in terms of AWCD, which was calculated at different times of incubation (24 h, 48 h, 72 h, and 96 h) as follows.

$$AWCD = \frac{1}{31} \sum_{i=1}^{31} (A_i - A_0)$$

Where,  $A_i$  represents the absorbance reading of well  $i$ , which is corrected by subtracting the absorbance value of

blank well  $A_0$  (without carbon source) from the value of each plate well.

### Species Richness and Shannon-Weaver Index

The calculated AWCD value is considered as the estimate of the total capacity of microbial communities to use sole carbon substrates, which was used to calculate different indices of microbial functional diversity (Fraq et al. 2012, Xu et al. 2015). Shortest incubation time that allows better resolution is used to calculate average well color development, richness, and Shannon-Weaver index (Fraq et al. 2012). Species richness (R) was calculated as the number of oxidized C substrates using the absorbance value of 0.25 as the threshold for a positive response (Garland 1997). Shannon-Weaver index (H) is related to the number of carbon substrates degraded by microbial communities and was calculated as  $H = -\sum pi (\ln pi)$ ; where,  $pi$  represents the ratio of activity on each substrate to the sum of activities including all substrates.

### Data Normalization

Before performing multivariate analysis, the data was initially normalized to reduce any biasness due to differences in inoculum densities between samples (Garland 1996). Normalization of the data involves the correction of each absorbance value by its corresponding blank and then dividing by the AWCD value calculated for that time point. The normalized absorbance for a particular well ( $k$ ) was calculated as follows.

$$\bar{A}_k = \frac{A_k - A_0}{\frac{1}{31} \sum_{i=1}^{31} (A_i - A_0)}$$

Where,  $A_i$  represents the absorbance reading of the well  $i$  and  $A_0$  is the absorbance reading of the blank well (without carbon source). Normalized absorbance value is coded as zero, where there is very little response or negative value in a well since this is physically meaningless.

### Statistical Analysis

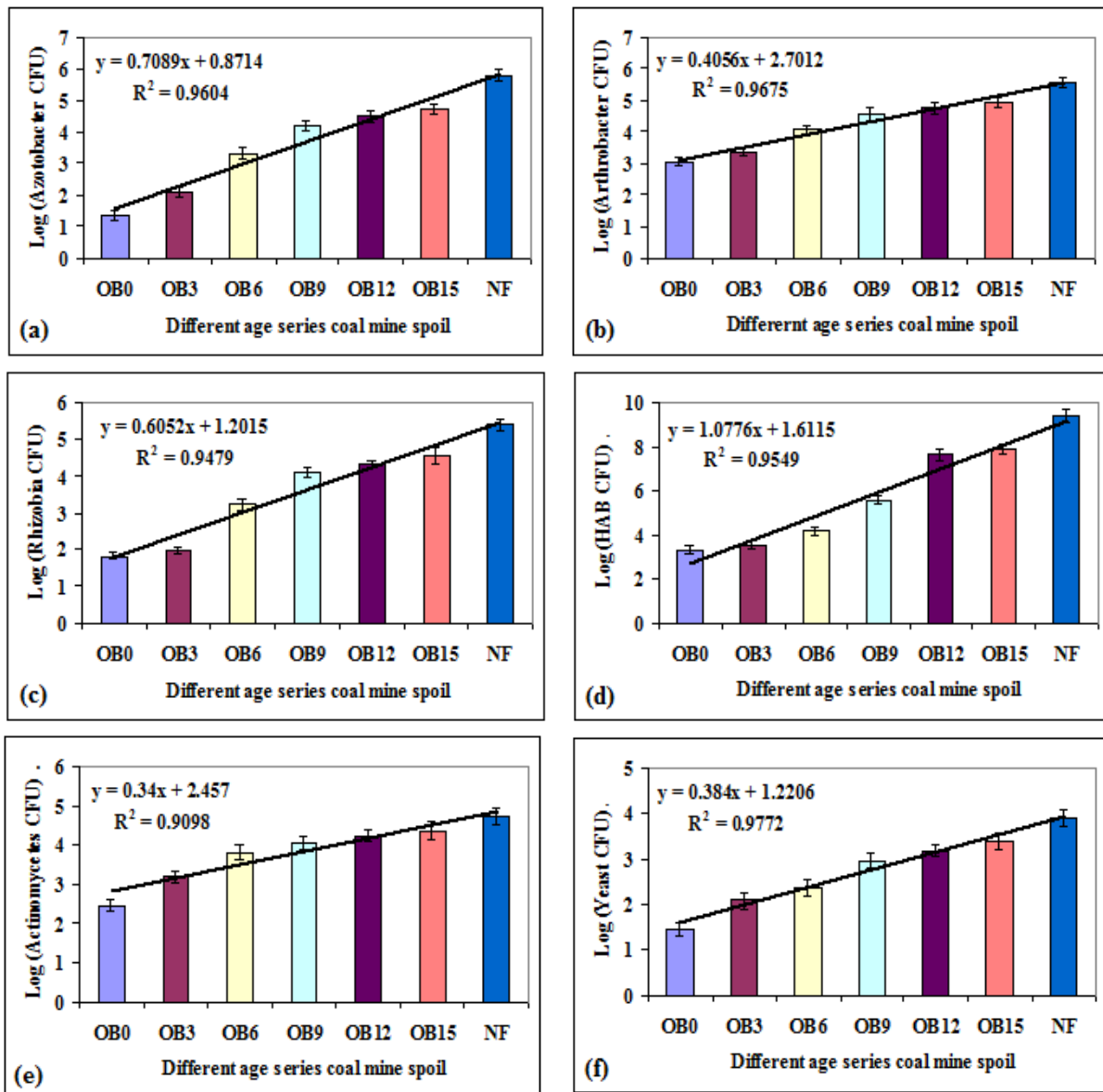
Principal component analysis was performed to analyze CLPPs based on normalized absorbance data (Weber et al. 2007, Urbanová et al. 2011) using SPSS (Version 18.0). Cluster analysis was performed using the similarity matrix based on substrate utilization by microbial communities in chronosequence coal mine spoil. RDA analysis was performed to elucidate the relationship between soil variables influencing microbial community structure in chronosequence coal mine spoil using Microsoft Excel XLSTAT-2014 (Version 2.03).

## RESULTS

### Microbial Enumeration

Relative distribution of microbial populations (expressed in  $\log_{10}$  CFU per g spoil) in chronosequence coal mine overburden spoil and nearby NF soil was presented (Fig. 1a-h), which revealed wide variation over time. Progressive increase in CFU in chronosequence coal mine overburden spoil with the minimum in OB0 and maximum in OB15 was exhibited by azotobacter ( $r = 0.980$ ;  $p < 0.001$ ), arthrobacter ( $r = 0.983$ ;  $p < 0.001$ ), rhizobia ( $r = 0.973$ ;  $p < 0.001$ ),

heterotrophic aerobic bacteria ( $r = 0.954$ ;  $p < 0.001$ ), actinomycetes ( $r = 0.953$ ;  $p < 0.001$ ), yeast ( $r = 0.988$ ;  $p < 0.001$ ) and fungi ( $r = 0.963$ ;  $p < 0.001$ ), which was found to be statistically significant. In contrast, the relative distribution of sulfur-reducing bacteria exhibited a declining trend with the increase in age of coal mine overburden spoil, which was statistically significant ( $r = 0.973$ ;  $p < 0.001$ ). However, the abundance and distribution of microbial populations in the nearby NF soil were found to be comparatively higher compared to different age series coal mine overburden spoil across the sites (Fig. 1a-h).



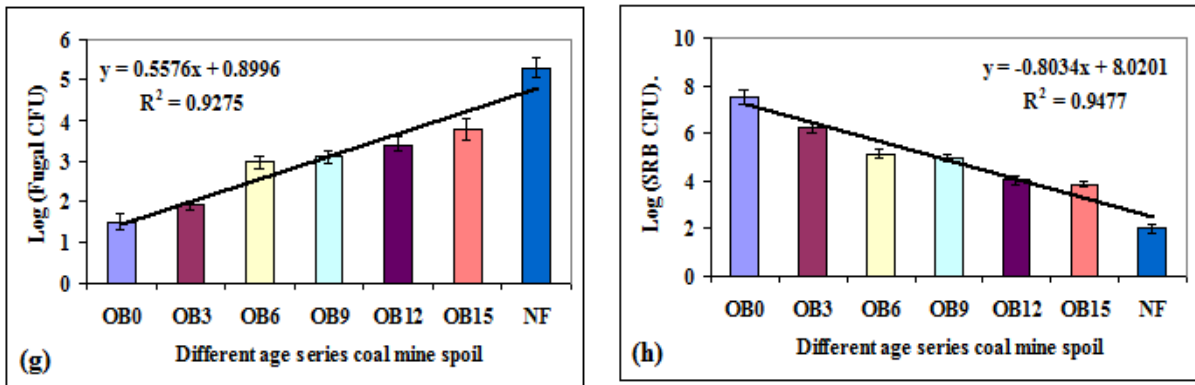


Fig. 1 (a-h): Relative distribution of microbial populations (expressed in log<sub>10</sub> CFU per g spoil) in chronosequence coal mine overburden spoil over time and nearby NF soil: (a) Azotobacter, (b) Arthrobacter, (c) Rhizobia, (d) Heterotrophic aerobic bacteria, (e) Actinomycetes, (f) Yeast, (g) Fungal counts (h) Sulfate-reducing bacteria.

**Average Well Color Development (AWCD)**

The average well-color development in BIOLOG™ Ecoplate revealed a differential pattern of responses exhibited by the microbial communities with respect to their metabolic potential in chronosequence coal mine overburden spoil, which exhibited an increasing trend with incubation time (Fig. 2). NF soil exhibited a relatively higher AWCD value compared to different age series coal mine overburden spoil over time across the sites. It is evident from the study that the shortest incubation time period (48 h) allows better resolution with respect to substrate utilization by microbial communities in chronosequence coal mine overburden spoil, which was used to calculate AWCD, species richness, and Shannon Weaver index.

**Patterns of Substrate Utilization**

Community level physiological profiling of chronosequence coal mine overburden spoil was performed using BIOLOG™ Ecoplate, which revealed wide variation in substrate utilization such as carbohydrates (0.0033-0.4758), carboxylic and ketonic acids (0.0026-0.3267), amino acids (0.0236-0.4126), polymers (0.0004-0.2316), amines and amides (0.0077-0.0348) by microbial communities with a minimum in OB0 and maximum in OB15 over time (Fig. 3). NF soil exhibited relatively higher utilization of carbohydrates (0.6131), carboxylic and ketonic acid (0.5228), amino acids (0.5826), polymers (0.2764), amines and amides (0.0536) compared to different age series mine spoil. The physiological responses exhibited by the microbial communities in chronosequence

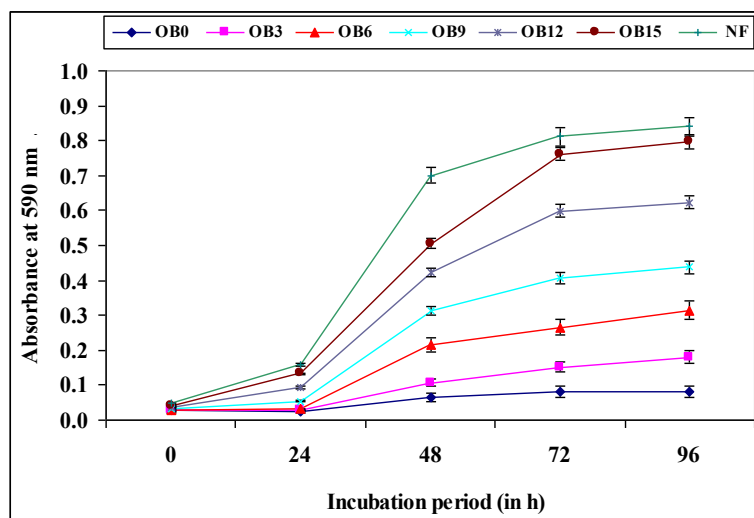


Fig. 2: Average well-color development of metabolized substrates using BIOLOG™ Ecoplate at different times of incubation (0, 24, 48, 72, and 96 h). Values were expressed as mean ± SD; (n =3).

coal mine overburden spoil revealed the following patterns of substrate utilization as carbohydrates > amino acids > carboxylic and ketonic acids > polymers > amines and amides over time (Fig. 3).

### Species Richness and Shannon Weaver Index

The study indicated a gradual increase in species richness from OB0 (03) to OB15 (24), which revealed relatively higher microbial diversity in OB15 with the increase in age of the mine overburden spoil across the sites (Table 1). The Shannon diversity index exhibited an increasing trend with a minimum in OB0 (0.56842) and a maximum in OB15 (2.13918) over time (Table 1). NF soil (2.27464) exhibited relatively higher microbial diversity compared to different age series mine overburden spoil. Pielou's evenness index based on the substrate utilization varied from 0.51740 (OB0) to 0.67311 (OB15) in chronosequence coal mine overburden spoil over time across the sites (Table 1).

### DISCUSSION

Wide variation in microbial community composition in chronosequence coal mine overburden spoil may be due to variation in microclimatic conditions, available soil nutrients, and heterogeneity in vegetational patterns. Being obligately aerobic and chemolithotrophic di-hydrogen fixing bacteria, the distribution of azotobacter exhibited an increasing trend from the nutrient-deficient OB0 to OB15 over time. The variability in the *Arthrobacter* population is due to nutritional versatility and starvation. The relatively higher rhizobial count was exhibited by OB15 compared to different mine

spoil due to the gradual establishment of vegetation with a symbiotic relationship with leguminous plants for nitrogen fixation, which revealed the sign of ecological restoration. Gradual decline in heterotrophic aerobic bacterial population from OB15 to OB0 is due to environmental extremities caused by extensive mining activities and heavy metal toxicity. The distribution of actinomycetes is influenced by temperature, pH, aeration, moisture, and organic C level, which may be the reason for relatively higher dominance in OB15 compared to different mine spoil. Being acid-tolerant, the minimal occurrence of actinomycetes was observed in OB0. The higher dominance of yeast in OB15 may be attributed to a gradual increase in different hydrological regimes, pH, organic C, aeration, and substrate availability over time. Being opportunistic (zymogenous), the fungal population

Table 1: Species richness, Shannon Weaver index, and Pielou's evenness index based on substrate utilization patterns by existing microbial communities in chronosequence coal mine overburden spoil over time and nearby NF soil across the sites.

Soil profiles	Species richness (R)	Shannon Weaver index (H)	Pielou's evenness index (J)
OB0	3	0.56842	0.51740
OB3	9	1.32470	0.60290
OB6	11	1.51897	0.63346
OB9	16	1.76324	0.63595
OB12	22	1.98635	0.64262
OB15	24	2.13918	0.67311
NF soil	28	2.27464	0.68262

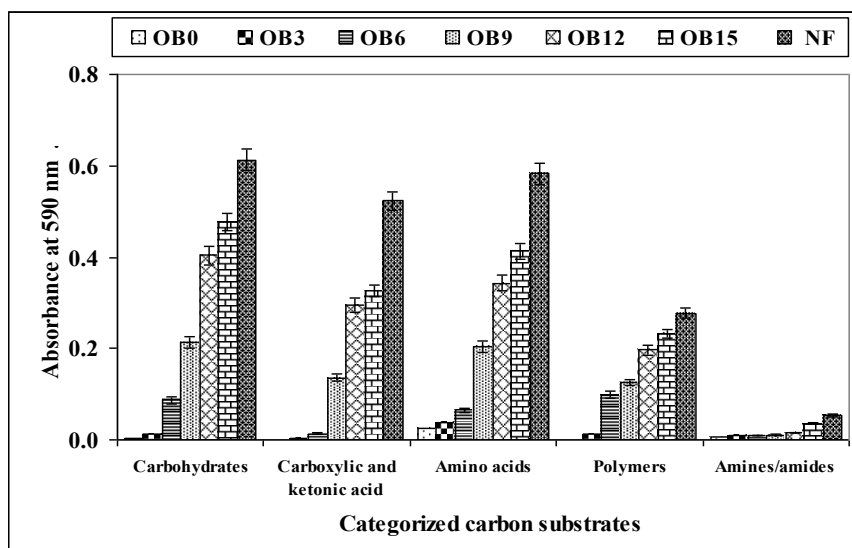


Fig. 3: Differential degree of substrate utilization (C1 – C31) revealed the variation in microbial community composition in chronosequence coal mine spoil and NF soil. Values were expressed as mean  $\pm$  SD; (n =3).

exists either as a free-living or mycorrhizal association to promote soil structural stability by forming macro aggregates. Relatively higher fungal dominance in OB15 may be due to the prevailing favorable moisture, improvement in pH, and available soil nutrients that enhance microbial colonization. The higher dominance of sulfur-reducing bacteria in OB0 may be due to their involvement in the utilization of sulfur compounds through oxidation of inorganic P and sulfur reduction that accounted for organic C mineralization.

Progressive improvement in AWCD from OB0 to OB15 may be due to the establishment of vegetation, available soil nutrients, and the presence of complex organic materials such as plant and root exudates (Frac et al. 2012), which promote microbial amelioration over time. A minimal AWCD value was recorded in OB0 due to the nutrient-deficient situation with an altered geomorphic system. The chemolithotrophs mostly dominate in OB0 with heavy metal contaminants and extreme environmental conditions, which proliferate through pyrite oxidation (Jha & Singh 1991). However, the root exudates were reported to stimulate microbial proliferation associated with increased microbial activities that influence the shift in microbial community structure (Van Der Heyde et al. 2020). Relatively lower AWCD value exhibited by the chronosequence coal mine overburden spoil compared to NF soil may be due to the heavy metal toxicity that influences the relative distribution and abundance of microbial community structure (Gremion et al. 2004). A similar pattern of time adaptation toward ecosystem recovery influencing AWCD has been substantiated (Kenarova et al. 2014, Fazekas et al. 2019, Martínez et al. 2021). Besides, the lower AWCD is due to heavy metal pollutants that restrict the availability of carbon sources for their utilization as well as toxic effects induced by metals and metalloids on microbial-mediated metabolic activities (Martínez-Toledo et al. 2021). The undisturbed NF soil harbors varieties of plant species with available soil nutrients are the possible reason for exhibiting relatively higher AWCD (Van Der Heyde et al. 2020). Microbial community composition and their activities vary in different mine spoil profiles in accordance with the physiological and nutritional status influenced by available soil nutrients and succession (Potthoff et al. 2006). The decline in microbial metabolic activities is due to the loss of microbial viability with specific functional attributes, which could be compensated by other microbial communities through microbial amelioration over time (Stefanowicz et al. 2008). Besides, the long-term adaptation of microbial growth in vitro is established using BIOLOG™ Ecoplate compared to the landscape-based environmental extremities revealing the inherent properties of resilience for adaptation exhibited by microbial communities (Kenarova et al. 2014, Martínez-Toledo et al. 2021). Changes in AWCD in different age series coal mine spoil revealed

improvement in the direction of OB15 through the shift in microbial community composition reflecting the progress of the ecological restoration.

Physiological responses exhibited by microbial communities revealed the following pattern of substrate utilization as carbohydrates > amino acids > carboxylic and ketonic acid > polymers > amines and amides (Kuźniar et al. 2018). Minimal substrate utilization by the microbial communities in OB0 is due to heavy metal contaminants caused by mining activities and their interference in assessing substrate for microbial-mediated activities (Tischer et al. 2008). Minimal utilization of carbohydrates in OB0 is due to the existence of chemolithotrophs as initial colonizers with a minimal tendency for carbohydrate catabolism. Colonization of other microbial populations over time may be the reason for the utilization of carbohydrates, carboxylic and ketonic acids, and amino acids as preferable nutrient sources. Microbial communities subsequently acquired the capacity to metabolize the complex and more recalcitrant substrates such as polymers, amines, and amides (Thouin et al. 2019, Chavan & Nadanathangam 2020). Several studies suggested that the catabolism of carbohydrates, carboxylic and ketonic acids and amino acids was sensitive to heavy metal toxicity (Lalor et al. 2007, Muniz et al. 2014). The study provides an insight into the multifaceted nature of physiological responses exhibited by the existing microbial community composition, which depends on available soil nutrients, the bioavailability of substrate for utilization, post-mining stress induced by heavy metal toxicity, and environmental heterogeneity that shapes the microbial community structure along with the supportive networks in chronosequence coal mine overburden spoil over time that influence the pace and progress of the ecological restoration.

The degrees of resilience exhibited by microbial communities against anthropogenic disturbances contribute to variation in microbial community composition. The diversity index is a quantitative measure used in microbial ecology studies that account for the existence of species richness (R) and distribution (evenness) as the measure of microbial community composition based on their substrate utilization using CLPP (Frac et al. 2012, Xu et al. 2015). Gradual increase in species richness in chronosequence coal mine overburden spoil revealed higher diversity among the microbial communities. Shannon diversity index exhibited an increasing trend in chronosequence coal mine overburden spoil over time, which revealed that the microbial communities in the less disturbed ecosystem may be dynamic in terms of functional responses to perturbations, but more resistant to the shift in microbial community composition (Waldrop et al. 2000). The evenness in the distribution of microbial communities is represented by Pielou's evenness index (J), which is con-

strained between 0 and 1 (Kaur et al. 2005). The increase in Pielou's evenness index in chronosequence coal mine overburden spoil suggested that the more even the distribution or less variation between microbial communities, the greater the diversity. Thus, the value of the diversity index increases when both the species richness and evenness increase.

Principal component analysis was performed based on the variation in AWCD, substrate utilization, species richness, and Shannon Weaver index of microbial community structure to discriminate the chronosequence coal mine overburden spoil and nearby NF soil across the sites (Ludwig et al. 1988). The Z1 and Z2 components explained 98.35% cumulative percentage of variance and revealed clear segregation of the chronosequence coal mine overburden spoil (Fig. 4a). Cluster analysis was performed based on ACWD using a similarity matrix, which revealed the existence of six clusters (I – VI) in the dendrogram, which exhibited the tree likeness of the original (unrandomized) tree was statistically well resolved (Fig. 4b).

Redundancy analysis based on the variations in AWCD, substrate utilization, species richness, and Shannon Weaver index explained the shift in microbial community composition based on substrate utilization patterns and AWCD in mine spoil profiles altering the microenvironment with possible effects on the efficiency of the readily mineralizable carbon substrate. About 99.05% variability in the patterns of substrate utilization was explained among microbial communities in chronosequence coal mine spoil based on fitted CLPP data from the canonical sum of eigenvalues (Fig. 5).

Site codes of mine overburden with a differential degree of substrate utilization (C1-C31) along with gradients arrows

were represented (Fig. 5). The species richness, Shannon diversity index with different microbial populations (AZB, ARB, RZB, HAB, ACT, YES) increased in the direction of OB12 and OB15, whereas the F: B ratio, FUN, and AWCD increased towards NF soil. Differential degree of different substrate utilization (C1 - C31) revealed by community level physiological profiling of chronosequence coal mine spoil suggested the shift in microbial community structure that influence ecological restoration.

## CONCLUSIONS

Microbial ecology studies provide valuable information about the shift in microbial community composition, which response quickly to natural perturbations and environmental stress due to their short generation time and intimate relationships with the biotic and abiotic components of terrestrial ecosystems attributed to their higher surface-to-volume ratio. Such studies emphasized the exposure of microbial communities to environmental extremities mediated by coal mining activities, which shift the microbial community composition with adaptive mechanisms of tolerance and substrate utilization in chronosequence coal mine overburden spoil. Although the microbial community dynamics are assessed through different ecological indices, the microbial community structure influencing ecological restoration is yet to be understood. The functional diversity of microbial communities is sensitive to environmental changes. Hence, exploration of microbial community dynamics by catabolic profiling based on substrate utilization was assessed through community-level physiological profiling, an effective approach essential for determining functional diversity influencing the pace and progress of mine spoil genesis

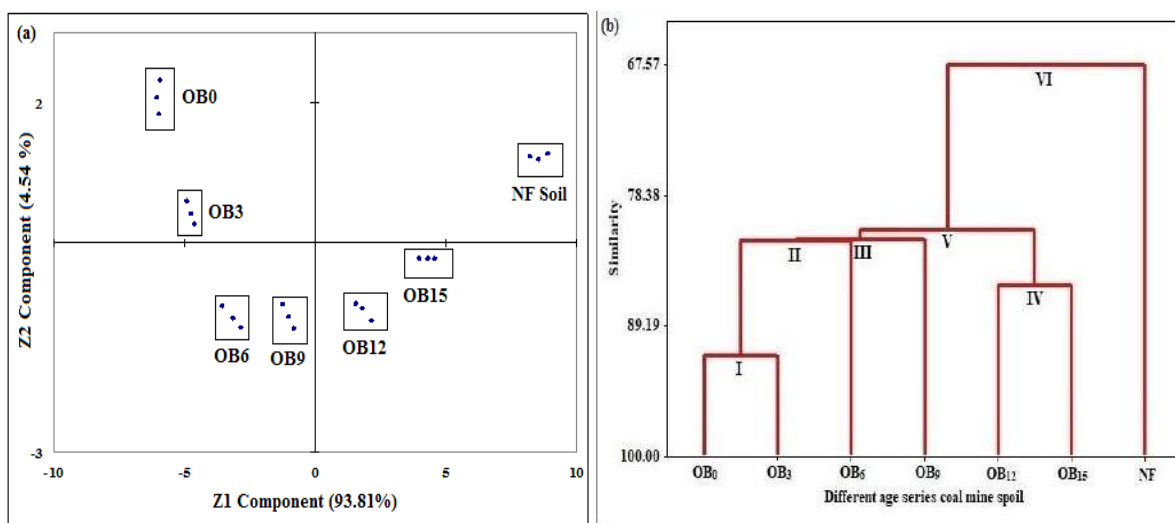


Fig. 4: (a) Principal component analysis, (b) Cluster analysis based on the variation in AWCD, substrate utilization in chronosequence coal mine overburden spoil, and NF soil.

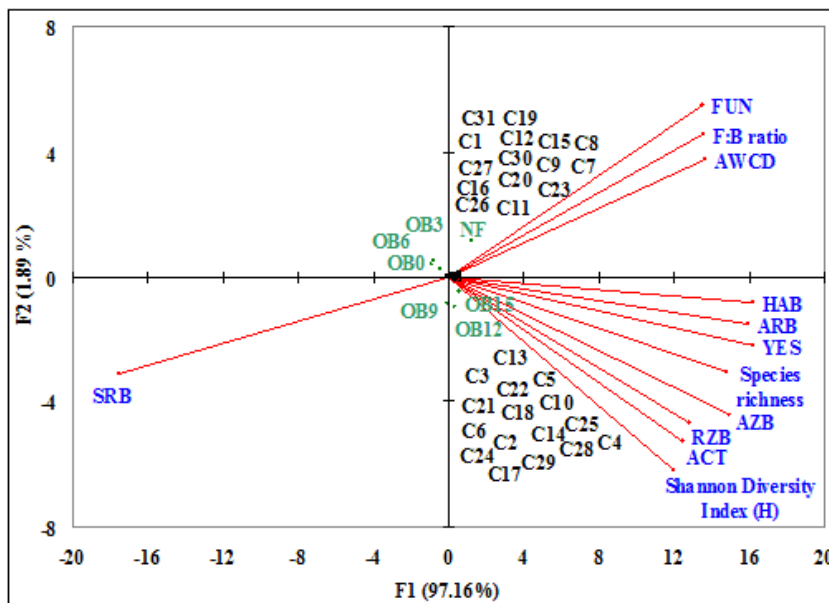


Fig. 5: Redundancy discrimination analysis based on the variation in AWCD, substrate utilization (C1 – C31), species richness, Shannon Weaver index, and different microbial CFUs in chronosequence coal mine overburden spoil and NF soil.

to support ecological restoration in chronosequence coal mine overburden spoil over time.

## ACKNOWLEDGEMENTS

The authors express their gratitude to the Head of the Department of Biotechnology and Bioinformatics, Sambalpur University for providing the necessary laboratory facilities to carry out the research work. The authors are thankful to Dr. Jitesh Kumar Maharana for helping in sampling mine spoil and statistical analysis.

## REFERENCES

- Chavan, S. and Nadanathangam, V. 2020. Shifts in metabolic patterns of soil bacterial communities on exposure to metal engineered nanomaterials. *Ecotoxicol. Environ. Saf.*, 189: 110012.
- Dangi, S.R., Stahl, P.D., Wick, A.F., Ingram, L.J. and Buyer, J.S. 2012. Soil microbial community recovery in reclaimed soils on a surface coal mine site. *Soil Sci. Soc. Am. J.*, 61: 915-924.
- de Quadros, P.D., Zhalnina, K., Davis-Richardson, A.G., Drew, J.C., Meneses, F.B., Flávio, A.D. and Triplett, E.W. 2016. Coal mining practices reduce the microbial biomass, richness, and diversity of soil. *Appl. Soil Ecol.*, 98: 195-203.
- Fazekaš, J., Fazekašová, D., Adamišin, P., Huličová, P. and Benkova, E. 2019. Functional diversity of microorganisms in metal- and alkali-contaminated soils of Central and North-Eastern Slovakia. *Soil Water Res.*, 14(1): 32-39.
- Fraç, M., Oszust, K. and Lipiec, J. 2012. Community level physiological profiles (CLPP), characterization, and microbial activity of soil amended with dairy sewage sludge. *Sensors*, 3: 3253-3268.
- Garland, J.L. 1996. Analytical approaches to the characterization of samples of microbial communities using patterns of potential C source utilization. *Soil Biol. Biochem.*, 28(2): 213-221.
- Garland, J.L. 1997. Analysis and interpretation of community-level physiological profiles in microbial ecology. *FEMS microbial. Ecol.*, 24(4): 289-300.
- Garland, J.L. and Mills, A.L. 1991. Classification and characterization of heterotrophic microbial communities based on patterns of community-level sole-carbon-source utilization. *Appl. Environ. Microbiol.*, 57(8): 2351-2359.
- Gasch, C., Huzurbazar, S. and Stahl, P. 2014. Measuring Soil Disturbance Effects And Assessing Soil Restoration Success By Examining Distributions Of Soil Properties. *Appl. Soil Ecol.*, 76: 102-111.
- Gomez, E., Garland, J. and Conti, M. 2004. Reproducibility in the response of soil bacterial community-level physiological profiles from a land use intensification gradient. *Appl. Soil Ecol.*, 26(1): 21-30.
- Gremion, F., Chatzinotas, A., Kaufmann, K., Von Sigler, W. and Harms, H. 2004. Impacts of heavy metal contamination and phytoremediation on a microbial community during a twelve-month microcosm experiment. *FEMS Microbiol. Ecol.*, 48(2): 273-283.
- Haferburg, G. and Kothe, E. 2012. Biogeosciences in Heavy Metal-Contaminated Soils. In Kothe, E. and Varma, A. (eds), *Bio-Geo Interactions in Metal-Contaminated Soils*. Springer, The Netherlands, pp. 17-34.
- Harris, J.A. 2003. Measurements of the soil microbial community for estimating the success of the restoration. *Eur. J. Soil Sci.*, 54(4): 801-808.
- Islam, R., Chauhan, P., Kim, Y., Kim, M. and Sa, T. 2011. Community level functional diversity and enzyme activities in paddy soils under different long-term fertilizer management practices. *Biol. Fertil. Soils.*, 47(5): 599-604.
- Jha, A.K. and Singh, J.S. 1991. Spoil characteristics and vegetation development of an age series of mine spoil in a dry tropical environment. *Vegetation*, 97(1): 63-76.
- Kaur, A., Chaudhary, A., Kaur, A., Choudhary, R. and Kaushik, R. 2005. Phospholipid fatty acid—a bioindicator of environment monitoring and assessment in the soil ecosystem. *Curr. Sci.*, 11: 1103-1112.
- Kelly, J.J., Häggblom, M.M. and Tate, R.L. 2003. Effects of heavy metal contamination and remediation on soil microbial communities in the vicinity of a zinc smelter as indicated by analysis of microbial community phospholipid fatty acid profiles. *Biol. Fertil. Soils.*, 38(2): 65-71.

- Kenarova, A., Radeva, G., Traykov, I. and Boteva, S. 2014. Community level physiological profiles of bacterial communities inhabiting uranium mining-impacted sites. *Ecotoxicol. Environ. Saf.*, 100: 226-232.
- Kennedy, A.C. and Gewin, V.L. 1997. Soil microbial diversity: Present and future considerations. *Soil Sci.*, 162(9): 607-617.
- Konopka, A., Oliver, L. and Turco, Jr. R.F. 1998. The use of carbon substrate utilization patterns in environmental and ecological microbiology. *Microb. Ecol.*, 35(2): 103-115.
- Kuźniar, A., Banach, A., Stępniewska, Z., Fraç, M., Oszust, K., Gryta, A., Kłos, M. and Wolińska, A. 2018. Community-level physiological profiles of microorganisms inhabiting soil contaminated with heavy metals. *Int. Agrop.*, 32(1): 101-109.
- Lalor, B.M., Cookson, W.R. and Murphy, D.V. 2007. Comparison of two methods that assess soil community level physiological profiles in a forest ecosystem. *Soil Biol. Biochem.*, 39(2): 454-462.
- Lehman, R.M., Colwell, F.S., Ringelberg, D.B. and White, D.C. 1995. Combined microbial community-level analyses for quality assurance of terrestrial subsurface cores. *J. Microbiol. Methods.*, 22(3): 263-281.
- Lenart-Boroń, A. and Wolny-Kotadka, K. 2015. Heavy metal concentration and the occurrence of selected microorganisms in soils of a steelworks area in Poland. *Plant Soil Environ.*, 61(6): 273-278.
- Li, P., Zhang, X., Hao, M., Cui, Y., Zhu, S. and Zhang, Y. 2019. Effects of vegetation restoration on soil bacterial communities, enzyme activities, and nutrients of reconstructed soil in a mining area on the Loess Plateau, China. *Sustainability*, (8): 2295-2311.
- Liu, Y., Lei, S. and Gong, C. 2019. Comparison of plant and microbial communities between an artificial restoration and natural restoration topsoil in coal mining subsidence area. *Environ. Earth Sci.*, 78(6): 1-3.
- Ludwig, J.A., Reynolds, J.F., Quartet, L. and Reynolds, J.F. 1988. *Statistical Ecology: A Primer on Methods and Computing*. Wiley-Interscience Pub., New York, pp. 331-337.
- Luo, R., Kuzyakov, Y., Liu, D., Fan, J., Luo, J., Lindsey, S., He, J.S. and Ding, W. 2020. Nutrient addition reduces carbon sequestration in Tibetan grassland soil: disentangling microbial and physical controls. *Soil Biol. Biochem.*, 144: 107764.
- Martínez-Toledo, Á., González-Mille, D.J., García-Arreola, M.E., Cruz-Santiago, O., Trejo-Acevedo, A. and Ilizaliturri-Hernández, C.A. 2021. Patterns in the utilization of carbon sources in soil microbial communities contaminated with mine solid wastes from San Luis Potosi, Mexico. *Ecotoxicol. Environ. Saf.*, 208: 111493.
- Mukhopadhyay, S., Maiti, S.K. and Mastro, R.E. 2013. Use of reclaimed mine soil index (RMSI) for screening of tree species for reclamation of coal mine degraded land. *Ecol. Eng.*, 57: 133-142.
- Muniz, S., Lacarta, J., Pata, M.P., Jimenez, J.J. and Navarro, E. 2014. Analysis of the diversity of substrate utilization of soil bacteria exposed to Cd and earthworm activity using generalized additive models. *PLoS One*, 9(1): e85057.
- Ngugi, M.R., Fechner, N., Neldner, V.J. and Dennis, P.G. 2020. Successional dynamics of soil fungal diversity along a restoration chronosequence post-coal mining. *Restor. Ecol.*, 28(3): 543-552.
- Pascual, J.A., Garcia, C., Hernandez, T., Moreno, J.L. and Ros, M. 2000. Soil microbial activity as a biomarker of degradation and remediation processes. *Soil Bio. Biochem.*, 32(13): 1877-1883.
- Potthoff, M., Steenwerth, K.L., Jackson, L.E., Drenovsky, R.E., Scow, K.M. and Joergensen, R.G. 2006. Soil microbial community composition is affected by restoration practices in California grassland. *Soil Biol. Biochem.*, 38(7): 1851-1860.
- Rath, M., Mishra, C.S. and Mohanty, R.C. 2010. Microbial population and some soil enzyme activities in iron and chromite mine spoil. *Int. J. Ecol. Environ. Sci.*, 36(2/3): 187-193.
- Rutgers, M., Wouterse, M., Drost, S.M., Breure, A.M., Mulder, C., Stone, D., Creamer, R.E., Winding, A. and Bloem, J. 2016. Monitoring soil bacteria with community-level physiological profiles using Biolog™ ECO-Plates in the Netherlands and Europe. *Appl. Soil Ecol.*, 97: 23-35.
- Scheffer, F. and Schachtschabel, P. 2010. *Bodenmikroflora. Lehrbuchder Bodenkunde* (in German) (Eds F. Scheffer, P. Schachtschabel). Spektrum Akademischer Verlag, Heidelberg. pp. 84-99.
- Stefanowicz, A.M., Niklińska, M. and Laskowski, R. 2008. Metals affect soil bacterial and fungal functional diversity differently. *Environ. Toxicol. Chem. Int. J.*, 3: 591-598.
- Thouin, H., Norini, M.P., Le Forestier, L., Gautret, P., Motelica-Heino, M., Breeze, D., Gassaud, C. and Battaglia-Brunet, F. 2019. Microcosm-scale biogeochemical stabilization of Pb, As Ba, and Zn in mine tailings amended with manure and ochre. *Appl. Geochem.*, 111: 104438.
- Tischer, S., Tanneberg, H. and Guggenberger, G. 2008. Microbial parameters of soils contaminated with heavy metals: Assessment for ecotoxicological monitoring. *Pol. J. Ecol.*, 56(3): 471-479.
- Urbanová, M., Kopecký, J., Valášková, V., Ságová-Marečková, M., Elhottová, D., Kyselková, M., Moëne-Loccoz, Y. and Baldrian, P. 2011. Development of bacterial community during spontaneous succession on spoil heaps after brown coal mining. *FEMS Microbiol. Ecol.*, 78(1): 59-69.
- Van Der Heyde, M., Bunce, M., Dixon, K., Wardell-Johnson, G., White, N.E. and Nevill, P. 2020. Changes in soil microbial communities in post mine ecological restoration: implications for monitoring using high throughput DNA sequencing. *Sci. Total Environ.*, 749: 142262.
- Veresoglou, S.D., Mamolos, A.P., Thornton, B., Voulgari, O.K., Sen, R. and Veresoglou, D.S. 2011. Medium-term fertilization of grassland plant communities masks plants species-linked effects on soil microbial community structure. *Plant Soil*, 344(1): 187-196.
- Waldrop, M.P., Balsler, T.C. and Firestone, M.K. 2000. Linking microbial community composition to function in a tropical soil. *Soil Biol. Biochem.*, 32(13): 1837-1846.
- Walker, L.R., Wardle, D.A., Bardgett, R.D. and Clarkson, B.D. 2010. The use of chronosequences in studies of ecological succession and soil development. *J. Ecol.*, 98(4): 725-736.
- Wang, L.P., Zhang, W.W., Guo, G.X., Qian, K.M. and Huang, X.P. 2009. Selection experiments for the optimum combination of AMF-plant-substrate for the restoration of coal mines. *Mining Science and Technology (China)*, 19(4): 479-482.
- Weber, K.P. and Legge, R.L. 2009. The one-dimensional metric for tracking bacterial community divergence using sole carbon source utilization patterns. *J. Microbiol. Methods*, 79(1): 55-61.
- Weber, K.P., Grove, J.A., Gehder, M., Anderson, W.A. and Legge, R.L. 2007. Data transformations in the analysis of community-level substrate utilization data from microplates. *J. Microbiol. Methods*, 69(3): 461-469.
- Winding, A. 1994. *Fingerprinting Bacterial Soil Communities Using Biolog Microtitre Plates*. In Ritz, K., Dighton, J., and Giller, K.E. (eds.), *Beyond the Biomass: Compositional and Functional Analysis of Soil Microbial Communities*. John Wiley & Sons, Chichester (United Kingdom), pp. 85-94.
- Winding, A. and Hendriksen, N.B. 1997. *Biolog Substrate Utilisation Assay For Metabolic Fingerprints Of Soil Bacteria: Incubation Effects*. In Insam, H. and Renger, A. (eds), *Microbial Communities: Function Versus Structural Approaches*, Springer, The Netherlands. pp. 195-205.
- Xu, W., Ge, Z. and Poudel, D.R. 2015. Application and optimization of Biolog eco plates in functional diversity studies of soil microbial communities. *MATEC Web Conf.*, 22: 04015.
- Zak, J.C., Willig, M.R., Moorhead, D.L. and Wildman, H.G. 1994. Functional diversity of microbial communities: a quantitative approach. *Soil Biol. Biochem.*, 26(9): 1101-1108.
- Zeller, V., Bardgett, R.D. and Tappeiner, U. 2001. Site and management effects on soil microbial properties of subalpine meadows: A study of land abandonment along a north-south gradient in the European Alps. *Soil Biol. Biochem.*, 33(4-5): 639-649.





# The COVID-19 Pandemic and Sustainable Tourism Development

M.A.H. Bhuiyan\*† and M.A. Darda\*\*

\*Department of Management, National University Bangladesh, Gazipur-1704, Bangladesh

\*\*Department of Statistics, National University Bangladesh, Gazipur-1704, Bangladesh

†Corresponding author: M.A.H. Bhuiyan; anowarlestari@gmail.com

Nat. Env. & Poll. Tech.  
Website: [www.neptjournal.com](http://www.neptjournal.com)

Received: 09-04-2022

Revised: 25-05-2022

Accepted: 30-05-2022

## Key Words:

COVID-19

Economic effects

Environmental effects

Tourism

## ABSTRACT

The Corona Virus (COVID-19) pandemic situation has posed a significant effect on the tourism industry. Tourism destinations have accepted emergency health care measures and restrictions imposed on human movement around the world. Beaches and resorts are empty, peoples' movements are stopped, and traveling between territories is strictly controlled. The COVID-19 lockdown around the world has imposed a negative impact on the livelihood of people and the world economy as well. The goal of the current study is to determine the potential for sustainable tourism growth in the near future given the social, economic, and environmental effects of the COVID-19 pandemic crisis.

## INTRODUCTION

More than 200 countries around the globe are affected by the Corona Virus (COVID-19) pandemic. The situation has been regarded as a symptom of discrimination and a deficit of social advancement in the affected countries. It also creates a social, economic, and political crisis in the infected territories (Chakraborty & Maity 2020). Walker et al. (2020) have estimated that the Coronavirus pandemic will be infecting 7.0 billion people and cause 40 million deaths worldwide. Most countries in the world have implemented lockdowns of cities, closure of borders, and other essential health measures to prevent the pandemic (Zhang et al. 2020a). The COVID-19 pandemic has created several uncertainties in global phenomena, such as negative effects on GDP (Baker et al. 2020), the relation between globalization and the pandemic (Zimmermann et al. 2020), effects on international business and trade (Bekkers & Koopman 2022), and the emergence of a crisis in the global value chain (Pahl et al. 2022). In the year 2020, the COVID pandemic reduced the world GDP by 4.2% (UNCTAD 2020). The indicators of the macroeconomy, such as employment, foreign investment, GDP, and health care system have been affected due to the lockdown and uncertainties during the lockdown situation (Idris & Oruonye 2020).

Tourism is one of the most negatively affected sectors by the COVID-19 pandemic globally. The pandemic situation has affected massively domestic and international travel,

accommodations, cruise lines, entertainment, restaurants, and other related segments in the tourism sector (Assaf et al. 2022). Most countries have taken various actions like lockdowns, travel bans, restrictions on movement, and quarantine which have had a significant impact on the global tourism industry (Gossling et al. 2021). For several weeks, there appear to be no formal activities in the world, which has a negative impact on every aspect of life. The pandemic situation has affected tremendously the tourism industry worldwide. Faus (2020) estimated that the tourism industry needs at least one year to recover the losses in the present situation. Most of the destinations in the world have embraced coronavirus-related restrictions.

In 2020, the World Tourism Organization (UNWTO) predicted that there will be 1.1 billion foreign tourist visits, down from 8.5 million in 2019. Due to this reduction, the global tourist industry has lost \$300 to 450 billion in revenue and five to seven years' worth of growth. During the first 8 months of 2020, tourism activities have decreased by 70% compared to the same period in 2019 in the globe. The pandemic situation has decreased US\$ 910 million to US\$ 1.2 trillion in export revenue and 100-200 million jobs around the globe (UNWTO 2020). According to World Travel and Tourism Council (WTTC), the pandemics COVID-19 situation has cut about 50 million jobs and about 75 million jobs are at risk worldwide. It is predicted that the tourism industry needs at least 10 months to recover after the outbreak of the

pandemic situation. The COVID-19 condition has affected Asia worst and Small Island Developing States (SIDS) has been impacted heavily because of their high reliance on tourism for economic growth (WTTC 2020).

Several crises like economic rescission, environmental degradation, and political instability have influenced tourism demand (Cró & Martins 2017). But present COVID-19 pandemic makes it difficult to manage and needs long-term survival approaches like the Ebola-related tourism crisis in African countries (Novelli et al. 2018). Moreover, Jiang et al. (2017) emphasized macro-level research to provide guidelines for crisis orientation in tourism. COVID-19 has negatively impacted the livelihood of people and economics around the world. During this pandemic span, social, economic, religious, and cultural activities have been disrupted due to maintaining physical and social distances. Furthermore, Dwyer et al. (2016) suggested that future research will be concerned to incorporate the measure of sustainability in terms of social, economic, and environmental aspects. The goal of the current study is to determine the potential for sustainable tourism growth in the foreseeable future given the social, economic, and environmental effects of the COVID-19 pandemic situation.

## THEORETICAL FRAMEWORK

Payne et al. (2021) emphasized policy response to mitigate negative impacts on the economy and focus on crisis management to overcome permanent shocks and changes in the pandemic situation. Government interventions are necessary for policy support and to restore the tourism sector to a pre-pandemic position (Payne et al. 2021). Assaf et al. (2022) have identified COVID-19 impacts in the tourism sector in terms of consumer behavior, demand and forecasting, destination and facility management, information technology, quality of life, and sustainability. Moreover, the COVID-19 pandemic is creating challenges for transformative impacts and practices in the future tourism sector. Kock et al. (2020) emphasized on possible positive settlement situation in tourism after the pandemic impacts future growth and competitiveness.

Fig 1 highlights the COVID-19 pandemic and sustainable tourism development in terms of social, economic, and environmental aspects. This pandemic situation is affecting the three aspects positively and negatively. The research initiatives in COVID-19 have covered two areas. Firstly, qualitative approaches are highlighting the management aspects to the policymakers so that they can prepare for future crises and pandemic situations (Gossling et al. 2021). Secondly, quantitative approaches are providing guidelines to analyze impacts in different aspects like social, economic, and environmental (Pham et al. 2021). Wut et al. (2020) argued that tourism has suffered as the most vulnerable sector worldwide during this pandemic situation. They have emphasized discovering the impacts of a pandemic to recover the situation.

Due to the pandemic situation, Gossling et al. (2021) urged for the resetting of the sustainable tourism model in place of the conventional model for embracing the tourism sector. They compared the COVID-19 impacts with the previous pandemics and events. They revealed travel pattern is responsible for the spread of the coronavirus and it creates significant impacts globally. Due to the correlation between opportunities, uncertainties, and crises, Hall et al. (2020) emphasized identifying strategic solutions for specific cases related to pandemics. It is necessary to find out the strategic responses in the tourism sector to recover from the crisis of the pandemic. Effective planning and guidelines are giving support to the tourism sector in terms of resistance and recovery of the losses as well as the transformation of this sector. These initiatives are helping the tourism sector collaborate with the other business sectors to recover from the losses of the pandemic (Do et al. 2021). Chen et al. (2022) identified several effects of the pandemic on the tourism sector in China, such as tourists' emotions, tourism venue management, national intention, and local reaction, conflicts in tourism activities, corporate initiatives in tourism, government support, tourism product, and post-crisis activities.

Dolnicar & Zare (2020) argued that due to the pandemic situation, the tourism industry needs innovative strategies to recover from economic damage and physical changes as well as achieve sustainable development. The tourism sector

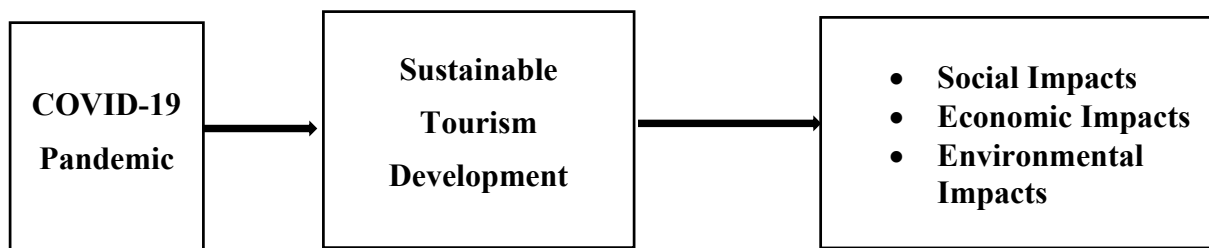


Fig 1: COVID-19 pandemic and sustainable tourism development.

has faced several crises due to the emergence of the COVID-19 pandemic which impacted the social and economic dimensions. Utkarsh & Sigala (2021) argued that the future of tourism research after post-COVID-19 depends on sustainability. Moreover, most of the research initiatives have emphasized responsible and sustainable post-pandemic tourism activities in the post-pandemic situation. Jones & Comfort (2020) emphasized sustainable tourism development with safe and clean consumption to remedy the damage in the tourism sector due to pandemic effects. According to Fennell (2021), the pandemic period's sustainable tourism activities and consumption were not identified. To manage the tourism sector in light of the pandemic recovery situation, Benjamin et al. (2020) emphasized sustainable tourism policies and practices, enforcing sustainable consumption, and ensuring economic benefits. The pandemic situation has caused social, economic, cultural, and psychological impacts on the different tourism stakeholders and they have suffered for a long time (Abbas et al. 2021). From the above discussion, it is indicated that the pandemic situation has affected immensely the tourism sector due to the spread of the infection. For the tourism sector to recover after the post-pandemic, ensuring sustainable tourism development is essential. It is necessary to identify the pandemic impacts from the perspective of social, economic, and environmental aspects and suggest necessary recommendations in this regard.

### **SOCIAL IMPACTS AND TOURISM**

COVID-19 becomes a major cause of infection and death of people in all age groups in the affected countries. Due to mass gatherings and panic, various social, cultural, political, and sports events have been canceled and some international occasions like Hajj, Umrah, Olympic Games, summits, conferences, and exhibitions are suspended for an indefinite time (Chakraborty & Maity 2020). The social, religious, and economic transformations face challenging circumstances in mass occasion arranging countries (Yezli & Khan 2020). Saudi Arabia has attracted 10 million pilgrims every year for Hajj and Umrah (Yezli et al. 2017). The maximum number of pilgrims will lose to the pandemic infection. The COVID-19 circumstances bring social and cultural changes in the world that lead to social segregation. This pandemic also has changed travel behavior and intention to travel willingness (Zhang et al. 2020b). Tourists have canceled their travel trips during this pandemic to ensure the safety of their health (Li et al. 2020).

Travel opportunities help people to fulfill their mental happiness and social well-being. The pandemic damaged the social fabric of people due to social distance, lockdown, and quarantine rules. The COVID situation made worse

different social problems like social and mental unrest, loss of freedom, isolation, and uncertainty in life (Saladino et al. 2020). The pandemic situation is affecting the behavior and well-being of tourists. Most of the destinations have ensured a travel ban for preventing the transfer of viruses among the local communities. Abbas et al. (2021) have identified several consequences in the tourism sector due to COVID impacts. The social consequences are health and mental issues for tourism workers, the virtual environment, human resources, social cohesion, tourism enterprises, and economic conditions.

The COVID-19 pandemic situation suggested avoiding mass gathering functions like conferences, sports events, business meetings, fashion shows, and marriage ceremonies, which have a great social impact (Ali & Alharbi 2020). The lockdown conditions worldwide have influenced labor productivity and caused lower tourism outputs. Tourism demand also decreased in this situation due to health risks to human mobility (WTO 2018). Sigala (2020) revealed that COVID-19 has impacted tourism at the employee, organization, and industry levels. This pandemic created significant losses in tourism employment which affected negatively livelihoods and societies. Nannia & Ulqinaku (2020) have suggested virtual tours for tourists in parks, museums, and other attractions due to COVID-19 lockdown circumstances. Tussyadiah et al. (2018) pointed out that virtual visits create a positive intention for tourists to visit a place physically. Ulqinaku and Sarial-Abi (2021) have suggested interactive tours through technological adoption when mortality threats increased.

The pandemic situation has created several social impacts on the tourism sector. Several factors can contribute to the development of sustainable tourism from a social perspective. The mentionable social aspects are guest-host interaction (Giovanardi et al. 2014), social motivation (Xing et al. 2014), social experiences (Nordvall et al. 2014), community perception (Kim et al. 2015), and socio-cultural impacts (Getz & Page 2016). Again, Nannia & Ulqinaku (2020) have suggested tourism development in experimental approaches, causal effects, virtual tours, and attitudes of tourists during the COVID-19 situation. Al-Mughairi et al. (2021) have identified some social impacts of a pandemic on the tourism sector in Oman, such as anxiety, irritation, depression, and stress among the tourism stakeholders regarding the possible consequences.

### **ECONOMIC IMPACTS AND TOURISM**

The COVID-19 pandemic crisis has had a significant impact on the aviation sector globally. Major international airline companies have deferred their flight operation. All airlines

have reduced air travel in this uncertain global situation. Other modes of transportation such as road, rail, and water were also hampered in this COVID-19 emergency (Goodell 2020). Millions of dollars have been lost in the aviation and tourism sectors in the related nations as a result of the travel ban. This also created shortage of medicines, agricultural products, food supply, and other commodities in affected countries (Ali & Alharbi 2020). As a result, the people related to tourism, aviation, and transportation are suffering extreme difficulties. Skare et al. (2021) conducted research on COVID-19 impacts on global tourism based on panel data from 185 countries. The research revealed that the pandemic caused a US\$ 4.1 to US\$ 12.8 trillion decline in tourism GDP, a decrease in jobs from 164 to 514 million, a loss of US\$ 4.8 billion to US\$1.9 trillion, and reduced investments from US\$ 362 billion to 1.1 trillion. The research recommended several initiatives for the recovery of the tourism sector such as policy support in public and private coordination, capacity building, and sustainable operation.

According to OECD Assessment, COVID-19-affected countries are facing high inflation and unemployment problems due to expenditure on treatment and rehabilitation of people (OECD 2020). Again, the affected countries have a lost 2% of their annual GDP growth every month during the pandemic. The tourism sector has faced a decrease in output from 50% to 70% (Chakraborty & Maity 2020). The outbreak control situation increases costs in the health sector, decreases the productivity of employees, and reduces economic activities as a whole. Yang et al. (2020) revealed that pandemic situations are causing several changes in the tourism industry, including market behavior, and economic transformation which is creating immediate impacts on the economy. Al-Mughairi et al. (2021) have revealed that the COVID pandemic created a negative impact on tourist demand, products and services, tourism supply chain, financial loss, distribution system, and relationships among the tourism stakeholders in Oman. Abbas et al. (2021) identified several economic impacts due to the COVID-19 situation such as job opportunities, tourism education, training, marketing support, sustainable opportunity, and required skills.

The continued social distance between people in this environment hinders tourism activity (Goodell 2020). Many Gulf countries like Saudi Arabia have invested a huge amount of money to develop the country as a tourism hub within Vision 2030 (KSA 2016). Their investment and vision fulfillment have been hampered by this pandemic situation. Moreover, investment in tourism-related amenities such as recreation centers, restaurants, coffee shops, museums, fitness clubs, shopping malls, swimming pools, and cultural centers is also affected by the pandemic condition (Yezli &

Khan 2020). In this pandemic condition, the output and labor productivity in the tourism sector are lower and the risk of health crises is higher (Yang et al. 2020). Subsidizing travel expenses and receiving financial aid from other industries will be crucial in the post-pandemic period for the tourism sector's recovery (Yan & Zhang 2012).

The COVID-19 pandemic situation has created great impacts on the tourism sector and the overall economy of the country. Future tourism development will be based on the evaluation of the different stakeholders-local communities, tour operators, accommodation owners, food businessmen, tour guides, and transportation providers' perceptions and aspects of tourism impacts (Dwyer et al. 2016). Moreover, several macro-level impacts such as the impact of climate change on tourism, and the effect on GDP, taxation, economic welfare, and employment in tourism (Dwyer et al. 2016) are also be considered in near future. Again, the post-pandemic situation will require sustainable tourism development based on tourists' behavior, destination choice, and tourism planning and strategies in new consequences (Wang & Ritchie 2012).

## ENVIRONMENTAL IMPACTS AND TOURISM

Within the context of the major global negative challenges, the COVID-19 situation generates certain positive situations. Environmental matters like pollution, global warming, climate change effects, and change in ecosystem and biodiversity are showing positive landmarks in this period due to less human pressure on the environment (Bremer et al. 2019). The pollution in natural tourist attractions such as forests, beaches, hill areas, and water bodies also decreases during this pandemic situation.

Beaches are a valuable natural resource that many nations rely on to support tourism, recreational activities, and the survival of the livelihood of coastal communities (Zambrano-Monserrate et al. 2018). However, the irresponsible use of these beaches by communities and tourists has resulted in pollution issues. (Partelow et al. 2015). The beaches around the world have decreased the arrival of tourists to maintain social distancing. As a result, the reduction of waste generation and beach clean-up activities can enhance during this pandemic period (Zambrano-Monserrate et al. 2020). Moreover, less waste generation also creates a positive impact on environmental issues such as water, soil, forest, and air (Schanes et al. 2018).

Noise pollution is one of the main sources of environmental degradation and cause health problem for people and disturbs the natural coherence of the ecosystem (Zambrano-Monserrate & Ruano 2019). The decrease in transpor-

tation use in tourist attractions is contributing positively to the reduction of noise (Zambrano-Monserrate et al. 2020). Moreover, some other aspects are suitable for post-pandemic tourism research such as tourism events and environmental consequences, event sustainability (Pernecky & Luck 2012), willingness to pay, and carbon footprint analysis (Andersson & Lundberg 2013). Abbasi et al. (2021) revealed that the COVID-19 pandemic has affected some global challenges which are influencing the global tourism sector. The challenges are carbon emission, renewable energy, industrialization, and the service industry.

The pandemic situation has created positive impacts on the environment due to maintaining social distance, lockdown conditions, producing less pollution, and limited use of natural resources. Future tourism development should consider various environmental aspects such as pollution, ecosystem and biodiversity, use of natural resources, recreational activities, and waste management. Table 1 highlights the future scope for sustainable tourism development related to the COVID-19 impacts with different themes in three areas- social, economic, and environmental.

Table 1: The COVID-19 pandemic impacts and sustainable tourism development.

Areas	Themes
Social	<ul style="list-style-type: none"> <li>• Crisis management and strategies</li> <li>• Emergency tourism package</li> <li>• Travel facilitation</li> <li>• Diversified tourism products and services</li> <li>• Tourism governance</li> <li>• Human capital development</li> <li>• Social distance and tourism</li> <li>• Knowledge management</li> <li>• Postponed tourism events</li> <li>• Stress among the population</li> </ul>
Economic	<ul style="list-style-type: none"> <li>• Employment and livelihood</li> <li>• Taxes and subsidies</li> <li>• Transportation</li> <li>• Consumer protection</li> <li>• Tourism investment</li> <li>• Stimulate demand</li> <li>• Tourism supply chain</li> <li>• Poverty and tourism</li> <li>• Sustainable profit</li> <li>• Tourism productivity</li> <li>• Loss of tourism demand</li> <li>• Slow revenue growth and poor cash flow</li> </ul>
Environment	<ul style="list-style-type: none"> <li>• Sustainable tourism</li> <li>• Sustainability and recovery</li> <li>• Embracing SDGs</li> <li>• Environmental pollution</li> <li>• Climate change impact</li> <li>• Energy efficiency</li> <li>• Carbon emission</li> </ul>

Sources: Adapted from UNWTO (2020), Haleem et al. (2020a), Haleem et al. (2020b)

## CONCLUSION

The COVID-19 lockdown around the world has imposed a negative impact on the livelihood of people and the world economy as well. The pandemic crisis also opens up new opportunities for sustainable tourism growth in the foreseeable future because of its effects on social, economic, and environmental factors. Foo et al. (2020) identified that government subsidies have stimulated the tourism sector during the pandemic situation. Ugur & Akbiyik (2020) suggested insurance packages for the recovery of the tourism sector due to the pandemic crisis. Sigala (2020) claimed the pandemic situation was a transformational opportunity for the tourism sector. The research recommended government efforts such as tax holidays, subsidies, and stimulus packages for enhancing alternative opportunities in tourism such as virtual services and e-tourism.

In the post-COVID-19 pandemic situation, sustainable tourism development will require studies on mortality conditions, pandemics, natural disasters, and economic crises (Ritchie & Jiang 2019, Nannia & Ulqinaku 2020). Ritchie & Jiang (2019) suggested on several aspects such as management strategies for post-crisis, tourism disaster lifecycle, micro-level emergency management, hospitality, small and medium enterprises (SME), technology trends, and knowledge management would be vital for sustainable tourism. Moreover, Getz & Page (2016) pointed to special interest tourism, impact assessment, and sustainability issues, and Yeoman et al. (2014) highlighted trend analysis for future tourism development.

## REFERENCES

- Abbas, J., Mubeen, R., Iorember, P.T., Raza, S. and Mamirkulova, G. 2021. Exploring the impact of COVID-19 on tourism: Transformational potential and implications for a sustainable recovery of the travel and leisure industry. *Curr. Res. Behav. Sci.*, 2: 100033.
- Abbasi, K.R., Abbas, J. and Tufail, M. 2021. Revisiting electricity consumption, price, and real GDP: A modified sectoral level analysis from Pakistan. *Energy Policy*, 149: 112087.
- Ali, I. and Alharbi, O.M.L. 2020. COVID-19: Disease, management, treatment, and social impact. *Sci. Tot. Environ.*, 728: 138861. <https://doi.org/10.1016/j.scitotenv.2020.138861>
- Al-Mughairi, H.M.S., Bhaskar, P. and Alazri, A.K.H. 2021. The economic and social impact of COVID-19 on tourism and hospitality industry: A case study from Oman. *J. Pub. Affairs*, 21: e2786. DOI: 10.1002/pa.2786
- Andersson, T.D. and Lundberg, E. 2013. Commensurability and sustainability: Triple impact assessments of a tourism event. *Tour. Manag.*, 37: 99-109.
- Assaf, A.G., Kock, F. and Tsionas, M. 2022. Tourism during and after COVID-19: An expert-informed agenda for future research. *J. Travel Res.*, 61(2): 454-457.
- Baker, S.R., Bloom, N., Davis, S J. and Terry, S.J. 2020. Covid-Induced Economic Uncertainty. Working Paper No. 26983. National Bureau of Economic Research, Cambridge, MA. DOI 10.3386/w26983

- Bekkers, E. and Koopman, R.B. 2022. Simulating the trade effects of the COVID-19 pandemic: Scenario analysis based on quantitative trade modeling. *World Econ.*, 45(2): 445-467.
- Benjamin, S., Dillette, A. and Alderman, D.H. 2020. "We can't return to normal": Committing to tourism equity in the post-pandemic age. *Tour. Geogr.*, 22(3): 476-483.
- Bremer, S., Schneider, P. and Glavovic, B. 2019. Climate change and amplified representations of natural hazards in institutional cultures. *Oxford Res. Encycl. Nat. Hazard Sci.*, 13: 54. <https://doi.org/10.1093/acrefore/9780199389407.013.354>
- Chakraborty, I. and Maity, P. 2020. COVID-19 outbreak: Migration, effects on society, global environment, and prevention. *Sci. Total Environ.*, 728: 138882.
- Chen, H., Huang, X. and Li, Z. 2022. A content analysis of Chinese news coverage on COVID-19 and tourism. *Curr. Issues Tour.*, 25(2): 198-205.
- Cró, S. and Martins, A.M. 2017. Structural breaks in international tourism demand: Are they caused by crises or disasters? *Tour. Manag.*, 63: 3-9.
- Do, B., Nguyen, N., D'Souza, C., Bui, H.D. and Nguyen, T.N.H. 2021. Strategic responses to COVID-19: The case of tour operators in Vietnam. *Tour. Hospital. Res.*, 22(1): 5-17.
- Dolnicar, S. and Zare, S. 2020. COVID19 and Airbnb- Disrupting the disruptor. *Ann. Tour. Res.*, 83(2): 102961.
- Dwyer, L., Forsyth, P. and Spurr, R. 2016. Tourism economics and policy analysis: contributions and legacy of the sustainable tourism cooperative research center. *J. Hospital. Tour. Manag.*, 26: 91-99.
- Faus, J. 2020. This Is How Coronavirus Could Affect the Travel and Tourism Industry. <https://www.weforum.org/agenda/2020/03/world-travelcoronavirus-covid19-jobs-pandemic-tourism-aviation/>.
- Fennell, D.A. 2021. Technology and sustainable tourism in the new age of disruption. *J. Sustain. Tour.*, 29(5): 767-773.
- Foo, L., Chin, M., Tan, K. and Phuah, K. 2020. The impact of COVID-19 on the tourism industry in Malaysia. *Curr. Issues Tour.*, 24(19): 2735-2739.
- Getz, D. and Page, S.J. 2016. Progress and prospects for event tourism research. *Tour. Manag.*, 52: 593-631.
- Giovanardi, M., Lucarelli, A. and Decosta, P. 2014. Co-performing tourism places: The "Pink Night" festival. *Ann. Tour. Res.*, 44: 102-115.
- Goodell, J.W. 2020. COVID-19 and finance: Agendas for future research. *Fin. Res. Lett.*, 35: 101512. <https://doi.org/10.1016/j.frl.2020.101512>
- Gossling, S., Scott, D. and Hall, C. M. 2021. Pandemics, tourism and global change: A rapid assessment of COVID-19. *J. Sustain. Tour.*, 29(1): 1-20.
- Haleem, A., Javaid, M. and Vaishya, R. 2020a. Effects of COVID-19 pandemic on daily life. *Curr. Med. Res. Pract.*, 10(2): 78-79.
- Haleem, A., Javaid, M., Vaishya, R. and Deshmukh, S.G. 2020b. Areas of academic research with the impact of COVID-19. *Am. J. Emerg. Med.*, 38(7): 1524-1526.
- Hall, C.M., Scott, D. and Gossling, S. 2020. Pandemics, transformations, and tourism: Be careful what you wish for. *Tour. Geogr.*, 22(3): 577-598.
- Idris, M. and Oruonye, E. 2020. Socioeconomic impact of COVID-19 in oil-exporting countries: An analytical review of the macroeconomic indicators in Nigeria. *Int. J. World Policy Develop. Stud.*, 6(5): 44-50.
- Jiang, Y., Ritchie, B.W. and Benckendorff, P. 2017. Bibliometric visualization: An application in tourism crisis and disaster management research. *Curr. Issues Tour.*, 22(16): 1-33.
- Jones, P. and Comfort, D. 2020. The COVID-19 crisis, tourism, and sustainable development. *Athens J. Tour.*, 7(2): 75-86.
- Kim, W., Jun, H., Walker, M. and Drane, D. 2015. Evaluating the perceived social impacts of hosting large-scale sport tourism events: scale development and validation. *Tour. Manag.*, 48: 21-32.
- Kock, F., Nørfelt, A., Josiassen, A., Assaf, A.G. and Tsonas, M.G. 2020. Understanding the COVID-19 Tourist Psyche: The Evolutionary Tourism Paradigm. *Ann. Tour. Res.*, 85: 103053
- KSA 2016. Kingdom of Saudi Arabia Vision 2030. <http://vision2030.gov.sa/download/file/ffd/417>.
- Li, J., Nguyen, H. and Coca-Stefaniak, J.A. 2020. Coronavirus impacts on post-pandemic planned travel behaviors. *Ann. Tour. Res.*, 86: 102964. <https://doi.org/10.1016/j.annals.2020.102964>
- Nannia, A. and Ulqinaku, A. 2020. Mortality threats and technology effects on tourism. *Ann. Tour. Res.*, 86(4): 102942. <https://doi.org/10.1016/j.annals.2020.102942>
- Nordvall, A., Pettersson, R., Svensson, B. and Brown, S. 2014. Designing events for social interaction. *Event Manag.*, 18(2): 141-151.
- Novelli, M., Burgess, L.G., Jones, A. and Ritchie, B.W. 2018. No Ebola... still doomed"—The Ebola-induced tourism crisis. *Ann. Tour. Res.*, 70: 76-87.
- OECD 2020. Coronavirus: The world economy at risk. OECD Interim Economic Assessment. [oecd.org/economic-outlook](https://oecd.org/economic-outlook)
- Pahl, S., Brandi, C., Schwab, J. and Stender, F. 2022. Cling together, swing together: The contagious effects of COVID-19 on developing countries through global value chains. *World Econ.*, 45(2): 539-560.
- Partelow, S., von Wehrden, H. and Horn, O. 2015. Pollution exposure on marine protected areas: A global assessment. *Mar. Pollut. Bull.*, 100: 352-358.
- Payne, J.E., Gil-Alana, L.A. and Mervar, A. 2021. Persistence in Croatian tourism: The impact of COVID-19. *Tour. Econ.*, 69: 1-7. DOI: 10.1177/1354816621999969
- Pernecky, T. and Luck, M. (Eds.). 2012. Events, Society, and Sustainability: Critical and Contemporary approaches. Routledge, Oxon.
- Pham, T.D, Dwyer, L., Su, J. and Tramy, N. 2021. COVID-19 impacts of inbound tourism on the Australian economy. *Ann. Tour. Res.*, 88(C): 103179.
- Ritchie, B.W. and Jiang, Y. 2019. A review of research on tourism risk, crisis, and disaster management: Launching the annals of tourism research curated collection on tourism risk, crisis, and disaster management. *Ann. Tour. Res.*, 79: 102812.
- Saladino, V., Algeri, D. and Auriemma, V. 2020. The psychological and social impact of Covid-19: New perspectives of well-being. *Front. Psychol.*, 11: 1-6.
- Schanes, K., Dobernig, K. and Gözet, B. 2018. Food waste matters—a systematic review of household food waste practices and their policy implications. *J. Clean. Prod.*, 182: 978-991.
- Sigala, M. 2020. Tourism and COVID-19: Impacts and implications for advancing and resetting industry and research. *J. Buss. Res.*, 117: 312-321.
- Skare, M., Soriano, D.R. and Porada-Rochon, M. 2021. Impact of COVID-19 on the travel and tourism industry. *Technol. Forecast. Social Change*, 163: 120469.
- Tussyadiah, I.P., Wang, D., Jung, T.H., and Tom Dieck, M.C. 2018. Virtual reality, presence, and attitude change: Empirical evidence from tourism. *Tour. Manag.*, 66: 140-154.
- Ugur, N. and Akbiyik, A. 2020. Impacts of COVID-19 on Global Tourism Industry: A cross-regional comparison. *Tour. Manag. Persp.*, 36: 100744.
- Ulqinaku, A. and Sarial-Abi, G. 2021. Tourism implications of online response to terrorism. *Ann. Tour. Res.*, 86: 102914.
- UNCTAD 2020. Covid-19 and Tourism: Assessing the Economic Consequences. UNCTAD, Geneva.
- UNWTO 2020. The Impact Assessment of COVID-19 Outbreak on International Tourism. <https://www.unwto.org/impact-assessment-of-the-covid-19-outbreak-on-international-tourism>
- Utkarsh, R. and Sigala, M. 2021. A bibliometric review of research on COVID-19 and tourism: Reflections for moving forward. *Tour. Manag. Persp.*, 40: 100912
- Walker, P., Whittaker, C. and Ghani, A. 2020. Report 12: The Global Impact of COVID-19 and Strategies for Mitigation and Suppression. Imperial College London MRC Centre for Global Infectious Disease Analysis, London, UK.

- Wang, J. and Ritchie, B.W., 2012. Understanding accommodation managers' crisis planning intention: An application of the theory of planned behavior. *Tour. Manag.*, 33(5): 1057-1067.
- WTO 2018. Managing Epidemics: Key Facts about Major Deadly Diseases.. <https://www.who.int/emergencies/diseases/managing-epidemics-interactive.pdf>.
- WTTC 2020. This is how coronavirus could affect the travel and tourism industry. <https://www.weforum.org/agenda/2020/03/world-travel-coronavirus-covid19-jobs-pandemic-tourism-aviation>
- Wut, T. M., Xu, J. and Wong, S. 2021. Crisis management research (1985-2020) in the hospitality and tourism industry: A review and research agenda. *Tour. Manag.*, 85: 104307.
- Xing, X., Chalip, L. and Green, B.C. 2014. Marketing a social experience: how the celebration of subculture leads to social spending during a sporting event. *Sports Market. Quart.*, 23: 138-147.
- Yan, Q., and Zhang, H.Q., 2012. Evaluation of the economic effectiveness of public tourism coupons in China in 2009: A corrected DEA approach. *Asia Pacif. J. Tour. Res.*, 17(5): 534-550.
- Yang, Y., Zhang, H. and Chen, X. 2020. Coronavirus pandemic and tourism: dynamic stochastic general equilibrium modeling of infectious disease outbreak. *Ann. Tour. Res.*, 83: 102913.
- Yeoman, I., Robertson, M., McMahon-Beattie, U., Smith, K. and Backer, E. (Eds.). 2014. *The future of events and festivals*. Routledge, Abingdon
- Yezli, S. and Khan, A. 2020. COVID-19 social distancing in the Kingdom of Saudi Arabia: Bold measures in the face of political, economic, social and religious challenges. *Travel Med. Infect. Dis.*, 10: 69. <https://doi.org/10.1016/j.tmaid.2020.101692>
- Yezli, S., Yassin, Y., Awam, A., Attar, A., Al-Jahdali, E. and Alotaibi, B. 2017. Umrah: An opportunity for mass gatherings health research. *Saud. Med. J.*, 38(8): 868-871.
- Zambrano-Monserrate, M.A. and Ruano, M.A. 2019. Does environmental noise affect housing rental prices in developing countries? Evidence from Ecuador. *Land Use Policy*, 87: 104059
- Zambrano-Monserrate, M.A., Ruano, M.A. and Sanchez-Alcalde, L. 2020. Indirect effects of COVID-19 on the environment. *Sci. Tot. Environ.*, 728: 138813.
- Zambrano-Monserrate, M.A., Silva-Zambrano, C.A. and Ruano, M.A. 2018. The economic value of natural protected areas in Ecuador: A case of Villamil beach national recreation area. *Ocean Coast. Manag.*, 157: 193-202.
- Zhang, D., Hu, M. and Ji, Q. 2020a. Financial markets under the global pandemic of COVID-19. *Fin. Res. Lett.*, 36: 101528. <https://doi.org/10.1016/j.frl.2020.101528>
- Zhang, K., Hou, Y. and Li, G. 2020b. The threat of infectious disease during an outbreak: Influence on tourists' emotional responses to disadvantaged price inequality. *Ann. Tour. Res.*, 84: 102993. <https://doi.org/10.1016/j.annals.2020.102993>
- Zimmermann, K.F., Karabulut, G., Bilgin, M.H. and Doker, A.C. 2020. Inter-country distancing, globalisation and the coronavirus pandemic. *World Econ.*, 43(6): 1484-1498.







# Green Campus Audit Procedures and Implementation to Educational Institutions and Industries

S. Rajalakshmi\*†, B. Mythili Gnanamangai\*, D. Vinoth Kumar\*, V. Sri Santhya\*, M. Priya\*, R. Mary Josephine\*, Ashutosh Kumar Srivastava\*\*, R. Sudhakaran\*\*\* and M. A. Deepa\*\*\*\*

\*South Zone Headquarters, Nature Science Foundation, Coimbatore-641 004, Tamil Nadu, India

\*\*Central Zone, Nature Science Foundation, Gorakhpur-273 001, Uttar Pradesh, India

\*\*\*North Zone, Nature Science Foundation, Faridabad-101 213, Haryana, India

\*\*\*\*Department of Botany, Government Arts College (Autonomous), Coimbatore-641 018, Tamil Nadu, India

†Corresponding author: S. Rajalakshmi; [directornsf@gmail.com](mailto:directornsf@gmail.com), [director@nsfonline.org.in](mailto:director@nsfonline.org.in)

Nat. Env. & Poll. Tech.  
Website: [www.neptjournal.com](http://www.neptjournal.com)

Received: 16-02-2022

Revised: 30-03-2022

Accepted: 09-04-2022

## Key Words:

Green audit  
Audit procedure  
Green campus  
Green audit procedures  
Green cover of campus  
Sustainable campus

## ABSTRACT

Nature provides a free lunch, but only if we control our appetites. As we are in the twenty-first century, modernization and industrialization are the two important outputs that have made human life more luxurious and comfortable. Simultaneously, they are responsible for several uses of exploitation of forests, natural resources, and wildlife, polluting the scarce, producing massive solid waste and sacred water resources, and finally making our planet Earth ugly and inhospitable. Today, people are getting more familiar with global issues like global warming, the greenhouse effect, ozone depletion, climate change, etc. Now, it is considered a final call by Mother Earth to walk on the path of sustainable development. The time has come to wake up, unite and combat together for a sustainable environment. The present study focuses on the concept of green audit and its importance with respect to the conservation of nature for future generations. Every organization should have its own green campus and environment policy with respect to nature conservation and environmental protection and should maintain a sizable amount of green cover area after building construction along with natural and planted vegetation. A maximum number of more oxygen-producing and carbon-di-oxide-absorbing plants should be maintained to provide a pure atmosphere to the stakeholders. The installation of a rainwater harvesting system, percolation, ponds, check dam, and drip irrigation system to conserve rainwater and groundwater should be noteworthy on the campus.

## INTRODUCTION

Green Audit is a tool of Management system used methodologically for the protection, conservation, and sustenance of the Environment. Green audit procedures are a set of guidelines framed on how to conduct a green audit at educational institutions and industrial sectors as per the checklist of Environment Management Systems and International Standards on ISO 14001:2015 and Indian Green Building Council at 360° views. In addition, it also speaks about an overall idea on green audits groundwork, auditing techniques, audit/non-conformity report preparation, and submission. It will be recording and verify the eco-friendly approaches and practices in educational institutions and industries. The audit process supports the nation as a whole for the noble cause of environmental protection and nature conservation which in turn enhances the quality of life of human beings (Arora 2017). It is a type of assessment to ensure that the Institution and Organization campus is greenish in terms of planting a

large number of trees and lawns on the campus. To ensure that the list of plants and animals/birds available on the campus, biodiversity conservation, water irrigation system, recycling of water, rain harvesting system, site preservation, soil erosion control, and landscape management will be evaluated (Gowri & Harikrishnan 2014). The first concept of Environment Audit was approved in the Earth Summit, Rio-1992. The audit ensures that the campus is greenish in terms of planting a large number of herbs, shrubs, and trees including lawns which in turn reduce environmental pollution, proper water irrigation system, natural topography or vegetation, biodiversity conservation, etc. implemented effectively for the benefit of the stakeholders. Similarly, it will also ensure a green campus, the environmental management system, maintenance of an eco-friendly campus that leads the environment clean and neat, solid-state management, recycling of water, disposal of sewage and waste materials including electronic wastes and biomedical wastes, landscape management, plastic use, etc. in the campus should be implemented effectively for the

benefit for the stakeholders. The Environment Management System is the quantitative and qualitative data to track air, water, and waste, and to gain actionable insights to improve operational performance. It is used to maintain a clean and green environment that leads to the stakeholders. It provides a 360° view of a surrounding campus and makes it easy for Owners/Managers/Environmentalists to collaborate, measure, control, and reduce environmental impacts. Finally, it leads to enhancing the quality of life for human beings, animals, and plants. Green campus initiatives are needed at present across the world due to changes in environmental conditions, global warming, and the increasing human population. It aims to make a sustainable and environmentally friendly campus for the stakeholders.

### WHAT IS A GREEN CAMPUS?

A green campus is an area of the organization or the organization as a whole itself that is contributing to having an infrastructure or development that is structured and planned to incur less energy, less water, less or pollution-free, and less or no CO<sub>2</sub> emission. In certain cases, the project zone of the green campus can be self-reliable in terms of energy and water consumption, and with higher ratings of the project zone, they can complement or support national energy and water needs as a part of corporate social responsibility. The green campus capitalization may incur some little investment but the vision of the green campus is to satisfy the organizational needs by its simple initiatives in a bigger vision to prevent the deterioration of environmental resources.

### THE GREEN CAMPUS OF AN ORGANIZATION

In the present scenario, with multiple options on the availability of all materials and gadgets with high carbon dioxide emission, the sole responsibility in choosing building materials and less emitting gadgets installed in the projected project area should be considered. In case the organization has to use many of the materials that add up a burden to the environment in terms of anything that disturbs the environmental cycle (in unavoidable circumstances), the organization should have taken proper steps to neutralize or nullify its emission and produce its own needs. A green campus is nothing but environmental-friendly practices and education combined to promote sustainable and eco-friendly practices along with user-friendly technology on the campus. It creates environmental culture, develops sustainable solutions to environmental problems, and provides solutions to various social and economic needs (Wang et al. 2013). It provides the concept of green building and oxygenated building which in turn is useful to provide a healthy atmosphere. Proper strategies and planning budgetary processes for a clean and green

campus also play an important role. Tool kit for members of staff and students for a sustainable green campus can be developed by using tools and resources from case studies and practices, which are intended to inspire, encourage and support educational institutions and industrial sectors to develop and implement their own transformative strategies (Suwartha & Sari 2013). Green campus audit is useful to detect and monitor sources of pollution, nature of vegetation, and topology which emphasizes the management of all types of waste, energy, water, soil, etc. It was implemented in the USA in 1970 for the first time but India is the first to implement environmental audit compulsory in later stages (Arora 2017). It enabled managers, environmentalists, and academicians, to check the compliance with

### GREEN CAMPUS AUDIT PROCEDURES

Green campus audit is a structured process of documenting the credentials in terms of measurable, recording, accounting, and investigating of used materials and their impact on the environment and its ecology. Green audit projects the best environmental practices and initiatives taken in the organization at the prescribed site of audit that brings added value to the organization in maintaining the eco-friendly campus. The first step of the audit is ensuring that the organization has a central role in building the green campus, to validate the same.

- Apply application forms of the green audit to any agencies that are Authenticated Professionals for people qualified to investigate and evaluate the campus for validating the best environmental practices.
- Once the application process is over the Professional team of Auditors will have an in-house visit to the mentioned site or organization for its claim.
- On accounting for all the green practices of the organization or the mentioned site or project site a detailed report will be given by the Auditing Professionals and the marks will be awarded to the respective heads.
- The report will be certified and returned to the applicants. If they wish to claim improved marks, they can re-apply with improved structures with a resting period of six months.
- If they wish to claim the neglected marks, they should re-apply within seven days after the receipt of the detailed GAR (Green Audit Report).

### OVERVIEW OF THE GREEN AUDIT FLOW

#### Establishing a Green Campus

Every campus needs to have a vision of self-reliability at the stage of designing itself. As there was no awareness in the

past about green buildings and green practices, the concept of converting the “go green” campus arrived. The campus should have restructured its existing facilities to establish or follow the “go green” campus practices. The “go green” structures and establishments should have a record of minimum documentation of existing records for three months. The Management of the Organization (Auditee) should show their inherent commitment towards making an eco-friendly atmosphere and be ready to encourage all types of green activities (Fig. 1). They should promote all kinds of green activities such as the conduct of environment awareness programs, campus farming, planting trees, maintenance of greenery, irrigation, use of biofertilizers and avoidance of chemical fertilizers and agrochemicals on the campus, etc., before and after the green auditing. The management should formulate ‘Green and Environment Policies’ based on a green auditing report. A clean and healthy environment should enhance an effective teaching and learning process and provide a conducive learning environment to the stakeholders. They should create awareness of the importance of the environment through environmental education among the student members. Green Audit is the most efficient and ecological way to manage environmental problems. In general, the Management should take responsibility to maintain a campus that is completely free from environmental pollution. Green campus audit may be beneficial to the campus in improving the greenery activities which in turn are used to save the planet for the future generation. Since green campus audit is

a kind of professional care and a simple indigenized system about the environment monitoring in terms of planting a large number of trees which is the responsibility of every individual who is part of economic, financial, social, and environmental factors. It is necessary to conduct a green audit frequently at least once in three years on campus because students and staff members should be aware of the green audit and its advantages. ‘Go green concept’ should be adopted to help the institution set environmental examples for the community, and thereby educate the young learners.

#### Aims and objectives of Green Campus Audit

- To recognize the initiatives taken towards the environment and threats to human health.
- To provide baseline information to assess threat and risk.
- To recognize, diagnose and resolve environmental problems.
- To identify the impact of the Institution on the Environment.
- To identify different pressures on the Institute to improve its environment.
- To ensure proper utilization of resources considering the health and welfare of the community.
- To set a procedure for disposal of all kinds of wastes

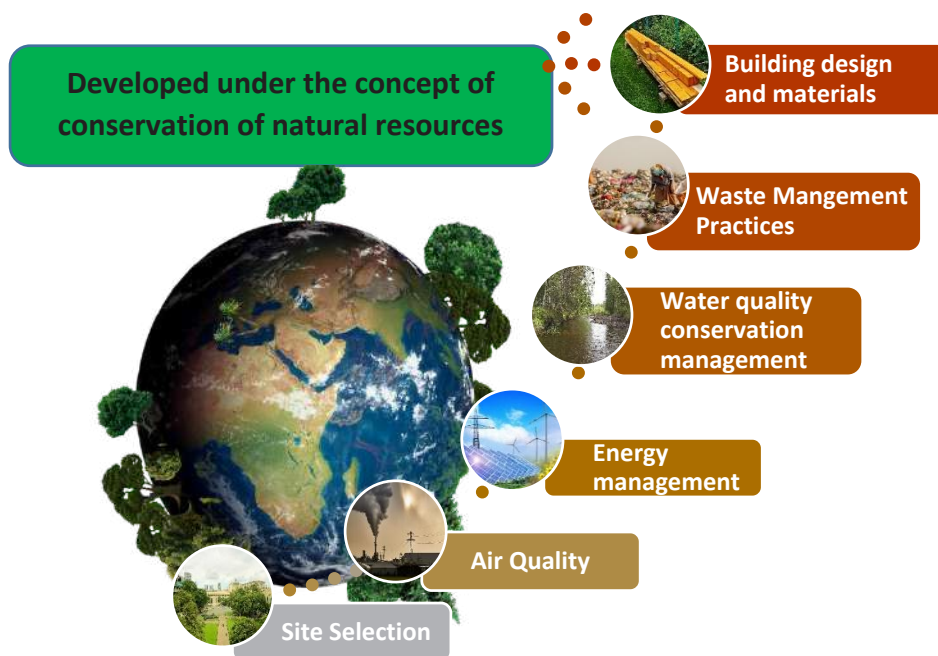


Fig. 1. Key steps for the ‘Go green’ concept at an Organization.

- To ensure the Green cover spread with pollution-free air and that provides working as a carbon sink.

### Definition of a Green Campus Audit

Green campus audit is a structured process of documenting the credentials in terms of measurable, recording, accounting, and investigating of used materials and their impact on the environment and its ecology. Green audit projects the best environmental practices and initiatives taken in the organization at the prescribed site of audit that brings added value to the organization in maintaining the eco-friendly campus to the stakeholders. The green campus should have a large number of trees, shrubs, herbs, climbers, twiners, and lianas which will provide an eco-friendly habitat to mammals, birds, flies, moths, earthworms, amphibians, termites, and various beneficial microorganisms in the soil and air. It will lead to giving a pure atmosphere without any environmental pollution and be available to the stakeholders in a sustainable manner (Ounsaneha et al. 2017).

### Benefits of the Green Auditing

There are several benefits to the conduct of a green audit by the Organization which may be useful to improve the campus significantly after receiving the report of the audit (Marrone et al. 2018). The green campus audit methodology follows both qualitative and quantitative measurements including physical observation of greeneries in terms of the growth of terrestrial and aquatic plants, animals, and microflora on the campus. The natural and planted vegetation and their maintenance in the organization's campus are also taken into consideration, through topography, landscape management design, and soil erosion control in environmentally sustainable development. The following are the major benefits of green auditing.

- Know the status of development of internal and external Green campus audit procedures and implementation scenarios in the Organization.
- Establishment of Green campus objectives and targets as of today as per the 'Green and Environment Policy', 'Indian Biodiversity Act', and 'Wildlife Protection Act' of the Ministry of Environment, Forests and Climate Change, New Delhi and World & Indian Green Building Council concepts.
- Assigning the roles and responsibilities of Environmental Engineer and Agriculture/Garden Staff to improve green initiatives.
- Development of ownership, personal and social responsibility for the Organization and its environment, and development of an environmental ethic and value systems for young generations.
- Enhancement of the Organization's profile and reaching the global standards in proving the green campus and eco-friendly atmosphere to the stakeholders
- Improving the drinking water / RO water / Bore well water / Open well water / Pond water / Municipal or Corporation water quality through the analysis of the Physico-chemical properties of water.

### PROCEDURES FOLLOWED IN GREEN CAMPUS AUDIT

The purpose of the green audit is to ensure that the practices followed on the campus are in accordance with the Green and Environment Policy developed by the Government and private agencies working with environmentally sustainable development adopted by the institution. The first step of the audit is ensuring that the organization has a central role in building the green campus, to validate the same (Adeniji 2008). A green campus is not intended for the self-sustainability of the building alone, it also involves the propagation of the green campus initiatives to be adopted by any individuals and organization at a minimum cost. A green campus audit should be conducted as per the guidelines of MoE. The audit should be conducted by authenticated Professionals who are to investigate and evaluate the campus. Professional team of ISO Environment Management Audit (14001:2015), Indian Green Building Council Accredited Professionals, Experts of Green campus Lead Auditors, and Botanists / Zoologists / Biotechnologists were selected to conduct the Green campus audit process. Labeling of common names and Botanical names of plants were observed. The operation of the water irrigation system, drip and sprinkler irrigation methods, and use of recycled water for irrigation purposes or any other purpose in the campus area was noted. The number of wells bore wells and water reservoir facilities on the campus were also noted as per the Audit Manual of Gnanamangai et al. (2021).

Attempts made for overcoming water scarcity during the summer season regarding the maintenance of plants and frequency of watering for plantations on the campus are noted. Biodiversity conservation education, projects, awareness programs, etc., through the Indian Biodiversity Act and Ministry of Environment, Forests and Climate Change, Government of India, and the conduct of outreach programs for dissemination of the Green campus motto is also recorded (Venkataraman 2009). During the audit process, the best environmental / greenery practices followed and new initiatives undertaken in the organization to reduce the environmental pollution and steps taken for nature conservation that brings added value to the organization in maintaining the eco-friendly campus to the stakeholders are assessed (IGBC 2021, WGBC 2021). The criteria, methods/

procedures, checklists, and recommendations used in the audit were based on the identified risks. The methodology includes: the preparation and filling up of questionnaire along with checklists, physical inspection of the campus, observation, and review of the document, interviewing responsible persons, and data analysis, measurements, and recommendations (Filho et al. 2015). Similarly, the methodology adopted for this audit was a four-step process comprising of data collection, data analysis, best practices followed on the campus, and recommendations and suggestions given to the organization to improve the greeneries practices further (Rajalakshmi et al. 2021).

### **Pre-Audit Stage Activities**

A pre-audit meeting (opening meeting) is conducted with Management and Administrative people along with staff coordinators of the Energy and Environment audit process, wherein, the audit protocol and audit plan are discussed in brief. The purpose of this meeting is to provide an opportunity to reinforce the scope and objectives of the audit and discussions held on the practicalities associated with the audit. Pre-audit stage activities are an important prerequisite for the green audit to meet the auditee and to gather information about the campus and necessary documents are collected directly from the Organization before the initiation of the audit processes. The audit team will be selected by the Audit organizations such as Nature Science Foundation, Coimbatore, as per the checklist comprised of Lead Auditor of ISO (QMS 9001:2015 and EMS 14001:2015), Botanist, Agriculture and Horticulture Scientists from Conventional and Technical Universities across India, Accredited Professionals from Indian Green Building Council, Hyderabad and Associated Chambers of Commerce and Industry of India, New Delhi.

### **Target Areas of Green Auditing**

Any Educational Institution such as colleges, Schools, Universities, Research Institutions, Industries, Service Industries, and Manufacturing Units that operates on a large scale, and cater to many stakeholders must undergo an audit for better environmental management. This will ensure the adequate measure taken to maintain the campus as a sustainable one.

### **Study Area of Flora and Fauna Diversity**

The audit site should be quite clean, and green and has much less pollution than the rest of the places. The campus is important not only from an education and product development point of view but also as a green lung. It is frequently visited by several nature enthusiasts to study the floral and faunal aspects. Biodiversity provides a useful measure of the qual-

ity of the environment and ecological studies are important aspects of the environment, in view of the consideration of environmental quality and protection of natural flora and fauna. Similarly, the topography is also very important with respect to the floral and faunal diversity studies. In the case of topography, altitude, longitude, and latitude are equally important in terms of natural flora and fauna diversity. Similar to that topology, geology, and soil conditions are playing important in green campus establishment. The study area of the audit site should be analyzed for soil type, presence of organic matter, and water holding capacity. Climatic conditions such as maximum and minimum temperature, maximum and minimum relative humidity, average annual rainfall, mean sunshine period, and wind speed during summer and winter periods covering both southwest and northeast monsoon periods are playing a pivotal role.

### **Accounting on Greenhouse Gas Emission**

CO<sub>2</sub> emission details in the campus accounting the direct and indirect sources need to be documented well in terms of usage, period of usage (hour), the number of persons practicing the emission, personnel availability inside the campus, operating time of each equipment in the campus, has to be documented. The carbon footprint data can be calculated based on the usage of electricity, usage of vehicles, usage of GHGs emitting equipment, consumption of fuel for generating electricity, food, and other work occurring. The accounting of green practices related to the neutralization of carbon footprint should be documented periodically. The possible reduction of greenhouse gas emissions can be achieved by enhancing agricultural practices, usage of free energy, usage of equipment with no greenhouse gases (GHGs) emissions, implementation of the vehicle-free zone, no electricity day, and the carbon-free zone should be accounted for and documented well.

### **Accounting on Energy Conservation and Management**

Frequent energy audits or daily energy audits help to maintain the record on their energy consumption. Separate metering for individual blocks helps to identify the energy consumption and leak. The reduction in the consumption of power leads to good green campus development. Documentation on using less power-consuming appliances like higher star-rated refrigerators and air coolers must be used. Usage of CFL (Compact Fluorescent Bulb), LED (Light Emitting Diode) bulbs, and solar lamps should be accounted for properly. Building structures should minimize energy usage and leak proof. Highly ventilated building structures and the usage of fewer energy devices can be documented well. Any practices to reduce energy consumption can be reviewed and documented as well.

### Accounting on Water Conservation

Metering water usage and use of fixtures and appliances that consume less water should be documented. Practices like water usage accounting for every need in individual blocks can help to reduce water usage. Rainwater harvesting, watershed management, and storage capacity should be documented. The establishment of the water recycling unit, its capacity, and the need for recycled water along with the quantity should be recorded. Determination of recycled water quality should be documented well to maintain a safe and hygienic atmosphere. Special initiatives like recycled water for enriching the ecology, and water conservation practices should be well documented and practiced effectively. Accounting on 3R water use efficiency, water-efficient plumbing fixtures enabled with dual flow faucet, sensors that prevent leak and overflow tankers, metering devices, rainwater consumption, and purification systems to improve water quality considerably.

### Waste Management Practice

Innovative practices related to waste segregation and management must be accounted well for any organization to have a green campus role. Many categories of wastes like hazardous and E-wastes released from the green campus should be as minimum as possible. If the organization pertains to the release of hazardous wastes, it should have a stringent methodology adopted for its management and release to the environment. If the organization is an academic Institution, then the practice related to the usage and disposal of harmful chemicals and harmful wastes should be well documented in their laboratory usage and release. Proper sanitation, management, and disposal methods will be accounted and their function should be transparent to be adopted and practiced effectively. In the case of E-waste management, although reduced usage of electronics and refurbishing activities plays a major role in the green campus audit, the practice of any level of e-waste management and innovative contributions to society as well should be documented and accounted for in terms of the adoption of the practices in their own academic as well as non-academic institutions.

### Indoor Environmental Quality

It relates to the well-being of the personnel with respect to the ambiance of the environment. The indoor infrastructure should provide proper light, heat, and ventilation for maintaining a good indoor quality for the stakeholders. The indoor ambiance is accounted for in terms of the breathing zone in the air-conditioned room that relates to indoor humidity and the age of the indoor structure.

### Green Building Materials

As of the accounting on the building materials the transportation on the recurring materials must be documented in terms of frequency of storage and the availability of the materials. Green campus auditing also complements the practices of utilizing the resources nearby and requiring materials from a consent which practices the 'go green concept'. Green building materials should be user-friendly without causing any adverse effects to the environment as well as on human beings. Moreover, if the materials are stored for a long time, the material strength, as well as the quality of those materials, should not be lost. During the transportation of green building materials, the materials should not harm the environment and the strength and quality of materials should not be mislaid.

### THE PRACTICE OF A GREEN CAMPUS AUDIT

A fresh green campus audit is required for any new (or) old organization to self-evaluate one's needs with respect to environmental objectives and implementation. To have continuous monitoring and implementation of self-sustainable practices, the green audit has to be practiced once a year with updated practices and with consistent improvement in all the mentioned sections of protecting the environmental objectives (Fig. 2). Mere practice and insist on a green campus audit is to create a self-sustainable organization that doesn't affect nature and assists in protecting the natural resources, earth, ecology, and biodiversity (Venkataraman, 2009). The audit helps to assess the strength and weaknesses of any organization on their self-sustainability in the long run in terms of green campus planning and efforts (Aruninta et al. 2017). The Indian Green Building Council (IGBC) is a division of the Confederation of Indian Industry (CII), which was set up in the year 2001. It is coming under the Confederation of Indian Industry (CII) to create and sustain an environment conducive to the development of India as a whole and civil society through advisory and consultative processes. The vision of the Green Building Council is, "To make a sustainable



Fig. 2. Green campus audit practice and benefits

environment for all and facilitate India to be one of the global leaders in the sustainable environment by 2025". IGBC also conducts examinations to qualify accredited professionals for green campus auditing. It also provides membership to individuals to promote sustainability and the environment through green building practices. It looks after and rates the organization starting from the designing of the project site to its implementation. Moreover, IGBC recognizes the initiatives taken toward environmental protection and offers solutions to various environmental problems (IGBC 2021, WGBC 2021).

### **Role of Plants, Animals and Microorganisms in Green Campus**

Ensuring rich biodiversity in the green campus is an important parameter. Plants are indicators for assessing the varying levels of environmental quality. In general, plants improve outdoor air quality with increased oxygen levels and reduced temperature and carbon-di-oxide. The green and varying colors of the flowering plants improve the ambiance of the environment. The record on maintenance of the plant biomass and its management are important with respect to green campus initiatives. The plants in the environment should account for 75% of wild or native plant traits in the green campus. The native plant traits promote the indigenous fauna at the site area. Hence the accountancy of 75% of the wild traits is leveraged for the native animals and birds to a particular region. The existence of such animals and birds in the green campus can be recorded for the rich flora and fauna in the proposed site which is considered a valuable addition to the campus. Similarly, accountability of the total beneficial microbial populations such as nitrogen-fixing, phosphate and potassium solubilizing bacteria, fungi, and actinomycetes are also considered for the rich biodiversity on the campus (Choy & Karudan, 2016).

### **Natural Topography, Vegetation and Rainwater Harvesting System**

Natural topography means the original geographical features of the campus, around 15- 20% of the organization should have natural features like rocks, water resources, slopes, landscape, pathways, etc. and the altered topography can be accounted for if it is facilitated. The vegetation in the land alone is considered as they are part of the natural topography. The vegetation in the artificially created structures is also accounted for audit when it is reported more than 30% of the claimed green campus audit site. The natural topography is well appreciated with wild vegetation than the artificially created topography like pathways and parking areas. Rainwater harvesting is mandatory in green campus audit sites. The main motto of the rainwater harvesting system is to

improve the water level underground which is important to reduce water scarcity (Khanal et al. 2020). For recharging dry bore wells, a pit is excavated around the bore well and a filter medium is filled into the pit (Fig. 3). This has led to self-sufficiency during water stress periods to the maximum extent (Musayev et al. 2015).

### **Landscape Design and Soil Erosion Control**

Landscape management is the care of the land to make sure that landscapes can fulfil the needs and aspirations effectively and sustainably of current and future stakeholders. It is an activity that forms a perspective of sustainable development, and ensures the preservation of a panorama, to help and harmonize changes that are added through social, monetary, and environmental methods. Landscape design is an important feature for any disasters to control especially with respect to soil erosion. In general, soil erosion occurs if the design of the land is not altered to prevent the slope features by strong vegetation and the use of plant buffer zone as safe for the escape of nutrients or fertilizers entering the streams. When the slope features are altered, adequate vegetation can alone be enough to prevent soil erosion. Un-altering the slope design adds value to natural topography, whereas, the vegetation in the same slope topography and plant buffer zone prevents the water from getting polluted.

### **Establishment of Lawns, Lianas, Trees, Herbs, Shrubs and Climbers on the Campus**

Lawns are gazing features of unutilized land made to cover the soil with green grass for the ambiance of the place to have a greenish look. The lawn provides a hollow space among the building structures. The shaded trees in between the grass lawn, pathways, and garden benches are meaningful lineaments to the green campus. In general, the campus should have a large number of trees, herbal plants, shrubs, climbers, lianas, twiners, and lawns that should be growing profusely



Fig. 3. Rainwater harvesting system

and showing healthier free from pests and diseases attack. The commonly available shrub species are Kakithapoo (*Bougainvillea spectabilis*), Madhanakamaboo (*Cycas revoluta*), Pigeon-berry (*Duranta plumieri*), Nilamulli (*Eranthemum roseum*), Sembaruthi (*Hibiscus rosa-sinensis*), Vetchi (*Ixora coccinea*), Malli (*Jasminum sambac*) and Arali (*Nerium odor*). Similar to that shrubs, the commonly available herbs are Kunukkuth thukki (*Micrococca mercurialis*), Melaanelli (*Phyllanthus maderaspatensis*), Keelanelli (*Phyllanthus niruri*), Otra mullu (*Priva leptostachya*), Adai-otti (*Pupalia lappacea*), Kirantinayan (*Ruellia prostrata*), Pattasukai (*Ruellia tuberosa*), Vettu kayathalai (*Tridax procumbens*) and Kattu paruthi (*Turnera ulmifolia*). The existence of climber, creepers, twiners, and lianas species commonly are Kayathalai (*Allamanda cathartica*), Kovai (*Coccinia indica*), Kattu-kodsi (*Cocculus hirsutus*), Amirtaval (*Tinospora cordifolia*) and Sinthal (*Monstera deliciosa*). The major grasses are Periapullu (*Aristida pinnata*), Chevvarakupul (*Chloris barbata*), Arugam Pillu (*Cynodon dactylon*), Korai Pollu (*Cyperus rotundus*) and Crowfoot grass (*Dactyloctenium aegyptium*). They are the type of herbs and shrubs that are green in color and grow vigorously without any pests and diseases attach which may be coincided with a healthier campus.

### Establishment of Different Types of Gardens on the Campus

Different types of gardens such as terrace gardens, vertical garden, kitchen garden, medicinal and herbal garden, ornamental garden and desert garden may be established at educational institutions and industrial sectors for demonstration as well useful purposes to the stakeholders (Fig. 4). Terrace gardens are the best utilization of roof spacing for gardening. They are intended to cultivate some purposeful herbs and shrubs including vegetables and fruits. Very recently the intention of growing trees on the terrace has been raised considerably. Although the initial facilitation is intense, once established the terrace garden yields a good amount of leafy vegetables and other vegetables. The growth of tubers, taproots, and vegetables from shrubs is cultivable in terrace gardens rather than through hydroponics and ver-

tical farming. Terrace gardens are achieved in the provided space by utilizing the grow bags and potteries. This can be grown with fertile and moist soil or coconut coir pith. Kitchen gardens are introduced in every house to utilize the kitchen wastes properly which may serve as the central feature of cultivating vegetables, fruits, ornamental plants, and landscape management.

Kitchen gardens are of two types one that is used to grow plants out of kitchen waste and another one is made to grow plants required for the kitchen like herbs, shrubs, and vegetables with an elevated ground setup. Both types of kitchen gardens add up value to the claim of green campus auditing. Growing many types of herbal plants having medicinal importance on the campus becomes more attractive and useful if concept gardens are maintained. Medicinal plant gardens can contain the locally available medicinal plants, RET (Rare Endangered Threatened) listed plants and those plants are most useful in terms of economic importance. It can also be arranged based on routine uses, herbal formulations, etc. The tree garden/arborea can be planted based on the zodiac signs which would attract the public and students, faculties, staff members, and employees and educate them based on their uses.

Medicinal and herbal plant gardens can be maintained in the backyard of the campus. In the tree gardens, trees as linings all over the campus can act as oxygen corridors. Native trees along with trees like *Azadirachta*, *Pongamia*, and *Ficus* species can be cultivated at the maximum as these plants are used to remove the dust particles and carbon lead from the air and purify the air considerably. Similarly, the ornamental plants with beautiful flowers can be maintained in the frontage gardens of campus for attraction and good ambiance. This will give an overall aesthetic look and also provide fresh air for healthy respiration to the stakeholders.

### Labelling of Common as well as Botanical Names of Plants

The calm and serene environment in an educational in-



Fig. 4. Establishment of different types of gardens



stitution and industry is the first and foremost important measure to keep the campus working towards its goal. The contribution of plants in bringing calmness to the minds of people is a well-known fact. Even though there are many restrictions for departments like forestry (Wood yielding trees), agriculture (Crop plants), and Botanical gardens (flowering plants and exotic plant collections) to grow a few types of plants, educational institutions, and industrial sectors do not have such boundaries. Growing plants of different categories are mandatory in educational institutions and industries to maintain the greenery on the campus. Naming the plants in the local language and botanical names (binomial nomenclature) will be an added advantage and also it will contribute to the familiarization of useful plants to the students and visitors (Fig. 5). Labeling the plants with a common name and the botanical name along with the family name (if possible) legibly using tags or hoardings should be done. Otherwise, a complete list of plants available on the campus may be prepared and listed as information for the visitors.

#### Operation of Water Irrigation System, Drip and Sprinkler Irrigation Methods

Maintaining the green campus and water conservation mechanisms should be applied efficiently on the campus. Well-planned water irrigation systems like sprinklers and drip should be implemented in the entire green area of the campus for an effective water management system. This can be implemented only when the plantations are well planned. The tree growing areas can be connected with drip irrigation and medicinal plants growing areas and flower gardens can be connected with sprinkler irrigation (Fig. 6). The water management system should be well planned and wastage should be minimized as much as possible. Rainwater harvesting should be implemented.



Fig. 5. Labelling of common as well as botanical names of Plants

#### Importance of Biodiversity Conservation

The campus should be a mini biodiversity conservation area, wherein, more greenery due to native plant species, medicinal plant gardens, concept gardens, and flowering plants that attract bees, birds, beetles, and other animals like squirrels should be monitored. Shade-giving trees in the paths, flowering trees in the avenues, and fruit trees in the back yards also would attract birds, bees, butterflies, and squirrels. Maintaining small ponds/open water sources and reservoirs will attract these small harmless animals to the campus. The Biology / Science departments should maintain a medicinal plant garden, economically important, rare, and endangered plant species or gardens that are the concept centric to the stakeholders. The campus should be free of exotic plants that cause a threat to the natural vegetation. This will aid in adding the necessary nutrients to the soil for the better growth of selected plants. The soil type will also help in choosing the irrigation system with respect to the water holding capacity (Venkataraman 2009). In view of the tremendous increase in human population, over-exploitation of natural resources, environmental pollution, global warming, deforestation, use of forest resources for human consumption, anthropogenic activity, climate change, and natural calamities are the major reasons for the loss of biodiversity (Lauder et al. 2015).

#### Use of Biofertilizers, Organic Manures, Green Manures and Chemical Fertilizers

Natural or eco-friendly methods should be used to grow plants vigorously on the campus. Use of biofertilizers, organic manures (cow dung, vermicompost, and plant wastes and litters), and green manures to grow healthy plants in the medicinal plant garden, kitchen garden, and terrace garden should be ensured to keep the campus organic. Plant waste such as fallen leaves, stems, fruits, nuts, seeds, and other plant parts should be used to make green manures. A concrete or ground-level green manure production unit and vermicomposting units will help to convert all the plant and animal-based wastes into green/organic manures. This will be a healthy way of solid litter waste management on campus. Minimal use of chemical fertilizers as part of the



Fig. 6. Operation of sprinkler irrigation methods

integrated nutrient management system is acceptable but nil use of chemical fertilizers is highly appreciable and also helps to keep the campus more of an organic ecosystem (Dominguez et al. 2019). Fortnightly the half-degraded plant manure can be removed and used as manure for the garden plants or used as feed for earthworms in the vermicompost pits (Dominguez et al. 2019). A vermicompost unit for decomposing kitchen wastes into vermicompost is considered a good initiative (Fig. 7).

### Acoustic Proof in Indoor and Outdoor Stadiums

Any campus of educational institutions as well as industrial sectors should be calm and serene which will bring peace to the stakeholders. At the same time, more enthusiastic expression of joy is also seen in indoor and outdoor stadiums. But this will always create noise above the permissible levels on the campus. Acoustic on-50 steel perforated panels will allow great sound reduction and also be durable. Acoustic baffles will be suitable for reducing reverberation times. So the construction plans or renovation plans should include these acoustical products which will make these indoor and outdoor stadiums (Fig. 8). Some plants absorb ultrasound around the indoor and outdoor stadiums and auditoriums which in turn are useful to reduce sound pollution to some extent. For example, Ferns, Baby's Tears, *Peace Lily*, *Leylandii*, *Aureo*, *Marginata*, *Tamarind*, *Polyalthia*, *Ecuadorian cactus*, *Espositoa frutescens*, etc. These plants are able to absorb ultrasound through cells and metabolized by biochemical methods.

### Establishment of Aquarium and Aquatic Plants

Growing fish in small ponds will keep the environment pleasant. In the closed environment like corridors and the front offices, auditoriums and gallery classes placing the fish aquarium as well as plant aquarium will improve the scenic value of the place bringing peace to the people. The fish water waste also can be used as manure for growing potted indoor plants. Growing *Lotus*, *Lilly*, *Hydrilla*, and other water plants will give a pleasant and calm environment and growing fishes like *Guppies* can keep the water clean



Fig. 7. Vermicompost Unit

and neat. The fountains and small ponds can be built in the frontages to give an aesthetic look and also growing water plants in these ponds will help to maintain the aesthetic sense of the environment greenish.

### Steps Taken During Hot Seasons to Maintain Plants

Just planting trees on the campus during functions and celebrations will not help in improving the green cover of the Educational Institutions and Industrial sectors. It requires a planned execution of watering them at the right intervals even during the summer vacations is highly important. Applying fertilizers and removing the weeds at the correct intervals should be scheduled and persons who are in charge should be taken care-off. The activities undertaken should be entered in the registers in detail. The Internal monitoring committee should review the activities and examine the results in the field periodically. Well-planned strategies should be implemented to save water and also supply water for the neighbouring residents in summer. Water conservation slogans should be displayed in all water resources, storage areas (water reservoirs), and utilization areas. There should not be any leakages and notices should be addressed immediately so that water wastage may be reduced significantly.

### Preservation of natural wells, water reservoirs, and water collection tanks

Preservation of natural wells, water reservoirs, and water collection tanks present on the campus should be well-maintained with high raised walls and removal of plants and shrubs around the wells without any contamination (Fig. 9). Well, restoration procedures are to be adopted and frequent checks on the water levels and water holding capacity, and purity of water should be monitored. Borewells should be made in the required places and instead of digging more bore wells the used and old bore wells can be recharged by connecting to the rainwater harvesting system. The water collected on every terrace of the huge institutions will be enough for recharging the bore wells. The rainwater harvesting unit can also be connected to the small pond, water tanks, and reservoirs to collect and store water to meet the water requirements of the entire campus throughout the year.

### An Account of More Oxygen Releasing and Carbon Dioxide Assimilating Plants in the Campus

Some plants are considered highly efficient in oxygen production and carbon dioxide absorption which in turn reflected the quality of the green campus. If more oxygen is made available on campus naturally, the stakeholders may be free from various cardiovascular and pulmonary problems and breathing troubles. The snake plant (*Sansevieria zeylanica*) otherwise known as the mother-in-law's

tongue and Gerbera Daisy (*Gerbera jamesonii*) plant are unique for their night-time oxygen production, and ability to purify air through the removal of various toxic gases in the atmosphere (Tiyarattanachai and Hollmann, 2016). In general, the campus should have a maximum number of more oxygen-producing and CO<sub>2</sub> absorbing plants such as *Areca Palm*, *Money plant*, *Neem*, *Tamarind*, *Ficus*, *Bamboo*, *Arjun*, *Magizhamboo*, *Marudhu*, *Maramalli*, *Nettilingam*, *Manjal*

*arali*, *Puvarasu*, and *Pongam* trees to give pure atmosphere to the stakeholders (Fig. 10).

## CONCLUSION

The green audit is an important key not only for sustainable development and also for a clean environment, at industries level, it detects some environmental problems. The pollution



Fig. 8. Features of indoor plants to absorb ultrasound (Acoustic).



Fig. 9. Water collection and reservoirs tanks.



Fig. 10. Oxygen releasing and carbon dioxide assimilating plants

problems are uprooted by equipping the industries with several maintenance measures. The audit is essential to provide indication management about the performance of the equipment and system of an environmental organization or institute. As a result, the best methods that are practicable can be applied to preserve water, air, soil plants, and animal life from adverse effects. Minimizing waste by developing a recycling system. Higher educational Institutes want to implement the green audit, also referred to as a green audit. One should understand the process of green auditing. It is a cyclic and continuous process. Still, there is a scope for further action, when academic institutes or organizations take part in restoring the environment. The economic development and rapid urbanization at the global, regional and local have led to ecological and environmental crises. In this background, for all the institutes it becomes essential to adopt the system of campus to be green for further development which will lead to sustainable development. NAAC, the National Assessment and Accreditation Council, New Delhi, has made it essential that all higher educational institutions should submit an annual Green Audit Report.

## ACKNOWLEDGMENT

The authors are thankful to the Trust members of the M/s. Nature Science Foundation, Coimbatore, Tamil Nadu, India for providing permission to publish articles for which all the relevant data and support have been provided. In addition, they are gratefully acknowledged for providing the necessary facilities and cooperation during the conduct of the audit process at different Colleges, Universities and Industries.

## REFERENCES

- Adeniji, A.A. 2008. Audit and Assurance Services, Lagos: Value Analyst Concept of Green Audit. New Age International, New Delhi, India.
- Arora, D.P. 2017. Environmental audit: Need of the hour. *Int. J. Adv. Res. Eng. Manag.*, 3(4): 25-31.
- Aruninta, A., Kurazumi, Y., Fukugawa, K. and Ishii, J. 2017. The integration of human thermal comfort in an outdoor campus landscape in a tropical climate. *Int. J. Geomate*, 14(44): 26-32.
- Choy, E.A. and Karudan, R. 2016. Promoting campus sustainability: A conceptual framework for the assessment of campus sustainability. *J. Social Sci, Human.*, 11(2): 112-118.
- Dominguez, J., Aira, M., Kolbe, A., Gomez-Brandon, M. and Losada, M. 2019. Changes in the composition and function of bacterial communities during vermicomposting may explain the beneficial properties of vermicompost. *Sci. Rep.*, 9: 1-11.
- Gowri, S. and Harikrishnan, V. 2014. Green computing: Analyzing power consumption using local cooling. *Int. J. Eng. Trends Technol.*, 15(3): 105-107.
- Gnanamangai, B.M. Muruganath, B.M. and Rajalakshmi, S. 2021. A Manual on Environment Management Audits to Educational Institutions and Industrial Sectors. Vol. I. Laser Park Publishing House, Coimbatore, Tamil Nadu, India, p. 127.
- IGBC 2021. Indian Green Building Council. <https://igbc.in/igbc/>
- Khanal, G., Thapa, A., Devkota, N. and Paudal, U.R. 2020. A review on harvesting and harnessing rainwater: an alternative strategy to cope with drinking water scarcity. *Water Supply* 20: 2951- 2963.
- Lauder, A., Sari, R.F., Suwartha, N. and Tjahjono, G. 2015. A critical review of a global campus sustainability ranking: Green Metric. *J. Clean. Prod.*, 108: 852-863.
- Filho, L., Muthu, N., Edwin, G. and Sima, M. 2015. Implementing Campus Greening Initiatives: Approaches, Methods, and Perspectives. Springer, London, UK.
- Marrone, P., Federico, O., Asdrubali, F. and Guattri, C. 2018. Environmental performance of Universities: Proposal for implementing campus urban morphology as an evaluation parameter in Green Metric. *Sustain. Cities Soc.*, 42: 226-239.
- Musayev, S., Burgess, E. and Mellor, J. 2015. A global performance assessment of rainwater harvesting under climate change. *Resour. Conserv. Recycl.*, 132: 62-70.
- Ounsaneha, W., Chotklang, N., Laosee, O. and Rattanapan, C. 2017. Predictors of behavior intention to develop a Green University: A case of an undergraduate university in Thailand. *Int. J. GEOMATE*, 15(49): 162-216.
- Rajalakshmi, S., Kavitha, G. and Vinoth Kumar, D. 2021. Energy and Environment Management Audit. AkiNik Publishing, New Delhi, India, p. 257.
- Singh, M., Singh, G. and Singh, H. 2012. Energy audit: A case study to reduce lighting cost. *Asian J. Comp. Sci. Inform. Technol.*, 2(5): 119-122.
- Suwartha, N. and Sari, R.F. 2013. Evaluating UI green metric as a tool to support green universities development: Assessment of the year 2011 ranking. *J. Clean Prod.*, 61: 46-53.
- Venkataraman, K. 2009. India's Biodiversity Act 2002 and its role in conservation. *Trop. Ecol.*, 50(1): 23-30.
- Wang, Y., Shi, H., Sun, M. and Huisingsh, D. 2013. Moving towards an ecologically sound society? Starting from green universities and environmental higher education. *J. Clean Prod.*, 61: 1-5.
- WGBC 2021. World Green Building Council. <https://www.worldgbc.org>.



# Medical Waste Management and Design of a Low-Cost Incinerator for Reduction of Environmental Pollution in a Multi-System Hospital

O. J. Oyebode† and J. A. Otoko

Civil and Environmental Engineering Department, Afe Babalola University, Ado-Ekiti Ekiti State, Nigeria

†Corresponding author: O. J. Oyebode; oyebodedare@yahoo.com

Nat. Env. & Poll. Tech.  
Website: [www.neptjournal.com](http://www.neptjournal.com)

Received: 29-04-2022

Revised: 27-05-2022

Accepted: 30-05-2022

## Key Words:

Pollution  
Incinerator  
Public health  
Environment  
Medical waste management

## ABSTRACT

Pollution of the environment and inappropriate management of medical wastes are major challenges facing developing countries and this must be tackled with recent technology for public health, enhanced natural ecosystems, and a better environment. This research is a two-step process that involves the assessment of the existing Hospital waste management practices in a multi-system Hospital in Ado-Ekiti, Nigeria. Excess air, kerosene (auxiliary fuel), single chamber, Batch-fed (Manual feeding), and controlled air incinerator were designed. Wastes were loaded once at the beginning of the combustion cycle followed by combustion, ash burnout, cool down, and ash removal to assist medical waste management. Findings revealed that personnel involved in handling medical waste were equipped with inadequate protective gear. Medical waste was handled together with municipal waste and both wastes were incinerated in an open dumpsite without engineered sanitary landfill at disposal locations constituting a nuisance with a high risk of pollution to the surrounding environment. The incinerator was designed for a waste load of  $269 \text{ kg}\cdot\text{day}^{-1}$ . It consists of four zones; the waste and combustion zone ( $2.7 \text{ m} \times 1.8 \text{ m} \times 1 \text{ m}$ ), the ash zone (0.23 m height), the combustion fumes and one-second retention zone (0.43 m height) as well as the excess air zone (0.46 m height). This low-cost medical waste incinerator has a lot of improvement, operational effectiveness, and efficiency to the currently available techniques. Viable recommendations made will improve the state of environmental health and reduce the harmful effects of medical waste.

## INTRODUCTION

In developing countries such as Nigeria, waste incineration is the primary method for managing hospital waste, with the economic advantages of destroying pathogens in the waste stream and reducing waste volume and reactivity. However, if handled improperly, incineration has a significant impact on the environment, releasing pollutants in the form of gaseous emissions and ash, which have environmental and public health implications (Adama et al. 2016). HWM has been regarded as minimal in studies undertaken in impoverished nations, with generators and handlers lacking in general awareness of relevant issues (Manyele et al. 2003). Although healthcare waste is classified as hazardous because it constitutes a serious direct threat to human health (WHO 1999), inadequate HWM is still prevalent in developing nations such as South Africa, Nigeria, Swaziland, Mozambique, Kenya, and Tanzania (Manyele 2004).

## Past Studies

Hospital waste generation varies not just between nations, but also within countries, depending on infrastructure, manage-

ment system, percentage of reusable items, and percentage of waste generated on an outpatient basis (WHO 2002). In developing countries like Nigeria, undeveloped open lands are often converted into waste disposal sites, even within planned residential areas; indiscriminate dumping of waste causes environmental and health hazards. Despite the controlled burning that is supposed to occur when using an incinerator, air pollution still occurs (Akpe et al. 2016). This is primarily due to insufficient design and the absence of air pollution control devices, which is a feature of most incinerators used in Nigeria for managing hospital waste. People migrated in substantial numbers to developed cities as a result of rapid industrial development, job opportunities, and urbanization (Lin et al. 2022, Patel & Burkle 2012, Muthukannan et al. 2019). Huff & Angeles (2011) and Cassidy et al. (2014) found that migration and industrial development had a negative influence on the environment, particularly on water, air, and soil. All kinds of life on Earth depend on clean air and water, and polluting any or both will be a severe problem. Human activities affect the regional ecological environment, climate, hydrology, vegetation, biogeochemical cycles, and biodiversity on a variety of temporal and spatial dimensions,

all of which contribute to environmental pollution (Collier et al. 2013).

The rapid rise of hospitals in both the commercial and public sectors has helped to rebuild the community's health (Agunwamba et al. 2013). Although not all hospital wastes are susceptible to disease transmission, biomedical waste makes up about 1-2 percent of the entire municipal solid waste (MSW) stream. 80-85% of hospital trash is non-infectious, 10% is contagious, and 5% is harmful (Gupta & Boojh 2006). Although hospitals' primary goal is to restore human health, hospital waste disposal is a major concern. Bio-medical waste has recently become a major source of worry for environmental law enforcement agencies, the media, and the general public, not only in hospitals and nursing homes (Ramesh et al. 2008). Bio-medical waste is generated in a variety of settings, including hospitals, laboratories, clinics, nursing homes, and medical, dental, and veterinary clinics. Some of these wastes pose major health and environmental dangers to people (Ramesh et al. 2008). Biomedical waste management has recently become a serious concern for hospitals, nursing homes, and the environment. The consequences of improper biomedical waste management have sparked global alarm, especially given its far-reaching implications (Mathur et al. 2012, Vasistha et al. 2018).

Medical waste has continued to pique public interest due to the health risks connected with human exposure to potentially hazardous wastes produced by HCEs (Adegbite et al. 2010). Although the treatment and disposal of hospital waste are intended to reduce hazards, secondary health risks may arise as a result of the release of harmful pollutants into the environment during treatment or disposal; improper handling of medical waste can have negative consequences and reduce the overall benefits of health-care (David et al. 2014). According to a 2002 assessment of HWM procedures in 22 developing nations, 18 to 64

percent of HCEs do not use suitable waste disposal methods (WHO 2002). In developing countries like Nigeria, the most common difficulties associated with HWM are a lack of understanding of health risks, poor management practices, insufficient financial and human resources, and poor waste disposal control (David et al. 2014). Although considerable research has been done on waste creation, segregation, and disposal, there has been minimal focus on public knowledge of the possible dangers connected with medical waste and the need for staff protection in rural and semi-urban areas. There is currently a knowledge and practice gap among health professionals, which must be filled not only in the study area but also across the country (David et al. 2014). Poverty was identified by developed countries as a fundamental factor impeding African efforts to manage hazardous waste in an environmentally sound manner (Walter 2010, David et al. 2014).

## MATERIALS AND METHODS

Afe Babalola University Multi-System Hospital, Ado -Ekiti was used as a case study as presented in Fig. 1. It is a 400-bed multi-system hospital that offers services such as Accident and Emergency, Surgery, Medicine, Pediatrics, Obstetrics, Gynaecology, Community Healthcare, Physiotherapy, Dental care, Fluoroscopy, Endoscopy, Colonoscopy, Gastroscopy, Bronchoscopy, Arthroscopy, Bone Densitometer, Pet-Scan, Nuclear Medicine, Echocardiography, ECG, and Treadmill Test, among others.

To effectively carry out this study, a field investigation was conducted in Afe Babalola University multi-system Hospital, Ado -Ekiti to obtain information such as the type of waste generated from each ward, the type of disposal, the time of disposal, the quantity of disposal, and so on. This information was used to analyze and characterize the profile of the HWM program adopted by the selected hospital for



Fig. 1: Afe Babalola University multi-system hospital (Field Study 2021).

their medical waste through site visits, and to complement the field investigation, a questionnaire will be administered.

**Low-Cost Medical Waste Incinerator Design**

The Low-Cost Medical Waste Incinerator is primarily based on modifications to the De Montfort Medical Waste Incinerator, Mark 9 designed by Professor D.J. Picken of De Montfort University, Leicester University, the United Kingdom over a period of about 8 years from 1996 to provide a low-cost and effective incinerator that could be built in almost any developing country and has been successfully applied in several African countries such as Burkina Faso, Kefalonia, and Kenya (Picken 2019, Picken et al. 2012). The incinerator to be developed is a single chamber, Batch-fed (Manual feeding), Controlled air incinerator with waste loaded once at the start of the combustion cycle, followed by combustion, ash burnout, cooldown, and ash removal as shown in Figs. 2, 3 and 4.

**RESULTS AND DISCUSSION**

The following is a summary of the existing HWM practices from point of creation to the dumpsite:

1. No segregation and absence of color coding for HWM, all hospital waste is dumped into a special container at the point of creation.
2. The hospital cleaners carry the waste containers daily to the much larger bins outside the premises of the hospital.
3. The cleaning personnel with inadequate protective gear offload these larger bins onto an open truck together with municipal wastes collected at different points to be transported to the dumpsite.
4. The cleaning personnel offloads the open truck into an already-dug ditch for treatment with open fire.
5. As seen in the questionnaires, there has been some form of training given to staff (Both principal and non-principal) on hospital waste management.

The following are limitations of the existing HWM practices in the unnamed hospital (Figs. 5, 6, 7 and 8).

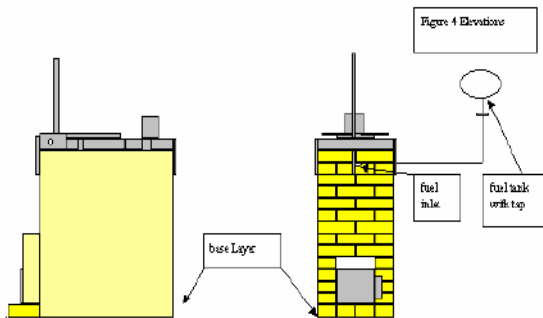


Fig. 2: De Montfort medical waste incinerator schematic diagram.

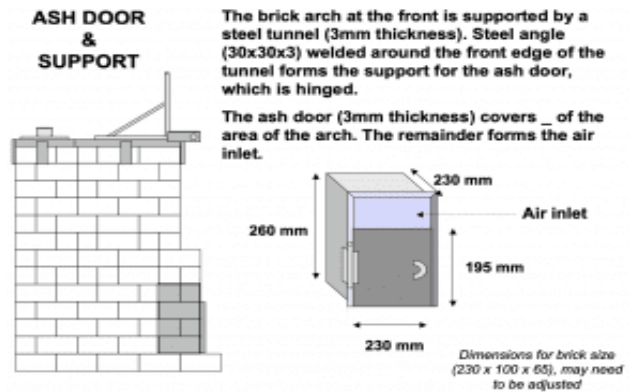


Fig. 4: De Montfort medical waste incinerator ash door and support.

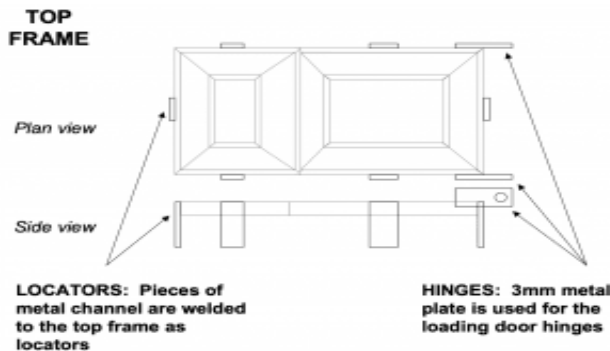


Fig. 3: De Montfort medical waste incinerator top steel frame.



Fig. 5: A hospital bed which is a point of creation of medical waste (Field Study 2020).

1. The lack of color coding and segregation is a poor practice that does not adhere to the WHO Standards for hospital waste management because all wastes are treated almost equally, which is not the case.
2. The inadequacy of protective gear of the cleaning personnel is also of great concern as they could easily be injured and get infected during the handling process
3. The use of an open truck used for handling both hospital and municipal waste shouldn't be practiced. Trucks should be covered to prevent disease vectors such as flies and rats from accessing such wastes and transmitting it directly or indirectly to humans
4. While using an open fire to treat wastes could help in some cases, doing so is not environmentally or ecologically friendly because the dump site is hidden behind homes, and smoke emissions can be harmful to people and pose concerns to both occupational and public health.



Fig. 6: Waste bins beside the hospital beds for temporary waste storage (Field Study 2021).



Fig. 7: Temporary storage bins for medical waste outside the hospital premises (Field Study 2021).



Fig. 8: Personnel offloading both medical and hospital waste onto the dump site (Field Study 2020).

### Design of the Single Chamber Batch-Fed Controlled Air Incinerator

The capacity of the incinerator and burning time is estimated from the quantity of waste load generated by the hospital using the equations developed by Walter (2010). No information was obtained on the quantity of waste generated per day by the Study Hospital because the study hospital is relatively new and is not operating at full capacity. It would be reasonable to infer that the hospital's daily waste generation is underestimated, therefore an assumed value of  $269 \text{ kg}\cdot\text{day}^{-1}$ .

### Determination of Incinerator Chamber Capacity

The volume of waste at an optimum incinerator of  $120 \text{ kg}\cdot\text{hr}^{-1}$  is dumped in the incinerator as a heap with a parabolic shape and assumed to be  $5 \text{ m}^3$  and the following formulas are used to estimate the volume of the combustion chamber.

$$\text{Volume of Combustion Chamber (V)} = L \times B \times H$$

$$V = 5 \text{ m}^3$$

$$\text{Length (L) to breadth (B) ratio} = 1.5: 1$$

$$\text{i.e. } L = 1.5B$$

Height (H) = 1m (assumed for easy Incinerator operation and maintenance)

$$\therefore 5 \text{ m}^3 = 1.5B \times B \times 1 \text{ m}$$

$$5 \text{ m}^2 = 1.5B^2$$

$$B \approx 1.8 \text{ m}$$

$$L \approx 2.7 \text{ m}$$

Combustion Chamber dimensions (L × B × H) = 2.7 m × 1.8 m × 1 m

### Determination of Heating Value Of Material Input

The Design Incinerator capacity was estimated at  $120 \text{ kg}\cdot\text{hr}^{-1}$ . Based on a 30% waste load, it is assumed to have the following compositions (Olanrewaju et al. 2019).



1. Dry Tissue: 6%
2. Moisture: 21%
3. Ash: 3%

Table 1 gives the total heat value per hour for 30% of the waste load of 120 kg.hr<sup>-1</sup> (36 kg.hr<sup>-1</sup>).

Based on a 70% waste load, it is assumed to have the following compositions (John & Swamy 2011).

1. Polyethylene: 21%
2. Polyvinylchloride: 2.1%
3. Cellulose: 36.4%
4. Ash: 10.5%

Table 2 gives the total heat value per hour for 70% of the waste load of 120 kg.hr<sup>-1</sup> (84 kg.hr<sup>-1</sup>).

$$\begin{aligned} \text{Total heat per hour of the waste load} &= 147,391.2 \text{ KJ.hr}^{-1} \\ &+ 2,091,416.88 \text{ KJ.hr}^{-1} \\ &= 2,238,808.08 \text{ KJ.hr}^{-1} \end{aligned}$$

**Volume of Combustion Chamber to Achieve One Second Residence Time at 1100°C**

Incinerators are required to operate at a minimum residence time of 1s (residence time for gas Fumes) at operating temperature.

**Combustion of Kerosene**

Moisture (H<sub>2</sub>O) at 1100°C temperature would exist in vapor (gaseous) form, hence the total quantity of vapor output is

calculated as follows:

Total H<sub>2</sub>O Mass = Total H<sub>2</sub>O Mass Output from Combustion of Hospital Waste + H<sub>2</sub>O from Combustion of Kerosene

$$\begin{aligned} &= 152.12 \text{ kg.hr}^{-1} + 36.35 \text{ kg.hr}^{-1} \\ &= 188.47 \text{ kg.hr}^{-1} \end{aligned}$$

$$\text{Molar Mass of H}_2\text{O (g.mol}^{-1}\text{)} = 18 \text{ g.mol}^{-1}$$

$$\text{Amount of substance, } n \text{ (mol)} =$$

$$\frac{\text{Mass of Substance (g)}}{\text{Molar mass of Substance (g/mol)}}$$

$$\text{Amount of H}_2\text{O (mol)} = \frac{188.47 \text{ kg/hr} \times 1000}{18}$$

$$\text{Amount of H}_2\text{O (mol)} = 10,468.9 \text{ mol/hr}$$

$$V_{H_2O} = \frac{10,468.9 \text{ mol/hr} \times 8.20573 \times 10^{-5} \text{ m}^3 \text{ atmK}^{-1} \text{ mol}^{-1} \times 1373 \text{ }^\circ\text{K}}{1}$$

$$V_{H_2O} \text{ (m}^3 \cdot \text{hr}^{-1}\text{)} = 1,179.48 \text{ m}^3 \cdot \text{hr}^{-1}$$

$$V_{H_2O} \text{ (m}^3 \cdot \text{s}^{-1}\text{)} = 0.33 \text{ m}^3 \cdot \text{s}^{-1}$$

$$\text{Total Volume Requirement} = V_{CO_2} + V_{N_2} + V_{H_2O}$$

$$= 0.17 \text{ m}^3 \cdot \text{s}^{-1} + 1.49 \text{ m}^3 \cdot \text{s}^{-1} + 0.33 \text{ m}^3 \cdot \text{s}^{-1}$$

$$= 1.99 \text{ m}^3 \cdot \text{s}^{-1}$$

$$\approx 2 \text{ m}^3 \cdot \text{s}^{-1}$$

Therefore, the active combustion chamber volume required to achieve one-second retention is 2m<sup>3</sup>. This active volume would be added to the calculated volume of the

Table 1: Total heat value per hour for 30% of the waste load of 120 kg.hr<sup>-1</sup>.

Component	Empirical Formula	Input [Kg.hr <sup>-1</sup> ]	HHV [KJ.kg <sup>-1</sup> ]	Total Heat [KJ.hr <sup>-1</sup> ]
Dry Tissue	C <sub>5</sub> H <sub>10</sub> O <sub>3</sub>	7.2	20,471	147,391.2
Moisture	H <sub>2</sub> O	25.2	0	0
Ash	-	3.6	0	0
Total (30%)	-	36	20,471	147,391.2

HHV (Higher Heating Value) sourced from (John & Swamy 2011)

Table 2: Total Heat value per hour for 70% of the waste load of 120 kg.hr<sup>-1</sup>.

Component	Empirical Formula	Input [Kg.hr <sup>-1</sup> ]	HHV [KJ.kg <sup>-1</sup> ]	Total Heat [KJ.hr <sup>-1</sup> ]
Polyethylene	(C <sub>2</sub> H <sub>4</sub> ) <sub>x</sub>	25.2	37,820	953,064
Polyvinylchloride	(C <sub>2</sub> H <sub>3</sub> Cl) <sub>x</sub>	2.52	38,154	96,148.08
Cellulose	C <sub>6</sub> H <sub>10</sub> O <sub>5</sub>	43.68	23,860	1,042,204.8
Ash	-	12.6	0	0
Total (70%)	-	84	99,834	2,091,416.88

HHV (Higher Heating Value) sourced from John and Swamy (2011).

combustion chamber (combustion chamber dimensions ( $L \times B \times H$ ) =  $2.7\text{m} \times 1.8\text{m} \times 1\text{m}$ )

The length and width of the combustion chamber are fixed, and the added height to the calculated height of 1m is calculated as follows.

$$V = L \times B \times H$$

$$2 \text{ m}^3 = 2.7\text{m} \times 1.8\text{m} \times H$$

$$2 \text{ m}^3 = 4.86 \text{ m}^2 \times H$$

$$H = 2 \text{ m}^3 \div 4.86 \text{ m}^2$$

$$H = 0.4 \text{ m}$$

$$\therefore \text{Overall Height of Combustion Chamber} = 1 \text{ m} + 0.4\text{m} \\ = 1.4\text{m}$$

$$\therefore \text{Minimum Combustion Chamber Dimensions (L} \times \text{B} \times \text{H)} = 2.7\text{m} \times 1.8\text{m} \times 1.4\text{m}$$

### Description of Primary Components of the Incinerator

The design of the low-cost incinerator is a modification of the De Montfort Medical Waste Incinerator, Mark 9 where necessary upgrades and removals would be made after which a comparative analysis of both designs would be shown in subsequent sections of this chapter. The following are descriptions of key components of the incinerator.

Please note that during construction, measurements may vary, all measurements are to be verified and or modified during construction.

### Waste Frame

The Waste frame is designed to the dimensions of the combustion chamber ( $L \times B \times H = 2.7\text{m} \times 1.8\text{m} \times 1\text{m}$ ) which is the active portion of the incinerator chamber that houses the hospital waste when placed in the Incinerator. The waste frame is made of a steel frame covered with wire gauze (Fig. 9) to facilitate the movement of ashes through the gauze after combustion and easy removal after cooldown. The legs of the waste frame are constructed to a height of 0.23m (Fig. 9) to allow easy removal of ashes after cooling down.

### Combustion Chamber

The combustion chamber consists of four zones (Fig. 10) bounded by the internal walls.

### Waste and combustion zone

This is where zone the hospital waste occupies which was designed for in section 4.2.2 ( $L \times B \times H = 2.7\text{m} \times 1.8\text{m} \times 1\text{m}$ )

### Ash zone

The height of this zone, 0.23 m which is also the height of

the waste frame legs allows for easy flow and collection of ashes during combustion and after cooling down respectively

### Combustion Fumes One-second Retention Zone

The height of this zone is 0.43m and was designed (section 3.2.8) to allow for a minimum of one-second retention time of combustion fumes

### Excess Air Zone

An additional spacing of 0.46 m is provided on all sides of the waste and combustion zone to allow for excess airflow from both the primary and secondary air inlets and would also serve as an allowance for the maintenance of the incinerator (Fig. 10)

### Base Slab

The base slab is a 6.21m x 5.31m, 150 mm thick concrete slab reinforced with DPC reinforcement (Fig. 11). The purpose

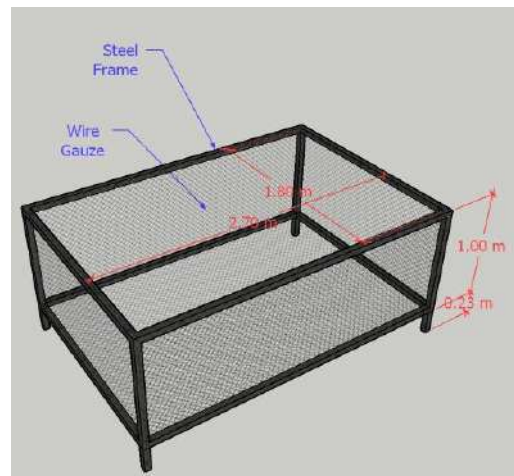


Fig. 9: 3-D Drawing of the hospital waste frame.

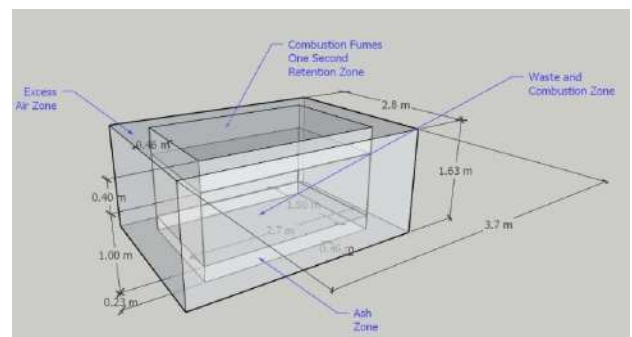


Fig. 10: 3-D Drawing of the combustion chamber zones.

Table 3: Stoichiometric oxygen requirement for combustion.

Component	Combustion Equation	Stoichiometric Air Requirement Per kg of Waste [kg.hr <sup>-1</sup> ]
Dry Tissue	$C_5H_{10}O_3 + 6O_2 \rightarrow 5CO_2 + 5H_2O$	11.7
Polyethylene	$(C_2H_4)_x + 3O_2 \rightarrow 2CO_2 + 2H_2O$	86.4
Polyvinylchloride	$2(C_2H_3Cl)_x + 5O_2 \rightarrow 4CO_2 + 2H_2O + 2HCl$	3.22
Cellulose	$C_6H_{10}O_5 + 6O_2 \rightarrow 6CO_2 + 5H_2O$	42.3
Total	-	143.62

of this base slab is to carry the weight of the walls and all of the other components of the incinerator.

**Internal Walls**

The internal walls are constructed using heat-resistant bricks or blocks. They are constructed over an internal perimeter of 3.7m x 2.8m (Fig. 12) making provisions for the primary and secondary air inlet, the combustion chamber, and the fume chamber, which would be explained in subsequent sections. The purpose of the internal walls is for the combustion

process, and to house the hospital waste for combustion and ashes from the combustion process.

**External Walls**

The external walls are also constructed using heat-resistant bricks or blocks to an overall height of 1.63 m. They are constructed over a perimeter of 4.91 m x 4.01m (Fig.12) also making provisions for the Primary and secondary air Inlet, the combustion chamber, and the fume chamber which would be explained in subsequent sections. An air gap clearance of 0.46 m (Fig.12) is provided to serve as heat insulation to prevent direct human contact with the heat of the combustion and heat of the internal walls.

**Primary Air Inlet**

The primary air inlet is a rectangular crosssection of 3.55m x 0.7m (Fig. 13) The purpose of the primary air inlet is to allow for air to enter into the combustion chamber to facilitate the proper combustion of the Hospital waste.

**Secondary Air Inlet**

The secondary air inlet is a steel pipe of diameter 0.3m (Fig.14). The steel pipe passes through both the external and



Fig. 11: 3-D Drawing of the base slab.

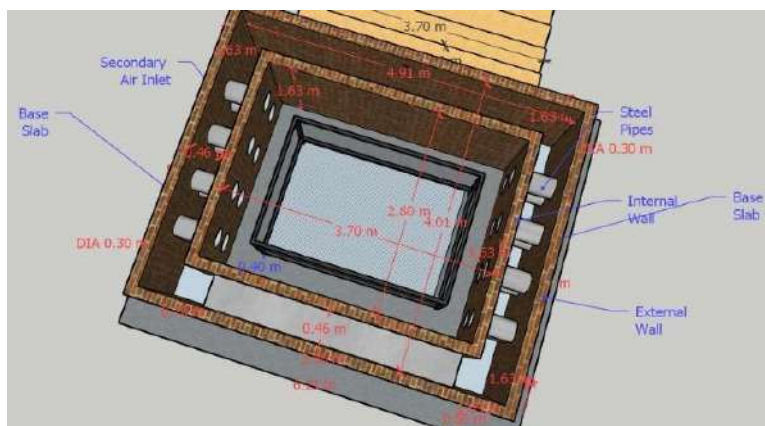


Fig. 12: 3-D Drawing of the internal and external walls.



Fig. 13: 3-D Drawing of the Primary Air Inlet.

internal walls and would be placed after both the external and internal walls have been constructed. The purpose of the secondary air inlet is to allow for additional air to enter the combustion chamber to allow for the proper combustion of the waste.

### Top Slab

The top slab is a  $4.31\text{ m} \times 5.21\text{ m}$ , 150mm thick with openings for connecting the Incinerator Operation and Maintenance door and the fume pipe (Fig. 15). The slab is precast and reinforced with DPC reinforcements after which it is placed on top of the walls after being underlain with mortar for firm placement.

### Operation and Maintenance Door

The operation and maintenance door on the top slab is constructed in a rectangular opening of  $2.7\text{ m} \times 2.8\text{ m}$  (Fig. 15). The operation and maintenance door is created to allow for the manual feeding of the hospital waste into the combustion chamber. The operation and maintenance door is constructed directly over the waste frame in the combustion chamber to allow the hospital waste to be placed directly into the waste frame.

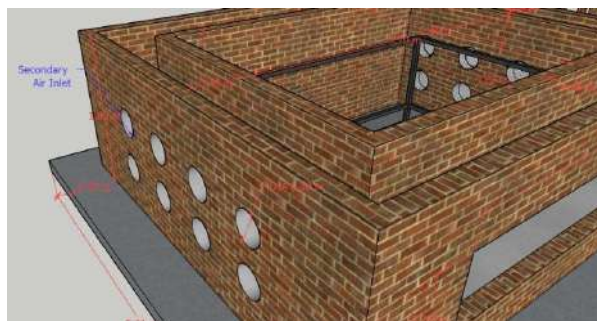


Fig. 14: 3-D Drawing of the secondary air inlet.

### Fume Pipe

The fume pipe is a metal pipe of diameter 0.45 m and a standing height of 1.5 m (See Fig. 16) above the Top Slab. The purpose of the fume pipe is for the upward displacement of combustion fumes through a specific channel to the atmosphere or pollution control device.

### Particle Filter

The particle filter is placed along the length of the fume pipe so that combustion fumes can pass through it and remove any tiny particles that could be hazardous to breathe in (Fig 16).

### Fume PIPE and Support Stand

They are constructed to hold the fume pipe firmly to prevent it from swaying.

Fig. 17, 18 and 19 show the 3D and section drawings of the whole incinerator.

### CONCLUSIONS

This study shows a similar trend of HWM practices observed in Afe Babalola University multi-system hospital in developing countries, particularly in Africa which is characterized by the absence of segregation of medical waste from point of generation. HWM practices in most developing countries do not meet WHO standards due to the lack of segregation

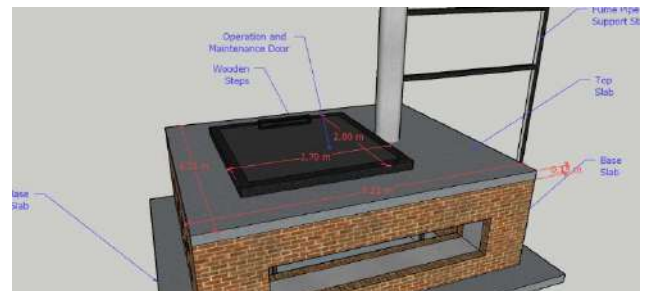


Fig. 15: 3-D Drawing of the top slab.

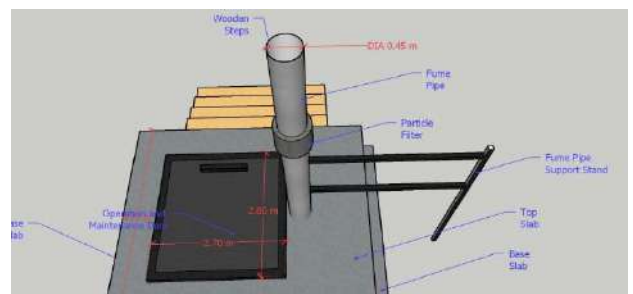


Fig. 16: 3-D Drawing of the fume pipe.

of medical waste at the point of generation, uncontrolled or open-air combustion of medical waste, collection and management of medical waste alongside municipal waste, use of inadequate protective equipment by the personnel involved in waste handling, open dumping of medical waste in

un-engineered dump sites, and poorly designed incinerators if they exist for the collection, transport, and disintegration of medical wastes. There is a high risk of environmental pollution particularly air and groundwater pollution as well as a high public health risk as a result of these poor management practices. Looking at De Montfort's design of a Low-Cost Medical Waste Incinerator, his design made no provisions for the quantity of kerosene to be used for the combustion of the medical waste. The combustion chamber's capacity was determined primarily by the quantity of waste to be incinerated, essentially creating a controlled environment for the combustion of medical waste while neglecting the reactions of medical waste components with kerosene. Since it's a kerosene-fueled incinerator, it's the major cause of black smoke from the chimney. However, the design of this study takes into account the combustion interactions of kerosene with various components of medical waste and is based on a daily loading of waste. Hence it is significantly larger compared to De Montfort's design although it retained certain features of his design such as the chimney/exhaust fume, access door for cleaning and maintenance of the incinerator, a concrete base, brick or sandcrete walls as well as openings/air inlets to allow for access air during combustion.

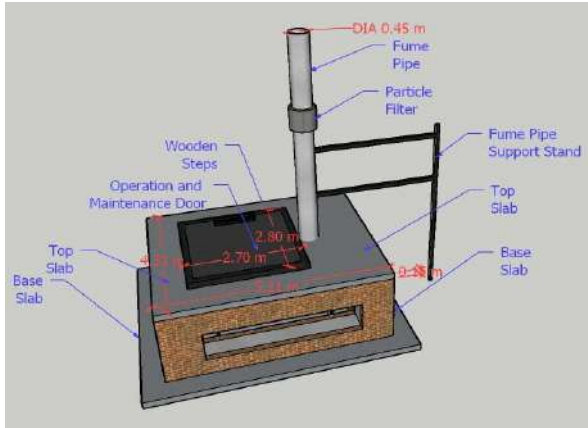


Fig. 17: 3-D Drawing of the incinerator.

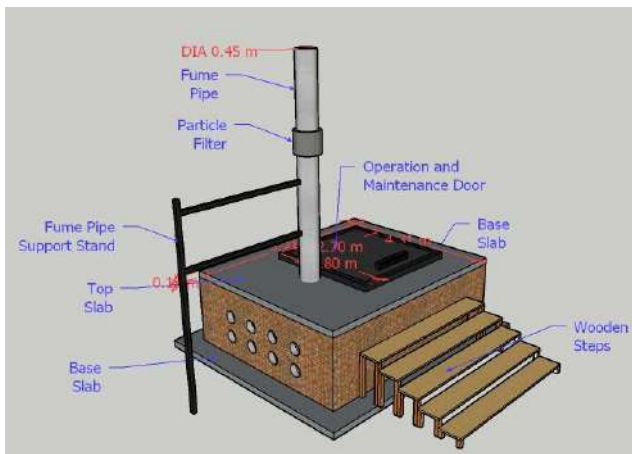


Fig. 18: 3-D Drawing of the incinerator.

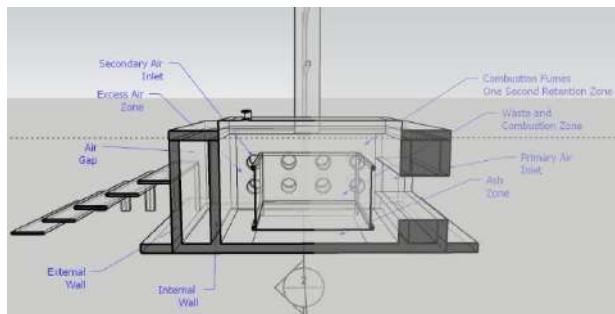


Fig. 19: 3-D, X-Ray, section drawing of the incinerator showing the combustion zone.

On completion of the design of the incinerator with an Incinerator capacity of  $120 \text{ kg}\cdot\text{hr}^{-1}$ , the optimum kerosene to a medical waste ratio of 1 L of Kerosene: 3.7 kg of medical waste was determined; aside from initial construction cost, the cost of fueling daily to combust the design daily waste load of  $269 \text{ kg}\cdot\text{day}^{-1}$  would require about 73 L which would sum up to N25,550 daily or about N9.3 Million yearly which seems like a significant amount. But compared to the financial implications of the potential health risks on humans as well as pollution of the environment, far more funds would be needed to rectify such problems when they arise. The hospital would need to allocate a fixed amount of funds from income generated towards the effective management of its medical waste to meet WHO criteria, avoid the negative impacts of poor HWM procedures, and increase the international rating of the Hospital. This design is untested, further research would be required into the construction and quantitative assessment of the effectiveness of this incinerator. Both designs do not include air control devices for the fumes produced from combustion. A low-cost design that can be implemented is the design of wet scrubbers which is effective towards this end.

**RECOMMENDATIONS**

The state of HWM practices in developing countries especially in Nigeria needs a lot of improvement and the following

are recommendations for achieving an improved state of HWM practices in Nigeria.

1. The Nigerian Government should create and enforce laws eradicating the dumping of medical as well as municipal wastes in un-engineered dumpsites; specific dumpsites should be made available and providing fencing to ward off scavengers.
2. All waste-handling staff should and must be outfitted with full safety gear.
3. Regulatory bodies must impose segregation practices in all healthcare facilities from the point of creation to the final disposal site.
4. Ensuring strict compliance with WHO standards on the collection, transport, and disintegration of medical waste
5. Hospitals should adequately allocate both human and financial resources in all HWM operations
6. Regular training and orientation of all staff involved in HCEs on HWM practices

## REFERENCES

- Adama, M., Esena, R., Fosu-Mensah, B. and Yirenya-Tawiah, D. 2016. Heavy metal contamination of soils around a hospital waste incinerator bottom ash dumps site. *J. Environ. Pub. Health*, 4: 53. doi:10.1155/2016/8926453.
- Adegbite, M.A., Nwafor, S.O., Afon, A., Abegunde, A.A. and Bamise, C.T. 2010. Assessment of dental waste management in a Nigerian tertiary hospital. *Waste Manage. Res.*, 28: 769-777. <http://doi.org/10.1177/0734242X09356017>
- Agunwamba, J.C., Emenike, P.C. and Tenebe, I.T. 2013. Comparative analysis of hospital waste management in Calabar metropolis and developed countries. *Int. J. Struct. Civil Eng. Res.*, 2(4): 600.
- Akpe, J.C., Oyelaran, O.A. and Abdulmalik, I.O. 2016. The design of a portable municipal waste incinerator with fuzzy logic-based support for emission estimation. *Aceh Int. J. Sci. Technol.*, 5(3): 748. doi:10.13170/aijst.5.3.5748.
- Cassidy, T., Inglis, G., Wiysonge, C. and Matzopoulos, R. 2014. A systematic review of the effects of poverty deconcentration and urban upgrading on youth violence. *Health Place*, 26: 78-87. doi:10.1016/j.healthplace.2013.12.009.
- Collier, K.J., Clapcott, J.E., Hamer, M.P. and Young, R.G. 2013. Extent estimates and land cover relationships for functional indicators in non-wadeable rivers. *Ecol. Indic.*, 34: 53-59.
- David, O.O., Dominic, E.A., Tunde, O.T. and Uchechukwu, E.O. 2014. Medical waste management practices among selected health-care facilities in Nigeria: A case study. *Sci. Res. Ass.*, 9(10): 431-439. DOI:10.5897/SRE2014.5863.
- Gupta, S. and Boojh, R. 2006. Report: biomedical waste management practices at Balrampur Hospital, Lucknow, India. *Waste Manag. Res.*, 16: 584-591.
- Huff, G. and Angeles, L. 2011. Globalization, industrialization, and urbanization in pre-World War II Southeast Asia. *Explor. Econ. Hist.*, 48(1): 20-36. doi:10.1016/j.eeh.2010.08.001
- John, E.S., Swamy, C.N. and Manilal, A. 2016. Bio-Medical Waste Incinerator Design for Smart Arbaminch City: Minimum Specifications for Health Care Waste Incineration. Environmental Council of Zambia, Zambia, pp. 1-22.
- John, S.E. and Swamy, C.N. 2011. Design of incinerator for the treatment of bio-medical solid waste in Chikmagalur city. *J. Ind. Pollut. Contr.*, 27(2): 173-179.
- Khurmi, R.S. and Gupta, J.K. 2015. A Textbook of Machine Design. Fourteenth Edition, Eurasia Publishing House (PVT.) Ltd, Ram Nagar, New Delhi.
- Lin, M., Yu, H. and Peng, W. 2022. Hydrochemical characteristics and irrigation water evaluation of suburban river: A case study of Suzhou City, Anhui Province, China. *Nat. Enviro. Pollut. Technol.*, 21(1): 640-659.
- Lúcio, F.B. and Douglas, M. 2004. *Clinical Engineering Handbook*. Elsevier Academic Press, Amsterdam.
- Manyele, S.V. 2004. Medical waste management in Tanzania: Current situation and the way forward. *Afr. J. Environ. Assess. Manage.* 8(1):74-99.
- Manyele, S.V., Anicatus, H. and Bilia, M.H. 2003. Globalization and its Effects on Medical Waste Management in Tanzania. IET Annual Conference and General Meeting, 4th-5th December, 2003, AICC Arusha, Tanzania, pp. 76-92.
- Mathur, P., Sangeeta Patan, S. and Shobhawat, A.S. 2012. Need of bio-medical waste management system in hospitals, an emerging issue: A review. *Curr. World Environ.*, 7(1): 117-124.
- Muthukannan, M., Aruna, S. and Chithambar, G. 2019. The environmental impact caused by the ceramic industries and assessment methodologies. *Int. J. Quality Res.*, 13(2): 315-334. Doi: 10.24874/IJQR13.02-05.
- Olanrewaju, M., Olawale, K. and Fasinmirin, R. 2019. Design of medical waste incinerator for health care facilities in Akure. *J. Eng. Res. Rep.*, 10: 1-13. 10.9734/jerr/2019/v5i216919.
- Patel, R.B. and Burkle, F.M. 2012. Rapid urbanization and the growing threat of violence and conflict: A 21st-century crisis. *Prehosp. Disas. Med.*, 27(2): 194-197. doi:10.1017/S1049023X12000568
- Picken, D.J. 2019. *The De Montfort „family“ of medical waste incinerators*. Springer, Singapore.
- Picken, J., Russell, A. and Nwaduikwe, C.J. 2012. Construction of a low-cost medical waste. *Int. J. Sci. Tech.*, 2(5): 141-163.
- Rai, D., Patel, N. and Srivastava, A.K. 2018. Assessment of biomedical waste disposal and management in three hospitals of Rishikesh, India. *Int. J. Res. Advent Tech.*, 6(9): 321-329.
- Ramesh, S.T., Jayanthi S. and Gandhimathi, R.A. 2008. Study on problems of management of bio-medical wastes and their remedial measures. *J. Ind. Pollut. Contr.*, 24(2): 147-150.
- Vasistha, P., Ganguly, R. and Gupta, A.K. 2018. Biomedical Waste Generation and Management in Public Sector Hospital in Shimla City. In Singh, V., Yadav, S. and Yadava, R. (eds.), *Environmental Pollution*, Springer Publications, Singapore, pp. 225-232.
- Walter, R.N. 2010. *Combustion and Incineration Process: Applications in Environmental Engineering*. Third Edition, CRC Press, Taylor and Francis Group, NJ.
- World Health Organization (WHO) (1999). *Unsafe injection practices and transmission of blood-borne pathogens*. WHO, Washington DC.
- World Health Organization (WHO) (2002). *Wastes from healthcare activities*. WHO, Washington DC.



# Effective Contribution of Air Pollutants to Physiological and Psychological Human Diseases: A Systematic Review

P. Chaitanya\*, Era Upadhyay\*†, Desh Deepak Singh\* and Virendra Singh\*\*

\*Amity Institute of Biotechnology, Amity University, Jaipur-303002, Rajasthan, India

\*\*Asthma Bhawan, Vidhyadhar Nagar, Jaipur-302039, India

†Corresponding author: Era Upadhyay; era.upadhyay@gmail.com

Nat. Env. & Poll. Tech.  
Website: [www.neptjournal.com](http://www.neptjournal.com)

Received: 17-02-2022

Revised: 06-04-2022

Accepted: 09-04-2022

## Key Words:

Criteria air pollutants  
Lung disorders  
Heart diseases  
Auto-immune diseases  
Blood disorders

## ABSTRACT

Increasing globalization, industrialization, population, and burning of fossil fuels have been adversely affecting the environment for a long time. The consequences of the effects can be seen even within a short period of time in the current scenario. The air pollutants such as SO<sub>2</sub>, NO<sub>2</sub>, CO, and PM are the main contributors to the adverse health effects. Long-term and short-term exposure to pollutants may cause acute and chronic effects on the human body as they can enter deep into the organ and circulate in the bloodstream. The ultimate purpose of this review is to develop a quantitative perceptible of the existing state of facts about potential health effects concerning the dose-response relationship between exposure level of air pollutants and induced diseases. We have drawn around 376 scientific research papers on high-impact factors related to air pollution and health. These publications were analyzed with consideration of experimental methods, design, observations, and reports on the exposure through inhalation which may emulate the normal direction of exposure inside the human organs. The present study suggests the effects of epidemiological studies on associations between pollutant concentrations and human health. Most of the inferences evidenced the severe adverse effects of particulate matter (PM<sub>2.5</sub> & PM<sub>10</sub>) on the respiratory and cardiovascular systems. Our present investigation reveals the health risk due to pollutants' exposure to the vulnerable population anguishing with asthma, COPD, cardiovascular disease, diabetes, cancer (physiological diseases); dementia, depression, and stress (psychological diseases).

## INTRODUCTION

Air pollutants are one of the major components of environmental pollution. The primary air pollutants released from the source such as biomass burning, vehicles, thermal power plants, etc. (Awadi 2018). NO<sub>x</sub> and VOCs react in the presence of sunlight and form highly reactive secondary pollutants. The reactions generate particulate and gaseous air pollutants and affect the health of children, the elderly, and vulnerable people adversely (Morakinyo et al. 2017). Source emission is increasing with increasing demands due to the rising population (Upadhyay et al. 2020). Increasing industrialization, urbanization, and vehicles emit injurious gases which form outdoor air pollution (Guarnieri & Balmes 2015). While biomass and fossil fuel burning generate indoor air pollution (Annesi-Maesano et al. 2013), may penetrate the respiratory tract and produce allergies. Indoor air pollution is more harmful as it covers less area and becomes more concentrated with the pollutants (Manisalidis et al. 2020). Weather conditions and geographical locations also affect the severity

and dispersal of the pollutants (Khamutian et al. 2015). Recently, pollution, unlike London smog, was noticed in Delhi, which required emergency measures thus all smog emitters were temporarily shut down to control the emissions (Singh 2016). The air quality was noticed with heterogeneous characteristics due to variation in correlations between different criteria pollutants in Delhi. This variation might have been established due to significant PM<sub>10</sub> emissions from construction sites, thermal power plants, industries, and vehicles mainly during the summer season (Biswas et al. 2011, Barik et al. 2021). While a distinct seasonality was recorded in winter by observing the PM<sub>10</sub> concentration level of 200 µg/m<sup>3</sup> in the residential area of Lucknow which is more than the prescribed level (60 µg.m<sup>-3</sup>) of the central pollution control board. On the other hand, the concentrations of SO<sub>2</sub> and NO<sub>2</sub> were measured as 8 µg.m<sup>-3</sup> and 30 µg.m<sup>-3</sup> respectively which are in the range of permissible limits (Upadhyay et al. 2017). Cifuentes et al. observed respiratory issues in the patients due to the endotoxins formed through exposure to PM (65.5 µg.m<sup>-3</sup> PM<sub>2.5</sub> & 153 µg.m<sup>-3</sup> PM<sub>10</sub>)

(Cifuentes 2019). While particulate matter combined with CO<sub>2</sub> (900-1500 µg.m<sup>-3</sup>) caused repeated respiratory issues enhanced by improper ventilation. Poor ventilation rapidly spreads the endotoxins due to limited area (Padhi et al. 2017) which deposits in the alveolar region of the lungs. The data showed that deteriorated air quality has become a severe issue that may cause non-communicable diseases that increase the risk to the health of 75% of the population (Schraufnagel et al. 2019). CO emission has greatly toxic effects on the sense organs which may cause numerous neuro-disorders. CO mixes with hemoglobin after entering the organism and may decrease the oxygen-carrying capacity across the system. People who had smoking habits were found as deficient in COHb (< 5-10%) levels (Schimmel 2018). The patients exposed to high levels of NO<sub>2</sub> concentration (30-90 µg.m<sup>-3</sup>) for even short-term had severe lung damage, shortness of breath, and chest pains (Karakatsani et al. 2010). The long-term exposure to these patients may cause mortality due to asthma by 3.1% (Weinmayr et al. 2010) CVD by 69%, pulmonary diseases by 28% whilst the short-term exposure of a combination of PM<sub>10</sub>, PM<sub>2.5</sub> & NO<sub>2</sub> (56.3 µg.m<sup>-3</sup>, 29 µg.m<sup>-3</sup>, 41.8 µg.m<sup>-3</sup>) increased the respiratory hospital admissions at all age groups (Çapraz et al. 2017). Short-term combined exposure to PM, O<sub>3</sub>, and high temperature caused diabetes mellitus, diagnosed by examining blood pressure (Hoffmann et al. 2012). High levels of PM<sub>2.5</sub> (10-33 µg.m<sup>-3</sup>) exposure may cause an increase in blood pressure and myocardial oxygen demand. PM exposure induced more mortality due to respiratory and diabetes illness in 65-year-old persons (0.64%) than in the younger population (0.34%) (Zanobetti et al. 2014).

An air quality monitoring program covering 11 fitness centers in Lisbon reported high temperature, humidity, and pollutants concentrations. The visitors to fitness centers were diagnosed with respiratory tract infections (Ramos et al. 2014). High toxicity is attributed to acute infections in the lower respiratory tract (bronchi, bronchioles, and alveoli) and upper respiratory tract (nasopharynx, oro-pharynx, and hypopharynx) (Lelieveld et al. 2015). High concentration of SO<sub>2</sub> (65.7 µg.m<sup>-3</sup>) exposure increases mortality due to the effect on FEV and FVC (He et al. 2010). Lower FEV1 (54mL) indicated respiratory illnesses in all aged groups of people. Exposure to 3.9-4.13 µg.m<sup>-3</sup> level of SO<sub>2</sub> caused allergy and acute respiratory inflammation in the young population (Alwahaibi & Zeka 2016). The present study is conducted to understand and infer the impact of pollutant concentrations on physiological as well as psychological disorders by analyzing their methodological approach, and diagnostic pattern, and reporting the results.

## MATERIALS AND METHODS

### Measurement Techniques for Air Pollutants

The foremost objective of the present study is to re-evaluate air pollutants' impact on human health considering indoor and outdoor exposure for short-term and long-term duration causing acute and chronic illnesses. To achieve this aim, we have used the published data obtained through a wide range of pollutants samples measured by various techniques and health impact through diagnosis. The degree of pollution was measured by using modeling data and systemically measured data to determine the quantity and quality of the pollutants. The data for pollutants and health effects was compiled from 1960 to 2020, obtained from the research methods and results pertaining to the assessment of 24 hour-counts with respect to hours/minutes by different monitoring and diagnostic approaches. Then the averaged data was analyzed critically to find out the correlations of individual pollutants with physiological and psychological diseases. This section of this paper includes the measuring methods for criteria air pollutants (PM<sub>2.5</sub>, PM<sub>10</sub>, CO, NO<sub>2</sub>, SO<sub>2</sub>) and their health impacts categorized as physiological diseases (chronic obstructive pulmonary disease, asthma, cardiovascular disease, diabetes, cancer) and psychological diseases (dementia, depression, and stress).

#### *Particulate Matter (PM<sub>10</sub> & PM<sub>2.5</sub>)*

The particulate matter was first measured in 1964 by using simple tools of statistics. Afterward, the methodological technique became advanced and stimulated good quality estimations (Halonen et al. 2011). About 70% of PM<sub>2.5</sub> and PM<sub>10</sub> concentrations from vehicular sources can be estimated from Chemical Mass Balance (CMB) model with seasonal variations in the city of Mangalore (Kalaiarasan 2018). The concentration level for 24-hour PM<sub>10</sub> was measured through poison regression analysis and gravimetric filter-based methods along with weather parameters (Achilleos 2016). The evaluation of concentration levels of particulate matter through regression analysis against hospital admissions revealed that respiratory illness was the reason for increased cases. The researchers also used another technique i.e. Lung Dose Evaluation Programme (LUPED) model to measure the concentrations of PM (PM<sub>10</sub>, PM<sub>2.5</sub>, and PM<sub>1</sub>). The LUPED model measures the endotoxins deposition inside the cellular regions of the respiratory tract and the rate of breathing (Padhi et al. 2017). PM is also measured by low pressure three cascade Dektai impactor ([www.dekati.com](http://www.dekati.com)).

#### *Carbon Monoxide (CO)*

The CO concentration level was observed first time in neu-



ropathy analytical studies through CT and MRI during the 1970s. Presently, CO estimation has been developed and the toxicity can be diagnosed through electrocardiography by using COx multivariate proportional hazards such as COHb levels, age, exposure duration, smoking habits, etc. to examine the acute myocardial infarction (AMI) (Kaya et al. 2016). The CO effects were examined through a simple questionnaire, CH<sup>2</sup>OPD<sup>2</sup> (community, home, hobbies, occupation, personal habits, diets & drugs) to get the historical exposure data (Abelsohn et al. 2010). The capillary gas chromatography, mass spectroscopy along with HP mole sieve plot column was used to analyze the blood sample of headspace and correlated between CO exposure and COHb levels through regression models. The results revealed an elevated level of COHb concentration with the rise in CO level (Rudra et al. 2010). The CO toxicity level in blood samples of two groups of 30-40 year aged people was measured through the Mann-Whitney U test and spectrophotometer (Nair et al. 2017).

### ***Nitrogen Dioxide (NO<sub>2</sub>)***

Earlier the health effects due to NO<sub>2</sub> exposure have been diagnosed in tissue through various techniques such as culture cells and regression models (Gezerman & Çorbacioğlu 2018). Recent studies on the association between air pollutants and chronic airway disease and cardiopulmonary diseases (asthma, idiopathic pulmonary fibrosis, etc.) have established diagnostic development (Conti et al. 2018). The effect of NO<sub>2</sub> was diagnosed with a decrease in lung functioning parameters such as FVC and FEV1 in adults (Cole-Hunter & de Nazelle 2018).

### ***Sulfur Dioxide (SO<sub>2</sub>)***

The simple questionnaire survey was used to examine breathing patterns of the responsiveness of SO<sub>2</sub> (Vahlsing & Smith 2012), the survey resulted in the need for some diagnostics in the tissues. Epithelial tissue injury due to SO<sub>2</sub> exposure was found through the biological marker in compound mucous cilia (Koenig 2016). The Elisa-based method was used to analyze the impact of SO<sub>2</sub> on health by observing inflammatory markers, fibrinogen, oxidative stress, and coagulation factors (Chuang et al. 2007). The correlation between SO<sub>2</sub> concentration (10 µg.m<sup>-3</sup>) and Fev1 (54ml) revealed lung functioning at a lower rate. Rajeswari reported pulmonary function test, thyroid profile, and absolute eosinophil count among male petrol pump workers to determine SO<sub>2</sub> toxicity (Rajeswari 2019). While Russell's analysis with regression modeling was used to find out the linkage between emissions of NO<sub>2</sub>, SO<sub>2</sub>, PM, and meteorological factors (Russell 2018).

## **Classification of Diseases**

Air pollutants are one of the most crucial contributors of the environment to the burden of disease. It is an important health risk factor for major non-communicable diseases. The efficiency of the pollutant concentration may be modified due to increasing population and industrialization which may affect even in a short period of time. Research reveals the linkages between several serious diseases among various age groups and air pollution. Based on the efficiency of the diseases, we have classified them into two categories namely physiological diseases and psychological diseases. The health effects due to individual air pollutants are discussed here under these two categories.

### **Association of the Pollutants with Physiological Diseases**

Diseases of the respiratory system are often evident by one or more symptoms that can be easily acknowledged. The presence of a meticulous symptom or a set of symptoms facilitates identifying an underlying disease in the respiratory system. We have reviewed several epidemiological studies in which the prevalence of respiratory symptoms has been assessed to obtain an insight into the occurrence of physiological diseases due to pollutants are CVD, COPD, asthma, diabetes, and cancer.

### ***PM<sub>10</sub>/PM<sub>2.5</sub> and Associated Physiological Diseases***

The PM exposure caused pulmonary inflammation and activates systemic hypercoagulability which increases the heart rate. Rising heart rate may become the sequel reason of myocardial infarction, heart attack, and mortality due to CVD (Lin et al. 2017, Chang et al. 2014). The women in the postmenopausal phase had suffered from obesity and found 76% increased mortality risk due to CVDs, they have regularly been exposed to 10 µg.m<sup>-3</sup> PM exposure (Miller et al. 2012). The associations of PM<sub>10</sub> (23 µg.m<sup>-3</sup>) and CO (1.66 µg.m<sup>-3</sup>) concentrations increased the cases of CVD by 2.8%. PM exposure causes a remarkable elevation in C-reactive protein (CRP), a protein produced by the liver that indicates inflammation, breast cancer, and CVD (Chandrasekhara 2014). The long-term air pollutants' exposure may cause hypercoagulability and thrombosis; which occur due to unfavorable effects on PT, ATPP, CRP, and tissue-type plasminogen activator (tPA), etc. (Mohammadi et al. 2016). Mölter et al. reported that long-term exposure to a combination of PM<sub>10</sub> and NO<sub>2</sub> decreased lung volume and airway resistance in children (Mölter et al. 2013). High levels of PM<sub>10</sub> (10 µg.m<sup>-3</sup>) increased by 0.72% increasing the CHF admission rate, while short-term exposure of 10 µg.m<sup>-3</sup> PM<sub>2.5</sub> increased by 13% cases of CHF, ischemic stroke, and

cerebrovascular diseases (Wellenius et al. 2012). Fine and ultra-fine particles reach the blood by entering deep into the alveoli of the respiratory system and then into cellular regions and lymph nodes. Long-term traffic exposure to  $PM_{2.5}$  ( $45.38 \mu\text{g}\cdot\text{m}^{-3}$ ) and  $PM_{10}$  ( $80.07 \mu\text{g}\cdot\text{m}^{-3}$ ) indicated the rising levels of InterLeukin-6 expression, fibrinogen, TNF-alpha, Soluble platelet selectin, t-Hcy, CIMT, PA-1, t-PA; that may be the cause of respiratory and cardiovascular diseases (Bauer et al. 2010, Wu et al. 2016). The association of  $PM_{10}$ ,  $NO_2$ , and CO at low concentration levels caused rising cases of allergic rhinitis (AR), whereas short-term exposure to  $PM_{10}$  &  $SO_2$  association revealed elevated levels of FVC and FEV1 (Chen et al. 2016). The concentration level of  $10 \mu\text{g}\cdot\text{m}^{-3} PM_{2.5}$  was found to be associated with high ERV1 (Xu et al. 2016).

Exposure to  $PM_{2.5}$  has adverse effects on glucose tolerance, insulin activity, and blood lipid concentration which may cause type-2 diabetes (Chen et al. 2016). A study revealed that long-term exposure to  $PM_{2.5}$  and/or in combination with  $NO_2$  may be an attributable factor to the risk of diabetes mellitus and hypertension (Bowe et al. 2018). Consequently, blood pressure and body mass index increased and resulted in obesity, CVD, respiratory diseases, and cancer even non-smokers may also be affected (Hansen et al. 2016, Katanoda et al. 2011). Exposure to  $PM_{2.5}$  and  $NO_2$  may increase HbA1C levels which is the reason for misbalancing glucose metabolism (Qiu et al. 2018).

### ***CO and Associated Physiological Diseases***

The poisonous gas, carbon monoxide mainly emitted from transportation means. Its exposure may cause an adverse impact on health such as severe headache, dizziness, CVD, premature births, low birth weight in infants, etc. The CO binds with hemoglobin (Hb) through the cell affinity of an oxygen molecule called hypoxemia. Hypoxemia restrains the oxygen binding capacity which may stimulate gasometrical and respiratory problems (Anand et al. 2017). A positive association was observed between Serum Ischemia modified albumin (diagnostic biomarker in blood COHb) and CO poisoning (Veronesi et al. 2017). The CO mixed with a low concentration of blood plasma was reported to have a high rate of morbidity and mortality due to a misbalance of the bilirubin which increases the risk of ischemic heart diseases, CAD-related diseases, and arteriosclerosis (Chi et al. 2013). The COex is a simple surrogate biomarker related to wealth consequences. Exposure to CO concentration increased the level of COex and increased the risk of myocardial infarction and respiratory infections in smokers (Zhang et al. 2013). A combination of exposure to CO,  $NO_2$ , and PM causes inflammation, COPD, exhaled CO may increase the risk of stroke, cardiovascular issues, hypertension, anemia, and

metal concentration, etc. (Nayor et al. 2016). The association of CO (0.9ppm for 8hrs; 6.0%) and  $NO_2$  (5.1 ppb for 24 h, 6.9%) enhances the risk of cardiac issues whereas the low concentration of CO showed severe cases of COPD (Yang et al. 2011). Exposure to CO and  $O_3$  also observed a rise in COPD and asthma cases in hospitals (Khamutian et al. 2015). The roadside workers were reported with some issues such as depression, forgetfulness, tidiness, fatigue, respiratory illness, high pulse rate, etc. while exposed to higher concentrations of CO (Mathur et al. 2017). Meteorological changes with CO exposure may cause coronary issues and heat stress which indicate the risk of CVD (Almendra et al. 2017). CO exposure during long and short-term reported inflammation due to rising WBC counts and ferritin (Lee et al. 2018).

$NO_2$  deeply penetrates the peripheral bronchi and causes mild and moderate asthma (Greenberg et al. 2017). Exhaled nitric oxide (eNO) increase neutrophilic inflammation in asthmatic person by reducing airway acidification & resistance and lung function (Zhang et al. 2013). Increased asthma visits were reported in the cold season while high annual mean temperatures were reported to enhance the risk of asthma and rhinitis due to  $NO_2$  exposure (Abe et al. 2009, Weaver & Gauderman 2017). An association between  $NO_2$  exposure and pollen was found with elevated emergency admissions of asthma (Galán & Simón 2015). The two-pollutant model concluded the CVD effects and inflammation, diagnosed through the measurement of the bow-like biomarkers and hsCRP (high sensitivity C - reactive protein) (Wu et al. 2016). Short-term vehicular  $NO_2$  and other pollutant emissions promote mortality due to cardiovascular and respiratory issues, and lung cancer (Atkinson et al. 2016). The association of  $NO_2$  and CO exposure was linked with a 2-3% increase in COPD hospitalizations (Peel et al. 2005). The short-term exposure to  $NO_2$  associated with  $PM_{10}/O_3$  caused acute lower lung function indicated by Fev1 measurements (Nkosi et al. 2016). Exposure to vehicular  $NO_2$  emission caused diabetes mellitus even in healthy non-smokers (Coogan et al. 2012). Short-term exposure to  $NO_2$  (2.67%) indicated increased CVD and diabetes (3.5%) (Goldberg et al. 2013).  $NO_2$  exposure with a concentration of  $5 \mu\text{g}\cdot\text{m}^{-3}$  in Taiwan caused rising levels of FBG and HbA1C (Honda et al. 2017). While the combination of PM and  $NO_2$  exposure caused the risk of increased diabetes through the C3c marker used in the inflammation process (Krämer et al. 2010). The  $NO_2$  with PM long-term exposure may cause mortality due to chronic diseases such as CVD and diabetes (Bowe et al. 2018).

### ***NO<sub>2</sub> and Associated Physiological Diseases***

$NO_2$  deeply penetrates the peripheral bronchi and causes mild and moderate asthma (Greenberg et al. 2017). Exhaled nitric

oxide (eNO) increase neutrophilic inflammation in asthmatic person by reducing airway acidification & resistance and lung function (Zhang et al. 2013). Increased asthma visits were reported in the cold season while high annual mean temperatures were reported to enhance the risk of asthma and rhinitis due to NO<sub>2</sub> exposure (Abe et al. 2009, Weaver & Gauderman 2017). An association between NO<sub>2</sub> exposure and pollen was found with elevated emergency admissions of asthma (Galán & Simón 2015). The Two-pollutant model concluded the CVD effects and inflammation, diagnosed through the measurement of the bow-like biomarkers and hsCRP (high sensitivity C - reactive protein) (Wu et al. 2016). Short-term vehicular NO<sub>2</sub> and other pollutant emissions promote mortality due to cardiovascular and respiratory issues, and lung cancer (Atkinson et al. 2016). The association between NO<sub>2</sub> and CO exposure was linked with a 2-3% increase in COPD hospitalization (Cheng et al. 2018). The short-term exposure to NO<sub>2</sub> associated with PM<sub>10</sub>/ O<sub>3</sub> caused acute lower lung function indicated by Fev1 measurements (Nkosi et al. 2016). Exposure to vehicular NO<sub>2</sub> emission caused diabetes mellitus even in healthy non-smokers (Coogan et al. 2012). Short-term exposure to NO<sub>2</sub> (2.67%) indicated increased CVD and diabetes (3.5%) (Goldberg et al. 2013). NO<sub>2</sub> exposure with a concentration of 5 µg.m<sup>-3</sup> in Taiwan caused rising levels of FBG and HbA1C (Honda et al. 2017). While the combination of PM and NO<sub>2</sub> exposure caused the risk of increased diabetes through the C3c marker used in the inflammation process (Krämer et al. 2010). The NO<sub>2</sub> with PM long-term exposure may cause mortality due to chronic diseases such as CVD and diabetes (Bowe et al. 2018).

### *SO<sub>2</sub> and Associated Physiological Diseases*

The meteorological conditions alter the ambient SO<sub>2</sub> concentration. A high concentration of SO<sub>2</sub> exposure may cause adverse health effects such as breathing problems, airway inflammation, asthma, cardiac issues, psychiatric alterations, etc. Mild optic asthma, high plasma viscosity, and low CBU (Cumulative breath units), Fev1, and FVC levels were reported in people exposed to SO<sub>2</sub> (200 ppb) and NO<sub>2</sub> (400 ppb) under meteorological conditions (Greenberg et al. 2017). The association of SO<sub>2</sub> with PM caused elevated blood pressure and lipid peroxidation, which altered the antioxidant enzyme activities (Kocamaz et al. 2012) and the risk of morbidity due to neuronal dysfunction and COPD (Tingting et al. 2017). The mortality due to lung cancer and respiratory issue was reported in Japan and Stockholm with high annual mean concentration levels of SO<sub>2</sub> (Katanoda et al. 2011). SO<sub>2</sub> exposure also stimulates the action of endogenous 2-AG which suppresses the inflammation associated with microvasculature dysfunction and brain inflammation (Greenberg et al. 2017). NO<sub>x</sub> and SO<sub>2</sub> exposed women

having early pregnancy and preconception may be affected by gestational diabetes mellitus (Robledo et al. 2015). The association of PM<sub>10</sub>, SO<sub>2</sub> & NO<sub>2</sub> exposure causes elevated FBG levels and lipid levels including low-density lipoprotein cholesterol, total cholesterol, triglycerides, etc. which indicate diabetes risk (Wang et al. 2014).

### **Association of the Pollutants with Psychological Diseases**

The efficiency of psychological behavior is measured in terms of stress or depression. Psychological behavior influences humans in twin folds: unhappiness, self-suffering, awful confrontations, depressing feelings, and various other sentiments that cause depression. Mainly adults are suffering from the symptoms of depression which are linked with hypotension and low lipid level. The study on the effect of air pollution on human behavior began in 1970. Further research on the relationship between air pollutants and human behavior may vary conceptually. Exposure to the high concentration level of particulate and gaseous air pollutants affects the process of psychology adversely which stimulate stress. This stress may proceed as a disruptive environmental pollutant which may create psychological issues in humans. This issue has been focused very less therefore; we decided to observe the air pollutants' effect on psychological as well as physiological diseases. This section includes the effect of PM<sub>2.5</sub>, PM<sub>10</sub>, SO<sub>2</sub>, NO<sub>2</sub>, and CO on stress, dementia, and depression.

### *PM<sub>10</sub> & PM<sub>2.5</sub> and Associated Psychological Diseases*

Exposure to SO<sub>2</sub>, NO<sub>2</sub>, PM<sub>2.5</sub>, PM<sub>10</sub>, and CO has been reported as a factor to enhance depression with the risk of asthma, CVD, diabetes, etc. (Hazlehurst et al. 2018). Individuals suffering from CVD were tending to have a 10.1% increase in stressful suicidal threats and 6.7% in dementia, and depression at 0-45 depression scales due to PM<sub>2.5</sub> exposure (Pun et al. 2017, Kim et al. 2010). A recent study revealed the strong correlation of PM<sub>2.5</sub> exposure with stress-induced toxicants based on gender, age, demographic, and socioeconomic status. The lung structure with its function and its immune function can be adversely impacted by stress (Sass et al. 2017). An erectile dysfunction, a sign of psychological stress was observed in people due to air pollutants exposure. The measurement of some blood markers such as IgE, interleukin-5, and interaction beta indicated chronic stress in asthmatic children (Cheng et al. 2018). Long-term association of PM<sub>10</sub> and O<sub>3</sub> exposure pollution caused dementia, mild cognitive impairment and Alzheimer's indication, and other psychological disorders (Oudin et al. 2016). However, emission from traffic exposure with APOE decreases cognitive impairment (Schikowski et al. 2015). The psychosocial

stress may be caused due to the secretion of plasma and adrenocorticotropic hormone (ACTH) which is enhanced by air pollution exposure (Cordella & Poiani 2003). The ambient pollutants may influence the risk of suicidal tendencies in people who are maintaining low social-economic status (Lee et al. 2018).

### ***CO and Associated Psychological Diseases***

High levels of pollutants emitted from diesel revealed the symptoms of acute psychological stress (Laumbach et al. 2011). The study on vehicular emission (NO<sub>2</sub> & CO) exposure reported a significant increase in the cases of dementia in Taiwan (Chang et al. 2014). An impaired cognitive behavior was observed due to the combination of HBO<sub>2</sub> (Hyperbaric Oxygen) and CO concentration (Weaver et al. 2007). The number of emergency hospital visits was also reported as a strong positive correlation between CO level and meteorological parameters (Szyzkowicz et al. 2016). The rural women were observed with increased depressive symptoms due to the CO emission from kerosene stoves resulting in higher cognitive impairment (Banerjee et al. 2012). This study also corroborates with cognitive impairment diagnosed in 43 years aged women due to exposure to high CO concentration (Mayer 2000).

### ***NO<sub>2</sub> and Associated Psychological Diseases***

Exposure to elevated concentration levels of air pollutants may cause stress due to neurological imbalance. The stress may disturb the parasympathetic activity which may cause inflammation. A questionnaire survey revealed that exposure to NO<sub>2</sub>, PM<sub>2.5</sub> & PM<sub>10</sub> caused depression in people (Zijlema et al. 2016). The women were diagnosed with more severe depression than men due to the concentration level of 10 µg.m<sup>-3</sup> NO<sub>2</sub> (Vert et al. 2017). Chang et al. conducted a population-based survey and found that the people were suffering from dementia due to NO<sub>2</sub> and CO exposure (Chang et al. 2014). The hereditary effect was noticed for decreasing lung function due to NO<sub>2</sub> exposure through the analysis of non-smokers (Shankardass et al. 2015). Elevated temperature with rising NO<sub>x</sub> concentration caused the risk of suicidal tendencies. A low level of gaseous air pollutant exposure may also report increased cases of psychiatric disorders along with the increased risk of suicidal distress (Oudin et al., 2018). The infants exposed to NO<sub>2</sub> were reported with inverse effects on mental development during prenatal and postnatal periods (Lertxundi et al. 2015).

### ***SO<sub>2</sub> and Associated Psychological Diseases***

The record revealed the impact of air pollutants exposure on physiological coordination and resulted in mood distortions

and stress. Short-term SO<sub>2</sub> exposure was reported with a high risk of depressive mood followed by chronic stress (Wang et al. 2014). Exposure to elevated concentrations of PM<sub>10</sub>, SO<sub>2</sub> & NO<sub>2</sub> affected pregnant women in the winter season and diagnosed with PSS 75-100 scores which indicate severe depression. The people exposed to high concentrations of PM<sub>2.5</sub>, BC, and SO<sub>4</sub><sup>2-</sup> were caused a high perceived stress scale (PSS) score (Mehta et al. 2015). The linkages of mechanisms between air pollutant levels and suicidal loss increase the depression probability (Lin et al. 2017). The air pollution exposure was measured and analyzed between prenatal and postnatal periods and the results indicated parental stress may cause the probability of childhood asthma (Deng et al. 2018). A recent study reported post-surgery cognitive disorder, which is an indication of dementia (Che et al. 2017).

## **RESULTS AND DISCUSSION**

### **Description of Study Material**

We have accessed a total of 369 high-impact factor research articles to carry out this review analysis. The articles having incomplete information, repetitive and outdated observations (n=82), and unknown time duration (n=02) were excluded. The remaining research papers for considering the study were 285. Further 60 papers out of 285 were excluded based on mislaid data for morbidity, mortality, sex, and age, related to diseases categorized as physiological and psychological diseases. Thus a total of 225 research articles were sorted out for this study. Regarding the number of patients, out of the records of 23 years (1997-2020) international publications which reported insufficient patients were excluded (n=22). The number of remaining patients (7781054) was integrated into the analysis. A primary cohort of 2754056 patients includes a record considering the effect of air pollution concentration levels on different age group populations. The methodology and results about the impact of air pollution in terms of physiological diseases (2088092 patients) and psychological diseases (665975 patients) were incorporated into the study for an efficient outcome. Figure 1 shows the detailed flow diagram for the description of the study material.

### **Authors' Interpretation of Systematic Evidence**

We have downloaded more than 200 peer-reviewed international research articles for interpretation based on analysis (all the considered articles are not included in the reference section of this study). Out of those, 50 research articles about each pollutant (PM<sub>2.5</sub>, PM<sub>10</sub>, CO, NO<sub>2</sub> & SO<sub>2</sub>) and associated diseases were taken into account. We have simplified the complex health effects due to air pollution exposure by classifying them into two groups of diseases-physiological

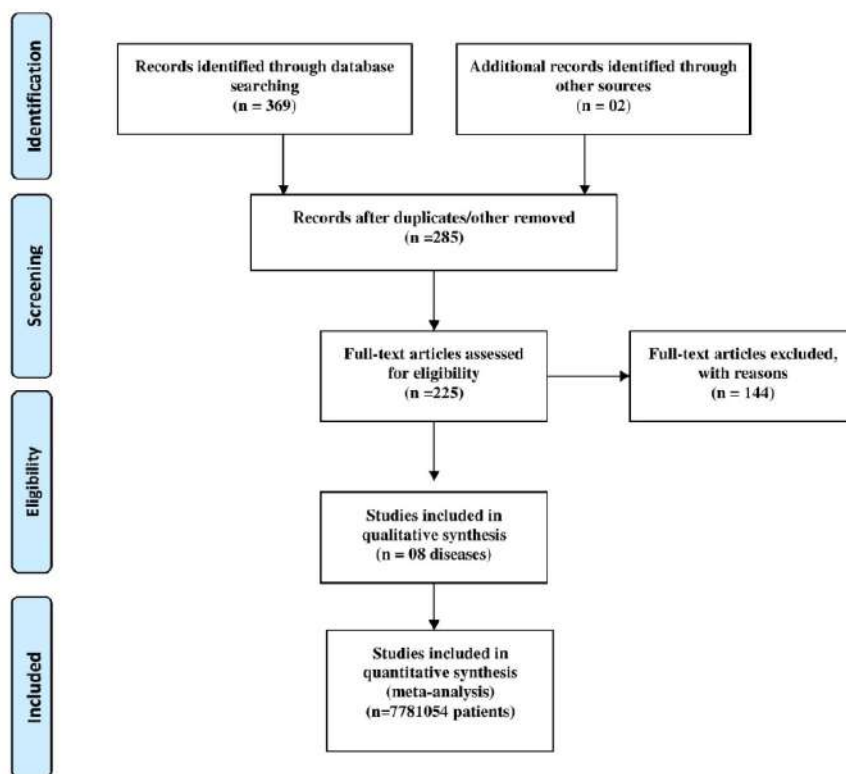


Fig. 1: Flow diagram representing the description of study material.

diseases and psychological diseases. Physiological diseases refer to CVD, COPD, asthma, diabetes, and Cancer, whereas psychological diseases include dementia, stress, and depression. Direct or combined exposure to air pollutants may cause physiological diseases. While psychological diseases occurred as a consequence of physiological disorders. The air pollutants cause direct or indirect effects on endocrine glands, deteriorate hormonal coordination, and may cause neuropsychological diseases. The mortality and morbidity due to short-term and long-term exposure to air pollutants and their acute and chronic effects have also been examined. Over the years trends for concentration levels of air pollutants, and associated age-wise effects on diseases were analyzed for critical assessment. The patterns helped us to analyze and realize the crucial interpretation for this study.

An overview of the diseases across the globe is shown in Fig. 2a. The figure depicts the hospital admissions for the physiological diseases that occurred due to air pollutants' direct and indirect exposure. The highest hospitalization was more than 50% for COPD cases associated with  $40 \mu\text{g.m}^{-3}$   $\text{PM}_{10}$  exposure and more than 15% of COPD cases were associated with  $50 \mu\text{g.m}^{-3}$   $\text{PM}_{2.5}$  exposure. About 50% of cases of cancer were associated with  $35 \mu\text{g.m}^{-3}$   $\text{PM}_{10}$ , 20

$\mu\text{g.m}^{-3}$   $\text{PM}_{2.5}$  &  $40 \mu\text{g.m}^{-3}$   $\text{SO}_2$  exposure. More than 30% of cases of diabetes were associated with  $30 \mu\text{g.m}^{-3}$  CO exposure and found as

the fourth highest disease as per our analysis.  $\text{PM}_{10}$  is again the key contributor to 15% of cases of asthma, however, more or less all five air pollutants were found to be responsible for asthma. CVD hospitalizations with more than 20% cases were associated with  $20 \mu\text{g.m}^{-3}$   $\text{SO}_2$  concentrations.

Figure 2b shows the effect of pollutants' exposure on hospitalizations due to the cases of psychological diseases pertaining to the direct and/or consequences of other ailments. CO ( $30 \mu\text{g.m}^{-3}$ ) and  $\text{SO}_2$  ( $35 \mu\text{g.m}^{-3}$ ) were observed as the key contributors to more than 50% of cases of dementia. Even a low concentration of CO ( $5 \mu\text{g.m}^{-3}$ ) was associated with more than 50% of cases of depression but it is the major contributor to depression.  $\text{PM}_{2.5}$  ( $15 \mu\text{g.m}^{-3}$ ) and  $\text{SO}_2$  ( $15 \mu\text{g.m}^{-3}$ ) are the second leading contributors associated with 25% of cases of depression.  $\text{NO}_2$  is also a notable contributor to depression as the stress was allied with 40% of cases due to  $\text{PM}_{10}$  ( $35 \mu\text{g.m}^{-3}$ ), 30%  $\text{NO}_2$  ( $13 \mu\text{g.m}^{-3}$ ), and 20% of cases due to  $\text{SO}_2$  ( $15 \mu\text{g.m}^{-3}$ ) concentrations.  $\text{PM}_{10}$  is the major air pollutant that was alone associated with 40-50% of cases of all three types of psychological diseases. However,

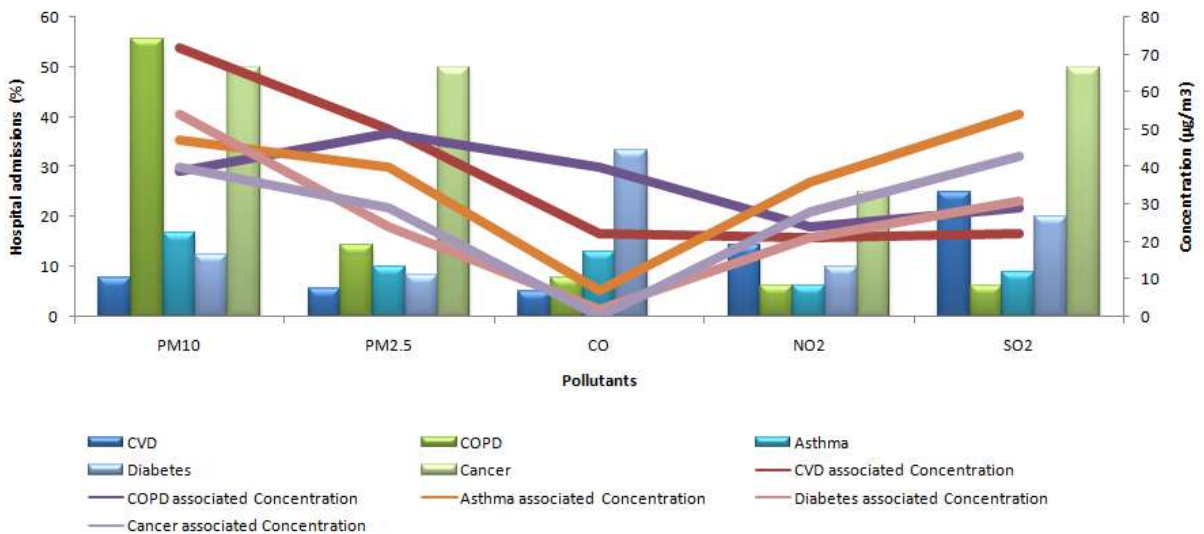


Fig. 2a: Overall outline of hospital admissions due to physiological diseases and associated concentration levels of PM<sub>2.5</sub>, PM<sub>10</sub>, CO, NO<sub>2</sub> & SO<sub>2</sub>.

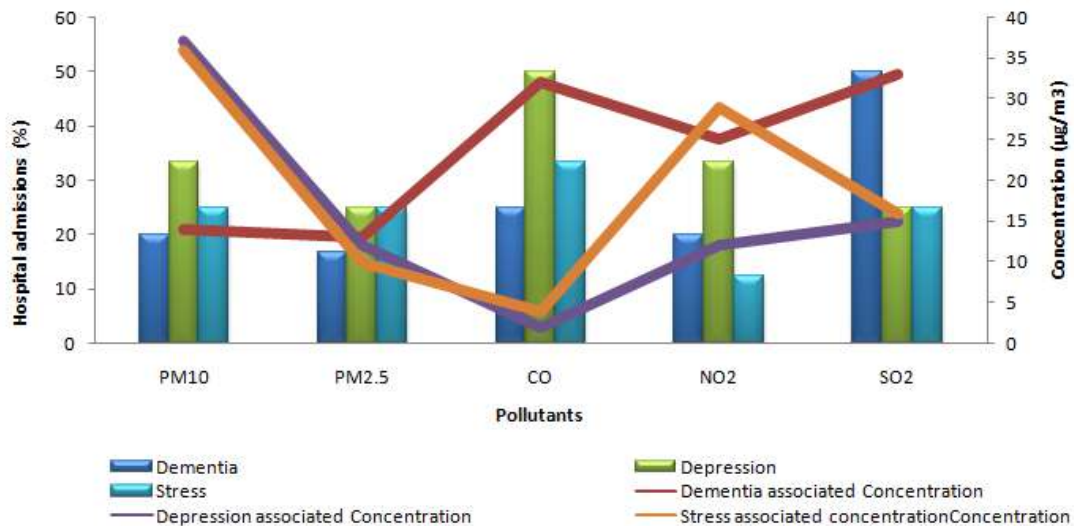


Fig. 2b: Overall outline of hospital admissions due to psychological diseases and associated concentration levels of PM<sub>2.5</sub>, PM<sub>10</sub>, CO, NO<sub>2</sub> & SO<sub>2</sub>.

PM<sub>2.5</sub> is the least contributor associated with 15% of cases of psychological diseases.

We have accessed a total of 369 high-impact factor research articles to carry out this review analysis. The articles having incomplete information, repetitive and outdated observations (n=82), and unknown time duration (n=02) were excluded. The remaining research papers for considering the study were 285. Further 60 papers out of 285 were excluded based on mislaid data for morbidity, mortality, sex, and age, related to diseases categorized as physiological and psychological diseases. Thus a total of 225 research articles

were sorted out for this study. Regarding the number of patients, out of the records of 23 years (1997-2020) international publications which reported insufficient patients were excluded (n=22). The number of remaining patients (7781054) was integrated into the analysis. A primary cohort of 2754056 patients includes a record considering the effect of air pollution concentration levels on different age group populations. The methodology and results about the impact of air pollution in terms of physiological diseases (2088092 patients) and psychological diseases (665975 patients) were incorporated into the study for an efficient outcome. Figure 1

shows the detailed flow diagram for a description of the study material.

Age is one of the important factors for measuring the degree of severity of the disease. The severity of the disease for diverse groups based on age versus hospital admissions due to physiological and psychological diseases is shown in figure 3. We have classified 6 major age groups (0-15, 15-30, 30-45, 45-55, 55-65 & >65). There were 60% cases of asthma, 30% COPD, and 10% cancer cases found to be associated with the age group of  $\leq 15$  years which is very sensitive mainly for children. The adult set of age (15-30 years) was associated with all diseases prominently except diabetes. However, 35% of cases of diabetes in the age group of 55-65, 45% of cases of CVD with >65 years, and 35% of cases of cancer were found in the  $\geq 65$  age group.

As per our study, psychological diseases prevail in the age group of  $\geq 65$ . This age group is mostly suffered from dementia ( $\leq 50\%$ ). The age group of 30-45 is the main age group that is burdened with stress, while the > 65 age group was found with high depression. The age group of 30-45 was more affected by stress levels that decreased as an increase in age was observed (45<55<65< above 65 years).

## CONCLUSION

The inference of this study from the data analysis of five air pollutants' concentrations versus five physiological and three psychological diseases will be an indication for further studies on diverse characteristics related to possible causes of impact. The study also provides an overview to categorize the strength of diseases for vulnerable population groups. It

was observed that particulate matter ( $PM_{10}$  &  $PM_{2.5}$ ) is the main contributor to all types of respiratory diseases. There is more than enough work done on the impact of  $PM_{10}$  and  $PM_{2.5}$  concentrations on physiological diseases, thus psychological diseases require more consideration.  $PM_{10}$  alone is the main pollutant that causes approx. 40%-50% cases of psychological diseases, whereas surprisingly  $PM_{2.5}$  with only 15% cases is the least contributor for psychological diseases. Among all five air pollutants, CO evidenced minimum effectiveness for cancer and CVD cases but highly effective for depression followed by  $PM_{2.5}$  and  $SO_2$ .  $NO_2$  was found to be a prominent cause of hospital admissions due to COPD and the second largest contributor to depression also. Adults are suffered from stress and increasing order of  $PM_{10}$ ,  $NO_2$ , and  $SO_2$  concentrations are responsible for stress. There are less data available for the effects of air pollutants on psychological diseases thus more rigorous research work is required for decisive health effects.

## ABBREVIATIONS

- APOE: Apolipo protein E
- CB1 & CB2 Receptors: Cannabinoid receptors
- COAD: Chronic Obstructive Airway Disease
- Coex: Exhaled Carbon monoxide
- CoHb: Carboxy Hemoglobin
- ERV<sub>1</sub>: Expiratory reserve volume 1
- FBG Levels: Fasting Blood glucose levels
- FEV: Forced Expiratory Volume

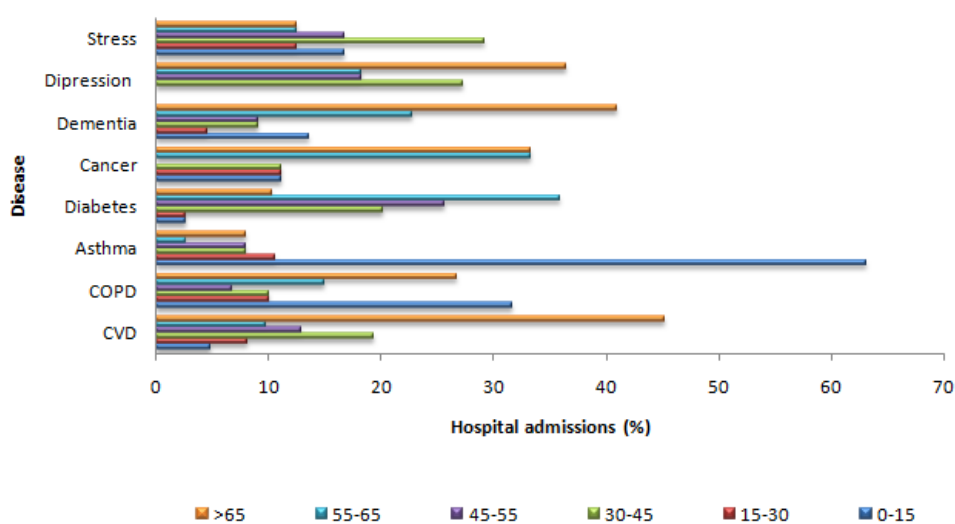


Fig. 3: The overall outline of hospital admissions due to physiological and psychological diseases as per age groups.

FVC: Forced Vital Capacity  
 HbA1C: Glycosylated Haemoglobin A1C  
 HBO<sub>2</sub>: Hyperbaric oxygen  
 IHD: Ischemic Heart Disease  
 LIDAR: Light detecting and ranging systems  
 PEF: Peak expiratory flow  
 SRAW: specific airway resistance z  
 TNF-alpha: Tumour necrosis factor-alpha  
 t-PA: tissue Plasminogen Ac

## REFERENCES

- Abe, T. Tokuda, Y. Ohde, S., Ishimastu, S., Nakamura, T. and Birrer, R.B. 2009. The relationship of short-term air pollution and weather to ED visits for asthma in Japan. *Am. J. Emerg. Med.*, 27(2): 153-159. <https://doi.org/10.1016/j.ajem.2008.01.013>.
- Abelsohn, A.R. and Sanborn, M. 2010. Lead and children: clinical management for family physicians. *Canad. Family Phys.*, 56(6): 531-535.
- Achilleos, S. 2016. Particle Pollution: Trends, Sources, Components and Health. (Doctoral dissertation). Harvard T. H. Chan School of Public Health, pp. 1-114.
- Almendra, R., Santana, P., Vasconcelos, J., Silva, G., Gonçalves, F. and Ambrizzi, T. 2017. The influence of the winter North Atlantic Oscillation index on hospital admissions through diseases of the circulatory system in Lisbon, Portugal. *Int J Biometeorol.*, 61(2): 325-333. DOI 10.1007/s00484-016-1214-z
- Alwahaibi, A. and Zeka, A. 2016. Respiratory and allergic health effects in a young population in the proximity of a major industrial park in Oman. *J Epidemiol. Community Health.*, 70(2): 174-180. doi:10.1136/jech-2015-205609.
- Anand, J.S., Schetz, D., Waldman, W. and Wiśniewski, M. 2017. Hyperventilation with Maintenance of Isocapnia. An Old New Method in Carbon Monoxide Intoxication. *PloS One.*, 12(1): e0170621. doi.org/10.1371/journal.pone.0170621
- Annesi-Maesano, I., Baiz, N., Banerjee, S., Rudnai P. and Rive S. 2013. Indoor air quality and sources in schools and related health effects. *J. Toxicol. Environ. Health*, 16(8): 491-550. doi.org/10.1080/10937404.2013.853609.
- Atkinson, R.W., Analitis, A. and Samoli, E. 2016. Short-term exposure to traffic-related air pollution and daily mortality in London, UK. *J. Expo. Sci. Environ. Epidemiol.*, 26(2): 125. <http://dx.doi.org/10.1038/jes.2015.65>
- Awadi, A.L. 2018. Assessment of indoor levels of volatile organic compounds and carbon dioxide in schools in Kuwait. *J. Air Waste Manag. Assoc.*, 68(1): 54-72. <https://doi.org/10.1080/10962247.2017.1365781>.
- Banerjee, M., Siddique, S., Dutta, A., Mukherjee, B. and Ray, M.R. 2012. Cooking with biomass increases the risk of depression in pre-menopausal women in India. *Soc. Sci. Med.*, 75(3): 565-572. <https://doi.org/10.1016/j.socscimed.2012.03.021>.
- Bauer, M., Moebus, S. and Möhlenkamp, S. 2010. Urban particulate matter air pollution is associated with subclinical atherosclerosis: results from the HNR (Heinz-Nixdorf-Recall) J. *Am. Coll. Cardio.*, 56(22): 1803-1808. DOI: 10.1016/j.jacc.2010.04.065
- Biswas, J., Upadhyay, E., Nayak, M. and Yadav, A.K. 2011. An analysis of ambient air quality conditions over Delhi, India from 2004 to 2009. *NPJ Clim. Atmos. Sci.*, 1: 214-224. doi:10.4236/acs.2011.14024.
- Bowe, B., Xie, Y., Li, T., Yan, Y., Xia, M. and Al-Aly, Z. 2018. The 2016 global and national burden of diabetes mellitus is attributable to PM<sub>2.5</sub> air pollution. *Lancet Planet Health*, 2: e301-e312. doi: 10.1016/S2542-5196(18)30140-2
- Çapraz, Ö., Deniz, A. and Doğan, N. 2017. Effects of air pollution on respiratory hospital admissions in İstanbul, Turkey, 2013 to 2015 *Chemosphere*, 181: 544-50. <https://doi.org/10.1016/j.chemosphere.2017.04.105>
- Chandrashekhara, S. 2014. C-reactive protein: An inflammatory marker with a specific role in physiology, pathology, and diagnosis. *Int. J. Rheumatol. Clinic. Immunol.*, 2(S1): 56-78.
- Chang, K.H., Chang, M.Y., Muo, C.H., Wu, T.N., Chen, C.Y. and Kao, C.H. 2014. Increased risk of dementia in patients exposed to nitrogen dioxide and carbon monoxide: a population-based retrospective cohort study. *PloS One*, 9(8): e103078. doi.org/10.1371/journal.pone.0103078
- Che, L., Li, Y. and Gan, C. 2017. Effect of short-term exposure to ambient air particulate matter on the incidence of delirium in a surgical population. *J. Sci. Rep.*, 7(1): 15461. DOI:10.1038/s41598-017-15280-1.
- Chen, C.C., Chiu, H.F. and Yang, C.Y. 2016. Air pollution exposure and daily clinical visits for allergic rhinitis in a subtropical city: Taipei, Taiwan. *J. Toxicol. Environ. Health Part A*, 79(12): 494-501. doi.org/10.1080/15287394.2016.1182002
- Cheng, N., Li, Y., Sun, F., Chen, C., Wang, B., Li, Q. and Cheng, B. 2018. Ground-level NO<sub>2</sub> in urban Beijing: Trends, distribution, and effects of emission reduction measures. *Aero. Air Qual. Res.*, 18: 343-356. doi: 10.4209/aaqr.2017.02.0092
- Chi, X., Winderlich, J., Mayer, J.C. and Panov, C. 2013. Long-term measurements of aerosol and carbon monoxide at the ZOTTO tall tower to characterize polluted and pristine air in the Siberian taiga. *Atmos. Chem. Phys.*, 13(24): 12271-12298.
- Chuang, K.J., Chan, C.C., Su, T.C., Lee, C.T. and Tang, C.S. 2007. The effect of urban air pollution on inflammation, oxidative stress, coagulation, and autonomic dysfunction in young adults. *Am. J. Respir. Crit. Care Med.*, 176(4): 370-376. DOI: 10.1164/rccm.200611-1627OC
- Cifuentes, P. 2019. Application of the public health exposes framework to estimate phenotypes of resilience in a model Ohio African-American Women's cohort. *J. Urban Health.*, 96(1): 57-71.
- Cole-Hunter, T. and de Nazelle, A. 2018. Estimated effects of air pollution and space-time-activity on cardiopulmonary outcomes in healthy adults: a repeated measures study. *Environ. Int.*, 111: 247-259. doi.org/10.1016/j.envint.2017.11.024
- Coogan, P.F. White, L.F. and Jerrett, M. 2012. Air pollution and incidence of hypertension and diabetes mellitus in black women living in Los Angeles. *Circulation*, 125(6): 767-72. DOI: 10.1161/CIRCULATION-NAHA.111.052753
- Cordella, M. and Poiani, A. 2014. Behavioral Oncology: Psychological, Communicative, and Social Dimensions. Springer, Netherlands. <https://doi.org/10.1007/978-1-4614-9605-2>
- Deng, Q., Deng, L., Lu, C., Li, Y. and Norbäck, D. 2018. Parental stress and air pollution increase childhood asthma in China. *Environ. Res.*, 165: 23-31. doi.org/10.1016/j.envres.2018.04.003
- Galán, I. and Simón, L. 2015. Assessing the effects of the Spanish partial smoking ban on cardiovascular and respiratory diseases: Methodological issues. *BMJ Open*, 5(12): e008892.
- Gezerman, A.O. and Çorbacioğlu, B.D. 2018. Air Pollution In Asia and Its Effect on Human Health: Air pollution in Asia. In Gezerman, A.O., Didem, B. and Gurjar, B.R. (eds), *Effective Solutions to Pollution Mitigation for Public Welfare*, IGI Global, MA, pp. 19-29. doi.org/10.4018/978-1-5225-3379-5
- Goldberg, M.S., Burnett, R.T., Stieb, D.M., Brophy, J.M., Daskalopoulou, S.S., Valois, M.F. and Brook, J.R. 2013. Associations between ambient air pollution and daily mortality among elderly persons in Montreal, Quebec. *Sci. Total Environ.*, 463: 931-42. doi.org/10.1006/enrs.2001.4242
- Greenberg, N., Carel, R.S., Derazne, E., Tiktinsky, A., Tzur, D. and Portnov, B.A. 2017. Modeling long-term effects attributed to nitrogen dioxide (NO<sub>2</sub>) and sulfur dioxide (SO<sub>2</sub>) exposure on asthma morbidity in a nationwide cohort in Israel. *J. Toxicol. Environ. Health Part A*, 80(6): 326-337. doi.org/10.1080/15287394.2017.1313800



- Guarnieri, M. and Balmes, J.R. 2015. Outdoor air pollution and asthma. *Lancet*, 383(9928): 158-1592. doi: 10.1016/S0140-6736(14)60617-6.
- Halonen, J.I., Zanobetti, A., Sparrow, D., Vokonas, P.S. and Schwartz, J. 2011. Outdoor temperature is associated with serum HDL and LDL. *Environ. Res.*, 111(2): 281-287.
- Hansen, A.B., Ravnskjaer, L. and Loft, S. 2016. Long-term exposure to fine particulate matter and incidence of diabetes in the Danish Nurse Cohort. *Environ. Int.*, 91: 243-250. doi.org/10.1016/j.envint.2016.02.036
- Hazlehurst, M., Nurius, P. and Hajat, A. 2018. Individual and neighborhood stressors, air pollution, and CVD. *Int. J. Environ. Res. Public Health*, 15(3): 472. doi: 10.1161/JAHA.116.003947.
- He, Q.Q., Wong, T.W. and Du, L. 2010. Effects of ambient air pollution on lung function growth in Chinese schoolchildren. *Respir. Med.*, 104(10): 1512-1520.
- Hoffmann, B., Luttmann-Gibson, H. and Cohen, A. 2012. Opposing effects of particle pollution, ozone, and ambient temperature on arterial blood pressure. *Environ. Health Perspect.*, 120(2): 241-6. doi.org/10.1289/ehp.1103647
- Honda, T., Pun, V. C., Manjourides, J. and Suh, H. 2017. Associations between long-term exposure to air pollution, glycosylated hemoglobin, and diabetes. *Int. J. Hyg. Environ. Health*, 220(7): 1124-1132.
- Kalairasan, G. 2018. Source apportionment studies on particulate matter (PM10 and PM2.5) in ambient air of urban Mangalore, India. *J. Environ. Manage.*, 217: 815-824. doi.org/10.1016/j.jenvman.2018.04.040
- Karakatsani, A., Kapitsimadis, F. and Pipikou, M. 2010. Ambient air pollution and respiratory health effects in mail carriers. *Environ. Res.*, 110(3): 278-285.
- Katanoda, K., Sobue, T. and Satoh, H. 2011. An association between long-term exposure to ambient air pollution and mortality from lung cancer and respiratory diseases in Japan. *J. Epidemiol.*, 5: 1102090211. doi.org/10.2188/jea.JE20100098
- Kaya, H., Coşkun, A. and Beton, O. 2016. COHgb levels predict the long-term development of acute myocardial infarction in CO poisoning. *Am. J. Emerg. Med.*, 34(5): 840-844.
- Khamutian, R., Najafi, F. and Soltanian, M. 2015. The association between air pollution and weather conditions with an increase in the number of admissions of asthmatic patients in emergency wards: a case study in Kermanshah. *Med. J. Islam. Repub. Iran*, 29: 229.
- Kim, C., Jung, S.H. and Kang, D.R. 2010. Ambient particulate matter is a risk factor for suicide. *Am. J. Psychiatry*, 167(9): 1100-1107. doi.org/10.1176/appi.ajp.2010.09050706.
- Kocamaz, E., Adiguzel, E., Buket, E.R., Gundogdu, G. and Kucukatay, V. 2012. Sulfite leads to neuron loss in the hippocampus of both normal and SOX-deficient rats. *Neurochem. int.*, 61(3): 341-346.
- Koenig, J.Q. 2016. Sulfur Dioxide exposure in humans. *Toxicology*, 15: 334.
- Krämer, U., Herder, C., Sugiri, D., Strassburger, K., Schikowski, T., Ranft, U. and Rathmann, W. 2010. Traffic-related air pollution and incident type 2 diabetes: Results from the SALIA cohort study. *Environ. Health Perspect.*, 118(9): 1273-1279. doi.org/10.1289/ehp.0901689.
- Laumbach, R.J., Kipen, H.M. and Kelly-McNeil, K. 2011. Sickness response symptoms among healthy volunteers after controlled exposures to diesel exhaust and psychological stress. *Environ. Health Perspect.*, 119(7): 945-950. https://doi.org/10.1289/ehp.1002631.
- Lee, H., Myung, W., Kim, S.E., Kim, D.K. and Kim, H. 2018. Ambient air pollution and completed suicide in 26 South Korean cities: Effect modification by demographic and socioeconomic factors. *Sci. Total Environ.*, 639: 944-951. doi.org/10.1016/j.scitotenv.2018.05.210
- Lelieveld, J., Evans, J.S., Fnais, M., Giannadaki, D. and Pozzer, A. 2015. The contribution of outdoor air pollution sources to premature mortality on a global scale. *Nature*, 525(7569): 367-371. doi:10.1038/nature15371
- Lertxundi, A., Baccini, M. and Lertxundi, N. 2015. Exposure to fine particle matter, nitrogen dioxide, and benzene during pregnancy and cognitive and psychomotor developments in children at 15 months of age. *Environ. Int.*, 80: 33-40. doi.org/10.1016/j.envint.2015.03.007.
- Lin, H., Guo, Y., Zheng, Y., Di, Q. and Liu, T. 2017. Long-term effects of ambient PM<sub>2.5</sub> on hypertension and blood pressure and attributable risk among older Chinese adults. *Hypertension*, 69(5): 806-812. doi.org/10.1136/thorax.55.11.930.
- Manisalidis, I.E., Stavropoulou, A., Stavropoulos and Bezirtzoglou, E. 2020. Environmental and health impacts of air pollution: A review. *Publ. Health Front.*, 8: 14. doi.org/10.3389/fpubh.2020.00014.
- Mathur, M., Mathur, G. and Mathur, M. 2017. Assessment of carbon monoxide at traffic signals, toll plazas, and in the main roadside built houses and impact of its chronic exposure on public health. *Int. J. Adv. Res. Ideas Innov. Technol.*, 3: 224-226.
- Mayer, M. 2000. Association of serum bilirubin concentration with risk of coronary artery disease. *Clin Chem.*, 46(11): 1723-1727.
- Mehta, A.J., Kubzansky, L.D., Coull, B.A. et al. 2015. Associations between air pollution and perceived stress: The veterans administration normative aging study. *N. Engl. J. Med.*, 14(1): 10. doi:10.1186/1476-069X-14-10
- Middleton, N., Yiallourou, P., Kleanthous, S. et al. 2008. A 10-Y time-series analysis of respiratory and cardiovascular morbidity in Nicosia, Cyprus: The effect of short-term changes in air pollution and dust storms. *Environ Health*, 7(1): 39. doi:10.1186/1476-069X-7-39
- Miller, M.R., Shaw, C.A. and Langrish, J.P. 2012. From particles to patients: oxidative stress and the cardiovascular effects of air pollution. *Future Cardiol.*, 8(4): 577-602.
- Mohammadi, A., Azhdarpoor, A., Shahsavani, A. and Tabatabaee, H. 2016. Investigating the health effects of exposure to criteria pollutants using AirQ 2.2.3 in Shiraz, Iran. *Aeros. Air Qual Res.*, 16(4): 1035-1043. doi: 10.4209/aaqr.2015.07.0434
- Möller, A., Agius, R.M. and de Vocht, F. 2013. Long-term exposure to PM10 and NO2 in association with lung volume and airway resistance in the MAAS birth cohort. *Environ. Health Perspect.*, 121(10): 1232-1238.
- Morakinyo, O.M., Adebowale, A.S., Mokgobu, M.I. and Mukhola, M.S. 2017. Health risk of inhalation exposure to sub-10 µm particulate matter and gaseous pollutants in an urban-industrial area in South Africa: An ecological study. *Br. Med. J.*, 7(3): e013941 dx.doi.org/10.1136/bmjopen-2016-013941.
- Nair, A.J., Nandini, M., Adappa, S. and Mahabala, C. 2017. Carbon monoxide exposure among police officers working in a traffic-dense region of Southern India. *Toxicol. Ind. Health*, 33(1): 46-52. https://doi.org/10.1177/0748233716654071
- Naylor, M., Enserro, D.M., Beiser, A.S., Cheng, S., DeCarli, C., Vasan, R.S. and Seshadri, S. 2016. Association of exhaled carbon monoxide with stroke incidence and subclinical vascular brain injury: Framingham Heart Study. *Stroke*, 47(2): 383-389.
- Nkosi, V., Hoek, G., Wichmann, J. and Vuyi, K.V. 2016. Acute respiratory health effects of air pollution on asthmatic adolescents residing in a community in close proximity to-mine dump in South Africa: Panel Stud., 11: 257-269. dx.doi.org/10.15739/irjpeh.16.032
- Oudin, A., Forsberg, B. and Adolfsson, A.N. 2016. Traffic-related air pollution and dementia incidence in northern Sweden: A longitudinal study. *Environ. Health Perspect.*, 124(3): 306-312.
- Padhi, B.K., Adhikari, A., Satapathy, P., Patra, A.K., Chandel, D. and Panigrahi, P. 2017. Predictors and respiratory depositions of airborne endotoxin in homes using biomass fuels and LPG gas for cooking. *J. Expo. Sci. Environ. Epidemiol.*, 27(1): 112-117.
- Pun, V.C., Manjourides, J. and Suh, H. 2017. Association of ambient air pollution with depressive and anxiety symptoms in older adults: Results from the NSHAP study. *Environ. Health Perspect.*, 125(3): 342-348. https://doi.org/10.1289/EHP494
- Qiu, H., Schooling, C.M. and Sun, S. 2018. Long-term exposure to fine particulate matter air pollution and type 2 diabetes mellitus in elderly: A cohort study in Hong Kong. *Environ. Int.*, 113: 350-356. https://doi.org/10.1289/EHP494

- Rajeswari, K.P. 2019. A Study on Pulmonary Function Tests, Thyroid Profile and Absolute Eosinophil Count among Male Petrol Pump Workers. Doctoral dissertation, Coimbatore Medical College, Coimbatore. <http://repository-tnmgrmu.ac.in/id/eprint/11116>
- Ramos, C.A., Wolterbeek, H.T. and Almeida, S.M. 2014. Exposure to indoor air pollutants during physical activity in fitness centers. *Build. Environ.*, 82: 349-360. doi.org/10.1016/j.buildenv.2014.08.026.
- Robledo, C.A., Mendola, P. and Yeung, E. 2015. Preconception and early pregnancy air pollution exposures and risk of gestational diabetes mellitus. *Environ. Res.*, 137: 316-322. doi.org/10.1016/j.envres.2014.12.020
- Rudra, C.B., Williams, M.A., Sheppard, L., Koenig, J.Q., Schiff, M.A., Frederick, I.O. and Dills, R. 2010. Relation of whole blood carboxyhemoglobin concentration to ambient carbon monoxide exposure estimated using regression. *Am. J. Epidemiol.*, 171(8): 942-951. doi.org/10.1136/thx.2007.094953
- Russell, A. 2018. Assessment of impacts of regulations on mobile emissions: Impacts of regulations on air quality and emergency department visits in the Atlanta metropolitan area. (1999–2013). *Res. Rep. Health Eff. Inst.*, 21: 195
- Sass, V., Kravitz-Wirtz, N., Karceski, S.M., Hajat, A., Crowder, K. and Takeuchi, D. 2017. The effects of air pollution on individual psychological distress. *Health Place*, 48: 72-79. doi.org/10.1016/j.healthplace.2017.09.006
- Schikowski, T., Sugiri, D. and Ranft, U. 2005. Long-term air pollution exposure and living close to busy roads are associated with COPD in women. *Respir Res.*, 6(1): 152. doi:10.1186/1465-9921-6-152.
- Schimmel, J., George, N., Schwarz, J., Yousif, S., Suner, S. and Hack, J.B. 2018. Carboxyhemoglobin levels induced by cigarette smoking outdoors in smokers. *J. Med. Toxicol.*, 14(1): 68-73.
- Schraufnagel, D.E.J.R. and Balmes, C.T. 2019. Air pollution and noncommunicable diseases: a review by the forum of international respiratory societies' environmental committee, part 2: Air pollution and organ systems. *Chest*, 155(2): 417-426. doi.org/10.1016/j.chest.2018.10.041
- Shankardass, K., Jerrett, M., Dell, S.D., Foty, R. and Stieb, D. 2015. Spatial analysis of exposure to traffic-related air pollution at birth and childhood atopic asthma in Toronto, Ontario. *Health Place*, 34: 287-295.
- Singh, K.D. 2016. Air Pollution in New Delhi Gets Dangerously High During Diwali Celebrations. *The wall street Journal, Indian Real-time wsj.com/indiarealtime/2016/11/01/* Accessed on 12 March 2017.
- Sun, X.W., Chen, P.L., Ren, L., Lin, Y.N., Zhou, J.P., Ni, L. and Li, Q.Y. 2018. The cumulative effect of air pollutants on the acute exacerbation of COPD in Shanghai, China. *Sci. Total Environ.*, 622: 875-881. doi.org/10.1016/j.scitotenv.2017.12.042
- Szyszkowicz, M., Kousha, T., Kingsbury, M. and Colman, I. 2016. Air pollution and emergency department visits for depression: a multicity case-crossover study. *Environ. Health Insights*, 10: 493.
- Tingting, X., Danming, Y. and Xin, C. 2018. Non-surgical treatment of obstructive sleep apnea syndrome. *Eur. Arch. Oto-Rhino-L.*, 275(2), 335-346.
- Tomie, A., Festa, E.D., Sparta, D.R. and Pohorecky, L.A. 2003. Lever conditioned stimulus-directed autoshaping induced by saccharin-ethanol unconditioned stimulus solution: Effects of ethanol concentration and trial spacing. *Alcohol*, 30:35-44.
- Upadhyay, E.J. Biswas, M. Nayak, S. Ghosh, Chaitanya, P. Manali, D. 2020. An Analysis to Understand the Air Quality Pattern of North Indian Cities. *Pollut. Res.*, 39(4): 257.
- Upadhyay, E., Nayak, M. and Biswas, J. 2017. Air Quality Status of Lucknow City—A Case Study. *Int. J. Eng. Res. Technol.*, 5(12): 69-74. 2017.
- Vahlsing, C. and Smith, K.R. 2012. Global review of national ambient air quality standards for PM10 and SO2 (24 h). *Air Qual. Atmos. Health*, 5(4): 393-399.
- Veronesi, A., Pecoraro, V. and Zauli, S. 2017. Use of carboxyhemoglobin as a biomarker of environmental CO exposure: a critical evaluation of the literature. *Environ. Sci. Pollut. Res.*, 24(33): 25798-25809.
- Vert, C., Sánchez-Benavides, G. and Martínez, D. 2017. Effect of long-term exposure to air pollution on anxiety and depression in adults: A cross-sectional study. *Int. J. Hyg. Environ. Health*, 220(6): 1074-1080. <https://doi.org/10.1016/j.ijheh.2017.06.009>.
- Wang, Y., Eliot M.N. and Koutrakis, P. 2014. Ambient air pollution and depressive symptoms in older adults: results from the MOBILIZE Boston study. *Environ. Health Perspect.*, 122(6): 553-558. <https://doi.org/10.1289/ehp.1205909>
- Weaver, G.M. and Gauderman, W.J. 2017. Traffic-related pollutants: exposure and health effects among Hispanic children. *Am. J. Epidemiol.*, 187(1): 45-52. doi:10.1093/aje/kwx223.
- Weinmayr, G., Romeo, E., De Sario, M., Weiland, S.K. and Forastiere, F. 2010. Short-term effects of PM<sub>10</sub> and NO<sub>2</sub> on respiratory health among children with asthma or asthma-like symptoms: a systematic review and meta-analysis. *Environ. Health Perspect.*, 118(4): 449-457. doi.org/10.1289/ehp.0900844
- Wellenius, G.A., Burger, M.R. and Coull, B.A. 2012. Ambient air pollution and the risk of acute ischemic stroke. *Arch. Intern. Med.*, 172(3): 229-234. doi.org/10.1016/j.amjcard.2005.08.061
- Wu, C.F., Shen, F.H. and Li, Y.R. 2016. Association of short-term exposure to fine particulate matter and nitrogen dioxide with acute cardiovascular effects. *Sci. Total Environ.*, 569: 300-305. <https://doi.org/10.1016/j.scitotenv.2016.06.084>
- Xu, Q., Li, X., Wang, S. and Wang, C. 2016. Fine particulate air pollution and hospital emergency room visit for respiratory disease in urban areas in Beijing, China, in 2013. *PLoS One*, 11(4): e0153099.
- Yang, A.C., Tsai, S.J. and Huang, N.E. 2011. Decomposing the association of completed suicide with air pollution, weather, and unemployment data at different time scales. *J. Affect. Disord.*, 3: 275-281. doi.org/10.1016/j.jad.2010.08.010
- Zanobetti, A., Dominici, F., Wang, Y. and Schwartz, J.D. 2014. A national case-crossover analysis of the short-term effect of PM<sub>2.5</sub> on hospitalizations and mortality in subjects with diabetes and neurological disorders. *Environ. Health.*, 13(1): 38. doi:10.1186/1476-069X-13-38.
- Zhang, Q., Li, L. and Smith, M. 2013. Exhaled carbon monoxide and its associations with smoking, indoor household air pollution, and chronic respiratory diseases among 512 000 Chinese adults. *Int. J. Epidemiol.*, 42(5): 1464-1475. <https://doi.org/10.1093/ije/dyt158>
- Zijlema, W.L., Wolf, K. and Emery, R. 2016. The association between air pollution and depressed mood in 70,928 individuals from four European cohorts. *Int. J. Hyg. Environ. Health*, 219(2): 212-219. <https://doi.org/10.1093/ije/dyt158>



# Radiological Study of Water for Human Use and Consumption in Rural Areas of the Central Zone of the State of Veracruz, Mexico

J.A. Vásquez-Contreras<sup>†\*</sup>, M.R. Castañeda-Chávez<sup>\*\*</sup>, O.P. Castellanos-Onorio<sup>\*</sup>, V. Alcántara-Méndez<sup>\*\*</sup>, P. Zuñiga-Ruiz<sup>\*\*</sup>, A. García-Saldaña<sup>\*\*</sup> and M. Díaz-González<sup>\*</sup>

<sup>\*</sup>Department of Chemical-Biochemical Engineering, Tecnológico Nacional de México/Instituto Tecnológico de Veracruz, Calzada Miguel Ángel de Quevedo 2779, Formando Hogar, 91897, Veracruz, Veracruz, México

<sup>\*\*</sup>Department of Postgraduate and Research, Tecnológico Nacional de México/Instituto Tecnológico de Boca del Río, Carretera Veracruz-Cordoba, km 12, 94290, Boca del Río, Veracruz, México

<sup>†</sup>Corresponding autor: J.A.Vásquez-Contreras; jorge.vc@veracruz.tecnm.mx

Nat. Env. & Poll. Tech.  
Website: [www.neptjournal.com](http://www.neptjournal.com)

Received: 26-03-2022

Revised: 06-06-2022

Accepted: 07-06-2022

## Key Words:

Radioactivity

Gross alpha and beta activity

Annual effective dose

Radiological study of water

## ABSTRACT

A study and spatiotemporal radiological characterization of water for human use and consumption in the main rural populations of the center of the State of Veracruz was carried out, covering 22 municipalities. The objective was to estimate the annual effective dose as a function of the concentration of gross alpha and beta activity. For this purpose, a low background proportional flux detection system calibrated with NIST-traceable radioactive standards was used. Sampling included only wells, springs, and lagoons in rural areas that supply water to these populations. The decision was based on the fact that these do not have a physicochemical treatment and was carried out during the dry and rainy seasons, which became factors of impact on the radiological material. The analysis included the results of 195 samples from 22 municipalities which showed ranges in the gross alpha of 0.052-0.95 BqL<sup>-1</sup> with a mean of 0.376 ± 0.101 BqL<sup>-1</sup> and a gross beta of 0.034-1.48 BqL<sup>-1</sup> with a mean of 0.389 ± 0.108 BqL<sup>-1</sup>. The comparison of the values obtained with respect to those of other countries and their complement with analysis of variance showed that there was a significant difference, particularly, for the results of gross alpha in the municipality of Alto Lucero de Gutiérrez Barrios and gross beta in Nautla and Tecolutla in dry and rainy seasons (at a probability of p ≤ 0.05 with the Tukey-Kramer HSD statistical test). A correlation between gross alpha and gross beta was also performed with an r of -0.18 and -0.44 in dry and rainy seasons. This means that among the radionuclides, the major sources of beta radiation are uranium and thorium decay series radionuclides. For the determination of gross alpha, the municipalities in the mountainous zones showed lower values of this activity than the municipalities in the coastal zone. Gross alpha activity values of 0.95 ± 0.11 BqL<sup>-1</sup> were detected in the municipality of Alto Lucero de Gutiérrez Barrios in the locality of Arroyo Agrio, which exceeded the limit of the Official Mexican Standard.

## INTRODUCTION

While water is an essential element for the life of all living beings on the planet, it is also a fundamental human right (Rickert et al. 2016). It is estimated that the composition of water on planet Earth is 97.5% saline and only 2.5% corresponds to fresh water; of that 2.5%, almost 30% is groundwater, 70% is in glaciers and other snow layers, and only less than 1% is surface water found in rivers, lakes and other bodies of water (CONAGUA 2011). The above confirms that little water is applied for human consumption and use and that it meets the requirements and quality from the sanitary point of view. Including chemical, physical and biological factors; highlighting that radioactivity is a physical factor; taking into account

that the monitoring of radioactive contamination has been established in several laws. All of this is a result of the citizenry's interest sparked by related human activity and accidents such as Chernobyl and Fukushima. This highlights the significance of population-wide water and food consumption being monitored for radioactivity.

According to data from the United Nations Scientific Committee (UNSCEAR 2000), the population of the planet receives a per capita radiation dose of 2.8072 mSv, of which 2.4 mSv are due to natural background, and 1.2 mSv are received through inhalation and 0.3 through ingestion. Despite this, studies of measurements made in Germany show that the average annual radiation exposure for children is 0.047

mSv, which is within the defined limits for alpha and beta activity concentration (Obrikat et al. 2004).

Italy presents studies of radioactivity in drinking water with values below the levels recommended by the WHO (Jia et al. 2009), as does Serbia (Jankovic et al. 2012).

In Pakistan, the values of mean concentrations of  $^{226}\text{Ra}$ ,  $^{232}\text{Th}$ , and  $^{40}\text{K}$ , were  $11.3 \pm 2.3$ ,  $5.2 \pm 0.4$ , and  $140.9 \pm 30.6$   $\text{mBqL}^{-1}$  (Fatima et al. 2007). In Kazakhstan, the calculated effective doses for adults resulting from consumption of the investigated waters are in the range from 1.0 to 18.7  $\mu\text{Sv}$  per year. These doses are lower than the WHO and IAEA reference value (100  $\mu\text{Sv}$  per year) for drinking water. (Yamamoto et al. 2010). In Tunisia, water analyses were found to be below the reference levels (Gharbi et al. 2010).

In South Africa, the minimum and maximum gross alpha activity obtained was  $0.0041 \text{ BqL}^{-1}$  and  $0.0053 \text{ BqL}^{-1}$  respectively, while the minimum and maximum gross beta activity obtained from the water samples was  $0.0083 \text{ BqL}^{-1}$  and  $0.0105 \text{ BqL}^{-1}$  respectively. The reference level used in this country of  $1.38 \text{ BqL}^{-1}$  for gross beta activity (Madzunya et al. 2020).

In Ghana, the radiation levels are within the natural background radiation levels found in the literature (Faanu et al. 2014).

## MATERIALS AND METHODS

### Study Area

The state of Veracruz measures approximately  $71,826 \text{ km}^2$  and has a population of approximately 8,062,579 as of 2020 (INEGI. 2020). West Longitude ( $98^\circ 40' 53.40''$ ,  $93^\circ 36' 28.44''$ ), North Latitude ( $17^\circ 08' 13.20''$ ,  $22^\circ 28' 18.48''$ ) 22 municipalities (Fig. 1).

### Water Sampling

The samples were collected in rural areas of the central part

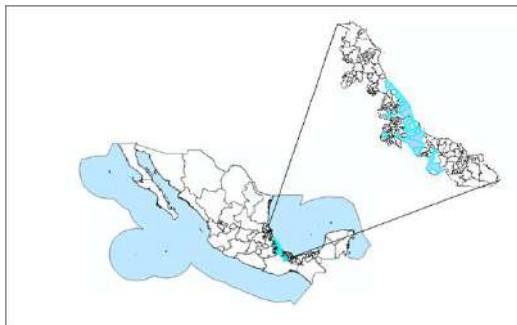


Fig. 1: Municipalities in the study area Veracruz, México.

of the state of Veracruz A total of 195 samples were collected in 22 municipalities, in dry and rainy seasons, where the different types of soil in the center of the state were considered. This was based on the fact that Veracruz is a state with a great diversity of types of geomorphology since it has been from coastal plains to significant mountains. To correctly locate the points, a Garmin GPS was used (GPSMAP64) and it was corroborated with UTM coordinates for geopositioning. The water was collected from supply sources such as aquifers, springs, and wells, using 3.7 L plastic containers with lids and covers, previously washed and rinsed with distilled water, then dried and marked with the sampling guide. The procedure for collecting the water was carried out according to the standard, fulfilling the following steps: the container was opened and submerged in water, which was allowed to run long enough so that the sample did not come from stagnant water. No reagents were added for the preservation or conditioning of the sample. Each sample was labeled appropriately and was not acidified since its radiological analysis did not exceed more than seven calendar days from the collection to receipt of the sample at the State Public Health Laboratory of Veracruz (Standard methods 2020).

### Test Method

The methods were validated and authorized by the Federal Commission for the Protection of Sanitary Risks (COFEPRIS 2020). With respect to the measurement of conductivity, its value is determined with the volume to be used, its purpose is to control the mass thickness for every  $20 \text{ cm}^2$  of counting area, methyl orange indicator solution is added at 0.05% and acidified to pH 4 with 1N nitric acid or at the change of color from orange to cinnamon yellow.

### Determination of Gross Alpha and Beta Activities by a Gas Flow Proportional Counter (GFPC)

Gross alpha and beta activity measurements, called the thin source deposition method, were performed as a first step in the radiological characterization of water samples, and this method included the standards.

The procedure is accredited by Federal Commission for the Protection of Sanitary Risks (COFEPRIS. 2020). For gross alpha and beta analyses, 2000 mL of each water sample was evaporated at  $\leq 90^\circ \text{C}$  (ensuring deposits with a mass thickness of less than  $1.48\text{E}-2 \text{ g.cm}^{-2}$ ). The residue obtained was transferred to a stainless steel planchet (2 inches in diameter and 1/8 inch deep). Each planchet was measured for gross alpha and gross beta activity during an interval of 60 or 120 minutes per sample depending on the conductivity of the samples at the state public health laboratory of the State of Veracruz using a Canberra Tennelec low-background. The

detector type was a gas flow proportional counter (GFPC) with a mixture of 90% argon and 10% methane (P-10) and an automatic transport of 50 samples. The high operating voltage of the detector was set at 1425 V. The background of each detector was determined by counting empty planchets for 60 min and 120 min.

The detectors were calibrated in 2020 for alpha and beta efficiency using <sup>241</sup>Am (11.0 Bq ± 1.44% at 1σ) and <sup>90</sup>Sr/<sup>90</sup>Y (16.3 Bq ± 1.25% at 1σ) standard solution sources, which were supplied by the Eckert & Zeigler Company.

The gross alpha efficiency was 0,0405±2.96 % at 1σ to 0.1740 ± 1.90 % at 1σ, with a mass thickness (3,07 E<sup>-3</sup>-1,48 E<sup>-2</sup> g.cm<sup>-2</sup>) and a mathematical model Ef=0,287 EXP(-139m) where *m* is the mass thickness of the deposit (g/cm<sup>2</sup>) while the gross beta efficiency was 0,3322 ± 1,36% at 1σ to 0,3909 ± 1,34% at 1σ, with a mass thickness (3,03 E<sup>-3</sup>-1,26 E<sup>-2</sup> g/cm<sup>2</sup>) and a mathematical model Ef=0,416 EXP (-17,4 m) where *m* is the mass thickness of the deposit (g/cm<sup>2</sup>). The seven solutions were carried out with the same sample preparation procedure analyzed; evaporated on a planchet and counted by the Canberra Tennelec GFPC.

The gross alpha and beta activity concentrations can be obtained as given in Equation (1)

$$A = \frac{cpmt - cpmf}{Ef * V * 60} \dots(1)$$

Where *A* is the gross alpha activity concentration or the beta activity concentration of the sample (BqL<sup>-1</sup>); *cpmt* is the gross sample count (alpha or beta); *cpmf* are background

counts (alpha or beta); *Ef* is the counting efficiency (alpha or beta); *V* is the sample volume(L); 60 is the Becquerel conversion to disintegrations per minute.

The minimum detectable concentration (MDC) for the gross alpha or gross beta activity concentration is calculated as given in Equation (2) (Currie 1968):

$$MDC = \frac{4.66 \sigma cpmf}{Ef * V * 60} \dots(2)$$

Where:

$\sigma = cpmf$  background uncertainty (alpha or beta).

**Estimation of the Annual Effective Dose**

The annual effective dose (AED) associated with human use and consumption, specifically with the ingestion of water, was not estimated because we worked with a gross alpha and beta activity concentration.

The radiological criteria for water quality in Mexico were established by the Ministry of Health in the NOM-201-SSA1-2015 (2015) and NOM-127-SSA1-2021 (2021), which contemplates gross alpha radioactivity parameters with a limit of 0.5 BqL<sup>-1</sup> and the gross beta radioactivity parameter with a limit of 1.0 BqL<sup>-1</sup>, regulations published in the Official Journal of the Federation. These values are 0.5 BqL<sup>-1</sup> for the gross alpha activity concentration and 1 BqL<sup>-1</sup> for the gross beta activity concentration according to the IAEA (IAEA 2016) and World Health Organization (WHO 2017). However, the

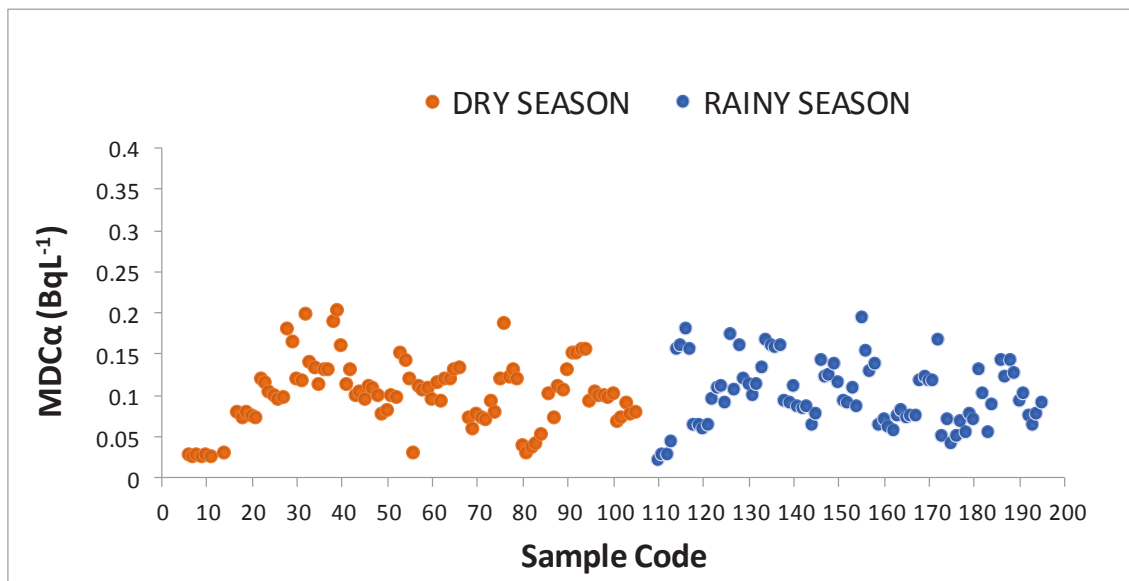


Fig. 2: The minimum detectable concentration of gross alpha in 2020.

annual effective dose value is as stated  $0.1 \text{ mSv}^{-1}$  and which is similar to the value recommended by the World Health Organization, WHO.

## RESULTS AND DISCUSSION

The minimum detectable concentrations MDCs of gross alpha and beta were calculated according to equation 2, the minimum detectable concentrations for gross alpha were found in a range of 0.025-0.202 with an average value of  $0.1009 \text{ BqL}^{-1}$  for the dry season and the rainy season in a range of 0.022-0.193 with an average value of  $0.1008 \text{ BqL}^{-1}$  (Fig. 2 and Fig.3).

The statistical test for comparison of means (t-test) reports that there is no significant difference ( $p > 0.05$ ) for the MDCs of alpha activity in the water samples in the dry and rainy seasons.

In Fig. 2, the values of the minimum detectable concentrations for the water sampled in the dry and rainy seasons for gross alpha and beta are of the order, with the MDC of the gross beta concentration for the dry season being 0.042-0.232 with an average value of  $0.1226 \text{ BqL}^{-1}$  and for the rainy season in a range of 0.049-0.232 with an average value of  $0.1262 \text{ BqL}^{-1}$ . According to the statistical test of comparison of means (t-test), the MDCs of beta activity in the water samples during the dry and wet seasons do not differ significantly ( $p > 0.05$ ).

## Determination of Gross Alpha and Beta Activity Concentrations

Of the 195 water samples analyzed in the dry and rainy seasons, only 16 samples exceeded the  $\text{MDC}_\alpha$ . In the dry season, only 11 samples presented an alpha activity concentration higher than the  $\text{MDC}_\alpha$  and 5 samples an alpha activity concentration higher than the  $\text{MDC}_\alpha$  in the rainy season; 115 samples recorded a beta activity concentration higher than the  $\text{MDC}_\beta$ , of which 58 samples presented a beta activity concentration higher than the  $\text{MDC}_\beta$  in the dry season and 57 samples presented a beta activity concentration higher than  $\text{MDC}_\beta$  in the rainy season.

Table 1 presents the gross alpha and beta activity concentration values in the dry and rainy seasons, with mean values, range and minimum detectable concentrations, the mean value of alpha activity concentration in the dry season was  $0.2409 \pm 0.0986 \text{ BqL}^{-1}$ ; with a range of 0.055-0.91  $\text{BqL}^{-1}$  and for the gross beta activity concentration was  $0.4208 \pm 0.1149 \text{ BqL}^{-1}$  with a range of 0.034-1.41  $\text{BqL}^{-1}$ , as for the rainy season the mean values for the gross alpha activity concentration were  $0.5102 \pm 0.1038 \text{ BqL}^{-1}$  with a range of 0.052-0.95  $\text{BqL}^{-1}$ , and for the mean gross beta activity concentration was  $0.3563 \pm 0.1008 \text{ BqL}^{-1}$ , with a range of 0.025-0.25  $\text{BqL}^{-1}$ . The performance of the statistical test (t-test) when performing the comparison of the gross alpha and beta activity concentrations in the dry and rainy seasons did not present a significant difference at a reliability value of ( $p > 0.05$ ).

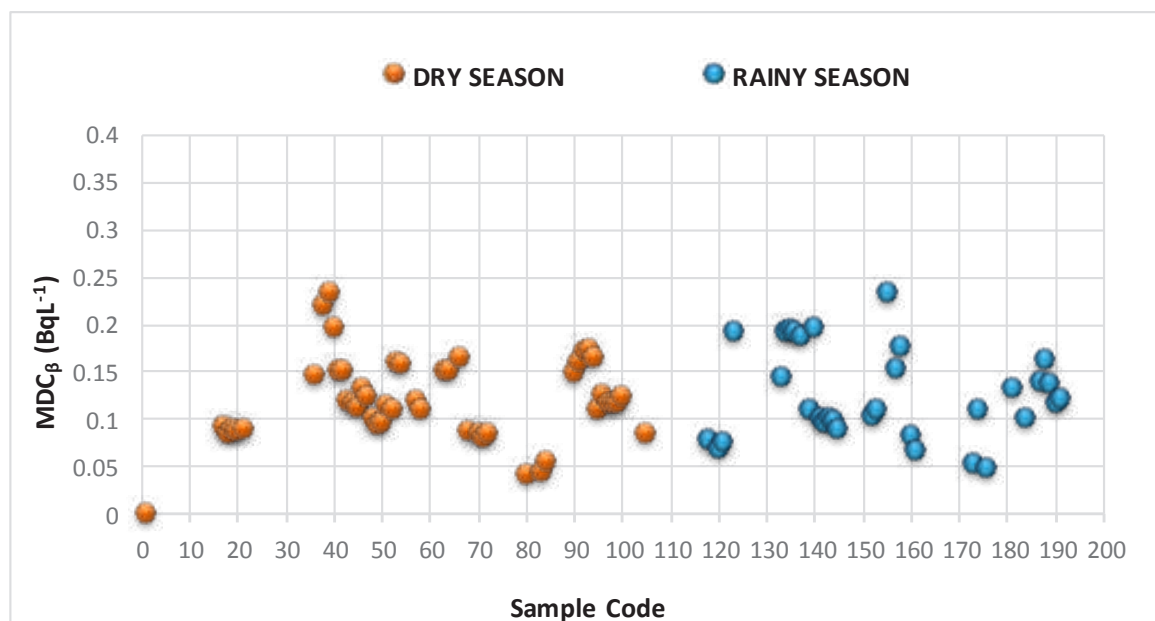


Fig. 3: The minimum detectable concentration of gross beta in 2020.

Although the results of the gross alpha activity concentration in the water samples taken in the municipality of Alto Lucero de Gutiérrez Barrios correspond to 56.25% of the total that was recorded, 45.45% of the samples in the dry season are from this locality, and the gross alpha activity concentration reached 80% with the samples taken in the rainy season. A gross alpha activity concentration of 0.95 BqL<sup>-1</sup> in the rainy season is reported as a maximum reached, so follow-up measures should be considered at this location. Monitoring should also be carried out in the municipalities of Nautla and Tecolutla because they reached values of interest.

It was demonstrated that none of the samples collected in the dry and rainy seasons in this study reached the limit established by Mexican regulations of 1.0 BqL<sup>-1</sup> for the gross beta.

Next, a comparative table was made of the mean values recorded from the different sampling sites in the 22 municipalities of the state of Veracruz, resulting in the construction of Table 2 for the determination of the concentration of gross alpha and beta activity. A comparative table of the concentration values of other studies in different countries was also elaborated (Table 3).

Table 1: Mean gross alpha and gross beta activity concentration of the sample with uncertainties.

Total Samples 105	Dry Season				Total Samples 90	Rainy Season			
	Gross Alpha A <sub>α</sub>	ΔA <sub>α</sub>	Gross Beta A <sub>β</sub>	ΔA <sub>β</sub>		Gross Alpha A <sub>α</sub>	ΔA <sub>α</sub>	Gross Beta A	ΔA <sub>β</sub>
Mean	0.2409	0.0986	0.4208	0.1149	Mean	0.5102	0.1038	0.3563	0.1008
Range	0.055-0.91	0.032-0.27	0.034-1.41	0.021-0.32	Range	0.052-0.95	0.03-0.14	0.057-1.48	0.025-0.25

Table 2: Mean values of the gross alpha and gross beta activity concentration in the dry and rainy stations.

Municipality	Latitude	Longitude	Mean Alpha in the dry station	Mean Beta in the dry station	Mean Alpha in the rainy station	Mean Beta in the rainy station
ALTO LUCERO DE GUTIERREZ BARRIOS	19.70641	-96.43159	0.418	0.596	0.625	0.755
BANDERILLA	19.58988	-96.94425	0.027	0.079	0.030	0.091
TECOLUTLA	20.25037	-96.94425	0.063	1.238	0.163	0.530
CAMERINO Z. MENDOZA	18.79346	-97.19874	0.076	0.088	0.063	0.081
COTAXTLA	18.82034	-96.34871	0.105	0.153	0.101	0.180
NAUTLA	20.15704	-96.71706	0.156	1.304	0.140	1.318
JAMAPA	19.03812	-96.22573	0.129	0.167	0.115	0.215
ACTOPAN	19.69853	-96.41605	0.160	0.190	0.161	0.191
VEGA DE ALATORRE	19.96973	-96.60164	0.104	0.121	0.095	0.146
JUCHIQUE DE FERRER	19.79197	-96.67081	0.091	0.103	0.078	0.097
LA ANTIGUA	19.36506	-96.36894	0.111	0.267	0.128	0.190
MEDELLIN	19.01771	-96.13743	0.105	0.127	0.094	0.115
NOGALES	18.82071	-97.16451	0.133	0.203	0.153	0.198
ORIZABA	18.86339	-97.07618	0.070	0.084	0.063	0.087
PASO DE OVEJAS	19.303	-96.439	0.086	0.142	0.075	0.150
TLALIXCOYAN	18.7439	-96.1375	0.136	0.354	0.128	0.398
PLAN DE LAS HAYAS	19.76176	-96.67541	0.040	0.044	0.052	0.068
PLAYA VICENTE	17.83254	-95.81519	0.098	0.482	0.068	0.378
SOLEDAD DE DOBLADO	19.04594	-96.42056	0.115	0.167	0.094	0.124
TIERRA BLANCA	18.63032	-96.15522	0.153	0.168	0.117	0.322
TRES VALLES	18.231	-96.132	0.099	0.118	0.097	0.119
YANGA	18.82543	-96.79071	0.077	0.175	0.077	0.164

Table 3: Gross alpha and gross beta activity concentrations in some countries.

Region/Country	$A_{\alpha}$ (BqL <sup>-1</sup> )		$A_{\beta}$ (BqL <sup>-1</sup> )		References
	Mean	Range	Mean	Range	
Wisconsin/USA	-	0.037-5.320	-	0.0925-1.924	Arndt and West (2004)
Albania	-	0.01-0.126	-	0.029-0.884	Cfarku et al. (2014)
Saudi Arabia	3.15	-	5.39	-	Alkhomashi et al. (2016)
Balaton/Hungary	-	0.026-1.749	-	0.033-2.015	Jobbagy et al. (2011)
Galati/Romania	0.022	<0.006-0.0852	0.076	<0.025-0.435	Pintilie et al. (2016)
Jordania	-	0.26-3.58	-	0.51-3.43	Alomari et al. (2019)
Katsina/Nigeria	-	0.080-2.300	-	0.120-4.970	Muhammad et al. (2010)
Turkey	0.164	0.007-3.042	0.555	0.021-4.845	Taskin et al. (2013)
TurKey	0.0493	-	0.1284	-	Osmanlioglu et al. (2007)
Southern/Vietnam	0.183	0.024-0.748	0.152	0.027-0.632	Ho et al. (2020)
South Africa	-	0.0041-0.0053	-	0.0083-0.0105	Madzunya et al. (2020)
Veracruz /México	0.376	0.052-0.95	0.389	0.034-1.48	Present study

### Annual Effective Dose Assessment for Ingestion of the Water Samples

The radionuclides causing the gross alpha and beta concentration results were not investigated in this work. The radionuclides that promote gross alpha activity in water are mainly due to uranium and its progeny, such as <sup>226</sup>Ra. The gross beta activity concentration is probably caused by the contribution of <sup>40</sup>K, <sup>210</sup>Pb, and <sup>228</sup>Ra. The sixteen samples with gross alpha activity concentration above the MDC and the ninety-five samples with gross beta activity concentration were contrasted to determine the strength of correlation between gross alpha and beta activity concentrations, presenting a negative Pearson correlation factor of -0.18 and -0.44 for the dry and rainy seasons respectively, which meant that there is a null correlation and that the radionuclides constituting this gross alpha and beta activity concentration are probably of natural origin such as mentioned by the Vietnamese author Ho et al. (2020) (Fig. 4 and Fig. 5).

During the research, the annual effective dose of the water samples was also evaluated with the respective compliance with national and international regulations. Therefore, the results presented are a reference that will allow an analysis to be made for decision-making, at some point there are significant changes in these values due to the contribution of radioactivity in the environment due to industrial and other anthropogenic activities in principle the great majority is below 0.1 mSv per year corresponding to not exceeding the guide value of the WHO.

### CONCLUSIONS

The present work can be used as a reference in the concentration of gross alpha and beta activity today, since the only nuclear power plant in Mexico, Laguna Verde, is located in the state of Veracruz, as well as the different anthropogenic activities that involve the use of radioactive material and that can increase with their contribution the concentration of activity in the studied area.

Future estimates should be carried out in the study area where there were higher concentrations of alpha activity, as is the case of Alto Lucero de Gutiérrez Barrios, and determine the specific activity of its constituents. At this site, it was observed that during the rainy season most of the measurements exceeded the official Mexican standard and the WHO and IAEA levels, and their increases were concentrated forcefully due to runoff phenomena as manifested during the rainy season.

It was possible to achieve all the objectives that were established in this work, as well as to have made the comparison of the results in the dry season and rainy season, complying with the sampling design and statistical analysis that included the variables regarding the dilution factor and location of the samples. This allowed for the internal and external validity of the research.

The performance of the method used by the Radiological Control of the LESP with respect to the WHO recommendations, in this part, by using as indicators the values of 1 BqL<sup>-1</sup> for gross beta activity and 0.5 BqL<sup>-1</sup> for gross alpha activity was adequate, complying with the limit requested by the current standard.



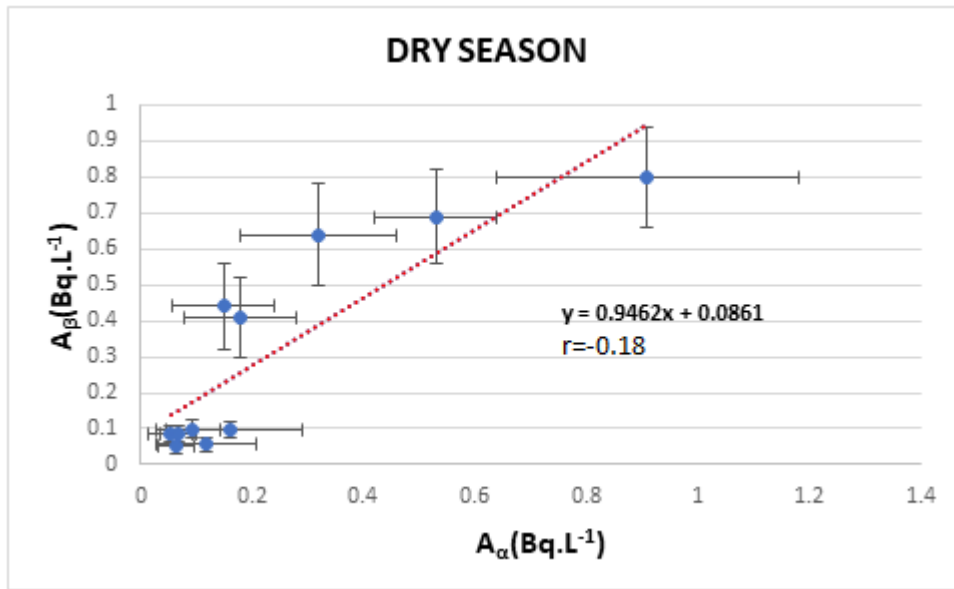


Fig. 4: The correlation function of the gross alpha and gross beta activity concentrations for the samples in the dry season of 2020.

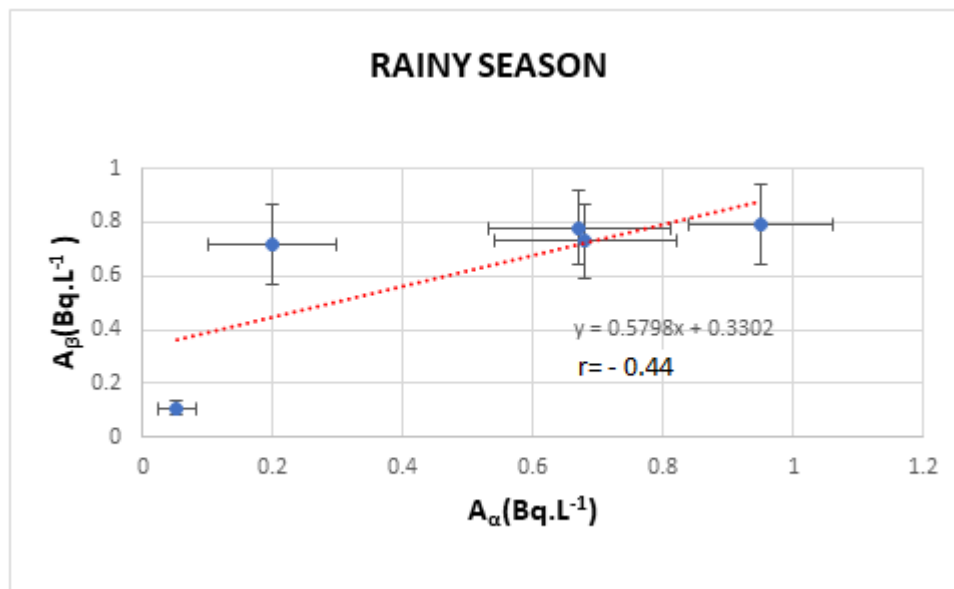


Fig. 5: The correlation function of the gross alpha and gross beta activity concentrations for the samples in rainy 2020.

**ACKNOWLEDGEMENTS**

The authors wish to express their gratitude to the State Laboratory of Public Health, and to the Instituto Tecnológico de Boca del Río, for providing their facilities for the development of this study. Last but not least, to the reviewers of this manuscript for their contributions and valuable criticisms, as well as to all the people who contribute to science through this article.

**REFERENCES**

Alkhomashi, N., Al-Hamarneh, I.F. and Almasoud, F.I. 2016. Determination of natural radioactivity in irrigation water of drilled wells in northwestern Saudi Arabia. *Chemosphere*, 144: 1928-1936.

Alomari, A.H., Saleh, M.A., Hashim, S., Alsayaheen, A. and Abdeldin, I. 2019. Measurement of gross alpha and beta activity concentration in groundwater of Jordan: groundwater quality, annual effective dose, and lifetime risk assessment. *J. Water Health*, 17(6): 957-970.

Arndt, M.F. and West, L. 2004. A Study of the Factors Affecting the Gross Alpha Measurement, and a Radiochemical Analysis of some

- Groundwater Samples from the State of Wisconsin Exhibiting an Elevated Gross Alpha Activity. Proceedings 51st Annual Conference on Radiobioassay and Radiochemical Measurement, Oct 30-Nov 4, 2004 Cincinnati, pp. 1-56.
- Cfarku, F., Xhixha, G., Bylyku, E., Zdruli, P., Mantovani, F., Përpunja, F. and Thoma, H. 2014. A preliminary study of gross alpha/beta activity concentrations in drinking waters from Albania. *J. Radioanal. Nucl. Chem.*, 301(2): 435-442.
- Comisión Federal Para Protección Contra Riesgos Sanitarios (COFEPRIS) 2020. oficio No.CAS/TA/08/2021.
- Comisión Nacional del Agua (CONAGUA). 2011. Estadísticas del Agua en México. Available in [http://www.conagua.gob.mx/conagua07/contenido/documentos/sina/capitulo\\_8.pdf](http://www.conagua.gob.mx/conagua07/contenido/documentos/sina/capitulo_8.pdf)
- Currie, L.A. 1968. Limits for qualitative detection and quantitative determination-application to radiochemistry. *Anal.Chem.*, 68: 586
- Faanu, A., Lawlubi, H., Kpeglo, D. O., Darko, E. O., Emi-Reynolds, G., Awudu, A. R. and Kpodzro, R. 2014. Assessment of natural and anthropogenic radioactivity levels in soils, rocks, and water in the vicinity of Chirano Gold Mine in Ghana. *Radiat. Protect. Dosimetr.*, 158(1): 87-99.
- Fatima, I., Zaidi, J.H., Arif, M. and Tahir, S.N.A. 2007. Measurement of natural radioactivity in bottled drinking water in Pakistan and consequent dose estimates. *Radiat. Protect. Dosimetr.*, 123(2): 234-240.
- Gharbi, F., Baccouche, S., Abdelli, W., Samaali, M., Oueslati, M. and Trabelsi, A. 2010. Uranium isotopes in Tunisian bottled mineral waters. *J. Environ. Radioact.*, 101(8): 589-590.
- Ho, P.L., Minh, V.T., Van Chinh, D., Thanh, T.T. and Van Tao, C. 2020. Simultaneous determination of gross alpha/beta activities in groundwater for ingestion effective dose and its associated public health risk prevention. *Sci. Rep.*, 10(1): 1-10.
- IAEA 2016. Criteria for Radionuclide Activity Concentrations for Food and Drinking Water, IAEA-TECDOC-1788.
- INEGI 2020. Anuario estadístico y geográfico de Veracruz, México. Available in: [www.inegi.org.mx](http://www.inegi.org.mx)
- Jankovic, M.M., Todorović, D.J., Todorović, N.A. and Nikolov, J. 2012. Natural radionuclides in drinking waters in Serbia. *Appl. Radiat. Isotop.*, 70(12): 2703-2710.
- Jia, G., Torri, G. and Magro, L. (2009). Concentrations of  $^{238}\text{U}$ ,  $^{234}\text{U}$ ,  $^{235}\text{U}$ ,  $^{232}\text{Th}$ ,  $^{230}\text{Th}$ ,  $^{228}\text{Th}$ ,  $^{226}\text{Ra}$ ,  $^{228}\text{Ra}$ ,  $^{224}\text{Ra}$ ,  $^{210}\text{Po}$ ,  $^{210}\text{Pb}$  and  $^{212}\text{Pb}$  in drinking water in Italy: Reconciling safety standards based on measurements of gross  $\alpha$  and  $\beta$ . *J. Environ. Radioact.*, 100(11): 941-949.
- Jobbagy, V., Kavasi, N., Somlai, J., Dombóvári, P., Gyöngyösi, C. and Kovács, T. 2011. Gross alpha and beta activity concentrations in spring waters in Balaton Upland, Hungary. *Radiat. Measure.*, 46(1): 159-163.
- Madzunya, D., Dudu, V.P., Mathuthu, M. and Manjoro, M. 2020. Radiological health risk assessment of drinking water and soil dust from Gauteng and North West Provinces, in South Africa. *Heliyon*, 6(2): e03392.
- Muhammad, B.G., Jaafar, M.S. and Akpa, T.C. 2010. A study of gross concentrations of alpha and beta activity in groundwater from the Katsina area of northern Nigeria. *Radiat. Protect. Dosimetr.*, 141(2): 127-133.
- NOM-127-SSA1-2021. 2021. Environmental Health, water for human use and consumption. Permissible limits of quality and treatment to which the water must be submitted for its purification. Norma Oficial Mexicana.
- NOM-201-SSA1-2015. 2015. Products and services. Water and ice for human consumption, packaged and in bulk. Sanitary specifications. Norma Oficial Mexicana.
- Obrikat, D., Beyermann, M., Bünger, T. and Viertel, H. 2004. Natural radionuclides in mineral water in Germany. *Kerntechnik*, 69(5-6): 223-226.
- Osmanlioglu, A.E., Kam, E. and Bozkurt, A. 2007. Assessment of background radioactivity level for Gaziantep region of southeastern Turkey. *Radiat. Protect. Dosimetr.*, 124(4): 407-410.
- Pintilie, V., Ene, A., Georgescu, L.P., Moraru, L. and Iticescu, C. 2016. Measurements of gross alpha and beta activity in drinking water from Galati region, Romania. *Roman. Rep. Phys.*, 68(3): 1208-1220.
- Rickert, B., Chorus, I. and Schmoll, O. 2016. Protecting surface water for health. Identifying, assessing, and managing drinking-water quality risks in surface-water catchments. World Health Organization.
- Standard methods for the examination of water and wastewater, 2017. 23rd edition, pp. 7-12.
- Taskin, H., Asliyukse, H., Bozkurt, A. and Kam, E. 2013. Natural radioactivity in bottled mineral and thermal spring waters of Turkey. *Radiat. Protect. Dosimetr.*, 157(4): 575-578.
- UNSCEAR. 2000. Sources and Effects of Ionizing Radiation. United Nations Publication, New York, pp. 35-36.
- World Health Organization (WHO) 2017. Guidelines for drinking-water quality. WHO Publications, Geneva, pp. 203-221
- Yamamoto, M., Tomita, J., Sakaguchi, A., Ohtsuka, Y., Hoshi, M. and Apalikov, K. 2010. Uranium isotopes in well water samples as drinking sources in some settlements around the Semipalatinsk Nuclear Test Site, Kazakhstan. *J. Radioanal. Nucl. Chem.*, 284(2): 309-314.



# An Assessment of Ongoing Developments in Water Resources Management Incorporating SWAT Model: Overview and Perspectives

S. K. Verma<sup>†</sup>, A. D. Prasad and M. K. Verma

Department of Civil Engineering, National Institute of Technology, Raipur, Chhattisgarh, India

<sup>†</sup>Corresponding author: S. K. Verma; shashiv50@gmail.com

Nat. Env. & Poll. Tech.  
Website: [www.neptjournal.com](http://www.neptjournal.com)

Received: 17-02-2022

Revised: 04-04-2022

Accepted: 09-04-2022

## Key Words:

Hydrological modeling  
Runoff  
Sediment yield  
Sensitivity analysis  
SWAT model

## ABSTRACT

Land and water are the most necessary natural resources because the entire life system depends on them. It requires proper management to achieve maximum utilization. When used in conjunction with Arc GIS, the Soil and Water Assessment Tool (SWAT) is a promising model for simulating the agricultural watershed since it can forecast runoff, sediment and nutrient transport, and erosion under various management scenarios. Furthermore, the model is better at evaluating both the spatial and non-spatial variation of hydrological methods under a very large watershed. This study uses the methodology employed by the SWAT model for the estimation of surface runoff and sediment yield and discusses in detail the setup of the model computer file needed by the model sensitivity analysis parameter and validation area unit. SWAT is a well-known hydrological modeling method used in many hydrologic and environmental simulations. Over 17 years (2005-2021), 212 studies were found from various peer-reviewed scientific publications listed on the SWAT online database (CARD). Applicability studies were divided into five categories: water resources, streamflow, erosion, land-use planning and agricultural settings, climate change scenarios, and model parameterization. Hydrologic phenomena and adaptations in various river basins have been investigated. They mostly examined environmental impacts and preventive techniques to ensure an understanding of effective environmental regulation. Streamflow susceptibility to climatic changes was shown in climate change studies. Modeling streamflow parameters, model modifications, and basin-scale calibrations were investigated. Future simulation aspects such as data sharing and the opportunity for improved future analysis are also discussed. A multimodal approach to future simulations, as well as more efforts to make local data available, are both very good ideas.

## INTRODUCTION

Simulators of hydrological and water resources have been widely utilized to overcome global water resource concerns. The assessments were mostly done using computer simulations, which save money by simulating real-world processes in space and time. They are also utilized to understand physical processes better and quantify water distribution in varied environments. Hydrologic models and new improvements in GIS have made this technique a good choice for water resources and environmental assessment. So, they have been used more recently to assess water resources (Krysanova & White 2015, Zhang & Al-Asadi 2019). The SWAT model is widely recognized as one of the key hydrological models used to address hydrologic and environmental concerns globally. Derived from the SWAT model, it is physically dependent, semi-distributed, and continuous-time to analyze water resources and anticipate the implications of land use/cover changes and land man-

agement strategies on soil degradation, sedimentation, and non-point source pollution (Arnold et al. 1998, Gassman et al. 2007). It has also been reported in peer-reviewed journals in curve number alteration, wetland applications, and best management practices (Akoko et al. 2021). Previous SWAT model uses have been studied. For example, compared to other models identified and reviewed, the historical development and applications of the SWAT model (mainly in the USA and parts of Europe) (Akoko et al. 2021, Arnold & Fohrer 2000, Harper et al. 1999). More than 20 peer-reviewed journal articles describing the SWAT model used in the Upper Nile Basin were identified and reviewed (Van Griensven et al. 2012). Since 2006, 126 articles have been highlighted and assessed in Southeast Asia, focusing on model applications, existing complexities, and potential research suggestions (Tan et al. 2019). Over 100 SWAT studies (published 1998–2016) were identified and reviewed in Brazil (de Almeida Bressiani

et al. 2015). This article review attempted to consolidate and classify SWAT applications into similar domains as the research mentioned above, even though some of these topics are strongly related or overlap. The objectives of this review study are to describe the significant findings of SWAT applications in various studies, examine the existing problems associated with SWAT model applications, and identify prospective SWAT model modifications that could be used in future research.

## OVERVIEW OF REVIEWED PAPERS

On April 30, 2021, the SWAT literature database (<https://swat.tamu.edu/>) returned almost 3500 articles using the keyword “SWAT”. After selecting the articles written in India, the number of papers was reduced to 212. The database contains peer-reviewed publications (CARD). Fig. 1 depicts the review methodological framework.

The SWAT model is a physically-dependent continuous time scale, deterministic and long-term simulation model (Mishra et al. 2006). It is an open-source model and was put together by the United States Department of Agriculture and Agriculture Analysis Service (USDA-ARS) and the Texas A & M University system (Mishra et al. 2006). This model’s major goal is to understand how

land management affects water, agriculture, and sediment outputs.

## Application Considering for Streamflow Simulations

Water resource studies have focused on extreme weather occurrences (floods and droughts) at several regional and national levels. For example, the SWAT model can simulate stream flows in ungauged basins (Chaibou et al. 2016). Analyze runoff processes to help build water resources (Dessie et al. 2014), and calibrate the rainfall-runoff model using remote sensing data (Milzow et al. 2011). The SWAT model was used to study surface and groundwater resources. In dry regions, measuring water supplies is important for simulating major hydrologic processes (Ouassar et al. 2009, Sultan et al. 2011).

## Application Considering as a Context of Climate Change

The SWAT model was used to evaluate future climate change impacts on water supplies. The research looked at water management, the availability of water, and agriculture, as shown in Fig. 2. The results were utilized to manage and develop water resources in the Nzoia catchment, Kenya (Githui et al. 2009), and emphasize the importance of the precipita-

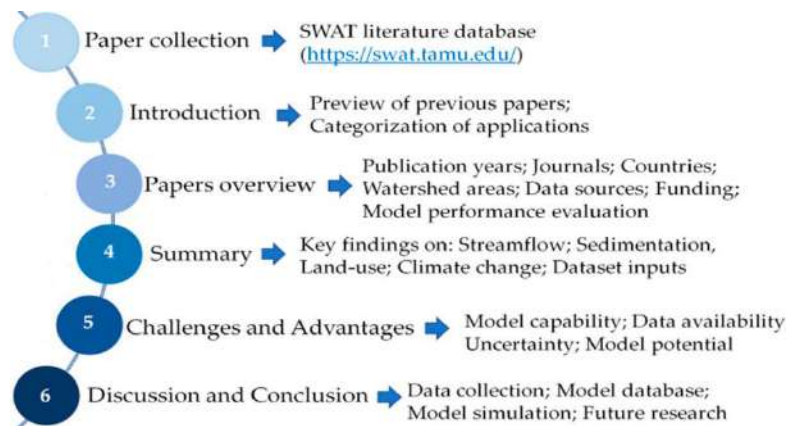


Fig. 1: Review methodology framework (Akoko et al. 2021).



Fig. 2: SWAT model application in climate change context (Githui et al. 2009).

tion–evaporation balance in the river Mitano basin, Uganda (Kingston & Taylor 2010). Increased rainfall and greater temperatures predicted by SWAT will put an enormous strain on Ethiopia's Keleta River watershed's hydrologic cycle (Bekele et al. 2019).

### Application Considering for Sediment Yield Erosion

The SWAT model was used to study sedimentation in numerous Indian river basins and designate and prioritize soil erosion-prone locations (Gessesse et al. 2015), and provide quantitative insight into the efficiency of erosion control strategies (Hunink et al. 2013). Various researchers found that installing filter strips, stone bunds, and forestry reduced current sediment outputs using the SWAT model. The SWAT model does not adequately reflect several physical phenomena, making the exact interpretation of quantitative data difficult (Betrie et al. 2011). The model was made to replace the sediment-rating curve and long-term sediment yield rate forecast. It was used to see how dams would affect semi-arid watersheds (Ndomba et al. 2008, Zettam et al. 2017).

### Model Application for the Agricultural Land Use/Land Cover Management

The use of the SWAT model to assess the influence of agricultural conservation strategies on water and sediment output helped to develop ecologically sound watershed management and development plans (Mwangi et al. 2015). The SWAT model was used to demonstrate how afforestation in dry sub-basins can counteract afforestation stress in wet sub-basins without affecting the basin's water balance (Nyeko et al. 2012). An analysis of daily flow sensitivity to changes in land use (converting a portion of the forestland to agricultural) found that a decrease in rainfall equals an increase in annual flow (Melesse et al. 2008). The SWAT model was used to investigate the effects of agriculture production on the hydrological processes and simulate the effects of agricultural conservation measures such as contour farming, grass strips, and filter strips on sediment and water yield (Mourad & Sang 2018).

### Model Application for the Parameter Selection and Input Dataset

According to Fig. 3, the following applications are included in the case of a model application for the selection of parameter and input datasets such as basin-scale calibration, water yield evaluation, and simulations using rain-gauge and worldwide rainfall data. The SWAT model was used to characterize and assess effective soil moisture capacity distribution across hydrological response units (HRUs) and systematically calibrate a complicated basin-scale model without explicitly matching model outputs to measured streamflow (Easton et al. 2011). By comparing uncalibrated SWAT model simulations of the leaf area index (LAI) utilizing the modified (SWAT-T) and normal SWAT vegetation growth modules, the structural improvements of SWAT's vegetation growth module for tropical forests were proved (Alemayehu et al. 2017). In the Wami River basin, the SWAT model was further constrained to reduce equivocality and forecast uncertainty, suggesting that adopting extra constraints leads to more reliable and accurate predictions (Wambura et al. 2018).

### SENSITIVITY ANALYSIS

SWAT model standardization and Validation first determine the most sensitive parameter for a given watershed or sub-watershed that considerably affects the model output at intervals of the given model input. SWAT may be a complicated model and manual standardization of the many parameters may be quite troublesome (Setegn et al. 2010). Sensitivity analysis helps to see the relative ranking of which parameters most affect the output variability (Shang et al. 2012). Sensitivity analysis indicates the necessity of the parameters in determining the sediment concentration, nutrient loss, and streamflow of the study space to reduce the maximum uncertainty in model output. It permits the attainable reduction in various parameters that must be tagged, thus reducing the standardization method procedure time. It also reduces the model's uncertainty and gives ideas for how to figure out the parameters for the standardization method. Table 1 and Table 2 represent the initial parameters utilized in the sensitivity analysis for the surface runoff

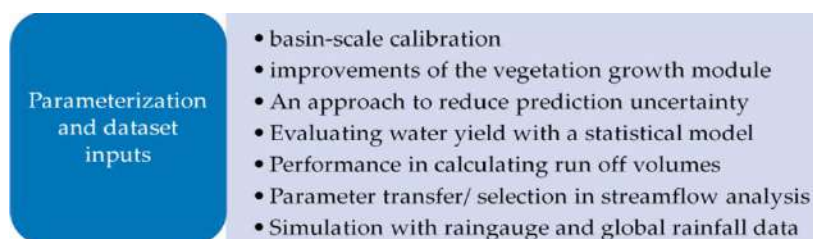


Fig. 3: Model application for the parameter selection and input dataset (Akoko et al. 2021).

and sediment yield standardization. Model standardization attempts to increase parameterization for a given set of native conditions, thereby reducing the prediction uncertainty. Standardization has been performed by rigorously choosing the model input parameters at intervals in their counseled uncertainty ranges. Calibration is nothing but adjusting the selected sensitive parameter within a recommended range to obtain a close agreement between observed and simulated due to uncertainty in model input, spatial variability, budget constraints, and access difficulties (Lweendo et al. 2017). Calibration becomes computationally extensive and complex when the number of parameters in the model is substantial.

Table 3: List of initially selected parameters for runoff modeling.

Parameter	Description of Parameters	Types of Parameters
SOL_K	Saturated hydraulic conductivity (mm.hr <sup>-1</sup> )	Soil water
SLP	Average slope steepness	Surface runoff
RCHRG_DP	Deep aquifer percolation fraction	Surface runoff
CN <sub>2</sub>	SCS runoff curve number for AMC-2	Surface runoff
ALPHA_BF	Base flow alpha factor	Groundwater
GW_DELAY	Groundwater delay	Groundwater
SOL_BD	Moist bulk density	Soil water
CH_N1	Manning's "n" value for the tributary Channel	Channel process
ESCO	Soil evaporation compensation factor	Evapotranspiration
SURLAG	Surface runoff lag time	Surface runoff
GW_REVAP	Groundwater revamp coefficient	Groundwater
CH_K1	Effective hydraulic conductivity in the tributary Channel	Surface runoff
GW_SPYLD	Specific yield of the shallow aquifer	Groundwater
CH_K2	Effective hydraulic conductivity in the main channel	Surface runoff
SOL_AWC	The available water content of the soil	Soil water
SLSUBBSN	Average slope length	Geo-morphology
BLA1	Maximum potential leaf area index	Evapotranspiration
SOL_ALB	Moist soil albedo	Soil water
CANMX	Maximum canopy storage	Surface runoff
EPCO	Plant uptake compensation factor	Evapotranspiration

Referring to Fig. 4, SWAT-CUP is a computer program used within the SWAT-CUP package for calibration of the SWAT model. SUFI-2 (Sequential Uncertainty Fitting Version 2 program) is used for the above model calibration process.

However, model validation is nothing more than re-running the simulation, employing a different statistic for the input file while not dynamically adjusting any parameter that can be adjusted throughout standardization. To utilize the graduated model for estimating the effectiveness of future potential management practices, the model was performed against the freelance set of measured knowledge. With each standardization and validation phase, the model's prognostic capability was incontestable, and also the model was also used for future prediction.

## MODEL EVALUATION

Several indices were used to evaluate the SWAT model outputs (see Fig. 5). The most widely used indexes were NSE, R2 (square of Pearson's product), PBIAS, IA, RVE, r bias, and VR (volume ratio). Each had one study. There were also RMSE, RSR (standardized RMSE), KGE (Kling Gupta efficiency), IVF (index of volumetric fit), and bR2

Table 2: List of initially selected parameters for sediment modeling.

Parameter	Description of Parameters	Types of Parameters
SPEXP	Exponential parameter for calculating sediment re-entertainment in the channel sediment routing	Channel
CH_N <sub>2</sub>	Manning's "n" value for the main channel	Channel
SLSUBBSN	Average slope length	Geo-morphology
CH_S <sub>2</sub>	The average slope of the main channel	Channel
OV_N	Manning's "n" value for the overland flow	Surface runoff
HRU_SLP	Average slope steepness	Surface runoff
SPCON	Linear amount of sediment that can be re-entertainment during channel sediment routing	Channel
CH_K <sub>2</sub>	Effective hydraulic conductivity in the main channel	Channel process
PRF	Peak rate adjustment factor	Channel
CH_W <sub>2</sub>	The average width of the main channel	Channel
CH_D	The average depth of the main channel	Channel
CH_I_2	The average length of the main channel	Channel

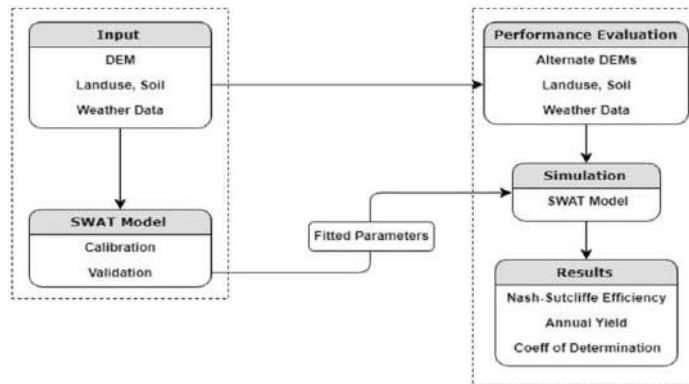


Fig. 4: Procedure for SWAT model run (Sedighi et al.2019).

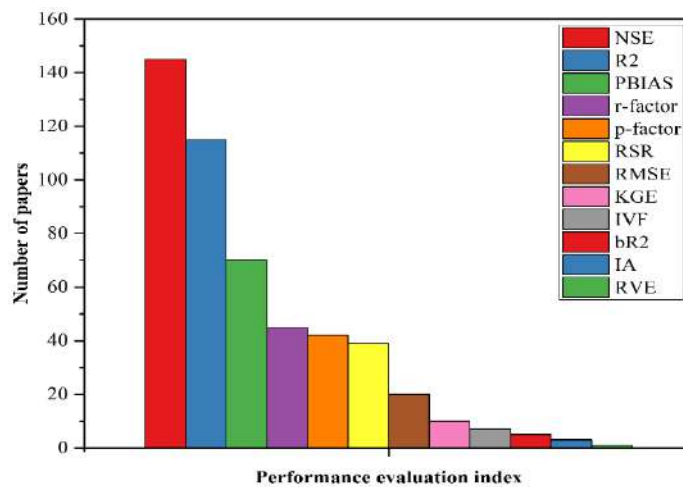


Fig. 5: Number of papers by different performance evaluation indexes.

(coefficient of determination x regression line between actual and predicted data).

## ADVANTAGES AND CHALLENGES OF THE SWAT MODEL

1. SWAT has got worldwide acceptance, to integrate various environmental processes and is used for sustainable and effective watershed management.
2. The SWAT model is mostly applied in large watersheds due to the availability of accurate data.
3. SWAT is a continuous time scale deterministic model capable of simulating the long-term effects of management changes.
4. It is highly capable of integrating with the Geographical Information System (GIS).
5. It incorporates DEM, soil map, and land use map, meteorological parameters to generate runoff at the basin scale.
6. It provides a useful tool to fill in the missing daily data in the observed records.
7. The SWAT studies reviewed in this review highlighted several concerns. Data availability/gaps, quality of data, and model restrictions were all concerns. The SWAT model could not reproduce the dynamics of sediment yield transport at a watershed outlet in some seasons, highlighting its limitations in small catchments (Shendge et al. 2018). Calibration and validation of runoff and sediment processes enhance the accuracy of SWAT model simulations (Mwangi et al. 2015). The SWAT model's poor performance in streamflow modeling was attributed to the insufficient spatial correlation of datasets (Le & Pricope 2017).
8. Despite its limitations, the SWAT model has many

advantages, prompting numerous scientists to use it for hydrological applications. Thus, the SWAT model may be implemented more simply with fewer parameters but possess higher data needs, compared to certain other well-known (continental scale) hydrological and land surface models (Trambauer et al. 2013).

9. The above model is useful in assessing the costs and advantages of adopting sediment control BMPs (Jayakrishnan et al. 2005, Briak et al. 2016). Assessing the implications of land-use changes (Gyamfi et al. 2016), and in drought planning and mitigating in data-scarce locations (Lweendo et al. 2017). These were all suggested for watershed management. As a result, the SWAT model can predict water productivity and assess alternative water management approaches (Ouassar et al. 2009).

### Limitation of SWAT model

1. SWAT does not simulate sediment routing and detailed flood routing because it was developed to predict the long-term erosion, sedimentation rates, and agriculture management impact.
2. It does not represent the heterogeneity of an aquifer, such as specific yield, spatially varying hydraulic conductivity, or hydraulic head.
3. It is limited to simulating stream seepage to the aquifer and groundwater discharge to the stream because it compares the shallow aquifer depth.
4. It does not consider the river bottom elevation and aquifer depth.
5. According to the SWAT user manual, it is better to use many sub-basins than many HRUs in a sub-basin. A maximum of 10 HRUs in a sub-basin is recommended.

### DISCUSSION

Dataset unavailability was cited as a problem in many of the articles identified. Numerous studies have identified inadequate land use/land cover data quality as a problem, especially in land-use analyses. In future SWAT model investigations, good spatial and temporal data will be needed to provide more precise assessments and findings and reduce uncertainty. Also, SWAT model simulations should collect enough data to enable future evaluations and analysis by other modelers. Developing databases using model parameterization data could improve SWAT+ (Bieger et al. 2017). Accessing additional data could help expand the SWAT+ dataset with data from around the world, minimizing model setup and parameterization time. The SWAT model

can predict how water will look in the future, and it can be used in agricultural development and strategic planning. The prior SWAT model featured a restricted number of concurrent components and no modeling of salt. SWAT+ provides the modeling of salt as a constituent, allowing for more extensive simulation of constituents and the routing of many pesticides simultaneously. Continued studies could use SWAT+ simulations to model nutrient transport, non-point pollution, and nutrient accumulation in water resources. The previous SWAT model included reservoirs on main channels at sub-basin exits, no pumping, canals, livestock herds, or managing water objects, and only one crop growing at a time. Water rights are described as spatial objects, and an endless number of crops can be planted simultaneously (Schuol et al. 2008). These changes allow for anthropogenic water evaluation. Future research could use SWAT+ to simulate future water availability for agriculture and other needs. Modeling of freshwater resources can help assess current sustainable water status and highlight areas requiring further investigation (Schuol et al. 2008). This is vital in creating regional and national agricultural infrastructure policies. Previous research has used the SWAT model to show the linkage between deforestation, sediment transport, and soil erosion. The model classifies water areas as HRUs and sub-basins as HRUs. SWAT+ separates water and land areas and identifies water areas as ponds/reservoirs (Bieger et al. 2017). Future studies could use this innovation to effectively understand environmental dynamics and incorporate population expansion and corresponding socio-economic challenges.

### CONCLUSIONS

A method based on SWAT and other models can be powerful. Local, national, and regional policies should be aligned with scientific investigations. Researchers should emphasize changes, trends, and related impacts using defined environmental thresholds at the local and regional levels. Obtaining additional data for future studies will allow other researchers to conduct new studies, for example, as supplemental material for journals. We should encourage governments to undertake more research (especially local data collection) that addresses/incorporates, or adopts integrated watershed management and associated environmental topics, with which the SWAT model has demonstrated proficiency. Local data for modeling is insufficient, so many researchers use global data instead. Some of the data needed for such studies can be acquired from worldwide datasets. Researchers at government agencies, universities, and other academic institutions should use SWAT and SWAT+ to plan and manage the larger ecosystem and develop policies. The SWAT model estimates sediment yield and runoff individually in the rout-



ing and soil phases, improving model simulation precision. This work is based on the principle of water balance. Soil runoff is calculated using the SCS curve number method, and the process of routing phase Muskingum method is most commonly used in the SWAT model. In addition, the SWAT model is also helpful in understanding the effect of land use on runoff, sediment, and the practice of agriculture. Because the SWAT model has a lot of uncertainties and flaws, the results may have been different.

## FUTURE SCOPE

1. SWATMOD can be used to overcome the limitations of the SWAT model in terms of groundwater modeling.
2. To study comparison and combination between SWAT and other models like ANN, EPIC, AGNPS, APEX, MIKE SHE, MIKE11, and NAM11 to predict the runoff and sediment load.
3. Research on water quality impacts due to sedimentation and different approaches to forecasting the effect of future climate change on dam sedimentation.
4. Between the upstream and downstream, complex soil erosion dynamics, sediment yield, and river sedimentation can be formed.

## ACKNOWLEDGEMENT

The authors are grateful to NIT, Raipur Chhattisgarh.

## REFERENCES

- Akoko, G., Le, T.H., Gomi, T. and Kato, T. 2021. A review of SWAT model application in Africa. *Water*, 13(9): 1313.
- Alemayehu, T., Van Griensven, A., Woldegiorgis, B.T. and Bauwens, W. 2017. An improved SWAT vegetation growth module and its evaluation for four tropical ecosystems. *Hydrol. Earth Syst. Sci.*, 21(9): 4449-4467.
- Arnold, J.G. and Fohrer, N. 2000. SWAT2000: current capabilities and research opportunities in applied watershed modeling. *Hydrological Processes: An International Journal*, 19(3): 563-572.
- Arnold, J.G., Srinivasan, R., Mutiah, R.S. and Williams, J.R. 1998. Large area hydrologic modeling and assessment part I: model development. *JAWRA J. Am. Water Resour. Assoc.*, 34(1): 73-89.
- Bekele, D., Alamirew, T., Kebede, A., Zeleke, G. and Melesse, A. 2019. Modeling climate change impact on the Hydrology of Keleta watershed in the Awash River basin, Ethiopia. *Environ. Model. Assess.*, 24(1): 95-107.
- Betrie, G.D., Mohamed, Y.A., van Griensven, A. and Srinivasan, R. 2011. Sediment management modeling in the Blue Nile Basin using SWAT model. *Hydrol. Earth Syst. Sci.*, 15(3): 807-818.
- Bieger, K., Arnold, J.G., Rathjens, H., White, M.J., Bosch, D.D., Allen, P.M., Volk, M. and Srinivasan, R. 2017. Introduction to SWAT+, a completely restructured version of the soil and water assessment tool. *JAWRA J. Am. Water Resour. Assoc.*, 53(1): 115-130.
- Briak, H., Moussadek, R., Aboumaria, K. and Mrabet, R. 2016. Assessing sediment yield in Kalaya gauged watershed (Northern Morocco) using GIS and SWAT model. *Int. Soil Water Conserv. Res.*, 4(3): 177-185.
- Chaibou, B.J., Jomaa, S., Benabdallah, S., Bazie, P., Afouda, A. and Rode, M. 2016. Multi-site validation of the SWAT model on the Bani catchment: Model performance and predictive uncertainty. *Water*, 8(5): 178.
- de Almeida Bressiani, D., Gassman, P.W., Fernandes, J.G., Garbossa, L.H.P., Srinivasan, R., Bonumá, N.B. and Mendiondo, E.M. 2015. Review of soil and water assessment tool (SWAT) applications in Brazil: Challenges and prospects. *International Journal of Agricultural and Biological Engineering*, 8(3): 9-35.
- Dessie, M., Verhoest, N.E., Pauwels, V.R.N., Admasu, T., Poesen, J., Adgo, E., Deckers, J. and Nyssen, J. 2014. Analyzing runoff processes through conceptual hydrological modeling in the Upper Blue Nile Basin, Ethiopia. *Hydrol. Earth Syst. Sci.*, 18(12): 5149-5167.
- Easton, Z.M., Walter, M.T., Fuka, D.R., White, E.D. and Steenhuis, T.S. 2011. A simple concept for calibrating runoff thresholds in quasi distributed variable source area watershed models. *Hydrol. Process.*, 25(20): 3131-3143.
- Gassman, P.W., Reyes, M.R., Green, C.H. and Arnold, J.G. 2007. The soil and water assessment tool: historical development, applications, and future research directions. *Trans. ASABE*, 50(4): 1211-1250.
- Gessesse, B., Bewket, W. and Bräuning, A. 2015. Model based characterization and monitoring of runoff and soil erosion in response to land use/land cover changes in the Modjo watershed, Ethiopia. *Land Degrad. Develop.*, 26(7): 711-724.
- Githui, F., Gitau, W., Mutua, F. and Bauwens, W. 2009. Climate change impact on SWAT simulated streamflow in western Kenya. *Int. J. Climatol. J. Royal Meteorol. Soc.*, 29(12): 1823-1834.
- Gyamfi, C., Ndambuki, J.M. and Salim, R.W. 2016. Hydrological responses to land use/cover changes in the Olifants Basin, South Africa. *Water*, 8(12): 588.
- Harper, D.M., Brierley, B., Ferguson, A.J. and Phillips, G. (eds.) 1999. *The Ecological Bases For Lake And Reservoir Management*. Volume 136. Academic Publishers Inc., Kolkatta, pp 3-11.
- Hunink, J.E., Niadas, I.A., Antonaropoulos, P., Droogers, P. and De Vente, J. 2013. Targeting of intervention areas to reduce reservoir sedimentation in the Tana catchment (Kenya) using SWAT. *Hydrol. Sci. J.*, 58(3): 600-614.
- Jayakrishnan, R.S.R.S., Srinivasan, R., Santhi, C. and Arnold, J.G. 2005. Advances in the application of the SWAT model for water resources management. *Hydrol. Process. Int. J.*, 19(3): 749-762.
- Kingston, D.G. and Taylor, R.G. 2010. Projected impacts of climate change on groundwater and stormflow in a humid, tropical catchment in the Ugandan Upper Nile Basin. *Hydrol. Earth Syst. Sci. Discuss.*, 7(2): 61.
- Krysanova, V. and White, M. 2015. Advances in water resources assessment with SWAT: An overview. *Hydrol. Sci. J.*, 60(5): 771-783.
- Le, A.M. and Pricope, N.G. 2017. Increasing the accuracy of runoff and streamflow simulation in the Nzoia Basin, Western Kenya, through the incorporation of satellite-derived CHIRPS data. *Water*, 9(2): 114.
- Lweendo, M.K., Lu, B., Wang, M., Zhang, H. and Xu, W. 2017. Characterization of droughts in a humid subtropical region, upper Kafue river basin (southern Africa). *Water*, 9(4): 242.
- Melesse, A.M., McClain, M., Wang, X., Abira, M. and Mutayoba, W. 2008. Modeling the Impact of Land-Cover and Rainfall Regime Change Scenarios on the Flow of Mara River, Kenya. In *World Environmental and Water Resources Congress 2008: Ahupua'a*, pp. 1-10.
- Milzow, C., Krogh, P.E. and Bauer-Gottwein, P. 2011. Combining satellite radar altimetry, SAR surface soil moisture, and GRACE total storage changes for hydrological model calibration in a large poorly gauged catchment. *Hydrol. Earth Syst. Sci.*, 15(6): 1729-1743.
- Mishra, S.K., Sahu, R.K., Eldho, T.I. and Jain, M.K. 2006. An improved I n S relation incorporating antecedent moisture in SCS-CN methodology. *Water Resour. Manag.*, 20(5): 643-660.
- Mourad, K.A. and Sang, J. 2018. Effectiveness of contour farming and filter strips on ecosystem services. *Water*, 10(10): 1312.

- Mwangi, J.K., Shisanya, C.A., Gathenya, J.M., Namirembe, S. and Moriasi, D.N. 2015. A modeling approach to evaluate the impact of conservation practices on water and sediment yield in Sasumua Watershed, Kenya. *J. Soil Water Conserv.*, 70(2): 75-90.
- Ndomba, P.M., Mtalo, F.W. and Killingtveit, Å. 2008. A guided swat model application on sediment yield modeling in Pangani river basin: Lessons learned. *J. Urban Environ. Eng.*, 2(2): 53-62.
- Nyeko, M., D'Urso, G. and Immerzeel, W.W. 2012. Adaptive simulation of the impact of changes in land use on water resources in the lower Aswa basin. *J. Agric. Eng.*, 43(4): e24.
- Ouessar, M., Bruggeman, A., Abdelli, F., Mohtar, R.H., Gabriels, D. and Cornelis, W.M. 2009. Modeling water-harvesting systems in the arid south of Tunisia using SWAT. *Hydrol. Earth Syst. Sci.*, 13(10): 2003-2021.
- School, J., Abbaspour, K.C., Yang, H., Srinivasan, R. and Zehnder, A.J. 2008. Modeling blue and green water availability in Africa. *Water Resour. Res.*, 44(7): 615
- Sedighi, M., Nasser, S. and Ghotbi-Ravandi, A.A. 2019. Degradation of 17 $\alpha$ -ethinylestradiol by *Enterobacter tabaci* Isolate and kinetic characterization. *Environ. Process.*, 6(3): 741-755.
- Setegn, S.G., Srinivasan, R., Melesse, A.M. and Dargahi, B. 2010. SWAT model application and prediction uncertainty analysis in the Lake Tana Basin, Ethiopia. *Hydrol. Process. Int. J.*, 24(3): 357-367.
- Shang, X., Wang, X., Zhang, D., Chen, W., Chen, X. and Kong, H. 2012. An improved SWAT-based computational framework for identifying critical source areas for agricultural pollution at the lake basin scale. *Ecol. Model.*, 226: 1-10.
- Shendge, R.B., Chockalingam, M.P., Saritha, B. and Ambica, A. 2018. Swat modeling for sediment yield: A case study of Ujjani reservoir in Maharashtra, India. *Int. J. Civil Eng. Technol.*, 9(1): 245-252.
- Sultan, M., Metwally, S., Milewski, A., Becker, D., Ahmed, M., Sauck, W., Soliman, F., Sturchio, N., Yan, E., Rashed, M., and Wagdy, A. 2011. Modern recharge to fossil aquifers: Geochemical, geophysical, and modeling constraints. *J. Hydrol.*, 403(1-2): 14-24.
- Tan, M.L., Gassman, P.W., Srinivasan, R., Arnold, J.G. and Yang, X. 2019. A review of SWAT studies in Southeast Asia: Applications, challenges, and future directions. *Water*, 11(5): 914.
- Trambauer, P., Maskey, S., Winsemius, H., Werner, M. and Uhlenbrook, S. 2013. A review of continental scale hydrological models and their suitability for drought forecasting in (sub-Saharan) Africa. *Phys. Chem. Earth A/B/C*, 66: 16-26.
- Van Griensven, A., Ndomba, P., Yalaw, S. and Kilonzo, F. 2012. A critical review of SWAT applications in the upper Nile basin countries. *Hydrol. Earth Syst. Sci.*, 16(9): 3371-3381.
- Wambura, F.J., Dietrich, O. and Lischeid, G. 2018. Improving a distributed hydrological model using evapotranspiration-related boundary conditions as additional constraints in a data-scarce river basin. *Hydrol. Process.*, 32(6): 759-775.
- Zettam, A., Taleb, A., Sauvage, S., Boithias, L., Belaidi, N. and Sánchez-Pérez, J.M. 2017. Modeling hydrology and sediment transport in a semi-arid and anthropized catchment using the SWAT model: The case of the Tafna river (northwest Algeria). *Water*, 9(3): 216.
- Zhang, S. and Al-Asadi, K. 2019. Evaluating the effect of numerical schemes on hydrological simulations: HYMOD as a case study. *Water*, 11(2): 329.



# Environmental Remediation of Contaminated Wastewater with Ammonium Using Clay-Based Adsorbents

Ibrahim Abdelfattah\*, Wael Abdelwahab\*\* and Ashraf M. El-Shamy\*\*\*†

\*Water Pollution Research Department, National Research Centre, El-Bohouth St. 33, Dokki, P.O. 12622, Giza, Egypt

\*\*Geological Sciences Department, National Research Centre El-Bohouth St. 33, Dokki, P.O. 12622, Giza, Egypt

\*\*\*Physical Chemistry Department, Electrochemistry and Corrosion Lab., National Research Centre, El-Bohouth St. 33, Dokki, P.O. 12622, Giza, Egypt

†Corresponding author: Ashraf M. El-Shamy; [elshamy10@yahoo.com](mailto:elshamy10@yahoo.com); [am.elshamy@nrc.sci.eg](mailto:am.elshamy@nrc.sci.eg)

Nat. Env. & Poll. Tech.  
Website: [www.neptjournal.com](http://www.neptjournal.com)

Received: 26-05-2022  
Revised: 17-06-2022  
Accepted: 22-06-2022

## Key Words:

Ammonium ions  
Removal efficiency  
Bentonitic clay  
Montmorillonitic clay  
Adsorbents  
Isotherms  
Drain wastewater

## ABSTRACT

Due to a lack of water treatment technology, developing and emerging nations have become significant polluters and water shortage is exacerbated by pollution. Ammonium toxicity is a huge global environmental concern with no clear solution. Population growth and industrialization destroy the ecosystem. Common and industrial products contain ammonium ions. Water pollution damages fish and other aquatic life. An inexpensive and green wastewater treatment method is adsorption. Adsorbent polymers that remove ammonium ions from wastewater have been explored. Ammonium ions are very hazardous when deposited into surface waters. Surfaces of bentonite and montmorillonite clay may attach sodium ammonium ions. They are cheap and abundant, therefore used to treat drain water. Bentonite outperformed montmorillonite in eliminating ammonium ions from water. Bentonite and montmorillonite clays were used to remove residual ammonium ions. These are utilized for bentonitic and montmorillonitic clays. Both clays were absorbed in a neutral pH, and it was free of sulfuric acid, ammonium ions, and phosphorus ions. Montmorillonitic clay boosted TDS by nearly 10% whereas bentonitic clay only raised TDS by 1%. Adsorption may inexpensively filter water and the surface charge of adsorbents affect their adsorption capacity. Ammonium ions may be recycled, and several bioreactors can remove ammonium ions from liquid and solid phases. Iterate over several models and the Freundlich isotherm model outperforms the Langmuir model by 5%. And bentonite clay adsorbs better due to iron oxide content.

## INTRODUCTION

Due to a lack of access to water treatment technology, emerging and fast-growing nations have become significant polluters. Growing pollution of aquatic sources endangers aquatic biota and promotes water shortages (Dey et al. 2021, Tse-Lun et al. 2021, Zahra & Mohammad 2013). The toxicity of ammonium ions is a significant global environmental problem, and it is difficult to define acceptable ecosystem boundaries. Population and industrial expansion emit ammonium ions, harming the ecosystem. Ammonium ions are found in numerous home and cleaning products, as well as commercial and industrial fertilizers (Rajoriya & Kaur 2014, Limbachiya et al. 2012, Mithra et al. 2012). Illegal municipal wastewater dumping allows ammonium ions to enter the aquatic environment, affecting fish and aquatic life. Adsorption is one of the most cost-effective and ecologically friendly wastewater treatment methods developed in recent decades. Several adsorbent materials

have gained academic attention for their capacity to extract ammonium ions from wastewater efficiently (Chopin et al. 2012, Neori et al. 1998). These contaminants are absorbed from wastewater via oxidation, osmosis, reduction, precipitation, ultra-filtration, electro-dialysis, ion exchange, and electrochemical methods. They create more sludge, are less efficient, and cannot remove as many ammonium ions. Adsorption is the preferred way of obtaining a broad variety of waste materials and natural resources (Duruibe et al. 2007, Young 2005). Clay is a particularly effective adsorbent for ammonium ions because clay is extremely effective, readily accessible, relatively affordable, and potentially reusable and cost-efficient (Buono et al. 2015, Rivett et al. 2008, Goody et al. 2014, Reda et al. 2018, 2022). Adsorption is the mass transfer of material from the gas or liquid phase to the surface or interface of a solid phase (i.e., adsorbent). The adsorption process has four stages: Diffusion from the bulk solution to the adsorbent surface through the boundary layer; Pore diffusion or intraparticle diffusion; physical and/or chemical

reaction: adsorption between adsorbate and adsorbent active sites (Aruna et al. 2021, Ibrahim et al. 2022). The first bulk diffusion phase may be avoided by uniformly distributing adsorbent and adsorbate in the solution. Adsorption kinetics is dictated by film diffusion or pore diffusion since the previous step, physical/chemical contact occurs quickly (Mahmoud et al. 2012). Adsorbent liquid volume and surface area affect film diffusion rate i.e., liquid membrane area. Relatively faster liquid-particle relative velocity means a thinner fixed liquid layer on particle surfaces and faster film diffusion (Park & Kim 2005). It is connected to the adsorbents' pore shape and distribution, as well as the adsorbate's molecular size and structure, but is less related to the liquid concentration or adsorbent particle surface area. Adsorption time squared determines pore diffusion rate  $t_{0.5}$ . Consequently, if the adsorption rate is linear with  $t_{0.5}$ , the pore diffusion mechanism likely dominates adsorption during these periods (Peez-Corona et al. 1998). Adsorption of ammonium ions from polluted water has great environmental and economic possibilities. Various laboratory studies may produce experimental values for field treatment plant design. Other system variables such as temperature, pH, and other ammonium compounds must be investigated further. Surface modification of adsorbents may improve removal efficacy and should be investigated. Solid waste adsorbents may minimize chemical consumption in water and wastewater treatment (Tian et al. 2010, Saad et al. 1997, El-Shamy et al. 2017a, 2017b, 2017c). Discoveries made in a continuous reactor system may be implemented more efficiently in the field. Research on ammonium ions removal in the presence of other contaminants is vital. Several elements affecting open-air scenarios must be understood (Shehata et al. 2019, Samar et al. 2022, Abdelfattah & El-Shamy 2022). This study is the first to compare two adsorbent media for the construction of community or home-based treatment facilities in industrialized nations. All the variables that occur in open natural environments must be acknowledged (Ashraf et al. 2018, Ibrahim et al. 2022). In batch processing, the adsorbent is combined with ammonium ion solutions for a specified contact time, and the adsorbate is separated by sedimentation or filtering (Farag et al. 2016). In a closed system, the data collected is typically inapplicable to real systems (Namasivayam & Sangeetha 2004). The batch method is used to investigate adsorption processes and compare adsorbents' capacities. Charged contaminants (such as inorganic and organic pollutants) adsorb on adsorbents with oppositely charged surfaces (Frisoni et al. 2001). Because most naturally polluted streams have modest quantities of certain contaminants, effective contaminant removal is critical. Contaminants at ultra-low concentrations should be reduced using adsorbents. Lower-loading adsorbents must be renewed for optimum utilization (Liu et al. 2011).

Researchers can improve adsorption rates by optimizing adsorbent design and experimental conditions. Single or more layers of nitrate molecules may be adsorbed on an adsorbent. Monolayer adsorption happens when an adsorbate only covers one molecular layer of the adsorbent surface. Adsorbent surfaces may adsorb more than one molecular layer of adsorbates (Tian et al. 2009, Zohdy et al. 2021). Physical adsorption may be multi-layer, happening on top of a chemically adsorbed monolayer. This study's goal was to prevent ammonium ions from reaching river water sources. Adsorbents were compared in batches using variables such as pH, starting concentration, adsorbent dose, and contact duration (Luo et al. 2010).

## MATERIALS AND METHODS

In this study, we will compare the physicochemical adsorption of montmorillonitic and bentonitic clays for the treatment of ammonium-contaminated synthetic wastewater as well as drain wastewater from Giza's El-Rahawy drain. Montmorillonitic clay samples from Ayash Clay Mine in the Cairo-Suez area, Egypt, and bentonitic clay samples from Norther Coast West Alexandria. ADWIC, Egypt produces ammonium ions dilutions at various concentrations using ammonium ions solution (pure reagent 33%). The investigation employed analytical-grade chemicals such as NaOH and HCl to modify the pH of the batches. All dilutions were prepared using double distilled water. The authentic drain discharge sample came from Giza's El-Rahawy drain. It was carefully bottled, acidified to pH 3, and sent to the lab for testing (Mehta et al. 2021). This study employed both montmorillonitic and bentonitic clay as active adsorbates. For future usage, they were desiccated after homogenous grinding by crushing into tiny bits and fine mesh-size particles throughout a US Standard Testing Sieve No 100 (150 microns). With the Jasco-FTIR-Spectrometer (Japan), FT-IR montmorillonitic and bentonitic clay powder absorption spectra were measured to identify functional groups that may contribute to the adsorption process. The pH of solutions was adjusted with HCl and NaOH using a Jenway 3510 bench pH meter. The amounts of ammonium ions were determined using the distillation-titration technique, which was utilized to characterize all raw and processed effluents (Wang et al. 2020).

### Batch Experiments

A multi-position magnetic stirrer at 200 rpm was used at room temperature ( $25^{\circ}\text{C} \pm 2$ ) for mixing beakers containing samples. The supernatant was filtered through the Whatman membrane filters ( $0.45 \mu\text{m}$ ). The residual ammonium ions concentration is measured according to Standard Methods

for Water and Wastewater Examination. The adsorbed  $\text{NH}_4^+$  ions are calculated as:

$$\text{Adsorption}\% = (C_0 - C_e)X \frac{100}{C_0} \quad \dots(1)$$

Where  $C_0$  and  $C_e$  are the initial and equilibrium concentrations of ammonium ions in ( $\text{mg.L}^{-1}$ ). The number of ammonium ions ( $q_t$  at time  $t$ ) adsorbed by adsorbent ( $M$ ) is estimated utilizing the subsequent equivalence:

$$q_t = (C_0 - C_t)V/M \quad \dots(2)$$

$C_t$  is the concentration ( $\text{mg.L}^{-1}$ ) of ammonium ions after time  $t$  min.,  $V$  is the volume of initial ammonium ions in one liter, and  $M$  is the adsorbent mass used in grams. The adsorption capacity ( $q_e$ ) is defined when equilibrium is reached (Gupta et al. 2011):

$$q_e = (C_0 - C_e)V/M \quad \dots(3)$$

**Adsorption Isotherms**

In addition, isotherm models assist in determining the needed dosage of adsorbent and the most appropriate sorbent for the situation. The most common isotherm models for a single solute are Langmuir and Freundlich (El-Kashef et al. 2019).

**Langmuir Isotherm**

It depends on maximum adsorption corresponding to a saturated monolayer of adsorbate molecules on the surface of the clay.

The Langmuir isotherm is presented in:

$$q_e = \frac{q_{\max} * K_L C_e}{1 + K_L C_e} \quad \dots(4)$$

The linearized form is:

$$\frac{C_e}{q_e} = \frac{1}{q_m K_L} + \frac{1}{q_m} * C_e \quad \dots(5)$$

$$\text{Slope} = \frac{1}{q_m} \quad \dots(6)$$

$$\text{Intercept} = \frac{1}{q_m K_L} \quad \dots(7)$$

Where  $q_m$  and  $K_L$  are Langmuir constants related respectively to the sorption capacity, and sorption energy,  $C_e$  ( $\text{mg.L}^{-1}$ ) is the equilibrium concentration and  $q_e$  ( $\text{mg/gm}$ ) is the adsorption capacity at equilibrium.  $R_L$  is the essential characteristic of the Langmuir dimensionless constant separation factor or equilibrium parameter which is defined by the following equation (El-Shamy et al. 2021).

$$R_L = \frac{1}{1 + K_L * C_0} \quad \dots(8)$$

$R_L$  calculated values from the above equation show the nature of the adsorption process to be either unfavorable ( $R_L > 1$ ), linear when ( $R_L = 1$ ), favorable when ( $0 < R_L < 1$ ), and irreversible when ( $R_L = 0$ ).

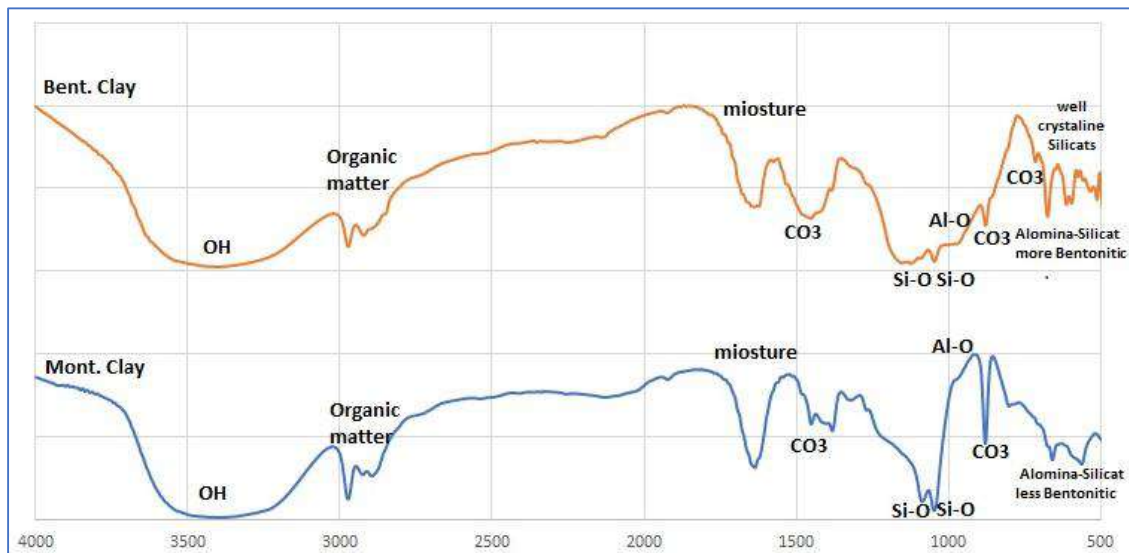


Fig. 1: FTIR Charts for bentonitic and montmorillonitic clay.

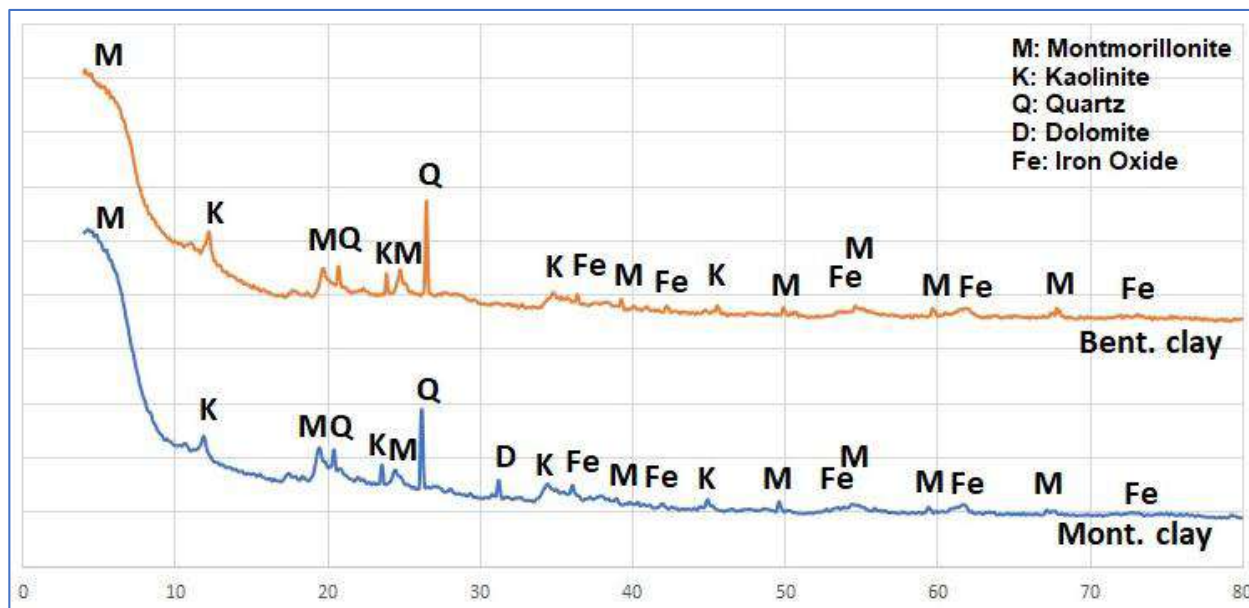


Fig. 2: XRD Charts for bentonitic and montmorillonitic clay.

### Freundlich Isotherm

It involves surface heterogeneity and the exponential distribution of active sites and their energies.

The Freundlich isotherm equation is presented as:

$$R_L = \frac{1}{1 + K_L * C_0} \quad \dots(8)$$

$$q_e = C_e^{\frac{1}{n}} \quad \dots(9)$$

The linearized form is:

$$\ln q_e = \ln K_F + \left(\frac{1}{n}\right) \ln C_e \quad \dots(10)$$

And the ((n)) calculated from the equation:

$$\text{Slope} = \frac{1}{n} \quad \dots(11)$$

And the ( $K_F$ ) is calculated as the anti-ln of the intercept as:

$$\text{Intercept} = \ln K_F \quad \dots(12)$$

Where  $q_e$  ( $\text{mg}\cdot\text{g}^{-1}$ ) is the adsorption capacity at equilibrium,  $C_e$  ( $\text{mg}\cdot\text{L}^{-1}$ ) is the concentration of ammonium ions at equilibrium,  $K_F$  is a constant related to the temperature, and  $n$  is a characteristic constant (Varshney et al. 1996).

### RESULTS AND DISCUSSION

The interaction of loaded clay molecules with ammonium ions was studied using FTIR (Fig. 1), XRD (Fig. 2), and XRF (Fig. 3). The adsorbent's surface area influences the adsorption process's potential effect. Because the clay particles were positively charged, the  $\text{NH}_4^+$  ions were likely adsorbed on the surface via complexing with the clay cations and attracting ammonium ions through hydrogen bonding.

#### Adsorbent Characterization

Adsorption of ammonium ions enhanced the surface clay/ammonium ions ratio. XRD, FTIR, and XRF were used to study  $\text{NH}_4^+$ -clay interactions. It is stretching at  $3049$  and  $2930$   $\text{cm}^{-1}$ , as well as two bending modes at  $1503$  (scissoring) and  $695$  (wagging)  $\text{cm}^{-1}$  were identified after integration with  $-\text{N}-\text{H}$ . A rare combination band at  $2003$   $\text{cm}^{-1}$  was also identified. It indicated that clay particles had replaced protons on the  $-\text{NH}_4^+$  groups of ammonium ions. Adsorption of  $\text{NH}_4^+$  produced a  $1403$   $\text{cm}^{-1}$   $\text{N}-\text{H}$  scissoring vibration peak of an ammonium compound. the  $-\text{NH}_2$  vibrations shifted blue from  $3046$  to  $3128$   $\text{cm}^{-1}$ , confirming the clay particles' incorporation of the  $-\text{NH}_4^+$  ligand. FTIR detected the chemical environment of the clay/ $\text{NH}_4^+$  species. The peak regions show that 86% of  $-\text{NH}_2$  groups protonated as  $-\text{NH}_4^+$  groups. After clay loading, the  $-\text{NH}_2$  groups complexed

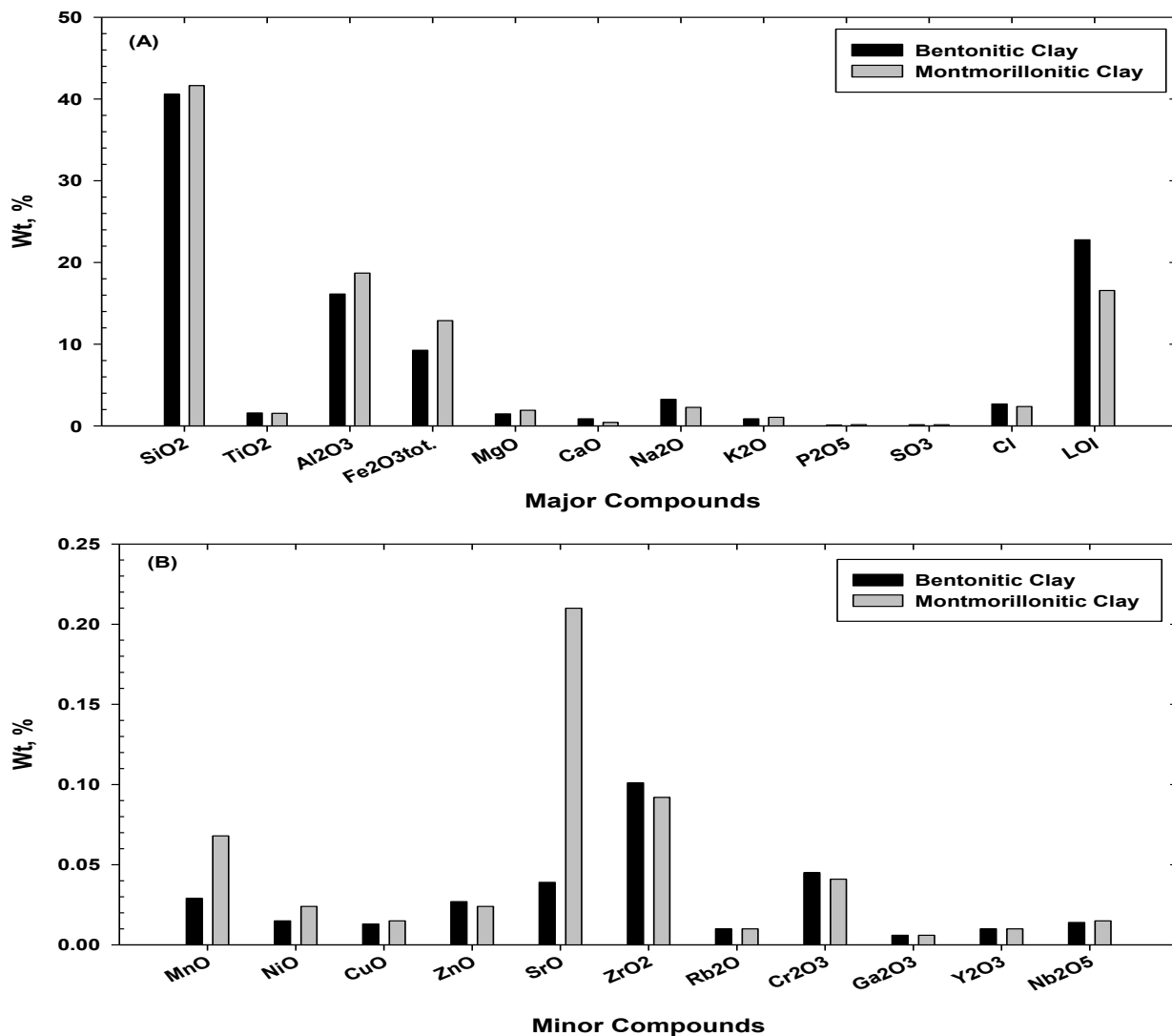


Fig. 3: XRF Charts for bentonitic and montmorillonitic clay.

with the clay particles, adding 402.4 eV to the binding energy (Benaissa & Benguella 2004).

### Effect of Adsorbent Dose

Fig. 4 shows the effect of various (B) and (M) dosages on ammonium ion elimination. The ammonium ions removal rate was less than 50% when the adsorbent concentration was less than 0.3 g.L<sup>-1</sup>. However, increasing the concentration from 0.6 to 1.2 g.L<sup>-1</sup> had no effect. Surprisingly, increasing the adsorbent concentration enhances the ammonium ion nitrogen removal rate. The adsorbent's active sites were less accessible when the ammonium ions concentration increased, according to one research. Because ammonium ions reached the adsorbent's lower active sites, the loading

rate decreased but the loading capacity rose. Ammonium ions diffuse into the low active sites in (B) and (M) as the concentration increases, speeding up ammonia removal. The ammonium ions removal method error was less than 4%, indicating that ammonium ions intake remained constant (El-Shamy et al. 2017).

### Effect of Initial pH

Fig. 5 shows adsorption data for B and M vs. contact time at 5 min intervals of up to 120 min. The number of ammonium ions absorbed by the material under investigation was determined using a cation exchange capacity and an adsorbent dosage (0.1 g.50 mL<sup>-1</sup>). The authors of this article tested at pH 6. The adsorption plots of ammonium ions on (B) and (M)

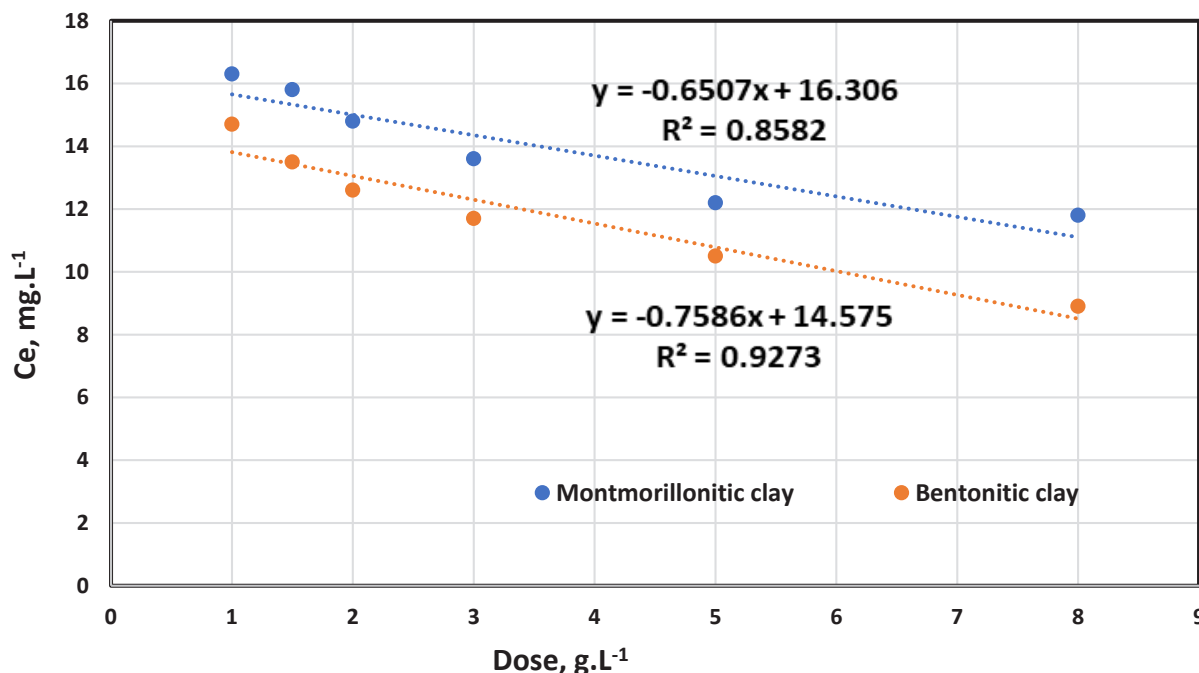
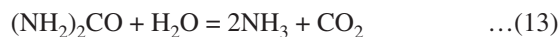
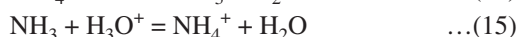


Fig. 4: Effect of weight volume % of bentonitic and montmorillonitic clay (Opt. of pH, 20 mg.L<sup>-1</sup> ammonium ions, dose of clay 0.5 g.100 mL<sup>-1</sup>, 100 mL solution, 1h stirring).

demonstrate three distinct phases: initial adsorption within 10 min, progressing equilibrium, and final equilibrium (El-Shamy et al. 2018).



Thus, unionized ammonia  $\text{NH}_3$  and  $\text{CO}_2$  are generated ( $\text{CO}_2$ ).  $\text{NH}_4^+$  ZZZ is formed when complex organic compounds in industrial, municipal, and animal wastes break down. Therefore, as previously explained, ammonium ions exist in two forms in aqueous solution: non-ionized ( $\text{NH}_4^+$  ZZZ) and ionized (N), as represented by the equations:



Ion exchange can only remove the ionized form of ammonium since it is pH-dependent. Because most ammonium install nitrogen is ionized at pH 8 and lower, these circumstances encourage elimination. In adverse circumstances, the balance changes quickly to a non-ionized form above pH 8. Because the pH of the solution affects the quantity of N removed, a series of experiments were done to determine the best pH range for ammonium removal. The ion exchange mechanism works best at pH 8 and below, with pH 6 providing maximum elimination. The equilibrium capacity is 50 meq.100 g<sup>-1</sup> at pH 6, but 42 meq.100 g<sup>-1</sup> at pH 8. Decreases in removal efficiency and equilibrium capacity to 35 meq.100 g<sup>-1</sup> occur at pH 2. The N removal effectiveness reduces

fast at pH 10, which may be explained by the fact that the ammonium ion is neutralized by the hydroxyl ion, leaving it uncharged. The performance diminishes below pH 6 due to increased hydrogen ions in the solution, which compete for exchange sites (Ho et al. 2000).

### Effect of Contact Time

Adsorption of Bentonite (B) and Montmorillonite (M) vs contact time is shown in Fig. 6. The number of ammonium ions absorbed by the clay sample was monitored over time. The batch experiment of this paper was tested at pH 6. The adsorption plots of ammonium ions on (B) and (M) demonstrate three distinct phases: initial adsorption within 10 min, progressing equilibrium, and final equilibrium (Dey et al. 2019).

### Kinetics of Adsorption Process

It was used to match experimental data and describe the relationship between adsorbate concentration and adsorption rate. The ammonia adsorption correlation ( $R^2$ ) was 0.9997 for montmorillonitic clay. The kinetic model has a higher  $R^2$  of 0.9985 for bentonitic clay (Fig. 7). Difficulty in experimental procedures creates unpredictable results. The qt error is large when t is fixed.  $q_e(\text{cal.})$  was found to be closer to the experimental data ( $q_e(\text{exp.})$ ). The fitted kinetic model is validated by comparing the calculated  $q_e(\text{cal.})$  to the measured  $q_e$ . In



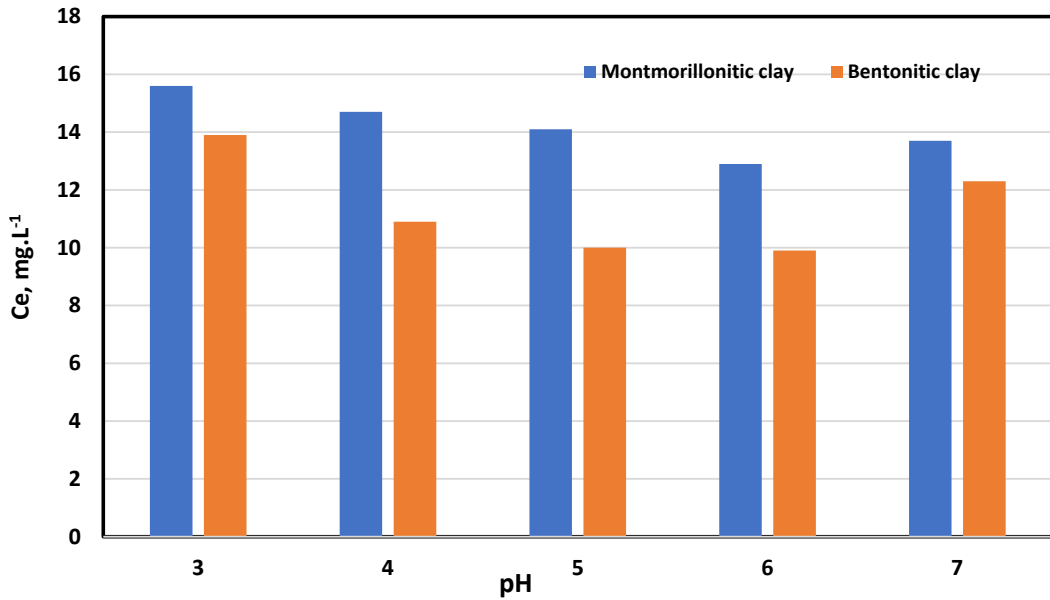


Fig. 5: Effect of pH on the adsorption capacity of bentonitic and montmorillonitic clay (Opt. of time, 20 mg.L<sup>-1</sup>, a dose of clay 0.5 g.100 mL<sup>-1</sup> clay, 100 mL, pH 6).

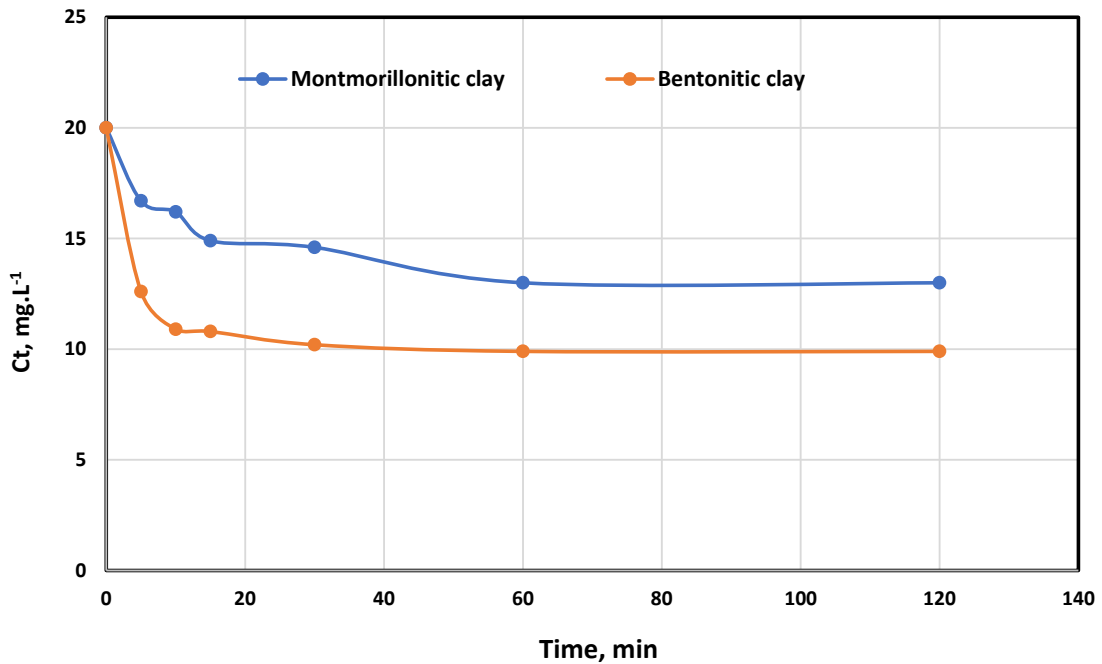


Fig. 6: Effect of contact time on the adsorption capacity of Bentonitic and montmorillonitic clay.

addition, coexisting cations influence the kinetic model for ammonia nitrogen adsorption (Aksu 2001).

**Adsorption Isotherms**

Fig. 8 demonstrates the batch multiple and simultaneous

ammonium ions adsorption using two clay types of Langmuir isotherm. This isotherm was fitted to the ammonium ion adsorption data.  $C_e/Q_e$  versus  $C_e$  over the concentration range produced a straight curve. The adsorbed ammonium ions increased with the equilibrium concentration.

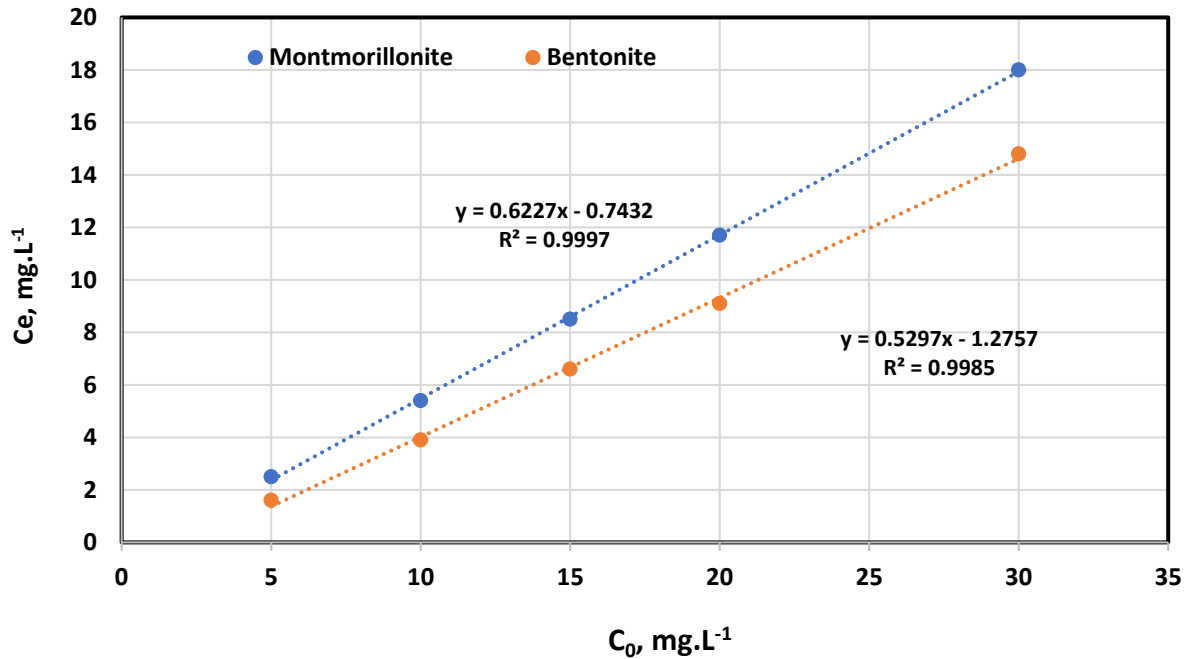


Fig. 7: Kinetics of adsorption using bentonitic and montmorillonitic clay (pH 6, a dose of clay 0.5 g.100 mL<sup>-1</sup>, 1 h stirring).

### Langmuir Isotherm

Fig. 8 shows the slope (b), intercept ( $Q_m$ ), and coefficient of determination as well as the statistical fit of the adsorption data to the Langmuir model is shown in Table 1. It demonstrates that numerous ammonium ion adsorptions match the Langmuir isotherm model well, with  $R^2 > 0.9$  for both clay types. Adsorption of ammonium ions is more favorable using Langmuir than using bentonite as an adsorbent. Similarly, ammonium ion adsorption data are applied to the Langmuir adsorption isotherm, but no linear form is obtained. The equilibrium data from the montmorillonitic clay adsorption isotherm fitted the Freundlich equation better than the Langmuir equation. The Langmuir adsorption paradigm fails in various situations because of its lack of material claim (Mehta et al. 2017).

Table 1: Langmuir data.

	Slope	Intercept	$q_m$	$K_L$	$R_L$	$R^2$
M	0.1575	4.9392	6.349206	0.031888	0.51-0.86	0.915
B	0.1813	2.3991	5.51572	0.07557	0.306-0.726	0.921

Table 2: Freundlich data.

	Slope	Intercept	n	$K_F$	$R^2$
M	0.789	-1.42	1.267427	0.241714	0.999
B	0.6714	-0.713	1.489425	0.490171	0.999

### Freundlich Isotherm

Fig. 9 shows the Freundlich isotherm for batch adsorption of ammonium ions onto clayey surfaces. In this case, the Freundlich isotherm was utilized to match the data. In Fig. 9  $q_e$  versus  $C_e$  was displayed linearly over the concentration range. The amount of adsorbed ammonium ions  $q_e$  increased with equilibrium concentrations  $C_e$ . Table 2 displays the Freundlich isotherm model parameters from Fig. 9 and the statistical fits of the adsorption data to this equation. Because the coefficient of determination  $R^2$  is larger than 0.9 for montmorillonitic clay, the isotherms are consistent for both montmorillonitic and bentonitic clay. Based on Fig. 9, the adsorption intensity (n) and the adsorption capacity ( $K_F$ ). If the  $1/n$  ratio is less than one, chemisorption is occurring, while co-adsorption is occurring. In bentonitic

clay, ammonium ions adsorption was chemisorption and cooperative adsorption. As seen in Table 2, the Freundlich model's ammonium ion constants  $n$  vary (1.2820 - 1.1074).  $n$  represents the adsorption processes' efficiency. According to the Freundlich model, montmorillonitic clay's resorption of ammonium ions is superior to bentonitic clay (Babarinde et al. 2009).

**Application of the Treatment Process for Real Drainage Wastewater**

The collected drainage water from the El-Rahawy drain in

Giza, Egypt, was physiochemically characterized (Table 3). After adding 10 g of clay to 1 L of collected sample and stirring for 60 minutes, the effluents were filtered and characterized physiochemically (Table 3). More than 79 percent of COD and BOD were removed using montmorillonitic clay, while over 84 percent were removed using bentonitic clay. Both clays removed 100 % of sulfide and 100% of total phosphorus. Overall, both clays efficiently eliminated contaminants from drainage water, although bentonitic clay was more effective owing to the presence of alumina silicate and iron oxide in their structure.

Table 3: Physicochemical characterizations of the raw and treated drainage water collected from El-Rahawy drain, Giza, Egypt.

	Raw Drainage water	Treated Effluents			
		Montmorillonitic clay		Bentonitic clay	
		M	% Removal	B	% Removal
COD, mg.L <sup>-1</sup>	108	22	79.63	13	88
BOD, mg.L <sup>-1</sup>	62	13	79	10	84
H <sub>2</sub> S, mg.L <sup>-1</sup>	1.6	0	100	0	100
NH <sub>3</sub> , mg.L <sup>-1</sup>	3.1	0.2	94	0.1	97
TDS, mg.L <sup>-1</sup>	920	1020	-10.87	930	-1.09
TP, mg.L <sup>-1</sup>	0.3	0	100	0	100
TKN, mg.L <sup>-1</sup>	23	6.8	70.4	4.9	78.7

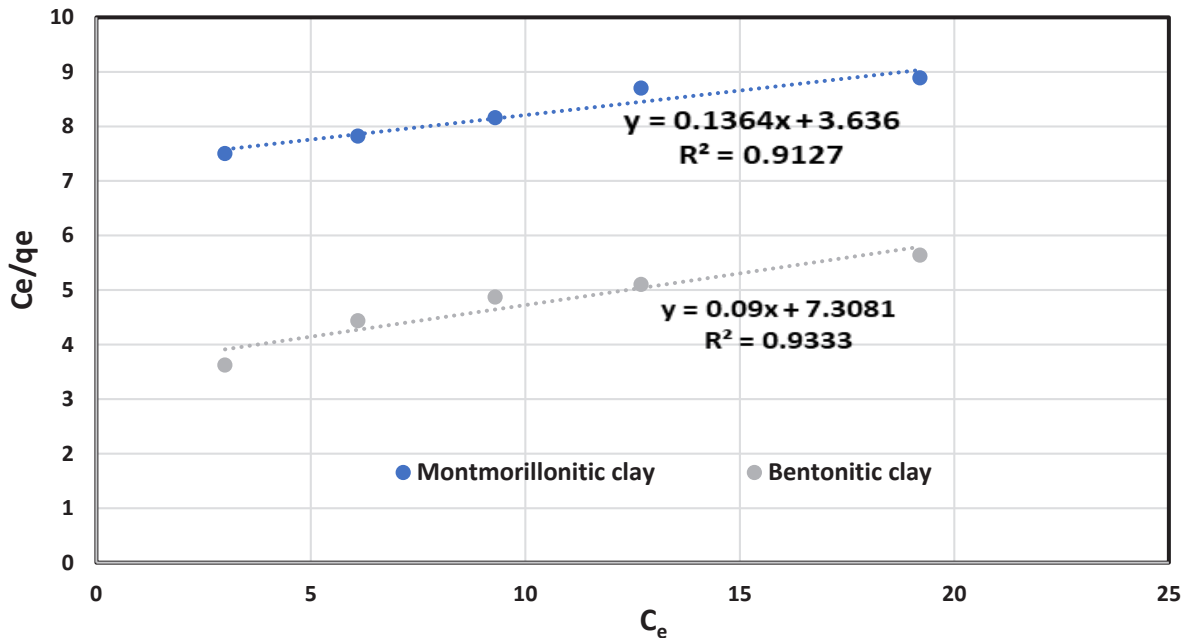


Fig. 8: Langmuir isotherm results for bentonitic and montmorillonitic clay.

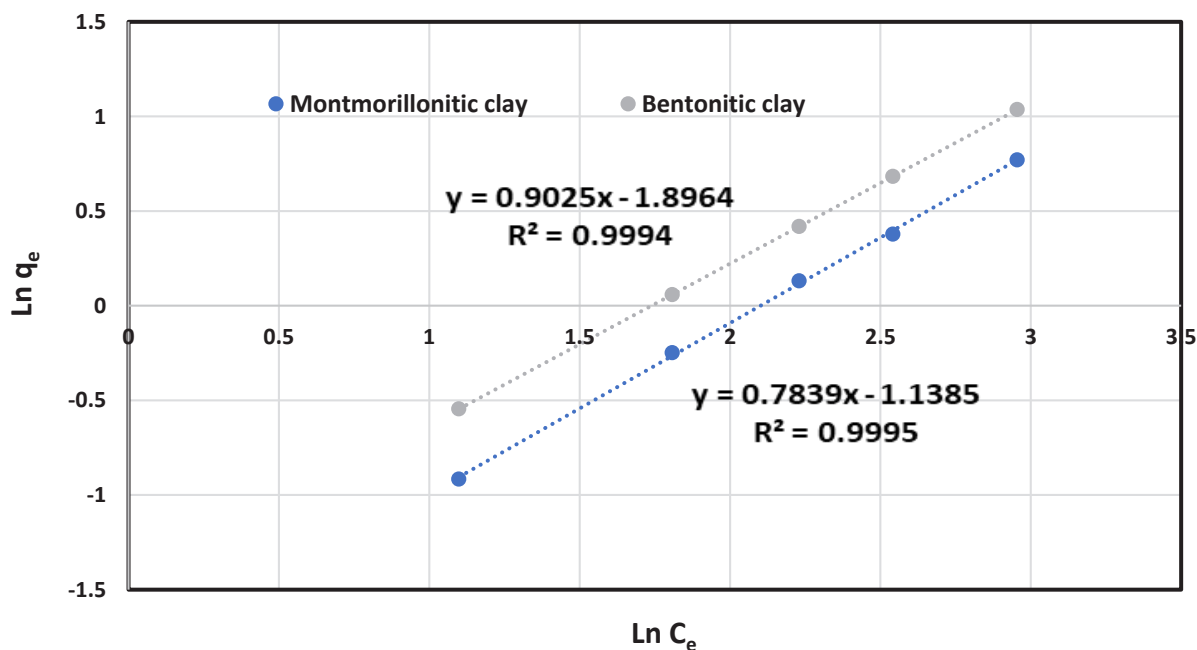


Fig. 9: Freundlich isotherm results for bentonitic and montmorillonitic clay.

## CONCLUSIONS

The adsorption method in the treatment of water pollutants is considered one of the most important and simple methods because it is a simple and sensitive way to remove many water pollutants, and these pollutants include ammonium ions present in sewage water. Besides all the above advantages, it is also a low-cost and environmentally friendly method. The process of removing pollutants is through the functional groups of the absorbents, which affect the surface charge and thus the ability to adsorb. It was classified as acidic or basic, which expanded its ability to remove pollutants, as it can deal with more than one type of pollutant with high efficiency. Added to its advantages is the ability to reuse after extracting ammonium ions, thus saving costs in purchasing additional materials from the absorbent material. Many bioreactors can remove ammonium ions from the water showing how ammonium ion molecules diffuse through the liquid and solid phases when equilibrium is reached. To choose a working model, it is necessary to fit isothermal data with different models. The adsorption properties of ammonium ions, which are often found in wastewater, were studied using two clay materials. The Freundlich, isotherm model fits the experimental data best for montmorillonitic clays alone, while the Langmuir model best fits both types of clays. The isometric models indicated that the absorption is physical and chemical. Both clays succeeded in removing

pollutants from wastewater, although bentonite clays were more effective due to the presence of iron oxide in their structure. Through the given results, we can say that these materials are suitable for practical application due to their ease of availability, low cost, and high efficiency in dealing with a wide range of water pollutants.

## REFERENCES

- Abdelfattah, I. and El-Shamy, A. M. 2022. Chitosan is a potential de-coloring agent for synthetic and textile industrial wastewater. *J. Environ. Account. Manage.*, 10(3): 305-319.
- Aksu, Z. 2001. Equilibrium, and kinetic modeling of cadmium (II) biosorption by *C. Vulgaris* in a batch system: Effect of temperature. *Sep. Purif. Technol.*, 21: 285-294.
- Aruna, N., Bagotia, N., Sharma, A.K. and Kumar S. 2021. A review on modified sugarcane bagasse biosorbent for removal of dyes. *Chemosphere*, 268: 129309.
- Ashraf, K., Eessaa1, El-Shamy, A.M. and Reda, Y. 2018. Fabrication of commercial nanoporous alumina by low voltage anodizing. *Egypt. J. Chem.*, 61(1): 175-185.
- Babarinde, N.A.A., Babalola, J.O., Ogunfowokan, A.O. and Onabanjo, A.C. 2009. Kinetic, equilibrium, and thermodynamic studies of the biosorption of cadmium (II) from solution by *Stereophyllum radiculosum*. *Toxicol. Environ. Chem.*, 91: 911-922.
- Benaissa, H. and Benguella, B. 2004. Effect of anions and cations on cadmium sorption kinetics from aqueous solutions by chitin: Experimental studies and modeling. *Environ. Pollut.*, 130: 157-163.
- Buono, D., Bartucca, M.L., Mimmo, T. and Cesco, S. 2015. Nitrate removal from polluted water by using a vegetated floating system. *Science*, 542: 803-808.

- Chopin, T., Buschmann, A.H., Troell, M., Kautsky, N., Neori, A. and Yarish C. 2011. Integrating seaweeds into marine aquaculture systems: A key toward sustainability. *J. Phycol.*, 37: 975-986.
- Dey, S., Dhal, G.C., Mohan, D. and Prasad, R. 2019. Synthesis of highly active Cobalt catalysts for low-temperature CO oxidation. *Chem. Data Collect.*, 24: 100283.
- Dey, S., Haripavan, N., Basha, S.R. and Babu, G. V. 2021. Removal of ammonia and nitrates from contaminated water by using solid waste bio-adsorbents. *Curr. Res. Chem. Biol.*, 1: 100005.
- Duruibe, J.O., Ogwuegbu, M.O.C. and Egwurugwu, J.N. 2007. Heavy metal pollution and human biotoxic effects. *Int. J. Phys. Sci.*, 2-5: 112-118.
- El-Kashef, E., El-Shamy, A.M., Abdo, A., Gad, E.A.M. and Gado, A.A. 2019. Effect of magnetic treatment of potable water in looped and dead-end water networks. *Egypt. J. Chem.*, 62(8): 1467-1481.
- El-Shamy, A.M., Farag, H.K. and Saad, W. 2017a. Comparative study of removal of heavy metals from industrial wastewater using clay and activated carbon in batch and continuous flow systems. *Egypt. J. Chem.*, 60(6): 1165-1175.
- El-Shamy, A.M., El-Boraey, H.A. and El-Awdan, H.F. 2017b. Chemical treatment of petroleum wastewater and its effect on the corrosion behavior of steel pipelines in sewage networks. *J. Chem. Eng. Process. Technol.*, 8: 1.
- El-Shamy, A.M., Shehata, M.F., Metwally, H.I.M. and Melegy, A. 2017c. Corrosion and corrosion inhibition of steel pipelines in montmorillonitic soil filling material. *Silicon*, 10(6): 2809-2815. <https://doi.org/10.1007/s12633-018-9821-4>
- El-Shamy, A.M., Abdelfattah, I., Elshafey, O.I. and Shehata, M.F. 2018. Potential removal of organic loads from petroleum wastewater and its effect on the corrosion behavior of municipal networks, *J. Environ. Manag.*, 219: 325-331.
- El-Shamy, A.M., Abdo, A., Gad, E.A.M., Gado, A.A. and El-Kashef, E. 2021. The consequence of magnetic field on the parameters of brackish water in batch and continuous flow system. *Bull. Natl. Resour. Cent.*, 45: 105.
- Farag, H.K., El-Shamy, A.M., Sherif, E.M. and El Abedin, S.Z. 2016. Sonochemical synthesis of nanostructured ZnO/Ag composites in an ionic liquid, *Z. Phys. Chem.*, 230(12): 1733-1744.
- Frisoni, G., Baiardo, M., Scandola, M., Lednicka, D., Cnockaert, M.C. and Mergaert, J. 2001. Natural cellulose fibers: heterogeneous acetylation kinetics and biodegradation behavior. *Biomacromolecules*, 2(2): 476-482.
- Goody, D.C., Macdonald, D.M.J., Lapworth, D.J., Bennet, S.A. and Griffiths, K.J. 2014. Nitrogen sources, transport, and processing in peri-urban floodplains. *Sci. Total Environ.*, 494: 28-38.
- Gupta, V.K., Agarwal, S. and Saleh, T.A. 2011. Chromium removal by combining the magnetic properties of iron oxide with the adsorption properties of carbon nanotubes. *Water Res.*, 45: 2207-2212.
- Ho, Y.S., Mckay, G., Wase D.J. and Foster, C.F. 2000. Study of the sorption of divalent metal ions onto peat. *Adsorpt. Sci. Technol.*, 18: 639-650.
- Ibrahim, A.F., Wael, A., and El-Shamy, A.M. 2022. Montmorillonitic clay as a cost-effective, eco-friendly and sustainable adsorbent for the physicochemical treatment of contaminated water. *Egypt. J. Chem.*, 65(2): 687-694. DOI: [10.21608/ejchem.2021.92320.4378](https://doi.org/10.21608/ejchem.2021.92320.4378)
- Ibrahim, A.F., Fathy, A., El-Saied, A.A. and El-Shamy, A.M. 2022. Biosorption as a perfect technique for purification of wastewater contaminated with ammonia. *Appl. Biochem. Biotechnol.*, 79: 379-794. <https://doi.org/10.1007/s12010-021-03794-4>
- Limbachiya, M.C., Nimavat, K.S. and Vyas, K.B. 2012. Physicochemical analysis of groundwater samples of Bechraji region of Gujarat state. *India Asian J. Biochem. Pharmaceut. Res.*, 2(1): 123-130.
- Liu, J., Wan, L., Zhang, L. and Zhou Q. 2011. Effect of pH, ionic strength, and temperature on the phosphate adsorption onto lanthanum-doped activated carbon fiber. *J. Coll. Interf. Sci.*, 364(2): 490-496.
- Luo, P., Zhao, Y., Zhang, B., Liu, J., Yang, Y. and Liu, J. 2010 Study on the adsorption of neutral red from aqueous solution onto halloysite nanotubes. *Water Res.*, 44(5): 1489-1497.
- Mahmoud, M.M., Osman, M., Ahmed, S.B. and Abdel-Fattah, T.M. 2012. Enhanced removal of lead by chemically and biologically treated carbonaceous materials. *Sci. World J.*, 60: 198.
- Mehta, N.S., Dey, S. and Majhi, M.R. 2021. Electro-mechanical characterization of alumina-based porcelain insulator doped with BaTiO<sub>3</sub> at high temperature with frequency variation. *Mater. Chem. Phys.*, 259(4): 124202.
- Mehta, N.S., Kumar, P., Tripathi, P., Pyare, R. and Majhi, M.R. 2017. Influence of alumina and silica addition on the physico-mechanical and dielectric behavior of ceramic porcelain insulator at high sintering temperature. *J. Span. Ceram. Glass Soc.*, 57(4): 151-159.
- Mithra, R., Sivaramakrishnan, S. and Santhanam P. 2012. Investigations on nutrients and heavy metal removal efficacy of seaweeds for wastewater remediation. *J. Algal Biomass Util.*, 3: 21-27.
- Namasivayam, C. and Sangeetha, D. 2004 Equilibrium, and kinetic studies of adsorption of phosphate onto ZnCl<sub>2</sub> activated coir pith carbon. *J. Coll. Interf. Sci.*, 280(2): 359-365.
- Neori A., Ragg, N.I.C. and Shpigel, M. 1998. The integrated culture of seaweed, abalone, fish, and clams in modular intensive land-based systems: II: Performance and nitrogen partitioning within an abalone (*Haliotis tuberculata*) and macroalgae culture system. *Aquacult. Eng.*, 17: 215-239.
- Park, S.J. and Kim, Y.M. 2005. Adsorption behaviors of heavy metal ions onto electrochemically oxidized activated carbon fibers. *Mater. Sci. Eng. A*, 39: 121-123.
- Peez-Corona, T., Madrid-Albamin, Y., Camara, C. and Beceiro E. 1998. Living organisms as an alternative to phyphenated techniques for metal speciation: Evaluation of baker's yeast immobilized on silica gel for Hg speciation. *Spectrochim. Acta B*, 53: 321-329.
- Rajoriya, S. and Kaur, B. 2014. Adsorptive removal of zinc from wastewater by natural biosorbents. *Int. J. Eng. Sci. Inv.*, 3: 60-80.
- Reda, Y., Yehia, H.M. and El-Shamy, A.M. 2022. Microstructural and mechanical properties of Al-Zn alloy 7075 during RRA and triple aging. *Egypt. J. Petrol.*, 31: 9-13. <https://doi.org/10.1016/j.ejpe.2021.12.001>
- Reda Y., El-Shamy, A.M. and Ashraf, K.E. 2018. Effect of hydrogen embrittlement on the microstructures of electroplated steel alloy 4130. *Ain Shams Eng. J.*, 9(4): 2973-2982. <https://doi.org/10.1016/j.asej.2018.08.004>
- Rivett, M.O., Buss, S.R., Morgan, P., Smith, J.W.N. and Bemment, C.D. 2008. Nitrate attenuation in groundwater: A review of biogeochemical controlling processes. *Water Res.*, 42: 4215-4232.
- Saad, A.E., Abass, S.M., Badr El-Din, F.H., Mohamed, S.A. and El-Shamy, A.M. 1997. Use of fungal biomass in batch and continuous flow systems for chromium (VI) recovery. *Afr. J. Mycol. Biotechnol.*, 5: 37-47.
- Samar, M., Mouneir, A., El-Hagrassi, M. and El-Shamy, M.A. 2022. A review of the chemical compositions of natural products and their role in setting current trends and future goals in Egypt. *J. Chem.*, 65(5): 491-506. DOI: [10.21608/ejchem.2021.95577.4486](https://doi.org/10.21608/ejchem.2021.95577.4486)
- Shehata, M.F.S., El-Shafey, N.A., Ammar, A.M. and El-Shamy, A.M. 2019. Reduction of Cu<sup>+2</sup> and Ni<sup>+2</sup> ions from wastewater using mesoporous adsorbent: effect of treated wastewater on corrosion behavior of steel pipelines, *Egypt. J. Chem.*, 62(9): 1587-1602.
- Tse-Lun, C., Li-Heng, C., Yupo, J.L., Chang-Ping, Y., Hwong-Wen, M. and Pen-Chi, C. 2021. Advanced ammonia nitrogen removal and recovery technology using electrokinetic and stripping process towards a sustainable nitrogen cycle: A review. *J. Clean. Prod.*, 309: 127369.
- Tian, S., Jiang, P., Ning, P. and Su Y. 2009. Enhanced adsorption removal of phosphate from water by mixed lanthanum/aluminum pillared montmorillonite. *Chem. Eng. J.*, 151(1-3): 141-148.
- Tian, Y., Yin, P., Qu, R., Wang, C., Zheng, H. and Yu, Z. 2010. Removal of transition metal ions from aqueous solutions by adsorption using a novel hybrid material silica gel chemically modified by tri eth-

- ylene tetra-amino methylene phosphonic acid. *Chem. Eng. J.*, 162: 573-579.
- Varshney, K.G., Khan, A.A., Gupta, U. and Maheshwari, S.M. 1996. Kinetics of adsorption of phosphamidon on antimony(V) phosphate cation exchanger: evaluation of the order of reaction and some physical parameters. *Coll. Surf. A*, 113: 19-23.
- Wang, L., Shi, C., Wang, L., Pan, L., Zhang, X. and Zou, J.J. 2020. Rational design, synthesis, adsorption principles and applications of metal oxide adsorbents: A review. *Nanoscale*, 15: 1-26.
- Young, R.A. 2005. *Toxicity Profiles: Toxicity Summary for Cadmium, Risk Assessment Information System*. RAIS, University of Tennessee, Tennessee.
- Zahra, A. and Mohammad, A. 2013. Adsorptive removal of  $\text{Co}^{2+}$  and  $\text{Ni}^{2+}$  by peels of banana from aqueous solution. *Univers. J. Chem.*, 1(3): 90-95.
- Zohdy, K.M., El-Sherif, R.M. and El-Shamy, A.M. 2021. Corrosion and Passivation Behaviors of Tin in Aqueous Solutions of Different pH. *J. Bio. Tribo. Corros.*, 7(2): 1-7. <https://doi.org/10.1007/s40735-021-00515-6>



# Fluoride Contamination of Groundwater from Semi-Arid Regions of Western India

Reema Mandal\*†, Anirban Das\*, A. K. Sudheer\*\*, Rajnee Ranjan\* and Mahesh Gaddam\*\*

\*Department of Sciences, Pandit Deendayal Energy University, Gandhinagar, Gujarat, India

\*\*Geosciences Division, Physical Research Laboratory, Ahmedabad, Gujarat, India

†Corresponding author: Reema Mandal; reema.mphd16@sot.pdpu.ac.in

Nat. Env. & Poll. Tech.  
Website: [www.neptjournal.com](http://www.neptjournal.com)

Received: 17-02-2022

Revised: 08-04-2022

Accepted: 10-04-2022

## Key Words:

Fluoride

Groundwater

Health risk assessment

Hazard quotient

Fluorosis

Empirical Bayesian Kriging

## ABSTRACT

A study on fluoride risk assessment was carried out in the semi-arid region of North Gujarat, India. The intricate link between groundwater fluoride and human health, lack of awareness, limited access to fluoride treatment facilities, and poor socio-economic conditions of the ~5.0 million rural population in the studied region make them vulnerable to fluoride. This study aimed to evaluate non-carcinogenic health risk, its severity, and the total population at risk in these regions due to chronic fluoride exposure. Fluoride in our samples ( $n=132$ ) exhibits large spatial variability, and it ranges from  $\sim 0.13$ - $8.64$   $\text{mg.L}^{-1}$  (average:  $1.64 \pm 1.50$   $\text{mg.L}^{-1}$ ) and 43% of them are more than the WHO limit of  $1.5$   $\text{mg.L}^{-1}$ . Hazard Quotient (HQ) was used to assess health risks through the ingestion exposure route. The comparison of the range ( $0.1$ - $8.55$  versus  $0.06$ - $4.11$ ), average ( $1.63 \pm 1.49$  versus  $0.78 \pm 0.72$ ), and median ( $1.26$  versus  $0.60$ ) of HQ between children and adults highlights that the former are at more risk compared to latter. Our conservative estimates suggest that  $\sim 0.45$  million children and  $\sim 1.06$  million adult population,  $\sim 55\%$  and  $\sim 20\%$  of the respective population classes, of the region, are potentially at risk. The empirical Bayesian Kriging model was used to produce risk-assessments maps. These can help policymakers in prioritizing the application of mitigation funding and resources, and in increasing testing efforts in high-risk areas. We believe this study should guide policymakers to adopt strategies in ensuring the public health safety of the rural population, children in particular, of the studied region.

## INTRODUCTION

Human health risk associated with high fluoride in drinking water continues to draw considerable attention even in recent years (Ahada & Suthar 2019, Zhang et al. 2020) as it used to draw about a few decades back (Dissanayake 1991, Ozsvath 2009). The intricate link between dissolved fluoride and human health necessitates a critical understanding of the problem and requires approaches (e.g., modeling and simulation, direct measurements, etc.) to determine the associated human health risk. Geogenic sources of fluoride include minerals like fluorite, amphiboles, apatite, and amphiboles (Handa 1975, Hem 1985) while anthropogenic sources include phosphatic fertilizers (Kundu & Mandal 2009), brick kiln industries (Datta et al. 1996), industries like aluminum smelting industries and coal-based power plants (Ali et al. 2016). Chronic consumption of drinking water with fluoride  $>1.5$   $\text{mg.L}^{-1}$  is known to cause different types forms of fluorosis such as degradation of dental enamel, skeletal deformities, ligament-calcification, osteosclerosis, and crippling deformities of joints and spine (Dissanayake et al. 1991, Biglari et al. 2016). Recent studies have also indicated that excess fluoride consumption may even be the cause of neurological effects

(Jiang et al. 2019); genetic effects (Cao et al. 2016); insulin resistance (Dey & Giri 2016); urinary tract diseases (Jha et al. 2011); thyroid hormone issues (Kravchenko et al. 2014); respiratory problems (Follin-Arbelet & Moum 2016) and may even cause cancer in bone, lungs, bladder, and uterus (Yang et al. 2000).

India accounts for  $\sim 50\%$  of the total fluorosis-affected world population (Vithanage & Bhattacharya 2015, Podgorski et al. 2018). With a  $\sim 60\%$  rural population, the Western state of Gujarat is one of the most severely affected states. The rural regions of Gujarat are mostly semi-arid and surface-water-scarce resulting in high reliance of residents on groundwater. Due to poor literacy rates and socio-economic conditions, these rural residents lack awareness about fluoride hazards, and with limited access to water/fluoride treatment facilities, they are coerced to consume untreated groundwater, resulting in their exposure to fluoride (and other contaminants). A few recent articles have highlighted the problem of high fluoride in Gujarat; for example, in Mehsana district Mandal et al. (2021) estimated that  $\sim 0.073$  million children and  $\sim 0.467$  million adults are at risk of fluorosis. Similarly (Shirke et al. 2020) reported  $>1.5$   $\text{mg.L}^{-1}$  in 40%

of the wells in groundwater of the Amba Dongar region. Both these studies inferred that children are at higher risk compared to adults. Additionally, it is also socially pertinent to assess the number of people potentially affected by fluoride-related morbidities in these rural regions. To the best of our knowledge, such studies on Gujarat are at best very sparse (Mandal et al. 2021) despite predictive modeling assessment (Podgorski et al. 2018) indicating that ~11 million population of the state are potentially at risk.

We hypothesize that given the similar level of groundwater contamination, rural populations are likely to be impacted more compared to urban counterparts as the former lack awareness about contamination/hazards, and rural regions lack infrastructure facilities such as fluoride treatment plants. To examine the same, as a case study we carried out a first-time investigation on groundwater fluoride contamination from two northern districts of Gujarat which covers a combined area of ~16000 km<sup>2</sup> with a present-day cumulative population of ~5 million. The hazard quotient is used to estimate the non-carcinogenic risk and its severity, and subsequently, the total population at risk in these regions due to chronic fluoride exposure in groundwater was evaluated. Furthermore, the Empirical Bayesian Kriging model was used to identify the high and low-risk zones in these districts.

## MATERIALS AND METHODS

### Study Area

**Banaskantha district:** Banaskantha district (23°33' N-24°25' N; 71°07' E- 73°02' E) consists of twelve sub-districts (viz. Danta, Amirgadh, Dantiwada, Tharad, Vav, Bhabhar, Vadgam, Deodar, Kankrej, Deesa, Dhanera, and Palanpur; (Fig. 1(a)) and have a geographical area of 10, 303 km<sup>2</sup>. It consists of 1249 villages with a population of ~3.12 million as per the 2011 census (<https://www.censusindia.co.in/district/banas-kantha-district-gujarat-469>). Long-term data suggest that average maximum and minimum temperatures were ~34°C and ~19°C respectively. The climate of the district is semi-arid, with an average yearly rainfall of 580 mm. Ephemeral rivers Banas and Saraswati constitute the drainage network of the district (CGWB 2011).

**Patan district:** Patan district is positioned between 23°24' and 24°09' N latitudes and 71°01' and 72°30' E longitudes in the northern part of Gujarat (Fig 1(b)). It occupies a geographical area of 5740 km<sup>2</sup>. The district is divided into seven sub-districts and consists of 517 villages with a total population of ~1.34 million as per the 2011 census (<https://www.censusindia.co.in/district/patan-district-gujarat-470>). The average maximum temperature is 34.4°C during summer and the minimum temperature is 19.5°C during winter. The district witnesses very low average annual rainfall (403

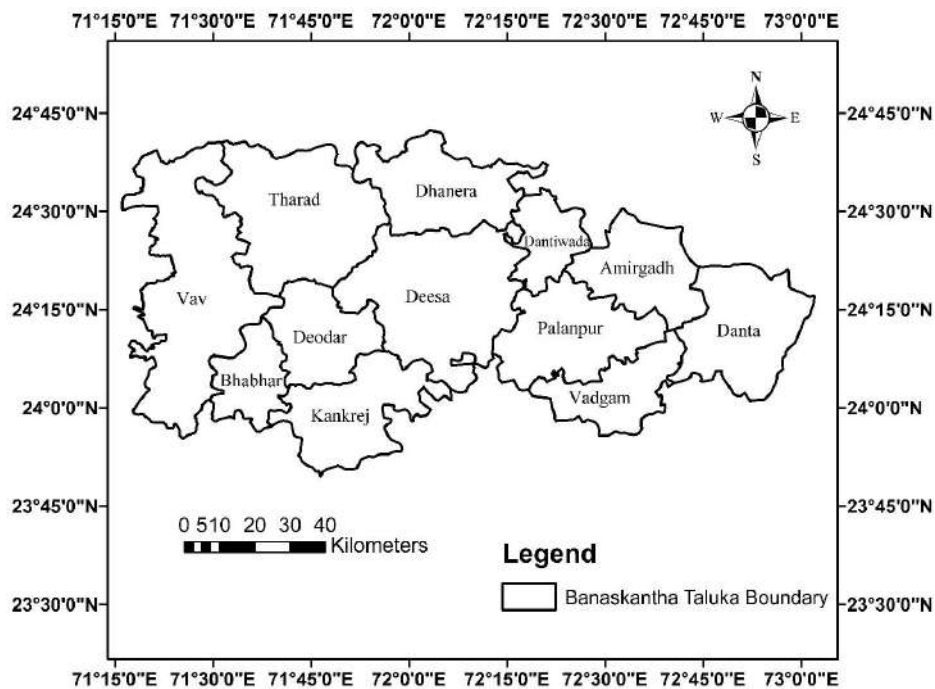


Fig. 1(a): Sub-district map of Banaskantha district.



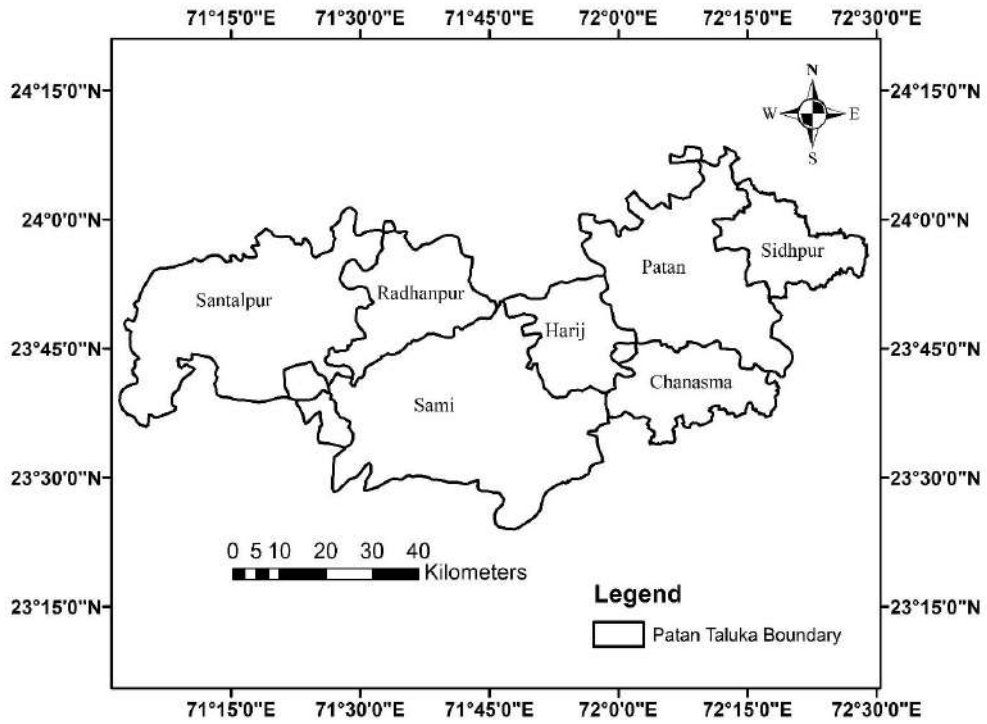


Fig. 1(b): Sub-district map of Patan district.

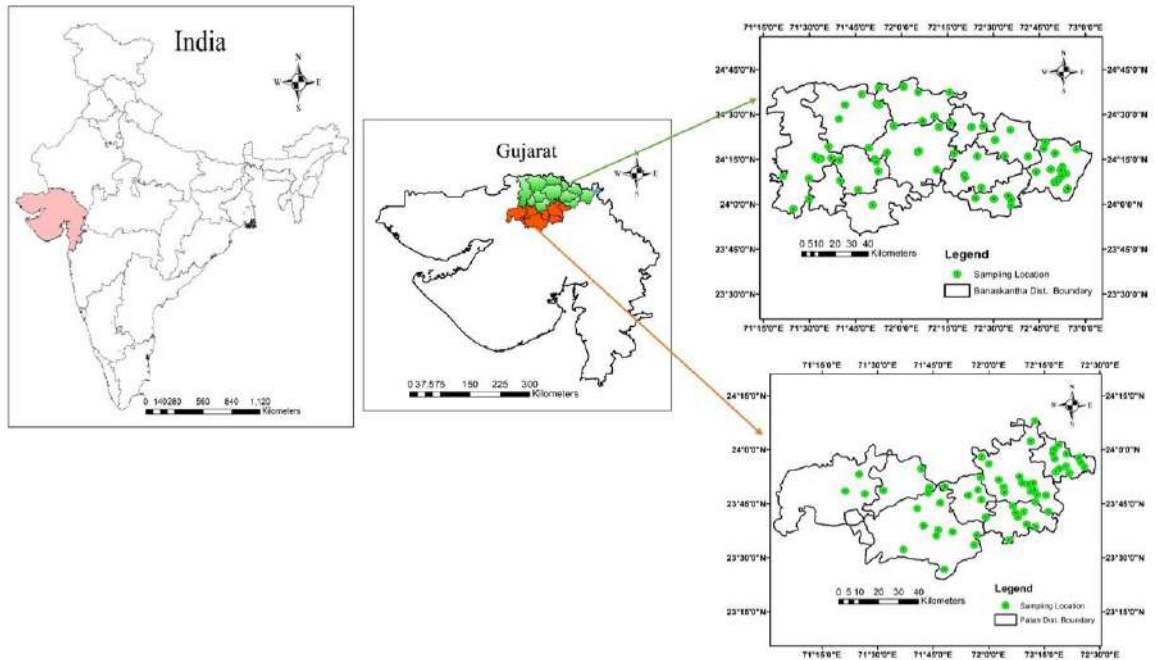


Fig. 1(c): Study area, and location map of the sampling sites in the Banaskantha and Patan districts.

mm) with Khari, Banas, and Umardasi being the three rivers basins (CGWB Report 2014). The district is predominantly covered by alluvium. It has a multi-layer aquifer system that comprises semi-consolidated Mesozoic and Tertiary formations and unconsolidated quaternary alluvial deposits.

### Sampling and Analyses

Groundwater samples were collected either from hand pumps, dug wells, or open wells of the study area. After sufficient purging, bottles were rinsed thoroughly and samples were collected without bubbles into separate bottles each for measurements of alkalinity and major ions, water isotopes, carbon isotopes, and trace elements. In total samples were collected from 132 locations - 72 from the Banaskantha district and 60 from the Patan district (Fig. 1(c)). In some areas of the western part of the Banaskantha district, groundwater samples were not collected as the local population is dependent on the treated river water source for their daily consumption. Random sampling was done from different villages of each sub-district.

In-situ parameters such as pH, temperature, and conductivity measurements were made using portable meters (Eutech PCD 650) with respective precisions better than 0.002 units, 0.1°C, 1  $\mu\text{S}\cdot\text{cm}^{-1}$ , and 1  $\text{mg}\cdot\text{L}^{-1}$ . After collection, samples were stored at 4°C in the laboratory until the analysis of anions. Fluoride and other anions ( $\text{Cl}$ ,  $\text{SO}_4$ , and  $\text{NO}_3$ ) were analyzed in (0.45  $\mu\text{m}$ ) syringe filtered samples by Ion-chromatography (Thermofisher Scientific). AG23 and AS23 columns were used for the separation of the anions, then eluted with a mixture of 0.8 mM  $\text{NaHCO}_3$  and 4.5 mM  $\text{NaCO}_3$  solution, and finally detected with a suppressed electrical conductivity detector. The detector response was calibrated using laboratory-made mixed standards and the consistency of the instrument performance was ensured by monitoring the detector sensitivity throughout the analysis. Overall reproducibility ascertained by a coefficient of variation in repeat measurements is within  $\pm 5\%$  for fluoride.

### Health Risk-Assessment

Non-carcinogenic risks due to fluoride can arise from both oral and dermal exposure routes. In this study, the dermal risk is not taken into consideration as it was found to be very insignificant. Estimation of daily intake (EDI) and Hazard Quotient (HQ) due to fluoride has been made for the oral pathway following USEPA (1989).

$$\text{EDI}_{\text{ORAL}} = (C \times \text{IR} \times \text{EF} \times \text{ED}) / (\text{BW} \times \text{AT}) \quad \dots(1)$$

$$\text{HQ}_{\text{ORAL}} = \text{EDI}_{\text{ORAL}} / \text{RfD}_{\text{ORAL}} \quad \dots(2)$$

In the above equations, C is the measured concentration of fluoride in groundwater ( $\text{mg}\cdot\text{L}^{-1}$ ); IR is daily water intake

rate ( $\text{L}\cdot\text{day}^{-1}$ ); EF is exposure frequency ( $\text{day}\cdot\text{y}^{-1}$ ); ED is exposure duration (y); AT is averaging time (day) and BW is average body weight (kg) of the consumer (e.g., adult or children).  $\text{HQ}_{\text{ORAL}}$  has been calculated separately for adults and children. Values of 350 days per year (EF), 30 years (ED), 10500 days (AT); 2  $\text{L}\cdot\text{day}^{-1}$  (IR), and 70 kg (BW) are used for adults while the corresponding values used for children are 350 days per year (EF), 6 years (ED), 2100 days (AT); 0.89  $\text{L}\cdot\text{day}^{-1}$  (IR) and 15 kg (BW).  $\text{RfD}_{\text{ORAL}}$ , the reference oral dose, has been taken as 0.06  $\text{mg}\cdot\text{F}\cdot\text{kg}^{-1}\cdot\text{body weight}\cdot\text{day}^{-1}$  (USEPA 1989, Ali et al. 2019). Using these values it is found that the product of EF and ED is equal to that of AT, thus equation 2 can further be simplified to:

$$\text{HQ}_{\text{ORAL}} = C \times \text{IR} / (\text{RfD}_{\text{ORAL}} \times \text{BW}) \quad \dots(2a)$$

The magnitude of HQ determines the probabilistic non-carcinogenic risk with HQ values  $< 1$  indicating that the water is safe for consumption while  $\text{HQ}_{\text{ORAL}} > 1$  indicates potential risks of fluorosis.

### Geostatistical Modeling

In our study, ESRI ArcGIS 10.7 software (License no - EFL000908614 ArcGIS Pro Geostatistical Analyst) was used to perform the geostatistical modeling. Empirical Bayesian Kriging (EBK) was applied to calculate HQ values to map its spatial variation and to identify the high-risk zones within the study area. The EBK model was preferred as it was reported to be more realistic and comprehensive than other interpolation techniques (Krivoruchko 2012, Mukherjee et al. 2019). It differs from the classical Kriging model as it automates the critical aspect of building a valid Kriging model through subsetting and simulation. In this interpolation technique, errors are estimated based on semivariograms obtained through repeated simulation (Emenike et al. 2018) whereas the other techniques need manual adjustment for accuracy. The accuracy and robustness of the EBK model were gauged by the calculated error parameters such as root-mean-square predicted (RMSP), mean standardized error (MS), root-mean-square-standardized (RMSS), and average standard (AS) error.

## RESULTS AND DISCUSSION

### Fluoride Distribution

Fluoride concentrations in our groundwater samples are reported in Table 1. The fluoride in our samples ( $n=132$ ) ranged from 0.13 to 8.64  $\text{mg}\cdot\text{L}^{-1}$  with an average of  $1.65 \pm 1.50$   $\text{mg}\cdot\text{L}^{-1}$  and a median value of 1.27  $\text{mg}\cdot\text{L}^{-1}$ . The observed range and average for the Banaskantha region are 0.13-6.03  $\text{mg}\cdot\text{L}^{-1}$  and  $1.68 \pm 1.27$   $\text{mg}\cdot\text{L}^{-1}$  while for the Patan region these values are 0.18-8.64  $\text{mg}\cdot\text{L}^{-1}$  and  $1.61 \pm 1.75$   $\text{mg}\cdot\text{L}^{-1}$

respectively. About 44% (32 of the 72) and 42% (25 of the 60) of the samples collected in Banaskantha and Patan districts respectively have fluoride above the WHO's maximum permissible limit (MPL) of 1.5 mg.L<sup>-1</sup> for safe drinking. The distribution pattern of fluoride levels across the study area indicates that ~20% of the samples had <0.5 mg.L<sup>-1</sup>; 22% within 0.5-1.0 mg.L<sup>-1</sup>; 15% fall within the regulatory limits of 1.0-1.5 mg.L<sup>-1</sup> while 43% of the samples having fluoride higher than MPL.

**Fluoride Risk-Assessment**

In our study area, fluoride >1.5 mg.L<sup>-1</sup> in 43% of the samples (n=132) underscores the significance of assessing the risk due to the consumption of groundwater. The dermal risk appears to be insignificant compared to oral intake. Health risk assessment (HQ; equation 2) depends on three parameters, of which, the concentration of fluoride is measured, while IR and BW are average values recommended by environmental/health/medical agencies (e.g., USEPA, and Indian Council of Medical Research and National Institute of Nutrition (ICMR-NIN); Health Canada).

USEPA recommends the use of IR value of 2 L.day<sup>-1</sup> and 0.89 L.day<sup>-1</sup> for adults and children respectively, whereas the corresponding values for BW are 70 kg and 15 kg. For India, where most of the regions are hot (semi)-arid or humid, average water consumption by working rural resident adults can be higher than 2 L.day<sup>-1</sup> and thus the fluoride exposure

may even be higher than calculated using USEPA parameters. Recently ICMR-NIN has reported values of water intake for Indian adult males (32-58 mL.kg<sup>-1</sup> BW), adult females (27-52 mL.kg<sup>-1</sup> BW), and children (60 mL.kg<sup>-1</sup> BW) —the lower limit and upper limit of the range are associated with sedentary-working and high-working persons (ICMR-NIN report, 2020). Similarly, the recommended average BW of adult males and adult females are 65 kg and 55 kg respectively. Based on these average BW values, the IR range translates to 2.1-3.7 L.day<sup>-1</sup> (adult male), 1.5-2.9 L.day<sup>-1</sup> (adult female) and 0.9 L.day<sup>-1</sup> (children). Calculated HQs using USEPA, and the range of ICMR-NIN parameters yield variable results (summarized in Table 1) showing that choice of average IR and BW values are critical. We have however used the lower-bound estimate of HQ (i.e., USEPA parameters) for evaluating risk and geospatial HQ mapping of the region. The distinction between males and females has not been made while calculating HQ values for adults though females are prone to more risk because of their lower BW (Table 1).

Calculated HQ values range from 0.06-4.11 for adults (average: 0.78 ± 0.72; median: 0.60) and 0.13-8.55 for children (average: 1.63 ± 1.49; median: 1.26) highlighting that children are more prone to risk because of their lower body weight though somewhat offset by their lower daily water consumption compared to adults. This inference is similar to the finding in previous studies (Adimalla et al. 2018, Ahada & Suthar 2019). To get better insight into the

Table 1: Calculated HQ<sub>Oral</sub> values for adults and children using USEPA and ICMR-NIN parameters. The HQ values show high variability.

Reference	Population class	IR [L. day <sup>-1</sup> ]	BW [kg]	HQ					
				Min.	Max.	Average	Standard deviation	Median	% samples with HQ>1
USEPA	Adult	2	70	0.06	4.11	0.78	0.72	0.6	28
USEPA	Children	0.89	15	0.13	8.55	1.63	1.49	1.26	58
ICMR-NIN, India	Adult (male)	2.1	65	0.07	4.65	0.88	0.87	0.68	35
	Adult (male)	2.9	65	0.1	6.43	1.22	1.2	0.94	45
	Adult (male)	3.7	65	0.12	8.2	1.55	1.53	1.2	56
ICMR-NIN, India	Adult (female)	1.5	55	0.06	3.93	0.74	0.73	0.58	26
	Adult (female)	2.2	55	0.09	5.76	1.09	1.08	0.85	43
	Adult (female)	2.9	55	0.11	7.59	1.44	1.42	1.12	52
ICMR-NIN, India	Children	0.9	15	0.13	8.64	1.65	1.5	1.27	58

potential risk to the population, HQ values were analyzed sub-district-wise. This approach is particularly beneficial to undertake mitigation measures at smaller space-domain and targeting smaller populations by the local authorities. Significant percentages of samples having  $HQ_{adult} > 1$  are observed for Danta (67%), Dhanera (43%), Vadgam (40%), Dantiwada (33%), Palanpur (25%), Amirgarh (25%), Sidhpur (44%), Patan (43%) and Harij (33%). Importantly, the fact that in the remaining 11 sub-districts less than 20% of the collected samples is having  $HQ_{adult} > 1$  underscores the lesser risk associated with the local population in them.

The oral exposure risk turns out to be more serious for children with 76 of 133 samples (58%) having  $HQ_{child} > 1$ . In our study area sub-districts with  $\geq 50\%$  of the collected samples having  $HQ_{child} > 1$  are Danta (100%), Dhanera (86%), Vadgam (60%), Dantiwada (100%), Palanpur (75%), Deesa (75%), Tharad (50%), Sidhpur (69%), Patan (57%), Radhanpur (67%) and Chanasma (55%). There are only three sub-districts (viz. Bhabhar, Sami, and Santalpur) in the entire region wherein the calculated exposure risk to children is nominal with no samples having  $HQ_{child} > 1$ .

### Population at Potential Risk

Translating the facts above (discussed in section 3.2) to the total adult and total child population potentially at risk in each of the sub-districts rests on the premise that the groundwater sampling is representative, and it requires population data in each sub-district and the % of risk-prone samples. High resolution and seasonal sampling address biases and uncertainties in representative sampling. Reliable estimates of sub-district level population data are available from the census of 2011. Two approaches can be adopted for determining the % of risk-prone samples in any given sub-district: either it can be taken as the same as that of % of samples with fluoride  $> 1.5 \text{ mg.L}^{-1}$  (e.g., Podgorski et al. 2018) or equal to the % of samples having  $HQ > 1$  (e.g., Mandal et al. 2021). Our calculations demonstrate that the latter approach provides a lower-bound estimate of the adult population at risk. An independent substantiation of the latter approach is made by calculating the total no of risk-prone villages in the Patan district and further matching it with reported data. We estimated the number of risk-prone villages in a sub-district by multiplying the % of samples with  $HQ_{adult} > 1$  in the sub-district by the total number of villages in it. Such exercise shows that there are 103 risk-prone villages in the Patan district- similar to/slightly lower than the 126 reported by Central Groundwater Board (CGWB 2014). Such could not be verified for the Banaskantha district due to a lack of available information on the number of risk-prone villages in it.

Estimates of adult and child populations at risk in each sub-districts are presented in Table 2. Calculations show that an estimated  $\sim 0.92$  million of the adult population and  $\sim 0.39$  million of the child population in the study area are potentially at risk due to the consumption of groundwater fluoride. With a projected increase of  $\sim 15\%$  in population during 2011-2020 (<http://www.population.u.com/in/gujarat-population>), currently, these values would translate to  $\sim 1.06$  million adults and  $\sim 0.45$  million children respectively. These values respectively are  $\sim 20\%$  of the adult population and  $\sim 55\%$  of the children population of the region. Our current estimate of  $\sim 1.51$  million reveals that  $\sim 30\%$  of the total (adult + children) population in the study area is potentially at risk.

An assessment of the potential risk severity was made based on Dissanayke's classification (1991). Results show that while 57% of the collected samples are conducive to tooth development and prevent decay, the probabilistic occurrence of dental fluorosis and dental-and-skeletal fluorosis is associated with  $\sim 37\%$  and  $\sim 6\%$  of the samples. With no samples having fluoride concentration  $> 10 \text{ mg.L}^{-1}$  the chances of crippling fluorosis are almost negligible. Furthermore, field photographs of children suffering from dental fluorosis (Fig. 2a and 2b) from the Danta region (within the Banaskantha district) are a testament to a real depiction of the fluoride problem in the study area.

### Geostatistical Modeling

Geostatistical HQ maps are depicted in Figs. 3(a-d). The validity, accuracy, and reliability of the geospatial modeling are assessed by parameters RMSS, MSE, RMSP, and ASE. In our case, the RMSS values obtained are 0.99 (Fig. 3a), 0.98 (Fig. 3b), 1.01 (Fig. 3c), and 1.02 (Fig. 3d); all values close to 1 are indicative of the significant accuracy in prediction estimates (Mukherjee et al. 2019). Furthermore, corresponding MSE values for these Figs. being close to 0 (0.02, 0.01, 0.02, 0.03) indicate valid predictions. Finally, the close values of RMSP and ASE with an average RMSP/ASE ratio of  $1.00 \pm 0.02$  signify the validity of the model output.

$HQ_{adult}$  mapping is shown for ranges (0.0 to 3.0) for Banaskantha (Fig. 3a) and (0.0 to 4.5) for Patan (Fig. 3c). It appears from Fig. 3a that adults are prone to the fluoride risk in Danta and eastern margins of the Amirgadh sub-districts (within Banaskantha region), and in parts of Sidhpur and Patan sub-districts (within Patan region; Fig. 3c). A significant yet concerning observation made from the comparisons of Fig. 3 (a, c) versus Fig. 3 (b, d) is that the children are more prone to risk compared to adults in both the sub-districts. In the Banaskantha region, very high  $HQ_{children}$  values ( $> 2.5$  to 6) were observed in the Danta sub-district (Fig. 3b) while others such as Dhanera, Dantiwada, Amirgadh, Palanpur, and

Table 2: Sub-district-wise statistical data of  $HQ_{oral}$  and the adult and children population at risk in Banaskantha and Patan districts.

Sr.No	Sub-district	Total samples	% of samples in $F>1.5$	% of samples in $HQ>1$	No of vil-lages in the sub-district		Population (Adult/Children)	Population at risk based on HQ	
Banaskantha	1	Danta	15	86	60	184	A	224839	134903
					100		C	46737	46737
	2	Palanpur	4	50	25	116	A	438773	109693
					75		C	56326	42244
	3	Vav	8	12.5	12.5	121	A	246156	30769
					25		C	41637	10409
	4	Tharad	6	16.6	0	134	A	327289	0
					50		C	56373	28186
	5	Dantiwada	3	100	33.3	57	A	115221	38407
					100		C	19051	19051
	6	Dhanera	7	71	42.9	77	A	230741	98889
					85.7		C	40759	34936
	7	Deesa	12	33	8.3	148	A	588123	49010
					75		C	94341	70755
	8	Deodhar	4	0	0	70	A	177919	0
					25		C	29161	7290
	9	Vadgam	5	40	40	109	A	240326	96130
					60		C	32382	19429
	10	Amirgadh	4	25	25	69	A	132354	33088
25					C		28030	7007	
11	Kankrej	2	0	0	101	A	275613	0	
				50		C	44364	22182	
12	Bhabhar	2	0	0	51	A	123152	0	
				0		C	21149	0	
13	Sidhpur	16	10	37.5	53	A	213087	79908	
				68.8		C	27375	18820	
14	Patan	14	7	42.9	139	A	449480	192634	
				57.1		C	58359	33348	
15	Harij	6	2	33.3	39	A	94562	31521	
				33.3		C	13127	4376	
16	Santalpur	3	0	0	73	A	128791	0	
				0		C	22074	0	
17	Radhanpur	3	1	0	56	A	144266	0	
				66.7		C	22416	14944	
18	Sami	7	0	0	98	A	182805	0	
				0		C	26560	0	
19	Chanasma	11	5	18.2	59	A	130743	23771	
				54.5		C	14868	8110	



Fig. 2a: Field photograph of a child suffering from dental fluorosis. The child is a resident of the Danta sub-district in the Banaskantha district.



Fig. 2b: Field photograph of another child (resident of Danta) suffering from dental fluorosis.

Vadgam are all associated with high fluoride risk,  $HQ_{\text{children}}$  values  $> 1.5$ .

## CONCLUSIONS

Fluoride contamination was investigated in groundwater from Banaskantha and Patan district, Gujarat, Western India. The five million residents of the studied region are vulnerable

to fluoride exposure as they are compelled to consume untreated groundwater due to the limited availability of surface water resources in the region, and their sparse access to water treatment facilities.

Health risks were assessed through the ingestion exposure route only while dermal contribution was found to be very insignificant.  $HQ_{\text{adult}}$  ranges from 0.06-4.11 (average:

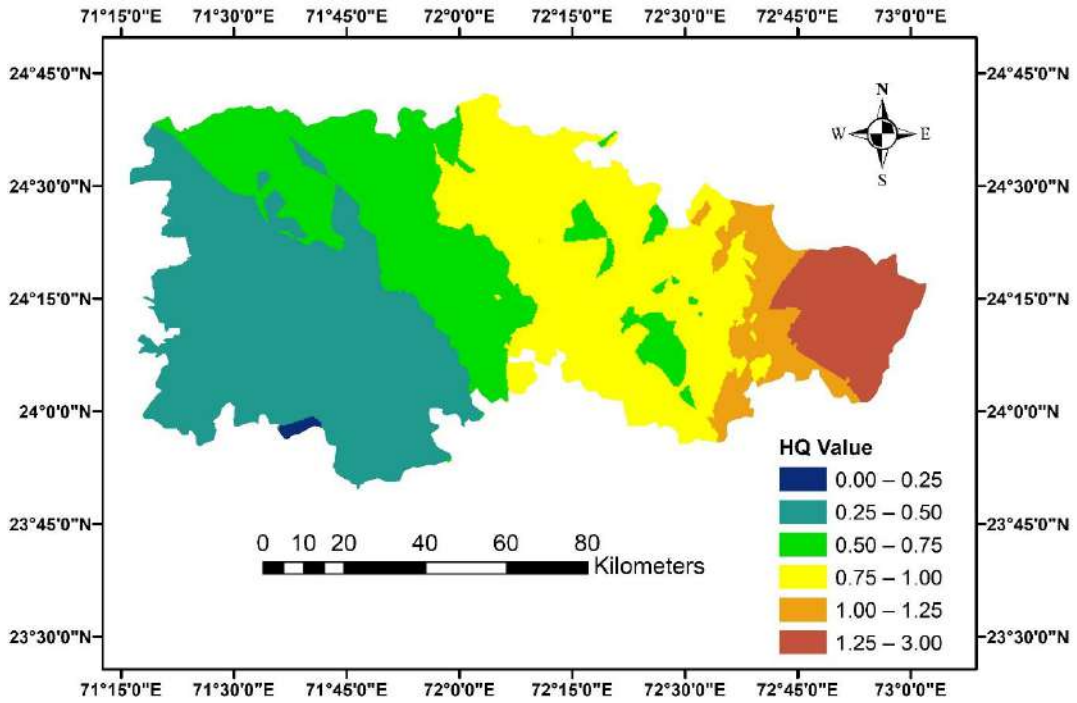


Fig. 3a: Health risk assessment (HQ<sub>oral</sub>) for adults in the Banaskantha district. The map was produced using Empirical Bayesian Kriging (EBK) model.

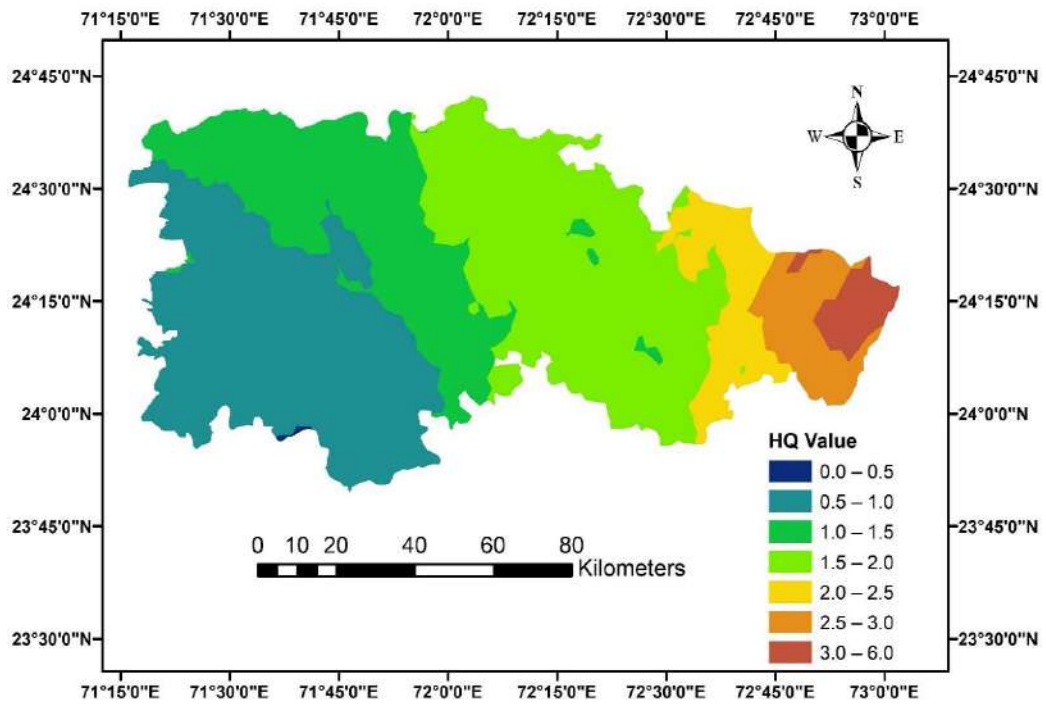


Fig. 3b: Health risk assessment (HQ<sub>oral</sub>) for children in the Banaskantha district. (Map produced by EBK model).

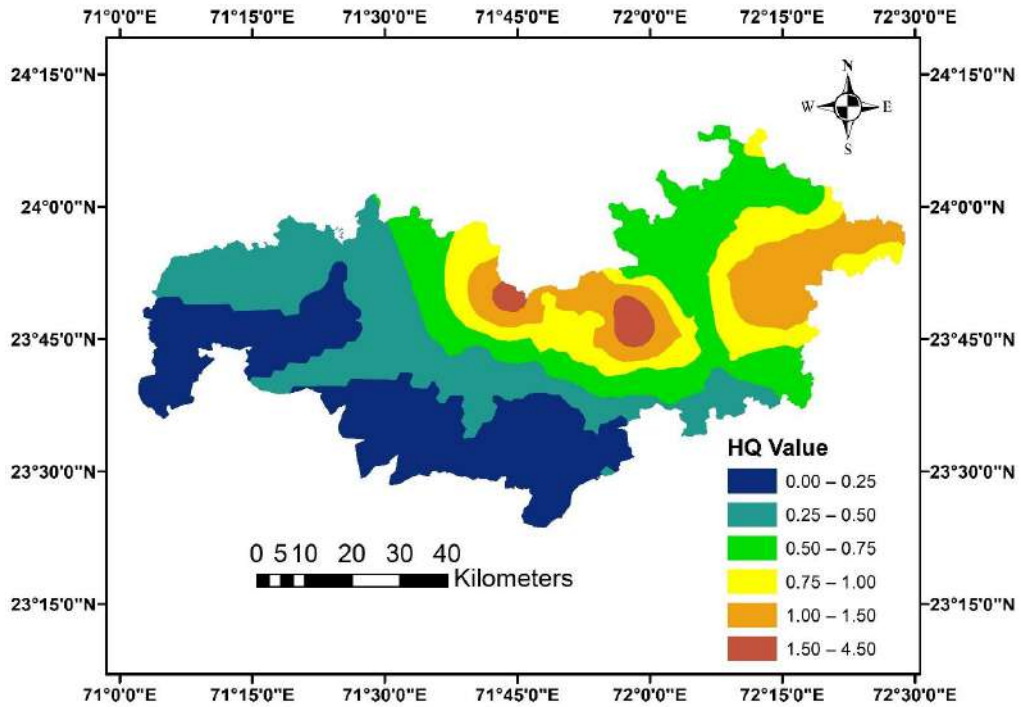


Fig. 3c: Health risk assessment ( $HQ_{oral}$ ) for adults in the Patan district. (Map produced by EBK model).

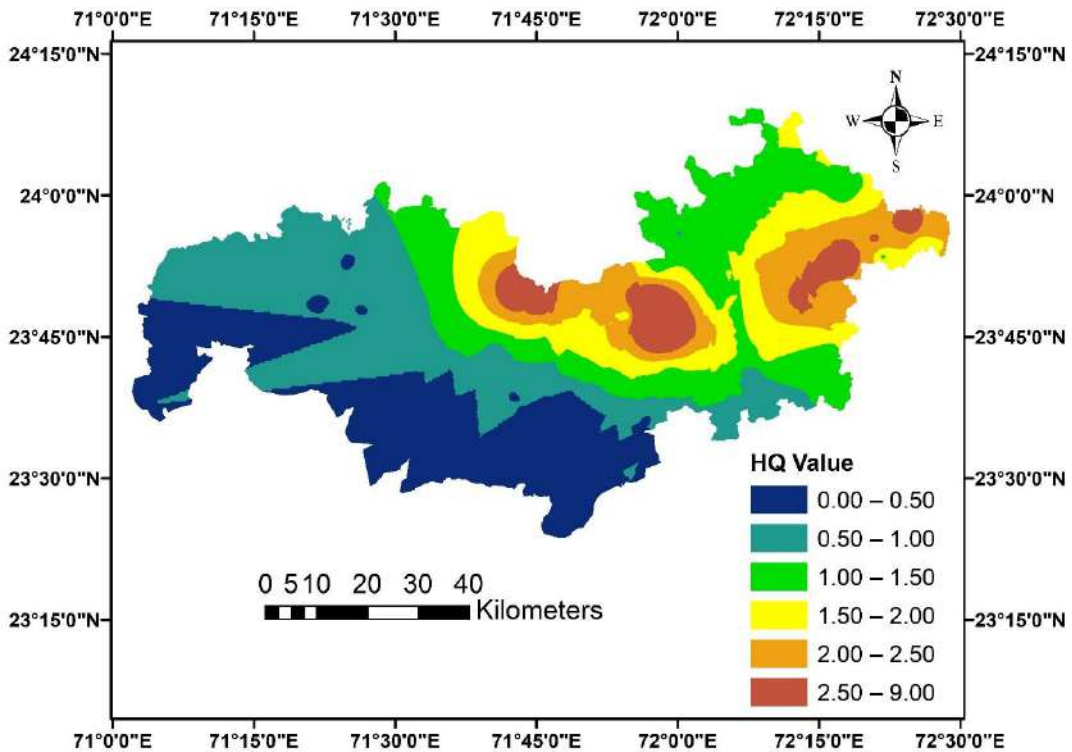


Fig.3d: Health risk assessment ( $HQ_{oral}$ ) for children in the Patan district. (Map produced by EBK model)



0.78 ± 0.72; median: 0.60) and values >1 were found in 28% of samples. In comparison, the range (0.1-8.55), average (1.63 ± 1.49), median (1.26), and 58% samples having  $HQ_{children} > 1$  all highlight that children are much more susceptible to fluoride risk compared to adults. Our conservative estimates suggest that ~20% of the adult population and ~55% of the child population of the region are potentially at risk. Photographs taken of children suffering from dental fluorosis are a testament to the real depiction of the hazard.

HQ maps of the endemic regions were produced by the Empirical Bayesian Kriging model. This mapping would help policymakers in channelizing mitigation funding and resources, and in increasing testing efforts in high-risk areas in Danta, Dantiwada, Dhanera, Vadgam, Sidhpur, and Patan sub-districts. Installation of fluoride treatment plants is suggested in these areas while rainwater harvesting is also suggested as a viable alternative. We hope that this study can help policymakers to adopt strategies to manage the regional groundwater resources better, in ensuring public health safety of the local population of the region, children in particular, from fluoride-related morbidities. We also believe that this article should stimulate further research concentrating on rural regions of India and other such countries, to estimate accurately the population impacted by fluoride contamination.

## ACKNOWLEDGEMENT

We acknowledge Physical Research Laboratory, Ahmedabad, India, for the technical support.

## REFERENCES

- Adimalla, N., Li, P. and Qian, H. 2018. Evaluation of groundwater contamination for fluoride and nitrate in a semi-arid region of Nirmal Province, South India: A special emphasis on human health risk assessment (HHRA). *Human Ecol. Risk Assess. Int. J.*, 14: 579 <https://doi.org/10.1080/10807039.2018.1460579>
- Ahada, C.P and Suthar, S. 2019. Assessment of human health risk associated with high groundwater fluoride intake in southern districts of Punjab, India. *Expos. Health*, 11(4): 267-275.
- Ali, S., Thakur, S.K., Sarkar, A. and Shekhar, S. 2016. Worldwide contamination of water by fluoride. *Environ. Chem. Lett.*, 14(3): 291-315.
- Biglari, H., Chavoshani, A., Javan, N. and Hossein Mahvi, A. 2016. Geochemical study of groundwater conditions with special emphasis on fluoride concentration, Iran. *Desalin. Water Treat.*, 57(47): 22392-22399.
- Cao, J., Chen, Y., Chen, J., Yan, H., Li, M. and Wang, J. 2016. Fluoride exposure changed the structure and the expressions of Y chromosome-related genes in the testes of mice. *Chemosphere*, 161: 292-299.
- CGWB Report 2014. Aquifer Mapping and Management of Groundwater Resources Banaskantha District, Gujarat. Central Ground Water Board Department of Water Resources, River Development and Ganga Rejuvenation, Ministry of Jal Shakti Government of India.
- CGWB. 2011. District Groundwater Brochure, Banaskantha District, Gujarat. Government of India, Ministry of Water Resources, Central Ground Water Board, West Central Region, Ahmedabad.
- CGWB. 2014. District Groundwater Brochure, Patan District, Gujarat. Government of India, Ministry of Water Resources, Central Ground Water Board, West Central Region, Ahmedabad.
- Datta, P.S., Deb, D.L. and Tyagi, S.K. 1996. Stable isotope ( $^{18}O$ ) investigations on the processes controlling fluoride contamination of groundwater. *J. Contam. Hydrol.*, 24(1): 85-96. DOI: 10.1016/0169-7722(96)00004-6
- Dey, S. and Giri, B. 2016. Fluoride fact on human health and health problems: A review. *Med Clin Rev.*, 2(1): 11.
- Dissanayake, C.B. 1991. The fluoride problem in the groundwater of Sri Lanka: Environmental management and health. *Int. J. Environ. Stud.*, 38(2-3): 137-155.
- Emenike, C.P., Tenebe, I.T and Jarvis, P. 2018. Fluoride contamination in groundwater sources in Southwestern Nigeria: Assessment using multivariate statistical approach and human health risk. *Ecotoxicol. Environ. Saf.*, 156: 391-402.
- Follin-Arbelet, B. and Moum, B. 2016. Fluoride: A risk factor for inflammatory bowel disease? *Scand. J. Gastroenterol.* 51: 1019e1024. <https://doi.org/10.1080/00365521.2016.1177855>.
- Handa, B.K. 1975. Geochemistry and genesis of fluoride-containing ground waters in India. *Groundwater*, 13(3): 275-281.
- Hem, J.D. 1985. Study and interpretation of the chemical characteristics of natural water (Vol. 2254). Department of the Interior, US Geological Survey, Virginia, US.
- ICMR-NIN. 2020. Nutrient requirements for Indians recommended dietary allowances and estimated average requirements.
- Jha, S.K., Mishra, V.K., Sharma, D.K. and Damodaran, T. 2011. Fluoride in the environment and its metabolism in humans. In: Whitacre, D.M. (ed.), *Environmental Contamination and Toxicology*, Springer, New York, NY, pp. 121e142. [https://doi.org/10.1007/978-1-4419-8011-3\\_4](https://doi.org/10.1007/978-1-4419-8011-3_4)
- Jiang, P., Li, G., Zhou, X., Wang, C., Qiao, Y., Liao, D. and Shi, D. 2019. Chronic fluoride exposure induces neuronal apoptosis and impairs neurogenesis and synaptic plasticity: Role of GSK-3 $\beta$ / $\beta$ -catenin pathway. *Chemosphere*, 214: 430-435.
- Kravchenko, J., Rango, T., Akushevich, I., Atlaw, B., McCormick, P.G., Merola, R.B., Paul, C., Weinthal, E., Harrison, C., Vengosh, A. and Jeuland, M. 2014. The effect of non-fluoride factors on risk of dental fluorosis: evidence from rural populations of the Main Ethiopian Rift. *Sci. Total Environ.*, 87: 595-606. <https://doi.org/10.1016/j.scitotenv.2013.12.087>
- Krivoruchko, K. 2012. Empirical Bayesian kriging. *ArcUser Fall*, 6(10): 71.
- Kundu, M.C. and Mandal, B. 2009. Assessment of potential hazards of fluoride contamination in drinking groundwater of an intensively cultivated district in West Bengal, India. *Environ. Monit. Assess.*, 152(1-4): 97. DOI: 10.1007/s10661-008-0299-1
- Mandal, R., Das, A., Sudheer, A.K., Kumar, S., Verma, S., Gaddam, M. and Deshpande, R.D. 2021. Sources, controls, and probabilistic health risk assessment of fluoride contamination in groundwater from a semi-arid region in Gujarat, Western India: An isotope-hydrogeochemical perspective. *Environ. Geochem. Health*, 11: 1-17.
- Mukherjee, I., Singh, U.K. and Patra, P.K. 2019. Exploring a multi-exposure-pathway approach to assess human health risks associated with groundwater fluoride exposure in the semi-arid region of eastern India. *Chemosphere*, 233: 164-173.
- Ozsvath, D.L. 2009. Fluoride and environmental health: a review. *Rev. Environ. Sci. Biotechnol.*, 8(1): 59-79.
- Podgorski, J.E., Labhasetwar, P., Saha, D. and Berg, M. 2018. Prediction modeling and mapping of groundwater fluoride contamination throughout India. *Environ. Sci. Technol.*, 52(17): 9889-9898.
- Shirke, K.D., Kadam, A.K. and Pawar, N.J. 2020. Temporal variations in hydro-geochemistry and potential health risk assessment of groundwater from lithological diversity of the semi-arid region, Western Gujarat, India. *Appl. Water Sci.*, 10(6): 1-20.
- USEPA. 1989. Risk Assessment Guidance for Superfund Volume I: Human

- Health Evaluation Manual (Part A). U.S. Environmental Protection Agency, Washington, DC.
- Vithanage, M. and Bhattacharya, P. 2015. Fluoride in the environment: sources, distribution, and defluoridation. *Environ. Chem. Lett.*, 13(2): 131-147.
- Yang, C.Y., Cheng, M.F., Tsai, S.S. and Hung, C.F. 2000. Fluoride in drinking water and cancer mortality in Taiwan. *Environ. Res.*, 82: 189e193. <https://doi.org/10.1006/enrs.1999.4018>.
- Zhang, L., Zhao, L., Zeng, Q., Fu, G., Feng, B., Lin, X., Liu Z., Wang, Y. and Hou, C. 2020. Spatial distribution of fluoride in drinking water and health risk assessment of children in typical fluorosis areas in north China. *Chemosphere*, 239: 124811.



# Payment for Environmental Services in Indonesia: Mutually Beneficial Watershed Environmental Management Model

N. Sunaedi\*†, S. P. Hadi\*\* and A. N. Bambang\*\*

\*Department of Geography Education, Siliwangi University, Jalan Siliwangi No. 24, Tasikmalaya 46115, West Java, Indonesia

\*\*Department of Environmental Science, Postgraduate School of Diponegoro University, Jalan Imam Bardjo SH No. 5-7, Semarang 50241, Central Java, Indonesia

†Corresponding author: N. Sunaedi; nedisunaedi@unsil.ac.id

**Nat. Env. & Poll. Tech.**  
Website: [www.neptjournal.com](http://www.neptjournal.com)

Received: 04-03-2022  
Revised: 02-04-2022  
Accepted: 06-04-2022

## Key Words:

Environmental services  
Watershed  
Environmental services users  
Environmental services providers

## ABSTRACT

Payment for Environmental Services (PES) is an effort and commitment of the world community in tackling the symptoms of global warming and damage to the ozone layer that will affect global climate change. Using field research methods, research data is collected through in-depth interviews with stakeholders in environmental services return programs in this research area. Research data is analyzed and described qualitatively for further conclusions. The concept developed upstream and downstream watershed relationships through the PES mechanism is based on the principle of voluntary agreement and awareness of maintaining the watershed ecosystem. The experience of implementing the PES Program in the Cidanau Watershed of Banten Province of Indonesia, managed by an independent institution. The PES program, in addition to its role as an environmental conservation program in the Cidanau watershed, also has socio-economical benefits for the community, environmental service (ES) users, and providers.

## INTRODUCTION

Land water flows naturally through the mechanism of the hydrological cycle (Easton 2015). As a result of forest destruction in the upstream watershed, rainwater will damage the soil and cause erosion, more runoff water than water enters the earth, and landslides occur in steep slope areas (Wasis et al. 2020). The impact of erosion is that in addition to causing a decrease in soil fertility, rainwater also carries soil particles along with surface runoff, which causes the water quality to become cloudy and poor.

Watersheds are producers of environmental services, namely: (1) carbon sequestration and storage; (2) biodiversity protection; (3) watershed protection; and (4) landscape beauty (Mayrand & Paquin 2004, Pagiola et al. 2005, Wunder 2006, Tacconi et al. 2012, Shrestha et al. 2021). The implementation of the PES program, especially water services, has been carried out to improve water quality through watershed improvements (Redondo-Brenes & Welsh 2006, Pissarra et al. 2021). To maintain the watershed environment has the value of sustainable environmental services, it is necessary to have ideal conditions for the forest environment that are well maintained and not damaged. The upstream watershed with rural characteristics is inhabited by farming communities

who live from agriculture and forest products. Meanwhile, in the downstream watershed, there are people with urban characteristics who use environmental services, especially water services to meet domestic and industrial needs. For the watershed environment to be well buffered, it is necessary to have a synergistic involvement between the two parties, namely the upstream watershed community to maintain and preserve the watershed environment that produces environmental services and the urban community in the downstream watershed utilizes environmental services. One of the efforts to achieve this goal is through the PES program.

PES is an environmental management model that involves at least two parties with mutually beneficial economic agreements with the voluntary principle that there is no coercion or pressure. This pattern contributes to the preservation and carrying capacity of the environment (Sommerville et al. 2009, Pirard 2012, Smith et al. 2013, Martin-Ortega & Waylen 2018, Aguilar-Gómez et al. 2020). PES is believed to be able to bridge the interests of natural resource users in the downstream watershed and environmental conservation communities in the upstream watershed (Wunder 2006). Even in the last decade, PES has spread widely throughout the world (Liu & Kontoleon 2018, Martin-Ortega & Waylen 2018, Rossi et al. 2021), in line with the increasing global

population and consumption of natural resources and increasing agricultural productivity, but on the other hand environmental degradation is also increasing.

Damage to the watershed environment is caused by the overexploitation of environmental resources, and poor farming families are accused of causing its damage. This group of poor farmers can be involved in the PES program and is expected to reduce poverty, especially by making payments to poor natural resource managers in the upstream watershed (Pagiola et al. 2005). The incentives for PES to overcome poverty are expected for environmental conservation through the PES program, and involving all stakeholders as participants by capturing local needs and interests (Ola et al. 2019).

The emergence of PES is motivated by concerns from experts, observers, and environmental researchers over global forest conditions. Mayrand & Paquin (2004), noted that since 1961 some tropical countries have lost more than 500 million hectares of forest, and consumption of forest products has increased by more than 50% worldwide. Such conditions have led to the loss of environmental services that are essential to life, economic development, and the health of the earth's population. These environmental services (ES) are generally unknown, poorly understood, or not accepted by policymakers, private companies, or local communities. As a result, these environmental services are rarely considered by the market, due to a lack of information or consumer awareness, or the absence of appropriate economic incentives that will influence the behavior of land users towards sustainable practice or conservation. The PES scheme attempts to remedy these market failures by internalizing benefits, thereby creating lost incentives for the provision of environmental services. The first step in this perspective is to define what environmental services are and what services can be internalized into market transactions.

The characteristics of the PES program are (1) voluntary transactions, (2) between environmental service users and environmental service providers, (3) expressed in the form of cooperation bonds for natural resource management, and (4) to produce agreed environmental services (Wunder & Wertz-Kanounnikoff 2009, Wunder 2015). In Indonesia, there are at least six locations (ICRAF 2013) namely: (1) Bungo in Jambi Province; (2) Singkarak in West Sumatra Province; (3) Sumberjaya in Lampung Province; (4) Cidanau in Banten Province; (5) Lembang in West Java Province; and (6) Kuningan in West Java Province.

Cidanau watershed has an important role as the main water supplier for the City of Cilegon located in the downstream part of the Cidanau watershed. Cilegon is an industrial city with more than 100 industries. These industries are dependent on the water supply of the Cidanau River for

their operational activities. Water needs for the community and industry will continue without knowing the seasons. On the other hand, water supply tends to decrease due to environmental damage due to erosion, floods, and landslides during the rainy season and drought during the dry season.

Environmental problems in the Cidanau watershed are mostly caused by human activities. Poverty is accused of causing environmental damage in this area. Almost all of the population inhabiting the upstream area of the river are small farmers with narrow agricultural land ownership, low income, and highly dependent on natural resource extraction. Along with the rapid rate of population growth which is always followed by efforts to meet the needs of human life, in the 1990s in the Cidanau watershed there has been a massive land conversion, natural forests are converted into dry agricultural land and swamp forests are converted into rice fields.

The research aimed to analyze the implementation of the PES program in Cidanau Watershed, Banten Province, Indonesia. The program is designed for the management of watershed natural resources that are mutually beneficial between people living in downstream watersheds as users of environmental services (Mayrand & Paquin 2004, Lipper & Neves 2011), especially water for industrial and domestic needs with farmers in upstream watersheds as environmental maintainers and environmental service providers.

## MATERIALS AND METHODS

The research sites are located at 06°07'18"-06°18'00" SL and 105°40'00"-106°04'00" EL. Cidanau watershed has an area of about 22,628.66 hectares, administratively located in Serang Regency and Pandeglang Regency, Banten Province, Indonesia which includes six sub-districts and 38 villages in the two districts (Sunaedi et al. 2019b). Cidanau watershed is a basin shaped like a bowl, the water source comes from the catchment area of several mountains (Mount Karang, Mount Haseupan, and Mount Pulosari) and empties into the Sunda Strait west of Java Island (Fig. 1).

This study uses a field research method (Bailey 2017), with data collection through focus group discussions (Nyumba et al. 2018), depth interviews, field observations, and documentation studies. Focus Group Discussion (FGD) is a data collection technique in which a researcher gathers a group of individuals to discuss a particular topic. FGD is a technique that aims to collect data based on the personal experiences, beliefs, perceptions, and attitudes of the participants through moderated interactions. FGDs are widely used in conservation research. FGD is a data collection technique that is often used as a qualitative approach to gain an in-depth understanding of social issues. This method aims to obtain data from a deliberately selected group of individuals, not from a statistically

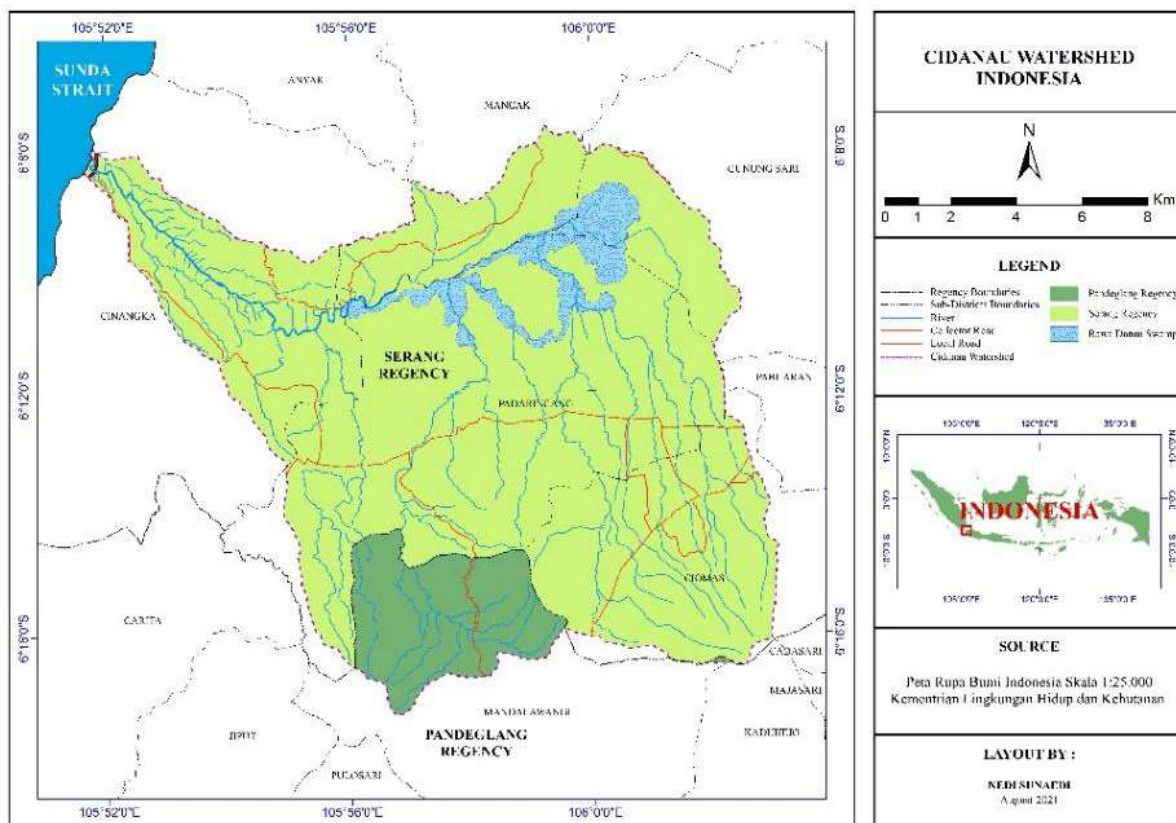


Fig. 1: Research site map.

representative sample of the wider population. Sources of data come from several informants consisting of; (1) a forest farmer group (FFG) as an ES provider, (2) KTI as an ES user, (3) the Cidanau Watershed Communication Forum (FKDC) which acts as a liaison in the PES program, and (4) the provincial government as the policy maker.

The main informants in this study were all parties involved directly or indirectly, including the people of the upstream watershed acting as providers of ES in Serang and Pandeglang, KTI, and other parties (local governments and NGOs) who act as facilitators and mediators of the PES program. Informants or sources from the selected farming community are the Chairman of FFG Karya Muda II Cinemas District of Serang Regency and the Chairman of FFG Maju Bersama in Padarincang District of Serang Regency. The considerations concerned are very understanding of the implementation of environmental service return programs at the level of environmental care providers or environmental service providers to provide in-depth information about environmental services. An informant from KTI is a Production Director who understands the IJL program because of its involvement from socialization, and negotiation to program

realization. Furthermore, informants from PES managers who are members of FKDC are the Secretary-General and an environmental activist from the Non-Governmental Organization (NGO) Rekonvasi Bumi.

This research was intensively carried out in 2019 - 2020 before the Covid-19 pandemic occurred. The data obtained are mostly qualitative and processed using an in-depth analysis of the focus under study, namely the PES program in the Cidanau watershed, Banten Province, Indonesia. Qualitative data processing techniques in this study consisted of data collection, data reduction, data presentation, and conclusion.

The data analysis technique used in this study is closely related to the research method used, namely the descriptive-qualitative method. Research data were analyzed qualitatively and equipped with tables or the like to facilitate understanding of research data. The data analysis technique used is the Miles and Huberman Model (Milies et al. 2020). Activities in qualitative data analysis are carried out inter-actively and continue to completion.

The steps of data analysis include (1) Data Reduction, which is quite a lot of data obtained in the field, then select-

ing, summarizing, and focusing on the important things, looking for themes and patterns. Thus the data that has been reduced will provide clearer answers and make it easier for researchers to conclude further data, and look for them if necessary; (2) Data Display, namely data presented in the form of brief descriptions, charts, relationships between categories, flowcharts, and the like. This step aims to make it easier to understand what happened, and plan further work based on what has been understood; (3) Conclusion Drawing/Verification, the data that has been analyzed is taken as preliminary conclusions that are temporary. This conclusion will change if there is no strong evidence to support the next stage of data inference. If the conclusions at the initial stage are supported by valid and consistent evidence when the research returns to the field, then the conclusions put forward are credible (Milies et al. 2020).

## RESULTS AND DISCUSSION

### Physical Environment Condition of Cidanau Watershed

The landforms consist of hills and wavy, and alluvial plains. Units of hill shape with moderate to high reliefs located to the North, East, and South form a horseshoe-like shape with a slope between ramps too steep. This hill unit is directly adjacent to the unit of form in the form of an intermountain depression with a slope of ramps to flat. In this form, The Rawa Danau (Swamp Lake) is located and drains the Cidanau

River as its main river. The Cidanau River drains water from the Rawa Danau and empties into the Sunda Strait.

The climatic conditions generally belong to a wet tropical climate with rainfall of more than 3000 millimeters per year. The wet season occurs from October to April and the dry season from May to September.

Table 1 and Fig. 2 showed that the average rainfall was relatively balanced with the average discharge. But, in certain years (2008, 2010, 2013, and 2017), the annual average of discharge is higher than the average rainfall. It was caused by the increasing discharge of some water sources from the wellsprings around the area.

Surface water conditions are characterized by the presence of rivers and their tributaries, swamps, and lakes. In the Cidanau watershed, there is the Cidanau River is the main river with 18 tributaries (sub-watershed). Rawa Danau is surface water in the form of swamps marked by typical swamp vegetation with an area of about 2,500 ha. The groundwater conditions in this area are classified into high, medium, and low groundwater potential. In some places, there are springs with the relatively high discharge with a flow rate between 100 m<sup>3</sup>/s to 300 m<sup>3</sup>/s with the main use being to meet domestic needs.

Land use in the Cidanau watershed is dominated by mixed plantations, paddy, and forest land (Table 2). The land use before the PES program was in the form of agricultural land with an open land-intensive system, such as dry land

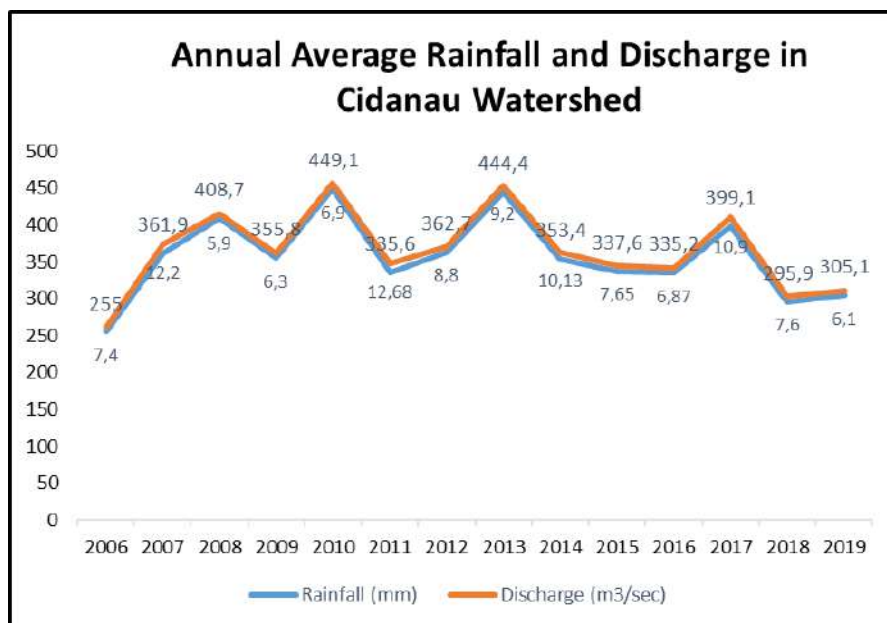


Fig. 2: Annual average rainfall and discharge at the Cidanau Watershed.

Table 1: Annual Average Rainfall and Discharge at the Cidanau Watershed (2006-2019).

Annual Average	Years													
	2006	2007	2008	2009	2010	2011	2012	2013	2014	2015	2016	2017	2018	2019
Rainfall (mm)	255	361,9	408,7	355,8	449,1	335,6	362,7	444,4	353,4	337,6	335,2	399,1	295,9	305,1
Discharge (m <sup>3</sup> /sec)	7,4	12,2	5,9	6,3	6,9	12,68	8,8	9,2	10,13	7,654	6,870	10,9	7,6	6,1

Source: Data from KTI Cilegon 2020.

rice and other seasonal secondary crops. The PES program has changed land use into a mixed plantation that resembles forest structures with the dominance of forest trees, fruits, and other commodities.

The inhabitants of the Cidanau watershed are 153,167 inhabitants. Most of them live as farmers with land ownership relatively narrow between 0.25-1.0 hectares. The composition of inhabitants' employment is very diverse, such as the agricultural sector with 53.03%, the manufacturing sector with 21.94%, the rest of it comes from trade, hotel, and tourism services. The level of education in the Cidanau watershed is low. Most people graduated from primary education because the educational facilities in each village are elementary schools and not sufficient. Higher schools only exist in the sub-district capital.

### PES Mechanism in Cidanau Watershed

At least four parties are involved in the implementation of PES in the Cidanau watershed: (1) KTI as ES user, (2) farmers living in upstream watersheds as ES provider, (3) FKDC which serves as a liaison of all watershed management interests, and (4) Local Governments (provinces and districts) as policymakers (Sunaedi et al. 2018). The concept is based on the principle of voluntary agreement between inhabitants of upstream and downstream. This Memorandum of Understanding was signed by the Governor of Banten who

acted as Chairman of the Regional Council of the Cidanau Watershed Communication Forum and by the President Director of KTI Cilegon (Sunaedi et al. 2018). To realize the memorandum of understanding, a month later on November 1, 2004, PES Agreement was signed between FKDC and KTI (Sunaedi et al. 2019a). The Agreement agreed, such as (1) environmental services are services produced by an ecosystem whose benefits both ecologically and economically, (2) environmental service products are the flow of substances, which are influenced by the type of land use and production system; and (3) PES is the payment of services produced by an ecosystem, which benefits ecologically and economically.

The basis of the environmental services payment agreement is a text of understanding based on the principle of voluntary agreement in maintaining the environment of the Cidanau watershed and on the benefits of the environment. Amaruzaman et al. (2017) state that the farming group must maintain at least 500 trees/ha and if the trees under contract are cut down during the contract period, the farmers should replace them. Any member who violates the agreement, all members will receive sanctions, and possibly contract termination.

The scope of the agreement includes (1) FKDC agreed to receive payments from KTI for the utilize ES from the Cidanau watershed, (2) FKDC agreed to carry out community forest development in the Cidanau watershed, the cost

Table 2: Land Use at Cidanau Watershed.

No.	Land Use	Area [ha]	Percentage [%]
1.	Forest	2814.41	12.44
2.	Swamp forest	1433.47	6.34
3.	Swamp lake	306.80	1.36
4.	Mixed plantation	8174.88	36.14
5.	Plantation	16.32	0.07
6.	Dry land agriculture	67.45	0.30
7.	Settlement	386.95	1.71
8.	Paddy field	6708.95	29.66
9.	Others	2710.77	11.98
	Total	22620.00	100.00

originally come from KTI funds, (3) KTI agreed to pay ES in the form of water usage, and (4) The payment from KTI based on the willingness.

Based on the results of an in-depth study with regard to various considerations, FFG Karya Muda II from Citaman Village and FFG Maju Bersama from Cibojong Village was selected as PES participants. Both villages were selected because these areas are critical in the Cidanau watershed and the socio-economic conditions are suitable. The land requirement for participation in the PES program is 25 hectares for one plot of a group of forest farmers. Land ownership in research areas is relatively low and generally less than one hectare. As an illustration, to reach an area of 25 hectares, it was collected as many as 43 farmers in Karya Muda 2.

In 2008, FKDC signed new contracts with FFG Alam Lestari from Cikumbueun Village, Mandalawangi District, Pandeglang Regency, and FFG Agung Lestari in Gunungsari District, Serang Regency for a 5-year contract period until 2013. Yet in 2009, FFG Agung Lestari failed and broke the contract for various reasons. In 2010, FKDC signed new contracts with FFG Karya Muda 3 in Citaman Village and FFG Karya Muda 2 also extend the contract as a result of renegotiation for the success as participants in the PES program. In 2014, the PES implementation in the Cidanau watershed entered its third period (Fig. 3). The main objective of this program, apart from protecting the watershed environment, is also to improve the standard of living of the people in the upstream watershed. The expected impact of the increase in the community's economic standard is the reduction in the community's habit of cutting trees on their land or in forest areas when they need cash.

Based on the field conditions, shows that the PES program is considered successful in improving the welfare of

forest farmers, so the program has motivated other forest farmers to join this PES program. Due to the limited funds available, the forest farmer groups that will join, are selected based on the priority targets and the readiness of the forest farmer groups to join. The determination of new members for the PES program is determined by the selection of proposals. In the preparation of proposals that are included in the selection of contracts for compensation for environmental services, applying the Participatory Landscape Analysis (PaLA) method that has been developed by ICRAF to identify environmental problems that exist in land or landscapes in a watershed area, and map existing local wisdom to solve these problems. The preparation of proposals and their selection was carried out in a workshop organized by FKDC.

Ha et al. (2011) stated that the background for the development of PaLA by ICRAF was based on the fact that the phenomenon of global population growth, migration between regions, and increasing community welfare had put pressure on the conversion of forest land into agricultural, residential and industrial land. PaLA was designed as an option to combine knowledge and multi-stakeholder perspectives for sustainable land use development from a plot of land towards sustainable agriculture and sustaining people's lives. PaLA is applied primarily to communities in the upstream watershed. Specifically, the goals of PaLA are: (1) to articulate and study farmers' perceptions of the relationship between land use and landscape function, (2) to understand farmers' choices in agricultural land management, (3) to understand the flow of water, sediment, nutrients, and organisms and internal filter functions that determine the function of the landscape based on the diversity of land use practices and interactions between landscape units, and (4) to understand the relationship between the goods and services of each land use decision made.

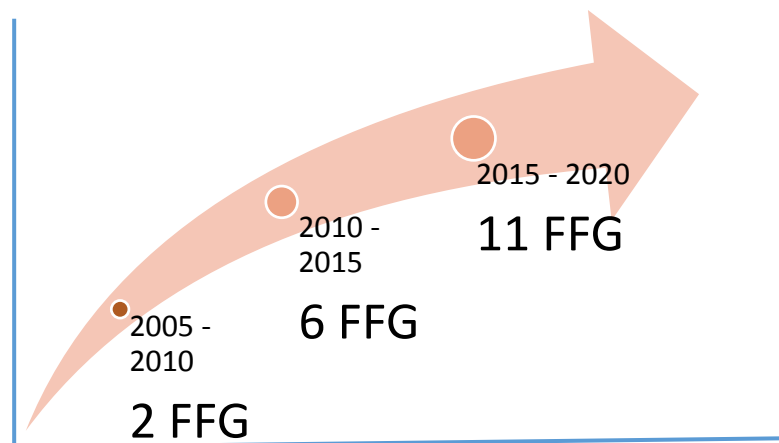


Fig. 3: Development of FFG as a participant in the PES program.

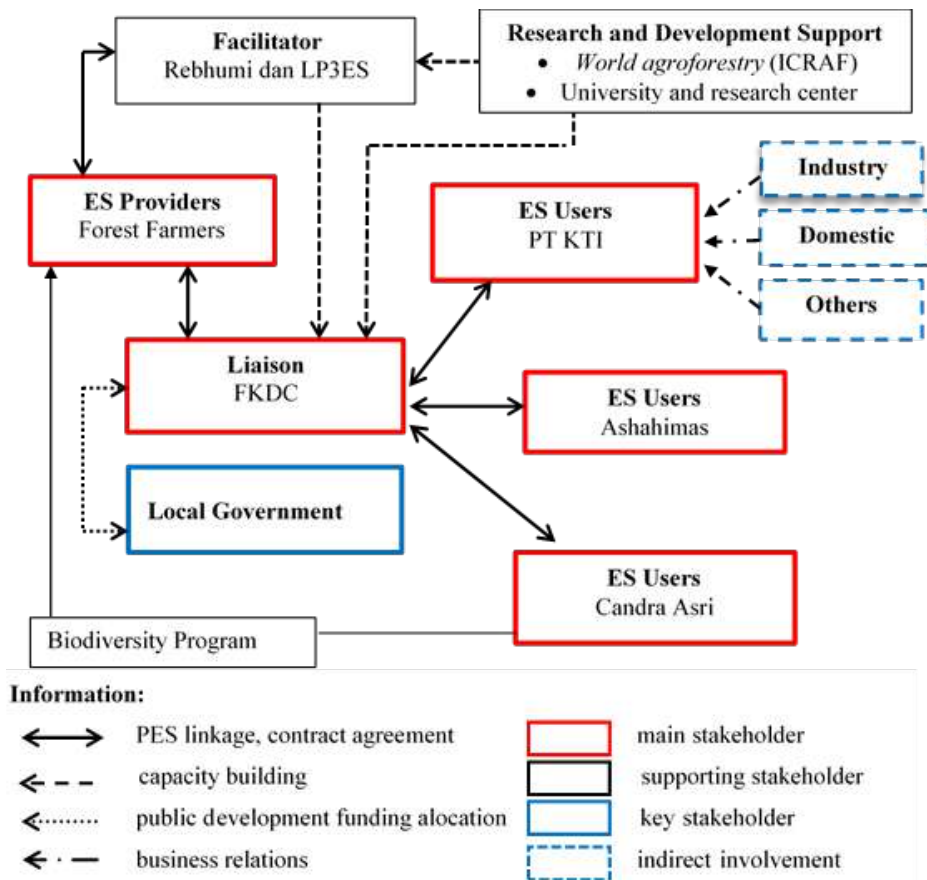


The implementation of the PES Program in the Cidanau Watershed includes several stages: (1) preparation of program plans and strategies, (2) identification of service providers and users of environmental services, (3) Socialization and activities at the FKDC level, at environmental service users, at service provider's environment, and (4) implementation of PES program. The implementation of the PES program begins with unifying the perception that all stakeholders need to understand the PES concept in the management of the Cidanau watershed. The unification of these various interests is contained in the vision and mission of FKDC, namely to build a balance of social and economic ecology in the utilization of natural resources in the Cidanau watershed to support sustainable development based on the concepts of one river, one planning, and one management. Its missions are (1) to preserve the natural resources of the Cidanau watershed; (2) to improve the welfare of the community in the Cidanau watershed area; (3) to maintain the sustainability of the water system to support sustainable development, (4)

foster an advanced investment climate and have the ability to compete.

The water environment service return scheme was also initiated and encouraged by FKDC which has also been a process dynamic since 2003 until now. In its development, many parties are concerned and contribute to the environmental services process in Cidanau, such as ICRAF which supports FKDC since 2007 and in 2014 awarded an environmental services contract to the group for applicative research. The concept of downstream-upstream payments was through the PES program, schematically shown in Fig. 4.

The PES management model in the Cidanau watershed (Fig. 4) is a model adapted from Leimona et al. (2010) which has been developing for a decade, namely by increasing users of ES. Initially from 2005 to 2010, the ES user who participated as a fund provider was PT KTI. In 2020, there were two additional ES users, namely Ashahimas and Candra Asri who donated funds to FKDC directly. One thing that



Source: adaptation from Leimona et al. 2010

Fig. 4: PES management model in Cidanau watershed.

attracted Candra Asri, apart from donating funds to FKDC, he also developed a biodiversity program in one of FFG's in the Cidanau watershed.

### Positive Impacts of the PES Program

In an activity or program, it is expected that there will be a positive impact under mutually agreed goals. Likewise, the PES program must have a good impact on all parties. In accordance with the main objectives of building and developing PES programs that have been agreed upon and contained in the FKDC, are (1) increasing the value of ecological, social, and economic benefits in a balanced watershed, (2) building community self-reliance to increase economic capacity, through the exploitation of natural resources that environmentally friendly, (3) improve the quality and quantity of water resources and other natural resources in the Cidanau watershed, and (4) build the synergy and integrity of integrated management based on the master plan and strategic plan for the management of the Cidanau watershed. In designing, building, and developing the PES program, it is necessary to refer to the above objectives, especially with regard to the fourth goal, namely to build synergy and integrity that affects all parties involved in it (Leimona et al. 2010).

**Environmental services beneficiaries:** KTI as an ES user, through this PES program, expects financial benefits in the form of raw water supply to be processed into clean water. In line with industrial growth in Cilegon City, which continues to increase, it is necessary to increase the water supply as well. Water is needed in industry as a component in the production process (such as cooling, as a mixture, etc.), and also serves as a supporter to meet the domestic needs of the employees. After the PES program, the average annual discharge of the river remained relatively constant in the range of 6 m<sup>3</sup>/second to 12 m<sup>3</sup>/second. The number and average river discharge are influenced by the amount of rainfall that occurs and land cover by vegetation in the upstream watershed. Land cover with dense vegetation provides an opportunity for rainwater to seep.

**Environmental services provider:** The PES program aims to increase the value of ecological, and socio-economic benefits of watersheds in a balanced manner, and build community empowerment to increase environmentally friendly economic capabilities. The PES program must be able to lift economic capabilities and improve the welfare of poor farming families.

The PES program has a positive impact on forest farmers (Sunaedi et al. 2019a), including (1) an increase in income, the most significant increase in income is not from PES but from the sale of fruits and spices from hetero plants cultures that have a high selling value, such as durian (*Durio zibethinus*), melinjo (*Gnetum gnemon*), cloves (*Syzygium*

*aromaticum*), and so on; (2) increasing family welfare, increasing the family's economic capacity has encouraged families to repair their homes and buy goods for family needs such as motor vehicles, electronics, and so on; (3) new job opportunities, this occurs at harvest time which provides opportunities for the emergence of traders of fruits and other commodities as well as the emergence of home industries for processing crops; and (4) the ability to send their children to school for farmer families participating in the PES program.

In the context of improving the watershed environment, the PES program must have the courage to change the order of farmers' activities for the better. Gorgens et al. (2021) used two approaches to PES implementation: (1) compensation for land that is discontinued from production, targeting low agricultural capacity, and (2) payment for low-capacity land already covered by natural vegetation. Facts showed that land is "sacrificed" for watershed conservation has increased productivity. Monoculture farming is more susceptible to crop failure compared to multicultural farming models which provide the possibility of choosing commodities that have high economic value without leaving the aspect of environmental preservation (Manhães et al. 2018).

**PES Program and poverty alleviation:** Landowners provide a variety of environmental services, from air services to biodiversity and carbon sequestration (Landell-Mills & Porras 2002, Pagiola et al. 2005). However, they often do not benefit from environmental conservation efforts, so forest farmers are tempted to convert their land to intensify agriculture that is less environmentally friendly. Initially, the PES Program was not a poverty alleviation program; rather it aims to address environmental issues and sustainable natural resource management. To achieve this goal, poverty cannot be used as a Criterion for Participation. However, the perception that areas with very high poverty rates are spatially correlated with areas that provide environmental services raises the expectation that PES programs can contribute to poverty reduction (Pagiola et al. 2010).

The PES program has the potential to reduce the poverty of farming communities that inhabit upstream watersheds. Some of the reasons that the PES program can improve welfare include: (1) the cash flow of funds received by the community participating in the PES program or a broad sense creates opportunities for land owners to convert natural capital into financial flows, (2) PES can provide opportunities for additional income other than land products to local communities, and (3) help reduce community vulnerability through the diversity of income sources (Tangisujit & Barnwal 2009).

Obtaining direct funds in the form of cash from agricultural land that is included in the PES program. The range of income earned varies from around a few hundred thousand

rupiahs to less than 1 million rupiahs which are paid twice a year. This is due to relatively narrow land ownership, which is less than 1 ha. Generally used to meet daily needs, more to pay for monthly electricity. According to several farmer sources, the amount of money obtained is not sufficient for their daily needs. However, greater income is obtained from the harvest of fruit and vegetable crops.

Currently, the income of group members is increasing because fruit and vegetable crops have started to produce. Durian (*Durio zibethinus*) is a superior fruit with a high selling price. In addition, dry cloves are extraordinary commodities that have advantages compared to other commodities, namely that they can be stored for a relatively long time and serve as savings for farmers. When the price of cloves is low, farmers store the cloves first and when the price is high they will sell them. To meet their daily needs, farmers rely on vegetable crops, such as petai (*Parkia speciosa*), jengkol (*Archidendron pauciflorum*), and melinjo (*Gnetum gnemon*). The melinjo plant can be used for fruit crackers and the leaves are processed into vegetables. The advantage of the melinjo plant is that it can be harvested almost every day. Thus, the existence of the PES program has increased community incomes in the upstream watershed (Sunaedi et al. 2018). Recently, many types of intercropping plants that have high economic value have been cultivated, namely the porang plant (*Amorphophallus muelleri*). Porang is a type of tuber plant that can live under the shade of a tree, so it does not interfere with the structure and composition of existing plants. The results of this study confirm findings written by other researchers who state that non-economic factors, such as trust and participation in designing schemes, have an important role in determining decisions made by land owners about whether to participate in PES schemes sustainably or not (Matheus et al. 2014, Khanal & Devkota 2020).

## CONCLUSIONS

The implementation of the PES program is inseparable from the participation of all parties who consciously and voluntarily realize the common ideal of integrated watershed management so that the environmental services it produces can be enjoyed sustainably. The concept developed upstream and downstream watershed relationship through the PES mechanism is based on the principle of voluntary agreement and awareness of maintaining the Cidanau watershed ecosystem. The parties involved are (1) KTI who act as users who can enjoy directly and benefit from environmental services, (2) environmental maintenance communities living in upstream watersheds and acting as providers, (3) local governments and technical institutions/bodies that act as policymakers, and (4) FKDC which acts as liaisons among the three.

The PES program in the Cidanau watershed has been running well and has benefited all parties such as (1) guaranteed raw water supply for urban communities as ES users to meet industrial and domestic needs, (2) increased socio-economic welfare for forest farming communities as ES providers, (3) the realization of government programs in preserving the watershed environment, and (4) increasing the carrying capacity of the watershed environment towards a sustainable green economy.

Experience in implementing an environmental services program in the Cidanau watershed managed by FKDC is the best practice to build environmental services. FKDC implements the program with the entire process of developing PES with the principle of integrated management through one river, one plan, and one management approach.

This field research is qualitative it takes a long time to discover new things. Researchers experienced several difficulties, such as determining competent sources and qualitative research data that must be analyzed in depth based on comprehensive and up-to-date references. These conditions provide opportunities for quantitative research with other variables.

## ACKNOWLEDGEMENTS

My gratitude to Mr. N.P. Rahadian is an informant from the Secretary General of FKDC who has provided very valuable and complete information about the PES program. Mr. A. Bachrani (Chairman of FFG Karya Muda 2) has provided information about the PES Program from environmental service providers. Director of PT KTI Cilegon who had provided information from environmental service users, especially water services. The Governor of Banten and the staff, especially the Head of Bappeda Banten Province, the Head of the Environment Office, and other related agencies thanked him for the permits, directions, and data that were very important in this study.

## REFERENCES

- Aguilar-Gómez, C. R., Arteaga-Reyes, T. T., Gómez-Demetrio, W., Ávila-Akerberg, V.D. and Pérez-Campuzano, E. 2020. Differentiated payments for environmental services: A review of the literature. *Ecosyst. Services*, 44: 101131. <https://doi.org/10.1016/j.ecoser.2020.101131>
- Amaruzaman, S., Rahadian, N.P. and Leimona, B. 2017. Role of Intermediaries in the Payment for Environmental Services Scheme: Lessons Learnt in the Cidanau Watershed, Indonesia. In: Namirembe, S., Leimona, B., Van Noordwijk, M. and Minang, P. (eds), *Co-investment in Ecosystem Services: Global Lessons from Payment and Incentive Schemes*. World Agroforestry Centre (ICRAF), Nairobi.
- Bailey, C.R. 2017. *A Guide to Qualitative Field Research*. Third Edition. Sage Publishing, New Jersey. <https://us.sagepub.com/en-us/nam/author/carol-r-bailey>
- Easton, Z.M. 2015. *Hydrology Basics and the Hydrologic Cycle*. Working Paper No. VT/1015/BSE-191P. College of Agriculture and Life Sciences, Virginia Tech., Virginia State University, Virginia.

- Gorgens, E.B., Mucida, D.P., Silva, B.H.L., Sperandio, H.V., de Azevedo, M.L., Martins, I.C., Nunes, T.K.M.R., Lima, V.O.B., Pereira, I.M. and de Moraes, M.S. 2021. Payment for environmental services to promote land aptitude. *Agri. Res.*, 10: 51-69. [10.31220/agriRxiv.2021.00051](https://doi.org/10.31220/agriRxiv.2021.00051).
- Ha, H.M., Quan, A., Degrande, H.N. and Hoa, N.T. 2011. Multi-scale Participatory Landscape Analysis (PaLA). *TUL-Viet (1)*: 27-39. In Hoang Minh Ha, Nguyen Hoang Quan (Editors). 2011. Tools for use in Integrated Natural Resources Management (INRM) and Payment for Environmental Services in Vietnam (TUL-Viet). Lecture Notes. Volume 1. ICRAF Vietnam. 89 pages.
- ICRAF. 2013. A Project by the World Agroforestry Centre and the International Fund for Agricultural Development: Research sites in Asia 2008–2012. World Agroforestry Centre Southeast Asia Regional Program, Bogor.
- Khanal, Y. and Devkota, B.P. 2020. Farmers' responsabilization in payment for environmental services: Lessons from community forestry in Nepal. *Forest Policy Econ.*, 118: 102237. <https://doi.org/10.1016/j.forpol.2020.102237>
- Landell-Mills, N. and Porras, I. 2002. Silver Bullet Or Fool's Gold? A Global Review of Markets for Forest Environmental Services and Their Impacts on the Poor: Instruments for Sustainable Private Sector Forestry Series. International Institute for Environment and Development, London.
- Leimona, B., Pasha, R. and Rahadian, N.P. 2010. The livelihood impacts of incentive payments for watershed management in Cidanau watershed, West Java, Indonesia. In: Tacconi, L., Mahanty, S. and Suich, H. (eds), *Payments for Environmental Services, Forest Conservation, and Climate Change: Livelihoods in the REDD?* Edward Elgar Publishing Limited.
- Lipper, L. and Neves, B. 2011. Payments for environmental services what role in sustainable agricultural development? ESA Working Paper No. 11-20. FAO Agricultural Development Economics Division, NY, pp. 11-20 [www.fao.org/es/esa](http://www.fao.org/es/esa)
- Liu, Z. and Kontoleon, A. 2018. Meta-analysis of livelihood impacts of payments for environmental services programs in developing countries. *Ecol. Econ.*, 149: 48-61. <https://doi.org/10.1016/j.ecolecon.2018.02.008>
- Manhães, A.P., Loyola, R.G., Mazzochini, G.G., Ganade, G., Oliveira-Filho, A.T. and Carvalho, A.R. 2018. Low-cost strategies for protecting ecosystem services and biodiversity. *Biol. Conserv.*, 217: 187-194 <http://doi.org/10.1016/j.biocon.2017.11.009>
- Martin-Ortega, J. and Waylen, K.A. 2018. PES What a mess! An analysis of the position of environmental professionals in the conceptual debate on payments for ecosystem services. *Ecol. Econ.*, 154: 218-237. <https://doi.org/10.1016/j.ecolecon.2018.08.001>
- Matheus A., Zanella, M.A., Schleyer, C. and Speelman, S. 2014. Analysis: Why do farmers join payments for ecosystem services (PES) schemes? An assessment of PES water scheme participation in Brazil. *Ecol. Econ.*, 11: 115
- Mayrand, K. and Paquin, M. 2004. *Payments for Environmental Services: A Survey and Assessment of Current Schemes for the Commission for Environment Cooperation of North America*. Unisféra International Centre, Montreal.
- Milnes, M.B., Huberman, A.M. and Saldana, J. 2020. *Qualitative Data Analysis, A Methods Sourcebook*. Fourth Edition. SAGE Publication, Inc., California, US, pp.8-10
- Nyumba, T.O., Kerrie Wilson, K., Christina J., Derrick, C.J. and Mukherjee, N. 2018. The use of focus group discussion methodology: Insights from two decades of application in conservation. *Ecol. Evol.*, 9: 20-32. <https://doi.org/10.1111/2041-210X.12860>
- Ola, O. and Menapace, L. 2019. Determinants of the environmental conservation and poverty alleviation objectives of payments for ecosystem services (PES) programs. *Ecosyst. Services*, 35: 52-66. <https://doi.org/10.1016/j.ecoser.2018.10.011>
- Pagiola, S., Arcenas, A. and Platais, G. 2005. Can payment for environmental services help reduce poverty? An exploration of the issues and the evidence to date from Latin America. *World Develop.*, 33(2): 237-253. [doi:10.1016/j.worlddev.2004.07.011](https://doi.org/10.1016/j.worlddev.2004.07.011).
- Pagiola, S., Rios, A.R. and Arcenas, A. 2010. Poor household participation in payments for environmental services: Lessons from the silvopastoral project in Quindío, Colombia. *Environ. Resour. Econ.*, 47: 371-394. [DOI: 10.1007/s10640-010-9383-4](https://doi.org/10.1007/s10640-010-9383-4)
- Pirard, R. 2012. Market-based Instruments for biodiversity and ecosystem services: A lexicon. *Environ. Sci. Policy*, 19: 59-68. <http://dx.doi.org/10.1016/j.envsci.2012.02.001>
- Pissarra, T.C.T., Fernandes, L.F.F. and Pacheco, F.A.L. 2001. Production of clean water in agriculture headwater catchments: A model based on the payment for environmental services. *Sci. Total Environ.*, 785: 147331. <https://doi.org/10.1016/j.scitotenv.2021.147331>
- Redondo-Brenes, A. and Welsh, K. 2006. Payment for hydrological environmental services in Costa Rica: The Procuencas case study. *Trop. Resour. Bull.*, 25: 19-25.
- Rossi, G.D., Jory, S.H. and Asim, Z. 2021. A mixed-methods analysis for improving farmer participation in agri-environmental payments for ecosystem services in Vermont, USA. *Ecosyst. Services*, 20: 10122. <https://doi.org/10.1016/j.ecoser.2020.101223>
- Shrestha, M., Piman, T. and Grünbühel, C. 2021. Prioritizing Key Biodiversity Areas for Conservation Based on Threats and Ecosystem Services Using Participatory and GIS-based Modeling in Chindwin River Basin, Myanmar. Elsevier, The Netherlands. <https://doi.org/10.1016/j.ecoser.2021.101244>
- Smith, S., Rowcroft, P., Everard, M., Couldrick, L., Reed, M., Rogers, H., Quick, T., Eves, C. and White, C. 2013. *Payments for Ecosystem Services: A Best Practice Guide*. Defra, London.
- Sommerville, M.M., Jones, J.P.G. and Milner-Gulland, E.J. 2009. A revised conceptual framework for payments for environmental services. *Ecol. Soc.*, 14(2): 34. <http://dx.doi.org/10.5751/ES-03064-140234>
- Sunaedi, N., Hadi, S.P. and Bambang, A.N. 2018. Essential water supply resources through payment for environmental services program in the Cidanau watershed, Banten Province, Indonesia. *IOP Conf. Ser.: Earth Environ. Sci.*, 145: 012133. [doi:10.1088/1755-1315/145/1/012133](https://doi.org/10.1088/1755-1315/145/1/012133)
- Sunaedi, N., Hadi, S.P. and Bambang, A.N. 2019a. Community-based environmental management through the payments for environmental services program in Cidanau watershed, Banten Province, Indonesia. *IOP Conf. Ser.: Earth Environ. Sci.*, 338: 12002. [doi:10.1088/1755-1315/338/1/012002](https://doi.org/10.1088/1755-1315/338/1/012002)
- Sunaedi, N., Hadi, S.P. and Bambang, A.N. 2019b. The role of forest farmers group through payment for environmental services scheme in preserving water resources in Cidanau watersheds at Banten, Indonesia. *Adv. Social Sci. Edu. Hum. Res.*, 320: 1106.
- Tacconi, L., Mahanty, S. and Suich, H. (eds). 2012. *Payments for Environmental Services, Forest Conservation, and Climate Change: Livelihoods in the REDD?* Edward Elgar Publishing Limited, Cheltenham, United Kingdom.
- Tangisujit, N. and Barnwal, P. 2009. *Innovative Socio-Economic Policies to Improve Environmental Performance: Payments for Environmental Services*. United Nations Publications, NY.
- Wasis, B., Harlan, D. and Wasis Putra, M.H. 2020. Impact of forest land cover on runoff, erosion, and sedimentation in the Karai Watershed, Simalungun Regency, North Sumatra Province, Indonesia. *Arch. Agric. Environ. Sci.*, 5(1): 40-49. <https://doi.org/10.26832/2456663.2020.050106>
- Wunder, S. 2006. Are direct payments for environmental services spelling doom for sustainable forest management in the tropics? *Ecol. Soc.*, 11(2): 23.
- Wunder, S. and Wertz-Kanounnikoff, S. 2009. *Payment for Environmental Services and the Global Environment Facility: A Scientific and Technical Advisory Panel (STAP) Guideline Document*. Working Paper No. GEF/C.35/Inf.12. Global Environment Facility (GEF) Council.
- Wunder, S. 2015. Revisiting the concept of payments for environmental services. *Ecol. Econ.*, 117: 234–243. <http://doi.org/10.1016/j.ecolecon.2014.08.016>



# Development of Flood Vulnerability and Risk Indices for Kelantan District, Peninsular Malaysia

A.M.A. Bahar\*, M. Muhammad\*, M. T. Anees\* and M. M. A. Khan\*†

\*Department of Geoscience, Faculty of Earth Science, Universiti Malaysia Kelantan, Campus Jeli, 17600 Jeli, Kelantan, Malaysia

†Corresponding author: Mohammad Muqtada Ali Khan; muqtada@umk.edu.my, muqtadakhan@gmail.com

Nat. Env. & Poll. Tech.  
Website: [www.neptjournal.com](http://www.neptjournal.com)

Received: 05-03-2022

Revised: 08-05-2022

Accepted: 22-05-2022

## Key Words:

Flood vulnerability

Natural hazards

Risk indices

Demographic variables

## ABSTRACT

Natural hazards are inevitable which required proper monitoring and application of mitigation measures to reduce vulnerability and risk. Flood is one of the most common natural hazards in Malaysia. The present study was conducted to identify vulnerable flood zones using flood vulnerability and risk indices and to minimize flood damage by suggesting mitigation measures. Four sub-districts of the Kelantan state, Peninsular Malaysia were selected based on the availability of the data and flooding history. For this purpose, demographic, social, economic, and flood event data were collected to develop flood vulnerability and risk index. Descriptive and inferential statistics were used to analyze the results. The results revealed that developed flood vulnerability and risk indices accurately predict high-priority zones. Overall, it was found that flood risk is relatively higher in a rural area compared to an urban area.

## INTRODUCTION

Flooding is a frequent natural hazard that causes the loss of human lives and the economy. Spatio-temporal patterns of flooding can be influenced by uncontrolled construction of buildings and land-use changes. The primary cause of the flooding is a storm which is due to high rainfall in a short duration. In high rainfall conditions, the intensity of flood is generally accelerated by settlements along the floodplains. Additionally, other factors include topographic variation, geomorphological changes, dense drainage networks, engineering structures, and dynamic climatic conditions.

Flooding is common in Malaysia which causes 90 percent losses due to natural hazards. The average annual flood damage is approximately US100 million (Chan 2015). In the state of Kelantan, the Kelantan River bank periodically overflow from November to February. Under the 50-year flood situation at Kusial Bridge, the projected flood volume is around 6 billion m<sup>3</sup>. In 1926 and 1967, significant flooding occurred and in the year 1967 floods, 84 percent of the population of Kelantan (537,000 people) was badly affected (Hassan & Rozi 2006). About 125,000 individuals have been evacuated and 38 have drowned.

Resilience principles must be implemented to provide adequate protection against the rising trend of flash flooding and its effects on civilization. To create a clear theoretical and practical foundation for flood resilience, the idea of flood

vulnerability in flood-prone areas needs to be addressed. Although, several methods of flood impact assessment have been developed (Penning-Rowsell et al. 2005, Yahya et al. 2016). Adaptation and advancement of theory, methodology, and practice in vulnerability assessment involve sudden changes in the present city areas. Although the definition of vulnerability is closely linked to susceptibility, impact assessment begins with a quantitative approach. This applies not only to retrospective evaluations but even to a large degree to prospective cases where future flood impact assessments can address the disruption of the socio-economic backbones of society and their effects on regional, national, and even transnational networks, due to the increasing availability of data. Due to the influence of several factors, vulnerability varies in different conditions (Ibrahim et al. 2017). The cumulative impact of several factors can be assessed using a vulnerability index. The primary task of vulnerability index development is to identify the most vulnerable area to flooding which is an important tool in flood management.

A significant unit of the population is affected by flood risk in Peninsular Malaysia. Rapid increment in settlement on floodplains causes exposure of a large number of people and property to flooding risk (JICA 1982). Vulnerability increases due to inaccurate responses from the public living in floodplains. Flood mitigation should be able to address severe risks in an area. Information about the level of danger,

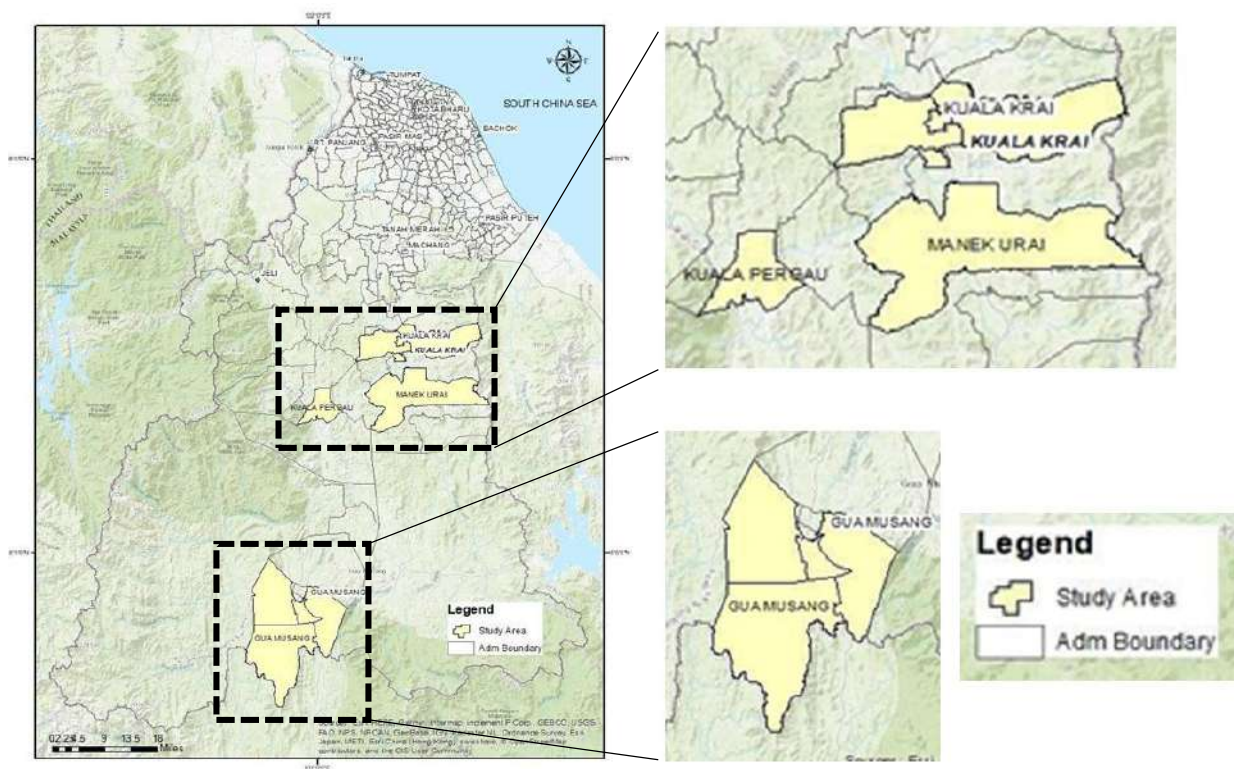


Fig. 1: Location of the study area.

exposure, and vulnerability is required for priority action in overcoming flood problems. Flood damage can be reduced by identifying flood-prone areas and applying proper mitigation measures (Lee & Choi 2018). Therefore, the objectives of the study are to identify vulnerable flood zones using flood vulnerability and risk indices and to minimize flood damage by suggesting mitigation measures.

## MATERIALS AND METHODS

### Location and Details of the Study Area

This work was conducted in the Kelantan state of Peninsular Malaysia. The area of the state is approximately 15000 km<sup>2</sup> (Anees et al. 2019). The highest elevation is 2187 m above mean sea level. The northern part of the state is surrounded by the South China Sea. Gua Musang Town of the district Gua Musang, Kuala Krai Town of the district Kuala Krai, and its two sub-districts such as Manik Urai and Kuala Pergau were selected based on administrative similarities in status and flooding exposure among locations (Fig. 1).

The area has a tropical and humid climate with mean variation in temperature as 20 to 30°C. High precipitation is generally recorded from November to January, while low

precipitation is in June and July. The mean annual precipitation is 3020 mm while the mean daily annual wind speed is 1.50 m.s<sup>-1</sup> (Anees et al. 2018).

### Data Used

Primary data was collected directly from main sources through interviews, surveys, and questionnaires. Whereas, secondary data was collected from the literature. Secondary data is accessible through different public and government records and online sources. The summary of the data is given in Table 1.

### Methodology

#### Primary Data Collection

Primary data include field surveys, field photographs, interviews with regional government offices, and household surveys with GPS locations. The survey was conducted within flood-prone areas. Factors considered for sampling were the vicinity of the flood-prone area, past flood records, and tenancy by infrastructure, land properties, and settlements in collaboration with community leaders.

- Interviews were conducted with representatives of stakeholders consisting of experts relating to floods, local government, and communities in various circles. Interviews were conducted with 200 respondents.

Table 1: Summary of data used in this study.

Data Type	Parameter/Variable	Frequency	Duration	Source/Remark
Demographic data	Population Size	Study Area	2014, 2015	Questionnaire Survey
Social Data	<ul style="list-style-type: none"> <li>• Household size</li> <li>• Gender of household</li> <li>• Educational level</li> <li>• Health status</li> <li>• Age</li> <li>• Occupation</li> </ul>	Household-level	N/A	Questionnaire Survey
Economy	Household income	Household	N/A	Questionnaire Survey
Flood events	Flood, flood extreme, flood hazard, exposure, and vulnerability.	Flood events in Kelantan and Malaysia	Various periods and time	Previous researcher, publication, and government records
Data Type	Parameter/Variable	Frequency	Duration	Source/Remark
Demographic data	Population Size	Study Area	2014, 2015	Questionnaire Survey
Social Data	<ul style="list-style-type: none"> <li>• Household size</li> <li>• Gender of household</li> <li>• Educational level</li> <li>• Health status</li> <li>• Age</li> <li>• Occupation</li> </ul>	Household-level	N/A	Questionnaire Survey
Economy	Household income	Household	N/A	Questionnaire Survey
Flood events	Flood, flood extreme, flood hazard, exposure, and vulnerability.	Flood events in Kelantan and Malaysia	Various periods and time	Previous researcher, publication, and government records

- Documentation study, which is to collect and study data or documents that support research, at least several relevant agencies such as the Malaysian Meteorological and Public work
- The questionnaire was given to 200 residents who experienced this disaster to find out their condition and response to the flood. The questions given in the questionnaire are important variables in analyzing flood risk. The components of the question are Flood hazard experience, related to depth, duration, and other flood characteristics such as distance from rivers and physical impressions. All questions are expected to become significant data in discussing flood hazards. Flood exposure, about the elements at risk that are affected around the respondent, especially those of vital value to the respondent, and flood vulnerability, which relates to the economic and social impacts of the respondent due to the flood, either directly or indirectly while flood risk, concerning vigilance and action in anticipation of floods.

### Development of Flood Risk Classification

Flood Risk is analyzed and grouped into four parameters, namely flood hazard, exposure, and vulnerability. The analysis was carried out with 2 analytical methods, namely spatial analysis, and scoring analysis. These results are then converted spatially using the Weighted Linear Combination (WLC) method to ensure that the weighted translations of different variables derived from the Analytic Hierarchy

Process (AHP) equation can be converted into maps in a relevant way. The WLC is the most common methodology in multi-scale evaluation analysis.

Development of spatial risk index using spatial layer overlay for all areal units (Census Tract) of each flood hazard region. The operation was between the hazard and the spatial layers of flood impact. Based on the spatial vulnerability intersection and exposed layers, the impact layers were formed. The Raster multiplication technique was used for the spatial intersection. The calculation of index value and map ranking for all raster grid cells were based on created index values (Rucinska 2014). Therefore, “the flood risk (RF) map” is the “spatial intersection of flood hazard, social (population) and exposure vulnerability” (Equation 1).

$$RF = HF_i \cap_n VP_i \cap VE_i \quad \dots(1)$$

where HF is a spatial layer of flood hazard which is equal to  $\cap_n HF_i$ , HF<sub>i</sub> is the several flood hazards related to areal components, VP is a spatial layer of social vulnerability which is equal to  $\cap_n VP_i$ , VP<sub>i</sub> is different population vulnerabilities related to the areal components, VE is a spatial layer of vulnerability due to infrastructure exposure which is equal to  $\cap_n VE_i$ , VE<sub>i</sub> is different infrastructure related to the areal components.

Scoring is a decision-making technique in a process that involves factors together by assigning a value to

each factor. In determining the scoring assessment can subjective scoring is carried out, namely by setting a score based on certain considerations and based on an understanding of the process, or objective scoring is by statistical calculations.

The scoring process is useful for assigning a score to each score parameter that affects flooding. The greater the influence, the higher the score. For scoring, a score of 1 is given to parameters that have a minor effect and a score of 5 is given to the parameter which has a major effect on flooding.

The procedure of the decision-making method using AHP analysis for the appropriate site selection zone is as follows:

- Hierarchy building at several levels. Hierarchy designing for all parameters of flood hazard, exposure, and vulnerability.
- Based on the couple, element comparison of the decision to reduce the decision-making concept.
- Determination of parameters by the normalization of the Eigenvector associated with the maximum Eigen matrix ratio. Comparison matrix couples are shown in Table 2.
- Calculation of each parameter weight using pair ratio with an assumption. If the consistency ratio (CR) value is 0.10, then the judgment is inconsistent or bad sensitivity value.

Spatial analysis is the aggregation weights relative that has been produced in the previous stage to produce composite weight as the final score of spatial decision making.

### Statistical Analysis

In general, the analysis used in this research is quantitative analysis techniques based on statistical analysis. This analysis is divided into two groups, namely:

- Use descriptive statistics to analyze collected data to avoid general conclusions or generalizations. The analysis is only in the form of an accumulation of basic data and descriptions, in the sense that it does

Table 2. Comparison matrix couples (Imanda & Andono 2015).

Value	Definition
1	Equally important
3	Quite important
5	High importance
7	Very high importance
9	Extremely high interests
2,4,6,8 Values between each criterion	

not seek or explain relationships, test hypotheses, make predictions, or draw conclusions. For example, in analyzing questionnaire data, field measurement data, and secondary data from Hyetograph and Hydrographs.

- Inferential statistics It is concerned with drawing conclusions and making assumptions based on observations, such as correlational analysis and comparative analysis, that have been carried out. Correlational research is to find an association or effect between the Independent Variables and the Dependent Variables. Comparative Analysis Comparative analysis is a method of mathematical analysis aimed at comparing the circumstances between two or more types. The measurement methodology used is often quite varied, depending on the type of data size and the number of categories, and the application of these analysis techniques. For example, the relationship between facets of floods, such as flood risk, exposure, and vulnerability, is studied.

## RESULTS AND DISCUSSION

In this study, flood vulnerability has been defined as a combination of three types of distinctive vulnerabilities such as economic, infrastructure, and social. Each of these three types can further be categorized in Table 3. To determine Infrastructure, a social and economic vulnerability that was impacted by the flood in 2014, a survey using a questionnaire and interviews with 200 respondents, as illustrated in figure (Fig. 2), was undertaken. The questionnaire containing seventeen questions was provided to the community of Gua Musang, Kuala Krai, Kuala Pergau, and Manik Urai to those who experienced the flood occurrence in 2014. The Analytic Hierarchy Process (AHP), a quantitative analysis technique, is used to compare flood vulnerability index components like the social vulnerability index, economic vulnerability index, and infrastructure vulnerability index, especially in determining the weight of all associated parameters.

### Economic Vulnerability

Economic vulnerability (EV) is represented by total loss data including losses in transportation, buildings, household, shop, and farms. For this study, economic vulnerability is classified into 3 classes based on the below calculation:

$$\text{Total loss (RM)} = \frac{(\text{high total loss}) - (\text{low total loss})}{3 \text{ (classes)}} \dots (2)$$

Based on data survey in the study areas (Gua Musang, Kuala Krai, Kuala Pergau dan Manik Urai), three classes of economic vulnerability can be determined - High total loss (H), Medium loss, and Low loss. Where,  $H > \text{RM } 100,000$ ,  $M < \text{RM } 100,000$  and  $> \text{RM } 50,000$ , and Low (L)  $< \text{RM } 50,000$ .



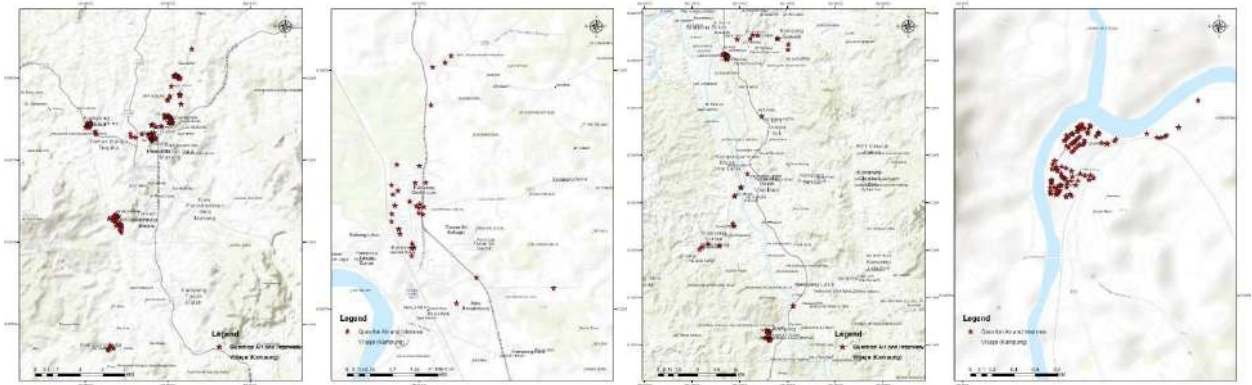


Fig. 2: Respondents' location of Gua Musang, Kuala Krai, Manik Urai, and Kuala Pergau for questionnaire and interview.

The results of the classification study Economic vulnerability in the 4 study areas can be seen in the graph (Fig. 3):

Based on the data above, economic vulnerability by area is calculated in Table 4:

**Social Vulnerability**

The focus of social vulnerability on occupation, gender, and age is shown in Fig. 4. These factors have important physical or mental characteristics which affect a

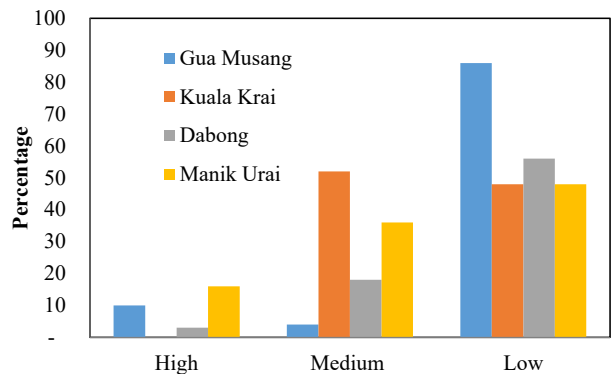


Fig. 3. Percentage of total losses by area.

Table 3: Categorization of distinctive vulnerabilities.

Category	Theme	Types
Economics	Total loss	1. Transportation 2. Household 3. house, 4. shop business 5. farm
Social	Age	6. 19 years and below 7. 20 years-39 years 8. 40 years-60 years 9. 61 years and above
	Occupation	10. Business 11. Farmer 12. Government 13. Housewife 14. Labor 15. Pensioner 16. Private 17. self-employed, unemployed 18. student
	Gender	19. Male 20. Female
Physical	Facilities	21. Roads 22. Railways 23. Bridges 24. schools and 25. hospitals

person's ability to take preventive measures against flooding.

Fig. 4 shows that, in December 2014 Kelantan flood, people below the age of 20 years are exposed more. It also showed that young people are more vulnerable to flooding than older people. In Fig. 4, fewer gender differences mean no effect in identifying the flood-level social vulnerability during the flood.

Fig. 5 shows the Respondents' classification based on their occupation. Based on collected data, most people are involved in the business which affects more during the flood. Additionally, unemployed people experienced the same. Overall results showed that flood vulnerability can be determined based on the impact experienced by the type of

Table 4. Economic vulnerability by area.

Area	Total Lost	EV Level
Gua Musang	2,600,000.00	Medium
Kuala Krai	5,100,000.00	High
Dabong	2,795,000.00	Medium
Manik Urai	4,140,000.00	High

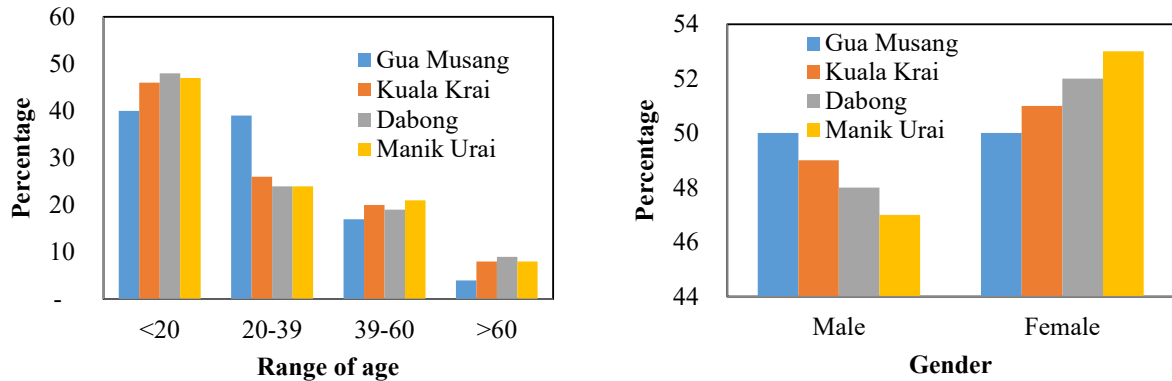


Fig. 4: Percentage of age and gender composition by area.

work. Furthermore, high flood vulnerability was experienced by business occupational people.

Calculation of the Social Vulnerability Index (SVI) is the result of accumulating all vulnerability parameters into the following equation:

$$SVI = \left( weight \times ratio \frac{F}{M} \right) +$$

$$(weight \times range\ of\ age) + (weight \times occupation) \dots(3)$$

Through calculations using AHP, the weight of each SVI parameter is shown in Table 5.

$$SVI = (0.24 \times ratio\ gender) +$$

$$(0.54 \times range\ of\ age) + (0.21 \times occupation) \dots(4)$$

By combining all elements of social risk, including multipliers, the overall score results are obtained as shown in Table 6.

### Physical Vulnerability

The final category is infrastructure vulnerability, which

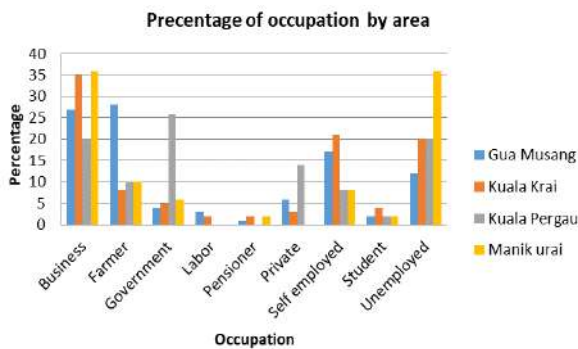


Fig. 5: Percentage of occupation composition by area.

includes road networks, railways, bridges, hospitals, and schools. Infrastructure is one of the basic requirements for population, communication, and safety which can be affected by floods. Schools can be used as evacuation places or centers of aid during a flood. Hospitals require special protection during floods. If hospitals get affected by flooding, it could worsen the treatments. As to be concluded, critical facilities tend to give special attention to vulnerability analysis to provide a more accurate estimate of the flood.

Table 5: Weight of elements of social vulnerability.

Parameters	Gua Musang	Kuala Krai	Kuala Pergau	Manik Urai	Weight
Age	40.00	46.00	48.00	47.00	0,54
Gender	1.00	1.04	1.08	1.13	0,24
Occupation	2.25	1.75	1.00	1.00	0,21

Table 6: Social vulnerability score, classification of social vulnerability, and social vulnerability class.

	Age	Gender	Occupation	SV Score
Gua Musang	22	0.24	0.47	22
Kuala Krai	25	0.25	0.37	26
Dabong	26	0.26	0.21	26
Manik Urai	25	0.27	0.21	26
Class score				SV Level
<8				Low
>8 and < 17				Medium
>17				High
Area				Score
Gua Musang				22
Kuala Krai				26
Dabong				26
Manik Urai				26
				SV
				High
				High
				High
				High

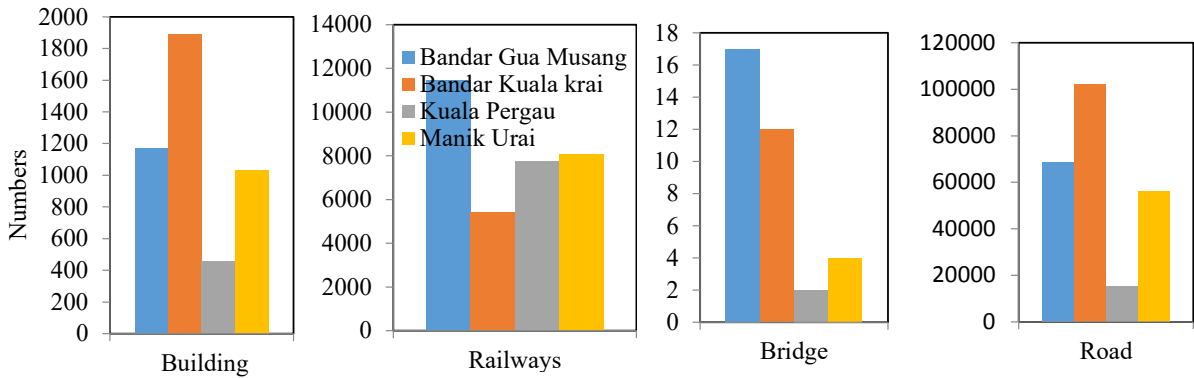


Fig. 6: Numbers of vulnerable buildings, railways, roads, and bridges.

The results of data processing related to physical vulnerability are shown in graphic images that represent each component (Fig. 6)

The physical vulnerability weight or index calculated by using the AHP method can be seen in Table 7.

The following method is used to calculate physical vulnerability across the entire study region. It adds up all components of physical risk, in this example, generally referred to as physical infrastructure, such as buildings, roads, railroads, and bridges, and multiplies them by their weights,  $PV = (0.411 \times building) + (0.288 \times road) + (0.185 \times railways) + (0.411 \times bridges) \dots(5)$

The results of calculations using Eq. 5 produce a total score as shown in Table 8.

Table 8 shows the physical vulnerability score from all areas based on their weight. Physical vulnerability is classified as Low (<8333), Medium (>8333 and <16666), and High (>16666). Based on the classification, Bandar Kuala Krai obtain the biggest score followed by Gua Musang, Manik Urai, and Kuala Perga. The results of the analysis shown in Table 8 also conclude that urban areas, Kuala Krai and Gua Musang Town are more vulnerable in terms of physical aspects than rural areas in Manik Urai and Kuala Pergau areas. By using the classification method in the table above, the level of Physical vulnerability can be determined as in Table 9.

Table 7: Physical vulnerability weight.

Parameters	Gua Musang	Kuala Krai	Kuala Pergau	Manik Urai	PV weight
Building	1.171	1.890	455	1.031	0.411
Road	68.629	101.984	15.047	56.192	0.288
Railways	11.445	5.407	7.742	8.074	0.185
Bridge	17	12	2	4	0.170

### Flood Vulnerability Classification

To determine the vulnerability index for the entire study area, the method used is in principle the same as the method used in calculating vulnerability in the portion of the study area. Based on calculations made, a comparison of the overall vulnerability class area can be seen in the following Table 10.

While the Total Vulnerability Index in the study area is shown in Table 11. Total vulnerability is obtained by adding up all the vulnerability component indexes throughout the blood of the study.

Since the index value is known, then the vulnerability index classification is determined from the entire study area. The vulnerability was classified as Low (<33), Medium (>33 and <66), and High (>66). Based on the classification, it is

Table 8: Physical vulnerability score.

Sub-district	Building	Railways	Road	Bridge	PV Score
Gua Musang Town	481	1,945	15,647	3	18,076
Bandar Kuala kraik	776	920	23,252	2	24,950
Kuala Pergau	187	1,316	3,430	0.3	4,933.3
Manik Urai	423	1,372	12,811	0.7	14,606

Table 9: Physical vulnerability class

Area	PVScore	PVLevel
Gua Musang	18.076	High
Kuala Krai	24.950	High
Dabong	4.933	Low
Manik Urai	14.606	Medium

Table 10: Vulnerability scores and vulnerability index of areas.

Parameters	Gua Musang	Kuala Krai	Kuala Pergau	Manik Urai	Weight
Social	22	26	26	26	0,541
Economy	1.00	1.04	1.08	1.13	0,241
Physical	2.25	1.75	1.00	1.00	0,211

Table 11: Total Vulnerability scores in all study areas

Parameters	Gua Musang	Kuala Krai	Kuala Pergau	Manik Urai
Social	22	26	26	26
Economy	16	51	28	41
Physical	18	24	5	14
Total	56	101	59	81

known that the Kuala Krai and Manik Urai areas are in the classification of areas with a high-level classification, while Dabong and Gua Musang are in the middle of the face in the Kelantan flooding event in 2014 (Table 12).

In terms of the economic impact at the community level, in remote rural areas, the loss of service facilities and shops can have a major impact on the community's economy. Urban areas typically see less of an economic impact than rural areas, in part because there are more options for amenities that can boost the local economy there.

The social impacts are discussed in two ways. First by direct examination of relationships between scarcity and density. Second particular social impacts indirect relationships between key demographic variables.

The population of old people is large in rural areas. Among them, mostly living alone increases flood vulnerability. Those people who migrate from urban to rural areas have less knowledge of flooding. It will also increase flood vulnerability. Migration, in general, is a key issue for both urban and rural areas.

### Risk Assessment

Flood risk is defined in this study as a function of flood hazard, Flood exposure, and Flood vulnerability. The risk assessment was done based on the flood hazard model

Table 12: Vulnerability level by areas.

Area	Score	VI Level
Gua Musang	56	Medium
Kuala Krai	101	High
Dabong	59	Medium
Manik Urai	81	High

simulation results, flood exposure data, and the identified vulnerable elements at risk. Two factors were considered while the assessment i.e., the magnitude and the probability of occurrence of the risk. Flood risk assessment is calculated qualitatively according to a certain class level and then spatially presented as a Flood Risk Map.

### Quantitative Risk Assessment

Flood risk can be considered as the actual threat. The estimation of flood risk results either in monetary or loss of life units, if the losses are measurable, or in qualitative terms (e.g. allocation in classes) in the case of intangible damages (social, environmental, cultural) to the affected areas. However, not all the values for the quantification of risk were available.

Based on flood hazard and the flood vulnerability for the different study areas using classes the qualitative assessment of risk was performed. The risk classes were weighted according to their level of importance. Follow the equation below:

$$\text{Flood Risk} = \Sigma FH + \Sigma FV + \Sigma FE \quad \dots(6)$$

The Flood Risk value of the data processing results shown in Table 13 shows that the greatest flood risk during the Kelantan extreme floods in 2014 based on the selected study area occurred in the Kuala Krai area, especially in terms of flood vulnerability.

Based on these data, flood risk is classified according to value into 3 classes High, Moderate and Low levels. Based on the classification, the class interval was obtained from Eq. (6):

$$\text{Class Interval} = \frac{273 - 0}{3} = 91 \quad \dots(6)$$

The highest flood risk value is 273, the lowest flood risk is 0. Flood risk in extreme flood conditions can be classified into 3 levels Low (0 to 91), Moderate (91 to 182), and High (>182). Based on the data collected, Gua Musang comes under the class Moderate while the rest is in the class High.

Based on Table 13, it can be said that flood risk is relatively higher in the rural area compared to the urban area as shown in Fig. 7. Risk assessment refers to the tolerability estimation based on the local society's acceptability criteria. The estimated risk comparison was based on the

Table 13: Flood Risk value in the study area

	FH	FV	FE	FR
Gua Musang	41	56	69	166
Kuala Krai	68	101	123	292
Manik Urai	63	59	129	251
Kuala Pergau	71	81	121	273

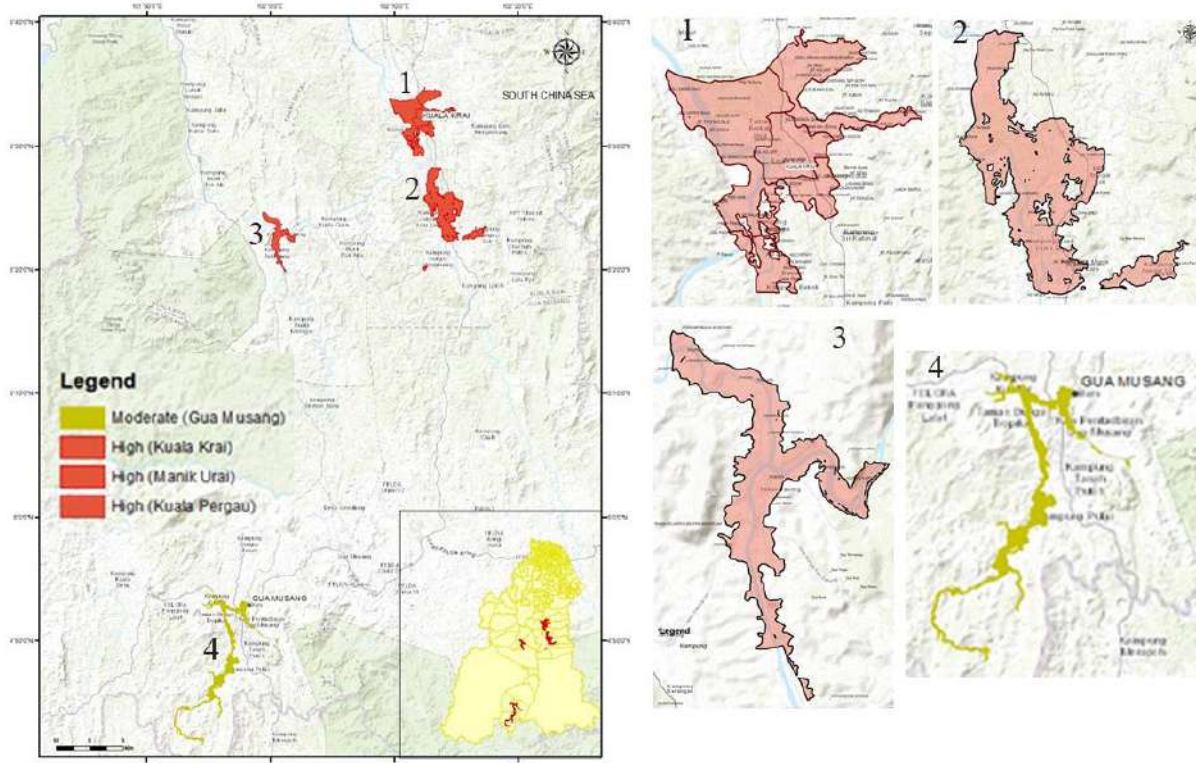


Fig. 7: Flood Risk Classes.

risk of the particular affected system and risk reduction application.

Research on economic flood impacts at the community level is lacking. As was already said, remote rural areas with little amenities and services were anticipated to have suffered greater economic losses. These setbacks further deplete rural residents' motivation to rebuild their businesses. It may also harm people's perceptions of the country as a desirable location for investments.

Before 2014, Kelantan experienced extreme flooding at least three times, in 1886, 1926, and 1967. However, because there was a lack of information at the time, it was unable to adequately prepare for the 2014 floods, which resulted in a loss of life and property. It may also be that the period between flood events is very long. The results of the survey and interviews only included one respondent who experienced severe floods in 1967. When there is extreme flooding, response actions should be expedited based on priority. This project is a methodical approach to addressing the flood issue in the field. It is vital to establish a specific value, whether it be the index, score of the extreme flood formula, or quantity, to ensure that this priority applies equally to all. All aspects of floods, including hazards,

exposure, and vulnerability, should be covered by this value.

In the case of extreme flooding, deforestation is not the main factor. It can be ascertained that deforestation in Kelantan in 1967 or earlier was still at a low stage, or not yet significant, and extreme flooding occurred. The results of the analysis show that the main cause of extreme flooding in Kelantan is the high intensity of rainfall. When a flood happened, the intensity of the rainfall in some places was very high. On the slopes of Mount Gagau, rainfall intensity of up to  $515 \text{ mm} \cdot \text{day}^{-1}$  was recorded for 3 days before the flood occurred.

## CONCLUSION

Three vulnerability classes such as economic, social, and physical were assessed using a questionnaire that contain 200 respondents' (flood 2014 affected people) interviews. In terms of economic vulnerability, Kuala Krai and Manik Urai are classified as High while Gua Musang and Kuala Pergau are classified as Medium. The social vulnerability which is focused on age, gender, and occupation, for all studies are classified as high. Physical vulnerability score from all areas shows Bandar Kuala Krai obtain the highest score followed by Gua Musang, Manik Urai, Kuala Pergau,

Kuala Krai and Bandar Gua Musang. Gua Musang Town is more vulnerable in terms of physical aspects than rural areas in this case the Manik Urai and Kuala Pergau areas. Total vulnerability is obtained by adding up all the vulnerability component indexes and the result is Kuala Krai and Manik Urai areas are in the high-level class, while Dabong and Gua Musang are in the medium class.

The risk classes were weighted according to their level of importance. The Flood Risk Value data processing results show that the greatest flood risk during the Kelantan extreme floods in 2014 based on the selected study area occurred in the Kuala Krai area, especially in terms of vulnerability. Flood risk is relatively higher in rural areas as compared to urban areas.

## ACKNOWLEDGEMENT

The authors gratefully acknowledged all staff of the Faculty of Earth Science, University Malaysia Kelantan for providing the facilities to carry out this research. The financial assistance provided by the short-term research grant project (Ac No: R/SGJP/A08.00/00644A/001/2012/000080), Universiti Malaysia Kelantan, and also from Fundamental Research Grant (FRGS) (Ac No: R/FRGS/A0800/00644A/003/2018/00556) is gratefully acknowledged.

## REFERENCES

Anees, M.T., Abdullah, K., Nawawi, M.N.M.A., Rahman, N.N.N., Ismail,

- A.Z., Syakir, M.I. and Abdul Kadir, M.O. 2019. Prioritization of flood vulnerability zones using remote sensing and GIS for hydrological modeling. *Irrigation and Drainage*, 68(2):176-190.
- Chan, N.W. 2015. Impacts of Disasters and Disaster Risk Management in Malaysia: The Case of Floods. In Aldrige, D.P., Oum, S. and Sawada, Y. (eds), *Resilience and Recovery in Asian Disasters, Risks, Governance, and Society*. Springer, Cham, pp. 239-265.
- Hassan A.J and Rozi A. 2006. Development of Flood Risk Map Using GIS for Sg. Selangor Basin. REDAC-USM, pp. 1-11.
- Ibrahim, N.F., Zardari, N.H., Shirazi, S.M., Haniffah, M.R.B.M., Talib, S.M., Yusop, Z. and Yusoff, S.M.A.B.M. 2017. Identification of vulnerable areas to floods in Kelantan River sub-basins by using the flood vulnerability index. *Geomate J.*, 12(29): 107-114.
- Imanda, A.R., and Andono, P.N. 2015. Utilization of Geographic Information System Using Analytical Hierarchy Process (Ahp) Method for Predicting Flood Prone Areas in Semarang City. Thesis. Dian Nuswantoro University Semarang.
- JICA. 1982. National Water Resources Study, Malaysia, Sectoral Report on River Conditions. Volume 5. Japan International Cooperation Agency, Kuala Lumpur.
- Lee, J.S. and Choi, H.I. 2018. Comparison of flood vulnerability assessments to climate change by construction frameworks for a composite indicator. *Sustainability*, 10(3): 768.
- Penning-Rowsell, E., Johnson, C., Tunstall, S., Tapsell, S., Morris, J., Chatterton, J. and Green, C. 2005. *The Benefits of Flood and Coastal Risk Management: A Handbook of Assessment Techniques*. Middlesex University Press, London, pp. 1-78.
- Rucinska, D. 2014. Spatial distribution of flood risk and quality of spatial management: A case study in Odra Valley, Poland. *Risk Anal.*, 35(2): 241-251.
- Yahya, H., Ahmad, M.N., Mohamad, R. and Rodzi, M. Z. M. 2016. Essential knowledge transfer process model to support disaster management. *J. Theoret. Appl. Inform. Technol.*, 87(3): 404.

... Continued from inner front cover

- The text of the manuscript should run into **Abstract, Introduction, Materials & Methods, Results, Discussion, Acknowledgement** (if any) and **References** or other suitable headings in case of reviews and theoretically oriented papers. However, short communication can be submitted in running with **Abstract and References**. The references should be in full with the title of the paper.
- The figures should preferably be made on a computer with high resolution and should be capable of withstanding a reasonable reduction with the legends provided separately outside the figures. Photographs may be black and white or colour.
- Tables should be typed separately bearing a short title, preferably in vertical form. They should be of a size, which could easily be accommodated in the page of the Journal.
- References in the text should be cited by the authors' surname and year. In case of more than one reference of the same author in the same year, add suffix a,b,c,.... to the year. For example: (Thomas 1969, Mass 1973a, 1973b, Madony et al. 1990, Abasi & Soni 1991).

### List of References

The references cited in the text should be arranged alphabetically by authors' surname in the following manner: (Note: The titles of the papers should be in running 'sentence case', while the titles of the books, reports, theses, journals, etc. should be in 'title case' with all words starting with CAPITAL letter.)

- Dutta, A. and Chaudhury, M. 1991. Removal of arsenic from groundwater by lime softening with powdered coal additive. *J. Water Supply Res. Techno. Aqua.*, 40(1) : 25-29.
- Hammer, D.A. (ed.) 1989. *Constructed Wetlands for Wastewater Treatment-Municipal, Industrial and Agricultural*. Lewis Publishers Inc., pp. 831.
- Haynes, R. J. 1986. Surface mining and wetland reclamation. In: Harper, J. and Plass, B. (eds.) *New Horizons for Mined Land Reclamation*. Proceedings of a National Meeting of the American Society for Surface Reclamation, Princeton, W.V.

### Submission of Papers

- The paper can be submitted by e-mail as an attachment in a single WORD file at **contact@neptjournal.com**
- The paper can also be submitted online in a single WORD file through the **online submission portal** of journal's website: **www.neptjournal.com**

### Attention

1. Any change in the authors' affiliation may please be notified at the earliest.
2. Please make all the correspondence by e-mail, and authors should always quote the manuscript number.

**Note:** In order to speed up the publication, authors are requested to correct the galley proof immediately after receipt. The galley proof must be checked with utmost care, as publishers owe no responsibility for mistakes. The papers will be put on priority for publication only after receiving the processing and publication charges.

# Nature Environment and Pollution Technology

**(Abbreviation: Nat. Env. Poll. Tech.)**

**(An International Quarterly Scientific Journal)**

Published by



**Technoscience Publications**

A-504, Bliss Avenue, Opp. SKP Campus  
Balewadi, Pune-411 045, Maharashtra, India

In association with

**Technoscience Knowledge Communications**

Mira Road, Mumbai, India

For further details of the Journal, please visit the website. All the papers published on a particular subject/topic or by any particular author in the journal can be searched and accessed by typing a keyword or name of the author in the 'Search' option on the Home page of the website. All the papers containing that keyword or author will be shown on the home page from where they can be directly downloaded.

**[www.neptjournal.com](http://www.neptjournal.com)**

©**Technoscience Publications:** The consent is hereby given that the copies of the articles published in this Journal can be made only for purely personal or internal use. The consent does not include copying for general distribution or sale of reprints.

Published for Proprietor, Printer and Publisher: Mrs. T. P. Goel, A-504, Bliss Avenue, Balewadi, Pune, Maharashtra, India; Editors: Dr. P. K. Goel (Chief Editor) and Prof. K. P. Sharma